unsaturated
SOILS

2006

EDITED BY
Gerald A. Miller
Claudia E. Zapata
Sandra L. Houston
Delwyn G. Fredlund

ASCE

GEO
INSTITUTE
/ASCE

UNSATURATED SOILS

2006

VOLUME ONE

PROCEEDINGS OF THE FOURTH INTERNATIONAL CONFERENCE
ON UNSATURATED SOILS

April 2-6, 2006
Carefree, Arizona

SPONSORED BY
The Geo-Institute of the American Society of Civil Engineers

IN COOPERATION WITH
The International Society of Soil Mechanics and Geotechnical
Engineering, Committee TC6 on Unsaturated Soils

The Canadian Geotechnical Society

EDITED BY
Gerald A. Miller
Claudia E. Zapata
Sandra L. Houston
Delwyn G. Fredlund

**GEO
INSTITUTE**

ASCE

Published by the American Society of Civil Engineers

Geotechnical Special Publications

This page intentionally left blank

Preface

Classical soil mechanics emerged in 1943 with the publishing of Karl Terzaghi's book entitled, "Theoretical Soil Mechanics". In 1948, the book titled "Fundamentals of Soil Mechanics" was written by Donald Taylor. These two books defined the context for classical saturated soil mechanics. These books focused on providing geotechnical engineers with the fundamental theories and formulations for three areas of application; namely, saturated flow through porous media, shear strength and its application to earth pressures, bearing capacity and slope stability, and volume change or settlement experienced when loading soft clay soils.

The scope of the application of soil mechanics was largely limited to saturated soils. In addition, moisture flux boundary conditions were not taken into consideration. In most cases an attempt was made to derive closed form solutions for either one-dimensional or two-dimensional characterization of the real world. Volume change problems were considered as a one-dimensional analysis with soil properties obtained from a one-dimensional consolidation test.

The original framework for soil mechanics served well for several decades but it gradually it became obvious that there were important "missing links" that remained outside the scope of soil mechanics. For example, the boundary conditions for a seepage analysis were limited to either a head boundary (i.e., such as water in a reservoir), or a zero flux boundary condition (i.e., such as an impervious soil). These boundary conditions have dominated the theory taught in soil mechanics at universities for many decades. There is a problem with such a limited scope of boundary conditions because we live in a "real world" with a moisture flux boundary condition at the ground surface. The moisture flux is controlled by climatic conditions at the site. Moisture flux boundary conditions become the primary forcing factor for many serious hazard related soil mechanics problems. Consequently, it is necessary to characterize the water balance conditions at the ground surface as well as modeling the infiltration of water into the soil.

Problems associated with expansive soils were the first class of unsaturated soil mechanics problems to be given serious research attention by geotechnical engineers. A series of international conferences were commenced to exchange ideas on how best to deal with expansive soils problems in 1965 at Texas A&M University. A series of conferences followed at approximately 4 year intervals. In the early 1990s it was realized that there would be merit in expanding the scope of problems addressed to include all types of unsaturated soils problems. Environmental engineering problems involving contaminant transport were also of paramount interest and concern. The first International Conference on Unsaturated Soils was held in Paris, France in 1995. This was followed by the Second International Conference on Unsaturated Soils in Beijing, China in 1998 and the Third International Conference on Unsaturated Soils in Recife, Brazil in 2002.

Historically, it is possible to look back and note that several major hindrances lay in the way of an early understanding of how best to formulate a science for unsaturated soil behavior. Most of these hindrances have now been thoroughly researched with the result that practical

engineering solutions have been proposed. It would now appear that it is time to force ahead with a full scale implementation of unsaturated soil mechanics into routine geotechnical engineering practice. The original hindrances that appear to have been sufficiently resolved can be stated as follows:

1.) the theories and formulations associated with unsaturated soil behavior for the classical subject areas have been proposed and verified,

2.) techniques and procedures have been developed for the estimation of nonlinear unsaturated soil property functions,

3.) the central role and importance of the soil-water characteristic curve (SWCC), or the water retention curve, has been realized,

4.) devices for the measurement of soil suction have been developed,

5.) new procedures for the solution of highly nonlinear partial differential equations have been discovered, and

6.) the teaching of unsaturated soil mechanics concepts, principles and solutions is increasingly becoming a part of the undergraduate and graduate teaching curriculum.

The Fourth International Conference on Unsaturated Soils held in Carefree, Arizona, provides yet one more opportunity to bring together researchers and practitioners in unsaturated soil mechanics from around the world. Significant strides have been made in the research of unsaturated soils problems and it is imperative that researchers be provided with a forum for the interchange of research findings and ideas. This is the primary purpose of the Fourth International Conference on Unsaturated Soils.

Each of the papers included in the proceedings received at least one positive peer review. All of the papers are eligible for discussion in the ASCE/G-I *Journal of Geotechnical and Geoenvironmental Engineering,* and all of the papers are eligible for ASCE Awards. Nearly eighty reviewers from around the world participated in the peer review process for abstracts and papers; the editors are sincerely appreciative for the efforts of all the anonymous reviewers. Special thanks go to the following persons for organizing and coordinating paper reviews for the following tracks:

- Evapotranspiration Cover Systems - Craig Benson, Charles Shackelford and Beth Gross (on behalf of the G-I Geoenvironmental Engineering Committee)
- Dynamic Soil Properties and Liquefaction Strength of Unsaturated Soils-- Mishac Yegian (on behalf of the G-I Earthquake Engineering and Soil Dynamics Committee)
- Geophysical Methods for Unsaturated Soils – Soheil Nazarian and Michael Rucker (G-I Geophysical Engineering Committee)
- Determination/Estimation of Unsaturated Soil Properties -- Claudia Zapata and Sandra Houston (on behalf of the G-I Soil Properties and Modeling Committee).

Delwyn G. Fredlund
Sandra L. Houston
Gerald A. Miller
Claudia E. Zapata

Contents

Volume One

Keynotes and Special Lectures

Field Investigations of Unsaturated Soil Systems and Equipment

Field Studies of Water Movement in Unsaturated Soil

Geophysical Methods for Unsaturated Soils

Evapotranspirative Cover Systems

Laboratory Investigations of Unsaturated Soil Systems and Equipment

Laboratory Investigations of Volume Change in Unsaturated Soil

Volume Two

Modeling Associated with Waste Repositories

Miscellaneous Analytical and Empirical Modeling for Unsaturated Soil

Indexes

This page intentionally left blank

Unsaturated Soil Mechanics Applied To Geotechnical Problems

E. E. Alonso and S. Olivella [1]

[1]Department of Geotechnical Engineering and Geosciences, Technical University of Catalonia (UPC), Building D2, Campus Nord, c/ J. Girona, 1-3 08034 Barcelona, Spain; PH (34) 934 016 866; FAX (34) 934 017 251; eduardo.alonso@upc.edu

Abstract

The paper presents an evaluation of the current state of development of unsaturated soil mechanics by directing the attention to the capabilities of existing methods of analysis to face real problems. A review of recent contributions in several fields of application: fills, embankments and dams; pavements, foundations; landfills; slopes; nuclear waste disposal and infiltration is presented. The review shows the increasing sophistication of available tools although well documented case records remain scarce.

Introduction

Unsaturated soil mechanics has traditionally been a specialized topic within the general field of Soil Mechanics and Geotechnical Engineering. One of the reasons for being "specialized" may be attributed to the small number of research groups interested in unsaturated soils. However, in recent years the number of professionals and research groups actively involved in a variety of aspects related to unsaturated soils has vastly increased. A good indication of this interest is the number of symposia and conferences being held worldwide. A review of major international journals reveals also an increased number of high quality papers being published in the field. A significant proportion of the published research deals with basic aspects: laboratory techniques and experimental results, theoretical developments and, in particular, constitutive models and numerical formulations of coupled flow-deformation models. In addition, and probably for a good reason, soils that exhibit non-typical characteristics (cemented and residual soils, saline soils, highly swelling materials, etc.), which are included under the general denomination of "special problem soils", are discussed in unsaturated soils conferences and workshops. However, engineering applications, especially those which involve well-documented case histories are more difficult to find. This review cannot possibly deal with all the aspects mentioned but,

in view of the relevance of engineering applications and its central position to judge the merits and to provide value to the vast basic research being performed, it was decided to focus this paper on the application of unsaturated soil mechanics to solve engineering problems.

Our present International Conferences on Unsaturated Soils were conceived as a generalization of the successful series of conferences on expansive soils which provided an extensive account of engineering problems associated with expansive soils, notably those which involve foundations and, to a lesser extent, other aspects such as slopes and pavements. It should be added, though, that many contributions had a strong empirical or semi-empirical character, rooted into practice, but difficult to generalize to a wider range of applications.

The purpose of this review is to show the wide variety of practical engineering problems now being covered by unsaturated soil mechanics. More specifically, the idea was to show how modern developments help to better understand the observed field performance. In this regard, applications which have a strong empirical character will not be discussed, despite the interest they may have in particular cases.

In recent years, the use of numerical tools in geotechnical engineering has generalized. However, a sound understanding of problems is as necessary now as it was before. The proper use of models, which exhibit an increasing sophistication, requires an adequate training in conceptual developments, theoretical issues and modelling techniques. An added difficulty is the need for a reliable estimate of relevant parameters. Application of unsaturated soil mechanics in practice will not escape from this general trend.

A typical feature of practical applications in unsaturated soil mechanics is the need to handle flow and deformation phenomena in an integrated manner. The reason behind is that changes in water content, or suction, generate deformations and stresses and, on the other hand, suction gradients -which generate flow- are almost inevitable in any practical situation. The implication is that most applied problems are "coupled". This flow-deformation coupling is sometimes solved in a very simple way. For instance, if one considers the long-term behaviour of a compacted embankment, an extreme scenario is to assume that it will saturate. Then, it is the change from "as compacted" to saturated conditions, which needs to be considered. When dealing with foundations on expansive soils, some methods of analysis require as input data the maximum expected potential heave of the soil and its spatial variation. These are examples of flow-deformation coupling being solved in a straight-forward manner. However, the hypothesis of full saturation may be unrealistic in some cases. But perhaps equally significant is the fact that the transient processes and the associated "intermediate" states are necessary to understand the field behaviour, especially if it is being measured by sensors.

In order to perform this review, engineering applications have been grouped in a few issues:

- *(a)* fills, embankments and dams;
- *(b)* pavements;
- *(c)* foundations;

(d) landfills;
(e) slopes;
(f) nuclear waste disposal, and
(g) infiltration.

A selective choice of available contributions and knowledge is unavoidable. The main purpose of the paper is to show the possibilities offered by modern unsaturated soil mechanics to make successful predictions and to provide an improved understanding of the observed behaviour. The reader may notice also some bias towards the work performed by the two authors and their colleagues. It is hoped that this limitation is compensated by a more in-depth knowledge of the cases presented.

Fills, Embankments and Dams

It is a common observation that fills, compacted to some extent, tend to change volume when wetted. Two case histories which involve collapse settlements have been reported by Charles et al (1984) and Brandon et al (1990). The first case is an example of "subsidence" of a loosely deposited fill of sandstone and siltstone (70m deep) induced by the progressive raise of the water table. The second case involves compacted fills of sandy clay which experienced a strong increase in surface infiltration at a given time after construction. In both cases the fills settled under their own weight. The ultimate cause of the collapse in both cases is the insufficient density of the compacted material. Embankment and dams are in general more carefully compacted although difficulties associated with deformations during the life-time of these structures are often reported.

The behaviour of compacted soils under laboratory and field conditions is a classic subject that may receive a more appropriate and precise analysis from the perspective of unsaturated soil mechanics. In fact, most of the basic experimental information used to validate constitutive models is obtained from compacted specimens. After construction, embankments experience changes in water content as a result of climatic factors and capillary rise from shallow phreatic levels. Suction will change in time at an essentially constant stress state. Volumetric, as well as distortion strains, may take place. Figure 1 shows the volumetric "shrinkage" experienced by a road embankment, insufficiently compacted on the dry side, after a heavy rainfall (Alonso et al. 1996). In this case, a simulation of the rainfall action on a 7 m-high embankment provided a clear understanding of the effect of collapse on the overall response of the structure (Fig. 2). The embankment experienced a volumetric contraction and not only a settlement. This is shown by the arrow lines in Figure 2, which follow the position of a few points in the embankment boundary. The horizontal displacement calculated in points of the slope, especially in the lower part, is confirmed by the actual behaviour (Fig. 1).

Computational models for coupled flow-deformation offer a powerful tool for the analysis of embankment performance. Consider as an example the design of a canal embankment on natural collapsible soils, a case described in Alonso et al. (2005b). One of the options examined to avoid excessive settlements of the

embankment was to substitute the collapsible soil (a low density carbonated soil) by the same soil compacted to a Normal Proctor optimum state. Tests were performed to characterise the natural and the compacted states by means of an elastoplastic model ("Barcelona Basic Model":BBM; Alonso et al, 1990). Then, several scenarios concerning the climate and the possible water losses from the canal were simulated. Figure 3 shows a schematic cross-section of the canal and the layers used to simulate the construction. The rainfall recorded during one year in a weather station located in the area is shown also in Figure 3. A suction equivalent to a relative humidity of 60% was imposed when no rain was recorded. In Figure 4 computed settlements of the concrete slab, for a period of 13 years, are represented for one of the design scenarios considered: heavy water losses from the canal start 2.5 yrs after the site beginning of the simulation. In the whole period rainfall infiltration is defined by a repetition of the one-year record shown in Figure 3. When infiltration comes only from the rain, settlements remain small irrespective of the type of embankment foundation: either the natural or the compacted soil.

However, in the case of natural foundation soil, some time after the start of canal losses settlement accelerates and it accumulates during a number of years. The period of slower rate of settlement corresponds to the dry weather: natural evaporation compensates in part the infiltration from the canal. When the embankment foundation is a compacted soil, settlements are small. The periodic sequence of infiltration and evaporation is reflected in the settlement record, but no accumulation of settlements is observed in this case.
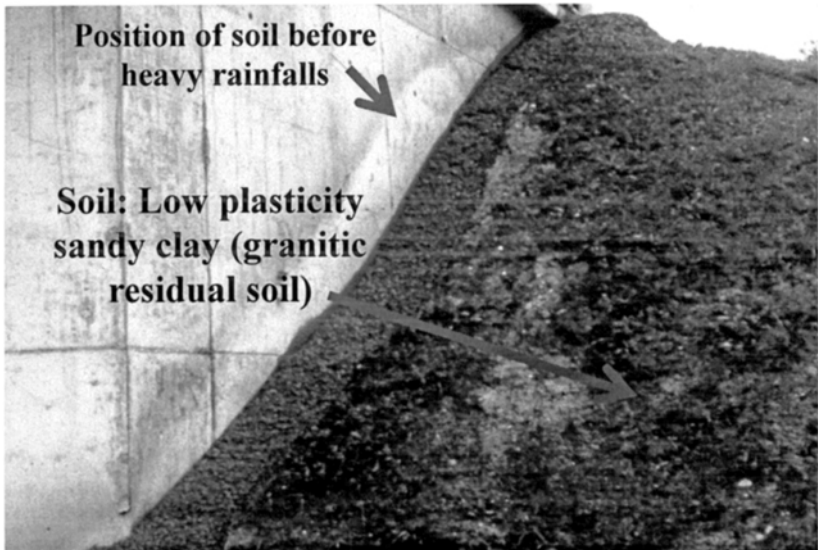
Figure 1. Collapsed embankment after heavy rainfalls. The black band close to the bridge abutment is a bituminous concrete which fills the empty volume left by the collapse of the embankment
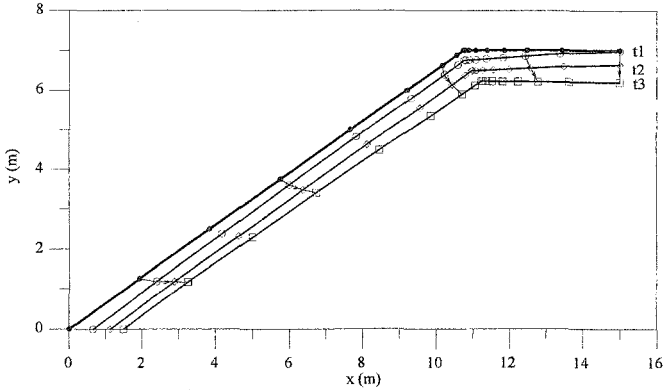
Figure 2. Computed surface profile of the embankment shown in Figure 1 at three different times Constant rainfall infiltration
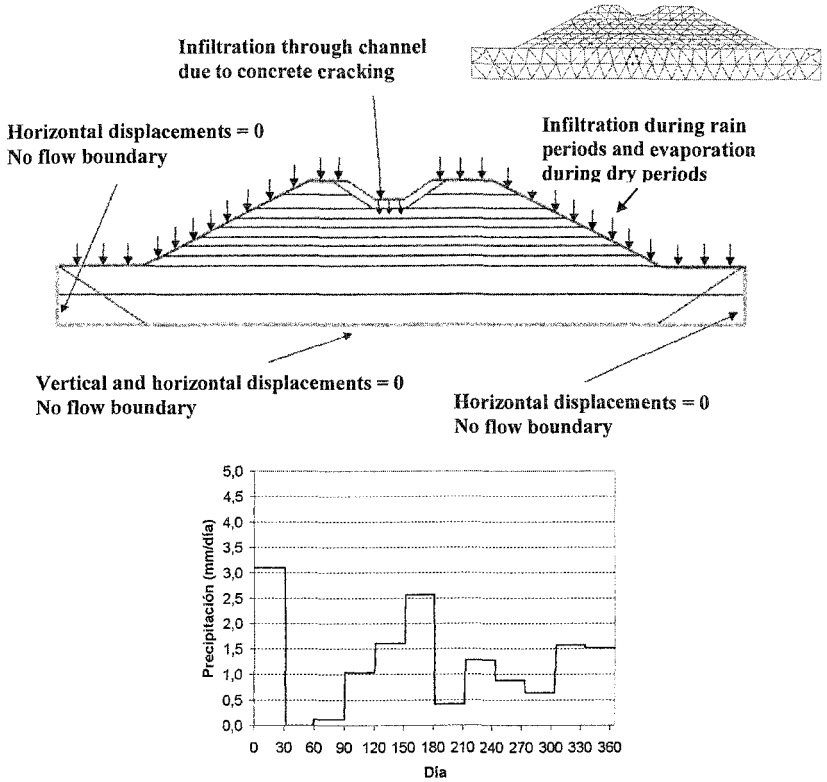
Figure 3. Canal Segarra-Garrigues. Geometry, discretization and 1-year rainfall record.
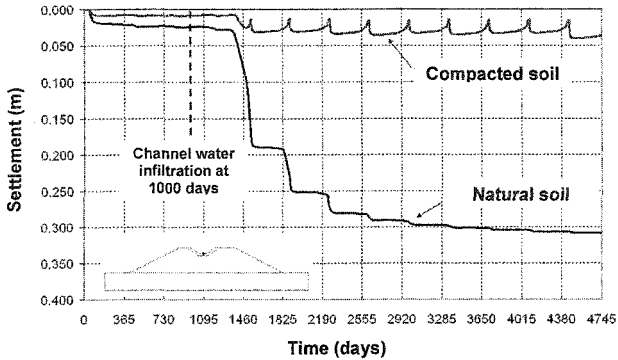
Figure 4. Settlements due to embankment construction, rainfall action and canal leakage.
Embankment founded on natural or compacted soil

The deformation analysis of embankments and earth-dams subjected to climatic effects requires an elasto-plastic formulation of the stress-strain behaviour. The topic is not merely academic since the rain action may induce settlements and horizontal deformations similar in magnitude to the movements induced by the full flooding of the upstream shell of a dam (an interesting case is the behaviour of Beliche dam, analyzed in a series of papers: Naylor et al., 1986, 1997; Alonso et al., 2005a). In this dam, as in many others, the rockfill collapse upon wetting was the main component of measured movements.

A characteristic feature of fill collapse induced by the weather action is its correlation with the rainfall records. This is shown in Figure 5, for a 40 m-high embankment (AVE embankment) made of compacted schist, whose behaviour was discussed by Soriano & Sánchez (1999). A good correlation between the rainfall intensity and the rate of settlement is observed during the period 1993-1998. Such a strong correlation has been reported in several dams: El Infernillo (Marsal et al., 1976), Beliche dam (Naylor et al., 1986, 1997), and Martin Gonzalo dam (Justo and Durand., 2000). However the rainfalls at the end of 1997, (Figure 5) having an intensity similar to those recorded in 1996, did not result in additional settlements. In the dams mentioned above the good correlation between rainfall and rate of settlements (and horizontal movements) was also lost a number of years after the end of construction. The modelling of the AVE embankment and of Beliche dam have been reported in Alonso (2003) and Alonso et al. (2005a). In both cases the rockfill and the compacted core (in the case of Beliche) were represented by an elasto-plastic constitutive model.

A comparison of measured and calculated settlement rates for the AVE embankment is shown in Figure 6. The agreement is good although the measured settlement rates tend to be higher than the computed values. The interesting point, however, is that the model correctly predicts that the strong rainfall events at the end

of 1997 did not induce any significant response of the embankment. A simple explanation for the behaviour is offered by the elasto-plastic constitutive model used to represent the embankment behaviour. At the beginning of 1997, the previous rainfall has been able to reduce the suction values within the embankment to such low levels that an additional rainfall was not able to induce any further yield of the compacted material. In constitutive terms, the elastic locus has now expanded and suction changes only induce reversible and (relatively small) elastic deformations. Even if the embankment becomes drier in the future, a new rainfall will not lead to significant displacements. The "time effects" are only a consequence of the evolution of infiltration and evaporation rates. "True" time effects can only be clearly identified once the suction-induced effects have ended. This distinction is important in the evaluation of dam performance and it has been further discussed in Alonso et al. (2005a), in the case of Beliche dam.
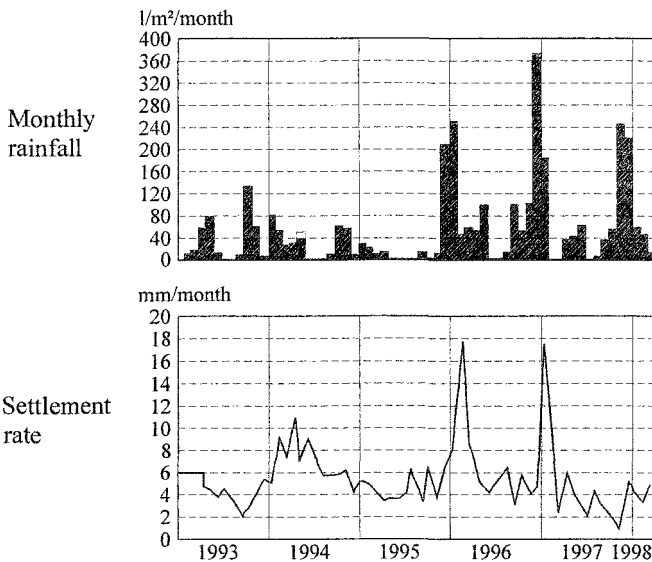
Figure 5. Settlement rates of a 40 m-high embankment belonging to the highspeed railway line between Madrid and Sevilla and rainfall records in the same area (Soriano & Sánchez, 1999).
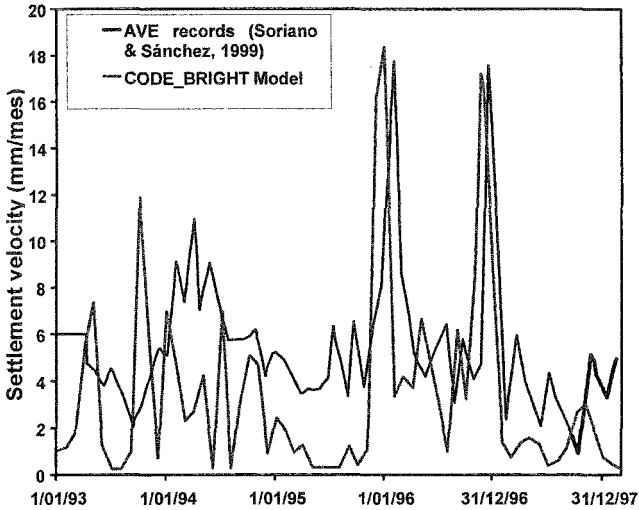
Figure 6. Comparison of measured and computed settlement rates of the AVE embankment.
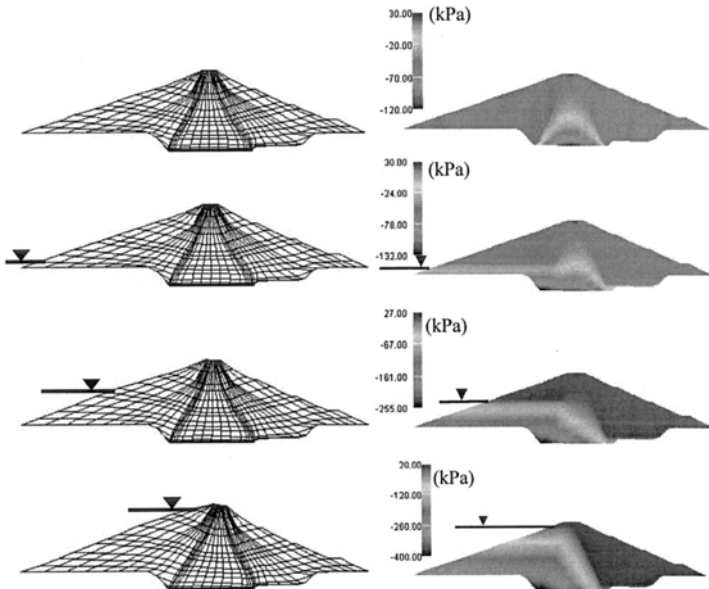
Figure 7. The calculated dam behavior during first reservoir filling, (a) Deformations in Case A displayed by 50 times and (b) Pore water pressure distributions in Case A. (Kohgo, 2005)
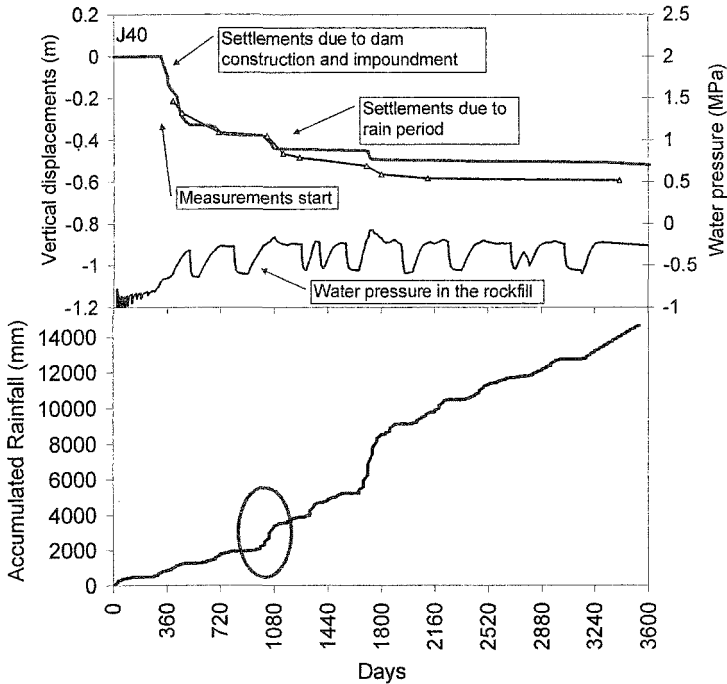
Figure 8. Calculated and measured vertical displacements of surface marker J40 of the doewnstrem shell of Beliche dam. The lower plot shows the accumulated rainfall

The application of unsaturated soil mechanics to the analysis of dams has been reviewed in the reports of Fry et al. (1995) and Kohgo (2003). A steady improvement in the techniques of analysis is apparent when the two reports are compared. A recent elasto-plastic fully coupled analysis of an actual dam was reported by Kohgo et al (2005). Figure 7 shows the evolution of flow within the dam and the parallel development of deformations. In the case represented, the dam had rather compressible rockfill shells. The insight that coupled flow-deformation analysis may provide into the behaviour of dams is shown in the review of Beliche dam reported in Alonso et al. (2005a). The dam was well-instrumented and large-diameter triaxial and oedometer tests of dam materials for dry and saturated records, as well as meteorological information were available. In the long-term simulation performed, dam materials were characterised by elastoplastic models previously calibrated with the help of the large-diameter tests. An interesting aspect in Beliche dam is the magnitude of the vertical and horizontal movements recorded in the downstream rockfill shell, not directly affected by the reservoir. Measured and calculated records are compared in Figure 8. The "jumps" observed correspond to periods of heavy

rains. Also indicated is the calculated suction in the rockfill. The acceleration of displacements coincides with peaks of low suction. However, only when the suction reaches values lower than any previous suction in the past history, irreversible deformations take place. This is well illustrated in Figure 9, where irreversible volumetric deformations in points of the upstream shell, core and downstream shell are plotted against time. Beyond an initial transient period of continuous accumulation of strain, irreversible deformations correspond to extremes of rain intensity.
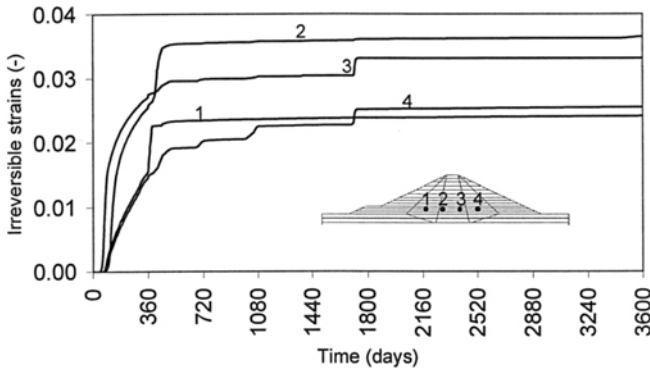
Figure 9. Calculated irreversible volumetric strains at the points of Beliche dam shown in the insert. Jumps correspond to periods of heavy rainfall.

The analysis of Beliche dam illustrates the relevance of suction (or relative humidity) to explain the behaviour of compacted clay (the core) and the coarse shoulder rockfill. Dams (and embankments) have been routinely analyzed by means of finite element techniques within the framework of Terzaghi's effective stress. These procedures, which are useful for some purposes, are unable to handle environmental factors. In fact, the climate was directly responsible for the behaviour of the downstream shoulder of Beliche. During construction and before full-impoundment, the deformations of the entire dam were largely controlled by the climate. The analysis within the framework of unsaturated soil mechanics helps also to distinguish the deformations associated with suction changes from pure creep effects. The former may be relevant for a number of years following dam completion. The period in which water-related effects are dominant depends on the specific climate and the permeability and retention properties of the dam materials.

Some of the current computer models for unsaturated soils include both air and water conservation equations. Air (or any other species in gaseous form) may flow in fully saturated or in occluded conditions as a dissolved species in the liquid. Air dissolution and exsolution in water is taken into account through Henry's law. On the other hand, the relative permeability (to water) depends strongly on the degree of

saturation. This background explains why the loss of saturation due to gas exsolution, a phenomenon that takes place when the liquid water pressure decreases, may lead to a significant reduction in permeability and therefore it may lead to a significant change in calculated pore water pressures. This mechanism has been invoked by Alicescu et al (1999) and LeBihan and Leroueil (2002) to explain the abnormal increase in water pressure observed in the downstream part of the clay core of some earthdams. They solved a one dimensional flow equation, which included the outlined effects and found that the calculated pore pressure distribution across the thickness of the dam core (an example of model calculations is reproduced in Figure 10) was close to actual measurements (Alicescu et al, 1999). Other explanations have also been suggested to explain this phenomenon, but the analysis of LeBihan and Leroueil is a novel and sensible approach which highlights the benefits of a joint saturated-unsaturated formulation of water flow in soils.
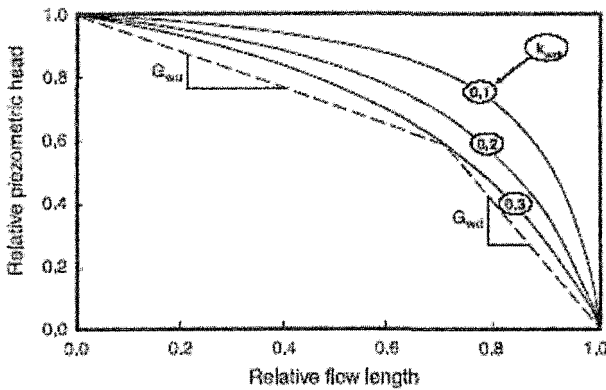
Figure 10. Envelopes of maximum relative piezometric heads as afunction of relative flow length for different values of kwrf. (LeBihan and Leroueil, 2002)

Pavements

Pavement structures experience a direct atmospheric action. Periods of infiltration and evaporation result in suction changes, which modify the initial state. Therefore, suction becomes an additional variable that has to be considered to interpret pavement performance. The effect of suction on base, sub-base and sub-grade properties has been reported by many authors. Suction effects on resilient and deformation moduli have been described by Fleckestein & Allen (1996), Sauer & Monismith (1968), Thompson & Robbnet (1979), Odeon et al. (1995), Edris & Lytton (1977), Uzan (1985), May & Witczak (1981), Phillip & Cameron (1995), Pappin & Brown (1992) and Jin et al. (1994), among others. The effect of suction on volume change and strength is, of course, also relevant in pavements, especially in sensitive sub-grades such as expansive soils.

Integrated analyses of pavement performance from the perspective of unsaturated soil mechanics are, however, scarcer. Flow (and temperature) models have been described by Wallace (1977), Pufahl et al. (1990) and McEnroe (1994). They lead to reasonable distributions of moisture conditions in the layered pavement structure under certain simplified boundary conditions. A simulation of pavement performance under environmental actions was described by Alonso (1998). A fully coupled thermo-hydro-mechanical (THM) finite element code (CODE_BRIGHT; Olivella et al., 1994; 1996; DIT-UPC, 2002) was the basic tool to perform the analysis. A reference pavement structure for heavy traffic was subjected to a Mediterranean type of climate, illustrated in Figure 11. The one-year record shown in Figure 8 was cyclically repeated for the multi-year simulations performed. The properties of the different layers were selected on the basis of previous experience and the specifications given for the reference pavement selected. Base and sub-base materials were granular pervious mixtures. For the sub-grade, a silty clay type of material was selected. For the bituminous pavement, two alternative conditions were examined: essentially impervious or "cracked". In the second case, a limited amount of infiltration and free evaporation is allowed.
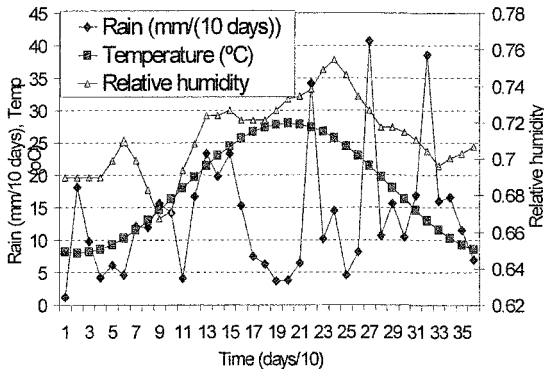
Figure 11. Yearly variation of Relative Humidity, rainfall and temperature in a representative Mediterranean climate.

The analysis included vapour transfer. The upper-pavement layers were considered rigid against suction changes. However, the subgrade was able to swell or shrink as suction changed. Thermal expansion and contraction of materials was also considered. A sketch showing the dimensions of the discretized domain is given in Figure 12. An initial suction condition, in equilibrium with a water table located at the lower boundary of the discretized domain, was assumed.
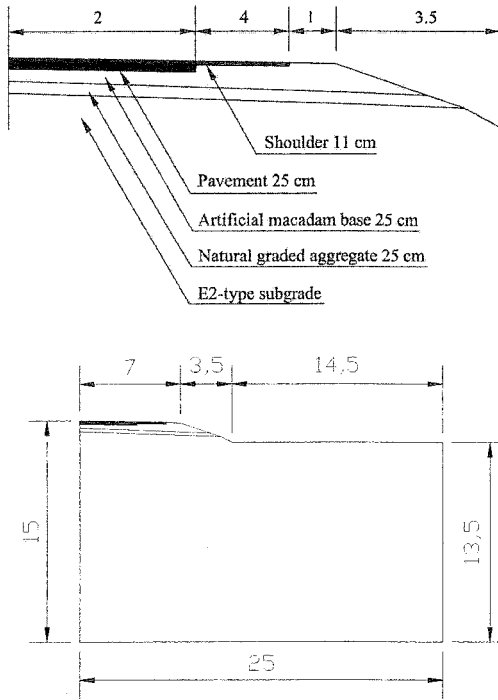
Figure 12. Discretized domain for the simulation of pavement performance.

The calculated changes of degree of saturation and vertical displacements for a few representative points of the impervious pavement are shown in Figures 13 and 14. The impervious pavement and the upper granular layers result in a very limited variation of the degree of saturation of points in the sub-grade. However, a slow accumulation of moisture was calculated with a marked cyclic character. This evolution resulted in a very moderate and irreversible heave, as shown in Figure 13. The unprotected surface (Point D) exhibited stronger cyclic changes in degree of saturation, which had a negligible effect on the pavement performance.
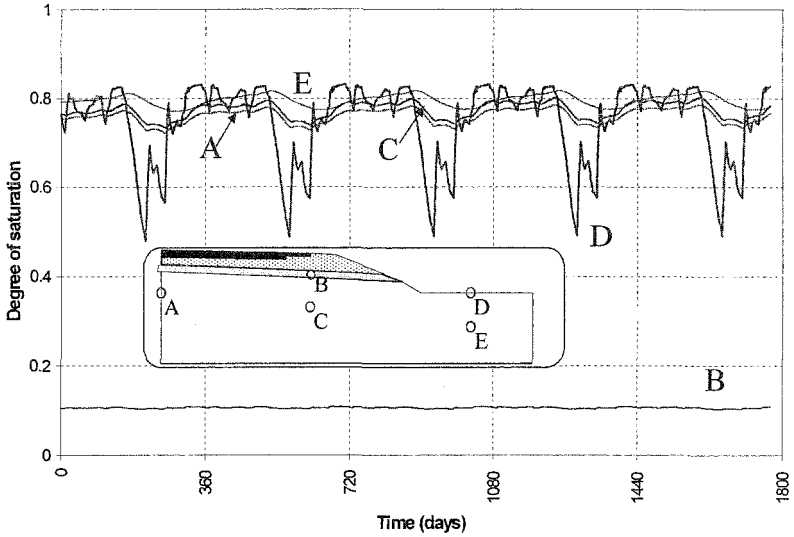
Figure 13. Impervious pavement. Variation of degree of saturation along time in some representative points.
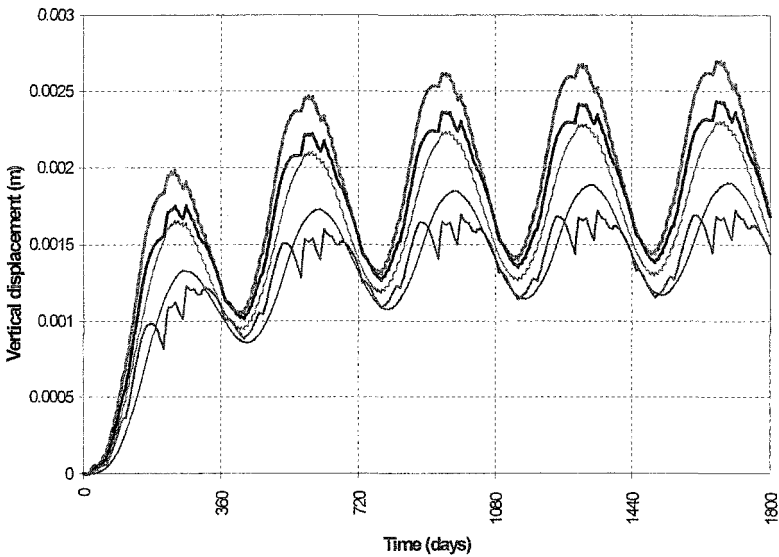
Figure 14. Impervious pavement. Variation of vertical displacement along time in some representative points.

When the pavement is cracked and evaporation is allowed, the situation changes. Points in the shoulder zone (Point C) experience now a settlement due to the shrinkage induce in the sub-grade. At the pavement axis (Point A), however, the computed displacements are almost negligible. This example has the purpose of showing the capabilities of coupled THM codes to model realistically the effects of environmental changes on a pavement. A particularly nice feature of these analyses is the possibility of investigating, at a limited effort, the effect of a number of design variables on the pavement performance: location and depth of drains, impervious barriers, median width and type of cover, permeability and retention properties of the different layers, etc.
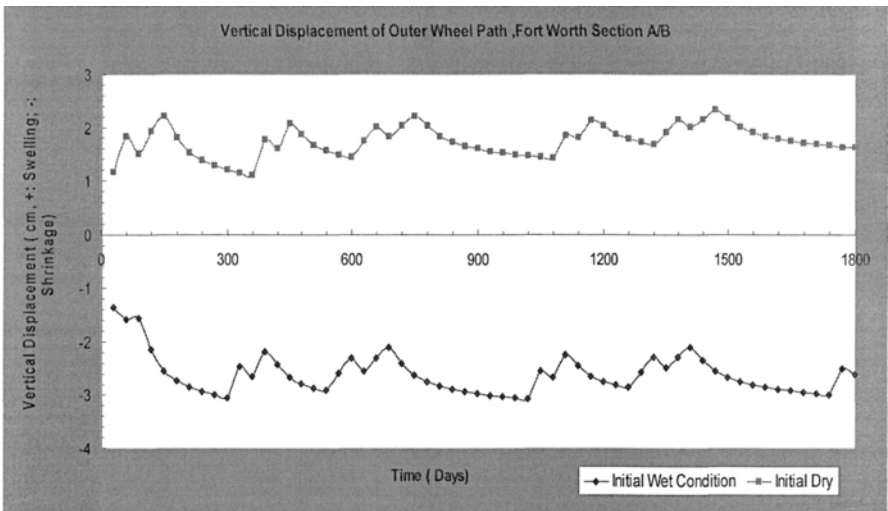
Figure 15. Effect of initial conditions on calculated vertical displacements (F.W. Section A/B)(Lytton et al., 2004).

The next step is to integrate this type of analysis in the design of the pavement. Lytton and his colleagues (Lytton et al., 2004; Hong et al., 2006a, b; Long et al., 2006; Bulut et al., 2005) have developed a design procedure for pavements in expansive soils, which includes a flow-deformation analysis of the pavement layers and the expansive sub-grade. The soil volumetric deformation is defined by means of a "state surface" which describes void ratio as a function of suction and confining stress (in fact, volumetric deformations are defined by means of two compressibility coefficients). They use the concept of soil diffusivity (Bulut et al., 2005), instead of permeability and water retention. An effort was made by the authors to provide a practical procedure to find all the relevant parameters in terms of basic soil parameters. The main idea behind the procedure is to find the expected maximum vertical displacement of the pavement during the simulation period. The difference between calculated vertical displacements along time for two widely different initial conditions ("wet" or "dry"; Fig. 15) provides the maximum expected displacement.

This value, in turn, is empirically related to the rate of pavement roughness development, which, in Texas practice, leads to design recommendations.

The flow deformation analysis provides, in this case, a systematic and consistent procedure to investigate a number of circumstances and design decisions that may affect he behaviour of the pavement (dimensions and position of vertical barriers, layers of inert materials, the thickness of a stabilized layer, the cover of the median, the width of shoulders, etc.). The procedure developed by Lytton et al. (2004) relies heavily on a local experience and it nicely shows how advanced models may be combined with empirical procedures to arrive to practical design decisions.

Foundations

Design criteria and construction techniques for building foundations on expansive soils are described in Nelson and Miller(1992). Design procedures rely on the free field estimate of heave and involve, in general, simple and robust criteria and calculation procedures. Poulos & Davis (1980) include the case of heaving ground in their analysis of single piles and pile groups. Several procedures are available for the analysis of slabs on swelling soils (Jiménez-Salas, 1965,1980; Lytton, 1973;). The key information for these procedures is the description of the soil profile after swelling.

Machado et al (2002) describe the use of plasticity models to analyze the behaviour of field tests on a single pile with enlarged base. The soil profile, a 7m deep colluvium on top of a residual soil was described by means of an elasto-plastic model developed by Machado (1998). Model parameters were determined by means of suction controlled tests on block samples collected in the field at several depths. The initial field suction profile was also determined. In one of the cases analyzed the soil was wetted before load application. A comparison of the measured and calculated load displacement curve is shown in Figure 16. The agreement is especially good for the initial part of the experiment. The unloading-reloading cycle is successfully reproduced.

Most of the design and calculation procedures mentioned do not link the soil swelling (or collapse) with the moisture transfer, which is at the origin of the observed phenomena. Moisture transfer, in turn, is controlled by climatic variables (type of cover, rainfall, wind velocity, solar radiation, etc.), design data (extent of the covered area, drainage or isolation barriers, if they exist, time of construction, etc.) soil profile and soil properties. It is a complex problem, which is coupled to the mechanical behaviour of the soil.
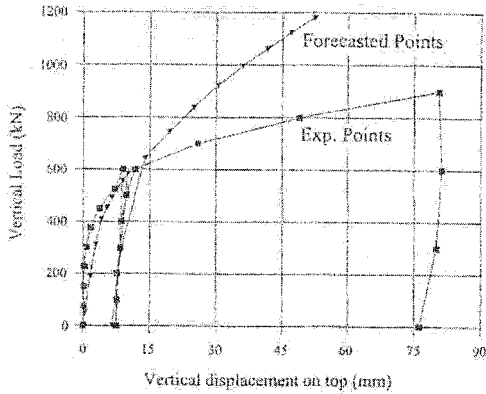
Figure 16. Experimental and predicted results obtained in Field test T-2. The soil was wetted before load application (Machado et al, 2002)

Coupled flow-deformation formulations for unsaturated soils have been developed in the last three decades. The initial developments followed the formulation of the "consolidation" problem for saturated soils and substitute formally Terzaghi's effective stress by a new formulation (generally Bishop's definition), which included the water suction (Alonso, Gens and Hight 1987). In several sections of the present paper, coupled formulations have been mentioned in connection with other engineering applications. In principle, a numerical program (generally based on a finite element approximation) handling the coupled flow-deformation in unsaturated soils may be used to analyze foundation problems. If a single effective stress (Bishop, in particular) is used to formulate the water continuity and the equilibrium equations and no additional and independent effect of suction (or water pressure) on the mechanical constitutive equations is introduced, the procedure may be useful to describe swelling-shrinkage phenomena. Recent examples are provided by the work of Ng & Small (2000) and Lytton et al. (2004).

An explicit consideration of two independent stress fields offers the opportunity to integrate into a single framework swelling and collapse phenomena. An example of such a formulation and its application to analyze the heave experienced by a nuclear power plant founded on expansive marls was described in Alonso et al. (1991) and Gens et al (1991).

Elastoplastic models for unsaturated soil behaviour offer an increased capability to model irreversible phenomena and coupling effects. Sheng et al. (2003) modified the original BBM, substituting the net stress by an effective stress:

$$\sigma'_{ij} = \sigma_{ij} + f(Sr) u_w \, \delta_{ij}$$

where f(Sr) is a function of degree of saturation, which in the examples solved was

taken as Sr or $\sqrt{Sr}$. They maintained other basic features of BBM and, in particular, the hardening effect of suction. The paper, which solves several cases of a footing on an unsaturated soil, places a particular emphasis on the numerical implementation of the equations and on stability and convergence criteria, Figure 17 shows the geometry of the foundation problem and Figure 18 reproduces the calculated displacements for one of the cases solved. The soil profile was initially saturated. It was later partially dried by applying a surface suction of 100 kPa. The footing load was added and a final surface wetting was simulated. The stressed points under the footing collapsed in this example, whereas the unloaded points under the free surface experienced a swell under the final wetting. This paper shows the capability of modern coupled formulations. A number of finite element programs are today available to solve similar problems.

An additional example is provided by the analysis of the "expanso-collapsometer", a field device, which was designed to measure "in situ" the heave or collapse potential of soils (Ferreira and Lacerda, 1995)(Fig. 19). Costa et al. (2004) compare the measured settlement of an experiment performed on a residual soil from Brazil with the calculations performed with CODE_BRIGHT (DIT-UPC, 2002). Soil parameters for a BBM model were in this case derived from flooding tests on block specimens (Fig. 20). A comparison between the calculated development of settlements in time and the measured values is given in Figure 21.
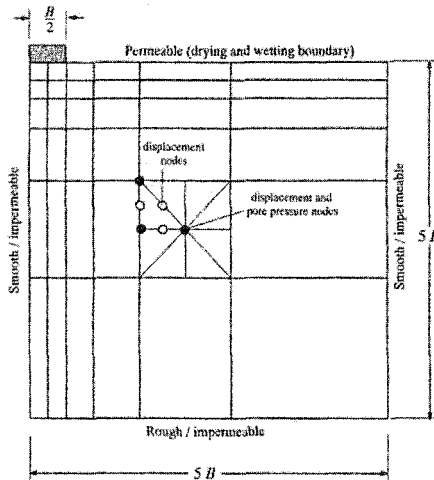
Figure 17. Footing mesh (625 nodes, 288 elements). (Sheng et al, 2003)
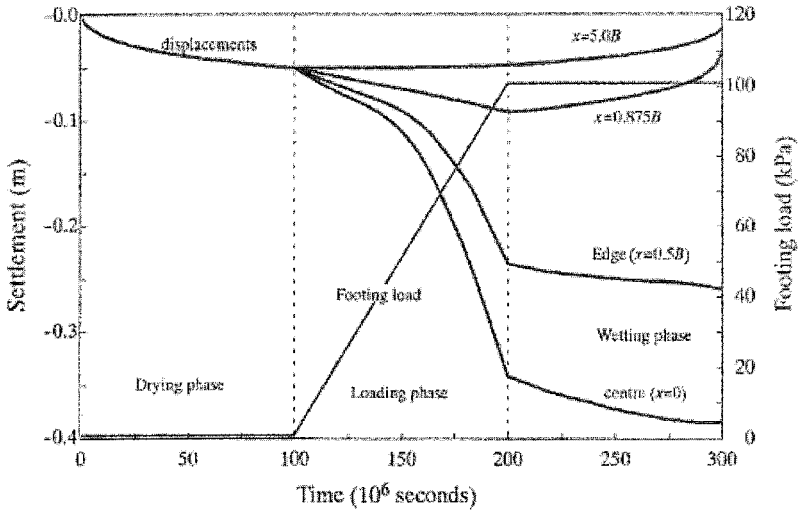
Figure 18. Predicted settlements at the ground surface (100 coarse time steps in each phase. Sheng et al (2004)
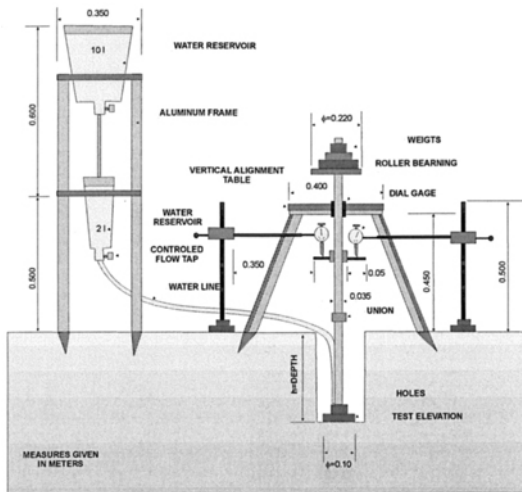
Figure 19. Scheme of the expanso-collapsometer (Costa et al, 2004)
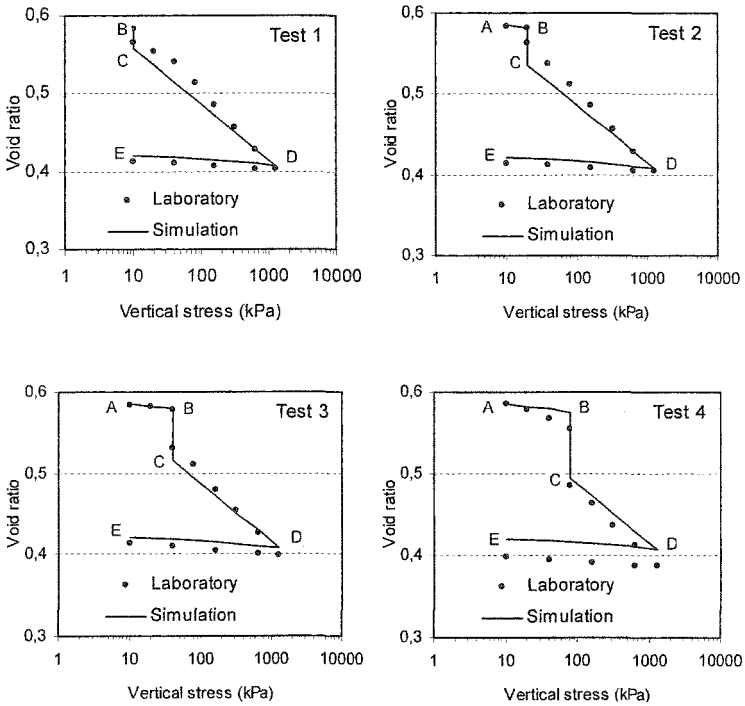
Figure 20. Oedometer test results and model simulation (Costa et al, 2004)
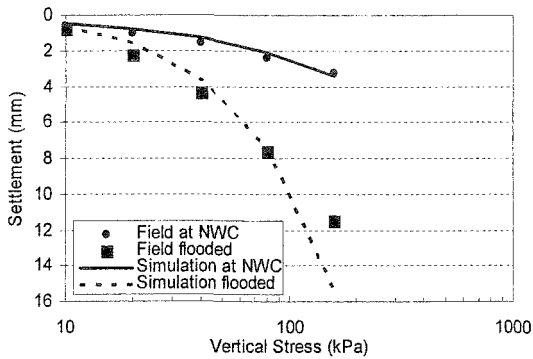
Figure 21. Measured and calculated settlements for a collapsometer test. Costa et al (2004)

Despite the availability of computational tools, well-documented case histories, which show the applicability of modern methods to foundation problems have seldom been reported. Much work remains to be done in this field before new computational procedures become an alternative to some of the more classical methods mentioned before.

Landfills

Liners for landfills are designed in different ways and contain several isolation elements, both natural and man-made. Impervious plastic soils are natural materials which are used for protection of the underlying aquifers and also in covers to prevent excessive infiltration. In both cases, desiccation - wetting processes deform the isolation materials. Desiccation may lead to cracking due to contraction. Increasing the thickness of the clay layer reduces the risk of infiltration in this case. If permeability increases due to the presence of cracks, both liquid and gas mobility increase and this may lead to unacceptable leakages.

Zhou & Rowe (2003) analyzed the desiccation of liners whose main component is clay. Clay liners are exposed to heating conditions induced by organic matter degradation and hence may suffer desiccation by water evaporation. This process, in turn, leads to contraction of the liner and to the development of fissures. This problem requires also THM modelling and, probably, the incorporation of chemical effects because leakages from municipal solid waste contain high concentrations of ions that may affect the clay properties. The presence of geomembranes may delay the process but it is assumed that its degradation will lead to conditions in which the clay layer should keep the waste under isolated conditions. Landfills are covered by evapotranspirative covers (Zhornberg et al., 2003). In this case the atmospheric conditions are of special importance since cyclic variations of suction affect the behaviour of the cover (Fig. 22). The evaluation of percolation into the deposit requires an accurate modelling of the cover because percolation is a small fraction of the total fluxes of infiltration and evaporation.

Mateus et al (2005) have demonstrated that further research into the behavior of synthetic clay liners should be performed because of the incorrect behaviour of a landfill lying on a granitic rock, which showed evidence of dispersion of pollutants. Fracturing of the liner under loading or shrinkage induced by differential wetting-drying processes may be the causes of such unexpected response.

Vangpaisal & Bouazza (2004) have investigated the gas permeability of bentonite-based clay liners (GCL) for waste isolation. Confinement stress, degree of hydration and original structure of the liner (made of granular or powdered bentonite) had a significant effect in the gas permeability, among other effects. Water content was not sufficient to explain the variations of gas permeability as it is normally assumed in conventional two phase flow. It is clear that a constitutive model for these materials (newly developed or adapted from existing models for unsaturated clays) is needed for understanding and predicting the behaviour of such liners, especially with regard to the coupling of fluid flow and mechanical effects (two way coupling) (e.g. Sánchez et al, 2005).
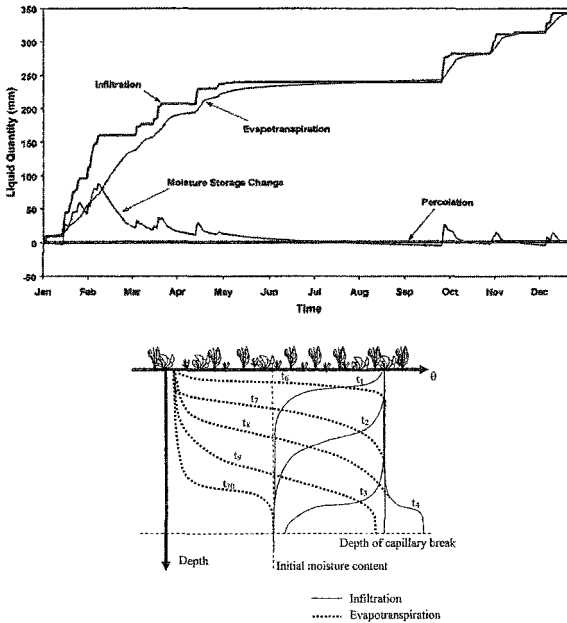
Figure 22. Seasonal variation in the water balance variables (Zornberg et al., 2003).

Slopes

Slope stability analysis within the framework of unsaturated soil mechanics is a step forward with respect to classical procedures, especially if the effect of climatic conditions is investigated. Different approaches, with varying complexity, have been reported in the past few years.

Cai & Ugai (2004) investigated the variation of safety factor depending on the rainfall intensity and duration (Fig. 23). Unsaturated flow and finite element analysis of slope stability are used in a sequential way by these authors. Stability analysis is performed by means of a shear strength reduction technique. With this method, charts can be developed to check the stability of slopes for different soils and rainfall conditions.
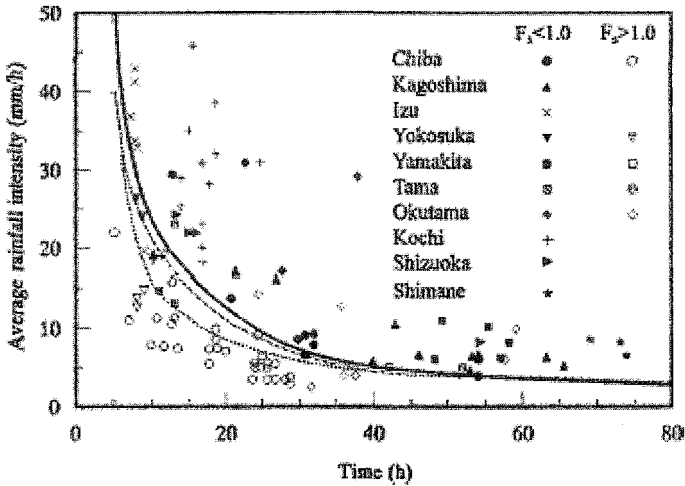
Figure 23. Effect of intensity and duration of the rainfall on the stability of different slopes (symbols:measured and lines:calculated results) after Cai & Ugai (2004).

A simple approach has been developed by Collins & Znidarcic (2004) by assuming one dimensional flow and an infinite slope analysis. The method allows establishing different extreme cases: for coarse materials and high infiltration rates, positive pressures develop and shallow failures are more likely, whereas for fine grained soils and low infiltration rates no positive pressures are developed and the failure is attributed to the loss of cohesion due to suction decrease thus leading to deeper failures.

Rahardjo et al. (2003) have investigated the response of a slope test site with simulated rainfall events. Some conclusions are drawn regarding rainfall intensity and the flux regime in the slope. Ng et al. (2003) analyzed also the behaviour of slopes in swelling soils subjected to artificial infiltration. Swelling processes, the increase in permeability induced by crack development and the development of horizontal stresses were measured. Modelling these experiments would be of great interest to improve the current knowledge of expansive unsaturated soils.

Griffiths & Lu (2005) use an analytical solution of the unsaturated flow problem to find the evolution of suctions in the slope. Suctions are then used to calculate the stability through standard finite elements, defining effective stress by means of the Bishop equation. The presence of suction increases stability because normal stresses increase if compared with the traditional case in which suction is not considered in the unsaturated zone (Figure 24)
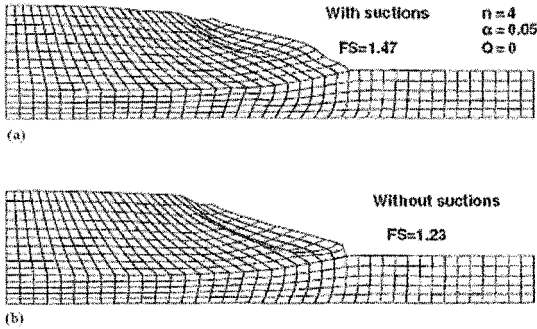
Figure 24. Failure mechanisms from finite element analysis of a silt slope with no infiltration: (a) with suctions, (b) without suctions above the water table (Griffiths & Lu, 2005)

Li et al (2005) developed a comprehensive formulation for slope stability analysis which is based on mixed finite elements and includes THM calculations. Figure 25 shows the map of degree of saturation and equivalent plastic strains for a slope in an unsaturated soil. Several aspects could be supported by the formulation such as localization and large strains.
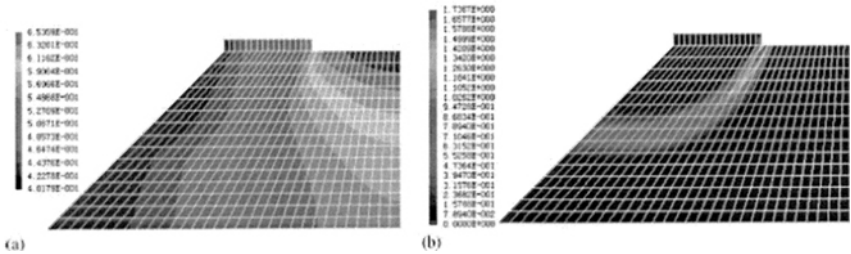
Figure 25. Degree of saturation (a) and equivalent plastic strain (b) for a slope in an unsaturated soil (After Li et al, 2005).

Ehlers et al. (2004) have presented a similar formulation and solved some slope stability problems including localization phenomena. Viscoplasticity is used as a regularization technique. The authors discuss cases of slope failure in the context of embankments subjected to water level increase and decrease at the upstream of an embankment dam. Figure 26 shows the case of water level increase.

The conditions for the initiation and propagation of rapid debris flows have received considerable attention in the recent past due to the catastrophic failures in Campania (Italy) in the period 1998-2005. Several research groups in Italy are currently investigating this problem using different techniques, notably among them the performance of 1-g infiltration tests in large flumes heavily instrumented. The debris flows affect relatively thin covers of pyroclastic soils deposited during

Vesubian eruptions (Figure 27). Olivares and Picarelli (2003) have described the phenomena. Coupled flow-deformation analyses in unsaturated-saturated soil offer a good potential to gain insight into the problem and to provide prediction tools. Within this context, Klubertanz et al (2000) presented a parametric study of the conditions leading to the initiation of debris flows. They found that the most significant factor was the time evolution of the infiltration flux.
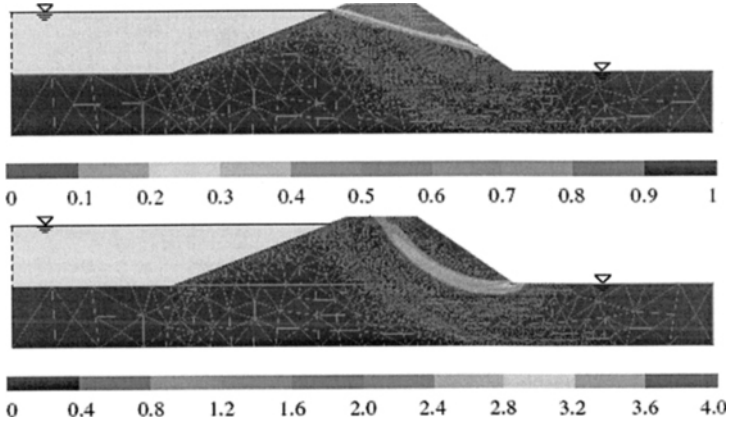
Figure 26. Degree of saturation and accumulated plastic strains for an embankment (After Ehlers et al, 2004).
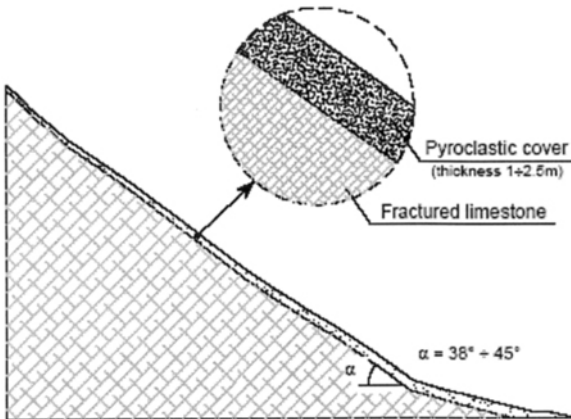
Figure 27. Typical cross section in the areas involved in catastrophic flowslides in 1998, 1999 in Campania. (Olivares and Damiano, 2005)

Nuclear waste disposal applications

Thermo-hydro-mechanical (THM) analyses of unsaturated soils has received considerable attention in nuclear waste disposal research because in current disposal concepts the engineered barrier designed to isolate the waste is generally made of compacted high plasticity expansive clay (bentonite or bentonite-based mixtures). Barriers are expected to swell as they become hydrated in a long and transient process governed by the permeability of the surrounding rock and the barrier itself and the temperature field imposed by the heat generated by the nuclear canister (in the case of high level waste isolation). Bentonite swelling leads to the sealing of discontinuities as stresses develop under confined conditions. The FEBEX in situ experiment in the Grimsel Test Site (Fig. 28, Huertas et al., 2000), the Kamaishi mine THM test (Chijimatsu et al., 2001) and the Prototype Repository Experiment based on the Swedish KBS-3 concept (Svemar and Pusch, 2000) are probably the most relevant large scale experimental investigations performed recently. In all these tests the clay barrier is subjected to the conditions expected in a real nuclear waste disposal scheme.

At present there is a high degree of understanding of the processes taking place in the FEBEX in situ test because a continuous modeling activity has contributed to different stages of the test, from its initial planning to the back-analysis of a comprehensive set of sensors. Predictive calculations, which were crucial for the design of the test, were reported by Gens et al., 1998. More recently the results of a series of benchmarking exercises based on FEBEX in situ measurements have been presented and discussed in Alonso et al., (2005). These modeling activities are complemented by extensive experimental laboratory work (e.g. Villar et al, 2005) and by theoretical developments (e.g. Sànchez et al., 2005). The Kamaishi mine test has also motivated research in experimental, theoretical and numerical areas. A comparison of different THM models for the behaviour of the bentonite barrier under in situ test conditions is the most recent work (Chijimatsu et al., 2005). The Prototype Repository Experiment is also being modeled as shown for instance by Ledesma & Chen (2005).

In order to illustrate the complexity of the THM behavior of clay based barriers for nuclear waster disposal two significant properties of bentonite are briefly discussed: The swelling pressure as a function of the dry density and the intrinsic permeability as a function of the accessible void ratio of the FEBEX bentonite (Figure 29).

Swelling pressure should be reproduced by a constitutive model for unsaturated materials, and this is not a straight forward exercise because of the possibility of having swelling and collapse deformations simultaneously during the wetting process. As shown in Figure 29 swelling pressure, which is a key property in barrier design, changes significantly with dry density. On the other hand, the standard Darcy's law with constant intrinsic permeability is not appropriate for bentonites because the water content variations induce structural changes and, in particular, changes in the amount of accessible pores. Even at constant volume (the barrier in situ is highly confined) the volume of connected pores is higher under low water

contents than under nearly saturated conditions. The joint consideration of near and far fields around a disposal area requires the interaction of THM processes at the scale of the barrier, with similar processes in the surrounding rock. Rutqvist et al (2002) describe the THM modeling approaches for fractured rock within the context of nuclear waste research.
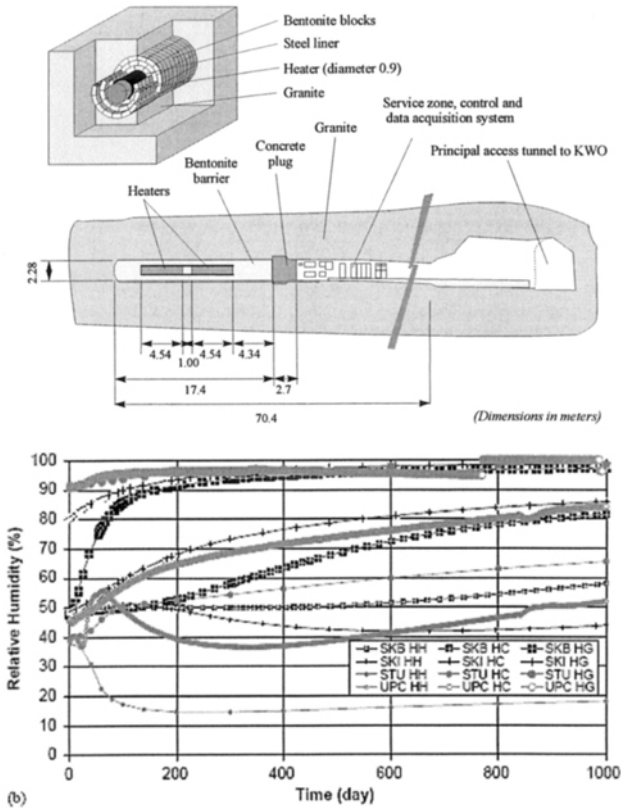
Figure 28. Febex experiment and relative humidity in the bentonite barrier (measured and calculated by different teams in a benchmark exercise). After Alonso et al (2005).

With the same objective, i.e. the investigation of the behaviour of nuclear waste disposal schemes, gas generation induced by corrosion and its migration through barriers is receiving an increasing interest. The in situ Gas Migration Test (GMT), performed at the Grimsel test site in Switzerland illustrates the modelling difficulties that are encountered. The test was designed to investigate forced gas migration through a compacted sand-bentonite mixture. A modelling work which considers the following mechanisms: diffusion, two phase flow in deformable porous media, and two phase flow including path dilation due to high pressures has been presented by Olivella et al. (2005).
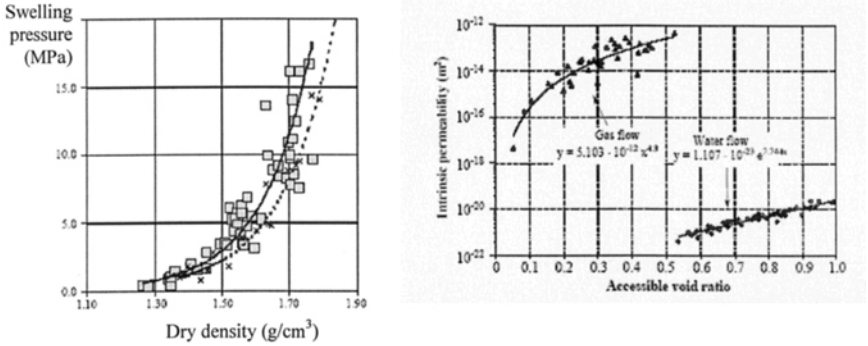
Figure 29. Swelling pressure and intrinsic permeability of bentonite barriers for nuclear waster disposal (Alonso et al 2005)

Infiltration

This subject is of increasing interest in geotechnics because unsaturated soils require a precise calculation of suction, which is strongly influenced by atmospheric conditions. Traditionally, saturated soil mechanics neglected almost completely this boundary condition since in most of cases a phreatic surface is assumed to exist at some elevation and pore water pressures can be easily calculated. In other cases saturated steady state flow conditions provides the necessary pore pressure information. The type of situations and engineering structures discussed in previous sections (embankments, earth dams, slopes, expansive soils etc.) require a precise knowledge of the water infiltration, which is necessary to predict suctions, intimately related with the mechanical behaviour.

Blight (2003), investigating the annual hydrologic balance, demonstrated that evapotranspiration is the most important component in the soil water – atmosphere balance. Traditionally only simple boundary conditions are considered. However, the hydro-thermal balance at the soil surface is difficult to establish and sometimes not all the required information is available.

As mentioned before, Griffiths and Lu (2005) use an analytical solution for the unsaturated flow equation in one dimension between the ground surface and the water table (assumed stationary). If permeability is described by means of an exponential function of suction a closed form solution for suction profiles under infiltration or evaporation regimes may be found. In this context, Rahardjo et al. (2003) have evaluated, using a test site, the ratio between infiltration and rainfall for different conditions of rainfall intensity. The ratio infiltration/rainfall decreases when the rainfall increases and, as a consequence, the ratio runoff/rainfall increases.

Soil scientists pioneered the use of a comprehensive approach for water and heat balance. As described by Milly (1984) the approach is based on the analysis of processes at the soil surface and atmosphere. Considered phenomena are aerodynamic diffusion (for estimating evaporation), turbulent diffusion of sensible heat into the atmosphere, radiation of heat and advection of heat. On the basis of 3-hourly

atmospheric data the boundary condition is developed for a numerical model simulating the water and heat flow in a soil column. This type of boundary condition is not commonly used in geotechnics but it needs to be considered for a realistic approximation in unsaturated soil analysis.
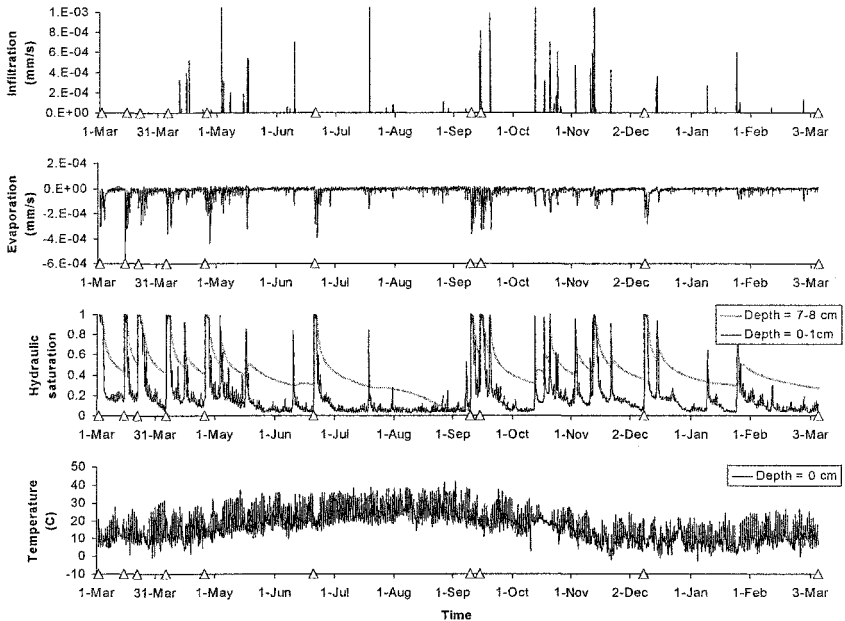
Figure 30: Unsaturated soil- atmosphere interaction (after Saaltink et al, 2002).

In the context of mine waste investigations Saaltink et al. (2002), who solved a coupled geochemical problem in an unsaturated soil (mine tailing deposits), used very precise atmospheric boundary conditions as outlined above in a daily time scale. This approach turned out to be crucial for water content prediction, which is in turn very important for calculating the oxygen diffusion into the soil (Fig 30). The geochemical reactions such as pyrite oxidation and other related reactions were strongly influenced by the amount of oxygen that could be supplied through the unsaturated soil diffusion. In summary, the accurate modelling of the infiltration process through the appropriate atmospheric boundary condition is a key point in the geochemical studies of tailings and their interaction with the underlying aquifers. Other scenarios related to modelling unsaturated soil performance may require similar approaches.

In their approach to model expansive soil movements beneath structures, Masia et al (2004) propose a model for suction prediction which uses atmospheric data and considers the foundation as an impervious element. The model is intended for the prediction of the seasonal and long term conditions during the life of the structure and hence it should be calibrated with climatic data. It also permits to investigate the optimum construction period, in order to reduce the effects of

expansion of the soils (doming) (Fig. 31).
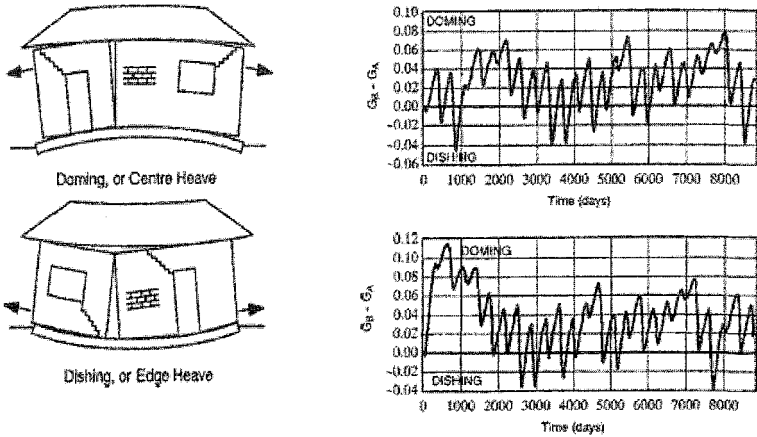
Figure 31: Doming and dishing beneath a structure due to seasonal movement of the ground surface induced by changes in humidity. Differential settlements and structural damage depend on the construction date. (After Masia et al 2004)

Final Remarks

The list of cases described in this paper does not cover all possible applications of unsaturated soil mechanics. Virtually all aspects of Geotechnical Engineering may be addressed under appropriate circumstances. Novel applications such as the volumetric behaviour of porous materials saturated with two liquids of different surface tension have been reported (Collin et al, 2002). The fundamental knowledge, the experimental techniques (especially in the laboratory) and the computational models have made significant progress in the past decade. In theory most of the field problems can now be addressed in a fairly consistent and complete manner. "Complete" in the sense of following some rational steps typical in Geotechnical Engineering: identification of the key characteristics of the problem; experimental determination of material parameters, initial and boundary conditions; application of a suitable computational model and real time validation against the measured field performance. However, the review made, even if it is judged as incomplete, reveals that the number of case histories in which such a methodology has been applied is very small. A significant proportion of the cases presented, show that existing models may solve interesting academic exercises. On the other hand, real cases are only partially addressed or they are interpreted in qualitative terms. It turns out that one of the pressing needs in unsaturated soil mechanics research is to demonstrate its capabilities and limitations in practical situations. Benchmarking exercises help to advance in this direction. To be of value they require the existence of a set of laboratory (or field) tests, carefully performed, and a recorded field performance. In addition to the geotechnical variables usually measured (stresses, deformations,

displacements) it is usually required to have information on suction changes and climatic conditions. This is an added difficulty which may explain, in part, the slow pace of publication of significant case histories.

Acknowledgements

References

Alicescu, V., J.-P. LeBihan and S. Leroueil (2000) Simulation of transient water flow through the LG-4 earth dam, Québec. *Proc. 53rd Canadian Geotechnical Conference*, Montréal, Vol. 1, pp 203-209.

Alonso, E.E., A. Gens and D.W. Hight (1987) Special Problem Soils. General Report. *Proc. 9th European Conference on Soil Mechanics and Foundation Engineering*. Dublin (Ireland) 3: 1087-1146.

Alonso, E.E., A. Gens and A. Josa (1990). A constitutive model for partially saturated soils. *Géotechnique*, 40(3), 405-430.

Alonso, E.E., A. Gens and A. Lloret (1991) "Double structure model for the prediction of long term movements in expansive materials". *Proc. 7th International Conference on Computer Methods and Advances in Geomechanics*. Cairns (Australia). 1: 541- 548.

Alonso E. and F. Batlle (1995) Construction and impoundment of an earthdam. In: Modern issues in non-saturated soils. Springer-Verlag: 357-396.

Alonso, E.E., A. Lloret and E. Romero (1996) Rainfall induced deformations of road embankments. In: Landslides. Balkema: 97-108.

Alonso E. E. (1998) Suction and moisture regimes in roadway bases and subgrades. *Proc.Int.Symp. on subdrainage in roadway pavements and subgrades*. Granada (Spain): 57-104.

Alonso, E. E. (2003) Exploring the limits of unsaturated soil mechanics: the behaviour of coarse granular soil and rockfill. The Eleventh Spencer J. Buchanam Lecture. College Station, Texas A&M University. (http://ceprofs.tamu.edu/briaud/buchanan.htm).

Alonso, E.E., J. Alcoverro, F. Coste, L. Malinsky, V. Merrien-Soukatchoff, I. Kadiri, T. Nowak, H. Shao, T.S. Nguyen, A.P.S. Selvadurai, p, G. Armand, p, S.R. Sobolik, M. Itamura, C.M. Stone, S.W. Webb, A. Rejeb, M. Tijani, Z. Maouche, A. Kobayashi, H. Kurikami, A. Ito, Y. Sugita, M Chijimatsu, L. Börgesson, J. Hernelind, J. Rutqvist, C.-F. Tsang & P. Jussila (2005), The FEBEX benchmark test: case definition and comparison of modelling approaches, *Int. J. Rock Mech. Min. Sci*,. 42: 611-638.

Alonso, E., S. Olivella, N-M. Pinyol (2005a) A review of Beliche dam. *Géotechnique*, 55(4): 267-285.

Alonso, E.E., E. Romero, D. Arnedo and S. Olivella (2005b). Geotechnical properties of low density unsaturated carbonated clayey silts and impact on the foundation of canal embankments. *Proc. of the 16th Int. Conf. on Soil Mech. and Geotech. Eng.* Osaka. Vol.3, 1823-1826

Blight, G.E. (2003) The vadose zone soil water balance and transpiration rates of vegetation. *Géotechnique,* 53(1): 55-64.

Brandon, T.L., J.M. Duncan and W.S. Gardner (1990) Hydrocompression settlement of deep fills. *Journal of Geotechnical Engineering,* Vol. 116, No. 10, 1536-1548.

Bulut, R., C.P. Aubeny and R.L. Lytton (2005) Unsaturated soil diffusivity measurements. *Proc. of an Int. Symp. on Advanced Experimental Unsaturated Soil Mechanics*, Trento, Italy, 281-286.

Cai, F. and K. Ugai (2004) Numerical Analysis of Rainfall Effects on Slope Stability. *International Journal of Geomechanics*, Vol. 4, No. 2, 69-78

Charles, J.A., D.B. Hughes and D. Burford (1984) The effect of a rise of water table on the settlement of backfill at Horsley restored open cast coal mining site 1973-1983. *Proc. 3rd Int. Conf. on Ground Movements and Structures*, 423-442.

Chijimatsu, M., T. Fujita, Y. Sugita, K. Amemiya & A. Kobayashi (2001) Field experiments, results and THM behaviour in the Kamaishi mine experiment. *Int. J. Rock Mech. Min. Sci.,* 38(1): 67-78.

Chijimatsu, M., T.S. Nguyen, L. Jing, J. De Jonge, M. Kohlmeir, A. Millard, A. Rejeb, J. Rutqvist, M. Souley & Y. Sugita (2005) Numerical study of the THM effects on the near-field safety of a hypothetical nuclear waste repository – BMT1 of the DECOVALEX III project. Part 1. Conceptualization and characterization of the problems and summary of results. *Int. J. Rock Mech. Min. Sci.,* 42: 720-730.

Collin, F., Y. J. Cui, C. Schroeder and R. Charlier (2002) Mechanical behaviour of Lixhe chalk partly saturated by oil and water: experiment and modeling. Int. J. Numer. Anal. Meth. Geomech. 26, 897-924.

Collins, B.D. & D. Znidarcic (2004). Stability Analysis of Rainfall Induced Landslides, *J. Geotech. and Geoenviron. Engng.,* 130(4): 362-372.

Costa, L.M., L.J.N. Guimaraes, I.D.S. Pontes Filho and S.M.R Ferreira (2004) Simulaçao do expansocolapsômetro em solos nao saturados. *Memorias 5° Simpósio Brasileiro de Solos Nao Saturados.* Sao Carlos, 135-141

DIT-UPC (2002) *CODE_BRIGHT. A 3-D program for thermo-hydro-mechanical analysis in geological media. USER'S GUIDE.* Centro Internacional de Métodos Numéricos en Ingeniería (CIMNE), Barcelona.

Edris, E.V. & R.L. Lytton (1977) Dynamic properties of fine grained soils. *9th Int. Soil Mach. And Found. Engng.* 2: 217-224.

Ehlers, W., T. Graff, M. Ammann (2004) Deformation and localization analysis of partially saturated soil. *Comput. Methods Appl. Mech. Engng.,* 193: 2885-2910.

Ferreira, S. R. M. and Lacerda , W. A. (1995) Volume Change Measurements in Collapsible Soil By Laboratory and Field Test., *Proceedings of the 1st International Conference on Unsaturated Soils*, 2, 847-854.

Fleckenstein, L.J. & D.L.Allen (1996)Evaluation of pavement performance.*TRR,*1519:28-35.

Fry, J. J., Charles, J. A. and Penman, A. D. M. (1996). Dams, embankments and slopes. *Proc. 1st Int. Conf. Unsaturated Soils*, Vol. 3, Paris, Balkema, 1391-1419.

Gens, A., E.E. Alonso, F. Batlle and A. Lloret (1991) "Prediction of ground movements in partially saturated soils". *Proc. 4th International Conference on Ground Movements and Structures*. Cardiff (U.K.): 1-24.

Gens, A., A.J. Garcia-Molina, S. Olivella, E.E. Alonso & F. Huertas (1998) Analysis of Full Scale In-situ Heating Test Simulating Repository Conditions. *Int. J. Num. Anal. Meth. Geomech.*, 22: 515-548.

Griffiths, D.V. & N. Lu (2005) Unsaturated slope stability analysis with steady infiltration or evaporation using elasto-plastic finite elements. *Int. J. Num. Anal. Meth. Geomech.*, 29: 249-267.

Hong, G.T., Bulut, R., C.P. Aubeny, R. Jayatilaka & R.L. Lytton (2006a) Design model for roughness and serviceability of oavements on expansive soils. *TRB*, to be published.

Hong, G.T., C.P. Aubeny, Bulut, R. & R.L. Lytton (2006b) Comparative design case studies of pavement performance on expansive soils. *TRB*, to be published.

Huertas, F., J.L. Fuentes Cantillana, F. Jullien, P. Rivas, J. Linares, P. Fariña, M. Ghoreychi, N. Jockwer, W. Kickmaier, M.A. Martinet, J. Samper, E. Alonso & F.S. Elorza (2000) Full scale engineered barrier experiment for high-level radioactive waste in crystalline host rock (FEBEX Project). Final Report, *European Commission Report no. EUR 19147 EN*.

Jiménez-Salas, J.A. (1965) Cálculo de los esfuerzos producidos sobre los edificios por las arcillas expansivas. Publicación nº 20 del Laboratorio del Transporte. Madrid

Jiménez-Salas (1980) Geotecnia y Cimientos III. Editorial Rueda. Madrid

Jin, M.S., K.W. Lee & W.D. Kovacs (1994) Seasonal variation of resilient modulus of sub-grade soils. *Jnl. Transp. Engng.*, 120(4): 603-616.

Justo, J.L. & P. Durand (2000) Settlement-time behaviour of granular embankments. *Int. Jnl. for Num. and Anal. Meth. in Geomech.*, 24: 281-303

Klubertanz, G., L. Laloui and L. Vulliet (2000) Parameters governing debris flow initiation. Debris-Flow Hazards Mitigation: Mechanics, Prediction, and Assessment, Wieczorek & Naeser (eds). Balkema, Rotterdam, 73-79.

Kohgo, Y. (2003), Review of constitutive models for unsaturated soils and initial-boundary value analyses, Proceedings of the 2nd Asian Conference on Unsaturated Soils, UNSAT-ASIA 2003, Osaka, 21-40.

Kohgo, Y., Hayashida, Y. and Asano, I., (2005). Analyses of rock fill dam by using a gereral elastoplastic model with two suction effects, *Int. Conf. on Computational and Experimental Eng. and Sciences*, ICCES, Chennai, India (to be published).

LeBihan, J.-P. and S. Leroueil (2002) A model for gas and water flow through the core of earthdams. *Can. Geotech. J.* 39: 90-102

Ledesma, A. & G.J. Chen (2005) THM modelling of the Prototype Repository Experiment: comparison with current measurements. In: *Advances in Understanding Engineered Clay Barriers*. Edited by E.E. Alonso and A. Ledesma. Taylor and Francis Group, London: 339-346.

Li, X., Z. Liu & R.W. Lewis (2005) Mixed finite element method for coupled thermo-hydro-mechanical process in poro-elasto-plastic media at large strains. *Int. J. Numer. Meth. Engng.*, 64: 667-708.

Long, X., C.P. Aubeny, R. Bulut & R.L. Lytton (2006) Two-dimensional moisture flow-soil deformation model for application to pavement design. *TRB*, to be published.

Lytton, R.L., C.R. Aubeny & R. Bulut (2004) Design procedure for pavements on expansive soils. Volume 1. *Report no. FHWA/TX-05/0-4518-1 NTIS*. Springfield, Virginia: 22161 (http://www.ntis.gov).

Lytton, R.L. (1973) Stiffened mat design considering viscoelasticity, geometry and site conditions. *Proc. 3rd Int. Conf. on Exp. Soils.*, Haifa, 2: 189-193.

Machado S.L. (1998) Application of elastoplasticity concepts to unsaturated soils. Doctoral Thesis. EESC/USP, Sao Carlos-SP. Brasil.

Machado, S. L., B.J.I. Carneiro, O.M. Vilar and J.C.A. Cintra (2002). Soil plasticity aspects applied in the prediction of the behaviour of field structures. *Proc. of the Third Int. Conf. on Unsaturated Soils.* Recife. Balkema., Vol.2, 697-702

Marsal, R. J., Arellano, L. R. Guzmán, M. A. & Adame, H. (1976). El Infiernillo. Behaviour of dams built in Mexico. Instituto de Ingeniería, UNAM, Mexico D.F.

Masia, M. J., Y. Z. Totoev and P.W. Kleeman (2004) Modeling Expansive Soil Movements Beneath Structures. *Journal of Geotechnical and Geoenvironmental Engineering*, Vol. 130, No. 6, 572-579

Mateus, A., J. Figueiras, F.M. Santos, R. Mota & H. Amaral (2005) The effectiveness of "clay" liners as basal isolation of landfills: a case study. *Environmental Geology*, 47: 1128–1137.

May, R.W. & M.W. Witczak (1981) Effective granular modulus to model pavement responses. *TRR*, 810: 1-9.

McEnroe, B.M. (1994) Drainability of granular bases for highway pavements. *TRR*. 1434: 23-28.

Milly, P.C.D. (1984) A simulation Analysis of Thermal Effects on Evaporation from Soil. *Water Resources Research*, 20(8): 1087-1098.

Naylor, D. J., Maranha das Neves, E., Mattar, Jr., D., Veiga Pinto, A. A. (1986). "Prediction of construction performance of Beliche Dam", *Géotechnique* 36, No. 3, 359-376.

Naylor, D. J., Maranha das Neves, E., Veiga Pinto, A. A. (1997). "A back-analysis of Beliche Dam", *Géotechnique* 47, No. 2, 221-233.

Nelson, J.D. and D. Miller (1992). Expansive soils. Problems and practice in foundation and pavement engineering. Wiley.

Ng, A.K.L and J.C. Small (2000) Use of coupled finite element analysis in unsaturated soil problems. *Int. Jnl. Numerical and Analytical Methods in Geomechanics*, 24,73-94

Ng, C.W.W., L.T. Zhan, C.G. Bao, D.G. Fredlund & B.W. Gong (2003), Performance of an unsaturated soil slope subjected to artificial rainfall infiltration. *Géotechnique*, 53(2): 143-157.

Odeon, H., J.P. Kerzreho, R. Kobish & J-L. Paute (1995) Ensayo de tres zahorras artificiales en la pista de ensayo sobre firmes del LCPC. *Carreteras*, 80 (Nov.-Dic.): 64-79.

Olivares L. and Picarelli L. (2003). Shallow flowslides triggered by intense rainfalls on natural slopes covered by loose unsaturated pyroclastic soils.*Géotechnique*: vol.52,2.

Olivares, L. and E. Damiano (2005) Post-failure mechanics of landslides: a laboratory investigation of flowslides in pyroclastic soils. Submitted for publication.

Olivella, S., J. Carrera, A. Gens & E.E. Alonso (1994) Nonisothermal multiphase flow of brine and gas through saline media. *Transport in Porous Media*, 15: 271-293.

Olivella, S., A. Gens, J. Carrera & E. E. Alonso (1996). Numerical formulation for simulator (CODE_BRIGHT) for coupled analysis of saline media. *Enginyering computations*, 13(7): 87-112.

Olivella, S., E.E. Alonso & C. Delahaye (2005), Modelling preferential paths of gas migration. Application to the Gas Migration Test. *2nd International Meeting on Clays in Natural and Engineered Barriers for Radioactive Waste Confinement*, March 14-18, Tours.

Pappin, J.W, S.F. Brown & M.P. O'Reilly (1992) Effective stress behavior of saturated and partially saturated granular material subjected to repeated loading. *Géotechnique*, 42, 3: 485-497.

Phillip, A.W. & D.A. Cameron (1995) The influence of soil suction on the resilient modulus of expansive soil subgrades. *Proc. 1st Int. Conf. Unsat. Soils. UNSAT '95*, 1: 171-176.

Poulos, H. G. and E.H. Davies (1980) Pile foundation analysis and design. Wiley

Pufahl, D.E., R.L. Lytton and H.S. Liang (1990) Integrated computer model to estimate moisture and tempertaure effects beneath pavements. TRR. 1286: 259-269.

Rahardjo, H., T.T. Lee, E.C. Leong, R.B. Rezaur (2003) Response of a residual soil slope to rainfall, *Can. Geotech. J.*, 42: 340-351.

Rutqvist, J., Y.-S. Wu, C.-F. Tsang & G. Bodvarsson. (2002) A Modeling Approach for Analysis of Coupled Multiphase Fluid Flow, Heat Transfer, and Deformation in Fractured Porous Rock. *Int. J. Rock Mech. Min. Sci.*, 39: 429–442.

Saaltink, M.W., C. Domenech, C. Ayora, C. Carrera (2002) Modelling the oxidation of sulphides in an unsaturated soil. *Mine Water Hydrogeology and Geochemistry*, Geological Society, London, 198: 187-204.

Sánchez, M., A. Gens, L.doN. Guimaraes & S. Olivella (2005) A double structure generalized plasticity model for expansive materials. 2005. *Int. J. Num. Anal. Meth. Geomech.*, 29: 751-787.

Sauer, E.K. & C.L. Monismith (1968) Influence of soil suction on behaviour of glacial fill subjected to repeated loading. *HRB*, 215: 18-23.

Sheng, D., D.W. Smith, S.W. Sloan and A. Gens (2003). Finite element formulation and algorithms for unsaturated soils. Part II: Verification and application. *Int. J. Numer. Anal. Meth. Geomech.*, 2003; 27:767–790

Soriano, A. & F.J. Sánchez (1999) Settlements of railroad high embankments. *Proc. XII European Conf. on Soil Mech. and Geotech. Eng.*, 3: 1885-1890.

Svemar, C. & R. Pusch (2000). Prototype Repository. Project description. *ASPO Hard Rock Laboratory. Progress Report, IPR-00-31*.SKB, Sweden.

Thompson, M.R. & Q.L. Robnett (1979) Resilient properties of subgrade soils. *Transp. Research Jnl. ASCE*, 105, TE1: 71-89.

Uzan, J. (1985) Characterization of granular material. *TRR*, 1022: 52-59.

Vangpaisal, T. and A. Bouazza (2004). Gas permeability of partially hydrated geosynthetic clay liners. *Journal of Geotechnical and Geoenvironmental Engineering*, Vol. 130, No. 1, 93-102

Villar, M.V., E. Romero & A. Lloret (2005) Thermomechanical and geochemical effects on the permeability of high-density clays. In: *Advances in Understanding Engineered Clay Barriers*. Edited by E.E. Alonso and A. Ledesma. Taylor and Francis Group, London: 177-192.

Wallace, K.B. (1977) Moisture transients at the pavement edge: analytical studies of the influence of materials and shear design. *Géotechnique*, 27(4): 497-516.

Wray, W.K., B.M. El Garhy & A.A. Youseff (2005) Three dimensional model for moisture and volume change prediction in expansive soils. *J. Geotech. and Geoenviron. Engng.*, 131(3): 311-324.

Zhou, Y. & R.K. Rowe (2003) Development of a technique for modelling clay liner dissication. *Int. J. Num. Anal. Meth. Geomech.*, 27: 473-493.

Zornberg, J.G., L. LaFountain & J.A. Caldwell (2003) Analysis and Design of Evapotranspirative Covers for Hazardous Waste Landfill. *Journal of Geotechnical and Geoenvironmental Engineering*, 129(6):427-438.

Geo-environmental and management aspects of the behaviour of mining and municipal solid wastes in water-deficient climates

Geoffrey E Blight[1]

[1]Professor Emeritus, Civil and Environmental Engineering, University of the Witwatersrand, Private Bag 3, Wits, 2050, South Africa email: blight@civil.wits.ac.za

Abstract

Geotechnical and Environmental Engineers face the challenge of managing ever-increasing quantities of mine and municipal solid waste, including disposal, rehabilitation of depositories and long term maintenance and monitoring. Waste management is a long-term process that may be required to continue for centuries into the future, as there are no walk-away solutions to the maintenance of waste depositories.

Climates that are water-deficient, to various degrees, cover 65% of the inhabited Earth. In some ways, waste management is simplified by a water-deficient climate, in others it is made more difficult.

After describing the characteristics and arising of mine waste (MW) and municipal solid waste (MSW), the paper proceeds to describe selected aspects of waste management in water-deficient climates, including:

.1 water retentivity,
.2 shear strength and slope stability,
.3 erosion of waste depository surfaces, and
.4 settlement of MW backfill and MSW landfill.

Introduction – the origins and quantities of mining and municipal solid wastes and the relationship with climate.

As the world market expands for commodities such as chrome, coal, copper, diamonds, fluorspar, gold, iron, manganese and zinc, so necessary for the functioning of the modern world, mining companies are exploiting ever lower-grade ore bodies.

Mining on a vast scale is usually necessary for profitability of a low-grade mine, and volumes of waste are commensurately large.

The actual volume of mine waste (MW) that has to be disposed of in dumps and tailings deposits, world-wide, is difficult to assess. In 1996 the International Commission on Large Dams (ICOLD) gave an estimate of: "almost certainly exceeds 5 thousand million tonnes per annum". Considering that some highly priced commodities occur in their ores in concentrations of grams or carats per tonne(T), and that many individual mines extract in excess of 50 million tonnes of ore per year (T/y), even ICOLD's estimate is probably much too low. For example, a single platinum tailings dam at Bafokeng, South Africa, has a design disposal capacity of almost 1 thousand million m^3 over a life of 50 years (Stuart et al, 2003).

The demand for the products of mining, e.g. power generation, chemical fertilizers and refined metals, comes from the ever-burgeoning population of the world, the people of which seek an improved or improving standard of life that, in turn, demands the acquisition of new goods and the discarding of old. As most of the world's population is urbanized, this produces an ever-increasing volume of municipal solid waste (MSW), most of which has to be disposed of in landfills. The amount of waste produced per head of population is related to the income level of the populace and varies from as low as 0.05 kg/person/day (0.018 tonne/person/year) (kg/p/d, T/p/y) for the very poor to as much as 2kg/p/d for the rich (e.g. Medina, 1997, Blight and Mbande, 1998). The relationship between wealth and waste is illustrated by Figure 1. The urbanized very poor invariably live in overcrowded conditions, whereas the rich have a generous living space. The net effect is that very poor communities generate about 45 T/ha/y of MSW, whereas rich communities generate only 10 T/ha/y (Blight and Mbande, 1998). This is also indicated in Figure 1. A very poor urban area in a developing country measuring, say, 10 km x 10 km, may generate 450 000 T/y of MSW. As the size of cities, especially in the developing world, is also rapidly increasing, the disposal of MSW has become a problem of insuperable proportions in many cities of the developing world, e.g. Manila and Jakarta. In addition to mining and municipal solid wastes, many industrial processes, e.g. thermal power station generation and metallurgical reduction, rival quantities of MW and MSW in the volumes of waste they produce. As an example, the production of power station ash and waste gypsum from fertilizer production in South Africa amounts to some 50 million T/y, or 1.25 T/p/y for the population of 40 million.

As shown by Figure 2, 65 per cent of the earth's inhabited land surface (i.e. excluding Antarctica) is annually or seasonally water-deficient. By definition, in an annually water-deficient climate, the monthly evaporation from a free water surface exceeds the monthly rainfall throughout the year, whereas in a seasonally water-deficient climate the annual evaporation from a free water surface exceeds the annual rainfall, although there may be seasonal excesses of rainfall over evaporation. The distribution of water-deficient areas in Figure 2 shows that many of the world's poorest and least developed continents and countries have water-deficient climates

(e.g. Africa and western South America) while many of the water-deficient areas are highly mineralized and support major mining activity (Africa, Australia, western South America, western and central North America and Asia). There is thus a strong case for considering the effects of water-deficiency, and the unsaturated land surface conditions it engenders, on the management of mining and municipal solid waste, especially as some of the effects may, with careful design and operating practices, be used to advantage. The geo-environmental management of MW and MSW has at least two aspects:

.1 the conventional geotechnical concerns with the stability of slopes and settlement of surfaces of waste repositories or impoundments, e.g. waste rock dumps, open cast mine backfill and tailings impoundments for MW, and landfills for MSW and

.2 the environmental concerns of surface erosion, surface and water pollution by acid mine drainage and other leachate from MW and MSW depositories, radon gas from MW deposits and landfill gas and odour emanations from MSW landfills.
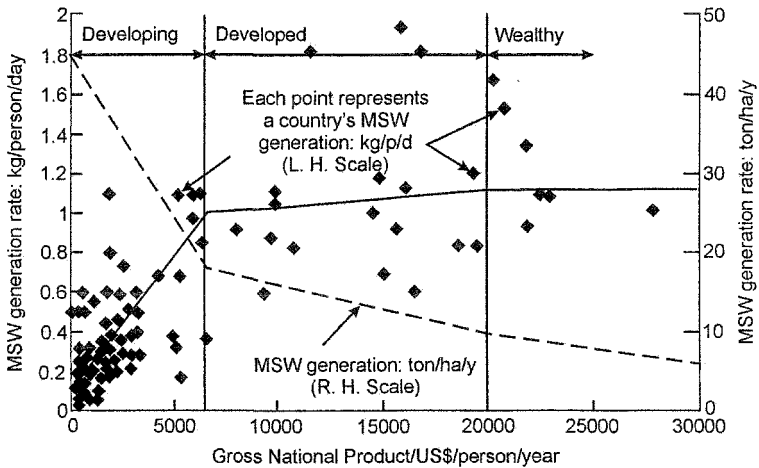
Figure 1: Relationship between rate of generation of municipal solid waste (MSW) as personal generation rate (kg/p/d) and gross national product (USD/p/y) as well as areal generation rate (T/ha/y). (After Medina, 1997 and Blight and Mbande, 1998)

Shaded areas are annually   65% of land surface (excluding Antarctica)
or seasonally water-deficient   is annually or seasonally water-deficient
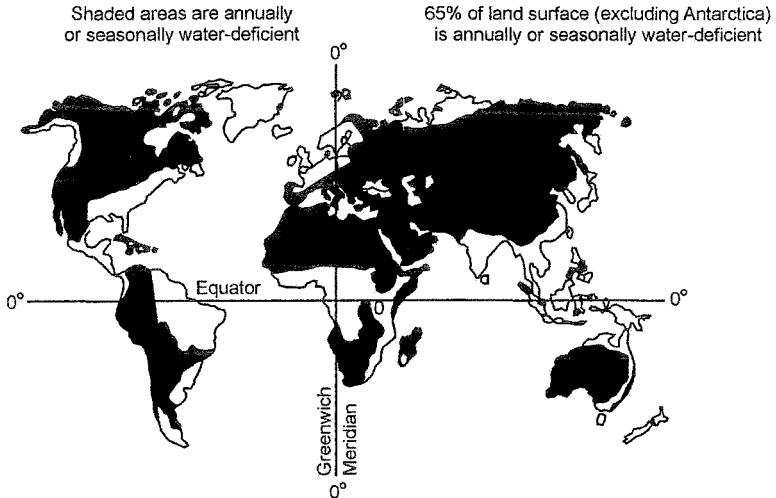
Figure 2:   Annually and seasonally water-deficient land areas of the inhabited
             world. (After Thornthwaite, 1958).

These problems are often worse in water surplus climates and the circumstances of
unsaturation can often be turned to advantage in water deficient climates.

After briefly describing and comparing the characteristics of mining wastes and
municipal solid wastes, a selection of the above topics will be discussed. They are:

  .1   water retention by mining waste and municipal solid waste;
  .2   the strength of unsaturated tailings and the stability of tailings slopes;
  .3   erosion of the surfaces of waste depositories; and
  .4   the settlement of strip-mining backfill and municipal solid waste landfills.

The origins and composition of mining waste and municipal solid waste.

Mine waste (MW)

        Mine waste may arise in a number of forms: as stripped soil and coarse
broken rock overburden in open cast or strip-mining operations, as development
waste rock in underground mining and as fine-grained tailings, the barren residuum
of the process of comminution and mineral-extraction from ores. The various wastes
are usually disposed of separately. The top-soil is stock-piled for eventual use in
rehabilitating the dumps of coarse wastes, or the surfaces of the back-filled mining
voids. The coarse broken rock is dumped either with or without compaction or is
used to backfill opencast or strip-mining voids. Although generally unsaturated,

because of their coarseness, any capillary water tension that may develop in these coarse wastes has little effect on their mechanical behaviour, either in terms of strength or settlement. They are also highly permeable and even in a water-deficient climate, rapid infiltration of rain renders capillary tensions ephemeral. However, capillary tension may have a considerable effect on the mechanical behaviour of fine tailings, and rain infiltration may lead to incremental collapse settlement of coarse wastes.

Figure 3 (Blight, 1994) shows typical particle size analyses for a range of tailings from various sources, as well as the industrial wastes, phospho-gypsum and pulverized fuel ash (PFA) from coal-burning power stations. Some of these wastes (e.g. PFA and gypsum) can be "dry-dumped" either by truck or belt conveyor, although they always contain some water to prevent dust pollution arising during transport and deposition. However, most of the tailings are transported hydraulically either as a slurry, as a "thickened tailings" or a "paste" and are deposited or "beached" into hydraulic fill tailings impoundments where the tailings flow under their own weight, settle and consolidate to form fine-grained silty deposits. A typical complex of hydraulic-fill ring-dyke tailings impoundments at a South African gold mine is shown in Figure 4. The retaining ring-dykes are usually constructed of tailings which are deposited around the dyke and flow down the beach toward a central drainage penstock. Because of the relatively fine grain size, in a water-deficient climate, tailings are capable of developing considerable capillary water stresses or suctions, as a result of the effects of incident solar radiation and consequent evaporative drying and lowering of the phreatic surface.

Municipal solid waste (MSW).

The composition, and hence the characteristics, of municipal solid waste are related to the financial status of the community and to cultural and dietary factors, in much the same way as the quantities of waste that are generated (Figure 1). Table 1 compares the composition of wastes from five different sources. On the left is the range of composition of MSW from the U.S.A. This features relatively large proportions of paper and cardboard, plastic and textiles. In comparison, waste from Cape Town, South Africa, (which, in this example, is sourced from the wealthier "leafy" suburbs), contains less paper than MSW from the U.S.A., but a greater proportion of organics – mostly garden waste. The analysis is also skewed by the relatively large proportion of building rubble. Metals and glass are almost absent from the waste because it is scavenged for these components on arrival at the landfill, but before landfilling.

The two South African cities of Soweto and Mdantsane , which house mainly poor people, differ mainly in that the predominant fuel for cooking and heating in Soweto is coal, burned in small cooking-cum-heating stoves whereas the fuel mostly used in Mdantsane is kerosene or liquefied petroleum gas. As a result, waste from Soweto contains a large proportion of ash and the proportions of paper, plastics and organics

are small because most of these materials are also used as fuel in the stoves. Finally, the semi-desert city of Gaborone, Botswana, has a waste analysis with even less paper than Mdantsane, but a surprisingly large content of organics and putrescibles, mainly food waste.

Table 1 does not give water contents for MSW, but they vary seasonally and typically range from 35 to 45 per cent by dry mass for wastes with a low organic content (e.g. Soweto) to 55 to 70 per cent if the organic content is high (e.g. Gaborone).

It must be emphasized that the composition of MSW is not constant, but is ever-changing as life-styles evolve. This is illustrated by Figure 5, which shows (a) how the composition of MSW in the United Kingdom evolved in the seven decades from the 1930s to the 1990s. Comparing Figure 5a with Table 1 shows that MSW in the U.K. during the 1930s to late 1940s was fairly similar in composition to present-day MSW in Soweto. Figure 5b shows how the uncompacted (as collected) density of the U.K.'s MSW reduced from nearly 300 kg/m^3 in the 1930s and 1940s to about 150 kg/m^3, mainly as a result of a decreasing ash content and increasing quantities of plastic film and cardboard and foam packaging.

Table 2 gives some typical geotechnical parameters for landfilled MSW of the composition shown to the left of the table. Readers who are unfamiliar with MSW should note the relatively low bulk and dry densities and the relatively large water content and void ratio. The degree of saturation (S_r) may appear relatively low, but it has been found that landfilled waste starts to exude leachate when S_r exceeds about 35% (e.g. Blight and Fourie, 1999). (See Figure 7 for further confirmation of this statement. At water contents of 35-40%, the suction in MSW approaches zero.) It should also be noted that the submerged density ($\gamma - \gamma_w$) is usually zero. Thus positive pore water pressures have an unusually large influence on in situ shear strength, and hence on shear stability.

Water retention of MW and MSW.

This subject has importance because it directly affects the water storage capacity of every waste depository. Figure 6a shows the suction-water-content relationship for drying and re-wetting of a coarse gold tailings (see coarse side of grading envelope in Figure 3a). The process is similar for finer materials, but the water contents involved are larger. As the tailings dried from a slurry, they shrank at very low suctions until they reached a water content of about 15%. Further drying developed suctions in the pore water that increased substantially with decreasing water content. Re-wetting caused the suction-water content curve to retrace its path with a small amount of hysteresis, and thereafter, re-wetting and re-drying followed substantially the same suction-water content path. This is typical for most tailings.
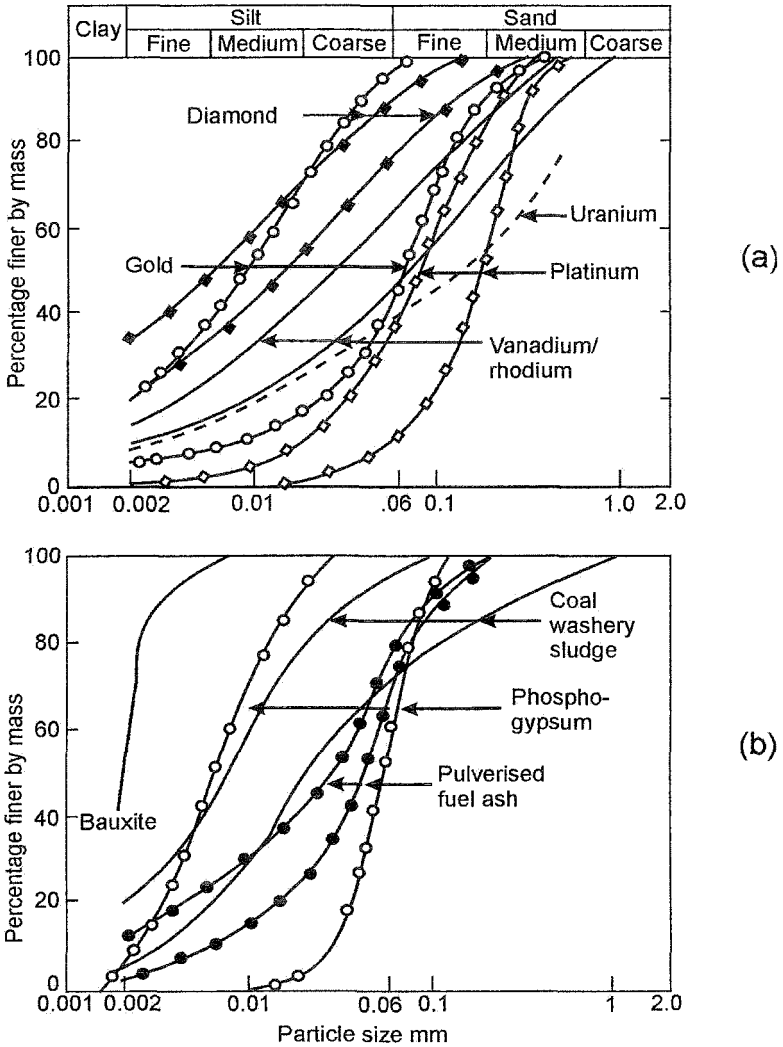
Figure 3:   Particle size analyses for (a) typical tailings from mineral extraction of various ores, and (b) fine-grained industrial wastes.

Figure 4:   A typical complex of hydraulic-fill ring-dyke impoundments for gold
                tailings at a South African gold mine. The impoundment at lower left
                is being reclaimed for further gold extraction.

Figure 6b shows an example of the consolidation behaviour of a fine gold tailings (on
the fine side of the envelope shown in Figure 3a). The process is closely related to
and occurs simultaneously with the processes of drying and re-wetting as successive
layers are deposited in a tailings impoundment.

After deposition on the beach of a tailings impoundment, a tailings slurry becomes
subject to two processes, either sequentially or simultaneously: The water content and
hence void ratio is decreased by evaporation engendered by solar radiation, and also
by compression under the superimposed load of additional layers of slurry. The net
effect is that the tailings consolidate under the combined effect of drying suction and
increasing overburden with each re-wetting cycle causing some over-consolidation.
In Figures 6a and 6b, lines AB are closely related and so are lines BC. The main
difference is that the total stress in Figure 6a remains at zero while the suction varies,
whereas in 6b both suction and total stress contribute to the consolidation pressure.

Table 1: Composition of waste from developed and developing communities

Component	% Composition by undried mass				
	USA	CapeTown	Soweto[*]	Mdantsane[**]	Gaborone[**]
		South Africa			Botswana
Ash, soil & building rubble	8-14	39	63	1	3
Paper and cardboard	34-44	19	9	31	12
Plastics and textiles	8-10	7[+]	3	15	5
Metals	11-13	2[+]	3	4	6
Glass	4-9	1[+]	12	3	6
Organics and putrescibles	12-22	32	10	46	68

+ Scavenged before landfilling.
* Predominant fuel: coal.
** Predominant fuel: kerosine or LPG.
Sources: Rathje and Murphy (1992) (USA) and author's analyses. (South Africa and Botswana).

Table 2: Typical composition of MSW and corresponding geotechnical parameters.

Component of MSW	% by dry mass	Component Solid Density Kg/m³	Overall Geotechnical parameter	
Ash, soil, & building rubble	62	2650	Bulk density kg/m³	1165
Paper and cardboard	10	1800	Water content % dry mass	37
Plastics & textiles	10	1000	Dry density kg/m³	850
Metals	2	7000	Void ratio e	1.8
Glass	1	2700	Degree of saturation S_r%	48
Organics & putrescibles	15	1800	Gas-filled void height $(1-S_r)$%	52
Overall solids density of waste kg/m³		2360	Initial storage of water Smm/m	312

As shown in Figure 7 suction-water content relationships can also be constructed for MSW, but because of the heterogeneity of MSW, it is very difficult to represent the behaviour of a large body of waste by a single curve, as each piece of component material will have its own suction-water content relationship. The suction may be uniform at a particular locality, but water contents will vary from fragment to fragment of waste. For example, a wad of paper that has been landfilled will have a very different water content to that of a fragment of building rubble in close contact with the paper, even though their suctions may be identical. In Figure 7 the laboratory curve represents the overall water content of a single composite sample consisting of many fragments. The in situ measurements were made by means of psychrometers buried in the wall of a pit excavated in a landfill which was sampled to estimate the water content associated with each suction measurement.
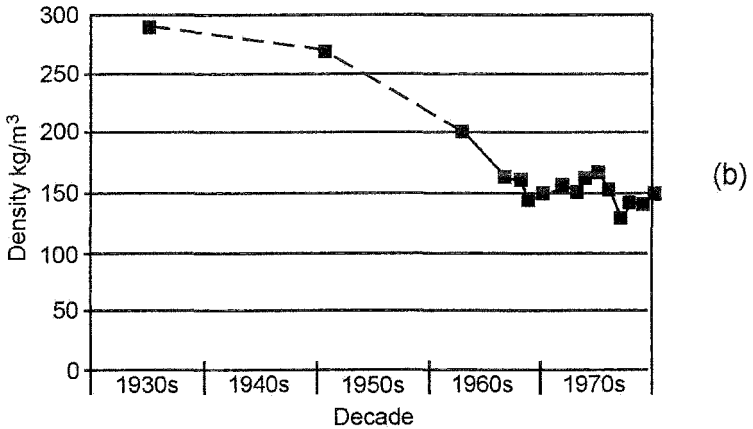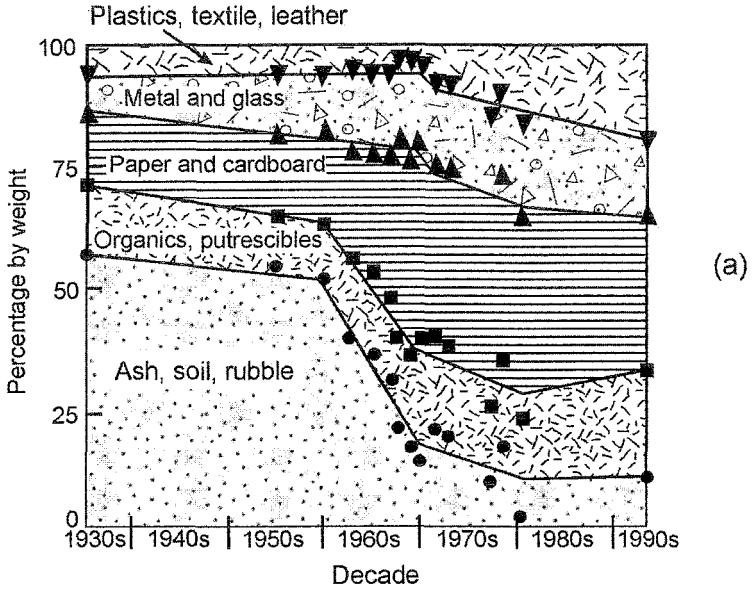
Figure 5: Changes in the composition and loose bulk density of MSW in the United Kingdom from 1935 to 1980: (a) Composition, mass % (b) Loose bulk density (After World Health Organization, 1991 and Watts and Charles, 1999).
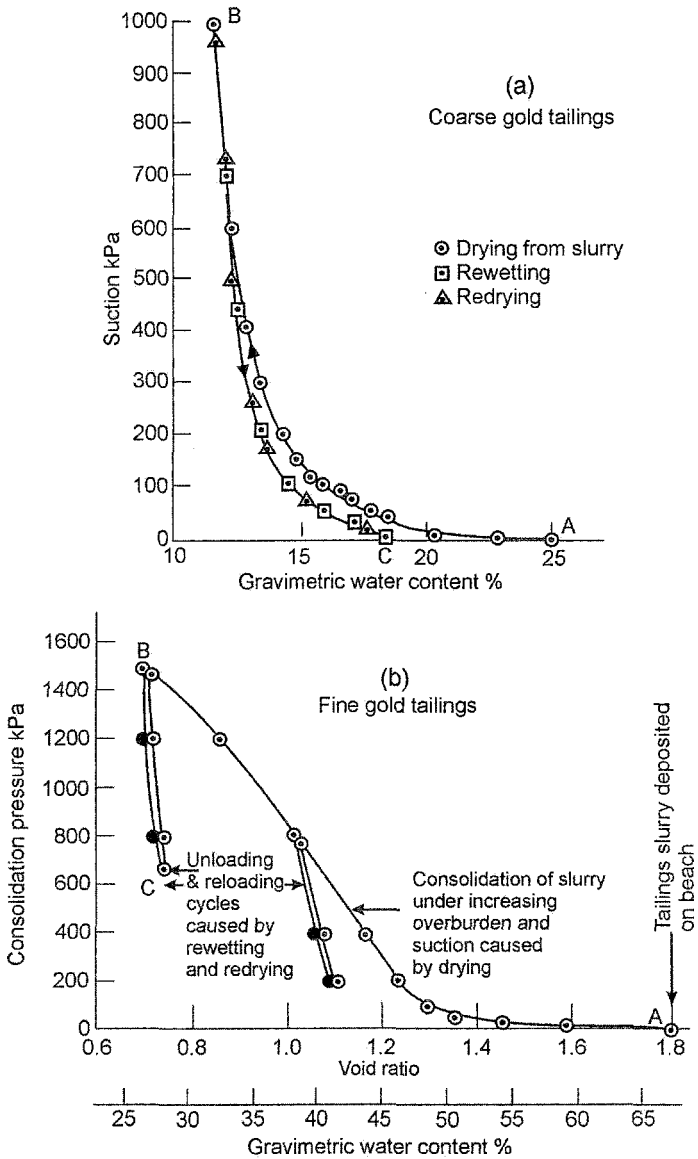
Figure 6:   (a) Suction-water content relationship for a coarse gold tailings.
            (b) Void ratio - consolidation pressure relationship for a fine
               gold tailings.
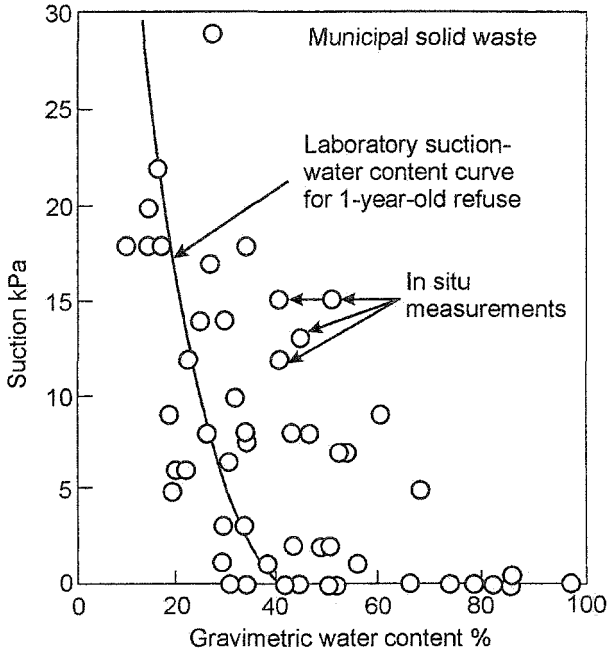
Figure 7:　Suction-water content relationship for municipal solid waste.

The shear strength of unsaturated tailings and the stability of tailings slopes.

In order to consider the geotechnical properties of shear strength and volume change for an unsaturated soil in terms of applied total stresses and suction, it is necessary to have a relationship linking these variables, i.e. an effective stress relationship is required. The first such relationship was proposed by Croney, et al. in 1958 and there have been many subsequent proposals over the past 48 years. Surprisingly, none of these has made any real advance on Bishop's proposal of 1959 that:

$$\sigma^{1} = (\sigma - u_a) + x\,(u_a - u_w) \tag{1}$$

i.e. that effective stress in an unsaturated soil, or any other porous material, can be represented by the sum of a total stress or stresses ($\sigma_i - u_a$) and a suction ($u_a - u_w$) multiplied by a modification or effectiveness factor (x) that is related to the extent of unsaturation. Appendix 1 lists ten of the effective stress relationships proposed by various authors between 1958 and 2002 and indicates how they are all equivalent to the Bishop equation, and also shows the progression of research over the past half-century.
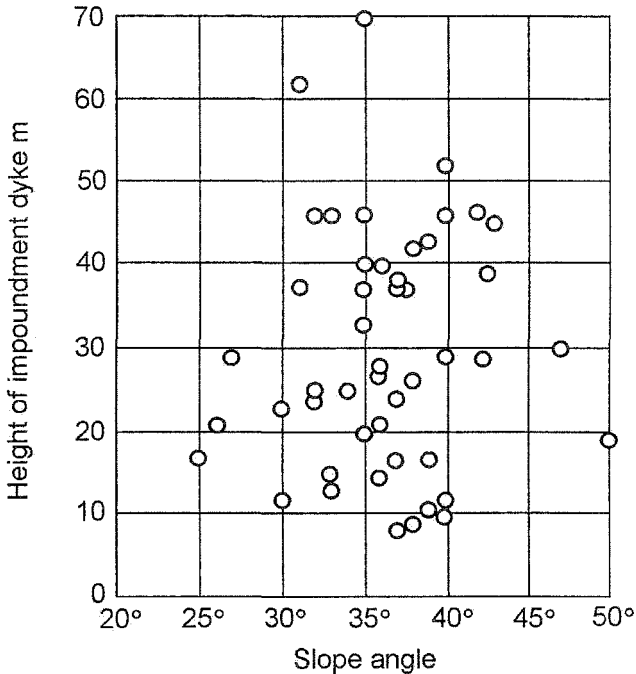
Figure 8:   Relationship between average slope angle and height for 46
             stable gold tailings impoundment dykes in the water deficient
             climatic zone of South Africa.

A striking demonstration of the strength that can be developed by slopes of
unsaturated tailings in a semi-arid climate is given in Figure 8 where the average
slope angles of 46 stable ring dykes in South Africa, built of gold tailings and
retaining gold tailings to their full height, have been plotted against the heights of the
slopes. All of these impoundments were operated in such a way that the bulk of the
deposits (and especially the all-important retaining embankments) were maintained in
a partly saturated state at all times. This so-called semi-dry operation was achieved
by providing adequate under-drainage to the retaining embankments to depress the
phreatic surface, by keeping the pool area of the hydraulic fill remote from the
embankments and by adopting a slow rate of rise (about 2 m per year) so that
successive layers of deposition could consolidate and dry thoroughly before being
covered by newly deposited material.

This practice, which is possible only in a water-deficient climate, enables stable
embankments to be constructed that may have almost incredibly steep slopes,
especially considering that gold tailings is a cohesionless silt with an angle of

shearing resistance of 30-35°. The average slope angle of these dykes is 35° while heights range up to 60 m and some dykes exceed 40° at heights in excess of 40 m. These are not the only examples of tailings impoundments with amazing outer dykes. Casagrande and McIver (1970) for example, reported a hand-built tailings dyke in Chile that was 30 m high at a slope of 63°!

That slopes of these dimensions can really be stable is supported by the simple analysis in Appendix 2 and its accompanying photograph that shows that if suctions in a slope are in static equilibrium with a water table at their base, and even if the tailings are cohesionless, then even a vertical slope can be stable, regardless of its height.

Figure 9 shows measurements of vane shear strength made in a deposit of gold tailings in which the water table was at 17 m below surface. The figure shows that the in situ strength can reasonably be represented by the equation:

$$\tau = \{\gamma H + \gamma_w (H_w - H)\} \tan \phi^1 \qquad (2)$$

In words, the strength of the cohesionless tailings equals $\tan \phi^1$ multiplied by the effective stress, as stated by equation (1) with $u_a = 0$, $u_w = -\gamma_w (H - H_w)$ and $x = 1.0$. In this case, because of the fine particle size of the tailings, the degree of saturation remained 100%, as did x, although the pore water pressure at the surface was at least -170 kPa.

Figure 10a shows a section through a gold tailings impoundment, 30 m high, with a 40° outer slope. The tailings impoundment had been abandoned 20 years previously and was completely stable. As part of a tailings re-mining project, it was decided to re-use the tailings impoundment to store re-mined tailings slurry. A piezometer installed in the tailings showed that the water table had subsided to the level of the soil surface underlying the impoundment. The impoundment was taken back into use, but a month afterwards, it was found that the phreatic surface had risen by 20 m. As a safety measure, it was decided to buttress the toe of the ring dyke. This was done by constructing a bund of compacted dry tailings at the toe and filling the space between the bund and the pre-existing dyke with re-mined tailings slurry. The result was an almost immediate failure of the dyke which is illustrated in Figure 10b.

Although the phreatic surface in the impoundment had subsided since abandonment, the tailings remained saturated, though subjected to a hydrostatic suction, as demonstrated by Figure 9. Very little addition of water was necessary to cause the loss of the suction and the re-establishment of a high phreatic surface (see Figure 6). The mechanism can be appreciated by reference to line BC of Figure 6b where a 2% increase in water content, from 8% to 10% was sufficient to reduce the suction from 1500 kPa to 650 kPa. The final straw was added by wetting the toe of the dyke with the well-intended "buttress" of tailings slurry. As the slurry had a very low shear strength, it provided no buttressing at all, but further raised the phreatic surface at the toe of the dyke.

Thus, adequate slope stability can be achieved at steep slope angles by the correct slope building practices, involving maximization of the effects of solar drying. However, unwary interventions that destroy the inherent soil suction can lead to disaster.

The Simmergo failure (Figure 10) occurred at 10 a.m. on a Saturday when deposition was not in progress. A maintenance workman was standing on the section of the wall that failed. According to him, there was a tremor and a loud rumbling. He clung to the tailings delivery pipe that is visible on either side of the failure (Figure 10b) and was let down gently as this subsided into the gap. Fortunately, no one was injured.
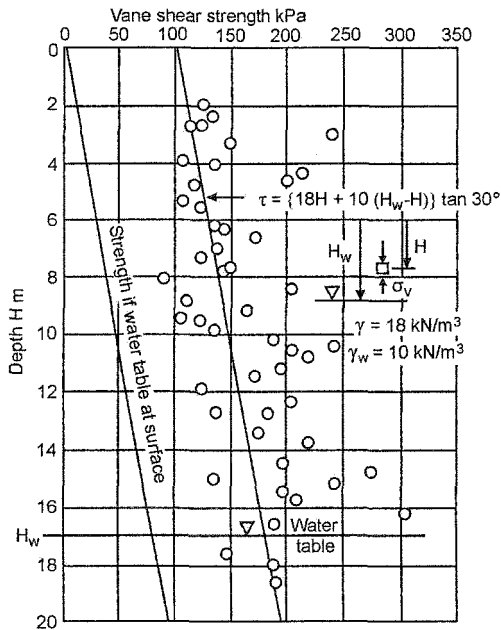
Figure 9:   Profile of in situ vane shear strength with depth in a deposit of gold tailings where the depth of the water table was 17 m.
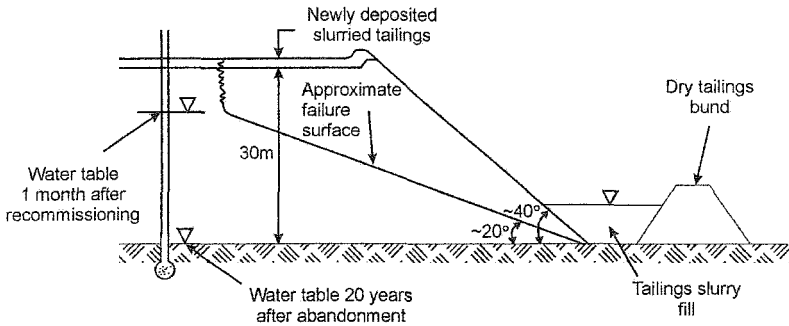
Figure 10:   (a) Section through the Simmergo gold tailings impoundment which failed as a result of a rising phreatic surface.

Figure 10:   (b) View of failure of Simmergo tailings dyke.

Erosion of the surfaces of waste depositories.

The topic of surface erosion may seem out of place in a dissertation on unsaturated soils. However, surface erosion is a process that, especially in water-deficient climates, occurs in the zone of the soil that is most likely to be unsaturated, unless rain is actually falling. Furthermore, erosion has two components – water erosion and wind erosion. In water-deficient climates, plant cover to surface soils is

usually much sparser than in water-surplus climates, thus exposing a greater proportion of the surface to the effects of water erosion. During the long dry seasons common to water-deficient climates, the soil surface dries out, powders or microcracks and becomes particularly susceptible to both water and wind erosion. Thus both water and wind erosion tend to be more severe in water-deficient climates than in areas of water surplus.
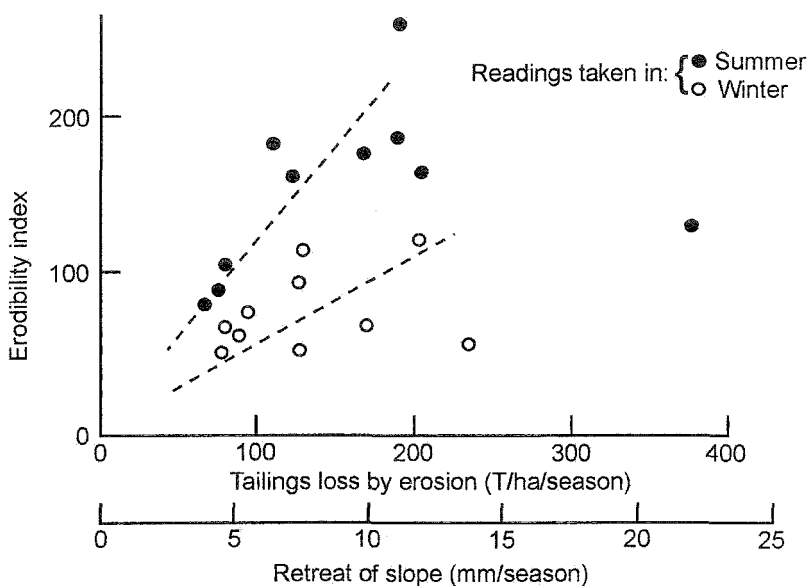
Figure 11:   Seasonal distribution of erosion losses in a water-deficient climate correlated with an erodibility index.

The use of very steep slope angles for the outer slopes of tailings impoundments in water-deficient climates such as those of Chile, South Africa and Western Australia, arose because, when tailings impoundments were first introduced in the early 1900's, the outer slopes were built by hand and it was convenient to adopt angles of 1 on 1.5 (34°), 1 on 1.25 (39°), etc. It became a matter of pride for a mine to build tailings slopes that were steeper than those of the rival mine down the road. These steep angles became accepted practice which continued until the early 1990's when (in South Africa) regulations were introduced requiring permanent rehabilitation of tailings impoundments before closure certificates were issued that relieved the mine of responsibility for the waste deposit. It slowly became accepted by mine owners that erosion from steep slopes by both water and wind can be large and that permanently rehabilitating excessively steep slopes becomes almost impossible. In the 1980's when the writer began to measure erosion rates from tailings slopes

(Dorren and Blight 1986, Blight, 1989) the measured rates proved to be so high that the mining industry found it difficult to believe the results and tried hard to discredit them. Eventually the truth prevailed. A more sensible view that is now gaining acceptance is that it is foolish to construct tailings slopes any steeper than the 15° (1 on 3.7) which is the maximum cross-slope on which agricultural machinery can work and which results in more moderate surface erosion. There is a similar temptation to make the slopes of MSW landfills very steep. Landfilled MSW, being fibrous, has a considerable component of strength that is independent of friction and will therefore stand stably at very steep slopes. However, the temptation should be resisted for similar reasons to those that apply to tailings dams.

Parameters affecting erosion from slopes

In a given climate, the main parameters that affect the rate of surface erosion of a slope are the slope angle and length and the surface cover. Early measurements of rates of erosion of the outer slopes of gold tailings dams (Dorren and Blight, 1986) showed that although surface hardness or shear strength, measured by a variety of means, does affect erosion rates, the effect is rather poorly defined. Figure 11 correlates an erodibility index (which is really a measure of how much strength the surface of a dry soil loses when wetted) with measured seasonal erosion losses from the side slopes of a number of gold tailings impoundments in South Africa. This is a summer rainfall region with a five month windy winter dry season. It can be inferred that erosion losses are not very well defined by the erodibility index, and also that, in the absence of rain, erosion occurring in winter must be caused by wind. However, surface cover (meaning a surface covering of a tailings slope by a gravel layer or by vegetation) can have a major effect on rates of erosion.

Figure 12 illustrates the results of erosion measurements on a moderately steep natural hillside formed in soil residual from a weathered greenstone schist. Figure 12a shows the profile of the slope which was interrupted at its upper end by large greenstone boulders. Figure 12b shows the rate of erosion of the slope, plotted from measurements of the slope surface elevation against a double row of steel pegs driven into the soil and observed over a period of 4 years. The upper part of the slope is eroding at rates approaching 50 T/ha/y at the top, reducing to zero at about half the slope length. The lower part is accreting at much the same maximum rate. The area under the erosion rate curve (in Tm^2/ha/y) is slightly less than that under the accretion rate curve, but erosion and accretion are close to being in balance. The measured difference of 150 Tm^2/ha/y in 1300 Tm^2/ha/y (11.5%) probably arose because erosion occurring above the boulders was not recorded, but contributed to the accretion. Similar patterns of erosion/accretion occur on the slopes of tailings impoundments, although rates of erosion/accretion of tailings slopes may be as high as 1000 T/ha/y (see Figure 13 and Table 3, to follow) rather than the 20-50 T/ha/y for natural slopes.

Figure 12c shows the composition of the surface cover to the slope, which is probably the key to the low rate of erosion. Bare soil and gravel and boulders predominate

near the top of the slope, where erosion is most active. Vegetation predominates near the toe where accretion is occurring. Without the vegetation, gravel and boulders that impede the rate of flow of water down the slope and shelter the bare soil patches from the wind, the rate of erosion would be much greater.
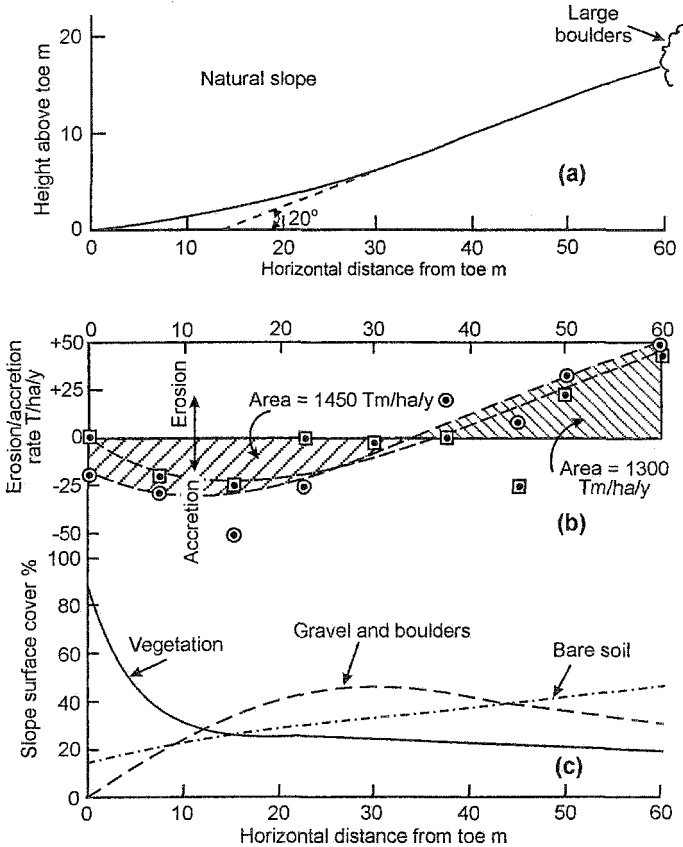
Figure 12:   Erosion of a natural residual soil slope in South Africa.
              (a) Profile of slope.
              (b) Distribution of erosion/accretion.
              (c) Surface cover of slope.

An erosion rate of 50 T/ha/y represents a change of slope surface of about 2.5 mm/y. Thus even this natural slope surface would erode or accrete by up to 200 mm in a human life span of 80 years. The surface of an unprotected tailings slope, in contrast, may change level by 4000 mm in the same time. Assuming that over the profile of a slope, erosion equals accretion, as shown in Figure 12b, this means that the angle of a

60 m long tailings slope would flatten from an initial $20°$ to $16.5°$ over 80 years. It is obviously sensible to construct the slope flatter in the first place. This observation is further illustrated by Figure 13 which shows the effects of slope angle and slope length on the rates of erosion of unprotected slopes of gold tailings in South Africa, measured over a period of 4 years (Blight, 1989). Much of the scatter of observations arises because slope erosion rates are affected by both angle and length. For any one slope angle (e.g. the most popular, $33°$. in Figure 13a) data is shown for slopes of various lengths. Similarly, for the most popular slope length between berms (25 m in Figure 13b), data is shown for several slope angles. The most notable conclusions from Figures 13a and b are that:

.1   Horizontal and vertical surfaces erode very little. The maximum rate of erosion occurs at slope angles of 60 to 75% ($31-37°$).

.2   Grassed and gravel-mulched surfaces (i.e. surfaces covered by a thin gravel layer) erode much less than untreated surfaces.

.3   Comparison with Figure 12 shows that unprotected slopes of tailings erode much more than natural soil slopes.

Figure 13c shows a three-dimensional erosion rate surface or "sail" that demonstrates how erosion loss depends on the interaction of slope angle and slope length. In this diagram, a more erodable surface would have the effect of allowing the sail to bulge out further, and heavier rain, or a higher annual rainfall would also cause the sail to bulge further out, increasing the erosion loss.

Concerning the effects of surface treatments of various types, Table 3 gives a summary of the results of a large-scale erosion-prevention test carried out on the outer slope of a gold tailings impoundment (Blight and Amponsah-Da Costa, 2004). Eleven experimental panels were set up on the slope, each measuring 10 m wide by 20 m long (up the slope). Precipitation and erosion were measured on all of the panels by means of rain gauges and a 5 m x 5 m grid of steel pegs driven into the slope surface (3 pegs across the width by 5 pegs along the length). Measurements were taken at the end of the wet season (March) and the end of the dry season (September) over a period of 4 years. As Table 3 shows, it appears possible, with an appropriate surface treatment, to reduce the rate of erosion of a tailings slope to values that are even less than those for a natural hillside. However, a longer period of observation is required to make sure that the various slope covers are sustainable with a minimum of maintenance.

Wind erosion of waste impoundment surfaces.

The discussion of erosion has so far not differentiated between water and wind erosion. Measurements of wet and dry season erosion in the South African gold fields area (which has a water-deficient climate with a 5 month long dry season) have shown that erosion losses caused by water are roughly twice those caused by wind

(see Figure 11). In drier climates, the expectation would be that wind erosion would increase relative to water erosion, and vice versa.

The rate of wind erosion of a loose (e.g. sand) surface is governed by an equation of the form (originally proposed by Bagnold, 1941)

$$q = R \, (v - v_{th})^3 \qquad\qquad (3)$$

where   q is the rate of soil particle movement (e.g. in $kg.m^{-2}.s^{-1}$)
   v is the wind velocity close to the soil surface (ms^{-1})
   v_{th} is the threshold wind velocity at which soil particle movement is initiated, and
   R is a constant of proportionality ($kg.m^{-5}.s^2$)

Wind arises from the movement of air masses across the surface of the Earth. As the air moves, its motion is retarded by interference or friction with the ground surface. The result is that wind speed increases with height above the surface. A feature that is higher than its surroundings, such as a sand dune, a tailings dam or a landfill, will force the air passing over it to rise, and in addition to retarding the wind by friction, introduces a venturi effect that accelerates the wind. As a result, prominent features of this nature produce their own distinctive profiles of near-surface wind velocity, two examples of which are shown in Figure 14.

Figure 14a shows the wind velocity profile for a coastal sand dune superimposed on the elevational profile. (Note that the vertical scale is exaggerated by a factor of 6.25) The wind amplification factor is the ratio of the wind velocity at a particular point on the dune surface to the velocity of the approaching wind. It will be seen that the wind profile has a similar form to the elevational profile, but there are differences. The wind amplification factor reaches a maximum shortly before the maximum elevation is reached. Hence, referring to equation (3), the maximum rate of sand transport will occur just before the crest of the dune is reached. Once the peak of the wind profile has been passed, the wind velocity falls rapidly to a very low value in the lee of the dune and sand picked up to windward of the crest is deposited to leeward.

Figure 14b shows the wind profile for the outer slope of a tailings dyke. Here, also, the peak wind velocity is experienced just to windward of the crest of the slope. The wind velocity then falls off rapidly and relatively little wind is experienced across the almost level surface of the impoundment. Even the 3 m width of the berm at elevation 104 m gives shelter from the wind. Figure 14 shows very clearly that certain portions of a slope are vulnerable to wind erosion, but other portions are not. The region in the vicinity, and up-wind of the crest clearly needs protection, as do the outer edges of berms. However, the top of the impoundment, and leeward slopes (in the case of prevailing winds) need no protection.. Protection against wind erosion can therefore be provided very specifically.
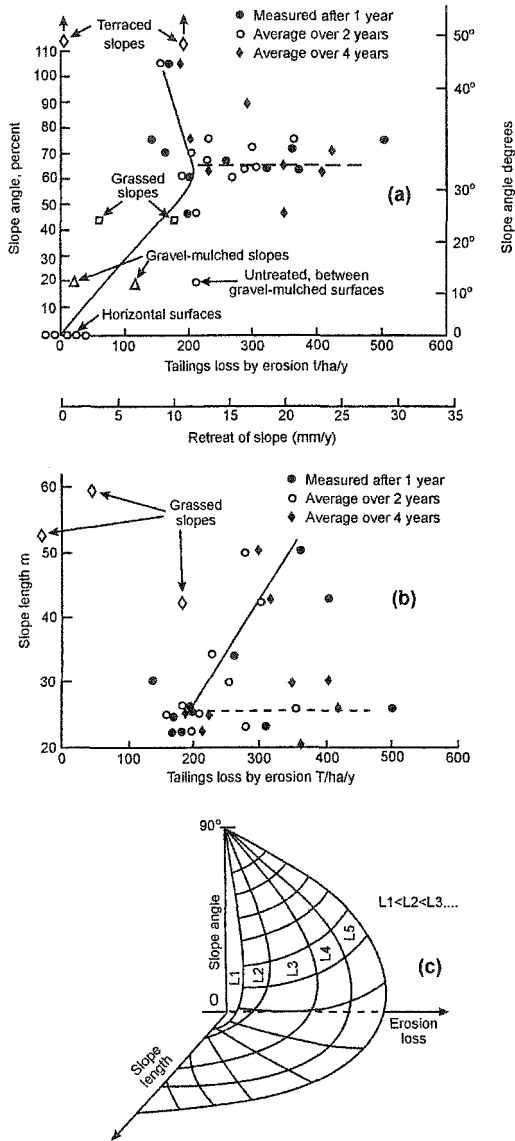
Figure 13:   Rates of erosion of the surfaces of gold tailings impoundments in
              South Africa.
              (a) The effect of slope angle on tailings loss.
              (b) The effect of slope length on tailings loss.
              (c) The three-dimensional erosion rate surface or "sail".

Table 3: Comparison of surface erosion rates of the slopes of gold tailings impoundment dykes treated in various ways, with erosion of a natural slope. (After Blight and Amponsah-Da Costa, 2004).

Description of slope	Cumulative rate of erosion measured over 4 wet seasons T/ha/y	Relative cost/ha %
Natural 20° hillside	25	-
33° Tailings slope: Treatment		
Untreated	1000	-
Grass (seeded)	160	100
Grass (sods placed on surface)	45	110
100 mm layer: 50 mm single sized stone	35	67
300 mm layer: run of mine waste rock	12	62
300 mm layer: fine waste rock	85	62
300 mm layer: fine waste rock on geofabric	15	120

Figure 15 shows wind-tunnel measurements on model tailings impoundment profiles that support and amplify the field measurements shown in Figure 14. Figure 15a shows the effect of a crest wall in deflecting air flow from the top surface of the impoundment, and Figure 15b shows that the amplification factor at the crest of a slope is linearly dependent on the slope angle and reduces progressively as the slope angle is reduced. Both of these observations agree with the data shown in Figure 13 for slope erosion by mixed causes.

The settlement of coal strip-mine backfill and landfilled municipal solid waste.

Settlement of strip-mine backfill:

Coal deposits usually occur as horizontal to sub-horizontal seams at relatively shallow depths of 20 to 70 m. If this is the case, the current most economical method of mining is to strip off and stockpile the top-soil - to use for later rehabilitation of the surface – and then to strip the overburden strata and excavate the coal. This process takes place over a working face that may extend for several hundred metres. While coal is being excavated and removed for beneficiation and sale, dragline excavators are occupied in stripping overburden and exposing the coal stratum ahead of the working face. The stripped overburden – usually consisting of soft to hard sandstone and shale fragments of random sizes – is cast by the dragline back into the void

behind the working face. The mine backfill is deposited in the form of a series of rows of conical piles with no attempt at compaction. At the end of the mining operation, the cones of spoil are flattened to form a regular surface, the top-soil is spread and the area rehabilitated. Because of the bulking of the rock when excavated, the final surface is usually above the original ground level, unless the coal seams removed are particularly thick.
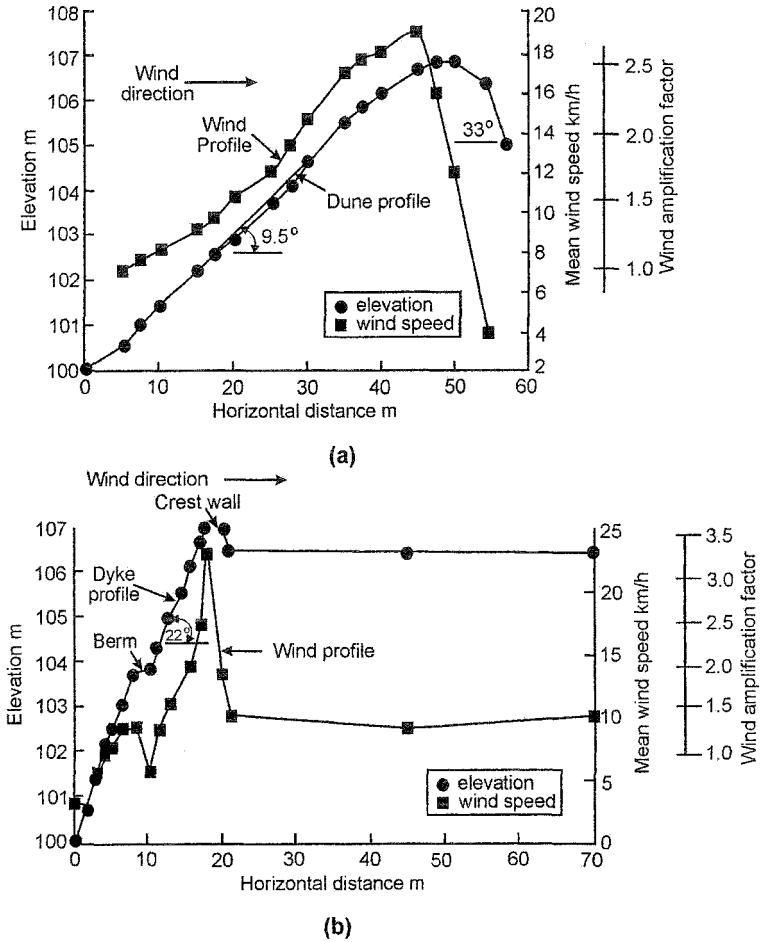
Figure 14:   Elevation and wind velocity profiles for
               (a) a coastal sand dune, and
               (b) the slope of a tailings dam.
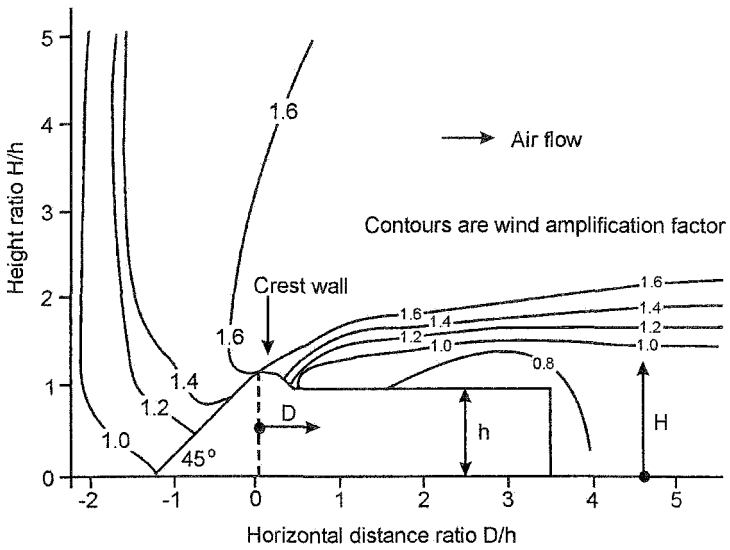
(a)
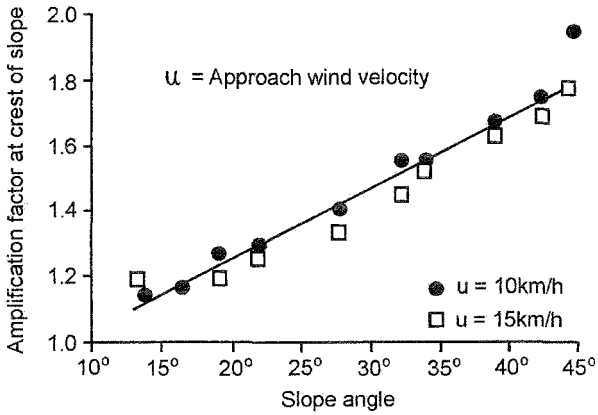
(b)

Figure 15: Results of wind-tunnel tests on model tailings impoundment profiles:
(a) Contours of wind amplification factor,
(b) Effect of slope angle on maximum wind amplification factor.

Because strip mining covers large areas, there has been an ongoing interest in the long term settlement of coal mine backfill and its effect on structures built over rehabilitated mine land. The results of several studies have been published (e.g. Charles, et al., 1977, Charles, et al., 1984, Reed and Hughes, 1990). These have established the following mechanisms for compression of the backfill, and hence settlement of the surface:

.1   Immediate compression of the backfill occurs under increasing overburden as particles are forced closer together causing distortion and crushing of point contacts.

.2   Time-dependent sloughing and slaking of rock fragments, resulting in creep settlement, occur because of relief of the original in situ stresses in the intact strata. Oxidation of minerals such as pyrite, now exposed to air, accentuate the particle breakdown.

.3   The regional water table has usually been lowered to below the level of the deepest coal seam to be mined. Once mining ceases, the water table will gradually recover and re-establish itself within the backfill. As a result, effective stresses in the rock fragments will be decreased and further "collapse" type settlement may occur as these crush.
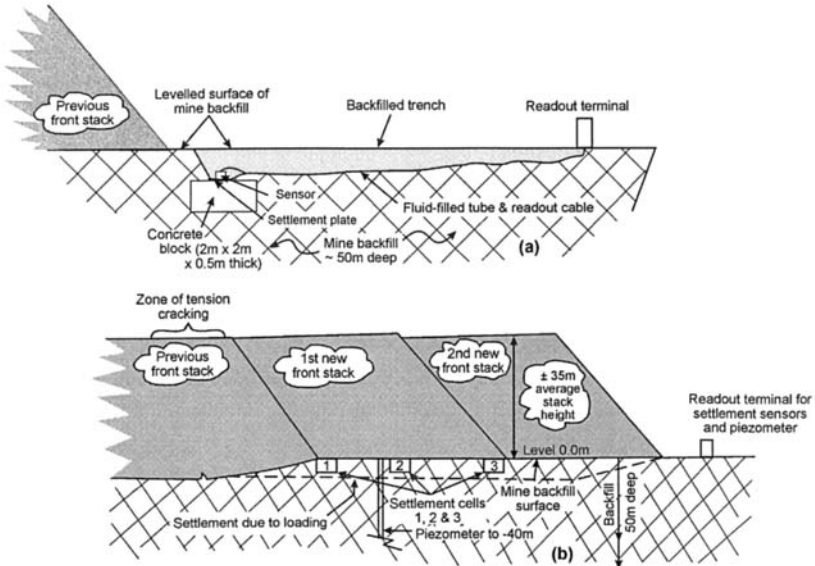
Figure 16:   Layout of full-scale settlement monitoring exercise, New Vaal Colliery, South Africa.

A survey of experience in the U.K. (Charles et al., 1977, Charles et. al., 1984, Reed and Hughes, 1990, Hills and Denby, 1996) showed that immediate compression may amount to 1 to 2% of the backfill thickness, time-dependent or creep settlement may amount to an additional 1%, and collapse settlement may be up to 2% of backfill thickness. However, these figures will depend on the nature and state of weathering of the backfill. Also, in water-deficient climates, permanent water tables are deep – often deeper than 30 to 50 m. Thus the collapse component of mine backfill settlement can be expected to be either absent, or considerably less than in the U.K., where permanent water tables are much shallower.

Settlement measurements at Lethabo, South Africa.

The Lethabo power station in South Africa is coal-fired and fed from an adjacent "captive" opencast colliery, the New Vaal Colliery. The power station has a dry ashing system that can handle 500-600 T/hour of ash (moistened to a water content of 15% to reduce dusting). To avoid sterilizing virgin ground, it was decided to stack the ash over the mined-out and backfilled area of the mine (van Wyk, 1998). The mechanical stacking system creates a front stack that is 35 to 38 m high above the level of the mine backfill, and then adds a backstack of between 8 and 12 m high above the top of the frontstack. The ash is not compacted and has a stacked density of about 1000 kg/m^3. Thus the loading superimposed on the surface of the mine backfill is up to 500 kPa.

There was a major concern that as each frontstack advanced, differential settlement of the backfill might compromise the stability and verticality of the mechanical stacker, at least resulting in misalignment and mechanical problems, and at worst causing the stacker to topple. A small-scale test embankment built after mining had started, but before the power station was commissioned, indicated that the settlement should not be excessive (Day, 1992). Nevertheless, it was decided to carry out settlement measurements under the full loading of the stacked ash at the start of full-scale operations.

The layout of the settlement monitoring exercise is shown in Figure 16. A series of 3 vibrating wire settlement sensors was installed (as indicated in Figure 16a) in a row ahead of the advancing series of frontstacks (as shown in Figure 16b). To protect the settlement sensors, each was mounted on a concrete block and covered by a metre of selected hand-placed fine backfill. The sensors were spaced 30 m apart, starting at the toe of the existing frontstack and spaced so that the second sensor would be under the center of the next frontstack and the third at its toe. A vibrating wire piezometer was installed at a depth of 40 m below the backfill surface to locate and monitor the level of the groundwater in the backfill.
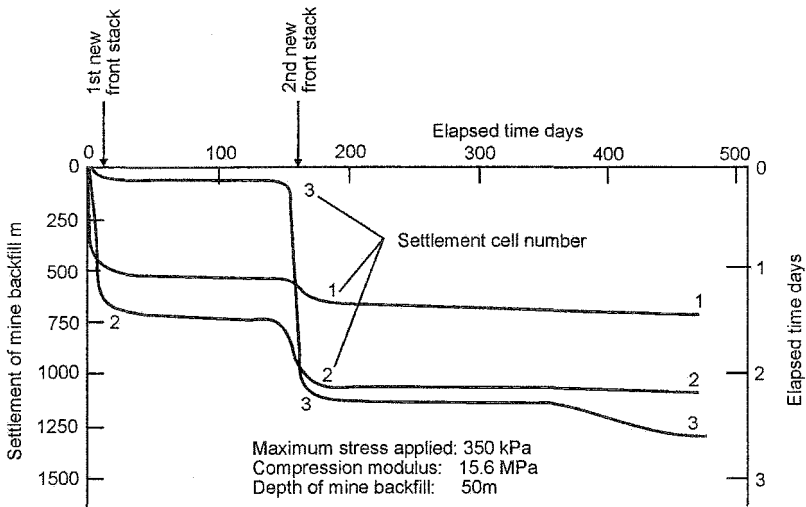
Figure 17: Settlement-time relationships observed in full-scale settlement monitoring exercise, New Vaal Colliery, South Africa.

Figure 17 shows the settlement-time curves recorded as two successive frontstacks of ash of 35 m average height were placed over the settlement cells. Cells 1 and 2 settled very rapidly as the first new frontstack advanced to cover them in a period of about 10 days. Cell 3 was only partly covered and therefore did not settle by much.

The site was left undisturbed for a period of about 150 days during which a slight time-dependent settlement was recorded by cells 1 and 2. The second new frontstack was then placed, completing the loading of all three settlement cells. During the 300 days after the second loading, slight time-dependent settlement was registered by all three cells, with cell 3 showing a second (unexplained) acceleration of settlement a year after loading had been completed. The piezometer showed no substantial change in water level during this time.

Relatively small (up to 200 mm) differential movements occurred that had little effect on the operation or stability of the stacker. However, because the ash self-cements itself within a short time after placing, settlement near the toe of the previous frontstack (see Figure 16) caused severe and deep tension cracks to open parallel to the crest. Similar cracks appeared in the first new frontstack as the second new frontstack was placed. These were closed by dozing, to keep out rainwater, as soon as they opened.

Settlement measurements at Matla, South Africa.

        The Matla power station, an older station than Lethabo, has a wet ashing system, with the ash being disposed of in hydraulic fill impoundments like mine tailings impoundments. A new ash impoundment was needed and it was decided to place it over a mined-out and backfilled section of the station's captive colliery the adjacent Kriel Colliery. Because of uncertainty as to how the hydraulically placed ash would react to differential settlement of the mine backfill, a large-scale test wall of ash measuring 280 m long by 110 m wide was placed hydraulically on the mine backfill, as shown in Figure 18 (see van Wyk and Blight, 1996). The chosen site was adjacent to one of the original mine access ramps, and this void was used as a return-water reservoir for the ashing. The water table had re-established at a depth of 16 m in the backfill and remained constant during building the test wall.

The settlement of the mine backfill was measured by a set of 8 sleeved rods set in concrete blocks on the mine backfill surface, and a second set of sleeved rods drilled into the mine backfill and anchored at depths of 1, 5, 10 and 16 m below the backfill surface. This enabled the distribution of settlement with depth to be measured.

The test wall was built to a height of 7 m, which with an ash bulk density of 1300 kg/m^3, represents a maximum loading of 91 kPa. As the ash and the mine backfill are relatively pervious and the ash was placed as a 1:1 ash:water slurry, the settlement, measured over the construction period of a year (368 days), probably includes some creep and collapse settlement, as well as immediate compression of the mine backfill.

The settlement versus imposed stress relationships are summarized in Figure 19. Figure 19a shows the distribution of settlement strain with depth, as measured by means of the sleeved rods set at various depths. The larger strains occurred between depths of 1-5 m and 5-10 m. The deeper layers, 10-16 m and 16-25 m, preloaded with larger overburdens, strained approximately half as much as the shallower layers.
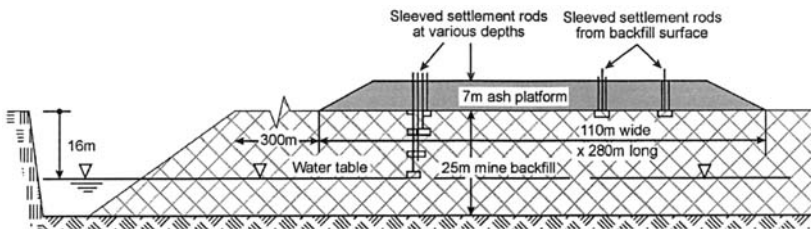
Figure 18:   Layout of 7 m hydraulic fill ash platform placed on mine backfill at Kriel Colliery, South Africa.
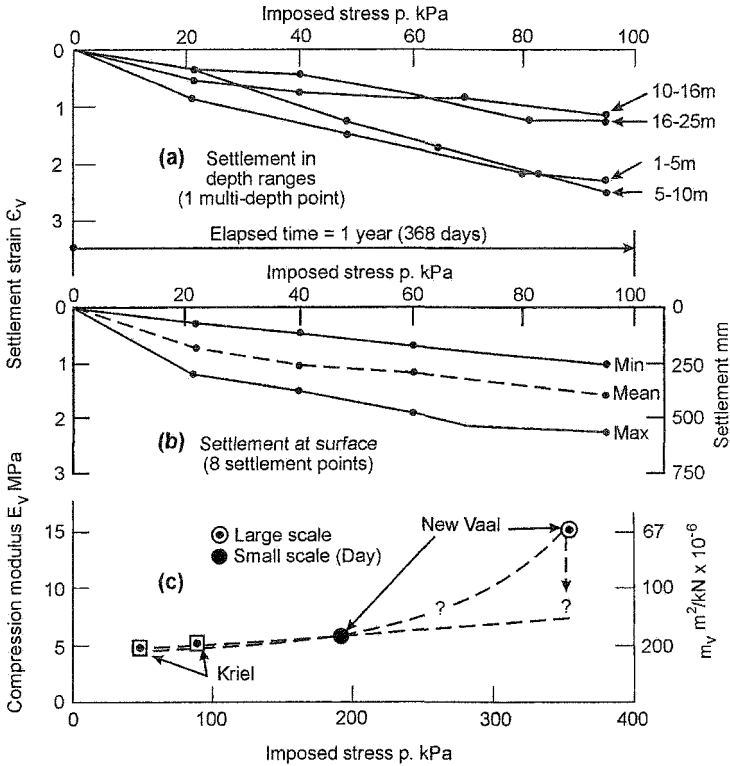
Figure 19: (a) and (b) Summary of results of settlement measurements on mine backfill loaded by hydraulically placed ash wall at Kriel Colliery. (c) Comparison of vertical compression modulus (E_v) and vertical compressibility (m_v) of mine backfill measured at Kriel and New Vaal Collieries.

In considering this result, it must be remembered that the backfill had been deposited in conical piles, with the lower material being dropped a considerable distance and then being covered by a considerable overburden, both of which would have produced more compaction than higher up. The tops of the backfill piles were then leveled off by dozing which must have resulted in a looser condition in the upper zone of backfill.

Figure 19b shows minimum, maximum and mean settlement-stress relationships measured by means of the surface settlement points. It is notable that the range of

settlement strains bracketed in Figure 19b is very close to the range covered in Figure 19a.

Summary of settlement measurements

The settlement measurements at New Vaal and Kriel collieries are summarized in Figure 19c as a relationship between average compression modulus, E_v (or its inverse, vertical compressibility, m_v) and the imposed stress p. The compression modulus is defined by

$$E_v = dp/d\varepsilon_v \text{ in kN/m}^2, \text{ kPa or MPa.}$$

The vertical compressibility is the inverse

$$m_v = 1/E_v = d\varepsilon_v/dp \text{ or } de/dp(1 + e_o) \text{ in m}^2/kN$$

where the subscript v indicates the vertical direction, ε_v is the vertical strain, e the current void ratio, and e_o the original void ratio.

The data for Kriel are quite comparable with the result obtained by Day (1992) for a smaller scale test at New Vaal, but the large scale test at New Vaal indicated a much higher compression modulus (15 MPa as compared with 5 to 6 MPa).

However, the large scale tests at New Vaal excluded the collapse settlement component, and the final value of compression modulus, as indicated in Figure 19c, may be less than that reached after 460 days (Figure 17) if the water table eventually rises above its present 40 m depth.

Settlement of land-filled MSW

Because of the excess of potential evaporation over rainfall, landfills in water-deficient climates are known to produce little or no leachate even if the landfill capping layers are pervious and almost all precipitation infiltrates (see, e.g., Fourie et al., 1999; Zornberg et al., 1999; Blight and Fourie, 1999 and Blight and Fourie, 2005). If the moisture storage capacity of the waste body is large enough, the entire annual rainfall infiltration could theoretically be stored and re-evaporated, and under these circumstances, the landfill would produce no leachate.

The Coastal Park Landfill in Cape Town is situated 500 m from the sea on permeable beach deposits of sands and silty sands, and the original landfill has no underliner. Water balance studies undertaken in 1985, a year before the landfill was commissioned, had indicated that little or no leachate would be produced, and as the

aquifer under the landfill is appreciably saline and does not constitute a usable water resource, an underliner was not considered necessary.

New landfilling regulations were introduced in South Africa in 1994 (Anon, 1994). According to these, landfills are classified in terms of the climate in which they are situated, and the climatic classification decides on whether or not a landfill is required to be under-lined. If the landfill is situated in a climate for which the estimated evaporation from the landfill surface during the wettest six months of the year has more than an 80% probability of exceeding the corresponding rainfall, no liner is required, and vice versa. The difficulty with the Coastal Park landfill was that the relevant probability was almost exactly 80%, and the national authority insisted that the existing landfill be closed and an extension, incorporating an underliner, be constructed. Because the existing landfill was at that time only 5-6 m high, there was a potential for raising it by at least 10 m, and if this were done, the moisture storage capacity would be increased considerably. Seeing that the leachate flow was a small percentage of the rainfall, it appeared possible that raising the height of the landfill would eliminate the leachate flow entirely, thus providing a large volume of usable air-space with a minimum of extra cost. It was therefore decided to embark on an experimental raising in which a section of the landfill incorporating four existing leachate measurement points would be raised by 7.5 m, and its behaviour monitored closely for a period of 5 years. The settlements described in this section resulted from this experiment. Observations of changes in the leachate flow rate and quality and of the density and composition of the waste have been reported elsewhere (Blight, 2005).

It was decided to raise the height of the test section of the landfill in two stages. In the first year (1998/1999) an additional 5 m would be added, and an additional 2.5 m would be added in the following year (1999/2000). The test section would be in the form of a compacted waste berm about 300 m long, 90 m wide at the base and 40 m wide at the crest, covering leachate measurement points numbered   2-5. Observations were made on the following levels, by means of surface points and sleeved depth points:

    .1 original waste surface
    .2 surface of first (5 m) raising
    .3 surface of second (2.5m) raising.

The full records of settlement for points 2-5 are shown graphically in Figure 20. Experimental point measurements have not been shown on Figure 20, but level measurements were made each week in year 1 and every two weeks in years 2 and 3 up to day 820. Thereafter, levels were measured monthly. Figure 20 shows the initial quick compression under the weight of the first 2.5 m raising, giving way to slow settlement which continued to increase as the waste crept and decomposed and, as a result, slowly compressed. Application of the 2 x 2.5 m first raising and the 2.5 m second raising caused the settlement to accelerate for the periods from 60 to 240 days and 700 to 750 days surface of the combined 7.5 m total raise and thereafter the

settlement rate started progressively reducing. Unfortunately, because of a misunderstanding between the project leader and the field staff, compounded by the introduction of staff new to the project, the settlement rods for the surface of the first 5m raising were not carried through to the surface of the 7.5 m raised surface, making settlement measurements impossible from day 840 onwards.

Only measurements on the original landfill surface and the final were possible after this. At the end of the experiment (5 years after the start) the lost settlement slabs were exhumed and levelled to establish their final settlement. The final settlements are shown on Figure 20 at a time of 5 years.

It is interesting to note that the waste above each leachate measurement point behaved differently. In particular, point 5 showed the least settlement under the first 2.5 m lift of the raising, but the underlying waste then appeared to yield, and under the second 2.5 m lift, settled to an extent similar to the other points. The building of trial landfill cap sections on the top of the raised landfill, but to one side of the test sections early in year 3 (Blight and Fourie, 2005), accelerated the settlement slightly, but this effect died away in a short time.

Compression characteristics of MSW.

The compression of the waste (Figure 20) is strongly time-dependent, as a result of conventional compression, creep of the organic and plastic components, and decomposition (and hence loss of mass) of the organic components. Figure 21 shows the compression of the original landfill and the raisings in the form of void ratio versus applied pressure or loading increment curves. These are shown for the original and new waste at 30 days, 0.5, 1, 2 and 3 years after loading. The slopes of chords to these compression curves have been summarized in Figure 21 as values of the vertical compressibility m_v or its inverse, vertical compression modulus E_v.

In Figure 21 the load increments for the original (5m) landfill represent the full weights of the 5 m raising (52 kPa) and the total 7.5 raising (88 kPa). For the 5 m raising, 26 kPa represents the weight of the lower 2.5 m of the raising. For the combined 7.5 m raising 44 kPa represents half of the weight of the raising.

The values of m_v recorded on Figure 21 have been compared in Table 4 with values calculated for settlement versus time curves published for four landfills of similar age to Coastal Park, situated in various parts of the world (Brazil, Colombia, Spain and England). Table 4 shows that, although on the high side, values of m_v for Coastal Park are similar to values calculated from time-settlement curves measured on comparable landfills in other parts of the world. In fact, considering possible differences in waste composition (e.g. Table 1), the agreement is remarkable.
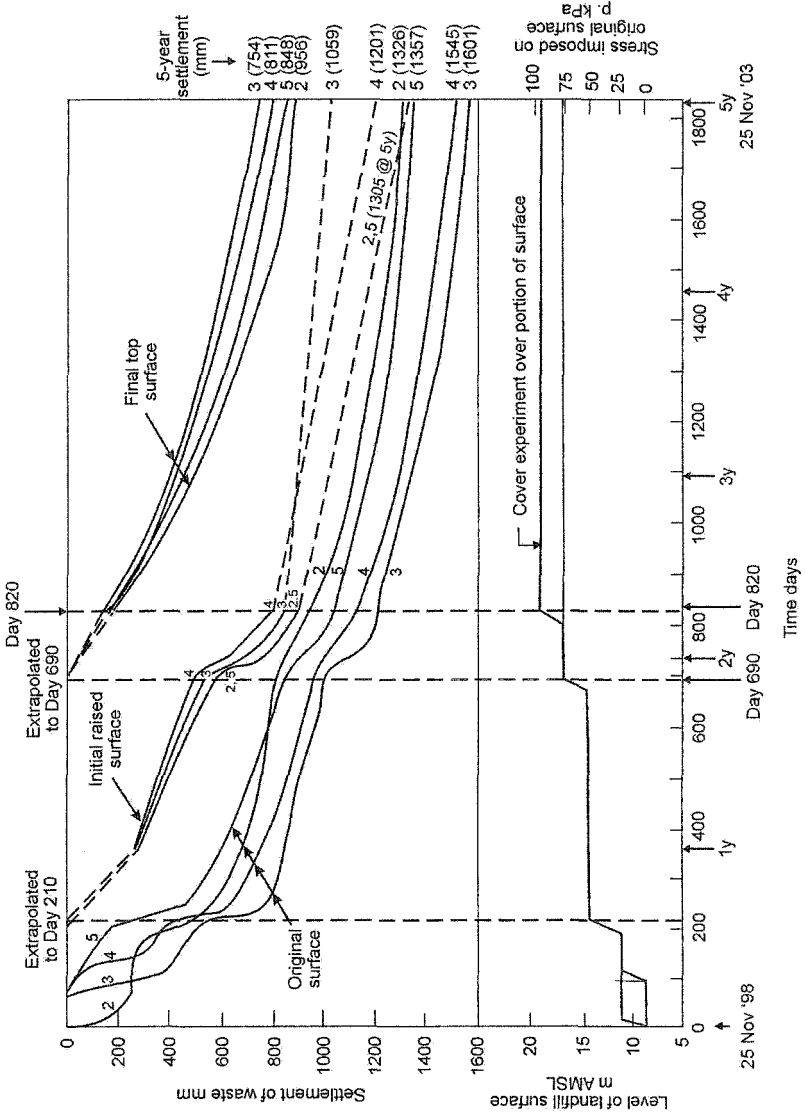
Figure 20: Settlement and imposed stress versus time relationships for test raising of Coastal Park landfill.

Table 4: Comparison of compressibilities of a number of landfills.

Reference and name of landfill	Height of Landfill m	Age Years	m_v m²/kN x 10⁻³	E_v MPa
Watts & Charles (1999). Brogborough, U.K.	11	6	3.8	0.2
Machado et al (2002). Bandeirantes, Brazil.	58	7	0.5 - 1	1 – 2
Rodriques & Velandia (2002). Dona Juana, Colombia	20	3	1.6	0.6
Pereira et al (2002). Valdemingomez, Brazil.	35	6	1.0	1
Coastal Park, South Africa. (Blight, 2005).	5-12.5	13-18	2.2-4.6	0.2-0.4

A comparison of Table 4 with Figure 19 will show that whereas E_v for mine backfill was measured to be 5 to 15 MPa, corresponding values for landfilled MSW are in the range of 0.2 to 2 MPa, i.e. mine backfill is 7 to 25 times less compressible than landfilled MSW.   Whereas the time-dependent settlement of mine backfill, as shown in Figure 17, is negligible, that of land-filled MSW, as shown in Figure 20, can be as large as, or larger than the instantaneous compression.

Apart from producing the data on settlement and leachate quality, the experimental raising was not completely successful, as the leachate flow did not completely cease as a result of raising the landfill and thus increasing the moisture storage capacity. The negative result appears to have been caused by the heterogeneity of the waste that allows a small proportion of infiltration to transit the waste via macro-pores and channels of coarse waste (e.g. building rubble) without being absorbed.
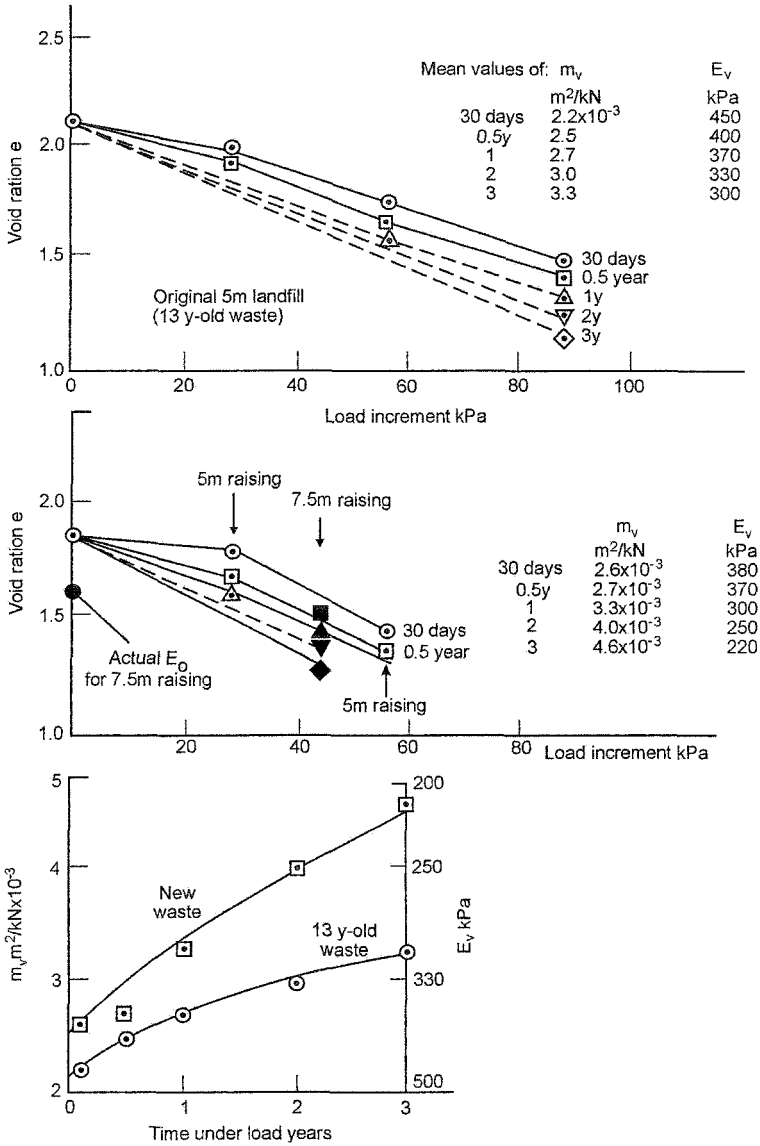
Figure 21: Values of vertical compressibility (m_v) and vertical modulus of compressibility (E_v) for the Coastal Park test raising.

Nevertheless, the leachate flow declined to 21/mm/year after 5 years and 16 mm/y after 6 years. The latter is not only within the maximum leakage rate through a liner, permitted for municipal solid waste landfills by the South African Minimum Requirements (Anon, 1994) of 30 mm/y, but is of a similar order to measured leakage rates reported for geomembrane linings, of up to 15 mm/y. (Koerner, 2001).

Summary and conclusions

Geotechnical and environmental engineers are faced with the problems of managing ever-increasing quantities of mine and municipal solid waste. Management includes both disposal and possible re-mining and re-disposal, as well as rehabilitation, maintenance and long term environmental monitoring. Long term decomposition of minerals contained in mine waste (e.g. pyrite) and decomposition of municipal solid waste, as well as the erosive effects of weather result in closed and rehabilitated waste deposits requiring monitoring and maintenance for the foreseeable future, which may extend to centuries hence. Waste management poses ongoing maintenance and monitoring problems for which there are no walk-away solutions.
Excluding Antarctia, 65 per cent of the Earth's surface has climates that are water-deficient, ranging from semi-arid with seasonal rainfall to absolute desert. In some ways, waste management is simpler in a water-deficient climate (e.g. the reduced leachate production and possible increased slope stability caused by capillary water tensions). In other ways it is more difficult (e.g. the increased difficulty of establishing and maintaining vegetation cover and increased water and wind erosion of rehabilitated surfaces).

After describing some of the characteristics of mine (MW) and municipal solid waste (MSW), including the circumstances of their arising, this paper has described, and in some cases compared, selected geoenvironmental aspects of the behaviour of these wastes in water-deficient climates. The aspects considered are:

.1   the water retention of MW and MSW which is so important in the water balance of waste deposits;
.2   the shear strength of unsaturated fine-grained MW (tailings) and the stability of tailings slopes;
.3   erosion of the surfaces of waste depositories by water and wind; and
.4   settlement of open-cast or strip mine backfill and MSW, including their similarities and differences, and recording some of the relevant compression characteristics.

Appendix 1: The search for a description of effective stress in an unsaturated soil.

Author(s)	Date	Equation for effective stress	Equivalency to Bishop equation
Croney, Coleman & Black	1958	Volume change $$\sigma^1 = \sigma - \beta^1 u_w$$	Assumed $u_a = 0$. With $u_a \neq 0$, $\sigma^1 = (\sigma - u_a) + \beta^1(u_a - u_w)$
Bishop	1959	$$\sigma^1 = (\sigma - u_a) + \times(u_a - u_w)$$	Suggested $\times$ approximated by S_r
Lambe	1960	$$\sigma = \overline{\overline{\sigma}} a_m + u_a a_a + u_w a_w + R - A$$	$\overline{\overline{\sigma}} a_m + R - A = \sigma^1$ $a_w = S_r$, $a_a = 1 - S_r$ Hence $\sigma^1 = \sigma - u_a(1 - S_r) - S_r u_w$, i.e. $\sigma^1 = (\sigma - u_a) + S_r(u_a - u_w)$
Aitchison Jennings	1961 1961	$$\sigma^1 = \sigma + \psi p^{11}$$	Assumed $u_a = 0$. Putting $p^{11} = u_a - u_w$ i.e. $\sigma^1 = (\sigma - u_a) + \psi(u_a - u_w)$
Richards	1966	$\sigma^1 (\sigma - u_a) + x_m(u_a - u_w) + x_s p_s^{11}$	$(u_a - u_w)$ = matric suction p_s^{11} = solute suction
Kassiff & Ben Shalom	1971	Volume change: $\alpha P_s = \Delta s - \Delta s_o$ s = suction, $P_s = \Delta(\sigma - u_a)$	$\alpha = \dfrac{\Delta(u_a - u_w)}{\Delta(\sigma - u_a)}$ Hence $\sigma^1 = (\sigma - u_a) - \underline{1}(u_a - u_w)\alpha$
Fredlund & Morgenstern	1977	Volume change $\varepsilon_v = \theta_w + \theta_a$ $\theta_w = \dfrac{(\varPhi_x + \varPhi_y + \varPhi_z - 3u_a)}{3H} + \dfrac{(u_a - u_w)}{R}$	For isotropic stress: $\theta_w = \dfrac{(\sigma - u_a)}{H} + \dfrac{(u_a - u_w)}{R}$ $\theta_w = \{1/H\}\{(\sigma - u_a) + H(u_a - u_w)/R\}$
Fredlund et al	1978	Shear strength $\tau = c^1 + (\sigma - u_a)\tan\varphi^1 + (u_a - u_w)\tan\varphi^b$	$\tau = c^1 + \{(\sigma - u_a) + \underline{\tan\varphi^b}(u_a - u_w)\}\tan\varphi^1$ $\tan\varphi^1$

		2 Decades later:	
Oberg & Sallfors	1997	$\tau = c^1 + \{(\sigma - u_a) + S_r(u_a - u_w)\} \tan \varphi^1$	
Sheng et al	2002	$\sigma^1 = \sigma - \delta_{ij}(S_r)u_w,$ $u_a = 0$	$\sigma^1 = (\sigma - u_a) - \delta_{ij}(S_r)(u_a - u_w)$
		and so on	

Appendix 2: Effect of suction on slope stability

Figure A1 shows a section through the outer dyke of a tailings dam that is built on marshy ground with the water table at the ground surface. The tailings dam has been in place for 30 years (as with the Simmer and Jack dam) and is fully consolidated. The water table under the tailings is also at ground level. Consider shear stability along a potential shear surface aa that passes through fully saturated tailings.

$$W = \gamma H^2/2 \ (\cot \alpha - \cot i) \tag{A1}$$

If φ^1 is the angle of shearing resistance of the cohesionless tailings and
$\quad \bar{u}$ is the mean pore pressure along aa
$\quad \bar{u} = -\gamma_w H/2$
$\quad aa = H/\sin \alpha$

The potential shearing resistance along aa is

$$T = (W \cos \alpha + \underline{\gamma_w H^2}) \tan \varphi^1 2 \sin\alpha \tag{A2}$$

The factor of safety against shear failure along aa is

$$F = T/W \sin \alpha, \text{ or}$$

$$F = \{\cot \alpha + \underline{\gamma_w/\gamma \sin \alpha}\} \tan \varphi^1 \tag{A3}$$
$$\quad\quad (\cot\alpha - \cot i)$$

Because the tailings is cohesionless, the problem is purely frictional and F is independent of the height H.

As an example, put $i = 90^\circ$ to get a vertical face, then

$$F = \{\cot \alpha + \sec \alpha \cdot \gamma_w/\gamma\} \tan \varphi^1 \qquad\qquad \text{(A3a)}$$

Putting $\varphi^1 = 30^\circ$, $\alpha = 45^\circ + \varphi^1/2 = 60^\circ$ and $\gamma_w/\gamma = 0.6$

$$F = 1.03$$

Hence such a slope would (theoretically) be marginally stable up to any height. However, if the height were such that $u = \gamma H$ were sufficient to exceed the air entry suction for the tailings, the upper part of the slope would crumble, although it would probably not fail completely.
As a second example, put $i = 60^\circ$ and $\alpha = 30^\circ$ with $\varphi^1 = 30^\circ$ and $\gamma_w/\gamma = 0.6$, then

$$F = 1.6$$
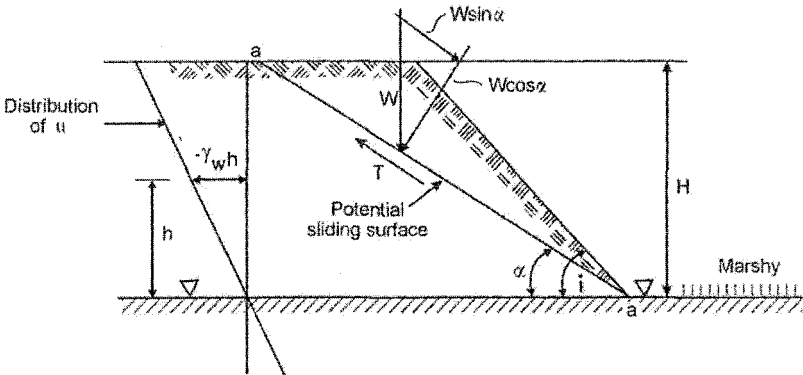
Figure 1A: Basis for analysing the effect of a depressed phreatic surface on the stability of a tailings slope.

Finally, setting the suction to zero

$$F = \cot \alpha \cdot \tan \varphi^1 = \tan \varphi^1/\tan \alpha \qquad\qquad \text{(A3b)}$$

and for the previous example,

$$F = 1$$

and the slope could not be made steeper than $\alpha = \varphi^1$.

To demonstrate the possibility of a stable vertical slope in a cohesionless material, Figure A2 shows a 10 m high vertical slope with the phreatic surface at its base, in

gold tailings. This slope had been standing, quite stably, for several years when the photograph was taken.

Figure A2: Photograph of a vertical tailings slope 8 m high, with the phreatic surface at its base.

References

Aitchison, G.D. (1961). "Relationship of moisture stress and effective stress functions in unsaturated soils." *In: Pore Pressure and Suction in Soils,* Butterworth, London, U.K., 47-52.

Anon, (1994). *Minimum Requirements for Waste Disposal by Landfill, 1ˢᵗ ed. Department of Water Affairs and Forestry,* Pretoria, South Africa.

Bagnold, R.A. (1941). *The Physics of Blown Sand and Desert Dunes.* Methuen, London, U.K.

Bishop, A.W. (1959). "The principle of effective stress". *Teknisk Ukeblad,* 106, 859-863.

Blight, G.E. (1989). "Erosion losses from the surfaces of gold tailings dams". *Journal, South African Institute of Mining and Metallurgy,* 89, (1), 23-29.

Blight, G.E. (1994). "The master profile for hydraulic fill tailings beaches". *Proceedings, Institution of Civil Engineers* U.K.,107, 27-40.

Blight, G.E. (2005). "Consequences of raising the height of a landfill in a water-deficient climate". *Waste Management,* In Press 1-16.

Blight, G.E., Rea, C.E., Caldwell, J.A. and Davidson, K.W. 1981. Environmental protection of abandoned tailings dams. 10ᵗʰ International Conference on Soil Mechanics and Foundation Engineering, Stockholm, Vol. 1 , pp. 303-308.

Blight, G.E. and Roussev, K.I. (1995). "The water balance for an ash dump in a water-deficient climate". *Unsaturated Soils,* Alonso, E.E. and Delage, P. (Eds). A.A. Balkema, Rotterdam, Netherlands, 2, 833-839.

Blight, G.E. and Mbande, C. (1998). "Waste management problems in developing countries." *In: Solid Waste Management – Critical Issues for Developing Countries,* E. Thomas-Hope, Ed. Canoe Press, Kingston, Jamaica, 11-26.

Blight, G.E. and Fourie, A.B. (1999). "Leachate generation in landfills in semi-arid climates". *Proceedings, Institution of Civil Engineers,* U.K., *Geotechnical Engineering,* 137, 181-188.

Blight, G.E. and Amponsah-Da Costa, F. (2004). "Towards the 1000 year erosion-free tailings dam slope – A study in South Africa". *In: Ground and Water Bioengineering for Erosion Control and Slope Stabilization.* Eds: Barker, D.H., Watson, A.J., Sombatpanit, S., Northcutt, B. and Maglinao, A.R. Science Publishers, Inc., Plymouth, U.K., 365-377.

Blight, G.E. and Fourie, A.B. (2005). "Experimental landfill caps for semi-arid and arid climates". *Waste Management Research,* 23, 113-125.

Casagrande, L. and MacIver, B.N. (1970). "Design and construction of tailings dams". Quoted by A.W. Bishop. (1973). "The stability of tips and spoil heaps". *Quarterly Journal of Engineering Geology,* 6, (3 and 4), 335-376, plus 15 of photographs.

Charles, J.A., Naismith, W.A. and Burford, D. (1977). "Settlement of backfill at Horsley restored open cast coal mining site". *1ˢᵗ Conference on Large Ground Movements and Their Effect on Structures,* Cardiff, U.K., 320-330.

Charles, J.A., Hughes, D.B. and Burford, D. (1984). "The effect of a rise of water table on the settlement of backfill at Horsley restored coal mining site, (1973-

1983)". *3rd Conference on Ground Movements and Structures*, Cardiff, U.K., 423-442.

Croney, D., Coleman, J.D. and Black, W.P.M. (1958). "The movement and distribution of water in soil in relation to highway design and performance". *Highway Research Board, Special Report 40*, Washington, U.S.A.

Day, P. (1992). "Determination of settlement parameters for opencast pit backfill by means of large scale tests". *Symposium on Construction over Mined Areas, South African Institution of Civil Engineering*, Pretoria, South Africa. 73-78.

Dorren, D.I. and Blight, G.E. (1986). "Erosion of the slopes of gold residue dams on the Transvaal Highveld – preliminary results." *Journal, South African Institute of Mining And Metallurgy"*, 86(12), 475-480.

Fourie, A.B., Blight, G.E., and Pinheiro, J. (1999). "Subsurface contamination by leachate at six unlined landfill sites in South Africa". *In: Sardinia (1999), 7th International Waste Management and Landfill Symposium*. S. Margherita di Pula, Cagliari, Italy, 133-140.

Fredlund, D.G. and Morgenstern, N.R. (1977). "Stress state variables for unsaturated soils". *Journal of the Geotechnical Engineering Division*, ASCE, 103(GT5), 447-466.

Fredlund, D.G., Morgenstern, N.R. and Widger, A. (1978). "Shear strength of unsaturated soils". *Canadian Geotechnical Journal*, 15(3), 313-321.

Hills, C.W.W. and Denby, B. (1996). "The prediction of opencast backfill settlement". *Proceedings, Institution of Civil Engineers, U.K., Geotechnical Engineering*, 134, 160-176.

International Commission on Large Dams, (1996). *A Guide to Tailings Dams and Impoundments, ICOLD*, Paris, France, 33-34.

Jennings, J.E. (1961). "A revised effective stress law for use in the prediction of the behaviour of unsaturated soils". *In: Pore Pressure and Suction in Soils*. Butterworth, London, U.K. 26-30.

Kassiff, G. and Ben Shalom, A., (1971). "Experimental relationship between swell pressure and suction". *Geotechnique*, 21(3), 245-255.

Koerner, R.M. (2001). "Do we need monitoring wells at double-lined landfills? *Civil Engineering, (*ASCE),(Feb.), 96.

Lambe, T.W. (1960). "A mechanistic picture of shear strength in clay*". Proceedings, ASCE Research Conference on Shear Strength of Cohesive Soils*, Boulder, Colorado, U.S.A. 555-580.

Machado, S.L., Vilar, O.M. and Carvalho, M.F. (2002). "An elastic-plastic framework to reproduce the MSW mechanical behaviour – long term analysis". *In: de Mello, L.G. and Almeida, M. (Eds), Environmental Geotechnics* (4 ICEG), (1), Swets and Zeitlinger, Lisse, Netherlands, 65-70.

Medina, L. (1997). Personal communication with author.

Oberg, A.L. and Sallfors, G. (1997). "Determination of shear strength parameters of unsaturated silts and sands based on the water retention curve". *Geotechnical Testing Journal*, 20(1), 40-48.

Pereira, A.G., Sopena, L., and Mateos, M.T.G. (2002). "Compressibility of a municipal waste landfill". *In: de Mello, L.G.and Almeida, M. (Eds),*

Environmental Geotechnics (4 ICEG),(l) Swets and Zeitlinger, Lisse, Netherlands, 201-206.

Rathje, W. and Murphy, C. (1992). *Rubbish! The Archaeology of Garbage*. Harper Collins, New York, U.S.A.

Reed, S.M. and Hughes, D.B. (1990). "Long term settlement of opencast mine backfills – case studies from the North East of England". *In: Reclamation, Treatment and Utilization of Coal Mining Wastes*. Balkema, Rotterdam, Netherlands, 141-155.

Richards, B.G. (1966). "The significance of moisture flow and equilibria in unsaturated soils in relation to the design of structures built on shallow foundations in Australia". *ASTM Symposium on Permeability and Capillarity*, Atlantic City, U.S.A.

Rodriques, J.A. and Velandia, E. (2002). "Geotechnical monitoring program in Bogota's municipal solid waste landfill after the 1997 landfill slide". *In: de Mello, L.G. and Almeida, M. (Eds.), Enviromental Geotechnics* (4 ICEG),(1). Swets and Zeitlinger, Lisse, Netherlands, 145-150.

Sheng, D., Smith, D.W., Sloan, S.W. and Gens, A. (2002). "An explicit stress integration scheme for unsaturated soil models. *3rd International Conference on Unsaturated Soils*", Recife, Brazil,(1), 125-131.

Stuart, R.J., Holmes, T.C., Jurcevici, M., Watt, I.B. and van Rensburg, G.D.J. (2003). "Influence of tailings dam settlement on decant towers and pipelines". *Tailings and Mine Waste'03*, Swets and Zeitlinger, Lisse, Netherlands, 95-100.

Thornthwaite, C.W. (1948). "An approach towards a rational classification of climates". *Geographical Review*, (38), 55.

van Wyk, W.J. (1998). "Settlement of Mine Backfill – Two Large Scale Field Tests". *M.Sc.(Eng) Dissertation*, University of the Witwatersrand, Johannesburg, South Africa.

van Wyk, W.J. and Blight, G.E. (1996). "Settlement of mine backfill under the overburden of a wet ash dam". *In : Environmental Geotechnics, M. Kamon (Ed)*. Balkema, Rotterdam, Netherlands,.423-428.

Watts, K.S. and Charles, J.A. (1999). "Settlement characteristics of landfill wastes". *Proceedings, Institution of Civil Engineers, U.K., Geotechnical Engineering*, (137), 225-234.

World Health Organization, (1991). *Urban Solid Waste Management. Compiled: Institute for Promotion of International Health Actions*, Copenhagen, Denmark.

Zornberg, J.G., Jernigan, B.L., Sanglerat, T.R. and Cooley, B.H. (1999). "Retention of free liquids in landfills undergoing vertical expansion". *Journal of Geotechnical and Geoenvironmental Engineering*, ASCE, 125(7), 583-594.

Suction Measurements

H. Rahardjo and E.C. Leong

School of Civil & Environmental Engineering, Nanyang Technological University, Blk N1, 50 Nanyang Avenue, Singapore 639798; email: chrahardjo@ntu.edu.sg and cecleong@ntu.edu.sg, respectively

Abstract

Application of unsaturated soil mechanics to practice requires measurement of soil suction. This paper examines several devices and techniques that are used for suction measurements in the laboratory and the field. Salient features of each suction measurement device are highlighted.

Introduction

Suction measurements have now become essential when dealing with unsaturated soils. Suction affects the engineering properties of unsaturated soils directly or indirectly. However, suction is affected more by climatic conditions rather than loading conditions as is the case with positive pore-water pressures in saturated soils. Due to the higher uncertainty in climatic conditions, suction is more variable with time than positive pore-water pressure. Theoretically, soil or total suction consists of matric suction and osmotic suction and their magnitudes can range from 0 kPa to 1 GPa. Currently, no single instrument or technique exists that can measure the entire suction range with reasonable accuracy. Suction measurement instruments are only available to measure suction up to about 10 MPa. A summary of suction measurement devices and their characteristics are shown in Table 1. All the devices listed in Table 1 except for the jet fill tensiometer are suitable for use in the determination of soil-water characteristic curve.

In this paper, the performance of suction measurement instruments with measurement range from 0 to 10 MPa will be examined and reviewed. Conveniently, suction measuring techniques are divided into three ranges in this paper: low range from 0 to 100 kPa, mid range from 100 kPa to 1 MPa and high range from 1 to 10 MPa for discussions. However, this paper is not intended to be a fully comprehensive and inclusive review of all suction measuring techniques due to space limitation.

Table 1. Summary of suction measurement devices

Device	Suction component measured	Measurement range (kPa)	Equilibrium time	Manufacturer & relative cost*
Jet fill tensiometer	Matric	0–100	Several minutes	Soil Moisture Equipment Skye Instruments Irrometer Co. Dynamax Inc. Cost: $
Small-tip tensiometer	Matric	0–100	Several minutes	
Null-type axis translation apparatus	Matric	0–1500	Several hours – days	Universities Cost: $$$
Miniature tensiometer	Matric	0–1500	Several minutes	Universities Cost: $$
Filter paper-contact	Matric	0–10000	2-5 days	Whatman Schleicher & Schuell Cost: –
Filter paper-non contact	Total	1000–10000	2-14 days	
Thermal conductivity sensor	Matric	10–1500	Several hours – days	Campbell Scientific GCTS Cost: $$
Electrical conductivity sensor	Matric	0–1500	6 – 48 hours	Soil Moisture Equipment Delmhorst Instrument Co. Dynamax Inc. Cost: $$
Psychrometer	Total	100–10000	Several minutes – several hours	Decagon Devices Soil Mechanics Instrumentation Wescor Cost: $$$$$

* Manufacturers listed are for information only and does not imply product endorsement. Relative cost is indicated by the number of dollar signs and – means negligible cost.

Low-Range Suction Measuring Techniques

Tensiometers can be used to measure negative pore-water pressures in a soil. A tensiometer consists of a small bore tube which is saturated with water. Water pressure in the tensiometer comes into equilibrium with the pore-water pressure in the soil through a high-air entry ceramic cup. A vacuum gauge or a pressure transducer is connected to the tensiometer for measuring the equilibrium water pressure. Cavitation of water in the tensiometer tube at water pressures less than – 90 kPa results in the maximum matric suction (difference between pore-air and pore-water pressures) that can be effectively measured is 90 kPa (Stannard 1990). Tensiometers come in different lengths and have been installed in the field to a depth of 3 m from the ground surface (Gasmo et al. 2000). The negative pore-water pressure recorded at the ground surface must be corrected for the difference in elevation heads between the pressure transducer and the ceramic cup (point of measurement). In general, tensiometer has been found to be the best measuring technique for low-range of

suction because it measures negative pore-water pressure directly and responds promptly to the changes in pore-water pressure.

Jet fill tensiometers

A jet fill tensiometer has a water reservoir with a jet fill system at the top of the tensiometer tube (Figure 1). During flushing a jet fill action will allow air bubbles in the tensiometer tube to rise to the water reservoir while water from the reservoir refills the tensiometer tube. Sluggish response of a tensiometer can be detected during calibration as shown in Figure 2 if the tensiometer is not fully saturated due to either poor sealing or using non-deaired water that cause air bubbles to develop in the tube.
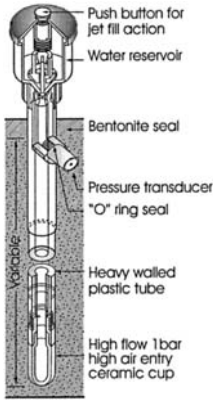
Figure 1. Schematic diagram of jet fill tensiometer.
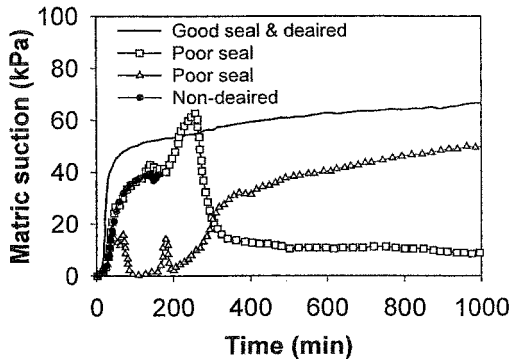
Figure 2. Readings of jet fill tensiometers.

Jet fill tensiometers have been used to monitor pore-water pressures in slopes and their performances have been found to be very good and reliable (Li et al. 2005, Rahardjo et al. 2005, Ng et al. 2003). Jet fill tensiometers are quite responsive to the changes in flux boundary conditions on slope surface. Figure 3(a) shows the contour lines of matric suctions across an entire slope profile during a dry period (before the occurrence of rainfall events). The matric suction were measured using jet fill tensiometers at depths of 0.5m, 1.1m, 1.7m, 2.3m and 2.9m. The slope crest experienced larger matric suction development than the toe. Figure 3(b) shows significant decrease in matric suctions across the slope profile after a series of rainfall events. Matric suctions of lower magnitude still exist near the slope crest. The results illustrate the usefulness of jet fill tensiometers in measuring pore-water pressure response to the changes in flux boundary conditions.
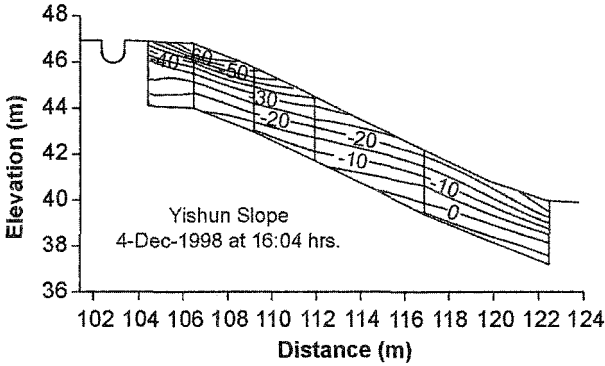
(a) Pore-water pressure from jet fill tensiometer measurements (kPa) at the end of the dry period
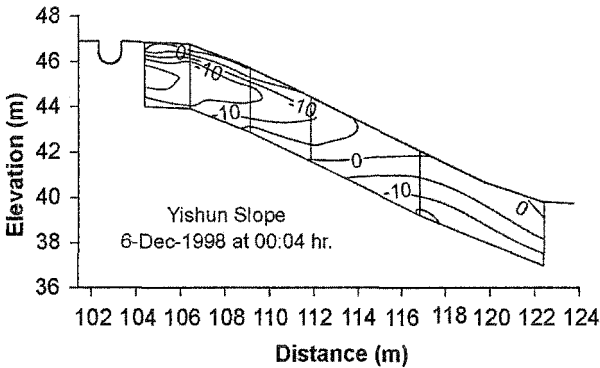
(b) Pore-water pressure from jet fill tensiometer measurements (kPa) after rainfall events

Figure 3. Contour plots of pore-water pressure obtained from jet fill tensiometer measurements

Small tip tensiometers

Small tip tensiometers (Figure 4) are very useful for measurements of negative pore-water pressures in laboratory tests. A small tip tensiometer has a small ceramic tip of 6 mm in diameter and 25 mm in length. The water reservoir of the jet fill tensiometer can be installed on top of the tensiometer tube for flushing the accumulated air bubbles. Small tip tensiometers have been used in infiltration column (Yang et al. 2004a) and slope model studies (Tami et al. 2004). The small tip tensiometers have provided reliable measurements of matric suction changes with sufficient accuracy of +/- 0.05 kPa during infiltration and drying tests (Yang et al. 2004b).
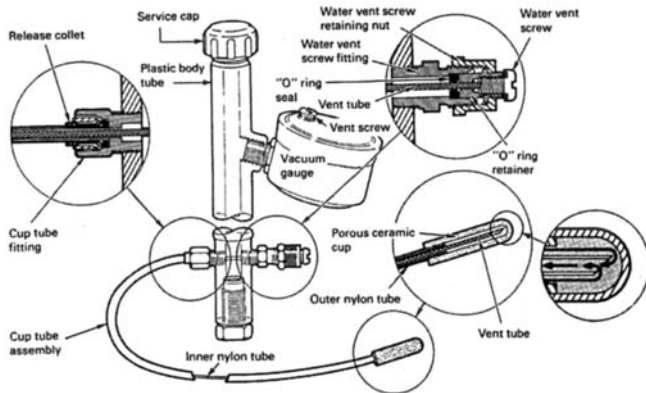
Figure 4. Small tip tensiometer with flexible coaxial tubing (From Soilmoisture Equipment Corp., 1999).

Mid-Range Suction Measuring Techniques

There is a need to extend the range of direct measurements of negative pore-water pressure beyond -100 kPa in order to measure typical matric suctions in the soil (Meilani et al. 2002, Wong et al. 2001, Guan and Fredlund 1997, Ridley and Burland 1993, Toll 1988). This can be done by using the axis translation technique and by creating conditions whereby cavitation in the measurement system can be prevented. These methods are described in the following subsections.

Null-type axis translation apparatus

Under atmospheric condition, highly negative pore-water pressures less than -100 kPa can lead to cavitation and nullify any attempt at measuring pore-water pressure. Hilf (1956) demonstrated that pore-water pressure increases if the ambient air pressure is increased. The magnitude of pore-water pressure increase is equal to the amount the ambient air pressure increase over atmospheric pressure. The null-type axis translation apparatus (Figure 5a) makes use of this technique to measure the negative pore-water pressure of a soil specimen by increasing the chamber air pressure to maintain a no-flow condition. The pore-water pressure of the soil specimen is usually increased to the atmospheric pressure i.e. 0 kPa. The matric suction of the soil specimen is then given by the difference between the chamber air pressure and the pore-water pressure. The equalization time for the null-type axis translation technique can be as short as 30 minutes to several hours as shown in Figure 5b for compacted residual soil specimens. Depending on the air-entry value of the ceramic disk, the null-type axis translation can be used to measure matric suction up to 1500 kPa.
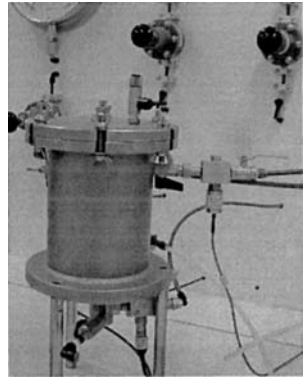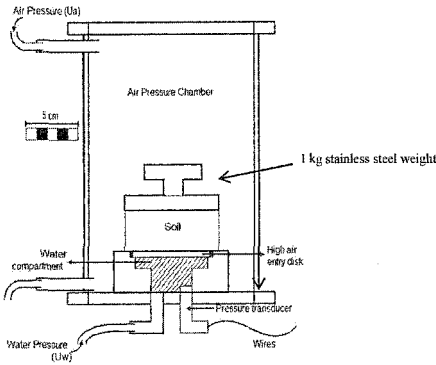
(a) Schematic of null-type axis translation apparatus   (b) Null-type axis translation apparatus
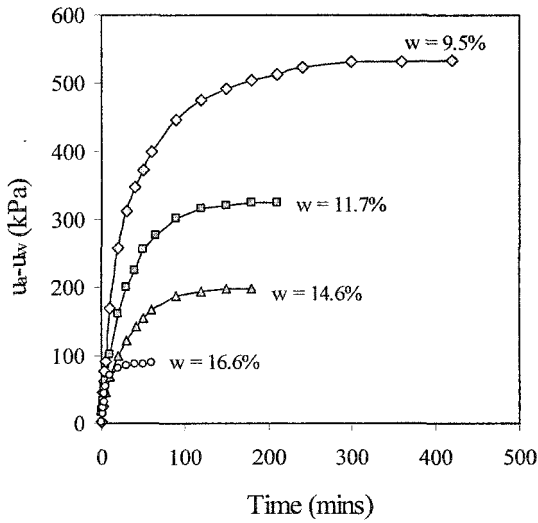
(b) Matric suction measurement

Figure 5. Schematic for null-type axis translation apparatus and matric suction measurements on compacted residual soils (from Widiastuti 2005)

NTU mini suction probe

NTU mini suction probe was developed in order to produce a sensor for direct measurements of matric suction higher than 100 kPa (Meilani et al. 2002, Meilani 2004). The probe uses a miniature pore-water pressure transducer, PDCR 81, manufactured by Druck Ltd. (Leicester, England) as shown in Figure 6. The PDCR 81 has the ability to measure pressure over a range of 15-bar and it only weighs 3 g with a cable of 20 cm length which can be immersed into water in a triaxial cell. The original 1 Bar high air-entry ceramic disk in the PDCR 81 was replaced with a new 5 Bar high air-entry disk (i.e., air-entry value of 500 kPa). Therefore, the probe can be used for direct measurements of matric suction up to 500 kPa. The new 5 Bar high air-entry disk has a low permeability (i.e., 1.21×10^{-9} m/s - Soil Moisture Equipment Corp. 1996) and therefore, it should be made as thin as possible in order to obtain high sensitivity of suction measurements. The original thickness (i.e., 6.8 mm) of the 5 Bar high air-entry disk had to be reduced to 1 mm by polishing it using sand paper into a shape shown in Figure 6a. Only 0.7 mm out of 1 mm thickness of the disk enters the PDCR 81 casing, resulting in a small gap of 0.4 mm between the diaphragm of the PDCR 81 and the bottom of the disk (Figure 6a). The small volume of water compartment between the diaphragm and the disk increases the responsiveness of the probe in measuring matric suction changes and reduces the potential for cavitation and air diffusion. The 5 Bar high air-entry disk was glued to the steel casing of the PDCR 81 using Araldite 2021 epoxy.

The performance of NTU mini suction probe has been verified in numerous calibration and triaxial tests. Figure 7 shows poor response of NTU mini suction probes to vacuum pressure when water compartment is not fully saturated. The probes can be saturated by submerging them into water in a triaxial cell and applying cell pressure up to 800 kPa. The probe is very responsive to pressure changes when it has been fully saturated. Figure 8 illustrates identical response of a fully saturated mini suction probe to the applied vacuum pressure that was varied rapidly. The probe also exhibited excellent response to varying positive cell pressures when water compartment is fully saturated (Figure 9).
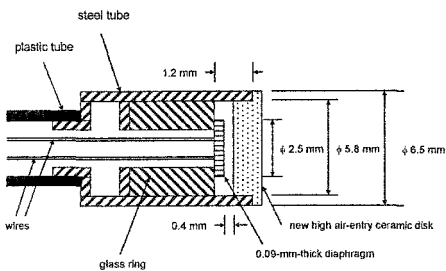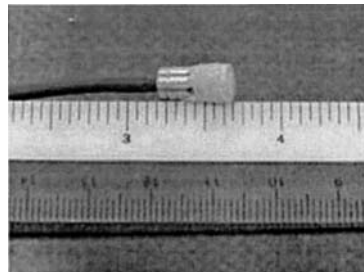
| (a) Schematic | (b) Actual |

Figure 6. NTU mini suction probe.
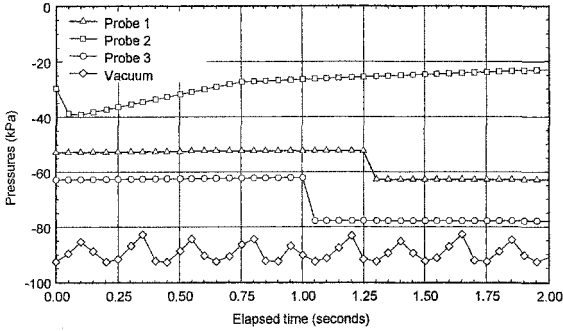
Figure 7. Response of NTU mini suction probes to vacuum pressure when water compartment contained some air bubbles (from Meilani 2004).
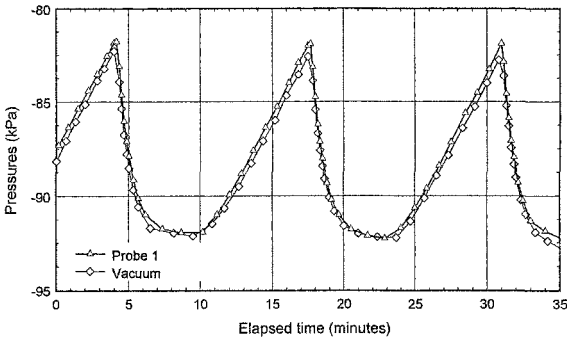
Figure 8. Response of probe 1 to vacuum pressure when water compartment was fully saturated (from Meilani 2004).
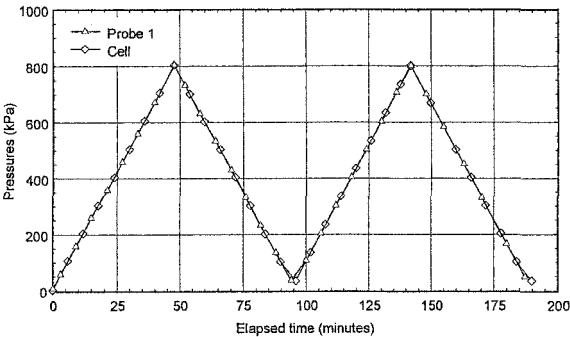
Figure 9. Response of probe 1 to positive cell pressure when water compartment was fully saturated (from Meilani 2004).

The theoretical response time of an NTU mini suction probe can be analyzed in accordance with the analyses given by Fredlund and Rahardjo (1993). Consider a mini suction probe that is submerged in water in a triaxial cell and a pressure is applied to water in the cell. The response time of the probe to the applied pressure can be calculated for each pressure increment as follows:

$$\left(t_j - t_i\right) = \frac{C_{aw}C_f\left(u_j - u_i\right)}{\left\{u_c - \dfrac{\left(u_i + u_j\right)}{2}\right\}}$$
(1)

where:

C_{aw} = compressibility of the air-water mixture
C_f = compliance factor for the measuring system
u_c = pressure applied to the water in the cell
u_i = compartment pressure at time, t_i
u_j = compartment pressure at time, t_j

The compressibility of the air-water mixture is calculated using the following equation:

$$C_{aw} = SC_w + \left(1 - S\right)/\overline{u}_a$$
(2)

where:

S = degree of saturation of the compartment
C_w = compressibility of water
$\overline{u}_a$ = absolute compartment air pressure
$= \left(\overline{u}_i + \overline{u}_j\right)/2$

The compliance factor of the NTU mini suction probe can be calculated using the following equation (Fredlund and Rahardjo 1993):

$$C_f = \frac{\rho_w g V_c L_d}{k_d A_d}$$
(3)

where:

ρ_w = density of water = 1 Mg/m^3
g = gravitational acceleration = 9.81 m/s^2
V_c = volume of compartment = 1.2769 x 10^{-8} m^3
L_d = thickness of the high air entry disk = 1 x 10^{-3} m
k_d = permeability of the high air entry disk = 1.21 x 10^{-9} m/s
A_d = cross-sectional area of the high air entry disk = 2.6421 x 10^{-5} m^2

The compressibility of the air-water mixture, C_{aw} should be updated for every pressure increment due to the change in the volume of water in the compartment. As the applied cell pressure is increased, water flows into the compartment causing an increase in the volume of water and consequently the degree of saturation of the

compartment, S. The volume of water flowing into the compartment can then be calculated using the following equation:

$$\Delta V_w = C_{aw} V_c \left(u_j - u_i \right)$$

(4)

where V_c = volume of compartment.

The computation is repeated from one pressure increment to the next until the maximum cell pressure is reached. The response time of an NTU mini suction probe with a high air-entry disk of 1 mm thick has been calculated for a maximum applied cell pressure of 500 kPa. Figure 10a shows that the calculated response time increases as the initial percentage of air volume in the compartment increases from 0.2 %, to 10 % and eventually to 25 %. Similarly for the same initial percentage of air volume in the compartment of 25 %, the response time also increases if the thickness of the high air-entry disk is increased from 1 mm, to 2 mm and eventually to 3 mm as shown in Figure 10b. It appears that the thickness of the high air-entry disk increases the response time more significantly than the initial percentage of air volume in the compartment does.

The actual response time of three NTU mini suction probes has also been examined experimentally. Three NTU mini suction probes with a high air-entry disk of 1 mm thick were saturated first prior to the experiment and then subjected to a sudden applied cell pressure of 500 kPa. Figure 11 shows that the response time of the three probes is less than 3 seconds which corresponds to an initial air volume in the compartment of 25 % (Figure 10a).
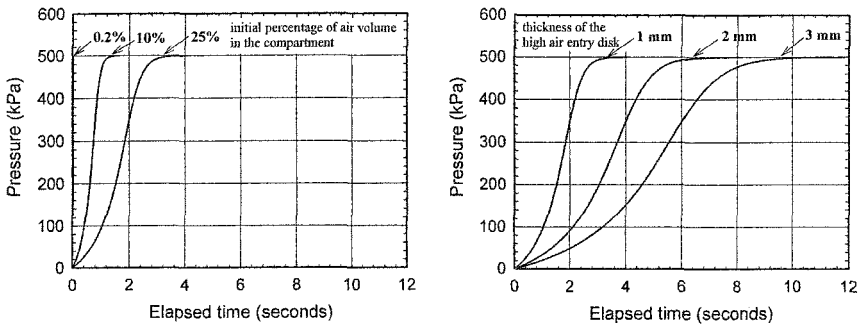
(a) Response time of NTU mini suction probe with a high air-entry disk of 1mm thick and at different initial percentages of air volume in the compartment.

b) Response time of NTU mini suction probe with a high air-entry disk of different thicknesses and at an initial percentage of air volume in the compartment of 25%.

Figure 10. Calculated response time of NTU mini suction probes
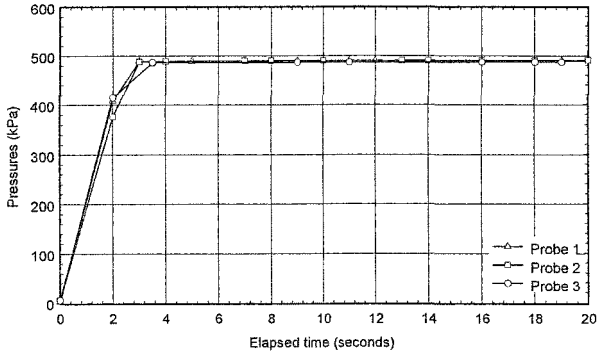
Figure 11. Experimental response time of NTU mini suction probes to a sudden cell pressure of 500 kPa (from Meilani 2004).

The maximum matric suction measurable by mini suction probes can be determined using the "free evaporation" test. The measurements in probes 1, 2 and 3 (Figure 12) decreased to − 426 kPa, − 400 kPa and − 495 kPa, respectively, before increasing rapidly to approximately − 100 kPa (i.e., atmospheric pressure) when the air-entry values of the disks were exceeded. Therefore, the air-entry values of the disks were at least 400 kPa.
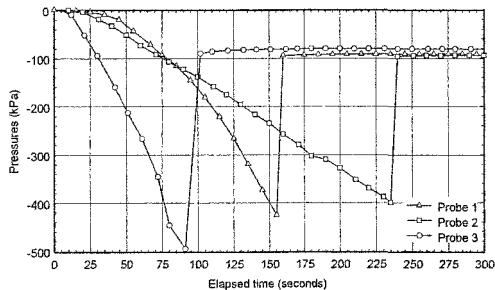
Figure 12. Response of the mini suction probes during evaluation using the "free evaporation" method (from Meilani 2004).

Since its development in 2002, NTU mini suction probes have been used in numerous triaxial tests with satisfactory performance. The probe can be installed along the soil specimen as illustrated in Figure 13. Figure 14 shows the typical pore-water pressure dissipation during isotropic consolidation of a saturated Kaolin specimen as measured using the three probes (top, middle and bottom) in a triaxial apparatus. The specimen was consolidated to an effective confining stress of 200 kPa under a single drainage condition to the top of the specimen. As a result, the top mini suction probe equalized first at 5 minutes, followed by the middle probe at 6 minutes and the bottom probe

equalized at 7 minutes. The measurements indicate the accuracy of the mini suction probes which measured pore-water pressure equalization as theoretically expected. Figure 15 illustrates the accuracy of NTU mini suction probes in measuring pore-water pressures along an unsaturated Kaolin specimen during a shearing-infiltration triaxial test using axis-translation technique (Hilf 1956).

It has been illustrated that NTU mini suction probes can be used to measure matric suction up to 400 kPa. It is possible to extend the range of matric suction measurements to 1500 kPa by replacing the 5 Bar high air-entry disk in the NTU mini suction probe with a 15 Bar high-air entry disk.
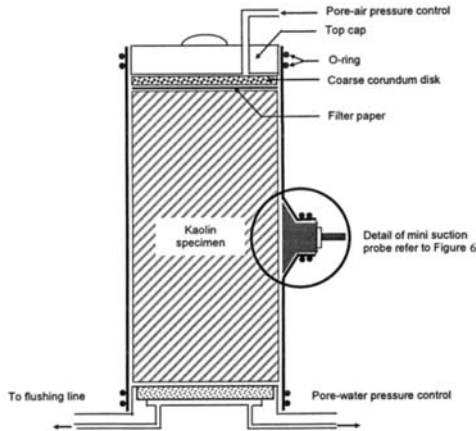
Figure 13. Installation of mini suction probe to the specimen (from Meilani et al. 2002).
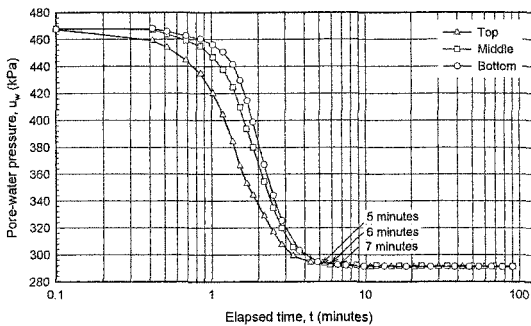
Figure 14. Dissipation of pore-water pressure during consolidation of a saturated Kaolin specimen (from Meilani 2004).
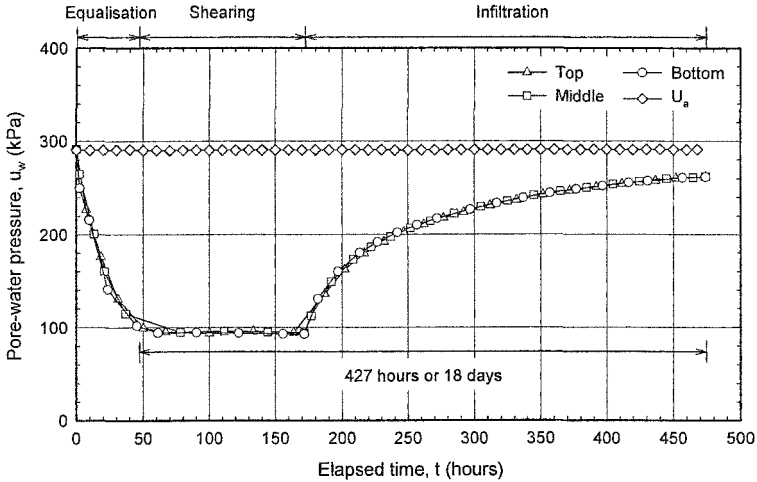
Figure 15. Pore-water pressure measurements throughout an unsaturated Kaolin specimen during a shearing-infiltration triaxial test using axis-translation technique (from Meilani 2004).

Filter paper: contact and non-contact

The use of filter paper as a soil suction sensor dates back to the work of Schull in 1916 in soil science (Marinho 1994). Currently the filter paper method is a standard test method for measurement of soil suction in ASTM D 5298-94 (1997). The test procedure and requirements are simple and can be performed in any soil laboratory without the need of any special equipment. The method involves placing filter paper in contact with a soil specimen in an airtight container for seven days. The seven-day period is required to achieve moisture equilibrium condition between the filter paper and the soil specimen. The moisture content of the filter paper is then determined, and the matric suction of the soil specimen is inferred from a calibration curve. A filter paper in contact with the soil specimen allows water in the liquid phase and solutes to exchange freely and therefore, matric suction is measured. A filter paper not in contact with the soil specimen only permits water exchange in the vapor phase only and prevents solute movement and therefore, measures total suction. A number of studies have been conducted on the filter paper method. More recent studies are by Bulut et al. (2001) and Leong et al. (2002).

Until the work of Houston and co-workers (El-Ehwany and Houston 1990; Houston et al. 1994), the calibration curves for both contact and non-contact filter paper methods are assumed to be the same. El-Ehwany and Houston (1990) reported a total suction calibration curve very different from the calibration curves by McKeen (1988) which is for matric suction. Lee and Wray (1992) found that the non-contact filter paper method tends to overestimate suction when the McKeen (1988)

calibration curve was used. Leong et al. (2002) showed different calibration curves for contact and non-contact filter paper methods. The calibration curves of the contact and non-contact filter paper methods have not been resolved. Walker et al. (2005) compared total suction measurements of a soil sample using transistor psychrometer and non-contact filter paper method. For the interpretation of the filter paper test results, the Hamblin (1981) filter paper calibration curve for matric suction was used. Walker et al. found the total suction given by the non-contact filter paper method to be consistently below the total suction given by the psychrometer. However, Walker et al. (2005) suggested that the discrepancy is due to insufficient equalization time and if sufficient time is allowed for equilibration, the total suction calibration curve will tend towards the matric suction calibration curve. Bulut et al. (2001) and Bulut and Wray (2005) stated that a single calibration curve based on water vapor measurements is adequate for both total and matric suction measurements. On the other hand, both Bulut et al. (2001) and Leong et al. (2002) indicated that an upper limit equalization time of 14 days is sufficient.

The most commonly used filter papers for suction measurement are Whatman No. 42 and Schleicher & Schuell (S&S) No. 589-WH. The calibration curves for these two filter papers are given in ASTM D 5298-94. The S&S No. 589-WH filter paper is now called grade 989-WH in the USA as the filter papers manufactured in the USA and Europe have different specifications (Bulut and Leong 2005). This could have accounted for the larger discrepancies observed for the S&S No. 589 as compared to the Whatman No. 42 filter paper by Leong et al. (2002). Leong et al. (2002) have also recommended that the calibration curves given in ASTM D 5298-94 should only be used for matric suction measurement below 1000 kPa, but above 1000 kPa they can be applied to both total and matric suctions. The Whatman No. 42 filter paper calibration curves for matric suction and total suction are summarized in Figures 16a and b, respectively. The equations suggested by Leong et al. (2002) for the Whatman No. 42 filter paper are as follows:

Matric suction:	$\log \psi = 2.909 - 0.0229 w_f$	$w_f \geq 47\%$	(5a)
	$\log \psi = 4.945 - 0.0673 w_f$	$w_f < 47\%$	(5b)
Total suction:	$\log \psi = 8.778 - 0.222 w_f$	$w_f \geq 26\%$	(6a)
	$\log \psi = 5.31 - 0.301 w_f$	$w_f < 26\%$	(6b)

Thermal conductivity sensor

Shaw and Baver (1939a, b) were the first to propose using thermal conductivity to measure the water content in a soil. In Shaw and Baver (1939b) device, the heating and temperature-sensing elements were in direct contact with the soil. To relate the thermal conductivity measurements to the moisture contents of the soil, a calibration curve for each soil must be developed as different soils have different thermal conductivities. To avoid separate calibration curves for different soil, Johnston (1942) used plaster of Paris to encase the heating and temperature-sensing elements. The thermal conductivity readings obtained were thus a function of the water content of

the plaster of Paris instead of the soil. Subsequent thermal conductivity sensor (TCS) consists of a rigid porous cylindrical block with a central heating element and a temperature-sensing element (Figure 17). As water content of a porous medium is related to its matric suction, matric suction can be inferred.
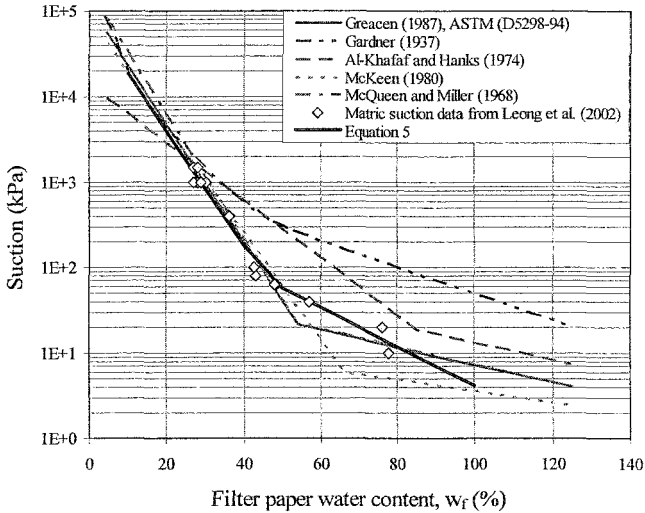
(a) Matric Suction
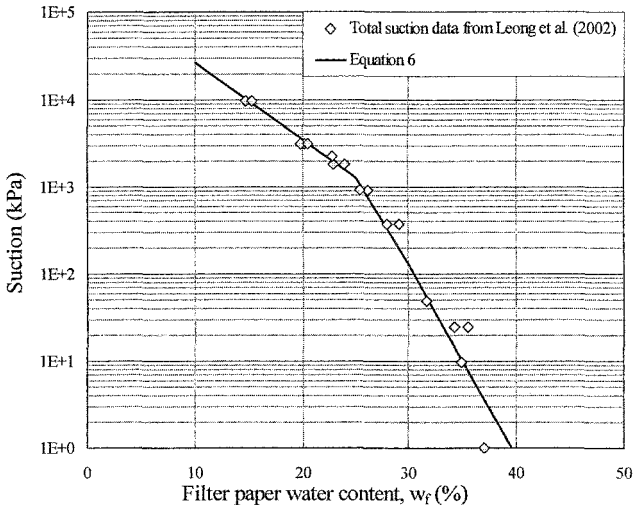
(b) Total Suction

Figure 16. Calibration curves for Whatman No. 42 filter papers.

When the TCS is embedded in a soil mass, a movement of moisture takes place between the soil and the TCS driven by the difference in pore-water pressure heads between the soil and TCS until equilibration of the pore-water pressure heads is achieved. Knowing the properties of TCS will enable the matric suction of the soil to be measured. In the TCS, the moisture content of the TCS affects its thermal conductivity properties. When a constant power supply is applied to its heating element, its temperature rise depends on its moisture content. The thermal conductivities of air and water at $20^{\circ}C$ are 0.026 W/mK and 0.6 W/mK, respectively. When a constant power supply is applied to the heater, the temperature-sensing element will detect a temperature rise dependent on the degree of saturation of the TCS cylindrical block. The effect of degree of saturation of the TCS cylindrical block on the temperature rise ΔT can be seen in Figure 18 for the case when the TCS is dry and when the TCS is in water.
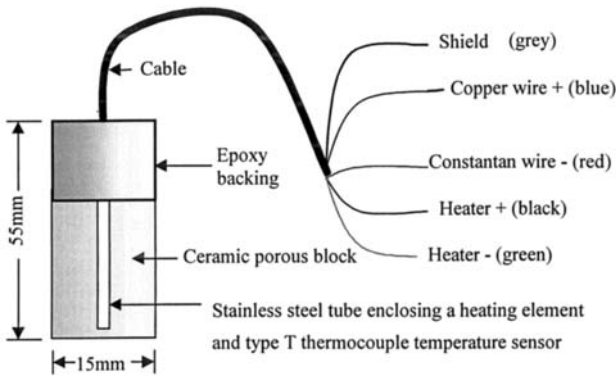
Figure 17. Schematic of CSI 229 thermal conductivity sensor.

Commercially available TCS is limited. In the mid 1970's, MCS 6000 TCS was available from Moisture Control System Inc. However, the production of MCS 6000 TCS was discontinued in the early 1980's. In 1981, Agwatronics Inc., USA, started manufacturing the AGWA TCSs but production of these sensors was also terminated. In late 1992, Campbell Scientific Inc., Australia, marketed the CSI 229 TCS. In 2000, Fredlund et al. developed a new TCS where improvements were made to heating and temperature-sensing elements and in terms of signal conditioning for better resolution and accuracy.

The more salient features of the TCS performance for matric suction measurements are illustrated in this paper with the study on the CSI 229 TCS by Zhang (2001) conducted at Nanyang Technological University. The CSI 229 TCS has a length of 55 mm and a diameter of about 15 mm shown schematically in Figure 17 and photographically in Figure 19. It consists of a stainless steel tube, 25 mm in length

and 0.9 mm in diameter, containing a heating element (resistance $\approx$ 34 Ω) and a thermocouple type T temperature sensor. The stainless steel tube is encased in a porous ceramic cylinder.
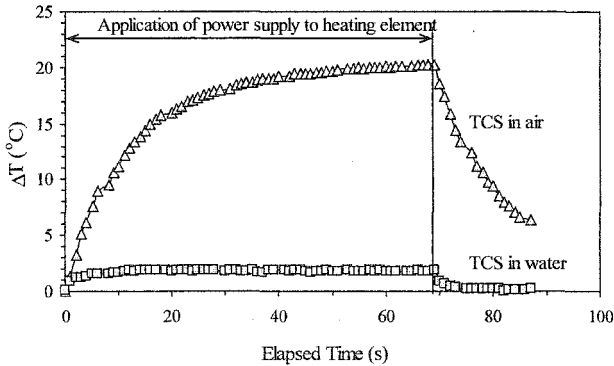
Figure 18. Responses of TCS in air and in water.
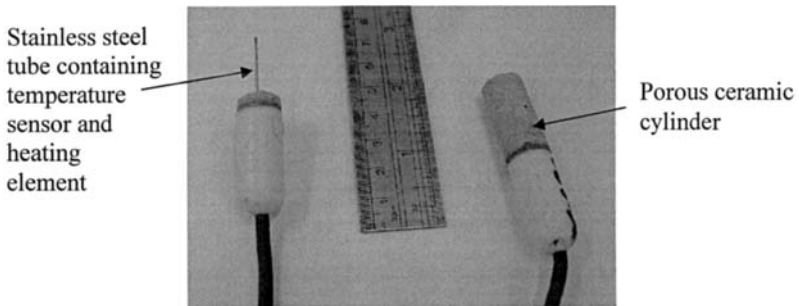
Figure 19. CSI 229 thermal conductivity sensor.

Heating time and temperature rise

Figure 20 shows a plot of temperature rise ΔT with elapsed time under different matric suctions from Zhang (2001). The temperature rise increases as matric suction increases. Except for the matric suction of 770 kPa, the temperature rise beyond a heating time of 30s was negligible. If the recommendation of Xing and Fredlund (1994) was used to estimate a heating time for the CSI 229 TCS which has a radius of 7.5 mm and a heating power 0.085 w, the heating time should be less than 30s. The recommended heating time of 24s by the manufacturer is therefore suitable for matric suctions up to 500 kPa. For higher heating time, the sensitivity of the CSI 229 TCS will deteriorate as it is affected by the surrounding soil.

Equalization time

Figure 21 shows the equalization time of the CSI 229 TCS for different matric suctions. Figure 21 shows that the equalization time can be as short as several hours or as long as 180 hours, independent of matric suction. This observation was attributed to the contact condition between the TCS and the soil during measurement, with good contact leading to shorter equalization times.

Hysteresis

All porous materials exhibit hysteretic behavior on drying and wetting. The amount of hysteresis depends on the pore-size distribution of the porous material. In order to ascertain the effect of hysteresis on measurement, two cycles of drying and wetting calibrations were performed. Figure 22 illustrates the effect of hysteresis on matric suction using the CSI 229 TCS. Figure 22 shows that the hysteresis was stable and reproducible as illustrated by the fact that the second drying-wetting-process calibration curves trace the first drying-wetting-process calibration curves, consistent with the observations of Wong and Ho (1987) and Fredlund et al. (2000) for other types of TCSs.
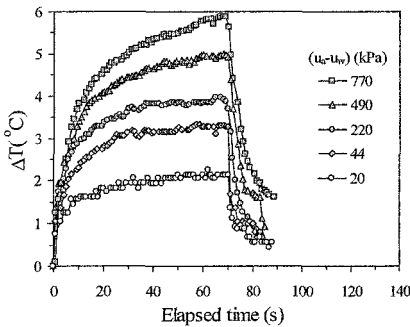
Figure 20. Temperature rise under different matric suctions.
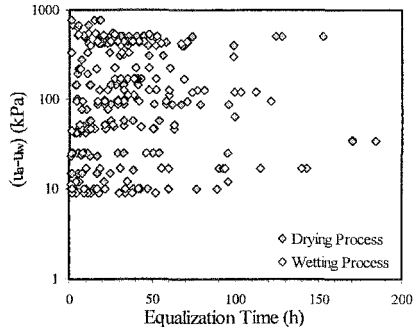
Figure 21. Equalization time of CSI 229 thermal conductivity sensor at different matric suctions.

Calibration curves

Figure 23 shows the calibration curves of a typical CSI 229 TCS using 24s heating time with the best-fit lines and the coefficient of determination R^2 values. For matric suction from 10 kPa to 800 kPa, the calibration curves are a straight line on a logarithmic matric suction scale. The distinctly different drying and wetting calibration curves once again illustrate the importance of the hysteretic behavior of TCS on the interpretation of matric suction. Figure 23 implies that the same temperature rise will give higher matric suction if the drying curve was used instead

of the wetting curve. Alternatively for the same matric suction, the TCS will have a smaller temperature rise when experiencing a drying process instead of a wetting process. As a result, the same temperature rise will correspond to different matric suctions depending on the TCS drying or wetting history. More noticeable is the hysteretic behavior is more significant at low matric suction than at high matric suction.
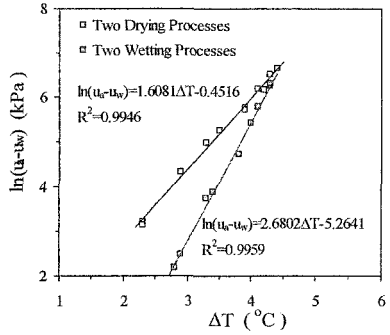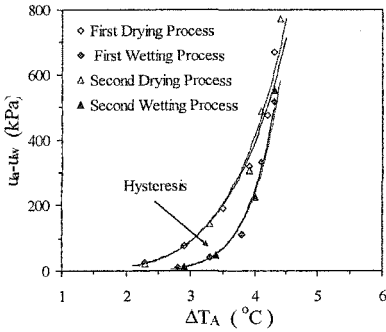
Figure 22. Effects of hysteresis on a typical CSI 229 thermal conductivity sensor.

Figure 23. Calibration curves for a typical CSI 229 thermal conductivity sensor.
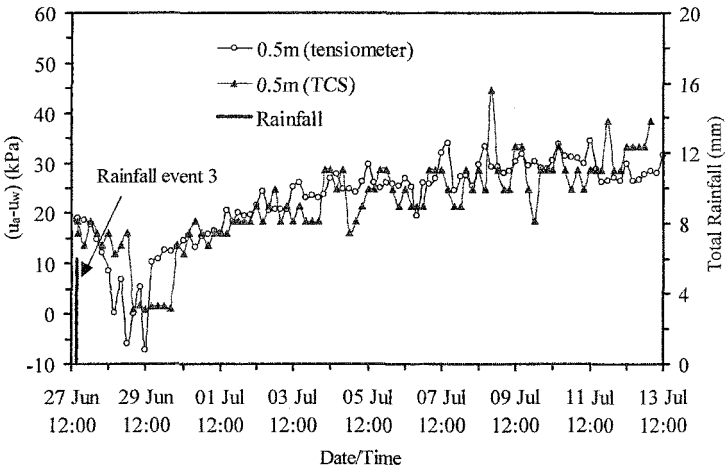
Figure 24. Typical CSI 229 thermal conductivity sensor readings in a residual soil slope together with tensiometer readings (after Zhang 2001).

In summary, the quality of the CSI 229 TCS is quite variable and reliability is a problem. Zhang (2001) used 32 CSI 229 TCSs in his study and 10 were found to be problematic, either problems with the heating and temperature-sensing elements or the porous block was damaged during installation. The range of matric suction measurement of the TCSs was also found to be variable, from 500 to 32000 kPa. However, the effective range may be up to about 600 kPa only (Zhang 2001). Hysteresis is present in the TCS and interpretation is difficult if the drying and wetting history of the TCS is not known. To date, the TCS is one of few matric suction measurement devices that can be deployed in the field. Typical field measurement of matric suction using the CSI 229 TCS in a residual soil slope at a depth of 0.5m is shown in Figure 24. Also shown in Figure 24 are the corresponding readings from a tensiometer showing that the TCS gave comparable readings.

High-Range Suction Measuring Techniques

Chilled-mirror psychrometer

The total suction of the soil is related to the water vapour pressure in the pore space of the soil which can be estimated from relative humidity. A range of devices is available to measure relative humidity. The chilled-mirror dewpoint technique is widely considered to be the most accurate method for dewpoint measurement and has been used in the laboratory to measure total suction (Bulut et al. 2002, Leong et al. 2003). Chilled-mirror psychrometer uses the chilled mirror dew point technique to measure relative humidity under isothermal conditions in a sealed container (Figure 25). In this device, the soil sample is placed into a sealed chamber containing a mirror and a detector of condensation on the mirror to measure the dewpoint. Relative humidity is given by the ratio of saturated vapour pressure of water at dewpoint to the saturated vapour pressure of water at the air temperature. At equilibrium, the relative humidity of the air in the sample chamber is the same as the relative humidity of the soil. The relative humidity readings with time for compacted mudstone residual soil specimens are shown in Figure 26. The equalization time to obtain the total suction of soil specimens was less than 20 minutes. In Figure 26, the equalization time for the compacted mudstone residual soil specimens were less than four minutes.

Leong et al. (2003) compared the total suction measurements on compacted samples to the sum of matric and osmotic suctions of the same soils that were measured independently. The range of total suction measured was up to 2500 kPa. The matric suction of the soils was measured with the null-type axis-translation apparatus and the osmotic suction of the samples was determined from the electrical conductivity of the soil water solution obtained from a pore fluid squeezer device. The matric suctions of the soil samples were in the range of 30 to 1200 kPa. The osmotic suctions of the soil samples were low, about 10 kPa, as tap water was used to compact the soil samples. The test results showed that total suctions obtained using the chilled mirror dew point device always overestimated the sum of the matric and osmotic suctions measured independently (Figure 27). This observation was consistent with those of Bulut et al. (2002) who found that the chilled-mirror psychrometer error was higher at low

suction levels, particularly when osmotic suction was below 1000 kPa. Further evidence of the limitations of the chilled-mirror psychrometer can be found in ASTM D6836-02 Method D (2003) which recommends using chilled-mirror hygrometer for determining the desorption soil water characteristic curve for suction range above 1000 kPa. Leong et al. (2003) suggested the following correction equation to reconcile the discrepancies between the sum of the matric and osmotic suctions and the total suction from the chilled mirror dew point device:

$$\psi_s = -0.00006\psi_{measured}^2 + 0.5866\psi_{measured} \tag{5}$$

where ψ_s = matric + osmotic suctions and , $\psi_{measured}$ = measured total suction.
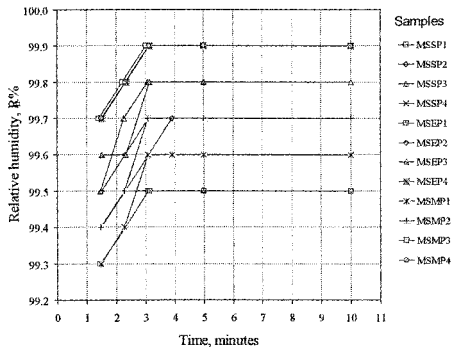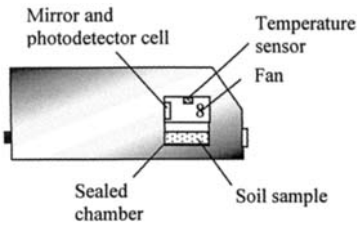
Figure 25. Schematic of chilled-mirror dewpoint device (from Leong et al. 2003).

Figure 26. Relative humidity readings with time for compacted mudstone residual soil specimens.

Conclusion

A number of field and laboratory suction measuring devices were examined in this paper. Arbitrarily the suction measuring devices were grouped low, mid and high range suction measuring devices. In the low range of suction measurement, jet fill and small tip tensiometers were discussed. In the mid range of suction measurement, null-type axis translation apparatus, NTU mini suction probe, contact and non-contact filter paper method and thermal conductivity sensor were discussed. In the high range of suction measurement, the chilled-mirror psychrometer was examined. Each device has its own limitation that can only be overcome with advancement in measurement technologies.

Acknowledgement
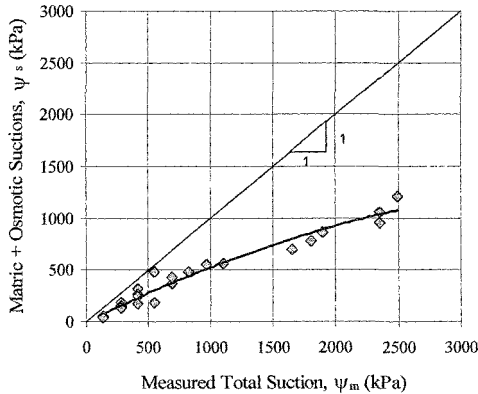
Figure 27. Comparison of sum of matric plus osmotic suctions and measured total suction.

References

ASTM (1997), "D5298-94 Standard Test Method for the Measurement of Soil Potential (Suction) Using Filter Paper," *Annual Book of ASTM Standards*, Vol. 04.09, Soil and Rock (II): D4943-latest, pp. 157-162.

ASTM (2003). "D6836-02 Standard test methods for determination of the soil water characteristic curve for desorption using a hanging column, pressure extractor, chilled mirror hygrometer, and/or centrifuge." *Annual Book of ASTM Standards*, ASTM, Philadelphia, PA.

Bulut, R., Hineidi, S. M., and Bailey, B. (2002). "Suction Measurements – Filter Paper and Chilled Mirror Psychrometer." *Proceedings of the Texas Section American Society of Civil Engineers*, Fall Meeting, Waco, Texas, October 2-5.

Bulut, R. and Leong, E.C. (2005). "Indirect Measurement of Soil Suction." Invited Paper, *Experus 2005 - Advanced Experimental Unsaturated Soil Mechanics*, Trento, Italy, June 27-29.

Bulut, R., Lytton, R. L., and Wray, W. K. (2001). "Soil Suction Measurements by Filter Paper." *Expansive Clay Soils and Vegetative Influence on Shallow Foundations*, ASCE Geotechnical Special Publication No. 115, Vipulanandan, C., Addison, M. B. and Hasen, M. (eds.), Houston, Texas, 243-261.

Bulut, R. and Wray, W.K. (2005). "Free energy of water – suction – in filter papers." *Geotechnical Testing Journal*, 28(4), 355-364.

El-Ehwany, M. and Houston, S.L. (1990). "Settlement and Moisture Movement in Collapsible Soils." *Journal of Geotechnical Engineering*, 116(10): 1521-1535.

Fredlund, D.G. and Rahardjo, H. (1993). *Soil Mechanics for Unsaturated Soils*, John Wiley & Sons Inc., New York.

Fredlund D.G., Shuai F. and Feng M. (2000). "Use of a new thermal conductivity sensor for laboratory suction measurement." *Proceedings of the Asian Conference on Unsaturated Soils*, Unsaturated Soil for Asia, Rahardjo H., Toll D.G. and Leong E. C. (eds.), 275-280, Balkema, Rotterdam.

Gardner, R. (1937). "A Method of Measuring the Capillary Tension of Soil Moisture over a Wide Moisture Range." *Soil Science*, 43, 277–283.

Gasmo, J.M., Hritzuk, K.J., Rahardjo, H. and E.C. Leong (2000). "Instrumentation of an unsaturated residual soil slope." *Geotechnical Testing Journal*, ASTM International, 22(2), 128–137.

Greacen, E. L., Walker, G. R., and Cook, P. G. (1987). "Evaluation of the Filter Paper Method for Measuring Soil Water Suction." *International Conference on Measurement of Soil and Plant Water Status*, 137–143.

Guan, Y. and Fredlund, D.G. (1997). "Use of the tensile strength of water for the direct measurement of high soil suction." *Canadian Geotechnical Journal*, 34, 604-614.

Hamblin, A.P. (1981). "Filter-Paper Method for Routine Measurement of Field Water Potential." *Journal of Hydrology*, 53, 355-360.

Hilf, J.W. (1956), "An Investigation of Pore-water Pressure in Compacted Cohesive Soils", *Ph.D. Dissertation*, Tech. Memo. No. 654, U.S. Dep. of the Interior, Bureau of Reclamation, Design and Construction Div., Denver, C.O.

Houston, S.L., Houston, W.R. and Wagner, A.M. (1994). "Laboratory filter paper measurements." *Geotechnical Testing Journal*, ASTM, 17(2): 185-194.

Johnston L. N. (1942). "Water permeable jacketed thermal radiators as indictors of field capacity and permanent wilting percentage in soils." *Soil Science*, 54: 123-126.

Lee, H.C. and Wray, W.K. (1992). "Evaluation of Soil Suction Instruments." *Proceedings of 7th International Conference on Expansive Soils*, Dallas, USA, pp 307-312.

Leong, E.-C., He, L., and Rahardjo, H. (2002). "Factors affecting the filter paper method for total and matric suction measurements." *Geotechnical Testing Journal*, ASTM International, 25(3), 322-333.

Leong, E.-C., Tripathy, S., and Rahardjo, H. (2003). "Total suction measurement of unsaturated soils with a device using the chilled-mirror dew-point technique." *Geotechnique*, 53(2), 173-182.

Li, A.G., Yue, Z.Q., Tham, L.G., Lee, C.F. and Law, K.T. (2005). "Field-monitored variations of soil moisture and matric suction in a saprolite slope." *Canadian Geotechnical Journal*, 42(1), 13 – 26.

Marinho, F.A.M. (1994). "Shrinkage Behaviour of Some Plastic Clays." *Ph.D. thesis*, University of London.

McKeen, R. G. (1980). "Field Studies of Airport Pavements on Expansive Soils." *4th International Conference on Expansive Soils*, 242–261.

McKeen, R.G. (1988). "Soil characterization using suction measurements," *25th Proc. Paving and Transp. Conf.*, University of Mexico, Albuquerque, N.M.

McQueen, I. S. and Miller, R. F. (1968). "Calibration of a Wide-Range Gravimetric Method for Measuring Moisture Stress." *Soil Science*, 106(3), 225–231.

Meilani, I., Rahardjo, H., Leong, E.C., and Fredlund, D.G. (2002). "Mini suction probe for matric suction measurement." *Canadian Geotechnical Journal*, Vol. 39(6), 1427-1432.

Meilani, I. (2004). "Shear Strength Characteristics of a Compacted Kaolin under Infiltration Conditions." *PhD Thesis*, Nanyang Technological University, Singapore.

Ng, C.W.W., Zhan, L.T., Bao, C.G., Fredlund, D.G. and Gong, B.W. (2003). "Performance of an unsaturated expansive soil slope subjected to artificial rainfall infiltration." *Geotechnique*, 53(2), 143-157.

Rahardjo, H., T.T. Lee, E.C. Leong and R.B. Rezaur (2005). "Response of a residual soil slope to rainfall." *Canadian Geotechnical Journal*, April, 42(2), 340 – 351.

Ridley, A.M. and Burland, J.B. (1993). "A new instrument for the measurement of soil moisture suction." *Geotechnique*, 43(2), 321-324.

Shaw B. and Baver L. D. (1939a). "Heat conductivity as an index of soil moisture." *Journal of the American Society of Agronomy*, 31: 886-891.

Shaw B. and Baver L. D. (1939b). "An electrothermal method for following moisture changes of the soil in situ." *Soil Science Society of America Proceedings*, 4: 78-83.

Soilmoisture Equipment Corp. (1999). *Commercial Publications*. P.O. Box 30025, Santa Barbara, CA.

Stannard, D.I. (1990). "Tensiometers - theory, construction, and use." In *Groundwater and Vadose Zone Monitoring*, ASTM STP 1053, D.M. Neilson and A.I. Johnson, Eds., ASTM, Philadelphia, PA, 34-51.

Tami, D., H. Rahardjo, E.C. Leong and D.G. Fredlund (2004). "A physical model for sloping capillary barriers." *Geotechnical Testing Journal*, ASTM International, March, 27(2), 173-183.

Toll, D.G. (1988). "The behaviour of unsaturated compacted naturally occurring gravel." *Ph.D. Dissertation*, Imperial College, London.

Walker, S.C., Gallipoli, D., and Toll, D.G. (2005). "The effect of structure on the water retension of soil tested using different methods of suction measurement." *International Symposium on Advanced Experimental Unsaturated Soil Mechanics*, Trento, Italy, June 27-29.

Widiastuti, S. (2005). "Measurement of suction and volume change behaviour in unsaturated soils." *MEng Thesis*, Nanyang Technological University, Singapore.

Wong D. K. H. and Ho A. (1987). *An evaluation of a thermal conductivity sensor for the measurement of soil suction*. Geotechnical Engineering Group, Dept. of Civil Engineering, University of Saskatchewan, Canada.

Wong, J.C., Rahardjo, H., Toll. D.G., and Leong, E.C., (2001). "Modified triaxial apparatus for shearing-infiltration test." *Geotechnical Testing Journal*, ASTM International, 24(4), 370-380.

Xing A. Q. & Fredlund D. G. (1994). "Numerical modeling of a thermal conductivity matric suction sensor." *Geotechnical Testing Journal*, ASTM International, 17(4), 415-424.

Yang, H., H. Rahardjo, B. Wibawa and E.C. Leong (2004a). "A soil column apparatus for laboratory infiltration study." *Geotechnical Testing Journal*, ASTM International, July, 27(4), 347 – 355.

Yang, H., H. Rahardjo, E.C. Leong and D.G. Fredlund (2004b). "A study of infiltration on three sand capillary barriers." *Canadian Geotechnical Journal*, August, 41(4), 629 – 643.

Zhang X.-H (2001). "Measurement of suction using thermal conductivity sensor." *MEng thesis*, Nanyang Technological University, Singapore.

A VOLUME-MASS CONSTITUTIVE MODEL FOR UNSATURATED SOILS IN TERMS OF TWO INDEPENDENT STRESS STATE VARIABLES

Delwyn G. Fredlund[1] and Hung Q. Pham[2]

[1] Professor Emeritus, Department of Civil and Geological Engineering, University of Saskatchewan, Saskatoon, SK, Canada, S7N 5A9. unsaturatedsoil@yahoo.com
[2] Assistant Professor, Department of Geotechnical Engineering, National University of Civil Engineering, 55th Giai Phong St., Hanoi, Vietnam. hqp802@mail.usask.ca

Abstract: This paper presents a description of a new volume-mass constitutive model for unsaturated soils. The model requires relatively simple laboratory tests to obtain the calibration information. Volume and water content changes can be independently computed using the model. The model is also capable of taking into account: i) the hysteretic nature of the soil-water characteristic curve; and ii) both elastic and plastic deformations in the soil. The predicted results for several artificial soils (i.e., sand, silt and clay) are consistent with observed behavior. A presentation of the model predictions for the volume-mass constitutive surfaces is also presented.

INTRODUCTION

Volume-mass constitutive relationships play an important role in modeling unsaturated soil behavior. The volume-mass relationships allow calculation of all volume-mass soil properties corresponding to any stress state. In addition, the volume-mass constitutive relationships can be used in the assessment of unsaturated soil property functions for shear strength and hydraulic conductivity. Many geotechnical problems should be solved as 'coupled' solutions of seepage, volume change and shear strength (Pereira 1996; Vu and Fredlund 2004). A rigorous volume-mass constitutive model will assist in achieving an integrated seepage, volume change and shear strength solution.

There are a number of volume-mass constitutive models that have been proposed for unsaturated soils (Pham 2005). Most models do not predict water content in terms of the stress state variables or assume that the degree of saturation is independent of net mean stress. Several models make use of two independent stress state variables (i.e., Alonso et al. 1990; Wheeler and Sivakumar 1995; Blatz and Graham 2003), while others make use of stress state variables incorporating soil properties (i.e., Kohgo et al. 1993; Jommi 2000; Wheeler et al. 2003; Tamagnini

2004).

In this paper, a new more rigorous volume-mass constitutive model has been proposed that is capable of: i) independently predicting water content, void ratio, and degree of saturation; ii) taking into account both elastic and plastic strains, and iii) taking into account hysteretic nature of the soil-water characteristic curve. The volume-mass constitutive model is proposed for isotropic loading/unloading conditions but is also applicable for K_0 loading/unloading conditions. A description of the volume-mass model and model predictions are presented in this paper.

TERMINOLOGY

There is no single, unique relationship between volume change and water content change for an unsaturated soil. Volume change and water content change in an unsaturated soil are controlled by two independent mechanisms: i) stress-strain (i.e., mechanical theory) behavior and ii) adsorption-drainage behavior (i.e., capillary theory). Therefore, water content change and volume change should be predicted separately within the context of a volume-mass constitutive model.

The soil particles are assumed to be incompressible; that is, deformations in the overall soil mass are directly related to changes in the volume of the pores. The soil-water appears only in pores; therefore, volume change and water content change are directly referenced to changes in the volume and shape of pores of the soil.

The "shape" of a pore can be defined by an "open pore diameter or neck pore diameter" and "body pore diameter" in relation to the capillary theory (Haines 1930). The "open pore diameter" is generally referred to as the "drying soil suction" or the air entry value of the pore (Neél 1942, 1943; Mualem 1973, 1974). The "body pore diameter" is generally referred to as the "wetting soil suction" or the water entry value of the pore.

The pores in a soil are comprised of various shapes and volumes. The pore-size distribution of a soil at any stress state provides information regarding both the total volume and the volume of water in the soil; therefore, in order to predict volume and water content, it is necessary to utilize the concept of the pore-size distribution of the soil. The pore-size distribution is changed when changing soil suction or net mean stress (Figure 1). It is required to predict changes in the volume and in the drying/wetting suction of each group of pores along the pores-size distribution at any stress states. In this paper, a reference pore-size distribution at a reference stress state is selected. The stress-strain relationship for the soil structure surrounding each pore group is then described.

The development of a volume-mass constitutive model includes: i) the proposal of basic assumptions for the response of a pore to changes in net mean stress and soil suction; ii) the formulation of the stress-strain relationship for the soil structure surrounding a pore including: changes in the air entry value, water entry value, yield stress, volume and water content; iii) the determination of the compression and unloading-reloading indices for each group of pores; and iv) the proposal of a model for the hysteretic nature of the soil-water characteristic curve within the context of a pore-size distribution.
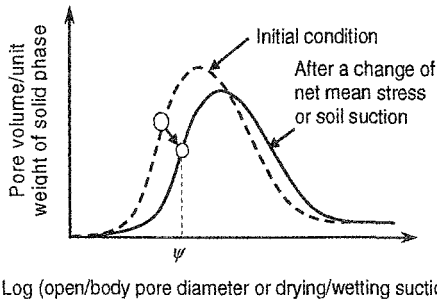
Figure 1. Schematic illustration of the change of the pore-size distribution due to a change in net mean stress or soil suction.

THEORY AND ASSUMPTIONS FOR THE MODEL
Stress state variables

The proposed model makes use of two stress state variables (Fredlund and Morgenstern 1977); namely, net mean stress, $(p = (\sigma_1 + \sigma_2 + \sigma_3)/3 - u_a)$, and (soil suction, $\psi = (u_a - u_w)$. The reference stress state is chosen to be a net mean stress = 1 kPa and soil suction = 0 kPa. This reference stress state is equivalent to the stress state where net mean stress = 0 kPa and soil suction = 1 kPa (i.e., assuming the air entry value of soil is greater than 1 kPa). The void ratio, e, of the soil is the primarily variable used to represent the overall volume of the soil. The gravimetric water content, w, of the soil is the primary variable used to represent the amount of water in the soil.

Reference Pore-Size Distributions

The pore-size distribution curve of a soil is generally plotted on a semi-logarithmic soil suction graph (Fredlund 1999; Simms and Yanful 2001). There are two types of the pore-size distribution curves for a soil; namely, i) the plot of the ratio of pore volume per unit weight versus open pore diameter (i.e., drying suction or air entry value of the pore) referred to as the *drying pore size distribution, DPD*, and ii) the plot of the ratio of pore volume per unit weight versus body pore diameter (i.e., wetting suction or water entry value of the pore) referred to as the *wetting pore size distribution, WPD*. For a soil that exhibits an insignificant volume change, the *DPD* and *WPD* are directly related to the initial/boundary drying and the boundary wetting soil-water characteristic curve of the soil (Figure 2).

The pore-size distribution of a soil with a significant volume change changes with soil suction and net mean stress. In order to predict changes in the pore-size distribution, it is necessary to select a reference pore-size distribution. The authors have observed that the drying pore-size distribution curve corresponding to an initially dry soil (i.e., at 10^6 kPa on the initial drying of a slurry soil) can provide a meaningful reference state. In the proposed model, *reference pore-size distributions* of a soil are chosen at completely dry conditions from the slurry. A soil has two reference pore-size distribution curves under completely dry conditions; namely, the *reference Drying Pore-Size Distribution (DPD),* denoted as $f_d(\psi)$, and the *reference Wetting Pore-Size Distribution (WPD),* denoted as $f_w(\psi)$.
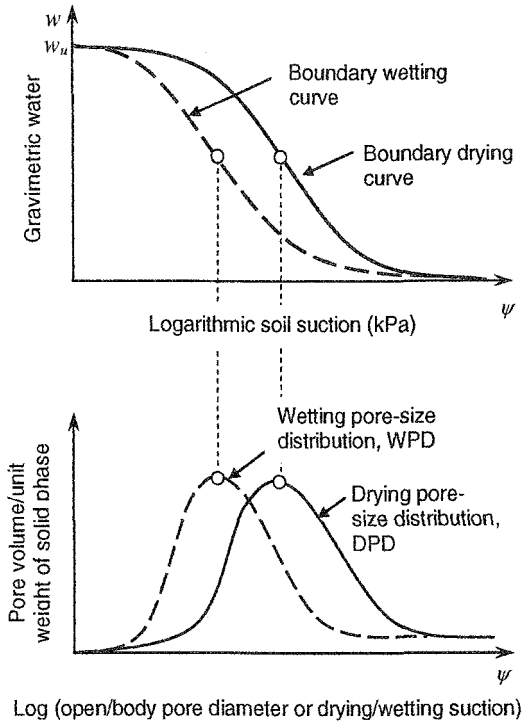
Figure 2. Schematic illustration of two pore-size distributions along with the drying and wetting soil-water characteristic curves of a soil.

Basic Assumptions

Seven assumptions are made in the development of the proposed volume-mass constitutive model. These assumptions are based on the findings of previous studies. The seven assumptions can be described as follows:

- *Assumption No. 1: In an unsaturated soil, a particular pore under consideration in the soil has only two states; namely, i) the pore is filled with water; or ii) the pore is empty.*

  Assumption No. 1 has been widely accepted in the development of a number hysteresis models for the soil-water characteristic curve (Paulovassilis 1962; Topp, 1971; Mualem 1973, 1974).

- *Assumption No. 2: Soil suction affects only the water-filled pores and does not affect the empty pores, while net mean stress has an effect on all pores in the soil.*

  Assumption No. 2 is similar to the explanation given for the mechanical behavior of an unsaturated soil by Alonso et al. (1994) and Wheeler and

Sivakumar (1995).

- **Assumption No. 3:** *Each water-filled pore in the soil has two indices; namely, i) virgin compression index, C_c^p and ii) unloading-reloading compression index, C_s^p.*

  The soil particles are assumed to be incompressible but it is reasonable to assume that a pore in the soil has two compression indices that are related to the elastic and plastic volume change of the pore. It can be shown that the summation of the compression indices of all pores in the soil is equal to that of the overall soil mass.

- **Assumption No. 4:** *There are two types of pore; namely, i) collapsible pores and ii) non-collapsible pores. The collapsible pores are relative large pores and the non-collapsible pores are relative small interconnected pores. The interconnected pores are assumed to be incompressible.*

  The assumption regarding collapsible and interconnected pores is similar to the explanation related to macro and micro structures that has been presented by several researchers (Alonso et al. 1994; Wheeler and Sivakumar 1995). Measured pore-size distribution curves for numerous soils under various loading and compaction conditions show that the micro pores do not seem to change with the change in volume of the soil (Sridharan et al. 1971; Ahmed et al. 1974; Delage and Graham 1995; Al-Mukhtar 1995; Alonso et al. 1995; Wan et al. 1995; Lloret et al. 2003). Therefore, interconnected pores are assumed to be incompressible.

- **Assumption No. 5:** *The virgin compression index and unloading-reloading compression index for a pore in the soil is proportional to the volume of the pore at the reference stress state (i.e., 1 kPa net mean stress and zero soil suction).*

- **Assumption No. 6:** *Pores are deformed and water is absorbed and drained through independently mechanisms.*

  The non-collapsible pores are assumed to be incompressible (assumption No. 4), and it is reasonable to assume that the collapsible pores deform independently.

- **Assumption No. 7:** *The unloading-reloading index of an air-filled pore is essentially equal to zero.*

  Silva et al. (2002) assumed that the unloading-reloading index of an unsaturated soil at a constant soil suction decreases with each increment of soil suction. The experimental data by Pham (2005) showed that the unloading-reloading index of an air-dried soil can be considered to be zero. Therefore, assumption No. 7 appears to be reasonable.

Volume change of a pore under different stress paths

The volume-mass constitutive relationships are stress path dependent (Alonso

1993; Pham 2005). The stress-strain relationship for the soil structure surrounding a pore needs to be considered for four different stress paths (i.e., loading, unloading, drying, and wetting). Let us consider a pore in a representative soil element with a volume of the solid phase equal to V_s. A description of four stress paths that the pore in the soil element could be subjected to is presented in this section.

Drying-wetting processes under zero net mean stress
    Let us consider a drying process where the soil suction is less than the air entry value and the pore is filled with water. The stress state acting on the soil structure surrounding the pore is equal to the soil suction $(u_a - u_w)$. When the soil suction is higher than the air entry value, the pore becomes filled with air and soil suction does not affect the soil structure surrounding the pore. The yield stress of the pore is equal to the air entry value of the pore. The volume of the air-filled pore is the same as that of the pore at a soil suction equal to the air entry value while the water content in the pore is equal to zero. A schematic illustration of the volume and water content changes of a pore along the initial drying process from an initially slurry condition are shown in Figure 3. The volume of a pore, $v^p(\psi,0)$, at a soil suction of ψ along a drying process can be calculated as follows:

$$v^p(\psi,0) = \begin{cases} v^p(1,0) - V_s C_c^p \log(\psi) & \text{for } \psi \leq \psi_{ae} \\ v^p(1,0) - V_s C_c^p \log(\psi_{ae}) & \text{for } \psi > \psi_{ae} \end{cases} \tag{1}$$

where ψ_{ae} = air entry value of the pore (i.e., reference air entry value = ψ_{ae}), C_c^p = virgin compression index of the pore, V_s = volume of the solid phase of the representative soil element, and $v^p(\psi,0)$ = volume of the pore at a soil suction of ψ and zero net mean stress. The volume of water in a pore, $v^w(\psi,0)$, along a drying process can be written as follows:

$$v^w(\psi,0) = \begin{cases} v^p(1,0) - V_s C_c^p \log(\psi) & \text{for } \psi \leq \psi_{ae} \\ 0 & \text{for } \psi > \psi_{ae} \end{cases} \tag{2}$$

where C_c^p = virgin compression index of the pore, and $v^w(\psi,0)$ = volume of water at a soil suction of ψ and zero net mean stress.
    The volume of the pore along the wetting process of an air-filled pore does not change until the soil suction is equal to the water entry value (Figure 3). When soil suction is less than the water entry value, the pore is filled with water and the soil continues to swell as soil suction decreases. The volume of the pore at any soil suction, ψ, along a wetting process (i.e., from initially air-filled) can be calculated as follows:

$$v^p(\psi,0) = \begin{cases} v^p(\psi_{ae},0) + V_s C_s^p \log(\psi_{ae}/\psi) & \text{for } \psi \leq \psi_{we} \\ v^p(\psi_{ae},0) & \text{for } \psi > \psi_{we} \end{cases} \tag{3}$$

where C_s^p = unloading-reloading index of the pore, and ψ_{we} = water entry value of the pore (i.e., reference water entry value = ψ_{we}). An equation for the volume of

water in the pore along a wetting process (i.e., initially air-filled) can be written as follows:

$$v^w(\psi,0) = \begin{cases} v^p(\psi_{ae},0) + V_s C_c^p \log(\psi_{ae}/\psi) & \text{for } \psi \le \psi_{we} \\ 0 & \text{for } \psi > \psi_{we} \end{cases} \tag{4}$$
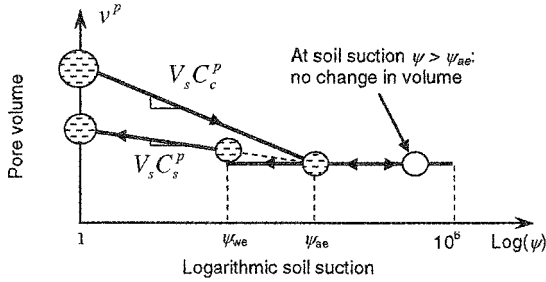
a) Volume change of a pore
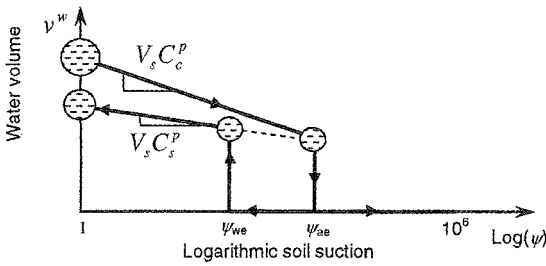
b) Water content change of a pore

Figure 3. Schematic illustration of volume and water content changes of a pore during the initial drying process.

Drying process under a constant net mean stress

The air entry value of a pore is a function of net mean stress and can be expressed as $\psi_{ae}(p)$. The volume of a pore can be presented as a function of both net mean stress, p, and soil suction, ψ. The volume of the pore under dry conditions (i.e., dry under zero net mean stress) can be calculated as follows:

$$v^p(\psi_{ae},0) = v^p(1,0) - C_c^p V_s \log(\psi_{ae}) \tag{5}$$

where ψ_{ae} = air entry value of the pore when drying under zero net mean stress, $v^p(1,0)$ = volume of the pore at the reference stress state (i.e., 1 kPa soil suction and zero net mean stress). When the soil is dried under a constant net mean stress, the air entry value of the pore is higher than that of the pore that is dried under zero net

mean stress (Figure 4). When the pore is filled with water, net mean stress and soil suction plays the same role; Therefore, the volume of a pore at a soil suction equal to the air entry value, $\psi_{ae}(p)$, and a net mean stress of p, can be presented as follows:

$$v^p(\psi_{ae}(p), p) = v^p(1,0) - C_c^p V_s \log(\psi_{ae}(p) + p) \tag{6}$$

where $v^p(\psi_{ae}(p), p)$ = volume of the pore at net mean stress, p, and soil suction equal to air entry value of the pore if dried under a net mean stress, p, $\psi_{ae}(p)$ = air entry value of the pore if the soil is dried under a constant net mean stress of p. An equation for the relationship between a change in soil suction and volume change of the pore can be derived by applying the capillary equation for the relationship between matric suction and the diameter of the capillary tube. The following equation can be obtained when assuming that deformation of the pore is isotropic (i.e., $\varepsilon_x = \varepsilon_y = \varepsilon_z$):

$$\frac{\psi_a}{\psi_b} = \frac{3V_0}{3V_0 - \Delta V} \tag{7}$$

where ψ_b = air entry value (or water entry value) of the pore *before deformation* (i.e., volume of V_0), and ψ_a = air entry value (or water entry value) of the pore *after deformation.*

The air entry/water entry value of a pore depends on the smallest/largest open pore diameter that is connected to the pore. The above equation may not be able to describe the change in the air entry value (or water entry value) under anisotropic loading conditions. For simplicity, a parameter called the pore shape parameter, η, is added to represent the relationship between the air entry value of a pore that is dried under zero net mean stress in relation to that of the pore when it is dried under a constant net mean stress, p:

$$\frac{\psi_a}{\psi_b} = \frac{3V_0}{3V_0 - \eta \Delta V} \tag{8}$$

where η = pore-shape parameter (≥ 1) depends on the soil and the stress history. An equation can be derived for the relationship between the air entry value of a pore when drying from slurry condition under zero net mean stress and that of the pore when subjected to a yield stress, p_0, and drying under a constant net mean stress, p, as follows:

$$\frac{\psi_{ae}}{\psi_{ae}(p, p_y)} = 1 - \eta \frac{\left[(C_c - C_s)\log(p_y) + C_s \log(\psi_{ae} + p) - C_c \log(\psi_{ae})\right]}{3\left[e_{sat} - C_c \log(\psi_{ae})\right]} \tag{9}$$

where $\psi_{ae}(p, p_y)$ = air entry value of the pore when yield stress is equal to p_y and drying under a net mean stress of p, p_y = yield stress of the soil and can be calculated as follows:

$$p_y = p_y(\psi_{ae}) = P(\psi_{ae}, p, p_0) = \begin{cases} p_0 & \text{for } (\psi_{ae} + p) \le p_0 \\ (p + \psi_{ae}) & \text{for } (\psi_{ae} + p) > p_0 \end{cases}$$ (10)

$$\approx \frac{(\tan^{-1}(\psi_{ae} + p - p_0) + 1.571)(\psi_{ae} + p - p_0)}{3.142} + p_0$$

where p_0 = yield stress of the pore prior to the drying process.
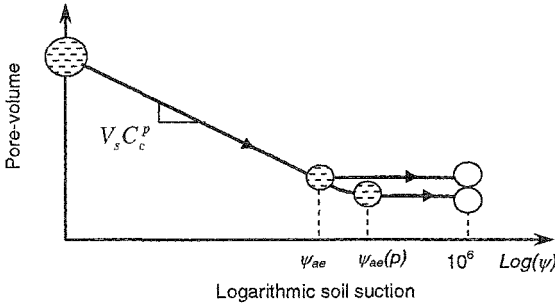
a) Relative comparison between volume changes of a pore
drying under zero and a constant net mean stress, p.
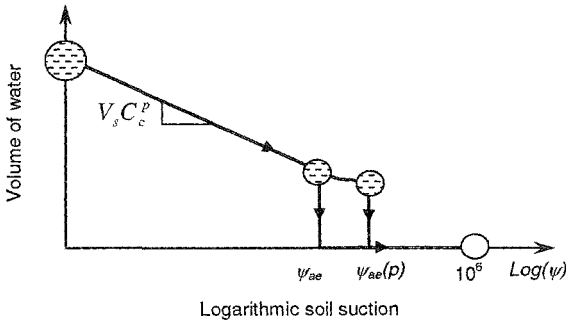
b) Relative comparison between water content changes of a
pore drying under zero and a constant net mean stress, p.

Figure 4. Schematic illustration of the effects of net mean stress to the air entry value, volume and water content of a pore along a drying process.

Wetting process under a constant net mean stress

The water entry value of a pore having a yield stress of p_y and wetted under a constant net mean stress, p, (i.e., $\psi_{we}(p, p_y)$) is higher than that of the pore when it is dried and wetted under zero net mean stress (i.e., reference water entry value, ψ_{we}). Similar to the procedure developed for the drying process, the relationship between the two values of the water entry values of the pore can be calculated as follows:

$$\frac{\psi_{we}}{\psi_{we}(p,p_y)} = 1 - \eta \frac{\left[(C_c - C_s)\log(p_y) + C_s \log(\psi_{we} + p) - C_c \log(\psi_{ae})\right]}{3\left[e_{sat} - C_c \log(\psi_{ae})\right]} \tag{11}$$

where ψ_{ae} = air entry value of the pore at zero net mean stress (i.e., reference air entry value), ψ_{we} = water entry value of the pore having zero yield stress and wetting under zero net mean stress (i.e., reference water entry value), $\psi_{we}(p,p_y)$ = water entry value of the pore when it has experienced a yield stress of p_y and is wetted under a constant net mean stress of p, where p_y, equal to the yield stress of the pore with a pore-shape parameter, η.

Alonso (1993) observed that any volume change related only to the wetting processes are stress path independent. Therefore, it is reasonable to assume that the volume of a pore that is wetted to a selected soil suction, ψ, and then subjected to a loading process by a net mean stress, p, is equal to that of the pore that is first loaded to a net mean stress, p, and then wetted to a soil suction, ψ. There are two types of pores after a wetting process; namely, i) water-filled pores and ii) air-filled pores. A pore that is filled with air after the wetting process is called the *continually air-filled pore*. For a water-filled pore, the volume of the pore at a soil suction of, ψ, and a net mean stress of, p, can be calculated as follows:

$$v^p(\psi, p, p_y) = v^p(1,0) - V_s C_c^p \log(p_y) + V_s C_s^p \log(p_y/(p + \psi)) \tag{12}$$

The yield stress of a pore that is filled with water after the wetting process can be calculated as follows:

$$p_y = p_y(\psi_{we}) = P(\psi_{we}, p, p_0) = \begin{cases} p_0 & \text{for } (\psi + p) \le p_0 \\ (p + \psi_{we}) & \text{for } (\psi + p) > p_0 \end{cases} \tag{13}$$

$$\approx \frac{(\tan^{-1}(\psi_{ae} + p - p_0) + 1.571)(\psi_{ae} + p - p_0)}{3.142} + p_0$$

where ψ_{we} = reference water entry value of the pore, p_0 = yield stress prior to the wetting process. In order to be consistent with the elasto-plastic theory for saturated soils, the volume-mass constitutive model for unsaturated soils must have a yielding of the soil structure surrounding *continually air-filled pores*. Three alternative assumptions for the stress-strain relationship of the soil structure surrounding a *continually air-filled pore* are as follows:

- *Alternative 1:*

The simplest alternative solution is to assume that *continually air-filled pores* are incompressible. In this case, the yield stress of a continually air-filled pore does not change when changing soil suction and net mean stress. The equation for the yield stress, p_y, can be written as follows:

$$p_y = p_y(\psi_{ae}) = p_0 \tag{14}$$

where p_y = yield stress of the *continually air-filled pore* (i.e., having a reference air entry value of ψ_{ae}) after the wetting process, and p_0 = yield stress of the pore prior to the wetting process.

• *Alternative 2:*

Let us assume that the compression curve of a *continually air-filled pore* at a constant soil suction on a logarithmic net mean stress scale can be expressed as a combination of two straight lines; namely, the virgin compression and unloading-reloading lines. The unloading-reloading index of an air-filled pore is equal to zero (i.e., assumption #7). Therefore, *volume change of an air-filled pore depends only on the yield stress of the pore.* The yield stress of a *continually air-filled pore* at a specific volume is a function of the virgin compression index of the pore (i.e., when it is filled with air).

The virgin compression index of a *continually air-filled pore* should be between the virgin compression indices of the pore when the soil is completely dry and that of the pore when soil suction is equal to zero. Figure 5 illustrates compression curves of a pore at three different soil suctions: i) at saturation (zero soil suction); ii) when soil suction equal to a certain soil suction, ψ, at which the pore is filled with air; and iii) at 10^6 kPa (i.e., soil is completely dry). The compression curve of the pore at soil suction of 10^6 kPa can be described by two straight lines; namely, i) from zero net mean stress equal to soil suction (i.e., horizontal line because the unloading-reloading index of the air-filled pore is equal to zero) and ii) at net mean stresses higher than the air entry value of the pore with a slope of C_{cd}^p. The compression curve of the pore at a soil suction of ψ, can also be described using two straight lines; namely, i) at net mean stresses less than air entry value of the pore (i.e., horizontal line because the loading-unloading of a air-filled pore is equal to zero), and ii) at net mean stresses higher than the air entry value with a slope of $C_{c\psi}^p$. The volume of an air-filled pore at a net mean stress less than the air entry value of the pore is equal to the volume of the pore at dry conditions (i.e., dried from slurry under zero net mean stress).

The virgin compression index of the *continually air-filled pore* is assumed to be a function of the following variables; namely, i) water content in the soil (i.e., as observed from the data measured by Sharma (1998)); ii) virgin compression index of the pore when soil suction is equal to zero (i.e., saturation); and iii) virgin compression index of the pore when soil suction is equal to 10^6 kPa (i.e., oven-dry condition). For simplicity, let us propose an equation for the virgin compression index of the *continually air-filled pore* (i.e., having a reference air entry value of ψ_{ae}) at a soil suction of ψ as follows:

$$C_{c\psi}^p = (S(\psi))^m (C_c^p - C_{cd}^p) + C_{cd}^p \tag{15}$$

where m = soil parameter (i.e., for the compressibility of dry pores), $C_{c\psi}^p$ = virgin compression index of the air-filled pore at soil suction of ψ, C_c^p and C_{cd}^p = virgin compression indices of the air-filled pore at soil suctions of zero and 10^6 kPa, respectively, and $S(\psi)$ = degree of saturation at soil suction of ψ on the corresponding soil-water characteristic curve of an initially slurried soil (i.e., when net mean stress is equal to zero).
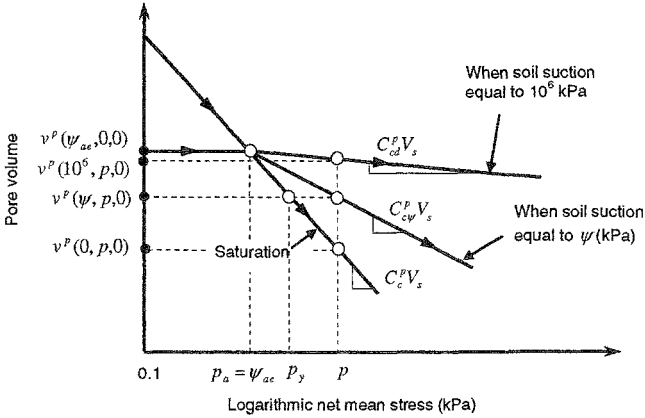
Figure 5. Schematic illustration of the compression curves of a pore at three different soil suctions (i.e., 0, ψ, and 10^6 kPa).

At a specific volume, the equivalent yield stress of a continually air-filled pore is assumed to be equal to the stress state variable that brings volume of the pore from the initial stress state to the same volume of the pore (i.e., when the pore is filled with water). The yield stress of the continually air-filled pore (i.e., reference air entry value = ψ_{ae}), can be obtained:

$$p_y^* = p_y^*(\psi_{ae}) = \psi_{ae}10^{\dfrac{\log\left(\dfrac{p}{\psi_{ae}}\right)\left[(S(\psi))^m\left[C_c^p-C_{cd}^p\right]+C_{cd}^p\right]}{C_c^p}} \tag{16}$$

- *Alternative 3:*

At completely dry conditions there is a certain amount of relative small particles and cementing material (i.e., chemicals) that act to bond the larger particles together. Along the wetting process, water gradually fills the pores and eliminates the bonding strength that keeps soil particles in position (Lawton et al. 1991a, 1991b; Pereira 1996). Let us assume that all bonds are removed when all interconnected pores (i.e., non-collapsible pore) are filled with water. This means that the *continually air-filled pores* reach maximum collapse and the equivalent yield stress on the soil structure surrounding a continually air-filled pore is equal to the magnitude of the net mean stress. It is reasonable to assume that the equivalent yield stress of the soil structure surrounding *continually air-filled pores* is a function of the amount of water in the interconnected pores and the net mean stress. The equivalent yield stress of the soil structure surrounding a *continually air-filled pore* is independent of the reference air entry value of the pore, ψ_{ae}, and can be calculated as follows:

$$p_y^*(\psi_{ae}) = \begin{cases} p\left(\dfrac{w(\psi,p)}{w_r}\right)^n & \text{for } w(\psi,p) < w_r \\ p & \text{for } w(\psi,p) \geq w_r \end{cases} \tag{17}$$

where $w(\psi, p)$ = water content in the soil at soil suction of ψ, and net mean stress of p, w_r = residual water content of the soil, and n = soil parameter.

- *Summary:*

The yield stress calculated using equation (16) or (17) is the yield stress for a continually air-filled pore inducing from only the wetting process at a constant net mean stress, p of an air-dried specimen from initially slurry. The actual yield stress of a *continually air-filled pore* at any stress state can be calculated as follow:

$$p_y = p_y (\psi_{ae}) = \begin{cases} p_y^* (\psi_{ae}) & \text{for } p_0 \leq p_y^* \\ p_0 & \text{for } p_0 > p_y^* \end{cases} \tag{18}$$

where p_y^* = yield stress calculated using equation (16) or (17), and p_0 = yield stress of the pore prior to the wetting process.

The volume of an air-filled pore is only a function of the yield stress of the pore (i.e., unloading-reloading index of the pore is equal to zero). The volume of an air-filled pore can be calculated as follows:

$$v^P (\psi, p, p_y) = v^P (1,0) - V_s C_c^p \log(p_y) \tag{19}$$

where p_y = yield stress of the pore.

Loading-unloading processes at a constant soil suction

Two types of pores are considered during loading-unloading processes of an unsaturated soil; namely, i) air-filled pores; and ii) water-filled pores. When the soil structure surrounding an air-filled pore is loaded, the pore will be compressed and the water entry value of the pore is decreased. If the soil suction is less than the water entry value, the pore absorbs water and becomes a water-filled pore. Loading-unloading processes of the soil structure surrounding a water-filled pore are similar to that of a saturated soil and have been described in the above sections. If soil suction is higher than the water entry value, the pore is still filled with air after the loading process and called the *continually air-filled pore*. Three alternative solutions for the volume have been described in the above section.

Mathematical formulations for the drying process of an initially slurry soil

Equations are presented in this section for the compression indices associated with each group of pores along the pore-size distribution. The equation for the reference pore-size distribution function is also described. Details of the mathematical derivation of each equation can be found in Pham (2005).

A curve-fitting model for the soil-water characteristic curve

The initial drying soil-water characteristic curve from the slurry of a volume change soil can be best-fit using the following equation:

$$w(\psi) = \left(\left[w_{sat} - \frac{C_c}{G_s} \log(\psi) - w_r \right] \frac{a}{\psi^b + a} + w_r \right) \left(1 - \frac{\ln\left[1 + \dfrac{\psi}{\psi_r} \right]}{\ln\left[1 + \dfrac{10^6}{\psi_r} \right]} \right) \tag{20}$$

where: C_c = virgin compression index of the soil; G_s = particles specific gravity; w_r = curve-fitting parameter represents the residual water content; w_{sat} = curve-fitting parameter represents the water content of the slurry soil at an effective stress of 1 kPa; a, b = curve-fitting parameters; and ψ_r = residual soil suction.

Equation for the virgin compression index of pores and the reference drying pore-size distribution

An equation for the virgin compression index of pores along the reference pore-size distribution is presented in this section. A soil is completely dry at a soil suction of 10^6 (Fredlund and Xing 1994). Some soils may be dry at somewhat lower soil suctions. Let us denote the lowest soil suction at which a soil is completely dry as ψ_{max} (i.e., $\xi_{max} = \log(\psi_{max})$ on a logarithmic soil suction scale). Consider a representative soil element of a slurry dried soil where the volume of solids is equal to V_s. The total volume of the pores in the soil element under dry conditions (i.e., at a soil suction $\geq \psi_{max}$) can be calculated as follows:

$$V_p = V_a = \int_0^{\xi_{max}} f_d(x)dx \tag{21}$$

where $f_d(x)$ = reference drying pore-size distribution function (*DPD*), and V_p, V_a = total volume of pores and total volume of air phase of the soil element at a soil suction of ψ_{max}, respectively. The water content and total volume of the soil at any stress states can be obtained in a similar manner. Taking into account assumptions No. 3 and 5, an equation for the virgin compression index of a pore group can be derived:

$$C_c^P(\xi) = \frac{d\left(\dfrac{-G_s w(10^\xi)C_c}{e_{sat} - C_c \xi}\right)}{d\xi} \tag{22}$$

where: e_{sat} = void ratio of the soil at reference stress state, $w(\psi)$ = water content along the initial drying soil-water characteristic curve. Similarly, an equation for the *reference DPD* can also be obtained as follow:

$$\int_0^\xi f_d(x)dx = V_{dry}^p - G_s V_s \left[w(\psi) - \int_\xi^{\xi_{max}} \frac{w(10^x)C_c}{[e_{sat} - C_c x]}dx \right] \tag{23}$$

Volume change of collapsible and non-collapsible pores

An equation for the prediction of the volume change along the drying process has been presented in the previous section. It was previously noted that there was no distinction between collapsible pores and interconnected pores. Non-collapsible pores are interconnected pores that exhibit no significant hysteresis between the wetting and drying processes. When soil suction exceeds the residual soil suction, water exists only in the non-collapsible pores. The total volume of the non-collapsible pores at residual soil suction is assumed to be equal to the volume of

water at residual soil suction.
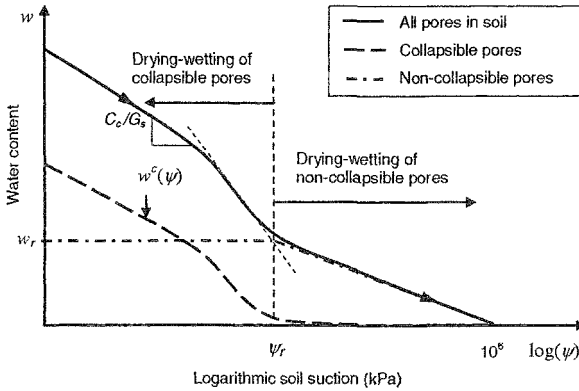
Figure 6. Schematic illustration of the gravimetric water content in collapsible and interconnected pores along the initial drying process.

The water content in a soil at a particular soil suction can be divided into two components; namely, the i) water content in collapsible pores and ii) water content in the non-collapsible pores. At soil suctions higher than residual soil suction, the water content in the soil is equal to the water content in collapsible pores (Figure 6). At soil suctions less than residual soil suction, the water content in the soil is equal to the water content in the collapsible pores and the water content at residual soil suction. Let us denote a function that presents gravimetric water content in the collapsible pores as $w^c(\psi)$. The function $w^c(\psi)$ can be calculated as follows:

$$w^c(\psi) = \begin{cases} w(\psi) - w_r & \text{for } \psi \le \psi_r \\ 0 & \text{for } \psi > \psi_r \end{cases} \tag{24}$$

where $w(\psi)$ = gravimetric water content along the initial drying curve for an initially slurried soil, and ψ_r = residual water content of the soil.

Summary of the compression indices of pores

Let us consider the existence of the non-collapsible pores. The virgin compression index of the group of pores having an air entry value, ψ, can be calculated as follows (i.e., by substituting Eq. (24) into Eq. (22)):

$$C_c^p(\xi) = -\frac{d\left(C_c \dfrac{a}{(10^\xi)^b + a}\right)}{d\xi} = -\frac{C_c ab \ln(10)(10^\xi)^b}{\left[(10^\xi)^b + a\right]^2} \tag{25}$$

where $\xi = \log(\psi)$, C_c = virgin compression index of the soil at saturation, a, b = curve fitting parameters obtained from a best-fitting of the SWCC of the soil at initially slurry conditions (Eq. (20)). Similarly, the unloading-reloading

compression index of the group of pores having logarithmic air entry value of ξ, can be calculated as follows:

$$C_s^p(\xi) = -\frac{d\left(C_c\dfrac{a}{(10^\xi)^b + a}\right)}{d\xi} = -\frac{C_s ab\ln(10)(10^\xi)^b}{\left[(10^\xi)^b + a\right]^2} \tag{26}$$

where C_s = unloading-reloading index of the soil at saturation. An equation for the *reference DPD* of the soil can be obtained by differentiating both sides of equation (23) and then simplifying.

$$f_d(\psi) = -\frac{d(w(\psi))}{d\psi} G_s \psi \ln(10) - \frac{aC_c}{\psi^b + a} \tag{27}$$

where $w(\psi)$ = gravimetric water content along the initial drying curve of an initially slurried soil. Similar to the compression indices of water-filled pores, it is possible to derive an equation for the virgin compression index of air-filled pores. The dried virgin compression index of the group of pore having logarithmic air entry value of ξ, can be calculated as follows:

$$C_{cd}^p(\xi) = -\frac{C_{cd} ab\ln(10)(10^\xi)^b}{\left[(10^\xi)^b + a\right]^2} \tag{28}$$

where C_{cd} = virgin compression index of the soil under dried condition.

Hysteresis model for soil-water characteristic curves

A new model for hysteretic soil-water characteristic curves based on the pore-size distribution curve is applied in the volume-mass constitutive model. A hysteresis model is developed in this paper using two one-dimensional pore-size distribution functions (i.e., wetting and drying pore-size distributions). Scanning soil-water characteristic curves are assumed to be horizontal with respect to the degree of saturation of the soil-water characteristic curve (Wheeler et al. 2003). This means that each group of pores has a unique relationship between the drying and wetting suction. The relationship between the *reference DPD* and the *reference DPD* can be described as follows:

$$f_w(\xi) = f_d(\xi - \Delta\xi) \tag{29}$$

where: $f_d(\xi)$ = reference drying pore-size distribution; $f_w(\xi)$ = reference wetting pore-size distribution, $\Delta\xi$ = difference between the air entry value and water entry value of the group of pores having an air entry value of ψ (i.e., log-cycles); and $\xi = \log(\psi)$.

Pham et al. (2005) presented a model for the three key hysteretic soil-water characteristic curves of a soil (i.e., initial drying, boundary drying, and boundary wetting curves). If the distance between curves and the slope ratio between the two boundary curves are known, the key hysteretic soil-water characteristic curves can be predicted. The *reference WPD and DPD* can be calculated from the boundary soil-water characteristic curves of the soil (Eq. (27)). Therefore, two reference pore-

size distribution curves can be calculated from: i) one of the three key soil-water characteristic curves; ii) the slope ratio and the distance between the two boundary curves.
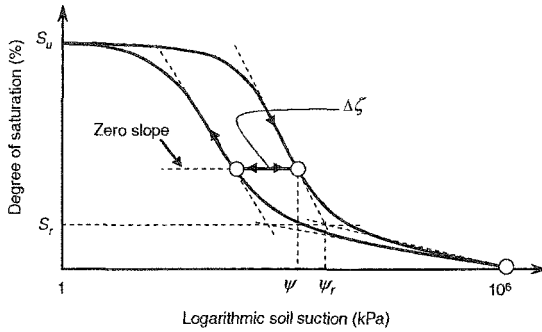
Figure 7. Schematic illustration of the distance between the two boundary curves in log-cycle.
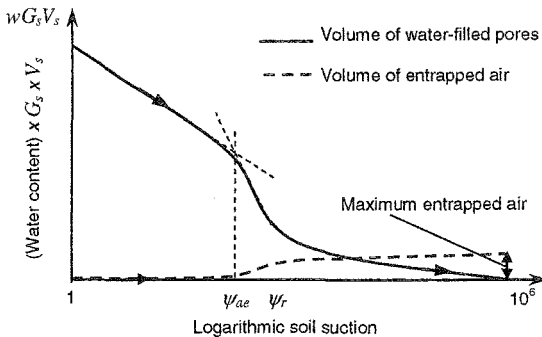
Figure 8. Volume of the water-filled pores and the air-filled pores during the initial drying process.

The proposed model also takes into consideration the effect of the entrapped air. At 100% saturation, no air is entrapped in the soil. Once a pore is filled with air, a certain amount of air is entrapped in the pore. It is assumed that the amount of air entrapped in a collapsible pore is proportional to the volume of the pore and denoted by an entrapped air parameter, β (Fig. 8).

A complete volume-mass constitutive model for soils

In summary, the following equations can be used to calculate the volume of a water-filled pore:

$$v^{p}(\psi) = v^{p}(1,0) - V_{s}C_{c}^{p}\log(p_{y}) + V_{s}C_{s}^{p}\log(p_{y}/(\psi + p))$$ (30)

The volume of an air-filled pore is stress path dependent. The volume of an air-filled pore after a drying process can be calculated as follows:

$$v^p(\psi) = v^p(1,0) - V_s C_c^p \log(p_y) + V_s C_s^p \log(p_y / (\psi_{ae}(p, p_y) + p)) \qquad (31)$$

The volume of an air-filled pore does not change after an unloading process. After a loading process or a wetting process, the volume of an air-filled pore can be calculated using the following equation:

$$v^p(\psi) = v^p(1,0) - V_s C_c^p \log(p_y) \qquad (32)$$

where $p_y =$ yield stress of the pore (i.e., can be calculated using one of the following Eqs. (14), (16) and (17)). When taking into consideration collapsible and non-collapsible pores, equations for the change in the air entry value of a pore can be obtained by modifying equations (15) as follow:

$$\frac{\psi_{ae}}{\psi_{ae}(p, p_y)} = 1 - \eta \frac{\left[(C_c - C_s)\log(p_y) + C_s \log(\psi_{ae} + p) - C_c \log(\psi_{ae})\right]}{3\left[e_{sat} - C_c \log(\psi_{ae}) - w_r G_s\right]} \qquad (33)$$

Similarly, an equation for the change in the water entry value of a pore can be obtained by modifying equation (16) as follow:

$$\frac{\psi_{we}}{\psi_{we}(p, p_y)} = 1 - \eta \frac{\left[(C_c - C_s)\log(p_y) + C_s \log(\psi_{we} + p) - C_c \log(\psi_{ae})\right]}{3\left[e_{sat} - C_c \log(\psi_{ae}) - w_r G_s\right]} \qquad (34)$$

If soil suction is less than the water entry value of the pore along a wetting path then the pore is filled with water, otherwise, it is filled with air. Along a drying process, the pore is filled with water if soil suction is less than the air entry value; otherwise, the pore is filled with air. The air entry value and water entry value of a pore can be calculated using equations (33) and (34), respectively.

At a particular stress state, the pore-size distribution of the soil can be calculated. The volume of water in a representative soil element can be calculated as a summation (i.e., integration) of volume of pores along the pore-size distribution from the current soil suction to 10^6 kPa. The volume of the representative soil element can be calculated as a summation (i.e., integration) from the zero soil suction to 10^6 kPa. The equations for the volume-mass constitutive surfaces are presented in the following section.

Equations for volume-mass constitutive surfaces
The volume-mass constitutive surfaces have been experimentally shown to be stress path dependent (Karube 1986; Alonso 1993; Pham 2005). Each volume-mass constitutive surface pertains to a particular testing stress path and an equation is required to describe the surface. The objective of this section is to show that it is possible to derive closed-form equations for the volume-mass constitutive surfaces (i.e., both overall volume and water content) corresponding to any stress path. Two equations are shown for the volume-mass constitutive surfaces followed by simple stress paths (Figure 9). The stress paths correspond to a slurry soil initially loaded to a net mean stress of p_0 at zero soil suction and then dried under various constant net mean stresses. For this stress path, the soil parameter, m, is not required since there is no change in net mean stress after pores filling with air.

a) Water content   b) Void ratio
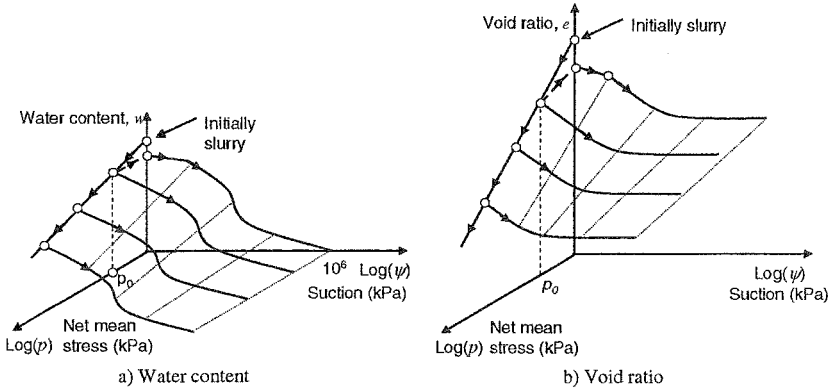
Figure 9. Schematic illustration of the volume-mass constitutive surfaces obtained from loading-unloading processes of an initially slurried specimen that is dried under various constant net mean stresses.

Equations for the water content and the void ratio constitutive surfaces can be written as follows:

$$w(\psi, p, p_0) = w(\psi_s, 0, 0) -$$
$$\frac{w^c(\psi_s)[(C_c - C_s)\log(P(\psi, p, p_0)) - \xi_s C_c + C_s \log(\psi + p)]}{(e_{sat} - C_c\xi_s - w_r G_s)} \tag{35}$$

$$e(\psi, p, p_0) = e_{sat} - G_s w(\psi_s, 0, 0) - \int_0^{\xi_s} \frac{G_s w^c(10^x) C_c}{[e_{sat} - C_c x - w_r G_s]} dx$$

$$+ w(\psi, p, p_0) G_s + \left(\left(\log(P(\psi, p, p_0)) - \xi_s \right) \left(\frac{G_s w^c(\psi_s)(C_c - C_s)}{(e_{sat} - C_c\xi_s - w_r G_s)} \right) \right)$$

$$- \int_0^{\xi_s} \left(\frac{G_s w^c(10^x)(C_c - C_s)}{(e_{sat} - C_c x - w_r G_s)} \right) \frac{d(\log(P(10^x, p, p_0)) - x)}{dx} dx \tag{36}$$

$$+ \left((\log(\psi + p) - \psi_s) \left(\frac{G_s w^c(\psi_s) C_s}{(e_{sat} - C_c\xi_s - w_r G_s)} \right) \right) - C_s \log(1 + p)$$

$$- \int_0^{\xi_s} \frac{G_s w^c(10^x) C_s}{(e_{sat} - C_c x - w_r G_s)} \frac{d(\log(10^x + p) - x)}{dx} dx - (C_c - C_s)\log(P(1, p, p_0))$$

where $w(\psi_s, 0, 0)$ = water content at soil suction, ψ_s, on the initial drying curve of the slurry soil, $P(\psi, p, p_0) = \dfrac{(\tan^{-1}(\psi + p - p_0) + 1.571)(\psi + p - p_0)}{3.142} + p_0$, $\xi_s = \log(\psi_s)$, $\psi_s = \left(1 - \dfrac{\eta[(C_c - C_s)\log(P(\psi, p, p_0)) + C_s \log(\psi_{ae} + p) - C_c \log(\psi_{ae})]}{3[e_{sat} - C_c \log(\psi_{ae}) - w_r G_s]} \right) \psi$,

e_{sat} = void ratio at the reference stress state, η = parameter for representing stress

history of the soil, $w^c(\psi) = \left((w_{sat} - \dfrac{C_c}{G_s}\log(\psi) - w_r) \dfrac{a}{\psi^b + a} \right)$, a, b = curve fitting parameters for the initial drying curve of the slurry specimen, G_s = Specific gravity of the soil particles, w_{sat} = gravimetric water content at reference stress state, C_c, C_s = compression indices of the soil at saturated condition (i.e., zero soil suction), p = net mean stress, p_0 = uniform yield stress, and w_r = residual water content of the soil. The equation for the degree of saturation surface can be derived from the equations for gravimetric water content surface (Eq. (35)) and void ratio surface (Eq. (36)) as follows:

$$S(\psi, p, p_0) = \frac{w(\psi, p, p_0)G_s}{e(\psi, p, p_0)} \tag{37}$$

Determination of the model parameters

The proposed volume-mass constitutive model requires relatively simple and conventional laboratory test data for calibration. The data required for calibration can be described as follows:

i. the initial drying soil-water characteristic curve of the initially slurry soil specimen.

ii. pore-shape parameter, η, represents the effect of net mean stress and stress history on the change in the air entry values of pores in the soil. It is suggested that this parameter be selected as equal to 2 (Pham 2005) if another soil-water characteristic curve at a different pre-consolidation pressure has not been tested.

iii. the parameters for the hysteretic nature of the soil-water characteristic curve of the soil; namely, i) the distance between the two inflection points of the two boundary hysteretic curves, D_{SL}; and ii) the ratio between the slopes of the boundary drying and the boundary wetting curves, R_{SL}. These values can be estimated as suggested by Pham (2001) and Pham et al. (2005).

iv. the virgin compression index of the air-dried specimen from an initially slurry specimen (i.e., completely dry specimen).

v. the soil parameter, m, is required to determine the compressibility of the soil structure surrounding a continually air-filled pores. In the case of no measured data, the soil parameter can be assumed to be equal to 1.

The compression index of an air-dried specimen becomes linear on a semi-log plot at the value of net mean stress beyond the residual soil suction (Figure 10). The dry virgin compression index, C_{cd}, of an air-dried can then be estimated as the same manner for saturated soils. For most soils, value of C_{cd} can be assumed to be equal to zero (Pham 2005).
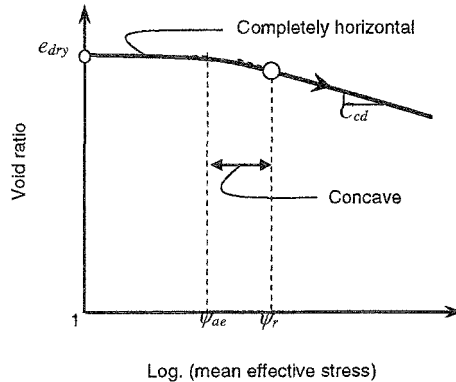
Figure 10. Compression curve of an air-dried from the slurry soil specimen and the method for the estimation of the virgin compression index of a dry specimen, C_{cd}.

PRESENTATION OF MODEL PREDICTIONS

The application of the proposed volume-mass constitutive model is presented for three artificial soils. The prediction results are presented for: i) several simple stress paths (i.e., 2D graphs) and ii) Several complete volume-mass constitutive surfaces (i.e., 3D graphs). Materials are described first, followed by a description of the stress paths and a presentation of prediction results.

Materials

Descriptions of the three artificial soils are presented in Table 1. The initial drying soil-water characteristic curves of the three soils starting from slurry conditions are shown in Figure 11. The virgin compression indices of the three soils under completely dry conditions, C_{cd}, are equal to zero.

Table 1. Characteristics of the three artificial soils

Soil name		Sand	Silt	Clay
Soil-water characteristic curve from initially slurried	w_{sat}	0.28	0.38	0.80
	a	500	2.0E+5	5.0E+9
	b	3	2.5	2.8
	w_r	0.03	0.08	0.10
Characteristics of the hysteretic SWCCs	D_{SL}	0.2	0.35	0.5
	R_{SL}	2	1.5	1.5
	β	0.1	0.1	0.1
Compression indices	C_c	0.01	0.2	0.5
	C_s	0.003	0.04	0.1
Specific gravity	G_s	2.6	2.7	2.8
Pore-shape parameter	η	2	2	2
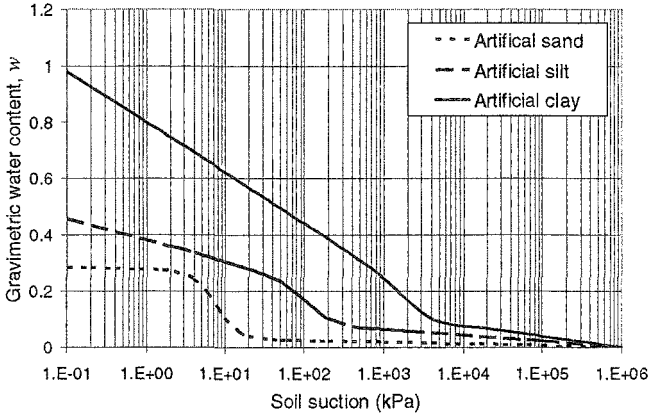
Figure 11. Initial drying soil-water characteristic curves for the artificial sand, silt and clay.

Prediction results for several simple stress paths

The shrinkage curve of a soil can be predicted using the proposed constitutive model by measuring both the void ratio and the water content along the drying process from slurry to 10^6 kPa soil suction. The predicted shrinkage curves for the three artificial soils are shown in Figure 12. The shrinkage curve for the sand soil is essentially a horizontal line since the sand does not change volume during a drying process. The computed shrinkage curve for silt and clay also appear reasonable. At high water contents, the shrinkage curves form 45 degree lines. The shrinkage curves are horizontal at water contents below the shrinkage limit. The transitions of the shrinkage curve between the low and high water contents appear to be smooth and have reasonable curvature.

For illustration purpose, let us predict void ratio, gravimetric water content and degree of saturation for the artificial silt when following several simple stress paths. The stress paths are described as follows (Figure 13). The soil is initially a slurry and subjected to a drying-wetting cycle to a soil suction of 100 kPa. The soil is then dried to 10^6 kPa and then subjected to a net mean stress of 2000 kPa. The soil is then subjected to a wetting process to 0.1 kPa, followed by an unloading process to a net mean stress of 1 kPa. The predicted void ratio, gravimetric water content and degree of saturation versus soil suction for the specified stress path are shown in Figure 14.
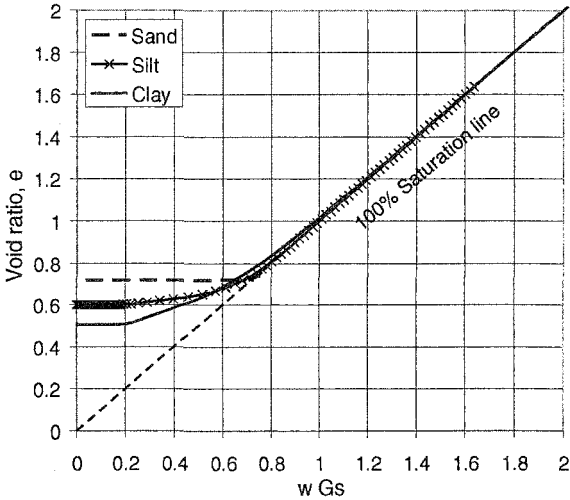
Figure 12. Shrinkage curves of the artificial sand, silt and clay.
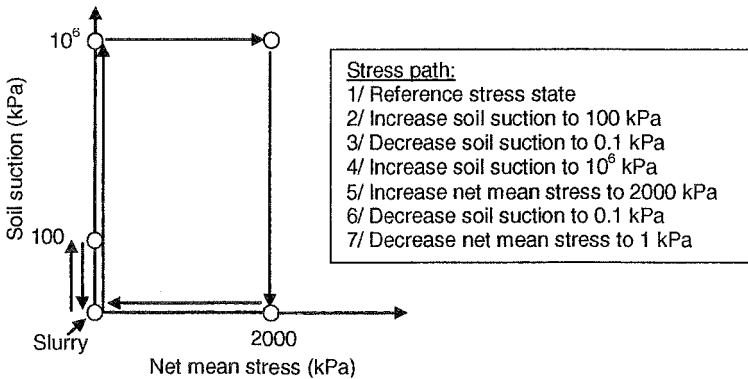
Figure 13. Stress path followed for the artificial silt.

Figures 14 shows the prediction results for the artificial silt followed stress path described in Figure 13. It is shown that the predicted results for the volume-mass constitutive relationships are reasonable. Hysteresis in the soil-water characteristic curve and plastic deformation have been taken into account in the simulation. The soil parameter m controls the collapse behaviour of the soil. The smaller the value for the soil parameter, m, the earlier the collapse occurs in the soil during the wetting process.
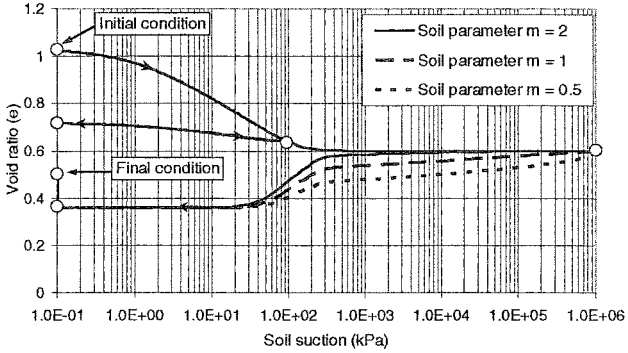
a) Void ratio
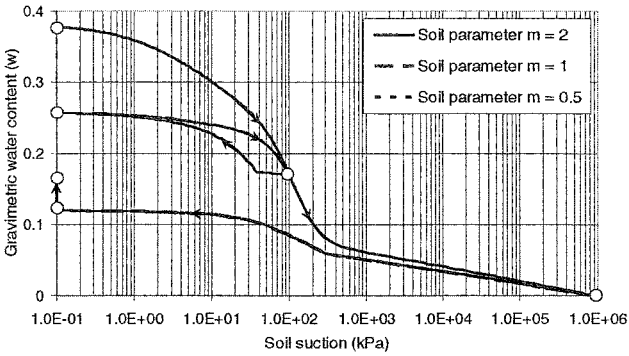
b) Gravimetric water content
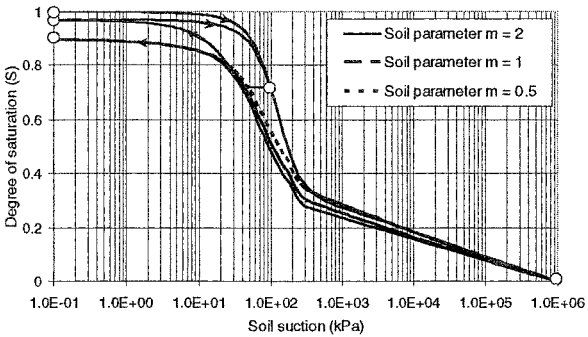
c) Degree of saturation

Figure 14. Degree of saturation for the artificial silt.

Prediction results for the volume-mass constitutive surfaces

It is necessary to select several series of stress paths to present the volume-mass constitutive surfaces for the three artificial soils. The selected stress paths should be simple but capable of showing several important characteristics of an unsaturated soil (e.g., swelling and collapsible behaviors).

The four series of stress paths for studying the volume-mass constitutive surfaces of an unsaturated soil are described in Figure 15. In stress path series #1, the soil is initially slurry, loaded to a certain net mean stress and then dried under the constant net mean stress to a soil suction of 10^6 kPa. In stress path series #2, the soil is initially slurry, then dried to a certain soil suction and loaded under constant soil suction condition to a net mean stress of 10^4 kPa. In stress path series #3, the soil is initially dried from a slurry, loaded to a certain net mean stress and then wetted under the constant net mean stress to a soil suction of 10^6 kPa. In stress path series #4, the soil is initially dried from a slurry, wetted to a certain soil suction and then loaded under the constant soil suction to a net mean stress of 10^4 kPa.
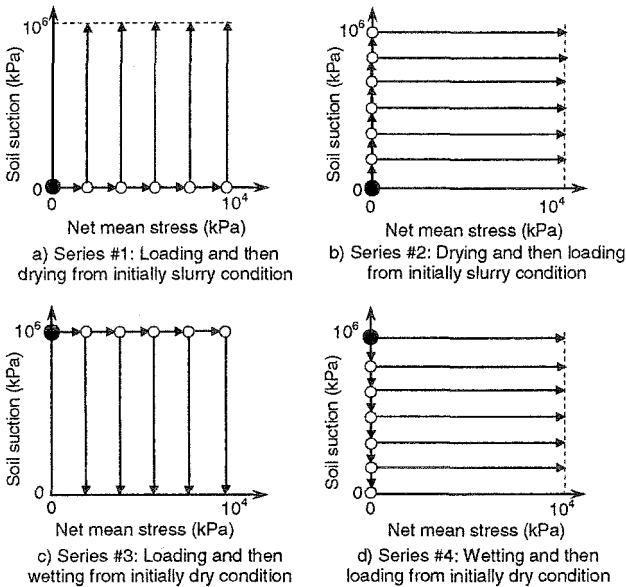
Figure 15. Four series of stress paths for studying volume-mass constitutive surfaces of an unsaturated soil.

The two stress path series #1 and #2 are used to study the mechanical behavior of various soil specimens when starting with the same initial slurry condition and ending at the same final stress state, but followed by two different stress paths during the drying process. Similarly, stress path series #3 and #4 are used to study mechanical behavior of various soil specimens with the same initial (i.e., dried from slurry) and final stress states but following two different stress paths that involve a wetting process.

Figure 16 shows that the calculated volume-mass constitutive surfaces agree well with all the postulates presented by Fredlund et al. (2000); namely, i) there is a one-to-one relationship between the effect of a change in net total stress and a change in soil suction, when the soil suction is less than air entry value of the soil (i.e., for both void ratio and water content surfaces); ii) there is a gradual curve that forms from the air entry value to the primary water content reference condition, corresponding to a particular water content on the water content surface; and iii) there is a gradual curve that forms from the air entry value to the second reference condition corresponding to a particular void ratio on the void ratio constitutive surface.
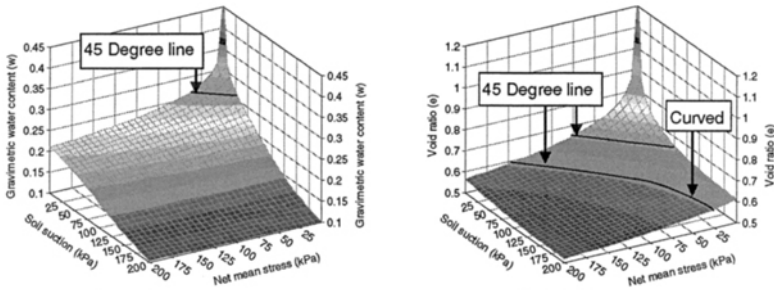
a. gravimetric water content   b. Void ratio

Figure 16. The constitutive surfaces for silt at low suctions and net mean stresses (stress path series #1 and #2).

Figures 17 to 19 show several volume-mass constitutive surfaces predicted for the three artificial soils. The predicted constitutive relationships at zero soil suction and zero net mean stress planes appear to be reasonable. The volume-mass constitutive surfaces starting from initially slurry seem to have steeper slopes than that starting from an air-dried condition. The shapes of the volume-mass constitutive surfaces predicted using the proposed model appear to be reasonable.
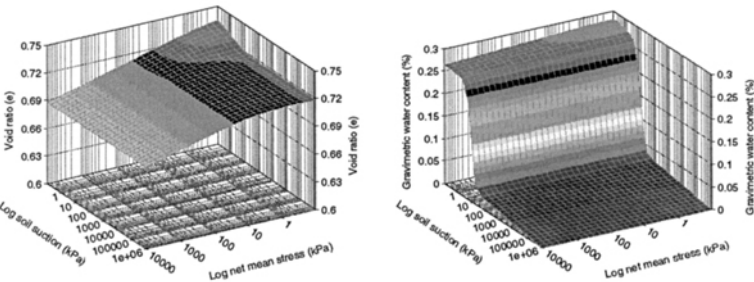
a. Void ratio   b. Gravimetric water content

Figure 17. The constitutive surfaces for sand (stress path series #1 and #2 in logarithmic scale).
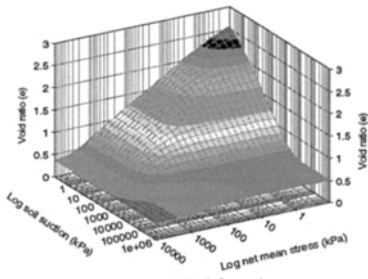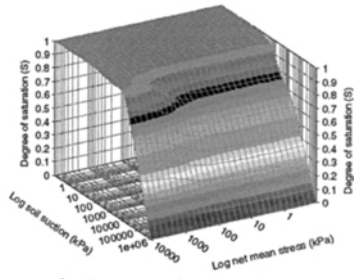
a. Void ratio   b. Degree of saturation

Figure 18. The constitutive surfaces for clay (stress path series #1 and #2 in logarithmic scale).
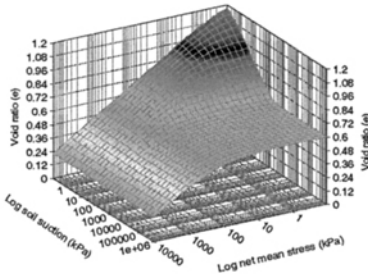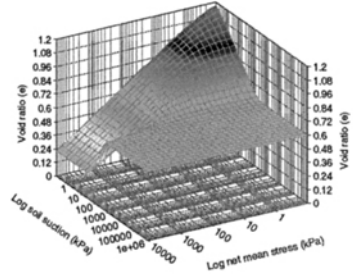
a. Stress path #1   b. Stress path #2
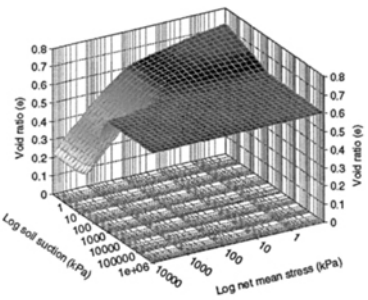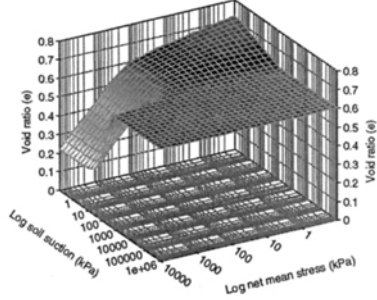
c. Stress path #3   d. Stress path #4

Figure 19. The constitutive surfaces for the artificial silt (stress path series #1, #2, #3 and #4 in logarithmic scale).

Figure 18b shows that the air entry value of a soil is increased with each increment of net mean stress. The void ratio constitutive surfaces obtained by following stress paths #2, #3 and #4 in Figure 19 seem to be somewhat unusual (i.e., at 10^6 kPa soil suction and 10^4 kPa net mean stress, the void ratio is higher than that at soil suction of 0.1 kPa and net mean stress of 10^4 kPa). However, the shape of the surfaces is similar to that measured by Matyas and Radhakrishna (1968). It shows that the proposed volume-mass constitutive model can predict both collapsible and swelling behavior in soils.

The void ratio surfaces measured for the artificial silt in Figure 19 show that the stress path related to a drying process is stress path dependent and the stress path related to only wetting processes is stress path independent. The proposed volume-mass constitutive model is capable of predicting volume-mass constitutive relationships that are stress path dependent.

CONCLUSIONS AND RECOMENDATIONS
The proposed volume-mass constitutive model is capable of: 1) predicting both volume and water content at all stress states corresponding to a wide variety of stress paths; 2) taking into account the hysteretic nature of the soil-water characteristic curve; and 3) predicting both swelling and collapsible behavior of an unsaturated soil. The model can predict volume-mass constitutive relationships that are stress path dependent. The prediction results appear to be consistent with observed laboratory data.

The hysteresis model for the soil-water characteristic curve makes use of two one-dimensional pore-size distributions. The two new parameters are: the pore-shape parameter, η, and compressibility of dry pore parameter, m. It is recommended that suggested ranges for the two parameters be the focus of future research programs.

REFERENCES
Ahmed, S., Lovell, C.W., and Diamond, S. 1974. Pore size and strength of compacted clay. Journal of the Geotechnical Engineering Division, ASCE, 100(GT4): 407–425.

Al-Mukhtar, M. 1995 Macroscopic behaviour and microstructural properties of a kaolinite clay under chemical and hydraulic state. *In* Proceeding of the first international conference on unsaturated soil, France. Alonso and Delage (eds), 1995 ISBN 90 5410 5836, pp.3-9

Alonso, E. E. Gens, A. and Josa, A. 1990. A constitutive model for partially saturated soils. Geotechnique 40(3):405-430.

Alonso, E. E., Gens, A. and Gehling, W. Y. Yuk. (1994) Elastoplastic model for unsaturated expansive soils. Numerical methods in geotechnical engineering, Smith (ed.), Balkema, Rotterdam, ISBN 9054105100, pp. 11-18.

Alonso, E.E. 1993. Constitutive modelling of unsaturated soils. Unsaturated soils: Recent Developments and Applications, Civil Engineering European Courses, 86 pp.

Alonso, E.E., Lloret, A., Gens, A., and Yang, D.Q. 1995. Experimental behaviour of highly expansive double-structure clay. Proc. 1st Int. Conf. Unsaturated Soils, Paris, pp. 11-16.

Blatz, J. A. and Graham, J. 2003. Elastic-plastic modelling of unsaturated soil using results from a new triaxial test with controlled suction. Geotechnique, 53(1):113-122.

Fredlund, D. G., and Morgenstern, N. R. 1977. Stress state variables for unsaturated soils. J. Geotech. Eng. Div., ASCE (GT5), 103: 447-466.

Fredlund, D. G., and Xing, A. 1994. Equations for the Soil-Water Characteristic Curve. Canadian Geotechnical Journal, 31(3): 521-532.

Fredlund, M. 1999. The Role of Unsaturated Soil Property Functions in the Practice of Unsaturated Soil Mechanics. PhD thesis at the University of Saskatchewan, Saskatoon, Canada.

Fredlund, M.D., Fredlund D.G., and Wilson, G.W. 2000. Estimation of Volume Change Functions for Unsaturated Soils. UNSAT-ASIA, Singapore, May 18-19, pp. 663-668.

Haines, W. B. 1930. Studies in the physical properties of soils - V: The hysteresis effect in capillary properties and the modes of water distribution associated therewith. Journal of Agriculture Science, 20: 97-116.

Jommi, C. 2000. Remarks on the constitutive modelling of unsaturated soils. In Proceeding of Experimental Evident and Theoretical Approaches in Unsaturated soils, Taratino & Mancuso, Balkema, Rotterdam, ISBN 90 5809 186 4, pp. 139-153.

Karube, D. and Kawai, K. 2001. The role of pore water in the mechanical behavior of unsaturated soils, Geotechnical and Geological Engineering, Special Issue on Unsaturated Soils, 19(3): 211-241.

Kohgo, Y., Nakano, M., and Miyazaki, T. 1993. (a) Theoretical aspects of constitutive modelling for unsaturated soils; (b) Verification of the generalized elastoplastic model for unsaturated soils. Soils and Foundations, 33(4): 49-73.

Lawton, E.C., Fragaszy, R. J. and Hardcastle, I.H. 1991a. Stress ratio effects on collapse of compacted clayey sand. Journal of Geotechnical Engineering, vol. 117, No 5, p. 714-730.

Lawton, E.C., Fragaszy, R. J. and Hethrington, M.D. 1991b. Review of wetting-induced collapse in compacted soil. Journal of Soil Mechanics and Foundations. Div., ASCE, Vol. 118, No 9, p. 1376-1394.

Lloret, A., Villar, M. V., Sanchez, M., Gens, A., Pintado, X., and Alonso, E. E. 2003 Mechanical behaviour of heavily compacted bentonite under high suction changes. Geotechnique 53(1): 27-40

Matyas, E. L., and Radhakrishna, H. S. 1968. Volume change characteristics of partially saturated soils. Geotechnique, 18(4): 432-448.

Mualem, Y. 1974. A conceptual model of hysteresis. Water Resources Research, 10(3): 514-520.

Mualem, Y. 1973. Modified approach to capillary hysteresis based on a similarity hypothesis. Water Resources Research, 9(5): 1324-1331.

Néel, L. 1942. Théorie des lois d'aimantation de Lord Rayleigh, 1. Cahiers de Physique, 12: 1-20.

Néel, L. 1943. Théorie des lois d'aimantation de Lord Rayleigh, 2. Cahiers de Physique, 13: 18-30.

Pereira, J.H.F. 1996. Numerical Analysis of the Mechanical Behavior of Collapsing Earth Dams during First Reservoir Filling. Ph.D. dissertation, University of Saskatchewan, Saskatoon, 449 p.

Pham, H.Q. 2001. An engineering model of hysteresis for soil-water characteristic curves. Master of Science thesis, University of Saskatchewan, Saskatoon, Canada (183 pages).

Pham Q. H. 2005. A volume-mass constitutive model for unsaturated soils. PhD thesis dissertation, University of Saskatchewan, Canada, 404 p.

Pham, Q. H., Fredlund, D. G. and Barbour, S. Lee 2005. A study on the hysteresis models for soil-water characteristic curves. Canadian Geotechnical Journal, 42(6): 1548-1568.

Poulovassilis, A. 1962. Hysteresis of pore water - an application of the concept of independent domains, Soil Science (92): 405-412.

Sharma, R. S. 1998. Mechanical behaviour of unsaturated highly expansive clays. PhD thesis dissertation of University of Oxford, 263 pages.

Silva, Filho F.C, Almeida, M.S.S, and Futai, M.M. 2002. Critical state modelling of unstaturated soils. *In* Proceeding of the third internayion conference on unsaturated soil, Recife, Brazil, March 2002. Swets and Zeitlinger, Lisse, ISBN 90 5809 371 9, pp. 133-137.

Simms, P. H., and Yanful, E. K., 2001. Measurement and estimation of pore shrinkage and pore distribution in a clayey till during soil-water characteristic curve tests. Canadian Geotechnical Journal, 38(4): 741-754.

Sridharan, A., Altschaeffl, A.G., and Diamond, S., 1971, Pore Size Distribution Studies. Journal of Soil Mechanics and Foundation Engineering, ASCE, Vol. 97, No. SM 5, pp. 771–787.

Tamagnini, R. 2004. An extended Cam-clay model for unsaturated soils with hydraulic hysteresis. Geotechnique. 54(3):223-228.

Topp, G.C. 1971. Soil-water hysteresis: The domain theory extended to pore interaction conditions. Soil Science Society of America Proceeding, 35: 219-225.

Vu, H. Q., and Fredlund, D. G. 2004. The prediction of one, two- and three-dimensional heave in expansive soils. Canadian Geotechnical Journal, 41:1-25.

Wan, A.W.L., Gray, M.N. and Graham, J. 1995. On the relation of suction, moisture content, and soil structure in compacted clays. *In* Proceeding of the first international conference on unsaturated soil, France. Alonso and Delage (eds), 1995 ISBN 90 5410 5836, pp. 215-222.

Wheeler, S. J., and Sivakumar, V. 1995. An elasto-plastic critical state framework for unsaturated soil. Géotechnique, 45(1): 35–53.

Wheeler, S.J., Sharma, R.J., and Buisson, M.S.R. 2003. Coupling of hydraulic hysteresis and stress-strainbehaviour in unsaturated soils. Geotechnique, 53(1):41-54.

Parameter Estimation From Stepped-Irrigation Tests On Instrumented Lysimeter Test Plots

G. Gjerapic[1] and M. Wickham[1]

[1]Golder Associates Inc., Lakewood, Colorado 80228; PH (303) 980-0540; FAX (303) 895-2080; email: ggjerapic@golder.com, mwickham@golder.com

Abstract

Calibration of soil-atmosphere models to in situ measurements of suction, moisture content, and lysimeter outflow in response to atmospheric conditions can be time consuming. Calibration usually involves iterative and often arbitrary adjustment to estimated or laboratory-determined material properties until an acceptable match is achieved between predicted and measured responses to atmospheric conditions. Stepped irrigation and draindown tests on instrumented lysimeter test plots, however, can provide an improved basis for estimating bulk material properties for use in model development beyond that available from laboratory measurements or calibration to measurements during normal atmospheric responses. Irrigation tests provide, in part, information regarding the change in the volumetric moisture content $(\Delta\theta_v)$ and unsaturated hydraulic conductivity, $K(\theta_v)$. The relationship $K(\Delta\theta_v)$ can be directly measured during the test. This provides valuable information for use in calibrating a numerical model, specifically for capturing scale effects and constraining the relationship $K(\theta_v)$ where standard models (e.g., Burdine, Mualem, van Genuchten) based on a proposed soil water characteristic curve are not valid. This paper describes a stepped-irrigation test conducted on an instrumented lysimeter in a mine waste rock pile. The irrigation portion of the test was conducted for seven days at two application rates. The draindown portion was monitored for 14 days following the test. The soil-atmosphere model based on the parameters from the irrigation test achieved a closer match to the observed conditions than the model calibrated to in situ measurements alone.

Introduction

To describe movement of water in the vadose zone, one needs to determine appropriate hydraulic properties for in situ materials, namely their suction-saturation relationships and unsaturated hydraulic conductivities. Laboratory methods for measurement of the soil suction-saturation relationship are relatively well established today. Some of the available methods for determining soil-water characteristic

curves (SWCC) are standardized (e.g. ASTM D5298 and ASTM D6838) and commercially available to practicing engineers and scientists. Laboratory methods to determine the unsaturated hydraulic conductivity, however, are not common in practical engineering applications due to difficulties associated with measurement accuracy, procurement of appropriate instrumentation, time constraints, cost of the equipment, and lack of standardized procedures. In the absence of laboratory data, the unsaturated hydraulic conductivity is commonly estimated from capillary flow models (Burdine 1953, Wyllie and Gardner 1958, Mualem 1976, van Genuchten, 1978, 1980). These models represent the porous matrix as an assembly of capillary tubes with different radii, each capillary radius corresponding to an appropriate suction (capillary rise) as determined from the soil-water characteristic curve. Assuming homogeneous soil conditions, the unsaturated hydraulic conductivity is determined by adding the flow contributions from the smallest to the largest capillaries that still remain saturated at a specific suction level. Capillary models are typically used to determine relative hydraulic conductivities defined as the ratio between the unsaturated hydraulic conductivity and the corresponding saturated conductivity value.

Laboratory measurements often fail to produce SWCC, $\theta(h_c)$, and unsaturated hydraulic conductivity, $K(h_c)$, relationships representative of field conditions. Thus, the laboratory-determined hydraulic parameters are often adjusted to account for differences between the laboratory and in situ material properties when implementing numerical models [e.g. Bouwer and Rice (1984) and Hendrickx et al. (1991)]. Calibration of numerical models to field measurements (e.g. suction, moisture content, lysimeters outflow) provides yet another basis for adjustments to laboratory-determined properties. In addition, calibration of numerical models can be used to independently develop suction-saturation and unsaturated hydraulic conductivity functions for specific field conditions. When infiltration and percolation are the processes of interest, calibration usually involves iterative and often arbitrary adjustment to estimated or laboratory-determined material properties until an acceptable match is achieved between predicted and measured in situ responses to atmospheric conditions. However, the calibration process is time consuming and can yield non-unique solutions or fail to reproduce an acceptable and convincing match to field conditions. Constraining the calibration with a well-controlled stepped irrigation and draindown test can expedite calibration and improve results.

For example, an initial set of one-dimensional soil-atmosphere models was constructed for an instrumented mine waste rock pile lysimeter using the material parameters displayed in Table 1. The SWCC parameters in Table 1 were derived from laboratory determined SWCC displayed in Figure 1. A comparison between the modeled and the measured lysimeter outflows is displayed on Figure 2. The initial condition for all soil-atmosphere models was the suction profile determined from the suction sensors within the lysimeter. The computer code UNSAT-H (Fayer, 2000) was used for all model simulations.

Table 1. Hydraulic properties based on measured laboratory data

Sample	Saturated vol. water content θ_{sat} (-)	Residual vol. water content θ_r (-)	van Genuchten parameters		Saturated conductivity $Ksat$ (cm/s)
			α_t (1/kPa)	n_t (-)	
WR-1	0.295	0.035	1.96	1.231	6.6E-02
WR-2	0.225	0	7	1.167	2.5E-02
WR-3	0.33	0.033	8.5	1.394	1.0E-03
WR-4	0.235	0	3	1.145	6.3E-02
WR-5	0.431	0.056	3.92	1.917	1.1
WR-6	0.343	0.041	2.94	1.8	4.0E-01

The initial set of model runs used the Mualem (1976) conductivity model to estimate the unsaturated hydraulic conductivity (see van Genuchten, 1978, 1980):

$$K(h_c) = K_{sat} \frac{\left\{1 - \left[1 - \left(1 + \left(\alpha_k \cdot h_c\right)^{n_k}\right)^{-1}\right]^{m_k}\right\}^2}{\left[1 + \left(\alpha_k \cdot h_c\right)^{n_k}\right]^{\frac{m_k}{2}}}, \quad m_k = 1 - \frac{1}{n_k} \quad (1)$$

with the corresponding suction-saturation relationship:

$$\theta = \theta_r + \left(\theta_{sat} - \theta_r\right)\left(1 + \left(\alpha_t \cdot h_c\right)^{n_t}\right)^{-m_t}, \quad m_t = 1 - \frac{1}{n_t} \quad . \quad (2)$$
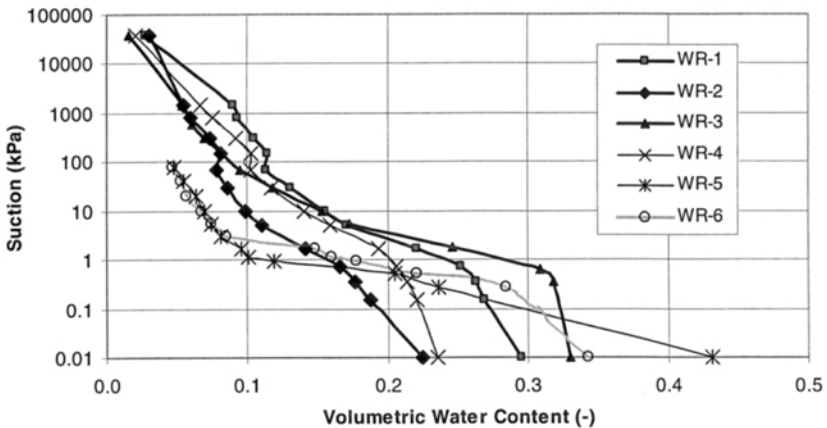
Figure 1. Laboratory determined SWCC

One should note that all initial soil-atmosphere models used a conventional van Genuchten model with the SWCC parameters, α_t and n_t, determining $K(h_c)$ relationship, i.e. $\alpha_k = \alpha_t$ and $n_k = n_t$.

The initial model runs failed to match both the seasonal lysimeter outflow and the magnitude of outflow for individual rain events even after significant calibration by varying hydraulic parameters in Table 1. Some of the calibration problems were ascribed to 1) uncertainties regarding snowmelt rates and volumes, and 2) the possible presence of preferential flow paths, resulting in a dual flow regime within the lysimeter (Smith et al., 1995).
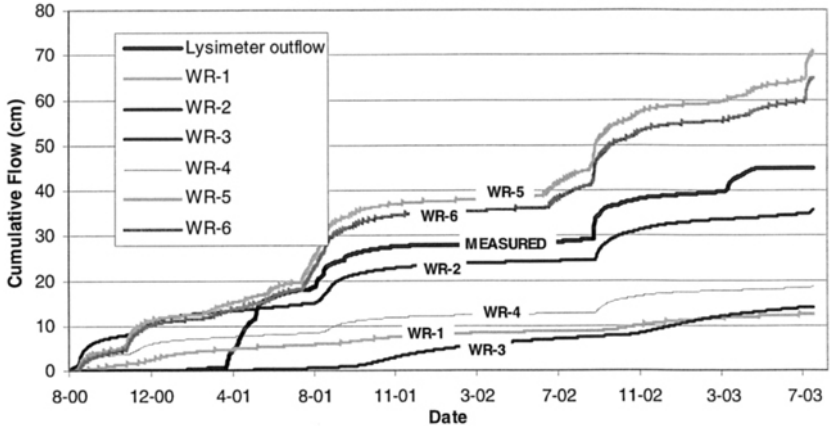
Figure 2. Initial model runs

To further investigate applicability of a one-dimensional soil-atmosphere model and to aid in model calibration, a well-controlled stepped irrigation and draindown test was conducted on a waste rock pile lysimeter. This paper describes the various aspects of the test and the subsequent methodology to estimate and test the unsaturated hydraulic conductivity parameters.

Test Approach and Methodology

The objectives of the irrigation test were to 1) encompass the range of moisture and suction conditions to be expected under atmospheric conditions, 2) provide controlled and measurable surface conditions (e.g. irrigation rate and evaporation), 3) minimize ponding and runoff, and 4) achieve near steady-state hydraulic responses. A stepped irrigation test was designed to allow for direct measurement of $\Delta\theta_v$ and unsaturated hydraulic conductivity $K(\theta_v)$. The test approach supplemented existing instrumentation for the test plot (meteorological monitoring, suction sensors, and barrel lysimeter) with additional equipment for the irrigation test.

The lysimeter was irrigated using a rotor sprinkler Rainbird 5000. Before the test, two types of sprinkler heads, spray and rotor, were tested to ensure that the irrigation rates on the order of 10^{-5} to 10^{-4} cm/sec could be sustained. The rotor sprinkler was chosen for two reasons:

1) *Superior performance with respect to the wind action;* the effective radius of the rotor sprinkler is more than twice the irrigation radius of the pop-up spray head. Therefore, the rotor sprinkler was chosen over the spray head because the irrigated area is less likely to shift under the strong wind conditions expected at the site.

2) *Flexibility in adjusting the irrigation rate.* Even though both rotor and spray heads can vary the irrigation rate by adjusting the spray arc, the variable nozzle sizes available for the rotor sprinkler provide for a larger range of watering rates.

The water for the sprinkler was supplied from a 1,700-gallon polyethylene tank during the test. In addition, two collapsible 1,500-gallon tanks were used for re-filling the 1,700-gallon supply tank. A water truck was used to replenish the water in the collapsible tanks. Water was transferred from the collapsible tanks to the 1,700-gallon tank as needed using a ¼-horsepower sump pump with a ball-float switch.

In order to provide a constant pressure to the sprinkler head, a ½-horsepower centrifugal pump was installed between the water tank and the rotor sprinkler. The water flow and pressure supplied by the pump were monitored with a flow meter and pressure gage. The irrigation rate was measured using a tipping bucket gage TE525WS.

The lysimeter outflow was directed to an adjacent manhole instrumented with the tipping bucket gage TE525WS. In addition, the lysimeter effluent was collected in a plastic container, and a sump pump was used to extract the collected effluent from the manhole. The volume of the effluent pumped from the manhole was recorded before disposal to provide an independent measurement of the tipping bucket gage readings. Both tipping bucket gages were recorded automatically using data loggers. A five gallon plastic bucket filled with water was used to monitor daily evaporation rates. Mechanical and electrical equipment used during the test is summarized in the following table:

Table 2   Electrical and mechanical equipment used for irrigation test

Equipment	Purpose
Jacuzzi 5CY ½ HP Cyclone Jet Pump (model 91020050) w/ Float Switch Quantity : 1	Provided positive pressure for the Rainbird 5000 rotor sprinkler
Hydromatic ¼ HP W/D/V-A1 Sump Pump w/ Ball Float Switch Quantity: 2	Extracted water from the manhole (1). Transferred water from the collapsible tanks to 1,700-gallon supply tank (1).
Dwyer 0-100 psi (g100) Liquid Filled Pressure Gage Quantity: 1	Measured hydrostatic pressure supplied to the Rainbird 5000 sprinkler head.
Blue-White Industries Digi-Flo F-1000-RB Flow Rate Meter Quantity: 1	Measured sprinkler head flow rate (water loss from the supply tank).
Texas Electronics TE525WS Rain Gage Quantity: 2	Measured irrigation rate (1). Measured lysimeter outflow (1).

The stepped irrigation test commenced on September 29, 2003 at 1700 hours. The initial effective irrigation rate was 3.5 x 10^{-5} cm/sec averaged over a 66-hour period (Table 3). The sum of effective irrigation and precipitation in Table 3 denotes total applied water corrected for evaporative losses. Prior to the start of the test, the lysimeter outflow was measured at approximately 4.9 x 10^{-7} cm/sec, which remained unchanged until September 30 at approximately 0700 hours. From September 30 at 7:00 a.m. to October 1 at approximately 0600 hours the lysimeter outflow gradually increased from 4.9 x 10^{-7} cm/sec to 3.5 x 10^{-5} cm/sec approaching steady-state conditions. The measured outflow rate reached the measured inflow rate on October 1 at approximately 0600 hours, approximately 37 hours after the test was initiated. A steady-state condition was maintained from October 1 at 0600 hours to October 2 at 0400 hours as illustrated by identical slopes of the inflow and outflow curves shown on Figure 3.

A rain event starting on October 2 at approximately 0400 hours increased the lysimeter outflow without notable increase in water storage. On October 2 at 1100 hours, about 66 hours since the test inception, the irrigation rate was increased from 3.5 x 10^{-5} cm/sec to 1.2 x 10^{-4} cm/sec, an increase by a factor of approximately 3.4. Steady-state conditions were attained approximately seven hours after the rate increase at approximately 1800 hours. The irrigation test was terminated on October 2 at 2030 hours.

Table 3 provides a more detailed summary of the quantities measured during the irrigation test.

Table 3   Irrigation test time-table and water budget

Elapsed Time (hrs)	Effective* Irrigation + Precip (cm/sec)	Lysimeter Outflow (cm/sec)	Cumulative Inflow Q_{in} (cm)	Cumulative Outflow Q_{out} (cm)	Storage Change (cm)	Storage Change (θ_v)
-	-	4.9 x 10^{-7}			-	
Start low irrigation rate of q=3.5 x 10^{-5} cm/sec						
14	3.7 x 10^{-5}	4.9 x 10^{-7}	1.9	0.02	1.9	0.8%
37	3.4 x 10^{-5}	< 3.5 x 10^{-5}	4.5	1.1	3.4	1.4%
59	3.3 x 10^{-5}	3.4 x 10^{-5}	7.1	3.8	3.3	1.4%
66	3.5 x 10^{-5}	≈ 5 x 10^{-5}	8.2	5.1	3.1	1.3%
Start high irrigation rate of q=1.2 x 10^{-4} cm/sec						
73	1.1 x 10^{-4}	<1.2 x 10^{-4}	10.9	6.9	4.0	1.7%
76	1.2 x 10^{-4}	1.2 x 10^{-4}	12.2	8.2	4.0	1.7%

* Effective irrigation and precipitation rates are average values from start of new irrigation rate
Measured average daily evaporation varied from approximately 4 to 4.6 mm/day;
θ_v is the volumetric moisture content change.

Interpretation

Test interpretation relies on the generalized Darcy's law for the water flux:

$$q = -K(\theta_v)\frac{\partial H}{\partial z} = K(\theta_v)\left[\frac{\partial h_c}{\partial z} + 1\right],\qquad\qquad (3)$$

where K denotes unsaturated hydraulic conductivity, The term θ_v denotes volumetric moisture content, H represents hydraulic head, h_c is suction head, and z represents downward vertical coordinate (note that $H=-h_c-z$). The purpose of the irrigation test is to establish steady-state conditions where total lysimeter inflow equals outflow from the lysimeter. For a specific range of inflow rates, it is possible to establish a unit gradient condition for which $q = K(\theta_v)$ (see Equation 3), thus implying a uniform moisture content profile throughout most of the lysimeter. Theoretically, for a steady-state condition with the constant inflow at the top and a unit gradient condition at the bottom boundary, all points within a homogeneous vertical soil column will have the same moisture content. Consequently, one can determine the unsaturated hydraulic conductivity as a function of a change in the average volumetric water content, $K(\Delta\theta_v)$, by simply monitoring general water balance components such as net inflow, net outflow, and change in the water storage for two consecutive stages with unit gradient conditions:

$$\Delta\theta_v\ L = \Delta Storage = Q_{in} - Q_{out}. \tag{4}$$

In our analysis, Q_{in}, represents contribution of the effective irrigation and precipitation (total applied water corrected for evaporative losses) and Q_{out} denotes lysimeter outflow. Cumulative values for the water balance quantities are shown on Figure 3.
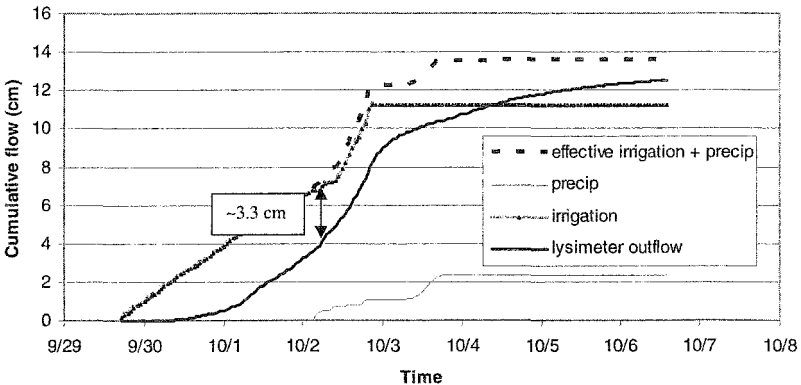
Figure 3. Measured cumulative outflows

Figure 3 displays a relatively rapid response to net infiltration during the irrigation suggesting that a significant portion of the flow at higher flow rates is conducted through "macro-pores" or preferential flow features. In addition, the measured draindown following the irrigation phase of the test is characterized by a rapid decrease in the lysimeter outflow at flow rates in excess of 5.0×10^{-5} cm/sec. However, both the irrigation and the draindown portions of the test (Figure 8) indicate the existence of the typical porous-type behavior for flow rates below about 5.0×10^{-5} cm/sec.

Figure 3 demonstrates that the measured outflow rate from the lysimeter reached the effective initial irrigation rate on October 1 at approximately 0600 hours, about 37 hours after the test was initiated. A comparison of the cumulative irrigation and the cumulative lysimeter outflow curves shows an increase in water storage within the lysimeter of approximately 3.3 cm during the initial transient period. For a lysimeter height of 94 inches (2.39 m), the corresponding increase in the "average" volumetric moisture content is approximately 1.4 % (Table 3).

Steady-state conditions for the second irrigation rate of 1.2×10^{-4} cm/sec were attained on October 2 at 1800, approximately seven hours after the rate increase. The additional change in storage from this higher irrigation rate was estimated to 0.9 cm. The storage change of 0.9 cm represents an increase in the "average" volumetric moisture content of 0.38% from the steady-state condition for the initial rate. The total change in moisture content was 4 cm, or about 1.7% change in the volumetric moisture content compared to conditions at the start of the test (Table 3).

The measured steady-state values from both applied irrigation rates (Table 3) were utilized to determine the $K(\Delta\theta_v)$ relationship assuming unit gradient conditions, the assumption supported by the suction sensor readings. The first steady-state $K(\Delta\theta_v)$ value is equal to the initial effective irrigation rate of approximately 3.4×10^{-5} cm/sec. The corresponding change in the moisture content, $\Delta\theta_v$, was 1.4%. Similarly, the second steady-state $K(\Delta\theta_v)$ value is the same as the effective irrigation rate of 1.2×10^{-4} cm/sec with a corresponding change in volumetric moisture content, $\Delta\theta_v$, of 1.7%. The measured $K(\Delta\theta_v)$ relationship is shown graphically on Figure 4.
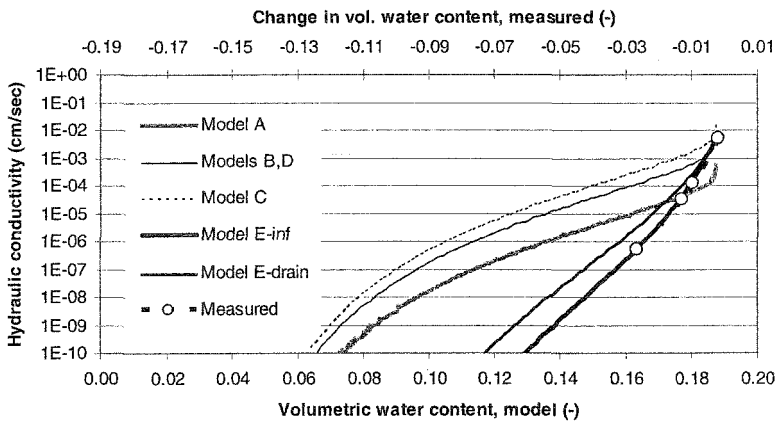
Figure 4. Model $K(h_c)$ curves and measured $K(\Delta\theta_v)$ values

The $K(\Delta\theta_v)$ information was used to calibrate a numerical model, specifically for constraining the bulk $K(\theta_v)$ relationship where standard models (e.g. Burdine [1953], Mualem [1976], van Genuchten [1978, 1980]) based on the proposed soil water characteristic curve were deemed invalid (Model E on Figure 4).

To expand the interpretation of the irrigation test results and test the interpretation of the measured $K(\Delta\theta_v)$ relationship, limited numerical modeling was performed. The draindown portion of the test was simulated using a numerical soil-atmosphere model. The model code used was UNSAT-H (Fayer, 2000) with the SWCC derived from the laboratory SWCC for the waste rock material WR-2 shown on Figure 1.

Numerical modeling

The SWCC that was initially adopted for numerical modeling was based on the laboratory data for WR-2 shown on Figure 1. Motivated by the model results on Figure 2, the initial WR-2 parameters were slightly altered as shown in tables 4 and 5. These modified WR-2 parameters were used for simulations A, B, C and D. However, the modified WR-2 suction-saturation relationship could not account for the observed changes in $K(\Delta\theta_v)$ during the irrigation test. Hence, the SWCC for simulation E was slightly altered as shown in Table 4.

Table 4   SWCC used for modeling stepped irrigation and drainage tests

Model	α (1/cm)	n -	θ_{sat} (cm^3/cm^3)	θ_r (cm^3/cm^3)
A, B, C, D	0.125	1.34	0.187	0.041
E	0.125	1.20	0.187	0.041

Both suction-saturation curves used to model the stepped irrigation and drainage tests are displayed on Figure 5.
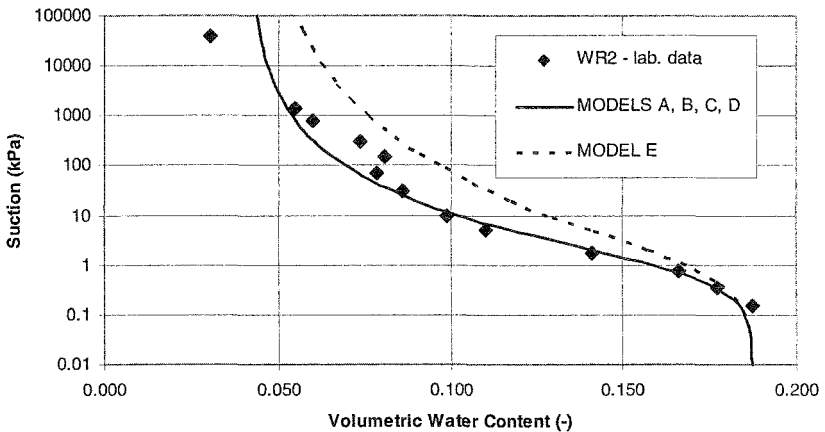
Figure 5. Model SWCC

Simulations A, B, C and D used a range of saturated hydraulic conductivity values to investigate model sensitivity. Different initial conditions were also used since the suction sensors readings are not reliable at low suction. The values for saturated hydraulic conductivities and initial suctions are listed in Table 5.

Table 5   Model Simulations

Model	K_{sat} (cm/s)	Initial flow rate** (cm/s)	Initial suction** (cm)
A	5.0×10^{-4}	4.9×10^{-7}	32.426
B	5.0×10^{-3}	4.9×10^{-7}	76.077
C	5.0×10^{-3}	4.9×10^{-6}	32.426
D	1.5×10^{-2}	1.5×10^{-5}	32.426
E*	5.0×10^{-3}	4.9×10^{-7}	14.205

*   modified hydraulic properties
**   initial conditions before start of irrigation test

Simulation E relied on a modified $K(\Delta\theta_v)$ relationship developed from the interpretation of the irrigation test to estimate the $K(\theta_v)$ relationship. The $K(\theta_v)$ relationship for all other scenarios were computed using the standard Mualem model (1976), i.e. using $\alpha_k = \alpha_t$ and $n_k = n_t$ in Equation (1). Each $K(\theta_v)$ relationship is shown graphically on Figure 4. It is clear that the slope of the measured function from the test is steeper than that computed by the Mualem method, likely due to the presence of larger pores and existence of preferential flow paths.

Draindown conditions were modeled separately for Simulation E using a separate $K(\theta_v)$ relationship (Figure 4). All draindown simulations used the initial suction profile as calculated from the corresponding irrigation runs at the maximum outflow rate. A comparison between the measured and the calculated values are shown on Figures 6, 7 and 8. Model results on Figure 6 display cumulative flow during the irrigation portion of the test. The cumulative outflow during the draindown portion following the cessation of irrigation is shown on Figure 7. A comparison between the measured and predicted flow rates for the draindown portion is displayed on Figure 8.
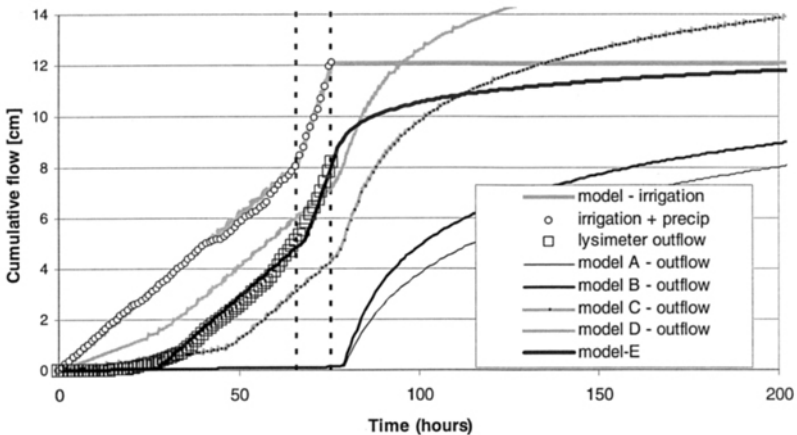
Figure 6. Stepped irrigation test – measurements and model predictions
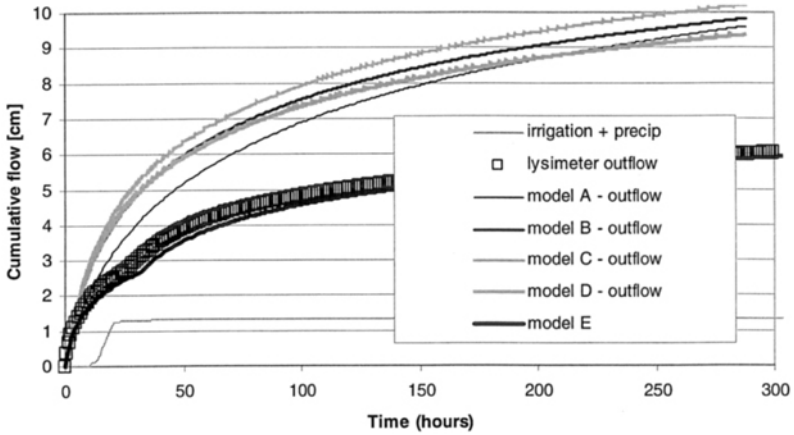
Figure 7.   Lysimeter draindown – measured and model predicted outflow
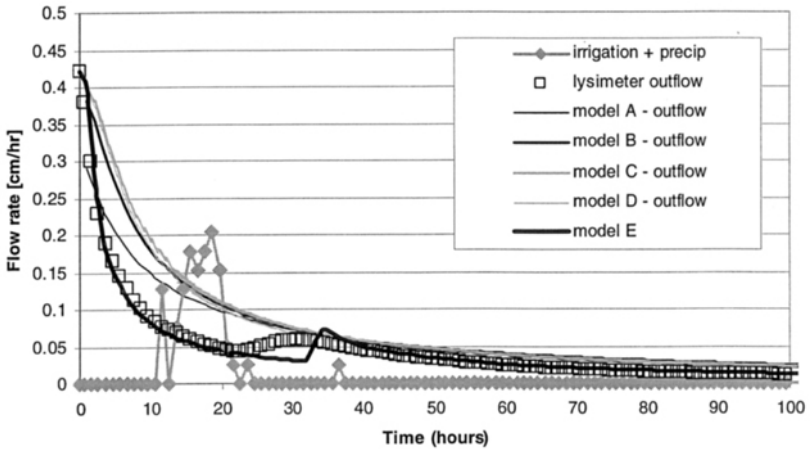
Figure 8.   Lysimeter draindown – measured and predicted flow rates

Conclusions

When a stepped irrigation test is used to independently evaluate the unsaturated hydraulic conductivity curve, model predictions are improved.

The following observations are offered based on the modeling results:

- A delay time of only 14 hours between the start of the test and the increased lysimeter outflow, as compared to models A and B, indicates existence of macropores. In addition, the approximately linear increase of the lysimeter outflow in

the early stages of the test supports the assumption of preferential flow paths of relatively uniform diameter throughout the soil column.

- Relatively large increases in the hydraulic conductivity for small increases in saturation, as observed during the infiltration test, are typical for the coarse grain material behavior. Therefore, for infiltration rates in excess of approximately 1 x 10^{-5} cm/sec, one can assume that the porous flow through the lysimeter is dominated by the interconnected network of macro-pore conduits.
- A relatively fast response to draindown conditions is an indication of the effective saturated hydraulic conductivity values larger than 1 x 10^{-3} cm/sec. Preliminary results indicate the effective saturated hydraulic conductivity for the waste rock pile lysimeter is on the order of 5 x 10^{-3} cm/sec or greater.
- In order to account for the existence of macro-pores in numerical modeling, the appropriate adjustments of the hydraulic properties are necessary as illustrated by model E. The semi-empirical approach for developing $K(\theta_v)$ relationship is likely to result in better predictive abilities since the hydraulic parameters are calibrated from the observed response curves rather than using the predetermined theoretical model relationships that may or may not be applicable to the problem at hand.

References

Bouwer, H. and Rice, R.C. (1984). *"Effects of stones on hydraulic properties of vadose zones"*, ASAE Winter Meeting, New Orleans, LA, Paper No. 84-2515, 11 pp.

Burdine, N.T. (1953). *"Relative Permeability Calculations from Pore-Size Distribution Data"*, Transactions AIME, Vol. 198, pp. 71-78.

Fayer, M. (2000). *"UNSAT-H Version 3.0: Unsaturated Soil Water and Heat Flow Model – Theory, User Manual, and Examples"*, Report No. PNNL-13249, Pacific Northwest National Laboratory, Richland, WA, USA.

Hendrickx, J.M.H., Khan, A.S., Bannink, M.H., Birch, D. and Kidd, C. (1991). *"Numerical analysis of groundwater recharge through stony soils using limited data"*, Journal of Hydrology, No. 127, Elsevier Science Publishers B.V., Amsterdam, pp. 173-192.

Mualem Y. (1976). *"A new model for predicting the hydraulic conductivity of unsaturated porous media."* Water Resour. Res. 12(3):513-522.

Smith, L., D.L. Lopez, R. Beckie, K. Morin and R. Dawson. (1995). *"Hydrogeology of Waste Rock Dumps"*, Final Report to Natural resources Canada, Contract No. 23440-4-1317/01-SQ. Available as an associated report through the Mine Environmental Drainage (MEND) Program.

van Genuchten R. (1978). *"Calculating the unsaturated hydraulic conductivity with a new closed-form analytical model."* Water Resources Program, Department of Civil Engineering, Princeton University, Princeton, New Jersey.

van Genuchten, M.T. (1980). *"A closed-form equation for predicting the hydraulic conductivity of unsaturated soils"*, Soil Sci. Soc. Am. J., 44: 892-898.

Wyllie, M.R.J. and Gardner, G.H.F. (1958).*"The generalized Kozeny-Carman equation I. A novel approach to problems of fluid flow"*, World Oil Prod. Sect., March, pp. 121-128.

Field Determination of Saturated and Unsaturated Hydraulic Conductivities Using the IP Method

J. L. Peace, Ph.D.,[1] P. Bandini, Ph.D., M.ASCE,[2]
and Z. A. Samani, Ph.D., P.E., M.ASCE[3]

[1] Principal Member of Technical Staff, Geophysics Department, Sandia National Laboratories, Box 5800; MS-0750; Albuquerque, NM 87185-0750; E-mail: jlpeace@sandia.gov

[2] Assistant Professor, Civil Engineering Department, New Mexico State University, P.O. Box 30001, MSC 3CE, Las Cruces, NM 88003-8001; Ph: (505) 646-2471; Fax: (505) 646-6049; E-mail: paola@nmsu.edu

[3] Professor, Civil Engineering Department., New Mexico State University, Las Cruces, NM 88003-8001; E-mail: zsamani@nmsu.edu

Abstract

An instantaneous profile (IP) test was conducted at Sandia National Laboratories, Albuquerque, New Mexico. The IP method was used to determine the field-saturated and unsaturated hydraulic conductivities of a natural soil profile. The soil profile was instrumented with two neutron probe access tubes and three clusters of paired tensiometers and time domain reflectometry (TDR) probes. The soil profile was flooded for a period of 48 hours. Flooding was discontinued when the soil was field-saturated. Neutron probe and tensiometer data were acquired on a continual basis for 890 days and 200 days, respectively. As the soil profile was allowed to drain, soil moisture and suction data were recorded throughout the soil profile. These data from the IP test were used to calculate the unsaturated hydraulic conductivity as a function of the volumetric moisture content of the soil profile. The curves representing hydraulic head, H, change with depth, z, exhibit a clear change in slope between 90 cm and 120 cm due to a caliche layer. Values of hydraulic conductivity were calculated from the slope of the $\partial H/\partial z$ curves corresponding to a given depth and time. The hydraulic conductivity of the soil profile is represented by a family of curves that represent the variations in soil characteristics within this soil profile.

Introduction

The determination of field-saturated and unsaturated hydraulic conductivities representative of the field conditions is of great importance in a variety of

engineering applications, including the design of clay liners, landfill covers, irrigation systems, contaminant flow, etc. Several direct and indirect methods have been described in the literature for *in situ* measurements of unsaturated hydraulic conductivity. The instantaneous profile (IP) test and the gypsum crust methods provide good results in terms of accuracy, but their cost is high (ASTM D 5126-90). Field tests are preferred over laboratory tests (Jaynes and Tyler 1980) and other indirect methods, as field tests provide direct measurements of the unsaturated hydraulic conductivity of soils on a realistic scale.

This paper describes the implementation and results of the IP test method on a natural soil profile. Field hydraulic conductivity data from this study were obtained to be used, together with additional laboratory data, in the development of the constitutive principles that govern the dynamics of unsaturated flow and water percolation through the natural soil profile for the design of vegetative soil covers for waste disposal in arid and semi-arid regions. The use of these site-specific parameters for model input reduces the level of uncertainty in the analyses compared to the use of empirical values from the literature.

Field Test Area

An IP test was conducted in Technical Area 3 (TA-3) at Sandia National Laboratories (SNL). SNL is located within the boundaries of Kirtland Air Force Base (KAFB), south of Albuquerque, New Mexico. Course-grained sediments dominate the shallow vadose zone in TA-3. Soils in the study area are very fine sandy loam according to the U.S. Department of Agriculture soil classification and silty sand (SM and and SC-SM) according to the Unified Soil Classification System (ASTM D2487). The soil in this site is mainly nonplastic. The dry unit weight of the soil ranges from 16.7 kN/m^3 to 18.9 kN/m^3 (106 to 120 lb/ft^3). The elevation of the study area is 1,640.1 m (5,381 ft) above sea level.

Instantaneous Profile Test

The IP method of Watson (1966) for field-determination of the unsaturated hydraulic conductivity of soil requires the construction of a soil profile that allows free vertical drainage of water. This technique is not applicable where significant lateral movement of water occurs. In the IP technique, frequent and simultaneous measurement of soil wetness and suction are made under conditions of free drainage. From these measurements, one can determine instantaneous values of the potential gradients and fluxes operating within the profile which are used to calculate the hydraulic conductivity of the soil.

Instantaneous Profile Test Site

An IP test site was constructed in the north-central portion of TA-3 at SNL to obtain site-specific, soil hydraulic parameters representative of the natural soil profile. Trenches were excavated around an undisturbed soil profile of 4.9 m x 4.9 m (16 ft x 16 ft) in area. The 31-cm(1-ft)-wide trenches were excavated to a depth of 1.8 m

(6 ft) and filled with a 10% bentonite-soil slurry. At the ground surface, a concrete retaining wall, 31-cm (1-ft)-high, was formed around the perimeter of the soil profile to allow for ponding of water.

The soil profile was instrumented with two neutron probe access tubes, three clusters of paired tensiometers and TDR probes (Figure 1). The neutron probe access tubes consisted of Schedule 80 PVC pipe with 5.1 cm (2 in.) inside diameter, installed to a depth of 2.74 m (9 ft). Each of the three instrument clusters, A, B, and C, contained tensiometers and TDR probes that were installed at depths of 30, 61, 91, 122, 152, and 180 cm (1, 2, 3, 4, 5, and 6 ft). Depths (ft) are indicated in Figure 1 next to the instrument location. Two additional neutron probe access tubes were installed outside the perimeter of the soil profile and close to the wall to determine if any leakage had occurred through the bentonite-soil barrier.
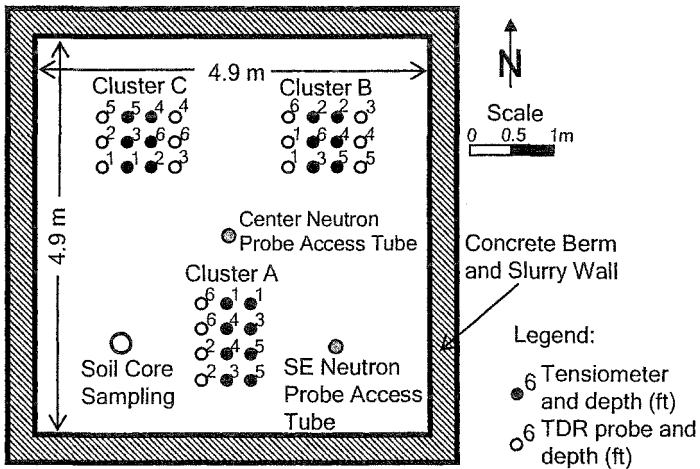
Figure 1. Schematic of the IP test site. Numbers indicate depth of instrument (ft)

All instrumentation was calibrated in the field or in the lababoratory before installation and operation. After installation, the instrumentation was tested for continuity and allowed to equilibrate with the soil profile. Tensiometers and TDR probes were multiplexed to a Campbell Scientific CR7 electronic data logger. Baseline neutron probe and tensiometer data within the soil profile were obtained before the test was initiated. Neutron probe data were recorded manually as counts of thermalized neutrons using a CPN Model 503DR neutron probe. Counts were obtained over 64 seconds at successive 31-cm (1-ft) intervals to 2.74 m (9 ft) in depth. Thermalized neutron counts were converted to volumetric moisture content using a soil calibration curve. Tensiometer data were obtained using Soil Moisture Systems, Inc. 1-bar porous cup tensiometers equipped with pressure transducers.

Instantaneous Profile Test—Flooding Phase. The soil profile was flooded with 20,845 lt (5,500 gal) of water over a period of 48 hours. Flow was monitored electronically with an EG&G flow meter. The pressure head within the concrete retaining wall was maintained at 5.1 cm (2 in.) during flooding. Flooding was discontinued once the instrumentation indicated that the 1.8-m (6-ft) of soil profile was field-saturated.

The advance of the wetting front was monitored with the neutron probe, tensiometers, and TDR probes. The wetting front moved quite rapidly through the soil profile due to redistribution of water within the profile. Over time, the wetting front slowed as the suction gradients diminished and the hydraulic conductivity of the soil increased. As the suction gradient decreased and the hydraulic conductivity increased, the flux diminished even more rapidly and the advance of the wetting front gradually dissipated.

The advance of the wetting front as recorded by the neutron probe in the center access tube is shown in Figure 2. Each curve in Figure 2 represents the moisture content at the depth indicated. Time in days is shown as negative because Day 0 represents the time, t_o, when flooding was discontinued and drainage of the soil profile was initiated. The data at 2.13 m, 2.44 m and 2.74 m (7, 8, and 9 ft) were measured below the depth of the bentonite-soil barrier and, therefore, the advance of the wetting front at these depths is more diffuse due to lateral flow.
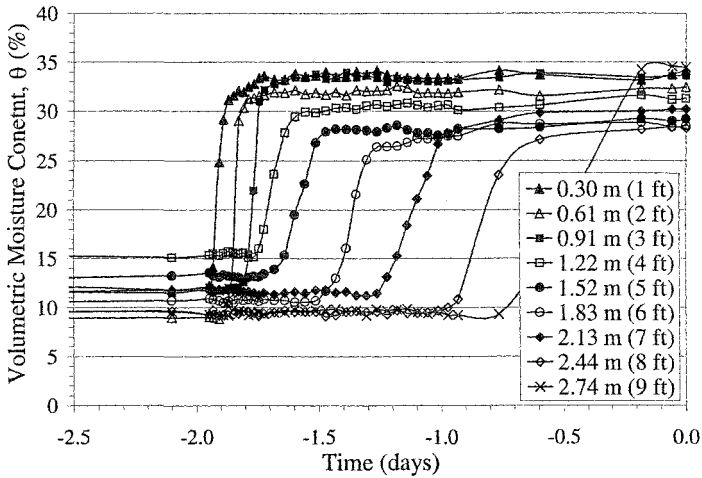
Figure 2. Advance of the wetting front at the center neutron probe access tube during flooding phase

Instantaneous Profile Test—Drainage Phase. When the IP test site instrumentation confirmed that the 1.8-m (6-ft)-thick soil profile was field-saturated (*i.e.*, the water

pressure reaches a value equal to, or greater than, the atmospheric pressure) and had attained steady-state conditions, flooding was discontinued and the soil profile was allowed to drain. (In the field, soil rarely attains complete saturation as some air remains within the soil matrix). The soil surface was covered with an opaque blue tarp to minimize soil heating and prevent evaporation. As the soil profile drained, data was obtained on the distribution of soil moisture and suction throughout the soil profile. Neutron probe data (volumetric moisture content) were acquired manually every hour for the first 32 hours of the test with the neutron probe and then every 4 hours for the next 48 hours. Thereafter, the frequency of moisture readings was decreased to one reading every 8 hours, every 12 hours, daily, weekly, and then monthly, as the rate of drainage decreased.

Collection of tensiometer data was computer controlled, allowing for more rapid data acquisition. Tensiometer data (suction) was acquired automatically with the Campbell CR7 data logger every 10 minutes for the first 32 hours of the test and then every 30 minutes for the next 70 hours. Thereafter, the frequency of tensiometer data acquisition was decreased to hourly and then twice daily. Neutron probe data were acquired on a continual basis for 890 days whereas tensiometer data was obtained on a continual basis for 200 days.

The neutron probe provided consistent data precision and reliable results throughout the entire range of moisture content in the soil profile. Tensiometer measurements were limited to values below 1 atm (1 bar); however, in the field, the useful limit of most tensiometers is approximately 0.85 atm. Although the suction range of 0 to 0.85 atm covers a minor part of the wider range of suction one could possibly encounter in the field, it actually encompasses a major part of the soil profile wetness range.

On the other hand, the tensiometers proved problematic during the IP test despite considerable instrumentation planning and care. A few tensiometers failed or operated intermittently as the test progressed. Very few tensiometers were operational beyond 200 days into the test. As a result, suction measurements were discontinued at 200 days. The TDR probes proved completely unreliable during this test. Therefore, TDR data were eliminated from consideration in this study.

Data Conditioning

Neutron probe and tensiometer data were evaluated for errors in data acquisition and instrument failure. All data were converted to appropriate units of volumetric moisture content, θ, or suction, Ψ. Suction describes the water pressure difference from atmospheric pressure. When the water pressure is equal to, or greater than, the atmospheric pressure, the soil profile is field-saturated. When the water pressure is less than the atmospheric pressure, the soil profile is unsaturated.

Volumetric moisture content and suction as function of time, $\theta(t)$ and $\Psi(t)$, were conditioned (e.g., smoothed) using Butterworth digital filters (Stearns 1975). Conditioned data were then fitted mathematically with low-order polynomials to obtain numerical arrays for determining the hydraulic properties of the soil profile.

Hydraulic Conductivity Function—Application

Moisture content data from the center neutron probe access tube is shown in Figure 3. The moisture content within the soil profile decreases rapidly during the first 60 days of drainage. Rapid initial drainage reflects much higher hydraulic conductivity at field-saturated and near-field-saturated conditions. Beyond 60 days, drainage decreases significantly with time, becoming near-asymptotic as one approaches 330 days. The section within the soil profile was found to increase rapidly during the first 10 days of drainage. The significant decrease in drainage with time observed during the drainage phase implying a simultaneous increase in suction and decrease in hydraulic conductivity.
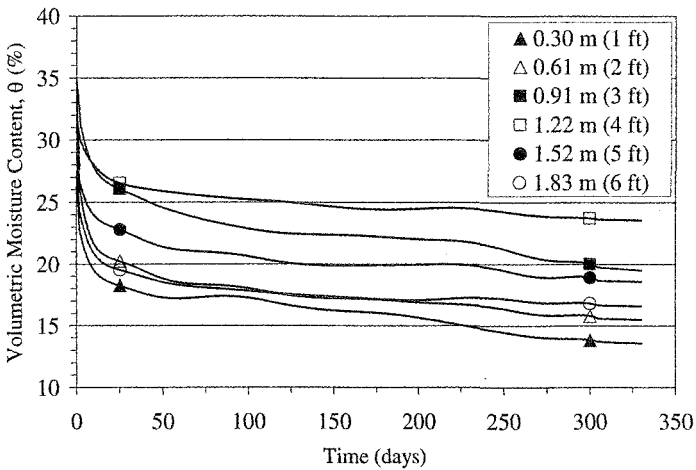
Figure 3. Volumetric moisture content recorded at the center neutron probe access tube during the drainage phase

Suction and volumetric moisture content data from the IP test were analyzed using the IP test method discussed by Hillel et al. (1972) to determine the unsaturated hydraulic conductivity, K, as function of volumetric moisture content, θ. This relationship was calculated at 30-cm (1-ft) intervals to 183 cm (6 ft) in depth for the center and southeast (SE) neutron probe access tubes by pairing volumetric moisture content data with suction data from tensiometer clusters A, B, and C. Data from days 1, 2, 4, 8, 16, 32, and 64 were analyzed to obtain specific points on the $K(\theta)$ curves.

Calculation of Hydraulic Conductivity Function

The flow rate (flux), Q, through each depth interval is calculated by integrating the moisture-time (θ, t) curves (Figure 3) with respect to depth, z. The slopes ($\partial\theta/\partial t$) of the moisture curves are determined at days 1, 2, 4, 8, 16, 32, and 64 using linear and polynomial regressions. These slopes are then multiplied by their respective depth increment, dZ, to obtain the per-layer rate of water content change, $dZ(\partial\theta/\partial t)$. The

flux, Q, through the bottom of each depth increment is obtained by accumulating the moisture content of each successive layer overlying that depth, *i.e.*, $Q = dZ(\partial\theta/\partial t)$. These data are presented in Table 1.

From suction data, the hydraulic (total) head, H, corresponding to the times for which the above flux values were calculated, is obtained by adding the depth of each tensiometer in clusters A, B, and C to their corresponding elevation head value. It was noted that the curves of hydraulic head change with depth ($\partial H/\partial z$) during drainage exhibit a distinct change in slope between the lower and upper halfs of the profiles. The slope change occurs at a depth of 90 cm to 120 cm (3.0 ft to 3.9 ft).

Hydraulic conductivity values were calculated from the slope of the $\partial H/\partial z$ curves corresponding to a given depth interval for a given time using linear regression, and the numerical values for the different depth intervals are provided in Table 1. The flux, Q, is equal to the product of the hydraulic conductivity, K, times the hydraulic head gradient, $\partial H/\partial z$. Thus, the hydraulic conductivity, K, was calculated by dividing the flux presented in Table 1 by the corresponding hydraulic head gradient. The coefficient of hydraulic conductivity was then plotted against the corresponding volumetric moisture content from Figure 3. The results are shown in Figure 4 and Table 1 for the center neutron probe access tube. The field-saturated hydraulic conductivity coefficient, K_s, for the soil profile was determined to be 4.05 x 10^{-4} cm/s under steady-state conditions during the flooding phase.

Discussion of Results

The dynamic range of measurements obtained from the IP test on the natural soil profile was limited to 30% to 35% volumetric moisture content (effective field saturation) and 15% to 20% volumetric moisture content. This limited range was due to the slow rate of drainage and the time and labor involved to continue monitoring incremental changes in soil moisture and suction within the profile. Even so, the IP test encompasses a significant portion of the soil profile-wetness range and provides valuable data describing the soil profile moisture, suction, and conductivity characteristics for the wet end of the soil profile.

The saturated hydraulic conductivity and conductivity near saturation are determined primarily by soil structural properties that are known to be subject to considerable spatial variability. This is in contrast to soil textural properties that generally are less variable and have a dominant effect on unsaturated conductivity. Saturated hydraulic conductivity is determined by an assemblage of macropores or channels of preferential flow that may have little effect on the overall pore-size distribution (texture) that determines the general shape of the predictive conductivity curve at intermediate water contents. The results show that there is a reduction of the unsaturated hydraulic conductivity in this soil profile at depths between 90 cm and 120 cm due to the presence of a horizon of carbonate cemented soil, locally called caliche.

Table 1. Calculated water flux, hydraulic head change, and hydraulic conductivity coefficients during drainage phase

Depth, z		Time, t	Q	$\partial H / \partial z$	K
(cm)	(ft)	(day)	(cm/day)	(cm/cm)	(cm/day)
30	1	1	1.067	0.49	2.177
30	1	2	0.201	0.61	0.330
30	1	4	0.149	0.67	0.223
30	1	8	0.082	0.72	0.114
30	1	16	0.026	0.79	0.032
30	1	32	0.014	0.94	0.015
30	1	64	0.002	0.90	0.003
61	2	1	2.134	0.49	4.354
61	2	2	0.622	0.61	1.019
61	2	4	0.363	0.67	0.541
61	2	8	0.195	0.72	0.271
61	2	16	0.053	0.79	0.067
61	2	32	0.031	0.94	0.033
61	2	64	0.007	0.90	0.008
91	3	1	2.515	0.49	5.132
91	3	2	0.917	0.61	1.504
91	3	4	0.533	0.67	0.796
91	3	8	0.293	0.72	0.406
91	3	16	0.086	0.79	0.109
91	3	32	0.049	0.94	0.053
91	3	64	0.018	0.90	0.020
122	4	1	2.682	1.13	2.384
122	4	2	1.021	1.18	0.869
122	4	4	0.622	1.17	0.531
122	4	8	0.357	1.16	0.309
122	4	16	0.117	1.20	0.097
122	4	32	0.058	1.24	0.047
122	4	64	0.023	1.09	0.021
152	5	1	2.981	1.76	1.694
152	5	2	1.183	1.74	0.680
152	5	4	0.750	1.67	0.449
152	5	8	0.427	1.59	0.268
152	5	16	0.140	1.61	0.087
152	5	32	0.077	1.53	0.050
152	5	64	0.027	1.28	0.021
183	6	1	3.591	1.76	2.040
183	6	2	1.378	1.74	0.792
183	6	4	0.905	1.67	0.542
183	6	8	0.515	1.59	0.324
183	6	16	0.168	1.61	0.104
183	6	32	0.090	1.53	0.059
183	6	64	0.032	1.28	0.025
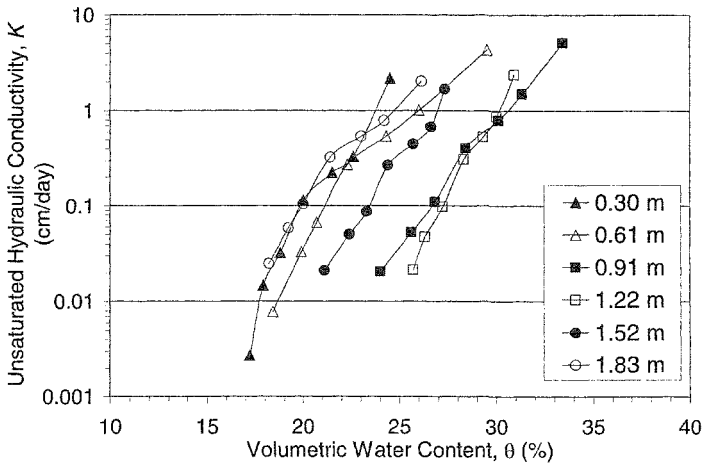
Figure 4. Unsaturated hydraulic conductivity as function of volumetric moisture content

The saturated hydraulic conductivity of the soil profile was determined under steady-state conditions during the flooding phase of the IP test. Field tests are preferred over indirect laboratory tests for determining the saturated hydraulic conductivity because the *in situ* soil structure and volume are usually altered during sample collection and preparation.

Summary and Conclusions

The IP test method was applied to determine the field-saturated and unsaturated hydraulic conductivities as functions of volumetric moisture content of a natural soil profile. The site was instrumented with neutron probe access tubes and tensiometers. During the fooding phase of the IP test, the field-saturated hydraulic conductivity was determined at steady-state conditions. As the soil profile was allowed to drain, soil moisture and suction data were recorded throughout the soil profile. It was found that the unsaturated hydraulic conductivity of this soil profile is not represented by a single function, but an envelop of curves that represent the variations in soil texture that govern water flow throughout the soil profile.

The IP test is an excellent method to obtain representatives values of the hydraulic conductivity function for an undisturbed soil profile and on a realistic scale. However, the IP method posses challenges in terms of proper and long-term functioning of the field instrumentation, data interpretation and conditioning, and high cost and intensive labor requirements. The additional difficulties and costs inherent to the IP test can be well justified by the significant reduction of

uncertainties in design and modeling when using direct field results instead of estimated values from the literature or results of indirect procedures.

Acknowledgements

References

Hillel, D., Krentos, V. D., and Stylianou, Y. (1972). "Procedure and test of an internal drainage method for measuring soil hydraulic characteristics in situ." *Soil Sci.*, 114, 395–400.

Jaynes, D. B., and Tyler, E. J. (1980). "Comparison of one-step outflow laboratory method to an in-situ method for measuring hydraulic conductivity." *Soil Sci. Soc. Am. J.*, 44, 903–907.

Stearns, S. D. (1975). *Digital signal analysis*, Hayden Book Company, Rochelle Park, NJ.

Watson, K. K. (1966). "An instantaneous profile method for determining the hydraulic conductivity of unsaturated porous materials." *Water Resources Res.*, 2, 709–715.

Predicting the hydraulic conductivity of unsaturated soils
from a soil moisture profile

T. Sugii[1]

[1]Department of Civil Engineering, Chubu University, 1200 Matsumoto-cho, Kasugai, Aichi, Japan, 486-8501, PH +81-568-51-9562; FAX +81-568-51-1495; email: nanto@isc.chubu.ac.jp

Abstract

A model of dynamic soil moisture distribution in unsaturated soil is proposed as a simple solution to Klute's equation. This model can represent relationships among soil moisture, depth and elapsed time using a sigmoid function. By substituting this model into Klute's equation (the governing equation of one-dimensional vertical seepage flow in the unsteady state), Klute's equation can be solved easily and the hydraulic conductivity of unsaturated soil can be obtained without suction data.

Introduction

Few practical cases adequately demonstrate in-situ hydraulic conductivity measurement in unsaturated soils due to difficulties in controlling matric suction and the water content of in-situ soils. Although permeability tests that can evaluate unsaturated hydraulic conductivity are proposed in soil science, they are not used in practical engineering to measure hydraulic conductivity of unsaturated soils because these methods cannot evaluate the hydraulic conductivities under a wide range of saturation conditions. In the current study, the author proposes a new function model that expresses the soil moisture profile during infiltration into the vadose zone using a sigmoid function. Only by measuring the volumetric water content, which changes with time while water is sprinkled on the ground surface, can parameters of the model be obtained easily. A logistic curve function is used as the sigmoid function.

Using the parameters of this model the relationship between the change in water content over time and the change in the water content with depth can be expressed. Klute's

equation can be solved easily with using this relationship. The present paper shows a method of predicting the hydraulic parameters of unsaturated soil using this model. Soil water diffusivity changes due to water content can be obtained by solving Klute's equation, moreover, the hydraulic parameters of unsaturated soil can be calculated using van Genuchten – Mualem model. To estimate all parameters, a versatile application program in Excel's Solver is used; therefore a special application program for seepage flow analysis is unnecessary when using this method.

Richards' Equation and Klute's Equation

Richards' governing equation (Richards, 1931) one-dimensional vertical seepage flow is written as:

$$C\frac{\partial \theta}{\partial t} = \frac{\partial}{\partial z}\left(k_{wu}\frac{\partial \psi}{\partial z}\right) - \frac{\partial k_{wu}}{\partial z} \tag{1}$$

where, ψ: pore water pressure; θ: volumetric water content; t: time; z: depth; k_{wu}: water conductivity of unsaturated soil; and, C: specific water capacity $(= \partial \psi / \partial \theta)$.

Klute substitutes the volumetric water content for the pore water pressure to derive the governing equation of one-dimensional vertical seepage flow as follows:

$$\frac{\partial \theta}{\partial t} = \frac{\partial}{\partial z}\left(D\frac{\partial \theta}{\partial z}\right) - \frac{\partial k_{wu}}{\partial z} \tag{2}$$

where, D : soil water diffusivity.

These equations are nonlinear, making them difficult to solve. The equations must be solved using Philip's solution (Philip, 1957) or a numerical analysis method.

One-dimensional seepage test

A seepage test was performed with Toyoura sand in a water tank as shown in Figure 1. Only one sensor (PR1), which can measure the dynamic data of volumetric
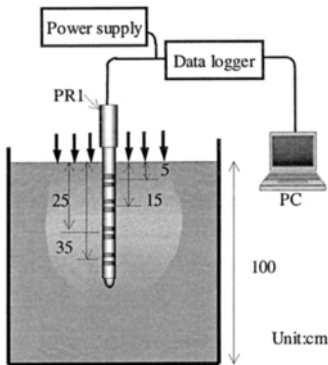
Figure 1. Laboratory apparatus.
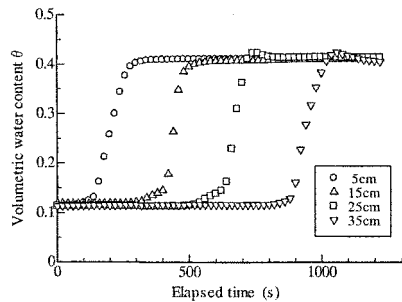
Figure 2. Measured volumetric water content during seepage into soils.

water content at four depths, is inserted into the ground. Water is sprinkled onto the dry ground surface (the initial water content is 0). In order not to prevent air from getting out, the intensity of sprinkling is less than 1.25 cm/s. Figure 2 shows the temporal distribution of the amount of moisture. Soil moisture begins to increase sequentially from a shallow position until the moisture at all points finally reaches a certain level. In the case of homogeneous soil, the four rates of the advance of the wetting front are similar at different depths.

Application of sigmoid function

A sigmoid function (Eq. (3)) is used to express the behavior of moisture in unsaturated soils (Sugii and Uno, 1996). The sigmoid function expresses some value from 1 to 0, continuously. Therefore, volumetric water content is converted to relative volumetric water content with final and initial volumetric water content. Various "S curve" lines can be drawn merely by changing the following two parameters:

$$\frac{\theta - \theta_{in}}{\theta_f - \theta_{in}} = \frac{1}{1 + \exp(b_0 + b_1 t)} \tag{3}$$

$$b_0 + b_1 t = \log_e\left(\frac{\theta - \theta_{in}}{\theta_f - \theta_{in}} - 1\right) \tag{4}$$

where, θ_{in}: initial volumetric water content; θ_f: final volumetric water content; t: elapsed time; b_0: fitting parameter concerning depth; b_1: fitting parameter concerning time (it has a negative sign).

By rearranging Eq. (3) as Eq. (4), it becomes easy to estimate these fitting parameters because the sigmoid function becomes a linear function with time. These parameters can also be estimated using the MS Excel Solver. In the current paper, these parameters were estimated using the latter method. The estimated parameters for each of the four depths

Figure 3. Fitting results of parameters.
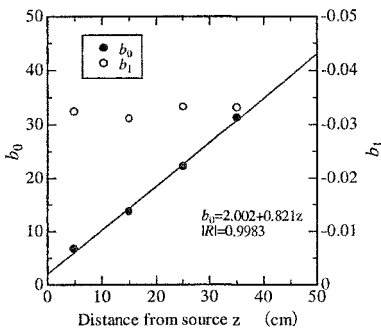
Table 1. Estimated parameters.

z (cm)	b_0	b_1	θ_f	θ_{in}
5	6.666	-0.0323	0.412	0.114
15	13.708	-0.0310	0.413	0.118
25	22.091	-0.0332	0.424	0.113
35	31.248	-0.0332	0.425	0.113
parameter	a_0	a_1	$b_1(ave)$	
	2.002	0.821	-0.0324	
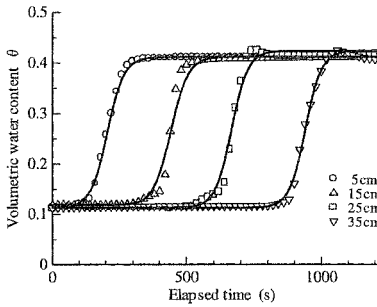
Figure 4. Measured and estimated volumetric water content.
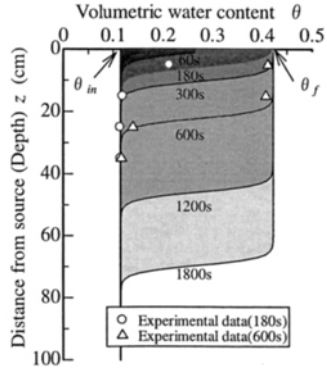
Figure 5. Measured and estimated soil moisture profile.

are shown in Figure 3 and Table 1. Although b_0 is a constant, b_1 is proportional to the distance from the source. Therefore, parameter b_1 is estimated by regression analysis:

$$b_0 = a_0 + a_1 z \qquad (5)$$

where, a_0, a_1: fitting parameters concerning depth.

The observed data and the estimated results using the estimated parameters (Table 1) are shown in Figures 4 and 5. A small error is identified in the increasing velocity of moisture at the depth of 15 cm, but the behavior of soil moisture can be simulated according to time and depth. In this paper, Eq. (6) is called the soil moisture profile model (SMPM).

$$\theta = \theta(z,t) = \frac{\theta_f - \theta_{in}}{1 + \exp(a_0 + a_1 z + b_1 t)} + \theta_{in} \qquad (6)$$

The lower the initial moisture, the more accurately Eq. (6) can estimate the hydraulic conductivity of unsaturated soil. If z and t are considered to be independent variables, Eq. (7) can be derived by substituting Eq. (6) for Eq. (2), and likewise with Eq. (8), using Eq. (7). Therefore, Eq. (9) can be derived by comparing Eqs. (7) and (8). This equation is an important characteristic of the proposed model.

$$\frac{\partial \theta}{\partial t} = \frac{\partial}{\partial t}\left(\frac{\theta_f - \theta_{in}}{1 + \exp(a_0 + a_1 z + b_1 t)} + \theta_{in}\right) = -(\theta_f - \theta_{in})\frac{b_1 \exp(a_0 + a_1 z + b_1 t)}{(1 + \exp(a_0 + a_1 z + b_1 t))^2} \qquad (7)$$

$$\frac{\partial \theta}{\partial z} = \frac{\partial}{\partial z}\left(\frac{\theta_f - \theta_{in}}{1 + \exp(a_0 + a_1 z + b_1 t)} + \theta_{in}\right) = -(\theta_f - \theta_{in})\frac{a_1 \exp(a_0 + a_1 z + b_1 t)}{(1 + \exp(a_0 + a_1 z + b_1 t))^2} \qquad (8)$$

The left-side expression of Eq. (9) can be rewritten as $\partial \theta / \partial t = -\partial \theta\, \partial z \cdot \partial z\, \partial t$,
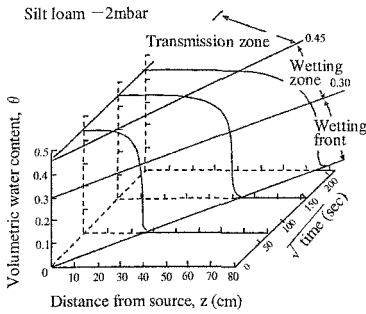
Figure 6. Relationship between wetting front and time (Yong and Warkentin (1975)).
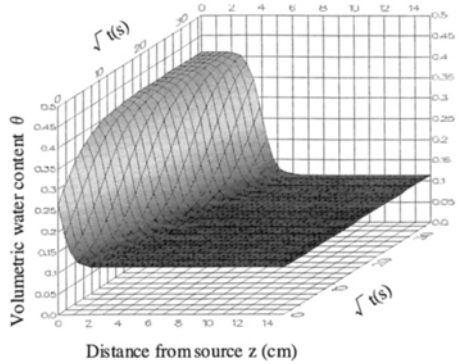
Figure 7. Relationship between wetting front and time (Soil Moisture Profile Model).

consequently b_1/a_1 in Eq. (9) is equal to $-\partial z/\partial t$ or the rate of the advance of the wetting front.

$$\frac{\partial \theta}{\partial t} = \frac{b_1}{a_1} \frac{\partial \theta}{\partial z} \qquad (9)$$

According to Table 1, the rate of the advance of the wetting front is estimated as approximately 0.039 cm/s.

Figure 6 shows the relationship between the wetting front and time, which Young and Warkentin, (1975) obtained for a horizontal seepage flow using the Boltzmann transformation method. Figure 7 drawn using SMPM and Figure 6 have the same shape despite the different types of soil.

Application of SMPM to permeability test for unsaturated soils

The Boltzmann transformation method can estimate hydraulic conductivity from Klute's equation. There are drying and wetting types in this method. However, neither type is applicable to vertical flow in which the gravity term dominates as is seen in Eq. (2). Therefore, this method can be used to measure the hydraulic conductivity of unsaturated soil in the laboratory only.

The current paper suggests that unsaturated hydraulic conductivity in vertical seepage flow can be determined simply by measuring the moisture during infiltration into unsaturated soil. Although knowledge of the specific water capacity of soils is needed, the possibility of measuring unsaturated hydraulic conductivity in vertical seepage flow is useful for field tests.

Calculation of hydraulic conductivity of unsaturated soil

Equation (10) can be derived from the relationship among Eqs. (2), (6) and (9).

$$\frac{b_1}{a_1}\frac{\partial\theta}{\partial z} = \frac{\partial}{\partial z}\left(-\frac{k_{wu}}{C}\left(\theta_f - \theta_{in}\right)\frac{a_1\exp(a_0 + a_1z + b_1t)}{(1+\exp(a_0 + a_1z + b_1t))^2}\right) - \frac{\partial k}{\partial z} \tag{10}$$

Equation (10) is the second partial derivative for only z, therefore it is easy to solve for θ :

$$\theta = -\frac{k_{wu}}{C}\left(\theta_f - \theta_{in}\right)\frac{a_1^{\ 2}\exp(a_0 + a_1z + b_1t)}{b_1(1+\exp(a_0 + a_1z + b_1t))^2} - k_{wu}\frac{a_1}{b_1} + c_1 \tag{11}$$

where, c_1 is an integral constant.

θ becomes θ_{in} for any depth when t equals 0. In addition, the first term of the right side of the expression is equal to zero because $\partial\theta/\partial t = 0$, therefore, $c_1 = \theta_{in} + k_{wu}a_1/b_1$ is given. The solution of Klute equation is given as follows:

$$\theta = k_{wu}\left(-\frac{\left(\theta_f - \theta_{in}\right)}{C}\frac{a_1^{\ 2}\exp(a_0 + a_1z + b_1t)}{b_1(1+\exp(a_0 + a_1z + b_1t))^2}\right) + \theta_{in} \tag{12}$$

from which soil water diffusivity is given by:

$$D = \frac{k_{wu}}{C} = -\frac{\left(\theta - \theta_{in}\right)}{\left(\theta_f - \theta_{in}\right)}\frac{b_1(1+\exp(a_0 + a_1z + b_1t))^2}{a_1^{\ 2}\exp(a_0 + a_1z + b_1t)} \tag{13}$$

If a specific water capacity, C, is measured from a soil water retention test in the laboratory, then the hydraulic conductivity of unsaturated soil can be obtained.

Figure 8 shows soil water diffusivity (water diffusion coefficient), which is obtained using Eq. (13). Although hydraulic conductivity of unsaturated soil can be calculated using a specific water capacity measured by a laboratory test, it can be obtained directly using a function model of soil water diffusivity.

Nonlinear regression of the parameter of van Genuchten-Mualem model (VG-M model) was conducted by the water diffusion coefficient obtained by Eq.(13) as an explained variable. According to the VG-M model, hydraulic conductivity and specific water capacity are shown as follows:

$$k_{wu} = k_{ws}\cdot Se^{0.5}\left\{1-\left(1 - Se^{1/m}\right)^m\right\}^2 \tag{14}$$

$$C = \alpha(n-1)(\theta_s - \theta_r)Se^{1\ m}\left(1 - Se^{1\ m}\right)^m \tag{15}$$

where, Se: effective saturation; k_{ws}: hydraulic conductivity of saturated soil; θ r: residual

volumetric water content; θ s: saturated volumetric water content; and, α, n, m are the van Genuchten model parameters.

The water diffusion coefficient expressed with VG-M serves as basis for the following equation:

$$D = \frac{k_{ws}Se^{0.5}\left\{1-\left(1-Se^{1/m}\right)^m\right\}^2}{\alpha(n-1)(\theta_s-\theta_r)Se^{1/m}\left(1-Se^{1/m}\right)^m} \qquad (16)$$

The parameters of VG-M model were estimated by regression analysis so that Eq.(13) and Eq.(16) might become equal. The MS-Excel Solver in the general-purpose application software was used to perform the nonlinear regression. Figure 9 shows the
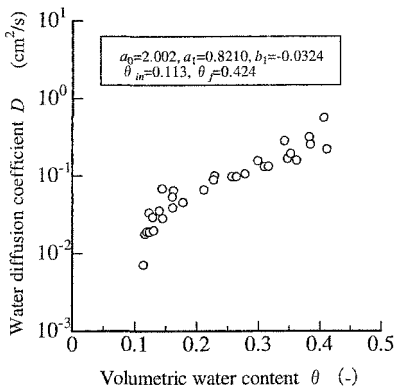
Figure 8.   Soil water diffusivity (calculated using Eq.(13)).
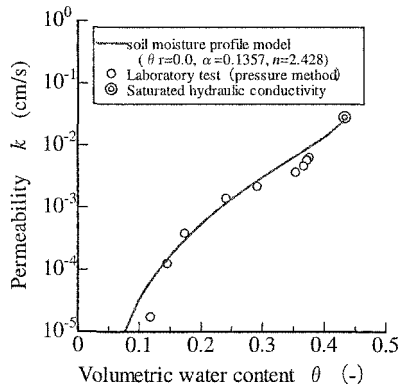
Figure 9. Comparison of proposed method and laboratory test.
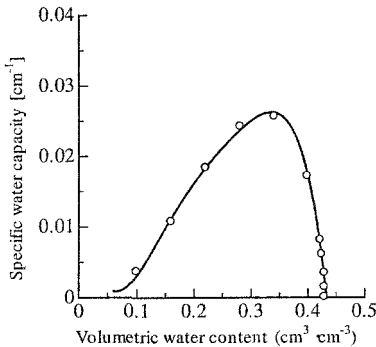
Figure 10. Specific water capacity from water retentivity test.
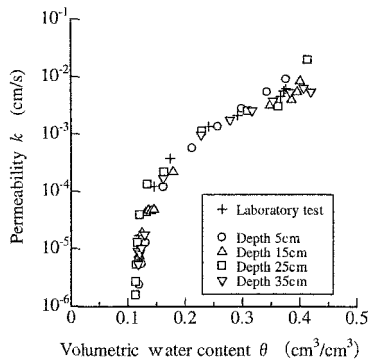
Figure 11. Comparison of proposed method and laboratory test.

comparison of estimated results and experimental results derived in the laboratory. It indicates that the proposed method strongly agrees with the experimental results. Hydraulic conductivity also can be obtained by using the experimental results of specific water capacity (Figure 10), thus they are shown in Figure 11.

Applicability of soil moisture profile model

The proposed model is applicable only in the case when velocity of wetting front is constant because it is based on the sigmoid function. Therefore, by using numerical analysis (Hydrus 2D (Rassam, et al. 2003)), velocities of the wetting fronts of three kinds of soil were investigated.

The hydraulic properties of the soils are shown in Table 2. Supposing an *in-situ* test, a cylindrical tube 60 centimeters in diameter is penetrated to a depth of 500 mm to control the vertical seepage flow. Zero pressure (i.e., the hydraulic conductivity of saturated soil) is given at A, and free drainage is given as boundary condition at B. The numerical analysis was calculated as the axial symmetry vertical flow (Figure 12).
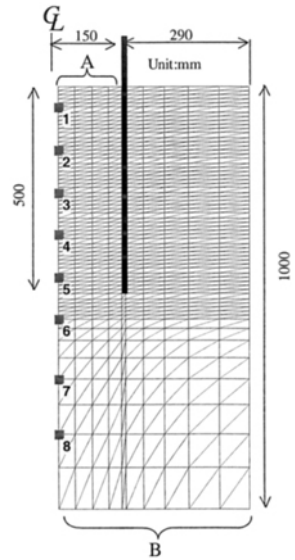
Figure 12. Finite element mesh and boundary conditions.

Table 2. Hydraulic properties (VG parameters)

	θr	θs	n	α (1/cm)	Ks(cm/s)
Sand	0.045	0.43	0.145	2.68	8.25E-03
Loam	0.078	0.43	0.036	1.56	2.89E-04
Silt	0.034	0.46	0.016	1.37	6.94E-5

Figure 13 (a) shows the change in volumetric water content at observed points with time. Although the velocity of the wetting front at No. 7 is slower than at other points, it is located at deeper than the cylindrical tube. Therefore, horizontal flow appears to have been generated. Figure 13 (b) shows that horizontal flow was also generated in soil deeper than 60 cm in depth. Meanwhile, in a shallow part of Silt by 2000 sec, the velocity of the wetting front is slow, but it shows a tendency of attaining constant velocity after 12000 sec (Figure 15(b)). We speculate that the tendency is attributable to the threshold hydraulic gradient or a boundary condition. These results (Figure 13-15) indicate that the
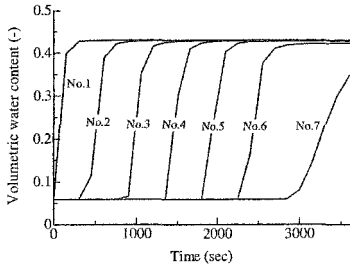
Figure 13 (a) Change of water content with time (Sand).
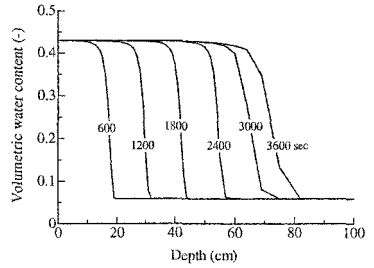
Figure 13(b) Soil moisture profile (Sand).
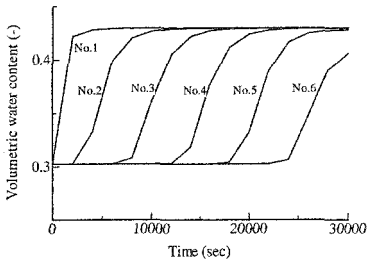
Figure 14 (a) Change of water content with time (Loam).
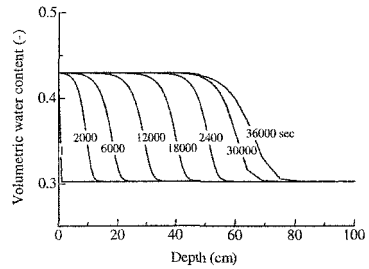
Figure 14(b) Soil moisture profile (Loam).
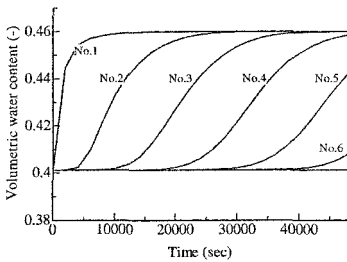
Figure 15 (a) Change of water content with time (Silt).
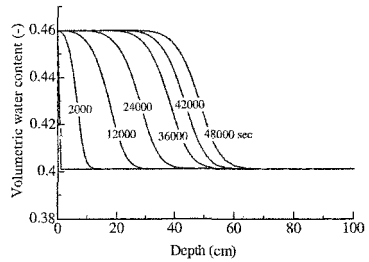
Figure 15(b) Soil moisture profile (Silt).

soil moisture profile model can be applied to general soil.

Conclusions

The model which can express relationships among soil moisture, depth and

elapsed time was proposed, and was applied to evaluation of the unsaturated hydraulic conductivity of the homogeneous sand. Moreover, to make applicability to other soils check, the numerical analytic tests were performed. The results are summarized below.

1)   The soil moisture profile, which changes with time and depth in vertical seepage flow, can be simulated using a sigmoid function.

2)   The differential coefficient of volumetric water content with respect to time is equal to the product of the velocity of the wetting front and the parameter ratio.

3)   In the infiltration test of one layer of general soil, the velocity of wetting front becomes a constant, and so the proposed model (soil moisture profile model) can be applied to sand, silt and loam.

4)   The hydraulic properties that were obtained using the proposed method are in good agreement with the results of other laboratory tests.

5)   This method is ideal for the in-situ test because of that earmark that does not need measurement of matric suction.

References

White, I., Sully,J.M. and Perroux, M. K. (1992). Measurement of suface-soil hydraulic properties: Disk Permeaters, Tension Infiltrometers, and other techniques, *Advances in measurement of soil physical properties:* SSSA Special publication ,30, 69-103.

Klute,A. (1952). A numerical method for solving the flow equation for water in unsaturated materials, *Soil Sci.*,73, 105-116.

Klute,A. (1972). The determination of the hydraulic conductivity and diffusivity of unsaturated soils, *Soil Sci.*, 113 (4), 105-116.

Philip, J. R. (1957). The theory of infiltration : 1: The infiltration equation and its solution, *Soil Sci.* 83 345-357.

Richards, L. A. (1931). Capillary conduction of liquids in porous mediums, *Physics* 1, 318-333.

Rassam, D., Simunek, J. and van Genuchten Th. (2003). *Modelling variably saturated flow with HYDRUS-2D.*ND Consult.

Sugii, T. and Uno, T. (1996). Modeling of the hydraulic properties for unsaturated soils, *Proc. of Symposium on Permeability and infiltration in unsaturated ground,* 179-184 (in Japanese).

Sugii,T., Yamada,K. and Uemura,M. (2000). Measuring hydraulic properties of unsaturated soils with unsteady method, *Proc. of the 2nd Asian Conference on Unsaturated Soils,* 439-444.

Sugii, T. (2005). Modeling of soil moisture profile during infiltration into vadose zone, Proc of the 16th International Conference on Soil Mechanics and Geotechnical Engineering, 2449-2452.

Yong, R.N. and Warkentin, B. P. (1975). *Soil Properties and behavior,* 155-163, Elevier Scientific Publishing Co.

Infiltration measurements in model embankments
composed of volcanic sandy soils

Y. Kiyohara [1], T. Unno [2] and M. Kazama [3]

[1] Department of Civil and Environmental Engineering, Hachinohe National College of Technology, 16-1 Uwanotai, Tamonoki, Hachinohe 039-1192, Japan; PH (81)178-27-7367; FAX (81)178-27-7367; email: kiyohara-z@hachinohe-ct.ac.jp.
[2] Department of Civil Engineering, Tohoku University, 6-6-06 Aza Aoba, Aramaki, Aobaku, Sendai 980-8579, Japan; PH (81)022-795-7438; FAX (81)022-795-7435; email: unno@soil1.civil.tohoku.ac.jp
[3] Department of Civil Engineering, Tohoku University, 6-6-06 Aza Aoba, Aramaki, Aobaku, Sendai 980-8579, Japan; PH (81)022-795-7434; FAX (81)022-795-7435; email: m-kazama@civil.tohoku.ac.jp

Abstract

To study seepage behavior caused by rainfall, field tests were carried out on model embankments that consisted respectively of Hachinohe Shirasu and Tsukidate soil. They are volcanic pyroclastic sediments with pumice that exist in Aomori and Miyagi Prefectures in Japan. Due to rainfall the maximum value of water content in earthfills which consist of Hachinohe Shirasu and Tsukidate soil were 40-42% and about 42% respectively. Their peak had tend to occur after each 1day and 2.5day of rainfall peak. Furthermore from the field test results, storage coefficient, which is normalized by porosity, at wetting process was 0.01-0.25 in Hachinohe Shirasu and Tsukidate soil.

Subsequently, using hydraulic properties determined from laboratory tests, finite element analyses of saturated-unsaturated seepage in those embankments were performed. Comparing the calculated behavior with measured one for about three months data, after 20 days we could conclude that the calculated seepage behavior agreed with observed one.

Introduction

Volcanic sandy soils and pyroclastic sediments with pumice are widely distributed in Japan; numerous embankments comprise those materials. During and after heavy rainfalls and severe earthquakes, slopes composed of such materials often fail.

Hachinohe Shirasu and Tsukidate soil, which were used in this experiment, are volcanic sandy soils and pyroclastic sediments; they are known in Japan as problematic soils. Their particles are characteristically crushable, extremely porous, and lightweight. Furthermore, it is known that water retention of those volcanic soils is greater than that for ordinary sand at the same suction because of the particle characteristics described above (Unno et al., 2005).

Road embankments that consist of Hachinohe Shirasu soil failed in the 1968 Tokachi-Oki earthquake (Sasaki et al., 1971) and an earth fill that consisted of Tsukidate soil also failed in the 2003 Sanriku Minami earthquake in Japan (Uzuoka et al., 2005). The retained water contents of the earth fills were inferred to be very high, contributing to their failure.

It is necessary to develop slope-failure predictions during rainfall to prevent disasters. Generally, slope stability depends on shear strength and water content in earth fills. Grasping long-term basic data related to infiltration behavior caused by rainfall can improve practical methods of stability prediction. Many studies of infiltration properties in earth fills, embankments, and so on have examined soils in numerous countries (Kitamura et al., 2000; Illias et al., 2003). Moreover, many studies have examined slope stability during rainfall (Ng et al., 2003).

For about one year, we used field monitoring to study infiltration characteristics and water retention properties of embankments consisting of Hachinohe Shirasu and Tsukidate soil. We verified a series of methods to predict seepage behavior using finite element method (FEM), then compared field data with calculated values.

Infiltration Characteristics observed in Field Monitoring

Engineering properties of model embankments. Field monitoring took place on two model embankments made of Hachinohe Shirasu and Tsukidate soil. Thereby, we examined seepage behavior during rainfall. These engineering properties are presented in Table 1. These materials are volcanic pyroclastic sediments with pumice obtained respectively from Aomori and Miyagi Prefectures in Japan. Particle sizes over 10 mm for Hachinohe Shirasu and over 20 mm for Tsukidate soil were removed by sieving. The coefficients of saturated permeability, obtained from laboratory tests, were about $4.27*10^{-3}$ cm/s for Hachinohe Shirasu and $1.10*10^{-4}$ cm/s for Tsukidate soil.

Table1   Engineering properties of the embankments

	Hachinohe Shirasu	Tsukidate soil
Soil particle density ρ_s (g/cm^3)	2.518	2.478
Optimum moisture content (%)	23.0	28.0
Maximum dry density (g/cm^3)	1.26	1.36
Moisture content during construction (%)	25.6	29.1
Dry density after construction (g/cm^3)	1.21	1.38
Porosity (%)	51.9	44.3
Coefficient of saturated permeability (cm/s)	4.27×10^{-3}	1.10×10^{-4}

Each model embankment is 1 m high and has an inclination of 33.7°(1:1.5; shown respectively in Fig. 1 and Fig. 2). The bottom of the embankment is put in a drained condition by gravel; surrounding sides are in an undrained condition by enclosure within wooden walls. They were constructed maintaining the optimum moisture content using a plate rammer to produce dense embankments.

Figure 2 shows six dielectric aquameter sensors, which measure the dielectric constant of the soil and are converted to water content (Craig et al., 2003). They were installed into the model embankments at depths of 0.15, 0.35 and 0.55 m from the slope surface. Each sensor was spaced horizontally 0.375 m from the others. Soil water contents in the embankments were measured continually at 10-min intervals. The amount of rainfall was also measured using a rainfall sensor.
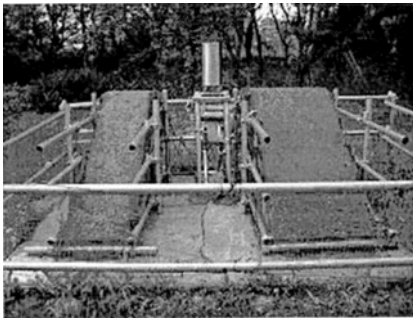
Figure 1. Model embankments consisting of Hachinohe Shirasu and Tsukidate soil.
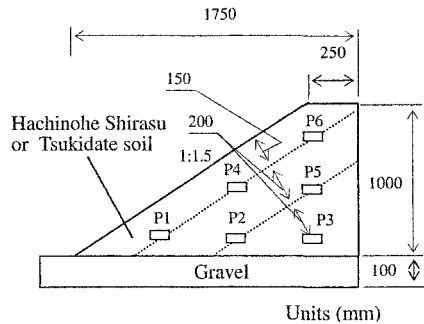
Figure 2. Model embankment cross-section.

Infiltration Characteristics. At field monitoring, the total rainfall was 1180 mm during the year (1 July 2004 – 30 June 2005). Figure 3 and Figure 4 respectively present results of water content in each embankment of Hachinohe Shirasu and Tsukidate soil recorded. Because of rainfall, the maximum value of water content was 40–42% for Hachinohe Shirasu and was about 42% for Tsukidate soil. In both cases water contents in subsurface soils were higher than surface soils.

The temporal variations in water content were more pronounced at smaller depth than those at larger depth. And the infiltration mainly occurred near the slope surface (near the points P1, P4, P6) for Hachinohe Shirasu and flow parallel to the slope mainly occurred. The infiltration was occurred near the top of slope (near the points P6, P4) for Tsukidate soil and vertical flow mainly occurred. It is thought that this difference had occurred by anisotropy of permeability.

For Hachinohe Shirasu, draining behavior suddenly appeared after infiltration, with reflecting the sharp peaks of volumetric water contents. For Tsukidate soil, the peak value continued two or three days before draining behavior appeared. This behavior was inferred to result from the lower hydraulic conductivity of Tsukidate soil than that of Hachinohe Shirasu; also, the water retention of Tsukidate soil is greater than that of Hachinohe Shirasu.

During the dry period (especially from late July 2004 to early August 2004), the water content declined to 23% for Hachinohe Shirasu and to about 17% for Tsukidate soil. In winter (late December 2004 – March 2005), soils of respective embankments had frozen because of sub-zero temperatures. So, the dielectric aquameter sensor could not measure the water contents containing in those embankments. And rainfall intensity which was measured during this season was mainly the value of snowmelt.
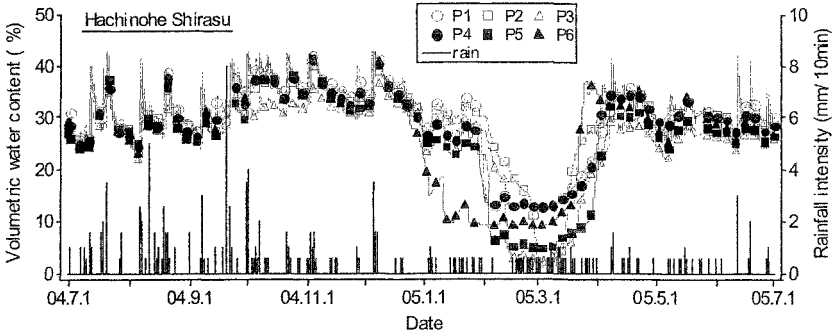
Figure 3. Water content of a model embankment made of Hachinohe Shirasu.
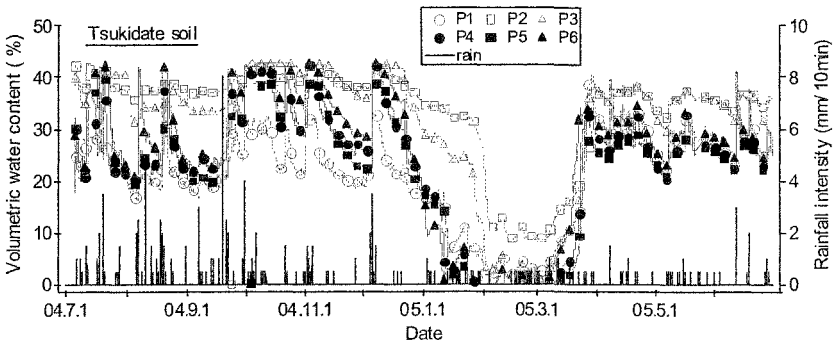
Figure 4. Water content of a model embankment made of Tsukidate soil.

Figure 5 shows the infiltration rate (the slope of increasing water content per time) and the draining rate (the slope of decreasing water content per time) and the lag time (the difference between the peak time of rainfall and that of water content) at the measuring point in Hachinohe Shirasu. The average infiltration rate of Hachinohe Shirasu was 28.8mm/h (21.9–38.4mm/h) at 0.15 m depth, 18.6mm/h (15.9–21.3mm/h) at 0.35 m depth, and 10.7mm/h at 0.55 m depth. The deeper the position from the slope surface, the slower the infiltration rate. This tendency probably occurred because the slope surfaces were more dried (absorbent), due to evaporation. The average draining rates of Hachinohe Shirasu were 1.4mm/h at 0.15 m depth,

0.9mm/h at the depths of 0.35 m and 0.55 m. The infiltration rate was about 11 times higher than the drainage rate.

The average lag time was 7.4 h (6.7–7.8 h) at 0.15 m depth, 16.3 h (13.7–18.8 h) at 0.35 m depth, and 23.7 h at 0.55 m depth. When roughly estimating the coefficient of permeability, by dividing the lag time into the distance from the upper to the lower parts (0.25 m), the average coefficient of permeability from field monitoring was $1.47*10^{-3}$ cm/s ($1.77*10^{-4}$ cm/s $-$ $5.95*10^{-3}$ cm/s). That value is of a similar order to values measured from laboratory tests.

Figure 6 shows the infiltration and draining rate and lag time at the measuring point in Tsukidate soil. The average infiltration rate of Tsukidate soil was 14.9mm/h (2.6–25.3mm/h) at 0.15 m depth, 2.5mm/h (0.5–4.5mm/h) at 0.35 m depth, and 5.8mm/h at 0.55 m depth. The deeper the position from the top of the slope, the slower the infiltration rate. The average draining rate of Tsukidate soil was 1.7mm/h at 0.15 m depth, 0.9mm/h at 0.35 m depth, and 0.1mm/h at 0.55 m depth.

The average lag time was 22.2 h (16.4–25.4 h) at 0.15 m depth, 40.8 h (36.1–45.6 h) at 0.35 m depth, and 69.7 h at 0.55 m depth. When roughly estimating the coefficient of permeability in the same manner as that for Hachinohe Shirasu, the average coefficient of permeability from field monitoring was $4.1*10^{-4}$ cm/s, which was of a similar order to the value measured using laboratory tests.
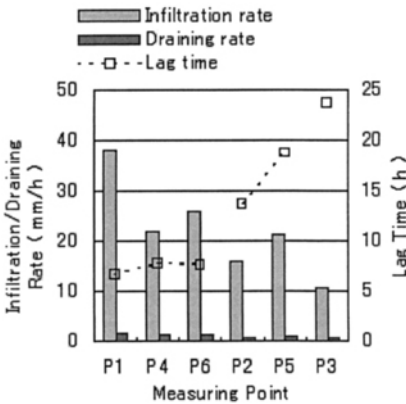
Figure 5. Infiltration and drainage rates and lag times for Hachinohe Shirasu.
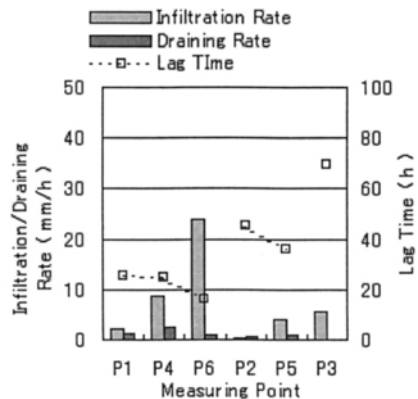
Figure 6. Infiltration and drainage rates and lag times for Tsukidate soil.

Storage Property. From field test results, the storage coefficient at wetting process were calculated using Eq. (1).

$$\beta_s / n = \frac{\max(\theta_t - \theta_i)}{n} \qquad (1)$$

In that equation, θ_i represents the initial water content at the beginning of rainfall, θ_t is the water content after t minutes, n indicates the porosity, and β_s is the storage coefficient.

Results are shown in Fig. 7. For rainfall events from June to November 2004, the storage coefficient rate β_s / n was 0.005–0.25 against θ_i / n was 0.45–0.77 and entrapped air during infiltration was 20–50% for Hachinohe Shirasu. The storage coefficient rate β_s / n was 0.01–0.25 against θ_i / n was 0.54–0.90 and entrapped air during infiltration was 10–40% for Tsukidate soil. Comparison of these field test results for the storage coefficient with laboratory test results (Uno, 1989) indicated that more air tends to be entrapped into those embankments. These results also indicate that the specific water retention of Tsukidate soil tends to be greater than that of Hachinohe Shirasu.
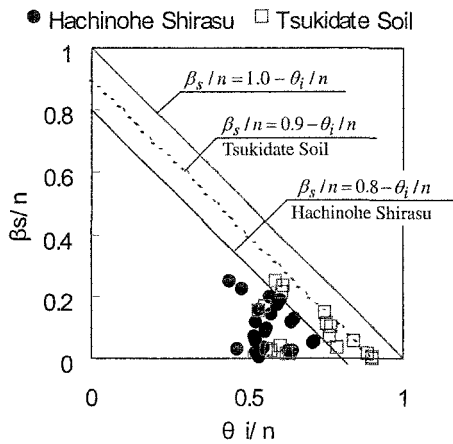
Figure 7. Distribution of the storage coefficient rate against initial water content.

Prediction of Infiltration by Finite Element Analyses

Numerical Model for Infiltration. This study used the *PlaxFlow* code, which is a finite element code for saturated-unsaturated seepage analysis (*PlaxFlow Manual*, 2003), to predict the behavior of rain infiltration into the embankments. In *PlaxFlow*, the Richard's equation (Eq. (2)) was used as a basic equation for the continuity condition. Van Genuchten's equation (Eq. (3) and Eq. (4)) (Van Genuchten, 1980) was used to determine the unsaturated permeability and water retention property. Those parameters are based on data from soil water characteristic curves of the wetting process obtained from laboratory tests.

$$\frac{\partial}{\partial x}\left(K_{unsat} \frac{\partial \phi}{\partial x} \right) + \frac{\partial}{\partial y}\left(K_{unsat} \frac{\partial \phi}{\partial y} \right) + Q = c \frac{\partial \phi}{\partial t} \tag{2}$$

$$S_e = \left[\frac{1}{1 + \left(\alpha |\phi| \right)^n} \right]^m = \frac{S - S_r}{S_s - S_r} \qquad m = 1 - \frac{1}{n} \tag{3}$$

$$K_{unsat} \approx K_{sat} \cdot S_e^{1/2} \left[1 - (1 - S_e^{1/m})^m \right]^2 \qquad (4)$$

In the equations shown above, K_{unsat} represents the unsaturated permeability, ϕ is the pore pressure head, Q is the source term, c is the effective capacity, S_e is the effective saturation, S_r represents the residual saturation, S_s is the saturation at $\phi = 0$, K_{sat} is the saturated permeability, and m, n, α are Van Genuchten's parameters.

Decision of Van Genuchten's parameters. Van Genuchten's parameters were decided as follows (Van genuchten, 1980 and Uno, 1989). First, estimate the S_s and S_r from measuring soil water retention curve (Unno et al., 2005), then calculate the neutral point P (the halfway between S_s and S_r) (Eq. (5)).

$$S_p = \frac{S_s + S_r}{2} \qquad (5)$$

Then, calculate the slope $dS/d(\log h)$ at point P on a semi-logarithmic scale (Eq. (6)).

$$SL_p = \frac{1}{S_s - S_r} \left| \frac{dS}{d(\log h)} \right| \qquad (6)$$

Finally, calculate the VG parameter as follows (Eq. (7) and Eq. (8)).

$$m = \begin{cases} 1 - \exp(-0.8 SL_p) & (0 < S_p \leq 1) \\ 1 - \dfrac{0.5755}{SL_p} + \dfrac{0.1}{SL_p^{\,2}} + \dfrac{0.025}{S_p^{\,3}} & (S_p > 1) \end{cases} \qquad (7)$$

$$\alpha = \frac{1}{h_p} (2^{\frac{1}{m}} - 1)^{1-m} \qquad (8)$$

Conditions of numerical analyses. Table 2 shows material properties used for analyses. Each coefficient of saturated permeability was a measured value from laboratory tests. Furthermore, to compare seepage properties of volcanic sandy soils with those of ordinary sand, analyses were also performed using material properties of Toyoura sand (Uno, 1989). The sand is fine clean sand that is produced in Japan.

Figure 8 shows the geometry of model embankment used in these analyses. Model geometry and drainage conditions correspond to field tests, as explained in the previous section. To improve the precision of calculation results, we tried to change mesh size which was finer than the model shown in Figure 8, but the results didn't so change satisfactory for these cases.

Rainfall data which had measured in field monitoring for three months, June 2004 – September 2004, were used in transient analyses in this study. The selected duration includes both wet and dry periods, which is reflecting the Japanese climate.

Table 2. Material properties of the embankments

Items	Hachinohe Shirasu	Tsukidate soil	Toyoura sand
Case	s1	t1	h1
Saturated Permeability (cm/s)	4.27×10^{-3}	1.10×10^{-4}	1.50×10^{-2}
Void ratio	1.08	0.796	0.72
Effective capacity (1/m)	0.4	0.15	0.01
Residual Saturation (%)	10	20	0
Saturation at $\phi = 0$ (%)	80	70	100
VG parameter n	1.308	1.321	3.586
VG parameter α (1/m)	18.17	12.551	5.23

$* \phi$: Matric suction
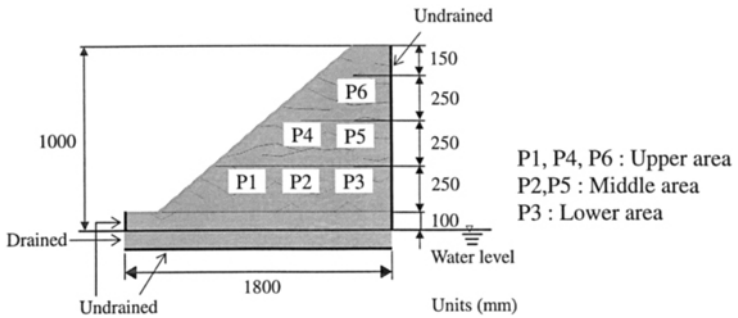
Figure 8. Model embankment geometry.

Example of calculation Results for Infiltration. Figure 9 and Figure 10 show the example of calculation results of volumetric water content in Hachinohe Shirasu, compared over three months field monitoring data with calculated behavior: June 2004 – September 2004. Upper part of monitoring points (P1, P4, P6) are shown in Fig. 9, middle and lower part of monitoring points (P2, P5, P3) are shown in Fig. 10. Comparison of calculated behavior with measured behavior reveals differences between calculated and measured values because of the instability of initial conditions during the first 20 days. Thereafter, the calculated seepage behavior relatively agreed with the observed one in every points. But the calculated maximum value and draining behavior of water content after rainfall were less than measured one. The differences between calculated and field monitored data of lower area were smaller than upper area.

In the same way, Figure 11 and Figure 12 show the example of calculation results of volumetric water content in Tsukidate soil. For Tsukidate soil, a difference is also apparent between calculated and measured values because of the instability of initial conditions during the first ten days. Thereafter, the minimum value of water contents and the behavior of infiltration process approximately agreed with measured values. Nevertheless, the maximum value and draining process after rainfall did not
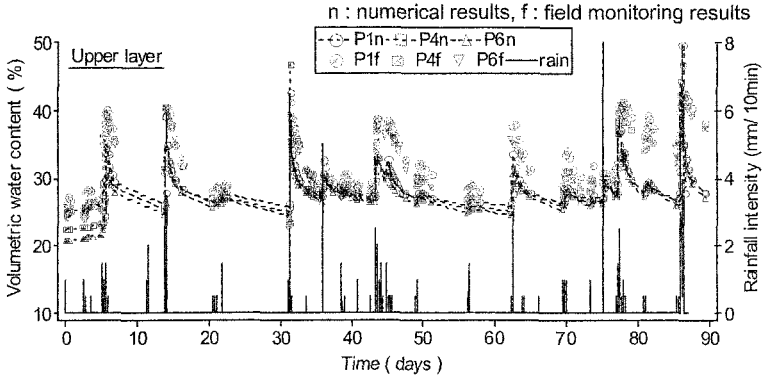
Figure 9. Calculated results of water content in an embankment made of Hachinohe Shirasu (Upper layer).
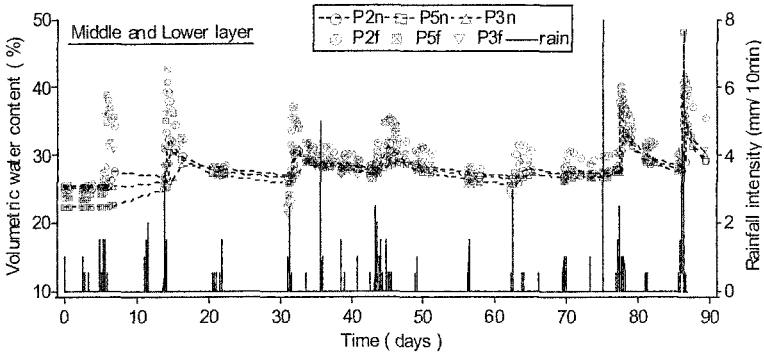
Figure 10. Calculated results of water content in an embankment made of Hachinohe Shirasu (Middle and Lower layer).
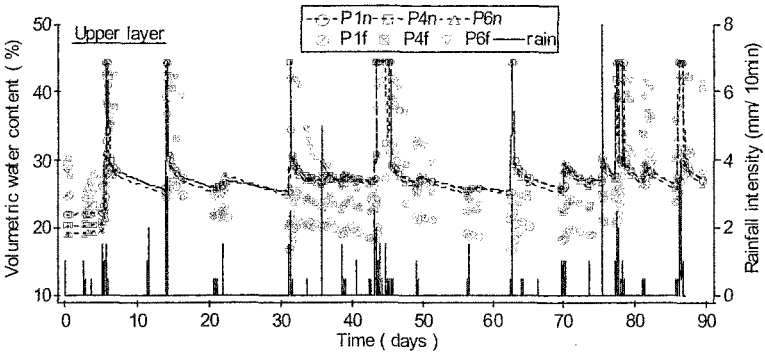
Figure 11. Calculated results of water content in an embankment made of Tsukidate soil (Upper layer).
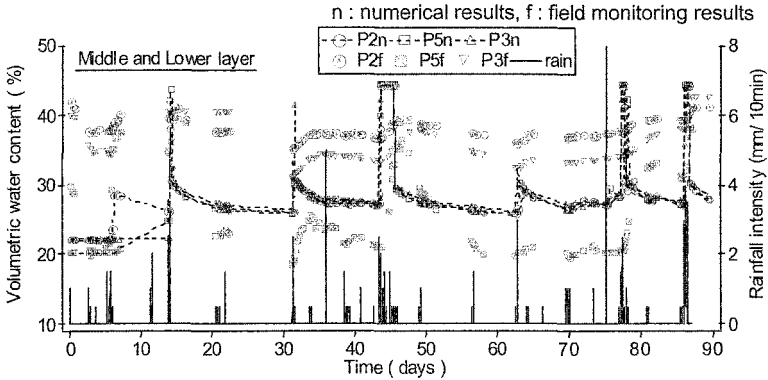
Figure 12. Calculated results of water content in an embankment made of Tsukidate soil (Middle and Lower layer).
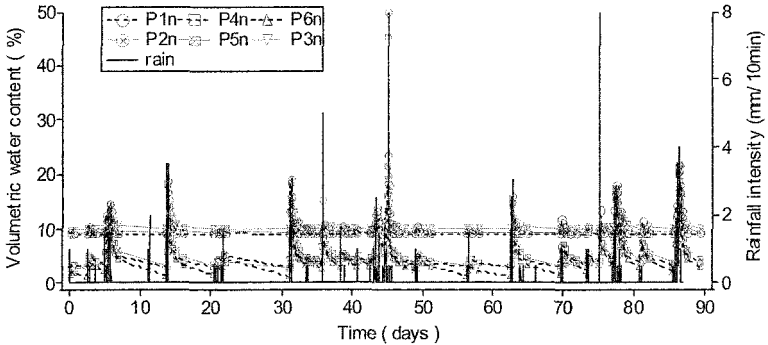
Figure 13. Calculated results of water content in an embankment made of Toyoura sand.

agree as well as those values for Hachinohe Shirasu. We infer that the difference resulted from the modeling accuracy of soil-water characteristics in the field model embankment (especially for the difference between wetting and drying processes) and the wide particle distribution used in the Tsukidate field model embankment, which might have caused heterogeneous particle distribution.

Furthermore, comparing results calculated using the parameter for fine clean sand (Toyoura sand) (shown in Figure 13), the water contents of embankments consisting of Hachinohe Shirasu and Tsukidate soil maintained higher values.

Conclusion

Field monitoring tests were performed for prediction and assessment of seepage properties of volcanic soil embankments. The following results were obtained.

For field tests, we produced model embankments consisting of Hachinohe Shirasu and Tsukidate soil, which are Japanese volcanic sandy soils. We measured soil water content distribution and infiltration behavior. We quantified the infiltration and draining rate, lag time, and the storage coefficient using rain infiltration.

Because of rainfall, the respective maximum values of water contents in embankments consisting of Hachinohe Shirasu and Tsukidate soil were 40-42%. Their respective peak values at 0.55 m depth occurred about 1 day and 3 days after rainfall peaks.

The average infiltration rates of Hachinohe Shirasu were 28.8mm/h at 0.15 m depth, 18.6mm/h at 0.35 m depth, and 10.7mm/h at 0.55 m depth. Deeper positions from slope surface revealed slower infiltration rates. The average infiltration rate of Tsukidate soil was 14.9mm/h at 0.15 m depth, 2.5mm/h at 0.35 m depth, and 5.8mm/h at 0.55 m depth. The deeper the position from the top of the slope, the slower the infiltration rate. The wetting rate of the infiltrating process was much faster than the drying rate. The storage coefficient β_s / n, which is normalized by porosity, of the wetting process was quantified (0.01–0.25) in both Hachinohe Shirasu and Tsukidate soil.

Finite element analyses of transient saturated-unsaturated seepage in embankments were performed using rain data observed from field tests and parameters based on the data from the soil water characteristic curves of wetting processes. Comparing the calculated behavior with measured behavior for about three months' data, we could conclude that the seepage behavior is predictable in these model embankments. To improve the analytical precision, especially for drying process behaviors, future studies about soil water retention properties and parameter study must examine.

Comparing water contents calculated using the parameter of fine clean sand with those of Hachinohe Shirasu and Tsukidate soils, the volcanic soils had higher values because of greater water retention properties and less permeability. So, compared with clean sandy soils, these volcanic sandy soils might cause the slope failure easily.

These results are measured or calculated less than 0.55m depth from the slope surface on the assumption of small model in order to grasp the seepage property. So, when we consider the slope stability of full size embankment, we must investigate the water content more deeper position and must check the stability of numerical models by changing the influence of mesh size, time interval, iteration number and so on (Rassam., et al 2003).

References

Akai, K., Ohnishi, Y. and Nishigaki, M. (1977). "Finite Element Analysis of Saturated-Unsaturated Seepage In Soil", *Japaniese. Geotech. Eng.*, 264, 87-96.

Craig, N., Leslie, S. and Roger, B. (2003). "Time domain reflectrometry measurements of water content in coarse waste rock ", *Can. Geotech. J.*, 40, 137-148.

Illias, T., Harianto, R., David G, T. and Eng-Choon, L. (2003). "Infiltration characteristics of two instrumented residual soil slopes", *Can. Geotech. J.*, 40, 1012-1032.

Kawamoto, K., Banyar, A., Per, M., Komatsu, T. and Oda, M. (2004). "Estimating soil water characteristic curves of water repellent volcanic ash soils by time domain reflectometry coil probe measurements", *Trans. of JSIDRE*, 233, 83-91.

Kitamura, R., Kawada, M., Abe, Hirofumi., Jomoto, K. and Terachi, T. (2000). "Deveropment of field measuring system for suction in unsaturated soil with rainfall", *Japaniese. Geotech. Eng.*, 652(51), 287-292.

Kono, I. and Nishigaki, M. (1981). "An experimental study on characteristics of seepage through unsaturated sandy soil", *Japaniese. Geotech. Eng.*, 307, 59-69.

Ng, C.W. W., Zhan, L.T., Bao, C.G., Fredlund, D.G. and Gong, B.W. (2003). "Performance of an unsaturated expansive soil slope subjected to artificial rainfall infiltrarion ", *Geotechnique*, 53(2), 143-157.

Ning, L. and William, L. (2003). *Unsaturated Soil Mechanics,* Wiley, New York.

PLAXIS manual. (2003) *PlaxFlow manual version 1,* Plaxis Ltd, Delft, The Netherlands.

Rassam, D., Simunek, J. and Van Genuchuten, M. T. (2003). *Modelling Variably Saturated Flow with HYDRUS-2D,* ND Consult, Brisbane, Australia.

Sasaki, Y. and Iijima, T. (1971). "Survey on disaster due to the Tokachi-oki earthquake 1968", *Research Report of PWRI*, 141, 67-78.

Unno, T., Takamura, H., Sento, N., Uzuoka, R. and Kazama, M. (2005). "Water retention characteristics of volcanic sands in Tohoku district which caused mud-flow type failure during earthquake", *Proc of 40th Japan National Conference on Geotechnical Engineering*, 875-876.

Uno, T. (1989). "Consideration on water retention and infiltration of unsaturated soils, *Engineering properties of unsaturated soils, Japanease Geotechnical Society Kansai branch,* 19-40 (in Japanese).

Uzuoka, R., Sento, N., Kazama, M. and Unno, T. (2005). "Landslides during the earthquakes on MAY 26, 2003 in Miyagi", *Soils and Foundations*, 45(4), to be appeared.

Van Genuchuten, M. T. (1980). "Closed-form Equation for Predicting the Hydrauric conductivity of Unsaturated soils", *Soil Sci. Am. J.* , Vol.44, 892-898.

Study of Infiltration Characteristics in the Field

I G.B. Indrawan[1], H. Rahardjo[2], and E.C. Leong[3]

[1]Research Scholar, School of Civil and Environmental Engineering, Nanyang Technological University, 50 Nanyang Avenue, Singapore 639798, PH: (65) 6790 6442, Fax: (65) 6791 0676; email: igbindrawan@ntu.edu.sg
[2]Professor and Vice Dean, School of Civil and Environmental Engineering, Nanyang Technological University, 50 Nanyang Avenue, Singapore 639798, PH: (65) 6790 4104, Fax: (65) 6791 0676; email: chrahardjo@ntu.edu.sg
[3]Associate Professor, School of Civil and Environmental Engineering, Nanyang Technological University, 50 Nanyang Avenue, Singapore 639798, PH: (65) 6790 5307, Fax: (65) 6791 0676; email: cecleong@ntu.edu.sg

Abstract

Infiltration characteristics of a single-layer soil and a two-layer soil were investigated in this study by conducting small-scale field infiltration tests and numerical analyses. The field infiltration tests were conducted using double-ring infiltrometers, where the water pressure head was maintained throughout the tests. Changes in pore-water pressure during the tests were measured using tensiometers installed at various depths in the soil. Simulations of the field infiltration tests were performed using a finite element program. The hydraulic properties of the soils used in the simulation were measured independently in the laboratory. The results showed that the difference in the hydraulic properties of the two-layer soil caused a delay in the downward water flow into the lower soil layer. The numerical simulation results and the field infiltration test results were found to be in reasonably good agreement.

Introduction

Water infiltration into single-layer and multi-layer soils under unsaturated condition has been a major concern, especially in slope stability analyses and waste management practices. In geotechnical engineering, numerous research works have been conducted to study water infiltration in unsaturated soils. The study has been performed using several methods including numerical analyses (e.g., Akindunni et al., 1991, Zhang et al., 2004), laboratory experiments (e.g., Barbour and Yanful, 1994; Stormont and Anderson, 1999; Yang et al., 2004), and field tests (e.g., Yanful et al., 1993; Woyshner and Yanful, 1995).

Transient processes of water infiltration in an unsaturated soil are a complex problem as the soil hydraulic properties are highly nonlinear. The complexity of the problem increases in multi-layer soils with a sharp contrast in hydraulic properties between the overlying soil layer and the underlying soil layer. In the field, the in-situ soil hydraulic properties are commonly measured using double-ring infiltrometers (e.g., Watson and Luxmoore, 1986; Bodhinayake et al., 2004). The use of double-ring infiltrometers, in conjuction with tensiometers for measuring pore-water pressures, can be extended to study water infiltration in unsaturated soils, as described in this paper.

This paper documents the results of field infiltration tests conducted to study infiltration characteristics of one-dimensional vertical flow of water through models of a single-layer soil and a two-layer soil. The initial objectives of the field infiltration tests were to measure the hydraulic properties of the existing sand at the study area and to study the performance of a two-layer soil model developed previously in the laboratory (Yang et al., 2004) under field conditions. Numerical simulations of the field infiltration tests were also performed in this study and the results are compared with those obtained from field tests.

Theory

SWCC and Permeability Function

Soil-water characteristic curve (SWCC) and permeability function are two important soil properties required in numerical modeling of water flow in unsaturated soils. SWCC expresses the relationship between volumetric water content and matric suction whereas permeability function shows the relationship between coefficient of permeability with respect to water phase, k_w and matric suction. SWCCs are commonly measured using a pressure plate extractor. Typically, a soil has two SWCCs, namely drying curve and wetting curve. The drying curve expresses the decrease in water content as matric suction increases and the wetting curve represents the reverse process.

Permeability function of an unsaturated soil is best measured directly in the laboratory or in the field. However, since direct measurements are tedious and time consuming, water coefficient of permeability of unsaturated soil is commonly estimated from SWCC and coefficient of permeability at saturation, k_s. This is due to the permeability function is generally assumed to be uniquely related to the SWCC.

Water Flow

Water flow in saturated and unsaturated soils is commonly described using Darcy's law. According to Darcy's law, the rate of water flow through a soil mass is proportional to the hydraulic head gradient as follows:

$$v_w = -k_w \frac{\partial h_w}{\partial y} \tag{1}$$

where v_w is the flow rate of water (m/s); k_w is the coefficient of permeability with respect to water phase (m/s); h_w is the hydraulic head (m); and $\partial h_w/\partial y$ is the hydraulic head gradient in the y-direction.

Under steady-state conditions, the governing partial differential equation for one-dimensional water flow in unsaturated soil is expressed as follows:

$$\frac{\partial}{\partial y}\left(k_{wy}\frac{\partial h_w}{\partial y} \right) = 0 \tag{2}$$

where $\partial h_w/\partial y$ is the hydraulic head gradient in the y- direction; k_{wy} is the coefficient of permeability with respect to water phase in the y- direction and is a function of negative pore-water pressure. Meanwhile, the governing partial differential equation for unsteady-state water flow in unsaturated soils is formulated as follows:

$$\frac{\partial}{\partial y}\left(k_{wy}\frac{\partial h_w}{\partial y} \right) = m_2^w \rho_w g\frac{\partial h_w}{\partial t} \tag{3}$$

where m_2^w is the coefficient of water volume change with respect to the change in matric suction; and t is the time.

Instrumentation and Test Set-Up

The infiltration tests were conducted at Changi reclamation area, Singapore. The reclamation material was about 12 m thick and the water table was about 3 m below the ground surface.

Three pits of 0.6 m deep were excavated in a parallel setting as shown in Figure 1. The pit located at the center was about $1 \times 1 m^2$ area and provided for the placement of pore-water pressure measuring devices. The pits located at both ends were $0.5 \times 0.5 \ m^2$ area and provided for setting up the models of a single-layer soil and a two-layer soil. The single-layer soil model consisted of a 0.6 m thick medium sand, the existing reclamation material. Meanwhile, the two-layer soil model comprised a 0.4 m thick medium sand overlying a 0.2 m thick gravelly sand.
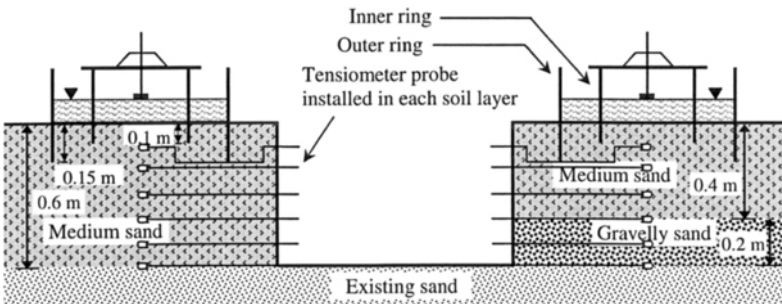
Figure 1. Schematic diagram of the field infiltration test.

A set of double-ring infiltrometer with a 0.3 m inner-ring diameter and 0.55 m outer-ring diameter was placed above each soil model. Using a driving plate, the inner ring was driven to a depth of 0.1 m, while the outer ring was hammered to a depth of 0.15 m below the ground surface. By this configuration, it was expected that a one-dimensional vertical flow of water occurred below the inner ring, where the infiltrating water through the outer ring acted as a barrier that reduced lateral movements of water from the inner ring.
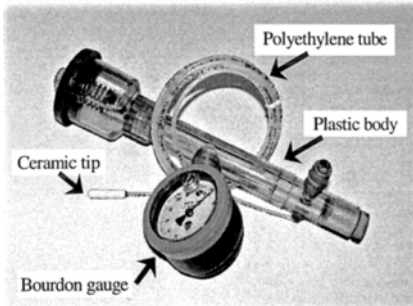
Figure 2. Tensiometer-bourdon gauge system.
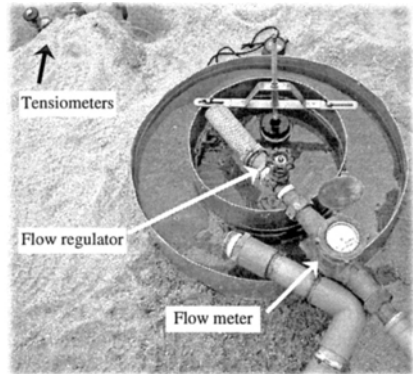
Figure 3. Field infiltration test setup.

Figure 2 shows a small tip tensiometer (Model 2100F Soilmoisture Probe, Soilmoisture Equipment Corporation, CA, USA) that was used to measure negative pore-water pressures during the field infiltration tests. Basic components of a tensiometer include a porous ceramic tip, a plastic body tube, and a pressure measuring device. The porous ceramic tip (Soilmoisture 2100F-200CR), which had a high air-entry value of 1bar, was 6 mm in diameter and 25 mm in length and it was attached to the plastic body tube via a coaxial polyethylene tube assembly of 1.8 m in length. Before use, the ceramic tip was saturated in a vacuum container filled with water. The readings of pore-water pressure changes during the tests were taken manually through a vacuum dial or bourdon gauge (Soilmoisture 2060FG4), which could be used to measure matric suctions ranging from 0 kPa to 90 kPa.

The ceramic tips of the tensiometers were installed during soil compaction. The medium sand of the single-layer soil model was re-compacted to its initial density, which was determined using sand replacement method as described in ASTM Designation D1556-00 (ASTM 2003). Meanwhile, the medium sand and gravelly sand of the two-layer soil model were compacted to a specified density. The soils were placed into the pits in 100 mm thick lifts and the mass of the soils for each lift was measured prior to compaction. The soils were compacted with a 2.5 kg Proctor hammer for 20 to 25 drops for each layer of 100 mm thick soil.

After compaction, the soils with the installed tensiometers were left for a few days to let the pore-water pressure in the soils to be in equilibrium with the surrounding existing sands and profiles of the maximum negative pore-water pressure to develop. The field infiltration tests were conducted using a constant head method by applying a maximum water pressure head of 20 mm in the double ring infiltration. The water pressure head was maintained throughout the tests by adjusting the flow regulator installed on the water pipe, as shown in Figure 3. Water used for the field infiltration tests came from the surrounding groundwater, which was pumped to the surface by a water pump and flown through a water pipe of 30 mm in diameter. The flow rates of the water infiltration were measured using a flow meter that was installed at the other end of the water pipe. Temperatures of the water and ground surface were measured during the field infiltration tests using a long-type thermometer (Traceable®) with a temperature measuring range from -50 to $150°$ C. During the tests, the readings of pore-water pressure changes were taken in each 30 seconds time interval. The test was stopped once the pore-water pressure of the bottom most layers reached zero.

Material Properties

Basic soil properties of the medium sand and the gravelly sand were investigated in the laboratory and the results are summarized in Table 1. The medium sand was greenish grey in color and contained some shells. The gravelly sand, which was essentially a mixture of coarse sand (50.1%) and fine gravel (49.9%), was light grey to white in color and was obtained commercially. Grain-size distributions of the soils were determined following ASTM D422-63 (ASTM 1998) and the results are presented in Figure 4. Specific gravity for the soils was measured as described in ASTM D854-02 (ASTM 2002a). The soils were classified in accordance with the Unified Soil Classification System (USCS) of the ASTM standard method D2487-00 (ASTM 2002b).

Table 1. Basic properties of the medium sand and the gravelly sand.

Description	Soil	
	Medium sand	Gravelly sand
Unified Soil Classification System	SP	SP
Specific gravity, G_s	2.67	2.66
Grain size distribution		
D_{60} (mm)	0.91	5.39
D_{30} (mm)	0.38	3.52
D_{10} (mm)	0.21	2.68
Coefficient of uniformity, C_u	4.33	2.01
Coefficient of curvature, C_c	0.76	0.86
Gravel content (> 4.75mm; %)	3.02%	47.51
Fines content (< 0.075mm; %)	0.46%	0
Dry density, ρ_d (Mg/m³)	1.73	1.62
Void ratio, e	0.55	0.64
Coefficient of permeability at saturation, k_s (m/s)	4.26×10^{-5}	7.60×10^{-2}

The SWCCs of the medium sand and the gravelly sand were obtained using a Tempe cell (model No. 1405 B01M3-3; Soilmoisture Equipment Corporation, USA), which

was operated using the same principle as the pressure plate described in ASTM standard method D2325-68 (ASTM 2000) (Fredlund and Rahardjo 1993).
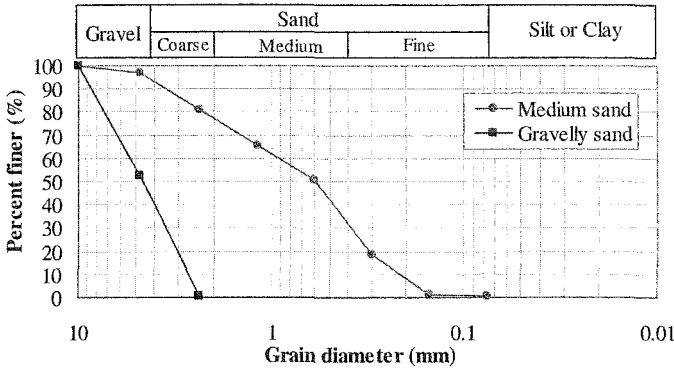
Figure 4. Grain-size distributions of the medium sand and the gravelly sand.
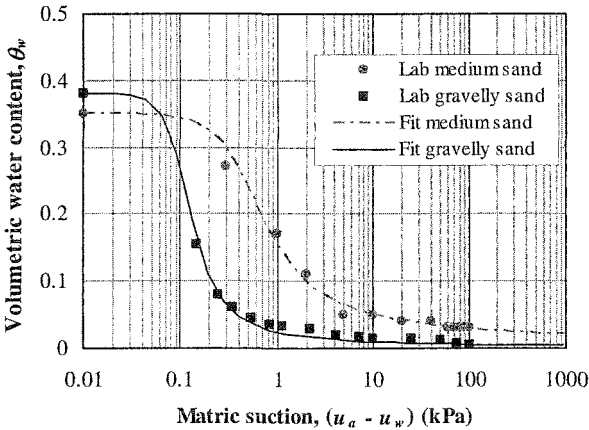
Figure 5. Soil-water characteristic curves of the medium sand and the gravelly sand.

Table 2. SWCC parameters of the medium sand and the gravelly sand.

Description	Symbol	Unit	Soil	
			Medium sand	Gravelly sand
Saturated volumetric water content	θ_s	-	0.352	0.382
Air-entry value	ψ_a	kPa	0.188	0.058
Residual matric suction	ψ_r	kPa	0.452	0.500
Residual volumetric water content	θ_r	-	0.021	0.026
Fitting parameters	a	kPa	0.321	0.100
	n	-	2.468	3.521
	m	-	0.937	1.322

In order to obtain a continuous SWCC, the measured SWCC was then fitted with the Fredlund and Xing (1994) function where the correction factor, $C(\psi)$, is taken as 1 as suggested by Leong and Rahardjo (1997a). The SWCCs of the medium sand and the gravelly sand are shown in Figure 5 and the SWCC parameters are listed in Table 2.

Figure 6 shows the permeability functions of the medium sand and the gravelly sand. Permeability functions of the medium sand and the gravelly sand were determined indirectly using the statistical method originally proposed by Childs and Collis-George (1950). The SWCC and the coefficient of permeability at saturation, k_s of the soil were used as the input. The predicted permeability functions were then best-fitted with the permeability functions suggested by Leong and Rahardjo (1997b) by changing parameter p. The curve-fitting results showed that the parameters p for the medium sand and the gravelly sand were 2.5 and 2.2, respectively.
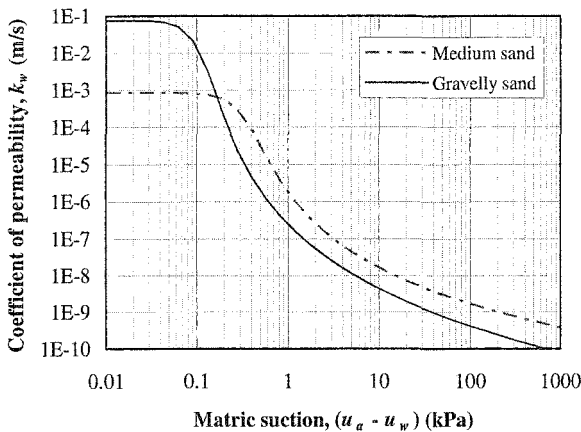
Figure 6. Permeability functions of the medium sand and the gravelly sand.

Numerical Simulations

Infiltration process in the field was simulated numerically using a finite element model, SVFlux (SoilVision Systems Ltd., 2003). The model used automatic adaptive mesh generation and refinement algorithms to solve each problem. Two soil columns of different soil profiles were developed in order to simulate the soil layer models developed in the field. The first soil column was divided into two regions of 0.6 m and 2.4 m high, representing the regions of the re-compacted medium sand and the existing sand, respectively. The second soil column was divided into three regions of 0.4 m, 0.2 m, and 2.4 m high, representing the regions of the re-compacted medium sand, the gravelly sand, and the existing sand, respectively.

The initial condition for the infiltration test simulations was obtained by performing a steady-state analysis with a constant water table at the bottom of the soil column. The bottom boundary condition of the constant water table was maintained

throughout the numerical simulations. Subsequently, a transient analysis of drying process of water infiltration was performed with the boundary condition at the top of the soil column being negative flux. A negative flux of 10^{-6} m/s was applied to the top of the re-compacted medium sand in each soil layer model in order to impose the initial pore-water pressure head profile of the numerical model to be similar to the one measured in the field.

Once the desired initial pore-water pressure profile was developed, a transient analysis of wetting process of water infiltration was performed. A total head boundary condition of 0.02 m was applied to the top of each soil layer model, representing the constant water pressure head maintained in the double-ring infiltrometer during the field test.

Results and Discussions

Figure 7 and Figure 8 show responses of tensiometers installed at various depths in the medium sand layer and medium sand overlying gravelly sand layer, respectively. As indicated by the responses of tensiometers installed at z = -0.1 m, z = -0.2 m, and z = -0.3 m, downward water movement through the medium sand of the single-layer soil model was relatively similar to that of the two-layer soil model.
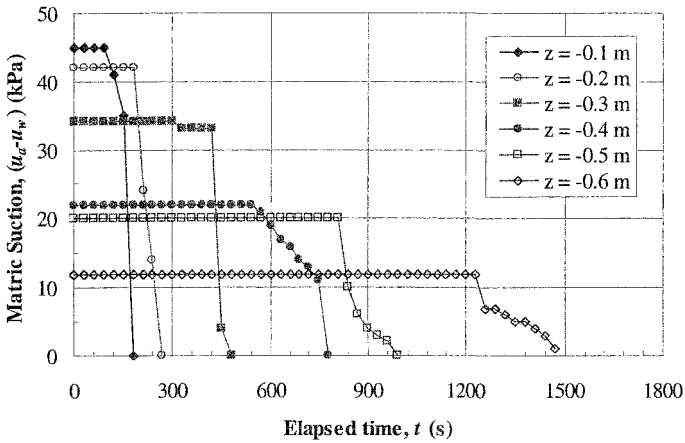
Figure 7. Tensiometer responses at various depths in the medium sand layer.

Relatively large differences of downward water infiltration in both soil layer models occurred at depths greater than z = -0.3 m. For instance, water infiltrated through the medium sand of the single-layer soil reached a depth of z = -0.6 m approximately at t = 1230 s and the matric suction in the soil layer at this depth reduced to 0 kPa at t = 1500 s. Meanwhile, water infiltrated through the gravelly sand of the two-layer soil model reached the same depth at t = 1650 s and matric suction in the soil layer decreased to 0 kPa at t = 1740 s.
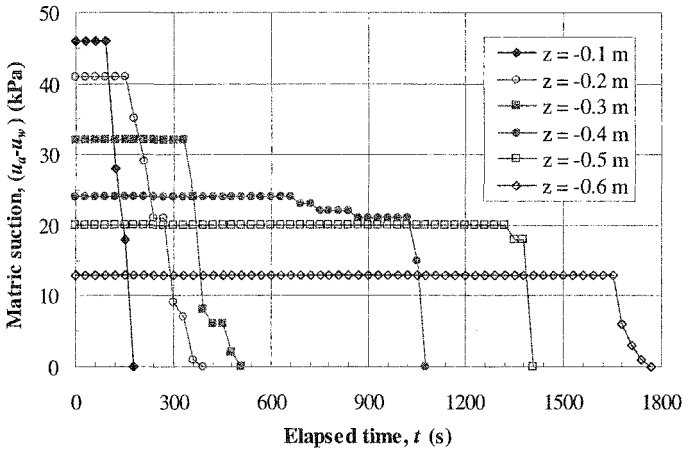
Figure 8. Tensiometer responses at various depths in the medium sand overlying gravelly sand layer.

The slower downward movement of water infiltration through the lower part of the two-layer soil model as compared to that of the single-layer soil model was most likely caused by the lower unsaturated permeability of the gravelly sand in the two-layer soil model as compared to the that of the medium sand in the single-layer soil model. The contrast in the unsaturated permeability between the medium sand and gravelly sand in the two-layer soil model, as shown in Figure 6, impeded the downward water movement into the underlying gravelly sand layer.

Figure 9 and Figure 10 show comparisons between the pore-water pressure profiles obtained from the field infiltration tests and the numerical simulations. In general, the numerical simulation results were in good agreement with the field test results. The infiltration characteristics of the single-layer soil model and the two-layer soil model as observed in the field test results were also indicated in the numerical simulation results.

The main discrepancies between the numerical simulation results and the field test results in both soil-layer models were observed at the late stage of the infiltration tests. The field data showed that the pore-water pressures particularly in the upper parts of both soil-layer models increased shortly after t = 10 min. At t = 25 min, the pore-water pressures in all soil layers of both models increased to zero, indicating water had reached the bottom part of the soil layers. On the other hands, the numerical simulation results at t = 25 min indicated that water had not reached the bottom parts of both soil-layer models as the pore-water pressures at the lower part of the soil-layer models remained negative.
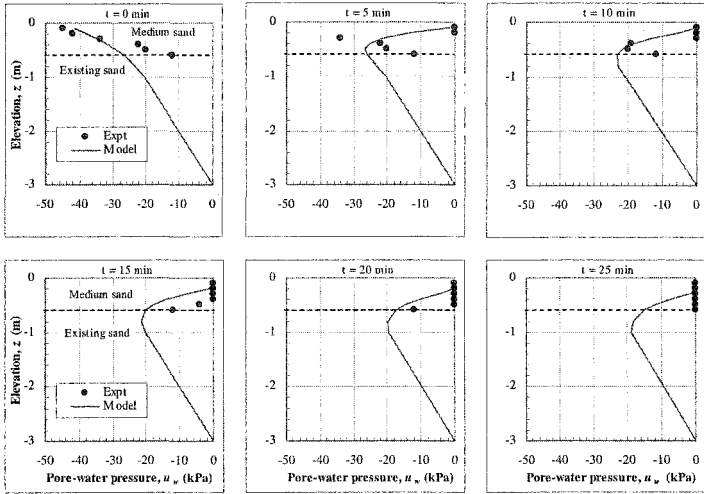
Figure 9. Comparisons of pore-water pressure profiles in the single-layer soil model.
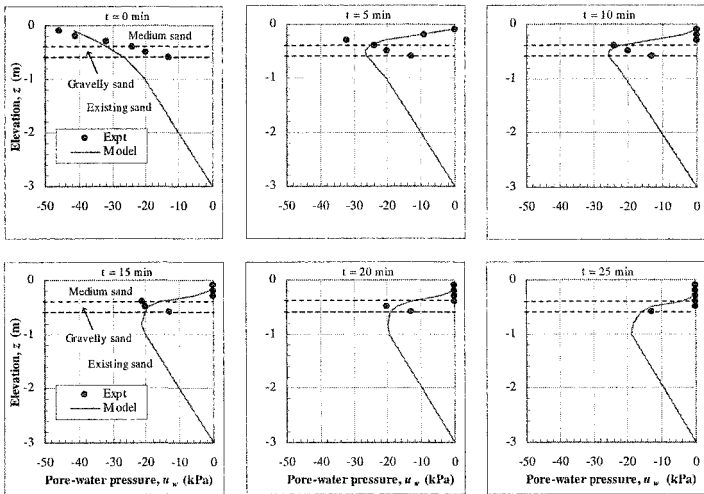
Figure 10. Comparisons of pore-water pressure profiles in the two-layer soil model.

The discrepancies between the numerical simulation results and the field data could be due to the soil hydraulic properties used in the numerical simulations. In this study, only the drying soil-water characteristic curves and drying permeability functions were available and used as input in the numerical simulations of both drying and wetting processes. If the wetting soil hydraulic properties were used to

simulate the wetting process during water infiltration, the pore-water pressures in the soil layers of both soil-layer models might increase faster during the wetting process. The wetting SWCC and permeability function are commonly characterized by having a steeper slope as compared to the drying SWCC and permeability function at low matric suction values. As a result, the volumetric water content and the permeability of the soil will increase at a faster rate and consequently, the pore-water pressures will increase very quickly during the wetting process at low matric suction values.

Conclusions

Small-scale field infiltration tests and numerical analyses were conducted in this study to investigate infiltration characteristics of a single-layer soil and a two-layer soil. The field infiltration tests were conducted using a double-ring infiltrometer. Changes in matric suctions during the tests were measured using tensiometers installed at various depths in the models. Simulations of the field infiltration tests were performed using a finite element program. The numerical simulation results were found to be in reasonably agreement with the field infiltration test results.

Acknowledgements

References

Akindunni, F.F., Gillham, R.W., and Nicholson, R.V. (1991). "Numerical simulations to investigate moisture-retention characteristics in the design of oxygen-limiting covers for reactive mine tailings." *Canadian Geotechnical Journal*, 28, 446-451.

ASTM. (1998). *Standard test method for particle-size analysis of soils (D422-63)*.

ASTM. (2000). *Standard test method for capillary-moisture relationships for coarse- and medium-textured soils by porous-plate apparatus (D2325)*.

ASTM. (2002a). *Standard test methods for specific gravity of soil solids by water pycnometer (D854-02)*.

ASTM. (2002b). *Standard practice for classification of soils for engineering purposes (Unified Soil Classification System) (D2487-00)*.

ASTM. (2003). *Standard Test Method for Density and Unit Weight of Soil in Place by the Sand-Cone Method (D1556–00)*.

Bodhinayake, W., Si, B.C., and Noborio, K. (2004). "Determination of hydraulic properties in sloping landscapes from tension and double-ring infiltrometers." *Vadose Zone Journal*, Soil Science Society of America, 3, 964-970.

Barbour, S.L., and Yanful, E.K. (1994). "A column study of static nonequilibrium fluid pressures in sand during prolonged drainage." *Canadian Geotechnical Journal*, 31, 299-303.

Childs, E.C., and Collis-George, G.N. (1950). "The permeability of porous materials." *Proceedings of the Royal Society of London*, 210A, 392-405.

Fredlund, D.G., and Rahardjo, H. (1993). *Soil mechanics for unsaturated soils*. John Wiley & Sons, Inc, New York.

Leong, E.C., and Rahardjo, H. (1997*a*). "Review of soil-water characteristic curve equations." *Journal of Geotechnical and Geoenvironmental Engineering*, ASCE, 23(12), 1106-1117.

Leong, E.C., and Rahardjo, H., (1997*b*). "Permeability functions for unsaturated soils." *Journal of Geotechnical and Geoenvironmental Engineering*, ASCE, 123(12), 1118-1126.

SoilVision Systems Ltd. (2003). *SVFlux user's guide, version 3.09*. SoilVision Systems Ltd., Saskatoon, Saskatchewan, Canada.

Stormont, J.C., and Anderson, C.E. (1999). "Capillary barrier effect from underlying coarser soil layer." *Journal of Geotechnical and Geoenvironmental Engineering*, ASCE, 125(8), 641-648.

Watson, K.W., and Luxmoore, R.J. (1986). "Estimating macroporosity in a forest watershed by use of a tension infiltrometer." *Soil Science Society of America Journal*, 50, 578-582.

Woyshner, M.R., and Yanful, E.K. (1995). "Modeling and field measurements of water percolation through an experimental soil cover on mine tailings." *Canadian Geotechnical Journal*, 32, 601–609.

Yanful, E.K., Riley, M.D., Woyshner, M.R., and Duncan, J. (1993). "Construction and monitoring of a composite soil cover on an experimental waste-rock pile near Newcastle, New Brunswick, Canada." *Canadian Geotechnical Journal*, 30, 588–599.

Yang, H., Rahardjo, H., Leong, E.C., and Fredlund, D.G. (2004). "A study of infiltration on three sand capillary barriers." *Canadian Geotechnical Journal*, 41, 629–643.

Zhang, L.L., Fredlund, D.G., Zhang, L.M., and Tang, W.H. (2004). "Numerical study of soil conditions under which matric suction can be maintained." *Canadian Geotechnical Journal*, 41, 569–582.

Monitoring field experiment in an unsaturated sandy soil slope in Switzerland

A. Thielen[1], S. M. Springman[2]

[1] Institute for Geotechnical Engineering, Swiss Federal Institute of Technology Zurich, ETH Hoenggerberg, CH-8093 Zurich; PH (41) 44-6333040; FAX (41) 44-6331079; email: andrea.thielen@igt.baug.ethz.ch
[2] Institute for Geotechnical Engineering, Swiss Federal Institute of Technology Zurich, ETH Hoenggerberg, CH-8093 Zurich; PH (41) 44-6333805; FAX (41) 44-6331079; email: sarah.springman@igt.baug.ethz.ch

Abstract:

The monitoring of saturation and desaturation processes is a critical issue for the assessment of potential landslides. In this study, results from the first year of a monitoring experiment on a 15 by 13 metre square test site in the vicinity of previous landslides are presented. A top layer of clayey sand overlies weathered sandstone just above the rock surface and this layering system allows rapid infiltration. Preceding geophysical investigations helped to optimize the configuration of the test site. Meteorological data (e.g. rainfall, temperature and air pressure), infiltration and outflow, suction and volumetric water content at different depths up to 1.5 m have been measured continuously using among others tensiometers, Time Domain Reflectometers and MoisturePoint devices. Interaction has been observed between suction and volumetric water content and between rainfall intensity and the reaction at different soil depths. Seasonal hydrological changes can also be presented in terms of the response characteristics of the soil to rainfall events.

Introduction

Steep slopes with an inclination greater than the friction angle of the soil can be stable due to the effect of suction, which augments the shear strength and can be represented as an apparent cohesion. The relationships between stress, strain, strength, suction and water content has been described by a large number of constitutive models with different approaches, well reviewed for example by Wheeler and Karube (1996). During infiltration of rainfall, the stabilizing effect of suction decreases with increasing saturation (S_r) and the following reduction of shear strength can result in failure, at worst culminating in a natural hazard.

Observations of this behaviour have been made for example by Springman et al. (2003) in a moraine slope with an inclination of 42°. The slope had been stable under unsaturated conditions and failed after 2 days of artificial rainfall irrigation. Also from former observations (and the daily newspapers), it is known that there is a strong historical link between extreme rainfall and landslide activity in Switzerland (e.g. Latelin et al., 2001) and overseas (e.g. Brand et al., 1984; Johnson and Sitar, 1990; Anderson and Sitar, 1994).

A series of 42 landslides occurred for example in May 2002 in North Switzerland near the river Rhine after an extreme rainfall event, in which 100 mm rain fell in 40 minutes (Fischer et al. 2003). The location of 6 such examples and pictures of two of them are plotted in figure 1. To investigate the relationship between rainfall, suction, volumetric water content and shear strength for the typical soil of this endangered area beside the river Rhine, a test site only a few metres away from already failed slopes and consisting of the same soil type has been equipped with various measuring devices for a monitoring experiment of two years duration.
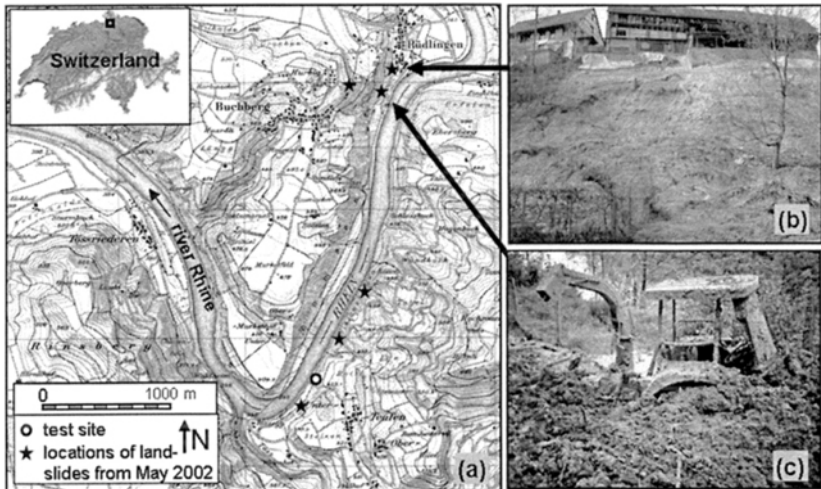
Figure 1. Location of the test site. (a) detailed map and map of Switzerland (after Bundesamt für Landestopographie 1976 and 2000), (b) and (c) pictures of landslides after the rainfall event in May 2002.

The main results of the first year of the monitoring experiment are reported in this paper.

Description of the test-site

The grass covered test slope (Fig. 2) has an average inclination of 27.° A top layer of clayey sand overlies weathered sandstone (silty sand) just above the rock surface. A combination of geophysical, geological and geotechnical methods was

applied for a site investigation prior to instrumentation (Thielen et al. 2005 and Friedel et al. 2005), which yielded a high resolution model of the subsurface. With the help of this model (Fig. 2) the placement of sensor probes was optimised for the monitoring experiment.
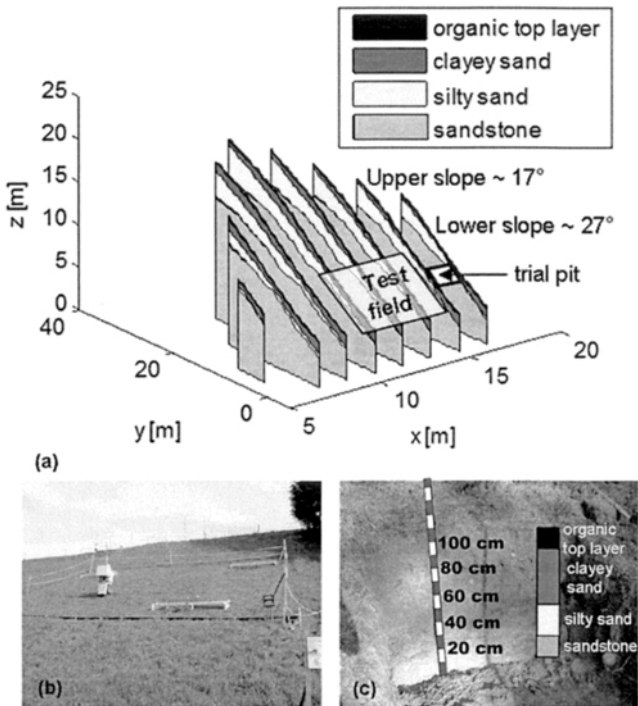
Figure 2. (a) model of the subsurface and location of the instrumented test site, (b) picture of the test field, (c) picture of the soil profile in the trial pit.

Characterisation of the soil

Classification of the two soil types (clayey sand and silty sand) was carried out following the Swiss Standards (VSS, 1997), based on USCS, including determination of the grain size distribution by sieving (VSS, 1986) and sedimentation (VSS, 1990a), determination of the density of solids (VSS, 1990b) and plasticity analyses (VSS, 1990c). In addition, permeability tests and determination of the dry bulk density was performed on undisturbed samples taken from the trial pit. Information about the grain size distribution, plasticity index, permeability and density for both soil types can be taken from table1.

Table 1. Results from laboratory tests

	Clayey sand	Silty sand
Grain size distribution		
Grain size [mm]	% passing	% passing
< 31.5	100	100
< 0.5	97	98.3
< 0.06	41.2	26.8
< 0.02	23.3	15.8
< 0.002	7.1	5.6
Plasticity analysis		
Ip [-]	7.3-17.75	3.29-5.85
w_L [-]	22.6-35.5	22.6-25.1
Permeability [m/s]	~$3*10^{-8}$	~$5*10^{-6}$
Dry bulk density [g/cm3]	1.29-1.49	1.29-1.40

Preceding investigation of the influence of rainfall

Contrary to geotechnical testing methods, geophysical imaging techniques can be used to derive a spatial image of the subsurface in landslide or instable slope areas (e.g. Hack, 2000). An especially suitable parameter for landslide investigations is electrical resistivity ρ that increases with porosity Φ and saturation ratio S_r, following the relationship from Archie (1942):

$$\rho = \frac{a}{\Phi^m S_r^n} \rho_W$$

The parameters a, m and n are empirical and ρ_W is the water resistivity, which is relatively constant. For a given material, the parameters a, m, n must be determined experimentally or taken from the literature (e.g. Schön 1983). For this example, it is assumed that full saturation in the areas of loose soil is reached with a resistivity of approximately 35 Ωm.

Electrical resistivity is today most effectively mapped using electrical resistivity tomography (ERT). Recently successful applications for landslide investigation include the works of Suzuki and Higashi (2001) and Lapenna et al. (2003). ERT-measurements on the test field were carried out in August 2003 and in July 2004 to get a first impression of the influence of rainfall on the degree of saturation. Figure 3 shows the resistivity images of 2003 compared to 2004 in the most interesting lower part of the slope. Low resistivity corresponds to high saturation and vice versa. The years 2003 and 2004 differ significantly in the amount of rainfall (more rainfall in 2004 than in 2003) and the resulting differences in water content were measured in the layer on top of the sandstone (Fig. 3). For this reason, the instrumented test site was located in the lower part of the field (see Fig. 2), where the above mentioned layer of interest could be reached with the sensor probes, whose lengths are usually restricted to a maximum of 1.5 m.
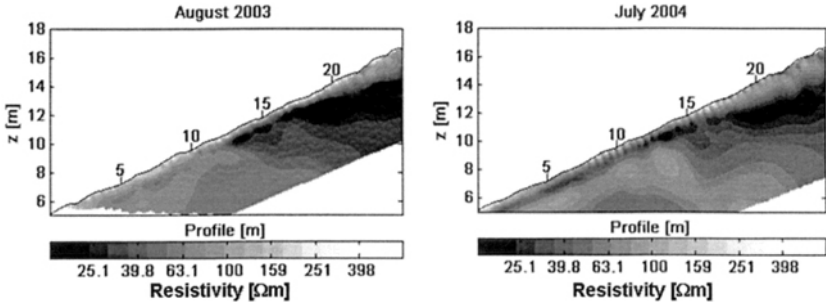
Figure 3. Comparison of resistivity tomograms (lower slope) taken in August 2003 and in July 2004.

The description of these and other geophysical investigations at the test site can be found in more detail in Friedel et al. (2005). Additional ERT-measurements in autumn, winter and spring will be done during this period. With this more complete plane image of saturation along the slope the understanding and significance of the data can be improved.

Instrumentation of the test site

Figure 4 shows the plane and the vertical distribution of the instrumentation used for this field study. The volumetric water content of the soil was measured using two types of Time Domain Reflectometry (TDR). A TDR device with 11 probes and a Moisture Point (ESI 2004) device with 4 probes each composed of 5 segments were installed at different depths in four locations on the test-site (Fig. 4). The TDR method is based on the significantly different dielectricity (K_a) of water ($K_a{\sim}81$) and of soil minerals ($K_a{\sim}3$-4) or air ($K_a{\sim}1$). The dielectricity of a bulk soil is therefore an indicator of its volumetric water content. The TDR system measures the propagation velocity (v_p) of a voltage pulse along the probe and dielectricity can be described as a function of v_p. With known dielectricity, volumetric water content θ can be calculated with the help of calibration functions (e.g. Topp et al. 1980). Calibration curves have been determined in the laboratory for the TDR systems and probes used in this monitoring experiment. More details of the calibration can be found in Thielen & Springman (2005).

TDR probes have a length of 15 cm and give point wise information about the water content. The Moisture Point devices are composed of 5 segments with segment lengths of 15 or 30 cm. Each operates similarly to the TDR probes and the water content along a vertical profile can be determined. Useful experience has been obtained with this combination of instruments in moraine by Springman et al. (2003). Two types of tensiometers were used for the measurement of suction: 15 tensiometers with electronic pressure transducers for continuous data logging, with

measurements taken every 10 minutes and 30 tensiometers for manual readout installed to verify the continuous data.
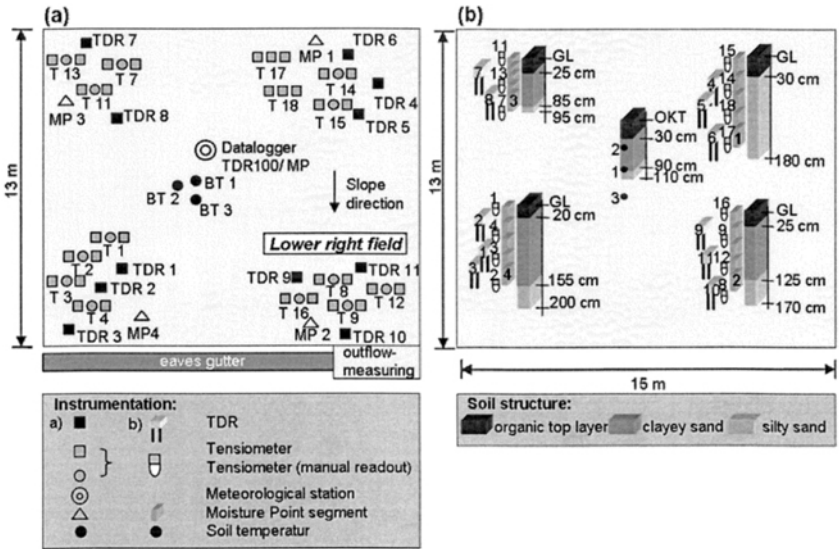
Figure 4. Instrumentation design of the test site (a) plan view, (b) vertical distribution of sensor probes.

Rainfall, soil temperature, air temperature, air pressure, air moisture and outflow were also measured within the scope of the monitoring experiment. In addition measuring devices for wind speed and solar radiation are installed at the moment in order to estimate the evapotranspiration rate. A more detailed description of the instrumental setup and the measuring devices used can be found in Thielen & Springman (2005).

Analysis and Discussion of Results

The results of the first year of the monitoring experiment are presented in this chapter. Attention is turned to the influence of rainfall at different soil depths and the interaction between measured volumetric water content and suction.

Annual characteristics of the data. Rainfall, suction and volumetric water content data for four depths from August 2004 till June 2005 are plotted in figure 5 for the lower right instrumentation field.

The Tensiometer data agrees with the corresponding TDR or Moisturepoint data. Increases in volumetric water content are accompanied by a decrease in suction, and with a volumetric water content decrease an increase in suction can be observed. The

lack of data from the middle of September to the middle of October was caused by an attack of mice which destroyed the cables connecting the instruments to the data logger.
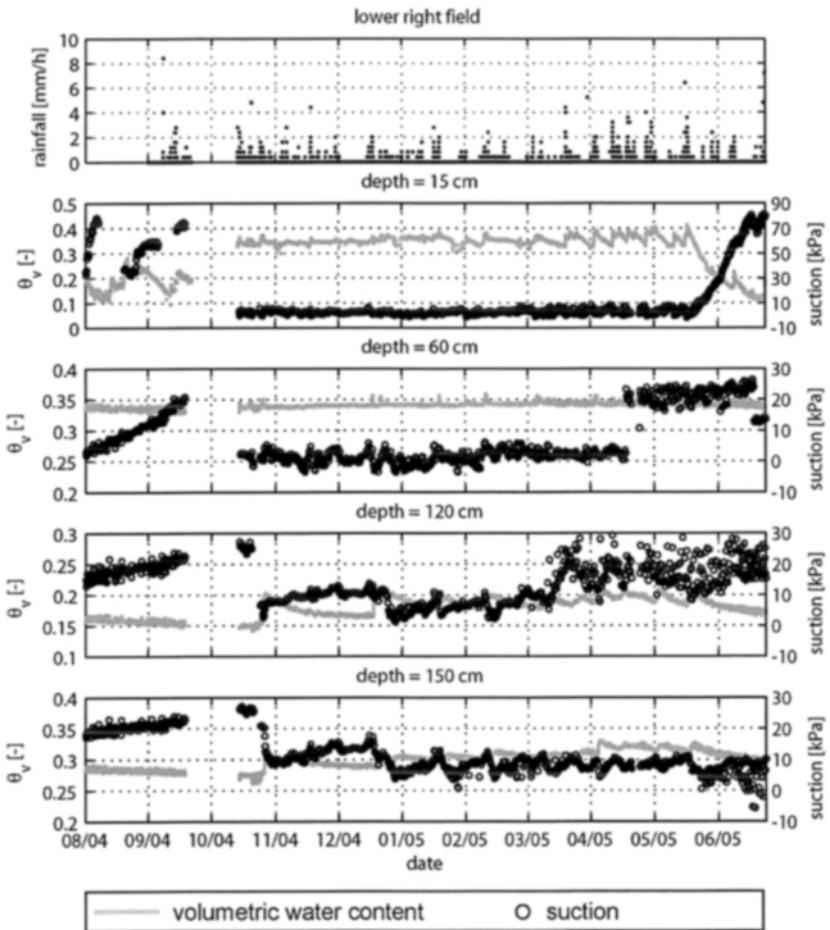
Figure 5 Rainfall, volumetric water content (Moisturepoint/TDR data) and suction (Tensiometer data) for the lower right field during the first year of the monitoring experiment.

Some short gaps in the data from tensiometers installed in the upper soil layer occurred when the instruments were dislodged by suction exceeding 80 kPa, which is a general problem of this type of tensiometers (Ridley et al., 2003). They had to be refilled by hand in a wetting period in order to resume work.

In soil layers deeper than 60 cm the average volumetric water content decreased from August 04 to October 04 and from April 05 to June 05 and increased between October 04 and April 05. There seem to be two periods with opposed average water content development, summer period between April and October and winter period between October and April. Data from the second year of measurements will give more information on this. At a depth shallower than 60 cm, this observation is also valid for the winter period. In summer, this layer was generally much less saturated but water content varied frequently often due to rainfall infiltration and evapotranspiration and a continual decrease in volumetric water content could not be observed.

The moisture retention capacity of the upper soil layer is high enough and its permeability is low enough to prevent flow to greater depths in summer even if the suction in deeper layers is higher generating an upwardly hydraulic gradient. In winter, the silty sand layer (>120 cm) shows the greatest response to rainfall events. The overlying clayey sand seems to be almost fully saturated and therefore cannot retain the water.

Response to rainfall in summer and in winter. Two rainfall events (Fig. 6) have been chosen to discuss in detail the differences between summer and winter. Suction and saturation data from five days around a rainfall event is plotted against depth at different time intervals.

A saturation ratio greater than 1 is not possible in this situation. It must, however be calculated using volumetric water content and soil porosity around the TDR probes. Actual porosity valves could not be measured and were assumed based on the dry densities of soil samples taken from the trial pit, which has led in some cases to a calculated saturation ratio greater than unity. The intensity and duration of the two rainfall events are very similar, so a valid comparison can be made.

In summer, a response to rainfall infiltration could only be observed in the upper soil layer (depth<60 cm). Already, at a depth of 60 cm no significant change in suction and saturation was observed. Before rainfall infiltration began, saturation of the upper soil layer was relatively low (S_r<0.5). The moisture retention capacity was high and hydraulic conductivity low. The saturation ratio in the same layer after the rainfall event was 0.7. At greater depth the soil was almost fully saturated and suction was lower than at lower depth generating an upwardly hydraulic gradient. The water content of the upper layer could decrease only by evapotranspiration.

During the winter, changes in suction and saturation due to the rainfall event could be observed at all depths. The main response to rainfall infiltration appears however at greater depth (>120 cm). Even before rainfall starts, the clayey sand layer (<120 cm) is almost fully saturated. The moisture retention capacity is very low or zero and hydraulic conductivity maximal. Regarding the suction distribution over depth the hydraulic gradient generates a downward water flow which increases saturation of deeper soil layers (see also figure 5).
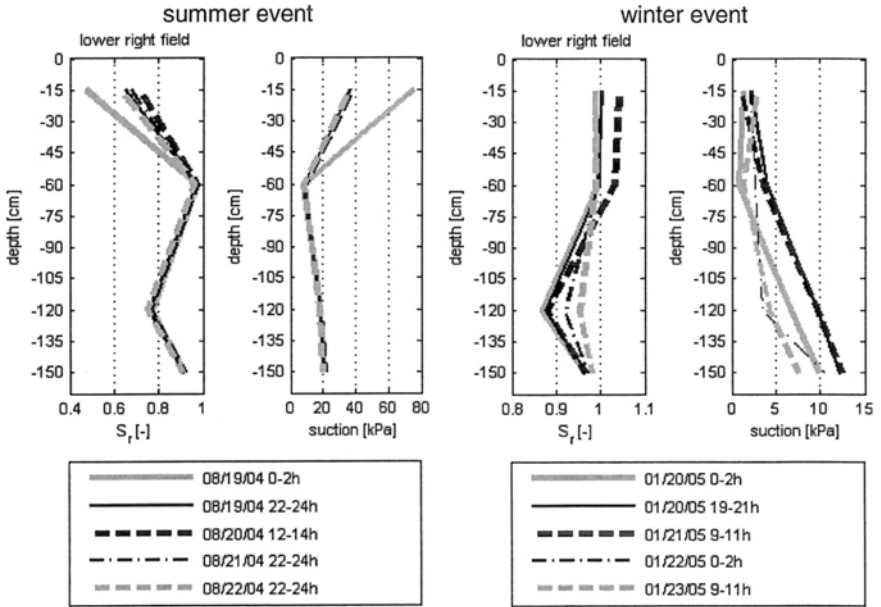
Figure 6. Saturation (Moisturepoint/TDR data) and suction (Tensiometer data) against depth for the lower right field during 5 days around a rainfall event in summer (left side) and in winter (right side).

Water retention curves. Saturation ratio of the soil is plotted against corresponding suction for the lower left field (Fig. 7) to determine the in situ soil water characteristics. A pair of variables is composed of the values from Tensiometer data and the TDR and Moisturepoint data at the same field, depth and time.

The soil remains fully saturated until suction augments to 10 kPa. Between suction valves of 10 kPa and 100 kPa the saturation ratio reduces to a value of 0.2. When a comparison is made between the in situ water retention curves (WRC) and usual results for silty sands (e.g. Nishimura & Fredlund 2000) the measured data seams very reasonable. Determination of the water retention curve of the two soil types in the laboratory is underway and data will be available soon to compare with field data. A hysteresis loop on the WRC can be observed in the data at depths of 90 cm and 150 cm.
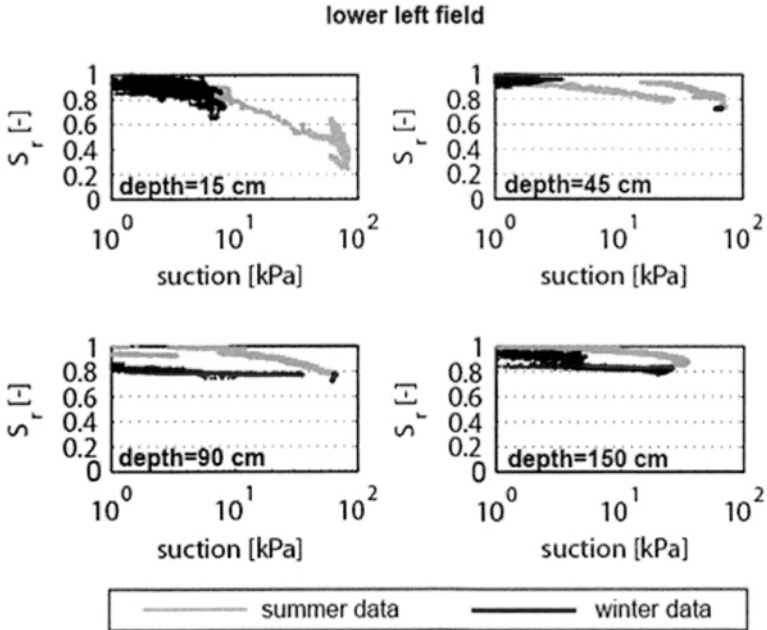
lower left field

Figure 7. **In situ water retention curves for different depths in the lower left test field. TDR or Moisturepoint data is plotted against data from a Tensiometer at the same depth and time.**

Implications on slope stability

A test site in the north of Switzerland has been equipped with various measuring devices to study the influence of rainfall infiltration on saturation ratio and suction, and its effect on the stability of the slope. Preceding investigations have shown that long term changes in water content occur in the soil layer on top of the sandstone basement. The field measurements have shown that during the summer months, a normal rainfall event does not cause saturation and suction changes in deeper soil layers. Consequently the shear resistance of the soil will not be influenced.

In winter, all soil layers are influenced by rainfall and suction often reduces to zero. Figure 7 shows a clear hysteresis effect in the WRC of the soil layers in depth of 90 cm and 150 cm. During winter months, data is on the wetting curve and with the same saturation ratio as in summer, which is associated with a lower suction contribution to stability.

The monitored slope with an inclination of 27° has been stable even without the suction contribution. If we consider that slopes with the same inclination failed

during the above mentioned event in May 2002, we can assume that the formation of perched water tables at interfaces between soil layers with different permeability could be the cause of this. The storm event in May 2002 was far more severe than those monitored during the first year of the experiment. Unfortunately, the saturation condition before this event is not known in order to decide, if only the heaviness of the event or also the preconditions were cause for the landslides. A second year of measurements will bring more information about the importance of long term and short term changes in water content concerning landslide initiation in this kind of soil.

Acknowledgements

References

Anderson, S.A.; Sitar, N. 1994. Procedures for the analysis of the mobilisation of debris flows. Proc. 13th Int. Conf. on SMFE, New Delhi, Oxford and IBH 1, pp. 255-258.

Archie, G. E. 1942. The electrical resistivity log as an aid in determining some reservoir characteristics. Trans. AIME 146, pp. 54-62.

Brand, E.W.; Premchitt, J.; Phillipson, H.B. 1984. Relationship between rainfall and landslides in Hong Kong. Proc. 4th Int. Symp. on Landslides 1, pp. 377-384.

Bundesamt für Landestopographie 3084 Wabern, 1976. Landeskarte der Schweiz 1:25000. Karte 1051 (Eglisau).

Bundesamt für Landestopographie 3084 Wabern, 2000. Atlas of Switzerland interactive, 3D Topography and Statistical Maps

ESI, Environmental sensors, 2004. (http://www.esica.com).

Fischer, C.; López, J.; Springman, S.M. 2003. Remediation of an eroded steep slope in weathered sandstone after a major rainstorm. International Conference on Landslides, Hong Kong, 8.-10. Dec. 2003, pp. 878-883.

Friedel, S.; Thielen, A.; Springman, S.M. 2005. Investigation of a site endangered by rainfall-induced landslides using 3D resistivity tomography and geotechnical testing. *J. Appl. Geophys.* (submitted).

Hack, R. 2000. Geophysics For Slope Stability. Surv. in Geophys. 21(4), pp. 423-448.

Johnson, K.A.; Sitar, N. 1990. Hydrologic conditions leading to debris-flow initiation. Canadian Geotechnical Journal, 27, pp. 789-801.

Lapenna, V.; Lorenzo, P; Perrone, A.; Piscitelli, S.; Sdao, F; Rizzo, E. 2003. High-resolution geoelectrical tomographies in the study of Giarrossa landslide (southern Italy). Bull. Eng. Geol. and Env. 62, pp. 259-268.

Lateltin, O, Bollinger; D.; Hegg, C.; Kreusen, H-R. 2001. The analysis of the 1999 landslides in Switzerland. Proc Int. Conf. on Landslides, Davos, ed. M. Kühne et al., VGE, Essen, pp. 159-167.

Nishimura, T.; Fredlund, D.G. 2000. Relationship between shear strength and matric suction in an unsaturated silty soil. *Unsaturated Soils for Asia*, Toll & Leong (eds) © 2000 Balkema, Rotterdam, ISBN 90 5809 139 2, pp. 563-568.

Ridley, A.M.; Dineen, K.; Burland, J.B.; Vaughan, P.R. 2003. Soil matrix suction: some examples of its measurement and application in geotechnical engineering. Géotechnique, Vol. 53, No. 2, pp. 241-252.

Schön, J. 1983. *Petrophysik. Physikalische Eigenschaften von Gesteinen und Mineralien*. Berlin: Akademie -Verlag.

Springman, S.M.; Jommi, C.; Teysseire, P. 2003. Instabilities on moraine slopes induced by loss of suction: a case history. *Géotechnique* Vol. 53, No. 1, pp. 3-10.

Suzuki, K.; Higashi, S. 2001. Groundwater flow after heavy rain in landslide-slope area from 2-D inversion of resistivity monitoring data. Geophysics 66(3), pp. 733-743.

Thielen, A.; Springman, S.M. 2005. First results of a monitoring experiment for the analysis of rainfall induced landslides -, International Symposium on Advanced Experimental Unsaturated Soil Mechanics- EXPERUS 2005, JUNE 27-29, 2005, Trento, Italy

Thielen, A.; Friedel, S.; Plötze, M.; Springman, S.M. 2005. Combined approach for site investigation in terms of the analysis of rainfall induced landslides. Sixteenth International Conference on Soil Mechanics and Geotechnical Engineering, Osaka, September 2005.

VSS, 1986. Mineralische Baustoffe und Lockergesteine – Siebanalyse. Schweizer Norm SN 670810c.

VSS, 1990a. Mineralische Baustoffe, Schlämmanalyse nach der Aräometermethode. Schweizer Norm SN 670816a.

VSS, 1990b. Versuche: Dichte des Bodens. Schweizer Norm SN 670335a.

VSS, 1990c. Konsistenzgrenzen. Schweizer Norm SN 670345a.

VSS, 1997. Identifikation der Lockergesteine – Labormethode mit Klassifikation nach USCS. Schweizer Norm SN 670 008a.

Wheeler, S.; Karube, D. 1996. Constitutive modelling. Proc. of the 1st Int. Conf. on Unsaturated Soils, UNSAT'95, Balkema, Vol.3, pp. 1323-1356.

Evaluation of Changes to Soil Suction Resulting from Residential Development

K.D. Walsh[1], C.A. Colby[2], W.N. Houston[3], and S.L. Houston[3]

[1]Department of Civil and Environmental Engineering, San Diego State University, 5500 Campanile Drive, San Diego, CA 92182-1324; PH (619) 594-0911; FAX (619) 594-8078; email: kwalsh@mail.sdsu.edu
[2]Automated Performance Monitoring, 5592 S. Moore, Littleton, CO 80127, PH (303) 973-7947; FAX (303) 973-0245; email: colbyc@wwdb.org
[3]Department of Civil and Environmental Engineering, Arizona State University, Tempe, AZ, 85287-5306, PH (480) 965-3589, FAX (480) 965-0557

Abstract

When new development occurs in arid regions, the boundary conditions and in particular the amount of water applied to the soil is usually changed. This change in the boundary condition at the surface can induce a change in the soil suction profile. In the case where the soils underlying structures exhibit volume change in response to a change in soil suction, a change in the soil suction can in turn induce volume change in the soil. As a consequence, the degree (amount by which the suction changes) and extent (depth over which a change occurs) of soil suction change are of interest to designers developing recommendations for many aspects of new construction, including grading, floor and foundation support, and landscaping. A series of suction measurements are reported for samples recovered from over 30 sites in the Denver metropolitan area where single-family residential structures have been in-place between 7 and 62 years. Samples were obtained to depths of approximately 12 meters. A companion set of results are presented for sites at which no development has yet occurred. In general, comparison of these results suggests that residential development affects the underlying soil suction profile in complex ways. In several cases, no effect can be observed. In most, suction decreased in the upper 3 to 7 meters, and in a few cases deeper wetting was suggested. The depth of suction decrease did not correlate to the age of the structure. However, operating characteristics, in particular landscaping choices and watering policies, have a significant influence over the degree and extent of suction changes.

Introduction

In areas where moisture-sensitive soils are prevalent, the foundation designer must consider the likely effect on the supported structure that will accrue from a change in the moisture regime in underlying soils. The estimation of the likely effect of such a change is conceptually simple: estimate the magnitude and direction of the change in the moisture regime and the zone over which this change will occur, estimate the volume change which will result from such a change, and integrate the volume change over the zone in which there is a change to calculate total movement.

Unfortunately, this simple concept is exceedingly difficult to accomplish in practice. As moisture-sensitive soils arise so often in arid regions, the "change" described in the previous paragraph is usually a wetting process in such cases. And, while we have improved our abilities to analyze moisture movement in the unsaturated zone, rigorous analysis of the phenomenon requires that we know in advance the *source* of water, the *volume* of water introduced and the timing of that introduction, and some rather significant detail about the *relevant soil properties*. These would include the soil water characteristic curve and the unsaturated permeability functions, as well as their variations in space. In the design process, we can rarely know these things in any detail. In fact, even in cases where there are allegations of damage, such as when a legal action is initiated by real or perceived deficiencies in the performance of a home, there are often substantial disagreements between engineers about the source, volume of water, and the past and future disposition of that water.

Conflicting views on the probable depth over which water content is likely to increase, and therefore suction is likely to decrease, as a result of residential construction can be found in the literature. In this paper, this depth will be referred to as the depth of wetting. There is general agreement that, in the absence of development, some equilibrium suction profile with depth will develop. Near the surface, one would expect precipitation or drought to cause perturbations from this equilibrium, which should decay with depth. The shape of the equilibrium profile about which these perturbations occur is depicted by some as constant with depth (e.g. Reed and Kelley 2000, Nelson et al 2003), and in other cases as a linear or near-linear decrease toward 0 at the groundwater table (e.g. Fredlund and Rahardjo 1993). It may be that this apparent disagreement is a matter of the vertical scale over which the suction profile is plotted; it seems unlikely that there is disagreement that the suction must ultimately reach zero at the water table. While some methods for estimating the equilibrium value at a given location based on climate have been proposed (e.g. PTI 2005), it is very clear that measurement of the equilibrium value is complex, and subject to significant scatter (McKeen 2003). Working from a database of about 50 homes, McOmber and Thompson (2000) identified a preconstruction profile and a post-construction profile, from which they estimated a depth of wetting due to construction in the range of about 6-9 meters (about 20-30 feet) for two different geological conditions in the Denver area. From their results, a depth of about 6.4 meters would be appropriate for the sites in this study. Diewald (2003) updated their

analysis with new data, and found a depth of wetting in conditions similar to those in this study to be on the order of 8 to 10 meters. By contrast, Nelson et al. (2003) propose a conservative approach of assuming the depth of wetting extends throughout the zone in which swell pressure exceeds overburden stress.

In order to provide some site-specific guidance on this question, a testing program was conducted in the Denver metropolitan area. Samples were obtained from the surface to a depth of approximately 12 meters below the surface at a number of houses. A range of geotechnical testing was performed on the samples obtained. Further, a database of samples taken from sites where no development had yet occurred was assessed, in order to obtain an estimate of the "undisturbed" condition. This paper reports the results of these two studies and a comparison of the suction profiles that were obtained, allowing some general statements to be made about the typical depth of wetting that arises from the changes to the moisture regime caused by residential development.

Initial Condition

Before one can make an assessment of the degree and/or extent of wetting that may have taken place as a result of construction of houses, it is of course necessary to first obtain information on the pre-construction condition. Soil suction measurements for sites without previous development were provided by a geotechnical engineering firm in the Denver area. This firm routinely conducts soil suction measurements on samples obtained for geotechnical exploration work, and so had available a significant number of such results, from which 423 individual suction readings from 25 project sites in the Denver metropolitan area were obtained. The samples were obtained using methods common to commercial geotechnical exploration, and ranged in depth from 1.2 to 10.3 m below the soil surface. Soil total suction readings were obtained via the filter paper method (ASTM D5298) on relatively undisturbed samples obtained via drive sampling. A range of soil classification tests was also performed.

The resulting suction profile is shown in Figure 1. Undisturbed samples were commonly obtained at increments based on the length of auger sections used, and samples in the database provided were obtained at depths of 1.2, 2.7, 4.3, 5.8, 7.3, 8.8, and 10.4 meters. The open squares represent the lowest values recorded at a given depth, or in other words the wettest conditions observed. The closed symbols represent the maximum values at a given depth, and thus the driest conditions observed. The solid triangles in the center are arithmetic averages of all of the values obtained at a given depth. The results came from a range of projects across the Denver metropolitan area, and from a range of soil types. However, all of the samples included here were taken from expansive soil deposits, and so were largely fine grained, plastic soils. Most of the samples would classify as CL or CH. As groundwater in the Denver metropolitan area is quite deep, it is unlikely that the near-surface suction profile is strictly controlled by the distance to the groundwater table. Rather, the assumptions implicit in this analysis are that the equilibrium suction in the

region near the ground surface is more controlled by the climate, that this climate is acceptably similar at all of the locations sampled, and that the averaging process will reveal the underlying equilibrium trend.
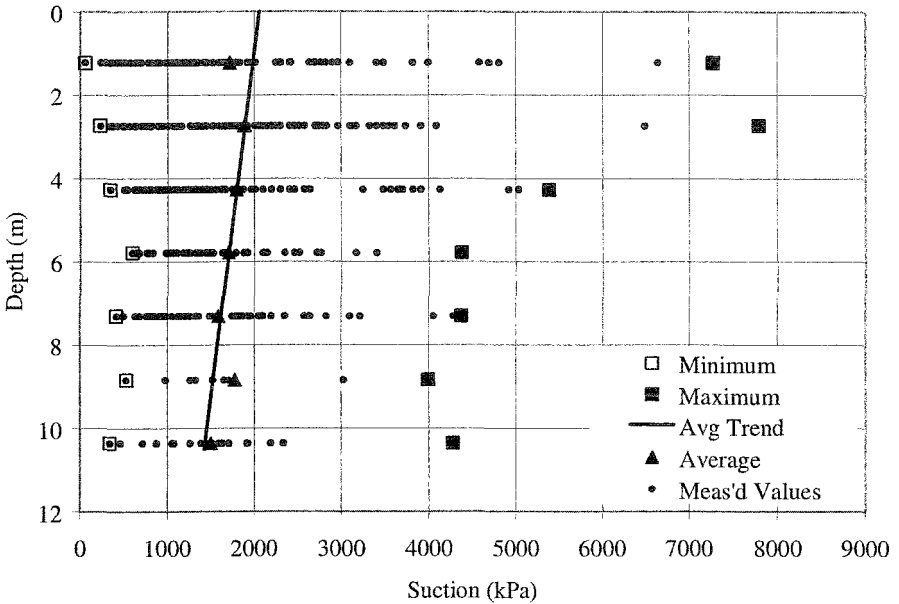
Figure 1. Range and average soil suction profiles for samples taken prior to construction, Denver metropolitan area

Interestingly, the results seemed to be independent of the soil type. No systematic differences in the average were observable for different soil types as classified by their McKeen expansion potential (McKeen 1992). Based on t-testing, there was no statistical support for differences between groups based on soil type, or between a given soil type and the average of all results. This finding is in keeping with the assumption that the relatively near surface equilibrium value is determined largely by climatic factors.

The resulting patterns have several expected characteristics. First, the range is highest near the surface and decreases with depth. However, the range between the highest and lowest values is still quite high at the maximum depths sampled. Second, the trend shows a decrease in suction with depth. The slope of this decrease is about 5 times higher than one would expect if the distance to the groundwater table controlled the suction at the near surface. The elevated slope is in keeping with a steady-state upward flow of moisture (Fredlund and Rahardjo 1993, p. 152), which is reasonable in an arid environment. The average trend indicated by the solid line in Figure 1 was used as an estimate of the pre-construction condition. For purposes of the following

comparisons, the existence of soil suctions lower than this line was taken as indication that a given site had been wetted. Note that this is a relatively weak argument from a statistical point of view, but in light of the enormous scatter in this type of data, it represents at least an unbiased assessment technique.

Sampling and Testing Program

A total of 32 sites were drilled between June of 2001 and February of 2003. Twenty-two of the sites had homes with standard full depth style basements, four had walkout style basements, four had crawlspace configurations, and two had garden level (i.e. partial depth) style basements. The homes on the sites drilled ranged from 7 to 62 years in age. Table 1 provides a summary of the age of the homes where testing was performed for this study. Only homes which had been in place for several years were selected, so that some degree of equilibration of the suction levels to the changes induced by development could occur.

Table 1: Summary of age of structures at boring locations

Age of Home (years)	Number of Homes
7-10	5
11-15	3
16-20	0
21-25	5
26-30	4
31-35	2
36-40	3
41-45	4
46-50	3
>50	1
Unknown	1
TOTAL	32

The borings were located as close to the house as was reasonably practicable and were drilled to a depth of approximately 12.2 meters (40 feet) below the ground surface. Bulk and drive samples were obtained in each boring at depths of intervals of approximately 0.3, 0.9, 1.5, 2.1, 2.7, 3.3, 4.0, 4.6, 5.2, 5.8, 6.4, 7.0, 7.6, 8.8, 10.4, and 11.9 meters (1, 3, 5, 7, 9, 11, 13, 15, 17, 19, 21, 23, 25, 29, 34, and 39 feet). The drive samples were obtained with a typical Modified California Barrel sampler having an inside diameter of 50.8 mm (2 inches) and equipped with 100 mm-long brass tubes. In most cases a CME Model 45 drill rig equipped with a 63.5-kg (140 lb) hammer powered by a rope and cathead arrangement was utilized. In two cases, a limited access rig mounted on a Mini-Sneaker tractor equipped with a 31.8-kg hammer was used instead. In all cases the hammer was dropped a distance of 0.76 m (30 inches).

After the completion of drilling, a PVC collar was placed in the top of each boring and cuttings from the boring were packed around the collar to preclude infiltration of surface water into the boring. A cap with expandable o-ring was also placed in the top of each collar. The borings were typically left open for seven days and were then backfilled with bentonite chips after completion of groundwater level readings in the open holes.

Laboratory testing was performed on 31 of the 32 sites drilled. No laboratory testing was performed on one site because the soil profile consisted of predominantly non-expansive sandstone. A series of six tests were performed on each sample obtained from the borings. These tests included total soil suction, swell-consolidation, liquid and plastic limits, sieve analysis including the % passing the number 200 screen, hydrometer, and specific gravity. A total of 438 suction tests, 411 swell tests, 395 liquid and plastic limit tests, 403 percent passing the number 200 screen tests, 367 hydrometer tests and 400 specific gravity tests were performed for this study.

The soil suction tests were performed using the filter paper method. Initially two laboratories were used to perform the suction testing. However, it became apparent that one of the two laboratories was unable to produce repeatable results, and so one lab was used for the remainder of the study. A total of six sites had suction tests that were not usable for this reason, leaving 25 sites with usable suction data. Initially nine different laboratories were used to perform the swell-consolidation testing, Atterberg limits testing, sieve analysis, hydrometer testing and the specific gravity tests. After the first ten sites were drilled and laboratory testing was completed, the study proceeded using one laboratory for all the suction and swell tests, and four laboratories for the Atterberg limits, sieve, hydrometer and specific gravity tests. The liquid limit, plastic limit, percent passing the #200 screen, hydrometer and specific gravity tests were performed in general accordance with applicable ASTM test procedures.

Conditions at Houses Tested

The principal results of interest in the present study are the soil suction profiles for the results at the occupied houses, and the comparison of those profiles to the average condition identified for sites without residential structures present. Soil suction profiles were developed using the measured total suction via the filter paper testing on relatively undisturbed samples. The filter paper method is a relatively difficult test to conduct consistently, and presents ample opportunities for contamination and errors.

As a check of data quality, the measured total suctions were compared to predicted matric suction values for each sample. These predictions were found by developing a correlated soil water characteristic curve (SWCC). Correlated SWCC's were obtained from the measured Atterberg limits and gradation information using the equations of Zapata et al. (2000). The SWCC was then entered at the degree of saturation

observed for the sample, and from this a predicted matric suction was obtained. These results provided a check on the reasonableness of the total suctions measured via the filter paper method. As expected, there was somewhat more variability in the SWCC-correlated matric suctions than in the measured total suctions, likely owing to the variability inherent in the correlation. Nonetheless, where predicted matric suction values significantly exceeded the total suction results, or showed noticeably different trends, the total suction values were assumed in error. Five of the sites gave very inconsistent results when the measured total suction was compared to the correlated matric suction, leaving 21 sites for this comparison.

A number of the sites tested showed a decrease in soil suction compared to the pre-construction benchmark value, over at least a portion of the depth of interest. Figure 2 shows an example of such a condition. For this particular site, in roughly the upper 3 to 5 meters, it is possible to conclude that the measured total suctions are below the average value observed in the pre-construction condition. Note that the correlated matric suction values are all below the measured total suctions, but that the correlated values show more scatter as would be expected. Figure 3 shows a case in which the depth over which there appeared to be reduced soil suctions compared to the pre-construction average was at least as great as the depth of the investigation. Interestingly, in some cases there was no evidence of a reduction in soil suction over any depth range observed in the samples. Figure 4 presents an example of this condition.
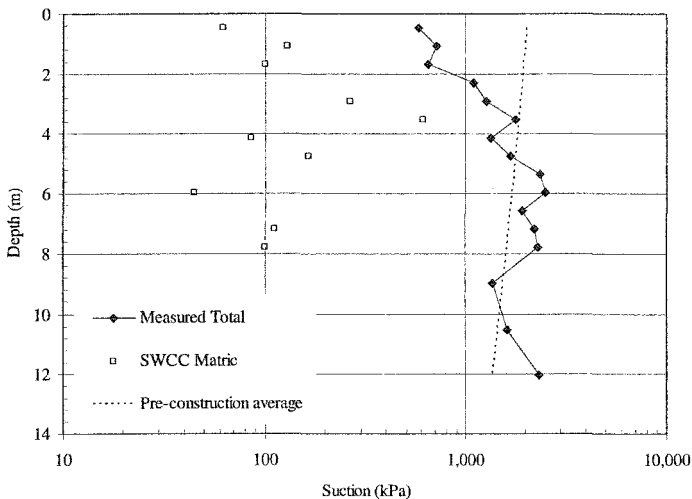
Figure 2: Suction profiles for site with reduced suction compared to sites prior to any development over a shallow depth.
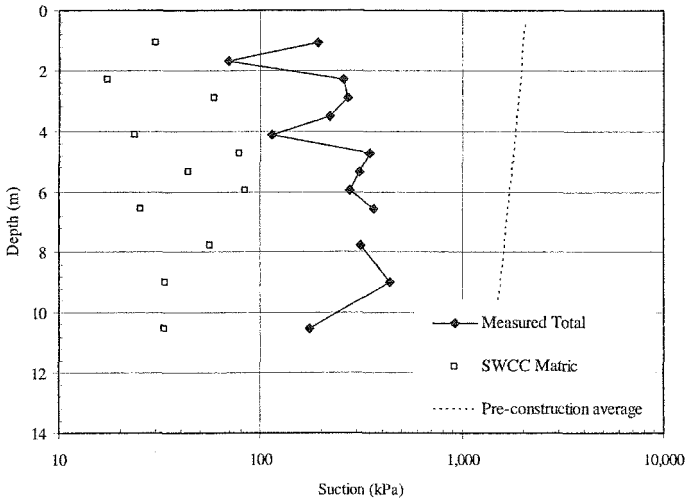
Figure 3: Suction profiles for site with reduced suction compared to sites prior to any development over a substantial depth.
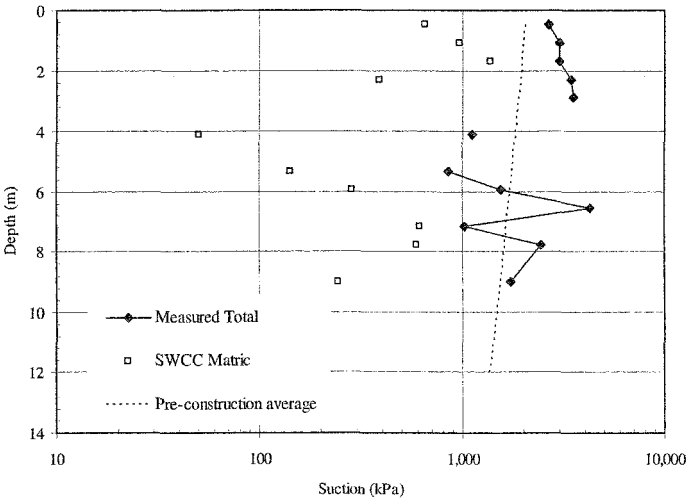
Figure 4: Suction profiles for site with no evidence of reduced suction compared to sites prior to any development

The depths to which suction appeared to have been reduced based on the process exemplified in Figures 2-4 was conducted for all 21 sites. The depth over which there

appeared to be a reduction (if present) can be thought of as the depth of wetting, and was estimated from the depth at which the measured suctions approached the pre-construction average condition and then remained at or above that level. Table 2 summarizes the depth of wetting observed for the sites included in this study.

Table 2: Summary of depth of wetting observations

Depth of Wetting	None	1.5-3m	3-4.5m	4.5-6m	6-7.5m	7.5-9m	9-10.5m	>10.5m
Number	2	3	5	3	3	1	1	3
% Observed	9.5%	14.3%	23.7%	14.3%	14.3%	4.8%	4.8%	14.3%
Cumulative %	9.5%	23.8%	47.5%	61.8%	76.1%	80.9%	85.7%	100%

No relationship was observed between the depth of wetting and parameters such as the age of the house or the soil type. Observations of the existing landscape conditions lead to a tentative conclusion that the sites showing the greatest depths of wetting tended to have very dense, lush landscapes implying heavy irrigation, and those with the shallowest depths of wetting tended to have modest landscaping, implying less irrigation.

Conclusion

Clearly there is substantial scatter in the results. Nonetheless, a few general conclusions are apparent. First, it is clear that while some of the sites show rather substantial depths of wetting, these sites do not represent the oldest homes in the data set (in one case, actually among the youngest). This means that the argument that wetting must occur at a given site to some substantial depth is not supported by these data. In most cases, the depths of wetting observed are in keeping with the results of McOmber and Thompson (2000), although deeper wetting was achieved in about 20% of the cases. Notably, the suction at the "wetted" state was found to be well above zero, with suctions in the upper portions of the sites where wetting was noted having a minimum of around 80-100 kPa.

References

Fredlund, D.G., and Rahardjo, H. (1993). *Soil mechanics for unsaturated soils*, Wiley-Interscience, New York.

McOmber, R.M., and Thompson, R.W. (2000). "Verification of depth of wetting for potential heave calculations." *Advances in unsaturated geotechnics.* proceedings of sessions of Geo-Denver 2000 held in Denver, Colorado, August 5-8, 2000, 409-422.

McKeen, R.G. (1992). "A model for predicting expansive soil behavior." *Proceedings,* 7th International conference on expansive clay soils, ASCE, 1-6.

McKeen, R.G. (2001). "Investigating field behavior of expansive clay soils." *Expansive clay soils and vegetative influence on shallow foundations,*

proceedings of Geo-Institute shallow foundation and soil properties committee sessions at the ASCE 2001 Civil Engineering Conference, 82-94.

Nelson, J.D., Overton, D.D. Durkee, D.B. (2001). "Depth of wetting and the active zone." *Expansive clay soils and vegetative influence on shallow foundations*, proceedings of Geo-Institute shallow foundation and soil properties committee sessions at the ASCE 2001 Civil Engineering Conference, 95-109.

Post-Tensioning Institute (PTI) (2005). *Design of post-tensioned slabs-on-ground*, Phoenix, Arizona.

Reed, R.F., and Kelley, M. (2000). "Impact of climatic variation on design parameters for slab on ground foundations in expansive soils." *Advances in unsaturated geotechnics*. proceedings of sessions of Geo-Denver 2000 held in Denver, Colorado, August 5-8, 2000, 435-455.

Zapata, C. E., Houston, W. N., Houston, S. L., and Walsh, K. D. (2000). "Soil-water characteristic curve variability." *Advances in unsaturated geotechnics*. proceedings of sessions of Geo-Denver 2000 held in Denver, Colorado, August 5-8, 2000, 84-124.

Pressuremeter Testing for Electric Power Transmission Line Structure Foundations in Desert Southwest Soils

Peter M. Kandaris, P.E. [1]

[1] Salt River Project, Mail Stop XCT317, P.O. Box 52025, Phoenix, Arizona, 85072-2025; PH (602) 236-8613; FAX (602) 681-2736; email: pmkandar@srpnet.com

Abstract

With the advent of improved foundation design and analysis methodologies, more accurate strength and stiffness values are required to yield reliable structure performance. In particular, lateral modulus of deformation values (synonymous with pressuremeter modulus in this paper) are needed in the design of drilled pier foundations for electric power transmission single pole structures. Parameter values can be developed from either in-place field tests or laboratory tests. More commonly, these parameters are estimated from published empirical correlations with Standard Penetration Resistance Test (SPT) N values or soil consistency. A number of researchers provide empirical pressuremeter relationships in both cohesive fine grained and granular deposits, but few look solely at unsaturated soils

The Salt River Project (SRP) has performed field pressuremeter testing for use in design of a number of its high voltage electric transmission structure foundations over the past 20 years. This paper presents the data and discusses the development of empirical correlations between field pressuremeter tests and standard penetration resistance blow counts obtained by the SRP in desert southwest unsaturated alluvial soils. Data from four projects within Maricopa County, Arizona are examined to develop the relationships. Data is supplemented with work performed by the Electric Power Research Institute at an SRP substation in the Phoenix area.

The purpose of the work is to provide more reliable estimates of lateral deformation modulus values for projects in the SRP service territory where it is not economical to perform site-specific pressuremeter testing. The correlations from this work appear to be very similar to those determined by previous researchers. The data from this work indicates somewhat less scatter than previously observed by others with the ratio of measured versus estimated deformation modulus values ranging from 0.3 to 2.5 for the linear regression average lines and 0.4 to 3.3 for the low bound 90% confidence interval curves.

Introduction

Single shaft steel pole structures offer an electric transmission line support method that is economic, aesthetic, rapid to erect and easy to construct. Typically, these structure types are founded on either short reinforced concrete drilled shaft piers or a direct embedment section of the steel pole shaft, with depth of embedment ranging from two to ten foundation diameters. Since primary forces on the foundations are the result of loading near the top of these tall structures (conductor weight, line tension and wind on conductors), foundations are subject to high overturning moments at relatively low shear values. The ability of the subgrade to resist lateral pressure from high moment forces and function within prescribed deflection ranges is the focus of transmission line foundation design.

Numerous methods have been applied to the design of laterally loaded pier foundations. Classical methods focus on the strength properties of supporting soils and calculate a state of static equilibrium assuming that the ultimate lateral capacity is based on passive soil resistance (Hansen, 1961; Czerniak, 1965, Broms, 1965). Soil strength does not generally control foundation design for unsaturated (and more often overconsolidated and cemented) desert southwest soils. Rather, maximum permissible deflection tends to dictate the depth and diameter of a transmission line pole foundation in this region. Rational solutions attempt to predict the lateral soil resistance along the pier as a function of the pier deflection where both static equilibrium and compatibility of deformation must be achieved simultaneously for all parts of the foundation system (Reese and Matlock, 1956; Matlock and Reese, 1960; Davisson and Prakash 1963; Reese and Allen, 1977; Poulos and Davis, 1980).

Computer model solutions incorporate both linear and non-linear components of rational solutions to model soil-structure interaction and load-deflection response. These improved foundation design and analysis methodologies require accurate strength and stiffness values to yield reliable structure performance. In particular, a computer program suite developed for the electric power industry (EPRI, 1996) uses lateral modulus of deformation values for design of single pole transmission structure drilled pier foundations. Geotechnical design parameter values can be developed from either in-place field tests or laboratory tests. More commonly, these parameters are estimated from published empirical correlations with Standard Penetration Resistance Test (SPT) N values or soil consistency.

Geology and Geomorphology

Inhabitable areas of the SRP service territory lie principally within the Basin and Range Physiographic Province – a region characterized by a series of elongated, and parallel mountain ranges separated by intervening valleys (see area map in Figure 1). The mountain ranges are typically uplift structural blocks composed of bedrock ranging from Precambrian to Tertiary age. Intervening valleys represent adjacent subsidence basins that have been filled with Tertiary to Quaternary sedimentary deposits. The two structural blocks generally are separated along mountain front

normal faults, with movement along the faults resulting from crustal extension during the Basin and Range Disturbance beginning in mid-Miocene time less than 15 million years ago (Menges, 1984).
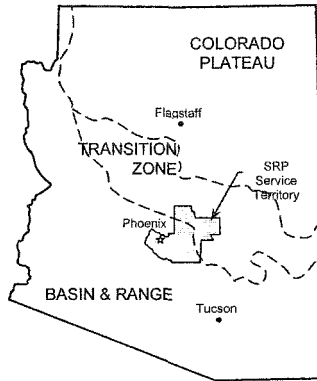
Figure 1. Area Map: Arizona Physiographic Provinces - SRP Service Territory.

Basin fills (up to 3000 m thick) are comprised of younger and softer materials than the surrounding uplift mountain blocks. Most basins were initiated as internally drained features with lake bed deposits of silt and clay, and evaporative deposits of halite and gypsum commonly forming in the central portions of the valleys. Upon infilling, the basins became externally drained, allowing removal of older sediments and deposition of younger alluvium (clay, silt, sand, gravel and cobble) near the surface. The older materials have become cemented and consolidated or indurated with age. The older consolidated or semi-consolidated basin fill materials became progressively buried below younger deposits toward the center of valleys and along drainage channels. The older deposits are the hardest and most cemented via calcium carbonate accumulation.

Near surface geomorphology of the SRP service territory is dominated by three major ephemeral stream/river channels: the Salt River, the Agua Fria River and Queen Creek Wash. Dissection and deposition from these rivers provide the complexity to the surface geology, removing older, more cemented or consolidated alluvium and replacing or overlaying with younger cohesive and cohesionless deposits containing minimal calcium carbonate content (Pearthree and Huckleberry, 1994). Since subsurface water tends to be well below transmission foundation depths (even near drainage channels), soils are unsaturated and weakly to non-cemented in many areas.

Background and Literature Review

Evaluation of a soil's deformation property (most often referred to as Young's modulus) can be performed using both laboratory and in situ test methods. Triaxial compression and uniaxial consolidation tests give stress-strain relationships, where

various slope points provide modulus values that are calculated as the ratio of stress to strain. Field in situ testing can be used to develop direct measurements of soil deformation modulus values. The best field measure of the lateral deformation modulus is offered by the pressuremeter test. For standard design work it is generally assumed that lateral and vertical modulus values are approximately equal.

Pressuremeter testing cannot be justified for many small foundations projects because of the cost and time required for such field work. In lieu of performing pressuremeter tests, the lateral (pressuremeter) modulus of deformation, E_p, is often estimated from empirical correlations with Standard Penetration Test (SPT) N values or Cone Penetrometer Test (CPT) cone tip resistance. CPT methods are not commonly used in desert southwest soils where strata are unsaturated, coarse grained and often cemented. In these conditions, SPT methods are typically employed both to measure soil consistency and for obtaining either split spoon or ring drive samples for laboratory testing. Corrected SPT values are required with larger diameter ring drive sampler blow counts to derive a common base for comparison with standard size sampler barrels.

A number of researchers have looked at the empirical relationship between SPT N values and pressuremeter modulus values in both cohesive fine grained and granular cohesionless deposits. A comprehensive review of estimating soils properties for foundation design was performed by Cornell University for the Electric Power Research Institute (EPRI) (Kulhawy and Mayne, 1990). When modulus values are plotted against blow counts, the data for cohesive soils show that more than one order of magnitude variation is possible when using N values as the sole predictor (Ohya et al., 1982). Cohesionless soil data also demonstrate considerable scatter when attempting to correlate the deformation modulus and SPT N values (D'Appolonia et al., 1970; Schmerttmann, 1970; Ohya et al., 1982).

An earlier EPRI research report provides empirical correlation charts relating the modulus of deformation to SPT N values for use in design of laterally loaded drilled pier foundations (Davidson, 1982). Correlations for cohesionless soils presented in this work are based on small plate load tests (Schmerttmann, 1970) as well as published correlations between pressuremeter modulus and SPT N values by others (Martin, 1977; Schultze and Biedermann, 1977). A similar design chart derives pressuremeter modulus and SPT N value correlations for cohesive soils (DiGioia, et al., 1975; Lukas, et al., 1976). Again, considerable scatter is observed in the data for all soils types, with the ratio of actual to estimated modulus of deformation values ranging from 0.2 to 5.0. The author recommends obtaining modulus values based on multiple correlations (SPT N values, unconfined compressive strength and soil consistency).

Few studies focus on unsaturated conditions or conditions where soils are cemented. GAI Consultants provide recommended modulus of deformation values for a variety of unsaturated strata ranging from fills, residual soils and decomposed rock to claystone, sandstone, shale, siltstone and limestone of various hardnesses (GAI,

1972). Recommended design values are step-wise functions of predominately low bound values of the data. Beckwith and Bedenkop compared deformation modulus and SPT N values in the unsaturated granular and cemented soils of the Phoenix, Arizona area as part of a foundation load test program (Beckwith and Bedenkop, 1973). Tests on hard clays and soft shales in Oklahoma showed similar results (Nevels and Laguros, 1993). A number of the empirical correlations noted in the literature review are presented in Figure 2.

(a) Schmertmann (1970): sandy gravel & gravel deposits; data from plate load tests – as reported by Davidson, 1982.
(b) GAI (1972): fills, residual soils and decomposed rock.
(c) Beckwith & Bedenkop (1973): cemented & coarse granular deposits.
(d) DiGioia, Donovan & Cortese (1975): cohesive soils – as reported by Davidson, 1982.
(e) Martin (1977): cohesionless silty sand to sandy silt residual soils.
(f) Nevels & Laguros (1993): hard residual clay and soft shale

Figure 2. Modulus of Deformation (E) versus Standard Penetration Resistance (N) Relationships Developed by Various Researchers.

Data

During the past 20 years SRP performed field pressuremeter testing for use in design of a number of its high voltage electric transmission structure foundations. This work incorporates 60 tests from four transmission line projects within the SRP service territory in Maricopa County, Arizona, and similar work performed by EPRI at an SRP substation in the Phoenix area. Project scope and pressuremeter test programs are summarized in Table 1 with data presented in Table 2 (moisture test data or observations shown only where provided in borelogs). Site locations are shown in Figure 3. Pressuremeter tests were terminated once the elastic soil behavior had been determined, generally not past creep pressure or to the limit pressure.

Table 1. SRP Pressuremeter Test Programs.

Project	Description	No. of Sites	No. of Tests per Site	Total Tests	SPT Method	PMT Method	Consultant
1. Browning 69/230/500kV Transmission Line (1999)	16.9 km long transmission line in Mesa, AZ	5	3-5	12	CME-75 drill rig w/ 165-mm dia. hollow stem auger; 61.5-mm ID open-ended ring drive sampler.	Menard GA-m with N-sized probe calibrated prior to use; test cavity prepared using an N-sized tool.	AGRA Earth & Environmental (Phx office)
2. Schrader 230kV Transmission System (1996)	23.3 km long transmission line and substation in Chandler, Gilbert & Higley, AZ	7	3-5	29[1]	CME-75 drill rig w/ 165-mm dia. hollow stem auger; 61.5-mm ID open-ended ring drive sampler.	Menard GA-m with N-sized probe calibrated prior to use; test cavity prepared using an N-sized tool.	AGRA Earth & Environmental (Phx office)
3. Santan to Kempton 69/230/kV Transmission Lines (1994)	6.4 km long transmission line in Mesa & Gilbert, AZ	4	3-4	15	CME-75 drill rig w/ 178-mm dia. hollow stem auger; 61.5-mm ID split-barrel (Dames & Moore-type) sampler.	GM with N-sized probe calibrated prior to use.	GAI Consultants (Pittsburgh office)
4. Mead to Phoenix 5000kV Project (1992)	414 km long transmission line: Marketplace Substation (Boulder City, NV) to Westwing Substation NW of Phoenix, AZ	2[2]	3	6	CME-75 drill rig w/ 165-mm dia. hollow stem auger; 61.5-mm ID open-ended ring drive sampler.	Menard GA-m with N-sized probe calibrated prior to use; test cavity prepared using an N-sized tool.	Sergent, Hauskins & Beckwith (Phx office)
5. EPRI Full Scale Foundation Test Program (1979)	Nation-wide testing program: 14 full-scale laterally loaded drilled pier foundation tests in a variety of soil conditions across the US. AZ tests at the SRP/APS Pinnacle Peak Substation in Scottsdale, AZ	1	6	6	Split barrel 51-mm OD, 35-mm ID sampler.	Geoprobe Ltd. Model GW-HR.	GAI Consultants (Pittsburgh office)

(1) Results from 8 tests were not included in the data. These tests either used pre-soaked holes, were not completed, or soils were too soft to test.

(2) Tests performed at 8 sites, but only 2 in Maricopa County, AZ
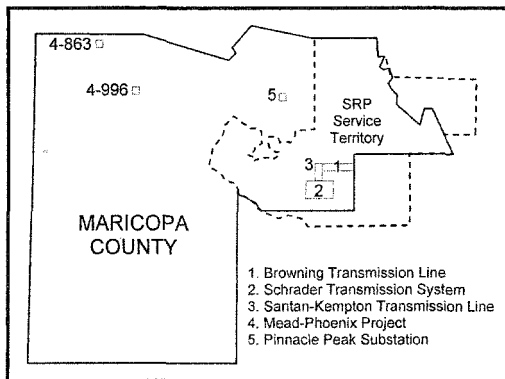
Figure 3. Test Site Locations.

Table 2. Soils Data from SRP Maricopa County Project Sites.

Proj	Boring	Depth (m)	USCS	w (%)	Type	N_{corr} (bl/ft)	E_p (MPa)
1	B1	1.68	CL	17.0	cohesive	8	0.90
1	B1	3.20	SC	17.7	cohesive	8	1.65
1	B1	4.42	CL	20.9	cohesive	8	0.90
1	B2	1.68	CL	11.8	cohesive	25	16.9
1	B2	3.20	CL	13.4	cohesive	31	47.2
1	B3	1.68	SP	9.4	cohesionless	8	3.93
1	B3	3.20	CL	14.4	cemented	21	29.8
1	B4	1.68	SC	7.6	cemented	83	90.7
1	B4	3.20	SC	2.6	cemented	27	47.0
1	B4	4.72	SC	8.9	cemented	76	129
1	B5	1.68	CL	6.2	cemented	55	98.3
1	B5	3.20	SC	5.6	cemented	73	89.5
2	2	1.83	SC-SM	20.2	cohesive	4	2.62
2	2	2.83	SC	13.8	cemented	45	24.1
2	2	4.48	SP	10.3	cohesionless	12	20.0
2	2	6.95	SC-CL	10.3	cemented	36	59.0
2	3b	1.95	SM	18.0	cohesive	15	6.34
2	3b	4.24	SW-SG	16.0	cohesionless	16	11.6
2	3b	8.11	SC-SP		cohesionless	54	77.9
2	4	1.25	SC-SP	12.3	cohesive	6	2.62
2	4	5.09	SP	3.3	cohesionless	27	26.5
2	4	7.96	GC-SC	5.7	cohesionless	29	56.1
2	4	9.51	SC		cemented	124	186
2	5	1.65	SM	7.0	cohesive	8	2.55
2	5	5.82	SP	5.2	cohesionless	36	19.7
2	6	1.00	CL	22.3	cohesive	11	4.07
2	6	2.04	CL	19.5	cohesive	15	5.72
2	6	5.09	SW		cohesionless	27	24.7
2	6	7.89	CL		cemented	97	138
2	7	1.40	ML		cohesive	13	15.2

Proj	Boring	Depth (m)	USCS	w (%)	Type	N_{corr} (bl/ft)	E_p (MPa)
2	7	3.51	CL		cemented	44	43.4
2	7	6.61	SW-GW		cohesionless	31	21.5
2	7	9.48	SM		cohesive	31	29.5
3	1	1.16	CL	18.8	cemented	14	20.0
3	1	2.87	SC	13.1	cemented	17	46.2
3	1	5.85	SC-CL	15.5	cohesive	64	84.8
3	2	1.13	CL	10.0	cemented	41	60.7
3	2	2.71	SP-SC	9.5	cohesionless	20	21.4
3	2	4.21	CL	16.5	cemented	59	60.7
3	2	5.64	CL	22.7	cohesive	34	26.9
3	3	1.43	CL-SC		cemented	30	64.8
3	3	3.11	SC	13.2	cemented	38	44.8
3	3	4.42	CL	13.9	cemented	56	68.3
3	3	6.00	CL	13.6	cohesive	35	37.9
3	4	1.28	CL	18.4	cemented	17	33.1
3	4	2.71	CL-SC	19.5	cemented	25	45.5
3	4	4.05	CL		cohesive	29	24.1
3	4	5.82	SC	14.3	cohesive	40	50.3
4	863	1.31	CL	moist	cemented	21	25.6
4	863	2.29	CL	moist	cemented	94	94.2
4	863	4.27	CL	moist	cemented	92	88.8
4	996	0.91	SC	dry	cemented	69	98.5
4	996	1.66	CL	dry	cemented	57	30.3
4	996	2.29	CL	dry	cemented	240	54.7
5	B-1	0.61	GP		cohesionless	6	6.13
5	B-1	1.52	GP		cohesionless	12	8.96
5	B-1	2.44	GP		cohesionless	43	26.5
5	B-1	3.35	GP		cohesionless	34	34.7
5	B-1	4.37	GP		cohesionless	30	196
5	B-1	4.72	GP		cemented	408	383

Results

Blow count and deformation modulus data values range across multiple orders of magnitude and generally show significant scatter when plotted arithmetically. Log transformation methods applied to the data convert the exponential changes to a more linear pattern when plotted on a log-log graph. Data is grouped by the general soil types of cohesive (non-cemented), cohesionless and cemented. Strata identified in the bore logs as weakly to strongly carbonate cemented are considered cemented and are evaluated separately from cohesive and cohesionless materials.

Linear regression of the log-transformed data is used to estimate average values (trends) for each of the data groups. The low bound of the 90% confidence interval is also calculated. Figures 4 through 6 graphically show the results of the analysis.

Data scatter from the estimated modulus of deformation values is evaluated in a manner similar to that done by others as described in the literature review. For all data, the results show that the ratio of actual to estimated modulus of deformation range as follows: Log-log average, cemented soil: 0.3 to 1.7, cohesionless soil: 0.6 to 2.0, cohesive non-cemented soil: 0.3 to 2.5; 90% confidence intervals, cemented soil: 0.4 to 2.1, cohesionless soil: 0.7 to 2.5, cohesive non-cemented soil: 0.5 to 3.3. About 34% of the calculated modulus values overestimate the actual measured values by

more than ten percent with linear regression average lines as compared to less than 17% with low bound 90% confidence interval curves.
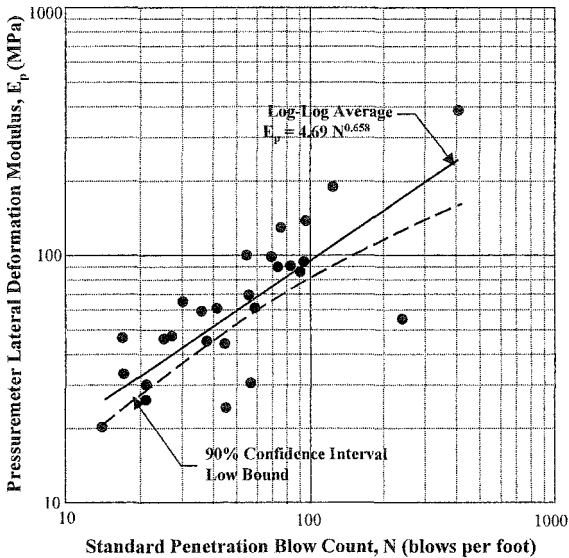
Figure 4. Lateral Deformation Modulus versus Blow Count: Cemented Soil Data.

Conclusions

The correlations from this work appear to be very similar to those determined by previous researchers. The majority of the deformation modulus data falls within the band of estimate curves developed by others shown in Figure 2. Most of this data plots above the lowest curve boundary with data trending in a similar manner.

The data from this work indicates somewhat less scatter than previously observed by others for the linear estimates of log transformed data of the average trend values and the lower bound of the 90% confidence interval for each soil grouping. The range of scatter for the ratio of measured versus estimated deformation modulus values from the earlier works is 0.2 to 5.0. Alternately, the range of deformation modulus values found from this data show that the ratio of actual to estimated modulus of deformation range from 0.3 to 2.5 for the linear regression average lines and 0.4 to 3.3 for the low bound 90% confidence interval curves. When examining the data, the largest deviations from the estimate curves occur when the moisture content is highest in cohesive soils. As the moisture content increases, the relationship between blow count and deformation modulus becomes more erratic. It is possible that the empirical relationship between deformation modulus and SPT blow count is more consistent in low moisture content unsaturated desert southwest soils.
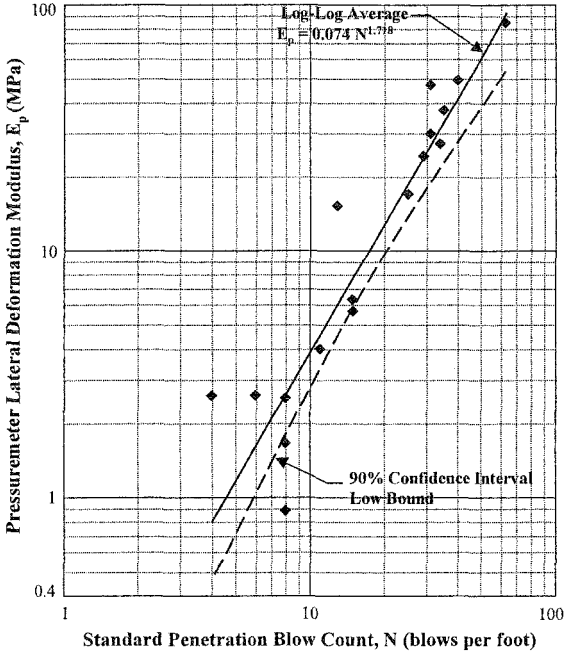
Figure 5. Lateral Deformation Modulus versus Blow Count: Cohesive Soil Data.
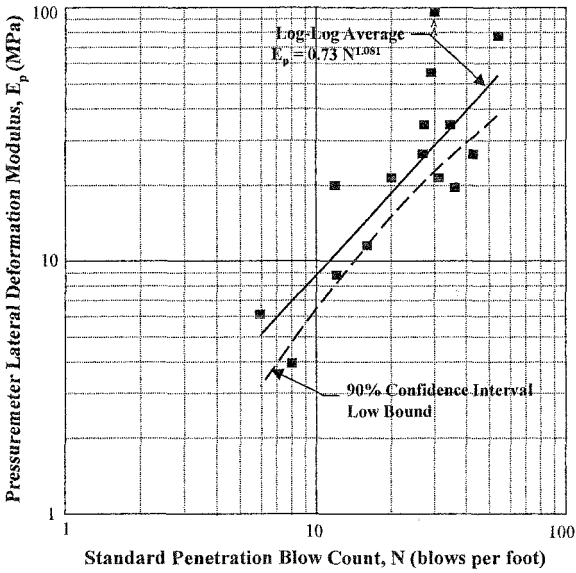
Figure 6. Lateral Deformation Modulus versus Blow Count: Cohesionless Soil Data.

A cursory examination was performed to evaluate variables contributing to data scatter. No improvement in the earlier log-log linear relationships was observed for the three soil categories when pressuremeter modulus values were normalized by overburden stress and compared to STP blow counts. Lower correlation coefficients were found with non-normalized data for all three soil categories. In addition, the moisture content and dry density data available were used to calculate degree of saturation (an indicator of negative pore water pressure in unsaturated soils). When grouped by soil category, a slight increase in deformation modulus was observed with 46% of the data as saturation decreased (blow counts held constant). The remainder of the data indicated no discernable pattern. Most likely, data scatter is the result of variations in SPT field procedures (probable with 5 investigations done over a 20-year period). Numerous variables such as type of hammer, borehole size, sampler liner size, cathead size, number of turns of the rope and rod length cause variance in hammer drop energy efficiency. Energy ratio has been reported to vary from 30% to 90% for particular drillers and SPT equipment (Kulhawy and Mayne, 1990).

Figure 7 gives the recommended correlation curves for all three soil groups. The curves represent the lower bound of the 90% confidence intervals for each soil group with the following exceptions: (a) a maximum deformation modulus value of 100 MPa is established for design of electric transmission line pier foundations in soil since minimum embedment will control pier deflection when soil stiffness exceeds
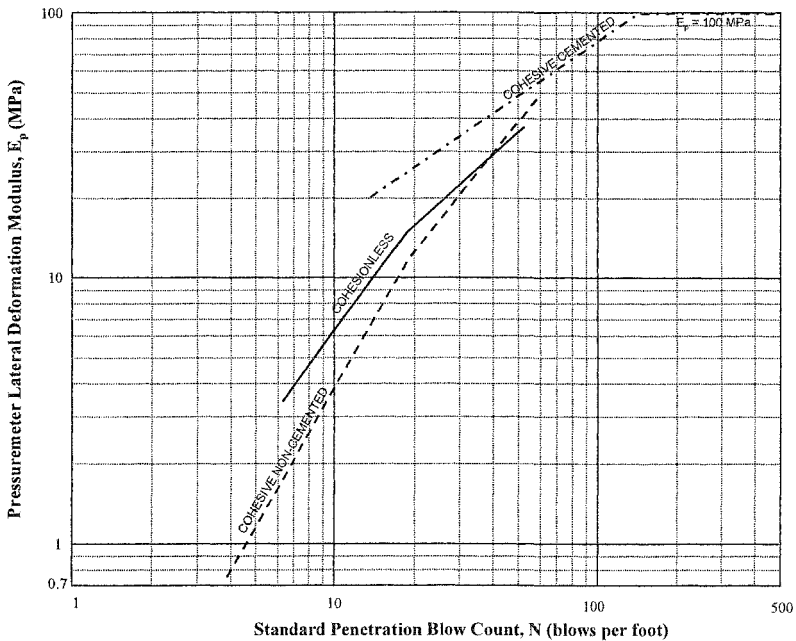
Figure 7. Lateral Modulus of Deformation (E_p) versus Standard Penetration Resistance (N): Design Curves developed from Maricopa County, Arizona Data.

this value, and (b) the log-log average value is used when the low bound 90% confidence interval is less than the low bound values observed by previous researchers. The second limitation applies only for cohesive soils with blow counts under 20. The use of confidence intervals also offers a rational method for selection of lower data bounds. The curves presented in Figure 7 establish a lower limit for 83% of the SRP data.

Local data may offer a path toward developing more reliable empirical correlations between deformation modulus and STP blow count values. As noted by another researcher, "the fact that some variation is inevitable in N value determination should not detract from the usefulness in predicting deflection modulus" (Martin, 1977). Empirical correlation charts, along with an understanding of local soil conditions can provide a reliable and cost effective design aid in foundation design.

References

Beckwith, G.H., and Bedenkop D. V. (1973). *An Investigation of the Load-Bearing Capacity of Drilled Cast-In-Place Concrete Piles Bearing on Coarse Granular and Cemented Alluvium Fan Deposits*, Rep. AHD-RD-10-122, ADOT, Phoenix.

Broms, B.B. (1965). "Design of Laterally Loaded Piles." *J. Soil Mech. and Foundation Engrg. Div.*, ASCE, 91(SM3), 79-99.

Czerniak, E. (1957). "Resistance to Overturning of Single, Short Piles." *J. Structural Div.*, ASCE, 83(ST2), 1-25.

D'Appolonia, D. J., D'Appolonia, E., and Brisette, R.F. (1970). Discussion of "Settlement of Spread Footings in Sands", *J. Soil Mech. and Foundation Engrg. Div.*, ASCE, 96(SM2), 754-761.

Davidson, H.L. (1982). "Laterally Loaded Drilled Pier Research - Volume 1: Design Methodology," Report EL-2197, Electric Power Research Institute, Palo Alto.

Davisson, M.T., and Prakash, S. (1963). "A Review of Soil-Pole Behavior." *Stresses in Soils in Layered Systems,* HRR 39, 25-48.

DiGioia, A. M., Donovan, T.D., and Cortese, F.J. (1975). "A Multi-Layered/Pressuremeter Approach to Laterally Loaded Rigid Caisson Design," presented at seminar on *Lateral Pressures Related to Large Diameter Pipes, Pile, Tunnels, and Caissons*, ASCE, Dayton.

Electric Power Research Institute (1996). *FAD (Foundation Analysis and Design - TLWorkstation™ Module) Version 3.0,* Computer Code SW-40077.

GAI Consultants, Inc. (1972). "Caisson Foundations – Transmission Pole Structures," presented at the ASCE National Structural Meeting, May 25.

Hansen, J. B. (1961). "The Ultimate Resistance of Rigid Piles Against Transversal Forces." *The Danish Geotechnical Institute Bulletin No. 12*, 5-9.

Kulhawy, F. H., and Mayne, P.W. (1990). "Manual on Estimating Soil Properties for Foundation Design," Report EL-6800, Electric Power Research Institute, Palo Alto.

Lukas, R.G. and de Bussy, B.L. (1976). "Pressuremeter and Laboratory Test Correlations for Clays." *J. Geotech. Engrg. Div.*, ASCE, 102(GT9), 945-962.

Martin, R.E. (1977). "Estimating Foundation Settlements in Residual Soils." *J. Geotech. Engrg. Div.*, 103(3), 197-212.

Matlock, H., and Reese, L.C. (1960). "Generalized Solutions for Laterally Loaded Piles." *J. Soil Mech. and Foundation Engrg. Div.*, ASCE, 86(SM5), 63-91.

Menges, C.M. (1984). *The Neotechtonic Framework of Arizona: Implications for the Regional Character of Basin-Range Techtonism*. OFR 83-19, Bur. of Geo. and Mineral Tech., Arizona.

Nevels, J., and Laguros, J.G. (1993). "Correlation of Engineering Properties of the Hennessey Formation Clays and Shales." *Proc*, Geotech. Engrg. Hard Soils – Soft Rocks, Athens, Vol. 1, p. 215.

Ohya, S. , Imai, T., and Matsubara, M. (1982). "Relationships Between N Value by SPT and LLT Pressuremeter Results." *Proc*, 2nd Eur. Sym. on Penetration Testing, Vol. 1, Amsterdam, 125-130.

Pearthree, P.A. and Huckleberry, G. (1994). *Surficial Geologic Map of the Mesa 30 x 60 Quadrangle, Arizona*, OFR 94-24, Ariz. Geological Surv.

Poulos, H.G., and Davis, E.H. (1980). *Pile Foundation Analysis and Design*, John Wiley & Sons, New York.

Reese, L.C., and Matlock, H. (1956). "Nondimensional Solutions for Laterally Loaded Piles with Soil Modulus Assumed Proportional to Depth." *Proc*, 8th Texas Conf. Soil Mech. Fndn. Engrg., ASCE, SP 29, B. of Engrg. Res., U. of Texas, Austin.

Reese, L.C., and Allen, J.D. (1977). "Structural Analysis and Design for Lateral Loading." *Drilled Shaft Design and Construction Guidelines Manual*, USDOT, FHWA, Office of Research and Development, Vol. 2.

Schmerttmann, J.H. (1970). "Static Cone to Compute Static Settlement Over Sand." *J. Soil Mech. and Foundation Engrg. Div.*, ASCE, 96(SM3), 1011-1043.

Schultze, E., and Biedermann, B. (1977). "Pressuremeter, Penetrometer and Oedometer Tests." *Proceedings*, 9th ICSMFE, Tokyo, Vol. 1, p. 271.

An In-Situ Ion Mobility Spectrometer Sensor System for Detecting Gaseous VOCs in Unsaturated Soils

Dick Sevier[1], Molly Gribb[1], Robert Walters[1], Jerome Imonigie[1], Kevin Ryan[1], Abu Kanu[2], Herb Hill[2], Feng Hong[3], Jake Baker[1], and Sin Ming Loo[1]

[1]Departments of Civil Engineering, and Electrical and Computer Engineering, Boise State University, 1910 University Drive, Boise, ID 83725; PH (208)-426-5707; FAX (208)-426-4800; e-mail: mgribb@boisestate.edu

[2]Department of Chemistry, Washington State University, Pullman, WA 99164, PH (509) 335-5648; FAX (509) 335-8867; e-mail: hhhill@wsu.edu

[3] Department of Physics, SUNY Canton College of Technology, Cornell Drive, Canton, NY 13617, PH 315-386-7154; e-mail: hongf@canton.edu

Abstract

Existing methods for the detection and measurement of volatile organic compounds (VOCs) in the vadose zone are often hampered by issues associated with ease of use, accuracy, and cost. As a result, there remains a need for inexpensive, minimally invasive, real-time instrumentation and sensor systems that can be used for characterizing or long-term monitoring of contaminated sites. A new sensor system to meet this need is under development at Boise State University, in collaboration with Washington State University.

A miniature Ion Mobility Spectrometer (IMS) has been fabricated from a machinable ceramic material and has been shown to have a resolving power comparable to a commercial IMS. The IMS system will be packaged in a probe housing for deployment using direct push methods and will be ultimately equipped with water content, temperature, and pressure sensors. The proposed system is designed for use in multi-probe arrays and features wireless transmission of data directly to the user. To our knowledge, an in-situ IMS for detection of subsurface gaseous VOCs has not been previously developed.

VOCs in Unsaturated Soils

If a VOC enters unsaturated soil as a result of a spill, it can be present in four different phases: gas (air), water, solid (soil), and as a free phase liquid. Partitioning

between the phases depends on the volatility, solubility, degree of saturation, amount of organic matter present, and temperature (Domenico and Schwartz, 1998). Compounds with large vapor pressures will volatize and move via diffusion in the gas or vapor phase. These vapors may escape to the atmosphere, dissolve in groundwater, or move into enclosed spaces such as basements, and impact indoor air quality. When a complete exposure pathway exists for vapor intrusion into structures, measurements of soil gas concentrations are needed to determine if the risk to human health warrants clean-up or other remedial action (EPA, 2002). Current methods for sampling and analyzing soil gas samples fall into two classes: passive sampling and active sampling. Passive sampling methods involve the shallow burial of a sorbent collector, which adsorbs the VOC from soil pore gas space as a result of diffusion (EPA, 1988). Passive sampling techniques require site-specific calibration for proper exposure time (typically 1-3 days) to ensure accurate results. Passive samplers are one-time use instruments, require offsite analysis and do not provide mass concentration data (Wong, 2003; EPA, 1988).

Active sampling involves the insertion of a sampling tube or probe into the soil. The gas sample is then extracted and brought to the surface for analysis, often using a field portable gas chromatograph (GC) for immediate results. However, these active sampling systems require the presence of a GC, a skilled technician, and all the systems and equipment needed for deployment and analysis. Thus, active sampling is typically expensive and labor intensive, which generally limits its use to short-term projects such as mapping contaminant plumes (EPA, 1988).

Limitations associated with existing methods led us to consider developing a new sensor system for collecting and analyzing soil gas samples in situ, based on ion mobility spectrometry.

IMS Sensor Applications and Theory

Ion Mobility Spectrometer (IMS) devices have been used in laboratory environments to analyze gaseous chemicals; more recently, these devices have been used in field applications to detect chemical warfare agents, explosives and narcotics. Ion mobility spectrometry is used to separate and quantify ions based on the drift of ions at ambient pressure under the influence of an electric field against a counter flowing neutral drift gas. Gas samples to be analyzed are introduced into the reaction chamber of the IMS system through a sample inlet by a carrier gas (typically nitrogen or air). In the reaction region the sample molecules are ionized and the resulting product ions (charged molecules) move under the influence of an applied electric field towards the ion gate which controls their entry into the drift region. When the ion gate is cycled, a given amount of the product ions is allowed to enter the drift region. The drift tube contains an electric field and a counter flowing drift gas which separates the ions according to their ion mobility. If a gaseous ion at atmospheric pressure is placed in a constant electric field, it will accelerate down the field until it collides with the neutral drift gas. Upon collision, the ion slows down, and, under the influence of the electric field, is accelerated again, resulting in another collision, and so forth. This chaotic sequential series of acceleration and collision at the molecular level translates into a constant ion velocity over macroscopic distances. As the ions

reach the ion collector (Faraday plate), a small current is generated. This current is recorded as a function of drift time; a microprocessor or other system is then used to identify each analyte and determine the concentration.

IMS Sensor System Overview

In this project, we have designed and fabricated a miniaturized IMS for use in unsaturated soils. The sensor system is comprised of many subsystems that reside either down-hole in the probe housing or up-hole on the surface. Figure 1 shows a block diagram of the system and Figure 2 shows the sensor system in its probe housing.
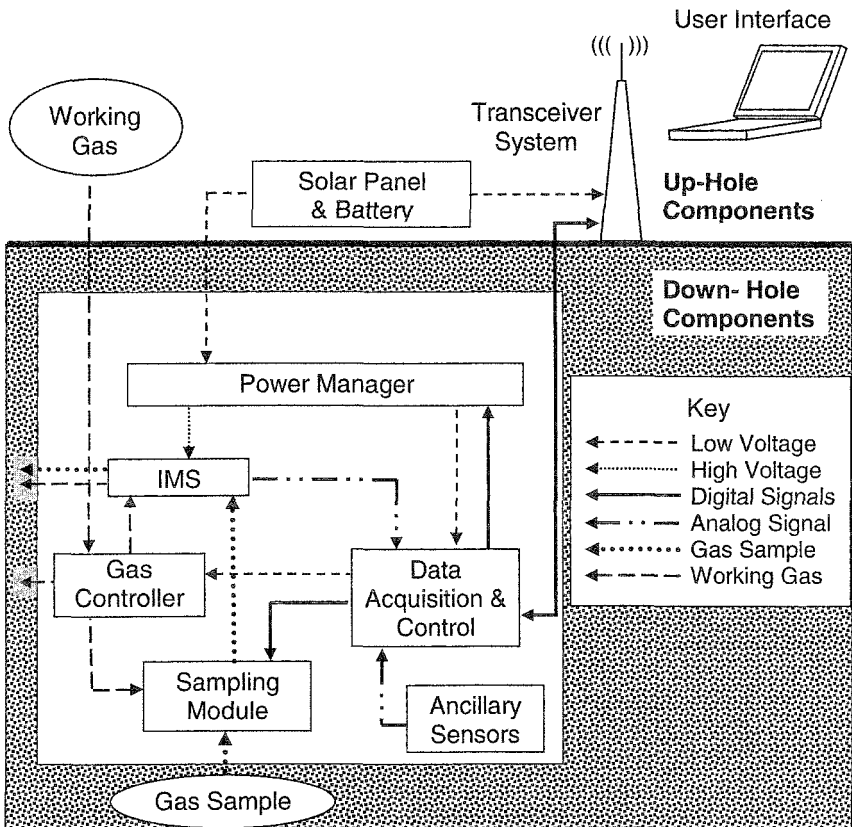
Figure 1. Block Diagram of the IMS Sensor System.

Once deployed, the IMS sensor probe will be connected to an "up-hole" system comprised of an electrical power source, a serial port for local data collection and/or device configuration, and a transceiver system to provide off-site data analysis. The transceiver will use either satellite or land wireless infrastructures to allow data collection and analysis by users in one or more global locations through a web interface.
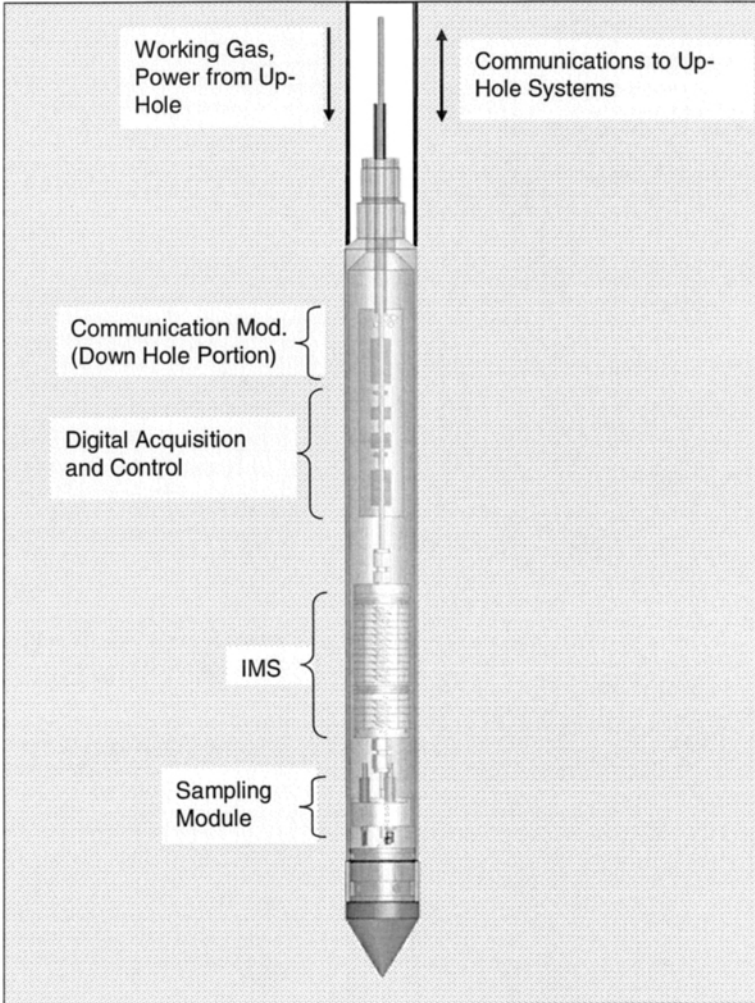
Figure 2. Layout of the IMS Sensor System in Probe Housing.

Our IMS sensor system is designed to provide real-time monitoring and in-situ identification and concentration values of target VOCs without the need for time consuming, off-site analysis. This sensor provides a method for long-term monitoring of sites and eliminates the need for expensive equipment and labor at a site associated with current active sampling methods. More information on the specific modules of the IMS sensor system under development is provided below.

IMS Sensor

The heart of the sensor system is the IMS sensor, which is compact enough to fit within the probe housing, yet offers the resolving power needed to accurately identify a variety of VOCs. The current dimensions of the IMS are an outer diameter of 3. 8 cm and a length ranging from 12 to 16 cm. Our IMS is composed of a reaction region with a Ni^{63} ionization source and a drift tube constructed of an alternating series of metal and insulating rings. The insulating rings were fabricated out of a machinable glass material called Macor (Dow Corning, Corning, NY). The conducting rings are connected with voltage divider network such that an electric field is created through the center of the tube. A Faraday plate at the end of the drift tube collects the ions that travel down the drift tube to generate a current that is sensed by the data acquisition and control module.

Gas Controller and Sampling Module

The gas controller moves gas samples extracted from the unsaturated soil through the sampling module and provides the counter-flowing drift gas to the IMS. We anticipate using nitrogen or air as the working gas for both of these functions. A venturi pump is used to generate a small vacuum to pull gaseous samples through a porous metal filter into the probe housing and introduce them into the IMS reaction region. The volume of soil impacted during sampling (i.e., the support volume for the measurement) will depend on the intrinsic permeability, degree of saturation and porosity of the soil. An increase in the intrinsic permeability results in an increase in the support volume. Conversely, an increase in degree of saturation will result in a decrease in the relative permeability to the gas phase and decrease in the support volume for a given sampling interval. Finally, an increase in the porosity (not accounting for a change in the intrinsic permeability) will also decrease the support volume. Work is currently underway to determine the working range of the sampling module with respect to these variables for different soil types.

Data Acquisition and Control (DAC) Module

This subsystem serves both the data sensing and harvesting roles. First, this subsystem amplifies the nano-ampere (nA) level current of the Faraday plate with a gain of ~1 Volt per nA. Then it digitizes the data and reduces noise prior to processing the data. This subsystem also controls other down-hole subsystems, such as the gas sampling module, gas controller, and power module, and exports the digital

data for subsequent communication from the down-hole probe location to the up-hole support system.

Communication Module

The two major communication pathways in the sensor system beyond the device interaction within the probe housing are:

- Communication between the down-hole (probe) system and up-hole system using the industry standard protocols.
- Communication between the up-hole sensor systems to the Internet using a satellite or other wireless communications infrastructure. The satellite communications link from the probe to the Internet has been simulated using existing tools by our industry partner, TenXsys (Eagle, Idaho), using a data source to the satellite in place of an actual sensor transmitter.

User Interface

The use of the Internet enables simple, flexible and intuitive data collection. Internet-based communication allows access by users across the globe. Also, no proprietary software is needed on the user's PC to access the data. An example of how the user interface may look is shown in Figure 3 below.
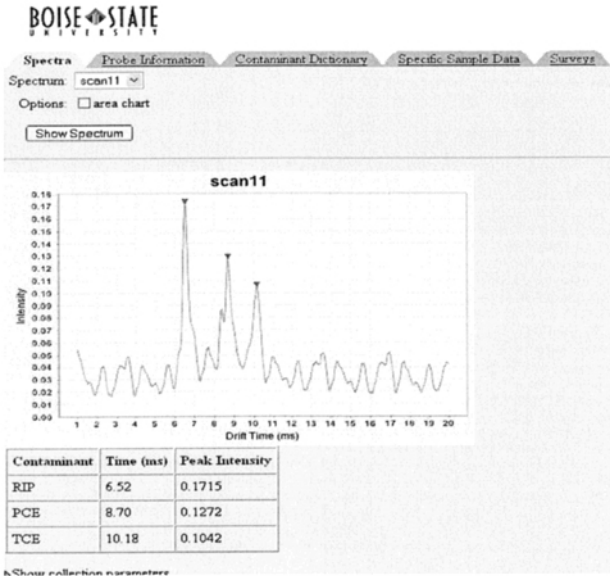
Figure 3. Example User Interface for the IMS Sensor System created by TenXsys (Eagle, Idaho).

Experimental Results

Two sets of experiments were conducted to evaluate the IMS prototype components. Additional experiments were carried out by the Washington State University team to characterize the IMS sensor itself for sensitivity and selectivity to various VOCs. These experiments verified the functionality of the IMS device, DAC, sampling module and high voltage power modules. The following sections describe the experimental results in more detail.

IMS Sensitivity

The IMS prototype's ability to detect target VOCs was evaluated using a reference laboratory amplifier, power supply and data acquisition system. Figure 4 shows the experimental setup for these tests.
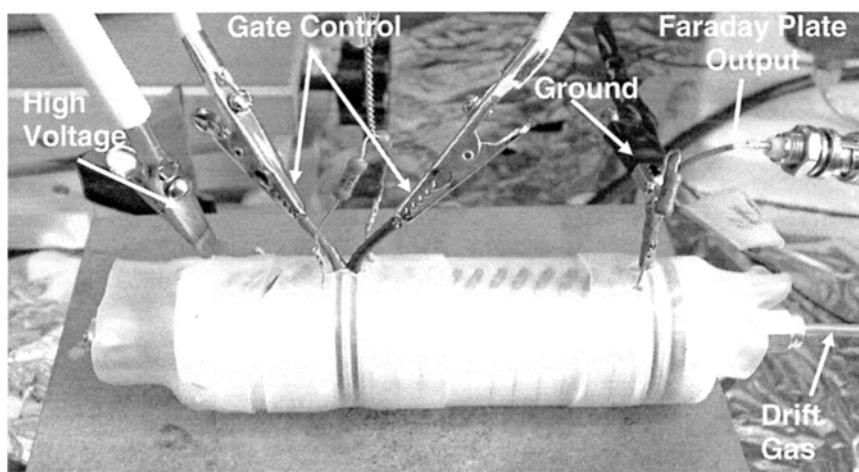
Figure 4. IMS Test Setup.

System Level Measurement

The IMS system was also tested to evaluate the behavior of the DAC module, power supply, sampling, and other modules. All modules were successfully integrated as a system and were demonstrated to perform the following tasks:

- Withdraw contaminant samples in controlled volumes and introduce the samples to the IMS.
- Provide and control the different high voltages needed by the ion gate and drift tube.
- Ionize the sample and control the drift event.
- Amplify and digitize current generated by the ionized sample.

- Provide data processing and storage of the current waveform.
- Provide automated control of the system through the DAC.

The IMS was able to identify the following compounds when introduced separately:

- Tetrachloroethylene (PCE)
- Trichloroethylene (TCE)
- Isobutyl methyl ketone (MIBK)
- Tert-butyl methyl ether (MTBE)

It was also able to identify the following compounds in mixtures:

- TCE and PCE
- MIBK and MTBE

A representative set of spectra that show that TCE and PCE can be detected by the IMS is presented in Figure 5. Preliminary results suggest that the detection limits will be in the ppm_v range. Optimization of the system may lead to detection limits in the ppb_v range. Thus, we expect the resolving power of the IMS to be comparable to commercial IMS systems.
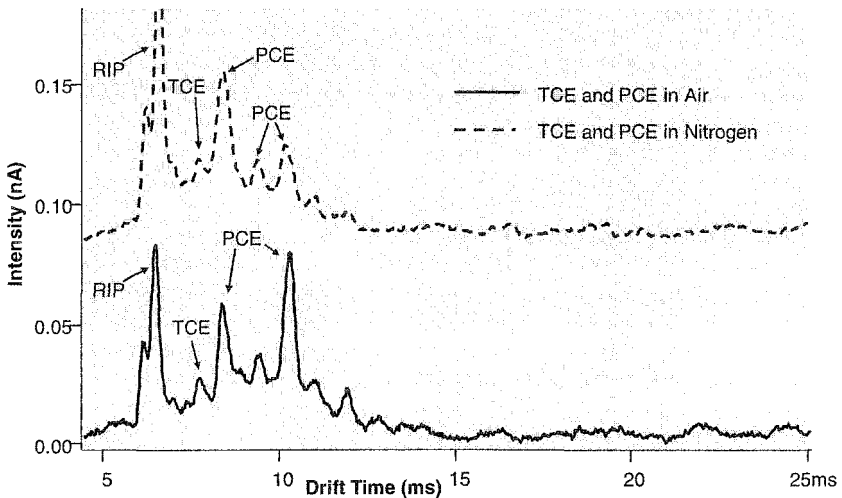
Figure 5. Preliminary Spectra of TCE and PCE from the IMS.

Figure 6 shows results of the end to end measurement of the IMS sensor system for a mixture of PCE and TCE. This measurement demonstrates the accuracy of the IMS sensor system in the time domain, but also reflects undesirable rounding of the peaks relative to the laboratory DAC system. We have identified the major

contributors to this problem as inadequate amplifier bandwidth and a noise reduction algorithm that is providing a low-pass filtration of the signal. As bandwidth is increased and an improved noise reduction algorithm is implemented in the DAC, less substantial rounding of the output should be possible. Overall, these experiments successfully validated the IMS sensor hardware as a platform for taking the technology forward for subsurface use.

Next Steps

The next major step is to redeploy these subsystems in the probe housing for in-situ measurement. This will require:

- Design and construction of the probe housing.
- Addition of pressure and temperature sensors to enable normalization of the ion mobility measurement.
- Construction and testing of a smaller sampling module and gas controller (designs are already completed).
- Completion of the down-hole to up-hole serial bus.
- Design and completion of the up-hole system power supply (battery, solar panels and controller).
- Completion of the up-hole system gas supply system.
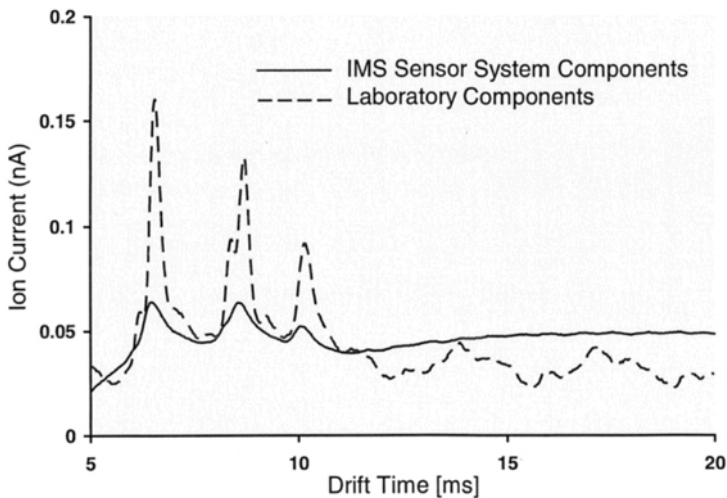
Figure 6. IMS Sensor System Measurement Relative to Lab System

In addition, refinements are expected to take place concurrently with the probe-based sensor in the following areas:

- Continued characterization and optimization of the IMS to achieve higher resolution.
- Investigation of the effects of interferences on IMS performance.
- Work to reduce noise and increase bandwidth of the DAC amplifier.
- Development of improved algorithms to enhance data processing in the DAC module.

Conclusions

We have designed, fabricated, and tested a miniaturized ion mobility spectrometer in the laboratory for use in unsaturated soils to detect gaseous VOCs. Preliminary experimental results suggest that this IMS will be able to detect PCE and TCE, and MTBE and MIBK in mixtures, with detection limits expected to be in the ppm_v range. Optimization of the system may lead to ppb_v-level detection limits. Additional characterization work is needed to determine the effects of interferents and verify the ability of the IMS to detect other VOCs of interest.

Acknowledgements

References

Domenico, P.A. and Schwartz F.W. (1998). *Physical and Chemical Hydrogeology*, 2nd Edition, John Wiley and Sons, New York, NY, 506 pgs.

Environmental Protection Agency (EPA). (1998). *Soil-Gas and Geophysical Techniques for Detection of Subsurface Organic Contamination*; Environmental Monitoring Systems Laboratory, Las Vegas, NV, EPA/600/S4-88/019.

EPA. (2002). *OSWER Draft Guidance for Evaluating the Vapor Intrusion to Indoor Air Pathway from Groundwater and Soils (Subsurface Vapor Intrusion Guidance)*, EPA-530-D-02-004.

Wong, T.T., Agar, J.G., and Gregoire, M.Y. (2003). "Technical rationale and sampling procedures for assessing the effects of subsurface volatile organic contaminants on indoor air quality," *Proceedings of the 56th Canadian Geotechnical Conference & 4th Joint IAH-CNC/CGS Conference*, Sept. 28-Oct. 1, 2003, Winnipeg, MB Canada.

Influence of Flooding on Borehole Shear Test (BST) Results in Unsaturated Soil

Charbel N. Khoury[1] and Gerald A. Miller[2]

[1,2] School of Civil Engineering and Environmental Science, University of Oklahoma, 202 West Boyd St., Room 334, Norman, OK 73019
[1] Ph.D. Student; PH (405) 325-9244; FAX (405) 325-4217; e-mail: ckhoury@ou.edu
[2] Associate Professor, PH (405) 325-4253; FAX (405) 325-4217; e-mail: gamiller@ou.edu

Abstract

This study was undertaken to begin evaluating the influence of soil suction on shear strength parameters determined from the Iowa Borehole Shear Test (BST) in unsaturated soil, namely the friction angle and cohesion intercept. A new technique, the Flooded Borehole Shear Test (FBST), was employed in this study. The BST, before and after flooding the borehole, was conducted for comparison of results. Suction was determined using the filter paper technique on undisturbed specimens in accordance with the ASTM D 5298 test method. Results showed that the friction angles determined from the FBST were much lower than those determined from the BST, as expected, apparently due to the reduction in suction due to flooding. The reduction in friction angle due to flooding generally followed a predictable pattern that was a function of the suction prior to flooding. However, the effect of suction on the cohesion intercept was much less pronounced. The cohesion intercepts from the FBST generally decreased slightly in comparison to the BST results, although cohesion intercepts were small in both cases. This paper discusses the practical implications associated with BST testing in unsaturated soil.

Introduction

Traditional soil mechanics typically involves assumptions appropriate primarily for the study of saturated or dry soil. However, many problems encountered in geotechnical engineering practice involve unsaturated soil, the behavior of which is significantly different than classical saturated soil. This study discusses the effect of suction on the shear strength parameters determined with the Iowa Borehole Shear Test (BST).

Laboratory and field tests were conducted at the University of Oklahoma to investigate the BST in unsaturated soil. Field testing included the BST and a modified test procedure called the Flooded BST (FBST), as well as laboratory testing including filter paper and multistage isotropically consolidated undrained (CIUC) triaxial tests on saturated specimens. Two test sites located within 10 miles of the University of Oklahoma were chosen for the research: the I-35 Interstate, and Westheimer Airport sites. At the I-35 Site, for the upper 1.37 m (4.5 ft) the soils consist of Fat Clay (CH) and then change to Lean Clay from 1.37 m (4.5 ft) to 2.13 m (7 ft). At the Airport Site, Fat Clay (CH) soils exist to a depth of 0.91 m (3 ft) and Lean Clay (CL) exists at depths from 0.91 m (3 ft) to 2.29 m (7.5 ft). Characteristic properties of the soil at both sites are presented in Table 1.

A main focus of this paper is the FBST used to study the influence of flooding and reduction of suction on BST parameters; the results are discussed relative to multistage CU triaxial test results.

Table 1- Characteristic Properties of Soil at I-35 and Airport Sites

Site	depth (m)	w_n %	LL	PL	PI	LI	Gs	% Finer 2μm	% Finer # 200	Activity	USCS Group Symbol	USCS Group Name
I-35	0.76	23.1	62	19	43	0.096	2.71	37	94	1.18	CH	Fat Clay
	1.07	17.4	56	19	37	-0.04	2.76	38	94	0.97	CH	Fat Clay
	1.37	19.9	56	18	38	0.049	2.74	21	98	1.80	CH	Fat Clay
	1.68	18.7	40	16	24	0.111	2.72	41	93	0.59	CL	Lean Clay
	1.98	22.6	41	16	25	0.264	2.76	47	97	0.53	CL	Lean Clay
Airport	0.30	---	55	23	33	---	2.71	37	94	0.892	CH	Fat Clay
	0.76	18.6	52	22	30	-0.106	2.70	39	93	0.770	CH	Fat Clay
	1.07	---	49	21	28	---	2.69	41	93	0.693	CL	Lean Clay
	1.37	18.8	46	15	31	0.126	2.70	41	98	0.764	CL	Lean Clay
	1.68	---	44	16	28	---	2.70	42	96	0.671	CL	Lean Clay
	1.98	17.5	30	17	13	0.011	2.65	33	98	0.392	CL	Lean Clay
	2.29	18.1	34	19	15	-0.048	2.71	41	97	0.382	CL	Lean Clay

Background

The Iowa Borehole Shear Test

The Iowa Borehole Shear Test (BST) (Handy and Fox, 1967) is an in situ test to determine the cohesion and friction angle of soil. It is a rapid and simple test, similar to performing a direct shear test on the sidewalls of a borehole (Figure 1). Details of the BST operation are provided by Handy and Fox (1967) and Lutenegger (1987). In summary, two diametrically opposed shear plates are lowered in a hole and then expanded against the borehole wall using gas pressure to increase the normal stress incrementally. Allowing a period for consolidation depending on the type of soil, a shearing stress is then applied by pulling the plates up along the hole until failure occurs. Finally, the shear and normal stress values are obtained for each test from which a Mohr Coulomb failure envelope is drawn.

The BST has been used on many projects in different site locations. For example, it was used in a shallow marine environment (Handy et al. 1985) as a part of a bridge foundation investigation and proved useful in landslide slope stability investigations (Handy 1986). Results of the BST were used in the prediction of uplift capacity of drilled shafts (Lutenegger and Miller 1994), and can be used to estimate soil-to-steel pile side friction by replacing the toothed BST shear plates with smooth plates (Handy et al. 1985). Several modifications of the BST device have also extended its use from sands, silts and clays to hard clay, overconsolidated clays and shales (Lutenegger et al. 1978).

Much previous research on the BST was focused on saturated soil. Results from the BST below the water table may compare favorably with laboratory effective stress-strength parameters for medium to stiff clays (Lutenegger and Miller 1994). In stiff clays it appears there is little excess pore water pressure developed during the test and therefore, the applied normal stress can be considered as effective stress. However, little emphasis has been placed on BST in unsaturated soil. Miller et al. (1998) have done a preliminary study on the influence of matric suction on the soil shear strength parameters determined using the BST. The BST was conducted in unsaturated silty soil compacted within a rigid wall calibration chamber; resulting friction angles and cohesion intercepts appeared to be strongly dependent on the matric suction in the soil.

Shear Strength of unsaturated soil

The shear strength of an unsaturated soil can be formulated in terms of two stress state variables (Fredlund et al. 1978), which are the net normal stress and the matric suction. Net normal stress is the difference between the total stress and pore air pressure ($\sigma - u_a$), and the matric suction is the difference between the pore air and

the pore water pressure ($u_a - u_w$). According to Fredlund and Rahardjo (1993), the shear strength of the soil can be written as,

$$\tau = c' + (\sigma_n - u_a)\tan\phi' + (u_a - u_w)\tan\phi^b \tag{1}$$

where: τ = shear stress at failure, c' = effective cohesion, σ_n = total stress normal to the failure plane, u_a = pore air pressure, ϕ' = angle of internal friction associated with the net normal stress variable, u_w = pore water pressure, and ϕ^b = angle of internal friction associated with the matric suction.

For many soils, ϕ' appears nearly constant over a significant range of suction, while ϕ^b varies with suction. The angle ϕ^b at low matric suction, below the air entry value, appears equal to ϕ', but at higher matric suction it decreases to a lower value (e.g. Fredlund and Rahardjo 1993).

With this behavior in mind, it was anticipated that in the case of the BST in unsaturated soil, possibly the failure envelope would achieve a slope inclination (ϕ_{BST}) similar to ϕ' if the matric suction did not vary during the test. Also, implicit in this possible outcome was the assumption that the pore air pressure remains equal to zero (gage pressure) during the test and the applied normal stress can be considered the net normal stress. It follows that the influence of suction should have been apparent in the values of the failure envelope cohesion intercept for tests conducted at different suction values. As discussed in the remainder of this paper, BST results were not as anticipated, and failure envelope parameters appeared strongly dependent on suction.

Determination of Soil Suction

Various techniques are available to measure soil suction: psychrometric, porous plate, pressure membranes, tensiometers, filter paper methods, and others. The filter paper technique was used in this study.

The filter paper is an inexpensive and simple laboratory test method used for total and matric suction determination. The filter paper method has been investigated by numerous researchers (e.g. Chandler and Gutierrez 1986, Houston et al. 1994, Swarbrick 1995, and Likos and Lu 2002).

The filter paper method is based on the assumption that a filter paper in close proximity to soil will achieve a moisture content at equilibrium with the moisture in a soil having a specific suction. The water content of the filter paper corresponds to a suction value determined from a calibration curve. Theoretically, the water content of the filter paper when placed in contact with the soil corresponds to the matric suction;

when not in contact with the soil, it corresponds to the total suction of the soil (Fredlund and Rahardjo 1993).

Methodology

Conventional BST

Borehole Shear Tests were conducted in hand-augered boreholes at several depths ranging from 0.46 m (1.5 ft) to 2.29 m (7.5 ft), at an interval of 0.305 m (1 ft). Multi-stage tests were performed where successively higher normal pressures were applied while leaving the shear head in place. The multi-stage test was conducted because it offers some advantages in simplicity, speed, dissipation of pore pressure and testing for individual layers; however, this method may produce invalid strength envelopes if the shear plates do not fully engage the soil (Handy et al. 1985). Research has shown that single and multi-stage tests generally result in similar failure envelopes (Lutenegger 1986).

Flooded Borehole Shear Test (FBST)

A novel technique was performed by flooding the borehole with water, and running the BST again at the depth locations used prior to flooding, to determine the flooded shear strength parameters of soil. For flooded tests, the shear plates were rotated 90 degrees from the previous orientation used before flooding. Specifically, after conducting the BST in the unsaturated soil at different depths, the borehole was successively filled with water. The FBST was performed starting from the bottom of the borehole and moving upward. The water was incrementally added to cover the desired test depth. A funnel having a hose attached to its bottom was used in order to minimize disturbance on the side of the borehole while adding water. The shear head of the BST was immediately lowered in the flooded borehole and the multi-stage test procedure was initiated. No time lag was allowed between flooding and BST testing to minimize soil swelling due to flooding. The Mohr-Coulomb failure envelope was plotted to determine the cohesion intercept, c_{FBST}, and angle of friction, ϕ_{FBST}.

As the borehole is flooded with water the unsaturated soil on the margins is believed to become nearly saturated, effectively eliminating the suction as illustrated in Figure 1. The extent of this wetting is currently unknown. The corresponding parameters determined from this new technique were expected to possibly represent the effective stress-strength properties of soil as previously observed in medium to stiff saturated clays. This hypothesis was examined by comparison with the multi-stage triaxial test results.

Soil Suction Measurement Using Filter Paper Technique

To estimate soil suction, the filter paper method was performed on thin-walled tube samples. Calibration of filter papers was performed in accordance to ASTM D

5298; calibration of filter papers on a batch-to-batch basis was conducted as recommended by Likos and Lu (2002). Total suction was determined when filter papers were not in contact with the soil specimen while matric suction was determined when the filter papers were in contact with the soil. The testing procedure for soil suction measurements using filter papers was conducted according to ASTM D 5298. Only total suction is reported in this paper as matric suction determinations were not reliable.
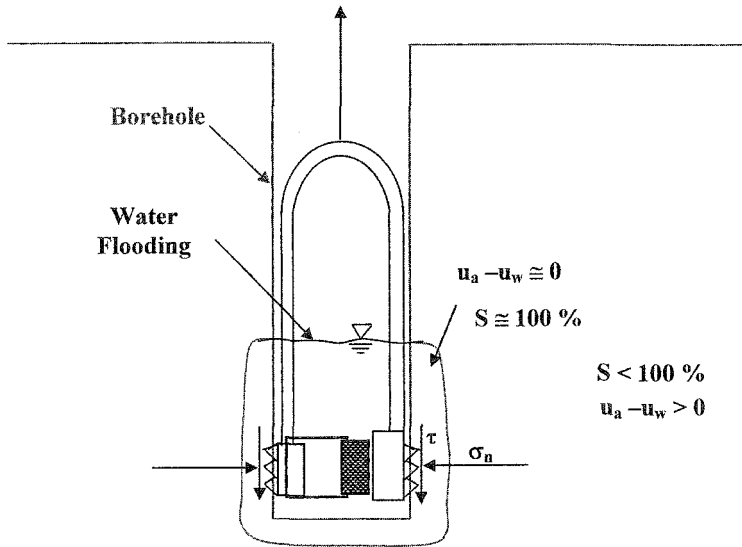
Figure 1- Flooded Borehole Shear Test

Results and Discussions

BST and FBST Results

Values of the BST angle of friction, ϕ_{BST}, ranged from $30°$ to $43°$; on the other hand, ϕ_{FBST} ranged from $12°$ to $26°$ using the FBST method. Cohesion intercepts obtained from both BST (c_{BST}) and FBST (c_{FBST}) were small. The BST gave much higher friction angles than the FBST, as clearly illustrated in Figure 2 for typical test results obtained at a depth of 1.37 m (4.5 ft) at the Airport Site. Results from the two sites and at different depths are summarized in Figure 3. The data in this figure show that the friction angle values decreased significantly after flooding the borehole. The BST and FBST results along with suction values are summarized in Table2.
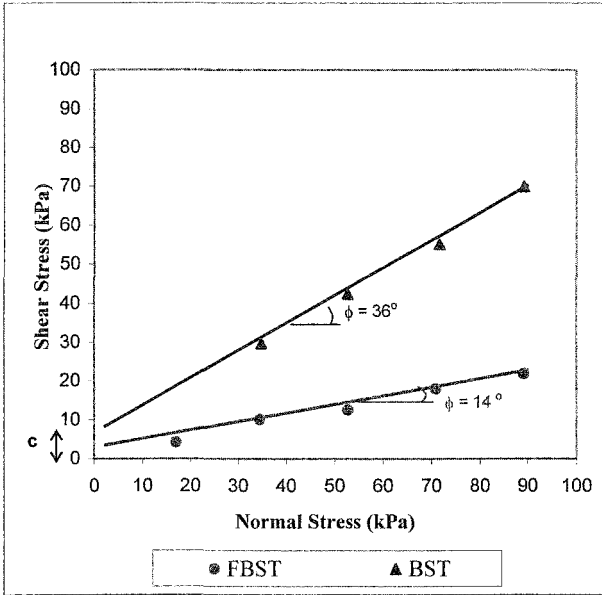
Figure 2- Typical Results (1.37 m depth, Airport Site) from BST and FBST
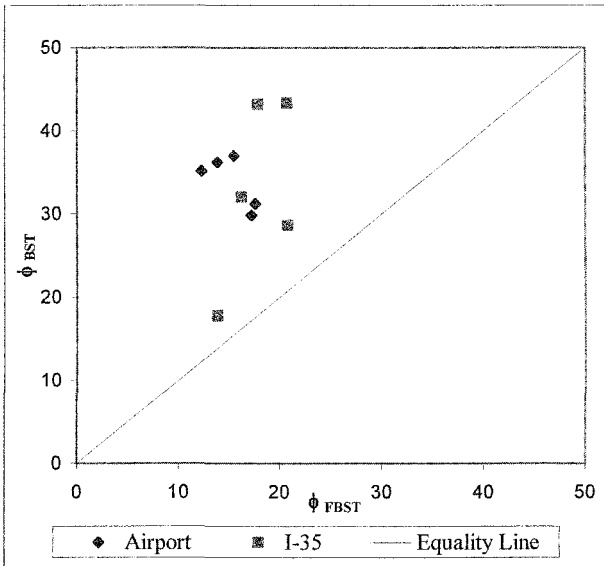
Figure 3- Comparison of BST and FBST Results

Table 2- BST, FBST and Suction Summary Results for the Two Sites

Site	depth (m)	c (kPa)		φ (deg.)		r²		Total Suction (kPa)
		BST	FBST	BST	FBST	BST	FBST	
I-35	0.76	0.0	1.9	43.2	17.9	0.993	0.999	1576
	1.07	0.0	0.3	43.4	20.7	0.983	0.953	805
	1.37	4.9	0.0	32	16.3	0.982	0.989	727
	1.68	8.6	2.0	28.6	20.8	0.997	0.997	339
	1.98	16	3.6	17.7	13.9	0.989	1.0	307
Airport	0.76	10.6	4.2	37	15.5	1.0	0.999	739
	1.37	3.9	0.0	36.2	13.9	0.998	0.990	586
	1.52	5.7	2.4	35.1	12.3	0.998	0.997	---
	1.98	7.8	0.0	31.2	17.6	0.999	0.997	118
	2.29	7.1	0.0	29.8	17.2	0.986	0.982	173

Correlation between Change in Friction Angle (Δφ) and Suction Results

The effect of flooding the borehole with water was examined with respect to the change of friction angle $\Delta\phi$ ($\phi_{BST}-\phi_{FBST}$) and suction. The relationship between the initial soil total suction and the change of friction angle ($\Delta\phi$) due to flooding of the borehole for the Airport and I-35 sites is presented in Figure 4. While data are limited, the plots show a good fit for a linear regression model with coefficients of determination (r^2) equal to 0.91 and 0.79 at the Airport Site and the I-35 Site, respectively. The plots and the data in Table 2 indicate a dependency of the BST friction angle on suction. As discussed previously, it was thought possible that the BST friction angle obtained would be similar to the ϕ' of the soil, assuming the suction remained constant during the test. Given the dependency of ϕ_{BST} on suction observed in the test results, it appears this is not the case. Possibly, changes in suction are occurring during the incrementing of normal stress or during shearing; this phenomenon is currently the subject of further research.

The regression models in Figure 4 indicate differences from one site to another even though both sites have relatively similar type of soil and geologic history. The Airport Site trend line is nearly parallel to the I-35 Site but shifted to the left. Possibly, this difference represents some natural spatial variability and/or hysteresis brought on by seasonal effects; I-35 site was tested in October after a drying period while the Airport Site was tested in January following a wetting period.
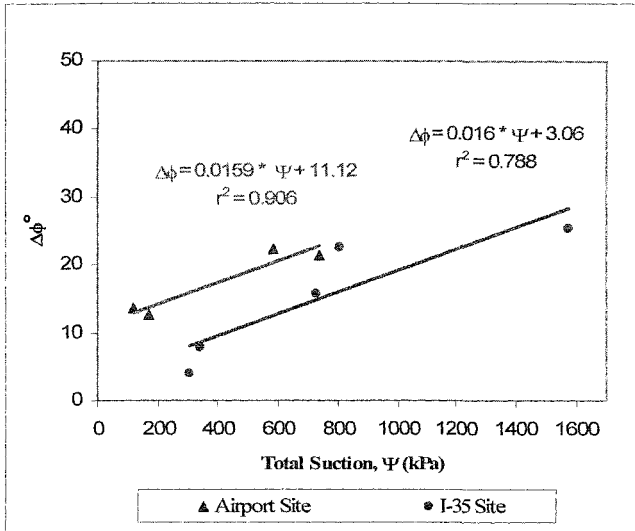
Figure 4- Variation of Δφ with Total Suction at Airport & I-35 Sites due to Flooding

Comparison of BST, FBST and Multistage Triaxial Test (MTT) Results

Comparison with Multi-Stage Triaxial Test results (MTT) in nearly all cases indicates that the angles of friction obtained from the BST in unsaturated soil are higher (Figure 5) and the cohesion intercepts (c) are smaller than the ones obtained from the MTT under similar ranges of normal stress. On the other hand, FBST values were much lower. As discussed previously, it has been observed that for medium to stiff clays the borehole shear test may provide a reasonable estimate of the effective stress strength parameters. Thus, it was thought that the flooding technique would eliminate the suction, effectively creating a nearly saturated soil, and possibly allow the BST to provide reasonable estimates of the effective friction angle and cohesion intercept. Results obtained from the FBST, are compared to MTT results performed on samples from the same depth. Results from the MTT and FBST are significantly different as shown in Figure 5. It is evident that the triaxial effective stress friction angles are generally much higher than the FBST values, where most of the points fall above the line of equality. One reason for this difference may be that after drilling the borehole and flooding it with water the unsaturated soil at the margins is weakened. Possibly during shearing the failure is occurring between the thin weak disturbed soil zone (affected by flooding) and the surrounding unsaturated soil, resulting in lower BST friction angles. Also, there is the possibility that positive shear induced pore water pressures are resulting in lower BST friction angles.

It is interesting to note that the friction angles determined from Multistage Triaxial Tests (MTT) were generally in between those obtained from the BSTs and FBSTs. The ranges of friction angles for normal stresses below about 100 kPa were 29° to 45°, 12° to 26°, 17° to 30°, for BST, FBST and MTT, respectively.
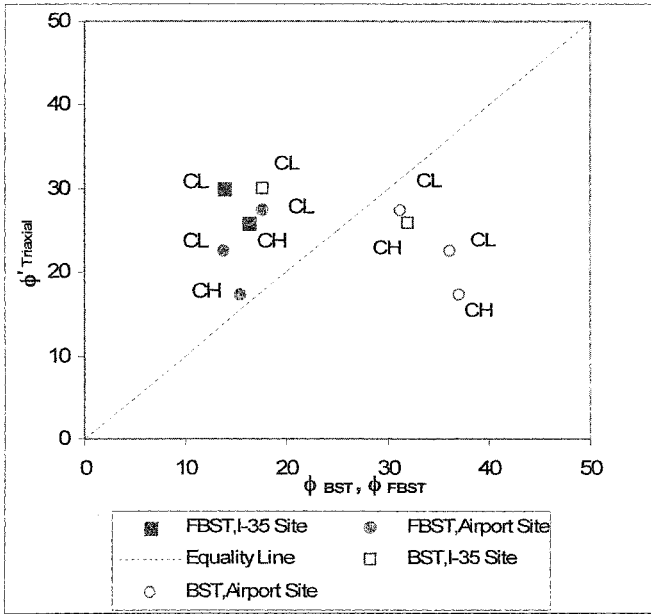
Figure 5- Comparison of φ between BST, FBST, and MTT results

Conclusions and Comments

In this paper, Borehole Shear Test (BST) results from unsaturated soil are examined. A novel test procedure, the Flooded Borehole Shear Test (FBST) was used to study the influence of borehole flooding on BST strength parameters. The Multistage Triaxial Compression Test (MTT) was conducted on selected back-pressure saturated samples to provide effective stress friction angles and cohesion intercepts for comparison to BST and FBST results. Total suction was determined on Shelby tube samples using the filter paper method. The following conclusions were developed based on this investigation:

- Friction angles determined from the FBST were much lower than those determined from the BST, as expected, apparently due to the reduction in suction due to flooding.

- The reduction in friction angle due to flooding generally followed a predictable pattern that was a function of the suction prior to flooding.
- Effective stress friction angles determined from Multistage Triaxial Tests (MTT) were generally in between those obtained from the BSTs and FBSTs. The ranges of friction angles for normal stresses below about 100 kPa were 29° to 45°, 12° to 26°, and 17° to 30°, for BST, FBST and MTT, respectively.
- Cohesion intercepts from the BST and FBST were generally small. The cohesion intercepts from FBST generally decreased slightly in comparison to the BST results. The ranges of cohesion intercepts for normal stresses below about 100 kPa were 0 to 11 kPa, and 0 to 4 kPa, for BST and FBST, respectively.
- Cohesion intercepts obtained from the MTTs were much higher than those obtained from both BSTs and FBSTs. The MTT cohesion intercepts fall in the range of 22 to 52 kPa.

There is much to be learned yet about the meaning of BST results from unsaturated soils. Currently, interpretation is limited to a total stress context since matric suction appears to be changing during the test. Thus, proper application of the BST results from unsaturated soils to geotechnical problems is not clear. Evolution of pore air and pore water pressures throughout the test is of particular interest; current research is focused on this topic.

References

American Society of Testing and Materials (ASTM) (1999), Annual Book of ASTM 1999, Vol.04.09.
Chandler, R.J and Gutierrez, C. I. (1986). "The Filter Paper Method of Suction Measurements," Geotechnique, Vol.36, pp.265-268.
Fredlund, D.G, Morgenstern, N.R, and Widger, R.A. (1978), "The Shear Strength of Unsaturated Soils," Canadian Geotechnical Journal, No.15 (3), pp.313-321.
Fredlund , D.G., and Rahardjo, H. (1993), "Soil Mechanics of Unsaturated Soils," John Wiley and Sons, NY.
Handy, R. L. (1986), "Borehole Shear Test and Slope Stability," Proceedings of In Situ '86 ASCE Specialty Conference on Use of In-Situ Tests and Geotechnical Engineering , Virginia Tech, Blacksburg, Virginia, pp. 161-175.
Handy, R. L., and Fox, N. S. (1967), "A Soil Borehole Direct-Shear Test Device," Highway Research News, No. 27, pp.42-51.
Handy, R. L., Schmertmann, J. H., and Lutenegger, A. J. (1985), "Borehole Shear Tests in a Shallow Marine Environment," Strength Testing of Marine Sediments: Laboratory and In-Situ Measurements, ASTM STP 883, R. C. Chaney and K. R. Demars, Eds., Philadelphia, pp.140-153.
Houston, S.L, Houston, W.N, and Wagner, A.M. (1994). "Laboratory Filter Paper Measurements," Geotechnical Testing Journal, ASTM, Vol.17, No.2, pp.185-194.
Likos, W. J., and Lu, N. (2002), "Filter Paper Technique Measuring Total Soil Suction," Journal of Transportation Research Board, Transportation Research Board 2002, Washington, D.C.
Lutenegger, A. J. (1986), "Pore Pressure Effects in Borehole Shear Testing," Proceeding Conference on Use of In-Situ Tests in Geotechnical Engineering, Samuel Clemence ed., pp. 752-764.

Lutenegger, A. J. (1987), "Suggested Methods for Performing the Borehole Shear Test," Geotechnical Testing Journal, ASTM, Vol. 10, No.1, pp.19-25.

Lutenegger, A. J., Remmes, B. D., and Handy, R. L. (1978), "Borehole Shear Test For Stiff Soil," Journal of the Geotechnical Engineering Division, ASCE, Vol. 104, No. GT11, pp.1403-1407.

Lutenegger, A. J. and Miller, G. A. (1994), "Uplift Capacity of Small-Diameter Drilled Shafts from In-Situ Tests," Journal of the Geotechnical Engineering Division, ASCE, Vol. 120, No. 8, pp. 1362-1379.

Miller, G.A, Azad, S., and Hassell, C.E, (1998), "Iowa Borehole Shear Testing in Unsaturated Soil," The Proceedings of the 2nd International Conference on Unsaturated Soils, Geotechnical Site Characterization, International Academic Publishing House, Beijing, P. R. China, Vol. 1, pp. 1321-1326.

Swarbrick, G.E. (1995), "Measurement of Soil Suction Using the Filter Paper Method," First International Conference on Unsaturated Soils, Eds.: E.E Alonso and P. Delage, Paris, 6-8 September, Vol.2, pp.701-708.

Analysis of Variations of Pavement Subgrade Soil Water Content

Andrew G. Heydinger[1] and B. O. A. Davies[2]

[1]Fellow Member ASCE, Ph.D., Professor; Mail Stop 307, Department of Civil Engineering, University of Toledo, Toledo, OH 43606-3390; PH (419) 530-8133; FAX (419) 530-8116; email: aheyding@eng.utoledo.edu
[2]Formerly graduate student, Department of Civil Engineering, University of Toledo, beresford_davies@yahoo.com.

Abstract

Seasonal Monitoring Program (SMP) data available in the Long Term Pavement Performance (LTPP) database DataPave was analyzed to investigate the variations of volumetric water content. The SMP data includes volumetric water contents from time domain reflectometry (TDR) probes in pavement sections located in the United States and Canada. Water content, or the associated degree of saturation, is used to compute resilient modulus for unsaturated unbound base and subgrade soils in the Mechanistic-Empirical Pavement Design Guide (M-EPDG) that was developed for the Federal Highway Administration. The purpose of this paper is to discuss results of analysis of volumetric water content data from the most recent release of DataPave (Release 19) and the resulting variations in resilient modulus that would occur.

Results from analysis of the data indicate that there are variations of volumetric water content that occur over time. For a few of the pavement sections, the variations of volumetric water content were seasonal. For most of the sections, it was not possible to determine consistent trends in the moisture variations on a temporal scale or when comparing the different climate zones, soil types (coarse or fine-grained), pavement types or depth to the water table. The volumetric water content variations typically were greater than 3% and less than 9%. These findings indicate that subgrade soils undergo varying degrees of saturation. The resilient modulus, computed using the water content variations and an empirical equation developed for the M-EPDG, can vary by as much as a factor of 2. The resilient modulus variations are generally higher in wet climates than in dry climates.

Introduction

Resilient modulus is a significant factor required for empirical and mechanistic-empirical methods for designing pavements so it is important to be able to predict variations of resilient modulus caused by variations in subgrade soil

volumetric water content. For unstabilized bases and subgrade soils, resilient modulus can be expressed in terms of the moisture condition using volumetric water content, degree of saturation or soil matric suction. Soil matric suction may be a better predictor of resilient modulus in unsaturated soils since it is a stress state variable, however soil suction is difficult to measure so there is very little soil matric suction data. Therefore, empirical equations have been proposed to predict resilient modulus as a function of water content or degree of saturation. From an example from a fine-grained soil by Drum, et al. (1997), a soil that is at optimum water content and undergoes an increase in gravimetric water content equal to 1.5%, equivalent to a change in saturation of 4.7%, would result in a decrease in resilient modulus by a factor of about 1.9. Findings from several researchers are depicted using plots of $\log(M_R/M_{R\ opt})$ versus $(w - w_{opt})$, which are typically linear (Witczak, et al., 2000a). For fine-grained soils, an increase of $(w - w_{opt})$ equal to just 1% results in decreases in M_R ranging from 10 to 60%. For course-grained soils and bases, the decreases ranged from 2 to 20%. If one can determine the moisture variations, then empirical equations can be used to predict the variations of resilient modulus for use with pavement design.

LTPP Seasonal Monitoring Program instrumentation was installed to measure temperature, volumetric water content, frost penetration and depth to the water table at 63 Specific Pavement Studies (SPS) pavement test sections to investigate climatic effects on pavements (FHWA, 2005a). Temperatures are measured at 18 depths using a temperature probe. Volumetric water contents are measured at 10 depths using time domain reflectometry (TDR) sensors. Frost penetration is measured using electrical resistivity probes. The sensors and probes were installed to a depth of approximately 2 meters below the pavement surface. The monitoring wells used to determine depth to the water table were installed to depths of approximately 5 meters below the pavement surface. The four climatic regions designated for the SMP testing are wet-no freezing (WNF), wet-freezing (WF), dry-no freezing (DNF) and dry freezing (DF).

Research on the use of TDR sensors to measure volumetric water content has shown that there is significant scatter when comparing computed and measured values of volumetric water content (Klemunes, 1998). Values of R^2 ranged from 0.68 to 0.77 for coarse-grained and fine-grained soils, respectively. Some error occurs when converting from gravimetric to volumetric water content if the dry density is not accurate. In spite of the fact that there is error in the TDR measurements, it is believed that the volumetric water content variations that were observed can be taken to mean that moisture variations do occur over time.

This paper discusses results of analysis of volumetric water content data obtained from the Season Monitoring Program (SMP) testing conducted as a part of the Long-Term Pavement Performance (LTPP) testing. The most recent release of DataPave (Release 19) was used to determine the variations of volumetric water content (FHWA, 2005b). Detailed information is provided on analysis of moisture variations at test sections that the primary author was involved with. Data from all sites included in the SMP testing were analyzed to determine if it would be possible to predict variations of volumetric water content on a seasonal basis. The moisture

variations are tabulated. The variations in resilient modulus resulting from the moisture variations are computed using an equation by Witczak, et al (2000a).

Mechanistic-Empirical Pavement Design Guide

The Mechanistic-Empirical Pavement Design Guide (M-EPDG) was developed for the FHWA for designing pavements (NCHRP, 2005). The M-EPDG incorporates a one-dimensional finite element solution that couples heat and moisture flow, the Enhanced Integrated Climatic Model (EICM), to predict variations of temperature and volumetric water content. The EICM uses the equation for soil-water characteristic curves by Fredlund and Xing (1994) and a relationship for hydraulic conductivity by Fredlund, et al. (1994). Empirical relationships are used to compute required soil parameters using the product of percent passing the #200 sieve and the plasticity index for fine-grained soils and using D_{60} for course grained soils (Zapata, et. al., 2002). According to the procedure described in the documentation, an equilibrium matric suction is computed by taking the product of the depth to the water table at equilibrium and the unit weight of water. The EICM typically predicts very small or no seasonal variations of moisture content (Witczak, et. al., 2000b and Heydinger, 2003b).

An equation was derived for predicting resilient modulus as a function of degree of saturation (Witzak, et al., 2000a). The equation is based on findings from several investigators that there is a log-linear relationship between the ratio of the resilient modulus at any degree of saturation and the modulus at optimum conditions. Recommendations are made for the model parameters a, b, B and k_s in Equation 1 for both fine and coarse-grained soils.

$$\log\left(\frac{M_R}{M_{Ropt}}\right) = a + \frac{b-a}{a+\exp(\beta + k_s(S - S_{opt}))} \tag{1}$$

Variations in resilient modulus were computed using Eqation 1 for this paper.

Seasonal Variations of Volumetric Water Content

Research was conducted on a limited number of pavement sections to investigate the seasonal variations in volumetric water content. Data from one asphalt concrete (AC) and one Portland cement (PC) pavement section from the Ohio Test Road was analyzed (Heydinger, 2003 a and b). The results from this research, shown in Figure 1, indicated strong seasonal trends for the two pavements at this one site. For the figure, the average volumetric water contents from the upper three TDR sensors in the fine-grained subgrade soil, about 0.5 meter, were plotted as a function of the day of the year. The variations in average volumetric water content are very similar to the variations of average soil temperature obtained from the same depths as the TDR sensors. The observed seasonal trends are that the volumetric water contents are the highest when the average temperatures are the highest and are the
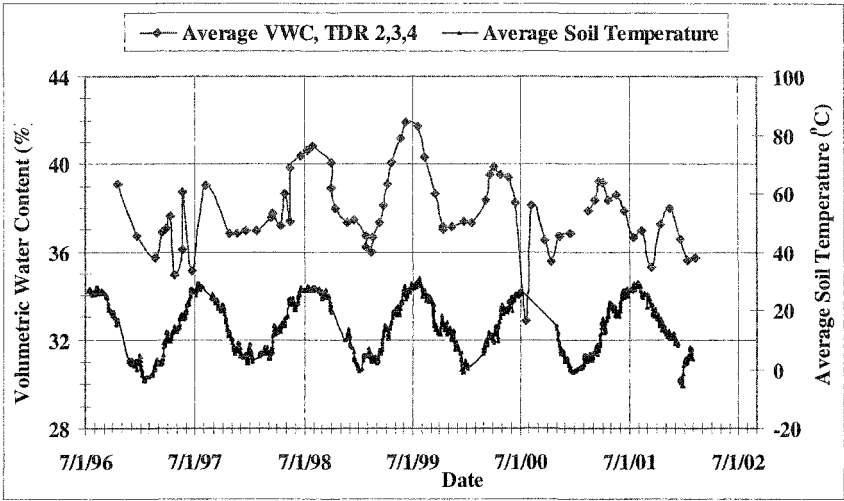
(b) Section 390204(PCC)
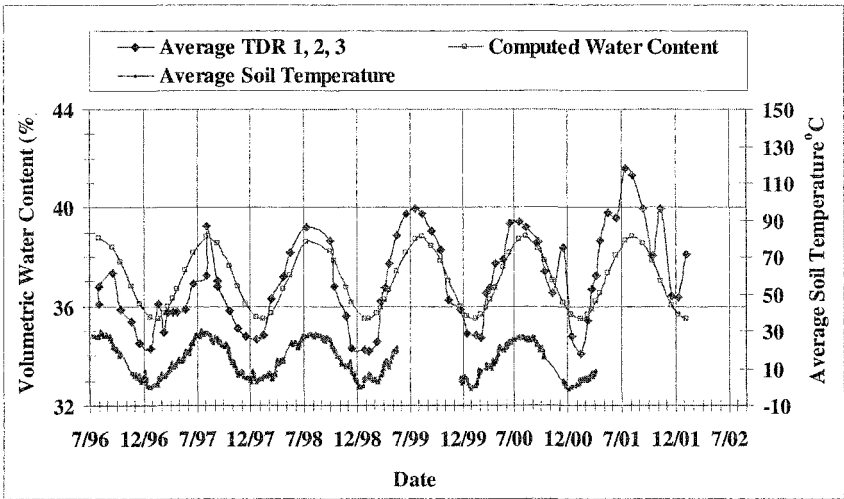
(a) Section 390104(AC)

Figure 1. VWC and average soil temperature (from Heydinger, 2003).

lowest when the temperatures are the lowest. Previous research has shown that an increase in temperature results in a decrease in dielectric constant, which means that the computed volumetric water content would also decrease (Selig and Mansukhani, 1975). Therefore, the water content variations cannot be attributed to temperature changes. TDR measured volumetric water contents decrease significantly when freezing occurs so water contents measured during freezing were excluded from the analyses. There appears to be an inverse relationship between volumetric water content and depth to the water table, water content increases as the depth to the water table decreases. The computed volumetric water contents were obtained using Equation 2, where t is the day of the year.

$$VWC(t) = 37.1 + 1.66 \sin[2\pi/365.25(t-130) \tag{2}$$

The mean volumetric water content (37.1), amplitude (1.66) and time factor (130) are material parameters. Figure 2 shows that the seasonal trends existed even for sensor 10 which was about 2 meters below the pavement surface. There appears to be no relationship between volumetric water content and precipitation. No strong trends were observed when volumetric water content was compared to cumulative precipitation from the previous 10 day or 30 day periods. Similar trends were observed on other test sections in other states using data obtained from the LTPP database, although the trends were not as strong as the pavements sections in Ohio (Davies, 2004).
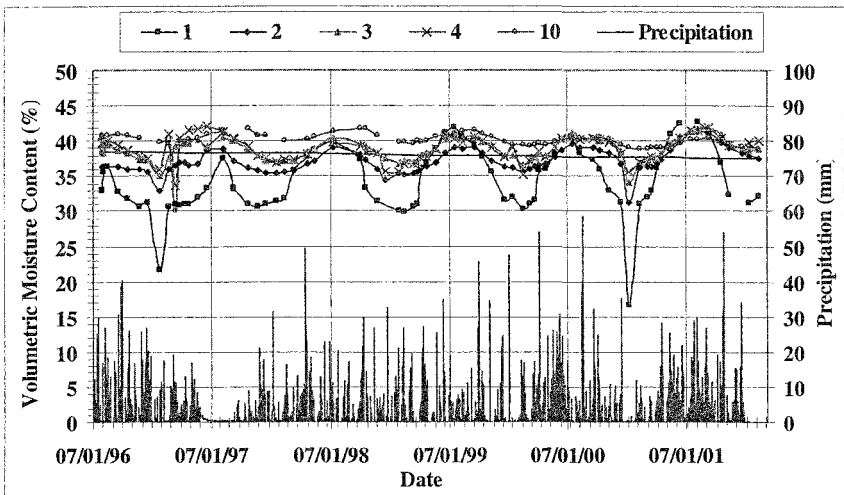
Figure 2. VWC and precipitation (from Heydinger, 2003).

Analysis of SMP Volumetric Water Content Data

        Data from the LTPP database was analyzed in order to investigate variations in volumetric water content using DataPave Release 19 (FHWA 2005b).   The analysis consisted of plotting average volumetric water contents, computed using the top three sensors in the subgrade soil, verses the day of the year. The figures were used to determine the water content variations and if the variations occurred on a seasonal basis similarly to Figure 1. The water content variations were tabulated. The months in which the maximum and minimum water contents occurred were also noted for sections where both the data was sufficient (at least 2 years) and where volumetric water content varied seasonally. Data from sections where freezing occurred was not included for computing the moisture variations so the moisture variations represent unfrozen soil. For some sections, the data was not sufficient to determine the moisture variations. The data was not continuous at many of the sections. Therefore, it was difficult to determine if there are seasonal variations of volumetric water content. Table 1 includes data from wet-freezing (WF) and wet-no freezing (WNF) climate zones and Tables 2 includes data from dry-freezing (DF) and dry-no freezing (DNF) zones.
        The data shown in the tables cannot be used to attribute any specific phenomenon to the variations of volumetric water content. For most of the sections the water contents did not appear to vary seasonally or there was insufficient data to make the determination. The ranges of moisture variations are similar when comparing wet and dry climates, freezing and no freezing climates, course and fine-grained subgrade soils and pavement types. There are no noticeable trends when comparing shallow depths to the ground water table to sections where the depth to the ground water table was greater than 5 meters.   The volumetric water content variations typically are 3% or more and did not exceed 9%. The moisture variations will result in variations in resilient modulus in the subgrade soils.

Resilient Modulus Variations

        The volumetric water content variations shown in the two tables were used to compute variations in resilient modulus. Values of soil porosity were computed using γ_d and w measured during installation of the TDR sensors and G_s obtained from DataPave Release 19 (FHWA, 2005b) in order to compute degree of saturation. S_{opt} was computed using γ_{dmax} and w_{opt} that were also reported in the database. Resilient modulus ratios ($M_R/M_{R\ opt}$) were then computed using Equation 1 and regression parameters for course and fine-grained soils determined by Witczak, et al. (2000a) for both the maximum and minimum volumetric water contents. The results of the analysis are shown in Table 3. Several sections included in the previous two tables were not included in Table 3 because of insufficient data or because of ill-fitting data, i.e. computed values of degree of saturation were significantly higher than 100%. A factor was computed by dividing the maximum ratio by the minimum ratio. The factors varied from 1 (no variation in resilient modulus) to 2 (resilient modulus varies

Table 1. Volumetric Water Content Data – Wet Climate

						Pave.	Base	Water	Averge of top 3 sensors					
State		SHRP	SHRP		Pave.	Thick	Thick	Table	Max.		Min.		Var.	No.
Code	State	ID	Climate	Soil	Type	(inch)	(inch)	Depth	VWC	Mo.	VWC	Mo.	VWC	Years
9	CT	1803	WF	C	AC	9.2	12.0	0.9->5	24	Dec	22	July	2	2
10	DE	0102	WF	C	AC	8.1	47.1	1.2-3.2	22	-	15	-	4 - 6	2
23	ME	1026	WF	C	AC	7.2	17.6	1.7-3.9	15	-	12	-	3	1
25	MA	1002	WF	C	AC	7.8	12.4	>5m	18	March	9	-	9	3
27	MN	1018	WF	C	AC	4.4	5.2	1.5-3.4	15	May	9	-	6	2
27	MN	1028	WF	C	AC	9.6	-	>5m	12	April	9	-	3	2
27	MN	6251	WF	C	AC	7.4	10.2	0.4->5	9	-	6	-	3	2
33	NH	1001	WF	C	AC	8.4	33.7	3.8-4.1	12	-	9	-	3	1
40	OK	4165	WF	C	AC	2.7	5.5	1.3->5	27	July	24	Dec.	3	1
50	VT	1002	WF	C	AC	8.5	25.8	0.8-1.4	16	-	8	-	8	2
87	ON	1622	WF	C	AC	5.9	33	>5m	12	-	8	-	4	2
31	NE	3018	WF	C	PC	11.9	5.6	1.4-3.9	12	-	9	-	3	2
36	NY	4018	WF	C	PC	9.4	-	1.9->5	23	-	18	-	5	2
89	QC	3015	WF	C	PC	8.2	13.3	1.7-3.4	12	-	8	-	4	2
20	KS	4054	WF	F	AC	9.5	3.4	3.7-4.1	39	Dec	36	Aug	3	2
24	MD	1634	WF	F	AC	3.6	17.8	1.4-3.6	24	-	18	-	6	2
31	NE	0114	WF	F	AC	6.7	36.0	4.0->5	45	-	42	-	3	1
39	OH	0901	WF	F	AC	3.8	33.9	1.6-4.2	36	July	35	Dec.	1	2
18	IN	3002	WF	F	PC	9.5	5.5	1.6-3	30	-	26	-	4	1
27	MN	4040	WF	F	PC	8.1	6	1.5->5	27	-	18	-	9	2
39	OH	0204	WF	F	PC	11.1	21.8	2.2-2.8	40	July	36	Dec.	4	5
42	PA	1606	WF	F	PC	9.9	7.8	>5m	40	-	36	-	4	3
83	MB	3802	WF	F	PC	9.8	10.8	0.3->5	40	-	36	-	4	1
13	GA	1005	WNF	C	AC	7.6	8.8	1.2->5	24	-	-	-	0	2
13	GA	1031	WNF	C	AC	11.2	8.8	1.3->5	18	-	12	-	6	3
28	MS	1016	WNF	C	AC	7.6	19.3	4.7->5	24	Feb.	15	-	9	1
28	MS	1802	WNF	C	AC	3.2	6.5	1.5->5	18	-	12	-	6	1
37	NC	1028	WNF	C	AC	9.8	-	1.3-3.1	24	-	18	-	6	2
48	TX	1060	WNF	C	AC	7.5	18.4	>5m	45	-	42	-	3	2
48	TX	1122	WNF	C	AC	3.4	24	>5m	22	-	18	-	4	1.5
53	WA	3813	WNF	C	PC	8	40.2	4.1->5	33	Sept.	29	July	3 - 4	2
1	AL	0101	WNF	F	AC	7.5	7.9	>5m	42	July	37	Dec.	5	4
48	TX	1077	WNF	F	AC	4.9	10.4	3.1->5	24	-	18	-	6	2
51	VA	0113	WNF	F	AC	4	13.9	>5m	40	July	39	Dec.	1	3
51	VA	0114	WNF	F	AC	7.2	17.9	>5m	29	-	28	-	1	2
13	GA	3019	WNF	F	PC	7.4	7.2	0.5->5	-	-	-	-	2	2
37	NC	0201	WNF	F	PC	9	17.3	>5m	42	-	39	-	3	4
37	NC	0205	WNF	F	PC	8	14.5	-	38	March	35	Oct.	3	3
37	NC	0208	WNF	F	PC	11.2	13.9	-	24	Oct.	21	March	2-3	2
37	NC	0212	WNF	F	PC	10.9	16.1	-	38	-	34	-	4	2

Table 2. Volumetric Water Content Data – Dry Climate

State Code	State	SHRP ID	SHRP Climate	Soil	Type	Pave. Thick (inch)	Base Thick (inch)	Water Table Depth	Averge of top 3 sensors				Var. VWC	No. Years
									Max. VWC	Mo.	Min. VWC	Mo.		
4	AZ	0113	DF	C	AC	9.3	15	>5m	11	Feb.	8.5	July	2 - 3	2
4	AZ	0114	DF	C	AC	14.1	24	>5m	22	-	16	-	6	1
4	AZ	1024	DF	C	AC	10.9	6.3	>5m	24	July	18	Dec.	4 - 6	2
16	ID	1010	DF	C	AC	10.9	5.4	2.4->5	12	-	6	-	3-4	2
30	MT	0114	DF	C	AC	7.2	12.4	>5m	12	-	9	-	3	1
30	MT	8129	DF	C	AC	3.2	22.8	2.6->5	9	-	6	-	3	1
32	NV	0101	DF	C	AC	7.2	43.3	>5m	15	-	15	-	3	2
49	UT	1001	DF	C	AC	5.5	5.8	4.5->5	19	-	13	-	5	2
56	WY	1007	DF	C	AC	2.8	6.2	>5m	20	July	16	Dec.	4	2
83	MB	1801	DF	C	AC	4.4	18.8	1.6->5	18	July	15	-	3	2
90	SK	6405	DF	C	AC	2.8	10.2	2.4->5	12	-	10	-	2	2
4	AZ	0215	DF	C	PC	11.0	6.3	>5m	30	-	22	-	8	1
49	UT	3011	DF	C	PC	10.2	7.2	4.3->5	36	-	27	-	9	1.5
46	SD	0804	DF	F	AC	7.2	12	>5m	35	-	30	-	5	3
32	NV	0204	DF	F	PC	11.8	38.7	>5m	21	-	18	-	3	1
35	NM	1112	DNF	C	AC	6.2	6.4	>5m	6	-	3	-	3	2
6	CA	3042	DNF	F	PC	8.8	10.3	0.6->5	-	-	-	-	4	2

by a factor of 2). A trend that can be observed is that the factors were lower in dry climates than the factors in wet climates. Data from resilient moduli computed from nondestructive testing are not available so it is not possible to compare the calculated resilient moduli with measured values. It can also be seen from Table 3 that the volumetric water contents at the laboratory optimum are generally higher than the water contents that were measured during installation of the TDR sensors, and the volumetric water contents usually increased after installation.

Conclusions

Seasonal Monitoring Program (SMP) TDR volumetric water content data from the LTPP database DataPave (Release 19) were analyzed in order to investigate volumetric water content variations in subgrade soils in 63 pavement sections located in the four climate zones. Average volumetric water contents from the top three sensors in the subgrade soil, representing a depth of about 0.5 meter below the pavement surface, were used. It is difficult to make definite conclusions concerning the seasonal variations of volumetric water content. Seasonal variations are shown for two sections at one site in Ohio and Equation 1 is presented for the variation at one pavement section. For many of the pavement sections, there was not sufficient data to observe seasonal trends so the volumetric water content variations were tabulated. The moisture contents did not appear to vary seasonally for many of the sections. There were no consistent trends in the moisture variations when comparing

Table 3. Resilient Modulus Variations

State	ID	Clim.	Soil Type	Pave Type	Max. VWC	Min. VWC	Max. S	Min. S	Instal. VWC	Opt. VWC	S_{opt}	Max. Ratio	Min. Ratio	Factor
AZ	0113	DF	C	AC	11	8.5	40.4	31.2	7.7	20.2	84.8	1.93	1.87	1.03
AZ	0114	DF	C	AC	22	16	68.5	49.8	10.8	17.0	53.0	1.08	0.71	1.52
AZ	1024	DF	C	AC	24	18	85.8	64.3	28.7	23.1	82.4	1.47	0.92	1.59
ID	1010	DF	C	AC	12	6	41.1	20.5	8.7	20.0	68.4	1.90	1.66	1.14
MT	8129	DF	C	AC	9	6	43.2	28.8	6.7	19.9	95.7	1.97	1.92	1.02
NV	0101	DF	C	AC	15	15	58.3	58.3	9.6	19.7	76.6	1.47	1.47	1.00
UT	1001	DF	C	AC	19	13	62.2	42.6	9.9	22.1	72.4	1.70	1.26	1.35
WY	1007	DF	C	AC	20	16	72.0	57.6	13.0	23.4	84.1	1.65	1.31	1.25
MB	1801	DF	C	AC	18	15	89.7	74.7	16.2	19.0	94.8	1.51	1.13	1.34
SK	6405	DF	C	AC	12	10	51.9	43.2	7.1	23.0	99.6	1.94	1.90	1.02
SD	0804	DF	F	AC	35	30	79.3	68.0	25.9	25.6	58.1	0.71	0.49	1.44
NV	0204	DF	F	PC	21	18	73.9	63.3	10.6	27.4	96.4	2.08	1.80	1.16
NM	1112	DNF	C	AC	6	3	15.7	7.9	3.5	21.2	55.6	1.90	1.83	1.03
DE	0102	WF	C	AC	22	15	100.2	68.3	12.6	19.5	89.0	1.53	0.77	1.98
ME	1026	WF	C	AC	15	12	68.1	54.5	9.4	17.0	77.4	1.58	1.24	1.27
MA	1002	WF	C	AC	18	9	54.1	27.1	4.2	12.6	37.7	1.28	0.70	1.83
MN	1018	WF	C	AC	15	9	48.3	29.0	15.9	20.4	65.8	1.80	1.45	1.24
MN	1028	WF	C	AC	12	9	50.1	37.6	8.6	13.2	55.2	1.46	1.13	1.29
MN	6251	WF	C	AC	9	6	30.2	20.1	9.7	19.7	66.0	1.88	1.79	1.05
NH	1001	WF	C	AC	12	9	62.1	46.6	12.0	22.1	114.4	1.97	1.92	1.02
OK	4165	WF	C	AC	27	24	55.2	49.0	16.7	21.3	43.6	0.88	0.77	1.15
VT	1002	WF	C	AC	16	8	47.6	23.8	10.0	15.4	45.7	1.55	0.96	1.63
ON	1622	WF	C	AC	12	8	41.5	27.7	4.9	22.5	78.0	1.91	1.80	1.06
NE	3018	WF	C	PC	12	9	38.2	28.7	7.1	16.3	51.8	1.58	1.35	1.17
QC	3015	WF	C	PC	12	8	46.1	30.7	11.3	14.2	54.5	1.59	1.22	1.31
KS	4054	WF	F	AC	39	36	110.4	101.9	31.0	33.0	93.4	0.74	0.56	1.33
MD	1634	WF	F	AC	24	18	74.4	55.8	16.4	21.0	65.0	1.33	0.72	1.85
NE	0114	WF	F	AC	45	42	105.6	98.6	23.0	32.7	76.7	0.48	0.40	1.20
OH	0901	WF	F	AC	36	35	88.6	86.1	20.0	20.0	49.1	0.35	0.33	1.04
IN	3002	WF	F	PC	30	26	89.1	77.2	34.7	23.3	69.3	0.76	0.51	1.48
MN	4040	WF	F	PC	27	18	79.1	52.7	34.2	29.2	85.6	2.08	1.23	1.69
OH	0204	WF	F	PC	40	36	98	89	20.0	20.0	49.1	0.33	0.30	1.12
MB	3802	WF	F	PC	40	36	78.1	70.3	40.4	28.8	56.3	0.62	0.48	1.27
GA	1031	WNF	C	AC	18	12	54.8	36.6	30.4	24.5	74.5	1.81	1.50	1.21
MS	1016	WNF	C	AC	24	15	73.5	46.0	24.3	22.5	68.9	1.57	0.89	1.76
MS	1802	WNF	C	AC	18	12	69.5	46.3	25.1	19.7	76.0	1.70	1.17	1.46
NC	1028	WNF	C	AC	24	18	56.6	42.5	10.3	22.7	53.6	1.29	0.93	1.39
TX	1122	WNF	C	AC	22	18	71.0	58.1	17.0	18.7	60.5	1.06	0.78	1.35
AL	0101	WNF	F	AC	42	37	114.6	100.9	28.4	33.3	90.9	0.71	0.46	1.53
TX	1077	WNF	F	AC	24	18	68.3	51.3	10.4	19.6	55.8	1.16	0.65	1.79
NC	0208	WNF	F	PC	24	21	89.4	86.4	18.9	42.3	87.0	1.02	0.92	1.11
NC	0212	WNF	F	PC	38	34	89.4	86.4	23.1	31.8	65.8	0.50	0.46	1.09

Note: The Max./Min. Ratio columns are under the heading $Log(M_R/M_{Ropt})$.

the different climate zones, soil types (coarse or fine-grained), pavement types or depth to the water table. The variations between the maximum and minimum volumetric water content are typically 3% or higher and can be as high as 9% so it is concluded that moisture variations do occur in subgrade soils.

Variations in resilient moduli were computed as a function of degree of saturation by using soils data in DataPave. Equation 2 was proposed for computing resilient moduli for unbound base and subgrade soils in the Mechanistic-Empirical Pavement Design Guide (M-EPDG). It is concluded that resilient moduli of subgrade soils vary because of moisture variations by as much as a factor of 2 but the variations are typically lower. Resilient modulus increases significantly in frozen soil at times when the unfrozen volumetric water contents decrease sharply. The resilient modulus variations are generally higher in wet climates than in dry climates.

The use of moisture content variations and the resulting variations in resilient modulus should improve predictions of pavement performance when using mechanistic procedures since pavement performance is dependent on cumulative damage that is incurred during traffic loading which can be modeled using mechanistic procedures. Therefore, it is necessary to be able to predict variations in volumetric water content. At this time, the SMP data is not sufficient to predict the variations accurately. There is a need for more TDR volumetric water content data and analysis of the data. The finite element program (EICM) used by the M-EPDG typically predicts very small water content variations after an equilibrium condition is reached. Additional data could be used to verify conclusively the EICM predictions, or the procedures used by the EICM could be modified.

References

Davis, B. O. A. (2004). "A model for the prediction of subgrade soil resilient modulus for flexible pavement design: influence of moisture content and climate change, *M.S. Thesis*, Department of Civil Engineering, University of Toledo.

Drum, E. C., Reeves, J. S., Madgett M. R. and Trolinger W. D. (1997). "Subgrade resilient modulus correction for saturation effects." *Journ. of Geotechnical and Geoenvironmental Engineering*, ASCE, 123(7), 663-670.

FHWA (2005a). Online information on the Long-Term Pavement Performance program http://www.fhwa.dot.gov/pavement/ltpp/ and Seasonal Monitoring Program http://www.fhwa.dot.gov/pavement/ltpp/smpdlr.cfm.

FHWA. (2005b). "Long-Term Pavement Performance, Standard Data Release 19.0." DataPave Online, http://www.datapave.com/.

Fredlund, D. G. and Xing A. (1994). "Equation for the soil-water characteristic curve." Canadian Geot. Jour., 31, 521-532.

Fredlund, D. G., Xing, A. and Huang, S. (1994). "Predicting the permeability function for unsaturated soils using the soil-water characteristic curve." Canadian Geot. Journ. 31, 533-546.

Heydinger, A. G. (2003a). "Evaluation of seasonal effects on subgrade soils." *Transportation Research Record 1821*, TRB, National Research Council, Washington, D.C., 47-55.

Heydinger, A. G. (2003b) "Monitoring seasonal instrumentation and modeling climatic effects on pavements at the Ohio/SHRP test road." Final Report, ODOT Project No. 14704(0), Department of Civil Engineering, University of Toledo.

Klemunes, J., Jr. (1998). "Determining soil volumetric moisture content using time domain reflectometry." FHWA-RD-97-139, Office of Engineering, R&D, FHWA, U.S. DOT, Mclean, Virginia.

NCHRP, (2005) Home page for the Mechanistic-Empirical Pavement Design Guide (M-EPDG), http://trb.org/mepdg/home.htm.

Selig, E. T. and Mansukhani, S. (1975). "Relationship of soil moisture to the dielectric property." Journ. of the Geot. Eng. Div., ASCE, 101(8), 755-770.

Witczak, M. W., Andrei D. and Houston, W. N. (2000a). "Resilient modulus as function of soil moisture – summary of predictive models." Appendix DD-1, NCHRP 1037 A.

Witczak, M. W., Houston, W. N. and Andrei D. (2000b). "Resilient modulus as function of soil moisture – A study of the expected changes in resilient modulus of the unbound layers with changes in moisture for 10 LTPP sites." Chapters 3 and 4 and Appendix DD-3, NCHRP 1037 A.

Zapata, C E., Houston, W. N., Houston, S. L and Walsh, K. D. (2002). "Soil-water characteristic curve variability." *Proc. on Advances in Unsaturated Geotechnics*, ASCE Geotechnical Special Publication No. 99, 84-124.

Monitoring Long-Term Subgrade Moisture Changes with Electrical Resistivity Tomography

Christopher R. Clarke

Geotechnical Branch, Materials Division, Oklahoma Department of Transportation, 200 N.E. 21st Street, Oklahoma City, OK 73105; PH (405) 522-4995; FAX (405) 521-0522; email: cclarke@odot.org

Abstract

Several models exist to predict the interaction between unsaturated soils and slab foundations or pavements. Validation of these models requires real-world data about the distribution and movement of water within the soil. Electrical resistivity tomography (ERT) offers an economical, non-destructive, and relatively non-invasive method of creating 2- and 3-dimensional views of moisture distribution.

This is a case study of an asphalt bicycling/walking path constructed on an expansive clay subgrade. A test section was underlain by a horizontal moisture barrier, in an attempt to minimize seasonal shrink/swell behavior. A string of electrodes was installed across the pavement section, beneath the barrier. By measuring the subgrade resistivity at monthly intervals, it was believed possible to estimate the depth of the active zone, the edge moisture variation distance, the long-term equilibrium moisture beneath the covered area, and seasonal fluctuations of moisture at the edge.

Introduction

The problem of moisture changes beneath pavements and foundation slabs is well-known and much studied. Even under essentially impermeable surfaces, subgrade soils will gain or lose moisture in response to hydraulic and thermal gradients, with resultant changes in stiffness, shear strength, and volume.

Three parameters of interest in understanding the soil-structure interaction are: a) the depth of the active zone, b) the edge moisture variation distance, and c) the long-term equilibrium moisture content beneath the pavement. In practice, these are often assumed, or estimated from semi-empirical equations. In the

simplest case (ignoring the effects of vegetation and utilities), they are controlled by soil properties, the local climate, and hydrology.

Active zone. Soil moisture varies over a large range at the surface, but this variation diminishes with depth, until at a certain depth the moisture is essentially constant. This is the depth of the active zone. It is controlled by soil properties, the amplitude and frequency of moisture variation at the surface, and fluctuation of the water table. Moisture moves vertically in the unsaturated soil profile in response to hydraulic and thermal gradients.

Edge moisture variation distance. When the soil surface is covered with a relatively impermeable barrier, such as pavement, moisture continues to move within the unsaturated soil profile, but also moves laterally due to hydraulic and thermal gradients between the covered soil and adjacent uncovered areas. As with the vertical profile, the most extreme variation occurs at the edge of the pavement, and diminishes with distance, until it reaches an essentially constant, equilibrium value at the edge moisture variation distance.

Long-term equilibrium moisture content beneath the pavement. As noted above, at a certain distance from the edge of the pavement, the moisture content is fairly constant. This may be greater or less than the moisture content at the time of construction, and is believed to be primarily dependant on soil properties and climate (Russam & Coleman 1961; Perera, *et al,* 2004). The time after construction required to reach equilibrium is not well established.

Monitoring moisture changes

Oklahoma has had chronic problems with heaving deformations and longitudinal cracking of asphalt pavements laid on expansive soils (Nevels 1995, 2001, and 2006). We have studied this problem repeatedly, and a weak area in the investigation is the lack of adequate moisture data.

Conventional methods to measure *in situ* soil moisture include electrical conductivity (gypsum block) and thermal conductivity sensors, nuclear methods, and time-domain and frequency-domain capacitance. Each of these requires careful excavation and placement of a sensor, or access casing, and each yield measurements of the moisture content of the soil immediately next to the sensor or casing. To obtain a complete picture of moisture distribution with depth and across the width of a pavement would involve extensive disturbance of the site by excavation or drilling, and monitoring the site under traffic.

Electrical resistivity and tomographic methods. The electrical resistivity of soil is a function of several variables, including mineral composition, density, composition of pore fluid, degree of saturation, and temperature. During monitoring of a site, most of these remain constant, and degree of saturation (or moisture content) and temperature become the only variables. The relationship between resistivity and

degree of saturation can be measured in the lab using undisturbed samples. The resistivity is roughly proportional to the inverse of the square of the degree of saturation.

Resistivity is a material property. In the field or in the lab, resistance is measured instead of resistivity. Resistance is a function of resistivity, the arrangement of electrodes, and the shape of the conducting body.

In the past twenty-five years, numerical analysis methods have allowed the back-calculation, or inversion, of resistivity data to estimate 2- or 3-dimensional cross-sections, or tomographs, of resistivity distribution. This method is becoming common in environmental monitoring, and in site investigation of regions with karst or mine works. Electrical resistivity tomography (ERT) has been used to monitor seepage into a pavement section (Buettner, *et al*, 1997) and a seepage-related slope stability problem (Jackson, *et al*, 2002).

Procedure

Data collection. In general compliance with ASTM G 57-95 and D 6431-99 (ASTM 2003), a series of electrodes are driven into the soil (or may be installed in a borehole) along the cross-section to be imaged. Typically the electrodes are equally spaced. The ratio between electrode spacing and electrode size is such that the electrodes can be considered point sources.

In the four-electrode method, a known current is passed between a pair of electrodes, the voltage across a pair of potential electrodes is measured, and the resistance calculated using Ohm's Law. Though many possible combinations of electrodes are possible, the Wenner array was used, with four equally-spaced electrodes, current electrodes on the outside and potential electrodes on the inside. The Wenner array is believed to provide good coverage in both horizontal and vertical directions, and does not have heavy demands on equipment sensitivity. The resistance is measured for all of the set of Wenner electrode combinations. The closer electrode spacings are more sensitive to surface resistivity; the longer electrode spacings are sensitive to deeper resistivities.

Inversion. The subsurface is modeled by a finite difference or a finite element distribution of resistivities. The objective is to adjust these resistivities so that the model produces resistances that match the field data. Typically, the number of elements far exceeds the number of measurements. The problem is solved iteratively, using smoothness-constrained non-linear optimization, so-called "Occam's method" (Constable 1987, deGroot-Hedlin 1990, Loke 1995). The objective function to be minimized is a weighted sum of the differences between the measured and modeled resistances, and the model roughness. The optimum solution is a compromise between best-fit and smoothest-fit.

Case History

In cooperation with the City of Norman, Oklahoma DOT constructed a new traffic signal and center turning lane at the intersection of Woods Avenue and Robinson Street. Incidental construction included removal and reconstruction of part of a paved bicycling/walking trail on the north side of Robinson Street. There was extensive longitudinal cracking in the existing pavement, with reason to expect the new pavement would end up the same way within a year.

The section consisted of 2 ½" (65 mm) of asphalt pavement, essentially at grade, underlain by 6" (150 mm) of cement kiln dust (CKD) stabilized base. The Geotechnical Branch proposed an experiment to evaluate the effectiveness of a horizontal moisture barrier in minimizing differential heave and longitudinal cracking of the pavement.

It was planned to monitor the site by periodic pavement condition surveys, cross-section surveys, and by nuclear density and moisture measurements in access tubes installed at the centerline, edge, and some offset from the trail. Test borings and piezocone tests were also planned. In addition, it was planned to estimate moisture distribution with ERT.

The plans for resistivity testing were at the level of a feasibility study. The Geotechnical Branch has had no experience with field resistivity testing. It was desirable to make the testing as simple and inexpensive as possible, and rugged enough to survive construction and function for at least a year.

We did have a soil resistivity meter, suitable for 4-pin testing in the lab or field, providing a 97 Hz input current at about 450 mA, with direct readout of resistance. Materials for the electrode array were obtained at home improvement and electronic stores. The array consisted of 20 electrodes at 1-ft. (0.31-m) spacing. The lead wires were insulated 20-gauge stranded copper wire. The electrodes were made from hot-dipped galvanized 20D nails, about 4" (100 mm) long. The lead wire was wrapped and twisted around the head of the nail, and covered with outdoor caulk. The nail was then painted with outdoor latex primer and paint, leaving ½" (10 mm) exposed at the tip. This was in compliance with ASTM G 57-95 (ASTM 2003) requirement that electrode length be less than 5% of the distance between electrodes, so that a point source can reasonably be assumed. The wires were threaded into a flexible conduit, with drilled entry holes for each wire.

Construction. After the stabilized base had cured, soil on both sides of the trail was excavated to the depth of the bottom of the stabilized layer. Three test sections and a control section were constructed. In each test section, a geomembrane was spread over the subgrade and stabilized base, and nailed to the underlying soil to prevent shifting during backfilling and paving. The test sections were approximately 30 ft. (10 m) long, and extended from the back of the curb on the south side of the trail to

the test width on the north side. The test sections had widths of 3, 5, and 7 ft. (1, 1.5, and 2 m) from the edge of the pavement on the north side; see Figure 1.

Placement of the membrane, the electrode array, and asphalt paving were done in one day. A crew from the Geotechnical Branch spread the membrane and nailed it into place on the exposed subgrade. Near the center of the 5' section, the membrane was folded back, the electrodes hammered into place, and the conduit was placed in a shallow trench scratched in the surface. Electrodes were installed beneath the membrane, and extended for some distance beyond the edge of the membrane. Elevations and horizontal offsets of the nails were then measured. The membrane was then laid back in place over the array, and nailed down. The heads of the nails used to nail down the membrane were covered with roofing sealant, to minimize short-circuiting of the array through the membrane. The bundle of lead wires was carefully wrapped and buried within the right-of-way, awaiting the end of construction to install an access junction box. Asphalt pavement was then laid directly on top of the membrane, and backfill was carefully placed over the exposed membrane. The finished cross-section is shown in Figure 2.

It was thought at the time that construction would soon be complete, and an initial reading could be taken. However, it was a month before an access junction box was installed, and another month before initial readings of resistivity were taken.

In the meantime, test borings were done, by SPT and thin-walled tube sampling, and several piezocone (CPTU) soundings. Survey nails were placed in the paved surface to provide references for cross-section surveys. A monitoring tube for nuclear moisture and density measurements was installed in May, 2005. For details of the site investigation and characterization, see the companion paper by Nevels (2006).

Results & Interpretation

A demonstration-copy of a commercially available 2-D resistivity tomography program, RES2DINV, developed by Loke (2004) was used to determine whether our home-made array produced any useful information. The results were surprisingly good. The array has been monitored on a roughly monthly basis to the present. Figure 3 presents a series of tomographs at 3-month intervals during the first year. Some aspects of the images are due to limitations of the demonstration copy, and some due to variations in material behavior. Nonetheless, the results were very promising.

Limits of analysis. As noted above, the measured and modeled resistances depend on the geometry of the conducting body. The model used by the demonstration-copy of RES2DINV is simply a half-space with the electrodes at the surface, which is significantly different from the actual cross-section in Figure 2. This departure from reality causes some distortions in the model tomographs in Figure 3. In general, the distortion is worst at the edge of the base and edge of the membrane, decreasing with distance from the edges. As such, it is not possible to overlay Figures 2 and 3.
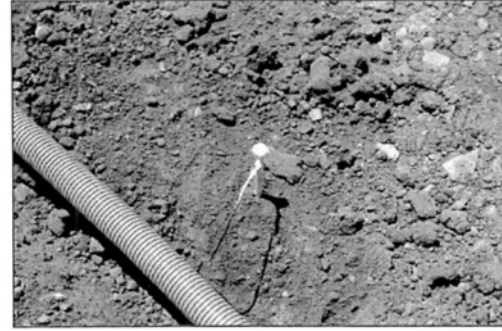
Figure 1. Test site construction: a) after paving, showing widths of membrane, b) electrode, c) conduit and electrode, d) graded and sodded.
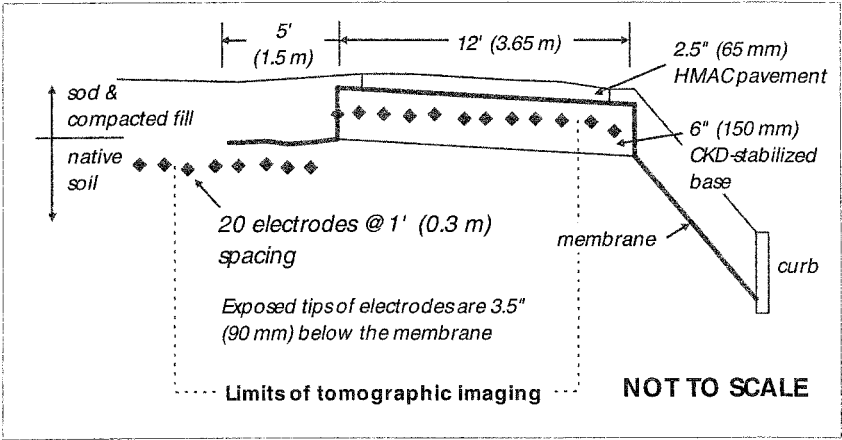
Figure 2. Cross-section of pavement, membrane, and electrode array.
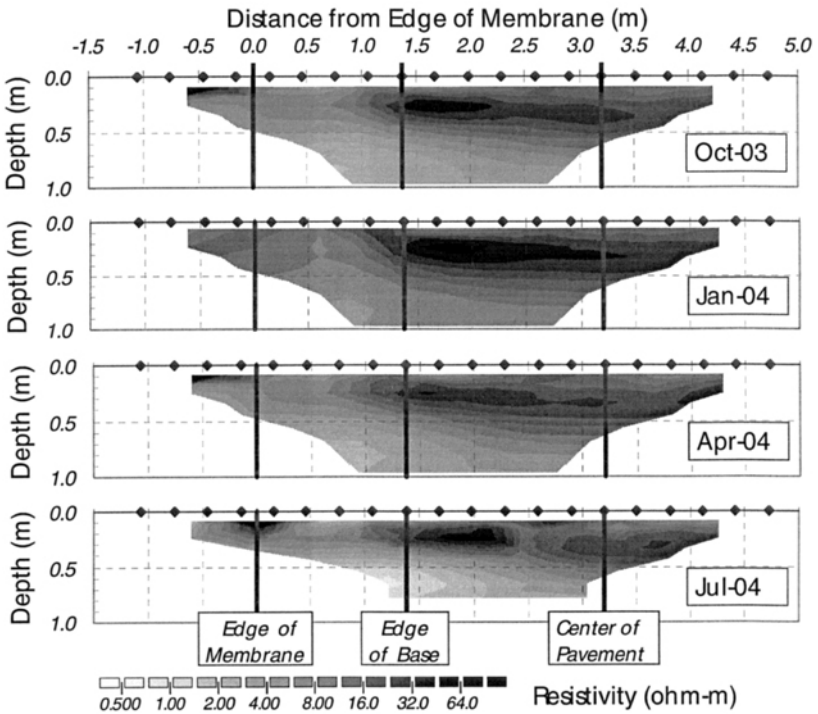
Figure 3. Tomographic images at 3-month intervals

The model used does not allow for *a priori* information, such as soil layers, in the inversion process. A smoothness-constraint is usually used in inversion, so that only the most distinct features appear, but requires some modification in this case. The actual parameter of interest in this case is soil suction, and it should be expected to vary smoothly (except at a wetting front). With distinct material layers, a smooth suction profile will not necessarily produce a smooth resistivity profile.

These limitations are in the demonstration-copy of RES2DINV only, and not in the licensed version (nor in licensed software by other suppliers).

Observations. The information in Figures 3 through 6 agrees qualitatively with expected moisture changes. Recall that moisture content decreases as resistivity increases.

The resistivity profiles at the edge of the membrane, as seen in Figure 4, display wetting and drying over the course of a year. The most extreme changes are at the surface, diminishing with depth. The profile for July, 2004 implies the moisture at about 0.5 m to be lagging the conditions at the surface, as expected. The depth of imaging was not sufficient to determine the depth of the active zone. Based on the companion paper (Nevels 2006), it believed that the depth of the active zone is about 1.6 m.

Figure 5 shows variation in resistivity as a function of edge distance. As expected the variation diminishes with distance, though it does not reach a constant, equilibrium value. The horizontal profiles resemble the vertical profiles in Figure 4, turned on their side. The horizontal profiles could yield the edge moisture variation distance if extended into the base; this was not done due to the distortions noted above.

Figure 6 shows compares changes in resistivity at the edge of the membrane to changes in resistivity at the center of pavement. The membrane is functioning as designed, to diminish moisture changes beneath the pavement. The moisture continues to change beneath the pavement, but over a much smaller range than at the edge, and the variation seems to be decreasing as the time since construction increases.

Shortcomings

There is, of course, room for improvement:

1. The array was not large enough to measure the full depth of the active zone. The length of the array can be increased, however electrodes installed in a borehole for cross-hole tomography would be more compact.
2. Some provision should be made for redundancy, to account for signal noise and loss of electrodes.
3. The effect of deterioration of the electrodes and wires should be measured and considered in analysis.

4. Installation of the electrode array should be modified so that an initial reading can be taken.

5. Moisture estimates should be verified by other means, such as nuclear moisture and density measurements.

6. A larger array practically demands equipment capable of higher currents, and automated switching and logging.

7. The electrodes should preferably be made of stainless steel, instead of galvanized steel.

8. Moisture-resistivity calibrations and soil-water characteristic curves base on undisturbed samples should be used to complete the model.
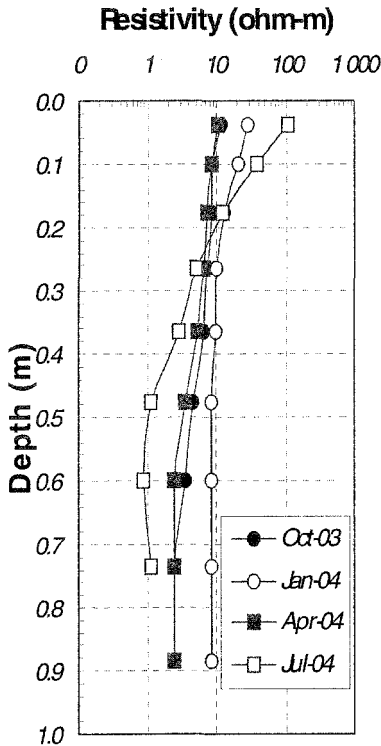
Figure 4. Vertical resistivity profile at the edge of the membrane.
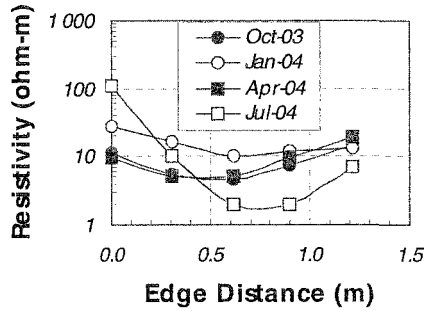
Figure 5. Horizontal resistivity profile from the edge of the membrane to the edge of the base.
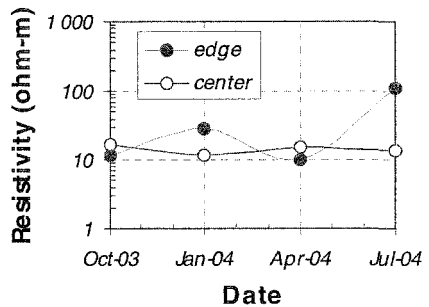
Figure 6. Comparison of variation of resisivity at the edge of the membrane and the center of the pavement.

Conclusions

This project demonstrated that ERT is a simple, inexpensive, and relatively non-invasive alternative to conventional methods of monitoring subgrade moisture, and can yield useful information about changes in subgrade moisture during the period after construction, and on a seasonal basis. Installation of the array required little disturbance of the construction site, and no heavy equipment.

The application of this method does require some caution in interpretation, as is common in the geotechnical field. The successes of this small project warrant application to larger studies.

Acknowledgements

References

American Society for Testing and Materials (ASTM). (2003). Annual Book of ASTM Standards, West Conshohocken, PA.

Buettner, M., Daily, W. and Ramirez, A. (1997). "Electronic (*sic*) resistance tomography imaging of spatial moisture distribution, moisture distribution, and movement in pavements ("Electrical resistance tomography for monitoring the infiltration of water into a pavement section.")." California Department of Transportation, FHWA/CA/OR-98-05.

Constable, S. C., Parker, R. L., and Constable, C. G. (1987). "Occam's inversion: a practical algorithm for generating smooth models from EM sounding data." *Geophysics*, 52, 289-300.

deGroot-Hedlin, C. and Constable, S. (1990). "Occam's inversion to generate smooth, two-dimensional models from magnetotelluric data." *Geophysics*, 55, 1613-1624.

Jackson, P. D., Northmore, K. J., Meldrum, P. I., Gunn, D. A., Hallam, J. R., Wambura, J., Wangusi, B., and Ogutu, G. (2002). "Non-invasive moisture monitoring within an earth embankment – a precursor to failure." NDT & E International, Elsevier Science Ltd., 35, 107-115.

Loke, M. H., and Barker, R. D. (1995). "Least-squares deconvolution of apparent resistivity pseudosections." *Geophysics*, 60, 1682-1690.

Loke, M. H. (2004). "RES2DINV ver. 3.42c." *Geotomo Software*, http://www.geoelectrical.com>_December 8, 2005.

Nevels Jr., J. B., (1995). "The use of soil suction in analysis of pavement cracking." Proc. Committee on Shallow Foundations and Soil Properties of the

Geotechnical Engineering Division of the ASCE and the 1995 ASCE Convention, W. Wray and S. Houston, eds., ASCE, GSP No. 48, 14-37.

Nevels, J. B. (2001). "Longitudinal Cracking of a Bicycle Trail Due to Drying Shrinkage." Expansive Clay Soils and Vegetative Influence on Shallow Foundations, C. Vipulanandan, M. B. Addison, and M. Hasen, eds., ASCE, GSP No. 115, 132-157.

Nevels, J. B. (2002). "Longitudinal Cracking of a Bicycle Trail Due to Drying Shrinkage." Proc. 3rd International Conference on Unsaturated Soils, UNSAT 2002, Recife, Brazil, Juca, J. F. T., de Campos, T. M. P., and Marinho, F. A. M., eds., Swets & Zeitlinger B. V., Lisse, The Netherlands, 687-69.

Nevels, J. B. (2006). "An Evaluation of Horizontal Membrane Barriers in Controlling Longitudinal Cracking." (submitted for publication) Proceedings of the Fourth International Conference on Unsaturated Soils, UNSAT 2006, Carefree, AZ, USA.

Perera, Y., Zapata, C. E., Houston, W. N., and Houston, S. L. (2004). "Long-term moisture conditions under highway pavements." *Proc. Geotechnical Engineering for Transportation Projects*, ASCE Special Publication No. 126, 1132-1143.

Russam, K. and Coleman, J. D. (1961). "The effect of climate factors on subgrade moisture conditions." *Geotechnique*, 11, 22-28.

An Evaluation of Horizontal Membrane Barriers in Controlling Longitudinal Cracking

James B. Nevels, Jr.[1]

[1]Geotechnical Engineer, Materials Division, Oklahoma Department of Transportation, 200 NE 21st Street, Oklahoma City, OK 73105-3204 ; PH (405) 522-4998; FAX (405) 522-0552; email: jnevels@odot.org

Abstract

This paper presents the results of a field experiment in applying horizontal membrane barriers to control longitudinal cracking in a bike trail pavement. A detailed site investigation of the test section was made to characterize the subsoil conditions which include classification, gravimetric and volumetric moisture content, engineering properties, matric suction versus depth, and soil water characteristic curve. The field experiment involves evaluating the effect that three widths of the horizontal membrane barrier beyond the edge of the pavement have on reducing longitudinal cracking. The premise controlling the behavior of this pavement is that changes in matric suction result in a horizontal shrinkage component that causes the longitudinal cracking. The evaluation of the effectiveness of the horizontal membranes involves the influence of the edge moisture variation distance and the active depth. In summary the horizontal membrane barrier was successful in eliminating the longitudinal cracking to date.

Introduction

This paper presents the findings of a field experiment in applying horizontal membrane barriers in order to control longitudinal cracking in a bike trail pavement. The experiment involves a 274.31 m length realignment of a five-year old bike trail due to a street-widening project in Norman, Oklahoma by the Oklahoma Department of Transportation (ODOT). The trail pavement cross-section was 3.05 m wide by 63.5 mm thick PG 64-22 asphalt concrete supported by a 152.4 mm thick cement kiln dust stabilized subgrade base, see Figure 1.

The original bike trail of similar design pavement had experienced extensive longitudinal cracking concentrated within 0.91 m of each pavement edge, see Figure 2b. Along the new realignment, a 27.43 m test section with an adjoining 27.43

Figure 1. Horizontal membrane test and pavement sections
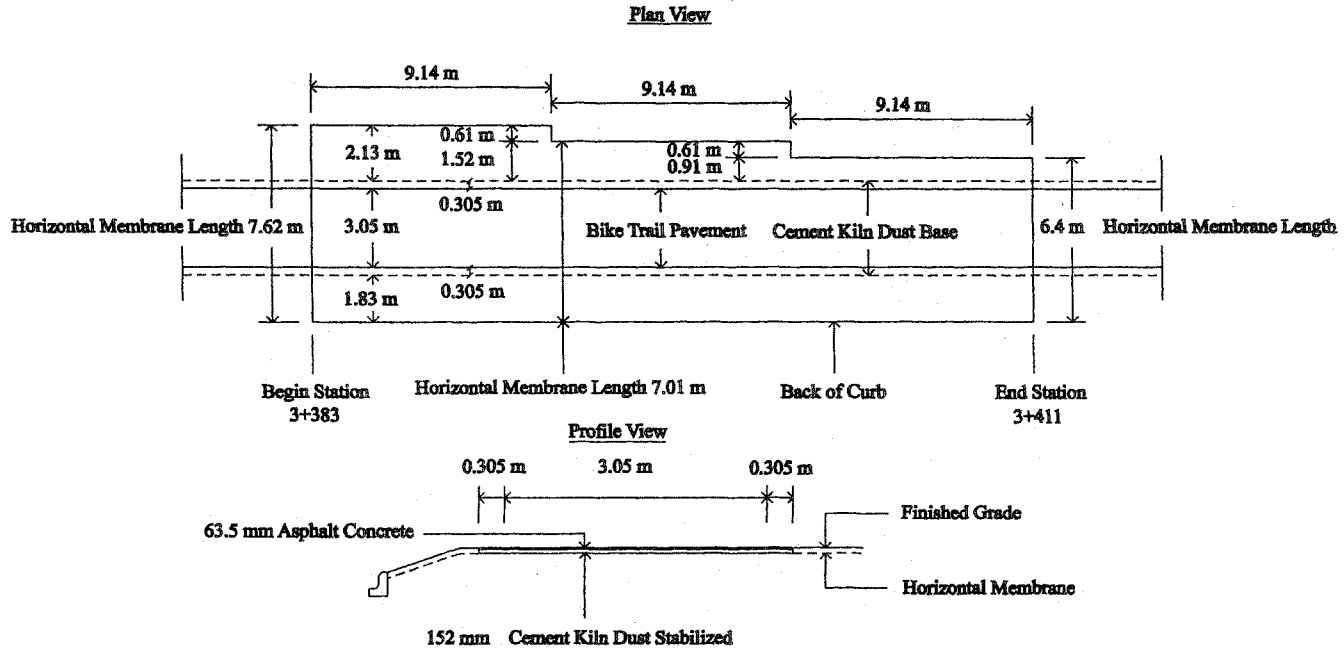
Figure 2a. Test section showing no cracks, looking west.

Figure 2b. Control section with longitudinal cracks, looking east.

control section was studied. The field experiment involves evaluating the effect that three widths of 0.5-mm PVC flashing in 9.14 m lengths have on reducing longitudinal racking. The horizontal barrier widths of 2.13, 1.52, and 0.91 m beyond the edge of the pavement base were evaluated while holding a constant width of horizontal barrier at the opposite pavement edge, see Figure 1. After 12 months of in-place service with a monitoring schedule, the longitudinal cracks reoccurred in the control section as well as the remainder of the 274.31 m bike trail realignment. However, no longitudinal cracks occurred in the test section, for a total of 22 months of observation.

The premise controlling the behavior of this pavement is that changes in matric suction result in a horizontal shrinkage component that causes the longitudinal cracking. During the course of the experiment monitoring, seven nail sets (five PK nails per set driven flush with the asphalt surface) were measured periodically by conventional survey level procedure with no discernible changes in the level of the asphalt surface, *i.e.* no center heave or edge heave. Horizontal shrinkage as reported by Wray and Ellepola (1991) can be analyzed by the Gardner-Lytton-McKeen method for predicting total shrinkage or swelling. This method is based on earlier moisture

flow findings by Gardner (1958) and the energy approach method of evaluating soil suction based on thermodynamic principles (Snethen et al. 1977). It has been shown that the Gardner-Lytton-McKeen method has to be modified to predict horizontal shrinkage (Wray and Ellepola 1991). Longitudinal cracking in pavements as related to the effect caused by soil suction has been reported in the literature (Nevels 1995 and Nevels 2001). This paper focuses on the horizontal barrier construction details, the geotechnical investigation, and the analysis made to explain the cause of the longitudinal cracking.

Horizontal Barrier Test Section

The construction of the 27.43 m length test section was completed in a planned construction sequence with the project contractor. The contractor first completed the 152.4 mm thick cement kiln dust stabilized subgrade base course. After this stabilized subgrade base was completed and the required curing period of a minimum of 72 hours after the final compaction, the contractor trimmed the grade as shown in Figure 1 from the back of the curb to a distance of 3.66 m from the opposite pavement edge. An ODOT crew installed the 0.5-mm thick PVC flashing, which is a black, non-reinforced, embossed on one side, PVC (poly-vinyl chloride), plasticized, impervious sheet. The flashing came in rolls 6.10 m long and was cut into 1.22 m strips. The 1.22 by 6.10 m strips were lapped 0.305 m between stations 111+00 and 111+90 and then the same strips were then lapped 0.305 m to finish forming the 7.62 by 9.14 m and 7.01 by 9.14 m horizontal membrane sections. As all the flashing strips were placed on July 24, 2003 on a hard and dry ground surface, approximately 600 16-penny nails were driven through 50.8 mm diameter by 1.59 mm thick aluminum washers to anchor the horizontal membrane down. The total time to complete these operations for the 27.43 m test section was 2 hours and 45 minutes. The contractor then placed the 63.5 mm thick asphalt concrete surface throughout the 274.31 m bike trail realignment. Following the asphalt pavement compaction, 254 mm of topsoil was placed and leveled up on both sides of the pavement, see Figure 1. Finally Bermuda slab sod was placed, rolled, and watered completing the pavement realignment including the test section and adjoining control section.

Geotechnical Investigation

The geotechnical investigation consisted of the following three phases: a geologic assessment, an in situ study, and a laboratory testing program. The geologic assessment reveals that the project lies on nearly level (0 - 1 percent slope) high terrace according to (Bingham and Moore 1983) running along the northeast side and paralleling the South Canadian River which is about 4.02 km to the southwest. The project lies near a drainage way, and the terrace may be thinner than normal. The rock underlying the terrace is mapped by (Bingham and Moore 2000) as the Hennessey shale formation.

The surface soils at the project are mapped as a Kirkland silt loam soil series (NRCS Cleveland County Soil Survey 1987). The Kirkland soil according to the NRCS soil description weathers from clay mantles (alluvial terrace) that are underlain by shale. The Kirkland soil series is a very deep (greater than 152.4 cm), moderately well drained, and a very slowly permeable soil. The series is formed in the alluvial terrace with the lower part formed in the fine-grained sandstone. This taxonomy for the Kirkland soil series is fine, smectitic, thermic, typic Naturstol. The soil series can be further characterized as overconsolidated clay due to dessication that has a medium to stiff consistency, blocky structure with slickensides, predominately a moist state, mottled color, and a high shrink-swell potential, as shown in Figure 3.

The in situ investigation involved 10 electric cone soundings within the 27.43 m test section tested according to ASTM D 5778 (ASTM 2003); see a composite tip resistance versus depth plot in Figure 4. The electric cone tip resistance versus depth profiles indicates relatively consistent soil profile underlying the test section. A continuous Standard Penetration Test (SPT) according to ASTM D 1586 (ASTM 2003) along with two continuously sampled thin-walled tube borings according to ASTM D 1587 (ASTM 2003) were made, to retrieve all necessary samples for laboratory testing; see Figure 3.

The laboratory testing program was specifically oriented to testing for moisture content, classification and index properties, and total wet density according to ASTM D 2216, D 422, D 4318, and D 2937 (ASTM 2003); see Figure 3. In addition, the testing program was directed toward estimating the matric soil suction versus depth through the active zone to a depth of 2.43 m in the stiff clay. In order to accomplish this estimate, the first step was to break the 2.43 m thickness into six layers. For each layer a number of clod tests (Nelson and Miller 1992) were made for each layer for the purpose of developing a volumetric moisture content versus gravimetric moisture content curve; see Figure 5. Next a soil water characteristic curve (SWCC) was developed for each of the six layers by measuring the matric suction in all of the clod shrinkage samples using the filter paper method according to ASTM D 5298 (ASTM 2003). Plotting all volumetric moisture content versus matric suction data on the same plot the SWCC's all plot on top of one another. These SWCC were all wetting curves, and the Fredlund and Xing (1994) curve fitting technique was applied to this data; refer to Figure 6 and Table 1.

Analysis

The site geology gives an essential clue for the pavement behavior at this site in that it describes a medium to stiff Kirkland mapped surface soil series underlain by lower plasticity clays of alluvial terrace origin. Further, the Kirkland series soil taxonomy indicates smectitic clay mineralogy. The stiff consistency of this Kirkland soil is also seen in the SPT N-value versus depth profile in Figure 3 and in the Qc versus depth profile in Figure 4. Based on the fact that the problem clay soil affecting the pavement is the Kirkland soil series, which has a maximum soil profile down to
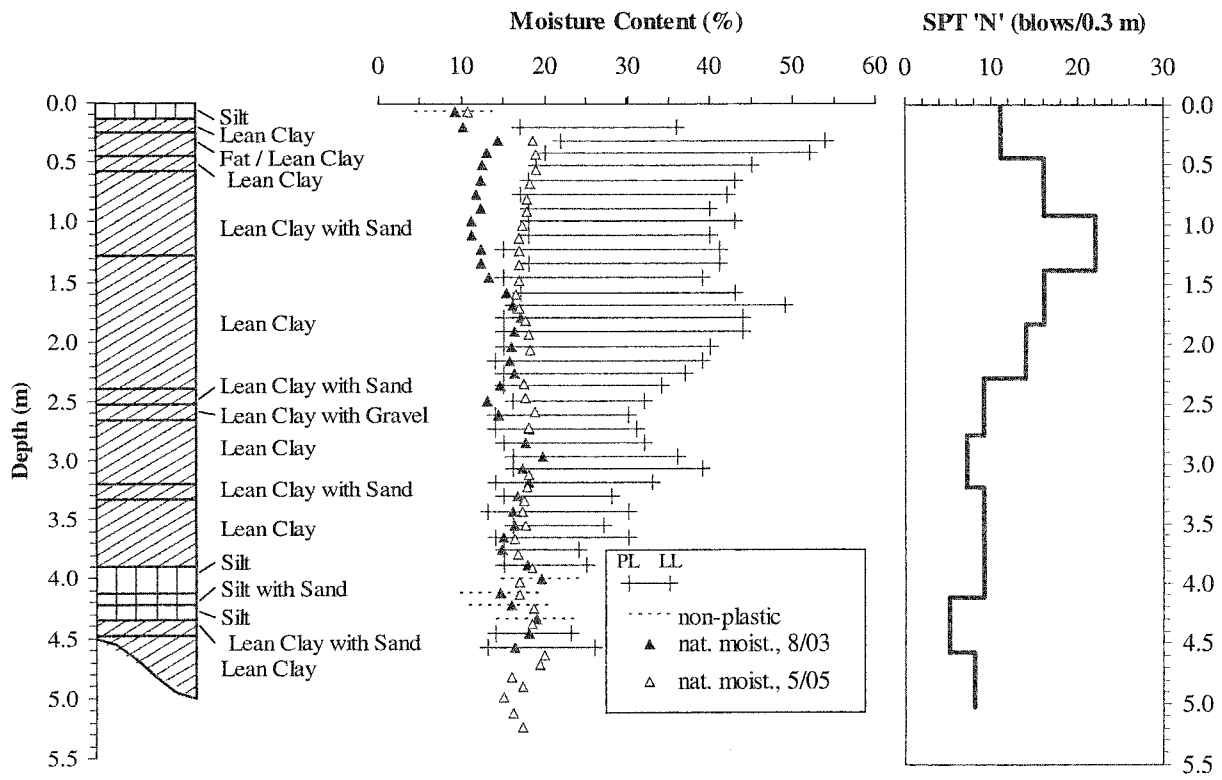
Figure 3. Site stratigraphy and *in situ* soil conditions.

Tip Resistance, q_c (MPa)
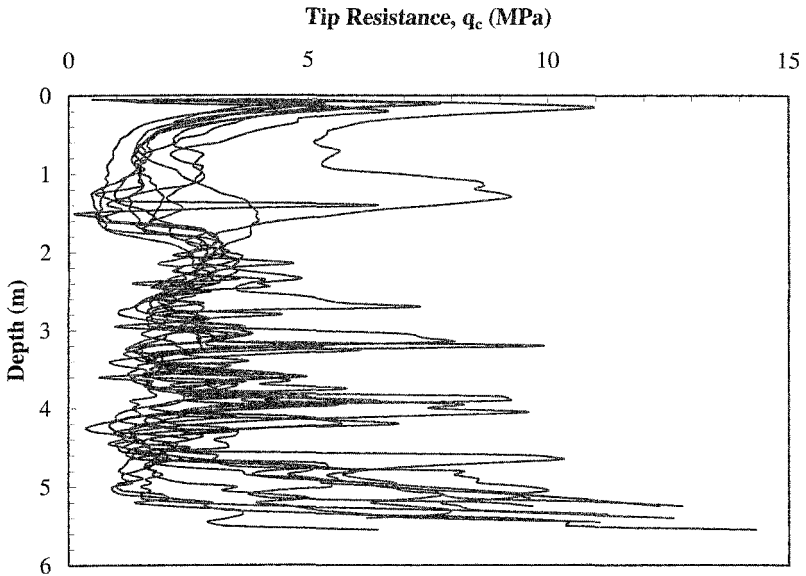
Figure 4. Composite tip resistance q_c versus depth.

$$\theta = 2.139w - 0.02146w^2$$
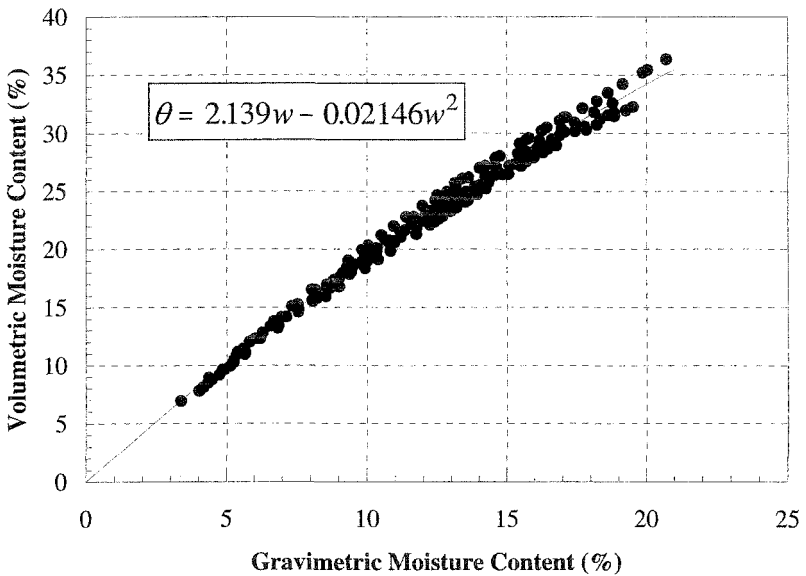
Figure 5. Volumetric vs. gravimetric moisture content relationship.
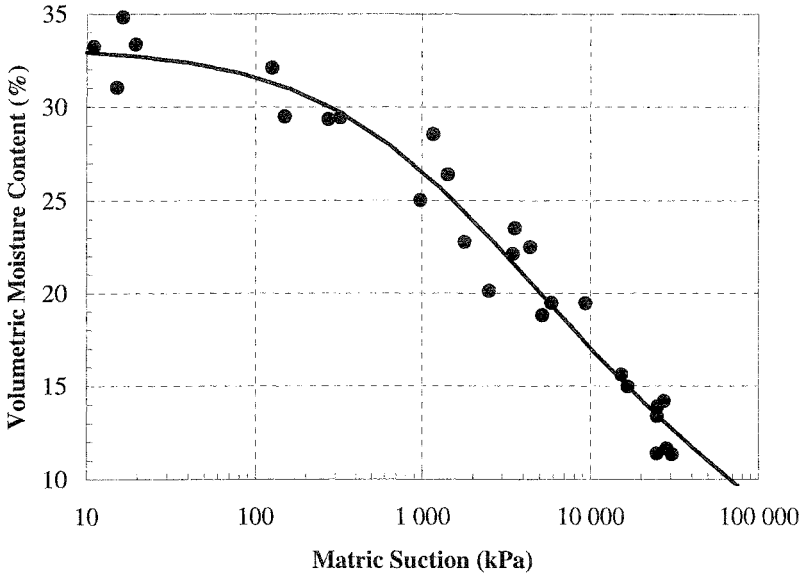
Figure 6. Soil-water characteristic curve.

Table 1. Fredlund and Xing model for the Soil-Water Characteristic Curve.

$\theta = C(\psi)\theta_s \left\{ \dfrac{1}{\ln\left[e + \left(\dfrac{\psi}{a} \right)^n \right]} \right\}^m$	Model parameters fitted to filter-paper suction data:
	ψ_r 10^6 kPa (assumed)
	θ_s 33.3 %
where the correction factor is:	
	a 1650 kPa
$C(\psi) = \left[1 - \dfrac{\ln\left(1 + \dfrac{\psi}{\psi_r} \right)}{\ln\left(1 + \dfrac{10^6}{\psi_r} \right)} \right]$	n 0.7
	m 1.08

2.08 m, and that the moisture profile convergence in Figure 3 is at 1.6 m, the active depth z is judged to 1.6 m.

Over the period of study at this site, the Thornthwaite Moisture Index (TMI) was utilized to show the impact of climate on the pavement performance (Thornthwaite 1948); see Figure 7. The climate based on the TMI in Figure 7 starts out very dry, becomes slightly wetter until September 2003, then steadily gets dryer until September 2004. Following this date a slow drying trend has occurred to August 2005. In the month of July 2004 the first longitudinal crack in the 27.43 m control section reoccurred; refer to Figure 2b; however, no cracks have occurred in the test section. Since July 2004 many additional cracks have reoccurred in the control section. The premise previously stated is that changes in matric suction result in a shrinkage component that causes longitudinal cracking. In order to access matric suction changes the gravimetric in situ moisture content profile August 2003 was used throughout the active zone down to a depth of 2.43 m. As stated by Briaud *et al.* (2003), moisture content is much more convenient and easier to measure than matric suction versus depth. The gravimetric moisture contents versus depth are converted to *volumetric moisture contents versus depth through the relationship presented in* Figure 5. The volumetric moisture contents from Figure 5 are then used along with the SWCC in Figure 6 to estimate the initial soil suction profile identified as the August 2003 suction, and a final soil suction profile identified as the May 2005 suction; see Figure 8. As indicated by Figure 8 the subgrade soil is shrinking.

After monitoring the pavement performance for 22 months, no longitudinal cracks have occurred in the test section while several longitudinal cracks have reoccurred in the control section. The widths of horizontal membranes studied beyond the edge of the pavement base course from Figure 1 were respectively 2.13, 1.52, and 0.91 m. Adding the base course overlap of 0.305 m makes the effective widths respectively 2.435, 1.825, and 1.215 m. The active depth for this site was established at 1.6 m. According to Nelson and Miller (1992), the width of the horizontal membrane barrier should be at least as wide as the edge moisture variation distance, e_m. A report by McKeen and Johnston (1990) shows that the barrier width could be much greater, approaching the distance equal to the active depth. In this experiment with horizontal membranes, an effort was made to evaluate the effect that e_m and z have on the development of longitudinal cracking.

The edge moisture variation was measured by the following two methods: McKeen and Johnston (1990) and El-Garhy and Wray (2004). The solution to the El-Garhy and Wray (2004) method requires the calculation of the soil diffusion coefficient, α. In this method, α is estimated by three empirical equations: McKeen and Johnston (1990), Bratton (1991), and Lytton (1994). In addition (Mitchell 1980), has established an upper and lower limit for the diffusion coefficient for expansive soils. All empirical equations and methods are discussed in (El-Garhy and Wray 2004). The *results of the e_m and z calculations from these equations and methods are presented in* Table 2.
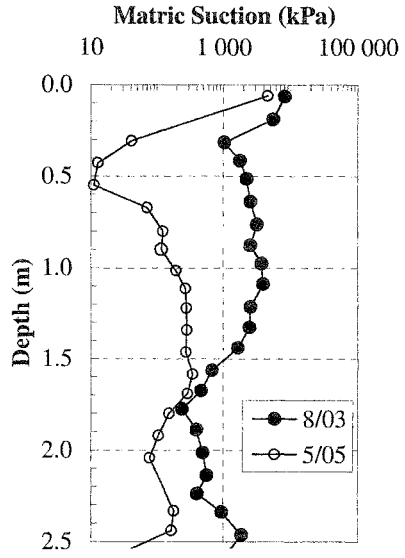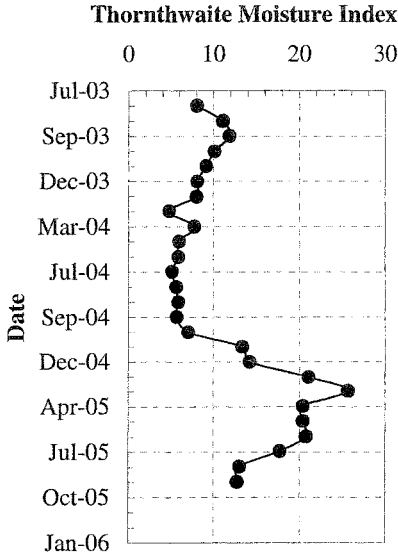
Figure 7. Thornthwaite moisture index (TMI) versus depth.

Figure 8. Matric suction versus depth.

Table 2. Edge moisture variation distance summary.

Method	Edge Moisture Variation Distance (m)				
McKeen and Johnson[1]	$e_m = 1.384$ F.S. $= 1.14$				
	McKeen			Mitchell	
El-Garhy and Wray[2]	and Johnson	Bratton	Lytton	Upper Limit	Lower Limit
	$\alpha = 0.0133$	$\alpha = 0.0062$	$\alpha = 0.0040$	$\alpha = 0.001$	$\alpha = 0.00001$
	$C_1 = 1.631$	$C_1 = 1.546$	$C_1 = 1.500$	$C_1 = 1.362$	$C_1 = 0.988$
	$C_2 = 0.452$	$C_2 = 0.426$	$C_2 = 0.412$	$C_2 = 0.370$	$C_2 = 0.259$
	$e_m = 1.95$	$e_m = 1.83$	$e_m = 1.76$	$e_m = 1.57$	$e_m = 1.09$
	F.S. $= 1.60$	F.S. $= 1.51$	F.S. $= 1.45$	F.S. $= 1.29$	F.S. $= 0.90$

[1] $e_m = z - D$, where z $= 1.60$ m and D $= 0.216$ m.

[2] $e_m = C_1 \left[\log\left(\frac{U_0}{0.1} \right) \right]^{C_2}$

Conclusion

Based on the findings of this field experiment, the following can be concluded:

1. The horizontal membrane barriers have been effective to date in controlling the longitudinal cracks in this pavement. In this experiment, the first and second membrane effective widths (2.435 and 1.825 m, respectively) were more than effective in stopping the longitudinal cracking, producing factors of safety of 2.00 and 1.50, respectively, using the third effective width as a reference.

2. A width of the horizontal moisture barrier at least as wide as the edge moisture variation distance e_m, with some factor of safety, would appear to be appropriate; refer to the third effective width (1.215 m) in Table 2.

3. The e_m is sensitive to the calculation of the diffusion coefficient α in the El-Garhy and Wray method.

Acknowledgements

References

American Society for Testing and Materials (ASTM). (2003). *Annual Book of ASTM Standards,* West Conshohocken, Penn.

Bingham, R. H., and Moore, R. L. (1983). "Reconnaissance of the water resources of the Oklahoma City quadrangle, central Oklahoma." Oklahoma Geological Survey and the United States Geological Survey, Hydrologic Atlas 4, Colorado Springs, Colo.

Briaud, J. L., Zhang, X., and Moon, S. (2003). "Shrink test-water content method for shrink and swell predictions." *Journal of Geotechnical and Geoenvironmental Engineering,* ASCE, Vol. 129, No. 7, 175-185.

El-Garhy, B. M. and Wray, W. K. (2004). "Method of calculating the edge moisture variation distance." *Journal of Geotechnical and Geoenvironmental Engineering,* ASCE, Vol. 130, No. 9, 945-955.

Fredlund, D. G., and Xing, A. (1994). "Equations for the soil-water characteristic curve." *Canadian Geotechnical Journal,* 31, 521-532.

Gardner, W. R. (1958). "Laboratory studies of evaporation from soil columns in the presence of water table." *Soil Science,* Vol.86, 2-24.

McKeen, R. G. and Johnston, L. D. (1990). "Climate-controlled soil design parameters for mat foundations." *Journal of Geotechnical Engineering,* ASCE, Vol. 116, No. 7, 1073-1094.

Natural Resources Conservation Service (NRCS). (1987). *Soil Survey of Cleveland County, Oklahoma,* Washington, D.C.

Nelson, J. D., and Miller, D. J. (1992). "Expansive soils: problems and practice in foundation and pavement engineering." John Wiley and Sons, New York.

Nevels Jr., J. B., (1995). "The use of soil suction in analysis of pavement cracking." *Proc., Committee on Shallow Foundations and Soil Properties of the Geotechnical Engineering Division of the ASCE and the 1995 ASCE Convention,* W. Wray and S. Houston, eds., ASCE, Geotechnical Special Publication No. 48, 14-37.

Nevels Jr., J. B., (2001). "Longitudinal cracking of a bicycle trail due to drying shrinkage." *Proc., Geo-Institute Shallow Foundation and Soil Properties Committee Sessions at the 2001 Civil Engineering Conference,* C. Vipulanandan, M. Addison, and M. Hasen, eds., Geo-Institute, ASCE, Geotechnical Special Publication No. 115, 132-157.

Perera, Y., Zapata, C. E., Houston, W. N., and Houston, S. L. (2001). "Long-term moisture conditions under highway pavements." *Volume 1 Geotechnical Engineering for Transportation Projects,* ASCE Special Publication No. 126, 1132-1143.

Russam, K. and Coleman, J. D. (1961). "The effect of climate factors on subgrade moisture conditions." *Geotechnique,* Vol. 11, 22-28.

Snethen, D. R., Johnson, L. D., and Patrick, D. M. (1977). "An investigation of natural microscale mechanisms that cause volume change in expansive clays." U.S. Army Engineer Experiment Station, Soil and Pavement Laboratory, Vicksburg, Miss.

Thornthwaite, C. W. (1948). "An approach toward a rational classification of climate." *Geographical Review,* Vol. 38, 55-94.

Wray, W. K., and Ellepola, C. B. (1991). "Prevention of longitudinal cracking in surfaces and fills." Texas Tech University, Research Study No. 11-8-89-121, Lubbock, Tex.

Interaction between trees and buildings on shrinkable soils – a detailed field study

Geoffrey E Blight[1]

[1]Professor Emeritus of Civil and Environmental Engineering, University of the Witwatersrand, Johannesburg. Private Bag, 3, Wits, 2050, South Africa; PH/FAX: -- 27 11 476 8759;
blight@civil.wits.ac.za

Abstract

A detailed investigation is reported of the effects of two deciduous trees on water contents in a shrinkable soil stratum supporting a small house on a shallow foundation. The trees involved are a willow (Salix tortuosa) presently 8.5 m high and growing 7.5 m from the west wall of the house, and an American ash (Fraxinus americana) presently 9 m high, growing 6.5 m from the south wall.

While it appeared that the growth of the Salix was not yet affecting the house, desiccation by roots from the Fraxinus were clearly causing the south wall to subside and crack. As a trial remedy, a root barrier was installed between the house and the Fraxinus.

Frequent (approximately two-monthly) measurements of soil moisture profiles between the trees and the house have been made over a period of a year and a half. Changes in soil moisture have been linked to the input and output variables for the soil water balance of rainfall, surface infiltration, evapotranspiration, soil water storage and deep infiltration, to both demonstrate the phenomena involved and aid in their understanding.

Introduction

In a recent review of the past 60 years of research on the desiccation of soil by vegetation (Blight, 2005) it was noted that most of the investigations of the interaction between trees and buildings, or other structures on shrinkable soils have sought urgent solutions to pressing problems, e.g. how to repair a cracked building or a distorted pavement quickly. Because of this, they have mostly been of a short-term, once-only nature. What seemed at the time to be the appropriate remedy has been

281

implemented, but follow-up observations to confirm success or note failure and its reasons have been few and far between. As a result, our knowledge has remained superficial and our understanding of the phenomena involved is limited.

Only one investigator (Biddle, 1983, 2001) has set out systematically to measure the effects of vegetation on soil water contents over a period of several years and thus gain a deeper understanding of the processes involved. Even Biddle's efforts, meritorious as they are, fall short because he has not linked the hydrological processes of rainfall infiltration and evaporation to the observed soil water contents, in more than a qualitative way.

A vertical root barrier would seem to be the obvious way of protecting a structure from the effects of shrinkage of clays caused by extraction of water by the invading roots of trees and other vegetation. However this method is so seldom described, as to be almost unknown in the literature of expansive/shrinkable clays. The following are selected experiences and comments: Newland (1965) described the use of a plastic-film moisture barrier to protect a house on expansive clay from changes in moisture content. Although not intended as a root barrier, this type of barrier, if not punctured and penetrated by growing roots, would have a similar effect. Root barriers are not mentioned in the landmark 1983 Geotechnique Symposium in Print on the Interaction Between Vegetation and Structures. The British Building Research Establishment (BRE) Digest 298 (1985) includes the following unenthusiastic, but valid statement, which is not likely to encourage readers to try root barriers in practice:

"Little is known about the effectiveness of root barriers in preventing root activity beneath house foundations. They are usually fairly expensive to install. As with underpinning, there is uncertainty about how extensive a root barrier should be, both laterally and in depth. If the trees are older than the building, a barrier that cuts off the root system beneath a house will cause swelling and heave as if the tree were entirely removed. Inserting root barriers close to trees can be dangerous. If sufficient of the root system is severed, the tree may lose lateral stability and fall. Even if rapid instability is not caused, the tree may slowly die and become unstable at a later date."

Nunn et al. (1992) describe the use of a root barrier to protect an extensive single storey office building from the effects of desiccation occurring in an adjacent garden. The barrier seemed to have been effective, although its behaviour was only observed for five months after installation.

More recently, Biddle (2001) has made a very similar statement to the 1985 BRE statement quoted above in which he discourages the use of root barriers. In the same symposium volume, the reader is told by Radevsky (2001) that "some local authorities (in Australia) believe in root barriers to prevent (insurance) losses and have been researching into appropriate specifications for the size, composition and optimum location of such barriers." In a third paper, Pengelly and Addison (2001) describe the remediation of a building that had been damaged by the roots of a line of

oak trees situated 2.4 m from one of the exterior walls. The remediation proceeded by injecting a potassium/ammonium solution through close-spaced holes (a 1.25 m square grid), drilled in the floor slab of the building, into the underlying soil. The rate of injection was 67 to 100 litres/m^3 of soil (6 to 8% water content). Following this irrigation, intended to reduce re-swelling of the soil, the roots of the trees were severed 900 mm from the walls of the building and a root and moisture barrier consisting of a plastic membrane backed by a concrete wall was installed, thus sealing in the injected water. Levels of the floor of the building taken over a period of $2^{1}/_{4}$ years showed that the underlying soil was successfully re-hydrated and the floor almost completely re-leveled, but do not show if the root barrier had any effect on the outcome.

Because of the lack of detail of the moisture movement processes involved, and of the action of a root barrier, and (indeed) the interaction between tree roots and buildings, it was decided that a series of detailed long term investigations of the phenomena involved was needed. This is the second report of this work, the first having been published recently (Blight, 2005).

The paper will report the early part of a detailed investigation of the effects of two deciduous trees on water contents in a shrinkable soil stratum supporting a small house on a shallow foundation. The trees involved are a willow (Salix tortuosa) presently 8.5 m high growing 7.5 m from the west wall of the house, and an American ash (Fraxinus americana) presently 9 m high, growing 6.5 m from the south wall. While it appeared that the growth of the Salix was not yet affecting the house, roots from the Fraxinus were clearly causing the south wall to subside and crack. As a trial remedy, a simple root barrier was installed between the house and the Fraxinus. The investigation considers both the south and the west walls, one protected by the root barrier, the other as yet unprotected.

The Experimental Site

The experimental site is at Clarens, which is situated in the Free State Province of South Africa at latitude $28°31^{1}$ south and longitude $28°26^{1}$ east at an elevation of 2000 m above sea level. Clarens is in the foothills of the Maluti mountain range, and is ringed by sandstone cliffs of the Clarens formation, which in turn are capped by strata of basaltic Stormberg lavas. The test site is situated on a gently sloping plain of colluvium consisting of silty clay deriving from the weathering of the sandstones and lavas. The colluvium is underlain by horizontally bedded sandstone. The soil is moderately expansive/shrinking, and contains closely spaced slickensides and extensive microfissuring between slickensides. The sand, silt and clay contents are close to constant with depth, and vary as follows: sand: 20-25%, silt: 47-53%, clay: 22-33%.

Index data for the Clarens soil are as follows: Liquid Limit: 46%, Plasticity Index: 18%, Linear Shrinkage: 9%. The soil properties are almost constant with depth and the transition from colluvium to unweathered sandstone occurs very suddenly over a

depth of 50-100 mm. At the location of the house the soil depth is only 500-600 mm. The water table lies within the sandstone at 5-7 m below the surface. The climate at the site is continental, with warm, moist summers (daily temperatures between + 10 and + 25°C) and cool dry winters (-10 to + 15°C). Being in the Southern Hemisphere, the summer solstice occurs on December 21 and the winter solstice on June 21.

In situ permeability measurements using the Guelph apparatus have shown that the soil is surprisingly permeable considering its particle size distribution. Infiltration through the surface, measured by means of an infiltrometer ring, averages 400 mm.h^{-1}. The in situ permeability at an average depth of 40 mm varies from 150 to 400 mm.h^{-1}, decreasing to 45 mm.h^{-1} at a depth of 150 mm and 35 mm.h^{-1} at a depth of 300 mm. This high permeability, due to the extensive micro-fissuring of the soil, combined with the near level grassed soil surface, means that run-off of incident rainfall is unlikely to amount to more than a very small proportion of rainfall, unless the rainfall intensity is extremely high.

Suction-water content relationships for soil

Figure 1 shows data on the suction-water content relationship for the soil. The figure shows suction-water content curves measured in the laboratory by means of calibrated gypsum blocks, for two undisturbed samples. It also shows a series of gypsum block measurements made in situ by means of gypsum blocks inserted into the side walls of a series of test pits. The method of gypsum block installation has been described in an earlier paper (Blight, 2002). The gypsum block readings were correlated with water content measurements from 50 mm diameter hand-augered holes made in undisturbed soil adjacent (200 mm) to the blocks. The results show considerable variability in the field suction-water content results, and that laboratory measurements also vary considerably from sample to sample. Even though the soil profile appears to the eye to be homogeneous from one point to another, its variability is sufficient to make it impossible to describe the suction-water relationship by a simple two-variable equation.

Inset in Figure 1 are suction measurements and contours on a developed elevation of the side-walls of one of the instrumented test pits. Each vertical line of numbers represents suctions measured by means of a line of three gypsum blocks running down the center of one face of the pit – twelve blocks in toto. Ideally, the contours would consist of a series of horizontal lines indicating a constant suction at each depth. In reality, the distribution of water content and suction is non-uniform, both in plan and with depth as a result of the fissuring of the soil that allows non-uniform wetting and drying to occur. The variability of water content within the soil profile will be amply illustrated by the water content contours presented in the remainder of the paper.
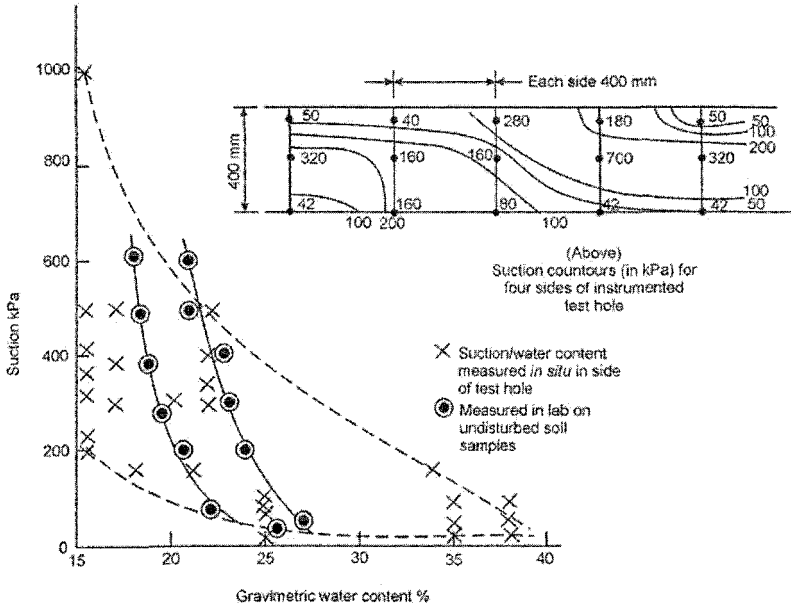
Figure 1: Suction-water content relationship for Clarens soil.

Effect of root barrier on soil water content

The diagram at the top of Figure 2 shows the location of the root barrier relative to the house and the tree (Fraxinus americana). The barrier was of very simple construction. A trench 500 mm deep was excavated, severing all the roots it crossed. The trench was lined with corrugated glass-fibre reinforced acetate sheeting, with the corrugations running vertically, and each 450 mm long sheet overlapped by two corrugations to form a barrier that extended from 500 mm to 50 mm below surface. The trench was backfilled with the soil excavated from it, the backfill being well compacted in layers placed at 100 mm depth intervals. The barrier was installed during July 2003 (winter) and the first soil water content measurements were taken at the end of October 2003. (spring). The months of July, August and September were dry and 16 mm of rain fell during October, before the first sampling on 31 October.

The lower part of Figure 2 shows water content profiles measured by sampling with a 50 mm diameter hand auger. Each sample hole was backfilled with the soil that came out of it. Care was taken to seal the hole by placing the soil back in 50 mm layers, ramming each layer and leaving the surface slightly proud. Each line of holes was marked and each line of samples was taken from an undisturbed line. Samples were taken at approximately two-monthly intervals and Figure 2 shows a series of water content profiles measured on 31 October 2003, 04 March 2004 (late summer), 06 May 2004 (autumn) and 25 October 2004. On each water content profile, the spot
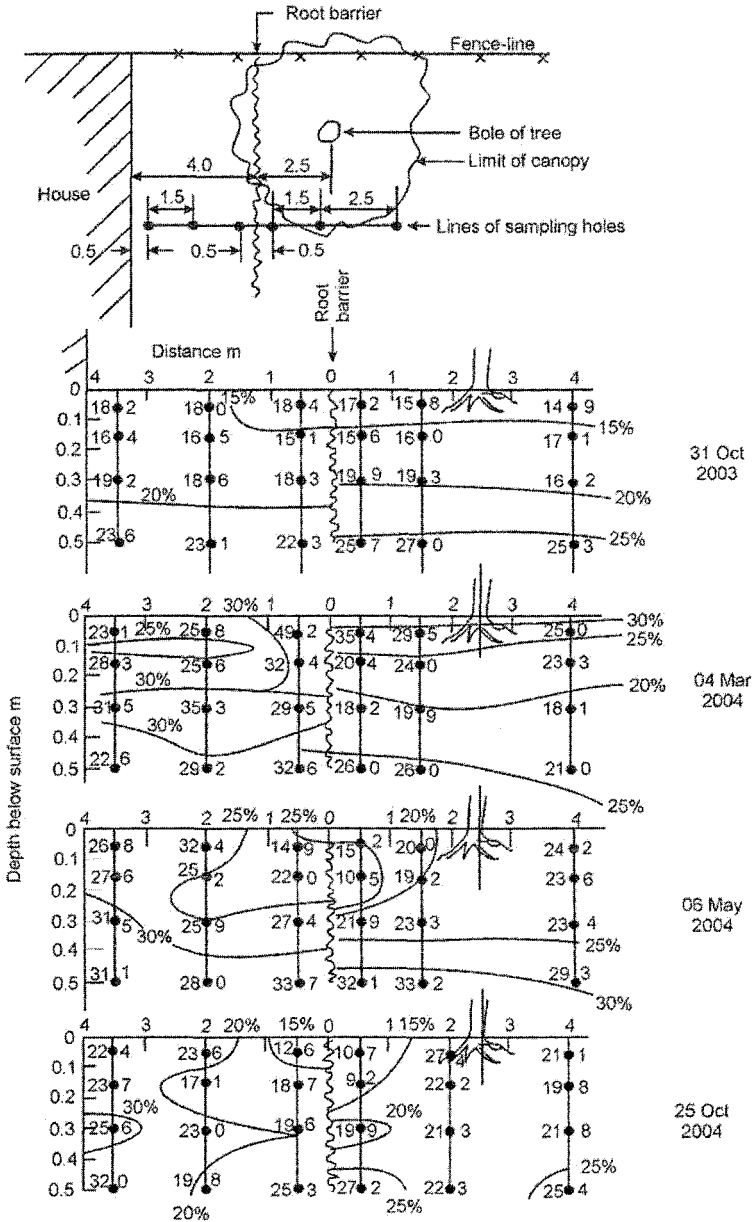
Figure 2: Effect of root barrier on soil water content at four times during the 2003/2004 year.

values represent the soil water content in per cent by dry mass with the decimal point (e.g. 14.9) representing the location of the corresponding sample.

The water content contours in Figure 2 should be examined in conjunction with Figures 3 and 4. Figure 3 shows the water content measurements consolidated into longitudinal profiles of water stored in the soil, expressed as mm of water (the equivalent of litres of water per m^2 of surface area) over the depth of sampling. Figure 4 shows the water balance for the site.

Time is recorded on the horizontal axis, rainfall and evapotranspiration from the soil (in mm or litres/m^2) on the left hand vertical axis and water stored in the soil as litres per m width for the 9 m length of the sections (i.e. the area under each section in Figure 3) on the right hand vertical axis. The water stored is indicated in Figure 4 by A for the water stored over the distance from the house to the barrier, and B for the distance from the barrier to the end of the section under the tree. A and B each represent the respective areas under the curves on sides A and B in Figure 3. The evaporation curve was established for the site by energy balance measurements made over a number of years and is an updated version of the measurements shown in an earlier paper (Blight, 2004).

Referring to Figure 2, the water content contours show that on 31 October 2003 (when the tree was in full leaf), the soil was slightly wetter under the tree than between the barrier and the house. On 04 March, 2004, the upper part of the soil on both sides of the barrier was wet from recent rain (see Figure 4) but the lower part of the profile under the tree was drier. By 06 May the soil under the tree was considerably drier than that between the root barrier and the house, and this situation persisted through to 25 October 2004.

The comments for Figure 2 are shown more clearly by Figure 3. At the start of the experiment (end October 2003) the soil under the tree was slightly wetter than that between the barrier and the house. Thereafter, the soil zone adjacent to the house was consistently wetter than the soil under the tree. It is also noteworthy that from 04 March onwards, soil water contents adjacent to the house remained high, even in late October 2004. Being on the south side of the house (and in the southern hemisphere), the area close to the house is perpetually in shade. Prior to October 2003, the invading tree roots dried out this area, as seen in the profile for 31 October 2003. Once installation of the root barrier had disabled the roots, this drying did not occur.

Figure 4 shows the data of Figures 2 and 3 even more succinctly. After December 2003, the A-line, representing the total water stored in the soil between the barrier and the house, lies consistently above the B-line, representing the total water stored in the soil under the tree. However, as far as the foundations of the house are concerned, the most important observation is that the soil water content adjacent to the house became relatively stable once the root barrier was in place. This has stabilized the south wall.
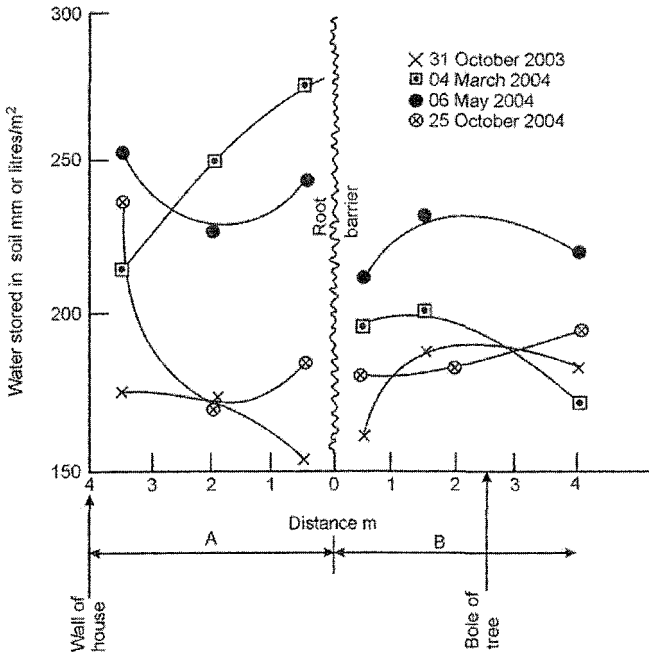
Figure 3: Longitudinal profiles of water stored in the soil on either side of the root barrier.

It is worth noting from Figure 4 that the cumulative evapotranspiration line for grassed areas coincided with the cumulative rainfall line at the end of October 2003 and the two lines almost coincided at the end of October 2004 showing that rainfall and evapotranspiration were close to balance at the Clarens site. The 2004/5 rainy season was, however rather wetter (758 mm from end October to end April, compared with 635 mm for the same period in 2003/4) and this would probably have resulted in greater runoff and/or deep percolation out of the base of the soil profile. (The wet season was not complete at the time of writing.)

Effect of tree without root barrier

Figure 5 shows the position of the willow tree (Salix tortuosa) relative to the house, and gives the present dimensions of the tree's branch and leaf canopy. Below the location diagram, four typical soil water content profiles are shown for 15 April 2004 (early autumn), 05 August 2004 (early spring), 30 November 2004 (early summer) and 30 April 2005. The corresponding sections showing the water stored in the soil profile are shown in Figure 6.
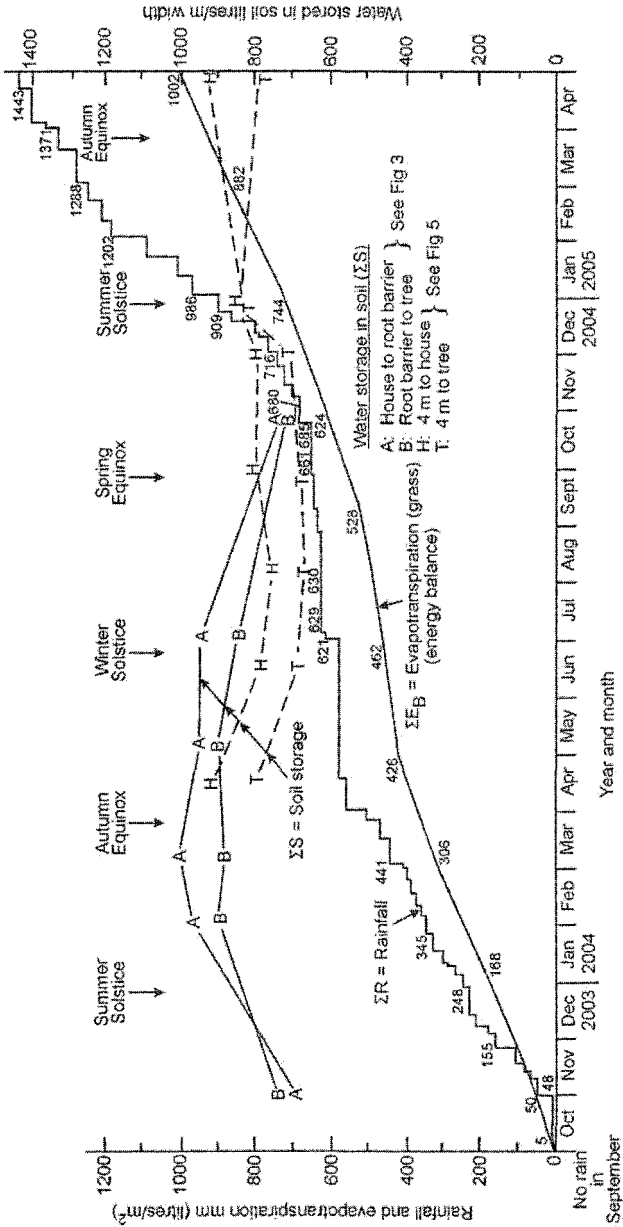
Figure 4: Water balance for the Clarens site showing soil water storage for root barrier-to-tree and tree-to-house measurements.
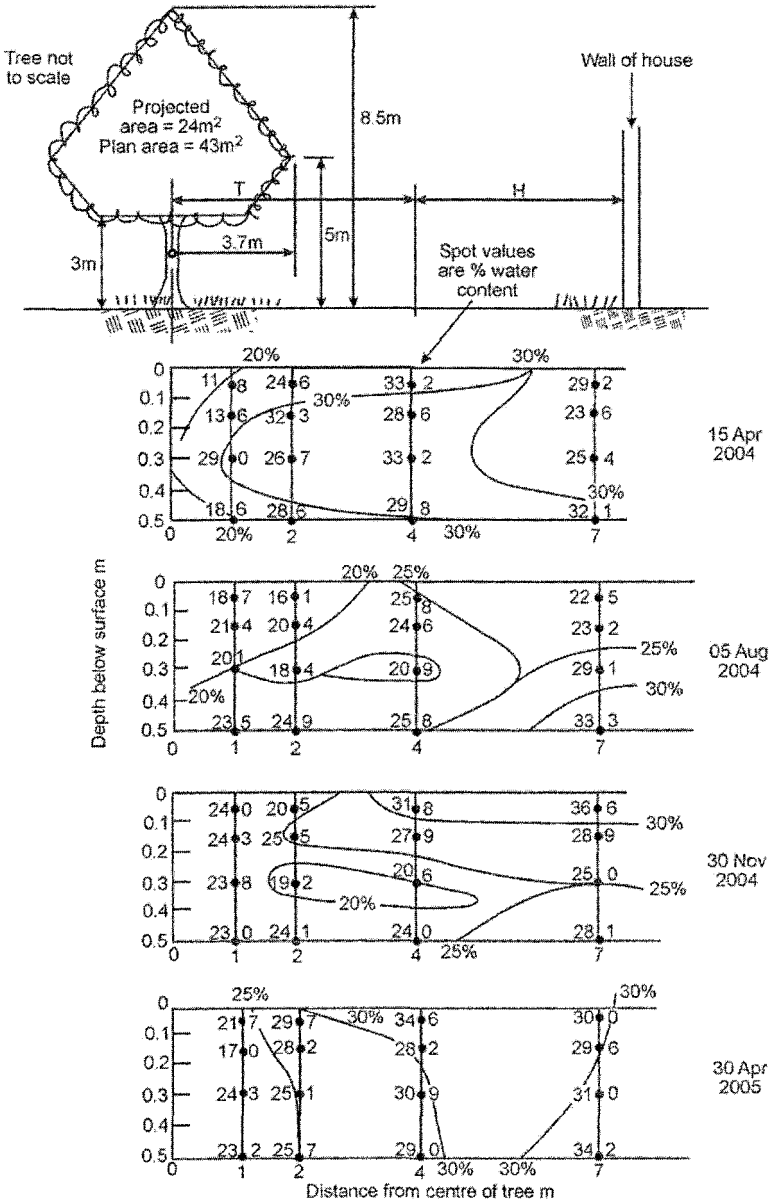
Figure 5: Contours of soil water content between tree and house at four times during 2004/2005 year.

The water content contours in Figure 5 are difficult to interpret umambiguously, but clearly show the persistent desiccation of the soil around the tree. The radius to which the tree exerts an influence on the soil water is difficult to judge, but is shown more clearly in Figure 6. This diagram shows that the main influence of the tree's root system extended to a radius of about 4 m from the tree, whereas the tree's leaf canopy had a radius of 3.7 m. Tree roots may have had some influence beyond a 4 m radius, but considering the variation through the year of the water stored in the soil close to the house (e.g. April 2004 and April 2005) the influence must have been minor beyond 4 m.

The water stored in the soil over distances T (tree to 4 m from tree) and H (4 m from tree to wall of house) have been shown on the water balance diagram (Figure 4). The plot confirms that the soil within the radius of main influence of the tree was consistently dryer than the soil beyond this radius. There are no signs of desiccation damage to the west side of the house, and it is likely that it is not yet being affected, even though it is about the same distance from the house as the Fraxinus to the south.

However, shortly before this paper was written, it was discovered that the Salix roots had managed to invade a sewer pipe running past the tree from the house. It may be that the tree's roots were less invasive of the soil than those of the Fraxinus because they had a readily available source of water in the sewer. The sewer pipe has now been repaired and future trends of soil water content between the house and the Salix will be monitored with interest.
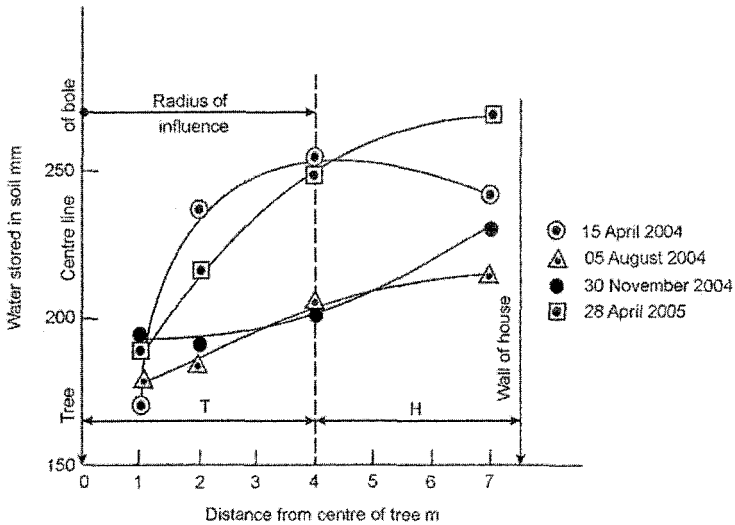
Figure 6: Radial profiles of water stored in the soil between house and tree.

Summary and conclusions

Although literature implicating the evapotranspiration activities of trees and other vegetation in damage to buildings extends over 60 years (Blight, 2005), only one investigator (Biddle, 1983, 2001) has made a detailed study of the effects of vegetation on soil water contents. The present paper adopts a similar detailed approach to the interaction between single trees and a structure and to the effect of a root barrier on soil water contents.

It is shown that a simple root barrier can have an almost immediate ameliorative effect on desiccation of soil adjacent to a building, caused by tree roots. Longer term effects have still to be observed. The effect of tree roots, unimpeded by a root barrier, have also been studied and the area of greatest effect defined. This area has not yet approached the building, and will continue to be observed, especially as an exterior source of water for the tree's growth has now been removed.

References

Biddle, P.G. (1983). "Patterns of drying and moisture deficit in the vicinity of trees on clay soils". *Geotechnique*, 33(2), 107-126.

Biddle, P.G. (2001). "Tree root damage to buildings". *In: Expansive Clay Soils and Vegetative Influence on Shallow Foundations, ASCE Geotechnical Special Publication* 115, 1-23.

Blight, G.E. (1997). "Interactions between the atmosphere and the earth", *Geotechnique*, 47(4), 715-767.

Blight, G.E. (2002). "Seasonal changes in the soil-moisture regime at shallow depths in an expansive soil in a semi-arid environment". *3rd International Conference on Unsaturated Soils*, Recife, Brazil, 2, 865-869.

Blight, G.E. (2004). "Water balances for soil systems". *3rd International Conference on Unsaturated Soils*, Recife, Brazil, 3, 1113-1124. *(Conference in 2002, 3 published 2004)*.

Blight, G.E. (2005). "Desiccation of a clay by grass, bushes and trees". *Geotechnical and Geological Engineering (in press)*.

Building Research Establishment (1985). *The influence of trees on house foundations in clay soils. Digest 298. Building Research Establishment*, Watford, U.K.

Newland, P.L. (1965). "The behaviour of a house on a reactive soil protected by a plastic film moisture barrier". *International Research and Engineering Conference on Expansive Soils, College Station*, Texas, U.S.A., 324-329.

Nunn, A.P., Holden, J.C., Ma, M. and Dimos, A. (1992). "Restoration of tree-affected building foundations". *7th International Conference on Expansive Soils*, Dallas, Texas, U.S.A., 143-148.

Pengelly, A. and Addison, M. (2001). "In-situ modification of active clays for shallow foundation remediation". *In: Expansive Clay Soils and Vegetative Influence on Shallow Foundations, ASCE Geotechnical Special Publication* 115, 192-214.

Radevsky, R. (2001). "Expansive clay problems – how are they dealt with outside the U.S.?" *In: Expansive Clay Soils and Vegetative Influence on Shallow Foundations, ASCE Geotechnical Special Publication* 115, 172-191.

Measuring evaporation from grassed surfaces and trees by energy balance

Geoffrey E. Blight[1]

[1]Professor Emeritus of Civil and Environmental Engineering, University of the Witwatersrand, Johannesburg. Private Bag 3, Wits, 2050, South Africa; PH/FAX: -- 27 11 476 8759;
blight@civil.wits.ac.za

Abstract

A companion paper submitted to this conference ("Interaction between trees and buildings on shrinkable soils – a detailed field study") investigates changes in the water content of a soil stratum caused by the activities of trees. The main activity is the abstraction of water from the soil by the trees' root systems. This must take place to provide for the evapotranspiration of water from the trees' branches and leaf canopies, that is necessary for growth.

Evapotranspiration from a tree can be measured by considering the tree's solar energy balance, because it is the energy absorbed by the tree branches and leaf canopy and the soil penetrated by the tree root system that drives the evapotranspiration and growth (photosynthesis) processes.

The paper describes the techniques developed to assess the solar energy balance for a tree and hence enable assessment of evapotranspiration from the tree branches and canopy as well as the soil shaded by the tree. The accuracy is checked by means of the soil-water balance for the grass-tree-soil system.

Introduction – the energy balance method for measuring evapotranspiration.

A companion paper submitted to this conference (Blight, 2006)"Interaction between trees and buildings on shrinkable soils – a detailed field study") describes an investigation of changes in the water content of a soil stratum caused by the growth activities of trees. The main activity is the abstraction of water from the soil by the trees' root systems. This must take place to provide for the evapotranspiration of

water from the trees' branches and leaf canopies, that is necessary for photosynthesis and growth.

The investigation was carried out at a site at Clarens, a small town in the Free State Province of South Africa. A full description of the site is given in the companion paper. The investigation concerned the water abstraction activities of two single deciduous trees, one an American ash (Fraxinus americana), the other a species of willow (Salix tortuosa). The measurements referred to in this paper were performed on the Salix and the grassed soil surface surrounding it.

Daily water usage, or evapotranspiration, ET, by grass, bushes and trees can be measured by an adaptation of the energy balance technique described by Blight (1997, 2002, 2003). This technique gives an estimate of the actual evaporation from the soil, whether drawn directly from the soil surface, or extracted from the soil by a root system and transpired by the vegetal cover. Incoming and reflected solar energy are measured, together with temperature changes of the near-surface soil and temperature and relative humidity gradients in the air above the soil surface. Wind speeds are also measured. Using these measurements, the net incoming solar energy (R_n) can be apportioned into energy consumed in heating the soil (G), heating the air (H), and latent heat of evaporation of soil water (L_e). R_n, G, H and L_e are measured in W/m^2 (i.e. $J/s/m^2$). The evaporation from the soil surface can be determined from the integrated surface energy balance linking L_e to the three solar power terms R_n, G and H:

$$\Sigma R_n = \Sigma L_e + \Sigma G + \Sigma H \tag{1}$$

In this equation, the terms are integrations of the power terms R_n, G, H and L_e over a day and have units of $kJ/m^2/day$.

As ΣH is always small compared with ΣG (see Blight, 2002) this can be simplified to

$$\Sigma L_e = \Sigma R_n - \Sigma G$$

(1a)

The summations are carried out over the period of measurement, usually from sunrise to sunset. The evapotranspiration for this period is then found by dividing ΣL_e by λ, the latent heat of evaporation for water (2470 kJ/kg) to give evaporation in kg of water per m^2 per day, which is equivalent to mm of water per day. There is little energy exchange during the hours of darkness and overnight water loss is usually neglected. The energy balance gives actual evapotranspiration from the soil, not potential evapotranspiration. When the soil is dry, and water is less available to be evapotranspired, the soil temperature becomes higher. Hence ΣG in equation (1a) increases, and ΣL_e (and hence evapotranspiration) decreases correspondingly.

If the measurements of received net solar energy are made, for example, above a grassed soil cover, the energy received by the soil surface will be less and thus ΣG

will be less and ΣL_c correspondingly more. The increase in ΣL_c is taken to have been consumed in transpiration of water by the grass. However, this obviously cannot apply if the grass is dead or dormant. In this case transpiration by the grass cover must be close to zero, and soil evaporation is reduced by insulation of the soil surface caused by the shading of the dormant grass. Hence the percentage of total evapotranspiration from a grassy surface, made up by soil evaporation, will vary from 100% when the grass is dormant to a lesser percentage, typically 80% when the grass is actively transpiring water abstracted from the soil by its roots.

Constructing the energy balance is not the only method available for measuring transpiration by trees. A method known as the heat pulse velocity technique (HPV) is very widely used for estimating transpiration by trees (Marshall, 1958, Swanson and Whitfield, 1981, Baker and van Bavel, 1987).
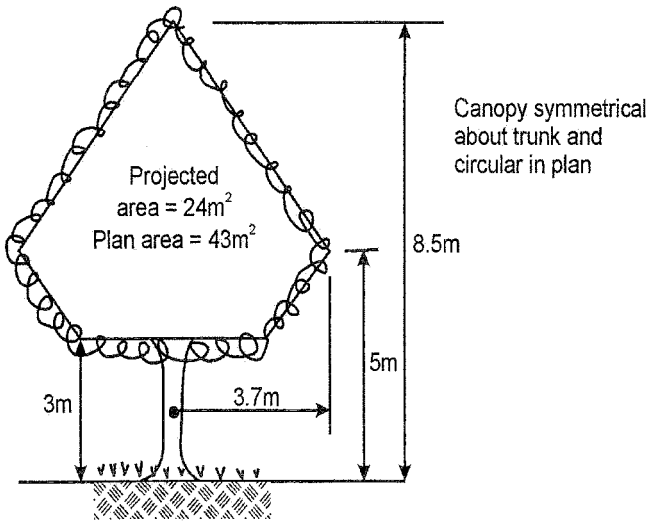
Figure 1: Formalized projected shape of tree.

HPV measures the rate of flow of sap up the stem of a tree or plant, by measuring the time for a pulse of heat applied to the sap at one level to be detected at a higher level. Lysimeter techniques, especially microlysimeters (e.g. Boast and Robertson, 1982) would be suitable for estimating evapotranspiration from a grassed surface, but cannot easily be applied to bushes and trees. In the microlysimeter technique a cylindrical core, including the grassed surface, is removed from the soil, weighed and replaced. The weighing is repeated daily to assess the rate of evapotranspiration from the soil. However, the energy balance method has the advantage of being readily applicable to trees, bushes and grass and was chosen for this reason.

Assessing the energy balance for the Salix

To assess the energy balance for a tree or bush, the shape of the canopy is formalized (as shown in Figure 1) to a vertical cylinder, cone, sphere or other suitable shape of appropriate dimensions. The formalized canopy shown in Figure 1 represents the Salix that is investigated in this paper.

Figure 2 shows the variation of the altitude of the sun measured during the day at Clarens (latitude $28°31^1$ south, longitude $28°26^1$ east) at the times of the summer solstice, the spring and autumnal equinoxes and the winter solstice.
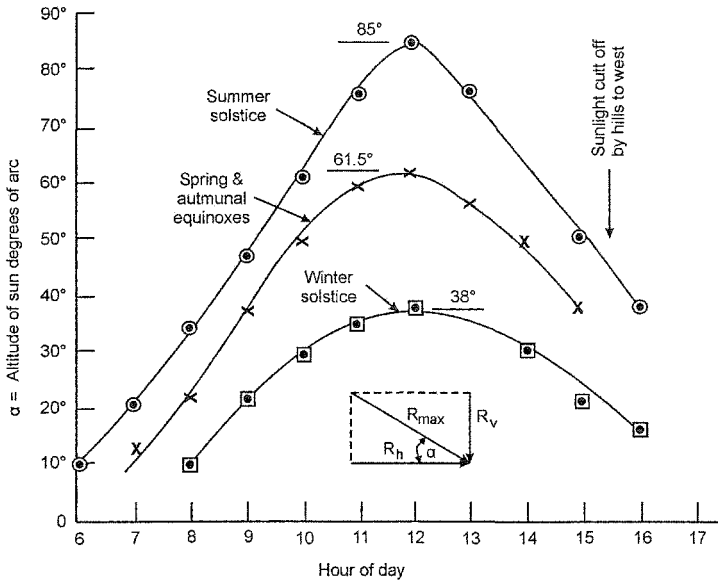
Figure 2: Variation of sun's altitude through the day.

The altitude of the sun in Figure 2 was measured by driving a stake vertically into the ground and measuring its height and the varying length of its shadow on the ground (allowing for the slope of the ground). R(max) can be measured by pointing a solar radiometer sensor at the sun and rotating it vertically and horizontally until it gives a maximum radiation reading (units of W/m^2). The radiation reflected from the ground at angle α must be subtracted from R(max). R_v can be measured directly by pointing the radiometer sensor vertically upwards. Measured values of R_v are close to values calculated as

$$R_v = R(max) \sin\alpha \qquad\qquad (2a)$$

R_h is the horizontal component of solar energy that impinges on the inclined sides of the formalized canopy.

$$R_h = R(max) \cos\alpha \qquad\qquad (2b)$$

R_v will shine on the plan area of the canopy and a proportion of R_v will penetrate the leaves and branches and shine on the grass and soil directly under the tree. $R(max)$ will shine on the sides of the canopy and the interception of these rays by the leaves and branches will cast a shadow behind the bush or tree. Part of $R(max)$ will penetrate the leaves and branches, and some of $R(max)$ will slant in beneath the canopy. The sunlight that penetrates vertically through the canopy or slants in from the side can be measured by measuring R_v under the tree or bush, and the sunlight that penetrates the canopy laterally can be measured as the maximum radiation $R(max)$, or its components, in the dappled shadow cast by the tree canopy.

Of the solar energy intercepted by the leaves and branches, part will raise their temperature, part will be used for photo-synthesis (about 2%, Salisbury and Ross, 1992) and the balance will evaporate or transpire water from the leaves. Approximately 220 kg of water are transpired to produce 1 kg of biomass (Salisbury and Ross, 1992).

The accuracy of the measurements in Figure 2 can be checked by noting that at noon the following should apply:

Summer solstice: $\alpha \approx 90° -$ (latitude of Clarens) + (latitude of tropic of Capricorn)
i.e. $\alpha = 90° - 28.5° + 23.5° = 85°$
Equinoxes: $\alpha = 90° -$ (latitude of Clarens)
i.e. $\alpha = 90° - 28.5° = 61.5°$
Winter solstice: $\alpha = 90° -$ (latitude of Clarens) $-$ (latitude of tropic of Cancer)
i.e. $\alpha = 90° - 28.5 - 23.5 = 38°$

Figures 3a, b and c show sets of observations of the following cumulative energy components (in kJ/m^2) measured during daylight hours on days close to the winter solstice, the spring equinox and the summer solstice:

$\Sigma R_v(0)$ = net vertical incoming energy for a grassed open (0) site near the Salix.
$\Sigma R_v(UT)$= net vertical incoming energy measured under the tree (UT).
$\Sigma R_v(T)$ = net vertical incoming energy intercepted by the tree canopy (T).
$\Sigma R_h(T)$ = net horizontal incoming energy intercepted by the tree canopy.
$G(0)$ = soil heat absorbed at open site.
$G(UT)$ = soil heat absorbed under tree.

Evapotranspiration from the open site was calculated as:

$$E\ (0)\ kg/m^2 = \{\Sigma R_v(0) - G\ (0)\}\ kJ/m^2 \div 2470\ kJ/kg$$

1 kg/m^2 is equivalent to 1 mm of evapotranspiration

Evapotranspiration from the soil under the tree was calculated in a similar way. For the tree canopy, the evapotranspiration was calculated separately for the plan and elevation, allowing 10 per cent of the intercepted energy for heating the leaves and branches and for photosynthesis, as follows:

E (T) (elevation) = 0.9 A(elevation) $\times$ ΣR_h(T) $\div$ 2470 kg of water
E(T) (plan) = 0.9 A (plan) $\times$ ΣR_v (T) $\div$ 2470 kg of water
Overall E(T) = E(T) (elevation + plan) $\div$ A$_i$ kg/m^2 $\equiv$ mm of water
Where A ( ) represents the area of either elevation or plan of the canopy and A$_i$ = Area of influence of the tree roots, i.e. area from which the evapotranspiration is drawn. (See companion paper for estimates of A$_i$.)

Numerical values for the three sets of measurements are summarized in Table 1.

Checking the realism of the result

Figure 4 shows the water balance for the site with month of year recorded on the horizontal axis and rainfall and evapotranspiration from grassed areas (open sites) on the vertical axis. The evapotranspiration line is a composite of many measurements taken on open grassed areas away from trees at the Clarens site from December 2000 onwards.

The water balance is not complete as it does not allow for possible downward flow of water from the shallow soil profile into the underlying sandstone or the reverse, recharge of the soil by upward flow from the sandstone under evaporation gradients. These are very likely to occur, but can only be quantified by separate measurements of soil suction or water content. The companion paper "Interaction between trees and buildings on shrinkable soils" gives detailed contours and profiles of water stored in the soil stratum in which the Salix is growing. On the assumption that soil moisture conditions are radially symmetrical about the tree, Pappus' theorem (concerning volumes of revolution) was used to estimate the quantity of water stored within the area of influence of the tree and this was then averaged over the area of influence. Six sets of measurements were available, and these are shown in Figure 4 as ΣS, the water stored in the zone of influence of the tree.
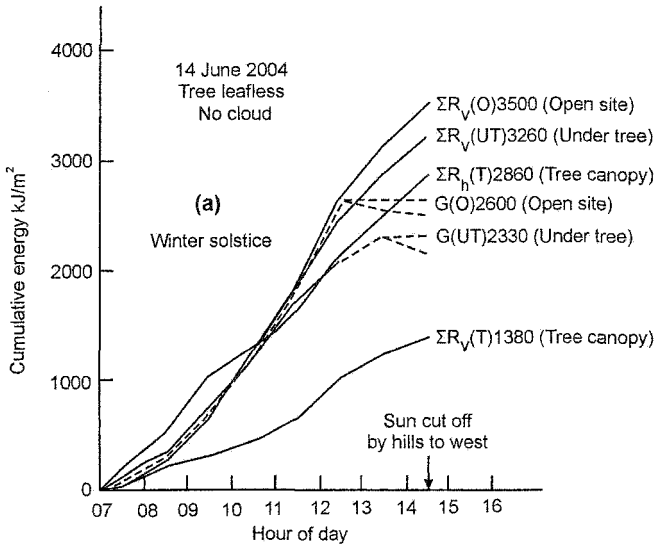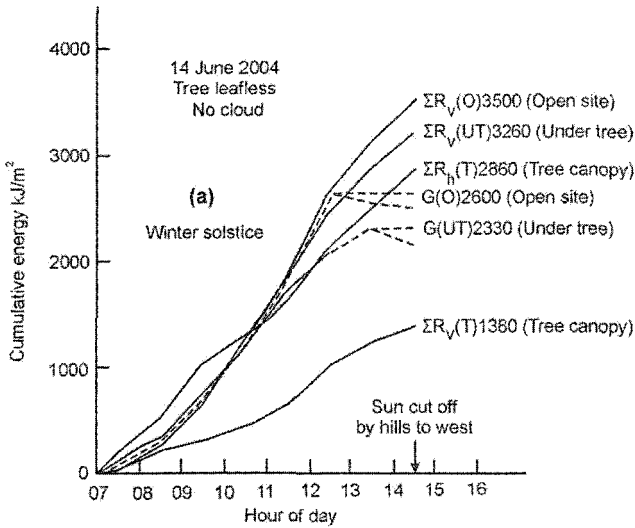
Figure 3: Energy accumulation related to tree
(a) Near winter solstice (21 June)
(b) Near spring equinox (21 September)
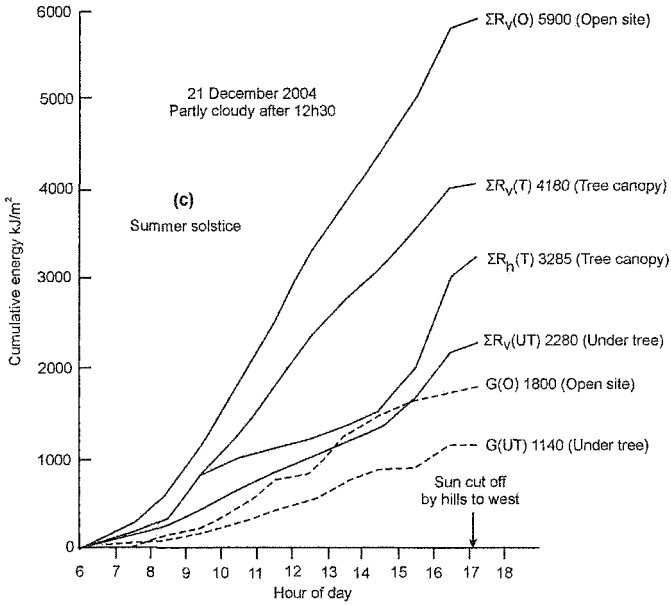
Figure 3: Energy accumulation related to tree
(c) Summer solstice (21 December).

The water balance equation for the soil stratum at the site is:

$$\Delta E = \Delta(R - RO) + \Delta S - \Delta OF \tag{3}$$

in which Δ indicates a change over a stated period of time,
E represents evapotranspiration (mm),
(R-RO) represents rainfall minus runoff, i.e. infiltration, taken as equal to rainfall (mm),
S is the water stored in the 500 mm thick soil stratum (mm), and
OF is outflow from the soil to the underlying sandstone or the reverse (mm).
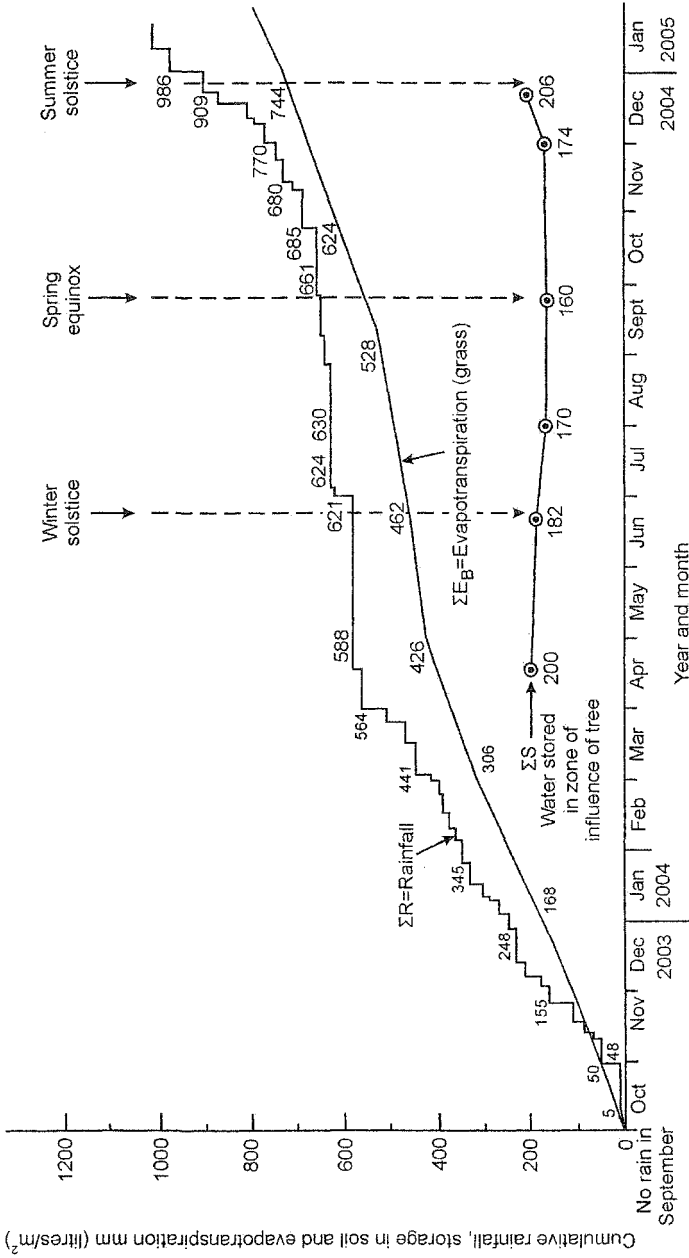
Figure 4: Water balance for Clarens site showing water stored in zone of influence of tree.

Table 1: Evapotranspiration from area of influence of the Salix

	Evapotranspiration in mm/day		
Source of evapotranspiration	Winter	Spring	Summer
Open grassed area	0.4	0.7	1.7
Canopy of tree	0.9	1.9	1.9
Soil under tree	0.2	0.3	0.5
Total for tree	1.1	2.2	2.4
Evapotranspiration from soil stratum $\Delta E = \Delta R + \Delta S$	0.9	1.2	2.2
	15 April-05 August	05 August-29 Nov.	29 Nov.-21 Dec.

Ignoring OF, Table 1 shows two things:

- that the evapotranspiration measured for the tree's area of influence consistently exceeds evapotranspiration from the open grassed area, and
- that for the winter and summer sets of measurements the total evapotranspiration from the tree's area of influence was fairly close to the corresponding figures derived from rainfall and water stored in the soil.

It should be pointed out that at the winter solstice the tree was leafless, but it has been assumed that evaporation would still take place from the surfaces of the branches. At the spring equinox the tree was in full new leaf and growing vigorously, but (see Figure 4) very little rain had fallen and the soil water was probably being maintained by upward flow from the underlying sandstone. The minimum saturated permeability of the soil (Blight, 2006) was measured at 35 mm/h or 840 mm/d. To reconcile the evapotranspiration figures in Table 1 for the spring set of measurements, an upward flow of only 1 mm/d under an upward suction gradient of 1 kPa/m is all that is required, and this seems very possible.

Conclusions

A method of measuring evapotranspiration from single trees and bushes has been described. The three sets of measurements presented appear to give realistic results when checked against changes in soil water stored in the soil within the area of influence of the tree.

References

Baker, J.M. & van Bavel, C.H.M. (1987). "Measurement of mass flow of water in the stems of herbaceous plants". *Plant, Cell and Environment*, 10, 777-782.

Blight, G.E. (1997). "Interactions between the atmosphere and the earth". *Geotechnique* 42(4), 715-766.

Blight, G.E. (2002). "Measuring evaporation from soil surfaces for environmental and geotechnical purposes". *Water S.A.*, 28(4), 381-394.

Blight, G.E. (2003). "The vadose-zone soil-water balance and transpiration rates of vegetation". *Geotechnique* 53(1), 55-64.

Blight, G.E. (2006). "Interaction between trees and buildings on shrinkable soils – a detailed field study". *4th International Conference on Unsaturated Soils. This conference.*

Boast, C.W. & Robertson, T.M. (1982). "A microlysimeter method for determining evaporation from bare soil: description and laboratory evaluation". *Journal, Soil Science Society of America*, 46, 689-696.

Marshall, D.C. (1958). "Measurement of sap flow in conifers by heat transport". *Plant Physiology*, 6, 385-396.

Salisbury, F.B. & Ross, C.W. (1992). *Plant physiology*, Wadsworth, California, U.S.A., 263-265.

Swanson, R.H. & Whitfield, D.W.A. (1961). "A numerical analysis of heat pulse velocity, theory and practice". *Journal of Experimental Botany*, 32(126), 221-239.

A SURVEY OF GEOTECHNICAL PRACTICE FOR EXPANSIVE SOILS IN TEXAS

William D. Lawson, P.E., Ph.D., M.ASCE[1]

[1] Visiting Assistant Professor, Department of Civil Engineering, and Deputy Director,
National Institute for Engineering Ethics, Texas Tech University, Box 41023,
Lubbock, TX 79409-1023, Tel (806) 742-3521, Fax (806) 742-0444,
email: William.D.Lawson@ttu.edu

ABSTRACT: This study describes geotechnical practice for expansive soils in Texas based on a controlled research survey of Texas geotechnical engineers conducted in April-May 2002. Expansive soils are Texas' defining geotechnical issue; however, the findings of this research show a remarkable amount of uncertainty in the geotechnical community as regards expansive soil movement prediction, analysis and design. The findings address the demographics of Texas geotechnical engineering practice, education in the expansive soil area, the frequency of use for several methods of expansive soil identification and characterization, the validity and procedures for expansive soil laboratory tests, the validity and frequency of use for several expansive soil movement prediction methods, and common practices for expansive soil analysis, reporting, and design. Despite the focus on Texas, the expansive soil practice issues described herein go beyond state boundaries and are of national and international interest with respect to the public health, safety and welfare.

INTRODUCTION

This research paper summarizes the results of an empirical study to identify and describe geotechnical engineering practice for expansive soils in Texas (Lawson 2003a). In addition to the demographics of the geotechnical engineer respondents, this study identifies the education of practitioners in the expansive soil area, the frequency of use for several methods of expansive soil identification and characterization, the validity and procedures for expansive soil laboratory tests, the validity and frequency of use for several expansive soil movement prediction methods, and common practices for expansive soil analysis, reporting, and design.

Despite the prevalence of expansive soils in Texas, research shows that most Texas civil engineers, geotechnical engineers included, receive practically no formal

education in expansive soils in their undergraduate program of study, and little exposure in graduate school (Lawson 2003b). Further, the author's conversations with geotechnical practitioners, service on state committees, and personal consulting experience suggest that most Texas geotechnical engineers hold isolated, or perhaps non-validated, views about many fundamental expansive soil practice issues. Stated another way, the Texas geotechnical practitioner community is lacking a broad context by which it might judge practical matters such as expansive soil identification, analysis and design procedures. This is exacerbated by the continued development of new theory and alternative methods for dealing with expansive soils. The point is that the geotechnical community – in Texas, nationwide and worldwide – can be strengthened if provided access to a controlled empirical study of geotechnical practice for expansive soil. This research is that study.

METHOD

Design of the Study

The findings of this research derive from responses to a 140-item, web-based questionnaire where the research questions were grouped into eight sections:

- Professional Status/Work Demographics
- Education
- Expansive Soil Identification/ Characterization
- Expansive Soil Laboratory Test Methods and Procedures
- Expansive Soil Movement Prediction Methods
- Expansive Soil Analysis
- Expansive Soil Reporting
- Expansive Soil Design Considerations

Apart from educational and professional status information, the author developed the technical survey questions from consulting experience and with reference to expansive soil texts, publications, and websites. These references were provided to the survey respondents. Prior to its administration, the survey instrument was pre-tested – both its scope and the individual questions – by submitting the survey to four respected geotechnical practitioners. Based on their review and comments, the survey instrument was finalized and published to the project website.

Definition and selection of the research sample posed several challenges. Ultimately, the selected sample population consisted of all members of the Texas Section, ASCE who identified 'geotechnical' as their primary or secondary discipline-specific interest area on their ASCE membership form.

Procedure

The research survey was administered through an Internet website which was principally active from April 11, 2002, through May 10, 2002, with survey respondents having been notified about the research by email and US Mail. The controlled log-in process assured respondents complete anonymity and confidentiality. Respondents were provided a link to the project website, accessed the questionnaire with prescribed log-on credentials, and took the survey on-line.

Respondents submitted their responses directly into a results database as they clicked through the on-line survey. This direct manner of data collection benefited the research by eliminating the need to hand-code survey responses, thereby minimizing opportunity for error. However, compatibility issues between the database and some Internet browsers created problems making certain parts of the survey inaccessible for some respondents, this despite extensive pre-testing of the system. Every problem which was brought to the author's attention was directly addressed and resolved. In some cases, respondents did not identify the error and thus submitted partial responses.

Analysis of responses was limited to simple statistical summaries such as identifying and ranking responses, calculating averages and median values, and discussing confidence intervals. These analyses required no sophisticated statistics and none are presented herein. While more rigorous data reduction can be done, for example, multivariate analyses identifying typical practices for predicting expansive soil movement as a function of education and/ or primary geographic practice location, this report does not address those more detailed analyses.

Evidence for Validity

The respondent sample population consisted of 607 persons, which was the control group for the survey. At completion, 236 persons from the control group had taken the survey for an overall response rate of 39 percent. An additional 53 respondents who were not in the control group also took the survey, but these data were excluded from analysis. Of the 236 surveys received, 46 were incomplete. After follow-up with respondents from the incomplete surveys, it was deemed appropriate to accept them as partial responses resulting from software compatibility problems associated with the web-based survey method and database.

As to face validity of the survey process, it is reasonable to conclude that members of the Texas Section, ASCE, who identify geotechnical as their primary or secondary interest area were appropriate survey candidates to represent the views of Texas geotechnical engineers with respect to expansive soil practices and procedures. While not all Texas geotechnical engineers are members of ASCE – US Department of Labor (Grigg 2000) and ASCE membership data (ASCE 2001) roughly estimate ASCE membership at 60 percent of the entire civil engineering community – ASCE represents the majority of civil engineers, and arguably the leaders of the geotechnical profession *are* members. The sample population also has the benefit of being clearly

defined and stable. Of course, not all respondents in the sampling frame practice in the expansive soil area. Survey responses showed that part of the control group (12 percent) focused on other practice areas such as off-shore, forensic, and environmental engineering and identified themselves as such. Another, smaller group of the respondents (fewer than 3 percent) were engineering faculty who did not claim practice experience. Notwithstanding the exceptions, the control group appeared to strongly represent the views of Texas geotechnical engineers as regards expansive soil practices and procedures.

Because the survey response rate was less than 50 percent which is customarily an adequate response for mailed surveys (Bailey 1994, pp. 147-72), the concern arises whether the respondents constituted a representative random sample of the survey population. One test criterion was available, the geographic distribution (Metropolitan Statistical Area) of the full control group. The distribution for the respondents (sample) was compared with the control group (universe) and yielded a very strong correlation.

In summary, the 39 percent survey response rate, the cohesive characteristics of the sample population, and the random sample of respondents indicate that the data from this survey are representative of the Texas geotechnical engineering community.

RESULTS

Professional Status/ Geotechnical Practice Demographics

The level of professional responsibility the survey respondents, is highly diverse and well-distributed, ranging from staff engineer to engineer faculty. Well over half of the respondents hold senior-level or higher technical positions, with the median level of responsibility being senior engineer. Most respondents (over 80 percent) are licensed engineers in Texas, many of these holding engineering licenses in other states. The average number of years of post-baccalaureate experience is 20 years total, 15 years geotechnical, and 11 years in expansive soils. Professional memberships for the group are heavily weighted toward ASCE (the control group – 99 percent) and ASFE (43 percent).

The respondents' annual project workload (fee basis) performed in the geotechnical and expansive soil areas shows a broad distribution, with half of the respondents (median value) doing 60 percent or more of their business in geotechnical, and half of the respondents doing 50 percent or more of their business in expansive soils.

Market sectors vary considerably, but about half of the respondents work primarily in the commercial market sector (52 percent, combined residential and non-residential). Also, about half (56 percent) of the respondents mostly perform geotechnical explorations for new construction. Geographically, as would be expected, most respondents practice in the major metropolitan areas of Austin, Dallas,

Fort Worth, Houston, and San Antonio. While the geotechnical practice areas generally correlate with the geographical distribution of the respondents, Houston is strongly under-represented as a practice area, and Dallas/ Fort Worth is over-represented; however, this is probably consistent with the comparative severity of expansive soil problems in these two population centers.

Education for Geotechnical Engineering and Expansive Soil Practice

Most respondents (58 percent) hold Master's degrees in engineering, with an additional 10 percent having a doctorate. As to coursework, 84 percent of the respondents completed two or more undergraduate geotechnical courses, and 56 percent of respondents completed four or more graduate geotechnical courses. However, three-fourths of the respondents (76 percent) took no *expansive soil* graduate courses. Most of the respondents who did complete graduate coursework in expansive soils took one course, and this was probably at Texas A&M University.

Expansive Soil Identification/ Characterization

This portion of the survey addressed qualitative identification and assessment of expansive soils, the goal being to identify which tests and methods Texas geotechnical engineers commonly use, or do not use. The research identifies 26 different tests and methods, ranked by weighted average from highest to lowest frequency of use. Respondents were mostly familiar with all the methods ("don't know" responses were less than 10 percent in all cases). The preferred choices for identification purposes were plasticity index, liquid limit, and moisture content, each of which garnered a frequency rating (combination of the 'often' and 'almost always' response) of more than 85 percent. These were closely followed by the USCS soil classification, dry unit weight, percent fines, and hand penetrometer, each of which had a frequency rating of 60 percent or more. In contrast, respondents infrequently use 14 of the 26 methods, these having a frequency rating of 15 percent or less. Infrequently-used tests included all suction test methods, mineralogical identification, expansion index, bar linear shrinkage, shrinkage limit, California bearing ratio, swell index, and Test Method ASTM D 4546, Method C. In addition to the identified tests, 40 respondents suggested 'other' test methods besides those shown, the most common being the TxDOT Potential Vertical Rise and knowledge of local geology.

Expansive Soil Laboratory Test Methods and Procedures

This portion of the survey dealt with expansive soil laboratory test methods and procedures, in particular the different types of swell tests and suction tests. These data offer a relatively fine-grained picture of several key issues that geotechnical practitioners must face and which may dramatically affect laboratory test results.

Seven swell test issues including specimen preparation, modification to prescribed test procedures, use of correction factors, and the like, were studied. Perhaps the most remarkable finding is that none of the identified swell test

procedures achieved a frequency rating greater than 13 percent. While these activities seem to be often discussed, they apparently are not often used. Of the seven items shown, the most frequently-used procedure was to reduce calculated swell test values to account for the fact that swell occurs in three dimensions even though the swell test constrains swell to one dimension; however, only 13 percent of respondents frequently make this correction, and 36 percent never do.

Suction test issues included specimen preparation and modification to prescribed test procedures. Perhaps the most remarkable finding from the suction test data is that, on the average, more than half (54 percent) of respondents indicated no knowledge of the suction test procedures. Of those who claimed knowledge, most made no adjustment to suction test procedures or specimens.

The research also evaluated respondent assessments of perceived validity of these different types of tests for design purposes. Note that the term "perceived validity" is used, since the response refers to the impression of the respondent and not to a controlled assessment of validity specific to the test method. Roughly one-fourth of respondents (26 percent) claimed to not know about the validity of the swell tests, and over one-half (60 percent) claimed to not know about the validity of the soil suction tests. Of those who offered an opinion, swell tests achieved a confidence rating (combination of 'highly valid' and 'reasonably valid' responses) of 39 percent, and suction tests had an average confidence rating of 13 percent.

Expansive Soil Movement Prediction Methods

This portion of the survey dealt with quantitative prediction, or estimates, of expansive soil movement. Whereas the expansive soil literature presents many methods to estimate expansive soil movement, this research survey attempted to identify which methods Texas geotechnical engineers use, and how much confidence they place in those methods. A total of 21 different approaches were discussed, and these were broadly grouped into three categories: OEDOMETER (having to do with predicting expansive soil movement based on laboratory swell tests), SUCTION (having to do with predicting expansive soil movement based on laboratory suction tests), and EMPIRICAL RELATIONSHIP (having to do with predicting expansive soil movement based on published data and correlations with soil index properties).

The research first identified the frequency with which respondents used the 21 different approaches to quantitatively estimate or predict the magnitude of shrinkage and swell of expansive soil, ranked by weighted average from highest to lowest frequency of use. Respondents were generally aware of the methods, with "don't know" responses varying from 12 percent to 26 percent. The preferred choice for quantitative movement prediction purposes was Potential Vertical Rise (TEX-124-E), having a frequency rating of 58 percent, and this is the *only* method with a frequency rating greater than 50 percent (recall that the frequency rating is the combined total of 'almost always' and 'often' responses). Three other approaches: Test Method ASTM D 4546 – Method B, the pressure swell test, and Test Method ASTM D 4546 – Method A, all of them oedometer methods, had frequency ratings of 20 percent or

more. In contrast, the remaining 17 of the 21 methods were used infrequently if at all, having frequency ratings of less than 15 percent.

These same 21 quantitative test methods were evaluated to identify the perceived *validity* which respondents assigned to swell values determined by each method, ranked by weighted average from highest to lowest perceived validity. By far, the most remarkable aspect of the data is that respondents do not have a feel for the validity of swell values determined by most of these methods. The best of the group, represented by 5 of the 21 approaches and all of them oedometer or empirical methods, had an average of 32 percent "don't know" responses. The remaining 16 methods had "don't know" responses ranging from 68 to 90 percent, average 82 percent.

Not only is the validity of quantitative swell values mostly unknown, but when validity is known it is typically suspect. For those engineers who offered their opinion about the validity of swell values obtained from the different methods, five methods achieved a confidence rating better than 10 percent, and none achieved a confidence rating better than 38 percent (recall that the confidence rating means that engineers feel that results determined by the prediction method are either 'highly valid' or 'reasonably valid'). The top performer, the pressure swell test, had a confidence rating of 36 percent, followed by Test Method ASTM D 4546 - Method B (38 percent), Potential Vertical Rise (TEX-124-E) (38 percent), and Test Method ASTM D 4546 - Method C (33 percent). Apparently, Texas geotechnical engineers do not trust most of their expansive soil movement predictions.

Expansive Soil Analysis and Reporting

This section of the survey dealt with expansive soil analysis and reporting methods. Here the goal was to gain some insight into how Texas geotechnical engineers approach the expansive soil analysis process, and the manner in which they report their results.

About one-fourth (28 percent) of respondents use only one method to determine quantitative values for expansive soil movement, but most respondents (53 percent) use two methods, and 19 percent use three or more methods.

Engineers approach their expansive soil analyses in many different ways. The survey identified nine different practices for performing expansive soil calculations, five of them based on individual boring approaches and four based on site-wide approaches. Respondents were roughly split on these approaches, with 44 percent basing their calculations on individual boring data and 56 percent performing their calculations at the project site level. The most common approach (25 percent) was to perform expansive soil calculations for the site based on statistically conservative conditions for the site.

Curiously, despite misgivings they may have about the validity of their expansive soil movement predictions, Texas geotechnical engineers tend to report exactly what they calculate. Most respondents (63 percent) use a factor of safety of 1.0 for their predicted heave value once they determine it. Only 25 percent of respondents use factor of safety values of 1.5 or more.

Expansive soil terminology varies, but most respondents (49 percent) refer to expansive soil movement as "shrink/swell" in their reports. They characterize this shrink/swell as either "potential" (46 percent) or "estimated" (37 percent) movement.

When reporting quantitative expansive soil movement values, both for a single boring or for the project site, respondents tend to round their calculated shrink/swell values up to the nearest ½-inch (12 mm) and this is the median threshold. On average, fewer than 15 percent of respondents report values with a precision of 1/10 inch (3mm) or more, and about 30 percent report to the nearest inch (25 mm) or greater. But again, reporting practices vary widely.

Expansive Soil Design Considerations

This portion of the survey addressed common design aspects of expansive soil problems. The context for this discussion was a hypothetical, moderately-loaded, low-rise, 40,000 square foot (3700 m^2) footprint, commercial retail/office building with 100 to 300 kip (445 to 1335 kN) column loads founded on expansive soil. In this scenario, the soil strata were assumed to be expansive to a depth of more than 20 feet (6 m), the expansive soil movement was determined to range from 4 to 6 inches (10 to 15 cm), and the allowable movement for floor slab design purposes was 1 inch (25 mm).

The survey posed a series of questions attempting to define the thresholds at which certain typical expansive soil design decisions were made. The first threshold was how expansive the native soil could be before the designer would not allow use of a soil-supported floor slab. Answers varied considerably, with the median response showing predicted movement of 2 inches (5 cm) or less; however, this question had cross-case validity concerns and the results are suspect. The second threshold was how expansive the native soil had to be before the designer would recommend a fully structural system as the *preferred option* for floor slab support. Again, the responses varied, with the median response showing predicted movement of 3 inches (7.6 cm) or more. The third threshold was how expansive the native soil had to be before the designer would recommend a fully structural system as the *sole option* for floor slab support. Here, the median response showed predicted movement of 5 inches (13 cm) or more.

Given this hypothetical scenario, another common design question is how to address potential floor slab movement. The survey explored geotechnical practices on this issue by identifying ten different techniques used to reduce expansive soil movements for floor slab support, and querying respondents as to their frequency of

use and perceived effectiveness. The ten movement reduction methods were then ranked by weighted average from highest to lowest frequency of use. Respondents were mostly familiar with all the methods ("don't know" responses were less than 10 percent in all cases). The most-used methods for movement reduction were removal of expansive clay and replacement with non-expansive select fill (frequency rating of 70 percent) and horizontal moisture barriers (frequency rating of 35 percent). Three other methods – vertical moisture barriers, water injection, and a combination of removal and replacement and water injection – had frequency ratings between 15 and 25 percent. None of the other methods achieved a frequency rating of better than 10 percent.

The survey then asked respondents to identify the *perceived effectiveness* which they assign to the methods, ranked by weighted average from highest to lowest effectiveness. The survey results indicate that respondents are unsure about the effectiveness of many of these methods. Besides the top performer (removal and replacement) the "don't know" response varied from 16 percent (horizontal moisture barriers) to 51 percent (chemical injection with sulfonated oil), average 33 percent. This suggests that, apart from the removal and replacement technique, engineers do not have much of a feel as to how effective the methods are. Among those engineers who offered an opinion about effectiveness of the methods, removal and replacement garnered a confidence rating of 85 percent, and this is a very strong showing since most engineers felt they could judge the effectiveness of this particular method. Movement reduction techniques judged least effective were injection with sulfonated oil-based chemical, and a dedicated sprinkler system, both of these having a confidence rating of less than 15 percent. Seven methods formed the remainder of the group. Removal and replacement in combination with chemical injection was judged the second most effective method, followed by removal and replacement in combination with water injection. However, none of the methods in the middle of the group varied appreciably in their confidence ratings, which ranged from 23 percent to 45 percent, average 35 percent.

Also with reference to the hypothetical design scenario, another design question dealt with the maximum amount of "removal of expansive soil and replacement with non-expansive fill" considered as a cost-effective solution. Respondents indicated a normally-distributed range from 1 foot (0.3 m) to 10 feet (3 m) or more, with the median response being 5 feet (1.5 m).

DISCUSSION

The data obtained from this research show many contrasts with regard to expansive soil practice in the geotechnical community. On the one hand, the Texas geotechnical engineers who work with expansive soils in their daily engineering practices are highly-experienced, senior level, professionally-active engineers with advanced degrees. However, most have not completed formal graduate coursework

in expansive soils, the geotechnical issue that accounts for more than half of their professional work.

When it comes to identifying expansive soils, geotechnical engineers tend to strongly rely on simple indicator tests such as the plasticity index and liquid limit. But when it comes to using or judging the validity of swell and suction laboratory tests specifically intended for the purpose of evaluating expansive soils, the data show a lot of ambiguity, in particular for the suction test methods. Few Texas geotechnical engineers use swell tests, far fewer use suction tests, and when they use them they do not trust the results.

Quantitative expansive soil prediction methods paint a similar picture. By far, the most commonly-used method to predict expansive soil movements is the empirical algorithm, Potential Vertical Rise, TEX-124-E, which is used roughly 60 percent of the time, almost twice as frequently as the next closest contender, a swell test. But engineers generally do not trust the numbers they calculate using PVR or any of the other methods, and in many cases, they have no feel for whether their expansive soil movement predictions are valid.

Expansive soil analysis practices vary widely, but considerable agreement exists on the number of prediction methods used (2), the factor of safety applied (1.0), and that expansive soils are reported as "potential shrink/swell" movements.

When it comes to design, perhaps the strongest area of agreement in the geotechnical community is that the best thing to do with expansive soils is get rid of them, or to isolate them through use of structurally-suspended floor systems. "Removal and replacement" is the most commonly-used and most trusted of all expansive soil movement reduction techniques, outstripping all other contenders by a factor of at least two.

CONCLUSION

This research describes geotechnical practice for expansive soils in Texas based on a controlled, statistically-valid survey of Texas geotechnical engineers conducted in April-May 2002. The findings are descriptive, not normative; that is, the intent of this research has been to show the way things are rather than what *ought* to be in the expansive soil practice area. While it will certainly be instructive for geotechnical engineers to get a better feel for the broad context and variation in practice for many expansive soil practice decisions, in no way does this research purport to either defend or to criticize any of the tests, methods, procedures or approaches identified herein.

However, the research findings do justify one normative claim. This research identifies a remarkable amount of uncertainty in the geotechnical community as regards expansive soil movement prediction, analysis and design.   Therefore,

engineers in Texas and throughout the world face the opportunity and obligation to promote the health, safety and welfare of the public by devoting increased effort and funding toward education and research, both practice and theory, in the expansive soil area.

APPENDIX I. REFERENCES

American Society of Engineers (2001), "The State of International Affairs," *A Civil Engineered World*, Volume 14, Issue 1, March 2001, available online at http://www.asce.org/pdf/2001intl_newsletter1.pdf, accessed 12/14/02.

Bailey, Kenneth D. (1994), *Methods of Social Research, Fourth Edition*, The Free Press, New York, 588pp.

Grigg, Neil S. (2000), "Demographics and Industry Employment of Civil Engineering Workforce," *Journal of Professional Issues in Engineering Education and Practice*, Vol. 126, No. 3, July 2000, pp. 116-124, ASCE.

Lawson, William D. (2003a), "Geotechnical Practice for Expansive Soils in Texas," TechMRT Research Report No. TTU-2003-2, Center for Multidisciplinary Research in Transportation, Texas Tech University, Lubbock, Texas.

Lawson, William D. (2003b), "Expansive Soils and Higher Education in Texas," TechMRT Research Report No. TTU-2003-1, Center for Multidisciplinary Research in Transportation, Texas Tech University, Lubbock, Texas.

ALTERNATIVE EARTHWORK PROCEDURE FOR EXPANSIVE SOILS

RONALD F. REED, P.E.

Reed Engineering Group, Ltd., 2424 Stutz Drive, Suite 400, Dallas, Texas 75235;
PHONE (214) 350-5600;
FAX (214) 350-0019; email: rreed@reed-engineering.com

Abstract

A wide variation in geologic conditions within the North Texas region allows for numerous methods to reduce the potential movement of a ground-supported floor slab constructed over expansive soils. Methods commonly used include isolation, removal and replacement of the expansive soils with inert fill, and preswelling via either mechanical excavation or high-pressure water injection. The preswelled soils are then capped to limit post-construction drying and to increase the subgrade modulus.

A brief description of each of the processes used to deal with expansive soils is provided. Specific emphasis is given to the use of the high-pressure water injection process to preswell soils. Typical moisture and suction profiles for varying geologic conditions are provided for background information.

An alternative procedure, designated the "picture frame method", consists of construction of an earthen, preswelled "dam" around the building perimeter to isolate the interior portion of the structure from moisture change. Analysis using antidotal information from observation of building performance was utilized to evaluate the width of the required dam. An 18-meter width was used for the case history. The depth varies with the geologic setting. A case history for a 59,130-square meter (sq.m.) office/warehouse is provided.

Introduction

Expansive soils present varying challenges to the design and construction of floor slabs in large industrial structures. The design is typically constrained by both use (such as heavy loads or super flat conditions), and by cost. The design must be functional for the intended use; however, excessively expensive designs are also unacceptable.

315

The purpose of this paper is to describe an alternative earthwork procedure to minimize the potential for movement below large industrial floor slabs. The procedure, designated the "picture frame method", consists of treating the perimeter zone subject to moisture changes while isolating the potential for moisture change within the building interior.

General background, design procedure and case history are presented in the following sections.

Geologic Setting

The north Texas area consists of a wide variation in geologic conditions. Within just the Dallas and Fort Worth area, there are 15 Cretaceous geologic formations overlain with varying thicknesses of Pleistocene and Holocene deposits. The Cretaceous formations vary from soft to hard limestone with interbedded soft shale to relatively massive formations of soft shale. The limestone generally weathers to hard calcareous clay of moderate to high plasticity. The shale generally weathers to form highly plastic clay (dual classified as severely weathered shale).

The variation in geologic formations results in a multiple of conditions relative to expansive soils. The seasonal depth of activity can extend the full depth of shallower soil profiles, or to depths of 5.5 meters or greater during drought years where the soil profile extends below seasonal drying.

The potential for "deep-seated heave", defined as movement originating from profiles below seasonal moisture variations but where the swell pressure exceeds overburden pressure, can extend to depths of greater than 7.5 meters. The highly plastic clay derived from the shale formations frequently result in profiles of this nature.

Potential Vertical Movements

The potential vertical movements associated with the expansive soils vary with the geologic formation and soil profile. Movements of 5 to 7.5 centimeters are common in profiles where the clay is less than about 1.5 meters thick. Deeper soil profiles can result in seasonal movement of 10 to 15 centimeters.

Movement associated with "deep-seated heave" in the deeper soil profiles weathered from the shale are frequently measured to be 10 to 25 centimeters. The largest documented movement by the author is approximately 40 centimeters. Because of the pattern of movement and its relevance to the picture frame method, a survey of this structure is included in this paper.

Typical Design Procedures

Typical design procedures within expansive soils can be divided into two general categories; isolation, and ground-supported. Isolation involves construction of piers below the active zone, then suspension of the structure. A suspended floor is feasible for many structures; however, it is generally not acceptable for large industrial buildings because of both cost and load considerations.

An alternative to a suspended floor consists of isolation of the structure on piers and use of a ground-supported or "floating" slab. Various methods are used to reduce the potential for movement of a ground-supported slab. The methods can be grossly divided into "dry" and "wet" approaches. Under dry philosophy, the expansive soils are totally or partially excavated and replaced with an inert or non-expansive soil. The main problem with this approach in the Dallas/Fort Worth area has been the potential for movement of the expansive soils below the inert fill.

The wet approach typically consists of preswelling the upper expansive soils then placement of a cap to limit moisture loss prior to placement of the floor. The type of cap is also generally dictated by the desired subgrade modulus.

Two alternative methods are presently used to preswell the upper clay; mechanical excavation and re-compaction and use of multiple passes of water pressure injection. Mechanical excavation and re-compaction consists of excavation, mixing the expansive soils to above optimum moisture, then compaction at a controlled moisture and density. Typical specifications require compaction at +1 to +5 percentage points above ASTM D-698 optimum moisture, at a density of between 92 and 98 percent of maximum density.

The pressure injection alternative is somewhat unique to the Texas market. This procedure involves mechanically forcing rods into the ground then injection of water under high pressure to mechanically fracture the soil. Water in the fractures is then absorbed by the clay. Multiple passes of water injection are then performed for both lateral and vertical coverage.

The rods are typically spaced at approximate 1.5-meter intervals and are forced into the ground at approximate 0.3 to 0.45 meter between injections. Each pass is offset approximately 0.75 meter orthogonally from the previous pass. The typical depth of injection has historically been 2.5 to 3 meters; however, recent improvements in the available pressures have allowed successful injection to depths of 9 meters. A photograph of a typical injection rig is provided on Figure 1.

The alternatives discussed above are effective in reducing post-construction movement to a ground-supported slab when applied in the appropriate geologic setting. However, for large industrial structures greater than approximately 40,000 square meters, each of these procedures can be cost- and/or time-prohibitive.
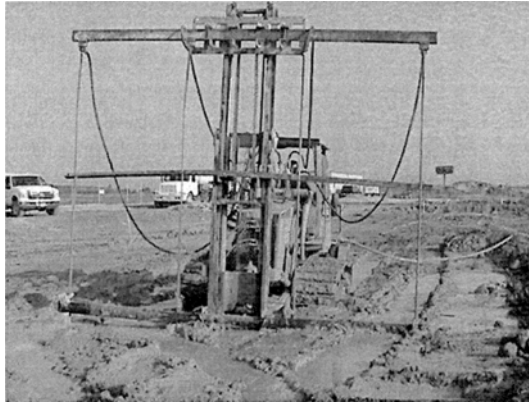
Figure 1.   Typical water injection rig used in DFW area.

Observation of ground-supported industrial office/warehouse floors within the Dallas/Fort Worth area that are not performing to an acceptable level typically finds differential movement along the building perimeter. Movement is attributed to moisture-induced heave and/or vegetation-induced drying and settlement. Instances of movement associated with a change in the ground water level have occurred. This type of movement is limited to specific geologic environments and is not addressed in this paper.

Limiting vegetation-induced drying and settlement is addressed by landscape design and/or root barriers. Moisture-induced heave, on the other hand, is associated with migration of a wetting front from the building perimeter into the drier soils in the interior of the structure. Preswelling the clay below the building has been effective in reducing this type of movement; however, preswelling all of the soil below a large structure is costly and time consuming. Thus, construction of some type of soil barrier is a logical alternative.

Other types of barriers have been in use within expansive soils for over 25+ years. The use of geomembranes to isolate roadway pavements has been extensively reported by Steinberg (2000).

Alternative Design Procedure
        An alternative procedure has been used by the author on large industrial structures within the Dallas/Fort Worth area for approximately four years. The procedure consists of extensively treating a strip of soil along the building perimeter (the "picture frame"). Treatment reduces the potential for movement within the zone of influence by preswelling the expansive soils and forms an isolation dam to limit the availability of moisture to interior expansive soils. Preswelling soils along the building perimeter reduces the rate of movement of the wetting front, effectively isolating the interior clay from moisture gain.

Appropriate geologic conditions should exist for application of the procedure. This alternative has been applied in profiles where expansive clay or weathered shale overlie unweathered bedrock and where thin alluvial deposits overlie weathered grading to unweathered shale. It is anticipated this alternative would not be effective where ground water is present which could influence hydration of clay isolated within the building interior.

Analysis of the effectiveness of the procedure was performed by evaluating the long-term building performance in expansive profiles where movement of the wetting front progressed inward from the building perimeter. A typical profile is shown in Figure 2. This profile developed over an approximate 28-year time frame.
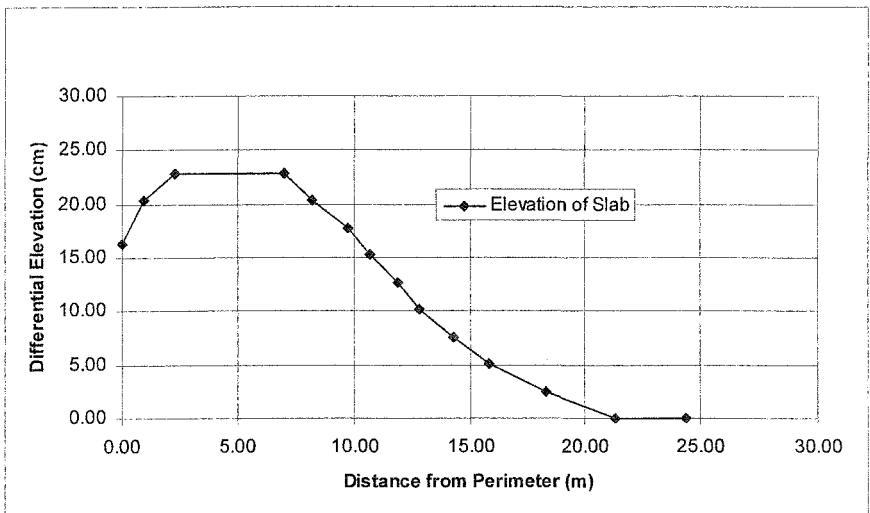
Figure 2. Typical pattern of differential movement of ground-supported floor slab where wetting front advances from building exterior to interior.

Case History

The design procedure was applied to a 59,130-sq. m. warehouse/distribution center (plan dimensions of 146 m. by 404 m.) located in Dallas within the Cretaceous Eagle Ford Shale. Subsurface conditions consisted of 2-1/2 meters of alluvial clay over highly plastic (CH) residual clay overlying dark gray shale. The top of unweathered shale was located at depths of 2 to approximately 7 meters below initial grades. A typical geologic profile with associated laboratory information is provided in Table 1. Typical absorption pressure-swell tests are shown in Figure 3. Swell tests were performed using the methods described by Johnson and Snethen (1978).

TABLE 1.
VERTICAL SOIL PROFILE AT TYPICAL BORING

Material Description	Depth, m.	Moisture %	Total Suction, kg/m^{2*}	Liquid Limit	Plasticity Index	-200 Sieve, %
Yellowish-Brown Clay w/Some Sand (CH)	0.5 – 1.0	17.2	115225			
	1 – 1.4	17.0	250468	70	50	93
	1.4 – 1.8	18.4	231915			
Yellowish-Brown Clay (CH) (Severely Weathered Shale)	2.75 – 3.0	17.0	198714			
	4.25 – 4.6	19.9	140125	66	45	
	5.8 – 6.0	21.1	118154			
	7.3 – 7.6	16.5	189926			
Dark Gray Shale						

*Total Suction preformed in accordance with ASTM D 5298.

Proposed finished floor resulted in required cut and fill of approximately 4.25 meters each. This resulted in the top of unweathered shale varying from approximately 1.8 meters to 9 meters feet below finished floor.

Potential vertical movements were estimated to vary from 23 to 38 centimeters. This movement was attributed to 7.5 to 12.5 centimeters associated with seasonal moisture changes in the upper 1.8 to 2.5 meters, and 15 to 25.5 centimeters associated with "deep-seated heave".

Alternatives evaluated included excavation and replacement of the upper clay with "select" fill, excavation and recompaction of the clay at elevated moisture and preswelling via injection. Both the mechanical and pressure injection preswelling alternatives included a thin "select" fill or lime-stabilized cap to limit moisture loss during construction.

The alternative "picture frame" procedure was developed to reduce the amount of required remedial earthwork, saving both time and money.
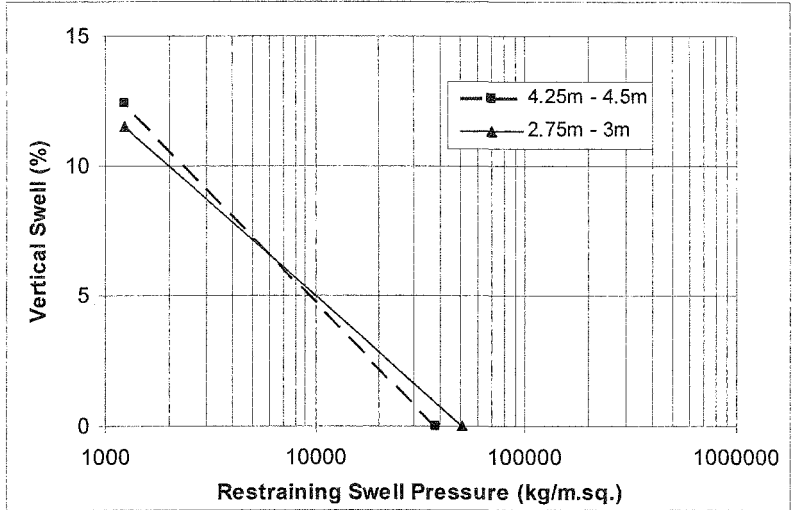
Figure 3.   Typical absorption pressure-swell test result.

Past experience indicated the majority of movement within the area occurred within the outer 9 to 12 meters of the building perimeter.   Based on these observations, a design width of 18 meters was recommended.   The perimeter strip was extended 4.5 meters beyond the foundation on the building exterior to reduce the potential for differential movement of site grade and paving adjacent to the foundation.

The constructed "picture frame" barrier was extended to a depth of 4.5 meters or top of unweathered shale, whichever was less.   A one-meter thick blanket of compacted clay was constructed over the balance of the building pad.   The purpose of the blanket was to provide limited protection against swelling of the upper soil associated with water which could pond adjacent to foundation elements during construction.

Clay blankets and sidewall protection consisting of recompacted clay were also installed along all underground utilities.   Utility line excavations were recompacted for a total width of 3 meters and a minimum of 1.5 meters below the flow line of the utility.   This was done to limit the potential for localized heave if a leak developed within the utility line.   Clay plugs were also constructed at the building perimeter at utility entrances to reduce the potential for water flowing below the structure within pipe bedding soils.

Observation of the building performance indicates no differential movement of the floor slab to date. Although the building is only five years old, performance to date supports the viability of the "picture frame" concept.

Conclusions

An earthwork procedure, designated the "picture frame" alternative, for large structures within expansive soils has been presented. The procedure consists of construction of a recompacted earthen dam along the building perimeter to effectively reduce the availability of water to the interior clay.

For the example provided, an 18-meter wide strip, varying in depth from approximately 2 to 4.5 meters, was constructed around the perimeter of a 59,130 sq. m. building within the Cretaceous Eagle Ford Shale. Based on post-construction visual inspection, no discernible differential movement of the slab has occurred after a five-year period.

References

Johnson, L.D. and Snethen, D.R. (1978). "Prediction of Potential Heave of Swelling Soil." *Geotechnical Testing Journal*, ASTM 1 (3), 117-124.

Steinberg, M. (2000). "Expansive Soils and the Geomembrane Remedy." *Advances in Unsaturated Geotechnics,* ASCE Geotechnical Special Publication No. 99.

Heave at Manufacturing Facility: Observations and Response

Bill Attwooll, Life M. ASCE[1], John Reins, M. ASCE[2], and Phil Lykosh, M. ASCE[2]

[1]Terracon, 301 N. Howes, Fort Collins, Colorado 80521; PH (970) 484-0359; FAX (970) 484-0454; email: wjattwooll@terracon.com
[2]Wiss Janney Elstner Associates, Inc. (WJE), 10881 West Asbury Avenue, Suite 110, Lakewood, Colorado 80226; PH (720) 962-8688; FAX (720) 962-8488; email: jreins@wje.com and plykosh@ wje.com.

Abstract

A manufacturing facility was completed in Loveland, Colorado in early 1993 on the clay shale Pierre Formation. As expansive subsurface materials were identified prior to construction, the facility was founded on drilled shaft foundations with a structurally supported basement underlain by a crawl space. The site was landscaped with bluegrass turf, and there were initially unlined ponds on the up-gradient side of the building.

Significant heave of almost 9 inches occurred under portions of the building within three years of occupancy. Early responses included replacement of damaged concrete masonry unit (CMU) partition walls and other cosmetic repairs. In addition, the ponds were lined, the lawn removed adjacent to portions of the building, and deep dewatering wells installed on the up-gradient side of the building.

Heave and distress continued in spite of these efforts, progressing slowly across the facility, and currently (2005) impact over three-quarters of the building. Maximum heave is almost 12 inches, and over half the building has heaved more than 6 inches. The locus of the maximum rate-of-heave is moving across the building at about 7 feet per year. Repairs have been performed over time as needed. Lateral heave has sheared a number of the 36-inch and 42-inch drilled shafts, which have been repaired by external banding with post-tensioned cables or carbon fiber wrap.

Heave appears to be associated with depths of wetting greater than typically documented in the area. Both construction details and geology appear to have contributed to the heave. Manufacturing has continued uninterrupted with only moderate inconvenience to the building occupants. Interestingly, single-family residences that abut the site have little reported heave damage.

Introduction

The facility was constructed in 1991 and 1992 and occupied in January 1993. Later that year displacements and cracking were observed. It was suspected the distress was caused by heave of the swell-potential materials on which the facility was founded. When a detailed elevation survey was performed in 1995, it was found that a portion of the building had heaved almost 9 inches. The building was resurveyed twice a year for the next three years, and annually since. The most recent survey, almost 12 years after the building was occupied, indicates damaging heave continuing beneath portions of the structure. The purpose of this paper is to describe the site conditions, present the history of movement, a geotechnical evaluation of heave, and the responses taken to mitigate the distress.

Existing Facility

The site is landscaped with trees, shrubs, and a bluegrass lawn. As the facility is in a residential area, to be good neighbors and meet municipality requirements, the building is set well back onto the site. Ponds storing irrigation water are located on the uphill side of the site between the building and the street. The general layout of the site is shown on Figure 1.
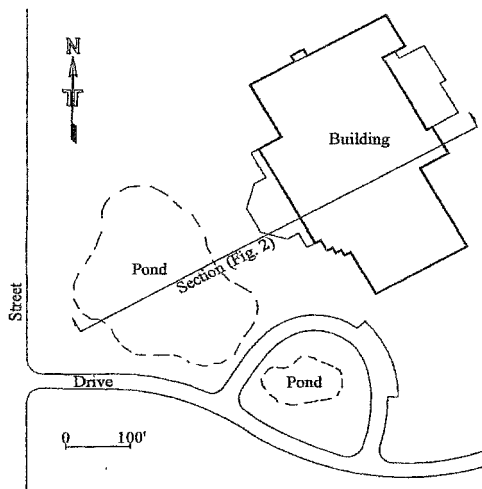
Figure 1: Site Layout

The manufacturing building is basically rectangular with 400-foot by 225-foot plan dimensions and 20-foot column bays. The structure is a single story steel framed masonry veneer building with a 16-foot deep basement. As swell potential was identified before construction, the basement floor is structurally elevated over a crawl

space. The bottom of the crawl space is about 20 feet below the exterior grade. Because of heavy machinery loads, the basement floor framing consists of precast concrete double tee beams with reinforced topping slabs. This construction creates a very stiff structural diaphragm. A schematic cross-section of the building and site is shown on Figure 2.
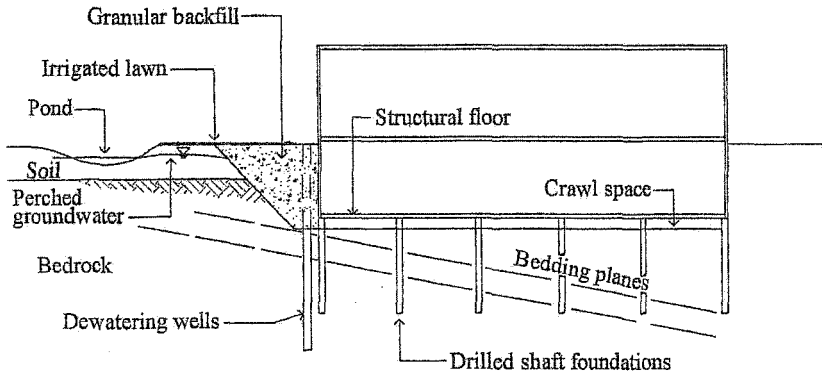
Figure 2: Schematic Cross-Section (Not to Scale)

The exterior basement walls are reinforced concrete and extend to the bottom of the crawl space. Drilled shafts on a 20-foot grid support the basement walls and building columns. Most of the drilled shafts extend about 22 feet below the bottom of the crawl space. Shaft diameters range from 18 inches to 42 inches depending on the magnitude of the load being supported.

Geology and Geotechnical Conditions

The site is located about 1.5 miles east of the foot of the Front Range of the Rocky Mountains in the Colorado Piedmont Section of the Great Plains Physiographic Province. The site is mantled by silty clay eolian and colluvial soils underlain at depths of 8 feet to 14 feet by claystone bedrock of the Lower Pierre Formation (Scott and Cobban, 1986). The upper portions of the bedrock are weathered. The bedrock becomes firmer with depth. The bedrock, which dips to the east at about 12 to 15 degrees, is relatively massive with indistinct bedding planes. The less weathered claystone is hard and blocky with numerous small joints and fractures. There are thin gypsum seams, some of which align with bedding planes. The bedrock is unsaturated in its native condition. The first aquifer is several hundred feet deep. As the site is located above the highest irrigation ditch, the native groundwater regimen was not altered until site development in 1991.

The pre-development borings indicated the claystone bedrock was unsaturated. Degrees of saturation typically ranged from about 90 percent near the top of bedrock to between 75 percent and 85 percent at depths in bedrock greater than 10 feet. The dry density of the bedrock increased from about 115 to 120 pounds per cubic foot

(pcf) in the upper 10 feet to about 125 pcf below. Atterberg Limits tests indicated that the claystone has generally low plasticity, with an average Liquid Limit of 46 percent and average Plasticity Index of 26 percent.

The pre-development geotechnical investigation identified the claystone bedrock as having high to very high swell potential based on a locally used, but non-standard test procedure. Denver swell tests performed during a post-construction distress investigation indicated moderate to high swell potential on samples inundated at about the in-situ overburden pressures (Terracon, 1996). A later distress investigation (SMI, 1998) used a similar test procedure but with samples inundated under a uniform but low confining pressure. The swell pressures indicated moderate to high swell potential. Overall, the swell tests indicated swell potential in the range of 1 to 4 percent. McKeen (1992) presented an alternative method that utilizes soil suction to evaluate swell potential. Filter paper suction tests performed during the Terracon (1996) investigation indicated low to moderate swell potential.

Building Movement

The measured heave represents upward movement of the drilled shaft foundations and not free-field movement of the soils in the crawl space. By the end of 1995, about 7 percent of the basement footprint had heaved 6-inches or more, with a maximum heave of about 9-inches, and about 25 percent of the building footprint had heaved in excess of 2-inches. The greatest heave was within about 60 feet of the southwest building corner, where heave was occurring at a rate of about 2-inches per year. Most of the heave was within about 80 feet of the west basement wall.

By late 2004, about 10 percent of the basement footprint had heaved 10 inches or more with maximum heave of almost 12 inches, 60 percent had heaved at least 6 inches, and the maximum rate of heave was about one inch per year. About fifteen percent of the basement footprint, in the east-central part of the building had not appreciably heaved. The distribution of heave in late 2004 is shown on Figure 3. The area of greatest active heave has been migrating eastward. By 2004 it was located roughly in the center of the building where the rate-of-heave was greater than 0.75 inches per year, as shown on Figure 3. The movement of the crest of active heave is summarized in Table 1.

Heave has been diminishing in the portions of the building that were first impacted. Since 2001, there has been little heave in the southwest portion of the building where the greatest total heave has occurred. Figure 4 shows heave with time for various portions of the building. The top two curves are of columns in the initial heave zone. Columns that had heaved 10 inches by 1998 were grouped, as were columns that had heaved 8 inches to 10 inches. The rate of heave of both column groups has diminished quite uniformly since then. By 1998, the maximum rate-of-heave had migrated to a group of columns north of those included in the first two groups. These columns were grouped as the third curve from the top. Heave of these columns has

Heave rate greater than 3/4"
per year, 2002 - 2004.

0   50'
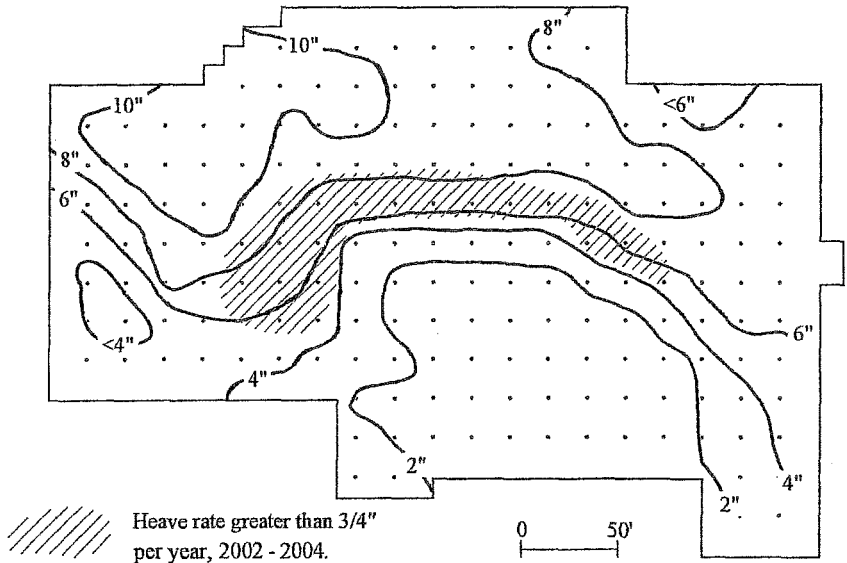
Figure 3: Distribution of Heave in Late 2004

Table 1: Movement of Greatest Active Heave

Year	Heave Crest*	Difference Bays**	Distance Feet	Years	Movement Ft/year
1995	6				
		1 ½	30	4	7.5
1999	7 ½				
		½	10	1	10
2000	8				
		1	20	4	5
2004	9				
Total to date			60	9	**6.67**

*Approximate Column Row on which active heave is centered
** Each bay is 20 feet

also greatly reduced. As the locus of heave has migrated, other groups of columns have become the most active. These were grouped as they were identified, and are represented by the lower three curves. Based on 11 years of data, as the heave has migrated through the building both the amount and rate of heave have diminished. Nevertheless, the ongoing rate of heave is significant and is producing localized distress.
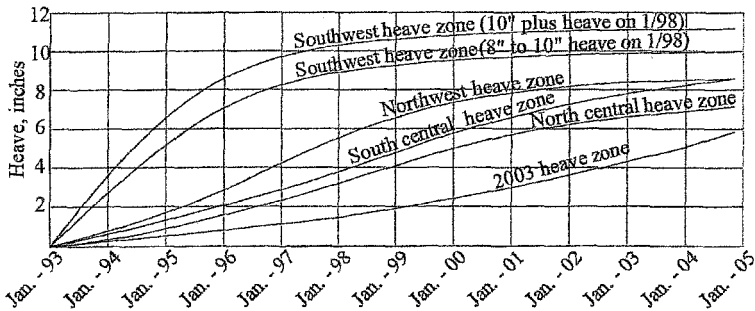
Figure 4: Heave Summary

Distress

Distress within the occupied portions of the building has been primarily in the form of shear cracking of the CMU partition walls, drywall distress and racked door frames. As heave has progressed across the building, damage has occurred to partition walls on the leading edge of the heave "wave." Initially the front of the wave in which the distress was occurring was broad, extending over two or more column bays. Recently, the front of the wave has tightened as the crest of the wave is approaching the relatively stable area on the east side of the structure. This is now concentrating the differential movement essentially in one column bay. Thus, even though the rate and amount of heave is diminishing, the degree of distress has locally intensified.

Another form of distress has been damage to the drilled shafts caused by lateral displacement of the ground as the bedrock has expanded. Although not visible to the building occupants, this has been the most significant structural distress. As the heave wave has moved beneath the building, the heaved bedrock to the west has pushed laterally on the drier bedrock to the east. This has imposed large lateral loads on the drilled shafts that are restrained at the top by the rigid double tee floor diaphragm. At a number of shafts, earth has piled up on the "uphill" side of the shaft and pulled away from the downhill side of the shaft. As a result, at least 10 drilled shafts with diameters as great as 42 inches have sheared at or near the ground line. Relative displacement across the shear cracks has been 2 inches or more. Tension gaps on the down movement side of a drilled shaft are shown on Figure 5, and a concrete column damaged by movement of the supporting drilled shaft is shown on Figure 6. Cracked and repaired drilled shafts are shown in Figures 7 and 8.

Geotechnical Evaluation of Heave

The data obtained have been evaluated in an attempt to understand why the heave is occurring, and to predict its likely extent. In the Front Range of
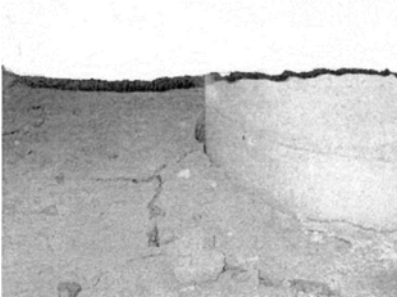
Figure 5: Tension Gaps due to Lateral Heave

Figure 6: Damaged Column due to Lateral Heave.
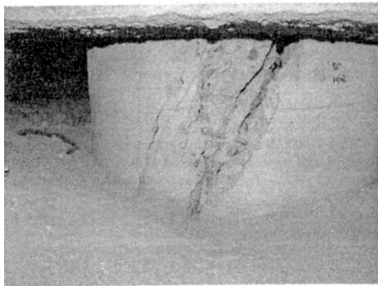
Figure 7: Cracked Drilled Shaft
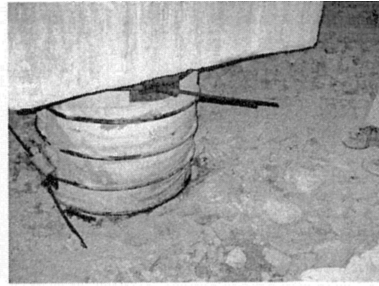
Figure 8: Repaired Shaft

Colorado, where there is much structural distress as a result of heave of surficial clays and bedrock with swell potential, there are ongoing discussions with respect to depth of wetting, as the amount and rate of heave can often be correlated to the depth to which wetting occurs (CAGE, 1999, Nelson, Overton and Durkee, 2001).

We have compared the subsurface moisture content distributions before site development to data from the post-distress investigations. Borings were drilled and piezometers established at various locations on the site, including the irrigated lawn between the pond and the west side of the building, and inside the building in areas with and without heaving. Two substantially different subsurface moisture conditions were found. The moisture content distributions for the exterior borings up gradient of the building are shown on Figure 9. The data indicate a modest increase in moisture content to a depth of wetting in 1998 of about 25 feet. This is within the observed range for a 5-year old facility (CAGE, 1996, CAGE, 1999).

Not included in Figure 9 were data from two borings next to the pond with elevated moisture contents in the upper 10 feet of the bedrock due to seepage from the then unlined pond. Heave estimates based on the moisture content increase and the depth

of wetting in the lawn area are modest. As similar estimates could apply to the single-family residences that abut the site, this is consistent with the absence of significant damaging heave to these residences.

Figure 10 shows the moisture content distribution below the building footprint obtained in 1996. Boring I-1 was drilled in the basement at the location of the then greatest heave of almost 9 inches. Boring I-2 was in a location that had heaved about 2 inches at that time. The third line is of data from two interior borings at locations then unaffected by heave. At the location of almost 9 inches heave (Boring I-1), the moisture content is elevated to a depth of about 40 feet below the bottom of the crawl space, or about 60 feet below the ground surface. At the location of about 2 inches heave, the moisture content was elevated to about 15 feet below the crawl space.
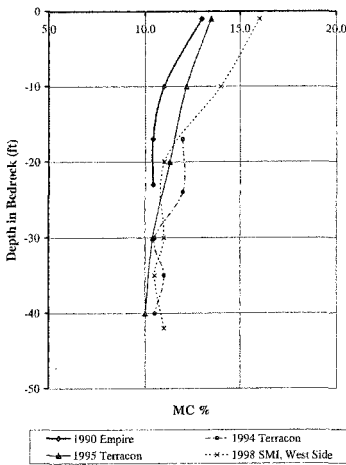
Figure 9: Upgradient Subsurface Moisture Distribution
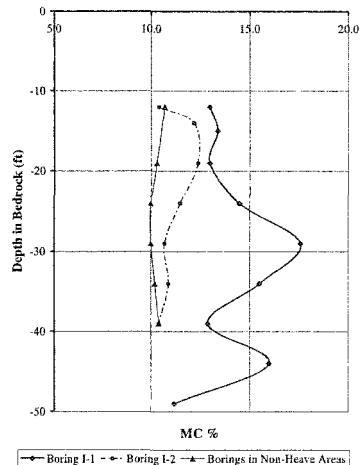
Figure 10: Subsurface Moisture Distribution under Building

The depth of wetting three years after building completion of 40 feet below the crawl space (60 feet below the ground surface), combined with the three-year heave of almost 9 inches is remarkable. Building construction was studied to better understand why this rapid moisture penetration occurred. For constructability reasons, the basement excavation extended about 10 feet beyond the basement walls and had a back slope of about one horizontal to one vertical (1H:1V). Thus, the top of the basement excavation was about 30 feet from the building line. As shown on Figure 2, this large excavation was backfilled with river-run sand and gravel (except for a thin clay cap at the top for landscaping purposes). The very pervious sand and gravel allowed infiltrating water to promptly flow to the bottom of the excavated zone, as demonstrated by wet conditions in the crawl space around the perimeter walls in particular on the west, upgradient, side of the building.

The piezometers in the lawn between the building and the pond indicated that a perched groundwater table developed on top of the weathered bedrock. The perched groundwater was "mounded", with flow to the pond on the west and towards the building to the east where it was intercepted by the sand and gravel. Infiltration over the sand and gravel was also being intercepted, as was water seeping from more pervious bedrock zones.

A review of the construction plans showed that on the west side of the building, the perimeter subsurface drains were not established at the bottom of the backfill zone. Rather they began above the bottom of the basement wall at the center of the building and sloped to sumps at the east side of the building. The perimeter drains do not pass below the bottom of the basement until some distance east along the north and south walls. In addition, the drains beyond that point were not functioning since no water was flowing into the discharge sumps. Thus, the large sand and gravel backfill bowl was acting as a water collector on the west side of the building that was not draining except where water flowed under the voided basement wall into the crawl space. In 1996, an interior drain system was installed to intercept this water, which was only a small part of the total infiltration as determined by a water balance study.

The building maintenance staff maintained excellent records of many building functions. For example, there were records of the quantity of irrigation water pumped from the ponds and of pond water levels. In addition, an official Loveland weather station with precipitation and evaporation data was close to the site. Using the on-site and weather data, the seepage rate from the pond and infiltration rate from lawn irrigation were estimated. On an annual basis, there was greater seepage from the pond, but growing season irrigation infiltration was also substantial. The resulting water budget allowed an estimate of the amount of water seeping under the structure, and a comparison with the amount of water removed from the dewatering wells and interior drains.

Another factor in the deep, rapid wetting was the character of the bedrock. The upper 5 feet to 10 feet of the claystone bedrock had weathered to a soil-like consistency. The weathering and subsequent wetting healed the joints creating a low permeability zone that supported the perched groundwater. The 20-foot deep excavation to the bottom of the crawl space removed the weathered bedrock, exposing the hard, fractured bedrock with the gypsum seams that can be seen in the crawl space. Thus, the sand and gravel introduced the infiltrating water directly into the hard bedrock with joint and gypsum seam permeability. Also, the stress relief of the 20-foot deep excavation of about 1 ton per square foot (tsf) may have allowed the natural joints and fractures to open slightly and accept the water more freely (Terracon, 1996).

The heave potential was evaluated analytically. In addition, the actual amount of heave provided a method to evaluate the original heave potential of the underlying materials. Foundation heave of about 12 inches with a depth of wetting of 35 feet to 40 feet indicates an average vertical heave in the wetted zone of about 2 to 3 percent, which is consistent with the swell test data.

The rapid deep wetting of the subsurface materials also explains the early absence of noticeable differential pier heave in the crawl space and voids remaining intact below the basement walls. As the depth of wetting extended well below the base of the drilled shafts, it appears that much of the drilled shaft heave occurred because the ground in which the shafts were embedded heaved. In recent years, there has been localized free-field heave in the crawlspace of several inches relative to the pier caps that is in addition to the deep heave that has lifted the piers.

Response to Heave

Based on subsurface investigations and discussions with the Owner, the structural consultants, WJE, prepared a mitigation plan that included both structural modifications to mitigate the internal building distress and site modifications to minimize water infiltration below the structure. Structural responses include:

- Replacing damaged CMU bearing walls with drywall and a slip joint detail to accommodate additional movement.
- As the distress progressed through the building and drilled shafts sheared due to lateral heave, WJE developed a method to repair the shafts, as shown on Figure 8.
- Significant shear cracks in certain columns supported on the pier caps have prompted additional repairs.

Site modifications included:

- Lining the pond.
- Removing the bluegrass and lawn irrigation within 30 feet of the building and replacing with xeriscape with minimal drip irrigation.
- Better control of and reduction of lawn irrigation.
- Installing a row of deep dewatering wells near the southwest corner of the building.
- Installing an interior drain system to remove water seeping under the basement wall.
- Installing water meters on the dewatering well and interior drain system discharge lines.

Predicted Heave

Once the extent of heave was discovered early in the life of the building, the Owner was anxious to know how much more the building would heave, since there were considerable costs associated with evaluating the problem and implementing the mitigation plan. This information was necessary to develop a management/maintenance plan to allow the building to continue to function despite the ongoing heave and needed repairs.

Terracon (1996) used traditional Denver methods and McKeeen's Method (McKeen, 1992) to evaluate heave potential. They also back calculated the heave potential based on the depth of wetting. These methods resulted in ambiguous future heave predictions. Therefore, a simple expedient was used. The survey data available at that time (see Figure 4) was extrapolated using a parabolic curve, indicating a likely maximum heave of about 12 inches.

Two years later, SMI (1998) estimated future heave using curve fitting techniques and analytical procedures outlined in Nelson and Miller (1992). They concluded that general pier movement would be about 15 inches, with an accuracy of about 5 inches, or a reasonable estimate of pier movement of from 10 to 20 inches.

By late 2004 maximum pier heave was almost 12 inches, with heave continuing in that location at the diminishing rate of about 0.05 inches per year. About 90 percent of the drilled shafts had heaved less than 10 inches.

Response to On-Going Movement

The response to the on-going movement has been periodic inspection and repairs, as needed. The Owner has shown admirable patience in coping with the slow heave wave propagating through the building. After 12 years, the locus of heave is only about half way through the building, suggesting they will be dealing with the problem for many years to come.

As heave continued, measures to mitigate the on-going heave have been considered. For example, in 1996 the possibility of flooding the crawl space to accelerate the heave was suggested. However, because of concerns of unknown risks and possibly greater localized distress than would otherwise occur over the life of the facility, flooding was not implemented at that time. As heave and distress have progressed, this option has been considered more seriously. Recent discussions have not been to flood the crawl space with standing water, as this would disrupt access to needed equipment. Rather, water could be introduced through slotted distributor pipes installed between the columns, or some other means. A supplier has proposed adding proprietary solutes to the infiltrating water to reduce the amount of resulting heave. As of yet, these proposals have not been implemented.

Conclusions

After 12 years, a manufacturing building in Loveland, Colorado has heaved differentially about 12 inches. Distress continues as a heave wave moves slowly across the building. The heave is the result of infiltrating moisture deeply wetting the underlying claystone bedrock that has moderate heave potential. Distress is being periodically repaired to maintain the building in a safe and operational condition.

References

Colorado Association of Geotechnical Engineers (CAGE) (1996). *Guideline for Slab Performance Risk Evaluation and Residential Basement Floor System Recommendations (Denver Metropolitan Area).*

CAGE (1999). *Drilled Pier Design Criteria for Lightly Loaded Structures in the Denver Metropolitan Area.*

McKeen, R. G. (1992). "A Model for Predicting Expansive Soil Behavior." Proc. 7th International Conference on Expansive Soils, ASCE & ISSMFE, Dallas, Texas.

Nelson, J. D. and Miller, D. J. (1992). *Expansive Soils: Problems and Practice in Foundation and Pavement Engineering,* Wiley, New York.

Nelson, J. D., Overton, D. D. and Durkee, D. B. (2001). "Depth of Wetting and the Active Zone." Expansive Clay Soils and Vegetative Influence on Shallow Foundations, ASCE Geotechnical Special Publication #115.

Scott, G. R. and Cobban, W. A. (1986). "Geologic, Biostratigraphic, and Structure Map of the Pierre Shale between Loveland and Round Butte, Colorado" U.S. Geological Survey Map I-1700.

Shepherd Miller, Inc. (SMI) (1998).   Geotechnical Investigation, Loveland Manufacturing Facility.

Terracon (1996). Geotechnical Engineering Report, Loveland Manufacturing Facility.

EQUILIBRIUM MOISTURE PROFILES AND GROUND HEAVE IN SWELLING SOILS

Jagath C. Ekanayake[1] and Mark S. Abshire, MS, PE[2]

[1]Landcare Research, P.O. Box. 69, Gerald Street, Lincoln, New Zealand, PH 3 325-6701; email: Ekanayakej@landcareresearch.co.nz

[2]MFG, Inc., Four Corners Regional Office, 1265 Ludwig Drive, Bayfield, Colorado, 81122, USA, PH 970-884-7431;
email: mark.abshire@mfgenv.com

ABSTRACT

The application of conventional non-swelling soil hydrology to predict wetting depths of submerged swelling soil suggests that equilibrium will only be achieved with moisture profiles having constant saturated moisture content throughout the entire depth. Considerable disparity has been observed between the wetting depths predicted by the conventional approach and equilibrium moisture conditions that have been empirically observed in swelling soil profiles many years after construction is complete. This paper uses well established water retention and volume change properties to introduce the mechanisms governing equilibrium moisture profiles in swelling soils as compared to non-swelling soils. The effort extends the work of previous researchers which has shown that the effect of overburden pressure on the volume change of swelling soils produces equilibrium moisture profiles entirely different from those predicted for non-swelling soil. It is shown that soil can be at equilibrium in both saturated and unsaturated states to great depths. Examples of equilibrium moisture profiles and ground heave in swelling soils are worked out using existing data to highlight the consequences of using non-swelling soil theory to analyse swelling soil hydrology.

1.0   INTRODUCTION

Despite advances in unsaturated soil geotechnics in the past 50 years, damages to structures, pavements and infrastructure caused by swelling soils continue to inflict heavy financial losses to the construction industry. Heave prediction methods commonly used in practice today include oedometer and soil suction methods. Both methods produce similar heave predictions when the same wetting depth is assumed (Abshire, 2003). It is becoming increasingly common to estimate wetting depths for both oedometer and soil suction heave prediction methods by evaluating the moisture profiles closer to equilibrium conditions based on soil water potential (suction) data. Therefore, interpretation of suction data and accurate estimation of equilibrium moisture profiles are critical for reliable heave prediction.

The volume change property of swelling soils makes the hydrostatics and hydrodynamics of swelling soils very different than those of non-swelling soils. One fundamental difference between the two types of soils is that the soil above the water table in swelling soil is wetter [has a higher water content] than soils below the water table (Philip, 1969; Talsma, 1977). In swelling soils, an additional soil water potential component known as the overburden potential component arises due to volume change against the overburden pressure (Coleman and Croney, 1952; Philip, 1969). This potential component usually makes the matric potential (soil suction) less negative.

2.0   LITERATURE REVIEW

2.1   Volume Change Properties of Swelling Soils

Because the soil geometry of swelling soils changes with the water content, it is advantages to use void ratio as a function of *moisture ratio*, $\vartheta = V_w/V_s$, rather than volumetric water content, to describe the hydrology and volume change behavior of swelling soils. Under a constant overburden pressure, soil volume changes take place from saturation to oven dry along the shrinkage curve, $e(\vartheta)$, in three different phases as shown in Fig. 1. They are called "normal", "residual and "zero" shrinkage phases. The three volume change phases are summarized in Table 1.
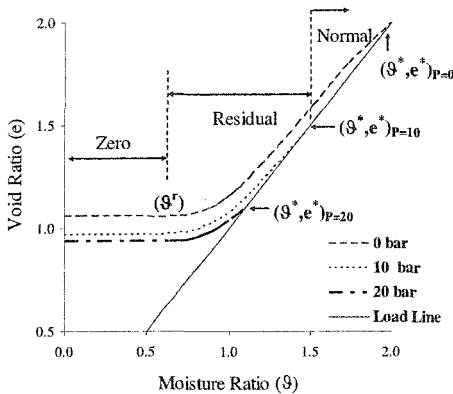
Figure 1   The shrinkage diagram ($e - \vartheta - P$) is a collection of shrinkage curves for a series of overburden pressures, Groenevelt & Bolt (1972).

Table 1   **Summary of Shrinkage Phases**

Phase	Condition	Range	Property
Normal	$e = \vartheta$, $de/d\vartheta = 1$	$\vartheta > \vartheta^*$	Total volume change = water volume change
Residual	$e > \vartheta$, $de/d\vartheta < 1$	$\vartheta^r < \vartheta < \vartheta^*$	Total volume change < water volume change
Zero	$e = constant$, $de/d\vartheta = 0$	$\vartheta^r > \vartheta$	Total volume change = 0 Water volume change > 0

A family of shrinkage curves for a series of overburden pressures is shown in the shrinkage diagram on Fig. 1. Air entry points for the three shrinkage curves for overburden pressures 0, 10, and 20 bars are shown by $(\vartheta^*, e^*)_0$, $(\vartheta^*, e^*)_{10}$, and $(\vartheta^*, e^*)_{20}$. The saturation line, where normal phases of all the shrinkage lines lie, is called the load surface ($e = \vartheta$, $de/d\vartheta = 1$). The soil volume change characteristics associated with the shape of the shrinkage diagram are well established (Philip, 1969; Talsma, 1977; Olsen and Haugen, 1998).

2.2   Overburden Potential and Equilibrium Moisture Profiles

Using the additional overburden potential component, Ω arises due to volume change properties of swelling soils, Philip (1969) used Eq.1, to describe three types of equilibrium moisture profiles in a swelling soil column.

$$\Phi = h_0 + \Omega - z \quad \text{Eq} - 1 \; ; \Omega = \alpha \left(P(0) + \int_0^z \gamma dz \right) \quad \text{Eq} - 2 \; ; \; \alpha = \frac{1}{P} \int_{P=0}^{P=P} \left[\frac{\partial e}{\partial \vartheta} \right]_P dP \quad \text{Eq} - 3$$

In Eq. 1, h_0 is the matric potential of an unloaded swelling soil and z is the soil depth. Ω is the overburden potential component given by Eq. 2, where α is called the load factor given by Eq. 3, γ is the wet relative density (Groenevelt and Bolt, 1972), and P is the overburden pressure (pressures and all potentials components are given in head equivalent units). Ekanayake and Painter (1995) showed that equilibrium moisture profiles in swelling soils are quite different than moisture profiles predicted by Philip (1969). Since only the volume change properties of the shrinkage diagram in Fig. 1 were used to derive Eqs. 2 & 3 without the water retention properties, predictability of the behavior of equilibrium moisture profiles was limited.

3.0   THEORY

The theoretical development of equilibrium moisture profiles presented in this paper is described using the moisture gradients derived across soil elements from the total potential gradients. The total potential gradient was determined using both water retention and volume change characteristics of swelling soils. The total soil water potential is the sum of the matric and gravitational potential components (assuming uniform ionic concentration in soil water).

3.1   Matric Potential and Water Retention Properties

The matric potential of non-swelling soils is independent of overburden pressure. Therefore a single water retention curve is sufficient to characterize the status of the soil water of an ideal non-swelling soil matrix. (Groenevelt and Bolt, 1972). On the other hand, the overburden potential component, Ω, arises due to volume change against overburden pressure, and is a component of the matric potential of swelling soils. The increase in the hanging water column height required to bring the system to equilibrium at the same moisture ratio after the removal of the overburden pressure, P_n, in Fig. 2(a,b) is called the overburden potential component, and is given by Eq. 4. The load factor α_n is given by Eq. 5 (Groenevelt and Bolt, 1972 and Yong, 1999).

$$\Omega_n = \alpha_n P_n = (h_n - h_0) \quad \text{Eq} - 4; \; \alpha_n = \frac{(h_n - h_0)}{P_n} \quad \text{Eq} - 5 \; ; h_n = h_0 + \Omega_n \quad \text{Eq} - 6$$

The matric potential, h_n, for the illustrations in Figs. 2 and 3 is given by Eq. 6, where h_0 is the matric potential of swelling soil under no overburden pressure.
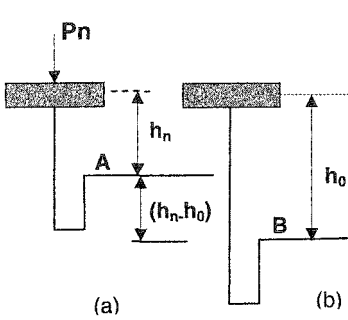
Figure-2
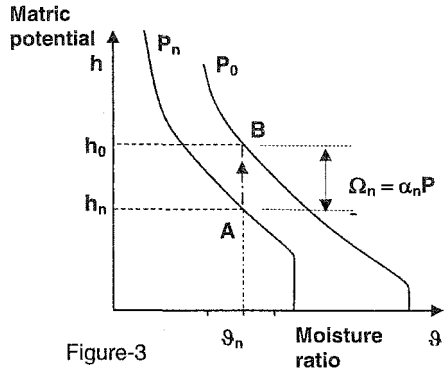
Figure-3

Figure 2 (a) A swelling soil sample under overburden pressure, P_n is in equilibrium with a hanging water column, h_n. **(b)** Soil sample is under equilibrium with h_0 hanging water column with no load.

Figure 3 Water retention curves corresponding to loaded (P_n) and unloaded (P_0) swelling soil

3.2   Multiple Water Retention Curves for Swelling Soils

According the illustration in Figs. 2 a,b, Fig. 3, and Eq. 6 (Groenevelt and Bolt (1972), a family of water retention curves can be produced for a series of overburden pressures $P_0, P_1 \ldots P_n$.
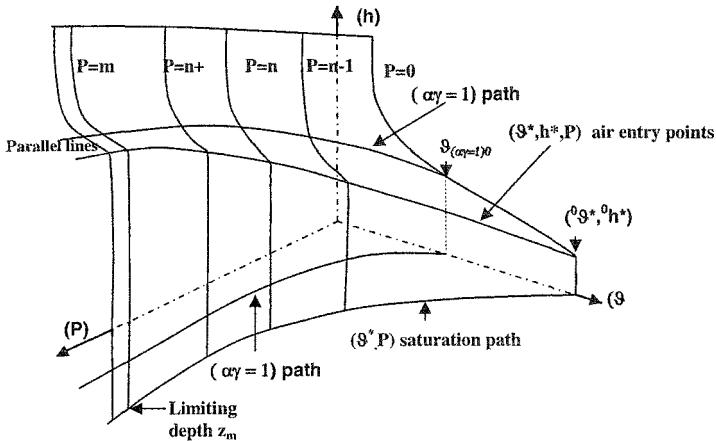
Figure 4   Idealized diagram of Matric potential (h), moisture ratio (ϑ), and overburden pressure (P). See **4.3** for more details.

The idealized water retention curve diagram, $h(\vartheta, P)$, shown in Fig. 4 is constructed according to Groenevelt and Bolt (1972). The potential swelling pressure, P_m, is balanced by the overburden pressure, P, at large depths, z_m. All water retention curves for $P > P_m$ converge to a single water retention curve where its shape $(dh/d\vartheta)$ remains unchanged. Below this point, swelling soils behave identical to non-swelling soils. The moisture ratio and void ratio, (ϑ^*, e^*), at the air entry points decrease with the overburden pressure while matric potential at the air entry point is increasing. Air entry and $\vartheta(\alpha\gamma=1)$ paths (see 4.3) are marked on the $h(\vartheta,P)$ surface. $d\vartheta/dz < 0$ for $\vartheta > \vartheta(\alpha\gamma=1)$, $d\vartheta/dz > 0$ for $\vartheta < \vartheta(\alpha\gamma=1)$ and $d\vartheta/dz = 0$ for $\vartheta = \vartheta(\alpha\gamma=1)$.

4.0   MOISTURE GRADIENTS AT EQUILIBRIUM

4.1   Moisture Gradient in Non-Swelling Soils

At equilibrium, the total soil water potential, Φ, of a non-swelling soil given by Eq.7 is constant relative to the depth. Therefore, $d\Phi/dz = 0$.

$$\Phi = h - z \quad \text{Eq} - 7; \qquad \frac{dh}{d\vartheta} = \frac{dz}{d\vartheta} \qquad \text{Eq} - 8$$

Since the soil geometry of non-swelling soil does not change with the overburden pressure, the moisture path direction $(dz/d\vartheta)$ at equilibrium follows the shape of a single water retention curve (either desorption or absorption) according to Eq-8 and Fig-5(a) $((\Delta h = h_n - h_{n+1}) = (z_n - z_{n+1})$ for $(\vartheta_n - \vartheta_{n+1}))$. On the air entry path (capillary fringe) in non-swelling soils,

$$dh/dz = 1 \quad \text{and} \quad \vartheta = \vartheta^*. \qquad\qquad \text{Eq-9}$$
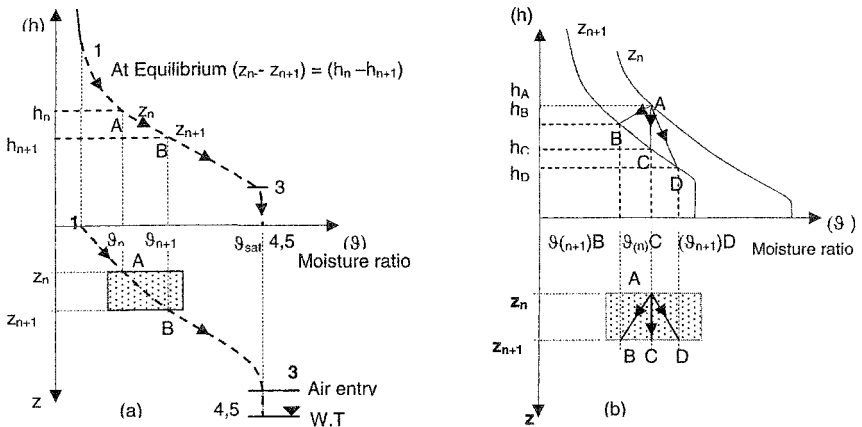
Figure 5   Single water retention curve for non-swelling soils (a) and for two water retention curves (b) for swelling soil for equivalent soil depths, z_n and z_{n+1}.

4.2   Moisture Gradient in Swelling Soils

Since the total potential of soil water, Φ, is constant relative to soil depth at equilibrium, Eq. 10 is obtained from the derivative of Eq. 1 with respect to z:

$$\frac{d\Phi}{dz} = \frac{dh}{dz} - 1 = 0, \qquad \frac{dh}{d\vartheta} = \frac{dz}{d\vartheta} \qquad \qquad \textbf{Eq-10}$$

The matric potential, h, in Eq. 10 now includes the overburden potential component, Ω, as given by Eq. 2. Conditions given in Table-3 and Fig. 5b suggest that the moisture path could take three different directions in order to satisfy the equilibrium condition given in Eq. 10.

Table 2   Options to Satisfy the Equilibrium Moisture Paths in Swelling Soils

Option		Condition	Equation
From [A] to [D]	$\Delta Z = [h_D - h_A]$	$d\vartheta/dz > 0$	**Eq-11**
From [A] to [B]	$\Delta Z = [h_D - h_A]$	$d\vartheta/dz > 0$	**Eq-12**
From [A] to [C]	$\Delta Z = [h_C - h_A]$	$d\vartheta/dz < 0$	**Eq-13**

Evaluation of $d\vartheta/dz$ across soil elements in a vertical soil column enables us to trace the equilibrium moisture profiles in a vertical soil column. From Eq. 1 and Eq. 2, the total potential of soil water of a thin soil slab in a vertical swelling at soil depth equivalent to overburden pressure, P_n is given by

$$\Phi = h_0(\vartheta) + \alpha_n(\vartheta, P_n) \left[P_n + \int_{z_n}^{z_{n+1}} \gamma_n(\vartheta, P_n) dz \right] - z \qquad \textbf{Eq-14}$$

where h_0 is the matric potential of an unloaded swelling soil at moisture ratio ϑ, and $\alpha_n(\vartheta, P_n)$ and $\gamma_n(\vartheta, P_n)$ are the load factor and wet relative density determined for overburden pressure P_n, respectively, and z is the gravitational potential component measured positive upward. The moisture gradient across the soil slab at overburden pressure P_n can be written (Ekanayake & Painter, 1995) as

$$\left(\frac{d\vartheta}{dz} \right)_n = \left[\frac{1 - \alpha_n \gamma_n}{\dfrac{dh}{d\vartheta} + \dfrac{d\alpha_n}{d\vartheta} \left(P_n + \int_{z_n}^{z_{n+1}} \gamma_n dz \right)} \right] = M_n(\vartheta). \qquad \textbf{Eq-15}$$

Philip (1969) and Ekanayake and Painter (1995) showed that the behavior of the moisture gradient ($d\vartheta/dz$) defined by Eq. 15 is determined by $(1 - \alpha_n \gamma_n)$.

4.3   The Behavior of $(1-\alpha_n\gamma_n)$

The wet relative density is given by Eq-16, where G_s is the particle specific gravity.

$$\gamma_n(\vartheta, P_n) = \frac{(\vartheta + G_s)}{1 + e_n(\vartheta)}$$ **Eq-16**

There exists a series of moisture ratios $(\vartheta_{(\alpha\gamma=1)0}, \ .... \ \vartheta_{(\alpha\gamma=1)n-1}, \ \vartheta_{(\alpha\gamma=1)n})$ satisfying the condition $\alpha_n\gamma_{n\,=\,1}$ on each water retention curve for overburden pressures from 0 to P_n (Phillip, 1969). The path satisfying the $\alpha_n\gamma_{n\,=\,1}$ condition is shown on the $P(\vartheta)$ plane and the $h(\vartheta, P)$ surface in Fig. 4.

4.4   Conditions Governing the Equilibrium Moisture Paths in Swelling Soils.

The equilibrium moisture distribution in a vertical swelling soil column is determined by either one or multiple combinations of five conditions defined for $d\vartheta/dz$. These conditions are summarized in Fig. 6 and Table. 3. Note that the first three conditions are derived from the function $(1- \alpha_n\gamma_n)$, which are directly related to conditions explained by Eq.s 11, 12 and 13.
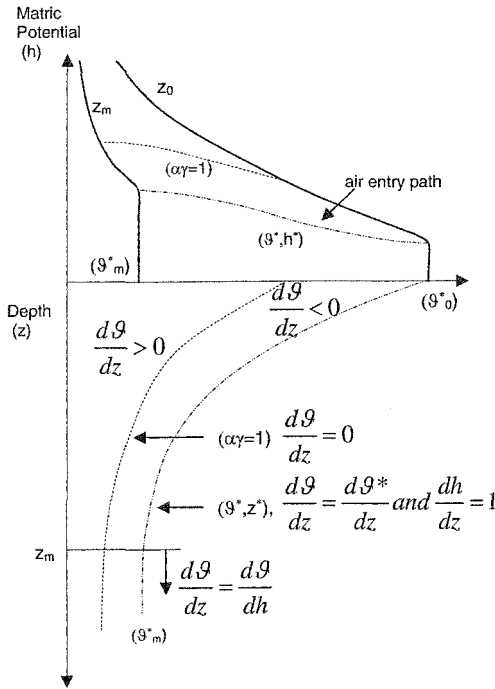
Figure 6   The controlling conditions of equilibrium moisture profiles in swelling soils on the (ϑ, z) and (ϑ, h) planes.

Table 3   **Conditions Controlling the Behaviour of Equilibrium Moisture Profiles in Swelling Soils.**

Condition No	Boundary	Condition
C1	$0 < \vartheta < \vartheta_{(\alpha\gamma=1)}$ $\alpha\gamma < 1$	$\dfrac{d\vartheta}{dz} > 0$
C2	$\vartheta > \vartheta_{(\alpha\gamma=1)}$ $\alpha\gamma > 1$	$\dfrac{d\vartheta}{dz} < 0$
C3	$\vartheta = \vartheta_{(\alpha\gamma=1)}$ $\alpha\gamma = 1$	$\dfrac{d\vartheta}{dz} = 0$
C4	On the air entry path and in the capillary zone	$\dfrac{dh}{dz} = 1, \dfrac{d\vartheta}{dz} = \dfrac{d\vartheta^*}{dz}$
C5	$z > z_m$ After limiting depth	$\dfrac{d\vartheta}{dh} = \dfrac{d\vartheta}{dz}$

5.0   IDEALIZED EQUILIBRIUM MOISTURE PROFILES

The following labeling procedure is used in our illustrations to indicate points where the equilibrium moisture profile intersects the ground surface, air entry point path, (ϑ^*, z^*), and $(\alpha\gamma - 1) = 0$ path: [1] Starting point of the moisture profile at the ground surface; [2] $\vartheta_{\alpha\gamma=1}$ boundary; [3] Air entry path, (ϑ^*, z^*); [4] Water table; and [5] z_m depth where the swelling diminishes. The following symbols are used in our examples to indicate the moisture ratios at different boundaries: ϑ_{10} - surface moisture ratio for unloaded condition; ϑ_{1n} - surface moisture ratio under overburden pressure, P_n; $\vartheta_{(\alpha\gamma=1)0}$ surface moisture ratio where $\alpha\gamma=1$ path reaches the surface (unloaded); and ϑ^*_0 - air entry point moisture ratio at the surface under no load.

5.1   Equilibrium Moisture Profile for Surface Moisture Ratio $\vartheta_{10} < \vartheta_{(\alpha\gamma=1)0}$, P=0

A surface moisture ratio, ϑ_{10}, is selected where $\vartheta_{10} < \vartheta_{(\alpha\gamma = 1)0}$ on the unloaded shrinkage curve Fig. 7. Since $d\vartheta/dz > 0$ for $\vartheta < \vartheta_{(\alpha\gamma=1)0}$ [C1], the moisture profile is beginning to move away from the vertical axis. The direction of the moisture profile changes once it intersects the $\vartheta_{(\alpha\gamma=1)}$ path at point 2. The moisture path then moves towards the vertical axis [C2]. At the air entry point 3, the soil becomes saturated and has a negative matric potential. From here on the moisture profile travels on the air entry path where matric potential increases linearly until it reaches the water table at point 4 .

5.2   Numerical Examples

The equilibrium moisture profiles given in Examples 1 and 2 were constructed using Olsen and Haugen (1999) volume change data obtained for field swelling soils in southern Norway. Soil physical properties for the field soils are given in Table 4. Air entry paths (ϑ^*, z^*) and (ϑ^*, h^*), plotted on the both planes, enable us to find where the soil becomes saturated.
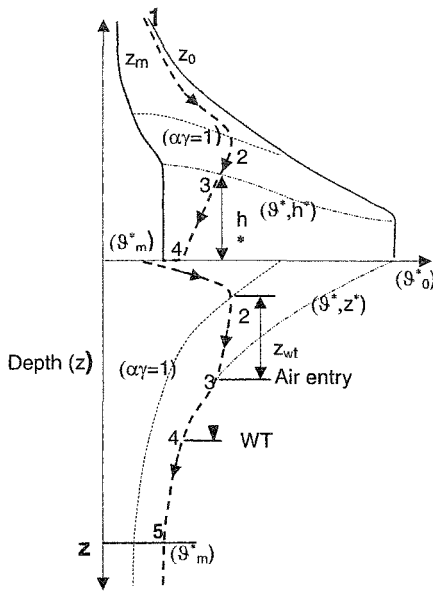
Figure 7   An equilibrium moisture profile for a dry surface condition & $P = 0$.

Table 4   **Soil Data From Olsen and Haugen (1999)**

Particle density (γ_s) g/cm^3	Sand (2-0.06) mm	Silt (0.06 – 0.002) mm	Clay (< 0.002) mm	Organic matter (g C/100g)
2.6	24%	40%	36%	2.2

Example 1 (Fig. 8a,b)

In this example we selected an unloaded surface moisture ratio, $\vartheta_{10} = 0.540$, $\vartheta_{10} < \vartheta_{(\alpha\gamma=1)0}$. Moisture ratio increases towards the $\vartheta_{(\alpha\gamma=1)}$ boundary where it intersects it at point 2: $\vartheta = 0.56 = 3.3$ m and changes the direction of the moisture profile. The moisture ratio decreases with depth where it intersects the air entry path at point 3: $\vartheta = 0.520$, z = 5.45m. Soil now enters the capillary zone, where the soil becomes saturated under capillary tension. Within the capillary zone, the decrease in soil matric potential, ($\Delta h = 800$ cm), is equal to the gravitational potential drop ($\Delta Z = 800$ cm) until the moisture profile reaches the water table at $\vartheta = 0.464$, z = 6.25 m). The gravitational potential drop 800 cm was estimated by projecting the point 3 at the air entry point graphically on to the water retention plane.

Example-2 (Fig. 8c,d)

In this example we selected a surface moisture ratio ($\vartheta = 1.36$) closer to the air entry value corresponding to 100 kPa surface load, $\vartheta_{(\alpha\gamma=1)1} < \vartheta_{11} < \vartheta^*_1$. The water retention curve for 100 kPa is also plotted on the (h,ϑ) plane in order to mark the starting point of the moisture path for the 100kPa loaded surface. Moisture ratio decreases towards the depth (Z) axis where it reaches the air entry path at $\vartheta = 1.28$, Z= 0.6 m. A further gravitational potential drop of 420 cm is sufficient for soil to reach the water table at 1.020 m. Similar moisture profiles given in examples 3 and 4 were observed by Talsma (1977) and Talsma and Lelij (1976).
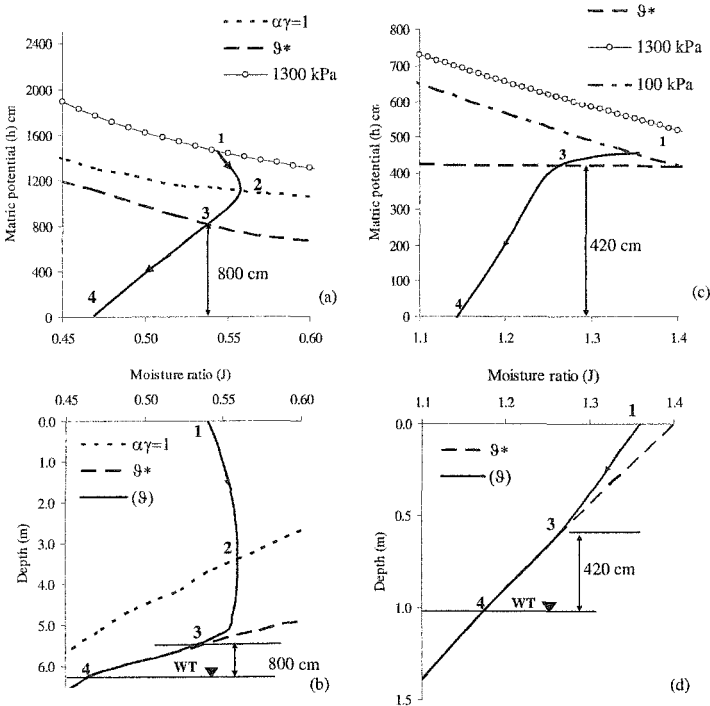
Figure 8 (a,b): Equilibrium moisture profile for conditions given in Example-1. Moisture profile starts at $\vartheta_{10} = 0.54$, point 1 at the surface. (c,d): Equilibrium moisture profile for the conditions given in example-2. This is a special case where the surface is under a overburden pressure 100 kPa.

5.3   Estimation of Soil Depth for Equilibrium Conditions (Ground Heave)

The soil depth for a known surface moisture ratio with the surface overburden pressure at equilibrium is simply given by the ('Y') depth axis of Fig 8 a, b, c, and d. Fig 9 is produced using 17 equilibrium moisture profiles similar to Fig 8 a and b.
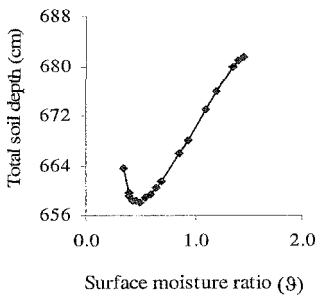
Figure 9   Total soil depths for different surface moisture ratios for different equilibrium moisture profiles.

6.0   CONCLUSIONS

It is noteworthy that a soil profile could be completely unsaturated, partially saturated or completely saturated under equilibrium conditions. Theory and examples presented in this paper and field observations (Talsma, 1977, Talsma and Lelij, 1976) showed that soil above the water table always has a higher water content than soil below the water table in swelling soils at equilibrium. Moisture ratio decreases with the depth below the water table. The application of non-swelling soil theory to swelling soils estimates a constant saturated moisture ratio with depth below the water table. The theoretical interpretation of moisture profiles based entirely on non-swelling soil hydrology predicts moisture profiles with higher water content. A moisture profile with higher water content overestimates the ground heave. Unfortunately, it is more common than not in practice to misinterpret a decreasing moisture profile below the water table as a non-equilibrium condition. The illustration in Fig 2 a, b, and Fig 3 showed that matric potential decreases (become more negative) when unloaded. Therefore, estimating wetting depths in the laboratory using the filter paper suction tests on unloaded soil samples could lead to a false interpretation of the status of the soil water potential in the field. Knowledge of the behavior of the entire equilibrium moisture profile enables a reliable estimation of volume change along the entire soil depth for known field conditions as derived by Eq. 10.

Reversing the Direction of the Wetting Front in Swelling Soils

There is always a possibility that the driving force at the wetting front (total potential gradient) could be reversed when the increase in matric potential is larger than the gravitational potential drop. The wetting front could move vertically upward instead downward if the conditions given in Eq. 17 and Eq. 18 are satisfied. In Eq. 17, although moisture ratio decreases with depth for $\vartheta_A > \vartheta_B$, water begins to flow upward. Talsma (1974) reported upward water movement against the moisture gradient.

$$(h_B - h_A) > (z_B - z_A) \quad and \quad \vartheta_A > \vartheta_B \qquad Eq-17$$
$$(h_D - h_A) > (z_D - z_A) \quad and \quad \vartheta_A < \vartheta_D \qquad Eq-18$$

In Eq. 17, although moisture ratio decreases with depth for $\vartheta_A > \vartheta_B$, water begins to flow upward. Talsma (1974) reported upward water movement against the moisture gradient. This suggests that in swelling soils, the wetting front movement is not only restricted by the overburden potential component which arises due to volume change against the overburden pressures, but also it could be reversed. The theory of conventional non-swelling soil hydrology would never be able to detect such phenomena in swelling soils.

REFERENCES

Abshire, M. S. (2003). Heave Prediction Using Indices Obtained from Oedometer Tests. Proc. 12th Panamerican Conference on Soil Mechanics and Geotechnical Engineering. Massachusetts Institute of Technology, Cambridge, Massachusetts, USA.

Coleman, J. D. and Croney, D. (1952). The Estimation of the Vertical Moisture Distribution With Depth in Unsaturated Cohesive Soils. DSIR Road Research Laboratory Report RN/1709/JDC.DC. March.

Ekanayake, J. C. and Painter, D. J. (1995). Gravitational Equilibrium Moisture Profiles in Swelling Soils. Water Resources Research, Vol. 31, No. 10. October.

Groenvelt, P. H. and Bolt, G. H. (1972). Water Retention in Soil. Soil Science, Vol. 113 (4), pp. 238-245.

Philip, J.R. (1969). Moisture Equilibrium in the Vertical in Swelling Soils 1: Basic Theory. Aust. J. Soil Res., Vol. 7, pp. 99-120.

Talsma, T. (1974). Moisture Profiles in Swelling Soils, Aust. J. Soil Res., Vol. 12, pp71-75.

Talsma, T., and Lelij, A. van der (1976). Infiltration and Water Movement in an In Situ Swelling Soil During Prolonged Ponding. Aust. J. Soil Res., Vol. 14, pp.337-349.

Talsma, T. (1977). A Note on Shrinkage Behaviour of a Clay Paste Under Various Loads. Aust. J. Soil Res., Vol. 15, pp. 275-277.

Van Genuchten, M.T. (1980). A Closed Form Equation for Predicting the Hydraulic Conductivity of Unsaturated Soils. Soil Science Society of America Journal, Vol. (44), pp. 892-898.

Yong R.N. (1999). Overview of Modelling of Clay Microstructure and Interactions for Prediction of Waste Isolation Barrier Performance. Engineering Geology, Vol. (54), pp.83-91.

Youngs, E.G., and Towner, G.D. (1970). Comments on "Hydrostatics and Hydrodynamics in Swelling Soils" by J.R Philip, Water Resorc. Res., Vol. 6(4), pp. 1246-1247.

COMPARISON OF BEAM DEPTHS FOR STIFFENED SLABS ON SHRINK-SWELL SOILS USING WRI, PTI 2004 AND AS 2870

Remon Abdelmalak[1], Jean-Louis Briaud[2]

1. Graduate Students, Dept. of Civil Engineering, Texas A&M University, College Station, Texas 77843-3136. (remon@neo.tamu.edu)
2. Professor and Holder of the Buchanan Chair, Dept of Civil Engineering (Geotechnical), Texas A&M University, College Station, Texas 77843-3136 (briaud@tamu.edu)

ABSTRACT : The most common foundation for light structures founded on shrink-swell soils is the stiffened slab on grade. The beam depth is an intrinsic design parameter for this type of foundation, it usually ranges between 0.6 and 1.2 m with common beam spacing of 3 to 6 m placed in both directions. The following methods are among the most common methods used to calculate the beam depth, spacing, and reinforcement needed for a safe and serviceable foundation: 1) BRAB Method (1968); 2) WRI Method (1980, 1996); 3) PTI Method (1996); 4) AS 2870 (1996); 5) PTI Method (2004). WRI and PTI Method (2004) are the most recently developed method in the USA while the AS 2870 is the most recent version of the Australian Standards. For the same input design data, applying these three design methods may result in different beam depths. In order to compare these methods, 27 cases are designed. They include three simple rectangular stiffened slabs subjected to three different weather patterns, built on three different shrink-swell soils, and loaded with a uniform pressure and perimeter line load. The resulting beam depths using the WRI, PTI 2004 and the AS 2870 methods in different soil and weather conditions are also presented and discussed.

INTRODUCTION

WRI Method (1981, 1996) (Wire Reinforcement Institute) was developed by Walter L. Snowden, P.E., of Austin, Texas. It is empirically derived by observing slab performance and modifying equations to give results approximating the foundations that had been found to give satisfactory results. WRI uses the same approach as the BRAB (1968) (Building Research Advisory Board) design method as it assumes a rectangular mound shape (i.e. the slab stiffness doesn't influence the unsupported distance), and introduces an empirical support index related to climatic rating and soil properties. Being considered as a modified version of BRAB, WRI introduces a design chart that relates the cantilever distance with the support index.

The Post-Tensioning Institute (PTI) design method (1980, 1996, 2004) is based on research work conducted at Texas A&M University by Wray and Lytton (Wray, 1978). This approach is based on analysis of a plate resting on a semi-infinite elastic continuum. The design equations included in the PTI manuals come from nonlinear regression analyses of parametric study results. Using these equations, design moment, shear, and deflection can be found for center heave and edge heave conditions.

Australian Standard AS 2870 method (1988, 1990, 1996) was prepared by the Standards Australia Committee BD-025, Residential Slabs and Footings. This standard recommends profiles of soil suction changes for different climatic zones of Australia and classifies the site using an index called the characteristic soil surface movement index.

The standard provides a table of recommended stiffened raft designs - based on the "Beam On Mound" Walsh model (BOM) modified to fit with previous experience for several site classes (Walsh and Cameron, 1997).

INPUT DESIGN DATA

Designing stiffened slabs on shrink-swell soils is a weather-soil-structure interaction problem as weather introduces moisture variations to the surface soil zone, the soil reacts with shrink- swell response according to the moisture variation, and the structure deforms as a result of the soil mound shape. These three design methods model this problem in different ways, consequently, the input design data differs from one method to another. For the sake of consistency in the input data the following assumptions were used:

Weather parameters

Three locations were chosen in Houston, College Station, and San Antonio, Texas, US representing wet temperate, temperate, and dry temperate climatic zones.

For WRI input weather data, the climatic rating indices (C_W) for these locations were found to be 17, 21, and 25, respectively, according to the Continental United States climatic rating map.

For PTI 2004 input weather data, the Thornthwaite Moisture index, I_m for these locations were found to be -16, 0, and 18, respectively, according to the Continental United States I_m map.

AS 2870 introduces a table for recommended H_s (depth of design suction change) values for each climatic zone. Correlating the average I_m in each climatic zone with the corresponding H_s, the following equation was concluded and used to calculate H_s for the three locations

$$H_s = 1.387 + 0.939e^{\left(\frac{-I_m}{24.843}\right)} \text{, where } H_s \text{ in (m)}$$

For AS 2870 input weather data, depths of design suction change H_s were found to be 3.3, 2.4, and 1.8 m, respectively.

The wet and dry suction profiles at the surface were assumed, for all locations, considering the guidance of the PTI recommended values (2.5 pF for the wettest condition as in the case of prolonged heavy rain and no drainage, 4.5 pF for the driest condition if the surface suction is controlled by vegetation).

Soil parameters

Three soils were chosen representing very high, high, and moderate shrink-swell potential.

For WRI and PTI 2004 input soil data, the liquid limits were assumed to be 90%, 70%, and 50%, respectively with corresponding plasticity indices of 60%, 45% and 30%.

For PTI 2004 input soil data, the % fine clay was assumed to be 70% and the % passing sieve # 200 was assumed to be 100% for all soils. Applying these input data

in PTI procedures, the Suction Compression Indices (γ_h) were found to be 0.133, 0.077, and 0.028 (pF^{-1}).

The Suction Compression Index represents the slope of the volumetric strain versus suction in pF units and the Shrinkage Index or the Instability Index without lateral restraint and without loading of the soil (I_{ps}) represents the slope of the vertical strain versus suction in pF units. The I_{ps} values were assumed to be one third of the corresponding γ_h values considering that the vertical strain is one third of the volumetric strain.

Consequently, for AS 2870 input soil data, the I_{ps} values were found to be 0.0443, 0.0257, and 0.0093.

Structural parameters

Three slabs were chosen of dimensions 12X12, 24X24, and 24X12 m representing different aspect ratios and different slab sizes. The beam spacing was chosen to be 3m in both directions. For all slabs a masonry veneer super structure was chosen.

RESULTS COMPARISON

The resulting beam depths are tabulated in the appendix. To compare these beam depths, the average beam depth for each design case was calculated and considered as the reference parameter in the comparison. Figures (1), (2), and (3) show the resulting beam depths using the three design methods.

The percentage difference between the design depth and the average design depth for all cases was also calculated. Figure (4) shows the percentage difference from the average beam depths for all cases.

Of the 27 design cases, only one case gives identical beam depths using the three design methods, this case was in a wet temperate climatic zone and has a very high shrink-swell potential soil and the smallest slab size (12X12 m).

Among these design methods, WRI beam depths and PTI 2004 beam depths shows the closest correlation, meanwhile PTI 2004 beam depths and AS 2870 beam depths shows the poorest correlation.

WRI

Of the 27 cases, 6 cases resulted in beam depths smaller than the average beam depths, 3 cases resulted in the average beam depths, and 18 cases resulted in beam depths larger than the average beam depth. The maximum beam depth was 0.9 m and the minimum was 0.4 m. The maximum percentage difference from the average beam depth was 21.62%, the minimum was -4.0%, and the average of all cases was 5.46%.

PTI 2004

Of the 27 cases, 4 cases resulted in beam depths smaller than the average beam depths, one case resulted in the average beam depths, and 22 cases resulted in beam depths larger than the average beam depth. The maximum beam depth was 1.05 m and the minimum was 0.45 m. The maximum percentage difference from the average beam depth was 44.0%, the minimum was -20.75%, and the average of all cases was 16.597%.
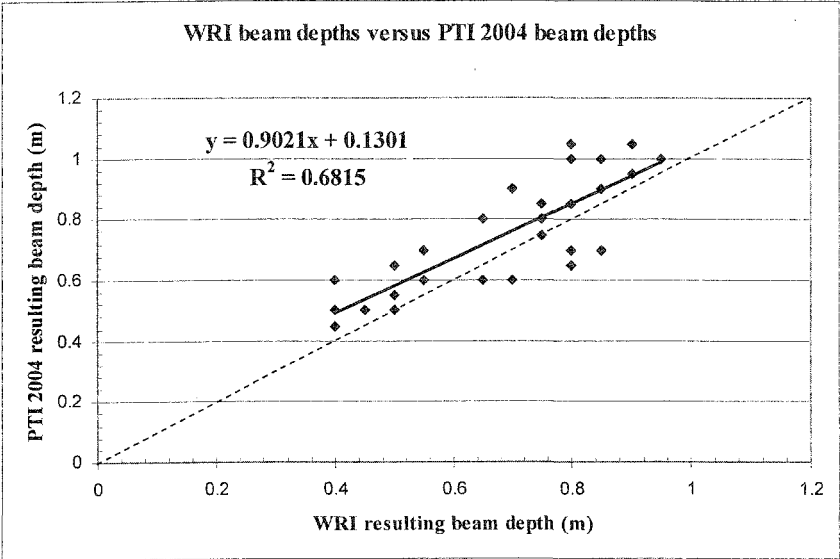
Figure (1), WRI beam depths versus PTI 2004 beam depths
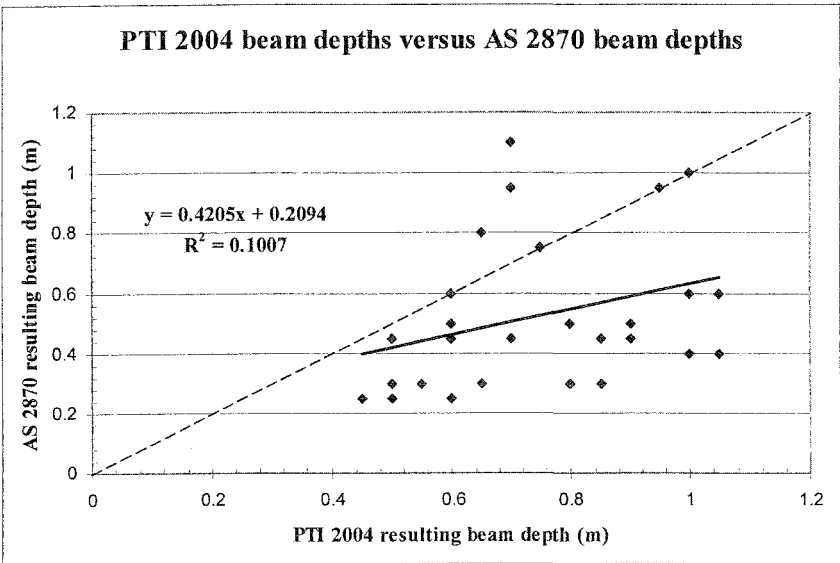
Figure (2), PTI 2004 beam depths versus AS 2870 beam depths
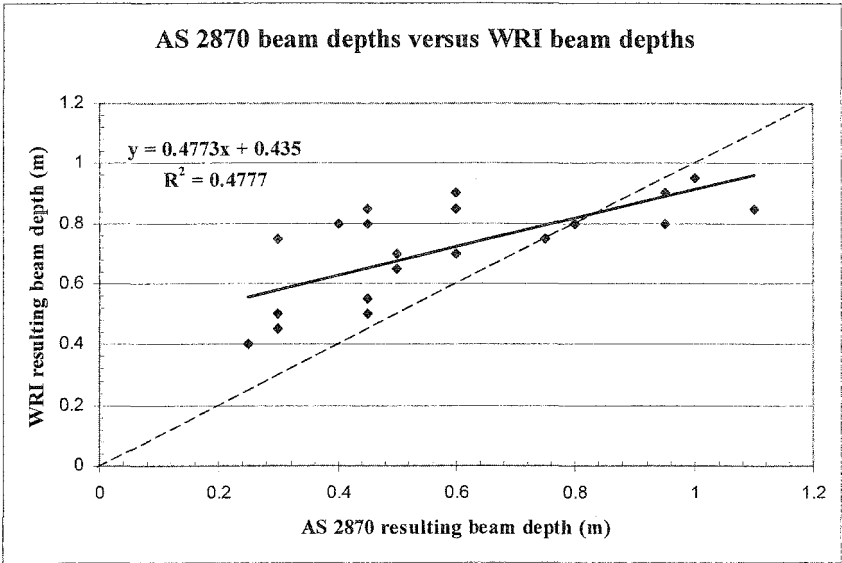
Figure (3), AS 2870 beam depths versus WRI beam depths
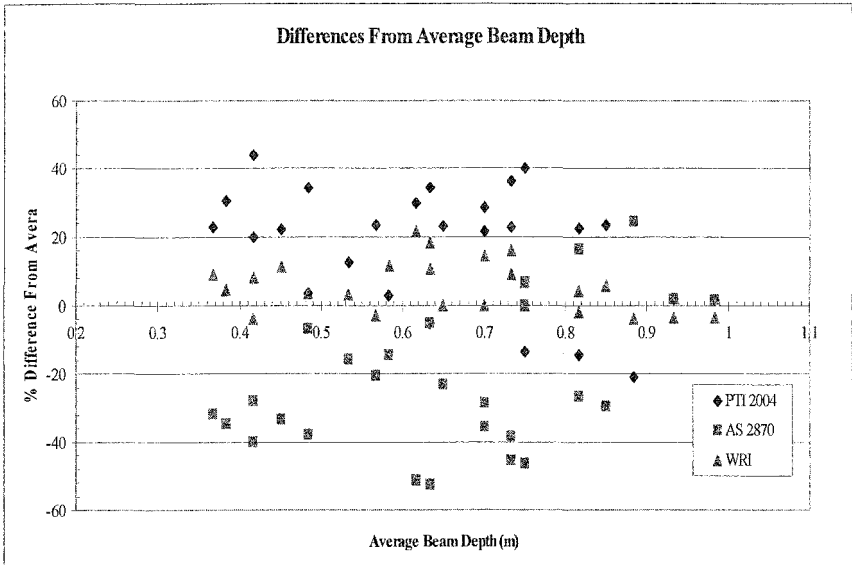
Figure (4), the percentage of the difference from the average beam depths

AS 2870

Of the 27 cases, 21 cases resulted in beam depths smaller than the average beam depths, one case resulted in the average beam depths, and 5 cases resulted in beam depths larger than the average beam depth. The maximum beam depth was 1.1 m and the minimum was 0.25 m. The maximum percentage difference from the average beam depth was 24.53%, the minimum was -52.63%, and the average of all cases was -22.63%.

CONCLUSIONS

This parametric study provides a table of resulting beam depths using three commonly used design methods for 27 cases that cover a range of soils of very high, high, and moderate shrink-swell potential, range of weather patterns of wet temperate, temperate, and dry temperate climatic zones, and range of slab sizes of dimensions 12X12, 24X24, and 24X12 m. The table of results may provide guidance for consultants who deal with similar design situations.

A technique was suggested to apply input design data for the three design methods with reasonable consistency, which enables consultants to use these three design methods despite the variation in the required input data for each method.

For the chosen 27 cases, the beam depth predicted by the WRI design method gives results closest to the average beam depth obtained by all methods with an average percentage difference of 5.46%, PTI 2004 gives beam depths larger than the average beam depth by 16.597%, and AS 2870 gives beam depths smaller than the average beam depth by 22.63%.

For the chosen 27 cases, applying these three design methods shows discrepancies between recommendations of beam depths that raise the need for comparison with observed field data.

Climate Parameters			Soil Properties				Slab Dim.		Beam Design Depth (m)			Average Depth (m)	% Difference from the average		
I_m	C_W	H_s (m)	γ_h	I_{pt}	LL%	PI%	L_L (m)	L_S (m)	PTI 2004	AS 2870	WRI		PTI 2004	AS 2870	WRI
-16	17	3.3	0.028	0.0093	50	30	12	12	0.5	0.45	0.5	0.483	3.45	-6.90	3.45
-16	17	3.3	0.028	0.0093	50	30	24	24	0.7	0.45	0.55	0.567	23.53	-20.59	-2.94
-16	17	3.3	0.028	0.0093	50	30	24	12	0.6	0.45	0.55	0.533	12.50	-15.63	3.13
-16	17	3.3	0.077	0.0257	70	45	12	12	0.65	0.8	0.8	0.750	-13.33	6.67	6.67
-16	17	3.3	0.077	0.0257	70	45	24	24	0.9	0.45	0.85	0.733	22.73	-38.64	15.91
-16	17	3.3	0.077	0.0257	70	45	24	12	0.85	0.45	0.8	0.700	21.43	-35.71	14.29
-16	17	3.3	0.133	0.0443	90	60	12	12	0.7	1.1	0.85	0.883	-20.75	24.53	-3.77
-16	17	3.3	0.133	0.0443	90	60	24	24	1	1	0.95	0.983	1.69	1.69	-3.39
-16	17	3.3	0.133	0.0443	90	60	24	12	0.95	0.95	0.9	0.933	1.79	1.79	-3.57
0	21	2.4	0.028	0.0093	50	30	12	12	0.5	0.3	0.45	0.417	20.00	-28.00	8.00
0	21	2.4	0.028	0.0093	50	30	24	24	0.65	0.3	0.5	0.483	34.48	-37.93	3.45
0	21	2.4	0.028	0.0093	50	30	24	12	0.55	0.3	0.5	0.450	22.22	-33.33	11.11
0	21	2.4	0.077	0.0257	70	45	12	12	0.6	0.6	0.7	0.633	-5.26	-5.26	10.53
0	21	2.4	0.077	0.0257	70	45	24	24	0.85	0.3	0.75	0.633	34.21	-52.63	18.42
0	21	2.4	0.077	0.0257	70	45	24	12	0.8	0.3	0.75	0.617	29.73	-51.35	21.62
0	21	2.4	0.133	0.0443	90	60	12	12	0.7	0.95	0.8	0.817	-14.29	16.33	-2.04
0	21	2.4	0.133	0.0443	90	60	24	24	1.05	0.6	0.9	0.850	23.53	-29.41	5.88
0	21	2.4	0.133	0.0443	90	60	24	12	1	0.6	0.85	0.817	22.45	-26.53	4.08
18	25	1.8	0.028	0.0093	50	30	12	12	0.45	0.25	0.4	0.367	22.73	-31.82	9.09
18	25	1.8	0.028	0.0093	50	30	24	24	0.6	0.25	0.4	0.417	44.00	-40.00	-4.00
18	25	1.8	0.028	0.0093	50	30	24	12	0.5	0.25	0.4	0.383	30.43	-34.78	4.35
18	25	1.8	0.077	0.0257	70	45	12	12	0.6	0.5	0.65	0.583	2.86	-14.29	11.43
18	25	1.8	0.077	0.0257	70	45	24	24	0.9	0.5	0.7	0.700	28.57	-28.57	0.00
18	25	1.8	0.077	0.0257	70	45	24	12	0.8	0.5	0.65	0.650	23.08	-23.08	0.00
18	25	1.8	0.133	0.0443	90	60	12	12	0.75	0.75	0.75	0.750	0.00	0.00	0.00
18	25	1.8	0.133	0.0443	90	60	24	24	1.05	0.4	0.8	0.750	40.00	-46.67	6.67
18	25	1.8	0.133	0.0443	90	60	24	12	1	0.4	0.8	0.733	36.36	-45.45	9.09

REFERENCES

1. Building Research Advisory Board, National Research Council Criteria for Selection and Design of residential Slabs-on-Ground," U.S. National Academy of Sciences publication 1571, 1968.
2. Post-Tensioning Institute, "Design and Construction of Post-Tensioned Slabs-on-Ground," Phoenix, Arizona, USA, Second Edition 1996.
3. Post-Tensioning Institute, "Design and Construction of Post-Tensioned Slabs-on-Ground," Phoenix, Arizona, USA, Third Edition 2004.
4. Standards Association of Australia, "Residential Slabs and Footings, Part 2: Guide to design by engineering principles," AS 2870.2 Standard House, Sydney NSW, Australia, 1990
5. Standards Association of Australia, "Residential Slabs and Footings," AS 2870 Standard House, Sydney NSW, Australia, 1996
6. Walsh, P. and Cameron, D. "The Design of Residential Slabs and Footings", Standards Association of Australia SAA HB 28-1997, [Homebush, NSW]: Standard Australia, (1997)
7. Wray, W. K., "Development of a Design Procedure for Residential and light Commercial Slabs-on-Ground Constructed over Expansive Soils," Ph.D. dissertation, Department of Civil Engineering, Texas A&M University, College Station, TX 1978.
8. Wire Reinforcement Institute, "Design of Slab-on- Ground Foundations," Findlay, Ohio, USA, August 1981.
9. Wire Reinforcement Institute, "Design of Slab-on- Ground Foundations, An Update," Findlay, Ohio, USA, March, 1996.

Geotechnical Evaluation of the Design of Post-Tensioned Slabs on Expansive Soils Using the PTI Third Edition Procedure for Arizona Conditions

H.B. Dye[1], C.E. Zapata[2], and S.L. Houston[3]

[1]Graduate Research Assistant, Arizona State University, Dept of Civil and Environmental Engineering, P.O. Box 875306, Tempe, AZ 85287-5306; PH (480) 965-3997; FAX (480) 965-0557; email: beata.czupak@asu.edu
[2]Faculty Research Associate, Arizona State University, Dept of Civil and Environmental Engineering, P.O. Box 875306, Tempe, AZ 85287-5306; PH (480) 727-8514; FAX (480) 965-0557; email: czapata@asu.edu
[3]Professor and Chair, Department of Civil and Environmental Engineering, Arizona State University, P.O. Box 875306, Tempe, AZ 85287-5306; PH (480) 965-3589; FAX (480) 965-0557; e-mail: sandra.houston@asu.edu

Abstract

Several changes have been introduced in going from the 2nd Edition to the 3rd Edition of the PTI procedure for the design of slabs-on-grade on expansive soils. The changes in the design procedure, when applied to desert regions, tend to result in doubling of the edge moisture variation distance and a change from center lift to edge lift design governing conditions. The new design parameters along with the change of critical mode of slab deformation lead, in general, to thicker slabs. It is the objective of this paper to examine the changes in the PTI design method and compare the results obtained with both the 2nd and the 3rd Edition design procedures for typical Phoenix, Arizona soils and climatic conditions.

Historical Background

Wray (1978) developed a procedure for determining the edge moisture variation distance based on the Thornthwaite Moisture Index, *TMI* for structures constructed on expansive soils. This method was later adopted by the Post-Tensioning Institute and was kept intact in the 1st Edition of the PTI design manual that is applicable to ribbed foundations only (PTI, 1980). Extensive clarifications of definitions and limitations of the design were added into the design manual published in 1996 as the 2nd Edition PTI design procedure (PTI, 1996). In this procedure the soil analysis remained unchanged and the design applicability was extended to both ribbed and uniform thickness foundations on expansive soils with provisions given to

stable and compressible sites. Currently, the 2nd Edition PTI design method is widely used.

Based on the research work done by Covar and Lytton (2001) significant changes have been introduced into the geotechnical evaluation of the PTI design procedure published as *Alternate Procedure for Determining Soil Support Parameters for Shallow Foundations on Expansive Clay Soil Sites* under *PTI Technical Note 12* (PTI, 2003). The *Alternate* 2nd Edition is applicable to sites with expansive soils and it is not applicable to soils with collapsible or compressible characteristics. In this procedure the soil analysis is based on soil index properties that are correlated to soil mineralogy. The estimated dominant clay type and soil index properties are both used to obtain a suction compression index for soil consisting of 100% clay, which is modified for gradation and used to calculate an unsaturated diffusion coefficient that is correlated to the edge moisture variation distance, e_m. The modified suction compression index is also used in the prediction of differential soil movement, y_m, based on the estimated variation in total soil suction.

The 3rd Edition procedure (PTI, 2004) introduces significant changes as compared to the 2nd Edition procedure (PTI, 1996), where only the method of constant suction at depth determination remains the same. At the same time, the 3rd Edition procedure is very similar to the *Alternate* PTI 2nd Edition, first published in 2003 (PTI, 2003). The main differences include modified sections on procedure applicability and updated figures and equations. The 3rd Edition also contains design provisions for compressible and stable soils, as well as additional methods of obtaining suction compression index modified for gradation. In addition, it includes an updated suction vs. TMI relationship first presented in the PTI 1st Edition procedure (PTI, 1980).

The 3rd Edition PTI procedure is in the process of being adopted by practicing engineers. This paper summarizes and provides a comparison of the design parameters obtained with the 3rd Edition procedure (PTI, 2004) and the results of the former 2nd Edition version (PTI, 1996) design method.

Definitions

The definitions of edge moisture variation distance, differential swelling mode and differential soil movement introduced in the 1st Edition (PTI, 1980) remained unchanged in the subsequent PTI design manuals. The edge moisture variation distance, e_m, is a distance measured inward from the edge of the slab over which the moisture content of the soil varies due to wetting or drying. Prior to the 2003 publication, the magnitude of the moisture variation distance depended mainly on climate. Starting with the *Alternate Procedure* (PTI, 2003) the unsaturated diffusion coefficient was recognized as the major factor influencing the edge moisture variation distance. Roots, fissures, fractures or joints in the soil increase e_m while moisture barriers at least 2.5 ft deep can be used in the procedure to reduce e_m.

Differential soil movement, y_m, also known in the 2nd Edition as differential swell, is the change in soil elevation between the two points separated by e_m. The amount of expansion or contraction that a soil stratum will undergo depends on the amount of clay minerals, thickness of stratum, depth and uniformity of clay layer below the ground surface, surcharge pressure, severity of climatic change, and the proximity to ground water table. It also depends on factors such as deep tree roots and zones of high osmotic suction. Moisture barriers of at least 2.5 ft deep can be used in the procedure to reduce y_m.

The swelling mode depends on the y_m value. The edge lift condition often occurs when the slab is constructed on a relatively dry pad. Due to wet environmental conditions the soil swells around the perimeter of the structure creating a dish-shaped deformed slab. Center lift condition often occurs when the slab is constructed on a relatively wet pad and dry environmental conditions lead to soil shrinkage around the slab perimeter. Both conditions are illustrated in Figure 1.
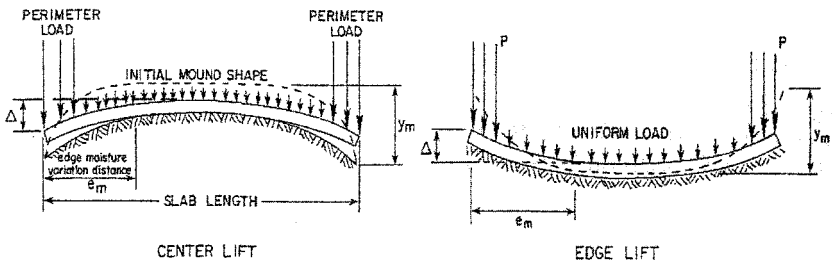
Figure 1. Deformation Modes of Slab-on-grade Constructed on Expansive Soil as per PTI (1996, 2001, 2005).

In all PTI procedures, e_m and y_m are computed under the assumption that the slab is perfectly flexible. Also, in all PTI procedures climate is assumed to be the main factor affecting differential soil movement, y_m, and edge moisture distance, e_m. The factors affecting soil behavior other than climate include: vegetation requiring large amounts of water, fence lines, trails and tracks which leave bare soil drier than the surrounding soil; cut and fill sections that experience differential soil movement; poor drainage that causes runoff water to collect near the structure; time of construction; and post construction practices. Factors not related to climate may induce soil movements much larger than the climate dependant movements; and even though the 3rd PTI Edition (Chapter 4 - *Design Commentary*) clearly states that the design procedure is invalid when the site is influenced to any significant degree by non-climate conditions, special provisions allow for their consideration in Chapter 3, *Geotechnical Investigation*.

PTI 2nd Edition Design Procedure, 1996

The 2nd Edition procedure (PTI, 1996) is applicable to ribbed and uniform thickness foundations on expansive soils with Plasticity Index (*PI*) equal to or greater

than 15 %. The applicability is extended to stable and compressible soils. In addition, this procedure is valid only when site conditions are governed by climate and the calculated differential soil movement, y_m, does not exceed 4 inches [10.2 cm]. The input parameters needed for the PTI 2nd Edition procedure include Liquid Limit (*LL*), Plastic Limit (*PL*), percentage of clay, *%clay* (defined as percent of soil particles smaller than 0.002 mm), predominant clay material, Thornthwaite Moisture Index (*TMI*) for the design region (Thornthwaite, 1948), suction at the active zone depth, and the depth to constant suction.

To determine e_m, for both edge lift and center lift conditions, the 2nd Edition procedure (PTI, 1996) makes use of a correlation with *TMI* (Figure 2). The *TMI* is determined for mean annual climate conditions (Thornthwaite, 1948). Engineers have adopted a value of − 40 as a representative value for the Phoenix area.
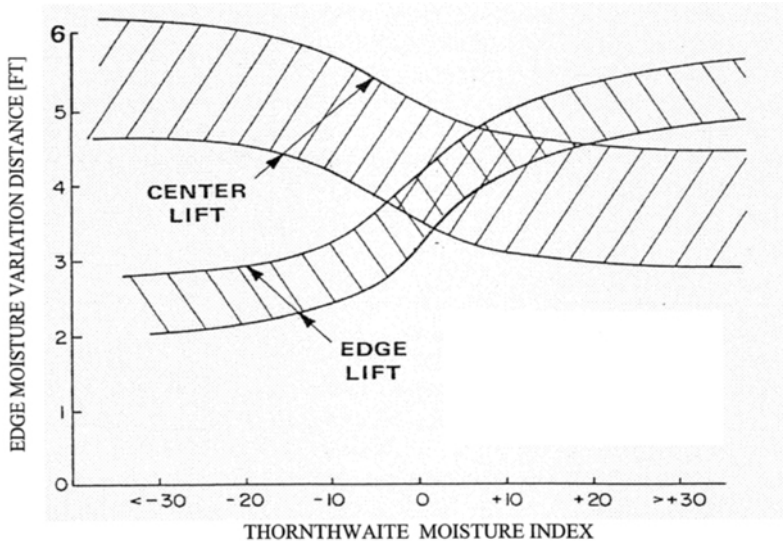
Figure 2. Edge Moisture Variation Distance as a Function of Thornthwaite Moisture Index (after Wray, 1978).

To determine y_m, the following properties shall be measured or estimated based on the following procedure:

1. Predominant clay mineral, which can be obtained from a figure presented in the PTI manual. The clay type is a function of Activity Ratio, *Ac*, defined as $\dfrac{P_{200}PI}{100\%clay}$, and Cation Exchange Activity, *CEAc* obtained by $\dfrac{P_{200}PL^{1.17}}{100\%clay}$, where Plastic Limit (*PL*), Plasticity Index (*PI*), percent soil passing US sieve # 200 (*P200*) and *%clay* are expressed as percentages. The use of Montmorillonite is

recommended if a conservative estimate is desired (Pearring 1963).

2. Depth to constant soil suction defined by $\dfrac{w}{PL}$, where w is the gravimetric water content. It occurs at the depth of inert material, unweathered shale or high water table. When sufficient data is not available, the depth to constant suction can be assumed to be 7 ft [2.1 m].

3. Equilibrium total soil suction, which in absence of measured values is estimated based on a correlation with *TMI* (Figure A3.6 in 2nd Edition PTI, 1996).

4. Moisture flow velocity defined by V = 0.5 *TMI*, where the magnitude of *TMI* is used. Though *TMI* is a dimensionless parameter, this is an empirical correlation that yields velocity in units of in/year. The moisture flow velocity is limited to values not smaller than 0.5 in/month [1.3 cm/month] or larger than 0.7 in/month [1.8 cm/month]. For Arizona conditions, where *TMI* = -40, the velocity has a magnitude of 1.7 in/month [4.3 cm/month], therefore 0.7 in/month [1.8 cm/month] ought to be used.

In absence of the computer program, VOLFLO 1.0 developed by Geostructural Tool Kit Inc., read off the magnitude of the differential soil movement from charts provided within the manual. The charts include all parameters determined in steps 1 through 4 above. Note that it the tables 'Percent Clay (%)' refers to $\dfrac{\%clay}{P_{200}}$ expressed as a percentage.

PTI 3rd Edition Design Procedure

The 3rd Edition procedure is applicable to two types of slabs. The first one is a ribbed foundation of uniform thickness slab with stiffening ribs projecting from the bottom of the slab in both directions. The second one is a uniform thickness slab foundation with no interior stiffening ribs. This Edition gives provisions for design on compressible and non-active soils, which are not summarized in this paper. In addition, it is possible to model the influence of vertical moisture barriers, planter areas and variable soil suction profiles with a commercial computer program, VOLFLO 1.5 developed by Geostructural Tool Kit Inc.

The 3rd Edition procedure is applicable to soils with Expansion Index, *EI*, greater than 20, as determined per ASTM standard D 4829, or where the following three requirements are met: Plasticity Index, *PI*, is equal to or greater than 15 %, more than 10 % of soil passes US sieve #200, and more than 10 % of soil particles are smaller than 0.05 mm in size. The parameters needed in this procedure include: initial and final suction profiles, *TMI*, moisture active zone depth, and mineral classification. Soil properties for each representative layer are required: *LL*, *PL*, *PI*, % passing US sieve #200, and *%clay*. In addition other soil parameters are suggested to be determined experimentally: dry density, moisture content, cohesive strength, confined or unconfined compressive strength, total suction, swell pressure, and Expansion Index.

Additional Definitions Provided in the Procedure. The following definitions are introduced in the 3rd Edition design procedure.

Moisture Active Zone Depth refers to the depth below the ground surface at which changes in moisture content (soil suction) can be expected due to environmental changes or other causes. This is also the location of the equilibrium moisture content.

Movement Active Zone Depth refers to the depth to which the soil experiences changes in volume. The movement active zone depth is usually smaller than the moisture active zone depth due to overburden restraint.

Soil Suction quantifies the energy level in the soil-moisture system. An imbalance of total suction between adjacent soils tends to drive moisture towards regions of higher suction. Total suction can be measured by filter paper method and psychrometers; while pressure membranes or ceramic pressure plates measure matric suction.

Equilibrium (Constant) Soil Suction represents a suction value that develops in a soil deposit at the depth of moisture active zone as a result of multiple weather cycles at the surface. The climate controlled equilibrium suction is expressed as a function of *TMI*. The constant suction is also dependant on local site conditions such as cemented soil, high osmotic suction, and presence of high water table or rocks, in which case the correlation with TMI is invalid.

Suction Compression Index is a soil property that is analogous to the Compression Index utilized in the settlement analysis of saturated soils. It is defined as the change in volume related to a change in suction for an intact specimen of soil.

Assumptions. In absence of the computer program VOLFLO 1.5, the 3rd Edition Stress Change Factor Chart procedure solves for the following simplified conditions.

- Steady state unsaturated flow;
- The active zone is assumed to be 9 feet below the ground surface;
- Suction Compression Index does not vary by more than 10% between layers;
- The suction at active zone depth is climate controlled. Although the initial correlation of equilibrium suction to TMI presented in 1st and 2nd Editions was developed for homogeneous profiles, in the 3rd Edition an assumption is made that the equilibrium suction is independent of soil type and profile homogeneity. This relationship was updated in version 3 and it is presented in Figure 3 (Fig. 3.4 in PTI, 2004). Resent studies have shown that the suction at a given TMI heavily depends on soil type (Perera, 2004), which agrees with the scatter of values and the poor statistical significance, R^2 equal to 0.36, of the proposed correlation. The correlation is not valid for soils with high osmotic suctions or where high water table is present.
- Initial suctions, h_i, at the soil surface below the edge of slab and at the edge moisture variation distance under the slab are assumed to be equal to the equilibrium suction at the moisture active zone depth as determined from the

suction vs. *TMI* correlation. Due to environmental and human induced flux at the soil surface, the soil at the edge becomes wetter or drier, resulting in different final suction values under the edge of the slab, h_f. The initial suction, h_i, is based on *TMI* while the final suction, h_f, is based on assumed, suction variations at the soil surface. These assumptions result in constant initial suction profiles at both ends of e_m and in a trumpet shaped final suction profile under the edge of the slab.
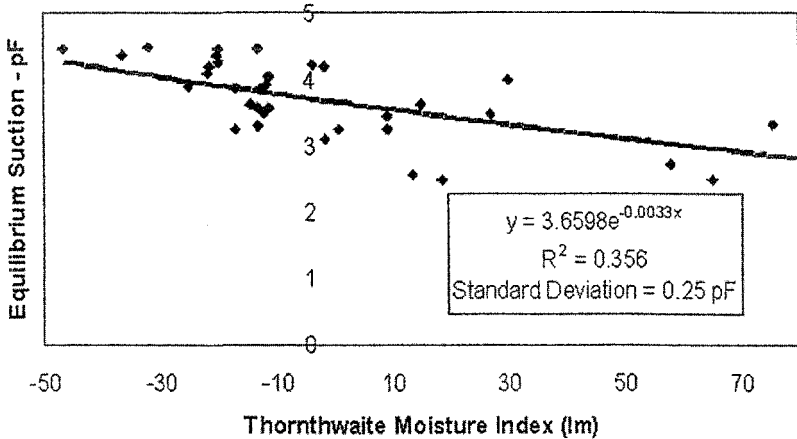
Figure 3. Variation of Soil Suction with Thornthwaite Moisture Index (PTI, 2004).

The PTI 3rd Edition procedure is also valid for a wider range of conditions through the use of the computer program VOLFLO 1.5. These conditions include but are not limited to deeper active zone, significantly different suction compression index values for adjacent layers, high osmotic suction zones, influence of vegetation, and initial soil suction profiles drier or wetter than equilibrium.

Procedure. A summarized step-by-step procedure for the 3rd Edition follows.

To calculate the edge moisture variation distance, e_m:
1. Determine the mineral classification zone for each significant layer. A chart that relates the mineral classification with Atterberg limits is provided in the procedure (Covar and Lytton, 2001).
2. Calculate percent fine clay, *%fc*, for each significant layer defined as $\%fc = \dfrac{\%clay}{P_{200}}100$, where P_{200} is the percent soil passing US sieve # 200.
3. Calculate Liquid Limit and Plasticity Index ratios for each significant layer. These ratios are defined as $LLratio = \dfrac{LL}{\%fc}$ and $PIratio = \dfrac{PI}{\%fc}$ respectively.

4. Calculate the Suction Compression Index, γ_h, for each significant layer. The 3rd Edition PTI procedure provides four methods as presented below. When procedures 2 through 4 are used, $\gamma_{h\ shrink}$ is read off from a figure which is based on the calculated $\gamma_{h\ swell}$ and which is presented in the 3rd Edition.

Procedure 1: Method based on mineralogical soil classification. A figure for each mineralogical soil class is provided within the 3rd Edition PTI procedure. It relates *LLratio and PIratio* to the suction compression index for soil consisting of 100% clay, γ_o. Once γ_o is read off from the graph, the actual soil suction compression index for swelling and shrinking conditions is calculated as follows:

$$\gamma_{h\ swell} = \left(0.01\gamma_o\%fc\right)e^{\left(0.01\gamma_o\%fc\right)} \quad ; \qquad \gamma_{h\ shrink} = \left(0.01\gamma_o\%fc\right)e^{\left(-0.01\gamma_o\%fc\right)}$$

Procedure 2: Expansion Index Procedure. Determine the Expansion Index, *EI*, per ASTM D 4829 (ASTM, 2005) and calculate the swell suction compression index by $\gamma_{h\ swell} = \dfrac{EI}{1700}$

Procedure 3: Consolidation Test Procedure. The γ_h is expressed in terms of the slope of the compression rebound curve, C_s, and the void ratio corresponding to the effective stress at the bottom of the curve, e_2, obtained from a consolidation test. The relationship reads $\gamma_{h\ swell} = \dfrac{0.7C_s}{1+e_2}$

Procedure 4: Overburden Pressure Swell Test Procedure. In the last procedure, $\gamma_{h\ swell}$ is correlated to the vertical strain $\left(\dfrac{\Delta H}{H}\right)$, due to increased water content and overburden pressure, *P*. The following relationship is used: $\gamma_{h\ swell} = \dfrac{\dfrac{\Delta H}{H}}{1.7 + \log_{10} P}$.

5. Calculate γ_h corrected if more than 10% of the soil passes US Sieve #10.

$$\gamma_{h(corrected)} = \gamma_h \dfrac{100}{F\dfrac{\gamma_{t(wet)}}{\gamma_{d(dry)}} + 100 - F} \quad ; \qquad F = \dfrac{100}{1 + \left(\dfrac{J}{100-J}\right)\left(\dfrac{\gamma_{t(wet)}}{\gamma_w G_{s(coarse)}}\right)}$$

where $\gamma_{t(wet)}$ is the moist unit weight of soil when soil suction is about 2.5 pF; $\gamma_{d(dry)}$ is the dry unit weight of soil at its natural water content (optimum water content or shrinkage limit); *J* is the % of soil by weight greater than US sieve #10 (2.0 mm diameter); $G_{s(coarse)}$ is the specific gravity of solids; and γ_w is the unit weight of water.

6. Find the modified suction compression index, γ_{mod}, for both swell and shrinkage. In this step, γ_h is weighted based on the location of different layers in the soil profile; for example: $\gamma_{mod} = \dfrac{3\gamma_{h\,topsoil} + 2\gamma_{h\,middle} + \gamma_{h\,bottom}}{6}$.

7. Calculate the modified unsaturated diffusion coefficient for each significant layer up to a minimum of 9 ft for both swelling and shrinkage modes:

$$\alpha'_{swell/shrink} = (0.0029 - 0.000162*S - 0.0122*\gamma_{h\ swell/shrink})F_f,$$

where S is the slope of the total suction in pF vs. water content relationship defined by: $S = -20.29 + 0.1555*LL - 0.117*PI + 0.0684*P_{200}$, and F_f is defined as the soil fabric factor, which is a function of the amount of roots and fractures present in the soil. F_f varies from 1.0 for soils with less than 1 root or fracture per vertical foot up to 1.4 for soils with five or more roots/fissures per vertical foot.

8. Calculate the weighted modified soil diffusion coefficient for both swell and shrinkage cases as a function of layer location within the soil profile:

$$\left(\alpha'\right)_{weighted} = \frac{3F_f\left(3\alpha_{topsoil} + 2\alpha_{middle} + \alpha_{bottom}\right)}{18}$$

9. Read off e_m from Figure 4 for both center lift and edge lift conditions. Use values of *weighted* α' and *TMI* for both conditions and choose the largest e_m value.
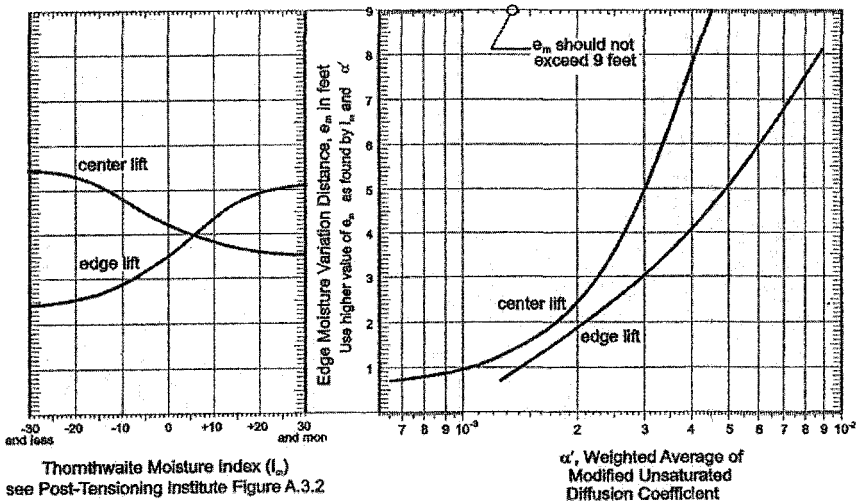
Figure 4. Edge Moisture Variation Selection Chart (PTI, 2004)

To find the differential soil movement, y_m:

1. Measure or estimate initial, controlling soil suction. This procedure assumes that the initial suction is the same at the soil surface at two locations separated by e_m and at the moisture active zone depth, where suctions in the horizontal plane do not vary. The magnitude and depth to constant suction is to be determined at a depth where soil suction does not vary by more than 0.0027 pF per ft (per 0.3 m). If direct estimation is not possible, the initial or equilibrium suction can be estimated directly from Figure 3, unless scenarios unrelated to climate conditions prevail. The most common cases are:

a. When shallow water table is present and osmotic suction is negligible. The method recommends using a suction equal to 2.0 pF.
b. When large trees are present at the site. In this case, the controlling suction should be equal to 4.5 pF throughout the tree root zone.
c. When soil is cemented or it is known to have high osmotic suction. In this case, the controlling soil suction must be determined experimentally.
2. Estimate final suction at the ground surface under the edge of slab. In absence of local measurements, final soil suction values at the ground surface are recommended to be 2.5 pF for the wettest condition; and 6.0 pF for surfaces controlled by evaporation from bare soil or wilted vegetation. For Phoenix conditions, limits of 2.9 pF and 4.5 pF are commonly used.
3. Calculate the differential soil movement, y_m, based on the modified suction compression index, γ_{mod}, and the Stress Change Factor, SCF. A set of Stress Change Factors is given in the procedure as a function of the difference between initial and final suction values at the edge of the slab.

$$y_m = \gamma_{mod} * SCF$$

Design Parameters for Arizona

Four expansive soils were collected from around the metropolitan Phoenix area. Laboratory testing was performed to determine typical Phoenix area input parameters needed for the calculation of e_m, y_m, and the slab thickness. The soil data are shown in Table 1 and analysis results in Table 2. In the 2nd Edition analysis, 7ft [2.1 m] moisture active zone depth was used. In the 3rd Edition analysis, 9 ft [2.7 m] active zone depth and final suctions at the edge of the slab of 2.9 pF (78 kPa) and 4.5 pF (3100 kPa) for the edge lift and edge drop mode respectively were used. From the PTI 2nd Edition suction vs. TMI correlation, the suction at the moisture active zone depth is 4.36 pF (2290 kPa) and from 3rd Edition (Figure 3) it is 4.18 pF (1500 kPa). The common practice in Phoenix is to use 4.2 pF (1555 kPa) for suction at depth, which is the value used in this analysis.

Table 1. Soil Index Properties Used in VOLFLO Input

Soil #	Layer Thickness [ft/m]	LL [%]	PL [%]	PI [%]	P_{200} [%]	%clay [%]
1	0.6/0.2	11	9	2	43	2
	2.6/0.8	45	18	27	41	19
	0.7/0.2	40	22	18	37	18
	5.1/1.5	27	19	8	28	9
2	1.2/0.4	41	20	21	66	24
	0.9/0.3	35	19	16	59	30
	0.9/0.3	49	22	27	72	38
	6.1/1.9	35	19	16	61	30
3	1.2/0.4	99	35	64	29	13
	0.9/0.3	93	33	60	46	13
	1.6/0.5	65	30	35	78	26
	5.4/1.6	68	30	38	47	24

Discussion

Several observations can be made from Tables 1 and 2. 1) The controlling swelling mode switches from Center lift to Edge lift in the transition from the 2nd Edition to the 3rd Edition PTI method; 2) In the 2nd Edition, e_m is environment dependent while in 3rd Edition e_m is also a function of the soil conductivity, i.e. the diffusion coefficient; 3) The 2nd Edition allows for a range of possible e_m and y_m values resulting in a range of slab thicknesses, while the 3rd Edition estimates unique values of slab thicknesses; 4) The slab thickness increases for all soils in these sample calculations in going from the 2nd Edition to the 3rd Edition PTI. The general observation is, the slab thickness increases as the *PI* increases. For Soil 1, which has the lowest average *PI*, the thickness increased by 25 to 67%, depending on the e_m value used in the 2nd Edition procedure; while for Soil 3, which exhibits the largest *PI*, the thickness increased from 90 to 140%. The range of slab thicknesses increased from 7.5 to 10 inches [19 to 25 cm] to a range of 12.5 to 18 inches [32 to 46 cm].

Table 2. Design Parameters

Soil		2nd Edition PTI, 1996[4]		3rd Edition PTI, 2004[4]	
Number		center lift[2]	edge lift	center lift	edge lift
1	e_m [ft]	4.6/6.1	2.0/2.8	9	5
	y_m [in]	1.59/4.59	0.41/0.83	0.12	1.02
	slab [in][1]	7.5/10			12.5
2	e_m [ft]	4.6/6.1	2.0/2.8	9	4.6
	y_m [in]	2.11/6.55	0.58/1.19	0.14	1.19
	slab [in][1]	8/10			14
3	e_m [ft]	4.6/6.1	2.0/2.8	7	3.7
	y_m [in]	1.81/4.03	0.5/0.67	0.27	2.73
	slab [in][1]	7.5/9.5[3]			18

[1] Assumed sub-rectangle 40 ft x 60 ft; perimeter load 800 psf; E_s = 1000 psi, μ = 1.0.

[2] y_m obtained with 2nd Edition PTI procedure exceeds the maximum 4" for soils 1 and 2. Results for 4" y_m value are presented. For the calculated 4.6" and 6.6" y_m values the soil thicknesses would be 10" and 10.5" respectively.

[3] The y_m values for large e_m values from 2nd Edition procedure were obtained with computer program VOLFLO 1.0 for soils 1 and 2. The procedure charts were used in the remaining calculations. The smaller of y_m values for soil 3 represent the limitations of the charts, where 3.6 pF is the maximum equilibrium suction value at depth.

[4] 1 ft = 0.3048m; 1 in = 2.54 cm

Conclusions

The comparison of PTI version 2 (PTI, 1996) and PTI 3rd Edition (PTI, 2004) can be summarized as follows: 1) The 2nd Edition provides a range in e_m and y_m values, while the 3rd Edition provides unique values; 2) The mode of failure changes from center lift (2nd Edition) to edge lift (3rd Edition) for the sample Arizona conditions conducted herein; 3) The slab thickness for Arizona conditions increased in going from version 2 to version 3 for the sample soils and conditions used in this

study. The change from center lift to edge lift for common Arizona conditions is consistent with the commonly observed field condition in Arizona of edge lift failure mode.

The PTI 3rd Edition procedure adds some rationality to slabs-on-grade design and covers a wider range of practical problems, with less empiricism than the PTI 2nd Edition procedure. Hence, it may lead to more appropriate design values, although it remains to be seen how conservative the design is and what are its limitations. Historical performance data covering a wide range of soils and environmental conditions is needed, however, for further evaluation.

Acknowledgments

References

American Society of Testing Materials. (2003). Standard ASTM D 4829-03. *Standard Test Method for Expansion Index of Soils*.

Covar, A. P. and Lytton R. L. (2001). "Estimating soil swelling behavior using soil classification properties". *Expansive Clay Soils and Vegetative Influence on Shallow Foundations*, Proceedings of Geo-Institute Shallow Foundation and Soil Properties Committee Sessions at the ASCE 2001 Civil Engineering Conference, Houston, Texas, Special Publication 115, 44-63.

Perera, Y. Y., Zapata, C. E., Houston, S.L., Houston W.N. (2004). Moisture Equilibria Beneath Highway Pavements. Transportation Research Board 83rd Annual Meeting - Session 410, Washington D.C., January 11-15.

Post-Tensioning Institute. (1980). *Design and Construction of Post-Tensioned Slabs-on-Ground*, 1st Edition, Post-Tensioning Institute, Phoenix, AZ.

Post-Tensioning Institute. (1996). *Design and Construction of Post-Tensioned Slabs-on-Ground*, 2nd Edition, Post-Tensioning Institute, Phoenix, AZ.

Post-Tensioning Institute. (2003). "Alternate procedures for determining soil support parameters for shallow foundations on expansive clay soil sites (Relating to the Post-Tensioning Institute manual Design and Construction of Post-Tensioned Slabs-on-Ground 2nd Edition)". *PTI Technical Notes*, Post Tensioning Institute Slab-on-Ground Committee, Phoenix, AZ.

Post-Tensioning Institute. (2004). *Design and Construction of Post-Tensioned Slabs-on-Ground*", 3rd Edition, Post Tensioning Institute, Phoenix, AZ.

Thornthwaite, C. W. (1948). "An approach toward a rational classification of climate". *Geographical Review*, 38, 55-94.

Wray, W. K. (1978). *Development of a Design Procedure for Residential and Light Commercial Slab-on-Ground Constructed over Expansive Soils*, Ph.D. Dissertation, Texas A&M University, College Station, Texas.

Investigation of a Leaking Water Line Beneath
Residential Foundation on Expansive Soils

B. M. El-Garhy, [1] and W. K. Wray, [2] Fellow, ASCE

[1] Associate Professor, Civil Engineering Department, Faculty of Engineering, Minufiya University, Shebin El-Kom 23511, Egypt. E-mail: belgarhy@hotmail.com.

[2] Professor, Department of Civil and Environmental Engineering, Michigan Technological University, Houghton, Michigan 49931, U.S.A.

Abstract

This paper presents the analysis of a slab-on-ground foundation influenced by a water line leak and the subsequent soil moisture condition and soil volume changes (shrink/ heave) in the supporting expansive soil. Several possible situations are considered: depth of leak and (1) edge swelling distortion mode resulting from a lengthy wet climate situation following a dry suction profile, (2) edge shrinkage distortion mode (center lift distortion resulting from a lengthy dry climate situation following a wet suction profile), and (3) edge shrinkage distortion mode resulting from a dry climate situation following an equilibrium suction profile. The analyses compares differential movements occurring from the no leak situation to that from a leak located at two different depths beneath the center of the slab foundation. The analysis also compares the resulting differential movements and the induced bending moments in the foundation structure. Some conclusions about the potential for water leaks beneath a slab foundation to cause structural distress to the supported superstructure are offered.

Introduction

When dealing with expansive soil, it is common to design a foundation system to withstand seasonal variation in soil moisture conditions, and to insulate the expansive soil mass beneath the foundation from extreme moisture condition changes. However, other non-seasonal changes in the soil moisture regime, such as those caused by ponding water adjacent to the foundation or large plants growing near the foundation, can cause structural distress usually not considered in the design of slab foundations.

A leaking water line beneath the foundation is often blamed for interior heaving of the soil beneath the foundation and the subsequent differential foundation movement

is blamed for the distress of the building superstructure. The available design methods for a slab-on-ground or raft foundation resting on expansive soil do not provide any specific guidance on how the leaking water line effects might be taken into account in the foundation design (Nelson and Miller, 1992; Lytton, 1994; Wray, 1995; Mills, 2000; PTI, 2004). There is also disagreement if a leaking water line could cause sufficient differential movement to cause damage to the building superstructure (Jackson and Moody, 1999).

This paper presents the analysis of a slab-on-ground foundation resting on expansive soil taking into account the effect of a leaking water line located beneath the center of the slab. The effects of a leak located at different depths beneath the center of the slab foundation on the soil suction distribution and the resulting soil movements or the initial distortion mound shape is presented and discussed. The effect of a leaking water line on the structural design parameters (i.e., moments, shears, and deflections) in slab foundation is also presented and discussed. The analysis is performed using the computer models SUCH and SLAB97 described by El-Garhy (1999).

Computer Models

A moisture diffusion and volume change model, named SUCH and developed by El-Garhy (1999), is able to predict the distribution of soil suction through the unsaturated soil mass beneath a covered area with respect to time and the resulting volume changes (shrink/heave) when the soil mass is subjected to different types of edge effects that can cause soil moisture condition changes, such as climate, trees, ponded water, and moisture barriers. To complete the framework, a soil structure-interaction model called SLAB97 was developed by coupling between the moisture diffusion and volume change model SUCH and the structural model to analyze the interaction between the slab foundation and the movements in the supporting expansive soils. The SLAB97 model is based on the finite element method and is able to calculate the structural design parameters (i.e., moments, shears, and deflections) in a raft foundation (stiffened or constant thickness) resting on expansive soil. Both models were described and validated against field measurements (El-Garhy et al., 2000; El-Garhy and Wray, 2004; Wray et al., 2005).

Studied Cases of Leaking Water Line

A water line leak may occur at any time during the lifetime of the structure. Therefore, a number of cases of leaking water line and subsequent formulation of different distortion mound shapes (i.e., edge heave and edge shrinkage) will be evaluated to determine the worst condition that produces the maximum structural design parameters (i.e., bending moment and differential deflection) in the slab foundation constructed over expansive soil.

Three main cases, denoted as A, B, and C, are investigated. Three sub-cases are studied (e.g., A1, A2, and A3) for each main case. The model SUCH was used for each case to calculate the distribution of soil suction in the expansive soil mass

beneath the slab and the associated soil movements or the initial distorted mound shapes. The SLAB97 model then was used to calculate the structural design parameters (e.g., bending moment and differential deflection) in the slab. The effect of the formation of the following distortion mound shapes resulting from the leak was studied: edge heave distortion mode resulting from a lengthy wet climate situation following an initially dry suction profile, Case A; edge shrinkage distortion mode resulting from a lengthy dry climate situation following an initially wet suction profile, Case B; and edge shrinkage distortion mode resulting from a dry climate situation following an initially equilibrium suction profile, Case C, a less severe condition than Case B. The soil suction at the location of the water leak within the soil mass is assumed to have reached an equilibrium condition and remains a constant 2.0 pF (9.8 kPa) throughout the year. Table 1 describes each Case.

Table 1. Case Descriptions

Case A: Edge Heave Resulting From a Long Dry Climate Followed by a Wet Climate		
Sub-Case	Description	Notes
A1	No leaking water line	Edge heave distortion mode is simulated by a one year wet climate following a dry suction profile. Soil suction at water leak location is assumed constant and equal to 2.0pF (9.8 kPa) throughout the year.
A2	Water line leak located 0.5m below the slab center	
A3	Water line leak located 1.0m below the slab center	
Case B: Edge Heave Resulting From an Initially Wet Climate Followed by a Long Dry Climate		
Sub-Case	Description	Notes
B1	No leaking water line	Edge shrinkage distortion mode is simulated by a one year dry climate following a wet suction profile. Soil suction at water leak location is assumed constant and equal to 2.0pF (9.8 kPa) throughout the year.
B2	Water line leak located 0.5m below the slab center	
B3	Water line leak located 1.0m below the slab center	
Case C: Edge Heave Resulting From Initially Suction Equilibrium Followed by a Long Dry Climate		
Sub-Case	Description	Notes
C1	No leaking water line	Edge shrinkage distortion mode is simulated by a one year dry climate following a long term equilibrium suction profile. Soil suction at water leak location is assumed constant and equal to 2.0pF (9.8 kPa) throughout the year.
C2	Water line leak located 0.5m below the slab center	
C3	Water line leak located 1.0m below the slab center	

In all the cases studied, a slab foundation of 8m (26.25 ft.) square resting on an Egyptian expansive soil was analyzed. The thin slab was stiffened by 250 mm wide x 400 mm (9.8x15.75 in.) deep stiffening beams and the spacing between the stiffening beams was 4m (13.1 ft.) in each direction. The thin slab was 100 mm (4 in.) thick and was loaded by 30.25 kN/m (2,073 lb./ft.) on the perimeter, 41.8 kN/m (2,865 lb./ft.) line loads along the central axis, and a uniformly distributed load of 2.2 kPa (46.45 psf)over the entire slab area.

The diffusion coefficient, the active zone depth, and the suction compression index for the Egyptian expansive soil were calculated and reported previously by El-Garhy (1999) to be 1.22×10^{-3} cm^2/sec, 6m (19.7 ft.), and 0.01975, respectively. The wet and dry soil suction profiles were calculated by the SUCH model for a soil profile initially at a constant suction of 4.0 pF (981 kPa), and was subjected to a constant wet surface suction of 2.0 pF (9.8 kPa) for a period of six months to produce the wet suction profile and to a constant dry surface suction of 6.0 pF (98,060 kPa) for a long period to produce the dry suction boundary profile. Figure 1 shows the predicted wet and dry suction boundary profiles used in the present study as the initial boundary profiles to predict the modes of distortion in each case.
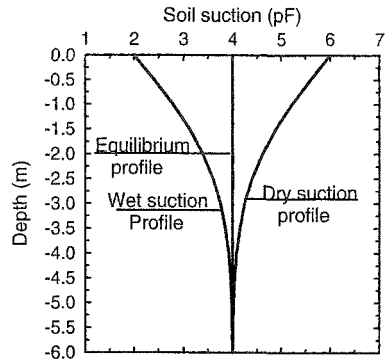
Fig. 1. Wet, equilibrium, and dry suction profiles used as the initial soil moisture suction distribution in the soil mass.

Analysis of the Results

Soil Suction and Distortion Mound Shapes
The soil suction distribution in the expansive soil mass and the associated volume changes or distortion mound shapes were predicted by the SUCH model for the 9 cases of Table 1. Figure 2 shows the distribution of soil suction in the supporting expansive soil mass beneath the slab foundation for cases A1, A2, and A3. Figure 3 shows the predicted distortion mound shapes for cases A1, A2, and A3. Referring to Figs. 2 and 3, and depicting the slab as rigid for illustration purposes, it is observed:

1. The effect of a leaking water line located 0.5m and 1.0m below the slab center on suction distribution extends approximately 1.0m from the point of the leak in each lateral direction for each leak location as shown in Figs. 2b and 2c.

2. The leaking water line located at 0.5m and 1.0m below the slab center causes localized heave that leads to the formation of an internal mound in the center of the

(a)

(b)

(c)
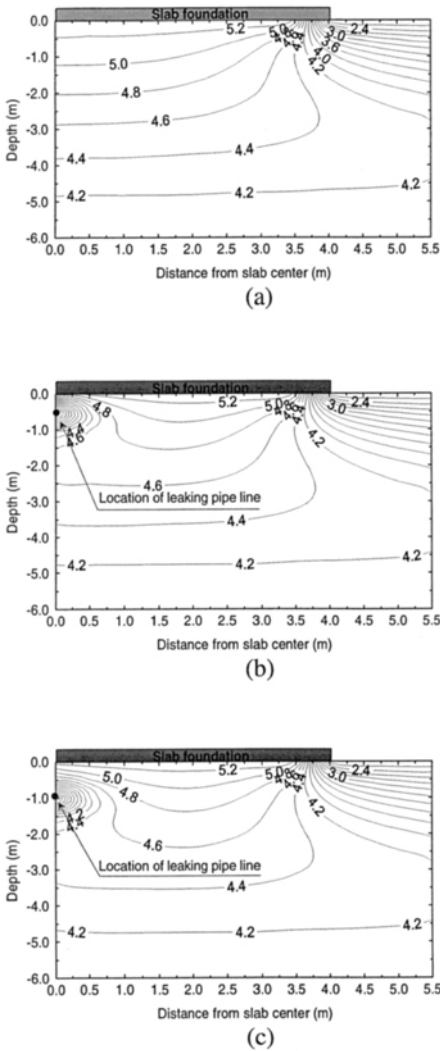
Fig. 2. Predicted soil suction distribution beneath slab foundation: (a) Case A1, no leaking water line; (b) Case A2, leaking water line located at 0.5 m below slab center; (c) Case A3, leaking water located 1.0m below slab center.

edge heave distortion shapes as shown in Figs. 3b and 3c. However, the magnitude of the localized heave in Case A3 (44.2 mm; 1.74 in.) is slightly greater than that in Case A2 (42 mm; 1.65 in.), this is because the depth of expansive soil subjected to wetting from leaking water line in Case A3 is greater than that in Case A2.

3. The leaking water line causes a higher value of localized heave due to the initial dry soil moisture suction condition assumed in the analysis beneath the slab.

4. The water line leak causes a decrease in the maximum differential heave as shown in Fig. 3.

Figure 4 shows the distribution of soil suction in the supporting expansive soil mass beneath slab foundation for Cases B1, B2, and B3. Figure 5 shows the predicted distortion mound shapes for Cases B1, B2, and B3. Referring to Figs. 4 and 5, it is observed that:

1. The effect of a water leak located 0.5m and 1.0m below the slab center on suction distribution extends a distance of approximately 0.5m laterally from the point of the leaks as shown in Figs. 4b and 4c.

2. A leak located 0.5m and 1.0m below the slab center causes a localized heave that leads to the formation of an internal mound in center of the edge shrinkage distortion mound shapes (Figs. 5b

Fig. 3. Predicted edge heave distortion mound shapes beneath slab foundations; (a) Case A1, no leaking water line; (b) Case A2, leaking water line located 0.5m below slab center; (c) Case A3, leaking water line located 1.0 m below slab center.

(a)

(b)

(c)
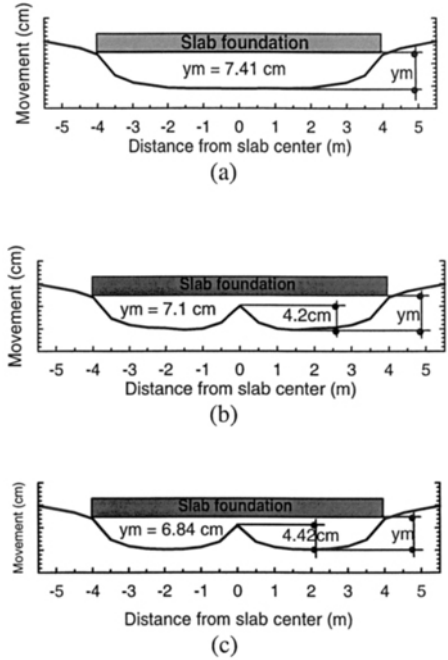
and 5c). The magnitude of the localized heave in Case B3 (90.3 mm; 3.91 in.) is slightly greater than that in Case B2 (90 mm; 3.54 in.).

3. A leaking water line causes a smaller magnitude of localized heave in the initial wet soil moisture suction condition assumed in the analysis than in the initially drier soil condition of Case A.

4. A water leak causes a greater maximum differential heave as shown in Fig. 5.

Figure 6 shows the distribution of soil suction in the supporting soil mass beneath the slab foundation for Cases C1, C2, and C3. Figure 7 shows the predicted distortion mound shapes for Cases C1, C2, and C3. Referring to Figs. 6 and 7, it is observed that:

1. The effect of a leak located 0.5m and 1.0m below the slab center on the suction distribution extends a distance of approximately 0.4m laterally from the point of the leak as shown in Figs. 6b and 6c.
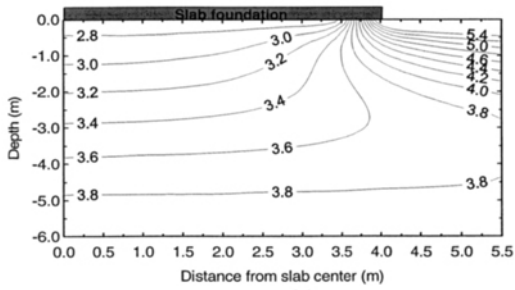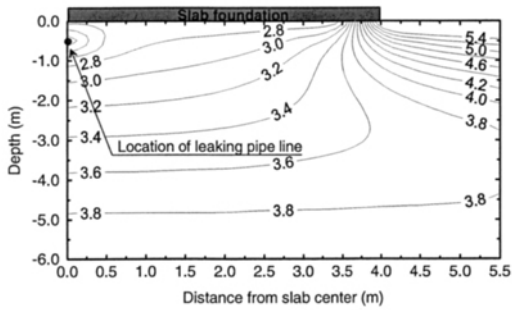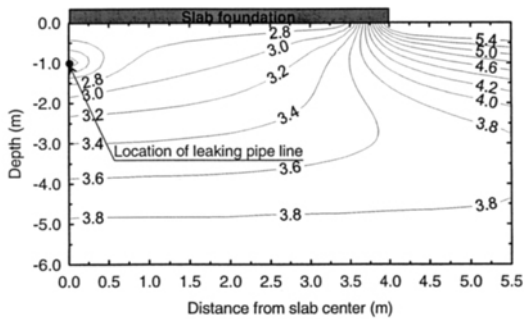
Fig. 4. Predicted soil suction distribution beneath slab foundation: (a) Case B1, no leaking water line; (b) Case B2, leaking water line located at 0.5 m below slab center; (c) Case B3, leaking water line located at 1.0 m below slab center.
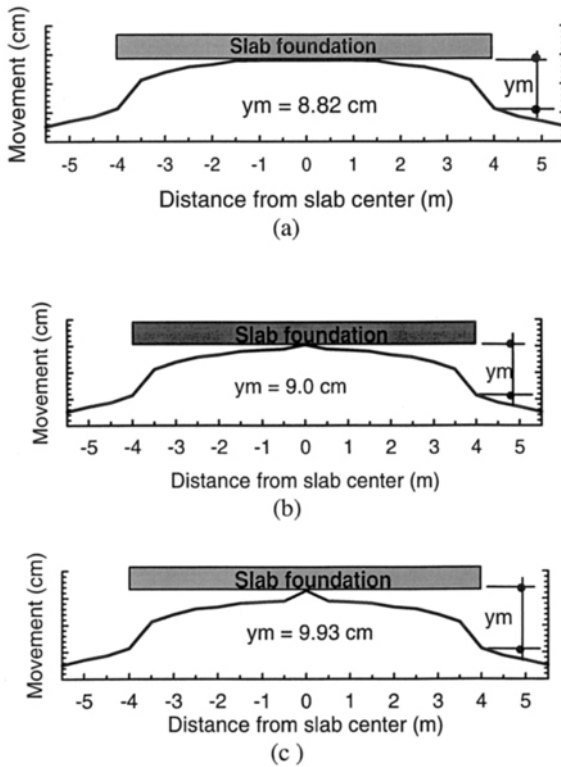
Fig. 5. Predicted edge shrinkage distortion mound shapes beneath slab foundation: (a) Case B1, no leaking water line; (b) Case B2, leaking water line located at 0.5 m below slab center; (c) Case B3, leaking water line located at 1.0 m below slab center.

2. A leak located 0.5m and 1.0 m below the slab center causes a localized heave that leads to the formation of an internal mound in the center of the distortion mound shapes (Figs. 7b and 7c). However, the magnitude of the localized heave in Case C3 (95.9 mm; 3.78 in.) is slightly greater than that in Case C2 (90.4 mm; 3.56 in.).

3. A leak causes a smaller value of localized heave due to the initial equilibrium soil moisture suction condition assumed in the analysis beneath the slab foundation.

4. A water leak causes greater maximum differential heave as shown in Fig. 7
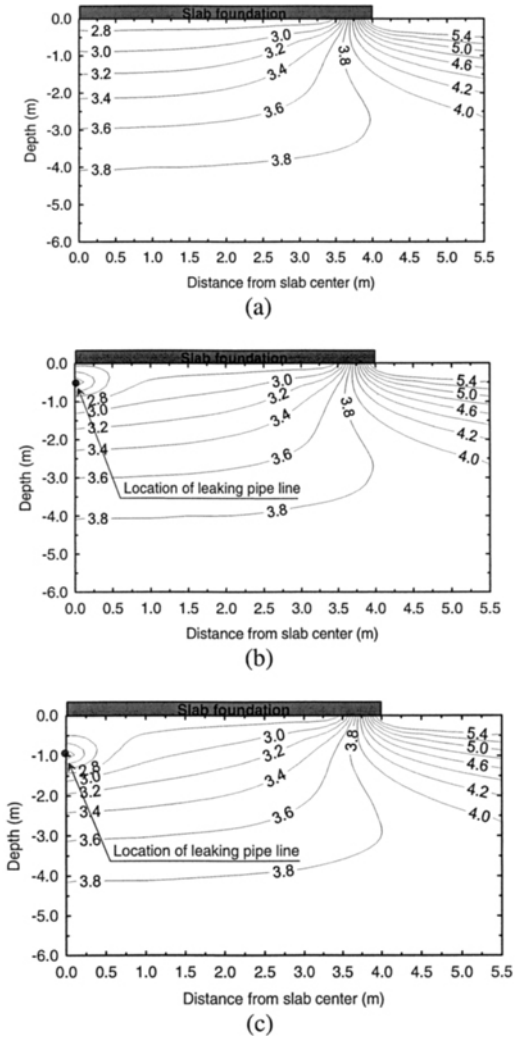
Fig. 6. Predicted soil suction distribution beneath slab foundation: (a) Case C1, no leaking water line; (b) Case C2, leaking water line located at 0.5 m below slab center; (c) Case C3, leaking water line located at 1.0 m below slab center.
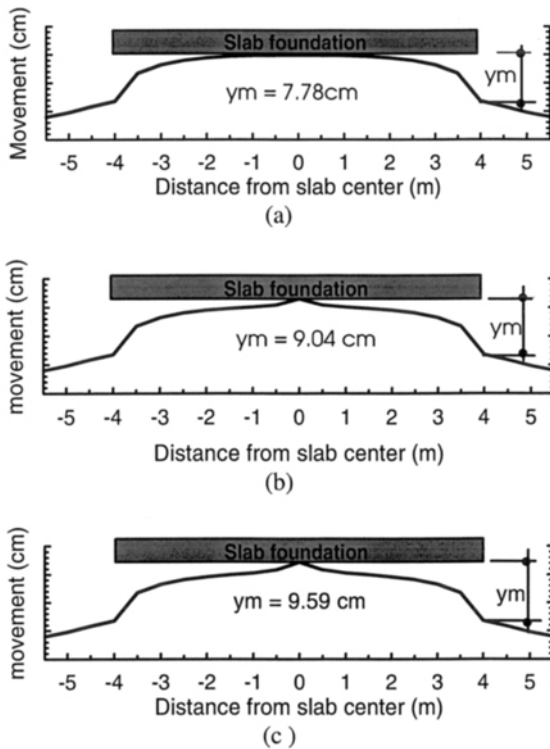
Fig. 7. Predicted edge shrinkage distortion mound shapes beneath slab foundation: (a) Case C1, no leaking water line; (b) Case C2, leaking water line located at 0.5 m below slab center; (c) Case C3, leaking water line located at 1.0 m below slab center.

Deflection and Bending Moment in Slab Foundation

The interaction between the stiffened slab and the distortion mound shapes was modeled using SLAB97. For all the studied cases, the maximum differential deflection and the maximum positive and negative bending moments were calculated and presented in Table 2 as a ratio from the values in cases of no leaking water line.

Referring to Table 2, it is observed that:

1. Cases B3 and C3 are considered the worst cases that produce the maximum design parameters (i.e., bending moment, deflection and shear) in the slab foundation. As shown in Table 2, in Case C3 the maximum differential heave, the maximum

Table 2. Comparison of maximum differential heave and structural
design parameters in slab foundation for the studied cases

Case	Ratio of Values Before the Leak Occurred to Values After the Leak Occurred			
	Maximum Differential Heave	Maximum. Differential Deflection	Maximum Positive Moment	Maximum Negative Moment
A1	1.00	1.00	1.00	0
A2	0.96	1.03	1.00	0
A3	0.92	0.95	0.99	0
B1	1.00	1.00	0	1.00
B2	1.02	1.03	0	1.14
B3	1.13	1.05	0	1.41
C1	1.00	1.00	0	1.00
C2	1.16	1.05	0	1.26
C3	1.23	1.07	0	1.44
	Note: Values of soil heave are indicated in Figs. 3, 5, and 7.			

differential deflection and the maximum bending moment increased by approximately 23%, 7% and 44%, respectively due to a water line leak. In Case B3, the maximum differential heave, the maximum differential deflection and the maximum bending moment increased by approximately 13%, 5% and 41%, respectively, due to a leak.

2. In Cases A2 and A3, the effect of leaking water line on the maximum differential heave, the maximum differential deflection and the maximum bending moment was less than 8%.

Conclusions

This paper introduces guidance on how the effect of a leaking water line might be taken into account in the analysis and design of slab or raft foundation resting on expansive soil. The following conclusions are reached from this study:

1. A leaking water line beneath a slab foundation may cause structural distress to the supported superstructure. However, the effect of a leaking water line is dependent on the soil moisture condition in the supporting expansive soil mass prior to the leak occurring.

2. A water line leak occurring during the formation of the edge shrinkage (center lift) distortion mode beneath a slab foundation can cause an increase in the maximum

differential heave experienced by the slab and the structural design parameters in the slab foundation (e.g., an increase in bending moment).

3. The effect of a water line leak on the maximum differential heave and the slab structural design parameters during the formation of an edge shrinkage (center lift) distortion mode decreases as the depth of leaking water line below the slab foundation decreases.

4. The effect of a water line leak on the maximum differential heave and the slab structural design parameters during the formation of edge heave distortion mode may be less than for edge shrinkage (center lift).

References

El-Garhy, B. M., (1999), "Soil Suction and Analysis of Raft Foundation Resting on Expansive Soils," Ph.D. Dissertation, Civil Engineering Department, Minufiya University, Egypt.

El-Garhy, B. M., Wray, W. K., and Youssef, A. A., (2000), "Using Soil Diffusion to Design Raft Foundation on Expansive Soils," Geotechnical Special Publication No. 99, ASCE, pp. 586-602.

El-Garhy, B. M., Wray, W. K., (2004) "Method for Calculating the Edge Moisture Variation Distance," Journal of Geotechnical and Geoenvironmental Engineering, , ASCE, Vol.130, No. 9, pp. 945-955.

Jackson, D. J., and Moody, E. D., (1999) "Plumbing Leaks and Their Influence on Foundation Movement and Associated Damage,) Texas Section ASCE, Spring meetings, pp. 73-79.

Lytton, R.L. (1994), "Prediction of Movement in Expansive Clay," Geotechnical Special Publication No. 40, ASCE, Vol. 2, pp. 1827-1845.

Mills, K.G., (2000), "A numerical Model of Ground Moisture Variation with Active Vegetation," Asian Conference on Unsaturated Soils, May 18-19, Singapore, pp. 237-242.

Nelson, J.D. and Miller, D.J. (1992), "Expansive Soils: Problems and Practice in Foundation and Pavement Engineering," John Wiley & Sons, Inc., NY.

Post-Tensioning Institute (2004), "Design of Post-Tensioned Slabs-on-Ground," 3rd Ed., Phoenix, AZ

Wray, W.K., (1995), Editor, "So Your House is Built on Expansive Soils," American Society of Civil Engineers, New York.

Wray, W. K., El-Garhy, B. M., and Youssef, A. A., (2005) "Three-Dimensional Model for Moisture and Volume Changes Prediction in Expansive Soils," Journal of Geotechnical and Geoenvironmental Engineering, ASCE, Vol. 131, No. 3, pp. 311-324.

Settlement of Coal-Fired Power Plant Foundations on Arid Soils

José L.M. Clemente[1], M. ASCE, Jeffrey O'Neal[2], and Charles G. Worthington[3]

[1]Principal Geotechnical Engineer, Bechtel Power Corporation, 5275 Westview Drive, Frederick, MD 21703, USA, jlclemen@bechtel.com
[2]Engineering Group Supervisor, Bechtel Power Corporation, 5275 Westview Drive, Frederick, MD 21703, USA, joneal@bechtel.com
[3]Assistant Project Engineer, Bechtel Power Corporation, 5275 Westview Drive, Frederick, MD 21703, USA, cworthin@bechtel.com

Abstract

A new 400 MW coal-fired power generating unit was planned to be constructed next to two existing units in the desert of central-eastern Arizona. An expansive clay layer was encountered at depth within the site of the two existing units. The clay layer was stiff to hard, and groundwater was located several hundred meters below the ground surface at the site. However, previous foundation heave experience obtained from another power plant built to the north of the site in the late 1970s/early 1980s led the designers to use drilled piers installed to a depth of about 24 m to support the two existing units. An extensive subsurface investigation program performed at the site of the new unit revealed the presence of alluvial sands and gravelly sands to a depth of about 8 m, where the top of the clay layer was encountered. Based on the results of field and laboratory tests and geotechnical analyses, it was decided to support the new unit using footings and structural mats placed directly on the alluvial soils. The use of these shallow foundations would result in significant schedule and cost savings for the project. Detailed foundation settlement monitoring for more than 1 year during plant construction indicated excellent foundation settlement performance and the adequacy of the selected foundation system.

Introduction

A coal-fired power generation unit was constructed at a site in the desert of central-eastern Arizona with subsurface conditions that included a layer of potentially expansive clay. The power unit includes one steam turbine, one boiler building, one baghouse, two induced draft fans, two scrubbers, and one 150 m high stack. A number of ancillary structures were also built, including a cooling tower, a main transformer, a coal handling facility, a lime unloading and storage facility, and water storage tanks. Figure 1 shows the layout of the power plant and the locations of selected

settlement markers that will be discussed later. The cooling tower, which is a few hundred meters to the west/southwest of the turbine building, and the coal handling facility, which is a few hundred meters to the north/northwest of the stack, are not shown on Figure 1. The power station cooling water is taken from onsite wells, circulated through the steam turbine, and cooled in the cooling towers in a closed cooling system.

The foundation system selected for the power station components consists of footings and structural mats. This paper includes summary descriptions of the site and subsurface conditions, geotechnical analyses, settlement calculations, and measured settlements. The measured settlements indicate excellent foundation settlement performance that validates the design assumptions and confirms the adequacy of the selected cost-effective foundation system.

Site Conditions

The site grade in the area of the existing power generating units was at Elevation 2,126 m based on the National Geodetic Vertical Datum of 1929 (NGVD 1929). The area proposed for construction of the new unit was adjacent to and west of the existing units. This area was flat with a loose surficial sand cover and lightly vegetated with grass and small brush.

The ground surface in the proposed water treatment area west of the new unit was relatively flat with elevations from about 2,122 to 2,124.5 m increasing in a north-to-south direction. The surface was moderately compacted due at least in part to occasional traffic through the area and was generally free of vegetation, except for a few scattered areas containing grass and/or small brush.

The proposed cooling tower area was southwest of the new unit in an undeveloped portion of the site resembling a typical high-desert environment. The ground surface was sandy, slightly irregular, and moderately vegetated with grass and small brush. The ground surface elevation varied from about 2,119.5 to 2,124.5 m.

The proposed coal handling facilities were north of the new unit in the area of the former 90-day coal storage pile and intermingled with the existing units' coal handling facilities. The ground surface in this area was generally at an elevation of about 2,123 m and consisted of loose to compacted sand. The area inside the west end of the railroad loop contained a light to moderate vegetation covering of grass and small brush. Portions of the area were covered with coal dust that was underlain by a layer of fly ash at a shallow depth. A drainage ditch leading to the coal pile runoff pond area at the west end of the railroad loop was just inside the railroad tracks.

Site Geology

The site lies in the southern part of the Navajo section of the Colorado Plateau physiographic province (Fenneman 1931). This area is characterized by the presence of badlands, valleys, and ridges. Terraces on the ridges reflect erosion cycles resulting from down-cutting by the Little Colorado River that flows through this area.
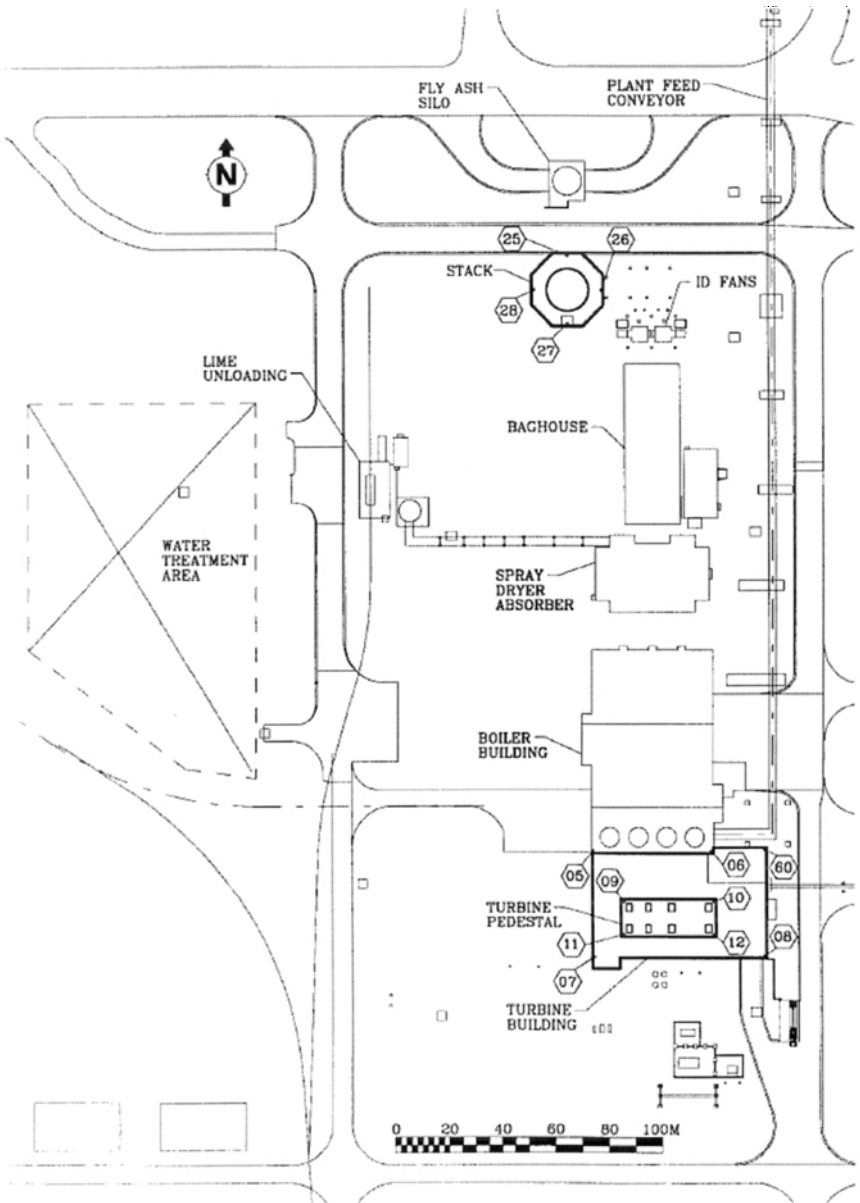
Figure 1. Layout of power plant and location of settlement markers.

Geologic units interpreted to be in the scope of the site subsurface investigation include relatively young alluvial deposits, the Pliocene Age Bidahochi Formation, and the Late Triassic Age Chinle Formation.

The alluvial deposits are composed primarily of sand with occasional gravel and cobbles and lesser amounts of clayey sand and sandy clay in generally discontinuous layers. The deposits likely result from erosion and sheet flow from the surrounding mountains and deposits from streams flowing across the area. Clayey layers contained within these deposits can have a significant effect on foundation design due to their expansion potential resulting from the generally dry nature of the deposits in this area and their ability to absorb water, increasing the volume of the deposit.

The alluvial deposits overlie and are often indistinguishable from the Bidahochi Formation due to similarities in the nature of the materials comprising the two formations. The Bidahochi Formation beneath the site consists of only the upper formation member, as subdivided by Repenning and Irwin (1954). Within the depth investigated beneath the site, the formation can generally be characterized as sand or silty sand, sometimes weakly cemented, with minor amounts of clay and gravel.

The Petrified Forest Member of the Chinle Formation underlies the Bidahochi Formation beneath the site. None of the borings drilled at the site encountered the Chinle Formation. However, previous borings drilled for the existing units encountered it at depths of 18 and 39 m, indicating the presence of a very irregular surface at the top of the formation, which was possibly caused by erosion before the Bidahochi sediments were deposited. The Petrified Forest Member is composed primarily of claystone with lesser amounts of siltstone and mudstone, while beds of sandstone and conglomerate may be present locally. The Chinle strata exhibit various colors ranging from light to dark gray or green to purple with a reddish tint.

Site Subsurface Conditions

The site subsurface conditions for the new unit were explored by 68 standard penetration test (SPT) boreholes that extended to depths ranging from 5 to 30 m. Two field electrical resistivity survey lines and one geophysical seismic crosshole/downhole test were also performed. A typical subsurface profile through the new unit is shown in Figure 2.

Ten SPT boreholes that penetrated through the Alluvial Deposit showed that the thickness for this layer ranged from about 9 to 18.5 m. The soils comprising this stratum included low-plasticity clayey sands and sands and occasional thin, low-plasticity clay layers. The SPT blow counts measured in the Alluvial Deposit ranged from 2 blows/300 mm to 50 blows/50 mm with a median value of 38 blows/300 mm and an average value of 49 blows/300 mm. A design SPT value of 30 blows/300 mm was adopted.

A discontinuous 1.5 to 3 m thick clay layer was encountered at a depth of about 8 m in several boring locations within the Alluvial Deposit. The liquid limit for this clay ranged from 41 to 76 percent with a median value of 63 percent and an average value of 61 percent, and the plastic limit ranged from 23 to 34 percent with a median value of 23 percent and an average value of 25 percent. This layer was potentially expansive.
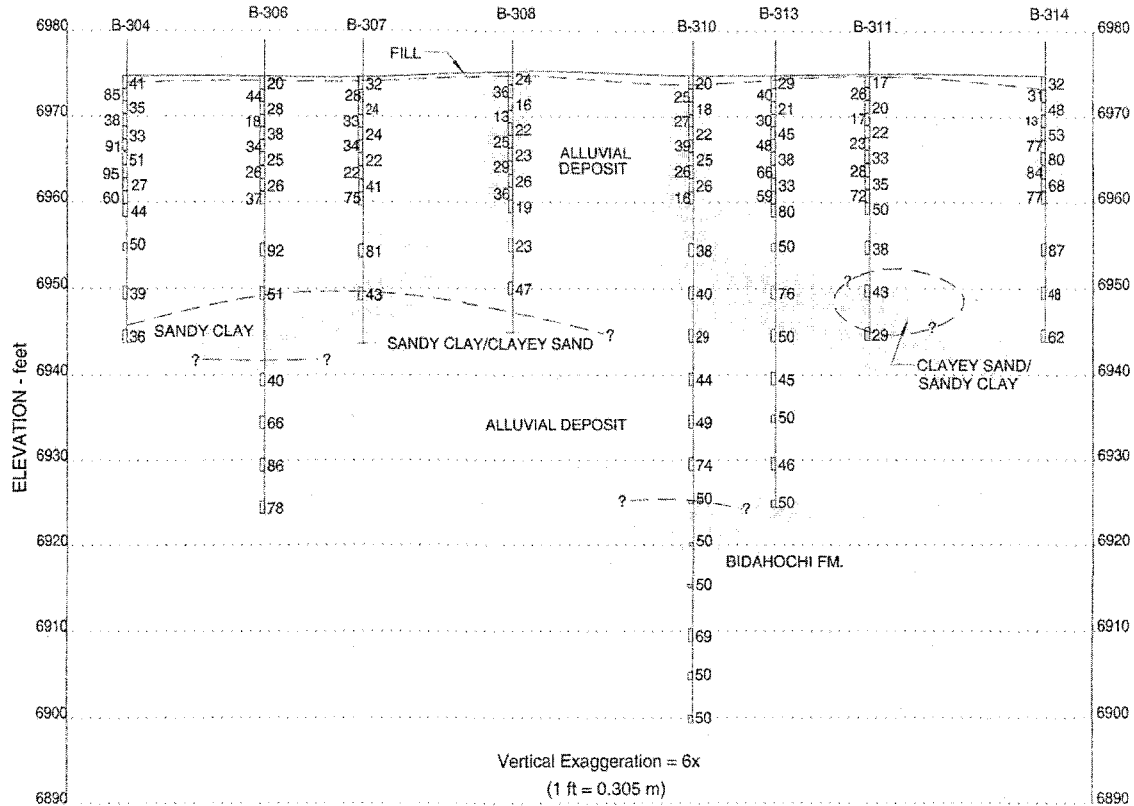
Figure 2. Typical subsurface profile.

Ten SPT boreholes were extended into and terminated in the Bidahochi Formation soils. These soils were classified as gravelly sandstone (local grading) to silty sandstone, clayey sandstone, and sandstone and were characterized by very high SPT blow counts that ranged from 60 blows/300 mm to 50 blows/75 mm with a median value of 120 blows/300 mm (linearly extrapolated) and an average value of 114 blows/300 mm (linearly extrapolated). A design SPT value of 100 blows/300 mm was adopted.

Groundwater was not encountered at the depths drilled at the site. The regional groundwater table is believed to occur in the Kaibab-Coconino aquifer at a depth of more than 200 m beneath the site. The fine-grained deposits of the Chinle Formation are considered to provide an impermeable barrier between the aquifer and the shallow formations beneath the site.

Seismic activity in the vicinity of the site is considered to be moderate to low (Fellows 2000).

Swell Potential of Clay Layer

Foundations for the existing units consisted of drilled piers to minimize settlements. Because of the presence of the potentially expansive clay layer at depth, the initial recommendations included the use of structurally suspended (separated from the soils) floor slabs and mats and drilled piers designed to resist tensile forces created by expansion of the clay layer. The recommendation to use structurally suspended slabs and mats was eventually eliminated. This heightened concern about the potential for clay layer expansion was caused by observed foundation problems at another plant built to the north of the site.

The groundwater was more than 200 m below the ground surface, so groundwater fluctuation was not expected to affect the clay layer. However, leaks from water pipes, although unlikely, could result in increased moisture content and swelling of the clay layer. For this reason, several swell potential tests were conducted on relatively undisturbed samples collected from the clay layer during the subsurface investigation for the new unit. The tests were conducted in accordance with American Society for Testing and Materials (ASTM) Standard D 4546 (1996) using either a small pressure (almost a free swell condition) or a pressure close to that produced by the existing soil overburden (foundation pressures not included). These test conditions resulted in higher swelling than if the foundation pressures had been used, providing more conservative swell potential estimates. Seventeen samples were tested, with the following test results: no swell (13 samples), swell of 0.3 percent or less (3 samples), and swell of 1.2 percent or less (1 sample). Based on these test results, it was concluded that swelling of the clay layer encountered in the Alluvial Deposit was not expected to adversely affect the performance of shallow foundations at the site. A decision was then made to consider the use of shallow foundations to support all structures and equipment, pursuant to the results of bearing capacity and settlement calculations. The use of shallow foundations was expected to result in significant schedule and foundation cost savings.

Engineering Properties for Bearing Capacity and Settlement Calculations

Subsurface material engineering properties for bearing capacity and settlement calculations were developed using correlations with the results of field (SPT) tests. These engineering properties are shown in Table 1. The layer thicknesses reflect average values over the plant foundation areas. The compressibility properties (E-values) reflect the assumption that settlements were expected to be mostly short term due to the granular or overconsolidated/dry nature of the soils at the site. Therefore, only elastic parameters were developed for all soil layers.

Table 1. Engineering properties for bearing capacity and settlement calculation.

Soil Layer	Layer Description	Thickness (m)	$s_u^{(1)}$ (kPa)	$\phi^{(2)}$ (degrees)	E (MPa)
1	Alluvial Deposit	15	0	35	$52.5^{(3)}$
1a	Clay (Discontinuous)	1.5-3	240	0	$143.5^{(4)}$
2	Bidahochi Formation	>15	0	40	$170^{(3)}$

[1] s_u was calculated from $s_u = 6N$ (Lowe III and Zaccheo 1975), where N is the design SPT blow count for the layer.
[2] ϕ was calculated from the design SPT blow count for the layer (Bowles 1982).
[3] E was calculated from $E = 1.72N$ (Davie and Lewis 1988), where N is the design SPT blow count for the layer.
[4] E was calculated from $E = 600s_u$ (Davie and Lewis 1988).

Bearing Capacity Calculations

For bearing capacity calculation purposes, it was assumed that the Alluvial Deposit soils extended to depths below the foundation zones of influence. This was expected to provide lower-bound bearing capacity estimates, since the possible beneficial effects from the hard clay layer and the very dense Bidahochi Formation soils would be ignored. The bearing capacity of shallow foundations was calculated according to the procedure outlined by Vesic (1975) for non-cohesive soils. The foundation depth was taken at 0.8 m, which was the minimum recommended frost depth at the site. Calculations were performed for typical anticipated foundation sizes, and a global factor of safety equal to 3 against bearing capacity failure was used. The results are shown in Figure 3.

The results shown on Figure 3 indicate that an allowable bearing pressure of at least 191 kPa (4 ksf) can be used to size wall (strip) and column footings at the site. The allowable bearing pressures for square and rectangular mats with widths ranging from 6 to 20 m placed at a depth of 0.8 m or deeper would be much larger than those presented in Figure 3. Therefore, no calculations were performed for large square and rectangular mats. An allowable bearing pressure of 191 kPa (4 ksf) was recommended for permanent building and equipment foundations.

Settlement Calculations

The bearing pressures applied by coal-fired plant equipment foundations are typically about 200 kPa for most dead and normal operating load combinations, but they can

reach localized values on the order of 250 kPa. The bearing pressures can exceed 250 kPa for some more extreme, short-duration load conditions. Only bearing capacity considerations are taken into account for the short-duration load combinations because these loads are not expected to cause permanent settlement. Because of equipment leveling requirements, strict differential settlement limitations are sought for the long-duration load combinations, which include mostly dead and normal operating loads. For satisfactory foundation performance, the maximum settlement is typically limited to 25 mm for column footings and to 50 mm for structural mats. Generally, these settlement limits are not imposed on tanks because they are very flexible and settlement tolerant. The foundation design goal is for settlements to be stabilized by the end of construction to prevent post-construction foundation movements that can be potentially detrimental to equipment performance.

The following simplified procedure was used to calculate elastic settlements:

1. Subdivide the subsurface profile into several sublayers of thickness Δz to the depth where the calculated pressure increase from the foundation is no more than 10 percent of the applied foundation pressure p. This depth is never taken as less than $2B$ (twice the foundation width) below the bottom of the foundation (note that Δz can be different for different sublayers).

2. Calculate the influence values I_σ and the pressure increase $\sigma_z = I_\sigma p$ beneath the center and corner/edge of the foundation at the center of each sublayer, assuming uniformly distributed, flexible foundation loads.

3. Calculate the strain ε at the center of each sublayer according to:

$$\varepsilon = \sigma_z / E$$

Where: E = modulus of elasticity for the sublayer.
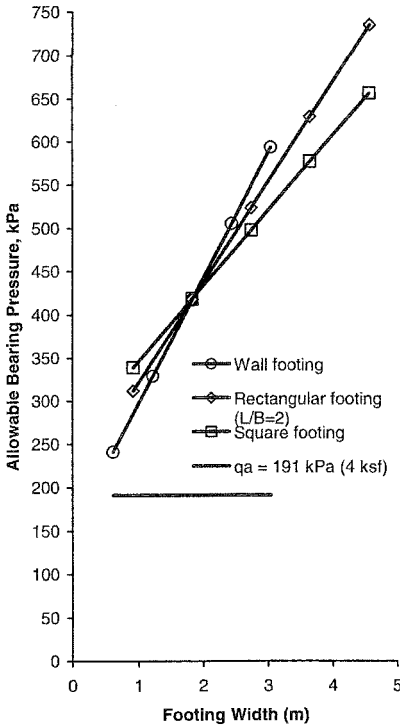
Figure 3. Calculated bearing capacity for footings.

4. Calculate the settlement of each sublayer according to:

$$\Delta H/\Delta z \;=\; \varepsilon = \sigma_z/E \Rightarrow \Delta H = \sigma_z \cdot \Delta z\, /E$$

Where: $\Delta H=$ settlement of sublayer and
Δz = thickness of sublayer.

5. Add the settlement of all sublayers to obtain the total settlement at the center and corner/edge of the foundation. The average of these two values is the estimated settlement of the rigid foundation.

Only the compressibility parameters for the Alluvial Deposit soils were used in the settlement calculations for footings, even if the zone of influence extended below 15 m. Compressibility parameters for both the Alluvial Deposit soils and the very dense Bidahochi Formation soils were used in the settlement calculations for mats.

Calculations were performed for typical anticipated foundation sizes and a bearing pressure of 191 kPa (4 ksf). The results are shown in Figures 4 and 5.

The results shown in Figures 4 and 5 indicate that acceptable foundation settlements were expected for an allowable bearing pressure of 191 kPa (4 ksf). Because the settlements were calculated using elastic parameters, a percent change in bearing pressure would result in an identical percent change in settlement for any given foundation size.
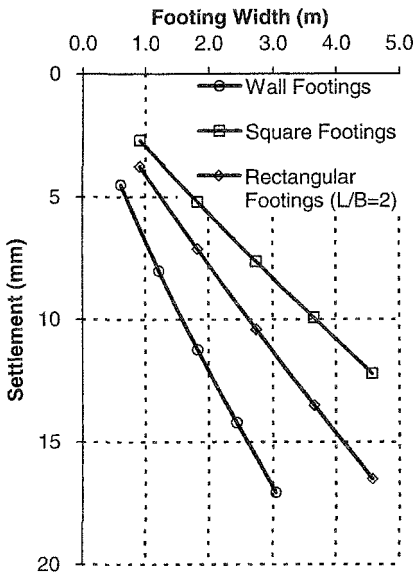
Figure 4. Calculated footing settlement under 191 kPa.
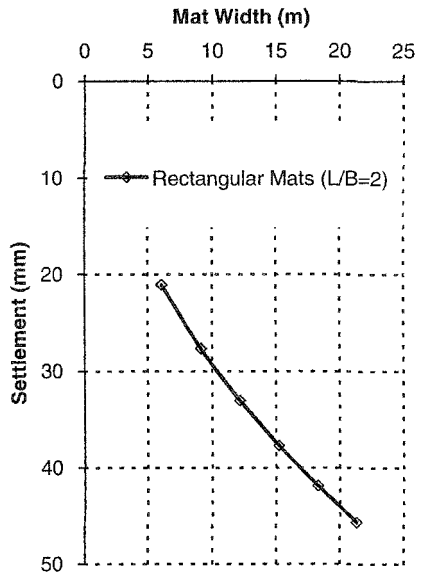
Figure 5. Calculated mat settlement under 191 kPa.

Measured Foundation Settlements

Measured settlements for selected foundations are shown in Figures 6 through 8. Each curve on these figures corresponds to data obtained from one of the settlement markers identified in Figure 1. An initial settlement reading was taken soon after the settlement monitoring markers were installed on the foundations. Subsequent readings were taken at about 2-month intervals. Settlement monitoring continued throughout construction for about 18 months, and the last values shown in Figures 6 through 8 correspond to full loading of the foundations.

Qualitatively, the settlement curves shown in Figures 6 through 8 generally follow the anticipated foundation settlement behavior at this site. Most of the settlement took place during load application, and only minor subsequent settlements were measured. This is particularly true with respect to the settlement measurements for the turbine pedestal shown on Figure 7. Also, most settlement markers showed signs of settlement stabilization when the last readings were taken, as shown in Figures 6 through 8.

Quantitatively, the settlement curves shown in Figures 6 through 8 show much smaller settlements for large mats than suggested by Figure 5. The smaller settlements are explained, in part, by the fact that the final design loads were smaller than the allowable bearing pressure of 191 kPa. For instance, the maximum design soil pressure beneath the stack foundation under sustained loading was about 144 kPa with a much lower average bearing pressure. The design soil pressure range beneath the turbine pedestal was 115 to 167 kPa under sustained loading with an average bearing pressure of about 141 kPa. These smaller bearing pressures still do not fully account for the fact that measured settlements were much smaller than the estimated settlements. The choice of elastic parameters was conservative, providing somewhat large settlement estimates. Note that the combination of design bearing pressure being smaller than the recommended allowable bearing pressure, and the use of conservative elastic parameters resulted in the acceptable design approach, as reflected in the magnitude of measured settlements.

Conclusions

A comprehensive subsurface investigation program and subsequent geotechnical analyses were used to develop a cost-effective foundation system for the coal-fired power plant. Concerns about possible adverse effects from swelling of the clay layer were eliminated by performing geotechnical laboratory tests that disclosed low swell potential. Measured settlements of permanent buildings and equipment were smaller than the calculated settlements, but the time-settlement history supports the design assumptions that short-term settlements would occur. The power station foundations were performing satisfactorily toward the end of construction in 2005.
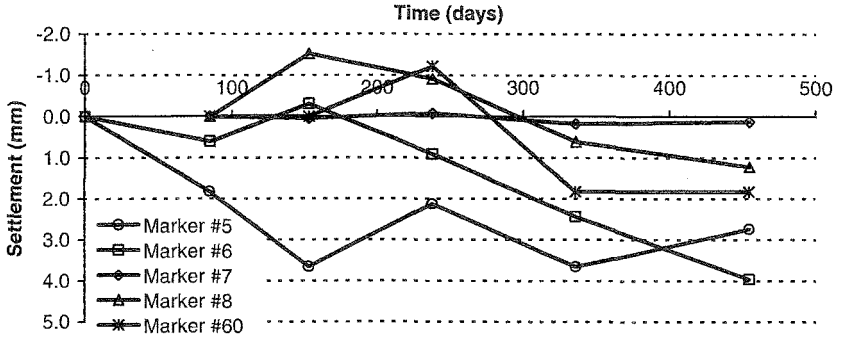
Figure 6. Settlement of turbine building foundation mat.
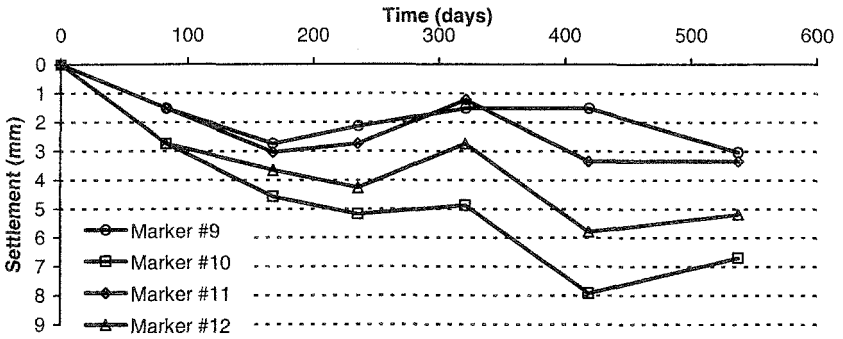
Figure 7. Settlement of turbine pedestal mat.
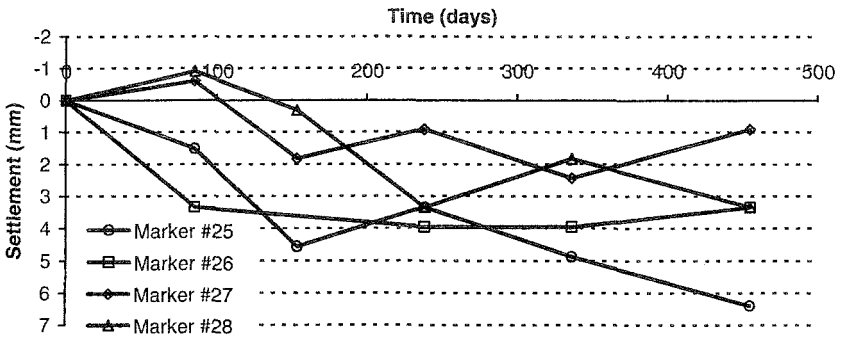
Figure 8. Settlement of stack foundation mat.

References

ASTM (1996). "Standard Test Method for One-Dimensional Swell or Settlement Potential of Cohesive Soils, D 4546," *Annual Book of ASTM Standards, Vol. 04-08*, Philadelphia, Pennsylvania.

Bowles, J.E. (1982). *Foundation Analysis and Design, 3rd. Ed.*, McGraw-Hill Book Co., New York, New York, p. 786.

Davie, J.R. and M.R. Lewis (1988). "Settlement of Two Tall Chimney Foundations," *Proc. 2nd. International Conference on Case Histories in Geotechnical Engineering*, St. Louis, Missouri, pp. 1309-1313.

Fellows, L.D. (2000). *Earthquake Hazard in Arizona*, "Arizona Geology," Arizona Geological Survey, Vol. 30, No. 1.

Fenneman, N.M. (1931), *Physiography of Western United States*, McGraw-Hill Book Co., New York, New York.

Lowe III, J. and P.F. Zaccheo (1975). "Subsurface Explorations and Sampling," Chapter 1 in *Foundation Engineering Handbook*, edited by H.F. Winterkorn and H.Y. Fang, Van Nostrand Reinhold Co., New York, New York, pp. 1-66.

Repenning, C.A., and J.H. Irwin (1954). *Bidahochi Formation of Arizona and New Mexico*, American Association of Petroleum Geologists Bulletin, Vol. 38, No. 8.

Vesic, A.S. (1975). "Bearing Capacity of Shallow Foundations," Chapter 3 in *Foundation Engineering Handbook*, edited by H.F. Winterkorn and H.Y. Fang, Van Nostrand Reinhold Co., New York, New York, pp. 121-147.

Salt Encrusted Desert Flats (Sabkha): Problems, Challenges & Potential Solutions

Waddah Akili

Professor of Civil Engineering (Retired), Principal, Geotechnical Engineering, 3222 Evergreen Rd. Ames, Iowa, email:w.akili@isunet.net

Abstract

The evaporative and sedimentary environment that has prevailed over the southern shores of the Persian Gulf region (eastern Saudi Arabia, Qatar, and United Arab Emirates) has produced salt-encrusted flat areas known in Arabic as "sabkha". Building activities on sabkha areas have posed problems and challenges to the construction industry, triggered primarily by the excessive salts present in both the sediments and their shallow ground waters. In general, sabkha sediments are cemented and uncemented layers of sand /silt material, interbedded with pockets of clay and mud, where calcium carbonate and more recent digenetic minerals (gypsum, anhydrite) serve as the principal cementing agent. The geotechnical aspects of sabkha are addressed with particular reference to building foundations. Simplified soil profiles from selected sabkha sites with Standard Penetration Test Results are shown. The effectiveness of some soil densification methods, as a means of improving engineering properties of sabkha sediments, is touched upon. The paper concludes by offering guidelines for proper field investigation in sabkha terrain, with a geochemical component as an essential part of the geotechnical investigation.

Introduction

Salt-encrusted flat surfaces, known as "sabkha" in the Arabic-speaking countries, are common in the coastal and inland areas of the Arabian Peninsula. These features are products of the evaporative environment that has dominated the southern shores of the Persian Gulf region for several thousand years. Location of major sabkhas along those shores is shown in Figure 1. Conditions leading to the formation of these salt flats and their properties in the coastal and inland areas are different, and Kinsman & Park (1969) refer to these features as "coastal sabkha" and "continental sabkha" respectively. The geomorphology, the geochemistry, and regional environmental parameters that influence the nature of

sabkha sediments have been reported on by a number of investigators (Kinsman 1969; Bush 1973; Butler 1969).

In general terms, coastal sabkha sediments are loose to moderately dense silt/sand material of varying: size, composition, texture, and origin. Muds and clays are often interbedded with the sands and silts, as seams or pockets, and are usually found down at the bottom of the profile. Distinguishing features of sabkha deposits include some or all of the following:(i) puffy and relatively hard surface often dotted with halite; (ii) lack of any vegetal cover over the surface; (iii) highly saline ground water table (usually within two meters from the surface); and (iv) readily visible precipitated salts (halite, anhydrite, gypsum, and calcite) within the upper portion of the profile. At most times, sabkhas' hard surface is sufficiently strong and durable to serve as a substitute for surfaced roads. Unfortunately, if the surface gets wet due to occasional rainfall, flash floods or storm tides, the soluble salts(mainly halite)-which provide the cementation in the crust, dissolve and the sabkha becomes impassible (Fookes 1976).

Documented engineering type information on sabkha with reference to foundations and potential problems associated with buildings on sabkha sediments has remained scanty. Fookes (1976) evaluated coastal sabkha in the United Arab Emirates as road bases. Akili & Torrance (1981) have simulated sabkha sands in the laboratory and have assessed strength associated with cementation using different percent cement in the sand. Further work on cemented sands, with reference to sabkha, using a laboratory penetrometer, was presented by Akili & Al-Joulani (1986).
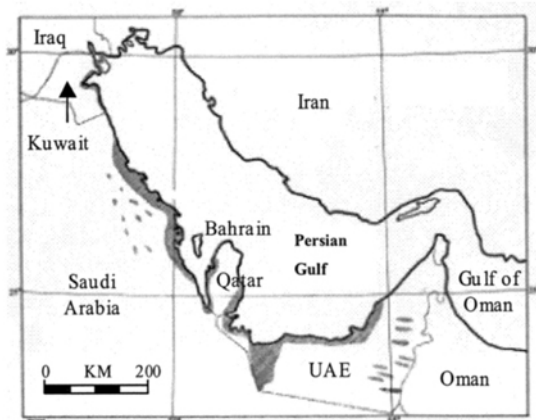
Figure 1. Map showing location of major sabkha flats along the southern coast of the Persian Gulf.

Fookes *et al.* (1985) have addressed chemical processes and geotechnical changes in sabkha soils and its waters, and have cited relevant case histories. Akili (1997) has evaluated some of the sabkhas along the western coast of Qatar Peninsula, by means

of open pits and borehole samples. The materials encountered in Qatar were, by and large, similar to those of the sabkhas of eastern Saudi Arabia.

This paper is an extension of earlier work by the author (Akili & Torrance 1981; Akili & Ahmad 1986; Akili 2004) on foundations in Sabkha terrain within the arid coastal margins of the southern shores of the Persian Gulf. Use is made of extensive field data collected from sabkha cites in eastern Saudi Arabia and Qatar. In this paper, the author sheds light on the nature of sabkha, its constituents, and common problems encountered in sabkha terrain. It also argues for the need to carry out an "appropriate" site investigation prior to design and construction of foundations in sabkha areas.

Sabkha Formation and Controlling Processes

Sabkha(s) are equilibrium geomorphic surfaces whose levels are largely determined by local ground water. Coastal sabkhas are supratidal and are commonly a wedge of sediments overlain by supratidal facies that are overlain by eolian facies. Figure 2 presents diagrammatically a generalized cross-section from the Gulf waters to the inland margin of a coastal sabkha. The inland portion of the sabkha plain tends to have a brownish, salt-encrusted surface while that portion which is only slightly above the high tide level is commonly covered with a greenish-black algal mat. Coastal sabkha brines are derived from the evaporation of percolating sea waters at or below the sabkha surface.
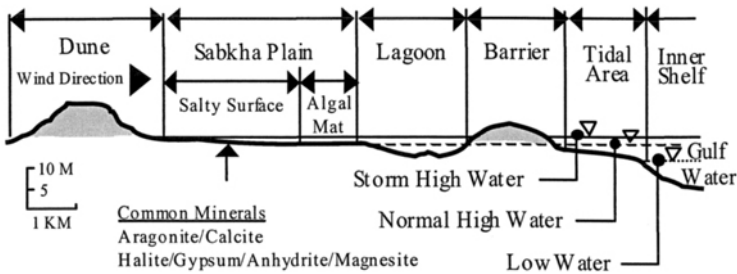
Figure 2. Generalized cross section across a typical coastal sabkha with typical surface features

Continental sabkhas are located inland and are often associated with areas of dune sands. They are considered as equilibrium deflation-sedimentation surfaces situated a set height (about a meter) above the ground water table (Kinsman 1969). Brines are the result of extensive evaporation losses of water vapor at the surface. Groundwater in nearby dune areas may have different ionic concentrations from sabkha brines. However, because the sabkha surface is very near the groundwater table, evaporation of incoming groundwater contributes to brine formation (Fookes *et al.* 1985).

Sabkha sediments, whether coastal or continental, reflect several sequences of sedimentation processes that are known to have occurred in the Persian Gulf region

during recent geologic history. Coastal sabkha sediments contain sands, silts, mud and clays that are either totally marine derived, or have been affected by marine environment during a sequence of ingressions and regressions of Gulf waters over the coast. As a result of these transgressions, the sands and silts were reworked by the waters and intermixed with marine sediments which resulted in the formation of: carbonate sands and silts, the bioclastic sands, the grey mud, and some of the clays. The most notable process occurring today is: the deposition of wind-transported sands over coastal and continental sabkhas (Fookes *et al.*1985). The depositional environment has produced quartzitic sand layers over original marine-derived and/or marine- affected sediments.

Secondary minerals (salts) have formed within host sediments (sands, silts, insoluble salts, clays, etc.) by precipitation from concentrated brines (as in the case of gypsum) or by reaction between the brines and the host sediments (as in the case of dolomite). The most prevalent secondary minerals in sabkha are: calcite, gypsum, anhydrite, dolomite, magnesite, aragonite and halite. New secondary minerals continue to form while older secondary minerals may undergo chemical and physical changes in response to the complex geochemical environment of the sabkha.

The formation of secondary minerals and their relative positions in sabkha sediments are largely dependent on the hydrology of the particular sabkha and the means by which the sabkha ground waters are replenished. The principal means of replenishment in coastal sabkha are horizontally moving sea water and/or vertical downward water which inundate the surface of the sabkha as a result of flash floods, high tides, or occasional rainfall. Continental sabkha waters are replenished from continental water sources (perched water) or rainfall. When the vertical water is rainwater, it will dilute the interstitial waters thus causing dissolution of soluble secondary minerals within the sabkha matrix.

The evaporative pumping mechanism is the most effective mechanism involved in causing the concentration of brines in sabkha waters, and in the formation of evaporite (secondary) minerals (Butler 1969). Evaporation from the sabkha surface provides the energy for the upward movement of the saline interstitial waters by capillary action. In the absence of flood tides and rainfall (both of which are infrequent), the water thus lost would be replenished by water entering laterally from the sea side. The upward movement of saline ground water and its evaporation from the surface readily accounts for the development of the crust dominated by halite and other soluble minerals. Back diffusion of ions along the concentration gradient, combined with the periodic reflux associated with storm tides, could lead to additional concentration of the saline interstitial waters (Hsu & Schneider 1973).

Profiles and Properties

The shores of eastern Saudi Arabia, Qatar peninsula, and the United Arab Emirates have extensive sabkha flats, both coastal and continental. They occupy roughly 15 to 20% of a coastal strip (50 km wide by 1000 km long) that extends from

Kuwait in the north to the Sultanate of Oman in the east. See Figure1 for details. For engineering purposes, the sabkha sediments of eastern Saudi Arabia and those on the western shores of Qatar are mostly sands and silts except in the shoreline extremities, where muds and clays tend to be more prevalent. The fines' content in the sands (silt & clay size) is significant. The sands are layered and often cemented Degree of cementation varies from weakly cemented to strongly cemented. Carbonate soils have been located at various sites, within the sabkha sediments, at different depths.

The author has examined a number of foundations investigations' reports and a large number of boreholes in sabkha terrain, looking for: common characteristics, distinctive features, and controlling factors. Despite the complex nature of sabkha sediments, i.e. varying: particle size, shape, degree and type of cementation, etc. it was possible to broadly view the sabkha profile as made up of three zones:

An **upper zone,** that extends from the crusty puffy surface down past the water table. This zone, one to three meters in depth, includes the water table and the stratified thin cemented sand/silt layers. Based on the Standard Penetration Test (SPT) values, the encountered sediments in this zone are generally medium dense to dense unless the surface has been inundated with rain water or high tide, which tends to wash away readily soluble salts responsible for particles' cementation.

An **intermediate zone,** which contains some or all of the following: loose quartzitic sands, calcareous sands, cemented sand-silt layers, clay layers interbedded with sands, muds, carbonate sands, and other marine-derived sediments. The general condition in terms of SPT varies from very loose to medium dense. This zone may vary in depth from few meters to about ten meters. Within this zone, foundations (mostly shallow) are laid; thus its geotechnical characteristics are critical in arriving at appropriate decisions and/or foundation geometries.

A **lower zone,** where sediments tend to exhibit high resistance to penetration by SPT. Materials encountered have included: dense to very dense sands and silts, strongly cemented sands, shale, stiff clays, or diagenetic rock. Based on SPT results, refusal is within one or two meters of penetration.

Range of SPT values, side by side with the description of materials encountered, for three selected sabkha cites, are shown in Figure 3.The SPT profiles shown tend to support the categorization of sabkha deposits into the three broad zones referred to earlier as: upper zone, intermediate zone, and lower zone respectively.

Design and Construction Considerations

It is appropriate when considering the broad categorization of sabkha, into three zones, to focus on conditions and sediments within the intermediate zone. This zone is the most critical when foundations recommendations are to be made.

The decision on the type of foundation and the selection of an appropriate site improvement method is highly dependent on: the type of sediments and their relative density; degree of cementation and the evaporites providing the cementation; percent fines within the uncemented layers; and % carbonates, chlorides, and sulphates in the brines. Some of the noted problems and potential safe guards are addressed below.

- Since sabkha sediments are highly variable materials in vertical and horizontal extents, chances are that these variations (layer thickness, relative density, degree of cementation, and type and percentage salts in sediments) would manifest themselves in extreme variations in compressibility characteristics. Precautionary measures need to be taken.
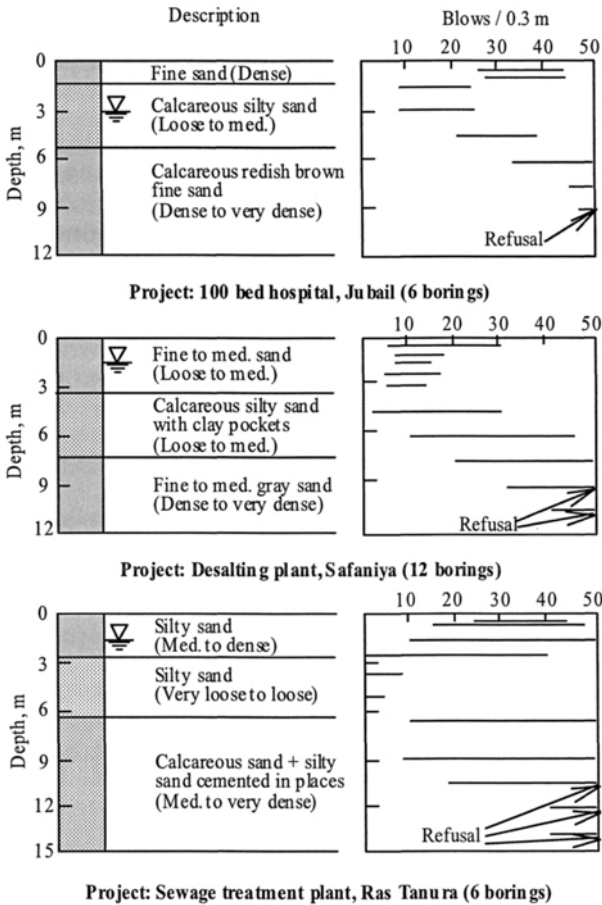
Figure 3. Simplified soil profile data from three selected sabkha sites typical of material encountered, showing ranges of Standard Penetration Test results (SPT) in terms of number of blows per 0.3 m.

- The corrosion problems in the concrete and steel, resulting from high concentration of chlorides and sulphates in sabkha brines.
- The inability to properly assess by conventional probes the degree of cementation of sabkha sands, particularly in the weak to moderately cemented range. Cementation has, both, positive and negative attributes in the context of foundation design over sabkha sites.
- Due to the high water table of sabkha and the nature of sabkha sediments, drainage of wastewater and irrigation water of built facilities (housing, industrial parks, etc.) is difficult and requires a well-planned disposal system. Discharge of waste and irrigation water through soak ways, as currently practiced, could cause a rise in groundwater level coupled with intermixing of water sources, leading to dissolution of some soluble salts thus undermining the strength and stability of the layers supporting the foundation.
- The evaporative pumping mechanism moves soluble salts from the water table towards the surface where they precipitate when water evaporates. The salt crystals thus developed may form blisters at man-made surfaces (pavements, concrete foundations, basements) causing cracking, particularly in pavements, but potentially in any porous material. Counter measures to deal with this problem and help reduce blistering have been outlined (French et al. 1982).
- Carbonate and gypsum contents in the sabkha sediments could be a trouble source of shallow foundations. High carbonate content (above 20 percent by total weight) may undermine foundations by carbonate leaching. Alternate hydration and dehydration of gypsum-rich layers under the hot and humid conditions that characterize the sabkha environment, is usually accompanied by volume changes that could contribute to differential settlement and thus foundation instability.
- The combination of loose sands with lightly cemented grains in sabkha sediments may be susceptible to collapse upon wetting or due to an increase in vertical stress. The collapse, referred to here, is not necessarily the sudden or the catastrophic break down of soil structure, but rather the slow type (years versus months) of relatively small magnitude(less than 1% percent). It is therefore highly recommended that the probable collapse potential of the sabkha site be addressed.
- Chemical reactions, precipitation and solution within sabkha sediments, are greatly enhanced if ground water flow, in and/or out of these sediments, is relatively high. Long range, these on-going activities (reactions, precipitation, and solution) could undermine the stability of a foundation unless precautionary measures are taken. It is highly recommended that the anticipated flow regime of groundwater, in and out of the site, be mapped out and parameters such as: hydraulic conductivity, porosity and flow velocity, be estimated.

As noted above, sabkha sediments are sensitive to changes in conditions that, directly or indirectly, affect the equilibrium chemistry of their sediments and properties. It is highly recommended that caution be exercised when considering foundations over sabkha. When design decisions are in the making; they should be preceded by: proper soil investigation, appropriate tests, and assuming worst-case scenarios.

Site Improvement by Densification of Sabkha Sediments

Sand/silt material encountered in sabkha (with particular reference to the intermediate zone) are usually in very loose to medium dense state, requiring intervention, often through densification, to sustain design loads safely within tolerable settlement limits. Experience with construction on sabkha flats has shown that some form of densification is required when shallow foundations are considered. The densification methods that have been attempted in the sabkhas have included: i) Placement and compaction of selected fill material over the sabkha surface, ii) Compaction without additional fill, iii) Vibro-compaction, and vi) Dynamic compaction. For highly settlement-sensitive structures, piled foundations have been used. The piles are generally end-bearing supported on rock, in dense sand, or on a hard pan. These materials are encountered within the lower zone of the profile.

Sabkha compaction by **vibratory rollers** has proven to be suitable for relatively small structures such as one to three story residential or commercial buildings. Such structures are usually supported on shallow footings with width rarely exceeding one or two meters. The stress influence zone of such footings is normally contained within two to four meters below footing grade. Adequate density is normally achieved by a predetermined number of passes using heavy rollers. Light rollers are generally not effective at a depth greater than two meters.

To increase the effectiveness of the compaction process, and largely within the intermediate zone, the sabkha crust should be broken down prior to compaction. Excavation to depth slightly above groundwater, replacement by a granular fill, and compaction of the fill by vibratory rollers, is practiced and appears effective in densifying deeper strata of sabkha sediments. However, if dewatering is required, this approach becomes uneconomical. In sabkhas where the crust is firm and the soil is medium-dense to dense in the upper zone all year round, the placement and compaction of a select fill on top of the surface may prove effective in sustaining the loads of a light structure. The thickness of the fill should be so that the pressure bulb developed by the footing is contained within fill. This approach may be considered only when structural and architectural constraints do not preclude raising site grade.

When sabkha deposits are loose and relatively thick, compaction at the surface is not effective. Deep compaction methods may be applied. Under this category, **vibrocompaction** has been used with mixed results. Vibrocompaction refers collectively to all methods involving the insertion of a vibrating probe into the ground with or without the addition of backfill material. The ability of any of these methods to accomplish the required improvement in density depends largely on:
  (1) soil gradation and fines' content,
  (2) degree of saturation and position of water table,
  (3) initial relative density of the deposit,
  (4) soil structure and degree of cementation, and
  (5) characteristics and the specifics of the method applied.

Vibroflotation is one of the methods categorized under vibrocompaction and consists of inserting a vibratory probe into the deposit at predetermined intervals. The induced vibration causes the loose to medium-dense granular soils to liquefy leading to subsequent densification. This method works well when the deposits are clean with little or no fines. Experience has shown that this method is ineffective when the percentage by weight of fines (particles finer than 0.075mm) exceeds 20%. This is because the hydraulic conductivity of materials containing fines is too low to permit rapid drainage of pore water, a requirement for densification, which follows liquefaction under the action of the vibratory forces. Details on vibroflotation's equipment and the process are discussed by Brown (1977). This method has worked well in densifying some loose sabkha deposits of eastern Saudi Arabia, down to about 6 meters below surface.

Vibro-replacement or stone column installations are accomplished using the vibro-replacement method in a manner similar to vibroflotation. A cylindrical vertical hole is made by a vibrating probe penetrating by means of jetting action and under its own weight. Gravel and/or gravel-sand backfill is dumped into the hole in increments of 0.4 to 0.8 m and compacted by the probe, which simultaneously displaces the material radially into the soft (or loose) soil. Column diameters are usually in the range of 0.6 to 1.0 m. Stone columns are placed in a grid pattern with center to center spacing of 1.5 to 3.5 m. The column should extend into a firmer stratum below. A blanket of sand and/or gravel, 0.3m or more in thickness, is usually placed over the top. This blanket has two functions; it acts as a drainage layer, and aids in distributing stress resulting from structures above. Useful guidelines on the application of this method are presented by ASCE Committee on Placement and Improvement of Soils (ASCE, 1978). The vibro-replacement method has been used on several sabkha sites in conjunction with vibroflotation application. Reports made available to the author appear favorable, and tend to support its use with caution. (Akili 1997; Akili 2004).

Site Investigation

To aid in planning of ground investigation of a sabkha site, preliminary information on the geology, geomorphology, and brine chemistry of the site should be made available. Relevant information under this category may include:
1) The land forming processes: past processes, present processes, and those that may be controlling after construction and development of the proposed site;
2) Types of sediments and their characteristics, bedrock/hard pan information, and buried algal mats, if any;
3) Salts in sediments: their type, amounts, presence of continuous and discontinuous cemented layers, particularly gypsum layers;
4) Groundwater flow characteristics: gradient, potential water ingress, capillary zone, surface water courses, and water table fluctuations; and,
5) Groundwater chemistry: major ions and their concentration, potential reactions, and the impact of construction and site development on: precipitation, dissolution, and crystal growth.

For large-size projects, it is recommended that site investigation be carried out in stages. Table 1 outlines a four-stage strategy; proven useful when sufficient lead time is available. Preliminary stage (Stage I), using walk over survey and/or widely spaced sampling procedure aids in the planning and execution of the three stages to follow. Because the soil-structure, and therefore stability of layers within the sabkha profile, are dependent on chemical cementation due to salts (chlorides, sulphates, carbonates); it is useful to identify layers that appear sensitive to the presence of salts versus those that are less sensitive. Therefore, it is imperative that chemical testing be performed (Stage IV) to determine type of salts in the sediments, and assess the manner in which these salts are present within the soil matrix.

Examination of relatively large exposures in open test pits, trenches, or through large diameter shallow borings, will aid in delineating sediments and layering, help identify crystalline salts, and at the same time, allow extraction of bulk and undisturbed samples. Specimens for determination of mechanical properties of soils are often obtained with open-end drive samplers which can be placed directly in consolidation or triaxial devices. In some cases, high quality Denison and Pitcher specimens are needed Block samples from open test pits have also been utilized. However, the presence of salts makes it extremely difficult to obtain good samples. Thus because of the difficulty of sampling, insitu testing is recommended for major projects Field tests including: plate bearing tests, CBR tests, Pressuremeter tests, foundation and embankment loading tests, dewatering, etc. have been used-with varying degrees of success- to investigate sites of major structures or to generate useful parameters for foundation design over sabkha sites.

Table 1. A proposed four-stage geotechnical investigation for a sabkha terrain.

Stage	Purpose	Major Tasks
I Preliminary	To plan subsequent stages	• Desk study • Walk over survey
II Defining	To determine type and extent of required field and lab work	• Identify land forms and controlling processes • Obtain preliminary in-depth information through open pits
III Main	To obtain all field and lab data at a standard, justified by size and complexity of project	• Mapping including: topography, outcrops, hydrology, water gradient • Perform fieldwork by: boreholes, sampling, in-situ testing • Perform lab tests: strength, compressibility, conductivity, etc. • Properties and classification
IV Auxiliary	Addressing chemical equilibrium of sediments and brines	• Chemical testing of soils and brines • Assessing chemical stability due to construction and development • Effect of leaching on stability and strength

When examining the behavior of granular materials in sabkha, it is important to distinguish between stable and metastable structures. The former derive their strength from particle interlock, while the latter are dependent to a large degree on weak

cementation bonds derived largely from the presence of salts. Some of the sand-silt layers in sabkha possess metastable particle structure, and are extremely susceptible to collapse upon loading or inundation. The author has noted collapse behavior on several sites, triggered by loading and/or an increase in moisture content (Akili 1997).

Concluding Remarks

The brisk pace of construction activities over sabkha flats along the southern shores of the Persian Gulf has necessitated consideration of their geological/ geomorphologic setting and their geochemical properties. Sabkha sediments are characterized by: highly saline groundwater, presence of significant amount of salts, high evaporation rate through the surface, rapid crystallization in the crust, and complex chemical reactions between the brines and the sediments.

Examination of a large number of boring logs and related field tests from several sabkha sites in eastern Saudi Arabia and Qatar, has confirmed that granular soils dominate sabkha profiles. Quartzitic sands, calcareous sands and silts, muds and clays make up the unconsolidated portion of the sabkha profile. Based on the Standard Penetration Test data, sabkha's granular sediments are generally dense within the **upper zone**, which contains also the cemented crust. This upper layer extends to the water table. Below the crust, an **intermediate zone** comprised of: loose to medium dense conditions of a granular matrix, a mixture of continental and marine-derived sediments, extends down to a maximum depth of ten meters below surface. Below the intermediate zone, dense sands, strongly cemented sands, diagenetic limestone or occasionally stiff clays are encountered and referred to, in here, as the **lower zone**.

Difficulties noted when using sabkha as building sites have been attributed to: (*1*) sediments' variability, which makes sabkha sites extremely susceptible to differential settlement; (*2*) sabkha's complex and changing geochemical setting, which adversely affects the mechanical properties of sabkha sediments; (*3*) the difficulty in assessing, by conventional probes, the degree of cementation of sabkha sands, particularly in the light to moderately cemented range; and (*4*) potential carbonate leaching with potential volume changes that are known to occur in layers containing gypsum.

Site improvement is often necessary for sabkhas to sustain shallow foundations. Improvement methods applied have included: surface densification by vibratory rollers, deep compaction by vibroflotation, vibro-replacement, and dynamic compaction. Observations, of available case studies, show some degree of success in increasing relative density on most jobs performed. Difficulties with deep compaction are bound to arise with higher fines and presence of undetectable cemented layers.

Site investigation in sabkha terrain should include an appraisal of the potential geochemical changes, likely to occur in sediments after construction. Although many of the chemical and physical processes that occur in sabkha are not fully understood, it is believed that sufficient knowledge exists today to assess the probable risks, and be able to design and construct safe foundations in sabkha deposits.

References

Akili, W. (1981). "On sabkha sands of eastern Saudi Arabia." *Proc. Symp. on Geotechnical Problems in Saudi Arabia*, 2,775-796.

Akili, W.and J.K. Torrance (1981). "The development and geotechnical problems of sabkha with preliminary experiments on the static penetration resistance of cemented sands." *Q. J. of Eng. Geol.*, 14,59-73.

Akili, W. and N. Ahmad (1986). "Arabian salt-encrusted flats (sabkha) as building sites." *Proc. Int. Conf. on Building on Marginal and Derelict Land*, Thomas Telford Ltd., London, 439-452.

Akili, W.and N.M. Aljoulani (1989). "Cone penetration tests on artificially cemented sands." *Proc. 1ˢᵗ Symp. on Penetration Testing*, Orlando, Florida, 2,607-611.

Akili. W. (1997). "Geotechnical properties of the sabkhas on the west coast of Qatar." *The soils of Qatar, An Internal Report,* The Univ. of Qatar.

Akili, W. (2004). "Foundations over salt-encrusted flats (sabkha): profiles, properties, and design guidelines."*Proc. Fifth Int. Conf. on Case Histories in Geotechnical Eng.*, New York, NY. Paper No.1.42.

American Soc.of Civil Engineers. (1978). *Proc. Symp. on Earth Reinforcement*, Pittsburg, PA.

Brown, R.E. (1977). "Vibroflotation compaction of cohesionless soils." *J. of Geotech. Eng.* 103(12), 1437-1451.

Bush, P. (1973). "Some aspects of the diagenetic history of the sabkha in Abu Dhabi, Persian Gulf."In: Purser, B.H.(ed.), *The Persian Gulf.* Springer-Verlag,395-407.

Butler, G.P. (1969). "Modern evaporite deposition and geochemistry of co-existing brines, the sabkha, Trucial Coast, Arabian Gulf." *J. of Sedimentary Petrology*, 39, 70-89.

.Fookes, P.G. (1976). "Road geotechnics in hot deserts." *The Highway Engineer, J.Inst.Higway Engineers*, (13).

Fookes, P.G. and W. J. French (1977). "Soluble salt damage to surfaced roads in the Middle East." *Highway Engineering*, 24, 10-20.

Fookes, P.G., W.J. French and M.N. Rice (1985). "The influence of ground and ground water geochemistry on construction in the Middle East." *Q. J. of Eng. Geol.*, 18,101-128.

French, W.J., A.B. Poole, P. Ravenscroft and M. Khiabani (1982). "Results of preliminary experiments on the influence of fabrics on the migration of groundwater and water-soluble minerals in the capillary fringe." *Q. J. of Eng. Geol.*, 15, 187-199.

Hsu, K.J. and J. Schneider (1969). "Progress report on dolomitization-hydrology of Abu Dhabi sabkhas, Arabian Gulf." In: Purser, B.H. (ed.), *The Persian Gulf,* Springer-Verlag, 409-422.

Kinsman, D.J.J. (1969). "Mode of formation, sedimentary association, and diagnostic features of shallow-water and supratidal evaporites." *Bull. of the Am. Assoc. Petrol. Geol.* 53,830-840.

Kinsman, D.and R.K. Park (1969). "Studies in recent sedimentology and early diagenesis, Trucial Coast, Arabian Gulf." *2ⁿᵈ Regional Technical Symp.*, Soc. of Petrol. Engineers of AIME, Saudi Arabia.

PULLOUT CAPACITY OF BLOCK ANCHOR IN UNSATURATED SAND

Naser Al-Shayea[1]

[1] *Civil Engineering Department, KFUPM, Box 368, Dhahran 31261, Saudi Arabia*;
PH (966 3) 860-2480; FAX (966 3) 860-2879; e mail: nshayea@kfupm.edu.sa

ABSTRACT

Block anchor is an interface element used to restrain horizontal movement of structures. This paper investigates the effect of moisture conditions (or degree of saturation) on the pullout capacity of block anchor embedded in sand at three different moisture conditions. The approach taken consists of experimental work, and analytical calculation. The experimental work is pullout tests, made in the laboratory, on 0.15 x 0.15 x 0.15m concrete block anchors embedded in sand, at a depth of 0.15m. The sand is deposited in a 1.2 x 0.6 x 0.8m box using a pluviation method to ensure a uniform and reproducible density. Materials used were characterized to find their properties, and the equipments used were calibrated before usage. The load and the corresponding horizontal and vertical displacements were recorded. In addition, visual observations were made on the failed soil body. The experimental results are compared with the analytical calculations (by Rankine, Coulomb, and log spiral theories). The 3-D effect was also considered.

The block anchor was found to have higher pullout capacity than a plate anchor. The results show that the moisture condition significantly affects the pullout capacity of the block anchor. The pullout capacity of the block anchor embedded in unsaturated (wet) sand is about double that for the block embedded in dry sand, while that for the block embedded in saturated sand is only about one half of that for the block embedded in dry sand. These findings have very significant implications in the analysis and design of the block anchor embedded in unsaturated sand. Also, these have contributions to the hazard risk assessment of block anchors embedded in sand subjected to variations in degree of saturation.

1. INTRODUCTION

Lateral earth pressure is a significant parameter in soil-structure-interaction problems involving underground substructures embedded in the soil body, such as

anchors. Anchors are interface elements between the ground and structures, and are used to stabilize earth structures by constraining displacement or movement. They transfer forces in a given direction from the structure to the ground (soil or rock). Anchor types include: anchor plates and beams (deadman), tie backs, vertical anchors, anchor beams supported by batter piles, and block anchors. Block anchor is a cast-in-place or pre-cast concrete member that may be square or rectangular in section with the necessary length to develop adequate passive resistance, Bowles (1997). They are specially designed to withstand pullout or thrust forces.

Review of literature reveals that many research studies have been conducted on the capacity of vertical anchor. Many studies were found to study anchor plate, including Hueckel (1957), Ovesen and Stromann (1972), Neely, et al. (1973), Das (1975), Akinmusuru (1978), Dickin and Leung (1983), and Ghaly (1997). But only few studies were found for block anchor, Bowles (1997) and Duncan and Mokwa (2001). Eleven researches were lab experimental works, one was a review work, and one was field experimental work.

This paper investigates the pullout capacity of block anchors embedded in sand using small scale laboratory models, with three different moisture conditions of the soil (dry, saturated, and saturated-then-gravity-drained). Experimental results are compared with those from analytical analyses.

2. THEORETICAL ANALYSIS
2.1 Theories of lateral earth pressure

There are three well-known analytical theories dealing with the passive earth pressures, namely: Rankine theory (smooth structure), Coulomb theory (rough structure), and Log spiral theory (curved failure surface). The theoretical value of lateral earth pressure is dependent on the theories used and on the assumptions made relative to the nature of the structure, the soil, and the soil-structure interface.

2.2. Forces acting on anchor block

Figure 1 shows a cross section of a short anchor block embedded in sand, with all forces acting on it and with friction considered. For an anchor block with the dimensions: width (B), depth (h), thickness (t), depth of embedment below soil surface (d), and the distance from the upper edge of the anchor to the pulling load (z); the forces are as follows:

P_u = ultimate pullout capacity of the block anchor embedded in sand,

P_p = effective passive force = $K_p * \gamma' * (d+h/2) * h * B$,

P_a = effective active force of soil= $K_a * \gamma' * (d+h/2) * h * B$,

F_t = effective friction force at the top of the block = $W_s * \tan \delta_b$,

F_b = effective friction force at the bottom of the block = $N * \tan \delta_b$,

F_s = effective friction force at two sides of the block = $2 * K_o * \gamma' * (d+h/2) \tan \delta_s * h * t$,
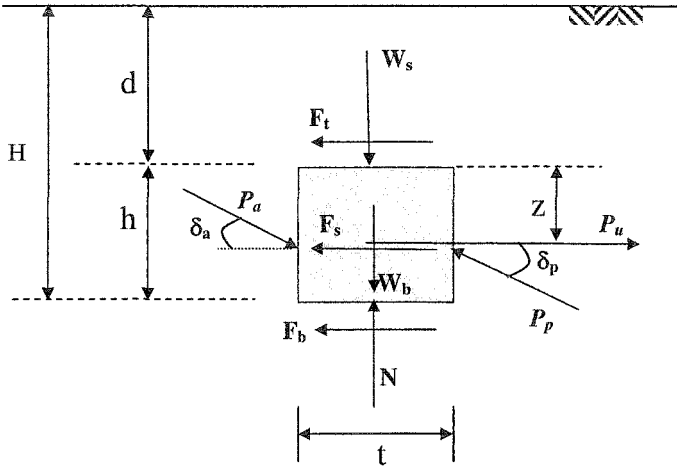
Figure 1.   Block anchor with acting forces.

W_s = weight of soil above the block anchor = $\gamma'*d* t*B$,

W_b = weight of the block anchor = $\gamma'_c * h * t *B$, and

N = normal force.

Where: γ' = effective unit weight of the soil,

γ'_c = effective unit weight of concrete,

K_p = coefficient of passive lateral earth pressure,

K_a = coefficient of active lateral earth pressure,

K_o = coefficient of lateral earth pressure at rest,

δ_t = angle of friction between soil and top surface of the block, and

δ_b = angle of friction between soil and bottom surface of the block.

The passive and active forces (P_p and P_a) are inclined by δ_p and δ_a, respectively to the normal-to-the-surface of the block side, where, δ_p is the angle of friction between soil and passive side surface of the block, and δ_a is the angle of friction between soil and active side surface of the block. The horizontal components of the passive and active forces ($P_{p,h}$ and $P_{a,h}$) are: $P_{p,h} = P_p * cos\ \delta_p$,and $P_{a,h} = P_a * cos\ \delta_a$.

The vertical components of the passive and active forces ($P_{p,v}$ and $P_{a,v}$) are the effective friction forces (F_p and F_a) at the passive and active side surfaces of the block anchor, respectively, and they are: $P_{p,v} = P_p * sin\ \delta_p$, and $P_{a,v} = P_a * sin\ \delta_a$.

2.3. Friction between Soil and Structure (δ)

Coulomb's theory considers friction between the soil and the structure. Notice that this friction is between the soil and the vertical sides of the structure. The

angle of friction between soil and structure is δ. Considering the δ–value, Coulomb's theory gives a higher value of passive pressure and a lower value of active pressure as compared to Rankine's theory, which likely produces overestimation (conservative), Bowles (1997).

As an approximation, Singh (1967) suggested the following values for δ: (1) $\delta = 1/3$ $\bar{\phi}$ for smooth structure (wall), (2) $\delta = 2/3$ $\bar{\phi}$ for ordinary retaining wall, (3) $\delta = 3/4$ $\bar{\phi}$ for rough walls with well-drained backfill, and (4) $\delta = 0$ when the backfill is subjected to vibrations, where $\bar{\phi}$ is the effective angle of internal friction of the soil. The range of values of δ between fine sand and concrete is 15-25°, Bowles (1997) and Das (1995). All values of δ suggested above are for the maximum value (δ_{max}).

The actual value is the mobilized friction angle ($\delta_{mobilized}$), which is less than the corresponding maximum value. The value of $\delta_{mobilized}$ is governed by the following factors:
a. Maximum possible value of the friction (δ_{max}), which depends on the roughness of the interface and the properties of the soil.
b. Relative shear displacement along the interface; which mobilize the interface friction.
c. Vertical equilibrium of the forces acting on the structure.
d. Weight of the anchor (light vs. heavy).

The angles for the horizontal friction δ_t and δ_b are taken to be equal to δ_{max}, and the angles for the vertical friction δ_p and δ_a are taken to be equal to $\delta_{mobilized}$. Notice that Ovesen and Stromann (1972) considered δ_a to be equal to the angle of internal friction of the soil (ϕ).

The mobilized friction angle ($\delta_{mobilized}$) can be found from the equilibrium of forces acting on the block shown in Figure 1. For light-weight anchor, the vertical components of the passive and active forces ($P_{p,v}$ - $P_{a,v}$) is greater than the weight of the block and the soil above it ($W_b + W_s$), and therefore slip does not occur on the interface between the block and the soil. This condition causes uplift of the anchor, making the normal force (N) equals zero. By summing forces along the vertical direction, with $N = 0$, yields:

$$\delta_{moblized} = \sin^{-1}\left(\frac{W_b + W_s}{P_p - P_a}\right) \qquad (1)$$

2.4. 3-D Effect

Based on the shape of the anchor, there are two types: long/continuous (plane strain, 2-D problem) and short (3-D problem). Theories of lateral earth pressures (Rankine, Coulomb, and Log spiral) were developed for 2-D situation. The

conditions at the ends of the structure are quite different from those at the center, which have significant influence on the passive resistance. Ovesen (1964) found that the passive earth pressure against short structures is higher than those predicted by conventional theories (Rankine and Coulomb theories), and the difference can be quite significant. Hansen (1966) developed a method for correcting the results of conventional pressure theories for shape (or 3-D) effects. For short anchors, the ultimate resistance should be multiplied by a correction factor (M) to account for 3-D effects. For a plate anchor, M is given as:

$$M = 1 + (K_p - K_a)^{0.67} \left[1.1E^4 + \frac{1.6F}{1 + 5(B/h)} + \frac{0.4(K_p - K_a)E^3 F^2}{1 + 0.05(B/h)} \right] \qquad (2)$$

where, $E = 1 - h/(d+h)$,
$\quad\ F = 1 - (B/S)^2$, and
$\quad\ S$ = center-to-center distance between two anchors.

The above equation considers both the embedment factor (E) and the shape factor (F). The value of E is 0.5 for d = h. The value of F is 0.0 for long/continuous anchor, and is 1.0 for single short anchor.

2.5. Capacity of Block Anchor

The ultimate capacity of block anchor (P_u) can be found from the equilibrium of forces acting on the block shown in Figure 1. By summing forces along the horizontal direction and multiplying the lateral earth pressure (passive and active) by the 3-D correction factor (M) given in Equation (2), yields:

$$P_u = M(P_{p,h} - P_{a,h}) + F_t + F_s + F_b \qquad (3)$$

For Coulomb and Log spiral theories, $F_b = 0$ (as $N = 0$). The allowable capacity of block anchor is $P_{all} = P_{all} / FS$, where, FS is a factor of safety of 1.2 to 1.5, as suggested by Bowles (1997).

3. EXPERIMENTAL INVESTIGATION
3.1. Material Characterization
3.1.1 Soil

The sand used in this research was selected to be the fraction of beach sand that passes sieve #30 and is retained in sieve #100. Various tests were made to characterize this sand according to the respective ASTM Standards. The grain size distribution curve of this sand indicated that D_{10}, D_{30}, and D_{60} are 0.18mm, 0.29mm, and 0.38mm, respectively. The coefficient of uniformity (C_u) equals 2.11, and the coefficient of concavity/curvature (C_z) equals 1.23. According to Unified Soil Classification System (USCS), this sand is categorized as poorly-graded clean sand

(SP). This sand has a specific gravity (G_s) of 2.679, and maximum and minimum densities of 1889.58 kg/m^3 and 1662.78 kg/m^3, respectively.

This research used pluviation method to produce uniformly dense, homogenous, isotropic, and reproducible sand deposits in the sand box. The optimum height of fall was found to be 100 cm. This height of fall was subsequently used to fill the box with sand for the pullout tests. The corresponding dry density is 1774 kg/m^3, i.e. the dry unit weight (γ_d) is 17.398 kN/m^3. This gives a relative density (D_r) of 60.3%; i.e., medium density. Using phase relationships, the void ratio (e) is 0.51, and the saturated unit weight (γ_{sat}) is 20.711 kN/m^3.

The above dry density was used for permeability and strength tests, as well as for analytical computations. The coefficient of permeability, at that was found to be 0.01476 cm/s (1.476×10^{-4} m/sec); i.e., within the range of medium permeability of fine sand.

Both direct shear tests and triaxial shear tests were performed to determine the angle of internal friction (ϕ) of this cohesionless sand. Direct shear tests were performed on dry sand at four different of normal loads; 20 kgf (196.1 N), 40 kgf (392.3 N), 80 kgf (784.5 N), and 160 kgf (1569.6 N). The resulted angle of internal friction (ϕ) is 44.9°. Three sets of drained CD triaxial tests were performed on sand at three different moisture conditions; dry, wet, and saturated. Tests were made at confining pressures (σ_c) of 25, 50, 100, and 200 kPa, so low to resemble those at shallow depths. A cycle of unloading and reloading was made for each test. Figure 2 shows typical plots for the deviator stress versus the axial strain for dry, wet, and saturation conditions of sand. The resulted angle of internal friction (ϕ) is 43.5°, a little lower than that from the direct shear test. For wet condition, the resulted apparent cohesion is about 17 kN/m^2, which is attributed to capillarity effects.

To assess the stiffness of the sand at shallow depths; the initial modulus (E_0), the secant modulus (E_{50}), and the dilatancy angle (ψ) were obtained from the results of triaxial tests at low confining pressure, and tabulated in Table 1. At a given confining pressure, the moduli are largest at wet condition, and smallest at saturated condition; while the dilatancy angle is largest at dry condition, and smallest at wet condition.

3.1.2 Friction between Soil and Concrete

Maximum friction angle between soil and concrete and between soil and steel were determined using the direct shear apparatus. Concrete or steel specimen having a dimension of 6 cm length, 6 cm width, and 1 cm thickness was placed in lower half of shear box, and sand at density of 1774 kg/m^3 was placed at the upper half. The angle of friction between soil and concrete were found to be 38.0°. The angle of friction between soil and steel were found to have an average value of 28.7°. This represents the value for δ_{max}.
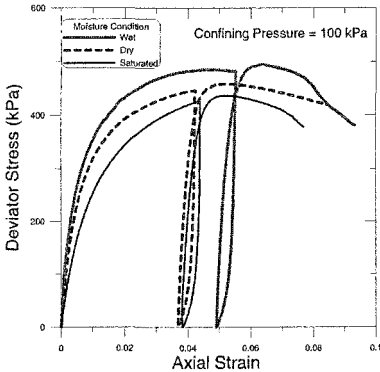
Figure 2. Results of triaxial tests on sand, under a confining pressure of 100 kPa, at dry, wet, and saturation conditions.

Table 1 Moduli of Elasticity and Dilatancy Angle

Moisture condition	σ_3 (kPa)	E_0 (kPa)	E_{50} (kPa)	ψ (°)
	25	19942	12085	18.4
	50	40130	23409	17.6
	100	83454	47145	15.8
	200	186378	103729	15.4
	25	23798	15109	16.0
	50	52648	29287	15.1
	100	110988	58079	14.6
	25	11337	7551	16.8
-	50	25633	15850	15.3
	100	47642	28714	14.9

3.1.3 Cable

Based on theoretical calculation for the predicted load capacity of block anchor, the cable used to pullout the block anchor was decided to be 5 mm diameter twisted steel cable. This cable has a breakout capacity of about 15.7 kN, at a maximum strain of about 3%. Additionally, the load-displacement behavior of the cable was obtained in terms of elongation (Δ) of cable vs. load level (P). The length of cable tested was 80 cm, equals to that used for the pullout tests of block anchor. This is essential to correct the displacement of the block anchor for the elongation of the cable. Tests were performed according to ASTM Standard. The maximum applied load to the cable is 3.9 kN (400 kgf), which is more than the maximum load capacity for block anchors predicted from theoretical solutions.

The soil-cable interface friction was tested to determine friction resistance of a cable having the same length as the cable used for pullout tests of the block anchor. The pullout test was performed on the cable using similar apparatus and procedure for block anchor pullout tests. The cable was embedded in the sand box at a depth of 225mm (the same depth of the cable for the block anchor). Measurements indicated that the maximum friction was only 32 N corresponding at a displacement of 0.5 mm. This is only about 2.4 % of the load for block anchor, its effect on the pullout load is neglected.

3.2 Model Preparation

A 150X150X150mm concrete block was tested in the laboratory to determine the pullout capacity of a scale model block anchor in sand. For comparison purposes, a 150X150mm steel plate anchor was also tested. During casting of concrete block, a steel cable was connected to reinforcements embedded into the block. The cable was positioned in the location of the pulling load, as estimated by theoretical calculation, $z = 80$mm.

Tests were made in a box, which is 1200mm long, 800mm wide and 600mm high. The box walls are watertight plexi-glass and are stiffened by steel bracing to sustain soil pressure. At the bottom of the box, a network of perforated ½ in PVC pipes enclosed with geotextile was installed for supply and drainage of water to allow testing at various moisture conditions. The box was filled with sand by pluviation method by an automated sand-laying machine to produce uniformly dense, homogenous, isotropic and reproducible sand; deposited by free-falling dry sand from a height of fall of about 1m. The showering continues in lifts until the bottom 300mm of the box is filled with sand to the desired elevation. The block anchor, with the two pressure transducers attached at bottom and the plate mounted on the top, is placed on the deposited sand at a distance 800mm from the front wall of the sand box (passive side) and in the middle between the two sides of sand box. The cable is stretched to the loading device, hooked at the load cell. Then, sand deposition is resumed until the box is filled with sand.

To reconstitute the model for the next test, the measuring devices were disconnected, the soil was excavated carefully down to 100mm below the bottom of the block anchor, the anchor block is taken, then the model is rebuilt.

For testing at saturation condition, water was gradually supplied to the sand through network of pipes at the bottom of the box, until the water spills from the top of the box. The valve was closed and the sand was kept saturated, for pullout testing of anchor at saturation condition.

For testing at wet/unsaturated condition, the sand is first saturated, then water was drained out through the pipes at the bottom of the box until the water reaches the bottom 100mm. The valve was closed and the pullout testing of anchor was made while the sand is at wet/unsaturated condition. To assess moisture conditions, soil samples were taken from random positions at depths between 15 cm and 30 cm from the surface. The water content (w) was found to be 12.5 %, which corresponds to a degree of saturation of 65.6%.

To measure the vertical pressure at the interface between soil and the bottom of the block anchor, two pressure transducers were used, one at the front-bottom and one at the back-bottom of the block anchor. The pressure transducers have diameter of 5 mm, maximum pressure of 200 psi.

Movements (vertical and horizontal) of the anchor placed inside the soil were monitored by four vertical and two horizontal LVDT's placed at an aluminum plate mounted on the block and extended above the surface. To minimize the earth pressure on this plate, its stem is oriented such that the 4mm thickness faces the direction of pulling.

3.3 Pullout Testing

Loading machine is mainly a gear box driven by fractional motor connected to screw-spindle to move backward (pulling motion) at a rate of 0.167 mm/min (1 cm/hour). A load cell was placed between cable and screw-spindle. The load cell is screwed to spindle screw. To connect cable to the load cell, a special high-strength hook was attached to the load cell. A load cell was used measure the pullout load generated by the loading machine. It is a medium range tension having maximum allowable capacity of 500 kgf. At the back of the gear box, a third horizontal LVDT was placed.

Load cell, LVDT's, and pressure transducer were calibrated before being used. Data logger was used to simultaneously record all ten measurements, consisting of one load cell, seven LVDT's (four vertical and three horizontal) and two pressure transducers. After each test, all data recorded were transferred to PC for post-processing.

Testing involves pulling the anchor until failure. Sets of pullout tests were made on block anchors at dry, wet and saturation conditions of sand. For comparison purposes, a set of pullout tests were made on plate anchors at dry sand condition. During testing, readings of various devices were monitored, and deformations of sand surface were visually observed, mapped (measurement of length, width and height were taken), and photographed. Failure conditions of the soil surface were observed at both the front of the anchor (passive side) and at the back of the anchor (active side).

4. RESULTS AND DISCUSSIONS

The effect of moisture condition of sand is presented for dry, wet and saturated condition. Figure 3 shows typical the load-displacement relationship for block anchor embedded in sand at dry, wet and saturated conditions. The displacement represents the actual displacement of the block anchor, which was obtained after correcting the measured displacement by the horizontal LVDT at the end of the cable from cable elongation and other connection displacements.

For the dry condition, the values of the ultimate pullout load and the corresponding displacement are 1310 N and 16.71 mm, respectively. For the wet condition, the values of the ultimate pullout load and the corresponding displacement are 2298 N and 28.3 mm, respectively. For the saturated condition, the values of the ultimate pullout load and the corresponding displacement are 705 N and 21.07 mm,

respectively. As a comparison, results from testing plate anchor in dry sand give the ultimate pullout load and the corresponding displacement to be 1200 N and 16.54 mm, respectively. It can be seen that the thickness of the block increases the ultimate load increases, due to the fact that the friction at the sides and top of the anchor contribute to the pullout capacity.

Figure 4 depicts the variation of the pullout loads versus moisture condition. It shows that the wet condition gives the highest pullout load, approximately 70 % higher than that for dry condition. This is due the increase of the bulk density and the present of apparent cohesion caused by the capillarity force. Saturated condition shows approximately 50 % reduction in pullout load compared to the dry condition, which is due to low effective unit weight.

The values of $\delta_{mobilized}$ for Coulomb theory are $11.2°$, $7.7°$, and $11.4°$ for dry, wet, and saturated conditions, respectively, for concrete block. The corresponding values for Log spiral theory are: $10.9°$, $7.3°$, and $11.0°$. For steel plate in dry sand, values of $\delta_{mobilized}$ are $2.2°$, and $2.1°$ for Coulomb and Log spiral theories, respectively.

The correction factor (M) to account for the 3-D effect, equation (2), is given in Table 2. Figure 5 presents results of the analytical solutions according to equation (3), with $F_t = 0$ (as it was observed that the top soil moves with the block not relative to it).

The vertical displacements measured using four LVDT's indicate uplifting and tilting of the block anchor towards the passive side. Pressure transducers at the bottom of the anchor block indicate uplifting of the block, although the one at the passive side is highly contaminated by the vertical component of the passive pressure.
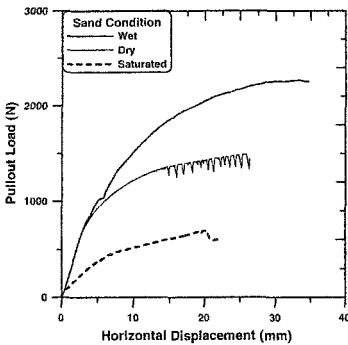
Figure 3. Load-displacement curves for anchor block in sand of different moisture conditions.
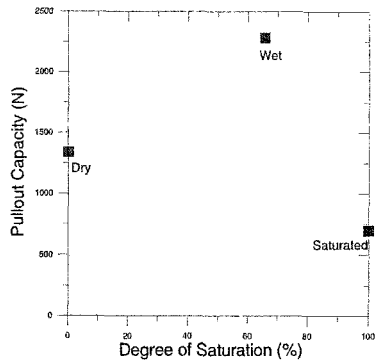
Figure 4. Pullout capacity of anchor block vs. degree of saturation of sand

Table 2. The correction factor (M) for the 3-D effect

Anchor type	Moisture condition	Theory		
		Rankine	Coulomb	Log Spiral
Block	Dry	2.76	4.26	4.39
	Wet	2.76	3.63	3.79
	Saturated	2.76	4.29	4.42
Plate	Dry	2.76	2.96	3.08
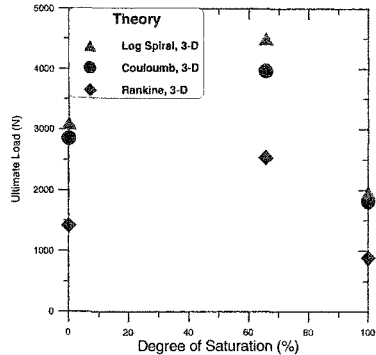
Figure 5. Results of the analytical solutions.

Typical failure conditions of the soil surface are presented in Figure 6 for dry and wet conditions. At the passive side, a bulging area was seen on the soil surface in front of the anchor for every test except for the wet condition. At the active side, an elliptic depression was found at the back of the anchor for dry condition. For saturated condition, a settlement of soil behind the anchor was observed. For wet/unsaturated condition, cracks were observed at both the passive side and the active side, with width varying between 1 and 5mm.

5. CONCLUSIONS

1. The moisture condition of the soil highly affects the pullout capacity of the block anchor. The wet condition gives the highest pullout capacity value, and the saturated condition gives the lowest.
2. Thickness of anchor contributes to the pullout capacity through friction forces. This contribution is not so significant as compared to the passive resistance.
3. Pullout capacity of block anchor by Rankine's theory, corrected for the 3-D effect with the frictions contributions, shows close agreement with experimental results.
4. The pressure below the block at the passive side is higher than that at the active side.
5. Vertical displacement indicated that there is an uplifting and tilting of the block
6. Horizontal displacements, needed to develop the maximum pullout capacity, were 16.71, 28.3, and 21.07 mm for dry, wet, and saturated conditions, respectively.
7. Failure manifested itself by a bulged area on the surface of the sand located at the passive side, and by a depression in the active side, for dry condition. For wet condition, cracks appeared at both passive and active sides.

ACKNOWLEDGEMENT

(a) Dry   (b) Wet/Unsaturated
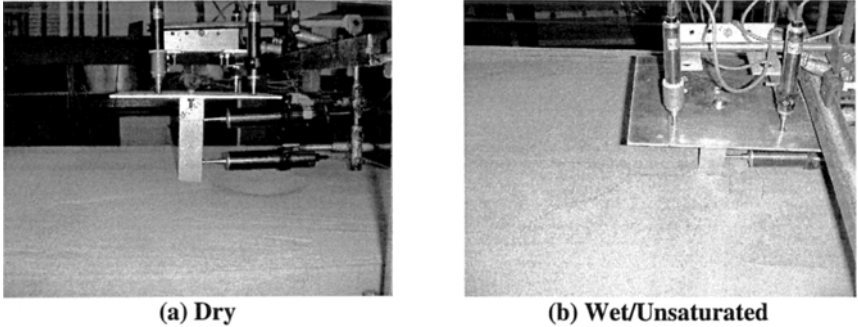
Figure 6. Failure conditions of the soil surface.

REFERENCES

Akinmusuru, J.O . (1978). "Horizontally Loaded Vertical Plate Anchors in Sand". *Journal of Geotechnical Engineering Division,* ASCE, Vol.104, pp. 283-286.

Bowles, J. E. (1997). *Foundation Analysis and Design (5th ed.).* New York: McGraw-Hill. 1175 p.

Das, B.M. (1975). "Pullout Resitance of Vertical Anchors". *Journal of Geotechnical Engineering Division,* ASCE, vol. 101 (GT1), pp. 87-91.

Das, B.M. (1995). *Principles of Foundation Engineering (3rd ed.).* California: Brooks/Cole Publishing Company.

Dickin, E.A., and Leung, C.F. (1983). "Centrifugal Model Tests on Vertical Anchor Plates". *J. of Geotechnical Engineering,* ASCE, Vol. 109 (12), pp. 1503-1525.

Duncan, M., and Mokwa, R. (2001). "Passive Earth Pressures: Theories and Test". *J. of Geotech. and Geoenvironmental Eng.,* ASCE, Vol. 127 (4), pp. 248-257.

Ghaly, A.M. (1997). "Load-Displacement Prediction for Horizontally Loaded Vertical Plates". *J. of Geotech. and Geoenvironmental Eng.,* ASCE, Vol. 123 (1), pp. 74-76.

Hansen, J.B. (1966). "Resistance of Rectangular Anchor Slab". *Danish Geotechnical Institute,* Copenhagen, Vol. 21, pp. 12-13.

Hueckel, S. (1957). "Model Tests on Anchoring Capacity of Vertical and Inclined Plates". *Proceedings of Fourth International Conference on Soil Mechanics and Foundation Engineering,* London, Vol. 2, pp. 203-206.

Neeley, W.J., Stuart, J.G., Graham, J. (1973). "Failure Loads of Vertical Anchor Plates in Sands". *Journal of Soil Mechanics and Foundations Division,* Proceedings of ASCE, Vol. 99 (9), pp. 669-685.

Ovesen, N.K. (1964). "Passive Anchor Slabs, Calculation Methods and Model Tests". *Danish Geotechnical Institute,* Bull. no. 4, pp. 5-39.

Ovesen, N.K. and Stromann, H. (1972), "Design Methods for Vertical Anchor Slabs in Sand", Proceedings, Speciality Conference on Performance of Earth and earth-Supported Structures. ASCE, Vol. 2.1, pp.1481-1500.

Singh, A.I. (1967). *Soil Engineering in Theory and Practice.* New York: Asia Publishing House, Inc.

Prediction of Roughness of Pavements on Expansive Soils

G. T. Hong[1], R. Bulut[2], C. P. Aubeny[3], R. Jayatilaka[4], and R. L. Lytton[5]

[1]Texas Transportation Institute, Texas A&M University, College Station, TX 77843-3135; gthong@tamu.edu, [2]r-bulut@ttimail.tamu.edu,[3]caubeny@civil.tamu.edu, [5]r-lytton@civil.tamu.edu, [4]Terracon, 8901 John Carpenter Freeway, Suite 100, Dallas, TX 75247; rjayatilaka@terracon.com

Abstract

A model was developed to predict pavement roughness due to both expansive soils and traffic in terms of serviceability index (SI) and international roughness index (IRI) by correlating the roughness analysis to the vertical movement estimated from a vertical movement model. The total vertical movement, including both swelling and shrinkage, at the edge of pavement sections, the geometry of the pavement, and site conditions were used as model parameters. Total movements calculated at the edge were based on exponential suction envelopes, volume change coefficients, pavement treatments and roadside conditions. Pavement treatments include vertical and horizontal barriers, inert soil and lime- or cement-stabilized layers. The movements in wheel paths at a distance from the edge of pavement are estimated based upon both field observations and the computed results of a transient finite element analysis. A relationship between IRI and SI was developed. The design equations that were developed for both flexible and rigid pavements include the effects of traffic and expansive soil and permit the selection of the desired level of reliability.

Introduction

This paper presents a design program for pavements on expansive soils, WinPRES, which estimates the development of pavement roughness on expansive soil subgrades. In addition to accounting for the effects of local soils, climate, and drainage conditions, the program has capabilities for evaluating the effectiveness of various design options, including vertical moisture barriers, soil stabilization, and replacement of active soils with inert soils. The program first predicts a so-called suction envelope, i.e., extremes of suction that occur in the soil profile due to seasonal variations in moisture, from which vertical shrink-swell movements are estimated. A one-dimensional analysis for shrink-swell deformations due to seasonal suction variations is performed at the edge of the pavement. Predicted deformations at the

415

edge of the pavement are then extrapolated to any wheel path of interest. The extrapolation algorithm was developed based on finite element studies calibrated to field observations. Predicted vertical shrink-swell deformations are used as a primary input parameter in estimating the rate of decline of serviceability index and the rate of increase in international roughness index. The pavement roughness and serviceability models can provide predictions for both rigid and flexible pavement systems. These models were developed from over 15 years of roughness measurements conducted by Texas Transportation Institute (TTI) on Texas pavements. This paper describes the formulation of the model. A companion paper (Hong et al., 2006) presents example implementation of the model.

Total Vertical Movement at the Edge of a Pavement

Volumetric strain due to suction changes

Lytton (1977) presented the following equation to estimate the volumetric strain, $\Delta V/V$, of an elemental volume of soil:

$$\frac{\Delta V}{V} = -\gamma_h \log_{10}\left(\frac{h_f}{h_i}\right) - \gamma_\sigma \log_{10}\left(\frac{\sigma_f}{\sigma_i}\right) \qquad (1)$$

where γ_h is the suction compression index, γ_σ is the mean principal stress compression index, h_i is the initial suction, h_f is the final suction, σ_i is the initial mean principal stress, and σ_f is the final mean principal stress. It is commonly sufficient to compute the final mean principal stress, σ_f, from the overburden, surcharge, and foundation pressure and treat the initial mean principal stress, σ_i, as a constant corresponding to the stress-free suction-versus-volume strain line. Because there is no zero on a logarithmic scale, σ_i may be regarded as a material property, i.e., a stress level below which no correction for overburden pressure must be made in order to estimate the volumetric strain. It has been found to correspond to the mean principal stress at a depth of 2.62 ft (Lytton et al., 2004). The final mean principal stress is estimated as follows:

$$\sigma_f = \frac{(1+2K_0)\sigma_z}{3} \qquad (2)$$

where σ_z is the vertical stress at a point below the surface in the soil mass, and K_0 is the lateral earth pressure coefficient.

The method to determine the suction compression index, γ_h, was developed based on the soil data of the Soil Survey Laboratory (SSL) of the National Soil Survey Center (Covar and Lytton, 2001). Most of the data in the present database were obtained over the last 40 years with approximately 75 percent of the data being obtained in the last 25 years. This data filtering produced a subset of the data containing approximately 6500 records. Next, the data records were partitioned based on Casagrande (1948) and the Holtz and Kovacs (1981) mineral classification (Fig. 1). This partitioning step

resulted in eight separate data groups, each representing a group with some mineralogical similarity. The zone III chart, one of eight groups, is shown in Figure 2. The two axes are given by the activity ratio, A_c (=PI/%fc), and LL/%fc where %fc is the percentage of fines comprised of clay (% clay/% fines). The method is "stable" in the sense that each mineralogical zone or group is explicitly defined; thus, no arbitrary distinctions can affect the results. Within each group, the practitioner needs only the liquid limit, plasticity index, and the fine clay fraction (%) to get an estimate of the soil compression index, γ_0. The actual suction compression index is proportional to the actual percent of fine clay in the soil. Thus, the actual γ_h is as follows:

$$\gamma_h = \gamma_0 \times \left[\frac{\text{percent of soil finer than 2 microns}}{\text{percent of soil passing the #200 sieve}} \right] \tag{3}$$
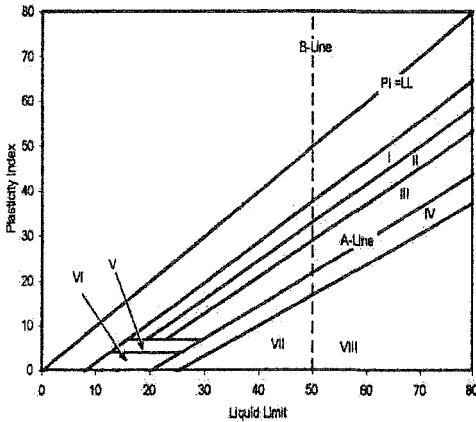
Figure 1. Data Filter for Partitioning Database on Mineralogical Types. (Covar and Lytton, 2001)
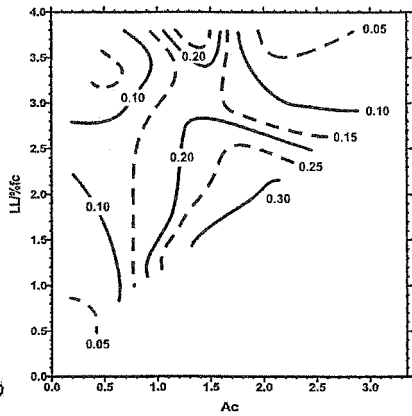
Figure 2. Predicted Soil Compression Index for Zone III. (Covar and Lytton, 2001)

The mean principal stress compression index, γ_σ, is related to γ_h by the following Eq. (4) based on Lytton (1994):

$$\gamma_\sigma = \gamma_h \frac{1}{1 + \dfrac{h}{\theta(\partial h / \partial \theta)}} \tag{4}$$

where θ is the volumetric water content, and $\partial h / \partial \theta$ is the slope of the suction-versus-volumetric water content curve. The suction compression index obtained is corrected to compensate for the different initial volume of soil mass during a wetting or drying process (Lytton et al., 2004):

$$\gamma_{h\,(\text{swelling})} = \gamma_h \exp(\gamma_h) \tag{5}$$

$$\gamma_{h\,(\text{shrinkage})} = \gamma_h \exp(-\gamma_h) \tag{6}$$

A suction compression index for stabilized soil can be estimated using Atterberg limits, soil particle size distribution of the natural soil to be stabilized, and the percent of stabilizing material such as lime or cement.

Suction envelopes

The volumetric strain defined by Eq. (1) is driven by changes in suction, h, as described earlier. Generally, the minimum and maximum suction at the ground surface of the site are considered as the suction at the field capacity, 2.0 pF, and wilting point, 4.5 pF, respectively. The suction at the field capacity should be adjusted with lateral slope and longitudinal drainage conditions of the pavement. The lateral slope conditions used are cut, flat, and fill. The longitudinal drainage conditions used are hill, slope, and valley. The minimum suction at the surface for different drainage and slope conditions are given in Table 1.

Table 1. Minimum Suction (pF) for Lateral Slope and Longitudinal Drainage Conditions.

Longitudinal Drainage	Lateral Slope		
	Cut	Flat	Fill
Hill	2.3	2.5	2.6
Slope	2.0	2.2	2.3
Valley	2.0	2.2	2.3

Note : For Thornthwaite Moisture Index (TMI; Thornthwaite, 1948) greater than +10.0, the values in the table are used. For $-20.0 \leq \text{TMI} < 10.0$, 0.2 is added to the values in the table. For TMI less than - 20.0, 0.4 is added to the values in the table.

Depth of root zone must be specified for sites that have trees near the edge of the pavement. A maximum suction at the site is the wilting point (4.5 pF) up to depth of root zone. The depth of moisture active zone (Z_m), the maximum possible depth of moisture flow, is assumed as a point where equilibrium suction begins. The value of equilibrium suction U_e at the site can be measured or considered as a calculated suction based on TMI, which is an approximated suction value based on the regression equation for the relation between field data and TMI:

$$U_e = 3.5633\exp(-0.0051\text{TMI}) \tag{7}$$

The exponential suction profile for the side of extreme dry and wet conditions is generated based on the equation for a transient state by Mitchell (1979):

$$U(Z) = U_e \pm U_0 \exp\left(-\sqrt{\frac{n\pi}{\alpha}}Z\right) \tag{8}$$

where U is the value of suction (pF) at a depth Z, U_e is the equilibrium suction, U_0 is the amplitude of suction change on different soil layers, n is the number of suction cycles per second, and α is the soil diffusion coefficient using Mitchell's unsaturated permeability. The value of α can be estimated from the Eq. (9) based on Lytton (1994):

$$\alpha = 0.0029 - 0.000162(S) - 0.0122(\gamma_h) \qquad (9)$$

where γ_h is the suction compression index and S, the slope of suction-versus-gravimetric water content, is estimated from the Eq. (10) based on Lytton (1994):

$$S = -20.29 + 0.1555(LL) - 0.117(PI) + 0.0684(-\#200) \qquad (10)$$

where LL is the liquid limit in percent, PI is the plasticity index in percent and $-\#200$ is the percent of soil passing the #200 sieve. The three typical suction envelopes generated for the case study sections (section A and B at the Fort Worth site, and one section at the Atlanta site) are shown in Figure 3. For the section A at the Fort Worth site, the result shows the suction profile is developed up to the depth of the moisture active zone, 15 ft. The initial suction 2.5 pF, for wetting at the surface is estimated using the climatic data and the drainage condition at the site. The equilibrium suction of 2.58 pF, which was obtained from lab tests of the soil sample, is attributed to a water table being near the depth of 17 ft and yields only a small amount of swelling. For the section B at the same site, the suction profile at this location is developed with the equilibrium suction of 3.45 pF; the limiting surface suction of 2.5 pF for wetting and 4.5 pF for drying is illustrated. The suction profile at the edge of the pavement at the site in the Atlanta District along U.S. 271 is generated with a root zone of 11.0 ft based on the root fibers found in the boring log.
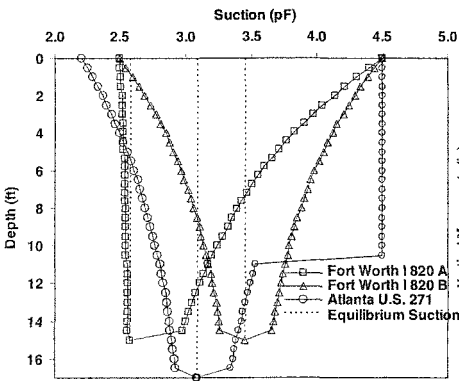
Figure 3. Suction Envelopes of Case Study Sections
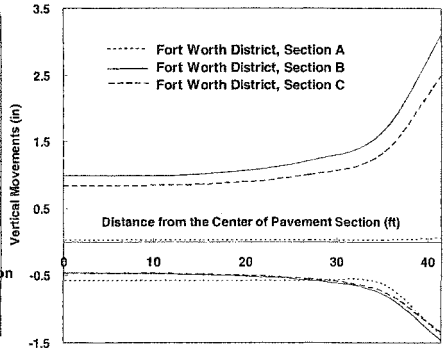
Figure 4. Transverse Distribution of Vertical Movements

Shrinkage and heave

The vertical strain estimated from the volumetric strain by using a crack fabric factor, f, is as follows:

$$\Delta H/H = f(\Delta V/V) \qquad (11)$$

where crack fabric $f = 0.67 - 0.33\Delta pF$. Typical values of f which have been back-calculated from field observations are 0.5 when the soil is drying and 0.8 when the

soil is wetting (Lytton, 1994). The total heave or shrinkage in a soil mass is the sum of the products of the vertical strains and the increment of depth to which they apply, Δz_i:

$$\Delta = \sum_{i=1}^{n} f_i \left[\frac{\Delta V}{V} \right]_i \Delta z_i \qquad (12)$$

where n is the number of depth increments, Δz_i is the depth increment, and $[\Delta V/V]_i$ is the volumetric strain in the ith depth increment.

Vertical movements extrapolated to a wheel path from the edge of pavement

Jayatilaka (1999) suggested a regression model to estimate the relationship between one- and two-dimensional vertical movements:

$$\frac{VM_{2D}}{VM_{1D}} = \xi_1 \exp\left[\left(\xi_2 \frac{d}{D} \right)^{\xi_3} \right] \qquad (13)$$

where VM_{2D} is the two dimensional vertical movement, VM_{1D} is the one dimensional vertical movement, d is the distance from the center of the pavement to the point where the vertical movement needs to be calculated, D is the half width of the pavement, and ξ_i (i=1,2,3) are the regression coefficients. The vertical movements for four types of soil in five different climatic conditions were estimated from both the MOPREC (one-dimensional vertical movement) and FLODEF (two-dimensional finite element flow and deformation) programs developed by Gay (1994). The FLODEF program calculates the transient unsaturated moisture flow and deformation in expansive clay using a sequential analysis of flow and deformation. The one-dimensional vertical movement program MOPREC was used in the development of regression equations for the estimation of vertical movement in a two-dimensional domain. The regression coefficients, ξ_i (i=1,2,3), developed using a multiple linear regression analysis depend on one-dimensional vertical movement, the depth of barrier, the depth of available moisture, the half width of pavement, the mean suction at a site, and TMI.

Transverse distribution of vertical movements

One of the case study sites, Fort Worth North Loop Interstate 820, is used to estimate a transverse distribution of vertical movements for each of three Cross Section A through C with the width of pavement of 83 ft. Cross Section A and B were embankment sections with Cross Section A being unusually wet and Cross Section B being closer to the normally expected moisture level. Cross Section C had an embankment on the north side of the roadway and was at grade on the South side. It too was at a higher moisture level than normally expected for the Fort Worth climatic zone.

Figure 4 shows that both swelling and shrinking expected without treatments increase from the center of pavement to the edge of pavement. The swelling that is expected in Cross Section A is very small because of the moist condition of the embankment, but the expected shrinkage is very large. The swelling expected in the Cross Section B is a little larger than that in the Cross Section C and the shrinkage expected in the Cross Section A, B and C is similar. The average swelling and shrinking expected, in Cross Section A and B, beneath the outer wheel path which is located at the distance of 27 ft from the center of pavement are 1.1 inches and 0.56 inches, respectively.

Pavement Design Based on Subgrade Movements and Traffic

The procedure described in the above paragraphs provides estimates of vertical deformations of expansive subgrade soils, with ΔH being the total vertical movement including both shrinkage and swell. The following paragraphs describe how WinPRES relates these predicted movements, together with projected traffic data, to obtain predictions of pavement performance for use in design. The program predicts pavement performance in terms of serviceability and international roughness index; the relationship between these measures is discussed below.

Relationship between serviceability index and international roughness index

Jayatilaka (1999) collected subgrade soil properties and surface profile measurements in several pavement sections in the state of Texas where moisture barriers have been installed. The pavement sections included Interstate-410, Interstate-10, U.S. 281, and General McMullen Drive in San Antonio, Interstate-30 in Greenvile, Interstate-10 in Sierra Blanca, Interstate-635 in Dallas, Interstate-10 in Seguin, and FM-1516 in Converse. The 690D Surface Dynamics Profilometer owned by the Texas Department of Transportation was used to obtain relative elevation profiles of the road surface in all of the test sites. The measurements are obtained at 6 inches intervals and saved in a computer file. The relative elevations of right and left wheel paths are recorded in two columns in units of thousandths of an inch.

This computer file is used as the input file for the computer programs that are used to obtain profile statistics. The profile statistics, International Roughness Index (IRI) and Serviceability Index (SI), are used to develop roughness predicted models in this study. In the AASHO road test (Carey and Irick, 1960), the serviceability of pavements was rated between zero and five. The IRI is based on the roadmeter measure and has units of slop such as m/km or in/mile. The IRI is influenced by wavelengths and is linearly proportional to roughness (Sayers and Karamihas, 1996). The computer program VERTAC (McKenzie et al., 1986) was used to obtain IRI and SI of all of the pavement sections. The program VERTAC is capable of calculating both IRI and SI.

The length of the roadway section that was used in the program depended on the lengths of barrier and control sections. The serviceability Indices and International

Roughness Indices obtained from this program were used in the development of roughness prediction models. In addition, these data were used to develop a relationship between the IRI and SI. A plot of IRI versus SI and the fitted model is shown in Figure 5. The relationship developed is as follows:

$$IRI = 8.4193 \exp(-0.4664SI) \tag{14}$$
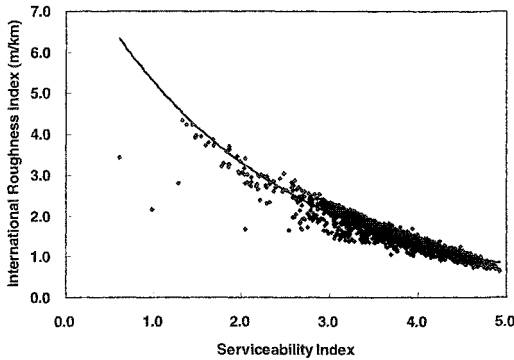
Figure 5. International Roughness Index versus Serviceability Index.

Correlating pavement roughness to total vertical movement

By plotting SI and IRI versus time, it was found that the pavement performance can be modeled through a sigmoidal type curve. The nonlinear regression technique was employed to fit the roughness indices versus time to the model and regression constants were obtained for each wheel path of each lane of each test section. The sigmoidal models with respect to present serviceability index (PSI) and IRI used in modeling pavement roughness with time are as follows:

$$PSI = PSI_0 - (PSI_0 - 1.5)\exp\left[-\left(\rho_s/t\right)^{\beta_s}\right] \tag{15}$$

$$IRI = IRI_0 + (4.2 - IRI_0)\exp\left[-\left(\rho_i/t\right)^{\beta_i}\right] \tag{16}$$

where PSI_0 is the initial present serviceability index of the pavement, t is time in months, IRI_0 is the initial roughness index (m/km), and ρ_s, β_s, ρ_i, β_i are roughness parameters. To estimate the roughness, ρ_s, β_s, ρ_i, β_i for each wheel path, the nonlinear regression analysis was carried out for the roughness data using the NLIN procedure in the statistical analysis software package developed by SAS Institute Inc. The results of analysis showed that the best values for β_s and β_i were found to be 0.66 and 0.56, respectively. Using these values, the final nonlinear regression analysis was performed for the data in all test sections and the roughness parameters ρ_s and ρ_i were estimated considering both traffic loading and expansive behavior of subgrade soil:

$$\rho_s = A_s - B_s \Delta H \tag{17} \qquad \rho_I = A_i - B_i \Delta H \tag{18}$$

where ΔH is the two-dimensional vertical movement in mm as predicted by Eqs. (12) and (13), A_s and A_i are the parameters that are function of traffic, structural number (SN) of pavement section, and resilient modulus of subgrade soil (M_r), and B_s, B_i are the constants. Since SN, M_r, and traffic are the same in a single lane of a pavement section, the two wheel paths of a single lane should have the same A_s and A_i values. Using this property, two simultaneous equations with two unknowns were obtained for each lane of a pavement section. Two simultaneous equations were solved for each lane and values of B_s and B_i were estimated for all the pavement sections considered for the development of roughness models. The values of B_s and B_i can be found for a site by assigning a reliability and using the following relationship:

$$B_s = 17.960 + 4.195Z_R \tag{19}$$

$$B_i = 35.817 + 8.158Z_R \tag{20}$$

where Z_R is the standard normal variable corresponding to the assigned reliability.

Design equations for flexible and rigid pavement

Roughness parameters A_s and A_i were estimated based on the AASHTO (1993) design equations for both flexible and concrete pavements. From the relation between the total loss of serviceability and the serviceability loss due to traffic, the roughness parameter, A_s, for flexible pavement is as follows:

$$A_s = t\left[\log_e\left(10^{-\lambda}\right)\right]^{\left(\frac{1}{0.66}\right)} \tag{21}$$

where a value of t of 480 months is assumed to be the time required for the roughness due to expansive clays to be complete, and λ is estimated for 40 years. The value of λ for flexible pavement is as follows:

$$\lambda = \left[0.4 + \frac{1094}{(SN+1)^{5.19}}\right] \times$$
$$\left[\log_{10} W_{18} - 9.36\log_{10}(SN+1) + 8.27 - 2.32\log_{10} M_r + Z_R S_0\right] \tag{22}$$

where W_{18} is the 18 kip (80kN) single-axle load applications, Z_R is the standard normal deviate, S_0 is the combined standard error, 0.44 based on AASHTO (1993), SN is the structural number of pavement, and M_r is the resilient modulus of subgrade soil (psi).

Since the AASHTO design equation is not available in terms of IRI, the parameter A_i cannot be estimated directly as in the case of A_s. From a regression relationship between SI and IRI, the initial IRI, which corresponds to PSI of 4.2, is estimated to be 1.19 (m/km). The roughness parameter, A_i is estimated using the same process to find A_s:

$$A_{\mathrm{i}} = t \left[\log_e \left(\frac{3.01}{8.4193 \exp\left(-0.4664\left(4.2 - 2.7\left(10^{\lambda}\right)\right)\right) - 1.19} \right) \right]^{\left(\frac{1}{0.56}\right)} \tag{23}$$

A similar process is used to find the A and B coefficients to predict the roughness and riding quality development for concrete pavement design. The roughness parameters, A_s, for concrete pavement is as defined by Eq. (21) and A_i is estimated based on the initial present serviceability index, 4.5, as follow:

$$A_{\mathrm{i}} = t \left[-\log_e \left(\frac{3.168}{8.4193 \exp\left(-0.4664\left(4.5 - 3.0\left(10^{\lambda}\right)\right)\right) - 1.032} \right) \right]^{\left(\frac{1}{0.56}\right)} \tag{24}$$

The value of λ for concrete pavement based on AASHTO (1993) pavement design program is as follows:

$$\lambda = \left[1 + 1.624 \times 10^7 / (D+1)^{8.46}\right] \times \lambda' \tag{25}$$

with $\lambda' = \log_{10} W_{18} - 7.35 \log_{10}(D+1) + 0.06$

$$-(4.22 - 0.32 p_t) \log_{10} \left[\frac{S_c' C_d \left(D^{0.75} - 1.132\right)}{215.63 J \left(D^{0.75} - 18.42 / \left(E_c / k\right)^{0.25}\right)} \right] + Z_R S_0 \tag{26}$$

where D is the thickness of concrete layer (inches), S_c' is the modulus of rupture of concrete (psi), J is the load transfer coefficient, C_d is the drainage coefficient, E_c is the modulus of elasticity of Portland cement concrete (psi), k is the modulus of subgrade reaction (pci), S_0 is the combined standard error, 0.34 based on AASHTO (1993), and p_t is the terminal present serviceability index. These equations for both flexible and rigid pavements are used to estimate the rate of increase roughness (IRI) and decrease of riding quality (PSI) due to both traffic and expansive clay movements.

Reliability levels for design

Reliability is a means of incorporating some degree of certainty into the design process to ensure that the various design alternatives will last the analysis period. The level of reliability to be used for design should increase as the volume of traffic and public expectation of availability increase. The table 2 presents recommended levels of reliability for various functional classes based on Huang (1993).

Table 2. Suggested Levels of Reliability for Various Functional Classifications.

Functional Classifications	Recommended Level of Reliability	
	Traffic (Huang, 1993)	Expansive Soil
For Prediction	50%	50%
For Design		
Interstate and other freeways	85 – 99.9 %	80 – 99.9 %
Principal arterials	80 – 99.0 %	75 – 95.0 %
Collectors	80 – 95.0 %	75 – 95.0 %
Local	50 – 80.0 %	50 – 80.0 %

Conclusions

The design program presented herein permits the designer to consider both flexible and rigid pavements, traffic expressed in 18-kip Equivalent Single Axle Loads, and multiple layers of subgrade soils characterized by their Atterberg Limits, percentage fines, clay fraction, and unit weight. The designer can evaluate the effectiveness of various treatments for reducing roughness caused by expansive clay subgrades including lime- or cement-stabilized layers, removal and replacement with a more inert soil, and vertical and horizontal moisture barriers. The designer can specify the level of reliability associated with the various predictions made by the program and can designate several different wheel paths in which to evaluate the effectiveness of the treatment. Both the present serviceability index and the international roughness index are calculated in each selected wheel path for a period desired. The program also calculates the expected amount of vertical swelling and shrinkage movement beneath each selected wheel path that controls the predicted performance. The design program is user-friendly, flexible, and capable of a wide variety of design tasks. It allow the designer to consider a wide variety of treatment options, drainage conditions, roadside vegetation, local climatic conditions, traffic conditions, and pavement type (asphalt and concrete).

While the design program WinPRES provides a comprehensive analysis package for a broad spectrum of site conditions, certain limitations should be borne in mind. One is a caution that the effect of sulfate swelling is not included in the design method presented this paper. At present, it should be sufficient to use this design program as it is intended, and that is under the assumption that no sulfate swelling potential is present in the subgrade soil. A second caution is related to the treatment of the stabilized layers in the program. The prediction of the reduction in swelling and shrinking potential of both lime-and cement-stabilized soils is based upon a limited number of laboratory tests that were run on stabilized soils from previous projects. The assumptions in WinPRES relating to shrink-swell characteristics of stabilized soils should be verified and perhaps modified in light of the results of further testing.

References

AASHTO (1993). *Guide for Design of Pavement Structures*. AASHTO, Washington, D.C.

Carey Jr., W. N., and Irick, P. E. (1960). "The Pavement Serviceability-Performance Concept.", Bulletin 250, Highway Research Board, National Research Council, Washington, D.C., pp. 40-58.

Casagrande, A. (1948). *Classification and Identification of Soils*. Transactions ASCE, Vol. 113, pp. 901-930.

Covar, A. P. and Lytton R. L. (2001). "Estimating Soil Swelling Behavior Using Soil Classification Properties." *Geotechnical Special Publication* No. 115, ASCE, Houston, Texas, pp. 44-63.

Gay, D. A. (1994). *Development of a Predictive Model for Pavement Roughness on Expansive Clay*. Ph.D. dissertation. Department of Civil Engineering, Texas A&M University, College Station.

Holtz R. D. and Kovacs W. D. (1981). *An Introduction to Geotechnical Engineering*. Prentice-Hall, Englewood Cliffs, New Jersey.

Hong, G. T., Aubeny, C. P., Bulut, R. and Lytton, R. L. (2006). *Design of Pavements on Expansive Soils*. Proceedings, 4th International Conference on Unsaturated Soils, Carefree, Arizona.

Huang, Y. H. (1993). *Pavement Analysis and Design*. Prentice Hall, Englewood Cliffs, N.J.

Jayatilaka, R. (1999). *A Model to Predict Expansive Clay Roughness in Pavements with Vertical Moisture Barriers*. Ph.D. dissertation. Department of Civil Engineering, Texas A&M University, College Station.

Lytton, R. L. (1977). *The Characterization of Expansive Soils in Engineering*, Presented at the Symposium on Water Movement and Equilibria in Swelling Soils. American Geophysical Union, San Francisco, California.

Lytton, R. L. (1994). "Prediction of Movement in Expansive Clay." *Geotechnical Special Publication* No. 40, ASCE, New York, NY, Vol. 2, pp. 1827-1845.

Lytton, R. L., Aubeny, C. P., and Bulut. R. (2004). Design Procedures for Pavements on Expansive Soils. FHWA/TX-05/0-4518-1, Texas Transportation Institute. College Station.

McKenzie, D. W., Riddle, P. and Crandell, J. (1986). VERTAC, *a Vertical Acceleration Program for the Calculation of Serviceability Index*, Version 6.0, Center for Transportation Research, University of Texas at Austin, Texas.

Mitchell, P. W. (1979). *The Structural Analysis of Footings on Expansive Soil*. Research Report No.1, Kenneth W. G. Smith and Associates, Newton, South Australia.

Sayers, M. W., and Karamihas, S. M. (1996). "The Little Book of Profiling." Transportation Research Institute, University of Michigan, Ann Arbor, Michigan.

Thornthwaite, C. W. (1948). "Rational Classification of Climatic." *Geographical Review*, Vol. 38, pp. 54-94.

Design of Pavements on Expansive Soils

G. T. Hong[1], C. P. Aubeny[2], R. Bulut[3], and R. L. Lytton[4]

[1]Texas Transportation Institute, Texas A&M University, College Station, TX 77843-3135; gthong@tamu.edu, [2]caubeny@civil.tamu.edu, [3]r-bulut@ttimail.tamu.edu, [4]r-lytton@civil.tamu.edu

Abstract

Vertical movements calculated by the new design method for each of the six case study cross sections, in three different climatic zones in Texas, were compared with the swelling movement predicted by the PVR method which has been used by Texas Department of Transportation (TxDOT) in the past. The vertical movements included both swelling and shrinking. Pavement treatments were selected to provide an acceptable predicted performance at high levels of reliability, and the vertical movements were calculated both at the edges of the pavements and beneath the outer wheel paths. The case studies were based upon a variety of traffic levels, site conditions, and sample testing. The treatments include lime- and cement-stabilized layers, removal and replacement with inert layers, and vertical and horizontal moisture barriers. The results of the case studies show that the PVR overpredicts the swelling movement that can be expected using the new method, and does not predict shrinkage movement. The resulting evaluation is that the PVR criterion is conservative.

Introduction

The performance of pavements constructed on expansive soils will be critically affected by vertical deformations of the supporting subgrade soils in addition to the traffic loading conditions that affect all pavements. A predictive model for pavement design on expansive soils must therefore reliably predict vertical deformations in the expansive subgrade soils. Further, the relationship between vertical deformations and pavement roughness and serviceability must be properly understood. A companion paper in this conference "Prediction of Roughness of Pavements on Expansive Soils" by Hong et al. (2006) highlights the comprehensive framework developed at Texas A&M University (TAMU) for predicting the roughness that is developed in a pavement over a period of time due to swelling and shrinkage of expansive clays. This paper compares predictions from the proposed new method to

427

those from the existing Texas Department of Transportation (TxDOT) procedure Tex-124-E, "Method for Determining the Potential Vertical Rise, PVR". Texas Transportation Institute (TTI) Research Report by Jayatilaka et al. (1993) provides much of the groundwork for the TAMU approach. The new method that is suggested to replace the PVR method is the culmination of several decades of effort by TxDOT, the Texas Transportation Institute. Key features of the new method include the following:

1. The depth of the moisture-active zone is limited by the moisture diffusivity properties of the soil. Further, the seasonal moisture-suction variations driving the shrink-swell processes are controlled by local climate, vegetation, and conditions of drainage. The new method accounts for all of these effects.
2. The reduction in soil swelling potential with increasing level of mechanical stress is implicit in the model. The new model was also formulated with the recognition that the existence of cracks in the soil mass influences the relationship between soil volume change and vertical deformations.
3. The model considers two-dimensional effects; e.g., differences in vertical deformations at the edge and center of the pavement. Other two-dimensional effects that can be considered include those due to horizontal or vertical moisture barriers.
4. The model can predict both shrinkage and swell of subgrade soil. Capability for prediction of soil shrinkage is important, since the total movement due to shrinkage and swelling will influence pavement performance.
5. In applying estimates of soil vertical deformations to predictions of pavement performance, a basic premise of the new model is that the total shrink-swell deformation contributes to the *rate of increase* of pavement roughness over time. Accordingly, a predicted vertical deformation by itself is not a reliable indicator of pavement performance. Rather, vertical deformations together with design traffic loads influence the time history of pavement performance, and this predicted history of roughness and serviceability should be used as a design basis.

Overview of Suction Based Method

The prediction of movement in expansive soil is important principally for the purpose of designing foundations and other ground supported structural elements such as pavements. In design, the principle interest is in making an accurate estimate of the range of movements that must be sustained by the foundation. It is for this reason that envelopes of maximum heave or shrinkage are important for design purpose.

There are three categories of methods of predicting movements in expansive clays: oedometer, empirical, and suction methods. The oedometer methods basically use the consolidation theory in reverse and are based on determining a swelling property of the soil by one of two tests: the constant volume or swell-pressure test and the consolidation-swell test. However, the oedometer methods always overpredict the in situ heave except in those rare cases where the capillary moisture conditions are met

in the field as in the case where high water tables are present on the site [e.g., Osman and Sharief (1987) and Dhowian et al. (1987)].

The empirical or semi-empirical methods are based on a correlation between laboratory or field measurements and soil indices such as the liquid limit, plasticity index, and clay content. There are large numbers of these empirical relations in the literature, but empirical relations all suffer from the same limitations of being confined to their locale of origin and having to rely upon an assumed final moisture condition. These limitations apply to both laboratory samples and to field measurements.

The methods using soil suction have the distinct advantage of using the moisture energy for predicting the heave and shrinkage of soil. Movements in expansive soils are generated by change of suction that is brought about by entry or loss of moisture. The volume change depends upon the total stress states that surround the soil. A companion paper by Hong et al. (2006) in this Conference details the philosophy behind the method and then outlines the comprehensive framework developed at Texas A&M University for predicting the movement of expansive soil based on changes of suction.

Design of Pavement with Remedial Measures for Three Case Study Sites

The design analysis for three study sites (Fort Worth North Interstate 820, Atlanta District U.S. 271, and Austin District State Route 1) is performed using the design program WinPRES with the data obtained from borehole logs, laboratory test results, climatic and drainage conditions, dimensions of road, and roughness and traffic information.

The typical soil properties in each analysis section are constructed considering all data such as Atterberg limits, particle size distribution, values of suction, and climatic and geometric conditions. The analysis cross sections of pavement for the six case study sections are constructed using the number of lanes and the width of shoulder. The pavement sections of both flexible and rigid pavement are estimated with various treatments and layer thickness. The typical value of the falling weight deflectometer modulus of the subgrade soil of 10,000 psi is used for the flexible pavement. A 28-day compressive strength of the concrete of 4,000 psi, mean modulus of rupture of concrete of 620 psi, drainage coefficient of 1.0, modulus of subgrade of 300 pci, and load transfer coefficient of 2.9 for the rigid pavements are used as design parameters. The average daily traffic (ADT) in one direction and the total 18 kip single axle loads in the traffic analysis period of 30 years for the three sites are assumed based on traffic information provided by the Fort Worth. The initial serviceability index for flexible and rigid pavement are assumed to be 4.2 and 4.5, respectively. Generally, the minimum acceptable SI after 30 years is considered as 2.5. The 50 percent reliability level is used for prediction and the reliability level of 95 percent is used for the design of both flexible and rigid pavement. The design analysis is performed with both

flexible and rigid pavements including treatments vertical moisture barriers, and lime stabilized and inert soil layers. The parameters used for three case study sites are presented in Table 1.

Table 1. Design Parameters for Structural Properties of Pavement and Traffic

Design Parameters	Study Sites			
	Fort Worth North Loop Interstate 820	Atlanta U.S. 271	Austin State Route 1	
			Main Lanes	Frontage Road
Number of Lanes	5	1	4	3
Distribution of Traffic (inner to outer)	0.16, 0.16, 0.16, 0.20, and 0.32	1.0	0.19, 0.19, 0.24, and 0.38	0.20, 0.33, and 0.47
Average Daily Traffic t=0 yr	13,712	10,000	16,283	4,028
of Outer Lane t=30 yr	21,744	20,000	25,821	6,837
Total W_{18} of Outer Lane (t=30 yr)	8,415,520	2,500,000	9,993,430	2,472,059
Width of Pavement (ft)	83.0	44.0	62.0	50.0
Distance from the Center of Pavement (ft)	27.0	9.0	21.0	15.0
Falling Weight Deflectometer Modulus of subgrade Soil	10,000 psi for Flexible Pavement, Modulus of Subgrade Soil for Rigid Pavement is 300 pci (k =FWD/19.4)			
28-day Compressive Strength of Concrete	4,000 psi			
Mean Modulus of Rupture of Concrete	620 psi			
Drainage Coefficient	1.0			
Load Transfer coefficient	2.9			
Initial Serviceability Index	4.2 for Flexible Pavement and 4.5 for Rigid Pavement			
Initial International Roughness Index	75.2 in/mile for Flexible Pavement and 65.4 in/mile for Rigid Pavement			
Reliability	50% for Prediction and 95% for Design			

Comparison of PVR Design Criteria with Case Study Results

The PVR computed for a given site is currently used in pavement design to determine what depth of the natural soil must be removed and replaced with a more inert soil or modified in place in order to reduce the computed PVR to 1 inch for Interstate/U.S., 1.5 inches for SHs, or 2 inches for FMs. The amount of movement that is predicted both at the edge of the pavement and beneath the outer wheel path by the method described in this paper is compared to the calculated PVR for the same cases. Contrary to the way the PVR is calculated, the predicted vertical movement is the sum of both shrinkage and swelling movements. The purpose of the comparison is to determine whether the previously used PVR criterion is conservative when compared to the movements that are calculated by the methods of this paper. A secondary purpose is to illustrate with the case studies the design advantages that are provided by having an estimate of both shrinking and swelling movements.

The new method of predicting the vertical movement uses this information to predict the accumulation of pavement roughness with time and traffic. It was discovered in the course of the analysis of the field monitoring data that were collected for a period of over 20 years in some cases that the total movement in the subgrade beneath a given wheel path governs the rate of increase of roughness rather than the level of roughness itself. Roughness is predicted as a decrease of present serviceability index (PSI) as well as an increase of the international roughness index (IRI). The computed

results for analysis pavement sections without treatment in the expansive subgrade
soil for three case study sites are summarized in Figure 1.
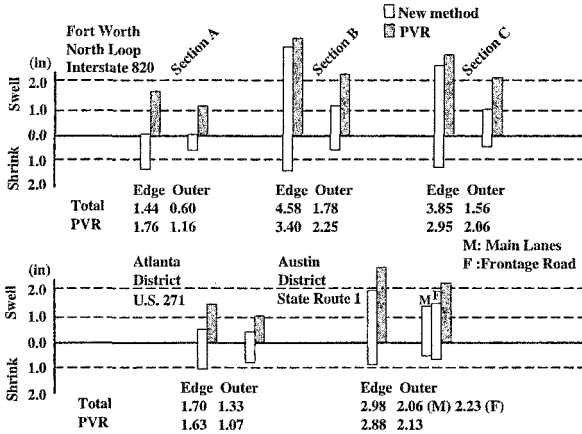
Figure 1. Subgrade Movements Compared with PVR (Tex-124-E) for the Pavement without Treatments.

Fort Worth north Interstate 820 case study

Three cross sections were used as separate case studies along the Interstate
820 Loop north of Fort Worth. Cross sections A and B were embankment sections
with Cross Section A being unusually wet and Cross Section B being closer to the
normally expected moisture level. Cross Section C had an embankment on the north
side of the roadway and was at grade on the south side. It, too, was at a more normally
expected moisture level for the Fort Worth climatic zone. Figure 1 shows the
calculated vertical movements for each of the cross sections as they were predicted by
the new method and also by the PVR method. The predictions were made at two
locations: at the edge of the pavement where the soil movement is not affected by the
weight of the pavement and beneath the outer wheel path where the weight of the
pavement will restrain the vertical movement to some extent. The new method
predicts both a swelling and a shrinkage vertical movement and a total movement,
which is the sum of the two.

The swelling expected in Cross Section A is very small because of the moist
condition of the embankment, but the expected shrinkage is very large. The new
method shows that not much additional swelling is to be expected in Cross Section A,
but a large amount of shrinkage is expected. The shrinkage figure is important
because it is an indicator of future longitudinal shrinkage cracking along the edge of
the pavement. The PVR for the same section is roughly in the same range as the total
movement predicted by the new method, but it is considerably larger than the swelling
that is predicted. The movement beneath the outer wheel path reflects the effect of the

weight of the pavement in the case of the PVR calculation but also indicates the added effect of the diffusion of moisture from the edge of the pavement in the case of the new method predictions. The new method expects to have less movement beneath the outer wheel path than does the PVR method. In Cross Section B, the swelling expected at the edge of the pavement using the new method is fairly close to the calculated PVR. However, the total movement is larger than the PVR because it includes the expected shrinkage. In Cross Section C, the new method predicts a swelling that is roughly close to that of the PVR at the edge of the pavement. The total movement expected by the new method is considerably larger than the PVR.

In all three cross sections, the new method predicted about the same amount of vertical shrinkage movement beneath the outer wheel path, indicating that longitudinal shrinkage cracks can be expected along the edge of the pavement in all of the cross sections. This shrinkage can be reduced by controlling the moisture influx and efflux beneath the edge of the pavement with the use of a vertical moisture barrier or wide paved shoulder.

Atlanta District U.S. 271 case study

The subgrade soil beneath the pavement at the Atlanta District case study site was not very expansive but there were trees growing within the right of way along the entire length of the case study site. The trees had extracted moisture from beneath the pavement and had caused a considerable amount of longitudinal shrinkage cracks. In the boring log taken beside the pavement in the roadside ditch, root fibers were logged at a depth of 13 ft. The predicted movements using the new method showed that more shrinkage should be expected at this site than at the Fort Worth site, which had even more expansive subgrade soil. So the longitudinal cracking that was observed at this case study site could have been expected using the new method. Figure 1 shows that the PVR predicts more swelling than is expected by the new method both at the edge of the pavement and beneath the outer wheel path. The total movement is close to the calculated PVR.

Austin District State Route 1 case study

The case study site in the Austin District was a sloping site in which the main lanes of State Route 1 were at a higher elevation than the frontage road. The frontage road had been overlaid several times to correct for the expansive clay roughness that had developed over time. There was a deep, grass-covered median between the main lanes.

The calculated PVR is greater than the swelling vertical movement predicted by the new method, but the total movement, is nearly the same as the PVR. Because the same composite boring profile was used in computing the movements beside and beneath the main lanes and the frontage road, the movements predicted at the edge of

pavement by the new method are the same for both cross sections. While the total movement predicted by the new method is nearly equal to the calculated PVR, the predicted swelling is only two-thirds of the total amount both at the edge of the pavement and beneath the outer wheel path for both the main lanes and the frontage road.

Pavement Treatments with Acceptable Predicted Performance

The movements reduced by treatments applied to the subgrade by both methods are compared. The treatments are used to provide a minimum acceptable predicted performance over 30 years with 95 percent reliability on the both flexible and rigid pavements (Table 2).

Table 2. Pavement Treatments with Minimum Acceptable Predicted Performance with the Reliability Level of 95 percent.

Case Study		Types of Pavement	Treatments for Minimum Acceptable Performance
Sites	Locations		
Fort Worth North Loop Interstate 820	Section A	Flexible	ACP 4.0 in, LTS 2.8 ft
		Rigid	CRCP 12.0 in
	Section B	Flexible	ACP 4.0 in, LTS 3.0 ft, Inert 1.0 ft
		Rigid	CRCP 12.0 in, LTS 1.2 ft
	Section C	Flexible	ACP 4.0 in, LTS 3.0 ft, Inert 1.0 ft
		Rigid	CRCP 12.0 in, LTS 1.0 ft
Atlanta District U.S. 271		Flexible	ACP 4.0 in, LTS 2.8 ft
		Rigid	CRCP 12.0 in
Austin District State Route 1	Main Lane	Flexible	ACP 4.0 in, LTS 3.0 ft, Inert 2.5 ft
		Rigid	CRCP 12.0 in, LTS 1.5 ft, Inert 1.8 ft
	Frontage Road	Flexible	ACP 4.0 in, LTS 2.5 ft, Inert 1.5 ft
		Rigid	CRCP 12.0 in

LTS-Lime-Treated Subgrade; ACP-Asphalt Concrete Pavement; CRCP-Continuously Reinforced Concrete Pavement; Inert-Inert Soil Layer.

The applications of a number of alternative treatments to each of the six cross sections in the case studies are performed. These alternatives included different pavement layer thickness, vertical moisture barriers, lime-treated subgrade layers, and removal and replacing of subgrade with a layer of a more inert soil. The criterion that was used in selecting these minimally acceptable treatments was for the pavement riding quality to remain above a present serviceability index (PSI) of 2.5 for the entire 30-year period without requiring any rehabilitation such as overlaying. This performance was to be maintained at a reliability level of 95 percent. Some of typical development of roughness with alternative treatments for the study sections A and B at the Fort Worth site are following session.

Typical development of roughness for case study

For flexible pavements in the study section A at the Fort Worth site with different treatments including lime-stabilized layers and inert soil, the loss of SI and the increase of IRI versus time are shown in Figure 2. A vertical barrier is not used in this case study because it is less effective than stabilized layers in controlling roughness. The results show that the loss of SI and the increase of IRI decrease after 30 years, as the structural number increases. The SI after 30 years is increased by 7 percent by adding an inert soil layer of 2.0 ft thick beneath flexible pavements with the same SN of 5.46. The pavement system with a stabilized soil layer of 3.0 ft thick and an inert soil of 2.0 ft thick is expected to reach PSI of 3.0 after 30 years.
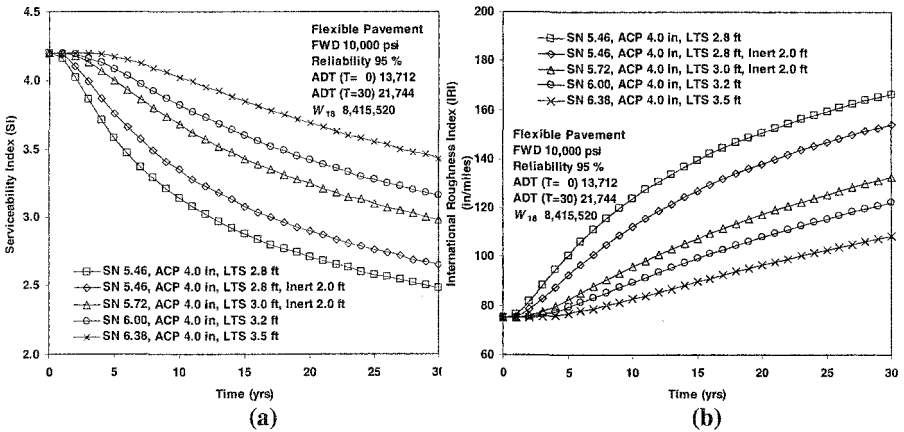
Figure 2. Predicted Performance with Alternative Treatments in the Flexible Pavement, Fort Worth North Loop Interstate 820, Section A: (a) Serviceability Index versus Time and (b) International Roughness Index versus Time.

In the rigid pavement design analysis, a lime-treated subgrade (LTS) of 1.2 ft and 1.5 ft thick and inert soil of 1.0 ft thick were used with a constant concrete thickness of 12.0 inches in Figure 3. The results show that the loss of SI or the increase of IRI with time is reduced by 18 percent by using the treatment including LTS of 1.2 ft thick and inert of 1.0 ft thick instead of using only a LTS of 1.2 ft thick. This rigid pavement system by adding inert soil of 1.0 ft is more effective than by increasing LTS thickness up to 1.5 ft from 1.2 ft. The results of the design calculations with treatments for the minimum acceptable performance in Table 2 in the six case studies are summarized in Table 3.
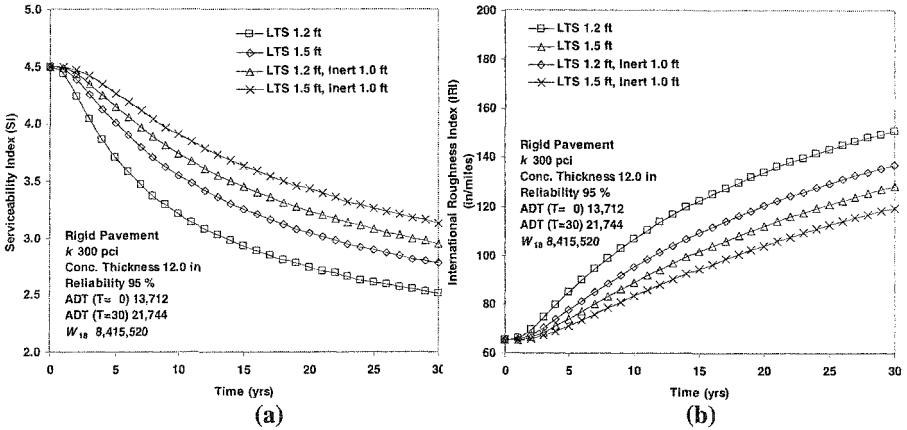
Figure 3. Predicted Performance with Alternative Treatments in the Rigid Pavement, Fort Worth North Loop Interstate 820, Section B: (a) Serviceability Index versus Time and (b) International Roughness Index versus Time.

Table 3. Subgrade Movements Compared with PVR (Tex-124-E) for the Pavement Design with Minimum Acceptable Predicted Performance.

Case Study		Types of Pavement	Movements (in)				PVR (in)	
Sites	Locations		Edge			Outer Wheel Path	Edge	Outer
			Swelling	Shrinkage	Total			
Fort	Section A	Flexible	0.02	1.12	1.14	0.42	1.21	0.81
Worth		Rigid	0.07	1.37	1.44	0.60	1.76	1.16
North	Section B	Flexible	0.78	0.72	1.50	0.61	2.08	1.20
Loop		Rigid	2.12	1.26	3.38	1.27	2.57	2.00
Interstate	Section C	Flexible	0.72	0.73	1.45	0.57	1.25	1.16
820		Rigid	2.03	1.25	3.28	1.28	2.35	1.80
Atlanta District		Flexible	0.30	1.06	1.36	1.08	1.28	0.88
U.S. 271		Rigid	0.67	1.03	1.70	1.33	1.63	1.07
Austin	Main Lane	Flexible	0.37	0.43	0.80	0.49	1.45	1.13
District		Rigid	0.88	0.64	1.52	1.02	1.72	1.22
State	Frontage	Flexible	0.66	0.58	1.24	0.84	1.94	1.17
Route 1	Road	Rigid	2.00	0.98	2.98	2.23	2.88	2.13

Subgrade movements at the Fort Worth site

Table 3 shows for each of the cross sections, A, B, and C, which of the treatments provided the minimally acceptable predicted performance for both flexible and rigid pavements. Cross Section A was unusually wet and the calculated swelling using the new method was small, less than 0.1 inch, at the edge of the pavement. By way of contrast, the PVR values at the same location were 1.21 and 1.76 inches beneath the flexible and rigid pavements, respectively. A similar imbalance is seen between the expected swelling beneath the outer wheel path as calculated by the new method and by the PVR method. The new method alerts the designer that shrinkage, and not swelling, will be the major problem at this cross section.

Cross Section B has a more typical moisture distribution in the embankment materials beneath the pavement. The new method shows that much larger movements, both swelling and shrinking, may be tolerated by the rigid pavement than by the flexible pavement. The expected total movements beneath the outer wheel paths are 0.61 and 1.27 inches in the flexible and rigid pavements, respectively. The corresponding swelling movements calculated by the PVR method are 1.2 and 2.0 inches beneath the outer wheel path in the flexible and rigid pavements, respectively. Both of these are greater than the 1-inch criterion that is presently used for the design of interstate highway pavements on expansive clay. As with the previous section, the PVR method overpredicts the amount of swelling in the outer wheel path and would lead to an overly conservative treatment to restrain the development of roughness due to expansive clay.

Cross Section C is nearly at grade and has a moisture level that is similar to that of Cross Section B. The new method calculates expected movements at the edge of the pavement that are larger than the calculated value of the PVR. The total movements of the subgrade beneath the outer wheel paths are 0.57 and 1.28 inches in the flexible and rigid pavements, respectively, while the amounts of swelling predicted by the PVR method are 1.16 and 1.80 inches beneath the same outer wheel paths. In each of the three cross sections, the PVR, which is a calculated vertical swelling movement, overpredicts the amount of total movement beneath the outer wheel path. A substantial amount of shrinkage movement, as is the case with all three cross sections, is a warning to the designer that some provision must be made to retain moisture beneath the pavement by use of a wider shoulder or a vertical moisture barrier in order to avoid longitudinal shrinkage cracking from reflecting through to the pavement surface.

Subgrade movements at the Atlanta site

In the Atlanta case study site, the soil is not particularly expansive but the presence of the tree roots so close to the paved surface leads to the expectation that shrinkage cracking will be found in both the shoulder and the traveled lanes. Photographs of this site revealed longitudinal cracks along the edge of the pavement, as expected. The swelling movements calculated at the edge of the pavement by the new method were 0.30 and 0.67 inches for the flexible and rigid pavements, respectively. As a contrast, the swelling movements calculated by the PVR method were 1.28 and 1.63 inches, respectively. The vertical shrinkage movements at the pavement edge were calculated to be 1.06 and 1.03 inches, respectively. The total movements beneath the outer wheel paths were 1.08 and 1.33 inches beneath the flexible and rigid pavements, respectively. With this level of predicted shrinkage, the designer is alerted to the fact that the pavement surface must be protected from the reflection of shrinkage cracks in the subgrade due to the drying influences of the trees.

Subgrade movements at the Austin site

The main lanes are about 20 ft higher than the frontage road and there is a deep grass-covered median between the northbound and southbound main lanes. There has been a considerable amount of differential movement along the frontage road, which has been corrected periodically by a sequence of asphalt concrete overlays. Table 4 shows the amounts of movement that are expected in the future starting from its current condition, and the treatments that will provide for an acceptable predicted performance.

The new method shows that swelling is expected roughly close to shrinkage movement for the flexible pavement. The PVR method predicts more than twice as much swelling at this site than does the new method except for the rigid pavement on the frontage road. The PVR also predicts more swelling beneath the outer wheel path than the movement predicted by the new method for the rigid pavement on the frontage road. Both of the total movements predicted by the new method beneath the outer wheel path of the flexible pavement are within the 1-inch criterion used with the PVR. However, none of the PVR values predicted for these acceptable treatments are within the 1-inch criterion. The PVR method would, in both the main lanes and the frontage road, require a more conservative treatment than the ones predicted by the new method to provide acceptable performance.

Summary and Conclusions

Vertical movements calculated by the new method, including both the swelling and shrinking, were compared with the swelling movement predicted by the PVR method for each of the six case study cross sections. Pavement treatments had been selected to provide an acceptable predicted performance at high levels of reliability, and the vertical movements were calculated both at the edges of the pavements and beneath the outer wheel paths using both the new method and the PVR method. A major purpose of the comparisons of the movements was to evaluate the PVR method in light of the new method, which was based upon many years of monitoring of pavements in several locations across Texas and careful modeling of the measured pavement roughness. A primary objective was to determine from these case studies whether the 1-inch PVR criterion, which has been used by the TxDOT in the past, required treatments to restrain the development of pavement roughness due to the expansive clay that were unnecessarily conservative.

The results of the case studies are that in every case, the PVR criterion of 1-inch proved to be unnecessarily conservative. The PVR overpredicts the swelling movement that can be expected using the new method both at the edge of the pavement and beneath the outer wheel path. Furthermore, the PVR does not provide a means of anticipating subgrade shrinkage that will result in longitudinal cracking along the edge of the pavement. In addition, both transverse and random cracks may reflect upward from shrinkage cracks in the subgrade.

The design criterion of lowering the PVR to 1-inch by removing and replacing the native soil with a more inert soil is conservative to differing degrees depending largely upon how wet the subgrade soil is at the time of construction. The wetter soils will not swell much but will shrink, and the pavement resting on them will get rougher than is estimated with the 1-inch PVR criterion. Also, if the soil is drier at the time of construction, it will swell substantially unless moisture control measures such as vertical and horizontal moisture barriers and stabilized and inert layers are used to control the moisture and the subsequent development of roughness. The new method shows that these control measures are more effective than is presently anticipated by the PVR method.

The design calculations with the new method have shown a total movement beneath the outer wheel path ranging between 0.42 to 1.08 inches for flexible pavements that had acceptable performance at a reliability level of 95 percent. On the same sites, rigid pavements were predicted to have acceptable performance when the total vertical movement beneath the outer wheel path ranged between 0.60 and 2.23 inches. This leads to the conclusion that neither the swelling movement, as in the PVR method, nor the total movement, as in the new method, is a reliable indicator of likely acceptable performance. Instead, all of these case studies show that it is important to use the predicted history of the present serviceability index and the international roughness index as the proper design guideline for an acceptable treatment of the subgrade of an expansive soil.

References

Dhowian, A., Erol, A. O. and Youssef, A. (1987). *Assessment of Oedometer Methods for Heave Prediction*. Proceedings, 6th International Conference of Expansive Soils, New Delhi, India.

Hong, G. T., Bulut, R., Aubeny, C. P., Jayatilaka, R. and Lytton, R. L. (2006). *Prediction of Roughness of Pavements on Expansive Soils*. Proceedings, 4th International Conference on Unsaturated Soils, Carefree, Arizona.

Jayatilaka, R., Gay, D. A., Lytton, R. L. and Wray, W. K. (1993). *Effectiveness of Controlling Pavement Roughness Due To Expansive Clays with Vertical Moisture Barriers*. Research Report 0-1165-2F, Texas Transportation Institute, Texas A&M University, College Station, Texas.

Osman, M. A. and Sharief, A. M. E. (1987). *Field and Laboratory Observations of Expansive Soil Heave*. Proceedings, 6th International Conference of Expansive Soils, New Delhi, India.

The New Engineering Treatment Techniques of Expansive Soils Subgrade for GuangXi Nanning-Youyi Guan Expressway

He-Ping Yang[1],   Jian-Long Zheng[2]

[1] Professor, School of Highway Engineering, Changsha University of Science and Technology, P.O. Box 410076, Chiling Road 45#, Changsha, Hunan, China.; email: cscuyang@163.com; PH (86) 731-2309581; FAX (86) 731-2309581;
[2] Professor, President, Changsha University of Science and Technology; email: jlzheng@126.com; PH (86) 731-2309080; FAX (86) 731-2309080;

Abstract

　　Treatment of expansive soil subgrades is a worldwide technical problem, which needs to be studied and solved urgently due to the rapid development of large-scale highway construction in China. In order to solve the problem, a research group have carried out a field survey in Ningming area. There the construction of Nanning to Youyi Guan Expressway (NYGE) has undergone serious geological disaster caused by Ningming expansive soil. On the basis of worldwide successful and unsuccessful experiences of treating expansive soil projects, the research group analyzed the causes of landslides and conducted a lot of laboratory and field tests on properties of expansive soil. Aiming at the three typical properties of expansive soil and the characteristics of subgrade failure, the group adopted enveloping techniques, and executed some creative schemes to treat slopes of embankments and cuts. All measures taken by research group were successful and have effectively solved the technical problem in the subgrade construction of NYGE. The research outcomes are also useful for railway construction, hydraulic works, and municipal works.

Introduction

　　Nanning to Youyi Guan Expressway (NYGE) is called the No.1 highway in Asia. In the construction of NYGE, the expressway traversed the edge of Ningming basin where the Ningming expansive soil is continuously distributed for about 14km long. The expected excavation volume in this section is 2,000,000 m^3. If all excavated expansive soil are discarded and replaced by borrowed earth to build embankment, it will be not only uneconomical but also easy to cause serious damages to environment. The project began in March 2003. After a rainy season, the excavated slopes in the

section slid in different scales. Some slopes were still unstable even after their grade had been flattened to 1:3, which caused the waste earthvolume sharply increase to 5,000,000 m^3 and brought great difficulty to the construction. Hence, expansive soils research group of ChangSha University of Science & Technology carried out many in-site geologic investigations for 23 slide slopes and systematically analyzed the causes of damage. Based on a series of tests and referring the successful experiences of treating expansive soils engineering projects at home and abroad, the research group put forward some new treating techniques and methods, and took it into practice, which successfully solved the technical difficulties in expansive soil subgrade construction of NYGE.

Properties and engineering geological characteristics of Ningming expansive soil

The investigation and research results have shown that Ningming expansive soil is a kind of residual expansive clay with brown or gray stripe (thickness ranging from 2m to 6m), and its mother rock is early Tertiary Nadu formation shale which is dark gray or light brown. Erosion (unloading) and chemical weathering process-especially the south Asian subtropical eluviation, not only caused minerals in eluvium to hydrolyze and transform, but also decreased the density and strength of soil while increased moisture content. All these changes led to a series of adverse engineering properties such as low density, high moisture content, high dispersing and high contractility, which are typical characteristics of eluvial expansive soil. And once excavated and exposed to the atmosphere , the dark-gray clay shale will crack , disintegrate into powder. Typical geological profiles exposed by excavated slope can clearly show that structural joints, fissures, and weathered fissures well developed. The fissures are mainly vertical, cross and horizontal, and layers are apparent. And through-fissures in layers were consistent with interlayers between soil and rock. Slope flows and landslides were mainly attributed to discontinuous structure surface. The data introduced in previous paper (Hand book of subgrade design, 1998) and some site-investigation results have shown that the depth of weathered-active zone for Ningming expansive soil is about 3m. Index properties of the expansive soil and shale were conducted in laboratory by many means in order to obtain the informations about their physical component, clay minerals, as well as the characteristics of engineering and compaction. The testing results were shown in Table 1-4.

Table 1. Material Composition of Ningming Residual Clay and Weathered Shale

Sample	Depth (m)	Particle Size Distribution (mm.%)				Activity (PI/< 2um)	OC (%)	EMC (%)	SSA (m²/g)	pH	CaCO₃ (%)
		>0.075	0.075-0.005	<0.005	<0.002						
No. 1	3.5-3.8	8.55	41.37	50.08	47.12	0.59	1.06	19.07	170.90	3.88	0
No. 2	9.9-10.2	0.77	63.83	35.40	28.24		2.69	17.64	161.11	6.98	0.11

Note: Sample 1= light-gray expansive soil   Sample 2 = dark-gray shale   OC = Organic
          Content   ECM = Effect Content of Montmorillonite   SSA =Specific Surface Area

Table 2.Quantitative Testing Result of Clay Mineral of Ningming Residual Clay and Weathered Shale

Samples	Changeable Cation (meq/100g)				Relative Clayey Mineral Content by XRD (%)				Mixed Ratio (%S)	Clayey Mineral Content (%)			
	Ca^{2+}	Mg^{2+}	K^+	Na^+	I/S	I	K	Ch		I/S	I	K	Ch
Sample 1	2.89	3.85	0.35	0.59	59	19	15	7	65	27.80	8.95	7.07	3.30
Sample 2	6.57	7.50	0.50	1.14	62	16	15	7	60	17.51	4.52	4.24	1.98

Note: XRD = X-ray diffractometer

Table 3. Engineering Properties of Ningming Residual Clay and Weathered Shale

Samples	Density (KN/m^3)	Moisture Content (%)	Dry Density (kg/m^3)	Specific Gravity	Void Ratio	Plasticity Index (%)	e_{Sl} (%)	Fs(%)
Sample 1	19.55	31.4	1488	2.77	0.86	39.8	3.50	57.5
Sample 2	21.59	25.0	1800	2.75	0.53	26.3	2.5	42

Note: e_{Sl} = linear shrinkage ratio   Fs = free swelling ratio
All specimens are undisturbed soils

Table 4. CBR testing result of Ningming residual clay and weathered Shale as fillers

Samples	98 times			50 times			30 times		
	CBR (%)	ρ_d (kg/m^3)	δ_e / w_{opt} (%)	CBR (%)	ρ_d (kg/m^3)	δ_e / w_{opt} (%)	CBR (%)	ρ_d (kg/m^3)	δ_e / w_{opt} (%)
Sample 1	1.4	1730	17.8/15.4	1.2	1650	16.8/15.4	1.4	1580	16.7/15.4
Sample 2	1.3	1780	10.5/15.0	1.3	1720	11.5/15.0	1.3	1640	11.9/15.0

Note: CBR=California Bearing Ratio ρ_d = Dry Density δ_e = soaking swelling ratio
w_{opt} = the optimum moisture content according to the heavy-pattern dry compacted standards
The energy of the compaction is $2684.9kJ/m^3$

Table1-4 showed that: (1) the Ningming expansive soils possess many properties such as high clayey particle content, high void ratio, high moisture content, low strength and large CBR soaking swelling ratio. The light-gray expansive soil can be identified as moderate -strong swelling potential one, and the dark-gray shale behaved as weak swelling potential, so both of them were not fit to build embankment directly; (2) the main clay mineral of Ningming expansive soil is I/S (illite/montmorillonite) mixed layer mineral with a high mixture ratio, and their effective montmorillonite content were 17.6% and 19% respectively. The exchangeable cation which are adsorbed by the clay mineral surface were mainly Mg^{2+}, and the soil is magnesian expansive clay with high physicochemical activity. Therefore, enveloping measure should be adopted immediately when slope was excavated.

Treatment measures of expansive soil embankment in NYGE

In the regions of expansive soils, the main problems in building embankment with expansive soils are post-consolidation, the slope's flow slide and continuous

over-deformation due to swelling and shrinkage of expansive soil in wet dry cycles. Replacement method is uneconomical and harmful to environment, while chemical improving method is also uneconomical and difficult to operate. Although numerous studies on building embankement with lime-improving expansive soil have been carried out in China. But as for Ningming expansive soil, its natural moisture content is very high, the soils are easy to conglobate, the operation of adding and mixing with lime is very difficult and the price of lime is almost near the price of cement, therefore the application of improving method is limited. Hence the research group determined to look for other ways to treat expansive soil embankment. After deeply studying on the fillers and the choice of materials, referring to the South African successful emperience of applying enveloping method (Katti, 2000), the research group carried out an embankment treatment technique basing on enveloping method.

Soil properties of filler and its water stability.   Three kinds of modifying tests and determination of the relative indices were conducted, respectively adding lime, portland cement and lime-cement mixture into two types of expansive soil. Results showed that the effect of lime-improved soil was the best. The light-gray expansive soil mixing 3% quick lime (W_{opt}=15.2%) was compacted into a specimen according to the heavy-pattern compacted standards (The compact energy is $2684.9kj/m^3$). After half of a month, the indices of the specimen, both CBR and δ_e, can meet the requirements of highway specification for fillers.

Table 3 and 4 showed that there was an obvious difference between the optimum moisture content and natural moisture content. Hence, the field compaction could not be controlled in the light of heavy-pattern dry compaction test. Meanwhile, the available filler in the excavation of subgrade is mainly weathered shale. Therefore a wet compaction test was also conducted as a complement, and test results showed that the optimum moisture content of weathered shale was 22% and the maximum dry density was 1620 kg/m^3, the two parameters were used as the controlling indices of filling compaction.

In order to study the feasibility of using envelope method to build un-immerseable embankement, the research group conducted unsoaking CBR tests, i.e. a soil property test that simulate the condition of enveloping expansive soil subgrade effectively. The test result is shown in Figure 1. Analyzing Figure 1, we can know that the CBR under unsoaking condition decreased along with the increase of specimen moisture content, however the falling trend of curve became moderate as the moisture content was over 25%; when moisture content was below 25%, the CBR was over 10%. Hence, the filler can meet the requirement of strength (Highway specification, 2004) as long as the changes of embankment moisture content could be controlled properly. Also results of previous studies have shown that the stable moisture content of embankment soil is 2%~3% higher than the average at the construction stage (Hu , 2004).

In order to master the varying speed of filler's swelling ratio on condition that the embankment has being soaked, the research group carried out a test on the variety of soaking swelling ratio of CBR sample along with time. The test result is shown in

Figure 2. It showed that soaking swelling ratio reached 3% in less than 2 hours, 7.5% after 9 hours, and continued increasing along with time. After 4 days, the CBR sample's soaking swelling ratio could rise up to 13.67%, and the swell percent was still increasing. Therefore, it is crucial to guarantee the effect of enveloping waterproof measures when Ningming expansive soil is used to build embankment directly. The following should be considered thoroughly when adopting enveloping method: treating of subgrade base, choice of enveloping material and proper enveloping thickness.
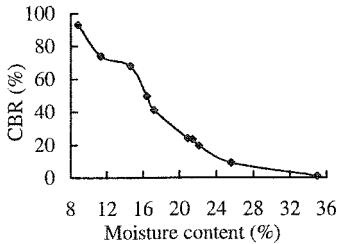
Figure 1. Change in CBR with moisture content
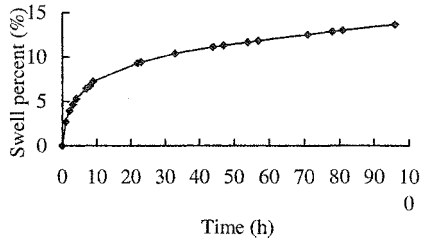
Figure 2. Change in swell percent of CBR sample with time

Treatment schemes of trial expansive soil embankment.   After considering several factors (including safety and reliability of engineering project, economic rationality of treatment measures, effects of environment protection after construction, and operational feasibility of construction) and referring to the research group's previous successful experience of adopting reinforcing side slope with geognet to build mid-strong swelling potential expansive soil embankment on Chu-Da expressway in Yunnan (Yang, 1999), the research group put forward four treatment schemes and built 530m-long trial embankment. They are following:

1. The stretch from K133+640 to K133+810 adopted the method that embankment sides were enveloped with inexpansive clay, shown in Figure 3.
2. The stretch from AK2+300 to AK2+500 adopted the method that reinforcing expansive soil side slope with geogrid, shown in Figure 4.
3. The stretch from K135+420 to K135+510 adopted the method of sandwiching expansive soil with crushed stone soil and reinforcing the side slope with geogrid , shown in Figure 5.
4. The stretch from K135+510 to K135+580 adopted the method of sandwiching expansive soil with lime-mixed soil and reinforcing the side slope with geogrid, shown in Figure 6.

To constrain post-consolidation of embankment, the total filling height of expansive soil body in the cross scection was controlled to be less than 6m, underneath the upper embankment. In light of the weathered depth of expansive soil in Ningming and the previous successful treating experience in Guangxi, the enveloping thickness for each scheme is designed to be 3m (but for the scheme 1. the thickness is 3.5m).
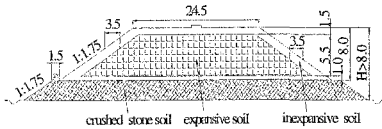
Figure 3. Envelope slope sides with inexpansive clay
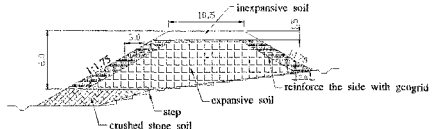
Figure 4. Reinforcing side slopes with geogrid
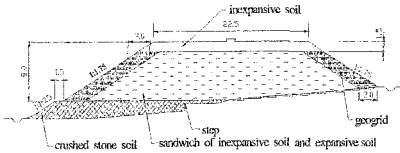
Figure 5. Sandwich expansive soil with crushed stone soil and reinforce side slopes with geogrid
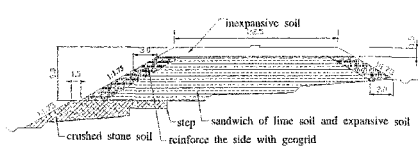
Figure 6. Sandwich expansive soil with lime-mixed soil and reinforce side slopes with geogrid

Besides lime-modified light-gray expansive soil, weathering smash dark-gray shale was used as main filler. By May 2004, the construction of trial embankments were all completed, the four stretches had totally used expansive soil nearly 80,000 m³. The research group set up seven monitoring profiles and buried lots of monitoring devices in order to obtain the foundational data and verify the effect of treatment measures. The monitoring items included consolidation of embankment, side deformation, change of moisture content, swelling deformation, as well as matric suction. It is rare that so many treating measures were adopted in building expansive soil trial embankments in the same expressway in China. So far, the trial projects have experienced two rainy seasons, the monitoring datum have shown that the trial embankments are stable, for example, the vertical deformation of the embankment in K133+720, which total filling height is 13m, is less than 0.13m, and no lateral deformation occurs in its side slope. Also the datum have proved that the enveloping measures are effective.

Treatment measures of expansive soil cut slope in NYGE

The landslide of expansive soil cut slope is the most serious geological hazard, which is also the easiest to occur, and the most difficult to be treated in regions of expansive soils, and so far there has not been any economic and effective treatment measure for it. The structures and properties of expansive soil or rock were very sensitive to the change of environmental condition due to wet dry cycle and the unloading relaxation caused by excavation. The three typical properties (swelling-shrinkage effect, crack effect and over-consolidation effect) are the origins that cut slopes slide frequently, and the cracking is the critical one. However it is pity that the working principle of crack effect has not been completely understood yet. Nevertheless, it is sure that cracks only come out when excavated surface is exposed and dehydrated, and the crack depth will not be larger than 3m usually. Therefore, the

possible solution to the engineering geological problem is as follows: (1) carry out field observation and survey on the characteristics of structure face, the types of structure body, and the variational rule of slope soil' moisture content along with wet dry cycle. In order to know the rule of the fissures' arising, development, and the soil's expansion and shrinkage. (2) master the relationship between over-consolidated unloading duo to excavation and the distribution of joints and fissures in the upper layer of slope, as well as get the process and characteristics of landslides. (3) Aiming at "the three typical properties" and the rules of slope failure, develop a reinforcing and protecting method combining rigid and flexible structures, preservation and resist percolation measures and supporting slope with flexible materials.

The sliding characteristics of expansive soil cut slope and analysis of the causes.
The rule and characteristics of landslide:

1. Landslides occurred in shallow layer. The 69% of slides, which were in small scale, all occurred in the layer of light-gray expansive clay, the 78% of landslides in larger scale occurred on the interface between soil and shale, or in the strongly weathered shale, whereas the interface were mainly distributed in the depth range of 3m-5.5m, and the depth of sliding surface rarely surpassed 6m.
2. Landslides were consequent upon the stratum's direction. The slides in small scale all were parallel to the same direction of stratum and slope, and the most (94%) of landslides in large scale were parallel to the stratum direction, therefore the stratified face of shale and eluvial expansive soil were the critical factor of slope failure.
3. Sliding surface was flat. The attitudes of shale layer were that: the dip direction were usually between $135°$ and $158°$, and the dip angle were from $2°$ to $16°$, most of dip angles were only from $2°$ to $5°$, whereas the slopes ratio were between 1:2.5 and 1:3.
4. The occurrence of landslides was seasonal. Most slides happened during the later of rainy season or after a heavy rain.
5. The shape of most sliding surfaces was fold line. The shape's formation was related to the distribution of soil and rocks stratum in the geological profile and all genetic types of cracks. The back of the sliding surface, controlled by the vertical cracks of the upper expansive soils layer, was in the form of precipitousness. Moreover, the height usually was the range of 1m to 3m. The mid and front of the sliding surface, controlled by the stratum joints and the structure surface of eluvial weak interlayer, were linear.

Analysis of landslide causes:

1. Geological structure. Both the shallow slips and the landslides occurred on the right side of the road direction because the right excavated slope was rock-bedded.
2. Soil structure. Because of extremely developed fissures and over-consolidation effects of expansive soil, free face was easy to be formed after excavation, which also caused stress to be released.

3. Weather condition. Ningming is located in subtropical zone, where drought and wet season are distinct. The runoff and infiltration of heavy rain caused landslide.
4. Incorrect construction steps. The enveloping and supporting measures for cut slope had not been adopted in time after slopes were excavated.
5. Vehicle Load. During the construction, the top of cut slope was used as a temporary construction road, therefore the repetition of vehicle load accelerated slopes sliding.

Analysis and thought on treatment measures. There are many technical measures to treat slopes in engineering practice, they can be classified as two types, rigid support method. and flexible support method. The rigid support method is a treatment measure consisting of masonry structure (self-weight retaining wall, anti-slidepiles and schistous slope wall) in conjunction with other necessary protective measures. This method is used most frequently in slope stabilization works. The working Principle of the method is to resist the slope body in imbalance and stress relief due to the over-consolidation during excavation by taking advantage of self-weight of masory structure. The slope soil body supported by the method is not permitted to deform, whereas the soil is bound to shrink and swell due to the effect of water and the influence of wet dry cycle. When the swelling deformation of expansive soil is large and could not be released, high swelling pressure will come out so as to destroy rigid support structure. It has been proved by the phenomenon occured that retaining walls are usually snipped or pushed away in the area of expansive soils.

The flexible support method means that a treatment structure for the slope body consist of chemical improving, reinforcement with geogrid, in conjunction with other necessary protective measures. The advantage of flexible support method is that it can not only bear super-pressure of soil but also permit soil deformation to a certain degree. Therefore, the flexible support body can absorb the stress relief duo to soil over-consolidation and the swelling pressure due to change of moisture content. Liao (1984) pointed out that if linear expansive ratio of the specimen is allowed to reach 0.3%, the swelling pressure can decrease about 25% ,compared with the condition that the deformation of expansive soil body is rigorously restricted. Hence, the flexible support method fits to treat expansive soil cut slope quite well.

Why did the research group put forward in NYGE and adopt the flexible support measure to treat landslide of expansive soil cut slope? In the last analysis, the reasons were the group's deep understanding on the "three typical properties of expansive soil" and the sliding rules of expansive soil cut slope. By placing and anchoring geogrid in separating filler layers, back-filling and compacting inexpansive soil or expansive soil to form reinforced body with enough thickness, then enveloping the top of slope and treating drainage system in the subbase and on the back of reinforced structure, the following can be taken into effect:
1. The friction and interlock between geogrid and filled earth, and the connection of geogrid and envelop in layers can afford enough shear strength and make the reinforced structure as a whole to resist landslide body.

2. The flexible reinforced structure permits the deformation of slope so that the stress and swelling pressure during the excavation of slope can be released.
3. The flexible reinforced structure, whose slope gradient is 1:1.5, reinforced body's thickness and height is over 3.5m and over 2/3 of cut slope's height respectively, can cover the main surface of fresh cut slope, and with enough self-weight to resist soil pressure.
4. The reinforced structure with enough thickness (surpassing weathering depth) can insulate and prevent the expansive soil slope from weathering, and avoid development of fissures and slide in surface layers.

The implemental schemes of trial cut slopes.   According to the above analysis, as well as the expansive soil properties, hydrogeologic condition, and the status of slope failure in NYGE, the research group, considering the requirement of environment protection and comparing the performance to cost ratio of many schemes, put forward and implemented three treating schemes:

1. The first scheme is to adopt root pile, build retaining wall at the toe of slope and modify the soil behavior in surface layer with DAH (applied to the left side slope from K138+440 to K138+750), shown in Photo 1.
The scheme fits the place where the stratum's direction is contrary to the strike of expansive soil cut slope. The slope is stable in general, but it has weak interlayer (weak structure face) or local with a few crashes and well-developed fissures. On one hand, applying root pile to treat local weak structure face can reinforce slope. On the other hand, root pile is a minitype of drill pile, the formed bores can be used in chemical grouting and make the good reinforcing and impervious effect. The scheme can be implemented not only during slope is excavated from the top to the toe, but also after the cut slope is completed and local weak interlayer is found. The advantages of the scheme are that the operational equipments are handiness, the construction is not complex and slope surface will not be disturbed strongly. In addition, drill can be done slantly to effectively resist horizontal swelling pressure. All these can benefit the slope stability.

2. The second scheme is to adopt supporting blind drain and build retaining wall at the toe of slope (applied to the right side slope from K139+100 to K139+400), shown in Photo 2.
The scheme fits high-excavated slope, whose stability is poor and stratum's direction is consistent with the strike of cut slope. Bedding slip is easy to occur in the slope. The supporting blind drain built on the slope surface can support the unstable slope body taking the advantage of the self-weight of large bulk masonry, and it has the effect of draining and depleting groundwater in slope body. Another advantage is that the blind drain can divide the slope into lots of parts in order to weaken the total swelling potential of slope body. Moreover, the slope can be supported better so that the slide can be well avoided by combining supporting blind drain with the slope-toe retaining wall. Usually, The construction operation is that built blind drain when slope is excavated from top to toe. And the scheme can also be applied to treat the slopes which have taken place flow and collapse.

3. The third scheme is to adopt flexible support with geogrid (applied to the right side slope from K137+800 to K138+050, from AK1+ 580 to AK1+660、from AK2+010 to AK2+120、from AK2+500 to AK2+700、from K134+010 to K134+360、from K136+200 to K136+600, the total length of six stretches of slopes is 1.3km long), shown in Figure 7.
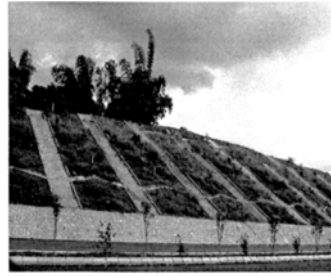
Photo 1. Treating slope with root pile

Photo 2. Treating slope with supporting blind drain
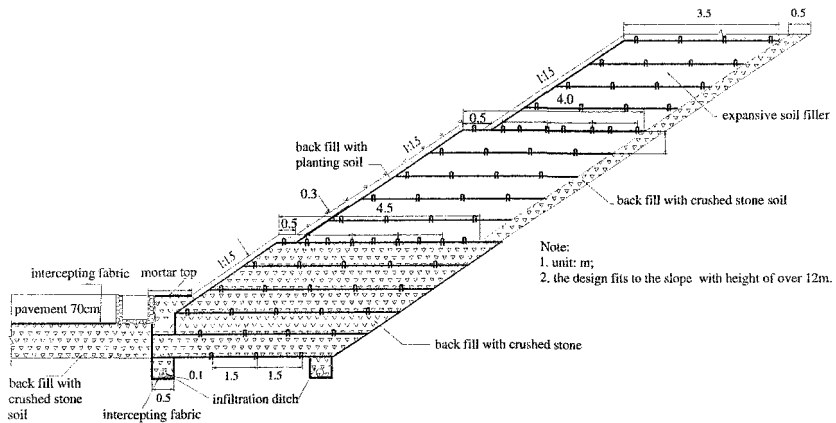
Figure 7. The flexible supporting structure

The scheme can be adopted to treat landslide, also to protect and support the fresh expansive soil cut slope. The basic processes of construction are as follows: overbreak the designed slope into a certain width, then back-fill and compact earth layer by layer after placing geogrid horizontally , back-envelop the filled earth with geogrid and connect the geogrids upper and under layers with connecting rod to form slope face so as to make the reinforced body as a whole to resist the influence of soil pressure and weathering. Compared with the rigid retaining wall, the flexible support structure is easier to be constructed, simpler in technique and lower in cost. For example, a scheme, building a reinforcing body of 7m high, has been adopted to treat

expansive soil cut slope of 300m long and 10m high in NYGE, the construction of structure was completed in only 20 days, and the cost did not surpass US $ 120,000 . But if self-weight retaining wall and masonry pitching slope had been adopted, the conservatively estimated cost would have been over US $ 147,000, and it would have been impossible to complete the project in one month (Zheng, 2004) , still more, it would be difficult to keep the stability of slope.

Just because of such good technique-economic benefits, the contractor of NYGE had adopted the same scheme actively to treat other two large landslides with 400m long after finish the construction of the six trial slopes. It have shown that the flexible support scheme have been well applied to treat the expansive soil cut slopes in the construction of NYGE.

Some noticeable problems in the construction of subgrade

1. The construction should be carried out in dry season and flexible reinforcement body should be built immediately after slope is overbroken.
2. Leaching layer at the back of flexible reinforcement body and blind drainage on the base of wall should be built well. In addition, it needs to be guaranteed that there is a distributary between the water from the leaching layer and the underwater in roadbed, and there is enough space to drain water current expedite.
3. The light-gray expansive soil should not be mix-filled with dark gray expansive shale, the lift of each layer loose should be not over 0.3m, and the grain size of large filler should be compacted to less than 0.05m during the filling of embankment.
4. The compacitve control in the construction of embankment should adopte the wet compaction standard. The moisture content of filler can be 2% more than the optimum moisture content (22%), and degree of compaction should be reached to 90%.
5. When the envelope scheme is adopted, the inexpansive clay used to envelope the side of embankment and expansive soil filler in the core of embankment should be placed, and rolling compacted layer by layer simultaneously.
6. When the reinforced slope is built and geogrid is back-enveloped, the geogrid between layers should be connected and tightened with connecting rod to guarantee its integration and effects.
7. Cover the geogrid with planting soil in time when building slope surface and back-enveloping geogrid in order to prevent aging of geogrid.

Conclusion

Ningming expansive soils are Tertiary shale and its weathered residual soil. They can not be used as fillers directly because of their poor engineering properties. If effective reinforcing and protective measures to the fresh cut slope can not be adopted in time, the slope is difficult to keep stable.

The measures of enveloping and waterproof, which are adopted to treat Ningming expansive soil subgrade, have effectively solved the expansive soil problem in the construction of Nanning to YouyiGuan Expressway.

The research group presented and excuted four schemes of building expansive soil embankment. Two of them are more convenient in construction and reliable. One is "Sandwich expansive soil with crushed stone soil and reinforce the side slope with geogrid", the other is "envelope slope sides with inexpansive clay". The two schemes can be used widely to treat expansive soil embankment.

It is a new attempt to treat expansive soil cut slope with flexible supporting structure in large scale. The expansive soils excavated are directly used as the filler of reinforcment body. It can take great economic benefits to the project and environmental benefits to the society. Maybe, the novel technique will become the best solution to the worldwide enigeering problem of "The cut slopes are bound to slide in expansive soils areas".

Acknowledgments

References

China Communications 2nd Highway Survey Design and Research Institute (1996) Handbook of design for highway subgrade(the 2nd edition), *Renmin communicatios Press*, 407 pp.

Hu M. J. Liu S. G. and Kong L. W. (2004) "Expansive soil character later test verification on freeway embankment treatment." *Rock and Soil Mechanics.* 25(9), 1418-1420.

Liao S.W. (1984). "Expansive soils and railway engineering." *The Railway Press*, China

Ramanath K. Katti. (2000). "Coulumbian Cohesion Approach to Engineering of Expansive Soil Deposites". *Advances in unsaturated geotechnics*, Reston, Virginia .156-162

Yang H. P. (1999). "Approach to Strengthening Expansive soil Embankment Side Slope with Geotechnical Screen." *Highway.* 3, 42-46.

Zheng J. L., Yang H. (2004). "The treatment theory, techniques and practice of expansive soils." *The People's communication Press*, Beijing China

China Communications 2nd Highway Survey Design and Research Institute (2004). "Specifications for Design of Highway Subgrades". *The People's communication Press*, Beijing China. 7 pp.

Recent Advances and Encountered Problems in Computing Air Losses in Compressed Air Tunneling by Consideration of Unsaturated Soil Mechanics

G. Steger[1], S. Semprich[1] and A. Chinkulkijniwat[1]

[1]Institute for Soil Mechanics and Foundation Engineering, Geotechnical Group Graz, Graz University of Technology, Rechbauerstraße 12, Austria; PH (+43) 316-873 6228; FAX (+43) 316-873 6232; email: gerhard.steger@TUGraz.at

Abstract

Compressed air tunneling is one of the rare cases in applied unsaturated soil mechanics, where air has to be considered as an active fluid phase. An excess air pressure inside the tunnel is applied to prevent groundwater inflow. As soil and also the shotcrete lining of the tunnel are permeable materials, a transient air flow from the tunnel into the surrounding ground takes place. In order to allow an accurate prediction of the amount of air losses in the design process and to provide pore pressure distributions for coupled flow-deformation analyses, a 3-D numerical tool considering unsaturated multiphase flow has been developed. The results of conducted case studies show a very good agreement with measured air losses for tunnels driven in sandy soils, whereas a big discrepancy for tunnels driven in silty soils was experienced. Recently performed laboratory tests are indicating that permeability increasing macro flow paths are likely to develop in cohesive soils. Therefore, a continuum mechanic based numerical approach to predict the air losses in cohesive soils requires the use of adapted relative permeability functions.

1 Introduction

One of the advance methods frequently applied in urban tunneling is the NATM (New Austrian Tunneling Method) in combination with compressed air. The construction process of this tunneling method consists of a sequence of excavation and applying a reinforced shotcrete layer and, if necessary, anchors as primary support to the tunnel lining. An applied excess air pressure inside the tunnel serves to prevent groundwater inflow. For this purpose, a bulkhead situated close to the beginning of the tunnel separates the excavation area from the atmosphere.

The magnitude of the air pressure p_a inside the tunnel is usually kept the same or slightly higher as the hydrostatic water pressure at the invert of the tunnel $p_{w,in}$. As

the gravity potential of air is negligibly small, a pressure difference Δp between air and water is acting at the tunnel walls. It reaches a maximum at the crown of the tunnel and is approximately zero at the invert of the tunnel, see Figure 1.
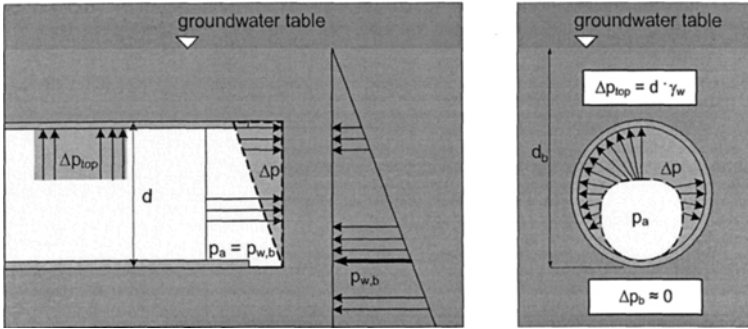
Figure 1. Difference of air and water pressure Δp at the tunnel walls.

Due to the pressure difference, an airflow both through the unsupported tunnel face and through shrinkage cracks and gaps in the shotcrete lining into the ground is induced. The air desaturates the soil and changes the pore water pressures in the surrounding soil of the tunnel. To maintain the excess pressure inside the tunnel, the air losses have to be replaced constantly by an air supply equipment.

The use of compressed air in NATM-tunneling is limited to soils with a water permeability $k_{w,100} \approx 10^{-4} - 10^{-7}$ m/s. At higher soil permeability, additional measures like grouting have to be taken, and at lower soil permeability compressed air is no longer necessary because of low water infiltration rates.

Especially for contractors, it is important to correctly estimate the maximum air loss rate q [m³/min] and the total amount of air losses Q [m³]. These data serve to evaluate the capacity of the air supply equipment and the energy costs of the generation of the compressed air respectively.

2 Numerical simulation of air flow in compressed air tunneling

2.1 TOUGH2

To develop a numerical tool for compressed air tunnel advance simulations, parts of the multi phase fluid and heat flow simulator TOUGH2 (for: Transport of Unsaturated Groundwater and Heat, Version 2) are used. The program is widely used in geothermal reservoir simulation, nuclear waste isolation, environmental assessment and remediation, and saturated and unsaturated zone hydrology.

The governing equations for multiphase fluid and heat flow have all the same mathematical form, regardless of the nature and number of fluid phases and components present. Acknowledging this, TOUGH2 is set up with a modular

architecture, in which the main flow and transport module can interface with different fluid property modules (Pruess et al. 1999), see Figure 2.
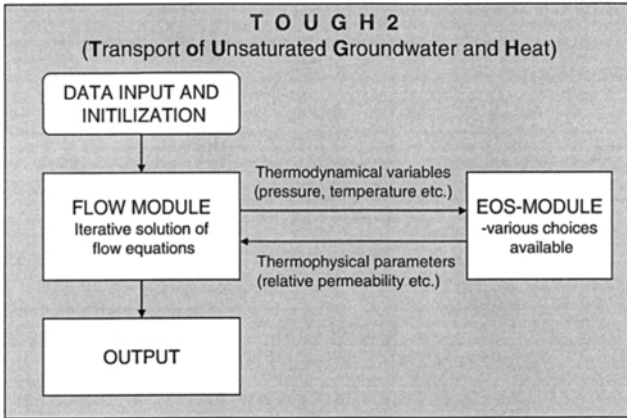
Figure 2. General program structure of TOUGH2.

The mass and energy balance equations for an arbitrary volume solved by the flow module have the general form

$$\frac{\partial}{\partial t}\int_{V_n} M^\kappa dV_n = \int_{\Gamma_n} F^K \bullet nd\Gamma_n + \int_{V_n} q^\kappa dV_n. \tag{1}$$

V_n is an arbitrary subdomain, which is bounded by the closed surface Γ_n. M represents the mass or energy per volume, with κ labeling the different mass components. F denotes mass or heat flux, and q denotes sinks and sources. The last term only appears in the mass balance equation if there are sinks and/or sources q present in the modeled problem. n is the normal vector on the surface element Γ_n, pointing inward V_n.

The introduction of the intrinsic permeability k allows a multiphase formulation of Darcy's law for computation of the phase fluxes F_β :

$$F_\beta = \rho_\beta u_\beta = -k\frac{k_{r\beta}\rho_\beta}{\mu_\beta}\left(\nabla P_\beta - \rho_\beta g\right) \tag{2}$$

Here u_b denotes the Darcy velocity (volume flux), $k_{r\beta}$ the relative permeability and μ_β the viscosity with respect to phase β. P_β is the fluid pressure in phase β, and is the sum of the pressure P of a reference phase (usually taken to be the gas phase) and the capillary pressure $P_{c\beta}$ (≤ 0). Vapor pressure lowering may also be modeled.

TOUGH2 offers two modules for simulating flow in unsaturated soils. The first of these modules, EOS9 (Equation of State 9), treats the air phase as a passive bystander at constant pressure, and conditions are assumed to be isothermal. No mass balance equations for air flow and heat flow are set up. The single water phase flow is described with a generalized form of Richards' equation for unsaturated flow

(Richards 1931), additionally considering variations in liquid phase density and viscosity:

$$\frac{\partial}{\partial t}(nS_w\rho_w) = div\left[k\frac{k_{rw}}{\mu_w}\rho_w\nabla(P_w + \rho_w gz)\right] \qquad (3)$$

In Equation (3) the subscript w indicates the water phase. EOS9 can describe flow under partially saturated as well as fully saturated conditions.

The second TOUGH2 module for flow in unsaturated conditions, EOS3, additionally considers air as an active fluid phase. Equation (1) is used to set up mass balance equations for water and air. All thermophysical properties contained in EOS3 are represented by the steam table equations as given by the International Formulation Committee (1987). EOS3 can handle isothermal problems as well as non-isothermal problems. Boundary conditions as pressure, saturation and temperature refer to the gas phase (Pruess et al. 1999).

Having in mind numerical simulation of compressed air tunneling, using TOUGH2 together with the EOS3 module seems a perfect choice. It is obvious that the EOS9 module, treating air just as a passive bystander, is not suitable for the simulation of active air flow as it occurs in tunneling under compressed air. Inside the tunnel, the excess air pressure prescribes a boundary condition with respect to the gas phase. On the ground surface respectively above the ground water table, the boundary condition is again given with respect to the gas phase by the (atmospheric) air pressure.

2.2 The program ASCATA

In the software-environment of TOUGH2-EOS3 the program ASCATA (for: Automatic Simulation of Compressed Air Tunnel Advance) was developed to simulate the occurring air flow in compressed air tunneling and its effects to the ground. ASCATA includes an automatic advance sequence and an integrated evaluation of the air flow data. It is important to simulate the advance, because the air flow changes with varying ground conditions and due to the continuous advance of the tunnel face the flow problem is transient.

To perform an advance simulation, first a numerical base model of the cross section of the tunnel in its starting position together with the ground conditions in the whole advance area is generated. The TOUGH2 pre- and postprocessor PetraSim is used for this purpose. The symmetry of the problem allows modeling just half of the cross section to reduce computation efforts, see Figure 5.

From the input-file of the model, ASCATA automatically locates the position of the tunnel face and initializes the flow computation. The simulation time corresponds to the advance rate of the tunnel. When the first simulation has finished, a subroutine relocates the position of the tunnel face in advance direction. Therefore, the soil grid blocks one layer ahead of the former tunnel face are transformed into "tunnel" grid blocks (= Dirichlet boundary conditions) simulating the excess air pressure inside the tunnel. Additionally, a new layer of shotcrete grid blocks is introduced along the perimeter.

When these changes have been made, a new input-file is generated according to the new position of the tunnel face and ASCATA performs the next flow simulation. Summarized, ASCATA is carrying out a series of flow simulations with input-files adapted to the different, consecutive positions of the tunnel face, see Figure 3.
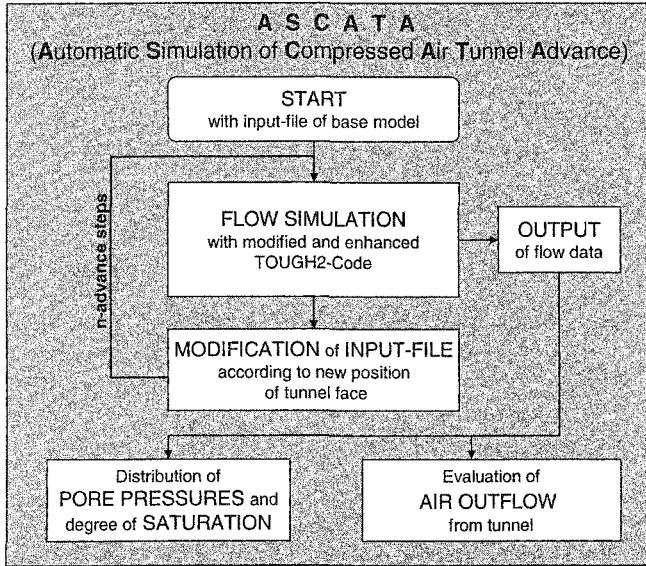
Figure 3. Program structure of ASCATA.

3 Case study: Subway tunnel Essen (Germany)

Several case studies for tunnels driven in grouted gravels and sandy soils using ASCATA have already been conducted (e.g. Steger & Semprich 2006). The computed air losses show a good agreement with measured values. A good agreement in context of predicting air losses means that the computed results are in a ± 25 % range of measured values. The formerly used analytical methods often lead to errors in the range of a whole magnitude and more. An unavoidable uncertainty in predicting air losses will always be the permeability of the shotcrete lining, which is supposed to vary in a certain range due to differences in the construction process.

In this paper, the advance of two single track subway tunnels driven in a silty soil layer in Essen (Germany) is simulated. During the construction of the tunnel tubes the occurring air losses were a lot higher than predicted (Kramer & Semprich 1989). The advance simulations are carried out for two different advance rates to assess the transient flow behavior. First, assuming difficult ground conditions, an advance rate of only 1 m/d is assigned, and then 5 m/d as an effective advance rate for NATM-subway tunneling is assigned. The investigated section length is 55 m.
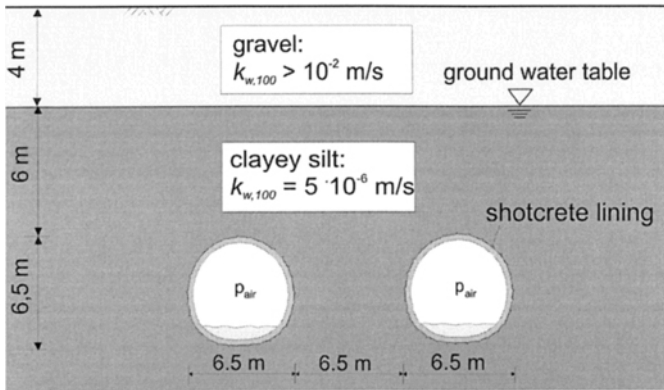
Figure 4. Characteristic geological and geometrical cross section.

3.1 Situation and soil parameters

The cross section of the tunnels (see Figure 4) is mouth shaped, with an average diameter of 6.5 m. In the investigated section, the tunnels are driven 12.5 m below the ground surface. The ground water table lies 6.0 m above the tunnel crown. The applied excess air pressure to counterbalance the hydrostatic pressure was 110 kPa. From the surface to a depth of 4.0 m the ground consists of a gravel of high permeability ($k_w > 10^{-2}$ m/s). Below the encountered soil is a slightly clayey silt with a water permeability of $k_{w,100} = 5 \cdot 10^{-6}$ m/s and a porosity $n = 40$ %.

To describe the unsaturated fluid conductivity of the soil, the relative permeability-saturation function (RP-function) of (van Genuchten-Mualem 1980, 1976) for the water phase and of (Corey 1954) for the air phase is used. For the WRC, the function of (van Genuchten 1980) is chosen. As no experimental testing was done, the parameters are taken as given by (van Genuchten 1980). The grain size distribution and the assigned conductivity parameters are shown in Table 1:

Mass fractions	Cl	FSi	MSi	CSi	FSa
[%]	7.5	2.5	20.0	60.0	10.0
Van Genuchten-Mualem	S_{lr}	S_{ls}	S_{gr}	m [-]	p_0 [kPa]
and Corey parameters	0.20	1.0	0.05	0.36	35.0
Intrinsic permeability K_i (fluid independent):	$6.7 \cdot 10^{-13}$ m²				
Water permeability $k_{w,100}$ at $S_w = 100\%$:	$5.0 \cdot 10^{-6}$ m/s				
Air permeability $k_{g,100}$ at $S_g = 100\%$:	$3.5 \cdot 10^{-4}$ m/s				

Table 1: Mass fractions and conductivity related soil parameters.

To the shotcrete an intrinsic permeability of $K_i = 7 \cdot 10^{-14}$ m² was assigned, as evaluated from laboratory tests of (Kammerer 2000). The relative permeability-saturation behavior is described with a linear relationship for both water and air.

3.2 Numerical model

The model's dimensions are 14 m, 70 m and 15 m in x-, y- and z-direction respectively (y-axis is advance direction). The total number of grid blocks is 46 200 and the corresponding number of connections between the grid blocks is 133 723. The cross section and a cut-out of the longitudinal section are displayed in Figure 5.

Grid block colours:

- ■ Gravel (high permeability, atmospheric pressure)
- ■ Clayey silt (Essener Schluff)
- ■ Tunnel (excess air pressure)
- ▢ Shotcrete lining
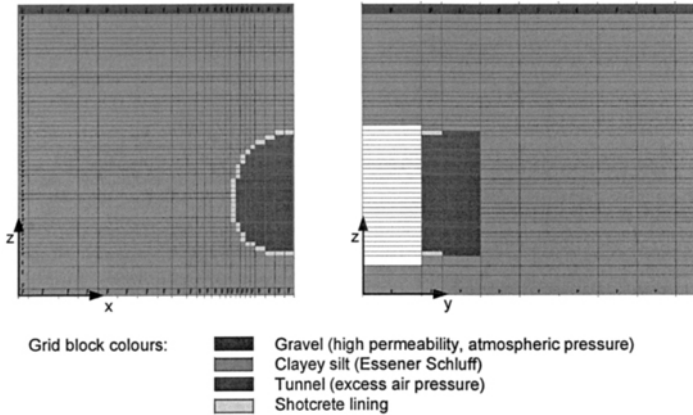
Figure 5. Cross section and longitudinal section of the numerical model.

The top boundary of the model (= atmosphere) consists of a thin layer of grid blocks with assigned Dirichlet-boundary conditions for a constant pressure of 100 kPa. Furthermore, full mobility for both water and air is assumed, as they are supposed to enter the atmosphere without resistance. In the presented model, the top layer does in effect not directly represent the air above ground surface, but atmospheric conditions are already assumed to prevail in the soil layer above the silt. This assumption can be made because of the high permeability of the gravel, which in comparison to the silt represents a negligible barrier to the air flow from the tunnel.

The simulation of the excess air pressure acting in the tunnel works in a similar way. The only difference is that instead of the atmospheric pressure now the excess air pressure of 110 kPa is assigned. It would not be necessary to assign tunnel-grid blocks all over the whole cross sections behind the tunnel face, but only to the lining and to the tunnel face directly. However, due to a convenience in programming ASCATA this procedure was chosen.

The bottom, the left lateral boundary and back side boundary are also simulated with Dirichlet-conditions, fixing the initial hydrostatic pressure distribution and the initial water saturation of 99 % there. To the front and the right lateral boundary (symmetry plane) a Neumann-condition with zero flux is assigned.

It is noted her again that beyond modeling the ground conditions in the total area of the numerical base model, only the modeling of a single cross section is required for the subsequent automatic advance simulation.

3.3 Computed air losses employing Corey's RP-function for air

The computed air losses for the advance of the two tunnel tubes are shown in Figure 6. The results are depicted separately for the shotcrete lining and the tunnel face. Every two meters there appears a discontinuity in the curves as a consequence of the stepwise simulation of the tunnel advance.
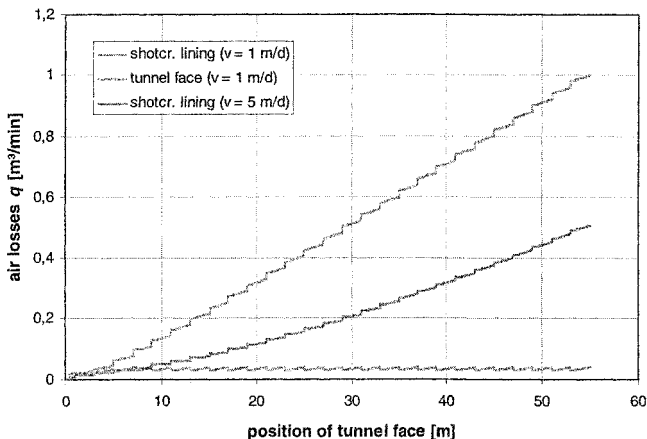
Figure 6. Computed air losses assuming validity of Corey's RP-function.

It can be seen that within the single advance steps, the curve sections describing the air losses through the tunnel face and also the shotcrete lining do not become horizontally. This indicates that the air flow in both cases is still transient, and that there would be a further increase of air losses if a lower advance rate was chosen.

Apart from the qualitative point of view, the computed air losses are extremely low. The air flow through the shotcrete lining is steadily increasing to a maximum value of only 0.5 respectively 1.0 m³/min after 55 m of tunnel excavation for the advance rates of 1 m/d and 5 m/d. The air losses through the tunnel face with 0.02 (not displayed) respectively 0.04 m³/min are likewise extremely low.

It is obvious that the calculated results are of no practical value since they are far from experience. The measured air losses during the advance of the two tunnel tubes in the modeled geological and geometrical section were 21 m³/min, which means that the computed results are more than 20 times to low.

The difference between measured and computed values in this order of magnitude is in contradiction to formerly conducted tunnel advance simulations in sandy soils, where the computed results did not differ more than ± 50 % from measured results. It has already been mentioned that due to the uncertainties in the estimation of soil and shotcrete fluid conductivity parameters this range can be considered as quite satisfying and as a good progress compared to the formerly used analytical methods for the prediction of air losses in compressed air tunneling.

However, the low computed values lead to the conclusion that the transient air-flow occurring in compressed air tunneling in cohesive soils is not correctly represented by the commonly known air RP-functions.

3.4 A new relative permeability-function for computing air losses in cohesive soils

(Kammerer 2000) performed laboratory experiments for air flow through a crack in a shotcrete element into unsaturated soil. The first soil type investigated was a slightly silty sand and the second was a clayey silt. The amount of air flow through the soil and the saturation in the soil were measured during the experiments. Back-analysis of the tests showed that the relative air permeability of the sand is well described by Corey's RP-function, in agreement with the experimental results of (Wyckoff & Botset 1936).

For the tests performed with the silty soil the development of macro flow paths was observed. The air flow occurred mainly in these erosion created pores, going along with a high increase of air permeability even for high degrees of overall water saturation. For example for $S_w = 0.85$, (Kammerer) found relative air permeabilities as high as 70 %. However, once the air entered the soil and the macro flow channels developed, the further desaturation of the soil occurred very slowly.

The described observations lead to the conclusion that an adapted RP-function for air should be used to compute realistic results for air losses occurring in cohesive soils. In Corey's function, the relative air permeability $k_{r,g}$ is given by

$$k_{r,g} = (1-\overline{S})^2 \cdot (1-\overline{S}^2),$$ (4)

where

$$\overline{S} = (S_w - S_{w,r}) \cdot (1 - S_{w,r} - S_{g,r}).$$

$\overline{S}$, the effective degree of liquid saturation, is equal to the water saturation S_w, if the residual water saturation $S_{w,r}$ and the residual gas saturation $S_{g,r}$ are zero. The new RP-function is received by curve fitting, according to the back-calculated values of (Kammerer 2000). The equation reads

$$k_{r,g} = 1 - \overline{S}^4$$ (5)

Here the effective degree of saturation is also used as modeling variable, but the air permeability is simply given by subtracting $\overline{S}$ to the power of 4 from 1.0. Figure 7 shows the new RP-function in addition to Corey's function.

It shall be noted, that due to the lack of more experimental data, the given equation can only be seen as a first approach. Furthermore, it only applies to air flow problems with high pressure gradients as it occurs in compressed air tunneling. For other transient air flow problems, Corey's curve may still be a suitable choice. It is also noted, that the described approach does not take into account changes of the water-relative permeability behavior and the WRC. However, as air is the prevalent flow phase and the taken approach is seen as a first step towards more realistic computation of air losses in cohesive soils, these simplifications seem to be justified.
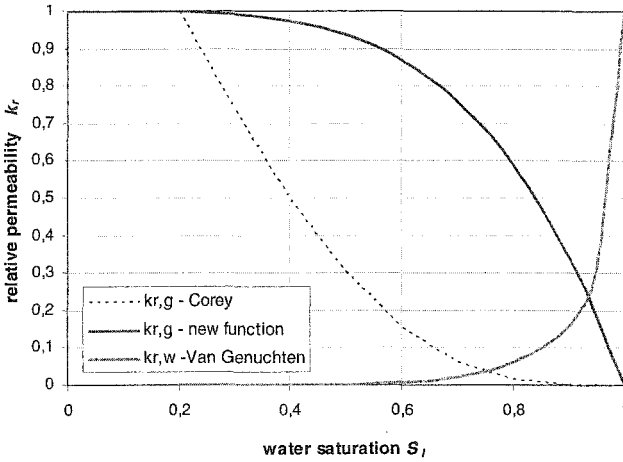
Figure 7. Comparison of Corey's RP-function and the proposed RP-function.

3.5 Results computed with the new air relative permeability function

Fig. 8 shows the computed air losses for the proposed air RP-function. Again the simulations were performed for the advance velocities of 1 m/d and 5 m/d. After the full advance length the air losses through the shotcrete lining reach approximately 35 m³/min in both cases. In comparison to measured values this means that the computed results are now about 65 % too high. Contrary, the computed air losses through the tunnel face are too low. They are hard to measure in field, but for these types of soils they are expected to be in the range of 10 – 20 m³/min.
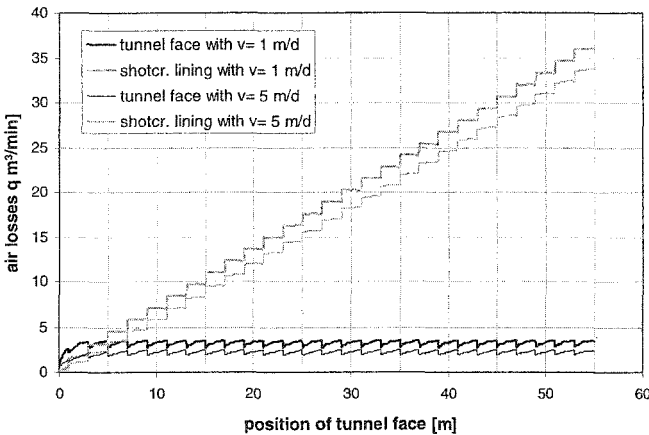
Figure 8. Computed air losses using the new RP-function.

The low difference for the simulations with differently assigned advance rates indicates that the air flow is close to reaching steady state conditions. This fact is also confirmed by the relatively linear increase of the air flow through the shotcrete lining. The opposite behavior, an upward curvature of the graphs, could be observed before, when Corey's RP-function for air was used.

Figure 9 shows the gas saturation and pore pressure distribution for a cross section 20 m behind the tunnel face. At the left lateral boundary the pressure with respect to the gas phase is according to the initial hydrostatic pressure distribution. Moving closer to the tunnel, the isobars steep strongly, caused by the compressed air escaping from the tunnel into the ground.

The gas saturation distribution (Figure 10, right) gives an idea of the extension of the air flow field. It can be seen that air flow is mainly taking place at the upper half of the tunnel cross section. Below, the air pressure does not exceed the air entry value of the soil and can therefore not penetrate into the ground. The overall degree of air saturation is quite low, with a maximum of 0.20 above the crown of the tunnel and a rapid decrease with increasing distance from the tunnel. This distribution is a result of the new RP-function for air, which already for low degrees of gas saturation shows high relative air permeability.

$100.0 < p_{air}$ [kPa] < 237.5 $0.01 < S_g$ [%] < 0.20
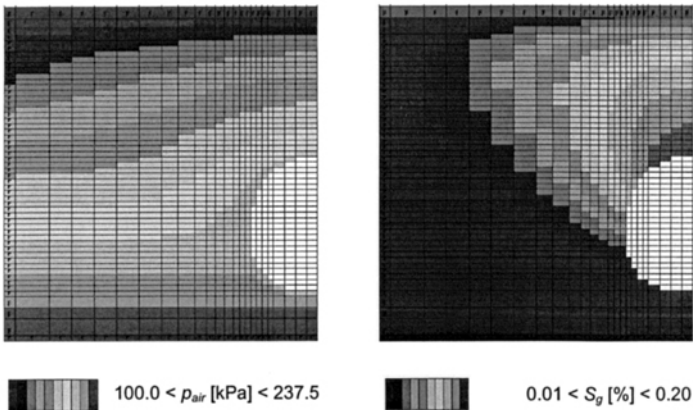
Figure 9. Gas pressure and gas saturation around the tunnel section.

4 Conclusions and outlook

A numerical tool to compute the air losses in compressed air tunneling has been presented in this paper. The developed program ASCATA uses TOUGH2 features to simulate the occurring unsaturated air and water multiphase flow.

Conducted case studies for tunneling in sandy soils have shown that a significant increase in the accuracy in the prediction of air losses could be reached with the program. Contrary, the case study performed for a section of two subway tunnels in Essen, which are situated in a silty soil layer, showed misleading results.

From laboratory tests performed by (Kammerer 2000) it was concluded that in cohesive soils macro pores created by erosion forces of the compressed air govern the flow behavior. According to these experimental findings, a new relative permeability function for air was estimated and employed for a second set of advance simulations. The computed results show a much better agreement with measured values. Still the air losses through the shotcrete lining results are a little too high whereas through the tunnel face are too low. A possible explanation for this performance is that the soil at the tunnel face is more affected by the erosion forces of the compressed air than the soil behind the shotcrete lining.

It is the aim of further research to extend the investigations into the erosion effects of compressed air flow and to determine reliable relative permeability curves. Moreover, the interaction between the relative permeability-saturation function and the WRC shall be studied. The purpose of this research is also to develop a sophisticated method to assess the risk of sudden air losses ("blow out") in compressed air tunneling.

References

van Genuchten, M.Th. (1980). A Closed-form Equation for Predicting the Hydraulic Conductivity of Unsaturated Soils. Soil Science Soc. of America, Vol. 44-5, 892-898.

International Formulation Committee (1987). A Formulation of the Thermodynamic Properties of Ordinary Water Substance. IFC Sekretariat, Düsseldorf, Germany.

Kammerer, G. (2000). Experimentelle Untersuchungen von Strömungsvorgängen in teilgesättigten Böden und in Spritzbetonrissen im Hinblick auf den Einsatz von Druckluft zur Wasserhaltung im Tunnelbau. Mitteilungshefte Gruppe Geotechnik Graz. Technische Universität Graz, Heft 8.

Kramer, J.; Semprich, S. (1989). Erfahrungen über den Druckluftverbrauch bei der Spritzbetonbauweise. Taschenb. für den Tunnelbau, Verlag Glückauf , Essen, 91-153.

Mualem, Y. (1976). A New Model for Predicting the Hydraulic Conductivity of Unsaturated Porous Media. Water Resources Research, Vol. 12, No.3 513-522.

Pruess, K.; Oldenburg, C.; Moridis, G. (1999). TOUGH2 User´s Guide. Version 2.0. Earth Sciences Division, Ernest Orlando Lawrence Berkeley National Laboratory.

Richards, L.A (1931). Capillary Conduction of Liquids through Porous Mediums. Physics, Vol. 1, 318-333.

Steger, G; Semprich, S. (2006, in print). 3-D Numerical Simulation of Air Losses in Compressed Air Tunneling. Proc. GeoShanghai International Conference, Shanghai.

Wyckoff, R.D; Botset, H.G (1936). The flow of gas-liquid mixtures through unconsolidated sands. Physics, Vol. 7, 1936.

Influence of reservoir level change on slope stability of a silty soil bank

Tony L. T. Zhan[1], W. J. Zhang[2] and Y. M. Chen[3]

[1] Associate professor, Department of Civil Engineering, Zhejiang University, 310027, Hangzhou, China; PH (0086) 571-87952415; FAX (0086) 571-87952269; email: zhanlt@zju.edu.cn
[2] PhD student, Department of Civil Engineering, Zhejiang University, 310027, Hangzhou, China
[3] Professor, Department of Civil Engineering, Zhejiang University, 310027, Hangzhou, China; PH (0086) 571-87951340; FAX (0086) 571-87952269; email: cym@civil.zju.edu.cn

Abstract

Seasonal change of water level in reservoirs is an important factor causing a slope failure of banks. Unsaturated-saturated seepage analyses were carried out to simulate the changes of phreatic line and pore-water pressure in a bank slope subject to a reservoir level change. On the base of the seepage analysis results and Fredlund's shear strength equation for unsaturated soils, limit equilibrium analyses were performed to evaluate the change in factor of safety (FS) with reservoir level. The analysis results demonstrate that the value of FS in the silty soil slope increases with the rising reservoir level, which is inconsistent with the result found in a literature. The increase of FS is attributed to an increase in the water thrust on the slope surface. During the drawdown process, there exists a critical reservoir level at which the value of FS is the lowest. The critical reservoir level is at a level equal to 1/3 of the slope height.

1 Introduction

Water level in a reservoir changes frequently due to seasonal climate change. This usually leads to a slope failure of banks around the reservoir. Jones (1981) investigated the landslides occurred in the vicinity of Roosevelt lake from 1941 to 1953. It was found that 49% of them occurred during the first filling period of reservoir from 1941 to 1942, and 30% of them occurred as a result of drawdown of reservoir. In Japan, about 40% landslides around reservoirs occurred during the rising of water level, and 60% happened under a drawdown condition (Zhong, 1990).

The hydrological process in the slope subject to a rising/lowering of water level is an unsaturated-saturated transient seepage. However, most of previous study on the influence of reservoir level change on slope stability was based on a saturated seepage analysis. On the basis of the Boussinesq's theory for an unsteady seepage, Zheng et al. (2004) established a simplified model for determining the phreatic lines in a slope under a drawdown condition. The obtained phreatic lines were input into limit equilibrium method to determine the factor of safety for the slope (FS). The analyses demonstrated that there exists a minimum FS when the reservoir level is lowered to a level at about 1/3~1/4 of the slope height. Ma et al. (2000) assumed that seepage in a bank slope was quasi-steady, and the shear strength parameters reduced once the soil layer became saturated. Their analysis results also showed that there existed a minimum FS during the changes of reservoir level. Both these two studies neglected the seepage in unsaturated zone and made a simplification on the shear strength of unsaturated soils.

In this paper, unsaturated-saturated seepage analyses were carried out by using the commercial program SEEP/W to simulate the change in pore-water pressures in a homogeneous silty soil slope subject to a reservoir level change. The obtained pore-water pressure fields were then imported into the limit equilibrium analysis program (Janbu's simplified method) to evaluate the change in factor of safety (FS) with reservoir level. In the limit equilibrium analysis, the contribution of negative pore-water pressure to shear strength was considered by the use of Fredlund's shear strength equation for unsaturated soils. On the base of the analysis results, the change of FS with reservoir level was interpreted in details.

2 Unsaturated-saturated seepage analyses

2.1 Finite element model

An ideal homogeneous and isotropic soil bank slope is used in this study. The soil type in the slope was specified as a silty clay with soil parameters shown in Table 1. Figure 1 shows the finite element mesh of the slope. The height of the slope is 10 m, and its slope angle is 33.5°. It is assumed a cyclic change of reservoir level happened to the bank within half a year (see Figure 2). The reservoir level rises from 6 m to 12 m during a rainy season (30 days), keeps at 12 m for 60 days, and then falls back to 6m during the subsequent dry season (30 days).

Table 1 Soil parameters for the silty soil considered in this paper

Soil parameters	Cohesion, c' (kPa)	Internal Friction angle, ϕ' (°)	Angle quantifying the contribution of suction to shear strength, ϕ^b, (°)	Air-entry value, $(u_a-u_w)_b$, (kPa)	Saturated permeability, k_s, (m/s)
Value	5	30	20	25	2.3×10^{-6}
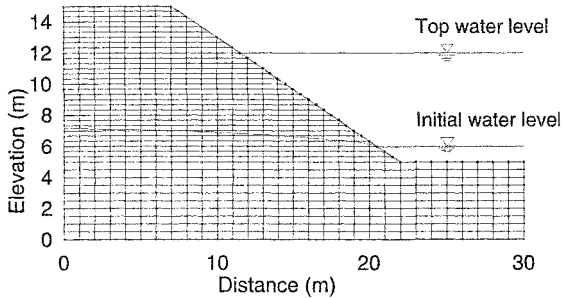
Figure 1 An ideal slope model and finite element mesh
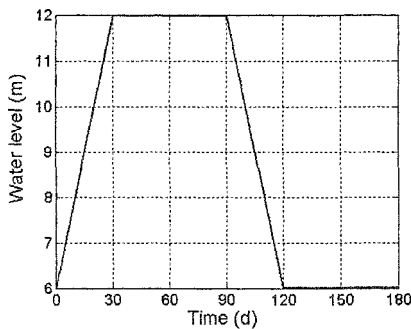
Figure 2 Change of reservoir level with time

To determine the changes of pore-water pressure in the slope with the reservoir level, unsaturated-saturated seepage analyses were performed using the commercial software SEEP/W (GEOSLOPE, 2003). During the analyses, the downstream boundary subject to the reservoir level change is defined as a total head boundary equal to the changing reservoir level shown in Figure 2. During the drawdown process, this boundary is defined as a review boundary. This means that the boundary is adjusted to a zero-flux boundary if the total head at a node is smaller than the corresponding elevation. All the other boundaries are specified as zero-flux boundaries. The initial condition is obtained by a steady state analysis in which the reservoir level maintains at a level of 6m and a rainfall intensity of 9.0×10^{-8} m/s was applied on the surface of the slope. The pore-air pressure in the slope is assumed to be at an atmospheric condition, i.e. $u_a = 0$. Hence, the value of pore-water pressure is equal to the magnitude of matric suction.

2.2 Model parameters

Soil-water characteristic curve (SWCC) and water permeability function are two prerequisite input parameters for the unsaturated-saturated seepage analysis. The SWCC of the silty soil is obtained from the literature published by Fredlund and Xing

(1994) (see Figure 3). Water permeability function for the soil was predicted from the SWCC by the use of the method proposed by Fredlund et al. (1994). The value of saturated permeability for the soil, k_s, is equal to 2.3×10^{-6} m/s. The predicted water permeability function is shown in Figure 4.
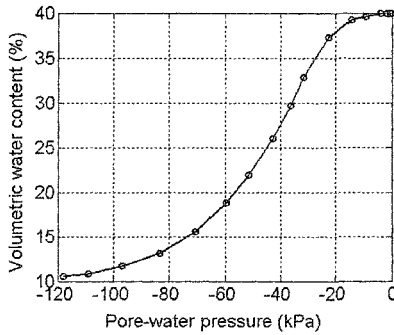
Figure 3 Soil-water characteristic curve for the silty soil
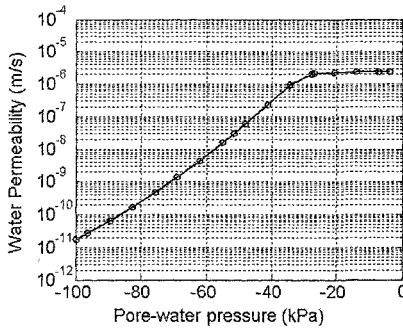
Figure 4 Predicted water permeability curve for the silty soil

2.3 Results from seepage analyses

The transient seepage analysis associated with the change of reservoir level shown in Figure 2 was carried out in 180 time steps, i.e. one day for each time step. Pore-water pressures and phreatic lines in the slope at each time step were obtained from the analyses. Figure 5 shows the change of phreatic line in the slope with the rising reservoir level, and Figure 6 shows the change of phreatic lines during the lowering of reservoir level. It can be seen that the phreatic level shows a delayed response with respect to the change of reservoir level because the seepage through a soil is generally slower than the flow at a free condition. During the rising and drawdown process, the phreatic lines take the shape of concave and convex, respectively. After the reservoir level maintains at the maximum/minimum level for about 10~20 days, the phreatic level tends toward the maintained reservoir level.
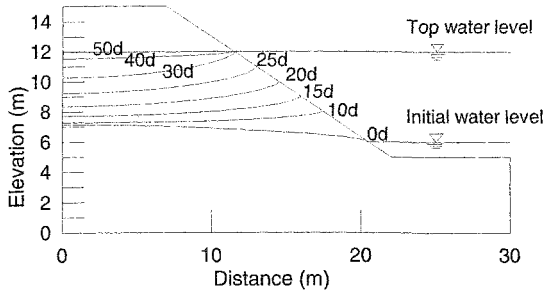
Figure 5 Change of phreatic line with the rising reservoir level
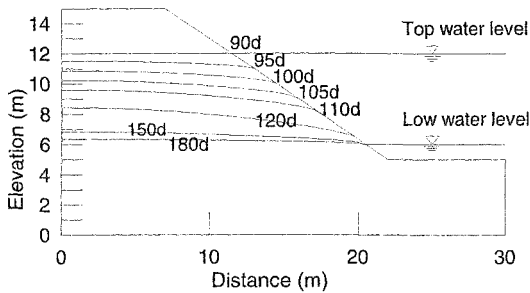
Figure 6 Change of phreatic line during the drawdown process

3 Slope stability analyses

3.1 Method for slope stability analysis

Janbu's simplified method was utilized to calculate the factor of safety for the slope subject to reservoir level change. Figure 7 shows the slope model and the forces acting on a typical slice. In the model, the influence of reservoir level is taken into account by applying a water pressure normal to the slope surface, which provides a support on the potential sliding mass. The total thrust force resulted from the water pressure (D) can be obtained by integrating the water pressure alone the slope surface, and it acts normal to the slope surface at a level equal to 1/3 depth of water. The changes of phreatic line and pore-water pressure inside the slope will alter the water content of the soil mass, and hence change the weight of the slice. On the other hand, the change of pore-water pressure will result in a change of shear strength along the bottom of each slice. The change of shear strength with the pore-water pressure can be described with the equation proposed by Fredlund & Rahardjo (1993):

$$\tau_f = c' + (\sigma_n - u_a)\tan\phi' + (u_a - u_w)\tan\phi^b$$

(1)

As mentioned previously, the pore-air pressure (u_a) in the slope was assumed to be zero. The influence of pore-water pressure on shear strength can be quantified by

$(-u_w)\tan\phi^b$. In a saturated zone (i.e., below the phreatic line), the value of pore-water pressure (u_w) is positive, and ϕ^b is equal to ϕ' (30°). In an unsaturated zone, the value of pore-water pressure (u_w) is negative, and ϕ^b is equal to 20°.
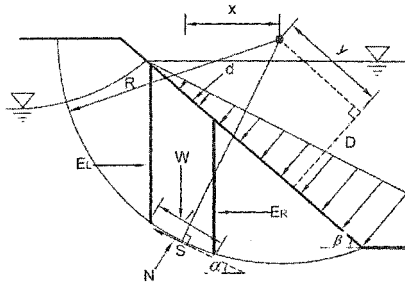
Figure 7 Analysis model and forces acting on a slice

By considering the limiting equilibrium conditions with respect to the forces in the vertical direction and the moments for all the slices, the factor of safety (FS) can be derived as follows:

$$FS = \frac{\sum\ [c'l + N\tan\phi' - u_w l \tan\phi^b]}{-Dy/R + \sum W \sin\alpha} \tag{2}$$

where

$$N = \frac{W + d\cos\beta - \dfrac{(c' - u_w \tan\phi^b)l\sin\alpha}{FS}}{m_\alpha}$$

$$m_\alpha = \cos\alpha + \frac{\sin\alpha\tan\phi'}{FS}$$

As the unknown FS is included in the term N, Eq. (2) must be solved through iteration procedures.

3.2 Results from slope stability analyses

It is known that the location of critical slip surface may change with the reservoir level. For simplicity, the slip surface is firstly assumed to be fixed as a circular slip surface passing through the toe of the slope (see Figure 8). The pore-water pressure at the bottom of each slice can be deduced from the pore-water pressure field obtained from the previous seepage analyses by the interpolation method. Thus, the contribution of negative pore-water pressure to shear strength at the bottom of each slice can be quantified by $(-u_w)\tan\phi^b$.
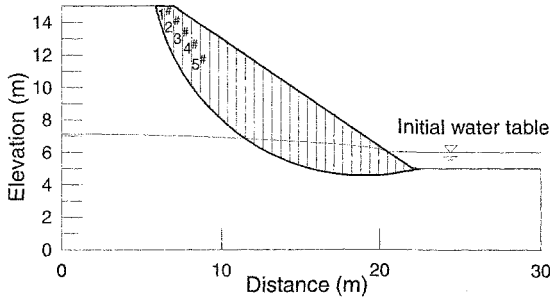
Figure 8 Soil slices on the fixed slip surface

Figure 9 shows the change in the contribution of negative pore-water pressure to shear strength for the first 11 slices during the rising of reservoir level. As shown in Figure 8, the initial phreatic line was just below the bottom of the 10th slice. Hence, at the initial condition (i.e., t = 0 d), the pore-water pressures at the bottom of the first ten slices are negative, and they have a contribution to the shear strength up to a maximum value of 20 kPa. As the reservoir level rises, a loss of negative pore-water pressure gradually happens to the bottom of the lower slices, and its contribution to shear strength loses accordingly. When the reservoir level reaches the top level and maintains for 10 days (i.e., t = 40 d), the contribution of negative pore-water pressure to shear strength only remains for the top two slices.
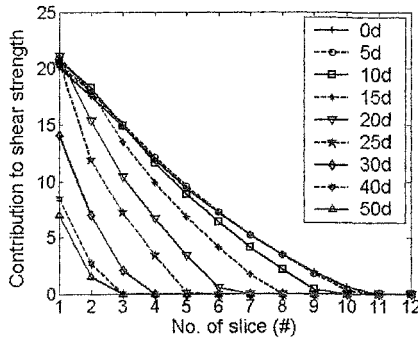
Figure 9 Contribution of negative pore-water pressure to shear strength during the rising of water level

Besides the changes in the shear strength along the potential slip surface, the change of water reservoir level also results in a change in the weight of the slices as well as a change in the thrust force of reservoir water. Effect of these changes on FS can be sorted out by looking into Eq. (2): ①The contribution of negative pore-water pressure to FS is described by the term $\sum u_w l \tan \phi^b$. ②The contribution of friction resistance to FS is described by $\sum (N \tan \phi' - u_w l \tan \phi')$. It takes account for the effects from the changes in the weight of slice and the positive pore-water pressure. ③The

contribution from the thrust force of reservoir water is described by $-Dy/R$. In addition, the cohesion of the soil has a contribution to FS. All these contributions to FS can be calculated for the fixed slip surface, and their changes with the rising/lowering reservoir level are shown in Figure 10.

As shown in Figure 10, at the initial condition (i.e., t = 0 d) both the negative pore-water pressure and the frictional resistance in the slope contribute significantly to FS (with values of 0.24 and 0.99 respectively), and the contribution from the thrust of reservoir water is negligible. As the reservoir level rises, i.e. from 0d to 30d, the contributions from negative pore-water pressure and the frictional resistance decrease by 0.16 and 0.25, respectively. But the contribution from the thrust of water to FS increases by a magnitude of 0.58, and it plays a dominant role. Hence, the value of FS increases from 1.47 to 1.66 during the rising of reservoir level. The increase of FS is mainly attributed to the delayed rise of phreatic line inside the slope relatively to the rise of reservoir level (see Figure 5). The result is inconsistent with the analysis results reported Ma et al. (2000), which is concerned with a sandy soil with a greater water permeability. The inconsistency may be attributed to the difference in water permeability between the two types of soil concerned. It should be noted that the contribution of cohesion increases slightly with the rising reservoir level. This is resulted from the change in the value of the denominator in Eq. (2).
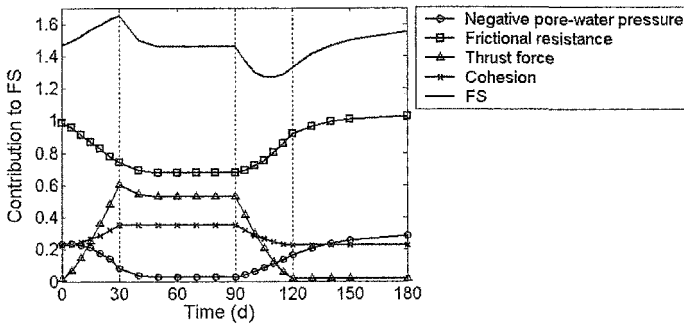
Figure 10 Change in the contribution of each term to FS

When the reservoir level reaches and maintains at the top level (from 30d to 90d), the value of FS firstly decreases, and then tends toward a constant value. The reason for the decrease is that the contributions from negative pore-water pressure and frictional resistance continue to decrease due to the delayed response of pore-water pressure. It should be noted that the thrust force is kept constant at this stage, and its contribution to FS shows a slight decrease due to a change in the value of the numerator in Eq. (2).

During the drawdown process, i.e. from 90d to 120d, the contributions from negative pore-water pressure and frictional resistance increase due to a regain in negative pore-water pressure and effective stress along the potential slip surface. However, the contribution from the thrust of reservoir water decreases with the lowering water

level. As shown in Figure 10, the drawdown process can be divided into two stages. For the first stage (i.e., from 90d to 110d), the change in the contribution from the thrust effect is more significant than the change in the contributions from negative pore-water pressure and frictional resistance, and hence the value of FS decreases from 1.46 to 1.27. It should be noted at this stage the drawdown of reservoir results in not only a change in water pressure on the whole slope surface but also a change in its acting area. For the second stage (i.e., from 110 to 120d), the change in the contribution from the thrust effect is relatively insignificant, and hence the value of FS increases from 1.27 to 1.33. Thus, the value of FS firstly decreases, and then increases during the drawdown process. In other words, there exists a critical reservoir level at which the value of FS is minimum. The reservoir level corresponding to the minimum FS is at a level equal to 1/3 of the slope height. This is essentially consistent with the analysis results reported by Ma et al. (2000) and Zheng et al. (2004).

When the reservoir level reaches and maintains at the lowest level, i.e. from 120d to 180d, the contributions from negative pore-water pressure and frictional resistance continue to increase. Hence the value of FS continues to increase until the phreatic line in the slope is equilibrated with the reservoir level.

As mentioned before, in a real case the critical slip surface may change with the reservoir level. Figure 11 shows the change of minimum FS with time corresponding to the critical slip surfaces, together the one corresponding to the fixed slip surface. It can be seen that the two curves are consistent in shape, and the difference only lies in the magnitude of FS at some time steps.
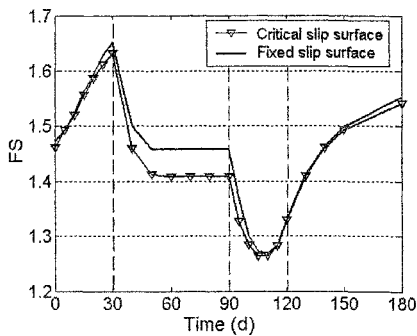
Figure 11 A comparison between the FS verse time curves corresponding to the critical and fixed slip surfaces

4 Conclusions

In this paper, unsaturated-saturated seepage analyses were carried out to simulate the changes of phreatic line and pore-water pressure in a bank slope subject to a reservoir level change. On the base of the seepage analysis results and Fredlund's shear strength equation for unsaturated soils, limit equilibrium analyses were

performed to evaluate the change in factor of safety (FS) with reservoir level. Based on the analysis results, it was found that the contribution of negative pore-water pressure to shear strength, the friction resistance and the thrust force of reservoir water are three important factors affecting the slope stability, and they exert a dominant role at different stages. The analysis results demonstrate that the value of FS in the silty soil slope increases with the rising reservoir level, which is inconsistent with the result found in a literature. During the drawdown process, there exists a critical reservoir level at which the value of FS is the lowest. The critical reservoir level is at a level equal to 1/3 of the slope height.

It should be noted the change of FS with the rising/lowering of reservoir level is quite complicated. It depends on slope dimensions, soil type, hydraulic parameters, rising/lowering speed of reservoir level and so on. The conclusions above only pertain to the special case concerned in this paper. More detailed analyses are necessary for a more general conclusion.

5 References

Fredlund D.G, Xing A., and Huang S.Y. (1994). "Predicting the permeability function for unsaturated soils using the soil-water characteristic curve". Canadian Geotechnical Journal, 31(3): 533-546.

Fredlund D.G., Xing A. (1994). "Equations for the soil-water characteristic curve. Canadian Geotechnical Journal", 31(3): 521-532.

Fredlund, D. G. & Rahardjo, H. (1993). Soil Mechanics for Unsaturated Soil Mechanics. Wiley Inter Science, New York.

GEO-SLOPE (2003). International Ltd. SEEP/W and SLOPE/W for finite element seepage analysis, vol.5. Users Manual. Calgary, Alberta, Canada, 2003.

Jones, J.A.A. (1981). The nature of soil piping, A review of Research. Geo. Books, Norwich, UK, 315p.

Ma C.W., Liu Z.Y., Miao T.D., Wang D.K. (2000). "The influence of water level changing on stability of river embankment". Journal of Lanzhou University (Natural Science), 36(3) : 56-60. In Chinese.

Zheng Y.R., Shi W.M., Kong W.X. (2004). "Calculation of seepage forces and phreatic line under drawdown condition". Chinese Journal of Rock Mechanics and Engineering, 23(18):3203-3210. In Chinese.

Zhong C. H.Z. (1990). "Discussion on reservoir landslides". Bulletin of Soil and Water Conservation, 10(1): 53-64. In Chinese.

Methodology for calculation of rain-induced slides

Øyvind Armand Høydal[1] and Håkon Heyerdahl[1]

[1]Norwegian Geotechnical Institute (NGI) and ICG, International Centre for Geohazards, P.O. Box 3930 Ullevaal Stadion, N-0806 Oslo, Norway, email: oah@ngi.no, hhe@ngi.no,

Abstract

A large number of slides occurred in the South-Eastern part of Norway during the autumn of year 2000. The slides were triggered by extreme duration of rainfall, leading to saturation of slopes that are partly unsaturated under normal conditions. On this background, a study aiming at establishing a methodology for assessment of stability of slopes prone to rain-induced landslides was started. The suggested methodology for calculation of the effect of rainfall on slope stability is described and applied on a typical example (model slope). Meteorological data together with assumed soil properties are used to define a yearly normal infiltration function and similar functions for extreme events. The normal infiltration function is used to calculate soil water content variation through a normal year using the computer code SEEP/W (2004). Extreme events are analysed by starting calculations from normal conditions. The resulting pore pressures are used to calculate safety factors for slopes during normal and extreme events.

Stability of the model slope is calculated using effective stresses based on changes in pore pressures and water content in the undrained and drained zones. Calculations have been performed for the normal year, for the 100-year situation, and for the extreme situation represented by the autumn of year 2000 for both shallow translatory slides and deep circular surfaces. The calculations have demonstrated a significant reduction in safety factors for both deep seated and shallow potential failure surfaces. A tentative conclusion from these calculations is that the safety level (margin) for climatically influenced slopes should be minimum in the order of 0.2 when considering the normal year situation (i.e. FS in a normal year > 1.2). This will ensure that stability of deep-seated shear surfaces do not drop to a critical level during a period of extreme rainfall, like the rain experienced in the South-Eastern part of Norway during the autumn of year 2000. For shallow slides, the safety margin must be evaluated based on top layer material properties.

INTRODUCTION

In the fall of year 2000, the South-Eastern part of Norway experienced the most extreme precipitation period ever recorded in this region (Dragset, 2002). During this period, Norwegian Geotechnical Institute was engaged in evaluation of 90 rainfall induced landslides (Jaedicke and Kleven, 2006), mostly shallow, translational slides in the Romerike district. The majority of these slopes are under normal conditions unsaturated in the upper soil layers. Geometries typical of problem slopes in the Romerike region in South-Eastern Norway have been modelled. The soils involved in sliding are mainly marine Quaternary deposits (silts and clays). No slides involving quick clay were triggered in the period, although such deposits are commonly found in the region. The general topography can generally be described as ravines cutting deeply into the originally relatively flat landscape, forming steep up to 40 m high slopes.

Triggering of slides during extreme climatic conditions will depend on the relationship between normal and extreme meteorological conditions. A procedure for calculating pore pressures condtions in slopes, and consequently resulting slope stability, for normal and extreme conditions is sketched in Figure 1. Calculation of pore pressures and slope stability during rainfall require a soil model that handles infiltration for both saturated and unsaturated soil conditions.
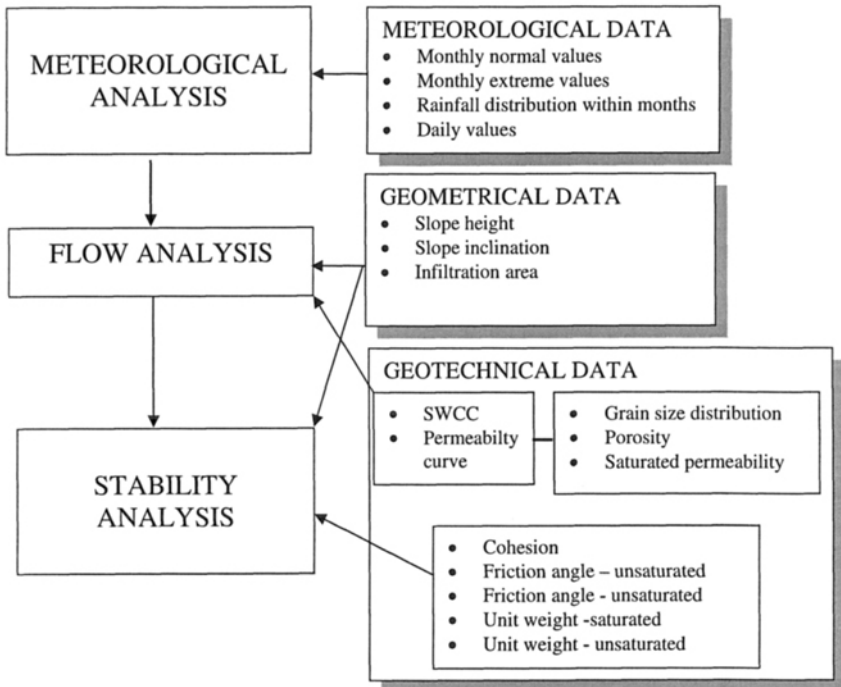
Figure 1. Flow chart - working procedure and minimum of necessary data

METEOROLOGICAL DATA AND ANALYSIS OF RAINFALL

Expected extreme rainfall values and durations can be calculated by various methods (Frøland, 1984, 1993). However, the distribution of rainfall during one rainfall event is usually an additional assumption. The importance of rainfall distribution with time is large, since the surface properties of the soil puts a check on the maximum infiltration and watercontent stongly influence soil permability. The variation in rainfall with time therefore will affect resulting pore pressures in the soil (suction), flow direction and position of the phreatic line ("water table"). Evaporation is also important for the resulting infiltration and will reduce net infiltration. By compering reginal runoff with rainfall, normal evaporation can be estimate. Application of more advanced analysis of the total surface-water balance, including evapo-transpiration, will increase the variation in suction further. The numerical flow calculation computer code SEEP/W (2004) used in the analyses will remove rainfall larger than the saturated permeability. However, the user must still know whether the data are "smoothed", i.e. intense showers are distributed over time to average values. Since rainfall often occurs in intense showers, infiltration periodically will be limited by saturated permeability. Using average (daily or monthly) values to represent normal or extreme situations, it is necessary to know the distribution of rainfall in time. For short, extreme rainfall, only a minor part of the water will infiltrate into the ground, especially in areas where silt and clay dominate the ground conditions. Table 1 presents typical saturated permeability values for different soils converted to mm/day, which is a standard unit for rainfall observations. Permeability about 10^{-7} m/s limits maximum infiltration to approximately 8 mm depth of rainfall per day when infiltration is driven by elevations only. For long term - or steady state - conditions, only a fraction of the saturated permeability can be used, since the overall hydraulic gradient, represented by the difference in total head divided by flow length, for a slope is always less than 1.

Table 1. Comparison between typical permeability values and rainfall

Typical soil	Typical saturated permeability *m/s*	Equivalent rainfall that may infiltrate *mm/day*
Sand	1.0×10^{-4}	$8.64 \times 10^{+3}$
	1.0×10^{-5}	$8.64 \times 10^{+2}$
	1.0×10^{-6}	$8.64 \times 10^{+1}$
Silt	1.0×10^{-7}	$8.64 \times 10^{+0}$
Lean clay	1.0×10^{-8}	$8.64 \times 10^{+1}$

Normal infiltration

In order to determine the normal water content in a slope, monthly precipitation rates were applied. Meteorological data representing the normal period 1961-1990 and data from the autumn of year 2000 from the meteorological station Gardermoen, Romerike (50 km North – North-East of Oslo) have been used. In the analyses, daily precipitation larger than 10 mm per day was set to 10 mm – equivalent to the permeability/infiltration capacity of silty soil. From this, new and corrected "normal" values were calculated. Table 2 shows the resulting values. In addition, infiltration

values must be corrected for snow and frozen ground conditions. A simplified approach was used, setting infiltration to zero in months with average temperatures below 0°C. The final curve is defined as the normal infiltration function for the specific soil. An equivalent calculation for the extreme rainfall that was measured during the autumn of year 2000 shows an infiltration correction factor (ratio of available water for infiltration of total rainfall) of approximately 0.6. Figure 2 shows normal rainfall, 20 and 100 year percentiles, calculated for every month of the year for Gardermoen. The observational period is from 1957 to 2002. The unit is m/day. In addition, 20 and 100 year percentiles for the periods September + October, October + November and September + October + November have been calculated. Extreme values calculated for single months cannot be put after each other in a series and normal conditions are defined as the start of an extreme period. It must be checked in each case whether it is the 1, 2 or 3 month extreme situation that is critical for the stability. Typically, for this data set, the situations that should be checked are: (i) 100 year September + October + November, (ii) 100 year October + November, and finally (iii) 100 year November.

Table 2 Corrected monthly normal rainfall at Gardermoen and infiltrating values from assumption of maximum infiltration capacity

Gardermoen	Normal rainfall (mm/month)	Corrected normal rainfall (mm/month)	Ratio of available water for infiltration, limited to max 10 mm/day	Average mm/day available for infiltration
Jan	59	52	0.89	1.7
Feb	49	42	0.86	1.5
Mar	53	47	0.89	1.5
Apr	48	41	0.85	1.4
May	61	50	0.82	1.6
Jun	73	58	0.79	1.9
Jul	79	62	0.78	2.0
Aug	90	64	0.72	2.1
Sep	96	68	0.71	2.3
Oct	100	73	0.73	2.4
Nov	89	69	0.78	2.3
Dec	65	56	0.86	1.8

The situation 100 year September + October will for this data set be irrelevant, since this corresponds to the 20 year value for October + November. Generally, the ground water level rises during the autumn, so that the last period will produce the highest total moisture content in the soil. From Figure 2 it appears that especially November gives a particularly high 100 years value. This is due to November 2000 being included in the data set. Hence, the observed values for November do not have the same distribution as the other months in the data set and the uncertainty in its return period increases.
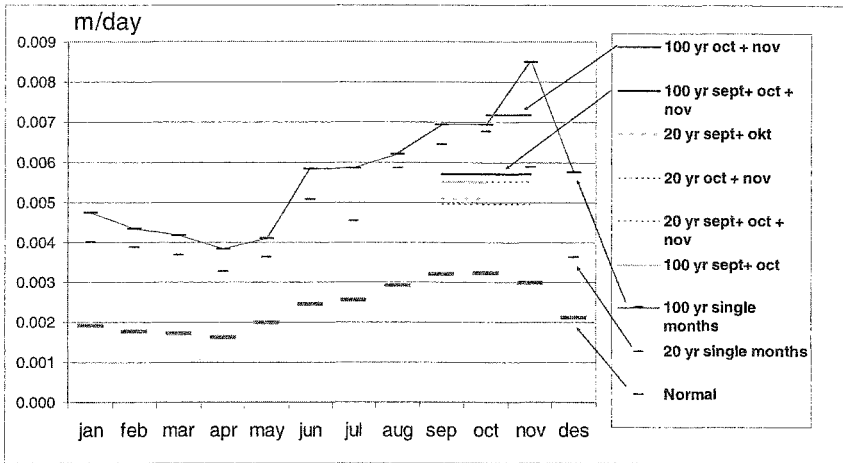
Figure 2 Normal- and extreme values for monthly rainfall at Gardermoen

FLOW ANALYSES

Flow analyses have been performed on a model slope, typical of a problem slope in the Romerike area during the autumn of year 2000. It has a height of 15 m and an inclination of ~27° (1:2). Behind the slope crest, there is a 30 m plateau which works as an infiltration zone, feeding water into the ground. The flow analyses are performed with the finite element program computer program SEEP/W (2004). The chosen soil model is homogenous, and represents a sandy silt (soil # 5, SEEP/W, 2004) with porosity 45 %, saturated permeability 4.80e-7 m/s and air entry value about 10 kPa. This soil is representative for numerous of the observed slides in Fall 2000. The elemet size used for daily precipitation rates is 12.5x 12.5 cm with secondary nodes in the upper 50 cm with transitional elements to courser elements in the inner part of the slope. Timestep and grid size is choosen so the model itself does not numerically smooth the applied boundary condition. Surface variation will be smoothed in a too course grid. Figure 3 illustrates the model.

Normal conditions

Normal water content and water table are defined by starting the numerical model with a yearly average normal infiltration value and thereafter cycle the normal infiltration curve for three years. The third year is defined as a normal year. Both the water table and soil water content are therefore expected to change through the normal year. The initial condition preceding an extreme period is defined as the preceding normal condition. The changes in the ground water level through a normal year are quite small. The largest changes are located in the lower part of the slopes. Here, the yearly variation in ground water level is ca. 0.5 m. The water content varies mainly in the top 5 m of the slope. Below this depth, the slope is saturated. The yearly variation in water content is shown in Figure 4 for the ground surface and at

three depths, 0.5, 2,0 and 5.0 m below the ground surface in the middle of the slope. The variations are largest just below the ground surface. From Figure 4 it appears that there is a time difference (phase lag) between the response at 2,0 and 5.0 m depth. The variation in capillary suction from the highest to the lowest water content corresponds to a change in suction of 20 kPa.
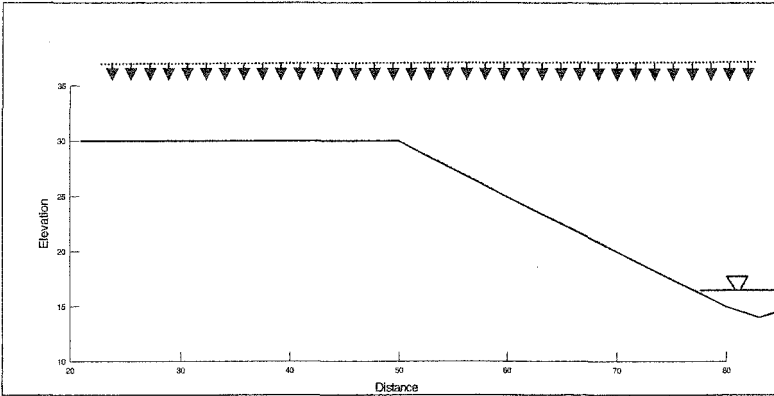
Figure 3. General slope geometry.
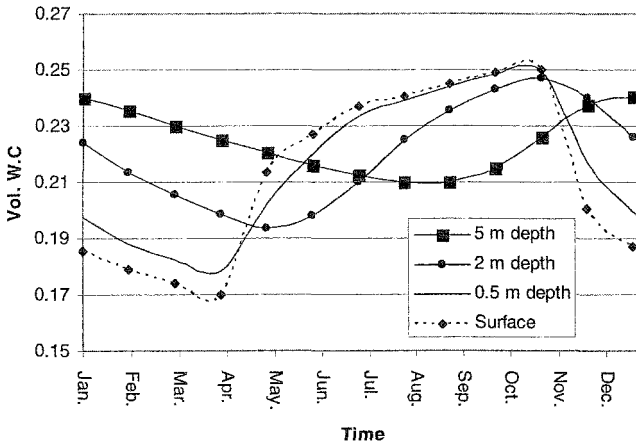
Figure 4. Variation in volumetric water content for a normal year shown for depths 0, 0.5, 2.0 and 5.0 m; vertical section in the middle of the slope

Monthly extreme events
The extreme situations are based on 100 years extreme rainfall values from Gardermoen. Infiltration has been taken as a factor of 0.6 times the monthly rainfall. In extreme periods there is s a general rise in ground water level (phreatic line) of 0.5 m. The water content in the top 5 m of soil increases. It is observed that a shorter

period of intense rainfall results in higher volumetric water content in the upper soil layer than a long period with lower rainfall depths. During extreme events the major changes occur in the unsaturated zone, while the position of the phreatic line changes very little. A detail study of the model's sensitivity towards varying geometric factors, boundary conditions etc. are given in Høydal and Skurtveit (2006).

Fall of year 2000

For analysis of the year 2000 event, daily precipitation rates and 6 hours time steps are applied. This result in large variations in suction close to the surface and changes in the flow patterns close to the slope surface. The water table gets another feeding compared with the average monthly data (Høydal and Skurtveit, 2006). The general ground water level increases by 0.9 m during the fall of year 2000. This is 0.9 m higher than for a normal year. Comparison of water content at 1.2 m depth shows that in year 2000, the maximum water content was 0.3 (Figure 5), but not higher than 0.25 at depth 0 - 5 m in the normal year (Figure 4). This corresponds to a drop in capillary suction of approximately 5 kPa in the extreme year. For a normal year, October is the month having the highest calculated water content in the ground, while in year 2000, November had the highest water content. Figure 5 also shows that the water content was higher than normally from April to August, but that the water content in the ground was normal in September just previous to the consecutive extreme autumn.
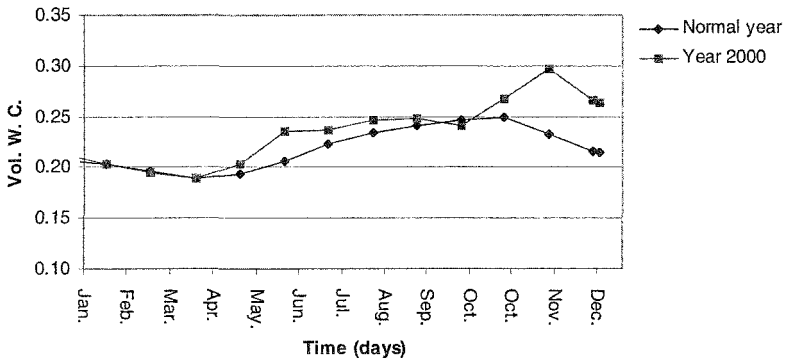
Figure 5. Comparison of water content for a normal year and in year 2000 at depth 1.2 m below ground surface (mid-slope).

SLOPE STABILITY

In the following, calculated slope stability through a normal year is compared with stability of the same slope calculated through the autumn of year 2000. Slope stability is calculated for deep-seated rotational failure surfaces and shallow slides.

Deep-seated, rotational failures

Reduced stability of deep-seated, circular shear surfaces may often be a result of a raised ground water level, and thereby reduced effective stresses. Also above ground

water level, effective stresses will be reduced, because the suction will be reduced due to increase in water content. However, the relative part of the shear surface which goes through the unsaturated zone will often be relatively small. Hence, the stabilizing effect of suction may be relatively small for deep-seated, circular shear surfaces.

Shallow slides

The mechanism for triggering of shallow (translational) slides in layers close to the surface are somewhat different from the mechanism for triggering of deep-seated, rotational failures. Commonly, water saturation reduces the strength of the top layer, which under normal circumstances is unsaturated. The depth of a shallow slide is strongly connected to presence of vegetation cover and its root system.

Stability model

The computer program SLOPE/W (2004) was used to calculate stability of the model slope shown above. The general shear strength formulations by Fredlund et al. (1978) for saturated and unsaturated conditions that are implemented in Slope/W are applied. The soil strength is characterized by the soil parameters cohesion c', effective friction angle ϕ', and contribution from suction given by ϕ^b, in addition to saturated and unsaturated weight. Different sets of shear strength parameters are applied where the cohesion ranges from $5-10$ kPa, unsaturated friction angle from $0 - 30°$, and saturated friction angle from $27 -$ to $30°$. For the stability calculation, a uniform soil model is applied. Circular shear surfaces and non-circular shallow shear surfaces and their corresponding safety factors have been calculated with the limited equilibrium method "Morgenstern-Price". Stability calculations were performed for each month and for specific events, using the pore pressure resulting from the corresponding flow analyses in SEEP/W (2004). During winter time, the safety factor is probably somewhat underestimated, because possible stabilizing effect of ground frost has not been included.

Figure 6 gives safety factor variation for circular failure surfaces in a normal year, friction angle 30°, cohesion of 5 kPa and unsaturated friction angle ϕ^b of 15°. It should be noticed that the safety factors do not represent the same shear surface from one month to the next. On the contrary, the most critical shear surface from each month has been picked.

Figure 7 summarises the variation in safety factor through a normal year and in extreme events as a function of soil parameters for deep circular shear surfaces. Figure 7 also shows that the duration (1, 2 or 3 months) of the extreme rainfall does not have a large influence on the resulting safety factor for the model slope. This may be due to establishment of close to stationary conditions for the groundwater flow in the slope, which remains more or less unchanged for these durations of rainfall. The difference between safety factor in the normal year and in the extreme events increase as a result of increasing value of ϕ^b.
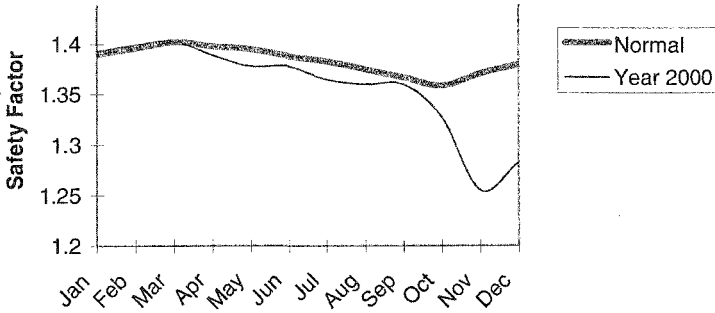
Figure 6. Seasonal variation of deep circular shear surfaces in normal year and throughout the extreme year 2000.
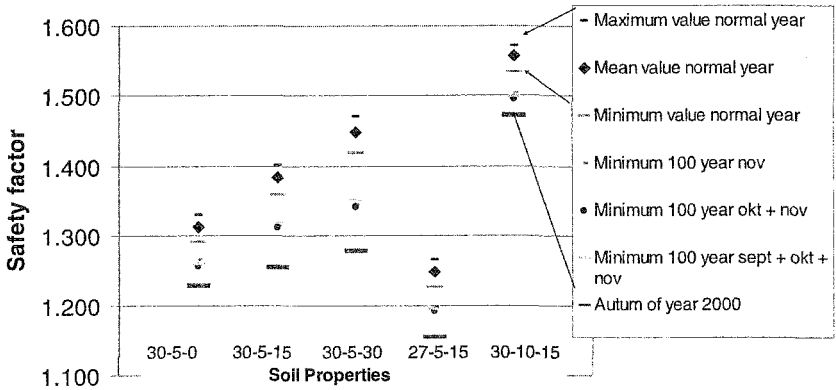
Figure 7. Variation of safety factor in the normal year and in the extreme year calculated for different sets of material parameters. The parameter set 30 – 5 – 0 means effective friction angle ϕ' of 30°, cohesion c of 5 kPa and ϕ^b of 0° etc.

Further, it should be noticed that the absolute value of the safety factor is strongly dependent on the choice of strength parameters. The value of the safety factor therefore is mainly a question of scaling the parameters. In a normal year, the critical shear surface is typically located as a circle centered horizontally 1/3 upslope from the toe, and concurrent crossing the toe and the top of the slope. The shape of the safety factor contours does not change considerably from the normal year to the extreme year, but the most critical shear surfaces are shallower, and centred more around the lower part of the slope in the extreme year (saturated zone). This has the effect that deep-seated rotational failures in such slopes are not primarily a result of reduced suction in the unsaturated zone, but follow a general rise in ground water level in the slope, and may be analysed by classical geotechnical calculation methods. Along parts of the critical shear circle, the pore pressure may change from a small suction (negative pore pressure) to a small positive pore pressure value. This is for instance the case at the toe of the slope, where the flow analyses have shown

that water may break the ground surface considerably higher up in the slope in an extreme year than during a normal year. Comparing the same critical circles in a normal year, the safety factor is reduced from 1.36 in the normal year to 1.29 in the extreme year. The safety factor for the most critical shear circle in the extreme year drops from 1.39 in the normal year to 1.25 in the extreme year. Using dayily precipityation rates compared with montly precipitation rates gives only small influence on ground water level corresponding safety factor for deep circular shear surfaces.

Shallow surfaces
Calculations were performed to check the stability of shallow, translational slides. Figure 8 shows the model set up with 3 shallow shear surfaces. Figure 9 shows the results from these calculations. Slides are observed shortly after intense periods as shown in figure 10. It has been found that daily precipitation rates and 6 hour time steps are needed to investigate the variation of suction in the top layer. Courser grid or time step smooth out the interesting events. It is important to notice that the pore pressure (suction) variations are much greater for shallow than for deep circular surfaces. The absolute value of the factor of safety is strongly connected to the choice of parameters and to the slope angle. A shallow surface only intersecting the saturated part of the slope is not stable for the chosen parameter set. The absolute value of the reduction in safety factor during the rainy season increases with reduced depth of the shear surface. The absolute value of the safety factor decreases with increased depth of the shear surface. The response of high daily precipitation rates appears almost immediately, and daily precipitatin rates are required to study stability of shallow surfaces.

Safety margins
In Norway, the building code says that for landslide events affecting safety of humans, the nominal yearly probability of an event shall be $\leq 1/1000$, i.e. dwellings and urbanizations are designed for a "1000-year event" (KAM/MD, 1997, Statens Bygningstekniske Etat, 1997). Such rainfall events are difficult to estimate based on existing data records. However, a 100-year event may be estimated from the meteorological records. The rainfall values during the autumn of year 2000 in the South-East part of Norway, and especially in the month of November, fall far outside all observations made during the last 100 years (or as long as data are available). Therefore, it is not possible to evaluate exactly how extreme the rainfall during the autumn of year 2000 actually was, except from concluding that it was more extreme than a 100-year event. Based on figure 6 and 7, the safty margin should be at least 0,2.

CONCLUSION
Instability from a transient situation requires data in the same resolution as the problem itself. Daily precipitation rates are used as input, require timestep smaller than a half day. For assessment of deep circular slides in fine-grained soils (silt/clay), normal conditions can be established by use of monthly data, since the location of the

phreatic line is little sensitive to short-term variations in rainfall values. Hence, use of monthly rainfall data results in a satisfactory location of the ground water level.

A usual way of designing after an extreme event is to require a safety level that includes the experienced extreme situation. For the model slope this means that there should be a safety margin of at least 0.2 for the safety factor with respect to extreme rainfall periods, when compared to the lowest safety factor computed for the normal year.

For shallow shear surfaces the safety margin must be evaluated together with top soil properties, vegetation cover and root depth. The performed calculations show that the necessary safety factor margin may be in the order of 1.0 for the shallowest slides, however, the consequences of the slides will be reduced successively as the thickness of the slide is reduced.
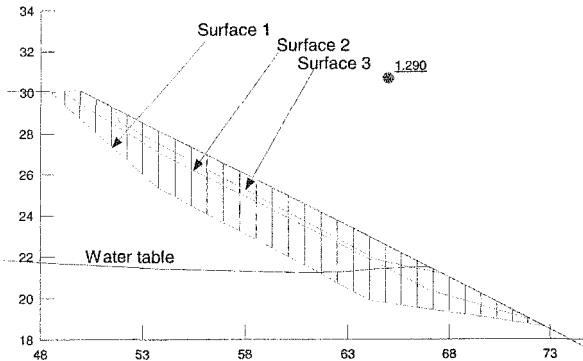
Figure 9. Arbitrary shear surfaces used for calculating safety factors through the fall 2000.
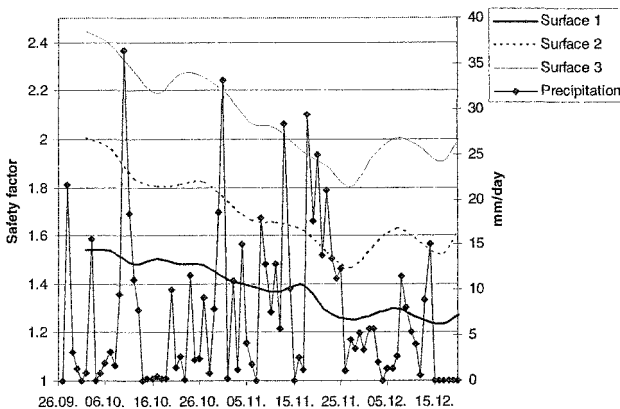
Figure 10. Variation in safety factor for the shear surfaces drawn in Figure 9 together with observed daily precipitation during the fall of year 2000.
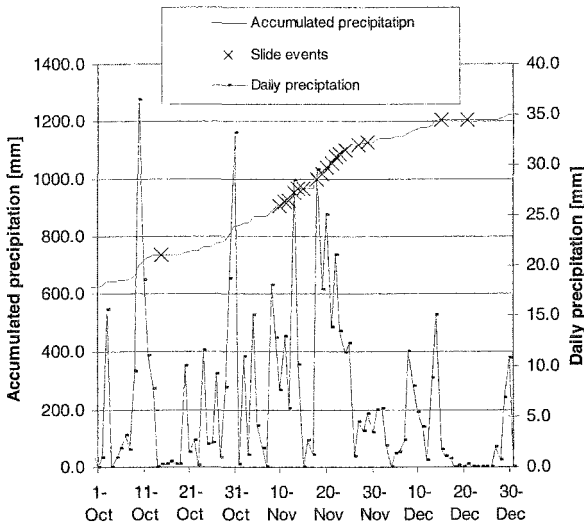
Figure 11. Rainfall data from Gardermoen meteorological station and slide events in the region

REFERENCES

-Dragset, T., 2002. *"Flommen på Sør- og Østlandet høsten 2000"*. Vann, mars 2002

-Fredlund, D.G. and Rahardjo, H. 1993. *Soil Mechanics for Unsaturated Soils*. John Wiley and Sons, Inc., pp. 517.

-Førland, E. J. 1992. *Manual for beregning av påregnelige ekstreme nedbørverdier*. DNMI rapport nr 21/92.

-Førland E.J 1984. *Påregnelige ekstreme nedbørverdier*. DNMI Fagrapport nr 3/84 Klima.

-Høydal, Ø. A., Skurtveit, E, 2006. *Experience from Modelling of Pore Pressure in a Partly Unsaturated Slope*, Submitted to Unsaturated Soils 2006.

-Jaedicke, C, Kleven, A, 2006. *Long term precipitation and slide activity in south-eastern Norway, autumn 2000*, submitted to Hydrological Processes

-KAM/MD (1997), *Arealplanlegging og utbygging i fareområder*. Rundskriv T-5/97.

-SEEP/W, Version 5.19. GEOSLOPE International, Copyright © 1991-2004.

-SLOPE/W, Version 5.19. GEOSLOPE International, Copyright © 1991-2004.

-Statens Bygningstekniske Etat (1997), *Forskrift til byggverk og produkter til byggverk,* Teknisk forskrift til plan og bygningsloven av 1985

Evaluation of the failure mechanism of an unsaturated tropical soil slope

de Campos, T.M.P.[1]; Moncada, M.P.H.[2]; Velloso, R.Q.[2]; Amaral, C.P.[3] & Vargas Jr. E.A.[4]

[1]PhD, DIC, Associated Professor, Civil Eng. Dept, Pontifícia Universidade Católica do Rio de Janeiro (DEC/PUC-Rio), Rua Marquês de São Vicente 225, Gávea, 22.451-900, Rio de Janeiro, RJ, Brazil, PH (21) 3114-1190, FAX 3114-1195, tacio@civ.puc-rio.br
[2]D.Sc Students, DEC/PUC-Rio, mopri@civ.puc-rio.br; raquelvelloso@yahoo.com.br
[3]D.Sc, Assistant Professor, DEC/PUC-Rio, camaral@civ.puc-rio.br
[4]PhD, DIC, Associated Professor, DEC/PUC-Rio, vargas@civ.puc-rio.br

Abstract

The paper presents results of studies performed at PUC-Rio to evaluate the mechanism of failure of a natural slope in Nova Friburgo, Rio de Janeiro, Brazil. The slide provoked the death of two people and important material losses. It happened in a profile of unsaturated gneissic residual soil. Failure occurred in a period of low precipitation, a few days after the rupture of a water pipe buried in its top portion. In an attempt to understand the mechanisms that caused failure, field and laboratory investigations were carried out and stability and flow analyses were performed. Flow analyses were executed using a 2D finite element saturated-unsaturated flow program. Resulting pore pressures were used in 2D stability analyses under different scenarios. Also analyses were run to have an assessment of 3D effects on the slope failure. It was verified that failure was caused by the rupture of the water pipe.

Introduction

The understanding of mechanisms or causes of failure of natural slopes is of utmost interest as it provides an insight on how to predict and, consequently, prevent the occurrence of such type of accident. This paper presents results of investigations performed at PUC-Rio aiming to evaluate failure causes of an unsaturated natural slope located in the city of Nova Friburgo, state of Rio de Janeiro, Brazil. Such failure, that occurred in the morning of April 12th, 2004, provoked the death of two people; the total destruction of a house; the partial destruction of another one, damages to circa of other three houses and the obstruction of a runway.

The investigations herein reported comprised a detailed geological survey, the execution of field and laboratory tests and of saturated-unsaturated flow and stability analysis.

Background Information: The area in which the accident occurred is described in de Campos et al. (2005). It is characterized by the presence of vegetated, plan-convex soil slopes, with inclination varying from 35° to 50°. The slopes are typically composed of biotita-gneiss weathered profiles, with a 1 to 3m thick mature soil layer (red-coloured mature residual soil and/or colluvionar soil, with a sandy-clay texture) and more than 15m thick saprolitic soil layer (white to yellowish coloured young residual soil, with a sandy texture). Outcrops of decomposed/sound rock are rare in the area.

The landslide (Figure 1) occurred between two streets, opened more than five years before. The movement had a typical tongue shape, with a length of some 25m and width of 15m. Besides the mature and saprolitic soil layers, it was identified the occurrence of a fill material, from 0 to 0.50m thick, as a top soil layer. Behind the destroyed houses there was a vertical cut of circa 2.5m contained by a brick wall with no drainage outlets.

Considering information from local people, the movement happened in two steps. The first, catastrophic, comprised a shallow movement at the upper part of the slope, encompassing essentially the mature/fill materials. The second movement occurred some half of an hour later, downstream of the first movement. It was characterized by a debris flow process associated with the material previously collapsed. This second movement is not considered in the investigations herein reported.

No natural water sources were observed, with a permanent water course being found some 60m below the base of the first movement. Thus the ground water table at the site would be fairly deep. On the other hand, local people indicated that a water pipe, connected to the main water supply pipeline, located in the road upstream of the accident, had been leaking for at least three days before, with the pressurized water reaching some 4m of height. Thus, it was understood that the main mass movement occurred in an unsaturated soil profile, with the landslide having been potentially caused by an increase of pore-pressures due to water infiltration in the natural slope.
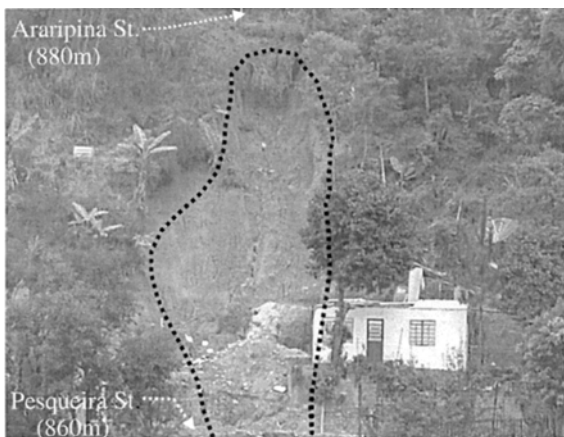
Figure 1. Frontal view of the accident (July, 2004)

Field and Laboratory Investigations

Field investigations comprised a topographic survey of the area, retrieval of undisturbed samples of the materials exposed in the scar of the landslide, execution of four SPT sounding boreholes (down to some 20m, with no indication of ground water table) and of hydraulic conductivity tests, and the determination of profiles of water content. Figure 2 shows a partial topographic plan of the site, with the location of the field investigation points, and Figure 3 shows the geological profiles corresponding to post and pre failure conditions.
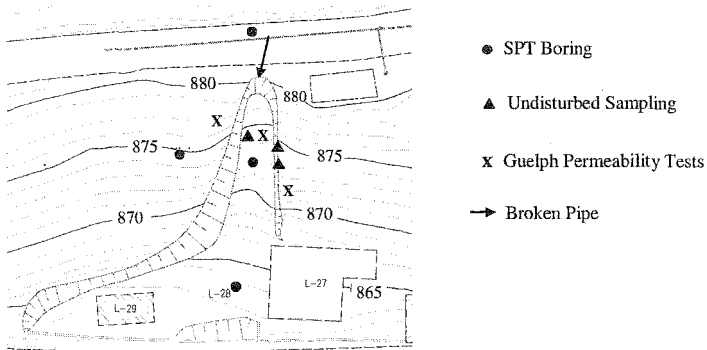
Figure 2. Topographic plant with location of site investigation points
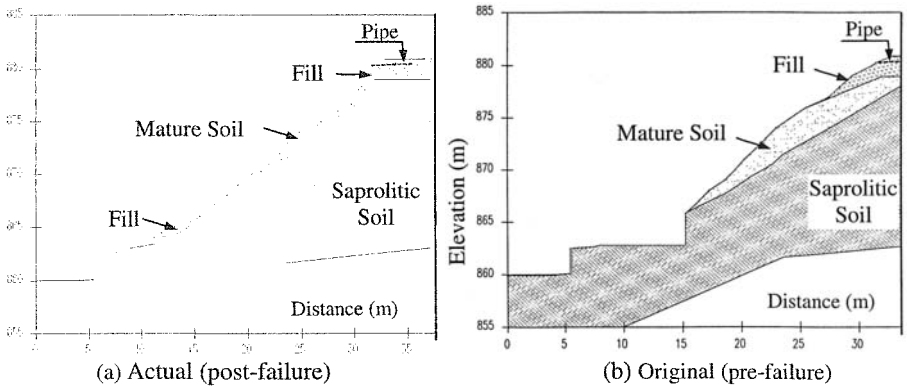
(a) Actual (post-failure)   (b) Original (pre-failure)
Figure 3. Soil profile

Hydraulic conductivity tests were run using a Guelph permeameter (e.g. Campos et al., 1992; Moreira et al., 1997). The results obtained, summarized in Table 1, indicate the occurrence, around the depth of 0.40m, of a saturated permeability, k_s, in the mature soil, some two orders of magnitude smaller than that observed in the underlying saprolitic soil. Field observations suggested that such hydraulic discontinuity would occur near the contact of the saprolitic with the mature soil.

Table 1. Results of hydraulic permeability field tests

Soil	Depth (m)	k_s (m/s)
Mature	0.20	4.5×10^{-6}
	0.40	5.5×10^{-8}
Saprolitic	0.20	2.8×10^{-6}
	0.40	9.3×10^{-6}

Besides soil characterization, laboratory tests comprised permeability tests on saturated samples, determination of soil-water retention curves and drained direct shear tests.

Characterization tests: Tables 2 and 3 show, respectively, results of characterization tests and average physical indices of the soils from the profile. The mature and fill materials have similar grain size distribution, presenting fines of low activity. The saprolitic soil is essentially a sandy material. Under an optical microscope it was observed that it is composed essentially of quartz and feldspar, which is in agreement with the obtained value of G_s (specific gravity of grains). The G_s values of the mature and fill materials, as well as their low activity, indicate that their main clay mineral may be kaolinite. Thus, *no expansive materials are present in the profile.*

Table 2. Results of soil characterization tests

Soil	Grain Size (%)				Atterberg Limits (%)			G_s
	Gravel	Sand	Silt	Clay	w_L	w_P	PI	
Fill	8.9	55.5	19.5	16.1	37.4	28.0	9.4	2.58
Mature	5.9	53.3	22.2	18.7	46.1	29.3	16.9	2.60
Saprolitic	2.5	85.5	9.2	2.8	-	-	NP	2.63

Table 3. Average physical indices

Soil	γ_t (kN/m³)	γ_d (kN/m³)	w (%)	e	S (%)
Fill	14.18	12.09	17.34	1.09	41.0
Mature	13.81	11.39	21.23	1.23	44.7
Saprolitic	15.21	14.08	8.02	0.79	26.0

Saturated Permeability and Soil Moisture Retention Curve: Saturated permeability was determined using flexible wall permeameters, with samples isotropicaly consolidated to two different effective stresses, σ', after back-pressure saturation. The results, shown in Table 4, were equivalent to those obtained in the field (see Table 1).

Table 4. Saturated permeability

k_{sat} (m/s)		Fill Soil	Mature Soil	Saprolitic Soil
σ' (kPa)	10	5.2×10^{-6}	6.2×10^{-6}	3.0×10^{-6}
	50	3.9×10^{-6}	1.9×10^{-6}	2.6×10^{-6}

The soil moisture retention curves (SMRC or SMCC) of the three materials (Figure 4), were obtained using the filter paper technique (e.g. Marinho, 1994; Vilar & de Campos, 2001). Following recommendations by de Campos et al. (1992), specimens were wetted or dried from their natural moisture content in order to obtain each data point of the curve. With this procedure it is believed that it is obtained a better representation of the SMRCs of the materials as they suffer non extreme processes of

wetting and drying from their natural water content. As no noticeable volume change was observed in the drying/wetting processes of the specimens of the three soils, the volumetric water content (Figure 4) was directly obtained from measured gravimetric moisture contents.
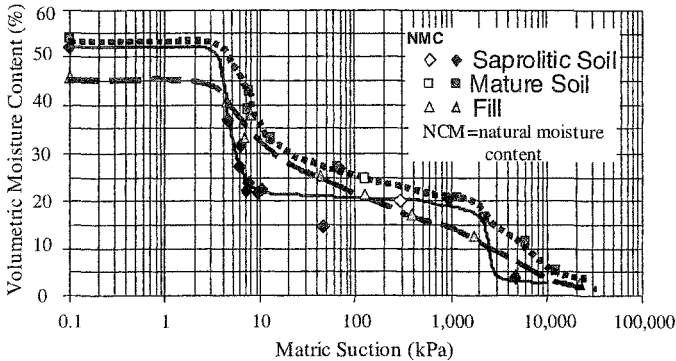
Figure 4. Soil-moisture retention curves

Shearing Strength: Table 5 shows the shear strength parameters of the tested materials, obtained from drained direct shear tests performed on vertically moulded samples, soaked prior to application of the vertical stresses. These results indicate that, under conditions close to saturation, the saprolitic soil has higher strength than the mature and fill soils, which essentially, have the same shearing strength.

Table 5. Shearing strength parameters

Soil	∅' (degree)	Cohesion c' (kPa)
Fill	30.6	0
Mature	30.9	0
Saprolitic	35.0	0

Flow Analysis

Saturated-unsaturated flow analyses were performed using the SWMS_2D computer code, developed by the U. S. Salinity Laboratory (Simunek et al., 1994). This software simulates 2D flow in a variable saturation media, solving Richards' equation (e.g. Lu & Likos, 2004) by the finite elements method. The geometry adopted in the flow analyses is shown in Figure 3a. The finite element mesh used, with 17.047 elements and 8.790 nodes, was refined in the contact between the mature and the saprolitic soil, being generated using pre-processors developed at PUC-Rio.

Hydraulic Properties: In the SWMS_2D programme, hydraulic properties are described by the equations of van Genuchten (e.g. Simunek et al.., 1994), which require the knowledge of the residual volumetric water content, θ_r, the saturated volumetric water content, θ_s, the saturated permeability, k_s, and of the fitting parameters n and α.

Values of the hydraulic parameters used in the present study are shown in Table 6. The saturated permeability was defined considering the results of both field and laboratory tests. The volumetric water contents θ_r and θ_s were taken from the SMRCs obtained in the laboratory. The parameters n and α were defined by fitting the model of van Genuchten to the experimental data shown in Figure 4.

Table 6. Hydraulic parameters

Soil	θ_r	θ_s	α (m^{-1})	n	k_s (m/s)
Fill	0.11	0.46	1.9	1.40	5.2×10^{-6}
Mature	0.19	0.54	2.4	1.55	6.2×10^{-6}
Saprolitic	0.10	0.52	5.0	1.50	3.0×10^{-6}

Boundary and Initial Conditions: The boundary conditions imposed in the flow modelling comprised atmospheric conditions (precipitation and evaporation) in the slope and impermeable contours at the streets, at the brick wall behind and at the base of the destroyed house, and at the bottom and right lateral limits of the flow domain.

Rain water precipitation data used in the simulations, taken from climatologic stations closer to the site, are reproduced in Figure 5. It is interesting to mention here that higher rain intensity and duration occurred in the area in previous years. A potential evaporation of 45.7 mm/month was adopted. That corresponds to the average potential evaporation for the month of April in the period from 1961 to 1990.
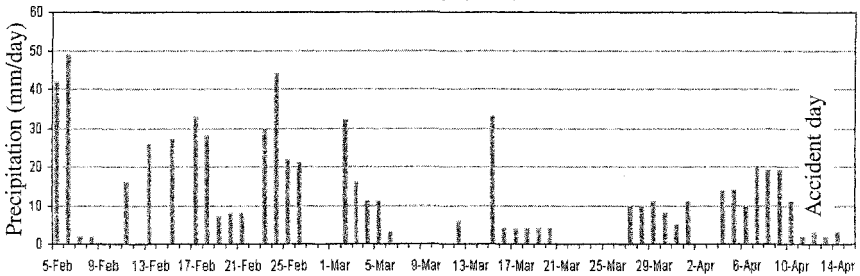
Figure 5. Rainfall data used in the flow analysis simulations

The adopted initial hydraulic heads, h_p, constant with depth for each soil, are presented in Table 7. These values were defined considering the soil moisture retention curves of the materials, taking as a basis a profile of natural water content obtained at the time of the field investigations as well as the average moisture content of the undisturbed samples collected in the field.

Table 7. Adopted initial suction conditions

Soil	$\theta_{initial}$ (%)	h_p (m)
Fill	0.22	-7.5
Mature	0.22	-20.0
Saprolitic	0.18	-2.0

Obtained Results: Four cases were considered in the flow analysis; all involving rain water infiltration and evaporation processes in the soil slope:

<u>Case 1a</u>: Soil profile with no hydraulic conductivity discontinuity and no leakage from the water pipe at the top of the slope;
<u>Case 2a</u>: Soil profile with no hydraulic conductivity discontinuity but with leakage from the water pipe at the top of the slope;
<u>Case 1b</u>: Soil profile with a hydraulic conductivity discontinuity at the contact of the mature and saprolitic materials and no leakage of the water pipe at the top of the slope;
<u>Case 2b</u>: Soil profile with a hydraulic conductivity discontinuity at the contact of the mature and saprolitic materials and leakage of the water pipe at the top of the slope.

To simulate leakage of the water pipe, constant water pressure heads of 0 and 1m were imposed at the point it was broken.

Full saturation of the slope did not occur in any of the simulated flow cases, as exemplified in Figure 6. This Figure shows the evolution of the hydraulic head with time in three points lying on the surface of the slope, defined after failure, for cases analysed with the hydraulic head in the broken pipe equal to zero. In Point 1, at the top of the slope, the saturation front nearly reached the after failure slope surface
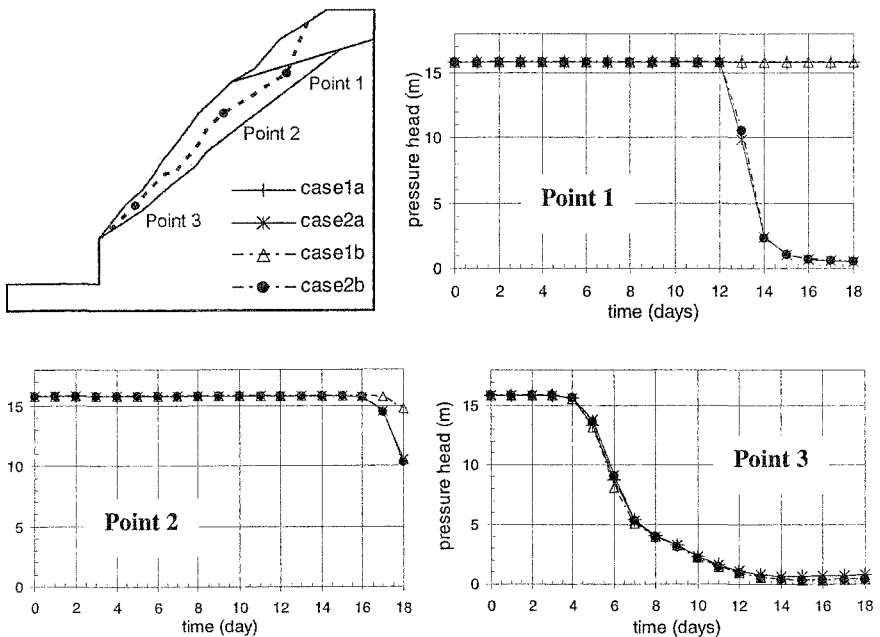
Figure 6. Hydraulic head evolution with time with $h_p = 0$ at the broken pipe

(AFSS) in which pipe failure was not accounted for, no change in suction occurred in this point. The same happened at Point 2 for the four cases considered. At this point some decrease in suction only started on the day the slope failed. At Point 3, at the bottom of the slope and much closer to the slope surface, no effect of the hydraulic discontinuity or of the broken pipe was observed. Suction started to decrease on the fourth day of simulation and the saturation front reaches the AFSS some two days before the day of failure.

In the simulations with a constant water pressure of 1m at the broken pipe, the same general flow pattern shown in Figure 6 was observed, with an important exception at the top of the slope for Case 2b, as will be seen later.

Slope Stability Analyses

Slope stability analyses were performed using limit equilibrium methods applied to planar and non-planar slip surface configurations.

Planar Slip Surface: Owing to the three-dimensional (3D) geometry of the accident, two-dimensional (2D) and 3D analyses using the infinite slope method were employed to evaluate 3D effects in the instability process. Following Wolle (1988) and including the Mohr-Coulomb shear strength envelope equation modified by Fredlund et al. (1978), the following general expression was used in the infinite slope analyses of the unsaturated slope to obtain the safety factor SF:

$$FS=\frac{c'(L+2z\cos\alpha)+u_s(L+2z\cos\alpha)\tan\phi^b+(K_0z+L\cos\alpha)(\gamma.z+\Delta p)\cos\alpha\tan\phi'}{(\gamma.z+\Delta p)L\sin\alpha\cos\alpha} \quad (1)$$

where: c', L, z, α, ϕ^b, K_0 and Δp are defined in Table 8, γ = total unit weight of the soil and u_s = matric suction.

Assuming that the failure surface occurred in the contact between the saprolitic and the mature soil, the following pore-pressure conditions were considered: (a) unsaturated profile, with the soil at its natural moisture content; (b) unsaturated profile with a constant suction of 10 kPa; (c) saturated profile without any pore-pressure generation (u=0) and (d) saturated profile, with positive pore pressures generated by flow parallel to the slip surface, with the phreatic surface positioned at different heights above the top of the saprolitic soil.

Table 8 shows the values adopted for the parameters required in the analyses. The value of K_0 derived from results obtained in laboratory tests performed in a gneissic residual soil using a suction controlled K_0 cell (Daylac & de Campos, 1994). The vegetation load surcharge, simulating conditions of an area lithely vegetated, was taken from Wolle (1988). The ϕ^b parameter was assumed as being equal to the ϕ' parameter, obtained in the drained direct shear tests earlier referred to. The other shear strength and geometric data show in Table 8 were inferred either from results of laboratory tests (Figure 5) or from field data.

Table 8. Parameters adopted in the infinite slope stability analyses

		2D	3D
Depth to slip surface	z (m)	2.30	2.30
Average width of the slip surface	L (m)	-	3.50
Angle of the slip surface with horizontal	α (rad)	0.52	0.52
Angle of shearing strength	ϕ'(rad)	0.54	0.54
Cohesion	c'(kPa)	0.00	0.00
Angle that shows the rate of increase in strength with suction	ϕ^b (rad)	0.54	0.54
Coefficient of earth pressure at rest	K_0	-	0.35
Vegetation load	Δp (kPa)	0	0

Table 9 shows results obtained. It is verified that three dimensional effects are important in the present case, implying in an increase of the safety factor above 30% from the 2D to the 3D analyses. Furthermore, it is verified that the slope would be stable under its natural moisture content, with instability occurring only if it were saturated, particularly if a water table would develop above the assumed slip surface.

Table 9. Safety factors obtained using the infinite slope method of analysis

Condition		2D	3D
Natural moisture content		7,96	14,8
Suction of 10 kPa		1,48	2,26
S=100%, Pore water pressure = 0		1,05	1,32
S=100%, Pore water pressure > 0 (flow parallel to slope)			
Position of the phreatic surface above the slip surface	1,00m	0,78	1,06
	0,50m	0,91	1,19
	0,10m	1,02	1,30

Non Planar Slip Surface: These were performed using the Morgenstern & Price limit equilibrium method provided in the software Slope/W (Krahn, 2004), which includes the possibility of analysing unsaturated soil slopes. The same shear strength parameters adopted for the previous set of analysis were employed in this second set, which comprised four series of 2D analyses considering different pore water pressure conditions and different ways to define the potential slip surface.

In the first series of analyses it was assumed that the whole profile would be fully saturated by rain water infiltration and that potential failure surfaces would be close to the defined non-planar after failure surface. Two situations were considered: (a) initial rupture of the upper part of the slope and, (b) initial rupture of the lower part of the slope. Figure 7 shows the position of such pre-defined slip surfaces as well as the safety factors (SF) obtained. In all three situations the safety factor was smaller than one. Considering the results obtained in the finite slope analyses, such results could be explained by the non consideration of 3D effects in the slope failure. On the other hand, the results indicated in Figure 7 suggest that failure of the slope would have been initialised by a movement at the lower part of the slope (smallest SF in Fig. 7). This, however, is not consistent with the information that initial rupture occurred in the upper part of the slope (highest SF in Fig. 7). Therefore, these results indicate that full saturation of the whole slope may have not happened.

Surface No.	Safety Factor
1 - Upper slip surface	0,89
2 - Lower slip surface	0,80
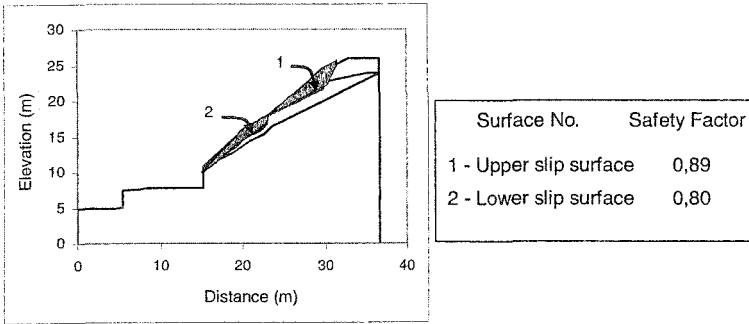
Figure 7. Pre-defined slip surfaces considered in the stability analyses

The second series of analyses comprised automatic search of critical slip surfaces in the saturated profile, including the possibility of existence of a crack in the fill material, at the top of the slope. Again, the lowest safety factor was obtained with failure happening first at the lower part of the slope. Furthermore, the results obtained were not satisfactory, as the generated critical surfaces did not show any agreement with field observations. This provided further evidence that full saturation of the slope was not responsible for its failure and reinforced the possibility of occurrence of a continuous layer of soil with lower permeability in the slope, as indicated in Table 1 and assumed in the flow analyses (Cases 2a and 2b in Figure 6).

In the third series of analyses it was considered the occurrence of pore pressures derived from rain water infiltration in the slope and from water infiltration under zero pressure head from the broken pipe, with the pore water pressures being given by the results of flow analyses corresponding to the day of failure. The lowest safety factor obtained in these analyses, with automatically generated potential slip surfaces compatible with field observations, was 1,22. As such results were not satisfactory, a further analysis was carried out.

In the fourth series of stability analysis it was considered the occurrence of a hydraulic discontinuity above the saprolitic soil and a water pressure head of 1m acting at the broken pipe positioned in the top of the slope. It is interesting to remember here that information collected at the site indicated that the broken pipe was spurting water to a height about 4m above ground level. Therefore, even considering that the water pressure in the broken pipe is unknown, the adopted hydraulic head was considered as being realistic. Figure 8 shows the obtained results.

As indicated in Figure 8a, positive pore water pressures arise in the slope near the point of rupture of the water pipe and at the bottom of the slope. Owing to that, an automatically generated critical slip surface, compatible with field observations, occur in the top part of the slope (Figure 8b). The safety factor obtained (SF = 0.90) is smaller than unity. Considering, however, the results from the 2D and 3D planar slip surface analyses performed, 3D effects would increase this obtained safety factor to a value close to 1.
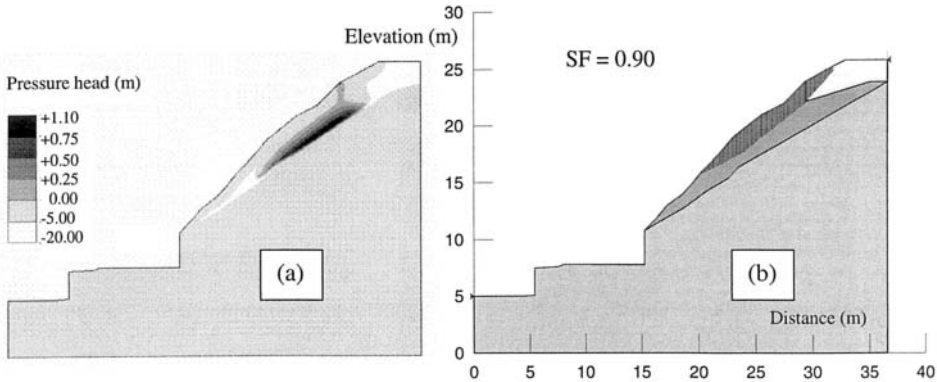
Figure 8. **Results of (a) flow and (b) stability analyses with hydraulic discontinuity in the profile and a hydraulic head of 1m at the broken pipe**

Conclusions

The studies herein presented comprised a vast range of field and laboratory investigations and of flow and stability analyses, designed to provide a definition of the mechanisms that may have caused the failure of a natural slope constituted by an unsaturated residual soil profile.

Even considering the inherent complexity associated to the type of problem in question, the employed methodology provided enough information that permit to conclude that failure of the slope was not due to full saturation of the residual soil slope, as it is usually assumed and would be expected in the case analysed.

A progressive saturation of the soil slope as a consequence of rain water infiltration, by itself, does not also explain the failure, even in the presence of a low permeability soil layer near the contact between the saprolitic and the mature soils. Indeed, if that were to be the cause of failure, the slope should have collapsed years before, when higher intensity and duration storms occurred in the area.

The rupture of a water pipe diversion at the top of the slope, when considered as leaking under zero water pressure condition, did not provide, as well an explanation for the failure. However, when a pressure head of 1m was imposed in the broken pipe and considered the presence of the hydraulic discontinuity layer, positive pore pressures developed in the top part of the slope. The simple, conventional infinite slope method of stability analysis indicated that such condition was required to take the slope to failure in both cases of 2D and 3D configurations. The more sophisticated, non planar stability analyses performed in sequence, confirmed that the slope failure was essentially due to the rupture of the pipe at the top of the slope. The final results of the stability analyses also indicated that slope failure occurred under 3D conditions.

References

Campos, J.L.E.; Vargas Jr., E.A. & de Campos, T.M.P. (1992). Field evaluation of the saturated-unsaturated permeability of soils in slopes. 1st Brazilian Conference on Stability of Natural Slopes - 1ª COBRAE, Rio de Janeiro, RJ, V. 1, 371-382 (in Portuguese).

Daylac R. & de Campos, T.M.P. (1994). Development of a K_0 cell with suction control. X Brazilian Congress on Soil Mechanics and Foundation Engineering, Foz do Iguaçu, PR, Vol. 2, 405-412 (in Portuguese).

de Campos, T.M.P., Delgado, C.C., Tibana, S., Aguilar, S.A.S. & Fonseca, E.C. (1992). Determination of the soil moisture characteristic curve in laboratory. 1st Brazilian Conference on Stability of Natural Slopes - 1ª COBRAE, Rio de Janeiro, RJ. V. 3, 853-871 (in Portuguese).

de Campos, T.M.P.; Amaral, C.P.; Moncada, M.P.H. & Veloso, R.Q. (2005). Preliminary evaluation of causes of failure of a natural slope in Nova Friburgo, RJ. IV Brazilian Conference on Stability of Natural Slopes – 4th COBRAE, Salvador, BA. (in Portuguese – in press).

Fredlund, D.G., Morgenstern, N.R. & Widger, R.A. (1978). Shear strength of unsaturated soils. Canadian Geotechnical Journal, 15,No. 3, 313-321.

Krahn, J. (2004). Stability Modeling with SLOPE/W. GEO-SLOPE/W Intern., Ltd.

Marinho, F.A.M. (1994). Suction measurement with the filter paper technique. X Brazilian Congress on Soil Mechanics and Foundation Engineering – Foz do Iguaçu, PR, V. 2, 515-522 (in Portuguese).

Moreira, B.D.M.; Vargas Jr., E.A.; de Campos, T.M.P. & Antunes, F.S. (1997). Study of a method for the determination of the saturated-unsaturated hydraulic conductivity of a soil from a natural slope in Rio de Janeiro. Unsaturated Soils. de Campos & Vargas Jr. Ed. - Editora Freitas Bastos, 3rd Brazilian Symposium on Unsaturated Soils, Rio de Janeiro, RJ, V. 2, 581-592 (in Portuguese).

Lu, N. & Likos, W.J. (2004). Unsaturated Soils Mechanics. John Willey & Sons, Inc.

Simunek, J., Vogel, T. & van Genuchten, M. Th. (1994). The SWMS_2D code for simulating water flow and solute transport in a two-dimensional variably saturated media. U. S. Salinity Laboratory, U. S. Department of Agriculture, Riverside, CA, USA.

Villar, L.F.S & de Campos, T.M.P. (2001). Obtaining the suction characteristic curve through the combined use of different methods. 4° Brazilian Symposium on Unsaturated Soils, Porto Alegre, RS, pp. 337-345 (in Portuguese).

Wolle, C. W. (1988). Analysis of translational landslides from an area of Serra do Mar within the context of a classification of natural slope instabilization mechanisms. D.Sc. Thesis. Escola Politécnica da Univ. de São Paulo. 406p (in Portuguese).

Cyclic Stress-Strain Behavior of Partially Saturated Soils

Selim Altun[1], A. Burak Göktepe[2]

[1]Department of Civil Engineering, Ege University, 35100, İzmir, Turkey; PH +90(232)388-6026; FAX +90(232)3425629; email: selim.altun@ege.edu.tr
[2]Department of Civil Engineering, Ege University, 35100, İzmir, Turkey; PH +90(232)388-6026; FAX +90(232)3425629; email: burak.goktepe@ege.edu.tr

Abstract

Although soils are generally assumed to be fully saturated below the groundwater table, they may be semi-saturated or near the state of full saturation under certain conditions. The situation of partial saturation may be caused by several factors, such as variation of water table level due to natural or manmade processes. It is known in geotechnical engineering that partially saturated soil is usually of higher strength and lower compressibility. Additionally, recent studies have shown that unsaturated soil can also cause much greater amplification in ground motion than a fully saturated model and has more resistance to liquefaction of sandy soils. The resistance of sand to onset of liquefaction tends to increase with a reduction in the saturation ratio of soil specimens; this was expressed in terms of the Skempton's pore pressure coefficient, B. Since the B-value is defined as the ratio of the induced pore water pressure to the applied effective confining stress, this can be easily obtained in the laboratory. The Skempton B-value method has been widely used to determine the state of saturation of laboratory soil specimens.

In order to examine the stress-strain behavior and the strain softening response of partially saturated cohesive soil, this study used a cyclic torsional shear apparatus, allowing for cyclic shear tests on the specimens under undrained conditions. This series of shear tests was conducted on partially saturated-undisturbed clay samples and the stress-strain properties were investigated to identify the saturation degree of the near-saturated samples. Undisturbed clayey specimens were subjected to multi-staged cyclic torsional shear stress, and deformation characteristics of soils, such as the variations of the shear modulus and damping ratios, were evaluated in terms of the saturation ratio. For the cyclic phase of torsional tests, the degradation curves were shown to move to the right with a decreasing Skempton B-value. It was also observed that the initial values of the shear modulus considerably affected the Skempton B-value.

Introduction

Compacted soils used in earth structures, especially in pavements, are in an unsaturated state during construction and, in some cases, during operating conditions. Therefore their behavior is influenced by the simultaneous existence of water and air in the pore spaces. Because of the difference in compressibility of the pore fluid phases and because of matric suction, the behavior of unsaturated soils is more complicated than completely saturated or completely dry soils. In spite of the clear facts of this behavior, there has only been minimal investigation into the response of soil used in construction (Deshpande and Muraleetharan 1998, Rampino et al. 1999). Water content, in addition to plasticity, mineralogy, etc., has been shown to have a large effect on cohesive subgrade material response, but attempts to quantify this effect have mainly been through empirical methods (Bishop and Blight 1963, Alonso et al. 1990, Li 2000).

Additionally, despite the fact that the small strain behavior of soil is the key function in estimating the performance of earth structures, only slightly interest has been devoted to this subject (Qian et al. 1991). Some investigations have recently been carried out to explore the small strain behavior of unsaturated soils using laboratory techniques or theoretical approaches (Drumm et al. 1997, Hardcastle and Sharma 1998, Butalia et al. 2002, Mancuso et al. 2002). However the studies performed on undisturbed samples in laboratory are rare (Talesnick and Frydman 1990).

Moreover, determining the large strain behavior of subgrade material is also crucial in evaluating the liquefaction or strain softening response of soils. There have been only limited investigations into large strain behaviors under unsaturated soil conditions for both granular and cohesive materials (Sherif et al. 1977, Xia and Hu 1991, Ishihara et al. 2001, Yang et al. 2004) These investigations have, however, demonstrated that these behaviors depend strongly on the degree of saturation, generally expressed in terms of the pore pressure coefficient B.

In this study, an experimental study was carried out using a torsional shear testing apparatus to investigate the small and large strain behavior of unsaturated-undisturbed silty clay. This study concerns the evaluation of the small strain and cyclic strength properties of cohesive materials as used in design and structural evaluation of flexible pavements. Based on the results of a cyclic torsional test program performed on undisturbed silty clay samples it has been shown that the cyclic response of cohesive materials is considerably by the degree of saturation. In detail, the small stress-strain and strength parameters for undisturbed cohesive soils were obtained for saturated and unsaturated conditions using the effective stress principle (Fredlund and Rahardjo 1993).

Saturation Conditions

Degree of saturation is a factor that reflects the combined effect of density and moisture content. The degree of soil saturation (S) can be described as

$$S = \frac{\omega \cdot G_s}{e} \qquad 0 \leq S \leq 1 \tag{1}$$

where e is void ratio, ω is gravimetric water content, and G_s is the specific gravity of solids. Gravimetric water contents in pavements are usually below 10% by mass of dry material, and dry soil unit weights (γ_d) are typically between 20.0 and 23.0kN/m^3.

Since the saturation ratio is a quantity requiring measurements of volume of a soil element, it is generally difficult to determine it precisely, particularly when the soil element is partly saturated and near the state of full saturation. In this case, the B-value has been used instead to quantify the state of saturation. As the B-value is defined as the ratio of the induced pore water pressure to the applied confining stress, this value is easily measured in the laboratory and accurate enough to indicate a state of partial saturation. Thus, the B-value has been widely used in laboratory soil testing to evaluate the degree of saturation of soil specimens. According to the earlier studies by Chaney (1978) and Yoshimi et al. (1989), the resistance to liquefaction has been shown to be roughly two times that of fully saturated samples, when the B-value drops to a level of about zero with a saturation ratio of about 90%. However, a crucial disadvantage of using either the B-value or saturation ratio is that it is practically impossible to monitor these quantities in soil deposits in the field. But in spite of this, evaluation of B-value in laboratory conditions and using this value is theoretically sufficient in some investigations.

Fredlund and Morgenstern (1977) suggested the use of two independent stress state variables to clarify the behavior of unsaturated soils. The most generally used state variables are the net normal stress, $\sigma - u_a$, and the matric suction, $u_a - u_w$, where σ is the total normal stress, u_a is the pore-air pressure, and u_w is the pore-water pressure. The pore air pressure can be calculated using pore fluid compressibility, and the pore-water pressure calculated by using the matric suction and the pore air pressure.

Test Material and Testing Procedure

The tested material

The tests were carried out on undisturbed tube samples of soft silty clay obtained from the Kocaeli Region in Turkey. These collected tube samples were extracted from a road construction area. The average depth of sampling was approximately between 7m to 8m. The soils typically comprised 2% gravel, 12% sand, 19% silt, and 66% clay, which can be described as low plastic silty clay with sand (CL) according to the Unified Soil Classification System (USCS), and their average value of specific gravity was $G_s = 2.69$. The liquid limit w_L measured was around 38%, and the plasticity index PI was 12%. The prior values of the moisture content were in the range of 20% and 24%. The classification tests on the soil were conducted in accordance with the procedures described in American Standards of Testing Materials (ASTM 1337 -2000). The above and other physical properties of the material are summarized in Table 1.

Table 1. Main physical properties of tested cohesive soil

G_s	Gravel (%)	Sand (%)	Silt (%)	Clay (%)	w_n (%)	w_L (%)	w_P (%)	I_p (%)
2.68~2.69	0~3	10~14	15~24	61~71	20~24	36~39	25~28	11~12

Test apparatus and specimen preparation method

In this study, hollow cylindrical torsional test apparatus was used to investigate the small and large strain behavior of unsaturated cohesive soil. The apparatus is capable of measuring and calculating many components (stresses, vertical and radial displacements, volume changes, variations of pore water pressure, etc.) using linear variable differential transducers (LVDT) and sensitive mechanical transducers during cyclic or monotonic shear tests. The specific volume changes of the specimen are inferred from the separate measurement of axial and radial displacements. The measurement of changes in water content was obtained through a system of two double-walled burettes coupled to a differential pressure transducer. The first burette was connected to the specimen drainage line and the second connected to the inner part of specimen.

The undisturbed tube sample of clay soil was obtained by using cutting tube methodology. The extricated soil sample was trimmed and drilled in order to obtain a hollow cylindrical specimen having 14cm in height, 4cm and 7cm in inner and outer diameter, respectively. During the process of trimming and drilling of hollow section, extra great care was paid because the soil samples were in unsaturated conditions. After the required measurements were made, the specimens were putted in flexible membranes both inner and outer sides.

Testing procedures and program

To investigate the small and large strain behavior of unsaturated soils, a torsional shear device was used at the İstanbul Technical University (Altun 2003). The testing procedure consists of three stages: evaluation of saturation level, compression, and cyclic torsional shear.

In the first stage, the specimen was subjected to a confining pressure of 20kPa. Then, the Skempton B-value was determined by increasing the confining pressure (σ_o) to 100kPa and measuring pore water pressure within the specimen. In the second stage, the confining pressure was increased to the required level, and the specimen was imposed to isotopic compression under this pressure. In this study, two values of confining pressure (100 kPa and 200 kPa) were used. Several series of cyclic torsional shear tests were performed at the end of the compression stages. To analyze strain-rate effects, each series was performed under stress-controlled condition and at loading frequency of 0.1Hz. Tests were initiated immediately after the end of compression to reduce time effects and thus obtain homogeneous data.

Two types of test were performed on undisturbed-unsaturated cohesive specimens. In the first type, in order to investigate small strain behavior of soil,

multi-stage torsional loading was applied to the specimen. In other words, very small cyclic shear stress level was initially utilized for five cycles, and then the stress level was increased progressively for each five cycles, not crossing over the elastic threshold strain of the soil. The elastic threshold was estimated from some methodologies using the criteria of Talesnick and Frydman (1992). Therefore, a very small strain behavior of soil could be evaluated with this methodology. In the second type, uniform cyclic loading was applied to the specimen to investigate the large strain behavior of soil. Thus, the effects of unsaturation on the strain softening response of cohesive soils were experimentally studied.

Test Results and Discussion

The testing of unsaturated cohesive specimens in hollow cylinder apparatus has rarely been reported in literature. The lack of such testing is in a large part due to difficulties in preparing undisturbed specimens from unsaturated samples. In order to overcome the difficulties of specimen preparation, some original techniques were developed.

Unsaturated tube samples were used in the tests. B-values of specimens measured during each experiment varied in the range of 0.27 and 0.72. The test results indicated the effects of B-value on small and large strain behavior of soil.

Small strain behavior

It has been believed that the stress strain behavior at small amplitude of a soil mass governs the velocity of wave spread through the soil. In addition, this is considered the most important factor in determining the dynamic response of foundations supported directly on soils. The characteristics of those stress-strain curves verify the range of strain associated with the elastic or inelastic response and identify the energy losses under cyclic loading.

In this study, a series of multi-stage stress amplitude tests were carried out on normally consolidated unsaturated cohesive samples in order to determine the influence of saturation level on the small strain response of soil. The maximum shear modulus, G_{max}, as well as the modulus degradation curves for each sample, were determined to evaluate the cyclic shear stress-shear strain properties and the difference between the soil samples with different water content. Some typical test records are given in Figure 1. In this figure, the variations of shear stress ($\sigma_{z\theta}$), shear strain ($\gamma_{z\theta}$) and pore water pressure (u) were obtained in terms of number of cycles. As seen in this figure, pore water pressure did not increase significantly at the beginning of loading.

In Fig 2, the variation of G_{max} depending on B-values was illustrated using the test results performed on samples having different B-values. It was concluded from this figure that initial shear modulus, G_{max}, decreases with increasing B-values. This result corresponds to those of similar researches recently performed and thus is expected result for clayey soil.
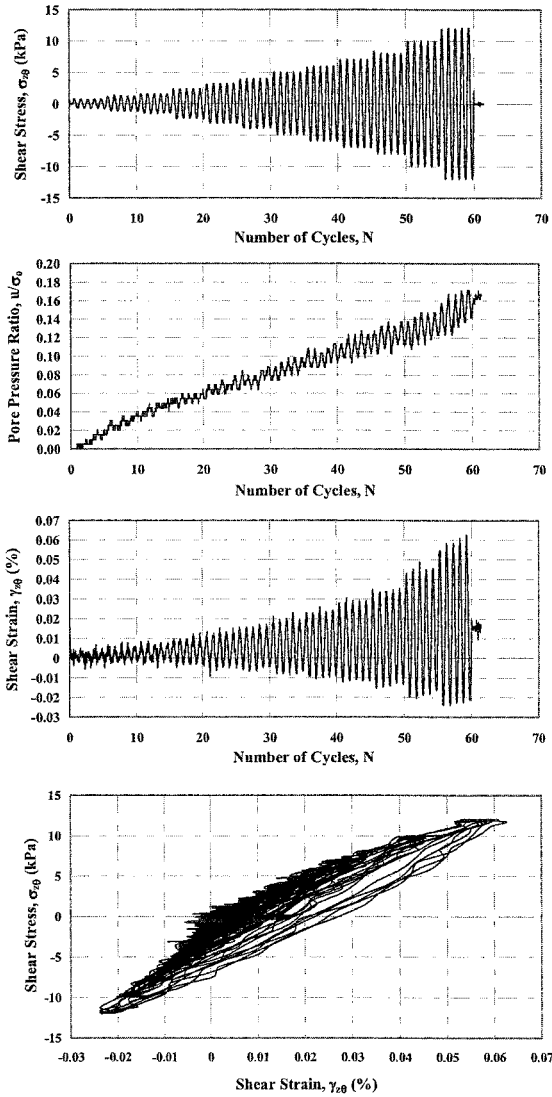
Figure 1. Typical test results in small strain state
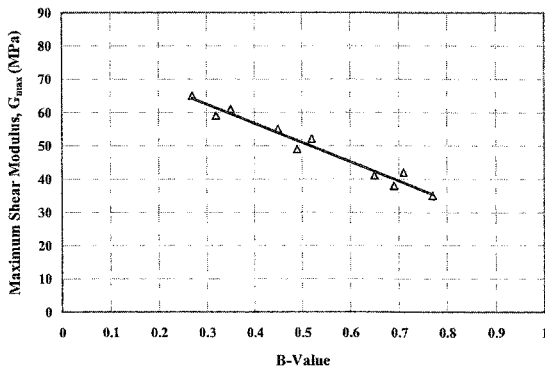
Figure 2. Effects of saturation condition on shear stiffness

Large strain behavior

The results of isotropic cyclic tests are showed in Fig 3. It may be seen in this figure that the pore water pressure did not develop sufficiently under uniform torsional shear stress. It was observed that shear strain amplitude increased progressively by the number of cycles. It is considered that differences in the stress--strain and strength characteristics from the literature are most likely due to the inherent variability of soil and testing procedure. Several studies (Yasuhara 1982, Talesnick and Frydman 1990, Usaborisut et al. 2001) have showed that unsaturated cohesive soil may exhibit limited flow deformation or strain softening behavior depending on the initial state, imposed stress amplitude and the number of cycles.

Test results under different B-values of pore pressure coefficient are illustrated in Fig. 4, in which the cyclic stress ratio is plotted against the number of cycles causing $\pm 5\%$ shear strain. It is clear that the strain softening resistance of clay increases significantly as the value of B decreases or, likewise, the degree of saturation decreases. In order to characterize the saturation effects observed, the strain softening strength is described here as the cyclic stress ratio required to cause strain softening at 20 cycles (Fig. 5). It can also be observed that the increment of saturation decreases the strength of soil against cyclic loading. In addition, it can be concluded from this study that the confining pressure (σ_o) has an important effect on cyclic strength of soil. As seen in Fig. 5 cyclic strength increases as applied confining pressure increases
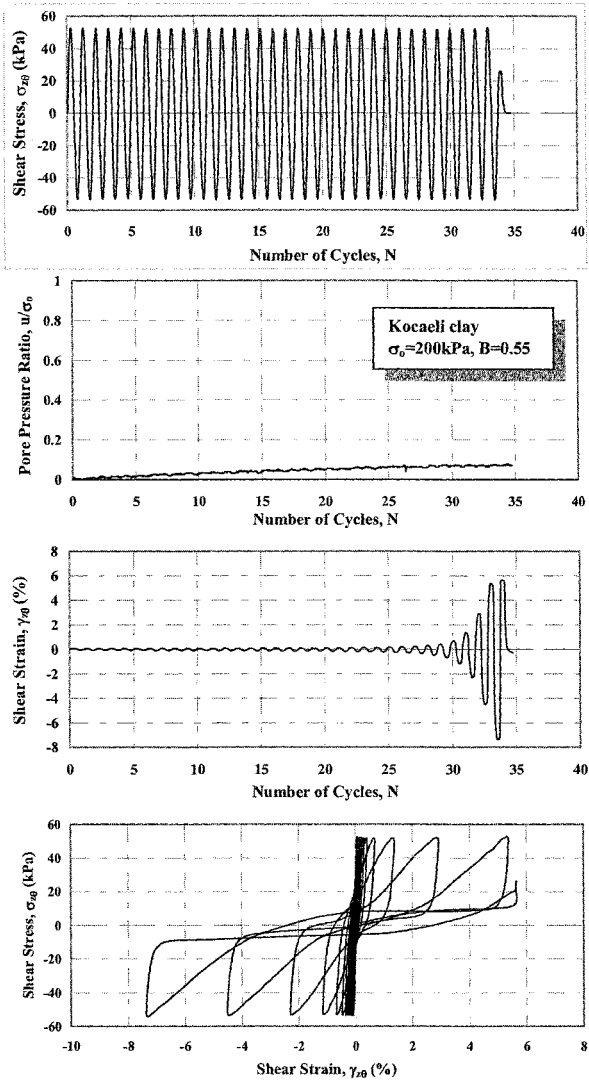
Figure 3. Typical test results in large strain state
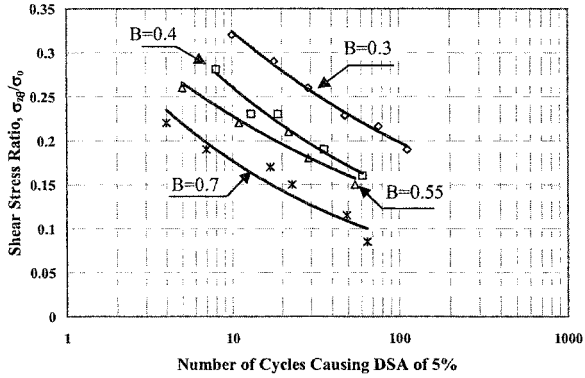
Figure 4. Large strain strength of clay at various B-values

As a result of the tests, the resistance to strain softening was found to increase with decreasing B-value. When the B-value decreases to 0.27 with the saturation ratio of S =93%, the cyclic strength is approximately twice that at the highest saturation with B=0.77.
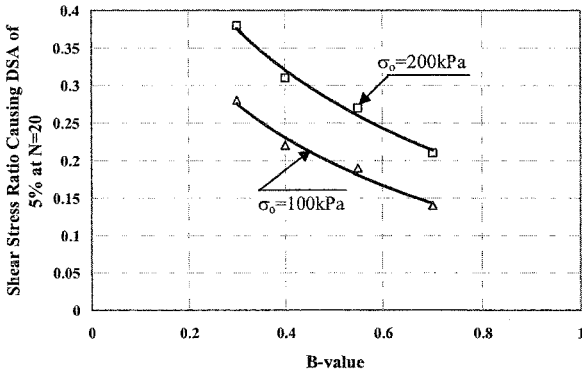
Figure 5. Cyclic strength versus B-values

Conclusion

An experimental program has been carried out using a Torsional shear test apparatus to investigate soil behavior in the small and large strain range. Undisturbed-unsaturated tube samples were used in the experiments. The response of soils to repeated loads can be evaluated under small and large amplitude dynamic strains with respect to saturation level.

As a result of the first group tests, saturation conditions were found to influence the initial shear stiffness of the undisturbed clay sample. If stiffness parameters are determined to be the crucial factors of subgrade and subbase materials, especially, in pavement, this finding should be taken into consideration.

It is known that a decrease in the degree of saturation tends to increase the resistance to liquefaction or strain softening response of soils. Based on laboratory test data, a correlation between the strain softening strength and the pore pressure coefficient B was evaluated. The strength in question was defined as the cyclic stress ratio required to cause $\pm 5\%$ shear strain at 20 cycles. It was found that the cyclic strength of clay is noticeably influenced by the saturation conditions.

References

Alonso, E.E., Gens, A. and Josa, A. (1990) "A constitutive model for partially saturated soils." *Géotechnique*, 40(3), 405-430.

Altun, S. (2003) "The evaluation of cyclic behavior of soil using torsional shear test apparatus." PhD Thesis, İstanbul Technical University.

Bishop, A.W. and Blight, G.E. (1963) "Some aspects of effective stress in saturated and partially saturated soils." *Géotechnique*, 13(3), 177-197.

Butalia, T.S., Huang, J., Kim, D.-G. and Croft, F. (2002) "Effect of moisture content and pore water pressure buildup on resilient modulus of cohesive soils in ohio." *ASTM Special Technical Publication*, 1437, 70-84.

Chaney, R. (1978) "Saturation effects on the cyclic strength of sand." *Proc., ASCE Special Conference on Earthquake Engineering and Soil Dynamics*, New York, 342–359.

Deshpande, S. and Muraleetharan, K.K. (1998) "Dynamic behavior of unsaturated soil embankments." *Geotechnical Special Publication,* No: 75-II, 890-900.

Drumm, E.C., Reeves, J.S., Madgett, M.R. and Trolinger, W.D. (1997) "Subgrade resilient modulus correction for saturation effects." *Journal of Geotechnical and Geoenvironmental Engineering*, ASCE, 123(7), 663-670.

Fredlund, D.G. and Rahardjo, H. (1993) *Soil mechanics for unsaturated soils*, John Wiley and Sons, Inc., New York.

Fredlund, D.G., and Morgenstern, N.R. (1977). "Stress state variables for unsaturated soils." *Journal of Geotechnical Engineering Division*, ASCE, 103(5), 447–466.

Hardcastle, J.H. and Sharma, S. (1998) "Shear modulus and damping of unsaturated loess." *Geotechnical Special Publication*, No: 75-I, 178-188.

Ishihara, K., Tsuchiya, H., Huang, Y., and Kamada, K. (2001) "Recent studies on liquefaction resistance of sand: Effect of saturation." *Proc., 4th Int. Conf. on Recent Advances in Geotechnical Earthquake Engineering and Soil Dynamics*, San Diego.

Li, J. (2000) "Nonlinear viscosity of subgrade soils under cyclic loading." *Geotechnical Special Publication*, No: 98, 119-128.

Mancuso, C., Vassallo, R. and D'Onofrio, A. (2002) "Small strain behavior of a silty sand in controlled-suction resonant column - Torsional shear tests." *Canadian Geotechnical Journal*, 39(1), 22-31.

Qian, X., Gray, D.H. and Woods, R.D. (1991) "Resonant column tests on partially saturated sands." *Geotechnical Testing Journal*, ASTM, 14(3), 266-275.

Rampino, C., Mancuso, C. and Vinale, F. (1999) "Laboratory testing on an unsaturated soil: Equipment, procedures, and first experimental results." *Canadian Geotechnical Journal*, 36, 1-12.

Sherif, M. A., Tsuchiya, C., and Ishibashi, I. (1977) "Saturation effect on initial soil liquefaction." *Journal of the Geotechnical Engineering Division*, ASCE, 103(8), 914–917.

Talesnick, M. and Frydman, S. (1990) The preperation of hollow cylinder specimen from undisturbed tube sample of soft clay, *Geotechnical Testing Journal*, ASTM, 13, 243-249.

Talesnick, M. and Frydman, S. (1992) Irrecoverable and Overall Strains in Cyclic Shear of Soft Clay, *Soils and Foundations*, 32, 47-60.

Usaborisut, P., Koike, M., Bahalayodhin, B., Niyamapa, T. and Yoda, A. (2001) "Cyclic torsional shear loading test for an unsaturated, hollowed specimen using Bangkok clayey soil." *Journal of Terramechanics*, 38, 71-87

Xia, H. and Hu, T. (1991) "Effects of saturation and back pressure on sand liquefaction." *Journal of Geotechnical Engineering*, ASCE, 117(9), 1347-1363

Yang, J., Savidis, S. and Roemer, M. (2004) "Evaluating Liquefaction Strength of Partially Saturated Sand." *Journal of Geotechnical and Geoenvironmental Engineering*, ASCE, 130(9), 975–979.

Yoshimi, Y., Tanaka, K., and Tokimatsu, K. (1989) "Liquefaction resistance of a partially saturated sand." *Soils and Foundations*, 29, 157–162.

Zienkiewicz, O.C., Xie, Y.M., Schrefler, B.A., Ledesma, A. and Bicanic, A. (1990) "Static and dynamic behavior of soils: A rational approach to quantitative solutions, II. Semi-saturated problem." *Proceedings of the Royal Society of London*, 429(1877), 311-321

Preparation and Cyclic Testing of Partially Saturated Sands

M. K. Yegian[1], E. Eseller[2], and A. Alshawabkeh[1]

[1]Professor of Civil Engineering, [2]Doctoral Student, Northeastern University, Boston, MA 02115; email: myegian@neu.edu

Abstract

A special laboratory experimental setup is described that permits preparation, and testing of large size partially saturated sand specimens. A unique liquefaction box was designed and built that has two of its walls hinged at the bottom of the box thus allowing rotation and inducing simple shear in the sample. A shaking table is utilized with the box to induce controlled shear strains in the sand specimen. Electrolysis technique was used to generate oxygen and hydrogen gases uniformly within the specimen without causing any change in the density of the loose sand. Experimental test results demonstrate that partially saturated sands have larger strength against liquefaction than fully saturated sands. Induced partial saturation can be a liquefaction mitigation measure. Further research is required to explore the technical and practical feasibility of this potential.

Introduction

During the past few years, there has been increased interest in the geotechnical research community to understand the dynamic properties and behavior of partially saturated soils. Partially saturated soils can be found in natural deposits where the ground water table fluctuates significantly or where there is significant capillary action above a water table. The effect of partial saturation on dynamic properties of soils is not very well understood. Recent laboratory investigations have demonstrated the potential influence of partial saturation on the shear and compressive wave velocities of sands (Yang et al. 2003, Ishihara et al. 2002). Also, preliminary research indicates that partially saturated sands exhibit larger cyclic strength against liquefaction than fully saturated sands at the same density (Xia and Hu et al. 1991, Ishihara et al. 2002, Chaney 1978, Yoshimi et al. 1989).

The authors have been conducting experimental research aimed at evaluating the effect of partial saturation on the liquefaction strength of sands. There are significant challenges in preparing laboratory samples of partially saturated sands and

in testing them under cyclic conditions. To induce partial saturation, air or gases need to be introduced uniformly within the sample and without affecting the density of the sand. Potential diffusion of the air/gas has to be minimized to ensure that the degree of saturation induced is maintained during sample preparation and testing. The cyclic shear stresses or strains induced in the sample need to be uniform to be able to make valid inferences from the pore pressure measurements made within the sample.

Triaxial setups have been used with some success to test small samples (Xia and Hu et al. 1991). Such a setup allows the calculation of the degree of partial saturation quite accurately using the pore pressure parameter B, and the testing of the sample can be conducted under undrained conditions. However, the small size of the sample used limits ability to create uniformly partially saturated sample, to accurately measure the pore pressures within the sample, and to test under cyclic simple shear condition, which is more representative of seismic excitation.

Large size fixed-walls or laminar boxes have also successfully been used to evaluate the dynamic response of partially saturated sands using a shaking table. Such experimental setups permit the preparation, testing, and monitoring of very large samples with uniform degree of saturation, thus addressing many of the challenges that were listed earlier in conducting experimental research on partially saturated sands. Because of the complexities involved in utilizing large samples in a laminar box on a shaking table, performance of many repeated tests in which the sample density, the degree of saturation, the method of inducing partial saturation and the testing of large number of samples under varying cyclic excitation amplitudes and frequencies, becomes quite a daunting task.

Understanding of the effect of partial saturation on dynamic soil properties and response is at its infancy. Further laboratory investigations need to be conducted to evaluate various techniques of inducing partial saturation and to determine the influence of various parameters on the properties and responses of such sands. For this purpose, the authors have developed a unique experimental setup that permits rapid preparation and testing of partially saturated sands.

This paper describes a special liquefaction box that was designed and built in which a large specimen of partially saturated sand can be prepared using various techniques and then tested under cyclic simple shear strain to assess the liquefaction strength of the sand. The paper also provides details of sample preparation, testing, and example test results.

Rotating-Wall Liquefaction Box

A special liquefaction box was designed to allow preparation and testing of partially saturated sands. Figure 1 shows the plan and elevation of the box. The box has four walls and a bottom plate all made of Plexiglas. The box is large enough to
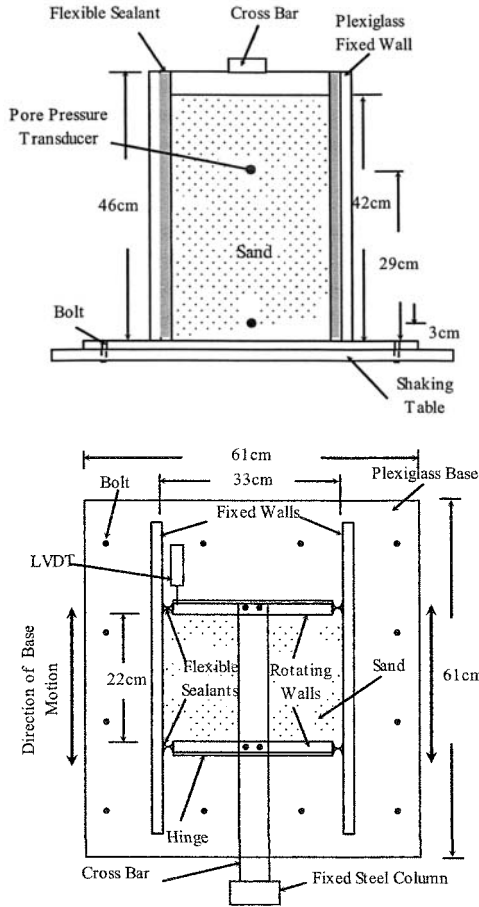
Figure 1. Details of the rotating-wall liquefaction box for testing fully and partially saturated sands.

allow preparation of 22 cm x 33 cm x 42 cm sand specimen. The uniqueness of the box is that two of the sidewalls are hinged to the bottom plate, and through rotation can induce simple shear strain within the sample.

Figure 2 shows a photograph of the empty box showing the hinge of one of the two rotating walls. The two rotating walls are connected to the two fixed walls and the bottom plate by a joint sealant that makes the joints water tight yet flexible allowing movements along the joints.
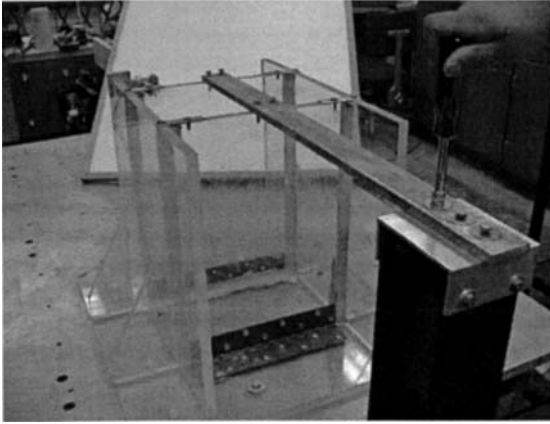
Figure 2. Photograph of the rotating-wall liquefaction box showing a bottom hinge and the cross bar.

The sand specimen in the box is tested under cyclic excitation through the use of a shaking table. Throughout the sample preparation and subsequent testing, the base plate of the box is fixed on the shaking table. Also, the tops of the two rotating walls are connected to one end of a cross bar. The other end of the cross bar is bolted on top of a steel column fixed on the floor of the lab, in front of the shaking table. This mechanism allows the use of the shaking table to induce controlled relative displacements between the tops and bottoms of the rotating walls. Since the box is fixed on top of the table and since the two tops of the rotating walls are also joined together by a stationary cross bar, a displacement history applied to the table induces a relative displacement between the bottom and top of the two rotating walls. A displacement transducer (LVDT) placed near the top of one of the rotating wall monitors this relative displacement. Dividing this relative displacement by the height of the LVDT location from the base of the box yields the simple shear strain history induced by the box within the sand specimen. It is noted that the same mechanism can be utilized to induce any random and transient strain history by exciting the shaking table with that history.

Preparation of Partially Saturated Samples

Another challenge faced in this research was to devise a procedure for preparing a partially saturated sand specimen in the rotating-wall liquefaction box. Ideally, the technique should allow the preparation of specimens with different degrees of saturation and that this degree of saturation be uniform within a specimen.

Various methods were evaluated and their advantages and disadvantages were noted (Eseller 2004). In this paper, one of the techniques for inducing partial saturation that showed good promise for use in laboratory experiments and possibly in field application is briefly presented.

Electrolysis (electrokinetic) is increasingly being used in geotechnical and geoenvironmental engineering for site remediation and dewatering of clays. The process of electrolysis involves the use of an anode and a cathode through which conduction of low amplitude current generates oxygen and hydrogen gases at the anode and cathode, respectively. Preliminary tests were conducted to asses the potential feasibility of electrolysis to generate gases in a large specimen of sand prepared in the liquefaction box. Figure 3 shows the amount of gases generated under 6 mAmp of current in a test tube of 4 cm in diameter and 25 cm in length. It was concluded that within a few hours large quantities of gases can be generated to reduce significantly the degree of saturation of a fully saturated sand specimen prepared in the liquefaction box.
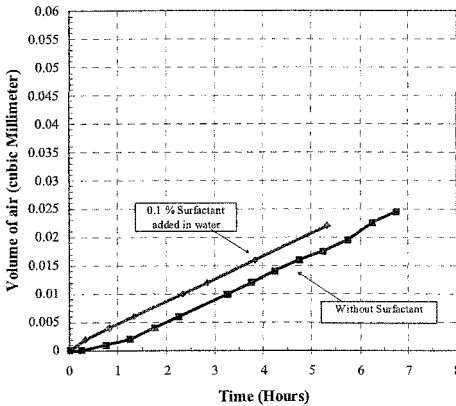
Figure 3. Small-scale test to determine gas generation rate in saturated sands (Ali 2003).

One of the phases of the research program reported in this paper was focused on using electrolysis to induce partial saturation of sand specimens within the box and then testing them under cyclic simple shear strains. Figure 4 shows an elevation of the box with the electrolysis setup.

To avoid oxidization of the electrodes and to ensure uniform generation of gases in a specimen of sand, titanium meshes were purchased and cut to desired sizes as shown in Figure 5.
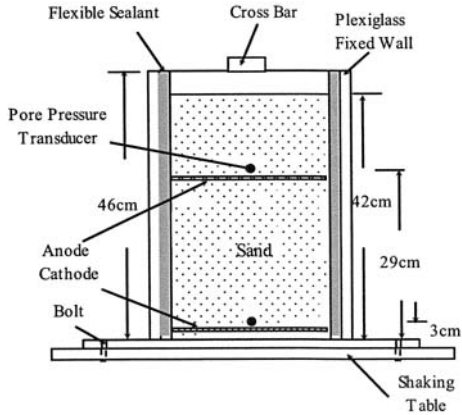
Figure 4. Setup used to induce partial saturation using electrolysis.
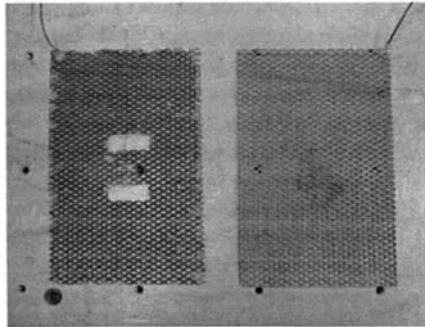
Figure 5. Titanium meshes used as anode and cathode in electrolysis to induce partial saturation.

The two holes in one of the meshes that were used as the anode in the upper region of a specimen were needed to allow insertion of radar antennas that was part of another phase of the research in which radar was used to detect partial saturation. Two pore pressure transducers were attached to each of the meshes and then the two meshes were placed at the desired depths within the box. A measured amount of water was placed in the box. Dry Ottawa sand was then poured slowly and uniformly into the box to achieve a fully saturated sample. This technique referred to as wet pluviation is known to be very well suited for preparation of large fully saturated sand

specimens. Figure 6 shows a photograph of the electrolysis setup showing the box full with the sand specimen and the wires extending to the current generator. It is noted that the free standing water on top of the specimen is the outcome of electrolysis where certain volume of gas has replaced equal volume of water in the pores of the sand specimen.
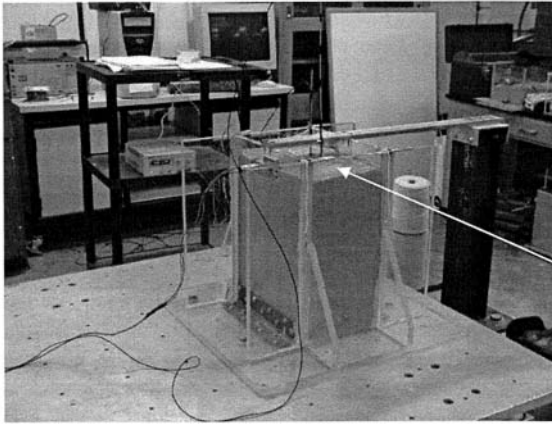
water ejected from
the specimen by
gases

Figure 6. Photograph of the electrolysis setup and an example of partially saturated specimen.

Typically, 525 mAmp current was used for a duration ranging from 1.5 to 3 hrs to achieve desired levels of degree of saturation. During the process of electrolysis, generation of bubbles could be observed within the specimen through the Plexiglas. Further evidence that bubbles were being entrapped could be seen by the accumulation of free water on top of the originally fully sutured specimen. The amount of displaced water was used together with phase relationships to compute the degree of saturation of a specimen at the end of electrolysis. Upon completion of the preparation of the specimen, it was immediately tested under controlled cyclic shear strain. It is noted that throughout the entire sample preparation, the liquefaction box was fixed on the 1.5 m x 2 m stable shaking table, and the two rotating walls were also rigidly connected to an external fixed column. Thus, during the sample preparation, the box experienced no external disturbances or vibrations ensuring that the density of the prepared specimen stayed constant and all initial pore water pressures were hydrostatic.

Example Test Results

The experimental research program included testing of many different fully and partially saturated sand specimens. Different types of sands were also utilized to assess the effect of particle angularity of the sands on the induced degree of saturation and liquefaction strength. One of the sand used was the commonly referred Ottawa

sand, which has a uniform gradation and has known minimum and maximum densities and porosity. In this paper typical result on the Ottawa sand are presented. Table 1 shows the index properties of the Ottawa sand used.

Table 1. Characteristics of the Ottawa sand used in this investigation. (Holtz and Kovacs 1981, modified after Hough, 1969)

Particle Size and Gradation				Voids			
Approx. Size Range (mm)		Approx. D_{10} (mm)	Approx. Range C_u	Void Ratio		Porosity (%)	
D_{max}	D_{min}			e_{max}	e_{min}	n_{max}	n_{min}
0.84	0.59	0.67	1.1	0.80	0.50	44	33
Density (Mg/m^3)							
Dry Density, ρ_d		Wet Density, ρ		Submerged Density, ρ'			
Min (Loose)	Max (Dense)	Min (Loose)	Max (Dense)	Min (Loose)		Max (Dense)	
1.49	1.78	1.51	2.12	0.93		1.12	

To evaluate the effect of partial saturation on liquefaction potential and pore pressure generation in sands, fully saturated and partially saturated sands were tested. A specimen of fully saturated sand was prepared using the pluviation method mentioned earlier. The resulting void ratio of the sample was 0.74. Comparison of this void ratio with the minimum and maximum values shown in Table 1 leads to the conclusion that the fully saturated sand had a relative density of about 20 %. The degree of saturation of the specimen was calculated to be 99.5 % using phase relationships and measured quantities of mass and volume.

The fully saturated Ottawa sand specimen was then subjected to a controlled level of harmonic shear strain with amplitude of 0.25 %, using the shaking table. Figure 7 shows the shear strain history that the fully saturated specimen was subjected to. The pore water pressures at the two locations shown in Figure 4 were monitored continuously during the test. The results are shown in Figure 8.
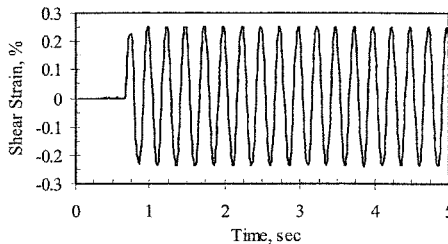
Figure 7. Harmonic simple shear strain history applied to the Ottawa sand specimens tested.
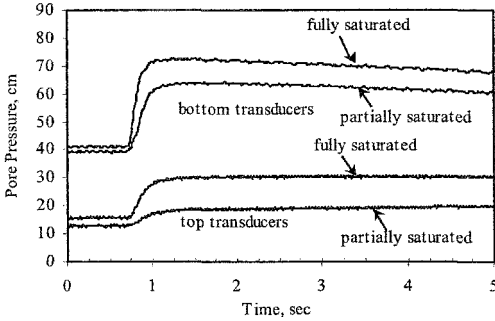
Figure 8. Pore water pressures measured during cyclic shear strain tests in fully and partially saturated sands.

From the results shown in Figure 8 it is noted that initial liquefaction was induced in the fully saturated sand within one to two cycles of application of shear strain.   Bottom and top transducers both show that the sand within the entire specimen liquefied. The maximum excess pore pressure ratio, r_u at the time of initial liquefaction was calculated to be 1 from the bottom transducer and 0.93 from the top transducer, thus confirming the visual observation of manifestation of liquefaction at the time of the testing.

A second sample of Ottawa sand was prepared using the same quantities of mass of water and sand and total volume of specimen that were used in the preparation of the fully saturated sand, but this time the titanium meshes were placed in the box for electrolysis.   After placing the sand through wet pluviation and accounting for the volume of the meshes in the specimen, the void ratio of the sample was calculated to be the same as that of the fully saturated specimen (0.74).

A current of 525 mAmp for 3 hours was used to generate gases in the specimen, thus inducing partial saturation. During the electrolysis, as a result of gases generated and entrapped in the specimen, a water layer accumulated on top of the originally saturated specimen. The resulting degree of saturation of the specimen after three hours of electrolysis was 96.3 %.

The partially saturated specimen was then subjected to the same shear strain history that was used to test the fully saturated sand (Figure 7). The resulting pore pressures measured again at the bottom and near the top of the specimen are shown in Figure 8. Clearly, the partially saturated sand did not achieve initial liquefaction. The maximum excess pore pressure ratio did not exceed 0.7 at the bottom of the specimen and 0.43 at the top.

This typical test result from the experimental research demonstrates that there is potential benefit in inducing partial saturation in a loose sand. A small amount of entrapped air or gases can minimize the generation of excess pore water pressures in liquefaction susceptible sand and may even prevent liquefaction.

Conclusion

An experimental setup was designed, built, and used to induce partial saturation in loose sands, and to test the specimens under strain controlled excitations. A special Plexiglas box was built that has two rotating walls that induce simple shear strains in a large specimen of sand. Flexible sealant connects the rotating walls of the box with the fixed walls, which makes the joints water tight and allows movements between the rotating and fixed walls of the box.

After preparing a fully saturated sand specimen in the box, partial saturation is induced using the process of electrolysis. Titanium meshes are used in the box acting as anode and cathode and current is passed through the system generating oxygen and hydrogen bubbles in the specimen. The experimental results lead to the conclusion that uniform degree of partial saturation can be induced in large specimen of sand in the laboratory using electrolysis.

Fully and partially saturated Ottawa sand specimens were tested using a unique setup that utilizes shaking table and induces uniform shear strains in the specimen. The experimental results demonstrate that small reduction in the degree of a fully saturated specimen can lead to significant reduction in excess pore pressures generated in loose liquefaction susceptible sand. Induced partial saturation can be a potential inexpensive liquefaction mitigation measure at sites where using conventional mitigation techniques are prohibitive. Further research is required to explore the technical and practical feasibility of this concept.

Acknowledgments

References

Ali, S. (2003). "Experimental Setup and Procedures for the Preparation and Cyclic Testing of Air Entrapped Sand." *Master's Report*, Northeastern University, Boston MA.

Chaney, R. (1978). "Saturation effects on the cyclic strength of sands." *Earthquake Engineering and Soil Dynamics*, Vol.1, pp.342–358.

Eseller, E. E. (2004). "Induced Partial Saturation for Liquefaction Mitigation." *Master's Thesis*, Department of Civil and Environmental Engineering, Northeastern University, Boston, MA, August.

Holtz, D. R., Kovacs, W. D., (1981) "An Introduction to Geotechnical Engineering" Prentice-Hall Civil Engineering and Engineering Mechanics Series, New Jersey

Hong, X., and Ting, H. (1991). "Effects of saturation and back pressure on sand liquefaction." *J. Geotech. Eng*, 117(9).

Ishihara, K., Tsukamoto, Y., Nakazawa, H., Kamada, K., and Huang, Y. (2002). "Resistance of partly saturated sand to liquefaction with reference to longitudinal and shear wave velocities." *Journal of Soils and Foundations*, JGS, Vol.42, No.6, p.93-105

Yang, J., Savidis, S., Sato, T., Li, X.S. (2003). "Influence of Vertical Acceleration on Soil Liquefaction: New Findings and Implications." *Proceedings of Soil and Rock America 2003*, Cambridge, Massachusetts, Volume 1, June

Yoshimi, Y., Yanaka, K., and Tokimatsu, K., (1989). "Liquefaction resistance of a partially saturated sand." *Journal of Soils and Foundations*, Vol.29, No.2, pp157-162.

Dynamic Response of Unsaturated Granular Soil Deposits: A Micro-Mechanical Study

Mourad Zeghal[1] and Claudia Medina[2]

[1]Department of Civil and Environmental Engineering, School of Engineering, Rensselaer Polytechnic Institute, 110 8th St., Troy, NY 12180-3590; PH (518) 276-2836; FAX (518) 276-4833; e-mail: zeghal@rpi.edu
[2]Department of Civil and Environmental Engineering, School of Engineering, Rensselaer Polytechnic Institute, 110 8th St., Troy, NY 12180-3590; PH (518) 276-2064; FAX (518) 276-4833; e-mail: medinc@rpi.edu

Abstract

A micro-mechanical study of the sedimentation process and dynamic response of unsaturated granular soils is presented in this paper. The discrete element method was used to idealize the granular soil skeleton. Suction forces were used to model the effects of interparticle water bridges in pendular state. Periodic boundaries and a high gravitational field were used to achieve a realistic simulation of a soil deposit with a computationally manageable number of particles. Numerical simulations were performed to investigate the impact of moisture content on the sedimentation and dynamic response of level ground deposits of unsaturated soils. The outcome of conducted simulations provided a valuable insight into the response mechanisms of these soils.

Introduction

A significant portion of the USA has semi-arid or arid climatic conditions where soils used as engineering materials are in an unsaturated condition. Unsaturated soils are used in the construction of civil systems such as compacted roadway embankments, earth dams, slopes, and fills. Prediction of the dynamic response of these soils is essential for the design of new systems as well health-assessment of rehabilitation of existing ones.

Unsaturated soils consist of a mixture of mineral particles with water and air filling the pores. The mechanical behavior of these soils depends not only on the rheology of the separate constituents, but also on the interaction among them. Depending on the moisture content, pore water may exist in pendular, funicular or capillary state (Newitt and Conway-Jones 1958). The pendular state is characterized by low moisture levels (degree of saturation lower than about 30%) and the particles are held together by the surface tension forces of the water-air-particle interface and suction force that develops within pendular water bridges. When the fluid has almost filled all the pores the capillary state is reached, and the particles are held by the suction force developed at the water-air interface. The intermediate stage between the pendular and capillary states, termed funicular state, is characterized by the co-existence of liquid bridges and liquid-filled pores.

The response of unsaturated soils has been modeled by researchers using continuum formulations. Water flow through such soils was addressed using an extension to Biot's saturated porous media theory (e.g., Li and Zienkiewicz 1992; Schrefler and Zhan 1993). Constitutive models based on a critical state framework involving two independent sets of stress variables (e.g., Alonso et al. 1990; Wheeler and Sivakumar 1995) and based on the fundamental principles of thermodynamics (e.g., Hutter et al. 1999; Borja 2004) were also used to describe the response of unsaturated soils. In addition, the discrete element method (DEM) has recently been used to study the micromechanical response of these soils (e.g., Gili and Alonso 2002; Liu and Sun 2002; Jiang et al. 2004). In spite of all these efforts, there is still a current need for a better understanding of the dynamic response of unsaturated soils.

A realistic modeling of pendular state unsaturated soils was achieved in this study by using a discrete formulation. The discrete element method (DEM) was used to idealize soil particles and interparticle suction forces were employed to model the effects of pendular water bridges.

A Micro-Mechanical Model of Unsaturated Granular Soils

A DEM model (Cundall and Strack 1979) was used to idealize a deposit of unsaturated granular soil as a collection of discrete particles. The particles are subjected to gravity and contact forces along with suction forces exerted by pendular water bridges. A new water bridge develops between any two particles that become in contact. A complete description of the motion of the deposit is provided by solving the equations of linear and angular momentum for each particle. For a particle p these equations are given by:

$$m_p \dot{\mathbf{v}}_p = m_p \mathbf{f}_g + \sum_c \mathbf{f}_c + \sum_b \mathbf{f}_b$$

$$I_p \dot{\boldsymbol{\omega}}_p = \sum_c \mathbf{r}_c \times \mathbf{f}_c$$

where v_p and ω_p are translational and rotational velocity vectors (a superposed dot indicates a time derivative), m_p and I_p are the particle mass and moment of inertia, f_c refers to the interparticle force at contact c ($c = 1, 2,...$), r_c is vector connecting the center of the particle to the location of the contact c, and f_b is the suction force exerted by the pendular water bridge b ($b = 1, 2,...$). These suction forces are assumed to be radial and do not generate a moment. When the particles are in contact, the contact force, f_c, and the suction force, f_b, (due to the generation of a water bridge) are taken into account. Only the suction force, f_l, is considered when two particles, formerly in contact are moving away from each other until the critical rupture distance of the pendular water bridge is reached.

A constitutive law provided the contact forces as a function of the relative movement of the particles. The normal contact forces were modeled using a nonlinear Hertz spring (Mindlin and Deresiewicz 1953) in parallel with a dashpot. The shear forces were idealized using a Kelvin model (elastic spring in parallel with a dashpot) in series with a frictional slider. The shear and normal forces are related by a slip Coulomb relationship (Itasca 2003). Suction forces develop when pendular water bridges form between particles. For a pendular state, the effects of gravity are negligible and the suction force accounts for the reduced hydrostatic pressure within the water bridge and the force caused by the water surface tension at the water-air-particle interface. These forces are given by: (Hotta et al. 1974)

$$f_l = \pi R^2 \Delta P + 2\pi T_s R$$

where R is bridge neck radius, T_s is surface tension of water and ΔP is the reduced hydrostatic pressure given by the Laplace-Young equation (Fredlund and Rahardjo 1993).

Numerical Simulations

Numerical simulations were conducted to analyze the impact of moisture content on the sedimentation process and dynamic response of a level-ground granular soil deposit. Soil particles where pluviated within a parallelepiped domain having periodic boundaries in the lateral directions to simulate a semi-infinite deposit (Fig. 1). The periodic deposit was subjected to a high gravity (g) field in order to reduce the number of particles to a computationally manageable value (using a concept similar to that of centrifuge testing of small-scale geotechnical models).

Specifically, the employed model consisted of a 60 mm height deposit that was subjected to 50 g gravitational field. Thus, this model represented a 3.0 m height prototype of a level site (Taylor 1995). The deposit grains were idealized using spherical particles with a uniform size distribution (with diameters ranging from 0.55 mm to 0.85 mm). The surface tension of the pore water was scaled up to account for

the employed high gravitational field. Figure 1 shows the deposit configuration after allowing the particles to settle under gravity.

Sedimentation process

The first simulations were performed to analyze the sedimentation process. Dry and then moist soil particles were pluviated within periodic domains (described above) under the employed gravity field. From a macro-scale point of view, the water content of 6% of the unsaturated deposit was spread uniformly among all locations. At the micro-level, this content was distributed among the pendular water bridges proportionally to the volume of involved particles, as suggested by the experimental investigations conducted by Kohonen et al. (2004).
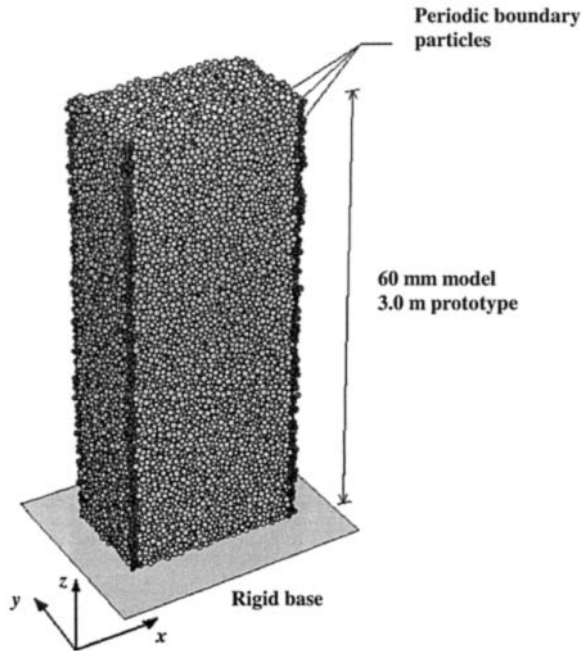
Figure 1. Three-dimensional view of the periodic granular soil deposit after sedimentation.

Figure 2 shows the final configuration and dry unit weight profile of the unsaturated deposit along with the corresponding dry one. The dry deposit was marked by a significantly denser configuration. The dry-unit-weight of this deposit was basically uniform with an average value of about 14.4 kN/m³ (i.e., 45 – 50% relative density). In contrast, the unsaturated one exhibited a loose configuration (Fig. 2). The associated dry-unit-weight increased with depth and corresponded to a negative relative density at all locations. Visual investigation of this deposit (Fig. 2) showed substantially large pores enabled by the suction associated with the pendular water bridges. This was especially the case near the free surface where the deposit had a "sponge-like" configuration.
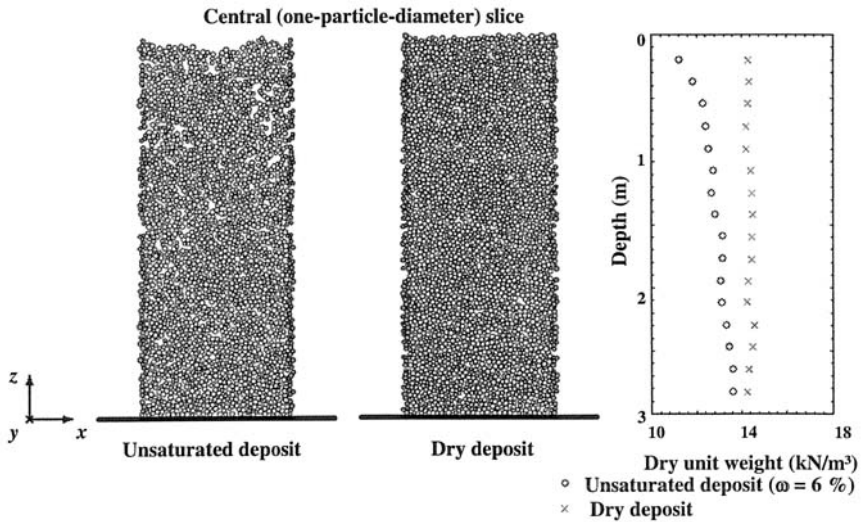
Figure 2. Effect of moisture content on the sedimentation process of dry and unsaturated granular soil deposits.

Dynamic response

The sedimented dry and unsaturated deposits were subjected to a dynamic base excitation consisting mostly of a sinusoidal motion of 2 Hz with maximum amplitude of 0.3 g. Average accelerations of these deposits were evaluated using spherical control volumes at a number of depth locations. Figure 3 exhibits the acceleration time histories along the central vertical axis of the deposits. Near the free
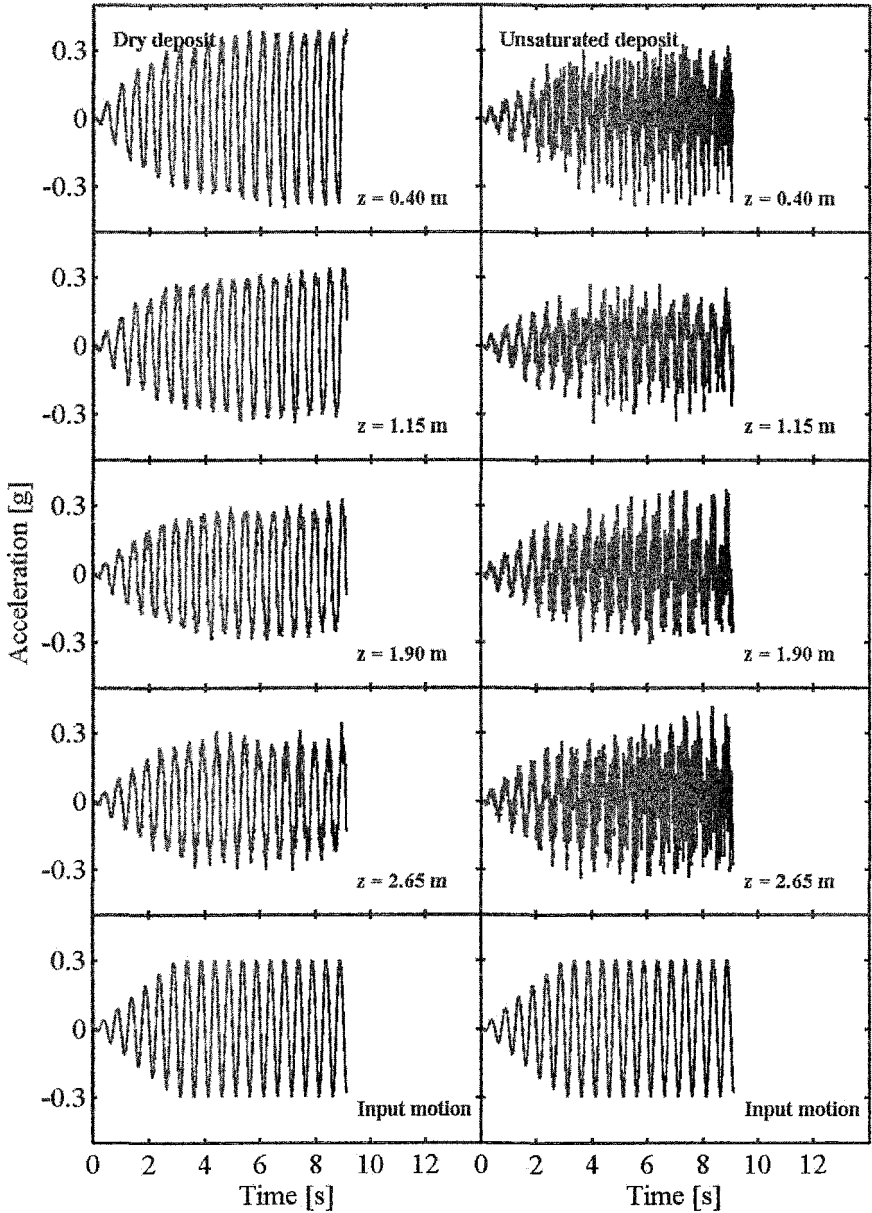
Figure 3. Acceleration time histories at selected depth of analyzed dry and unsaturated (6% moisture content) deposits.

surface, the dry deposit exhibited accelerations that were slightly larger than those of the unsaturated one. The corresponding stress-strain histories (Fig. 4) showed contrasting patterns. The response of the dry deposit was characterized by large strains, especially near the free surface (as large as 3.0% at 0.4 m depth and 0.9% at 2.65 m depth). These large strains were associated with significant hysteretic energy dissipation as indicated by the large areas of the stress strain cycles. As the shaking progressed, this deposit densified and experienced a decrease in shear strain amplitudes as well as level of hysteretic energy dissipation. The decreases in the vicinity of a depth of about 1.15 m were the largest from a relative point of view. However, the densification was generally uniform with depth. Indeed, Fig. 5 shows that the porosity decreased from a value exceeding 0.42 to a value approaching 0.39 at all locations (only the first 3 s of the porosity at 0.4 m depth are shown since the reminder of the time history is affected by the process of emptying of the upper measurement sphere). The densification led to a total surface settlement of about 19 cm (Fig. 5).

The unsaturated deposit exhibited a contrasting and essentially linear response at all levels with very minor hysteretic damping (Fig. 5). The cyclic excitation had only a slight impact on the stress-strain response that was perceptible only near the base. This may be explained by the fact that the deposit porosity remained constant and was affected in a noticeable fashion only at depths higher than about 2.5 m. The associated surface settlements were less than 2 cm. Obviously, the cohesive forces of the pendular bridges were large enough to ensure that deposit experiences only minor normal and shear deformations for the employed 0.3 g input motion. The results presented in this paper are part of an ongoing research effort and further results will be reported in future publications.

Conclusions

A discrete element model was used to study the sedimentation process and response of level ground deposits of pendular state unsaturated soils when subjected to dynamic base excitations. The effect of associated pendular water bridges was considered using interparticle suction forces. Simulation of the natural process of sedimentation let to a significantly loose deposit with a negative relative density (especially near the free surface). The analyzed unsaturated deposit exhibited an essentially linear response associated with minor hysteretic damping and surface settlements when subjected to a moderate cyclic loading. The employed model captured qualitatively the mechanisms and response patterns of unsaturated soils and provided an effective tool to shed light on the intricate response mechanisms of these soils.
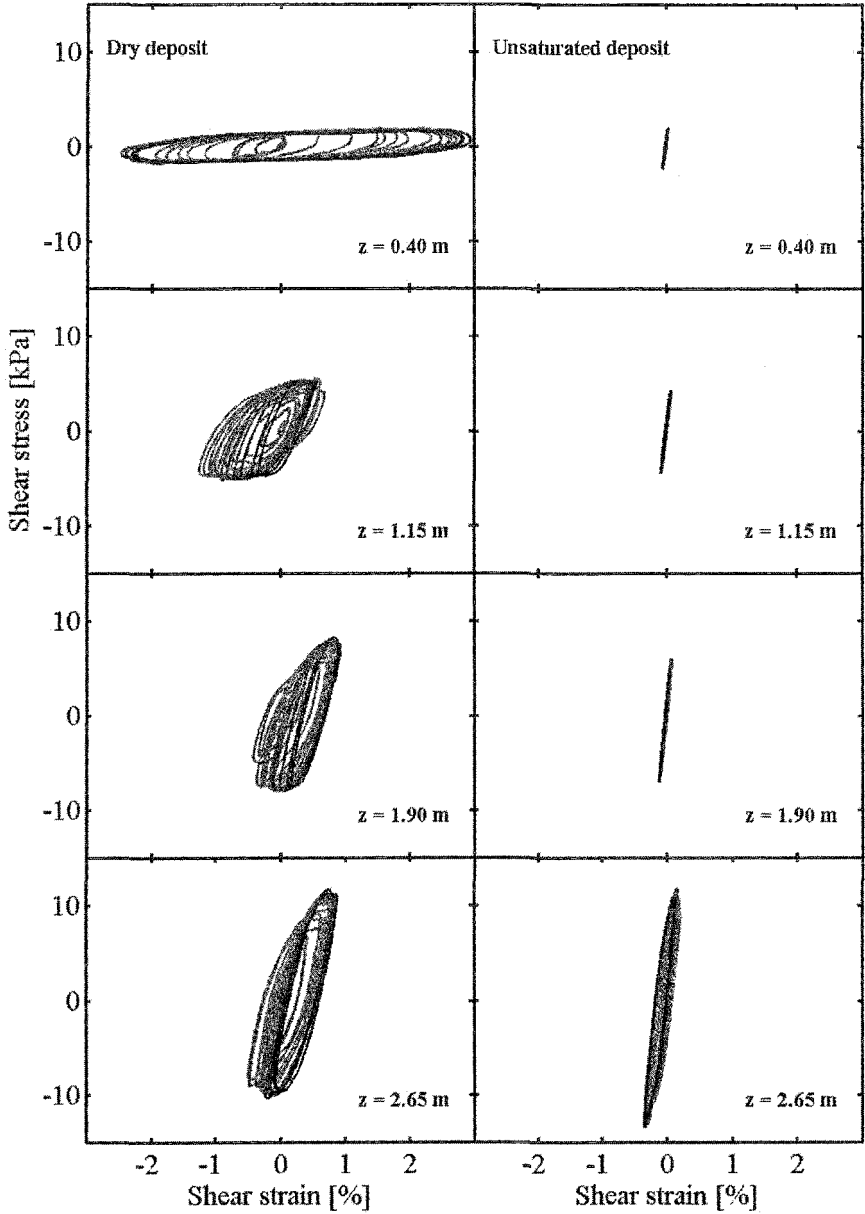
Figure 4. Shear stress-strain histories at selected depth of analyzed dry and
unsaturated (6% moisture content) deposits.
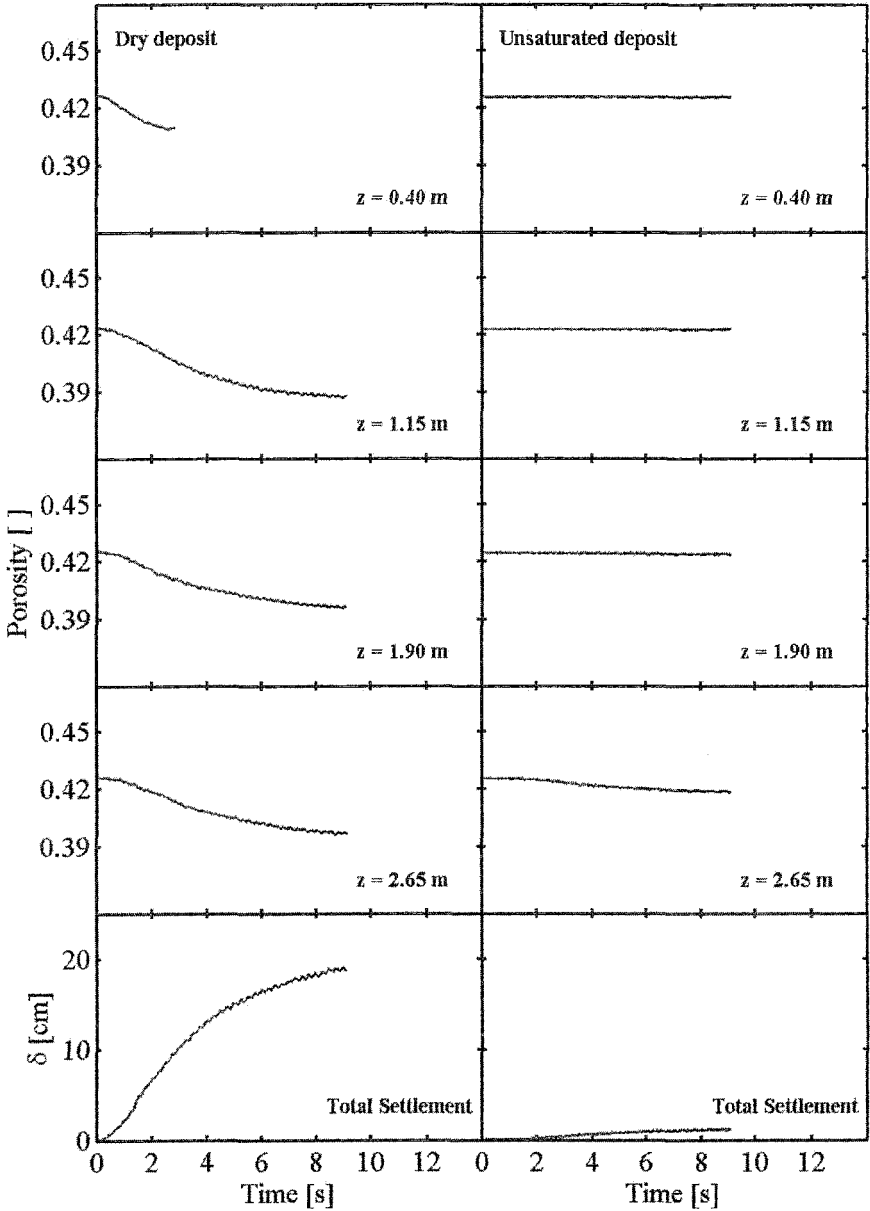
Figure 5. Porosity histories at selected depth and total settlement of analyzed dry and unsaturated (6% moisture content) deposits.

References

Alonso, E. E., Josa, A., and Gens, A. (1990). "A constitutive model for partially saturated soils." *Géotechnique*, 40(3), 405–430.

Borja, R. I. (2004). "Cam-Clay plasticity. Part V: A mathematical framework for three phase deformation and strain localization analyses of partially saturated porous media." Computer Methods in Applied Mechanics and Engineering, 193, 5301–5338.

Cundall, P. A. and Strack, O. D. L. (1979). "A discrete numerical model for granular assemblies." Géotechnique, 29(1), 47–65.

Fredlund, D. G. and Rahardjo, H. (1993). Soil mechanics for unsaturated soils. John Wiley and Sons, Inc.

Gili, J. A. and Alonso, E. E. (2002). "Microstructural deformation mechanisms of unsaturated granular soils." International Journal for Numerical and Analytical Methods in Geomechanics, 26, 433–468.

Hotta, K., Takeda, K., and Iinoya, K. (1974). "The capillary binding force of a liquid bridge." Powder Technology, 10, 231–242.

Hutter, K., Laloui, L., and Vulliet, L. (1999). "Thermodynamically based mixture models of saturated and unsaturated soils." Mechanics of Cohesive-frictional Materials, 4(4), 295–338.

Itasca (2003). Particle Flow Code, PFC3D, release 3.0. Itasca Consulting Group, Inc., Minneapolis, Minnesota.

Jiang, M. J., Leroueil, S., and Konrad, J. M. (2004). "Insight into shear strength functions of unsaturated granulates by DEM analyses." Computers and Geotechnics, 31, 473–489.

Kohonen, M., Geromichalos, D., Scheel, M., Schier, C. and Herminghaus, S. (2004). "On capillary bridges in wet granular materials." Physica A, 339, 7–15.

Li, X. and Zienkiewicz, O. C. (1992). "Multiphase flow in deforming porous media and finite element solutions." Computer and Structures, 45(2), 211–227.

Liu, S. H. and Sun, D. A. (2002). "Simulating the collapse of unsaturated soil by DEM." International Journal for Numerical and Analytical Methods in Geomechanics, 26, 633–646.

Mindlin, R. and Deresiewicz, H. (1953). "Elastic spheres in contact under varying oblique forces." Journal of Applied Mechanics, ASME, 20, 327–344.

Newitt, D. M. and Conway-Jones, J. M. (1958). "A contribution to the theory and practice of granulation." Transactions of the Institution of Chemical Engineers, 36, 422–442.

Schrefler, B. A. and Zhan, X. (1993). "A fully coupled model for water flow and airflow in deformable porous media." Water Resources Research, 29, 155–167.

Taylor, R. N. (ed.) (1995). Geotechnical Centrifuge Technology. Chapman and Hall, London, UK.

Wheeler, S. J. and Sivakumar, V. (1995). "An elasto-plastic critical state framework for unsaturated soils." Géotechnique, 45(1), 35–53.

Influence of the Suction on the Stiffness at Very Small Strains

C.E. Mendoza[1] and J.E. Colmenares[2]

[1]Department of Civil and Agricultural Engineering, National University of Colombia, Bogotá, Carrera 30 No 45-03, Building 406, Office 208; PH (571) 3165000, Ext 13312; FAX (571) 3165184; email: cemendozas@unal.edu.co

[2]Department of Civil and Agricultural Engineering, National University of Colombia, Bogotá, Carrera 30 No 45-03, Building 401, Dean Office; PH (571) 3165000, Ext 13552; FAX (571) 3165184; email: jecolmenaresm@unal.edu.co

ABSTRACT: This paper presents the results of an investigation on the variation of the stiffness at very small strains of an unsaturated clayed soil subjected to drying processes. The soil stiffness was measured by using the wave velocity technique (ultrasonic pulse transmission method and bender elements testing). The test were conduced on samples of kaolinite clay derived from volcanic ash. Those samples were prepared by using a static compaction method known as the flouting mould. Compacted samples of kaolin were allowed to dry gradually up to air-dry condition. At intermediate equilibrium stages, the Shear and Young`s modulus and the matrix suction were measured. The effects of initial void ratio, compaction water content and matrix suction on the dynamic response of the soil were investigated. The experimental results suggest that suction significantly increases the stiffness at very small strains. An S-shaped relationship between the initial stiffness and the degree of saturation was observed. The modulus increased significantly at early stages of the drying process, with the changes becoming more gradual as drying continued. However, at final stages, near to air-dry condition, the effect of suction on the stiffness was important again. The initial void ratio appears to have more influence on the stiffness than compaction water content. Contours of equal suction in the plot of the modulus versus degree of saturation, during drying processes, were analyzed. Additionally, changes in the soil fabric during drying and wetting were analyzed considering changes in void ratio.

INTRODUCTION

Capillary forces produce significant differences in the behavior of partly saturated soils depending of the degree of saturation. These differences are due to the fact that the meniscus between particle contacts of an unsaturated soil increases the

interparticle forces, producing an additional effective confining pressure in the soil structure which in turn increases the stiffness at very small strains. The development of interparticle forces by the menisci around particle contacts depends principally of the difference in pressure between the two phases inside the pores: air pressure and water pressure. This pressure difference is known as matrix suction and it is a state variable used often to describe the effects of interparticle forces, generated by the menisci, on the soil behavior.

The influence of the matrix suction on the stiffness at very small strains has been studied for different materials using devices such as: resonant column (Qian et al. 1993), ultrasonic pulse transmission method (Inci et al. 2003), bender elements test (Marinho et al. 1995) and controlled-suction resonant column (Mancuso et al. 2002). However, in those investigations either the range of values of suction studied was narrow or the matrix suction was not measured. The results have been presented in terms of the degree of saturation.

This paper presents the results of an experimental investigation developed to study the influence of the matrix suction on the Shear and Young's modulus of a partly saturated compacted cohesive soil at very small strains (i.e. G_{max} and E_{max}). The effects of the compaction water content and the initial void ratio on the path followed by the modulus during drying were studied.

BACKGROUND

Previous Research
The variation of G_{max} with suction during drying appears to depend of the kind of soil: if the soil is cohesive or if it is well-graded, the relationship between the modulus and the suction is proportional (Mancuso et al. 2002, Inci et al. 2003). See figure 1. But if the soil is cohesionless or if it is poorly graded, there is an optimum value of the degree of saturation which corresponds to the degree of saturation where the shear modulus has a maximum value (Marinho et al. 1995, Wu et al. 1984, Qian et al 1993). See figure 2. That optimum value maybe due to: (i) development of micro fracture of the soil samples during drying (Marinho et al. 1995) due possibly to abrupt changes in water content, or (ii) the development of menisci failure between particles separated a short distance during shearing perturbation. Shear deformation involves particle displacement and particle rotation. When an unsaturated soil is subjected to shear, menisci are strained and may eventually break causing a reduction of the capillary effects (Cho & Santamarina 2001). Therefore, G_{max} decreases with increase in suction. Menisci failure occurs first between particles separated a short distance than when those are in contact. When the soil is uniformly graded there are big voids in its structure yielding menisci between separated particles. For that reason, uniformly graded soil may show an optimum degree of saturation. Instead, in well-graded soils and cohesive soils the G_{max} always increases with the increase of suction: for sands, the strains for menisci failure between particles in contact (ε = 0.01 to 1%, Cho & Santamarina 2001) are higher than the threshold strain determined from the shear modulus degradation curves where G is maximum (Alarcón-Guzman 1986, Georgiannou et al. 1991). The strain at menisci failure decreases with the decrease in water content, (Cho & Santamarina 2001), the contribution of menisci to

the internal forces does not vanish suddenly, but gradually with the drying. Therefore, the G_{max} decreases slowly as drying continue.
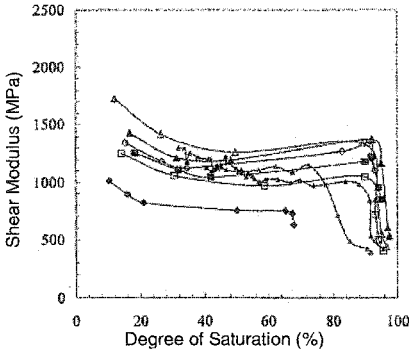
Figure 1. Variation of shear modulus with degree of saturation (Inci et al. 2003).
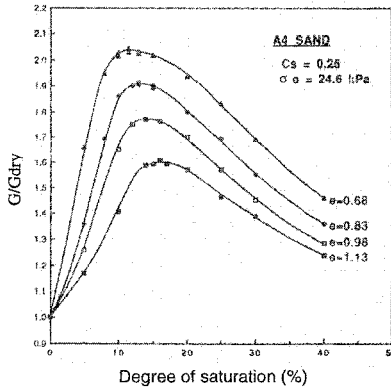
Figure 2. G/Gdry versus degree of saturation (Qian et al. 1993).

Wave Equation

The wave equation relates a temporal variation of particle motion to its spatial variation, and predicts two types of body waves or modes of propagation: shear waves and longitudinal waves. Using theory of elasticity, the relationships shown in equations 1 and 2 can be used to relate measured wave velocity with the appropriate modulus.

$$G_{max} = \rho V_S^{\,2} \qquad\qquad\qquad (1)$$

$$E_{max} = \rho V_L^{\,2} \qquad\qquad\qquad (2)$$

Where ρ: total density
V_S : shear wave velocity

V_L : longitudinal wave velocity
E_{max}: maximum Young`s modulus
G_{max}: maximum Shear modulus

TESTING PROGRAM

The testing program involved the determination of physical properties (i.e. void ratio, degree of saturation, etc.), longitudinal, L, and shear, S wave velocities and matrix suction of statically compacted clayey soils in laboratory. In order to change the degree of saturation of the soil samples, they were allowed to dry gradually in the laboratory up to air-dry condition. Then, water was added following a wetting path to reach the initial moisture content. Several measurements of S and L were performed at equilibrium stages, during drying and wetting. The relationship between the dynamic elastic parameters of the soil and its corresponding matrix suction was evaluated. Details of the methods used for drying and wetting of the soil samples are shown in Dineen (1997) and Mendoza (2004).

Materials

The type of cohesive soil used in this experimental study was commercial kaolin originated from volcanic ash. The material is clay with a high fraction of colloids (> 80%).The liquid limit is 80% and the plasticity index is 35%. The soil lies below the line A in the USCS plasticity chart therefore it may be classified as MH. However, the X Ray Diffraction Test indicates that the soil is mainly composed by kaolin (more that 40% was kaolin). In addition, the fraction analysis of soil oxides indicated that there is silicon ($SiO_2 > 47\%$) and aluminium ($Al_2O_3 > 31\%$). Therefore, the soil tested corresponds to kaolin. The above and other physical properties of the material are summarized in table 1.

Table 1. Basic material properties

LL %	PL %	SL %	PI %	ω_{nat} %	G_S
80	45	35	35	1.81	2.61

Samples

Tests were conducted on cylindrical samples prepared by using a static compaction method known as the flouting mould (Shackel 1970). The flouting mould method consists of two pistons travelling in opposite direction, at the same velocity, in a mould flouting filled with soil between the two pistons. With this method, the uniformity of the sample is independent of its dry density and its degree of saturation. Additionally, the uniformity of the sample is not dependent on the velocity of the applied load (Shackel 1970).

Each sample had dimensions of approximately 38-mm-diameter and 76-mm-high. The specimens were prepared at different initial void ratio and moisture contents. A total of five samples were prepared for the testing program. The initial characteristics of the specimens tested are shown in table 2. Each sample was prepared with different compaction effort, therefore applying a different energy input per unit volume. This fact may result in the generation of different fabric and structure within each soil sample.

Table 2. Initial characteristic of the samples tested

Sample	W %	γ_d g/cm³	e	Sr %	Matrix Suction kPa
1	37	1.31	0.99	97	258
2	37	1.14	1.29	75	293
3	29	1.14	1.29	58	529
4	37	1.2	1.18	85	168
5	23	1.14	1.29	46	799

Laboratory Equipment

The G modulus at very small strain was measured by using bender elements of the type developed at the Norwegian Geotechnical Institute by Dyvik & Madshus (1985). The bender transducers employed were able to generate and detect shear and longitudinal waves throughout unsaturated soil samples (Mendoza & Colmenares 2004a). In order to have good coupling between the soil and the bender elements, small slots (with dimensions a little smaller than the bender elements) were made at the top and bottom of the specimens to accommodate the bender transducers. To avoid damage during the introduction of the transducers, it was necessary to lubricate the piezoelectric elements with silicon grease. A measurement system consisting of a Philips-Fluke function generator model 5138A, a Fluke digital oscilloscope model 105B series II, piezoelectric elements (transmitter and a receiver), and a PC-based data acquisition setup was used for this study (Fig. 3).

Complimentary Test

Retention curves and volume changes

In this study, the matrix suction of the soils was measured using the filter paper technique (Ridley et al 2003). The filter paper employed was the Schleicher & Schuell 589 (S & S 589), and the soil matrix suction was calculated from the filter paper water contents using the correlation proposed by Greacen et al (1987). Figure 4 shows the retention curves of the five soil samples tested. Volume changes during drying and wetting were analyzed in terms of the void ratio. Figure 5 shows the variation of the void ratio with the degree of saturation.

The influence of the initial void ratio and compaction water content on the retention curve, and volume changes during drying and wetting was discussed by Mendoza et al (2005). They found that the compaction water content has more influence than the initial void ratio on drying and wetting paths, Shrinkage during drying occurs also for moisture contents smaller than the shrinkage limit. Additionally, there is a water content for which there is no more volume change if drying continues. This moisture content does not appear to depend on the compaction water content.
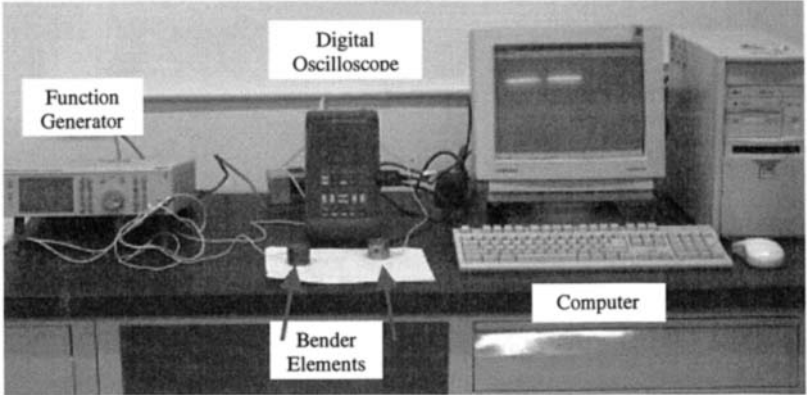
Figure 3. Test setup.
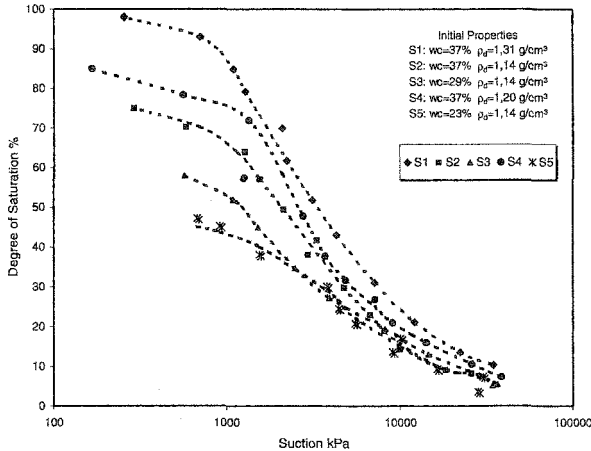
Figure 4. Variation of matrix suction with degree of saturation.

RESULTS AND DISCUSSION

The variation of both initial shear modulus and maximum Young's modulus with the matrix suction during drying is shown in figure 6 and 7, respectively. Both shear modulus and Young's modulus, for all samples, increased with the matrix suction. The trend line is a straight line (semi logarithmic scale) with high correlation ($r^2 >$ 0.96). However, with the experimental data it is possible to identify three stages of behavior during drying: initially a sharp increase in the stiffness occurs due to volume changes in the soil, then a small variation in stiffness is presented as suction increase. Finally, at residual conditions, a sharp increase in the stiffness is displayed again. The same behavior has been observed by Cho & Santamarina (2001), Inci et al. (2003) and by Mendoza et al. (2005). Mendoza et al. (2005) found the limits of the three stages of behavior are related with the three main zones defined in the retention

curve. They suggested that the retention curve may be useful to predict the variation of the stiffness at very small strains with the degree of saturation.

In general, for a fixed matrix suction, the higher the initial degree of saturation, the higher the stiffness at very small strains (Fig. 6 and Fig. 7). On the other hand, the strained line moves away when increases matrix suction. The strained line slopes are proportional to the value of the initial degree of saturation. These results suggest that the initial degree of saturation affects both the value of the stiffness at very small strains and the path followed by the modulus with the matrix suction during drying.
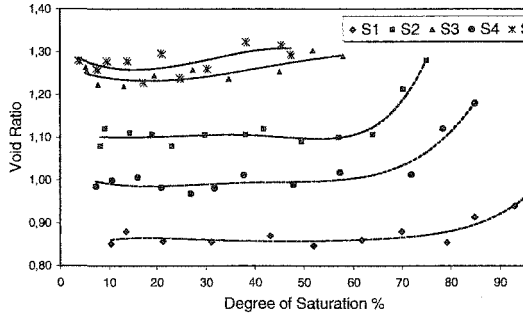
Figure 5. Variation of void ratio with degree of saturation.
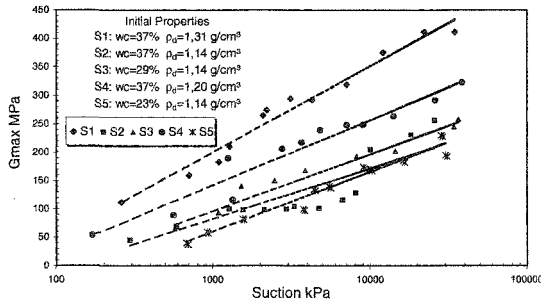
Figure 6. Variation of shear modulus with matrix suction.
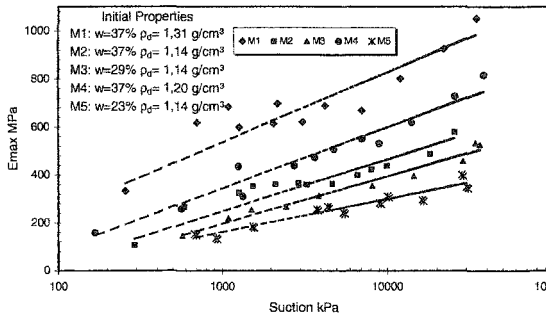
Figure 7. Variation of Young's modulus with matrix
suction.

Influence of the initial void ratio

In order to investigate the effects of the initial void ratio on the stiffness, at very small strains, results of three samples prepared with the same initial water content and different void ratio were compared (samples 1, 2 and 4 in table 2). The dry density was higher and smaller than the maximum of the standard proctor curve, and the water content was on the wet side. The experimental results for the shear modulus are shown in figure 8. It appears that for a fixed matrix suction, the smaller the initial void ratio, the higher the stiffness at very small strains. This is due to the fact that the lower the void ratio, the higher the coordination number (i.e. average number of contacts per particle). In general, the greater the coordination number, the higher the stability of the packing (Santamarina 2001).

Influence of the compaction water content

In order to examine the role of the compaction water content, similar drying processes were followed with samples prepared at three different initial water contents, on the dry and wet side of standard proctor conditions. The initial density of the samples was smaller than the maximum density of the standard proctor curve. The samples tested were 2, 3 and 5 (see table 2). Results for the Young's modulus are shown in figure 9. In a similar way that for the initial void ratio, the compaction water content also influences the modulus at very small strains: for a fixed matrix suction, the higher the compaction water content, the higher the stiffness. For samples with the same initial void ratio, the higher the water content, the lower the pore size (Mendoza et al. 2005), and therefore, the coordination number is bigger. However, samples prepared at the same compaction water content but different initial void ratio show important differences in stiffness for a given value of matrix suction. Therefore, the initial void ratio seems to have more influence on the stiffness at very small strain than the compaction water content.
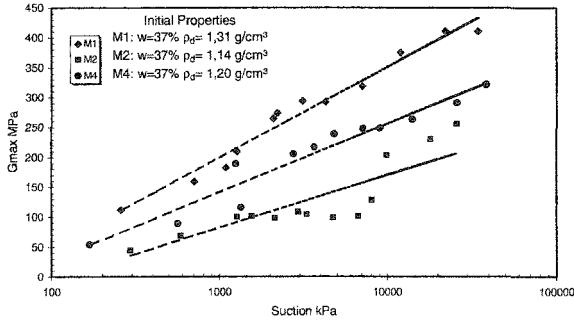
Figure 8. Influence of the initial void ratio on the relationship shear modulus - matrix suction for samples prepared at the same initial water content.
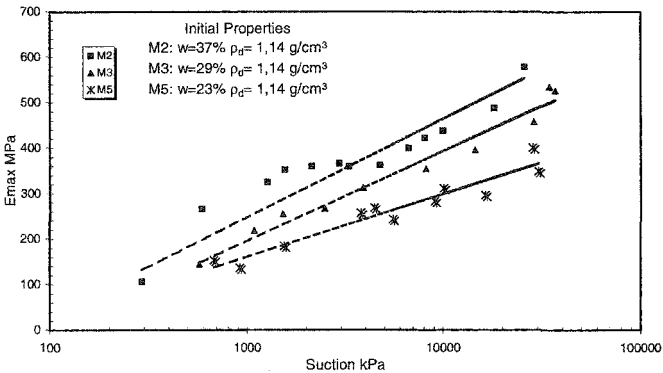
Figure 9. Influence of the compaction water content on the relationship Young's modulus - matrix suction for samples prepared at the same initial dry density.

Contours of equal suction

The relationship between Young's modulus and degree of saturation with contours of equal suction is shown in figure 10 (similar curves are displayed for shear modulus). At the beginning of the drying process, it appears that E_{max} is independent of the initial water content (horizontal contours of equal suction). With continued drying, the water content becomes more important affecting the value of the modulus. In general, the contours of equal suction change during drying: they become more vertical as the drying take place. In other words, the matrix suction, or degree of saturation has more influence on the soil modulus when the sample is close to its residual stages.

Particle displacements and particle rotation without volume change

At the beginning of the drying process a strong increase in the density of the soil occurs (Fig. 5). As the drying takes place, the increase in suction does not produce major volume changes, but eventually might cause particle displacement and particle rotation, which in turn may produce a more "efficient structure". This fact may explain the different path followed by void ratio during wetting of the sample 2

(Fig. 11), where two identical samples were allowed to dry gradually: one until no further shrinkage occurred (M2HI) and the other up to air-dry condition (M2H). Then, a wetting path was followed to the reach initial water content. The data obtained from drying paths are indicated by full symbols and the data from wetting paths, by empty symbols (Fig. 11).The experimental results shows that the sample which reached the air-dry condition displayed more swelling than the other sample during wetting. This swelling is due, possibly, to both the increase in the coordination number, occurring during drying, and changes in the water double layer thickness at the clay surface. If there is not volume changes, the increases in the coordination number is due only to particle displacements and particles rotation.
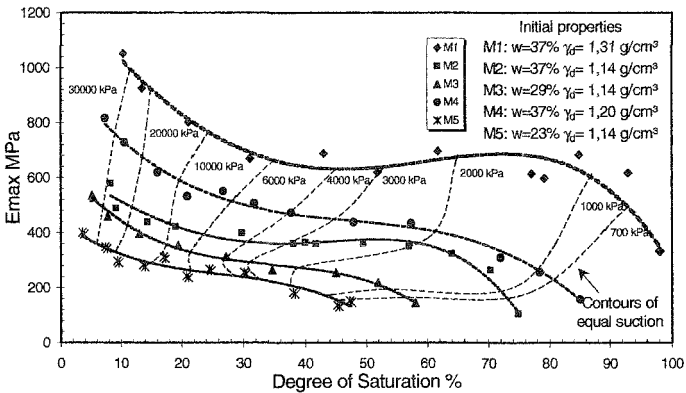
Figure 10. Influence of the compaction water content on the relationship Young's modulus - matrix suction.

On the other hand, it appears that the increase in the coordination number, during drying is related to both the initial void ratio and the compaction water content: the lower the void ratio the higher the coordination number (the lower the initial void ratio, the greater the slope at the straight line Fig. 8), and the higher the compaction water content, the higher the coordination number (the higher the compaction water content, the greater the slope of the straight line Fig. 9).

CONCLUSIONS

The main conclusions obtained from this study, which are related to the soil used, are:

1. Suction significantly increases the stiffness of unsaturated statically compacted clay. This effect is more pronounced in samples with low initial void ratio and high initial degree of saturation.

2. The matrix suction produces an additional effective confining pressure in the soil structure. An increase in the coordination number also occurs as the suction increases. This in turn increases the stiffness of the soil at very small strains.
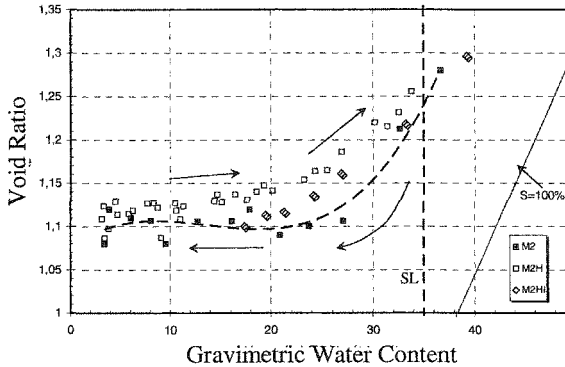
Figure 11. Volume changes during drying and wetting.

3. A low initial void ratio and high compaction water content produce smaller pores sizes (i.e. higher coordination number) and therefore major stiffness.

4. The initial void ratio seems to have more influence on the stiffness at very small strains than the compaction water content.

5. The initial degree of saturation appears to influence the path followed by the stiffness at very small strains with the matrix suction during drying.

6. When no more shrinkage occurs in the soil, displacements and rotation of particles may continue to occur as drying continues.

REFERENCES

Alarcón-Guzman, A. (1986). "Cyclic Stress-Strain and Liquefaction Characteristics of Sands." Ph.D Thesis. Purdue University.

Alarcón-Guzman, A., Chameau, J.L., Leonards, G.A. & Frost, J.D. (1989). "Shear Modulus and Cyclic Undrained °Behavior of Sands." Soils and Foundations, Vol 29, N° 4, pp 105-119.

Atkinson, J.H. (2000). "40th Rankine Lecture. Non – Linear Soil Stiffness in Routine Design." Géotechnique 50, N° 5, pp 487-508.

Cho, G.C., & Santamarina, J.C (2001). "Unsaturated Particulate Materials – Particle – Level Studies." Journal of Geotechnical and Geoenvironmental Engineering, Vol. 127 N° 1. ASCE. pp 84 – 96.

Clayton, C.R. & Heymann, G. (2001). "Stiffness of Geomaterials at Very Small Strain." Géotechnique 51 N° 3 pp 245-255.

Dineen, K. (1997). "The Influence of Soil Suction on Compressibility and Swelling." Ph.D Thesis. University of London.

Dyvik, R. & Madshus, C. (1985). "Laboratory Measurements of G_{max} Using Bender Elements." Proc ASCE Annual Convention: "Advances in the Art of Testing Soils under Cyclic Condicions", Detroit.

Georgiannou, V.N., Rampello, S. & Silvestri, F. (1991). "Static and Dynamic Measurement of Undrained Stiffness of Natural Overconsolidated Clay." Proceeding of the X ECSMFE, Florence. Vol. 1, pp 91-96.

Greacen, E.L., Walker, G.R. & Cook, P.G. (1987). "Evaluation of the Filter Paper Method for Measuring Soil Water Suction." Int. Conf on Measurement of Soil and Plant water status, pp 137-143.

Hight, D.W., Bennell, B, Davis, P.D., Jardine, R.J. & Porovic, E. (1997). "Wave Velocity and Stiffness Measurements of the Crag and Lower London Tertiaries at Sizewell." Géotechnique 47, N° 3, pp 451-474.

Inci, G., Yesiller, N. & Kagawa, T. (2003). "Experimental Investigation of Dynamic Response of Compacted Clayey Soils." Geotechnical Testing Journal, Vol. 26, N° 2, pp 125 – 141.

Jamiolkowski, M., L o Presti, D. & Pasqualini, E. (1986). "Behavior of Soil at Small Strains." Proceedings of the International Symposium on Engineering Geology Problems in Seismic Areas. Bari.

Mancuso, C., Vassallo, R. & d'Onofrio, A. (2002). "Small Strain Behavior of a Silty Sand in Controlled – Suction Resonant Column – Torsional Shear Tests." Canadian Geotechnical Journal, 39, pp 22 – 31.

Marinho, F. Chandler, R. & Crilly, M. (1995). "Stiffness Measurements on an Unsaturated High Plasticity Clay Using Bender Elements." Proc 1st Int. Conf. On Unsaturated Soils. Vol 2 pp 535 – 539.

Mendoza, C.E. (2004). "Influence of Suction on the Shear Modulus at Very Small Strains on Compacted Soils." MSc Dissertation. National University of Colombia. Bogotá (In Spanish)

Mendoza, C.E & Colmenares, J.E. (2004a). "Mounting and Calibration of the Bender Elements." Proc. X Colombian Congress of Geotechnics. Paipa. pp 33-43. (In Spanish).

Mendoza, C.E & Colmenares, J.E. (2004b). "Shear Modulus and Capillary Forces." Proc. X Colombian Congress of Geotechnics. Paipa. pp 117-123. (In Spanish)

Mendoza, C.E, Colmenares, J.E. & Merchán V.E. (2005). "Stiffness of an Unsaturated Compacted Clayed Soil at very small Strains." Proc. International Symposium on Advanced Experimental Unsaturated Soil Mechanics, Trento, Italy 27-29 June 2005, pp 199-204.

Qian, X, Gray, D & Woods, R. (1993). "Modulus of Unsaturated Sands." Journal of Geotechnical Engineering, Vol. 119, N° 2, pp 295 -314.

Ridley, A.M., Dineen, K., Burland, J.B. & Vaughan P.R. (2003). "Soil Matrix Suction: Some Examples of its Measurement and Application in Geotechnical Engineering." Géotechnique 53, N° 2, pp 241-253.

Santamarina, J. C. (2001). "Soil and Waves." John Wiley and Sons, Ldt. New York.

Shackel, B. (1970). "The Compaction of Uniform Replicate Soil Specimens." Journal of the Australian Road Research Board. Vol 4, N° 5, pp 12 – 31.

Vanapalli, S.K., Fredlund, D.G. & Pufahl, D.E. (1999). "The Influence of Soil Structure and Stress History on the Soil-Water Characteristics of a Compacted Till." Géotechnique 49, N° 2. pp 143-159.

Viggiani, G. & Atkinson, J.H. (1995). "Stiffness of Fine-Grained Soil at very Small Strain." Geotechnique, 45, N° 2, pp 249 – 265.

Wu, S., Gray, D.H. and Richart, F.E. Jr. (1984). "Capillary Effects on Dynamic Modulus of Sands and Silts." J. Geotech. Eng.,ASCE, 110(9), p.p. 1188-1203.

Resilient Modulus and Plastic Strain of Unsaturated Cohesive Subgrade Soils

Johnson H. S. Kung[1], H. D. Lin[2], Shu-Jung Yang[3], Wei-Hsing Huang[4]

[1]Department of Construction Engineering, National Taiwan University of Science and Technology, P. O. Box 117-653, Taipei, 106, Taiwan, R. O. C; PH(886)953726099; FAX:(886)2-27376606; johnsonlive@yahoo.com.tw

[2]Department of Construction Engineering, National Taiwan University of Science and Technology, #43,Sec.4,Keelung Rd., Taipei, 106, Taiwan, R. O. C; PH(886)2-27376559; FAX(886)2-27376606; hdlin@mail.ntust.edu.tw

[3]Department of Civil Engineering, National Central University, Jungli, Taoyuan, Taiwan 32054; PH(886)3-4257062; FAX(886)3-4252960; s9322079@cc.ncu.edu.tw

[4]Department of Civil Engineering, National Central University, Jungli, Taoyuan, Taiwan 32054; PH(886)3-4257062; FAX(886)3-4252960; t321655@ncu.edu.tw

Abstract

Construction specifications generally require that subgrade soils be compacted in the field at or near optimum moisture content (OMC). As such, subgrade soils should be treated as unsaturated soils. In addition, moisture content in the pavement components changes over time as a result of environmental and traffic factors. Numerous studies indicated that the moisture content of the subgrade, after construction, would attain an equilibrium with the environment and this is referred to as the equilibrium moisture content (EMC). However, the influence of water content or soil suction on the unsaturated cohesive subgrade soils has not been systematically considered in the conventional subgrade soil design. This paper aims to evaluate the variations of resilient modulus and plastic strain with the post-construction moisture content and soil suction for cohesive subgrade soils.

This study carried out the resilient modulus and plastic strain tests via the MTS cyclic triaxial system. To simulate subgrade soils at in-service conditions, soil specimens were compacted at the optimum moisture content, and then placed in the damp room to increase the moisture content to equilibrium condition for resilient modulus and plastic strain test. Based on the above test results, the characteristic of

resilient modulus and plastic strain of two unsaturated cohesive subgrade soils were investigated. The experimental results demonstrated that the stress state, moisture content, and soil suction influenced the resilient modulus and the plastic strain. Unsaturated subgrade resilient modulus reduces with increasing deviator stress and decreasing matric suction. The subgrade plastic strain increases as the deviator stress increases and the matric suction decreases. Furthermore, the high subgrade moisture content or low soil suction would result in sharp decrease in subgrade resilient modulus, and should be avoided for pavement design. Finally, based on the concept of effective stress of unsaturated soils, a prediction model incorporating cyclic deviator stress and matric suction for unsaturated cohesive subgrade soils was established. The matric suction of soil proved to be a good prediction variable for resilient modulus. Also, the effects of seasonal variation of moisture content on the resilient modulus of subgrade soils are reflected in the deviator stress-matric suction model for the prediction of resilient modulus.

Key Words: unsaturated soils, resilient modulus, plastic strain, matric suction

INTRODUCTION

Resilient modulus (M_r) and plastic strain represent the repeated elastic and excessive plastic stress--strain behavior of subgrade soils respectively. The design procedures for flexible pavements, presented in the 1986 AASHTO Guide for Design of Pavement Structures (1986), use resilient modulus in the pavement design to represent the deformational characteristics of pavement materials, replacing the empirical "soil support value" used in the previous design guide. The plastic strain induced by the repeated traffic load was treated to be the important parameter for flexible pavement system recently (Puppala et al. 2004). Both parameters are determined in the laboratory in accordance with AASHTO T292-91 under conditions of maximum dry density and optimum water content. As such, subgrade soils should be treated as unsaturated soils post compaction.

In service period, moisture content in the pavement components changes over time as a result of environmental and traffic factors. Also, subgrade moisture is sensitive to rising in water table, infiltration of water, or evaporation (Khoury et al. 2003). Thadkamalla and George (1995) indicated that subgrade soils exhibited increased average moisture content at the shallow part of the subgrade and a decreased fluctuation of water content over time. Quintus and Killingsworth (1998) examined the subgrade of 137 LTPP test sites, including 59 sites with cohesive subgrade soils and 78 sites with granular subgrade. They reported that the in-situ moisture content of the 59 cohesive subgrades was always at the wet side of OMC and is referred to as the equilibrium moisture content (EMC). This finding confirmed that the moisture content of cohesive subgrades increased after construction and the degree of saturation of cohesive subgrades was mostly less than 100%. Consequently, the theory of unsaturated soil mechanics is used to study the characteristics of resilient modulus and plastic strain for cohesive subgrade soils.

The matric suction is defined to be the independent stress variable by the extended Mohr-Coulomb theory (Fredlund and Morgenstern 1977). The matric suction controls the mechanical behavior of unsaturated soils. This paper aims to evaluate the

variations of resilient modulus and plastic strain in terms of soil suction. Relationship between the resilient modulus and soil suction has been proposed by some researchers (Sauer and Monismith 1968 ; Khoury et al. 2003 ; Fredlund and Rahardjo 1993 ; Yang et al. 2005). They showed that the resilient modulus increased with increasing matric suction.

Resilient modulus and plastic strain test procedures require that subgrade soils undertake five deviator stresses of 21, 34, 48, 69 and 103 kPa in sequence. It is difficult to measure soil suctions corresponding to each deviator stress using the filter paper method in a test. Axis-translation technique, widely used in triaxial testing of unsaturated soils, is considered as an appropriate approach for resilient modulus testing under controlled matric suction. However, this technique has not been used for repeated loading tests before. Therefore, this study examines the effect of matric suction on the resilient modulus and plastic strain of compacted subgrade soils using axis-translation technique, with emphasis on the variation in matric suction with the deviator stress. Three initial matric suctions were chosen to simulate the stress state of in-service subgrade soils. Resilient modulus and plastic strain tests were conducted at these 3 matric suction levels to examine how saturation and matric suction influenced the resilient and plastic stress–strain behavior of cohesive subgrade soils.

TEST EQUIPMENT

The cyclic resilient modulus and plastic strain tests were performed using an MTS closed loop hydraulic loading system and the 458 controller. The axial deformation of the specimen was measured using the linearly variable displacement transformers (LVDTs) with a maximum stroke of 10 mm outside the triaxial chamber, and the deviatoric stress was measured using an external load cell with a capacity of 10 kN. The data acquisition system was programmed to take 200 readings per second for each channel monitoring the axial loading and deformation.

Matric suction was applied to a specimen through one water pressure controller and one air pressure controller. Positive pore water pressure was maintained by using the axis-translation principle proposed by Hilf (1956). The use of the axis-translation technique requires independent control of pore-air pressure and control or measurement of pore-water pressure. Pore–water pressure was applied or measured at the base of the specimen through a saturated fine ceramic disk, which had an air entry value of 500 kPa. Pore–air pressure was applied at the top of the specimen through a coarse corundum disk. The applied pore–air and pore–water pressures were allowed to equilibrate within the whole soil specimen for up to about 7 days in some cases. The end of the equilibration was determined by the rate of water flowing in and out of the specimen.

MATERIALS AND SAMPLE PREPARATION

Material

The soils used in this study are residual lateritic soil and pulverized mudstone. Both soils are frequently encountered subgrade soils in the construction of highways in

northern Taiwan. The soils were classified as A-7-6 and A-6; both are cohesive according to AASHTO T 292-91(1992). Their basic properties, including specific gravity (Gs), liquid limit (LL), plastic index (PI), and clay content were evaluated and the results are summarized in Table 1.

The drying soil-water characteristic curve tests were performed using pressure-plate apparatus in accordance with ASTM D 2325-68.The results for the two soils are shown in Fig. 1. Test results show that the A-7-6 and A-6 soils start to desaturate at a matric suction of about 10 kPa. When matric suction is higher than 50 kPa, the A-6 soils with low plasticity retained the small suction and A-7-6 soil with high plasticity retained the high suction at specified water content.

Table 1. Properties of the soils

Soil	G_s	LL	PI	Clay Content (%< 0.002mm)	AASHTO Classification	USUC Classification
1	2.71	46	19	55.4	A-7-6	CL
2	2.67	37	15	41.5	A-6	CL
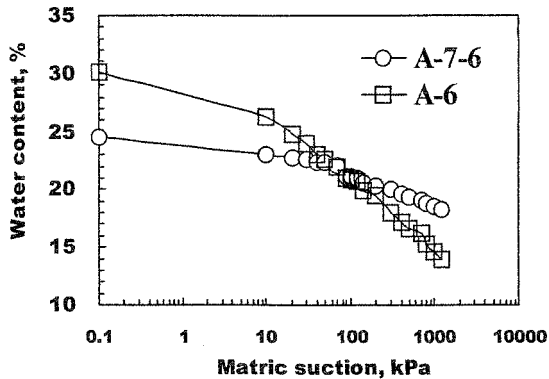
Figure 1. Soil–water characteristic curves for A-7-6 and A-6 soils.

Sample Preparation

Soil specimens were 50 mm in diameter and 100 mm in height and compacted at OMC, in accordance with AASHTO T-180. After compaction, the sample was extracted from the mold, and its initial weight, height, and diameter were measured. The sample was then placed in a split mold and subjected to the wetting process addressed by Yang et al. (2005). The moisture content of the samples was increased to different moisture contents predetermined to represent different stages of the subgrade in-service. This helps to reduce the time required to reach equilibrium of the initial matric suction and the moisture condition in the specimen when using the

axis-translation technique.

TEST METHODS AND PROCEDURES

Test Methods

The AASHTO T 292-91 test method was used to determine the resilient modulus and plastic strain of each specimen. The test consists of applying a cyclic load that has a square-shaped load pulse with fixed cycle duration of 1.0 second and load duration of 0.1 second. Specimens were loaded according to the T 292-91 test method. The conditioning process of 1,000 loading cycles is needed, since it can reduce bad contact between the specimen and the top disk or the specimen and the bottom disk. After conditioning, T 292-91 undertakes five deviator stresses of 21, 34, 48, 69 and 103 kPa in sequence at a constant confining pressure of 21 kPa. The loading process is under undrained pore-water condition. Each loading process has 50 loading cycles. However, matric suction in specimen is hard to reach steady during 50 loading cycles. It is necessary to increase number of loading cycles to observe variation of matric suction in 10,000 loading cycles. For each loading sequence, the load and the vertical displacement were measured and used to determine the resilient modulus and plastic strain as matric suction reaches equilibrium.

Test Procedures

To ensure no air in water compartment and saturation of high air entry ceramic disk, six-hours of flushing any diffused air bubbles is needed. Cell pressure is 600 kPa for flushing (Fredlund and Rahardjo 1993). Specimen was compacted at OMC. After compaction, the specimen was extracted from the mold and then wetted to simulate the in-service moisture.

After compaction and wetting, specimen was placed on the saturated ceramic disk, and then sealed onto the pedestal by a membrane. The cell was filled with water and all drainage valves were opened. Cell pressure (σ_3) and air backpressure (u_a) were equally and simultaneously increased to prevent premature consolidation. Water backpressure (u_w) continued to increase until matric suction (u_a-u_w) reached the designated initial matric suction (50, 150, and 450 kPa). The moisture contents corresponding to these initial matric suctions are all at the wet side of OMC, as shown in Table 2. Table 2 summaries the moisture content of the two soils at compacted, wetted, and equilibrium conditions. Also shown in Table 2 (the last column) are the corresponding water content derived from soil-water characteristic curves at the predetermined matric suctions. It is noted that the water contents at equilibrium conditions are very close to those corresponding to the drying soil-water characteristic curve at the 3 matric suction levels. Hence, the control of initial matric suction in the axis-translation technique is considered satisfactory.

Consolidation stage was initiated by elevating cell pressure above air backpressure to a net confining pressure (σ_3-u_a) of 21 kPa. During consolidation, air backpressure and water backpressure were controlled. Hence, specimens were held at a desired matric suction and net confining pressure. In addition to consolidation, equilibrium of initial matric suction was completed at this stage. If specimens are too dry (i.e. matric

suction in specimen is higher than initial matric suction), specimens will absorb water. Otherwise water will be drained out of the specimens. Consolidation is assumed to have reached an equilibrium condition when there is no longer a tendency for the overall volume change. The changes level off gradually and an equilibrium of moisture condition and matric suction in the specimen is reached in 2–3 days.

The specimen was then tested for resilient modulus under drained pore-air condition and undrained pore-water condition. During repeated loading, the pore-air pressure was maintained, however, the pore-water pressure changed. Thus, the net confining pressure remained constant throughout the test, whereas the matric suction varied.

Table 2. Results of the water contents of the soils under various conditions.

Soil	Initial Matric Suction (kPa)	Compacted (%)	Wetted (%)	Equilibrated (%)	Soil–water characteristic curve (%)
A-7-6	50	18.1	21.3	21.8	22.4
	150	18.1	22.3	20.8	20.5
	450	18.1	20.9	19.7	19.6
A-6	50	16.8	24.4	23.2	22.6
	150	16.8	21.2	20.2	19.9
	450	16.8	20.5	19.1	18.2

RESULTS AND DISCUSSION

Resilient Modulus

The resilient modulus is defined by the ratio of deviator stress to resilient strain. For each loading sequence, the load and the vertical displacement for the last five cycles after 10,000 loading applications were measured and used to determine the resilient modulus.

The relationships between the resilient modulus and the deviator stress for A-7-6 and A-6 soil at various initial matric suctions is shown in Fig. 2. Regardless of soil type, the resilient modulus was found to increase with increasing deviator stress at initial matric suction of 450 kPa. However, the resilient modulus decreases with increasing deviator stress at initial matric suctions of 50, 150 kPa. This can be explained by plotting the resilient strain at different matric suction levels for A-6 soils, as shown in Fig. 3. It is noted that, at low matric suction (high saturation) levels, the soil becomes so soft and vulnerable to deformation that the resilient strain increases sharply and exhibits declining resilient modulus with deviator stress accordingly. On the contrary, the soil becomes harder to deform that the resilient strain increases unapparent and exhibits rising resilient modulus with deviator stress accordingly at high suction level.
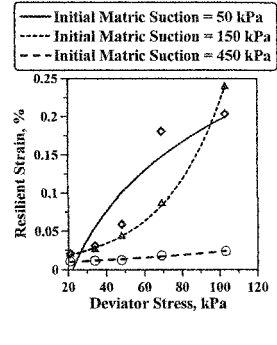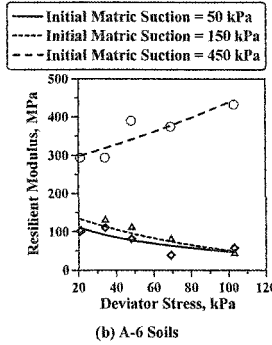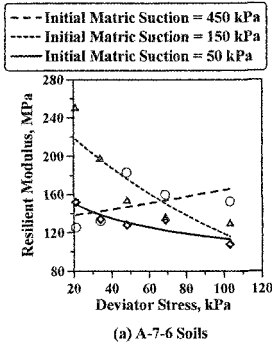
Figure 2. Variation of resilient modulus with deviator stress for A-7-6 Soils and A-6 Soils.

Figure 3. Variation of resilient strain with deviator stress for A-6 Soil.

The variations of resilient modulus with matric suctions corresponding to different deviator stress at different initial matric suctions for A-6 soils are shown in Fig. 4. The resilient modulus increased with increasing matric suction except at initial matric suction of 450 kPa. This can be explained by plotting the resilient strain at different deviator stress and matric suction levels, as shown in Fig. 5. It is noted that, at low matric suction levels, the resilient strain decrease sharply with increasing matric suction (increasing deviator stress at the same time) and exhibits rising resilient modulus with matric suction accordingly. On the contrary, the resilient strain decreases unapparent with increasing matric suction and exhibits declining resilient modulus with matric suction accordingly at high suction level. However, as the matric suction increases, the resilient strain decreases for all specimens. This indicates that high matric suction increases the effective stress in the specimen and thus reduces the deformation under different deviator stress.

Notably, the resilient modulus shows a decrease, representing reductions ranging from 15% to 40%, as the initial matric suction decreases from 450 kPa to 50 kPa for A-7-6 soil. However, sharper decreases in resilient modulus were observed with decreasing initial matric suction for A-6 soil. Reductions in resilient modulus varied from 40% to 85% depending on the deviator stress. This is because A-6 soil has a larger increase in moisture content than A-7-6 soil as the matric suction is reduced from 450 to 50 kPa. Hence, A-6 soil exhibits more pronounced decreases in resilient modulus than A-7-6 soil.
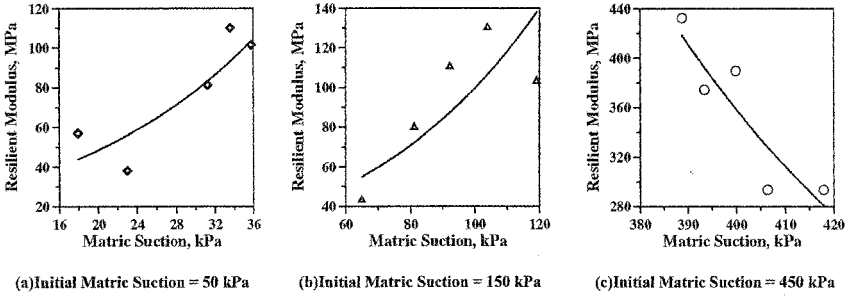
Figure 4. Variation of resilient modulus with matric suction for A-6 Soil.
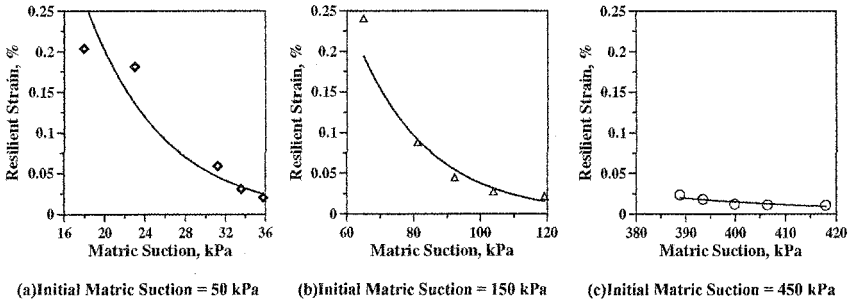
Figure 5. Variation of resilient strain with matric suction for A-6 Soil.

A Prediction Model for Resilient Modulus

The deviator stress model was widely used in the past to represent the resilient modulus of cohesive subgrade soils. The following form is suggested by AASHTO T 292-91 (1992):

$$M_r = k_1 (\sigma_d)^{k_2} \tag{1}$$

Where M_r = resilient modulus; σ_d = deviator stress; k_1 and k_2 are regression parameters. Since the deviator stress model does not reflect the effect of moisture content on resilient modulus, Yang, et al. (2005) incorporated the matric suction in the model to account for moisture conditions in the soils. Based on the effective stress concept, the deviator stress-matric suction model is proposed to describe the relationship between resilient modulus and matric suction.

$$M_r = k_3 (\sigma_d + \chi \psi_m)^{k_4} \tag{2}$$

Where M_r = resilient modulus; σ_d = deviator stress; ψ_m = matric suction, i.e., $(u_a - u_w)$; χ = parameter initially thought to be a function of degree of saturation ($\chi = 0$ for dry soils, $\chi = 1$ for saturated soils); and, k_3 and k_4 are regression parameters. In this model, the resilient modulus is expressed as a function of deviator stress and matric suction. The matric suction is negative pressure, the opposite value to atmospheric pressure, and is expressed as a positive value.

In Eq. (2), χ represents the contribution of matric suction to the effective stress and can be considered as the weight of matric suction on effective stress. For saturated soils, parameter χ is equal to 1. For unsaturated soils, Khalili and Khabbaz (1998) found a unique relationship between χ and the ratio of ϕ_e / ϕ_m,

$$\chi = \left(\frac{\psi_e}{\psi_m} \right)^{0.55} \tag{3}$$

Where ϕ_e = air entry value. At suction levels lower than the air entry value, soils are practically saturated. Fig.6 shows the air entry values are 13 kPa and 5 kPa for A-7-6 and A-6 soils, respectively. Experimental results derived in this study from resilient modulus tests using axis-translation technique are used to test the validity of the AASHTO model and proposed model. Table 3 summarizes the results of regression analysis using the deviator stress model and the deviator stress-matric suction model in conjunction with Eq. (3). In general, the deviator stress-matric suction model exhibits improved correlation over the deviator stress model. More importantly, the incorporation of matric suction makes the resilient modulus model more reasonable, because it is derived based on the effective stress concept. The proposed model can be used for characterizing the resilient modulus of unsaturated in-service subgrade soils.

Table 3. k1 to k4 constants for deviator stress model and deviator stress-matric suction model.

Soil	Initial Matric Suction (kPa)	Deviator Stress Model			Deviator Stress-Matric Suction Model		
		k_1	k_2	R^2	k_3	k_4	R^2
A-7-6	50	262.30	-0.1813	0.802	409.70	-0.2698	0.808
	150	297.08	-0.1796	0.965	677.98	-0.3397	0.970
	450	138.67	0.0739	0.156	84.99	0.1628	0.115
A-6	50	611.06	-0.5526	0.602	1430.30	-0.7258	0.600
	150	692.29	-0.5379	0.593	3504.30	-0.8740	0.683
	450	62.84	0.3332	0.909	16.59	0.5855	0.846
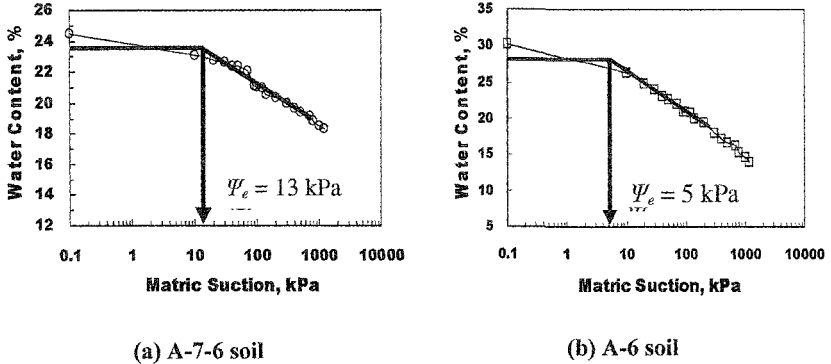
(a) A-7-6 soil   (b) A-6 soil

Figure 6. Air entry values for A-7-6 and A-6 soils.

Plastic Strain

The plastic strain is defined by the un-rebound deformation during the cyclic loading process. For each loading sequence, the load and the vertical displacement for the last five cycles after 10,000 loading applications were measured and used to determine the plastic strain.

The relationships between the plastic strain and the deviator stress for A-7-6 and A-6 soil at various initial matric suctions is shown in Fig. 7. Regardless of soil type, the resilient modulus was found to increase with increasing deviator stress at all specimen. The plastic strain of A-7-6 is considerable smaller than A-6 soil at different deviator stress. This shows that the A-7-6 soils will perform better than the A-6 soils under the cyclic load in service period.

The variations of plastic strain with matric suctions corresponding to different deviator stress for A-6 soils are shown in Fig. 8. The plastic strain decreased sharply with increasing matric suction at all specimen. This verifies once again that high matric suction increases the effective stress in the specimen and thus reduces the deformation under different deviator stress. The relationship of plastic strain versus matric suctions for A-7-6 soils are plotted in Fig.9. A slightly difference from A-6 soils, the plastic strain increased unobvious with increasing matric suction at different deviator stress. This is because A-7-6 soil has a smaller decrease in moisture content than A-6 soil as the matric suction is increased from 50 to 450 kPa. Hence, the effect of matric suction for A-7-6 soil is unpronounced under the selected suction range.

CONCLUDING REMARKS

Two cohesive soils were tested for resilient modulus and plastic strain using the axis-translation technique to evaluate the effect of matric suction on resilient modulus and plastic strain. Moisture content derived from various specimen conditions demonstrate that control of matric suction in the specimen through the

(a) A-7-6 Soils   (b) A-6 Soils
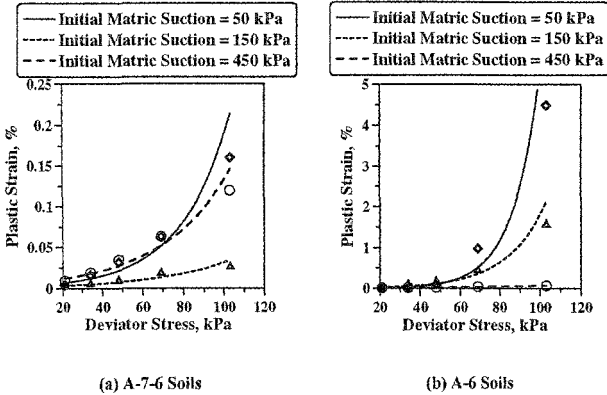
Figure 7. Variation of plastic strain with deviator stress for A-7-6 Soils and A-6 Soils.
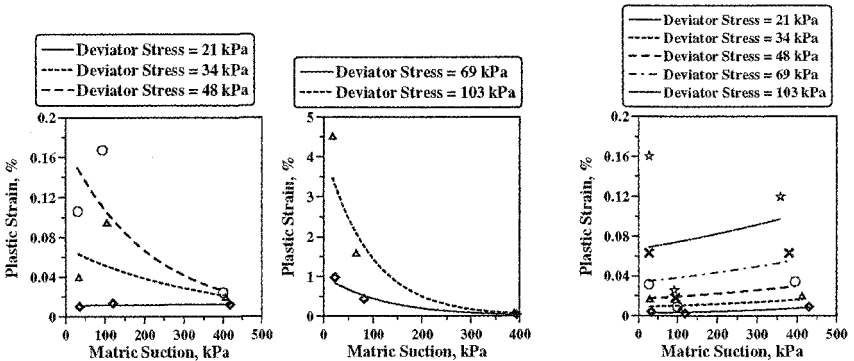
Figure 8. Plastic strain and matric suctions for different deviator stress of A-6 soils.

Figure 9. Plastic strain and matric suctions for different deviator stress of A-7-6 soils.

axis-translation technique is satisfactory. Laboratory data indicate that increases in matric suction would result in decreases in deformation and hence increases in resilient modulus. For subgrade soils at moisture conditions approaching saturation, very sharp declines in resilient modulus can occur due to the low matric suction level in the soil. The subgrade plastic strain increases as the deviator stress increase and matric suction decreases. Based on the concept of effective stress and experimental results, matric suction is judged to be an important factor for characterizing the resilient modulus of unsaturated soils. With the incorporation of matic suction in the resilient modulus model, the effect of moisture conditions at various in-service situations can be reflected. The deviator stress-matric suction model suggested in this paper provides an alternative that has better fundamental meaning over the deviator stress model.

ACKNOWLEDGEMENTS

REFERENCE

1. AASHTO, (1986). *Guide for Design of Pavement Structures*. American Association of State Highway and Transportation Officials.
2. Puppala, A. J., Chomtid S., and Wattanasanticharoen, E. (2004). "Plastic deformation potentials of sandy clay from repeated load triaxial test." Geotechnical Engineering for Transportation Projects, GeoTrans.
3. Khoury, N. N., Musharraf, Z. M., Nevels, J. B., and Mann, J. (2003). "Effect of soil suction on resilient modulus of subgrade soil using the filter paper technique." CD- ROM, Transportation Research Board, National Research Council, Washington, D.C.
4. Thadkamalla, G. B., and George, K. P. (1995). "Characterization of subgrade soils at simulated field moisture." In *Transportation Research Record: Journal of the Transportation Research Board, No. 1481,* TRB, National Research Council, Washington, D.C., 21-27.
5. Quintus, H.V., and Killingsworth, B. (1998). "Analyses relating to pavement material characterizations and their effects on pavement performance." Publication FHWA-RD-97-085, FHWA, U.S. Department of Transportation.
6. Fredlund, D. G., and Morgenstern, N. R. (1977). "Stress state variables for unsaturated soils." *Journal of Geotechnical Engineering,* ASCE, GT5, Vol.103, 447-446.
7. Sauer, E. K., and Monismith, C. L. (1968). "Influence of soil suction on behavior of a glacial till subjected to repeated loading." *Highway Research Record,* No. 215, 8-23.
8. Fredlund, D. G., and Rahardjo, H. (1993). *Soil mechanics for unsaturated soils.* John Wiley & Sons, Inc., New York.
9. Yang, R. R., Huang, W. H., and Tai, Y. T. (2005). "Variation of resilient modulus with soil suction for compacted subgrade soils." CD-ROM. Transportation Research Board, National Research Council, Washington, D.C.
10. Hiff, J. W. (1956). *An investigation of pore water pressure in compacted cohesive soils.* Technical Memo 654, Bureau of Reclamation, Denver.
11. AASHTO, (1992). Designation T292-91 : standard method of test for resilient modulus of subgrade soils and untreated base/subbase materials. American Association of State Highway and Transportation Officials.
12. Khalili, N., and Khabbaz, M. H. (1998). "A unique relationship for χ for the determination of the shear strength of unsaturated soils." *Geotechnique,* Vol. 48, No. 2, 1-7.

Soil Property Variation by Time Domain Reflectometry

Xiong Yu[1], Vincent P. Drnevich[2], Robert L. Nowack[3]

[1] Assistant Professor, Department of Civil Engineering, Case Western Reserve University, 10900 Euclid Avenue, Bingham 210, Cleveland, OH 44106-7201, xxy21@po.cwru.edu
[2] Professor, Department of Civil Engineering, Purdue University, 550 Stadium Mall Drive, West Lafayette, IN 47907-2051, Drnevich@purdue.edu
[3] Professor, School of Earth Science, Purdue University, 550 Stadium Mall Drive, West Lafayette, IN 47907-2051, Nowack@purdue.edu

Abstract

Time Domain Reflectometry (TDR) is widely applied for measuring soil water content and electrical conductivity. The method works by analyzing the signal responses under the excitations by a small magnitude electrical pulse, which are used to estimate the properties of the soil sensed by the TDR measurement probe. The commonly used method of TDR signal analysis empirically determines the characteristic reflection points. The soil properties obtained with this method are the average values over length of the TDR probe. The variation of material properties with distance along the probe are generally ignored, which otherwise could provide supplementary information of practical importance. The study of vadose zone is an example where the soil moisture varies with depth. This paper presents an approach for obtaining soil property variation within the probe from TDR measurements. It makes use of a forward model that consists of a frequency domain model for a non-uniform TDR system and a simplified model for soil dielectric permittivity. Inversion analysis was used to determine the geometry and soil properties for each layer within the probe. Both the forward model and the inversion method are first illustrated by numerical examples. They are then applied to analyze data from experimental measurements on layered soils. The preliminary results indicate that the framework provides accurate determination of soil properties, including the thickness of each layer as well as the corresponding soil properties. The capability of obtaining material profiles could further enhance the current TDR-based field monitoring system. It could also be incorporated into the existing cone penetrometers to obtain more information on soil properties.

Introduction

Time Domain Reflectometry (TDR) is a useful technology for various material and infrastructure applications (Dowding and O'Connor 1999). It utilizes transmission line principles and measures the reflections due to the change of material properties or probe geometry. The TDR signal is generally analyzed in the time domain to empirically determine the characteristic reflection points. The measured soil properties are averaged values over the length of measurement probe. More detailed information about material properties can be obtained by model based inversion analysis.

The numerical models for a TDR system generally assume the system can be described by the uniform transmission line model, i.e., that there are no internal reflections in the TDR system except those taking place at the interfaces of the specimen (Heimovarra et al. 1994; Friel and Or 1999). This puts strict requirements on hardware design and reduces the flexibility in probe geometry. Directly applying these models to analyze the TDR devices in practice will generate errors due to the non-uniform characteristics of these devices. Models for non-uniform TDR system such as by Feng (1999) or Lin (1999) are more appropriate for this case.

With the model at hand, another important task to investigate is whether it is feasible to back calculate the material properties in heterogeneous media. Lin (2003a, b) has shown that it is possible to determine the moisture content and dielectric spectrum using inversion analysis. However, determination of layered soil conditions remains a challenging task due to the issue of non-uniqueness in the interpretation of the data. This paper describes the work to determine the layered soil distributions. It utilizes a simplified two-parameter model for soil dielectric permittivity (Huisman et al. 2002). Constrained optimization is incorporated for soils to obtain robust results in inversion. The developed approach is illustrated by numerical simulations and by analyzing the actual measured signals.

Background

Time Domain Reflectometry
Time Domain Reflectometry (TDR) is an established methodology in electrical engineering for locating discontinuities in electrical cables (Ramo 1965). Previous research indicated that TDR was also a useful tool for characterizing material dielectric properties (Fellner-Feldegg 1969). Since the pioneering work by Topp et al. (1980), TDR has been a topic of extensive research and is widely used in engineering practice. The applications include measuring soil water content and density, monitoring slope deformation, estimating porewater salinity, etc.

A TDR system for field measurement generally includes a TDR device (which consists of pulse generator and sampler), a measurement probe, and a connecting cable (Fig. 1). The pulse generator sends out an electrical pulse (which generally is a step pulse with a very fast rise time) and the sampler records the response from the system. The dielectric constant and electrical conductivity are two pieces of important information that can be obtained from direct analysis of a time domain TDR signal. The speed of the electromagnetic defines the dielectric constant of the material within

the probe. It is analogous to Young's modulus which is related to the speed of the stress wave. The attenuation of the electromagnetic wave defines the electrical conductivity, which is analogous to material damping. Analyses and experimental results have shown that the determined values are averaged properties over TDR measurement probe length (Topp et al. 1982).
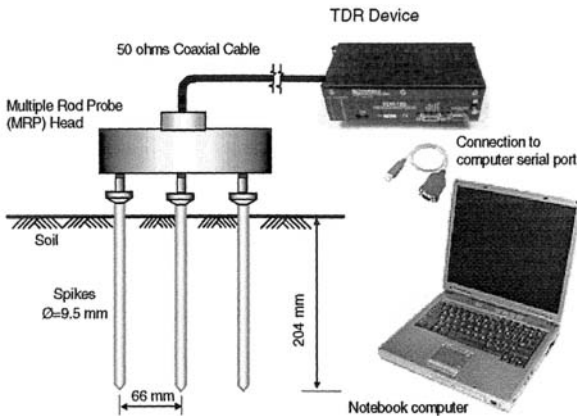
Figure 1. Components of a Typical TDR System

Frequency Domain Representation of a Non-Uniform TDR System by Impedance Transform

Obtaining more information from TDR signal requires incorporating an accurate model to describe the electromagnetic wave phenomena in the TDR system. Most models for TDR system utilize the uniform transmission line assumption (Heimovaara et al. 1994, Friel and Or 1999). This is generally not true unless strict constraints on the system hardware design are satisfied so that the only appreciable reflections are those from the measurement sample. The non-uniform transmission line models by Feng et al. (1999) and by Lin (2003a, b) are more appropriate to describe the actual TDR system responses. The model developed by Lin (2003a, b) is selected for this research due to its simplicity in describing the complex responses in TDR system.

In the model by Lin (2003a), the electromagnetic wave propagation in the TDR device is described by spectral solution of a non-uniform transmission line. The time domain wave equation is first transformed into spectral form, where the response at each individual frequency can be described by an equivalent circuit model consisting of a pulse generator and an equivalent complex resistance. The equivalent resistance represents the non-uniform transmission line making up the TDR device. An important concept for obtaining the lumped equivalent complex resistance is the impedance transform, where the equivalent impedance at a given location is obtained from the load impedance and the characteristic impedance of the connection lines in a

bottom-up fashion (Eq. 1). The process continues to the connection point where the voltage of TDR signal is sampled by the TDR sampler (Eq. 1 and Fig. 2).

$$Z_{in}(z_n) = Z_L$$

$$Z_{in}(z_{n-1}) = Z_{c,n} \frac{Z_L + Z_{c,n} \tanh(\gamma_n l_n)}{Z_{c,n} + Z_L \tanh(\gamma_n l_n)} \tag{1}$$

where Z_L is the load impedance, $Z_{in}(Z_n)$ and $Z_{in}(Z_{n-1})$ are the input impedance of the nth section and $n-1^{th}$ section respectively, $Z_{c,n}$ is the characteristic impedance of the nth section, γ_n, l_n are propagation constant and length of the nth section.

Front Panel, Cable,..., Measurement Probe
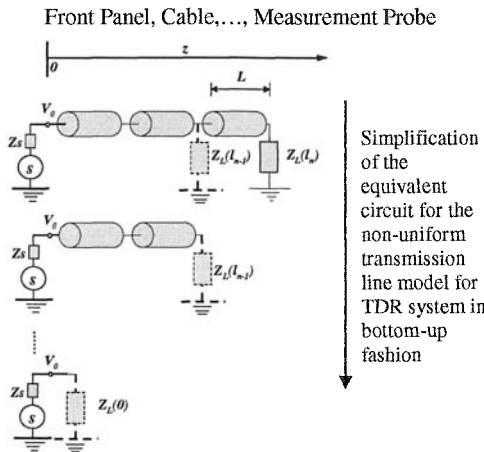
Figure 2. Equivalent circuit model based on impedance transform for non-uniform TDR system

The predicted sampling voltage of the TDR signal can be obtained from the final equivalent circuit at the bottom of Fig. 2 as:

$$V(0) = \frac{Z_L(0)}{Z_s + Z_L(0)} V_s \tag{2}$$

where V_s and $V(0)$ are the source and output voltage represented in the frequency domain respectively, Z_s is the internal impedance of TDR electronics which typically is 50 ohms, and $Z_L(0)$ is the lumped impedance at the point where the signal is sampled.

The voltage, $V(0)$, can be transformed into a time domain signal by Inverse Fast Fourier Transform (IFFT). The predicted signal can then be compared with actual measured signal. Optimization algorithms can then be used to obtain the model parameters.

Dielectric Model for Soil

Due to the heterogeneity and non-uniform characteristics of soils as well as the complex microscopic electrochemical phenomena, the complete description of true

soil dielectric properties is practically impossible. Although various models have been used to describe mixtures of soil solids and pore fluids, no complete model is available that can describe the dielectric properties of soils (Hilhorst et al. 2000). Most of the models used for research on soils refer to the research results of liquids, solid materials, or simple mixtures. This includes many famous formulations such as Debye's model (Debye, 1929), Cole-Cole's model (Cole and Cole, 1941), Maxwell Garnett formula (1904), and Schwarz formula (1962). All these models explain phenomena due to certain relaxation mechanisms or within a certain frequency range. In addition to these models, the semi-empirical power-law volumetric mixing model also is frequently used for soils (Birchak et al. 1974). Huisman et al. (2002) compared several approaches for analysis of TDR waveforms including the use of two different inversion models, i.e., (1) fitting a simulated waveform based on a model with frequency-dependent permittivity, and (2) fitting a waveform based on a model with an apparent dielectric permittivity (Eq. (3)). The comparison showed that the results by the frequency-independent (apparent) permittivity were as accurate and reproducible as other models.

$$\varepsilon = K_a - j\frac{\sigma}{\varepsilon_0 \omega} \tag{3}$$

where K_a is the apparent dielectric constant, σ is the electrical conductivity, ω is the angular frequency, and ε_0 is the dielectric permittivity of a vacuum (8.854×10^{-12} F/m).

The advantage of this simplified model is that it captures two of the most important pieces of information from the TDR signal, the apparent dielectric constant and the electrical conductivity. This model was selected in this study to alleviate the problem of non-uniqueness associated with more complex models.

Experiment and Analysis

Calibration of TDR System

Equation (2) shows that the input signal and the properties of each connecting section (including the front panel, cable, and probe head) in TDR instrument system are necessary to predict the measured signal.

Different approaches can be used to measure the input signal. A commonly used method is to measure the signal with a shunt of 50 ohms connected to the TDR device. However, this signal obtained by this method is a distorted version of the true input signal as it does not account for the impedance mismatching inside the TDR device (front panel). There are several approaches to determine the true input signal. Heimovaara (2001) used an error function (Erf) to fit the measured input signal. Huisman et al. (2000) minimized the effects of internal reflection by subtracting the signals measured with open or shorted calibration loads. In this study, the input signal was first measured by using a 50 ohms matched impedance shunt. The signal was then smoothed to remove the jittering in the signal. The smoothed signal is assumed to be the input signal with the jittering assumed to be due to the impedance mismatches in front panel. The properties of the front panel were then determined by a calibration procedure to account for the effects of these mismatches inside the TDR device.

The properties of each connecting section in the TDR system were determined by calibration. Several reference signals are taken to accomplish the calibration processes. These include 1) signal measured with a shunt of 50 ohms directly connected to the pulse generator; 2) signal measured with the connection cable and the shunt of 50 ohms connected to the cable end; 3) signal measured with the probe head connected to the cable; and 4) signal measured with the measurement probe in a standard reference material (water in this case). The calibration procedure is implemented successively to determine the properties of each section by matching the predicted signal with the measured signal, which can be mathematically described as:

$$\arg\min\left(\left\|v_{measure} - v_{cal}\left(L_i, Z_i, \varepsilon_i\right)\right\|\right), \ i=1, 2, 3, 4 \tag{4}$$

where 1, 2, 3, 4 indicate front panel, cable and probe head and probe respectively.

For each section, there are three unknown parameters, i.e., the section length, L, the section characteristic impedance, Z, and the dielectric permittivity of the insulation material, ε. The low loss dielectric permittivity of cable insulation materials can be assumed to be constant or be described by Debye's model. Given one of these parameters, the other two can be determined.

The calibration was carried out from top to bottom, i.e., the front panel was first calibrated, followed by connection cable, probe head, and measurement probe. After all the calibration procedures were accomplished, another step was carried out on the whole TDR sections to achieve the best matching to further reduce the effects of error accumulation,. Figure 3 shows the matched signal versus measured signal to the multiple probe head for system using a Campbell Scientific TDR100 device.
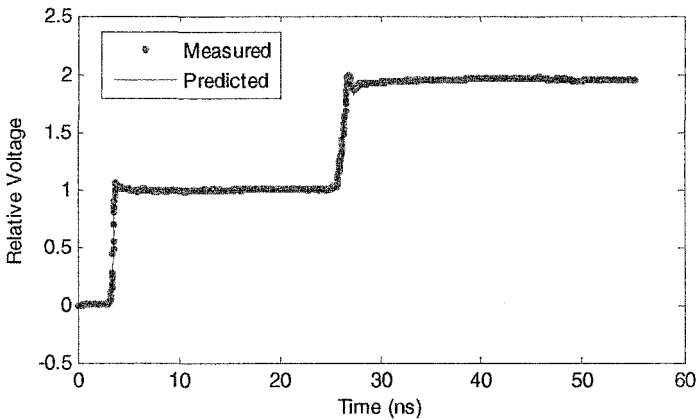
Figure 3. Example of measured and predicted signals for multiple rod probe head

The comparison indicates that the predicted signal correctly describes the major phenomena (reflections) inside the TDR system. Some locations in the signal where high frequency signal jittering exists cannot be perfectly matched. Figure 4 shows the predicted and measured signals for deionized water using the calibrated

parameters. The close match indicates that the calibration correctly determined the parameters of the TDR system.
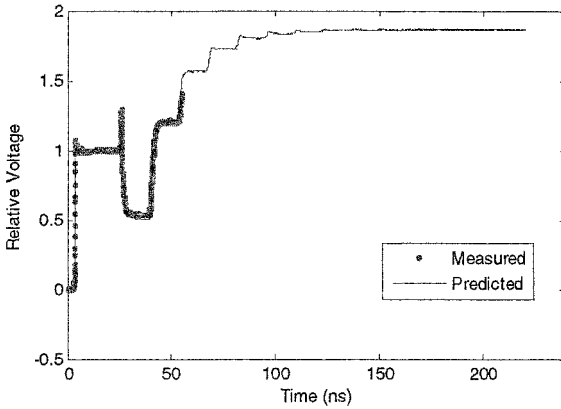
Figure 4. Measured and predicted signal for deionized water using TDR100

Problem Statement for Profile of Soil within the Probe

To determine the properties of each layer of soil within the probe, the objective is to minimize the differences between the measured and predicted TDR signals as described in Eq. (5).

$$\left\| v_{measure} - v_{cal}\left(K_{a1}, EC_{b1}, L_1; K_{a2}, EC_{b2}, L_2, \cdots\right) \right\| \tag{5}$$

where $v_{measure}$ is the measured TDR signal and v_{cal} is the predicted signal by the non-uniform transmission line model, which is a function of the layer thickness (L), the dielectric permittivity (K_a), and electrical conductivity (EC_b) for each layer.

The optimization is carried out by a constrained optimization procedure. The purpose of adding constraints is to alleviate the problem of non-uniqueness and increase the accuracy of inversion results. Major constraints include the geometric relationship (Eq. (6)), the dielectric constant relationship (Eq. (7)), and the electrical conductivity relationship (Eq. (8)) between the individual layers and the whole specimen.

$$L = L_1 + L_2 + \ldots \tag{6}$$

$$\sqrt{K_a}L = \sqrt{K_{a1}}L_1 + \sqrt{K_{a2}}L_2 + \ldots \tag{7}$$

$$\sigma L = \sigma_1 L_1 + \sigma_2 L_2 + \ldots \tag{8}$$

where L is the total length of the measurement probe in soil, L_i, K_{ai}, σ_i represent the length, the dielectric constant, and the electrical conductivity of the ith layer, respectively.

Additional constraints are based on physics; dielectric constant must be greater than or equal to one (Eq. (9)) and electrical conductivity must be greater than or equal to zero, (Eq. (10)).

$$K_{a,i} \geq 1; \tag{9}$$

$$\sigma_i \geq 0 \tag{10}$$

Considering these constraints, the problem to determine layer profile is described as: minimize Eq. (5), subjecting to the constraints in Eqs. (6) to (10).

Illustration of Model and Optimization Procedures with Simulated Examples

The model and optimization procedure were first evaluated with numerical examples. The simulation was carried out by assuming the soil specimen consisting of two layers. Soil dielectric properties were described by the Debye's model. Three different cases were simulated. The first one simulated the traveling of electrical pulse from dry soil layer to wet soil layer of equal thickness. The second one simulated the traveling of electrical pulse from wet soil to dry soil of equal thickness. The third case was similar to the first one but the thicknesses of the two layers were assumed to be different.

A two parameter model (Eq. (3)) was used for soil in the inversion analyses. Thus, there were three unknowns to determine for each layer, i.e., apparent dielectric constant, electrical conductivity and layer thickness. Constrained optimization was used to estimate these parameters using the simulated signals as the target signals. The initial seed values were set to be equal to the bulk dielectric constant and bulk electrical conductivity (Yu and Drnevich 2004). Figure 5 shows the target signals and the predicted signals after the completion of the optimization. The signal predicted by the seed parameters were also plotted for comparison. The figure indicates that the predicted signal using parameters obtained by inversion analysis very closely matches the target signals.

The values of the parameters used to simulate the target signals and the corresponding parameters determined by inversion analysis are listed in Table 1. This further indicates that results of inversion are satisfactory.

Table 1. Parameters for simulation and results of inversion

		Top Layer			Bottom Layer		
		$\varepsilon_s (K_a)$	σ (S/m)	L(m)	$\varepsilon_s (K_a)$	σ(S/m)	L(m)
Case I(a) (Dry-to-wet equal thickness)	Target	5.50	0.005	0.116	26.0	0.05	0.116
	Seed value	15.7	0.025	0.120	15.7	0.025	0.120
	Inverted	5.55	0.0057	0.115	25.75	0.044	0.117
Case I(b) (Dry-to-wet unequal thickness)	Target	5.50	0.005	0.050	26.0	0.050	0.150
	Seed value	15.7	0.025	0.100	15.7	0.025	0.100
	Inverted	5.55	0.0073	0.05	25.95	0.049	0.150
Case II (Wet-to-Dry equal thickness)	Target	15	0.002	0.119	3	0	0.119
	Seed value	15.7	0.025	0.120	15.7	0.025	0.120
	Inverted	15.27	0	0.124	3.02	0.0025	0.118
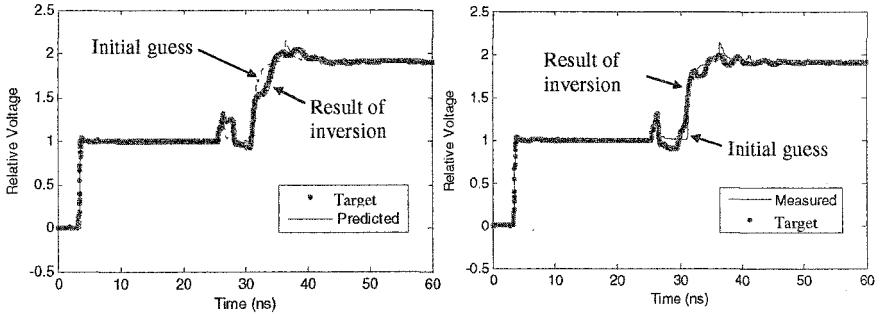
Figure 5. Inversion analysis using simulated signals in layered soils as target (left: dry (top) to wet (bottom); right: wet (top) to dry (bottom))

Measurement and Inversion Analysis of Layered Soils
Results from the simulated examples indicate the numerical model and inversion procedure are valid. Measured signals from experiments were used to further evaluate the performance of this approach. The experiment was carried out using ASTM standard graded sand. Soil was compacted into a 23.3cm (around 9 inch) metallic mold in two layers. For one test set, dry soil was first compacted with an aluminum rod to fill half of the mold. The surface of the soil was made flat and the remaining height of the mold was measured to determine the exact height of bottom layer. The amount of soil used for the bottom layer was also measured. A thin layer of plastic film was placed on top of the bottom layer. The film was cut to fit exactly into the cylinder. A hole with diameter slightly larger than that of the center rod was cut in the middle of the wrapper. After the wrapper was put in place, wet soil was placed and compacted to fill the upper portion of the mold. The surface was made flat and the amount of soil in the upper layer was determined. Following this, a steel rod was driven into the soil along the center of the mold. The rod and the metallic mold simulated a coaxial cable where the soil acted as the insulation material (Drnevich et al. 2003). A TDR signal was then acquired. After TDR testing, water content determinations were made, by oven drying, on samples carefully obtained from the top and the bottom layers.. The dry densities of soil in the bottom and top layer were then determined. Another set of experiments followed similar procedures. The only difference was that wet soil was placed in the bottom layer and dry soil was placed on the top layer. Table 2 summarizes the geometry and physical properties of the soil layers in these two experiments.

Inversion analyses were performed with the measured TDR signal as targets. The initial seed values were again set to be the bulk values determined by empirical time domain analysis. Figure 6 shows the comparison of measured signal versus predicted signals for the case where dry soil is at top and wet soil is at the bottom. From the figure, it can be seen that the predicted signal using parameters determined by inversion analysis is very close to the measured signal.
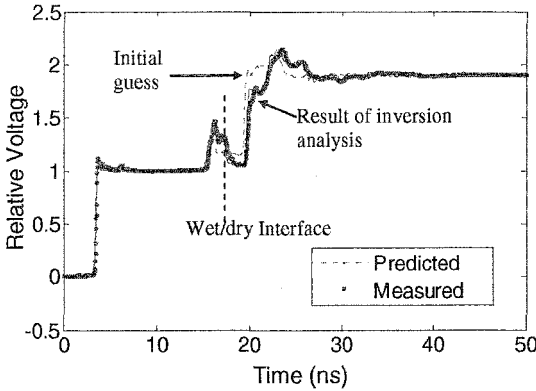
Figure 6. Results of inversion analyses for measured dry (top) to wet (bottom)
condition

The parameters determined by inversion analysis of the measured signals on layered soils are summarized in Table 2. The estimated volumetric water content for the inversion analysis was calculated using Topp's equation (Topp et al. 1980). Comparisons provided in Table 2 indicates that the results of volumetric water contents calculated by the inverted dielectric constants using Topp's equation show similar trends and magnitude of variations compared with those of actual measurements. Relatively large errors happened for the case where drier soil was located at the bottom. A tentative explanation was given below: material with low dielectric constant generally causes a hump in the reflected signal. The reflection at the end of the measurement probe also causes the TDR signal to rise up. These made it difficult to differentiate the effects of these two factors and might result in the relatively larger level of errors for the case where soil was drier at the bottom. Measures to alleviate these effects will be investigated.

Table 2. Results of inversion analysis on measured soil profile

		Layer	Length (m)	Dry Density	Gravimetric Water Content	Volumetric Water Content (θ)
Case I (top dry-bottom wet)	Measured data	Top	0.119	1.723	1.34%	2.3%
		Bottom	0.114	1.600	6.41%	10.3%
			Length (m)	K_a	σ (S/m)	θ (by Topp's equation)
	Results of Inversion	Top	0.136	1.86	0	0.0%
		Bottom	0.106	6.00	0.01	10.3%
		Layer	Length (m)	Dry Density	Gravimetric Water Content	Volumetric Water Content (θ)
Case II (top wet-bottom dry)	Measured data	Top	0.119	1.521	6.81%	10.4%
		Bottom	0.114	1.747	0%	0%
			Length (m)	K_a	σ (S/m)	θ (by Topp's equation)
	Results of Inversion	Top	0.126	7.94	0.0025	14.6%
		Bottom	0.115	2.47	0.0006	1.6%

Conclusions

This paper introduces work toward obtaining variation in soil properties within the probe from Time Domain Reflectometry measurements. A general model for non-uniform TDR system was incorporated as forward model. A simplified model for soil dielectric permittivity was utilized. Constrained optimization was used in inversion analyses to determine the layer properties. Results by use of numerically simulated TDR signals and by analysis of actual measured signals in layered soils indicate the developed approach has promise. Since the simplified dielectric model for soil was originally developed for cohesionless soils, the applicability to cohesive soil needs to be evaluated. Work will continue to refine and develop robust procedures to use TDR for soil profiling.

Acknowledgements

References

Birchak, J. R., Gardner, C. G., Hipp, J. E., and Victor, J. M. (1974), "High Dielectric Constant Microwave Probes for Sensing Soil Moisture", *Proc. IEEE*, Vol.62, pp. 93-98.

Cole, K.S. and Cole, R.H. (1941), "Dispersion and Adsorption in Dielectrics: I-Alternating Current Characteristics", *J. Chem. Phys.* Vol. 9, pp. 341-351.

Debye, P. 1929, Polar Moleculars, New York, Chemical Catalog Co.

Dowding, C.H. and O'Connor, K. (1999), *Geo Measurements by Pulsing TDR Cables and Probes*, CRC Press, Boca Raton, FL

Drnevich, V.P., Yu, X., and Lovell, J., (2003) "Time Domain Reflectometry for Water Content and Density of Soils: Test Procedures and Typical Results," *Proceedings of TRB Annual Meeting*, Washington, D.C., January

Fellner-Feldegg, J. (1969), "The Measurement of Dielectric in the Time Domain", *J. Phys. Chem.*, Vol. 73, 612-623

Feng, W., Lin, C.P., Deschamps, R.J. and Drnevich, V.P. (1999), "Theoretical model of a multisection time domain reflectometry measurement system", *Water Resources Research*, 35(8): 2321-2331.

Friel, R., and Or, D. (1999). "Frequency analysis of time-domain reflectometry (TDR) with application to dielectric spectroscopy of soil constituents", *Geophysics* 64(3):1–12.

Heimovaara, T. J. (1994). "Frequency analysis of time domain reflectometry waveforms: 1. A four-component complex dielectric mixing model for soils", *Water Resource Research*, Vol. 30, No. 2, (1994) 201-209.

Heimovaara, T.J. (2001). "Frequency domain modeling of TDR waveforms in order to obtain frequency-dependent dielectric properties of soil samples: A theoretical approach", *Proc. Int. Symp. and Workshop on Time Domain Reflectometry for*

Innovative   Geotechnical   Applications,   Infrastructure   Technology   Inst.,
     Northwestern University, Evanston, IL.
Hilhorst, M.A., Dirksen C., Kampers, F.W.H., and Feddes, R.A. (2000), "New
     Dielectric Mixture Equation for Porous Materials Based on Deporlarization", *Soil
     Sciences Society America Journal*, 64: 1571-1587.
Lin, C.P. (2003a), "Analysis of nonuniform and dispersive time domain reflectometry
     measurement systems with application to the dielectric spectroscopy of soils".
     Water Resources Research, 39(1): art-1012.
Lin, C.P. (2003b), "Frequency domain versus travel time analyses of TDR waveforms
     for soil moisture measurements", *Soil Science Society of America Journal*, 67(3):
     720-729.
Maxwell Garnett, J.C. (1904), "Colours in Metal Glasses and Meta Films", *Trans. Of
     the Royal Society*, (London), CCIII, pp385-420.
Ramo, S., Whinnery, J. R., and Van Duzer, T. (1965), *Fields and Waves in
     Communication Electronics*, 1st ed., John Wiley, New York
Schwarz, G. (1962), "A Theory of the Low Frequency Dielectric Dispersion of
     Colloidal Particles in Electrolyte Solution", *J. Phys. Chem.*, Vol 66, pp2636-2642.
Topp, G. C., Davis J. L. and Annan, A. P. (1980), "Electromagnetic determination of
     soil water content: Measurements in coaxial transmission lines", *Water Resource
     Research*, Vol. 6, No. 3, 574-582.
Topp, G.C., J.L. Davis, and A.P. Annan (1982), "Electromagnetic determination of
     soil water content using TDR: I. Applications to wetting fronts and steep
     gradients", *Soil Sci. Soc. Am. J.* 46:672-678.
Yu, X. and Drnevich, V. P. (2004). "Soil water content and dry density by time
     domain reflectometry." *Journal of Geotechnical and Geoenvironmental
     Engineering*, 130(9), 922-934.

Comparison of Viscous Damping in Unsaturated Soils, Compression and Shear

Paul Michaels, PE[1] Member ASCE

[1]Associate Professor, Boise State University, 1910 University Drive, Boise, Idaho 83725 <pm@cgiss.boisestate.edu> 208 426-1929

Abstract

Geophysical down-hole surveys can be used to measure the small strain dynamic properties of soils by the effects these properties have on wave propagation. The relevant effects include amplitude decay (corrected for beam divergence) and velocity dispersion. In this paper, down-hole data collected during the GeoInstitute's Denver 2000 field day are presented and analyzed as a Kelvin-Voigt solid. Findings for these unsaturated soils include viscous damping and stiffness which differ significantly for shear and compressional waves. A strong viscous damping is observed in compression, but weak damping is presented in shear. Lumped parameter constitutive models are discussed which mathematically represent the soil dynamics.

It appears that, in the case of unsaturated soils, the relatively low level of viscous damping in shear may be explained by the low mass of the air in the pores. That is, it is difficult for inertial decoupling to occur between the soil frame and the pore fluid when the pore fluid (air) is of such low density. Thus, a pore fluid in coupled motion with the frame can not produce significant viscous drag. On the other hand, large viscous damping is observed for compressional waves. This larger damping may be due to the larger relative motions between air and frame which can be forced by compression of the frame matrix. These observations may be relevant in areas such as the design of driven piles and the estimation of potential for damages from vibrations due to construction.

Introduction

As one of the participants in the GeoInstitute's Denver 2000 field day, the author collected down-hole data in an unsaturated granular soil. It was a unique opportunity since other participants measured related soil properties by different methods in the same general vicinity. These included ConeTec direct push surveys as well as surface

wave demonstrations by Olson Engineering. The field site was at the Asphalt Recycling and Stabilization Inc. (ARS) quarry. The author demonstrated a method by which the soil stiffness and damping properties (Kelvin-Voigt constitutive model) could be determined. These soil properties are derived from measurements of seismic wave velocity and amplitude decay as a function of frequency (Michaels, 1998).

The ConeTec demonstration was conducted about 100 meters from the author's down hole survey, and produced soil behavior types (SBT) which indicated a silty sand layer about 4.6 meters thick over a gravely sand which extended to depth of about 9 or 10 meters. Differences in ground elevation were not surveyed, and the distance between the two sites was large enough to prevent more than a qualitative comparison between the two locations.

The Olson Engineering surface wave demonstration was closer, perhaps within 50 meters to the down-hole work. Handouts of Olson's analysis indicated a shear-wave velocity profile that varied between 140 m/s and 230 m/s (0 to 3 meters depth) ending with a constant value of 230 m/s (3 to 6 meters depth). Olson and the author employed different sources. Since our sources were different, the source spectra were also different. Spectral plots handed out by Olson indicated that frequencies used in the SASW inversion extended from about 20 to 280 Hz. The author's down-hole source produced a spectral content from about 10 to 100 Hz, with the most reliable data between 20-80 Hz. The author's hammer delivered blows at 135 degrees from the vertical and is shown in Figure 1.
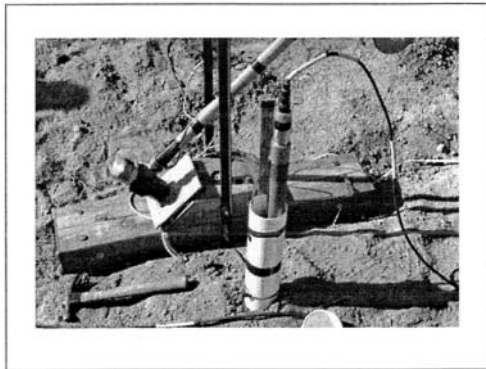
Figure 1. Hammer source used in down-hole survey

Also shown in the Figure 1 is the stick-up of casing (2.5 inch PVC, schedule 40) and the GeoStuff BHG-2 down-hole 3-component geophone, clamped by a worm driven bowspring. The source is nailed to the soil (0.35 m south of the hole) and the hammer can be pivoted to strike blows from opposing directions. Typically, 3 to 5 blows are stacked from each direction at any depth station and stored as two separate recordings. Subtraction of recordings enhances shear waves, addition of recordings

enhances compressional waves. Principal component analysis is used to determine the down-hole tool orientation and is described in Michaels (2001). The geophone elements were 14 Hz velocity phones, and a 3 component stationary reference phone was planted 0.6 meters south of the source. The purpose of the reference phone is to provide data to correct for minor variations in the source waveform and triggering. Triggering of the Bison engineering seismograph was by contact closure (between the wired hammer head and the aluminum covered strike plate.

Waveform Data

Figure 2 shows horizontal and vertical component waveform data collected down-hole on the 8th of August, 2000. The horizontal component data were rotated to align with the source polarization (parallel to the 1m source beam) and the vertical component data are taken simply from the single vertical component.
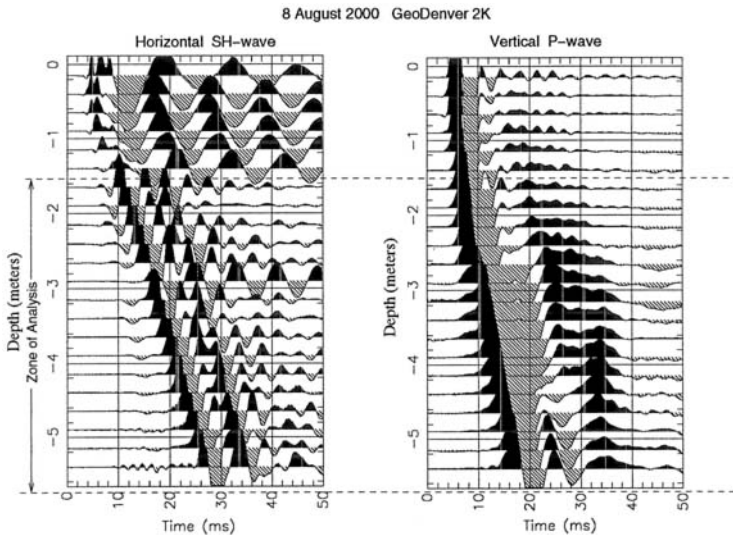
Figure 2. Horizontal and vertical component waveform data.

Data were collected every 0.25 meters, from the bottom of the hole upward. The sample interval was .0001 seconds. Only the first .05 seconds of a 0.5 second recording is shown to display the direct arrival waves with the best clarity. The amplitudes have been rescaled at each depth station by the L2 norm of the signal for that depth. Since true amplitudes decay rapidly with depth and distance propagated, this is the best way to present the waveforms in a single display. The bore hole did not appear to be well coupled to the soil in the first 1.5 meters from the surface. This view was formed by observing poor coherence and a high noise level, especially in

the horizontal motion (observe the persistent ringing in the horizontal data above 1.5 meters depth). An additional consideration is that surface waves dominate both the horizontal and vertical components at the surface, close to the source. For that reason, only the data from 1.5 to 6.0 meters depth is presented in the analysis which follows. This deeper data presented consistent and coherent wave fields which one would expected for body waves propagating in the soil.

Viscoelastic Analysis

Under the Kelvin-Voigt (KV) constitutive model, both phase velocity and amplitude decay are functions of frequency. The author's analysis method is to jointly invert phase velocity dispersion and inelastic decay observed over a range of frequencies. Velocity dispersion is computed in the time domain. Narrow band (2 Hz) filtered versions of the data are aligned in a depth window using trial velocities. For each alignment velocity, a semblance is computed (objective function to be maximized). A golden section search determines the best velocity for that frequency band. Amplitude decay is observed from the amplitude (after correction for beam divergence) of each filtered version of the data for each depth in the depth window. A least squares linear fit to the logarithmic amplitude decay with depth is performed at each frequency. The slope of that linear solution is the determined decay value for that frequency. A least squares inversion jointly solves for the two coefficients of the 1-D inelastic wave equation (Michaels, 1998). The governing wave equation is

$$\frac{\partial^2 u}{\partial t^2} = C_1 \frac{\partial^2 u}{\partial x^2} + C_2 \frac{\partial^3 u}{\partial t \partial x^2} \quad , \tag{1}$$

where u is particle displacement, x is the direction of wave propagation, and t is time. The stiffness coefficient is C_1 (m^2/s^2) and the damping coefficient is C_2 (m^2/s). The method is robust when done over a large enough depth window. Effects associated with scattering, mixed or multiple wave fields within the aperture, and near-field waves tend to average out over intervals greater than a few meters. The reader is cautioned not to interpret individual measurements of velocity or decay at any one frequency, as this may be misleading. Rather, the reader should focus on the joint inversion results (C_1 and C_2) which are determined statistically by the data's presentation of Kelvin-Voigt specific behavior.

Figure 3 plots the measured velocity dispersion and amplitude decay for both the P-wave and SH-wave data collected on 8 August, 2000. The depth range analyzed extended from 1.5 to 6 meters depth. Error bars are for 95% confidence limits. The results for the vertical component signals, labeled P-wave, are shown in Figure 3 (a) and (b). The results for the horizontal component signals, labeled SH-wave are shown in c) and d) of the same figure. The reader is urged to observe the solid curves which are computed from the solutions for C_1 and C_2. Note that, for example, the solid velocity curve for P-waves is always faster than the solid curve for S-waves.

We note that the velocity variation with frequency is significantly greater in the case for the P-wave data. Consistent with that observation, the variation of amplitude decay with frequency is also very much larger in the case for P-waves than for SH-waves. Further, the response is nearly elastic for SH-waves, the propagating wavelet largely retains its shape as the wave propagates. For P-waves, the propagating wavelet stretches its shape with distance propagated, consistent with KV damping. In other words, the damping of P-waves is greater than for SH-waves.

The least squares solution for the wave equation coefficients, C_1 and C_2 are given for the two cases (compression and shear) in Table 1. Note that the damping, C_2, for compression is about 40 times greater than for shear. Confidence limits are for 95%.

The shear-wave velocity solution shown in Figure 3(c) varies from a low of about 245.45 m/s to a high of 245.48 m/s. This extremely low level of dispersion is due to the minimal damping in shear. The average shear velocity magnitude is in general agreement with the analysis from the Olson Engineering SASW survey conducted about 50 meters distant from the borehole. The GeoDenver attenuation is
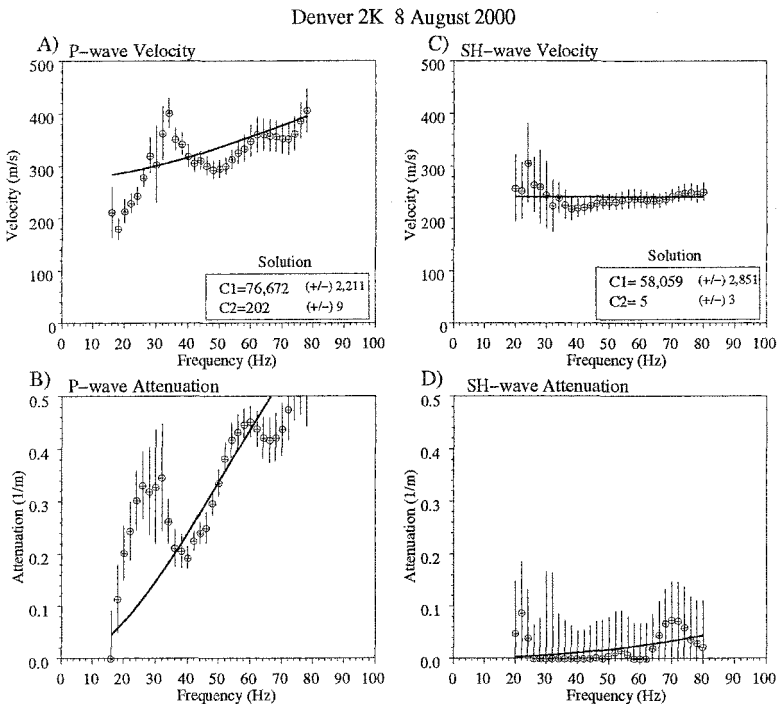
Figure 3. Velocity dispersion and attenuation measurements

Table 1. Inversion results for P- and SH-waves 1.5< depth <6 meters

Wave Type	C_1 (m^2/s^2)	C_2 (m^2/s)
P-wave	76,672 (+/-) 2,211	202 (+/-) 9
S-wave	58,059 (+/-) 2,851	005 (+/-) 3

very modest compared to determinations made at GeoLogan 1997 (saturated sand, C_2=14 m²/s) and in Idaho (saturated gravel and sands, C_2 as large as 255 m²/s) Michaels (1998).   While no water content measurements were made at the GeoDenver bore hole, the soil was clearly unsaturated, no water table was observed in the bore hole or neighboring quarry pit.

The compressional P-wave velocity solution shown in Figure 3(a) varies significantly over frequency (from a low of about 300 m/s to a high of 400 m/s). Consistent with a viscoelastic model, the attenuation also varies greatly (from 0 to almost 0.5 nepers per meter). The author has no comparable results for saturated soils, since the Biot type 2 wave generally appears to be present and limits the aperture available for this type of analysis. However, it has long been recognized in the exploration seismic industry that the best signal is returned from reflections when the source is located below the water table (Sheriff and Geldart, 1995, p202). This suggests the possibility that P-waves may differ from S-waves significantly in terms of damping at saturated conditions; greater damping for S-waves, less damping for P-waves.

Comparing Oscillations to Waves, Damping Ratio and Loss Tangent

The equation (1) coefficients C₁ and C₂ are ratios of stiffness and viscosity to density. That is,

$$C_1 = \frac{G}{\rho} \quad C_2 = \frac{\eta}{\rho} \quad , \tag{2}$$

where G is the shear modulus, η is the viscosity, and ρ is the density of the soil (combined matrix and pore fluids). All of the above are specific properties of the soil, they are constants, and they are invariant with frequency. They become lumped parameters when a specific volume of soil is considered (ie. density becomes mass).

Some authors, Kramer (1996), Schnabel et al. (1972), and Stoll (1985), to name just a few, have expressed shear modulus as a complex quantity,

$$G^* = G_R + i G_I \quad , \tag{3}$$

where i^2=-1 . The real part, G_R , is frequency invariant, but the imaginary part, G_I, depends on frequency. Specifically,

$$G_R = \rho C_1 , \quad G_I = \rho C_2 \omega = \eta \omega \quad . \tag{4}$$

Loss tangent is given by (Stoll, 1985),

$$\tan(\delta_L) = \frac{G_I}{G_R} = \frac{C_2 \omega}{C_1} \quad , \tag{5}$$

and this is frequency dependent as well. Kramer (1996, p.176-177) and others give damping ratio as

$$\xi = \frac{\eta \omega}{2G} = \frac{C_2 \omega}{2C_1} \quad , \tag{6}$$

from which it can be seen that damping ratio is also frequency dependent. Unfortunately, the vast majority of resonant column reports are for dry samples, and results for shear have revealed damping ratios which appeared to be frequency independent. In an attempt to explain that, Hardin (1965) suggested that viscosity varied with frequency in such a way as to remove the frequency dependence in damping ratio. This new viscosity has been termed "equivalent viscosity" by Kramer. Damping ratios computed from "equivalent viscosity" are not consistent with the Kelvin-Voigt representation, and should not be compared with this work. One should only consider frequency variant determinations of loss tangent or damping ratio when working within a true KV representation.

Shear testing by Stoll (1985) reported loss tangents for frequencies from 2 to 1000 Hz in 20-30 Ottawa sand. The loss tangent for dry sand was largely independent of frequency (.006), but rose significantly with frequency for saturated sand (from .006 to .04). If we substitute Table 1 results for shear into equation (5), we obtain loss tangents for GeoDenver soil which vary from .005 to .054 for the frequency range 10 to 100 Hz. These results suggest that some water was present in the GeoDenver soil, but more detailed conclusions are not possible since neither grains size distributions nor water content were determined.

Beyond the Kelvin-Voigt (KV) Representation for Shear Waves

Figure 4 (a) shows the traditional KV constitutive model as lumped elements in an oscillator. Also shown is how an assemblage of single degree of freedom (SDF) oscillators can be used to represent shear-wave propagation. The KV representation has traditionally been used to mathematically describe the dynamics of soils in engineering practice. Examples include consolidation (ASTM-D2435, 1996) and resonant column (ASTM-D4015, 1996) tests, as well as the response of soils under impact (Roesset et al., 1994). A significant limitation is the single mass element in the model. Soils do not consist of a single component, but are in general a medium consisting of 2 to 3 physical components. These include a solid component and 1 or more pore fluids.

Since the solid and pore fluid elements may move independently of each other, a better model would allow for those possibly separate motions. Pioneering

work on this topic was done by Biot (1956 a, 1956 b). The essential problem with the KV model is in accounting for the dashpot. Stoll (1985) demonstrated that saturating pores with water produced significantly more viscous damping than was the case for pores filled with air. This observation suggests that damping depends on the pore fluid, and may be due to relative motion between fluid and frame. If the dashpot is to be due to the viscous friction between pore fluids and frame, these materials can not be bound together as a single mass element. Further, even small amounts of water can significantly increase damping values, as reported in studies of lunar soils (Tittmann et al., 1974).

Recent theoretical work by the author has posed an alternative model for saturated media (Michaels, in press). This representation has been named the Kelvin-Voigt-Maxwell-Biot (KVMB) representation, being inspired by those existing models. The lumped element KVMB oscillator is shown in Figure 4 (b). Also shown is how an assemblage of these 2DF oscillators can be constructed to represent shear-wave propagation. In that work, a mathematical mapping between the traditional KV and the KVMB representations is formulated using the decoupling principal (Sadun, 2001).

Air vs. Water as Pore Fluids (Shear)

As can be seen from Figure 4(b), the production of viscous friction through the action of the dashpot depends on the relative motion between pore fluids and the solid frame. This relative motion depends in large part upon the resistance of the pore fluid to motion by virtue of its inertia and the available permeability. The more massive the fluid component, the greater its ability to resist being dragged along with the moving solid frame for a given permeability. The fluid mass increases with both porosity and the density of the fluid. For a given porosity, we should expect a dense fluid to produce greater damping than a less dense fluid, like air. This is what the KVMB model predicts as can be seen in Figure 5. The small level of shear wave damping in the Denver 2000 data may be explained by the lack of inertia for a pore
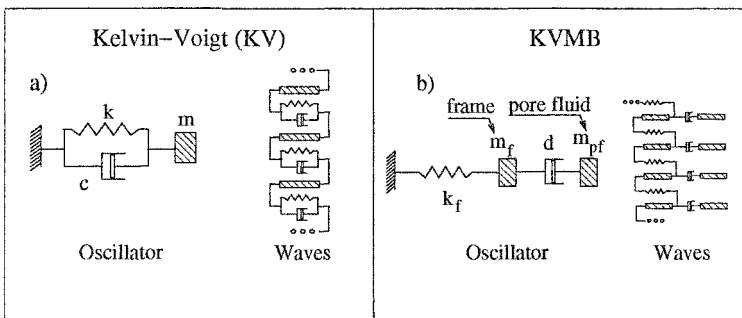
Figure 4. Kelvin-Voigt and KVMB representations of a soil.

fluid composed largely of air.

The theoretical computation shown in Figure 5 is based on the KVMB representation, and includes an assumption of cylindrical pores, as was the case in Biot (1956a). The vertical axis is an equivalent KV damping ratio mapped from the KVMB representation. The details of this theory for saturated conditions is given in Michaels (in press). The published theory is appropriate for saturated conditions, with either water or air being the fluid completely filling the pore space. The extension to unsaturated conditions is discussed below.

The solid curves in Figure 5 are shown for some selected degree water saturations and the corresponding water contents. The case of completely dry (S=0%) is not shown as it would fall below the chosen axes.

Starting at the left edge of Figure 5 (low frequencies), the pore fluid and frame are largely coupled, moving together. With little relative motion, KV damping is computed to be at a low value. The level of damping increases with frequency as the fluid and frame begin to separate and experience more relative motion due to reduced inertial coupling. The soil is represented by a capillary tube model where all tubes have the same, uniform cylindrical shape and diameter (0.3 mm in this example). This capillary model is the same used by Biot (1956a). Resistance to flow is a result of the fluid viscosity, and this resistance is gradually overcome by inertial forces with increasing oscillation frequency. Maximum KV damping is produced at a peak of the solid curve. Here, the relative motion between frame and fluid is at a maximum, with the frame moving one way and the fluid lagging in phase, moving in an opposite direction producing a large *relative velocity* between the two. As frequency increases, inertial forces dominate. The relative velocity between frame and fluid actually decreases with decreasing absolute velocity of the fluid. That is, in the very
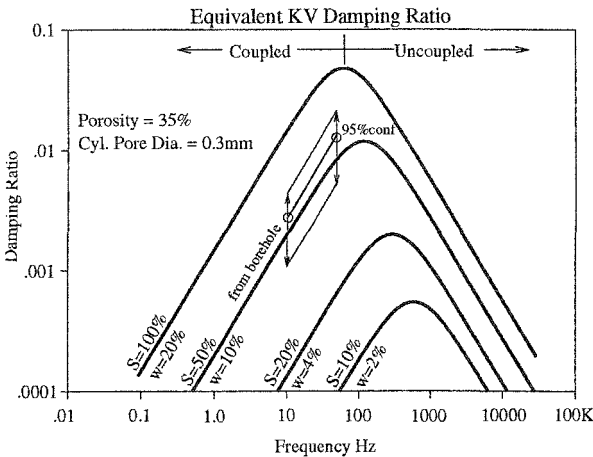
Figure 5. Equivalent KV damping ratio as a function of frequency.

high frequency limit, the fluid tends to slow down and remain at rest, no longer moving out of phase with the frame. At that point the frame is moving through what is essentially a stationary fluid.

The borehole determined values of C_1 and C_2 (see Table 1) have been converted to damping ratio using equation (6). The borehole computed damping ratios are plotted in Figure 5 between the two circles.

Estimating Damping Ratio for Intermediate Saturations

The computations shown in Figure 5 include estimates of what might be expected at intermediate saturations. The assumptions which lead to the intermediate saturations shown are as follows:

1. Pore fluid mass is a weighted blend of air and water, set by degree saturation.
2. Pore fluid viscosity is a weighted blend of air and water, set by degree saturation.

The equations which implement these assumptions are as follows:

$$m_{fluid} = m_{air} + S m_{water} \quad , \tag{7}$$

$$m_{frame} = m_{solid} + (1 - S) m_{water} \quad , \tag{8}$$

$$\mu_{blend} = (1 - S) \mu_{air} + S \mu_{water} \quad . \tag{9}$$

Here, S is the degree of water saturation, μ is viscosity, and the masses, m, are computed from porosity and saturations for a relevant volume of interest by the usual method found in any soil mechanics text. In equations (7) and (8), the assumption is that at low water saturations, the moisture clings to the frame and only the air moves relative to the pore throats. At high saturations, the pore fluid flows through the pores by inertia. The extra mass due to water density is essential in creating a significant amount of damping because air, being so light, lacks the needed inertia.

Conclusions

Shear waves appear to have less damping than P-waves in unsaturated soils. This may be due to the relative reduction in pore fluid density that occurs when water is replaced with air, and this results in less inertia to drive fluid flow through pores.

Shear waves are significantly easier to represent than P-waves. The representations shown in Figure 4 are for shear only. The pore fluid (be it air or water) possesses no shear strength, thus requires no spring to represent the fluid component. The situation is quite different in compression, since fluids possess a compressibility (air is highly compressible, water less so).

P-wave damping has been represented by combining volumetric compression of the soil with the diffusion equation (Bardet, 1995). Bardet derives the theoretical

response of a "Biot Column" and predicts the dynamic behavior in terms of several parameters, including soil stiffness, degree of saturation, porosity, specific gravity, and permeability. Since volumetric strain is key to this representation of a soil, Bardet expresses the view that water will not damp a poroelastic shear beam (because no water diffusion is expected in the absence of shear-volume coupling). This view neglects the alternative possibility of inertial coupling in shear.

A summary observation may be this. It appears that, for the case of shear, inertial coupling is the key mechanism by which pore fluids may be driven through the frame. On the other hand, diffusion is the key mechanism by which pore fluids may be driven through the frame in compression. Thus, a low density pore fluid like air can result in high levels of damping for P-waves, but not for SH-waves. A dense pore fluid is required to increase the damping in shear. This is evident when the author compares SH-wave damping in saturated soils with those in unsaturated soils.

Finally, the author's theory predicts that low levels of damping may result even in saturated conditions when the permeability of the soil is either very low or very large. This is because very small pores prevent fluid-frame motion, and very large pores produce less friction when fluid-frame motion occurs. The theory also predicts less damping at very low or very high frequencies as described above. Thus, field observations of shear wave damping may lead to a method for determining permeability of saturated soils, and possibly a method for the estimation of degree water saturation in unsaturated soils.

Acknowledgments

References

American Society of Testing and Materials (SSTM). (1996). "Standard test method for one-dimensional consolidation properties of soils", D2435, W. Conshohocken, Pa.

American Society of Testing and Materials (SSTM). (1996). "Standard test methods for modulus and damping of soils by the resonant-column method", D4015, W. Conshohocken, Pa.

Bardet, J.P. (1995). "The damping of saturated poroelastic soils during steady-state vibrations", Applied Mathematics and Comp., 67, Elsevier 3-31.

Biot, M. (1956a). "Theory of propagation of elastic waves in a fluid-saturated porous solid". I Low-Frequency range", *J. Acoustical Soc. Am.*, 28(2), 168-178.

Biot, M. (1956b). "Theory of propagation of elastic waves in a fluid-saturated porous solid". II High-Frequency range", *J. Acoustical Soc. Am.*, 28(2), 179-191.

Hardin, B.O. (1965). "The nature of damping in sands." J. Soil Mech. and Found. Div., ASCE, 91(1), 63-97.

Kramer, S.L. (1996). *Geotechnical Earthquake Engineering*, Prentice Hall, New Jersey.

Michaels, P. (1998). "In situ determination of soil stiffness and damping." *Journal of Geotechnical and Geoenvironmental Engineering*, ASCE, 124(8), 709-719.

Michaels, P. (2001). "Use of principal component analysis to determine down-hole tool orientation and enhance SH-waves." *Journal of Environmental and Engineering Geophysics*, EEGS, 6(4), 175-183.

Michaels, P. (in press). "Relating damping to soil permeability", *International Journal of Geomechanics*, ASCE.

Roesset, J., Kausel, E., Cuellar, V., Monte, J., and Valerio, J., (1994). "Impact of weight falling onto the ground", *Journal of Geotechnical and Geoenvironmental Engineering*, 120(8), 1394-1412.

Sadun, L., (2001). *Applied linear algebra: The decoupling principle.* Prentice Hall, New Jersey.

Sheriff, R.E., and Geldart, L.P. (1995). *Exploration Seismology,* Cambridge University Press, Cambridge England.

Schnabel, B., Lysmer, J. and Seed, H.B. (1972). "Shake, A computer program for earthquake response analysis of horizontally layered sites", *EERC 72-12*, University of California, Berkeley, California.

Stoll, R. (1985). "Computer-aided studies of complex soil moduli", *Proc., Measurement and use of shear wave velocity for evaluating dynamic soil properties,* ASCE, Reston, Va., 18-33.

Tittmann, B.R., Housley, R.M., Alers, G.A., and Cirlin, E.H. (1974). "Internal friction in rocks and its relationship to volatiles on the moon", in *Proc. of the Fifth Lunar Conference,* Supplement 5, Geochimica et Cosmochimica Acta, Vol. 3, 2913-2918.

Role of Practical Geophysics in In-situ Characterization for Underground Construction in Phoenix, Arizona

D.B. Durkee[1], M.L. Rucker[2], D.E. Smith[1], and A.F. Ackerman[1]

[1] Gannett Fleming, Inc., 4722 North 24th Street, Suite 250, Phoenix, AZ, 85016-4852; PH (602) 553-8817; FAX (602) 553-8816; email: ddurkee@gfnet.com
[2] AMEC Earth & Environmental, Inc., 1405 West Auto Drive, Tempe, AZ, 85284; PH (480) 940-2320; FAX (480) 785-0970; email: michael.rucker@amec.com

ABSTRACT

The application of surface and downhole geophysical methods for site characterization can provide data, information and insight into the subsurface that often cannot be achieved by traditional drilling and sampling techniques. Geophysical measurements applied over a broad area can complement geotechnical sampling methods applied at discrete locations. From a practical perspective, access to areas that cannot be drilled provides subsurface coverage that would otherwise be missing or could only be achieved at extreme cost. This paper presents the results of a comprehensive investigation and characterization program that included the use of state-of-the-art surface seismic microtremor surveys and downhole geophysical methods to complement rotosonic drilling and sampling methods and an innovative method of pressuremeter testing. Refraction microtremor surveys provided continuous simplified vertical shear wave profiles and associated low strain modulus profiles in 36-m (120-foot) increments along an 1,800-m (6,000-foot) alignment profile. Downhole geophysical methods included resistivity logging using an induction electrical sonde to provide vertical subsurface profiles to high resolution (about 0.5 m) that were then correlated back to estimates of clay content in the coarse sand-gravel-cobble (SGC) formation. Geophysical measurements were correlated to downhole pressuremeter test results to verify the relationships between the surface and downhole geophysical methods and in-situ high-strain borehole modulus results. Results from these methods were used to estimate the depth of the Holocene-Pleistocene contact, estimate strength and modulus parameters, and identify the extent and frequency of clean lenses and boulders within the geologic profile. The results of the investigation provided a detailed geologic characterization that was used to optimize tunneling depth, perform engineering analyses for support of excavation and underpinning, and evaluate standup time and tunneling methods.

PROJECT DESCRIPTION

The City of Phoenix, Arizona proposes to build an Automated People Mover (APM) at Sky Harbor International Airport to connect parking facilities, terminals, a new consolidated rental car facility, and the Light Rail Transit System currently under construction. Approximately 3.2 km (2 miles) of the APM will be underground, in dual bored tunnels each approximately 6.7 m (22 ft) in diameter and 13.5 m (40 ft) below grade. Stations will be constructed using a cut and cover technique requiring extensive support of excavation and underpinning.

Soil conditions at the airport are composed of coarse grained alluvial deposits from the nearby Salt River. The non-cohesive nature of the shallower alluvium and presence of large particles in the alluvium have made site characterization, parameter selection, and construction particularly challenging for previous underground projects in the Phoenix area. In particular it is difficult to obtain samples, determine strength and modulus parameters, and maintain excavation stability. Previous underground construction projects have been completed successfully in Phoenix but not without a wide range of consequences. Generally, tunnels constructed within the Pleistocene-aged geologic unit have experienced far better performance than tunnels constructed in the younger overlying Holocene-aged geologic unit primarily due to minor amounts of clay present, low degree of cementation, and low matrix suction potential.

SOIL CONDITIONS

Soil conditions at the airport are composed of alluvial deposits from the Salt River. The riverbed deposits are composed of sands, gravels, and cobbles (SGC) with boulders as large as 1 m (3 ft) in diameter with inter-bedded lenses of cohesionless running soils. The SGC deposit comprises two main geologic units; the Holocene-aged "B2" and Pleistocene-aged "B3" which have been identified within the depths of interest for the bored tunnel and cut and cover portions of the APM project. The B2 and B3 soils vary little in gradation, the primary difference being the presence of slightly greater clay content in the deeper B3 soils. The B2 soils have less than 4 percent clay and the B3 soils have more than 4 percent clay with an average of 7 percent. Table 1 illustrates the trends in laboratory test results of typical B2 and B3 soils. Frequent lenses of clean sands, cobbles, and boulders exist within both units.

Table 1. Trends of Laboratory Test Results

Geologic Unit	USCS	Plasticity Index	Clay Content	Fines Content
B2	SM, GM, GP, GP-GM, GW-GM	< 3	< 4 %	< 10%
B3	SM, SC/SM, GM, GC, GC/GM, GP-GC	> 5	> 4 %	> 10%

Given the subtle differences noted by classification methods, an investigation was developed based on the assumptions that the modulus of SGC is profoundly influenced by the presence of cohesion in the SGC matrix. Generally, the shallower, younger SGC without clay cohesion has relatively low modulus, and thus lower s-wave velocity and high resistivity; and the deeper, older SGC with clay cohesion has relatively high modulus, and thus higher s-wave velocity and lower resistivity.

GEOTECHNICAL AND GEOPHYSICAL INVESTIGATION METHODS

Previous investigations at the airport and nearby locations with similar soil conditions have been performed using a Becker hammer drill rig. This method does not allow for undisturbed sampling or accurate determination of subtle changes in stratigraphy since the process of reverse circulation with air separates out and blows away the clays. Analyses for design of underground structures have thus been performed using conservative values obtained from the literature for similar soil types.

The geotechnical investigation employed for this project consisted of a variety of techniques, including Rotosonic drilling and lab testing of select samples; seismic microtremor (ReMi) vertical profile shear wave surveys; various downhole geophysical tools including dual induction logging, neutron and gamma logging, and boring diameter measurements with a three arm caliper; and pressuremeter tests performed at various depths in borings adjacent to downhole geophysics borings.

Rotosonic Drilling and Sampling

Rotosonic drilling (see Figure 1) utilizes a steel drill casing that is vibrated while being pushed allowing continuous soil core extraction. This method provided visual evidence of minor changes in stratigraphy as well as select sampling at critical locations for identifying subtle changes in clay content.
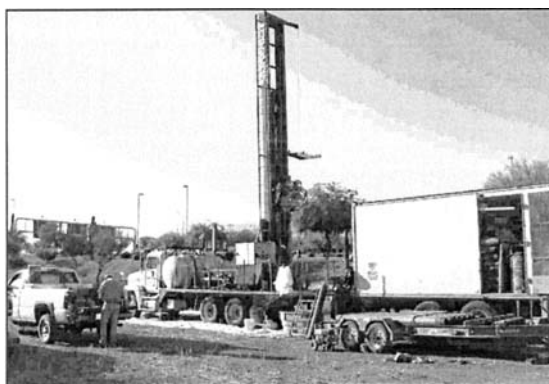
Figure 1. Rotosonic drill rig operation.

Seismic Microtremor (ReMi) Profiling

ReMi is a recently developed seismic shear wave profiling technique (Louie, 2001; Rucker, 2003) that can be implemented with the same engineering seismograph equipment used for seismic refraction surveys (see Figure 2). It is a surface wave method utilizing an array of geophones deployed in a line on the ground surface. Processing and analysis of the field data is accomplished using PC-based software. Seismic energy sources can be ambient ground vibrations such as traffic noise as well as discrete energy sources. Being a surface wave method, velocity reversals, where lower shear wave velocity (V_s) horizons underlie higher V_s horizons, can be detected and quantified.

In a test program in an unpaved area prior to the full investigation, the B2/B3 interface depth was estimated using seismic refraction compression wave velocity surveys and ReMi - V_s profiles correlated with rotosonic borings and laboratory index testing. Generally, the deeper B3 unit with slightly greater clay content had considerably higher V_s than the shallower B2 unit with little or no clay. Since ReMi surveys could be effectively completed on paved as well as unpaved areas, they were then performed continuously across the entire underground project alignment.
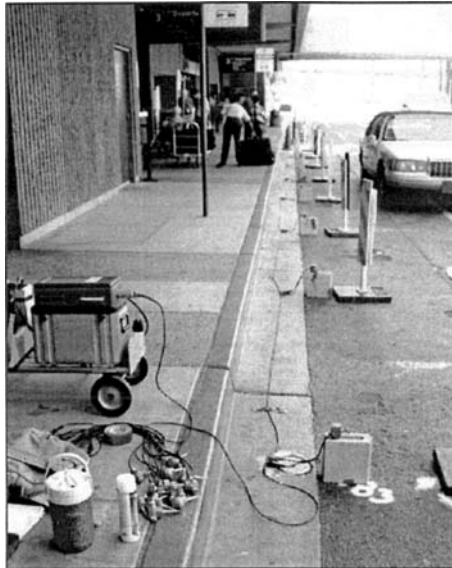
Figure 2. Seismic refraction microtremor (ReMi) equipment and setup for data acquisition.

ReMi arrays were set up on paved areas as well as open areas along the project alignment, and traffic was used as an ambient noise surface wave energy source. Arrays with lengths of 36 m (120 ft) and depths of investigation greater than 18 m (60 ft) were used to develop a continuous V_s profile along the project alignment. Each array consisted of 12 geophones, one geophone for each seismograph channel, set in a line with 3 m (10 ft) of space between each geophone (see Figure 2). To facilitate rapid geophone placement on and coupling to paved surfaces, a cinder block with a slot in the top was placed at each geophone location to accommodate the geophone spike normally used to place the geophone in the ground surface. A geophone was then set on top of the cinder block. Where a soil surface was available, the spike was used for geophone placement and coupling to the ground. Both 4.5 Hz and 28 Hz vertical geophones, with different data collection events for each geophone set, were used. Results from the 4.5 Hz geophones were used for the deeper portions of the interpretations and results from the 28 Hz geophones were used for the shallower portions of the interpretations. Results using the 4.5 Hz geophones were typically sufficient for the investigation work. A Geometrics S-12 twelve channel signal enhancement seismograph was used for data collection. The typical sample rate for the 12 channels of seismic signals was 1 millisecond with a length of recording of 12 seconds. No filters were employed during data collection. Ambient noise from the adjacent traffic, including bus and truck traffic, had a typical useful frequency range of 5 Hz to 40 Hz.

Downhole Geophysics

Downhole geophysical measurements (see Figure 3) offered an excellent compromise in scale between the relatively small laboratory test points and the large scale seismic refraction surveys. The dual induction resistivity tool uses electromagnetic induction to measure electrical resistivity, and works in open holes with or without borehole fluid, and in plastic (PVC, etc.) cased holes. The tool has both a vertical resolution and depth of investigation around the borehole of about 0.5 meter (1.6 ft). Variations in resistivity were measured continuously to that resolution through the select borings. Neutron logging measures the properties of the surrounding soil using a known radioactive source by bombarding the surrounding soil and measuring the amount of neutron return and return time. The neutron return indicates the hydrogen content in rocks and liquids in pore spaces, which can be used to estimate porosity. Generally, saturated clays have lower counts and sands have higher counts.

Figure 3. Downhole geophysical methods operation.

Pressuremeter Testing Program

Although the soil profile along the project alignment was clearly characterized through the investigations described above, stress-strain properties of the major soil units were still not quantified. Shear strength parameters and soil deformation properties can be determined using pressuremeter tests. The pressuremeter is typically lowered into a borehole, and pressurized laterally against the sidewalls at discrete locations to develop a relationship between pressure and radial deformation. Modulus values are then obtained by applying traditional stress-strain theory to the measured pressure-deformation relationships. To successfully perform pressuremeter tests it is critical that the borehole be stable and generally smooth along the soil-pressuremeter interface. However the coarse granular SGC deposits of the Salt River presented special problems relating to hole formations, stability, and hole integrity thereby requiring a specialized method for maintaining hole stability.

A method was developed specifically for this project, for forming a suitable hole utilizing a cased oversized borehole with a lean grout to provide borehole support. A full description of the test method, data reduction, and results is presented in Durkee, et al. (2005). Pressuremeter tests were performed in four boreholes all in close proximity to the downhole in situ test holes.

DISCUSSION OF RESULTS

Seismic Surveys and Rotosonic Drilling Results

The combination of ReMi surveys, laboratory testing, and field logging provided a good estimate of the Holocene/Pleistocene contact and general assessment of the clay content of each geologic unit. ReMi survey results indicated a consistent abrupt increase in V_s at depth, and laboratory test results indicated an increase in clay content at depth. Field logging of the continuous rotosonic cuttings verified the increased clay contents, but also indicated embedded clean cobble and boulder lenses within the Pleistocene B3 deposits.

The increase in V_s at the Holocene/Pleistocene interface is readily seen in Figure 4. S-wave velocities are shown in meters per second, and are based on ReMi interpretations. Depth interpretations deeper than about 10 to 15 meters are anticipated to be more approximate than shallower depth interpretations. Locations of Rotosonic borings are shown as vertical dashed lines, and the B2/B3 contacts based on boring results are shown as grey lines. Typically, V_s in the upper 6 to 7.5 m (20 to 25 ft) ranged from approximately 270 to 460 m/sec (900 to 1,500 ft/sec) while below 7.5 m (25 ft) V_s ranged from approximately 610 m/sec (2,000 ft/sec) to as high as 1,070 m/sec (3,500 ft/sec).
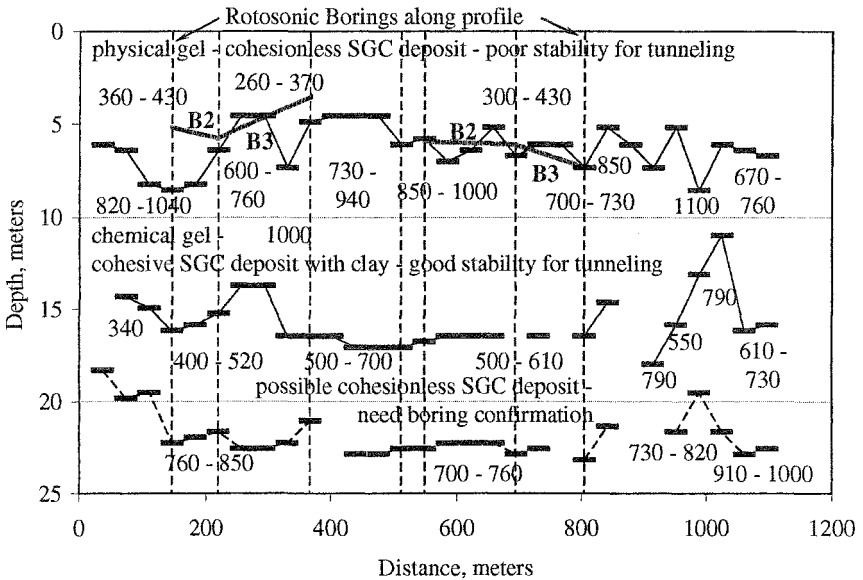
Figure 4. Subsurface profile along part of project based on ReMi V_s profiles.

Increases in V_s by factors of about 2 to 3 at the B2/B3 interface reflected an increase in clay content. Equivalent low-strain modulus values increased between roughly a factor of four up to a factor of ten at the B2/B3 interface. Using a simple relationship of modulus to confining pressure (increasing depth) such as Richart, et al. (1970), the modulus might double at a gradually increasing rate between depths of 3 m to 12 m (10 ft to 40 ft); that modulus pattern is not consistent with the measured V_s profiles. One explanation for the significant modulus increase is that the higher clay content in the B3 material provides sufficient cohesion for the SGC to behave as a cohesive mass rather than a cohesionless collection of particles. Rucker (2004) describes a percolation theory approach to modulus and density where, depending upon a relevant volumetric scale, geo-material masses exist in one of two states, either as a cohesionless physical gel or as a cohesive or cemented chemical gel. At similar geo-material mass densities, a chemical gel geo-material could have a modulus up to about a factor of ten greater than a physical gel geo-material. The B2 unit, lacking sufficient clay, tends to behave as a physical gel and the B3 unit, having sufficient clay tends to behave as a chemical gel. Tunneling conditions should be considerably more stable in the chemical gel ground than in the physical gel ground.

Although the difference in shear wave velocity between Holocene and Pleistocene soils was abrupt and distinct, a deeper low V_s layer was also identified. This was attributed to Pleistocene era scour and redeposition from meandering of the adjacent Salt River around an underground bedrock ridge. The discovery of the low velocity layer at depth also emphasized the limitations of the "averaged" nature of the large-scale ReMi survey. Several smaller lenses of cobbles and boulders were identified in rotosonic borings that were not detected by ReMi. Ground-truthing of the ReMi surveys with actual boring data and consideration of alternative in situ measurements is very important for effective characterization.

Clay Content vs. Depth Using Dual Induction Resistivity Logging

The project is located immediately adjacent to the Salt River, which flows intermittently (interrupted by long dry periods) during heavy runoff or releases from dams located upstream. The water table at the project location is typically 10 or more feet below the proposed tunnel invert and the zone of interest in the B2/B3 materials was well above the groundwater table at the time of this investigation. Hence, the basic assumption was made that a variation in minor amounts of clay in the unsaturated SGC could be identified through dual induction resistivity logging. This assumption is predicated on the fact that clean, dry granular materials are generally considered to be non-conducting. In SGC soils, the slight moisture on the surface of the granular particles provides the only paths for electrical currents, resulting in very high resistivity (low conductivity) measurements.

As noted above the clay content is slightly higher in the B3 SGC soils. In these soils the measurable amounts of clay in the interstitial spaces are capable of providing pathways for electric currents. This was assumed since clay particles, with their ion

double layers at the particle surfaces mobilized when moist or wet, will have higher electrical conductivities than clean SGC (granular) soils.

Quantification of clay electrical resistivity was not feasible due to sampling limitations and clay and moisture content variability within the interstitial spaces in the SGC. However, by conceptually equating conductive clay to a conductive fluid in the SGC pore spaces, Archie's Law for formation resistivity and formation factor (Schlumberger, 1972) was applied to estimate the percent clay in the SGC through resistivity measurements. Utilizing Archie's Law, the measured resistivity of the SGC changes approximately as the inverse of the square of the change in the amount of clay present. Thus, if the SGC resistivity at 4 percent clay is about 200 ohm-m, the SGC resistivity at 8 percent clay is about 50 ohm-m.

Resistivity values were compared to laboratory test results of clay percentages to calibrate an approximate Archie's Law-based resistivity to clay content relationship. Correlations of the various data indicated that SGC could generally be considered to be the B3 unit, or cohesive and high modulus, if the measured resistivity was less than about 80 ohm-m. That resistivity was consistent with a clay content of about 6 percent rather than the 4 percent used to differentiate B2 and B3 units, but most measured clay contents were either above or below the 4 to 6 percent range.

Vertical resolution of the dual induction resistivity logging results also provides an image of the variability of the subsurface materials. The electrical logs presented in Figure 5 show large swings in resistivity down to a depth of approximately 9 m (30 ft). These swings are consistent with zones of clean SGC materials (no clay) interbedded with more clayey materials. Also, from the data presented in Figure 5 it is evident that when there is sufficient clay to provide continuous pathways (4 to 6 percent) through the SGC (such as in the B3), the electrical resistivity became relatively low, approaching 80 ohm-m's or less.

The implications of this condition have been experienced during construction of another tunnel in similar SGC materials. During construction of ADOT's East Drainage Tunnel interbedding of zones with and without clay resulted in intermittent events of face loss (loss of ground support at the face of the tunnel excavation) and ultimately several severe cases of ground runs (soil loss into the newly excavated tunnel prior to placement of support). Based on the resistivity logging in select boreholes at the airport, similar conditions can be anticipated on this project.

Nuclear Logging

Abrupt decreases in the neutron return at a depth of about 9 m (27 ft), agreed well with the B2/B3 interface indicated by the other methods previously discussed. The response is probably due to moisture retained in the clays, to confirm the B2/B3 interface.

Gamma logging records the natural decay of Potassium 40 in most clay minerals and is used as an indicator of clay content. However, some types of clay have little or no gamma response, and naturally occurring uranium in rock formations may give false results. Total clay contents were small and gamma logging was not considered useful for characterization of these soils.

The three-arm caliper measurements served predominantly to identify unstable borehole walls and correct the results from the other geophysical tools.
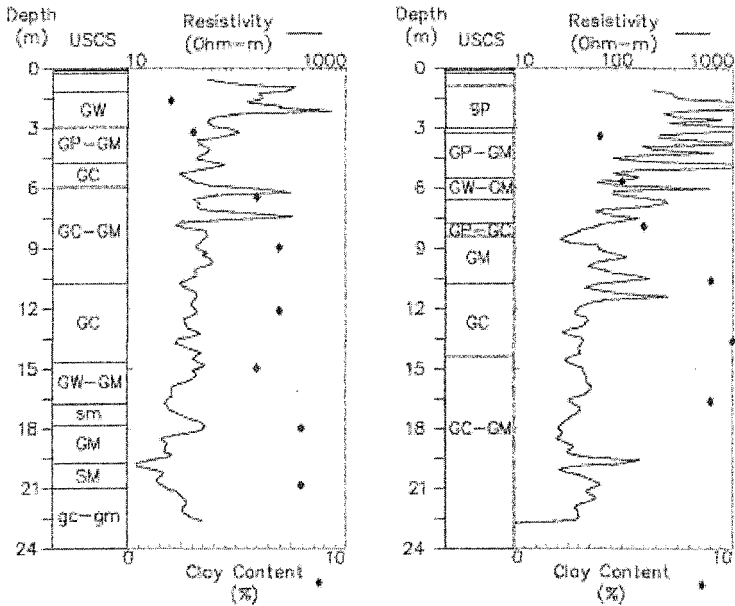
Figure 5. Clay content vs. resistivity.

Pressuremeter Test Results

The procedure described above was used to drill four boreholes to depths of 25 m (80 ft) at locations spaced along the project alignment. A total of 90 pressuremeter test attempts were made at 0.5-m (1.5-ft) intervals which resulted in 45 usable test results that were of good to excellent quality. The other 45 tests were judged as unsuitable primarily because the hole was too large in diameter to obtain satisfactory data.

Of these 45 usable tests, 20 were completed in the B2 subunit of the SGC and 25 were completed in the B3 subunit. The results of the 45 usable tests, in terms of shear modulus for initial loading conditions are shown in Figure 6. From Figure 6 it

is evident that the modulus values obtained from the pressuremeter tests varied over a relatively large range. The shear modulus for initial loading conditions ranged from 3.5 MPa (500 psi) to over 100 MPa (15,000 psi). The results presented in Figure 6 illustrate the variability within the soil mass but also indicate the distinct difference between the B2 and B3 soil.
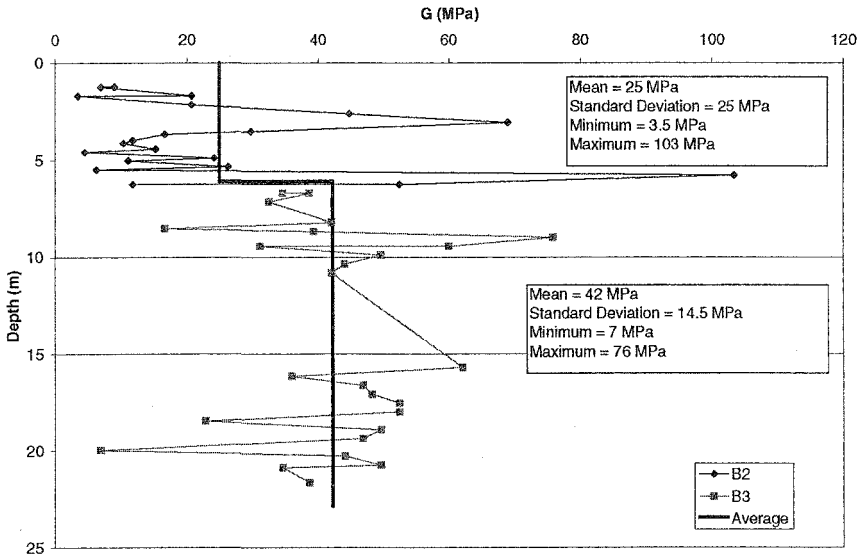
Figure 6. Shear modulus values from 45 of the pressuremeter tests.

CONCLUSIONS

Excavation and drilled shaft construction are commonplace in Phoenix and the local contractors are well prepared to deal with sloughing and difficult conditions associated with SGC soil. Tunneling operations, although successfully completed in the past, are relatively rare and require a much better understanding of the subsurface soil to properly prepare for adverse conditions.   Tunnel construction without sufficient B3 cover is highly susceptible to ground runs and large amounts of settlement. Tunneling in the B3 soil does not guarantee uniformly sufficient clay content because of the frequent lenses of clean soil, thus ground runs and settlement are still possible, albeit less likely.

In addition to the anticipated tunnel performance and associated ground losses, the clay content and even more so the presence of clean cobbles and boulder lenses, greatly affects the method of tunneling to be used. Large particles can not pass the TBM face and tunneling operations must be shut down in order facilitate their removal.

The slight changes in clay content important to anticipating tunneling performance in SGC were detectable using a combination of exploration methodologies operating on a variety of scales. Access for drilling was extremely constrained throughout the project, and only a few locations could be efficiently drilled within the confines of airport infrastructure and operations. Traditional drilling and sampling was not possible due to the large particle sizes, and the regionally preferred methods of drilling and sampling these coarse materials did not yield representative samples. A combination of rotosonic drilling and sampling and borehole geophysics in select borings and continuous surface seismic geophysics has provided the information needed for appropriate geotechnical assessment for the project. The effectiveness of these characterization concepts will ultimately be determined during project construction. In addition, pressuremeter test results confirmed these observations in terms of measured soil parameters, in situ.

In conclusion it is evident from the results presented in this paper that the combination of investigation and testing techniques utilized provided consistent confirmation of the site conditions and anticipated performance during tunneling. The results indicated a distinct difference in the stress-strain properties of the Holocene (B2) soils and the Pleistocene (B3) soils. It is the intent of the authors to continue this study during construction of the project through a comprehensive monitoring program that will provide measured data for comparison with predictive models used for design.

REFERENCES

Durkee, D.B., Langer, J.A., Hughes, J.M.O., and Smith, D.E. (2005). *Pressuremeter Tests in Sand Gravel and Cobbles*, Symposium International ISP5/PRESSIO August 2005.

Louie, J.L. (2001). "Faster, Better: Shear-wave velocity to 100 meters depth from refraction microtremor arrays", *Bull. of the Seismological Soc. Am.,* 91:347-364.

Richart, F.E., Hall, J.R. Jr. and Woods, R.D. (1970). *Vibration of Soils and Foundations*, Prentice-Hall, Englewood Cliffs, New Jersey.

Rucker, M.L. (2003). "Applying the refraction microtremor (ReMi) shear wave technique to geotechnical engineering", *Third International Conference on the Application of Geophysical Methodologies to transportation Facilities and Infrastructure*, Orlando, Florida, FHWA, December 8-12.

Rucker, M.L. (2004). "Percolation theory approach to quantify geo-material density-modulus relationships", *9th ASCE Specialty Conf. on Probabilistic Mechanics and Structural Reliability*, Albuquerque, New Mexico, July 26-28.

Schlumberger (1972). *Log Interpretation Charts*, Schlumberger Limited, Houston, Texas.

Characterizing Unsaturated Cemented Soil Profiles for Strength, Excavatability and Erodability using Surface Seismic Methods

Michael L. Rucker[1], Member ASCE and Kenneth C. Fergason[1]

[1]AMEC Earth & Environmental, Inc., 1405 West Auto Drive, Tempe, Arizona 85284; PH (480) 940-2320; FAX (480) 785-0970; email: michael.rucker@amec.com; ken.fergason@amec.com

Abstract

Unsaturated soil profiles with cementation varying from non-existent to rock-like in nature are typical in the arid and semi-arid regions of the American Southwest. Geotechnical sampling of these materials can be difficult, especially as the materials become more rock-like. Furthermore, excavation of the harder cemented materials may require rock excavation methods, so that effective material characterization is needed for selection of appropriate excavation methods. Geological characterization of cementation strength, excavatability and erodability can be accomplished through various means. Surface seismic methods such as seismic refraction for p-wave velocities and refraction microtremor for s-wave velocities can provide subsurface profiles to effectively characterize geomaterial strengths as well as subsurface profiles. Without a water table to interfere with p-wave velocities, seismic refraction is very effective for obtaining depths to materials with increasing strengths. Velocity reversal conditions can be interpreted from the refraction microtremor s-wave results. Visual observations of stage cementation in test pits excavated using various sized backhoes and trackhoes and other geotechnical test data for dams, highways and other infrastructure are correlated with shallow seismic p- and s-wave velocity results. These correlations provide empirical testing for excavatability as a function of seismic velocity and stage cementation that is consistent with and correlated to the Kirsten excavatability criteria. The Kirsten excavation criteria have been expanded by others to address erodability and scour.

Introduction

Prediction of excavation and erodability conditions is a basic geotechnical engineering characterization task. Effective characterization of excavation or erodability conditions can have profound impacts on project design and construction

methods and costs, while effective characterization of erodability can be essential to assure public safety associated with dams, bridges and overland flooding. Unsaturated soil profiles with cementation varying from non-existent to rock-like in nature that present complex characterization challenges are typical in arid and semi-arid regions including the American Southwest. These challenges include large to extreme lateral depth and strength variability in the shallow subsurface and the common occurrence of relatively more cemented, stronger horizons overlying less cemented, weaker horizons. Standard geotechnical sampling methodologies often are limited or not applicable in these 'intermediate' materials where gravels are common and cementation and/or coarse gravel often result in soil sampler refusal, yet the materials are not sufficiently rock-like to be sampled well using rock coring methods.

Prediction of rock excavation conditions by bulldozer ripping has been largely solved for decades using criteria based on seismic refraction compression wave (p-wave) seismic velocity measurements (CAT, 1984, 1993, 2000) or other borehole-based rock mechanics criteria such as rock mass criteria. Those criteria do not address less competent 'intermediate' materials. Kirsten (1982 and 1988) developed an excavatability criteria based on subsurface sampling with geotechnical and geologic testing, not including geophysics, and qualitative observation, that estimates excavation conditions for the full range of geologic materials from soft soil to hard rock. NRCS (2001) has codified this characterization method, including qualitative aspects, to estimate geomaterial erodability to assess dam spillway adequacy. Nowatzki and Almasmoum (1988) reported on a limited laboratory-scale study of caliche excavatability without extensive field-scale observations of measurements. Stage cementation (Machette, 1985) provides a qualitative means to visually categorize cemented material strength and estimate excavatability or erodability.

At project sites in the southwest investigated by the authors, there appears to be good to excellent cross-correlation between actual documented excavation equipment performance and interpreted seismic velocities, geologic description of stages of cementation as logged in test trenches and test pits, and prediction of excavation characteristics based on Kirsten criteria.

Surface Seismic Measurement Methodologies

Surface seismic work is performed by the authors using a standard 12 channel signal enhancement seismograph and a sledgehammer energy source for seismic refraction measurements. Details of seismic refraction field procedures and interpretation methods used to characterize cemented soil profiles are described by Rucker (2000a). For geotechnical characterization typical depths of investigation are less than 9 m (30 ft). A 36 m (120 ft) geophone array with 3 m (10 ft) geophone spacing and 1.5 m (5 ft) hammer spacing to the nearest geophone provides sufficient depth of investigation and effective near surface resolution. When better shallow detail is needed, geophone and hammer spacing is typically halved. Field operations with a two person crew can proceed quickly and efficiently. When terrain or project requirements prevent vehicle access, the equipment can be backpacked to

investigation locations. Such mobility makes seismic an effective tool for preliminary subsurface evaluations before drill rig or heavy equipment access must be prepared.

An example completed interpretation is presented in Figure 1. Subsurface horizon p-wave velocities and interface depths are interpreted using the intercept time method (ITM) applied to five shotpoints at array endpoints, center and quarterpoints, along each 12-geophone array. Shallow interfaces with large velocity contrasts are readily interpreted using ITM. By breaking each line into four subparts, up to four local p-wave velocities with variable interface depths can be interpreted laterally along a soil or rock horizon. The interpreted profile in Figure 1 includes a cemented soil horizon (solid line, confirmed by test pit) based on eight individual depth interface points along the subsurface profile at depths of about 1.5 to 1.8 m (5 to 6 ft). Multiple interpretations of the uncemented surficial horizon at 0 to 1.5 m results in a p-wave velocity of 370 meters/sec (m/s) (1,200 f/s). The underlying cemented horizon has laterally varying p-wave velocities with four interpreted velocities ranging from 880 to 1160 m/s (2,900 to 3,800 f/s). As will be shown in this paper, a rubber-tired backhoe may be able to excavate a test pit deep into the cemented horizon at the 12 m location on this seismic line, but may refuse at or near the top of the cemented horizon at the 32 m location.
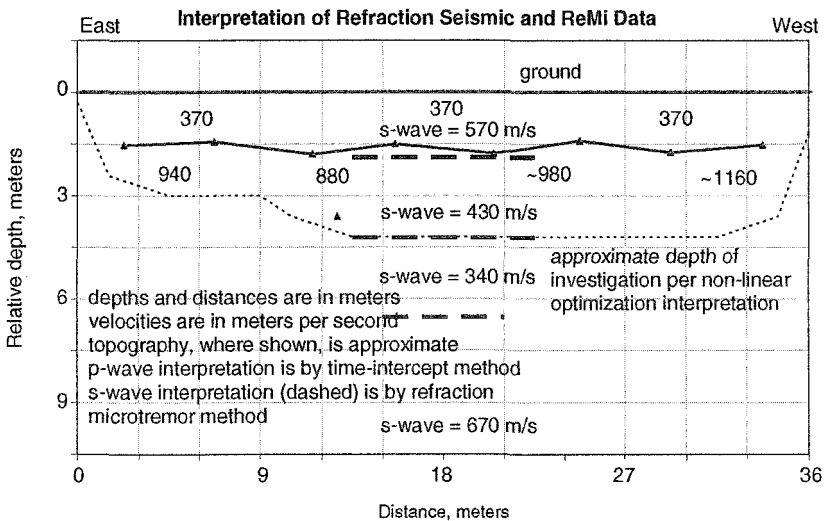
Figure 1. Example seismic line with both seismic refraction p-wave and refraction microtremor s-wave results. Energy source shotpoints are 0, 9, 18, 27 and 36 m.

A second, 'automated' seismic refraction interpretation utilizing a software package implementing a non-linear optimization technique (Optim, 2004) is also performed on the p-wave data. The resulting gradational seismic velocity changes across a mesh

with 0.6 m grid dimensions serves as effective check to the ITM interpretation but does not model the discrete cemented soil interface as well as ITM. By optimizing and presenting ray paths, the non-linear optimization result does provide an effective depth of investigation interpretation that cannot be obtained using standard refraction interpretation (Rucker, 2002). In the Figure 1 example, the p-wave depth of investigation is about 4 m. There is no seismic refraction interpretation result below that depth; this interpretation detail can be of great significance to geotechnical site characterization.

Recent surface wave developments, including the refraction microtremor (ReMi) method (Louie, 2001), enable collection and analysis of surface wave data using the same seismograph and field setup (using low frequency 4.5 Hz geophones) as seismic refraction as described by Rucker (2003). When collecting refraction data, only a few additional minutes are needed to collect ReMi data using a field vehicle, field crew jogging or ambient noise as the surface wave energy source. Concurrent p-wave and s-wave interpretations utilize strengths of each method to complement weaknesses of the other. Seismic refraction p-wave interpretation constrains the shallow portion of the s-wave interpretation while the deeper ranging s-wave interpretation can characterize a velocity reversal. An s-wave velocity is typically 0.5 to 0.6 times the corresponding p-wave velocity. The Figure 1 interpretation includes constraining the upper two s-wave velocity layers of 170 and 430 m/s (570 and 1,400 f/s) to about half the interpreted p-wave velocities. A velocity reversal with s-wave velocity of about 300 m/s (1,000 f/s) is then interpreted to underlie the cemented horizon at a depth of about 4 to 7 m (14 to 22 ft). Finally, a higher s-wave velocity of 670 m/s (2,200 f/s) is interpreted to underlie the subsurface profile.

Cementation Stage, Geologic Description and Geotechnical Characteristics

Stages of soil cementation in the southwest, primarily calcium carbonate or $CaCO_3$ as summarized in Table 1, have been described and codified by Birkeland (1999) with original compilations from Gile and others (1981) and Machette (1985). Since relatively large areas of intact soil fabric must be observed for effective cementation classification, samples from borings cannot be classified with precision. Drilling operations destroy the fabric of a soil, so that cementation stage cannot be accurately observed. Presence or absence of grayish or whitish color indicates the presence or absence of cementation minerals, but not degrees of cementation. In general, soil cementation is categorized visually into 5 stages with subcategories in the lesser stages of cementation. At higher cementation stages (typically Stage V, VI and possibly Stage IV), cemented soil behaves more as a rock or rock-like material.

Geotechnical parameters were applied to cemented calcareous soils by Beckwith and Hansen (1982) by the early 1980's. Their classification system included early application of stage cementation in the soil class descriptions, with emphasis on observation from boring samples. That dependence on boring samples, and additional decades of experience in both refinement of field geologic observation for stage cementation classification and geotechnical testing, require modification of

these stage cementation identifications. Beckwith and Hansen's typical geotechnical parameters, with both original and revised stage cementation, are presented in Table 2. Given the additional project experience accumulated since 1982, a study to reconfirm and revise the typical parameters presented in Table 2 may be appropriate. Descriptions of weak, moderate and strong cementation from boring samples may especially be subject to revision. When adequate material is available for observation, the description of stage cementation replaces the concept of weak to strong cementation. Further complexities can arise when clays are present in a calcareous soil and clay cohesion contributes to the material matrix strength.

Table 1. Descriptions of Calcium Carbonate ($CaCO_3$) Soil Cementation Stages from Birkeland (1999) with original compilations from Gile and others (1981) and Machette (1985)

Stage	Gravelly Parent Material	Nongravelly Parent Material
I	Thin discontinuous clast coatings; some filaments; matrix can be calcareous next to stones; about 4% $CaCO_3$	Few filaments or coatings on sand grains; <10% $CaCO_3$
I+	Many or all clast coatings are thin and continuous	Filaments are common
II	Continuous clast coatings; local cementation of few to several clasts; matrix is loose and calcareous, enough to give somewhat whitened appearance	Few to common nodules; matrix between nodules is slightly whitened by CO_3 (15-50% by area), and the latter occurs in veinlets and as filaments; some matix can be noncalcareous; about 10-15% $CaCO_3$ in whole sample, 15-75% in nodules
II+	Continuous clast coatings; local cementation of few to several clasts; matrix is loose and calcareous, enough to give somewhat whitened appearance; CO_3 in matrix is more pervasive	Common nodules; 50% - 90% of matrix is whitened; about 15% calcium carbonate in whole sample
Continuity of fabric high in carbonate		
III	Horizon has 50-90% K fabric with CO_3 forming an essentially continuous medium; color mostly white; CO_3-rich layers more common in upper part; about 20-25% $CaCO_3$	Many nodules, and carbonate coats so many grains that over 90% of horizon is white; carbonate-rich layers more common in upper part; about 20% calcium carbonate
III+	Most clasts have thick CO_3 coats; matrix particles continuously coated with CO_3 or pores plugged by CO_3; cementation more or less continuous; >40% $CaCO_3$	Most grains coated with CO_3; most pores plugged; >40% $CaCO_3$
Partly or entirely cemented		
IV	Upper part of K horizon is nearly pure cemented CO_3 (75 - 90% $CaCO_3$) and has a weak platy structure due to the weakly expressed laminar depositional layers of CO_3; the rest of the horizon is plugged with CO_3 (50 – 75% $CaCO_3$)	
V	Laminar layer and platy structure are strongly expressed; incipient brecciation and pisolith (thin, multiple layers of CO_3 surrounding particles) formation	
VI	Brecciation and recementation, as well as pisoliths, are common	

Table 2. Typical geotechnical parameters for calcareous soil classes by Beckwith and Hansen (1982) with bold print showing updated geotechnical parameters from borings and current stage cementation description based on undisturbed material test pit observations rather than disturbed sample observations from borings.

Class	Description - *Current Stage Cem in Bold*	Friction angle	Cohesion KPa	SPT N	UCS MPa
1	Holocene "collapsing" soils; Stage I, **Uncem., Stage I**	30°	10	<15	
2	Moderately cemented; Stage II **Weakly cem., Stage I+, II**	33-37°	50 - 140	5-25 **15-30**	
3	Strongly cemented; Stage III **Moderately cem., Stage II, II+**	35-42°	140 - 290 **100 - 190**	25-60 **30-75**	
4	Very strongly cemented with soft rock properties; Stage IV **Strongly cem., Stage III, III+**		Note: 1 psi = 6.9 KPa	60- 200+ refusal	0.5- 1.0
5	Moderately hard rock; Stage IV **Stage IV and higher**			200+ refusal	1.0- 35

Test Pit / Trench Stage Cementation and Seismic Velocity Correlation

The authors have been involved in three significant projects with logging of test trenches and test pits by geologists and overlapping seismic lines using procedures outlined in this paper. Stage cementation logging and seismic velocity correlations from these projects are presented in Figure 2. A project east of Kingman, Arizona, included subsurface materials consisting primarily of Stage I to Stage II+
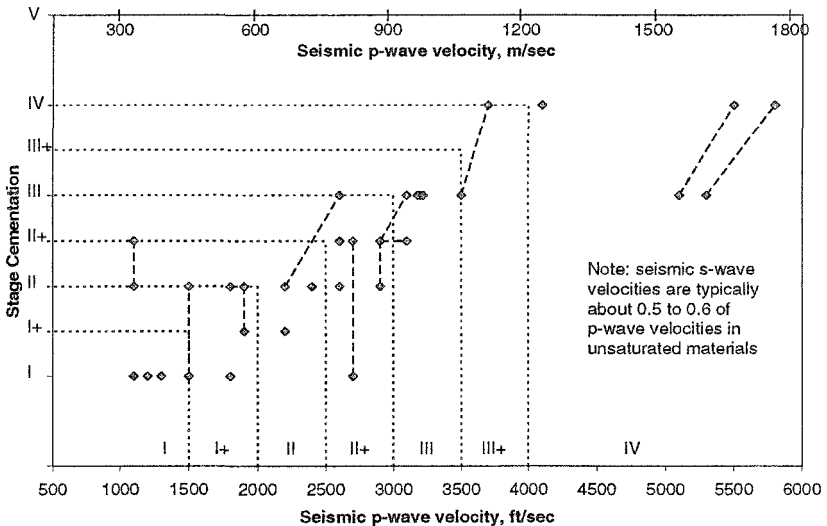
Figure 2. Correlation of stage cementation classifications from test pits and trenches with overlapping seismic velocities from three projects in Arizona. Data points connected by a dashed line indicate a range in either stage cementation or velocity.

cementation with no refusal encountered by the rubber-tired backhoe used for test pit excavation. A flood control dam project in the western Salt River Valley, Arizona, included test pits and trenches with primarily Stage I to Stage III cementation excavated using both a rubber tired backhoe and small trackhoe. The rubber tired backhoe refused on Stage III material. A highway project at a flood control structure in the eastern Salt River Valley, Arizona, included test pits with Stage I to Stage IV cementation and several excavation equipment sizes where some encountered refusal.

Qualitative and quantitative trends are apparent from Figure 2. First, in spite of inherent variability in the geologic materials and issues of observation and measurement at different size scales, there is a good relationship between stage cementation and seismic velocity. In these cemented soils, a reasonable seismic velocity and velocity range can be assigned to characterize stage cementation. Stage I, II, III and IV cementation can be anticipated in subsurface horizons with p-wave velocities less than about 610 m/s (2,000 f/s), 610 to 910 m/s (2,000 to 3,000 f/s), 910 to 1,220 m/s (3,000 to 4,000 f/s), and greater than 1,220 m/s, respectively. Reasonable scatter is present in the data, but this is typical of geotechnical parameters.

Test Pit / Trench Equipment Refusal and Seismic Velocity

Excavation of project test pits and trenches also provided an opportunity to correlate seismic velocity to equipment power and refusal as presented in Figure 3.
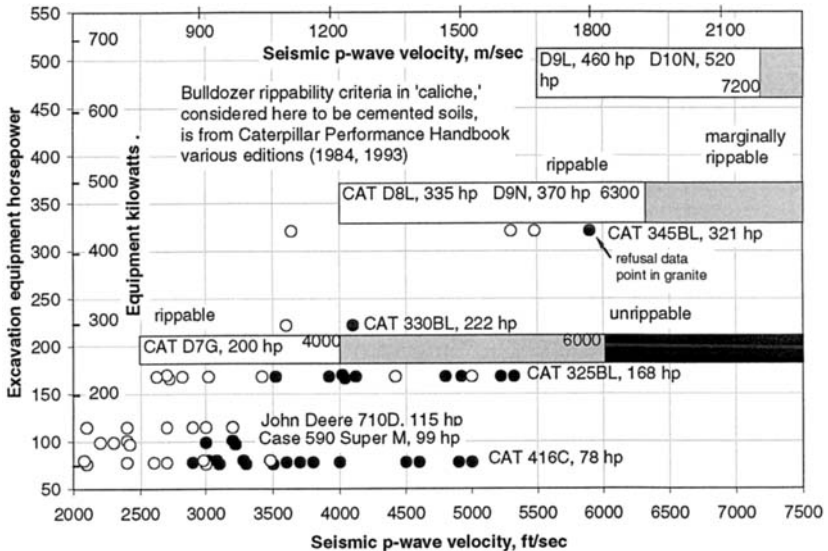
Figure 3. Seismic velocity and backhoe or trackhoe excavatability and published bulldozer rippability criteria for 'caliche.' Backhoe or trackhoe refusal data at test pits or trenches is indicated by solid circles while non-refusal is indicated by open circles. Equipment type and horsepower are listed beside data points.

Seismic velocity has been a standard means to assess bulldozer rippability in rock masses for decades (Cat, 1984 and 1993). However, those published relationships have been for bulldozers of 150 kw (200 hp) or more and did not include analogous excavatability criteria for backhoe loaders or trackhoe excavators. Kirsten (1982) did link equipment power across equipment type (bulldozers, backhoes, trackhoes) to equivalent excavation capability. An appropriate machine would be used to apply excavation force in a particular manner for an excavation task. Stacy and Noble (1975) indicated that rubber tired backhoes would typically encounter refusal at material seismic p-wave velocities greater than about 910 m/s (3,000 f/s).

As shown in Figure 3, rubber tired backhoes smaller than 75 kw (100 hp) generally encountered refusal at a seismic p-wave velocity above 910 m/s (3,000 f/s). Not only are these results consistent with Stacy and Noble, they indicate that such backhoe refusal can generally be anticipated in materials with Stage III cementation. Larger trackhoes with power of 86 to 164 kw (115 to 222 hp), could be anticipated to encounter refusal at about 1,070 to 1,220 m/s (3,500 to 4,000 f/s). That is consistent with materials at Stage III+ to IV cementation and consistent with marginal rippability for a 150 kw D7G bulldozer. Finally, the much larger 240 kw 345BL trackhoe, consistent with a D8L bulldozer, did not refuse in Stage III to IV materials with p-wave velocities up to 1,680 m/s (5,500 f/s), although digging was difficult.

Estimating Uniaxial Compressive Strength for Cemented Materials

Uniaxial or unconfined compressive strength (UCS) values, or an estimate of equivalent strengths, are needed to assess excavatability using the Kirsten Excavation Classification System. Correlation of seismic velocities with UCS values from boring core samples on two of the projects is presented in Figure 4. Many of the p-wave velocities are based on s-wave velocities at deeper subsurface velocity reversal zones. Samples with UCS greater than a megapascal generally came from cemented material masses with seismic p-wave velocities greater than 910 m/s (3,000 f/s) and Stage III or higher cementation. An outlier data point of 0.07 MPa (10 psi) at 1,340 m/s (4,400 f/s) p-wave velocity was logged as a thin weaker zone (about 0.3 m thick) at a depth that cannot be detected or interpreted using these surface seismic methods.

Rucker (2000b) has related typical anticipated UCS values and seismic p-wave velocities through a common parameter of modulus. Using this concept, p-wave velocities and typical anticipated UCS values for intact material masses, without joints and fractures to reduce modulus and seismic velocity, have been estimated as a conservative prediction of UCS as shown in Figure 4. At Stage I to IV cementation, actual measured UCS values for samples at a seismic p-wave velocity are generally much higher, typically by a factor of 2 or more, than the predicted UCS. This is consistent with the presence of fractures, joints, or uncemented zones within a cemented material mass that are not sampled but reduce the modulus and seismic velocity of the material mass. The harder cemented zones are sampled and can be tested. Increasing seismic velocity and cementation may be analogous to increasing rock mass strength by increasing RQD and reducing joints and fractures.
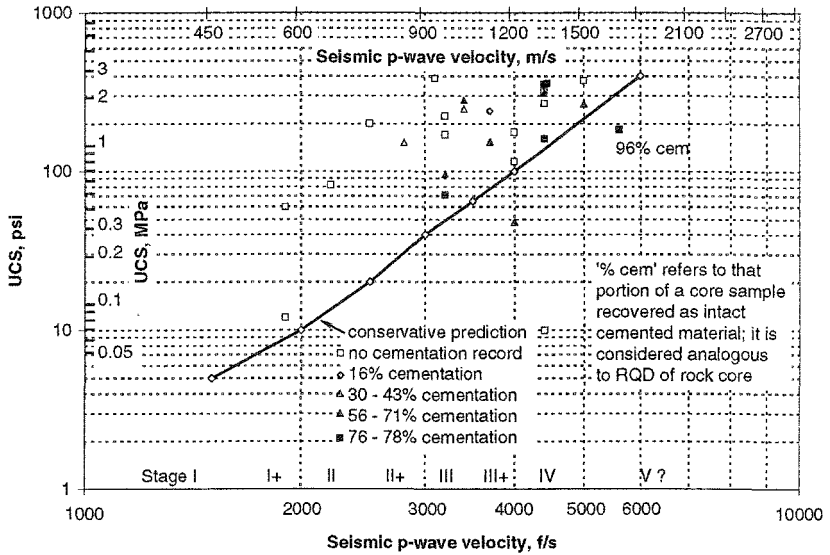
Figure 4. UCS values from core samples with overlapping seismic p-wave velocities. The solid line shows a conservative UCS prediction as a function of p-wave velocity.

Kirsten Excavation Classification System

This excavation system uses a Class Rating to categorize ground into 8 classes of excavatability based on excavation power as shown in Table 3. It has been adapted for analysis of erodability as documented in the 'Field Procedures Guide for the Headcut Erodability Index' (NRCS, 2001). Excavation class ratings are numeric and based on powers of 10 of the product or quotient of various ground mass parameters. The wide range of ground strength addressed and variety of usable parameters makes the Kirsten method especially useful for cemented soils.

Table 3. Kirsten excavatability classes; check current models for power. In Figure 3, Case 590 and Cat 416C are Class 2, John Deere 710D and Cat 325BL are Class 3, Cat D7G and 330BL are Class 4, Cat 345B and D8L are Class 5, and D9L is Class 6.

Class	Excavation Class Range N	Excavatability Description	Trackhoe/ Dozer Type	Trackhoe/ Dozer Power
1	< 0.01	Hand spade		
2	0.01 – 0.099	Hand pick and spade	Cat 215	63 kW 85 hp
3	0.1 – 0.99	Power tools	Cat 225, D6D	101 kW 136 hp
4	1.0 – 9.99	Easy ripping	Cat 235, D7G	145 kW 195 hp
5	10 – 99	Hard ripping	Cat 245, D8K	242 kW 325 hp
6	100 – 999	Very hard ripping	Cat D9H	306 kW 411 hp
7	1000 – 9999	Extreme rip/blasting	Cat D10	522 kW 701 hp
8	10000 +	Blasting		

The overall calculation for Class Rating is as follows:

Class Rating $= M_s * (RQD / J_n) * J_s * (J_r / J_a)$

Where M_s = mass strength $\quad J_s$ = relative ground structure number
$\qquad RQD / J_n$ = block size $\quad J_r / J_a$ = joint strength number

Each of these parameters will be discussed relative to cemented soils. The mass strength or consistency parameter M_s is based on uniaxial (UCS) strength, either estimated or measured, and is characterized in Table 4.

Table 4. Mass strength or consistency parameter M_s. Tested UCS values for individual samples of various cementation stages may be higher (factor of 2-3 or more) than the estimated UCS values based on mass behavior.

Material Type	Consistency _Cementation stage_ _See Figure 4_		Average UCS psi	Average UCS MPa	Average Mass Strength M_s
Granular / cohesive soil	V loose / v soft	**I**	5	0.035	0.02
	Loose / soft	**II**	10	0.069	0.04
	Med dense / firm	**II+**	20	0.14	0.09
	Dense / stiff	**III**	41	0.28	0.19
	V dense / v stiff	**III+**	80	0.55	0.41
Rock	V soft rock	**IV**	160	1.1	0.87
			319	2.2	1.9
	Soft rock		638	4.4	4.0
			1276	8.8	8.4
	Hard rock		2552	17.7	17.7
	Very hard rock		5104	35.4	35
	Extremely hard rock		20400	141.3	140

Block size is determined as the RQD divided by the joint set number J_n. At shallower depths of perhaps about 8 m (25 ft) or less, cementation is sufficiently incomplete at Stages I through III that RQD is taken to be 5. At greater depths or possibly Stage IV at near surface, cementation may be sufficiently complete at Stage III or IV that RQD of 100 can be used. The joint set number J_n is 5 for multiple joint or fissure sets and intact granular materials. For cemented soils discussed in this paper, block size is typically 1 (RQD/J_n or 5/5) at shallower depths and 20 (RQD/J_n or 100/5) for Stage III or higher materials at greater depths or possibly Stage IV near surface.

The relative ground structure number J_s is taken to be 1.0 since defined joint sets with dip and joint spacing ratio are typically not present in these cemented soils.

Joint strength number is the joint roughness number divided by the joint alteration number. Joint roughness number J_r is 1.0 for cemented soils drillable with hollow stem auger, and J_r is 3.0 for intact granular material such as sand-gravel-cobbles. Joint alteration number J_a in cemented soils drillable with hollow stem auger is less

than or equal to 6.0. For the soils discussed in this paper, joint strength number ranges from 0.5 (J_r/J_a or 3/6) to 0.17 (J_r/J_a or 1/6).

Excavatability Classification in Cemented Soil Masses

A summary of excavatability conditions for cemented soils as discussed in this paper is presented in Table 5. Overall, very good correlation exists between actual field performance of excavation equipment, stage cementation, excavatability class ratings and seismic velocity at the material behavior change point between cementation Stage II+ and III, 910 m/s (3,000 f/s) seismic p-wave velocity and Excavation Class 2 to 3. Variations in actual machine power and selection of UCS values lead to less distinct boundaries between cementation Stage III to III+ to IV at a seismic p-wave velocity range of 1,070 to 1,220 m/s (3,500 to 4,000 f/s), but trends between material strength and excavation power are still apparent. Example correlations between the Kirsten excavatability criteria and seismic velocity at ground class 6 and 7 in weathered granite rock (Rucker, 1999) have been presented elsewhere. The effectiveness in cross-checks between these methods is encouraging towards applying these methods to erodability, although it is appropriate to use lower estimated mass strength parameters estimated from seismic velocities to predict lower erodability thresholds than would be predicted based on measured UCS values.

Table 5. Excavatability conditions in cemented soils as classified by seismic velocity, stage cementation, and Kirsten excavation Class. Case 590 Super M and Cat 416C backhoes consistently refused at Stage III, seismic p-wave velocity > 910 m/s.

Cementation Stage & P-wave Vel., m/s (f/s)	Class Rating N $M_s*(RQD/J_n)*J_s*(J_r/J_n) = N$	Excavation Class & Onsite Equipment
Stage I < 460 (1500)		1 shovel
Stage I+ 460 (1500)	0.02 * (5/5) * 1 * (3/6) = 0.01	2 Case 590, Cat 416C
Stage II 610 (2000)	0.04 * (5/5) * 1 * (3/6) = 0.02	2 Case 590, Cat 416C
Stage II+ 760 (2500)	0.09 * (5/5) * 1 * (3/6) = 0.05	2 Case 590, Cat 416C
Stage III 910 (3000)	0.19 * (5/5) * 1 * (3/6) = 0.1	3 John Deere 710D
Stage III+ 1070 (3500) Higher sample UCS	0.41 * (5/5) * 1 * (3/6) = 0.2 to 1.23 * (5/5) * 1 * (3/6) = 0.6	3 Cat 325 refused Cat 330BL succeeded
Stage IV 1220 (4000) Higher sample UCS	0.87 * (100/5) * 1 * (1/6) = 2.9 2.61 * (100/5) * 1 * (1/6) = 8.7	4 Cat 330BL refused Cat 345BL succeeded

Acknowledgements

References

Beckwith, G.H. and Hansen, L.A., 1982, Calcareous soils of the Southwestern United States, *Geotechnical Properties, Behavior and Performance of Calcareous Soils,*

ASTM STP 777, K.R. Demars and R.C. Chaney, eds., American Society for Testing and Materials, pp. 16-35.

Birkeland, P.W., 1999, *Soils and Geomorphology*, Oxford Univ. Press, New York.

Caterpillar Tractor Company, (Cat), 1984 and 1993, *Caterpillar Performance Handbook*, Edition 15 and 24, Peoria, Illinois, October.

Gile, L.H., Hawley, J.W. and Grossman, R.B., 1981, Soils and Geomorphology in the Basin and Range area of southern New Mexico – Guidebook to the Desert Project, New Mexico Bureau of Mines and Mineral Resources Memoir 39.

Kirsten, H.A.D., 1982, A Classification System for Excavation in Natural Materials, *Civil Engineer in South Africa*, Vol. 24, No. 7, July, pp. 293-308.

Kirsten, H.A.D., 1988, Case Histories of Groundmass Characterization for Excavatability, *Rock Classification Systems for Engineering Purposes, ASTM STP 984*, Louis Kirkaldie, Ed., American Society for Testing and Materials, Philadelphia, Pennsylvania, pp. 102-120.

Louie, J.L., 2001, Faster, Better: Shear-wave velocity to 100 meters depth from refraction microtremor arrays, *Bull. of the Seismological Soc. Am.*, 91:347-364.

Machette, M.N., 1985, Calcic soils of the southwestern United States, Soils and Quaternary Geology of the Southwestern United States, Ed. David Weide, 1-21.

NRCS, 2001, Field procedures guide for the headcut erodability index, Chapter 52, Part 628, National Engineering Handbook, U.S. Department of Agriculture Natural Resources Conservation Service, 210-VI-NEH, rev. 1, March.

Nowatzksi, E,A, and Almasmoum, A.A., 1988, A method for estimating the excavatability of caliche, *Geotech. Testing J.*, GTJODJ (11)2, June, 148-154.

Optim L.L.C., 2004, SeisOpt@2D v4.0, Optim Software and Data Solutions, UNR-MS-174, 1664 N. Virginia St., Reno, Nevada, 89557.

Rucker, M.L., 1999, A Rippability Index Approach for Characterizing Weathered Granites, *Rock Mechanics for Industry*, Amadei, Kranz, Scott & Smeallie (eds), Balkema, Rotterdam, 101-107.

Rucker, M.L., 2000a, Applying the seismic refraction technique to exploration for transportation facilities, *First International Conference on the Application of Geophysical Methodologies to transportation Facilities and Infrastructure*, St. Louis, Missouri, FHWA, December 11-15.

Rucker, M.L., 2000b, Earthwork factors in weathered granites by geophysics, in Nazarian, S. & J. Diehl (eds), *Use of Geophysical Methods in Construction, Geotech. Spec. Publ. No. 108*: 201-214. Reston, Virginia: ASCE.

Rucker, M.L., 2002, Seismic refraction interpretation with velocity gradient and depth of investigation, *Second International Conference on the Application of Geophysical and NDT Methodologies to transportation Facilities and Infrastructure*, Los Angeles, California, FHWA, April 15-19.

Rucker, M.L., 2003, Applying the refraction microtremor (ReMi) shear wave technique to geotechnical engineering, *Third International Conference on the Application of Geophysical Methodologies to transportation Facilities and Infrastructure*, Orlando, Florida, FHWA, December 8-12.

Stacy, T.R. and Noble, G.W., 1975, Seismic Evaluation of Soil Trenchability, *Proceedings of the Sixth Regional Conference for Africa on Soil Mechanics and Foundation Engineering*, Vol. 2, 185-186.

Surface Seismic Methods for Locating and Tracing Earth Fissures and other Significant Discontinuities in Cemented Unsaturated Soils and Earthen Structures

Michael L. Rucker[1], Member ASCE and Otto C. Holmquist[2]

[1]AMEC Earth & Environmental, Inc., 1405 West Auto Drive, Tempe, Arizona 85284; PH (480) 940-2320; FAX (480) 785-0970; email: michael.rucker@amec.com
[2]GEOLINES L.L.C., 3170 Broad Leaf Street, Las Vegas, Nevada, 89135; PH (702) 732-8778; FAX (702)732-8778

Abstract

Seismic refraction methods have been used for more than a decade to locate earth fissures and other significant discontinuities in unsaturated, cemented soils that present potential risks to various facilities. Recently, these methods have been adapted to locating areas of potential significant cracking within earthen structures, including large flood control embankments. Earth fissures and connected cracks in normally dry embankments have potential under flood induced erosion to cause failures in such structures or at linear infrastructure such as roads and canals. The essence of these methods is to identify anomalous large signal attenuations and (or) first arrival time delays in standard multi-channel seismic refraction data. Locations of anomalous attenuation or time delays are interpreted in the field and marked on the ground. Using a series of profiles along an earth fissure or other discontinuity trace, actual positions of the features can be determined. Once the locations of such features have been determined, further geologic investigation, including test pits, are typically used to verify and assess the features and potential hazard. These methods have been used to locate and trace earth fissures in Arizona and Nevada, including in urbanized areas of Las Vegas and at industrial ponds and flood control dams.

Introduction

Earth fissures are typically a result of ground tension developed by differential ground subsidence due to groundwater depletion or other geologic phenomena. Although actual tension cracks may be only fractions of an inch to an inch or two in aperture, water piping and erosion can rapidly widen fissures into gully-size erosion features. In 1984, about 1,500 acre-feet of effluent disappeared from a paper mill waste water storage lake in northeast Arizona after earth fissures opened in the

601

reservoir (Neal and others, 1998). A previous event in a nearby playa lakebed led to the loss of about 6,000 acre-feet of effluent in the early 1960's, and another fissure intercepted a canal in the area in 1995. In 1993, a newly opened earth fissure was discovered in the southern portion of a proposed combustion waste disposal facility site in southeast Arizona, including lined ponds, after heavy winter rains and runoff (Keaton and others, 1998). That fissure system also crosses transcontinental pipelines and damaged county roads in 2004. In 2002, an earth fissure system was discovered extending under a flood retention structure (FRS) in the western Salt River Valley in central Arizona (Rucker and Fergason, 2004) and is being mitigated.   An earth fissure system was discovered adjacent to the Central Arizona Project canal in east Scottsdale in 2003 (CAP, 2005). In August 2005, rainfall runoff opened previously filled earth fissures, threatening homes in a rural neighborhood in the southeast Salt River Valley (Arizona Republic, 2005). Earth fissures are a recognized geologic hazard requiring mitigation by developers in the Las Vegas area (Bartlett, 2002), and have recently been revealed in southwestern Utah by flooding (Lund, 2005).

Cracking in earth embankments, especially at flood control structures, presents another erosion hazard induced by either ground tension or desiccation of FRS material in arid climatic settings. Piping erosion through an FRS embankment during flood storage induced by interconnected cracking could lead to catastrophic structure failure. Identifying presence and location of embankment cracking is a critical issue for assessing safety and risk of flood retention structures and dams.

Earth Fissure / Crack Characteristics Relevant for Geophysics

Once piping (Figure 1) or gully erosion has developed, an earth fissure or embankment crack can generally be readily identified and mapped by surface geologic reconnaissance.   However, before such surface features become evident, or

Figure 1.   An erosion piping hole at an earth fissure west of Phoenix, Arizona. Various geophysical methods were tested at this typical elongated feature.

once such surface features along a fissure trace cease, subsurface exploration is required to positively identify or trace a fissure. An uneroded fissure may be less than a millimeter (Figure 2) up to perhaps 25 to 50 mm (1 to 2 inches) wide, and usually has the shallowest soils bridging that aperture at ground surface. Backhoe test pits (Figure 3) or shallow excavation can confirm the presence, location and aperture of a fissure exposed by excavation.
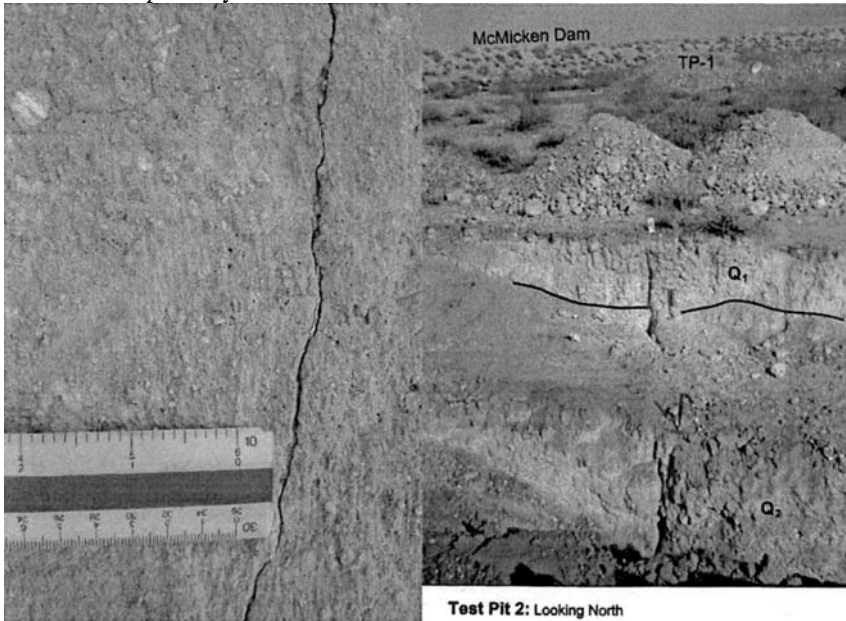
Figures 2 and 3. Earth fissures located using seismic refraction methods. Figure 2 shows a clear but small (inch scale) aperture uneroded earth fissure feature found in a confirmatory test pit. Figure 3 shows a larger earth fissure in a confirmatory test pit with no surficial exposure but considerable subsurface aperture.

A critical feature of an earth fissure is the interconnected and organized nature of the tension cracking through the typically cemented alluvial soil mass. This nature separates earth fissures into a more discrete or discontinuous geophysical and hydraulic behavior controlled by the earth fissure discontinuity itself as compared to a more continuous or homogeneous behavior in more typical geomaterial mass settings without considerable large-scale tension. Even if erosion or piping features are not present at ground surface, aerial photography, especially low sun angle aerial photography (Beckwith and others, 1991), can identify linear trends on the ground surface and vegetation that may indicate the presence of earth fissuring.

The challenge presented by earth fissures and embankment cracks to the geotechnical and geological community is to be able to reliably indicate the presence and locations of these features in an effective and efficient manner. Once the presence of such features are indicated, then verification and quantification by geologists and engineers

can proceed through test pits or other excavation methods. Once quantified, mitigation measures can be determined, designed and applied to these hazards.

Non-Seismic Geophysical Methods Applied to Earth Fissures

Earth fissures are typically associated with areas where rapid changes in bedrock depth or basin lithology are occurring. Depths of investigation of hundreds of feet are typically needed to provide useful basin and bedrock characterization; drilling is costly and inefficient. Geophysical methods are successfully applied for general subsurface characterization. Gravity is frequently employed to identify areas with rapid changes in bedrock depth and estimate bedrock depth (Slaff, 1993; Rucker and Fergason, 2004). Electrical resistivity methods can provide useful information concerning basin lithology (Rucker and Fergason, 2004), especially if large variations in basin material clayeyness contribute to ground strain and earth fissuring. Such methods are especially effective if they are guided by remote sensing satellite data using interferometry by synthetic aperture radar (InSAR) that identifies differential subsidence across a region to a scale smaller than 50 meters and vertical resolution to a few millimeters (Weeks and Panda, 2004). However, all of these methods are large scale that only indicate areas where earth fissures may be present or likely to occur.

Seismic methods to indicate the presence and location of earth fissures are being routinely used by the authors and will be discussed shortly. In 2004, one of the authors (Rucker) tested small scale electrical methods across a known earth fissure (see Figure 1) as possible faster, more efficient alternatives to seismic methods for fissure identification. An ideal measurement system would allow rapid coverage of long profiles with clear geophysical anomaly indications or other readily interpreted measurements to identify presence and location of potential fissures. Electromagnetic (EM) measurements can be performed without the need to make contact with ground. Capacitive coupling, where an electrode array is dragged along the ground, typically in a dipole-dipole arrangement, could also meet such ideal criteria. Figure 4 presents results from EM and surface resistivity measurements (to emulate capacitive coupling measurements) using Wenner and dipole-dipole arrays deployed in profiles perpendicular to the fissure and sufficiently long to indicate non-fissured ground versus ground at the earth fissure. An ideal fissure in unsaturated ground would be an opening that behaves as a thin, vertically oriented infinite resistivity. Anticipated results from a Wenner array passing over such an electrical feature are included in Figure 4. However, actual fissure behavior as an electrical medium, such as partial filling by loose material, may be far from ideal. Given the empirical results presented in Figure 4 that did not indicate an electrical anomaly at a fissure, simple field resistivity measurements could not be counted on to provide interpretable information concerning the presence or absence of an earth fissure as shown in Figure 1.

Ground penetrating radar (GPR) might be anticipated to be a useful tool for locating earth fissures. However, GPR performance as a geophysical tool in the basin soils of the desert southwest U.S. has been disappointing. In studying archeological sites in southern Arizona, McGill (1995) found 500 MHz GPR penetration to be less than 1
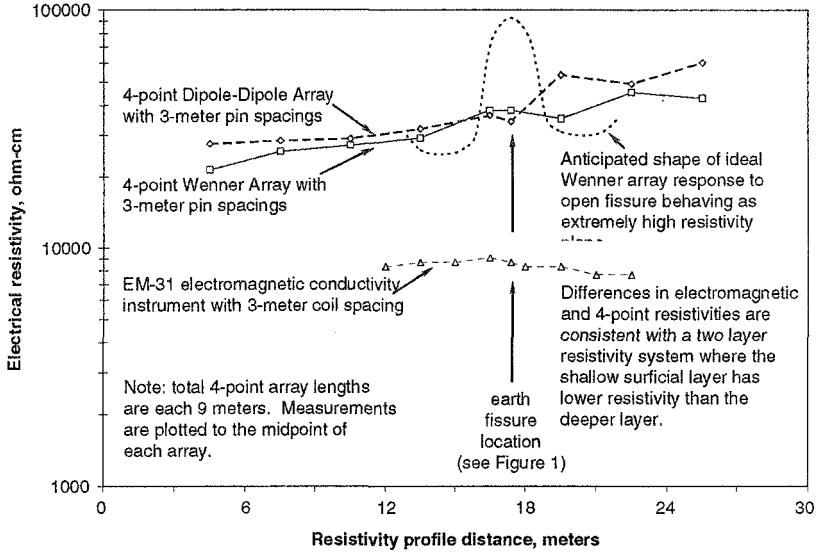
Figure 4. Results of small scale (not exhaustive) testing of electrical resistivity methods at earth fissure shown in Figure 1. Resistivity profile is perpendicular to earth fissure trend. Ground was moist from recent precipitation during winter season.

meter, and 80 MHz GPR penetration to be only slightly greater than 1 meter. Sternberg (2004) has also indicated that GPR penetration of less than 1 meter can be anticipated in slightly moist to moist clayey soils, including sites in southern Arizona. Recent experience by one author's firm at a relevant FRS site using 100 and 200 MHz GPR to locate abandoned metal corrugated pipe met with limited success. In some circumstances, an earth fissure with significant subsurface piping and erosion may provide a suitable GPR target. However, the potentially small target presented by an uneroded fissure aperture such as shown in Figure 2, or a larger fissure overlain by clayey soils that attenuate GPR signal, may not be detectable using GPR.

Surface Seismic Detection of Earth Fissures and Cracks

An earth fissure or interconnected embankment crack presents a discontinuity that effectively attenuates, delays or blocks the propagation of elastic energy (seismic signal) through a ground or embankment material mass. Seismic energy can be compression wave (p-wave), shear wave (s-wave) and other elastic waves. Seismic s-wave attenuation across an earth fissure in south central Arizona was reported by Wrege and others (1985). Presented with the need to trace an earth fissure beyond surface features across a proposed pond facility in 1994, one author reviewed the s-wave method, and while in the field, observed that p-waves were attenuated and delayed. Since p-wave seismic data could more readily and rapidly be acquired through standard seismic refraction methods and equipment, an effective procedure

using p-waves from a sledgehammer energy source was developed (Rucker and Keaton, 1998). These procedures have been modified since to reflect current seismic refraction procedures and capabilities. A critical part of the procedure is field interpretation of the data so that the presence or absence and location of discontinuities are staked in the field as data collection proceeds. A twelve channel signal enhancement seismograph with sledgehammer energy source and geophone spacing of 3 m (10 ft) is used. Fissure or crack detection, location and verification is not complete until subsurface ground truthing is done using test pits. Since that time, this seismic refraction method has been used by the authors to trace earth fissures, or verify the absence of earth fissures, at a number of sites in Arizona and Nevada.

A typical set of expected seismic refraction traces for ground without discontinuities such as an earth fissure or a significant embankment crack, will have a pattern similar to that shown in Figure 5. First arrival times increase at regular time intervals across the array consistent with the expectations of the seismic refraction method. Gains for each channel are adjusted so that the first arrival pulses are of similar height across the geophone array and relative signal amplitudes (through gain settings) can be compared. An excellent indicator of a fissure-type discontinuity is a signal attenuation of 12 decibels or more between two geophones, a factor of 4 in amplitude, at least 3 geophones from the energy source that persists through the seismic array.
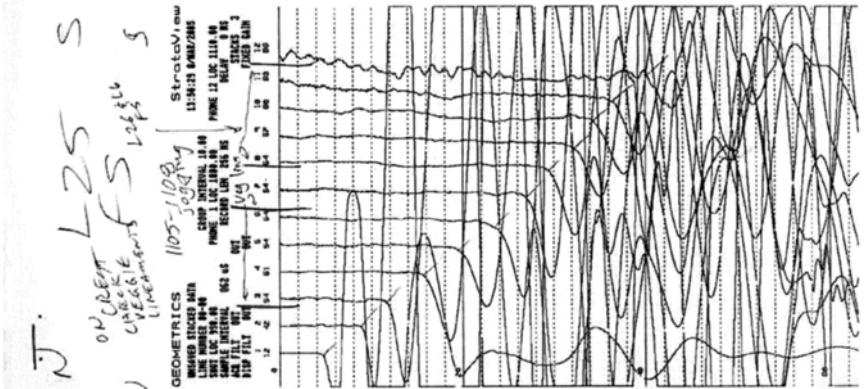
Figure 5. Typical 12-channel seismograph traces adjusted for fissure or crack detection. Geophone spacing is 3 m (10 ft), the energy source is 1.5 m (5 ft) from geophone 1, trace length is 256 milliseconds and sampling rate is 62 microseconds. First arrival picks are manually marked in the field. A total of 5 trace sets, with energy source at the array endpoints, center and quarterpoints, are usually obtained. This trace is from an embankment crest. Vegetative lineaments hinted at embankment cracking, but no discontinuities were indicated from the seismic data.

An example set of seismic refraction traces for ground with an earth fissure could have a pattern similar to that in Figure 6. Geophone signals from energy source to the earth fissure (geophones 12 to 7) are normal for seismic refraction similar to the traces in Figure 5. Once the earth fissure severely attenuates seismic signal propagation (between geophones 7 and 6), the rest of the seismic signals are distorted.

Time delays of several milliseconds or more to apparent loss of signal beyond the seismic anomaly (Figure 6) are also typical indicators of an earth fissure-type discontinuity. Based on field interpretations using energy source locations along the geophone array for forward and reverse seismic anomaly determination, interpreted discontinuity locations are staked in the field before the geophone array is picked up.
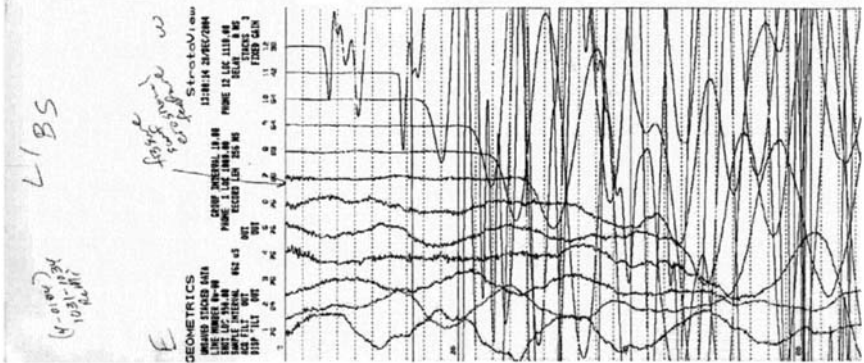
Figure 6.   Example 12-channel seismograph traces adjusted for fissure or crack detection with an earth fissure present. This line was set with the earth fissure shown in Figure 1 between geophones 6 and 7. The energy source is 1.5 m (5 ft) beyond geophone 12 at the top. Signals at geophones 6 through 1 are severely attenuated and delayed, indicating the fissure presence and location between geophones 6 and 7.

Search patterns to locate or verify the presence or absence of earth fissuring vary with the requirements of a project. Discovery or previous knowledge of an earth fissure in the vicinity of a project based on surface observation will suggest a seismic line pattern for tracing the fissure (Rucker and Keaton, 1998; Rucker and Fergason, 2004). A seismic line is completed and interpreted across the last surficial evidence of the fissure to verify seismic signal discontinuity. That point is staked. The anticipated fissure trend is then projected for a distance, typically 60 m (200 ft), and another seismic line is centered on that point, completed and interpreted for discontinuity. The interpreted discontinuity position on the new line is staked, the projected earth fissure trend is taken along the line of the staked discontinuity interpretations, and the trend is again marked at the new projected fissure trend location.   Another seismic line is centered there, performed and discontinuity interpreted, and that discontinuity location staked. This process is repeated across the site until a geophysical trace of the earth fissure is complete. If at any point there is no indication of a discontinuity, then seismic lines offset from the projected trend are completed until the new fissure trace location is found or the fissure is indicated to have ended. Rucker and Keaton (1998) detail the use of this procedure to trace an earth fissure in southeast Arizona across a facility site for 700 m (2,300 ft) beyond the last surficial expression. Test pits at selected locations across the trace ground truth the existence of and quantify characteristics of the earth fissure.

A need to verify the absence of or locate an unknown fissure(s) may require the use of continuous seismic coverage across a portion of a facility or structure. This may

be of critical importance for dam, FRS or pond safety assessment, such as described by Rucker and Fergason (2004). It provides, if needed, the additional benefit of collecting considerable shallow seismic data for geotechnical characterization. Continuous coverage requires that seismic lines be partially overlapped so that a seismic discontinuity under line endpoints is not missed. Current procedures include a typical advance of 23 m (75 ft) for each 36 m (120 ft) seismic line to provide an overlap of 14 m (45 ft) to avoid missing a feature at a line end. Test pits at seismic discontinuity interpretations provide ground truth for the presence of earth fissures.

Detection of Significant Embankment Cracks

Conceptually similar to earth fissures, significant, interconnected cracks in normally dry flood control or other embankments can become a risk for piping erosion and catastrophic failure when times of water impoundment do occur. Surface expression of piping erosion in an embankment, often due to infrequent heavy rains, may be the only visible evidence of potential problems evident for routine inspection. Traditional methods to investigate internal cracking in these structures have been limited to trenching for coverage of large areas or test pits or other excavation for isolated areas, as shown in Figure 7.

Figure 7. Upstream slope of flood retention structure in arid environment in central Arizona with upper 1 m (3 ft) of material removed. Note visible transverse cracking extending from crest. This FRS had a central drain installed with deep trenching at the crest in conjunction with embankment crack mapping in the early 1980's.
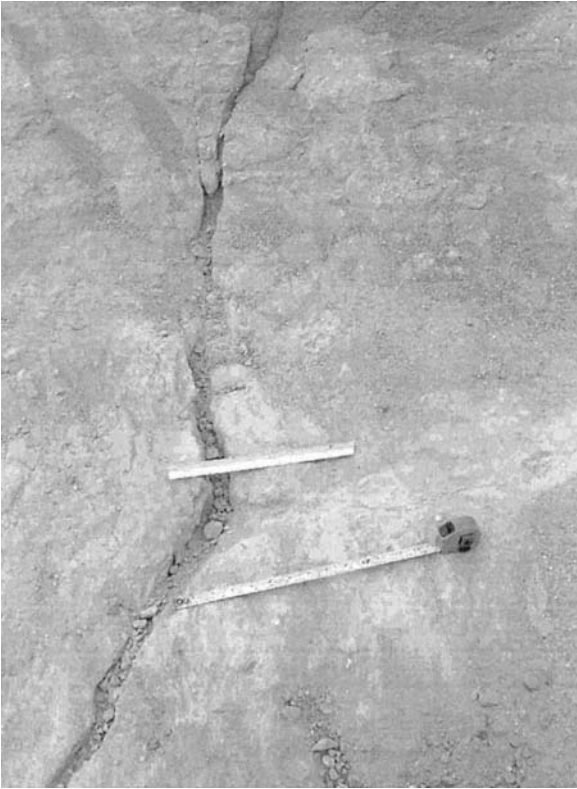
Figure 8. Closeup of significant crack visible in Figure 7. Darker embankment fill material at top edge of photo was test pit backfill from an earlier investigation. Surficial exposures of piping erosion at the embankment crest originally guided investigators to evaluate this location.

Similar to earth fissures, the seismic refraction method provides a means to evaluate the presence or absence of significant interconnected embankment cracking. The traces presented in Figure 5 were collected at the crest of an FRS where strong transverse vegetative lineaments across the embankment crest, especially between geophones 6 and 7, were a surface hint of possible significant transverse cracking. However, a seismic line across these features did not exhibit the attenuation or arrival time delays consistent with internal transverse cracking. In that situation, the seismic method indicated that an internal transverse cracking problem was not present at that location in spite of the surface vegetative lineament. Invasive test pit evaluation of those lineaments was not needed.

Examples of seismic signal attenuation and time delay from a seismic line completed at the embankment crest location shown in Figures 7 and 8 are shown in Figure 9. These traces demonstrate forward and reverse indications of significant embankment

cracking, with interpretable indications of seismic discontinuities at two locations along the line. Seismic work was completed at this site before excavation was begun. The interpreted seismic discontinuity locations were staked and later verified to be consistent with the cracking exposed by excavation.
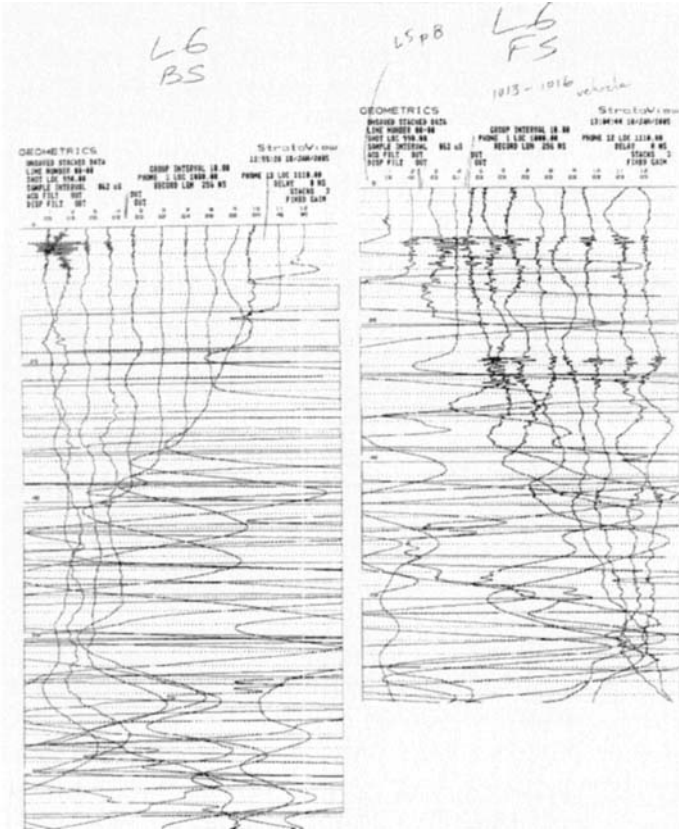
Figure 9.   Traces from both the backshot (BS) end and the foreshot (FS) end of a seismic line completed at the embankment location shown in Figures 7 and 8. Multiple seismic anomalies are indicated. The BS traces show a very clear time delay between geophones 4 and 5 while the FS traces show significant signal attenuation between geophones 4 and 5.   The BS traces also show a significant time delay between geophones 9 and 10 while the FS traces show a further signal attenuation or loss at about geophone 9.

Success and Limitations of Method

To date, understanding of the successful applications and limitations of this method are project specific examples.   Because it is being applied to dam safety investigations in Arizona, a formal review and documentation of the method's history is planned for 2006.   Furthermore, earth fissure initiation and development is a poorly

understood dynamic geologic process that, in some circumstances, can be difficult to ground truth for verification of success or failure of a seismic anomaly interpretation.

In Arizona and northern Nevada, the seismic method has been successfully used to trace multiple confirmed earth fissures beyond visual surface expressions (see Figure 1) at two industrial sites, a major flood retention structure (FRS, Figures 1 through 3) and two canals. In addition, previously unknown fissures were found using the seismic method at one industrial site and that FRS. Earth fissure presence and locations were verified by test pits. Sites with areas suspected of containing earth fissures, but lacking visual surface erosional features, have also been evaluated using the seismic method. These include parts of the abovementioned sites and an additional four major flood retention structures. Earth fissures were not identified based on the seismic method at these suspected sites; no earth fissures were found in test pits and trenches completed in these suspect areas. Depending upon project needs, from 20 to 50 to over 100 seismic lines were performed to achieve adequate coverage for determining the presence or absence of earth fissures in critical areas.

Use of the seismic method to identify significant embankment cracking has begun only recently and has been applied to selected locations at four embankments, including three flood retention structures. Seismic signatures (Figure 9) of significant cracking (Figures 7 and 8) have been interpreted at three embankments. Seismic signatures of no significant cracking (Figure 5) have been interpreted at one embankment.

Limitations of the seismic method include geometric constraints that limit seismic line deployment over a fissure or crack target and site noise that limits effective p-wave data collection. Interference from the energy source impact noise can occur at p-wave velocities below the speed of sound in air, although such low strength soils may not be able to maintain an earth fissure or crack. S-wave or surface seismic methods may be able to overcome some limitations of the p-wave method.

Summary and Conclusions

Evaluation of seismic anomalies indicated from seismic refraction measurements provide an effective, non-destructive means to identify the presence and locations of earth fissures in unsaturated soils in arid and semi-arid environments. These methods have been successfully applied to earth fissure investigations for over a decade. More recently, these methods are beginning to be applied to evaluations of significant transverse cracking in normally dry, desiccated flood control structures and other embankments where piping erosion through such interconnected cracking could lead to catastrophic failure during rare impoundment events.

References

Arizona Republic, 2005, Big storm wreaks devastating havoc, Holly Johnson and Judi Villa, *The Arizona Republic*, Thursday, August 11, p. 1 and 12.

Bartlett, K., 2002, Las Vegas: A Thirsty, Sinking City, in *When Cities Face Geologic Forces, Geotimes*, October, http://www.geotimes.org/oct02/feature_cities.html.

Beckwith, G.H., Slemmons, D.B. and Weeks, R.E., 1991, Use of low-sun-angle photography for identification of subsidence induced fissures, in *Land Subsidence, Proceedings of the Fourth International Symposium on Land Subsidence*, ed. A.I. Johnson, held in Arvada, CO, May 12-17, IAHS Publ. No. 200, Oxfordshire U.K., International Association of Hydrological Sciences Press.

Central Arizona Project (CAP), 2005, Subsidence and Earth Fissure Monitoring Presentation, Well Rules Stakeholder Group Meeting Summary, January 26. Http://www.water.az.gov/WaterManagement/Content/WellRules/2005/1-26-05_well_rules_minutes.doc.

Keaton, J.R., Rucker, M.L. and Cheng, S.C., 1998, Geomechanics analysis of an earth fissure induced by ground-water withdrawal for design of a proposed Ash and sludge impoundment in Southeastern Arizona, *Land Subsidence, Case Studies and Current Research, Proceedings of the Joseph F. Poland Symposium on Land Subsidence*, ed. J.W. Borchers, Special Publ. No. 8, Association of Engineering Geologists, pp. 217-226.

Lund, W.R., 2005, Earth Fissures near Beryl Junction in the Escalante Desert, Prelim. Report, Jan. 26. http://www.geology.utah.gov/utahgeo/hazards/fissures.htm

McGill, J.W. and Sternberg, B.K., 1995, Archeology studies in southern Arizona using ground penetrating radar, *J. of Applied Geophysics*, Vol. 33, pp 209-225.

Neal, J.T., Colpitts, R. and Johnson, K.S., Evaporite karst in the Holbrook Basin, *Land Subsidence, Case Studies and Current Research, Proceedings of the Joseph F. Poland Symposium on Land Subsidence*, ed. J.W. Borchers, Special Publ. No. 8, Association of Engineering Geologists.

Rucker, M.L. and Keaton, J.R., 1998, Tracing an earth fissure using refraction-seismic methods with physical verification, 1998, *Land Subsidence, Case Studies and Current Research, Proceedings of the Joseph F. Poland Symposium on Land Subsidence*, ed. J.W. Borchers, Special Publ. No. 8, Association of Engineering Geologists, pp. 207-216.

Rucker, M.L. and Fergason, K.C., 2004, Role of practical geophysics to investigate and mitigate a distressed flood control dam, presented at Dam Safety 2004, ASDSO 21st Annual Conference held in Phoenix, Arizona, September 26-30, Association of State Dam Safety Officials.

Slaff, S., 1993, Gravity and Magnetic Surveys at Brady Earth Fissure, Picacho Basin, Pinal County, Arizona, Arizona Geological Survey Open-File Rpt. 93-1a, April.

Sternberg, B.K., 2004, Electromagnetic geophysics techniques for location of abandoned underground mines, *5th Biennial Workshop on Interstate Technical Group on Abandoned Underground Mines*, Tucson, Arizona, April 21-23.

Weeks, R.E. and Panda, B.B., 2004, Defining subsidence-induced earth fissure risk at McMicken Dam, presented at Dam Safety 2004, ASDSO 21st Annual Conf. held in Phoenix, Arizona, September 26-30, Association of State Dam Safety Officials.

Wrege, B.M., Hasbrouck, W.F. and Schumann, H.H., 1985, Seismic surface-wave attenuation across earth fissures in the alluvium, south-central Arizona, Surface and Borehole Geophysical Methods in Ground Water Investigations, 2nd National Conference and Exposition, National Water Well Association, p. 121-131.

An Investigation of Factors that Influence the Water Diversion Capacity of Inclined Covers with Capillary Barrier Effects

M. Aubertin[1*], E. Cifuentes[1], V. Martin[1], S. Apithy[1],
B. Bussière[2], J. Molson[1], R. P. Chapuis[1], A. Maqsoud[2]

[1]École Polytechnique de Montréal, Dept. CGM, C.P. 6079, Centre-Ville, Montréal, QC, Canada, H3C-3A7 ; Ph (514) 340-4711 (Ext. 4046) ; FAX (514) 340-4477 ; *email : michel.aubertin@polymtl.ca
[2]Université du Québec en Abitibi-Témiscamingue, 445 boul. de l'Université, Rouyn-Noranda, QC, Rouyn-Noranda, Qc, Canada, J9X 5E4 ; Ph (819) 762-0971 (Ext. 2531) ; FAX (819) 797-4727

Abstract

Covers with capillary barrier effects (CCBEs) can be used as an alternative to more traditional covers that rely on materials with a low saturated hydraulic conductivity. A typical CCBE includes a fine-grained soil layer placed on a coarser material. Other layers can also be added to help the cover play its role(s) efficiently. In a cover built on a flat area, the capillary barrier effect at the interface between the fine and coarse materials allows the finer soil layer to store incoming water, which can later be released by evaporation. Such Store-and-Release covers can be quite convenient in arid and semi-arid conditions. In sloping areas, a CCBE also acts as a lateral water diversion system. Part of this diversion occurs along the sloping interface between the two superimposed soils. It can contribute significantly to the reduction of water percolation deeper into the underlying wastes. However, inclined CCBEs are more complex, as they are influenced by many factors that are not yet fully understood. In such layered covers, moisture is not evenly distributed along the length of the slope. Under some conditions, the moisture-retaining layer can reach a critical degree of saturation at a certain down dip location, which increases infiltration of water into the coarse material and reduces the cover efficiency. This paper presents some of the main results of an ongoing investigation of inclined CCBEs that includes testing on a physical model, field work on large scale covers, and numerical analyses of various cover scenarios. Emphasis is placed here on numerical simulations to assess some of the influence factors that affect the diversion capacity and moisture distribution. The numerical results show how the diversion capacity is affected by the saturated hydraulic conductivity of the fine-grained soil, by the precipitation rate and duration, and by the layer thickness. The findings presented here can be useful for the design of inclined CCBEs.

Introduction

Cover systems typically aim at reducing water infiltration into waste disposal sites. Covers can also serve other purposes, such as controlling surface erosion, preventing bio-

intrusions, and limiting gas emission from wastes (i.e. methane, CO_2, radon) or gas influx from the atmosphere to the reactive materials underneath (i.e. O_2, the case of acid generating tailings and waste rock).

Various materials and configurations are used to design and construct covers. In this regard, an interesting solution, which is still under development, is to make use of capillary barrier effects to control the exchange of fluids (water and gas) at the surface of the waste disposal sites. Such engineered systems, which have been labelled covers with capillary barrier effects (CCBEs) by the authors (e.g. Aubertin et al. 1997a; Bussière et al. 1998), are attracting considerable interest as they may represent an advantageous alternative to more traditional covers that rely on materials having a low saturated hydraulic conductivity. A capillary barrier effect appears under unsaturated conditions when a relatively fine-grained material overlies a coarser one. The contrast in hydraulic properties between the two materials, due to the different grain size and porosity, restricts water flow at the interface. The lower unsaturated hydraulic conductivity k_u of the coarser material, at similar suctions, contributes to this effect by limiting the downward flow of water from the fine-grained material. A more detailed description of unsaturated flow and capillary barrier effects in layered systems can be found in many publications, (e.g. Morel-Seytoux, 1994; Aubertin et al. 1995, 1997a, 1997b; Morris and Stormont, 1997; Bussière et al. 1998, 2000, 2003a, 2003b; see also the corresponding lists of references, not repeated here because of space limitations).

The main advantages of a CCBE lie in its relative simplicity, long-term stability, and potentially lower construction costs compared to more traditional covers (e.g. Morris and Stormont 1997). Such multilayered cover systems have been extensively studied over the last decade or so. The authors' initial investigations focussed mainly on CCBEs in which the water retention layer is designed to act as an oxygen barrier, for applications on acid generating tailings (e.g. Aubertin *et al.* 1995, 1997a). Hindering oxygen from penetrating into the reactive mine wastes is an effective control method that is well suited to relatively humid climates, particularly on flat areas. However, at some sites, such as those with large tailings dykes and waste rock dumps, the geometry makes it difficult to maintain an effective oxygen barrier along the entire sloping area (Bussière *et al.* 2003b). In such cases, it may be necessary to design the cover primarily to minimize water infiltration.

"Store-and-Release" covers (also bearing various other names such as "alternative", "water balance", or "evapotranspirative" covers; e.g. Ogorzalek et al. 2005) can be quite effective for preventing infiltration in arid and semi-arid conditions (e.g. Williams *et al.* 1997). In such a cover built on a flat area, the fine-grained material is able to store water due to its high retention capacity and due to the capillary barrier effect at the interface with the coarse material underneath. This water can later be released by evaporation or evapotranspiration.

Some studies indicate that, when properly designed, the performance of a CCBE can match or even exceed that of a cover with a low saturated hydraulic conductivity (Morris and Stormont 1997), particularly when the layered system is inclined. However, inclined CCBEs are fairly complex systems, which can be influenced by many factors. A sloping CCBE takes advantage of the unsaturated properties of soils to favour lateral drainage during wetting periods, a process that complements the evaporative role associated with upward water flux during dry spells. Such inclined systems, sometimes referred to as Store-Divert-and-Release (SDR) covers, have been shown to work well as a means of diverting water in relatively dry climates (e.g. Zhan *et al.* 2001).

A particular aspect of inclined CCBE behaviour is that moisture is not evenly distributed along the slope length. A higher water content is usually observed at lower elevations along the slope, within the moisture retaining layer. In some cases, the moisture-retaining layer can reach a critical degree of saturation at a certain location along the slope, reducing the capillary barrier efficiency. Infiltration of water into the coarse material then becomes possible as its water entry value (WEV) is reached. The climatic conditions play a very important role on how the cover behaves. Depending on the intensity and duration of the expected precipitation, the cover system might have to manage large amounts of water which can then exceed its diversion capacity (Bussière *et al.* 2003a). In the following section of the paper, the authors briefly recall the main features of inclined CCBEs used to reduce water infiltration. The results presented here are part of a broad investigation on the use of cover systems to control the production of acid mine drainage (Aubertin *et al.* 1995, 1999; Bussière *et al.* 2003b).

Diversion capacity of inclined CCBEs

When a fine-grained soil overlies a coarser material in a relatively dry state (i.e. unsaturated conditions well above the phreatic surface), it retains the infiltrating water by capillary forces. The retention is more pronounced in finer materials, which typically show a higher air entry value (AEV) on the water retention curve (WRC). When placed on a material that desaturates more easily due to a coarser pore structure, the finely textured soil can thus store the infiltrating water. Water storage in the fine material is also favoured because water does not easily move downward into the coarse material underneath, due to its low hydraulic conductivity at a low degree of saturation. The water then accumulates above the interface until the local negative pressure reaches the water entry value WEV (or water entry pressure) of the coarse material. The WEV corresponds, on the WRC, to the suction ψ at which water starts to penetrate the material on a wetting path (provoking an increase in the water content). Once water moves across the interface, it increases the degree of saturation and hydraulic conductivity of the coarse material, hence dissipating the capillary barrier effect. Hysteresis of the hydraulic functions may play a role in this regard, but this issue has been addressed elsewhere and will not be considered here.

The behaviour of a CCBE largely depends on its geometry. The response of horizontal covers is now fairly well understood, but the same cannot be said for inclined (dipping) CCBEs, which show a more complex response under natural conditions. It is known, however, that infiltration at the interface between two soils can be reduced when the contact between the materials is tilted. In this case, the moisture that builds up above the contact tends to flow along the sloping interface. However, when there is a significant inflow of water, the fine soil may become wet enough, and at a certain point downdip, the pressure at the interface may reach the WEV of the coarse-grained material. At this location, water infiltration into the coarse material becomes significant, and the capillary barrier effect progressively disappears. The location of this "point" along the slope (which is actually a zone, as discussed below) is called the Down Dip Limit or DDL point (Ross, 1990). The amount of water flowing laterally down to the DDL point (see breakthrough point in Figure 1) is called the diversion capacity of the CCBE. The distance between the top of the slope and the DDL point is referred to as the effective or diversion length of the capillary barrier (L_d).

A few analytical solutions have been proposed to evaluate the diversion capacity and length of idealised sloping capillary barriers (e.g. Ross, 1990; Morel-Seytoux, 1994; Lu and Likos,

2004). These solutions have typically been developed for steady-state conditions, with a pressure (or suction) that does not depend on the location along the slope (except for the Morel-Seytoux solution). Also, they usually consider the coarse-grained material layer to be infinitely thick, and the phreatic surface to be far from the interface. Some of these analytical solutions have been reviewed and compared by the authors (e.g. Bussière *et al.* 1998, 2000). The analysis showed that existing solutions have a limited applicability in practice, due to their inherent simplifying assumptions. Hence, further investigation was deemed necessary to better define the response of inclined CCBEs used to store, divert and release (SDR) water.
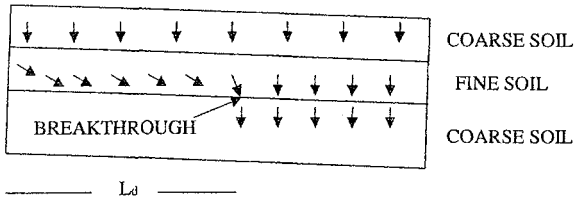
Figure 1. Schematic representation of a layered cover, showing water movement in an inclined CCBE following a precipitation event; water breaks through the coarse grained soil when the suction reaches its WEV (adapted from Bussière et al. 1998, 2000)

Laboratory and field studies

The initial part of this investigation consisted of evaluating, under controlled laboratory conditions, the hydraulic response of layered systems. First, a number of tests were performed in instrumented columns, which were used to validate, under simplified 1D conditions, the main concepts and the modelling tools being used (i.e. Aubertin *et al.* 1995, 1997a). Another series of tests were then performed using a specially developed set-up to look at the diversion length, with different slope angles and precipitation rates. This apparatus is made of an instrumented rectangular box (2.5 m long, 1 m high, and 0.25 m thick), built with a steel frame and Plexiglas walls, in which pressure transducers and TDR probes are installed. The system is also equipped with a rain simulator. To identify the breakthrough location, the base of the box includes holes that collect infiltration along its length. Different variables have been studied with this layered system, such as the amount of precipitation, moisture and pressure distributions, and water flow with local desaturation during drainage. Detailed results have been presented in Bussière *et al.* (1998, 2003b). These showed that the capillary barrier effect along the interface between the two tested materials (i.e. fine sand on coarse gravel) tends to disappear progressively and not at a pin-point location. Pressure measurements during the tests confirmed the observed trends with water flux measurements. The data obtained from these experiments correlated well with unsaturated flow modelling results. The numerical calculations predicted the diversion length more precisely than analytical solutions for these particular inclined capillary barriers. The study also showed that the precipitation rate and inclination angle of the layered system have a large influence on the location of the DDL point (or zone). These laboratory tests were useful to better understand the phenomena involved and to validate the modelling tools (which are used below), but they did not offer the practical solutions necessary for field applications.

The laboratory studies were complemented by field data obtained from instrumented sites. These included experimental test plots to compare various scenarios, and to identify how the

various layered cover systems would behave from a hydrogeological and geochemical standpoint (i.e. Aubertin *et al.* 1999). Because of their geometry, these test plots were mainly relevant for assessing flat cover behaviour. The field work has also included investigations on inclined CCBEs, under semi-arid (Zhan *et al.* 2001) and humid (Bussière *et al.* 2005) climatic conditions. These studies have shown that the actual behaviour of inclined covers was affected by many factors. The field data confirmed the existence of a DDL zone, where the capillary barrier effect is progressively reduced and where the CCBE becomes less effective to limit water infiltration. The field data gathered for these projects have been successfully compared to numerical calculations. The results also highlighted the need for further (and more elaborate) studies to optimise the design of inclined CCBEs for reducing water infiltration. Numerical analysis is a useful means to investigate the various factors that may influence the response of inclined CCBEs.

Numerical analysis of large scale covers

Numerical modelling is a convenient tool to investigate the unsaturated flow behaviour of a CCBE (Aubertin *et al.* 1997a, 1997b, 1999; Bussière *et al.* 2000, 2003a, 2003b). Numerical results complement the information obtained from physical models at the laboratory scale (Aubertin *et al.* 1995, 1997a) and at the field scale (Aubertin *et al.* 1997c). Previous work has shown that it is possible to predict water movement and distribution in horizontal or inclined CCBEs with commonly available unsaturated-saturated numerical codes. The Authors show here some results from a series of numerical analyses, inspired by typical field cases encountered on mine sites. These were performed to investigate the effect of different parameters on the performance of CCBEs used to limit water infiltration. The base case involved the use of a cover, made of a silty soil, installed on a waste rock pile (e.g. Zhan *et al.* 2001). The first objective of the study was to look at the short-term response of the cover following major storms, for different precipitation rates, material properties, and cover configurations. The main program used for these calculations is the commercial finite element model SEEP/W developed by GEO-SLOPE International Ltd. (2002). This code uses Richards' equation to simulate problems in two dimensions, including variably saturated flow for both steady-state and transient conditions. SEEP/W was chosen because it has been successfully used for several unsaturated flow studies on layered systems (e.g. Bussière *et al.* 2003a).

Short- term behaviour

The first model represents a covered circular waste rock dump (under axi-symmetric conditions) having a height of 24.5 m, a base radius of 50 m, and a slope angle of 40° (Apithy 2003). The density of the mesh, which contained more than 3200 elements, was adapted to improve the precision of calculations in critical zones where the gradients were the most pronounced. This model contains three different materials: a homogeneous waste rock that has the properties of a gravel, a thin silty cover material (0.5 or 0.25 m thick, depending on the simulation), and a 6 cm drainage/runoff material layer. The latter is a "virtual" layer that was used for water accumulation and movement at the surface of the cover (as runoff), but it may not exist in reality. In this particular case, the cover is made of only one material since the waste rock can create the necessary capillary barrier effect at the interface with the silty soil (Zhan *et al.* 2001).

A toe drain was simulated by applying a boundary pressure equal to atmospheric pressure at the bottom of the slope (in the cover at $x = 55$ m and $z = 0.5$ m). The water table was placed at the base of the grid ($z = 0.5$ m). The initial pressure head at each node, required for

transient calculations, was obtained from a steady-state analysis using the same model; for the steady-state simulations, a precipitation rate P of 1 mm/day was applied on top of the cover. During the transient analyses, the boundary condition P applied on top of the model ranged from 0.5 to 30 cm/day.

The main hydraulic properties of the different materials used in this numerical investigation are given in Table 2. The waste rock (Material 1) has a low air entry value ψ_a of about 0.5 m of water and a saturated hydraulic conductivity k_{sat} of 10^{-3} cm/s. The residual and saturated volumetric water contents, θ_r and θ_s of this material are respectively 0.06 (for a WEV of 85 kPa, or about 8.5 m of water) and 0.39. Four different silty material properties were used. The difference between the four materials lies in their saturated hydraulic conductivity k_{sat} (see Table 1), which varies from 10^{-3} to 10^{-6} cm/s (Apithy 2003).
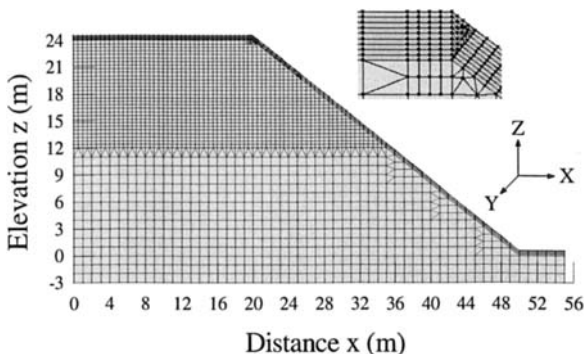
Figure 2 Typical mesh used in the unsaturated flow calculations, with a close-up view of the top part of the slope (adapted from Apithy 2003). The properties of the surface (top) layer, the silt (dark) layer, and the waste rock in the pile are given in Table 1.

Table 1 . Main hydraulic properties of the materials used in the numerical calculations conducted with the model shown in Figure 2 (After Apithy, 2003).

Material	ψ_a (m of water)	θ_s (or n)	k_{sat} (cm/s)	θ_r	WEV (m of water)
Surface	0.5	0.39	1×10^{-3}	0.06	8.5
Silt A	1.5	0.38	1×10^{-3}	0.06	10.0
Silt B	1.5	0.38	1×10^{-4}	0.06	10.0
Silt C	1.5	0.38	1×10^{-5}	0.06	10.0
Silt D	1.5	0.38	1×10^{-6}	0.06	10.0
Waste rock	≈ 0	0.3	1×10^{-0}	0.005	<1

Overall, more than 30 different simulations were performed for this case. Different precipitation rates P were used: 0.5, 1, 2, 5, 10, 20, and 30 cm/day. The precipitation was applied for 5 days and the system was then allowed to drain for 23 days. For each P value, the response of four different cover materials with different k_{sat} values was investigated (see Table 1). Also, for precipitation rates of 10 and 20 cm/day and for a cover material with a k_{sat} of 10^{-4} cm/s, two cover thicknesses were considered: 25 and 50 cm. Some of the main modelling results are shown below. The emphasis of this investigation was placed on

identifying the location (called z_{85}) of the theoretical DDL point in the slope, where the capillary barrier effect begins to disappear. The DDL location was defined as the point where the pressure near the interface became equal to the WEV of the coarse material (i.e. WEV of 8.5 m of water, or about 85 kPa). This large WEV was identified conservatively on the water retention curve of a waste rock that contains a fair amount of fine grained particles. A larger WEV means that there are more possibilities for suction to become lower than this critical value, hence providing a "pessimistic" view of the DDL location and of the cover diversion capacity. The diversion length given here must thus be taken as a lower bound for the problems at hand (see details in Apithy 2003).

The effect of precipitation rate on the location of the DDL point, expressed here as elevation z_{85}, is shown in Figure 3. For these simulations, the cover material was Silt A. For the boundary conditions applied to the model, the z_{85} value varied from 9 to 12.7 m from the base of the pile. The results indicate there is a critical value of P above which the DDL point starts to move from its initial position ($z = 9$ m) towards the top of the slope. In this series of calculations, the critical P value was between 2 and 5 cm/day. For precipitation less than this critical P value, the cover is able to divert water along the slope, up to the maximum length imposed by the position of the water table and by material properties. At higher precipitation rates, the water starts to significantly infiltrate below the cover at (or very near) the DDL point. It was observed that the diversion length tends to diminish as P increases. For relatively large P values (i.e. above approximately 5 cm/day), the system does not reach a steady-state condition after 5 days of precipitation; the diversion length is still decreasing as the DDL point continues to move upward.
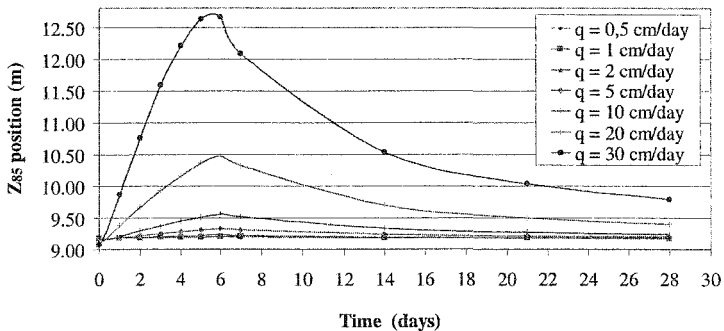
Figure 3. Evolution of the DDL point z location (z_{85}) during the 28 day simulations for different precipitation rates; an increasing z_{85} gives a shorter diversion length (adapted from Apithy, 2003).

Another series of simulations revealed the influence of the saturated hydraulic conductivity (k_{sat}) of the cover material on its ability to limit water infiltration. Four different k_{sat} values were used (see Table 1). The results show that for materials having a k_{sat} less than (or equal to) 10^{-5} cm/s, the position of the DDL point does not appear to vary with precipitation P. However, the diversion length is reduced when the hydraulic conductivity becomes higher than this critical k_{sat} value (of 10^{-5} cm/s). These results have confirmed the expected influence of k_{sat} on the diversion capacity of this type of inclined CCBE. Numerical simulations were also performed with covers having two different thicknesses: 25 and 50 cm. For these simulations, two large P values (of 10 and 20 cm/day) were applied as boundary

conditions; Silt B (Table 1) was used for the cover material. For a P value of 10 cm/day, the z_{85} locations are around 10.2 m and 9.6 m (from the base of the pile) for cover thicknesses of 25 and 50 cm, respectively. When the precipitation rate P is increased from 10 to 20 cm/day, the z_{85} moves upward by about 2 m, for both thicknesses. Shorter diversion lengths are obtained for higher P values, and for lower cover thicknesses. This means that increasing the thickness of the cover can help reduce the water infiltration, which was not an unexpected outcome.

Increasing the diversion length

As part of this study, different cover configurations are being investigated to assess the conditions for which the diversion length would be exceeded by large precipitation events. Means to increase the diversion length are also evaluated. Different configurations have been compared. A schematic representation of one such SDR cover system is shown in Figure 4. The cover shown on the left hand side of Figure 4 is made of 3 layers. The top layer is composed of relatively fine-grained material used to promote run-off and store the infiltrating water. The middle layer made of a coarser material (which creates a capillary barrier effect) also serves as a diverting layer for the water that would percolate through the first layer, and thus would be rapidly drained along the slope. The bottom layer, composed of fine-grained material, serves as another line of protection, being a transition layer between the cover and the coarse-grained material (waste rock) underneath. This additional water retention layer insures that water in the above layers would not easily percolate into the reactive waste, favouring a longer diversion down the sloping system. Many combinations of fine-grained materials (made of crushed waste rock, non reactive tailings, or natural sandy silts) and coarse-grained materials (typically non reactive waste rocks) can be used to create an effective SDR cover of this type.

The modelled case involved a cover composed of 2 m of waste rock sandwiched between two layers of silt (1 m thick); the slope is also 2.5H:1.0V. The geometry of the models represents one bench having a height of 36 m. The slope of the waste rock dump is 2.5H:1.0V (the figure is not to scale). An artificial (virtual) 12.5 cm thick layer of drainage material was again placed on the surface. This material is used to deal with runoff from a precipitation event (which is not taken into account in SEEP/W). It could also represent an erosion barrier placed on the cover; its saturated hydraulic conductivity (k_{sat}) is assumed to be relatively high (1 cm/s). The bottom and left boundaries of the model are assumed to be no-flow boundaries. The model drains from the toe of the dump. Several simulations were made with an applied infiltration function that corresponds to three consecutive 24-hour storms with a return period of 100 years (i.e. intensity of 9.07×10^{-5} cm/s). Similar conditions were used by Zhan *et al.* (2001) to model the efficiency of the cover system placed on the leach pad at Barrick Goldstrike Mines Inc. (Elko, NV). Under the imposed conditions, a mono-layered cover (as above) and a multilayered cover (Fig. 4, left) worked well in limiting the infiltration into the waste rock (results are not shown here because of space limitations). There was no significant water inflow, as the diversion length exceeds the slope length.

The cover response is sensitive to many factors, such as variations in the material properties, slope angle and length, potential evaporation of the area, precipitation duration and intensity (e.g. Bussière *et al.* 2003a). Other calculations were conducted to evaluate how covers would perform under more demanding conditions. For the case shown here (Fig. 4), the AEV and WEV of the main cover material (silt) were reduced by one order of magnitude (for the AEV: from about 1 m to 0.1 m of water; for the WEV, from about 100 m to 10 m); this is comparable to using a sandy soil instead of a silt to create the SDR cover. The precipitation

intensity was also increased by one order of magnitude to a value of 9.07 x 10^{-4} cm/s. Figure 4 (right hand side) shows the distribution of water in the multilayer SDR cover following the 72-hour storm.
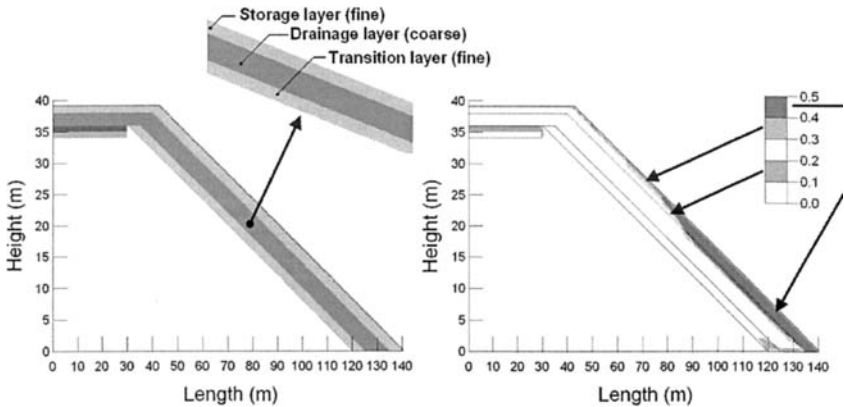
Figure 4. Representation of the waste rock dumps with a multilayer SDR cover (left), with the water content distribution (right) following a 72-hour storm with the alternate cover material and increased precipitation (adapted from Martin 2003, and Martin *et al.* 2005).

With this scenario, it was observed that the water was penetrating below the monolayer cover as its diversion length is exceeded (results not shown here because of space limitation). The DDL of this monolayer cover was located at a height of about 14 metres. In the case of the multilayered cover, Figure 4 shows that water penetrates into the coarse material layer and then flows along the slope. Only a minimal amount of water penetrates into the transition (fine grained) layer at the base of the CCBE. No water infiltrates into the waste rock, even under such an extreme precipitation event. Hence, this alternate configuration would provide an additional protection against infiltration under such extreme precipitation events.

Long-term behaviour

The cases shown above represent situations that may limit the applicability of an inclined CCBE in a relatively dry environment. In such cases, the design of SDR covers is controlled largely by the response following large precipitation events (i.e. intense, but relatively short duration events). On the other hand, when an inclined CCBE is used in a humid climate to prevent water infiltration into the waste, it can be expected that the diversion capacity may also be exceeded due to the annual regime of climatic conditions that exist at the site. Various scenarios of layered cover systems have been analysed for the climatic conditions of western Quebec as input parameters. These climatic data have been used in other modelling calculations (e.g. Fala et al. 2005), to evaluate the response of various disposal and reclamation schemes (not presented herein due to space limitations). The case shown here, which loosely represents an actual mine site, is that of a waste rock pile covered by layered systems upon closure. Again, the authors have looked at the diversion length (among other issues) obtained from the modelling results, for various conditions.

The results shown below pertain to a circular pile with a height of 25 m, and a base diameter of 110 m. In these analyses, the top surface (crest of the dump) is inclined slightly outward, at an angle of about $3°$ (5% slope), while the main external slope has an angle of $37°$ (4.0H:3.0V). The waste rock in the dump is considered homogeneous, and its hydraulic properties have been defined by in situ and laboratory tests at the reference site; the waste rock hydraulic conductivity k_{sat} is 4.3×10^{-4} cm/s, its AEV is about 10 cm of water, and its WEV is about 60 cm of water. The cover is made of a layer of silt (placed on the waste rock) on which a layer of coarse sandy soil is added to control runoff and erosion. The properties of the silt (with a variable layer thickness) and the coarse sand of 1 m thickness are respectively: k_{sat} of 5.0×10^{-5} cm/s and 9.9×10^{-2} cm/s; an AEV of about 200 cm and 10 cm of water; a WEV of 7000 cm and 100 cm of water.
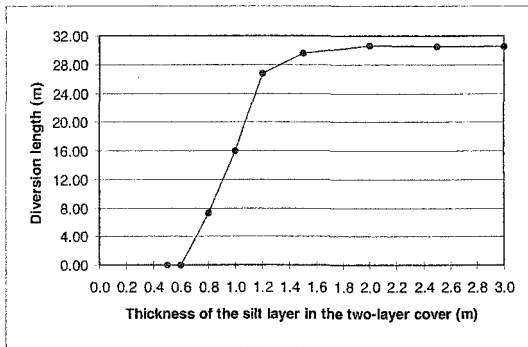
Figure 6 Effect of the silt layer thickness on the diversion length of a sand-on-silt cover placed on the slope of a waste rock pile (adapted from Cifuentes, 2006).

This part of the study aims at evaluating various cover scenarios, and the effect of changing cover characteristics on the diversion length. The investigation also involves an assessment of the means available to maximize the diversion length, in order to prevent infiltration below the cover. The results shown in Figure 6 illustrate some of the main observed trends. The figure shows the effect of the silt layer thickness on the diversion length, based on the results at the end of a one year climatic cycle (i.e. in December, at the onset of winter when infiltration stops due to freezing). This figure shows that a minimum thickness (of about 0.6 m in this case) is required to produce a significant diversion of water along the inclined CCBE. The diversion length then increases with the silt layer thickness until a quasi-plateau is reached; for the situation analysed, the plateau is reached at a thickness of about 1.6 m. Beyond this point, the diversion length is not much influenced by the silt layer thickness. The analyses leading to this figure have also shown that the diversion length evolves over time during the year, being at its minimum at the end of the Fall (when precipitation is high and evaporation is minimal). Many other calculations have been conducted, using different materials, cover configurations, and climatic regimes. The overall results, presented in Cifuentes (2006), indicate that the optimisation of a SDR cover must take into account the above mentioned factors (more detailed results will be presented elsewhere).

Conclusion

Inclined covers with capillary barrier effects (CCBEs) can be used to limit water infiltration. In this regard, the efficiency of the CCBE is mainly assessed using the location of the DDL point (or the effective length of the capillary barrier). This point corresponds approximately to a location where the suction in the coarse grained material, acting as the capillary break, reaches its water entry value WEV at the interface with the water retention layer placed on top of it.

This study focuses on how the diversion length of a CCBE is affected by various factors, such as climatic conditions and rate of precipitation, the properties of the soils used in the cover, and the thickness of the different cover layers. After briefly recalling the physical processes involved in the use of layered systems to create a SDR (Store, Divert, and Release) cover and considering the previous results obtained from physical models in the laboratory and from instrumented field sites, the authors have presented some key results from numerical modelling investigations. The cases shown here mainly relate to covers installed on waste rock piles. The results indicate that an inclined CCBE can efficiently divert water along the interface between coarse and fine-grained soils. The maximum diversion length corresponds to the DDL point. At this location, the fine-grained soil is sufficiently wet that the pressure applied to the coarse-grained soil reaches its WEV; water ingress then becomes possible. The disappearance of capillary barrier effects at the DDL location is gradual and does not occur at a pin-point location as postulated by analytical solutions. As expected, the precipitation rate and slope angle of the layered system affect the diversion capacity of an inclined capillary barrier. A critical precipitation rate P exists, above which the diversion capacity of a given inclined CCBE is reduced; beyond that, the DDL point moves upward along the slope with an increasing P value. The saturated hydraulic conductivity k_{sat} of the cover material is another critical factor affecting the diversion capacity of an inclined CCBE. Decreasing k_{sat} increases the effective length of the SDR cover. Results shown here also indicate that increasing the thickness of the cover may help to reduce the infiltration of water.

This study illustrates why it is essential to evaluate the position of the DDL point, at critical precipitation rates, when designing efficient CCBEs for diverting water. To do so, 2-D transient modelling can be quite useful to ensure that the DDL location will not be along the cover area, even under critical climatic conditions. This is required to prevent water infiltration into the wastes.

Acknowledgments

References

Apithy, S.A. (2003). *Étude du comportement de couvertures à effets de barrière capillaire placées sur des haldes à stériles en climat semi-aride*. MASc. Thesis, Ecole Polytechnique de Montréal.
Aubertin, M. Bussière, B. Monzon, M. Joanes, A.M., Gagnon, D. Barbera, J.M., Aachib, M. Bédard, C. Chapuis, R.P., Bernier, L. (1999). *Étude sur les barrières sèches construites à partir de résidus miniers* : Phase II Essais en place. MEND Report 2.22.2c. .

Aubertin, M., Aachib, M., Monzon, M., Joanes, A-M., Bussiere, B. and Chapuis, R.P. (1997a). *Étude de laboratoire sur l'efficacité des barrières de recouvrement.* MEND Report 2.22.2b.

Aubertin, M., Chapuis, R.P., Bouchentouf, A. and Bussière, B. (1997b). *Unsaturated flow modeling of inclined layers for the analysis of covers.* Proc. of the 4th ICARD, Vancouver, B.C., 2 : 731-746.

Aubertin, M., Chapuis, R.P., Aachib, M., Bussière, B., Ricard, J.-F. and Tremblay, L. (1995). *Évaluation en laboratoire de barrières sèches,* MEND Report 2.22.2a.

Bussière B., Maqsoud A., Aubertin M., Martschuk J., McMullen J., Julien M. (2005) *Cover performance at the LTA site, Malartic, QC, CAN.* CIM Bulletin (March 2005)

Bussière, B., Apithy, S., Aubertin, M. and Chapuis, R.P. (2003a). *Diversion capacity of sloping covers with capillary barrier effect.* Proc. 56th Ann. Canadian Geotechnical Conf., Winnipeg, 9 p. [CD-ROM].

Bussière, B., Aubertin, M. and Chapuis, R.P. (2003b). *The behaviour of inclined covers used as oxygen barriers. Canadian Geotechnical Journal,* 40 : 512-535.

Bussière, B., Aubertin, M., Chapuis, R.P. (2000). *An investigation of slope effects on the efficiency of capillary barriers to control AMD.* Proc. 5th ICARD, Denver, Colorado, USA

Bussière, B., Aubertin, M., Morel-Seytoux, H.J. and Chapuis, R.P. (1998). *A laboratory investigation of slope influence on the behaviour of capillary barriers.* Proc. 51st Canadian Geotechnical Conference, Edmonton, 2 : 831-836.

Cifuentes, E. (2006). *Modélisation numérique des écoulements non saturés dans des couvertures à effets de barrière capillaire inclinées.* Master Report, École Polytechnique de Montréal.

Fala, O., Molson, J.W., Aubertin, M., Bussière, B. (2005) *Numerical modelling of flow and capillary barrier effects in unsaturated waste rock piles.* Mine Water & the Environment (in press).

GEO-SLOPE International Ltd. (2002). *SEEP/W for finite element seepage analysis, User's guide,* Version 5. GEO-SLOPE Int. Ltd. Calgary, Alberta, Canada, p.549

Lu, N. and Likos, W.J. (2004) Unsaturated Soil Mechanics, John Wiley and Sons.

Martin, V., Aubertin, M., Zhan, J. Bussière, B. and Chapuis, R.P. (2005). *An Investigation into the Hydrological Behaviour of Exposed and Covered Waste Rock Dumps.* Proc. SME Annual Meeting. Salt Lake City, [CD-ROM].

Martin, V. (2003). *Étude des propriétés non saturées des stériles miniers.* MASc. Thesis, Ecole Polytechnique de Montréal.

Morel-Seytoux, H.J. 1994. *Steady-state effectiveness of a capillary barrier on a sloping interface.* 14th Hydrology Days, Ed. Hubert J. Morel-Seytoux, Hydrology Days Publications, 335-346.

Morris, C.E. and Stormont, J.C. (1997). *Capillary barriers and Subtitle D covers: estimating equivalency.* Journal of Environmental Engineering, 123: 3-10.

Ogorzalek, A.S., Shackelford, C.D. and Benson C.H. (2005). *Comparison of model predictions and field data for an alternative cover in a semi-arid climate.* Mines and the Environment, CIM.[CD].

Ross, B. (1990). *The diversion capacity of capillary barriers.* Water Resour. Res., 26 : 2625-2629.

Williams, D.J., Wilson, G.W. and Currey, N.A. (1997). *A cover system for a potentially acid forming waste rock dump in a dry climate.* Tailings and Mine Waste 97, 231-235. Balkema.

Zhan, G., Aubertin, M. Mayer, A., Burke, K. and McMullen, J. (2001). *Capillary cover design for leach pad closure,* SME Transaction 2001, 1: 104-110.

Design and Installation of Zero-Tension Lysimeters in an Inclined Cover

By S-É. Parent[1], A. Cabral[2], G. Gras[3] and F. Marinho[4]

[1] Ph.D. Candidate, Dept. Civil Eng., Université de Sherbrooke, Quebec, Canada; PH (819) 821-8000 2235; FAX (819) 821-7974; email: s-e.parent@usherbrooke.ca
[2] Professor, Dept. Civil Eng., Université de Sherbrooke, Quebec, Canada;
PH (819) 821-7906; FAX (819) 821-7974; email: alexandre.cabral@usherbrooke.ca
[3] Formerly Undergraduate Research Assistant, Université de Sherbrooke; email: supgael.gras@wanadoo.fr
[4] Associate Professor, Escola Politécnica, Universidade de São Paulo, SP, Brazil; PH +55 11 3091-5703; FAX +55 11 3091-5181; email: fmarinho@usp.br

Abstract

The infiltration component of the water budget in a soil cover layer is difficult to measure under field conditions. Often, zero-tension (or pan) lysimeters are used for that purpose. Although they are relatively cheap and easy to build, as well as easy to install, their design may be more complex than one thinks. Indeed, the design depends on the unsaturated properties of the soil in which it is installed, in particular the hydraulic conductivity function. The latter is often derived from the water retention curve and the limitations inherent in this process may lead to errors, resulting in the lysimeter being dysfunctional. The walls of a zero-tension lysimeter must be high enough to permit the development of a pressure greater than atmospheric at the base of the container, from where the infiltrated water drains. Using theoretical and numerical approaches, and considering construction constraints (in terms of layer thicknesses), this paper presents a procedure to determine the height of zero-tension lysimeters that were installed in a 300 m² experimental cover (a double capillary barrier constituted of a layer of deinking by-products, sand and gravel) placed above a municipal solid waste facility. Numerical simulations were used to evaluate lysimeter performance.

Introduction

Lysimeters, which are widely used to monitor infiltration through cover systems, consist of a container that is buried within the soil mass. The water that is collected often drains out of the container through a pipe by gravity. Depending on the design, the installation of a lysimeter will modify the pore-pressure distribution within the cover, a perturbation that leads to measurement errors, usually underestimations of the quantity of infiltrating water.

There are two major difficulties in the design of lysimeters. First, due to the variability in climatic conditions, infiltration rates can vary over several orders of magnitude. Second, the design depends highly on the unsaturated properties of the porous material in which the container is buried (and that also fills it), namely the water retention curve (WRC) and the hydraulic conductivity function (*k*-function). Both curves may be difficult to obtain and are subject to heterogeneities.

The design procedure described in this paper has been applied for the design of two sets of zero-tension lysimeters that were installed on an experimental inclined capillary barrier, constructed in July 2005 at the Saint-Tite-des-Caps municipal landfill facility, Quebec, Canada. The goal of the lysimeters is to monitor infiltration through a layer of deinking by-products (DBP) that was employed as alternative construction material. As the first step in the design procedure, the unsaturated properties of the cover materials involved were determined. The procedure was validated using numerical simulations to evaluate lysimeter performance.

Background and Theory

There are several types of lysimeters. The most common types are zero-tension lysimeters, wick lysimeters and ceramic cup lysimeters. Fine reviews of lysimeter types, including pros and cons of each type, can be found in Brye et al. (1999), Zhu et al. (2002) and Gee et al. (2004). In this study, zero-tension lysimeters were selected for their simplicity to build and to install.

Zero-tension lysimeters

The zero-tension lysimeter is a container placed at the desired depth within the cover system that captures infiltrating water. The bottom of the container is connected to a pipe that diverts water to a collection device at atmospheric pressure.

Collection efficiencies of less than 10% have been noted for zero-tension lysimeters (Zhu et al. 2002) due to flow bypass. In order to avoid flow bypass, Bews et al. (1997) proposed high-wall lysimeters. The purpose is to meet the two following conditions. First, the pore water pressure at the base of the lysimeter must be greater than or equal to atmospheric pressure. If the pore water at the base of the lysimeter is not at atmospheric pressure, water is retained in the soil, causing the flow to bypass the container. Second, the pore pressure at the top of the container must be equal to the pore pressure outside of the container. In order to achieve the second condition, use of coarser materials (i.e. coarser than the soil surrounding the lysimeter) to fill the lysimeter is to be avoided. Indeed, use of a coarser material causes the infiltrating water to be diverted away from the container due to the creation of a capillary barrier, i.e. a lower unsaturated hydraulic conductivity into the lysimeter than outside (Chiu and Shackelford 2000).

The suction profile is key to the understanding the flow into zero-tension lysimeters. As a first step to explain how the suction profile develops in a capillary barrier, a soil column is examined (Figure 1). At hydrostatic conditions above the water table, with no flow crossing the capillary barrier, the pressure head decreases linearly (at 45°) with increasing height and the total head is null. If a steady-state vertical infiltration rate is imposed to a sufficiently thick medium, the pressure head profile breaks away from the 45° line to become constant with height. Above this height z_c (Figure 1), the hydraulic gradient is equal to unity and the vertical flow (or infiltration rate, q) is equal to the unsaturated hydraulic conductivity.
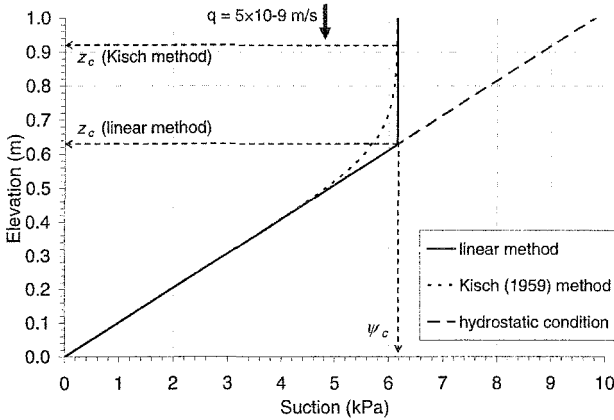
Figure 1. Suction profile developed into a sand column submitted to a steady-state flow

The variation of suction with height can be predicted using the linear (Bews et al. 1997) or the Kisch (1959) method. The linear method consists in the determination of the maximum suction value existing in a porous material submitted to an infiltration rate under a unit gradient. This suction value can be determined graphically using the k-function. For example, as shown in Figure 2, for an infiltration rate, q, of 5×10^{-9} m/s, the maximum suction for the sand is slightly greater than 6 kPa, which is equivalent to a 0.6-m high column of water, i.e. $z_c = 0.6$ m.
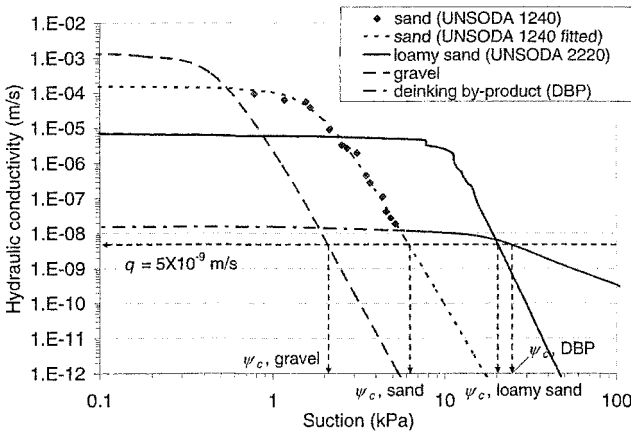
Figure 2. Hydraulic conductivity functions of the materials used in this study, with linear method.

The linear method does not model the asymptotic behavior that is observed at elevations below z_c, when suctions converge towards z_c (Akindunni et al. 1991). Alternatively, the Kisch (1959) model can be used to determine suction profiles with more precision (Figure 1). The use of the linear model will always give lower z_c's (Parent and Cabral 2005).

Materials and Methods

The instrumented cover consists of an inclined double capillary barrier, as shown in Figure 3. Two sets of lysimeters were installed to monitor infiltrations along the slope; one set placed in the gravel layer and the other placed in the overlying sand layer. The unsaturated properties of the loamy sand, sand, and gravel had to be estimated from their grain-size distributions, shown in **Figure 4** (Section 3.1). The infiltration rate was determined using the widely known HELP model, Hydrologic Evaluation of Landfill Performance (Schroeder et al. 1994). The finite element software SEEP/W (Geo-Slope 2004) was also used.
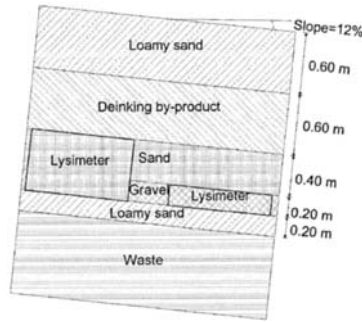
Figure 3. Profile of the experimental capillary barrier built at the Saint-Tite landfill
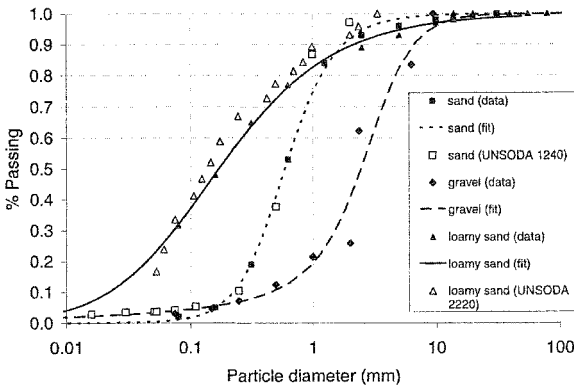
Figure 4. Particle-size distributions of loamy sand, sand, and gravel

Determination of the unsaturated properties of the materials

The hydraulic conductivity function of the deinking by-products was determined using the water retention curve. The latter was measured using a special apparatus that allows monitoring of volume changes during the test (Cabral et al. 2004).

The unsaturated properties of the sand, the gravel and the loamy sand were derived from their particle-size distribution shown in **Figure 4**. Equivalent particle-size distributions to the ones obtained for the loamy sand (soil 2220) and the sand (soil 1240) were found in the UNSODA database (**Figure 4**). Water retention data for soils 2220 and 1240 were retrofitted using the Fredlund and Xing (1994) functions to describe the WRC, while the van Genuchten (1980) model was used describe the k-function. The saturated hydraulic conductivity and the porosity of the loamy sand and the sand were estimated using the neural network in the RETC code (van Genuchten et al. 1991). The WRCs and k-functions obtained are presented in **Figure 5** and **Figure 2**, respectively.

In order to estimate the WRC of the gravel, the modified Kovacs model (Aubertin et al. 2003) was applied (**Figure 5**). To predict the saturated hydraulic conductivity (k_{sat}), the equation proposed by Chapuis (2004) for sands and gravels was used. The k-function was estimated with the van Genuchten (1980) model (**Figure 2**).
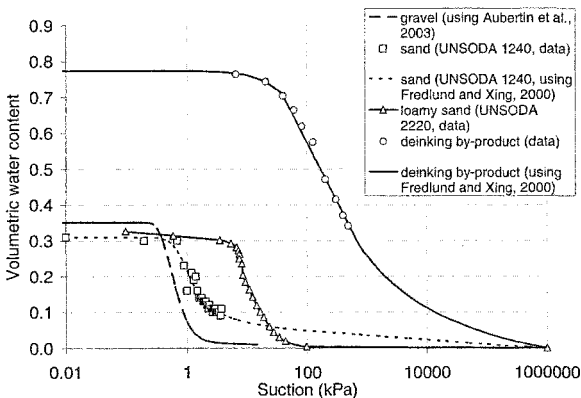
Figure 5. Water retention curves of gravel, sand and loamy sand.

Determination of the percolation rate

In order to determine the lysimeter heights as explained above, a representative percolation rate must be obtained. A simulation was performed using the HELP model to estimate the potential infiltrations through the DBP layer for the cover system shown in **Figure 3**. Climatic data for Montreal/Dorval were used. The average percolation over five years is presented in **Figure 6**.

If the design flow rate is set to $q = 5 \times 10^{-9}$ m/s, the lysimeter should be able to recuperate at least 85% of the total infiltration reaching the base of the DBP layer. If the design had imposed a 100% recuperation rate, lysimeters would need to be designed to collect flows as low as 2×10^{-12} m/s, requiring 1.5-m walls, i.e. walls higher than the entire cover system.
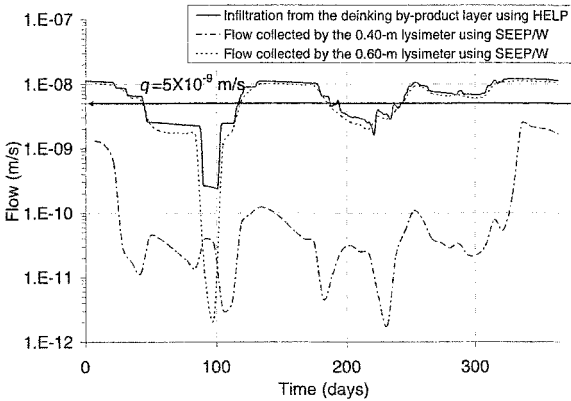
Figure 6. HELP and VADOSE/W simulations: percolation with time through the deinking by-product layer.

Lysimeter Design

Heights of the walls

Based on the linear method and adopting an infiltration rate of 5×10^{-9} m/s, the values of z_c for the sand and the gravel are, respectively, 0.60 m (6.2 kPa) and 0.20 m (2 kPa) (**Figure 2**). Since the sand in the capillary barrier was not thick enough to accommodate containers with the above mentioned heights, the lysimeter had to be extended into the underlying layer, i.e. into the gravel.

It is relevant to remind that the goal of the lysimeters placed in the loamy sand and the sand is to monitor infiltrations through the DBP layer. Lysimeters were not installed in the DBP layer because a 2.25-m height container would be needed.

Numerical simulations

Only the results of numerical simulations to evaluate the performance of the lysimeter installed in the sand layer forming the capillary barrier are presented. The weekly inflow obtained from the HELP simulation was eventually used as the top boundary condition in all subsequent simulations of the performance of the lysimeters using SEEP/W. The top boundary condition coincides with the top of the sand layer. The lower boundary condition was set as a water table (pressure=0), placed at a significant depth into the waste mass. The inside bottom boundary of the

lysimeter was set to no flux source with possible boundary review, i.e. pressure can not reach positive values (drain condition). Indeed, a water table, instead of the boundary review, led to a source of water that eventually drained out of the lysimeter. Two lysimeter heights were simulated. First, a container of 0.40 m-high, corresponding to the thickness of the sand layer, was simulated. Second, a simulation with a container of 0.60 m-high was performed, corresponding to the height prescribed by the design procedure.

The variations of the collected flow at the bottom of the 0.40-m and the 0.60-m lysimeters with time for a one-year simulation are shown in Figure 6. The curve representing the collected flow for the 0.40-m lysimeter is far lower than the applied flow rate, while the collected flow for the 0.60-m lysimeter nearly coincides with the one representing the applied flow rate. The differential can be calculated by subtracting the collected flow from the infiltration rate, and by multiplying the difference by time (a year). An error of 5.85 m over 6.11 m, or 94% is thus obtained for the 0.40-m lysimeter. As for the 0.60-m lysimeter, an error of 0.13 m over 6.11 m, or 2 %, is obtained. In the latter case, this error is associated with lower infiltration rates than that adopted. The error shows the major importance for accurate wall-heights design. For example, Figure 7a and b presents the results of the simulation in terms of flow vectors for a particularly dry week, for the 0.40-m lysimeter and the 0.60-m lysimeter respectively. For both cases, some water diverges away from the lysimeter due to a pressure gradient. As discussed above, the lysimeter whose height was determined based on the design infiltration rate (0.60 m) should function properly most of the time. Indeed, the vertical vectors at the entrance of the 0.60-m lysimeter (Figure 7d) indicate that, for a typical period, practically no water by-passes the lysimeter, which is not the case for the 0.40-m lysimeter (Figure 7c).

Conclusions

A zero-tension lysimeter design procedure was applied for the design of a set of lysimeters installed in the 300 m^2 experimental capillary barrier cover at the Saint-Tite-des-Caps municipal landfill. The design parameter of concern was the wall heights. If there are properly determined, the introduction of a lysimeter should not cause any disturbance in terms of pressure gradients in the porous material in which the container is buried (and that fills it); otherwise, infiltrating waters by-pass the lysimeter. In addition, an appropriate height would ensure that the pressure at the base of the lysimeter is equal to zero, allowing water to be drained out.

For a suction profile associated with a hypothetical soil column submitted to a specific infiltration rate, the height of the walls of a fully functional lysimeter corresponds to the vertical distance from the water table to the elevation where suction no longer varies with elevation. In order to determine the suction profile within the experimental cover, the infiltration rate had to be determined and the hydraulic conductivity functions of the materials had to be obtained. The infiltration rate was determined using the HELP model.

A numerical simulation using SEEP/W was performed to evaluate the performance of the lysimeters installed in the sand layer. The design of the capillary barrier limited the thickness of this layer to 0.4 m, whereas the required lysimeter wall height was found to be 0.6 m. As a consequence, the lysimeters had to be extended beyond the sand/gravel interface. It was decided not to install lysimeters in the DBP layer because the required height for the lysimeters would be 2.25 m, which exceeds the total thickness of the cover system.
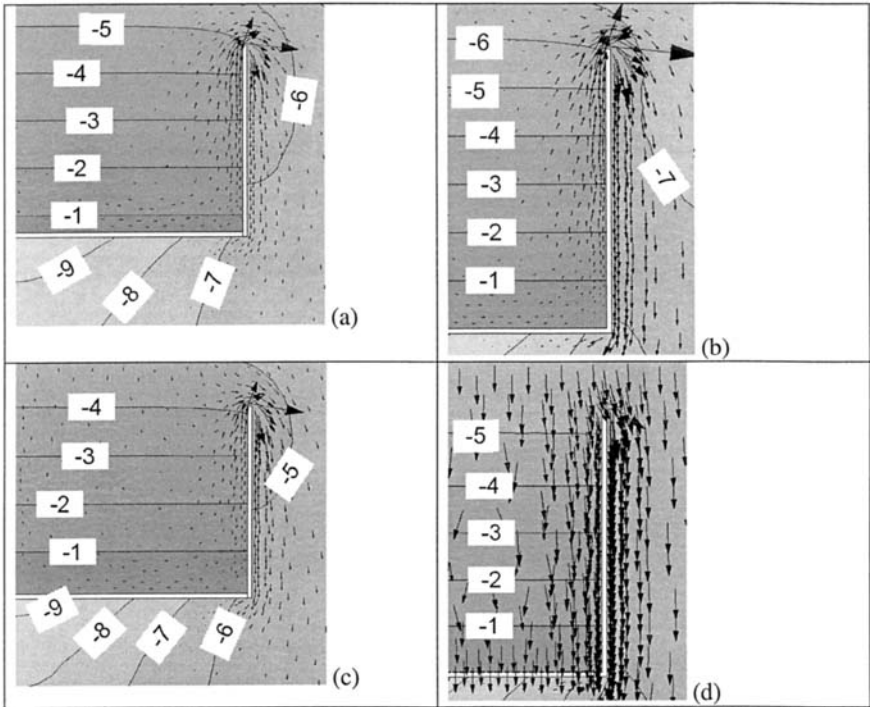
Figure 7. Cross sections showing flow vectors and iso-pressure (kPa) contours: (a) 0.40-m lysimeter in particularly dry week; (b) 0.60-m lysimeter in particularly dry week; (c) 0.40-m lysimeter in typical conditions (85% of the time); (d) 0.60-m lysimeter in typical conditions (85% of the time)

The numerical simulation showed that, for the infiltration rate applied, it can be expected that the lysimeter will be functional, with the exception – perhaps – of the driest month. Moreover, if lower wall heights were prescribed, a significant amount of water would by-pass the lysimeter, distorting the actual water infiltration that reaches the sand layer.

References
Akindunni, F. F., Gillham, R. W., and Nicholson, R. V. (1991). "Numercial

simulations to investigate moisture-retention characteristics in the design of oxygen-limiting covers for reactive mine tailings." *Canandian Geotechnical Journal*, 28, 446-451.

Aubertin, M., Mbonimpa, M., Bussiere, B. R., and Chapuis, R. (2003). "A model to predict the water retention curve from basic geotechnical properties." *Canadian Geotechnical Journal*, 40(6), 1104-1122.

Bews, B. E., O'Kane, M., Wilson, G. W., and Williams, D. "The design of a low flux cover system, including lysimeters, for acid generating waste rock in semi-arid environments." *Fourth International Conference on Acid Rock Drainage*, Vancouver, B.C., 747-762.

Brye, K. R., Norman, J. M., Bundy, L. G., and Gower, S. T. (1999). "An equilibrium tension lysimeter for measuring drainage through soil." *Soil Science Society of America Journal*, 63(3), 536-543.

Cabral, A. R., Planchet, L., F.A., M., and Lefebvre, G. (2004). "Determination of the soil water characteristic curve of highly compressible materials: Case study of pulp and paper by-product." *Geotechnical Testing Journal*, 27(2), 154-162.

Chapuis, R. P. (2004). "Predicting the saturated hydraulic conductivity of sand and gravel using effective diameter and void ratio." *Canadian Geotechnical Journal*, 41(5), 787-795.

Chiu, T. F., and Shackelford, C. D. (2000). "Laboratory Evaluation of Sand Underdrains." *Journal of Geotechnical and Geoenvironmental Engineering*, 126(11), 990-1001.

Fredlund, D. G., and Xing, A. Q. (1994). "Equations for the Soil-Water Characteristic Curve." *Canadian Geotechnical Journal*, 31(4), 521-532.

Gee, G. W., Zhang, Z. F., Ward, A. L., and Keller, J. M. "Passive-wick water fluxmeters: theory and practice." *SuperSoil 2004, third Australian New Zealand Soils Conference*, University of Sydney, Australia.

Geo-Slope. (2004). *SEEP/W User's Manual*.

Kisch, M. (1959). "The theory of seepage from clay-blanketed reservoirs." *Géotechnique*, 9, 9-21.

Parent, S.-E., and Cabral, A. R. (2005). "(Accepted) Design of Inclined Covers with Capillary Barrier Effect." *Geotechnical and Geological Engineering Journal*.

Schroeder, P. R., Dozier, T. S., Zappi, P. A., McEnroe, B. M., Sjostrom, J. W., and Peyton, R. L. (1994). "Hydrologic Evaluation of Landfill Performance (HELP) Model: Engineering Documentation for Version 3." Army Engineer Waterways Experiment Station, Vicksburg, MS.

van Genuchten, M. T. (1980). "A closed-form equation for predicting the hydraulic conductivity of unsaturated soils." *Soil Science Society of America Journal*, 44, 892-898.

van Genuchten, M. T., Leij, F. J., and Yates, S. R. (1991). "The RETC code for quantifying the hydraulic functions of unsaturated soils." *EPA/600/2-91/065*, U.S. Department of Agriculture, Agriculture Research Service.

Zhu, Y., Fox, R. H., and Toth, J. D. (2002). "Leachate collection efficiency of zero-tension pan and passive capillary fiberglass wick lysimeters." *Soil science of America journal*, 66.

Unsaturated Flow Flux Assessment for Evapotranspirative Cover Compliance

Edward Kavazanjian, Jr.[1], Beth Ann Gross[2], and Tarik Hadj-Hamou[3]

[1]Department of Civil and Environmental Engineering, Arizona State University, Tempe, Arizona, 85287-5306, PH (480) 727-8566, FAX (480) 965-0566, email: edkavy@asu.edu
[2]GeoSyntec Consultants, 3600 Bee Caves Road, Suite 101, Austin, Texas, 78746, PH (512) 451-4003, FAX (512) 306-8042, email: bgross@geosyntec.com
[3]GeoSyntec Consultants, 2100 Main Street, Huntington Beach, California, 92648, PH (714) 969-0800, FAX (714) 969-0820, email: thadj-hamou@geosyntec.com

Abstract

Assessment of liquid (soil water) flux under unsaturated flow conditions is an important factor in permitting and design of evapotranspirative final cover systems (ET covers) for landfills. Unsaturated flow flux assessments are employed to demonstrate regulatory compliance for permitting of ET covers, to develop construction specifications for approved ET covers, and to establish performance criteria for monitoring of constructed ET covers. Ideally, unsaturated flow flux assessments for ET covers should be based upon site-specific data and should be made using boundary conditions and soil profiles as close as possible to prototype conditions. In practice unsaturated flow flux assessments for ET cover performance have typically been based upon either direct flux measurements from lysimeter test sections or unsaturated flow modeling. The unsaturated flow model may often be calibrated using either percolation and run-off data from lysimeter test pads or internal soil moisture content data from the as-built cover. Lysimeter test pad data are adversely impacted by unrealistic lysimeter boundary conditions, difficulties in accurately measuring small values of percolation, and the inability of unsaturated flow models to accurately predict runoff, while flux values predicted using models calibrated solely upon internal soil moisture content data are of questionable reliability. Therefore, choice of the appropriate approach with which to demonstrate regulatory compliance is often a question of "the lesser of two evils." However, consideration of the limitations of these two approaches suggests that for municipal solid waste landfills in arid and semi-arid climates the use of internal soil moisture measurements from a prototype cover in situ may be preferable for both regulatory compliance evaluation and design of ET covers due to a more accurate simulation of prototype conditions as well as other practical engineering considerations.

Introduction

Evaluation of liquid (soil water) flux through an unsaturated soil layer is an important consideration in several aspects of geoenvironmental engineering, including permitting and design of evapotranspirative alternative final cover systems for solid waste landfills. Unsaturated flow evaluations are employed to demonstrate regulatory compliance for permitting of proposed ET covers, to develop construction specifications for approved ET covers, and to establish performance criteria for monitoring of constructed ET covers. Unsaturated flow evaluations for ET cover compliance and design purposes are generally conducted in one of two ways: either through direct monitoring of a large-scale lysimeter test sections (Benson et al., 2001) or through unsaturated flow modeling. When an unsaturated flow model is employed, it is often calibrated using either lysimeter test pad data or internal moisture content measurements in the as-built cover (Hadj-Hamou and Kavazanjian, 2003). Ideally, an ET cover performance evaluation should employ prototype soils, prototype boundary conditions, and direct measurements of unsaturated flow. While lysimeter test sections and internal moisture content measurements can both employ prototype soils, each of these sources of data for ET cover flux evaluation are subject to significant drawbacks. The lysimeter induces changes in the boundary conditions at the base of the cover. Flux cannot be directly measured using internal measurements of soil moisture content. Therefore, the selection of the preferred method is often considered to be a matter of personal preference. However, field monitoring of moisture content profiles indicates that for municipal solid waste landfills the changes in the boundary condition at the base of the cover are potentially of great significance, as the base of the lysimeter cuts off heat and moisture flow from the landfill below which in some cases can dramatically change the unsaturated flow regime. Furthermore, while the flux calculated from internal soil moisture measurements may not be reliable in an absolute sense, regulatory compliance demonstrations and cover design often only require consideration of the relative flux between different cover configurations. Taking into account that in situ moisture content measurement is significantly easier and cheaper than lysimeter test pad construction and monitoring, internal moisture content measurements of the as-constructed cover may well be preferable to lysimeter tests sections for regulatory compliance evaluation of ET covers.

Evapotranspirative Final Cover Systems

Final cover systems functions for landfills include control of percolation of surface water into the waste, control of gas emissions from waste, isolation of the waste from the environment, and prevention of disease vectors and other nuisances. Final cover systems generally must also meet aesthetic and site end-use criteria. Final cover systems are often intended to fulfill these functional requirements for periods of from several decades to hundreds or even thousands of years with minimal maintenance. A final cover containing a low permeability soil barrier is the "prescriptive" minimum standard for municipal solid waste (MSW) landfills the United States (USA) in accordance with Title 40, Section 258 of the *Code of Federal Regulations* (the USA "Subtitle D" landfill regulations). However, due to concern

with the degradation of compacted low permeability soil barriers, the use of alternative ET cover systems is becoming increasingly popular at semi-arid and arid sites. Figure 1 illustrates a typical "low permeability" barrier type of final cover system for a MSW landfill, while Figure 2 shows an alternative ET cover. While concerns with the degradation of low permeability soil barriers include differential settlement, frost heave, and root penetration, the use of ET covers at semi-arid and arid sites is driven to a large extent by concern over desiccation cracking of the low permeability soil barrier (Kavazanjian, 2001).
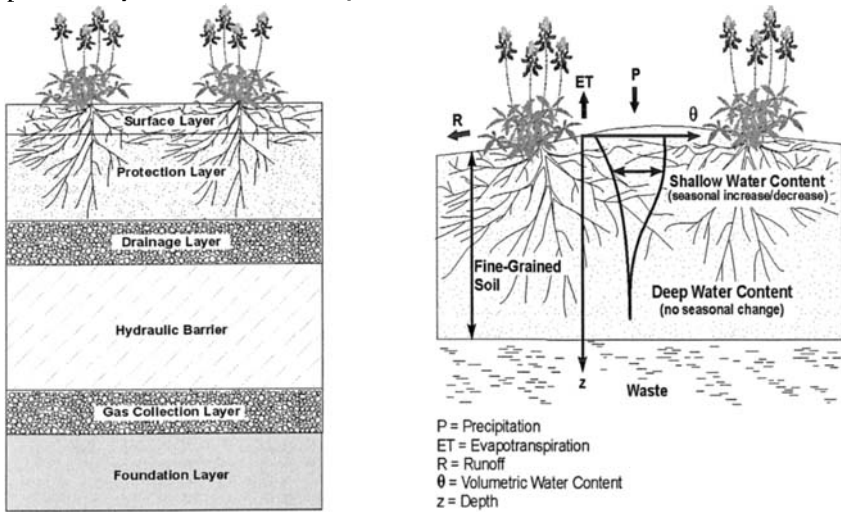
Figure 1 Low Permeability Barrier Final Cover

Figure 2 Evapotranspirative Final Cover

ET covers control percolation through storage of infiltrating surface water during periods of precipitation and subsequent release of the stored water through evaporation and transpiration. An ET cover typically consists of a thick layer of relatively fine-grained soil, such as silty sand or sandy clay, that is capable of supporting vegetation. The water storage capacity of the fine-grained soil allows the ET cover to store a significant amount of water by surface tension and capillary action until it can be removed by evapotranspiration. The relatively low hydraulic conductivity of the fine-grained soils, even at high degrees of saturation, limits advancement of the wetting front during seasonal wet periods (rainfall or snow melt). Because they are constructed drier and generally with less compactive effort than compacted clay low permeability barriers, ET covers are less prone to desiccation cracking than compacted clay barriers. Furthermore, water that infiltrates into cracks in an ET cover may still be drawn into the cover by soil suction and ultimately released by transpiration without percolating through the cover.

In order to employ an alternative final cover system such as an ET cover, USA regulations generally require a demonstration of "hydraulic equivalence" or

"equivalent protection to groundwater" for the ET cover. These requirements are generally interpreted as requiring a demonstration that percolation (liquid flux) through the ET cover will be less than or equal to the percolation through a prescriptive final cover with a low permeability barrier. However, little guidance is provided on how these performance demonstrations should be made.

One approach to demonstrating the hydraulic equivalence of an ET cover is to construct side-by-side lysimeter test sections using both the ET cover and a prescriptive low permeability barrier cover and then measure percolation through the prescriptive and alternative final covers directly. While this lysimeter test section approach is intuitively satisfying, it is subject to a variety of limitations. Figure 3 shows a typical lysimeter cross section. Lysimeter conditions that may not be representative of prototype conditions include the cutting off of the heat and moisture flow from landfill below, reinforcement provided by geosynthetic materials that inhibit cracking of the test section, and the "capillary break" provided by the liquid collection layer at the base of the lysimeter. In addition to these limitations, even if monitored for as much as five years, test sections may not capture extreme climate conditions or the long-term performance of a cover expected to function for decades. Furthermore, test sections are expensive and cannot be constructed at every site that employs an alternative final cover and test section performance is not readily extrapolated to other cover configurations even at the same site with the same soils.
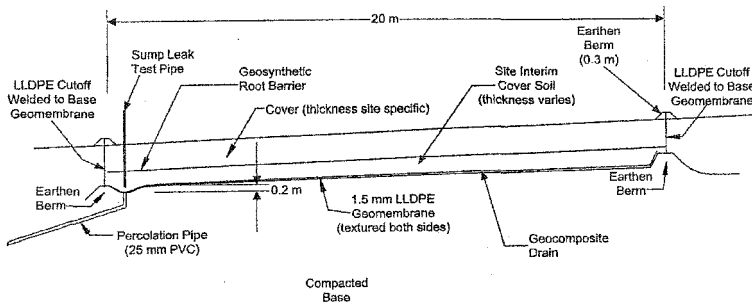
Figure 3 Lysimeter Test Section (Benson et al., 2001)

ET Cover Performance Modeling

ET Cover Water Balance Modeling. Unsaturated flow models for performance evaluation of ET covers are typically referred to as water balance models. The water balance for a cover system can be expressed as follows:

$$D = P - R - \Delta W_{surface} - \Delta W_{plants} - \Delta W_{soil} - ET - L \qquad (1)$$

where D = vertical drainage (percolation) from the cover system, P = precipitation (rain, snow, irrigation), R = runoff, $\Delta W_{surface}$ = change in water storage on the soil

surface, ΔW_{plants} = change in water storage in plant leaves, stems, and litter (interception), ΔW_{soil} = change in water storage in the soil, ET = evapotranspiration, and L = lateral drainage. Equation 1 assumes no contributions to water balance from surface water run-on, lateral groundwater flow, freezing of water, or condensation from the vapor phase (e.g. landfill gas). Considering only the mass balance of above-ground water and assuming no evaporation during precipitation, Equation 1 becomes:

$$I = P - R - \Delta W_{soil} - \Delta W_{plants} \qquad (2)$$

where I = infiltration and the other variables are as defined previously. Considering only the mass balance of the subsurface water, we can then write that:

$$D = I - ET - \Delta W_{soil} - L \qquad (3)$$

Except for the few models that consider interception (surface storage) by vegetation and frozen water, the water balance models used in engineering practice employ some form of Equations 2 and 3 to evaluate the water balance and employ an unsaturated flow model to compute I, ΔW_{soil}, and L.

Accuracy of Water Balance Models. Though Equations 2 and 3 appear simple, the components of these water balance equations are difficult to quantify. It can be especially difficult to quantify drainage (percolation) in arid and semi-arid environments because evapotranspiration is limited by water availability, i.e. in drier climates actual evapotranspiration is generally much less than potential evapotranspiration due to the lack of available water. Because the magnitude of drainage in drier climates is so much smaller than that of precipitation and evapotranspiration, relatively small errors in evapotranspiration (i.e. errors due to water availability-limitations) can result in relatively large errors in estimated drainage. In addition to the evaluation of drainage when evapotranspiration is water limited, a number of other factors affect the accuracy of water balance analyses. These factors, discussed briefly below, are described in detail by Gross (2005) and summarized in Table 1.

In evaluating the mass balance of water at the soil surface (Equation 2), it is generally assumed that there is no evaporation during precipitation. Furthermore, the models typically do not allow infiltration and evapotranspiration to occur at the same time, unless they treat evaporation and transpiration as sink terms. When using meteorological forcing (climatic conditions) to model the upper boundary of the flow field, the boundary varies from prescribed-flux to prescribed-head based on the condition at the boundary. These boundary conditions cannot be simulated simultaneously, though they are sometimes accounted for simultaneously during rainfall by applying a reduced precipitation rate at the upper boundary.

Water balance models employ a number of different constitutive relationships to describe the soil-water characteristic curve (SWCC) and the unsaturated hydraulic conductivity function of soils. The functions most commonly used to characterize

SWCCs in water balance models, the Brooks and Corey (1964) and van Genuchten (1980) functions, often give poor results when they are extrapolated to low matric potentials e.g., potentials somewhat lower than -150 m (-1500 kPa), as water retention in this range is controlled more by adsorption theory than capillary theory. However, some of the less common water balance models do use water retention functions that incorporate adsorption theory at low matric potentials.

Table 1

Processes and Parameters that Affect Water Balance Analyses (after Gross, 2005)

Processes that may not be Considered in a Water Balance Model
Precipitation intensity
Evaporation during precipitation
Interception
Effect of surface slope on runoff
Freeze and thaw of cover system surface
Snow accumulation and melt
Formation of a surface crust
Lateral flow in a sloping cover system
Preferential flow
Hysteresis in SWCC and hydraulic conductivity functions
Change in soil hydraulic conductivity over time
Temperature effect on hydraulic conductivity
Empirical methods used to evaluate transpiration
Multiple plant species
Plant growth dynamics
Isothermal and thermal vapor flow
Thermal water flow
Processes and Parameters Difficult to Assess or Infrequently Measured
Precipitation intensity
Field SWCC and hydraulic conductivity functions
SWCC and hydraulic conductivity function at high matric potentials
Plant parameters (leaf area index, root depth)
Initial conditions (representative matric potential or water content)

The hydraulic conductivity functions most commonly used in water balance models are based upon the theoretical pore size distribution models of Mualem (1976) or Burdine (1953). Pore-size distribution models for unsaturated hydraulic conductivity are based on capillary bundles and become less accurate as the soil dries and adsorption forces, rather than capillary forces, dominate. Stephens (1992) has suggested that values of soil unsaturated hydraulic conductivity at matric potentials less than -10 m (-100 kPa) should be measured rather than calculated. Accurately measuring unsaturated hydraulic conductivity, however, is difficult. At the Hanford Site, unsaturated hydraulic conductivity determined by five different methods varied

by more than three orders of magnitude (Gee et al., 2002). In addition to difficulties with assessing the SWCC and hydraulic conductivity function of a soil when it is initially placed, natural dynamics act to change these properties over time. Most of the models currently available to evaluate the performance of ET covers do not include these evolutionary processes.

The SWCC relationship is hysteretic. Hysteresis affects all of the water balance components that involve the movement of water through soil (infiltration, evapotranspiration, redistribution, and drainage). However, hysteresis is currently only included in a few water balance models. Most of the commonly used computer models for water balance are one dimensional and do not consider the effect of either surface slope on runoff or lateral drainage. Furthermore, most models typically treat runoff as equal to the amount of precipitation in excess of that stored on the surface, lost to evaporation, or infiltrated into the soil and ignore interception of runoff.

The methods used to predict potential evapotranspiration vary widely and sometimes erratically in their performance (Allen et al., 1998). Most methods used to predict evapotranspiration assume isothermal conditions and energy-limiting conditions. In semi-arid and arid climates, where water availability limits evapotranspiration, excess energy is transferred to the soil and atmosphere as sensible heat, creating a thermal gradient for water flow in both liquid and vapor phases. Thermal flux of water may also affect drainage for municipal solid waste landfills. The relatively high temperatures (due to waste decomposition) in these landfills relative to ambient temperature can generate thermal vapor fluxes out of the landfill. These thermally-induced flows are generally not considered in water balance analyses. Though evaporation can occur under matric potential and temperature gradients, most water balance models only consider vapor density gradients under isothermal conditions.

Plants are very important to the performance of an ET cover system. Important plant parameters include root depth and wilting point. Most published data on root depths are for crops in tilled soils or natural plant communities in uncompacted soils and may not accurately represent the root depth of compacted soils. The wilting point is often assumed, by convention, to occur at a matric potential of approximately -150 m (-1500 kPa). However, it is actually plant specific and lower values have been reported for vegetation in semiarid and arid climates.

Calibration of ET Cover Performance Models

Model Calibration. Given the variety of factors influencing unsaturated flow models used to assess ET cover performance, calibration of these models is an important element of their application in practice. Calibration, defined as the process of adjusting model soil and vegetation parameters to give the best possible agreement between predicted and observed performance, ideally should employ a field data set with boundary conditions (e.g. meteorological forcing data, bottom boundary head/gradient/flow) and a soil profile representative of prototype conditions. Ideally, model calibration should be based upon both internal soil state variables (e.g. soil water content, bottom drainage boundary conditions) and dependent variables (e.g.

runoff, soil water storage, percolation through the cover) and "good" agreement should be achieved among both sets of variables. However, complete sets of internal and external variables are rarely available, particularly for prototype ET covers where measurement of percolation (vertical drainage) is essentially impossible without altering the boundary conditions unless the cover has a capillary break or drainage layer in it. Furthermore, when a complete data set is available, it is often difficult to achieve "good" agreement with both internal and external variables using the same set of soil properties. In such cases, the engineer must decide which parameters he will base his calibration on, i.e. which parameters are most important to his application. Both internal moisture content and dependent variables (e.g. runoff and percolation) have been used in practice for model calibration.

Calibration Using Runoff, Storage, and Percolation. Roesler et al. (2002) describe calibration of ET cover performance models using runoff and percolation collected from large pan lysimeters like the one in Figure 3. Figure 4 shows runoff, storage, evapotranspiration, and precipitation for two unsaturated flow models (HELP and UNSAT-H) calibrated using data collected at a site in Albany, Georgia for the United States Environmental Protection Agency Alternative Cover Assessment Program (ACAP) (Roesler et al., 2002). The advantage of this approach is that percolation, often the parameter of primary interest with respect to the hydraulic performance of the cover, is directly measured by the lysimeter and the model is calibrated using measured percolation values. Problems with this approach include difficulty in obtaining simultaneous agreement among all dependent variables, as illustrated by Figure 4. Another problem is that in many cases measured percolation values may be very small, often less than precision of measuring devices. In the extreme case no percolation may be measured, as in the first years of monitoring the ET cover for the Altamont site in the San Francisco Bay area (Roesler at al., 2002). Furthermore, due to the interdependence of percolation and runoff on a variety of different processes, the "best-fit" solution may be non-unique: different combination of vegetative and soil properties may yield similar percolation and runoff values.

A further concern with using percolation and runoff data for calibration is that there has not been good agreement between simulated and measured runoff at ET cover sites. While some researchers have reported underestimation of runoff for ET cover models (Scanlon et al., 2002), other researchers have reported the opposite (Roesler et al., 2002). The lack of agreement between calculated and measured runoff has been attributed to uncertainties in hydraulic conductivity and antecedent moisture content of the surface soil and the effects of precipitation intensity, surface slope, interception of precipitation by plants, and frozen ground and snowmelt (Khire et al., 1999). Inaccuracies due to the hydraulic conductivity of the surface layer and precipitation intensity may be particularly important at arid and semi-arid sites. Scanlon et al. (2002) suggest that to accurately simulate runoff, water balance models may need to be calibrated by modifying the hydraulic conductivity of the soil at the surface of a cover system. Gross (2005) showed that if the precipitation intensity assumed for the simulations is significantly greater than the representative precipitation intensity for a site, runoff may be over-predicted and drainage may be under-predicted.
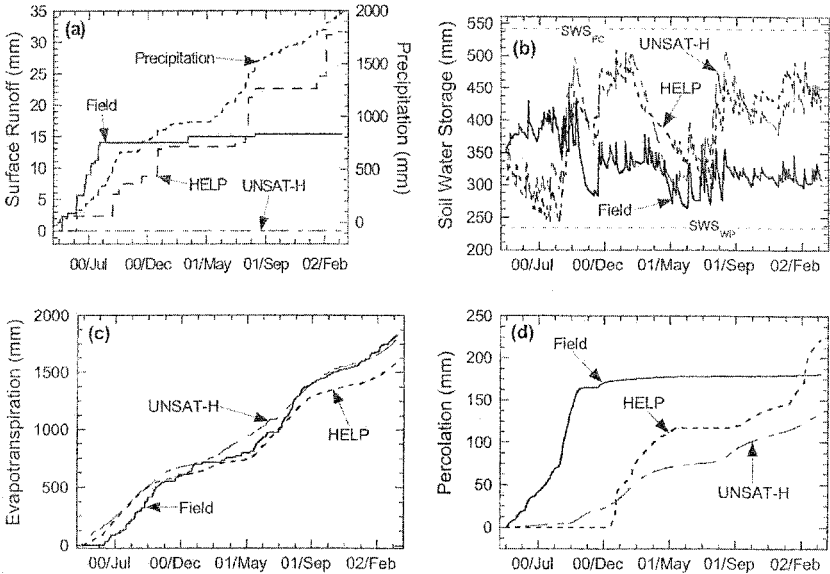
Figure 4 Model Calibration Using Runoff, Storage, Evaporation and Percolation for the Albany, Georgia ACAP Site (Roesler et al., 2002)

The use of lysimeter data to evaluate ET cover performance also suffers from the aforementioned difference in bottom boundary conditions between the lysimeters and the prototype. Most importantly, the lysimeter cuts off heat and moisture flow from below at MSW landfill sites. The geomembrane at the base of the lysimeter also inhibits cracking and the formation of macro-permeability zones within the cover and the lysimeter collection system introduces a capillary break into the cover. Thus, extrapolation of the results from a lysimeter to a prototype cover is suspect.

Calibration Using Soil Moisture Measurements. Hadj-Hamou and Kavazanjian (2003) describe calibration of an ET cover performance model using data from time domain reflectometry (TDR) monitoring devices placed within an as-built cover. The TDR measuring devices were installed at various depths within the soil after cover construction and monitored over time. Figure 5 shows the comparison between observed and predicted moisture content for the second and third year of monitoring at the City of Los Angeles Lopez Canyon Landfill at a depth 0.15 m using UNSAT-H calibrated with data collected during the first year of monitoring. The advantage of this approach is that it monitors the actual field performance of the prototype. The primary disadvantage of this approach is that it does not directly measure percolation. It is possible to create a model that accurately predicts soil moisture content changes but inaccurately predicts percolation due to compensating errors in the SWCC and unsaturated hydraulic conductivity relationships. Furthermore, this approach does not consider "macro-permeability" due to cracks, root penetration, and other discontinuities and non-homogeneities in the cover in the calculated percolation.
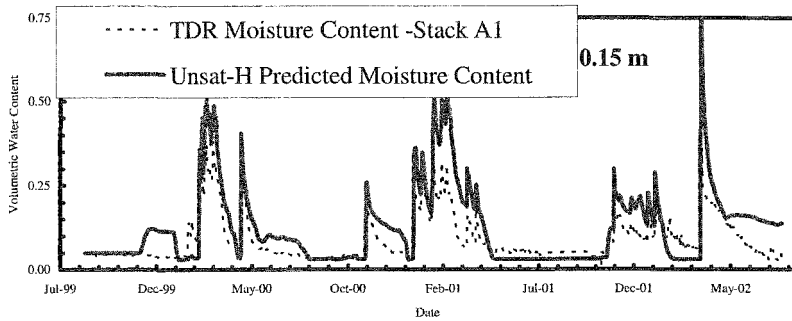
Figure 5 Measurement and Prediction of Soil Moisture Content at a Depth of 0.15 m, Lopez Canyon Landfill, Los Angeles, CA (Hadj-Hamou and Kavazanjian, 2003)

While the absence of direct percolation measurement is a shortcoming of calibration using soil moisture measurements, proponents of this approach maintain that a model that accurately predicts soil moisture content change to varying meteorological boundary conditions should reliably predict soil storage and flux.

Calibration using internal soil moisture measurements is also susceptible to inaccuracies in measurement of soil moisture content. Gross (2005) discusses sources of inaccuracy in soil moisture content measurement. One source of inaccuracy particularly important with TDR measurements is drift in the transducers. Figure 6 presents TDR moisture content versus depth profiles at the Lopez Canyon landfill over a period of 27 months. Laboratory measurements on samples recovered from depths of 0.6 m to 0.7 m adjacent to the TDR probes indicated that the increase in moisture content shown by the TDR readings at this depth is in fact drift of the transducers and that below a depth of 0.6 to 0.7 m soil moisture content for the subject site is unaffected by seasonal climate changes. This knowledge alone may often be sufficient for regulatory approval. Furthermore, the decrease in moisture content from approximately 0.7 m to 0.5 m below grade within the relatively homogeneous ET cover indicates an upward gradient and upward flux in the cover. This effect is likely due in large part to the heat and moisture flux from waste decomposition in the landfill below and will not captured in a lysimeter test section.

Conclusions

ET cover performance may be evaluated using lysimeter test sections or unsaturated flow models. The unsaturated flow models are often calibrated using either runoff and percolation data from a lysimeter or soil moisture measurements made in the cover in situ. Because lysimeters cut off the heat and moisture flux from below, the use of lysimeter test sections for ET cover evaluation for MSW landfills is suspect. Use of lysimeter runoff and percolation data for model calibration is limited by the inability of most models to accurately predict runoff and by difficulties in measuring percolation accurately, particularly in arid and semi-arid climates where evapotranspiration is water limited and the percolation values are very small.
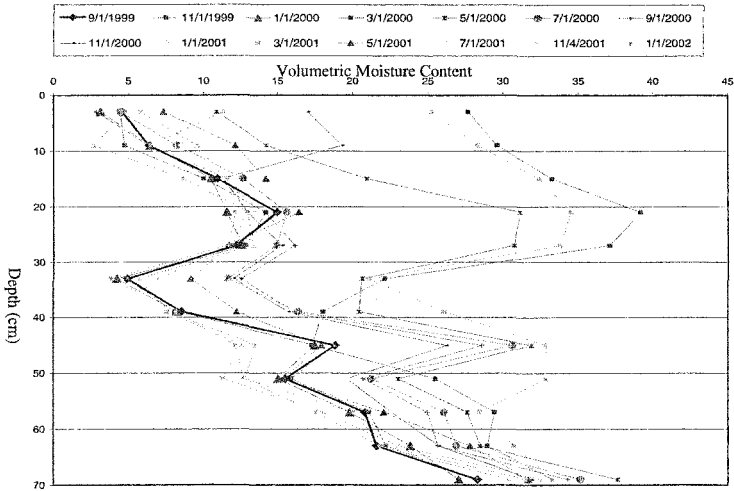
Figure 6 Moisture Content versus Depth, Lopez Canyon Landfill, Los Angeles

A primary advantage of calibration using soil moisture contents is that it can be conducted using data from the prototype cover and therefore can account for heat and moisture flux from below. The accuracy of percolation calculated using this method is questionable due to concerns over the non-uniqueness of the solution, measurement accuracy, and the influence of cracks and other macro-features on flux. However, for regulatory compliance the relevant question is often the relative flux through an ET cover compared to a prescriptive cover system with a low permeability soil barrier. A model calibrated using internal soil moisture measurements subject to variable meteorological conditions at the surface should give reliable estimates of the relative flux for different "intact" cover configurations subject to the same boundary conditions and the additional flux due to high permeability zones in the cover will be less for an ET cover than for prescriptive cover with a low permeability soil barrier. Furthermore, soil moisture content measurements alone may be sufficient for regulatory compliance if they can demonstrate an upward gradient within the cover or that the bottom of the cover is isolated from seasonal moisture fluctuations, as shown by the data in Figure 6. These considerations suggest that carefully obtained soil moisture content measurements within a prototype landfill cover section in situ should be the preferred approach for both regulatory compliance (e.g. comparing prescriptive and alternative soil covers) and design (e.g. evaluating the necessary cover thickness to minimize climate effects on percolation) of ET covers for MSW landfills in arid and semi-arid climates.

References

Allen, R.G., Pereira, L.S., Raes, D., and Smith, M. (1998). "*Crop Evaporation Guidelines for Computing Crop Water Requirements,*" FAO Irrigation and

Drainage Paper No. 56, 2nd ed., Food and Agricultural Organization of the United Nations, Rome, Italy.

Benson, C., Abichou, T., Albright, W., Gee, G., and Roesler, A. (2001). "Field Evaluation of Alternative Earthern Final Covers," *International Journal of Phytoremediation*, Vol. 3, No. 1,

Brooks, R.H. and Corey, A.T. (1964). *"Hydraulic Properties of Porous Media,"* Hydrology Paper No. 3, Colorado State University, Ft. Collins, CO, 27 p.

Burdine, N.T. (1953). "Relative Permeability Calculations from Pore-Size Distribution Data," *Petroleum Transactions*, American Institute of Mining, Metallurgical, and Petroleum Engineers, Vol. 198.

Gee, G.W., Ward, A.L., and Wittreich, C.D. (2002) *"The Hanford Site 1000-Year Cap Design Test,"* PNNL-14143, Pacific Northwest National Laboratory, Richland, Washington.

Gross, B.A. (2005) "Water Balance Evaluations for Monitored Evapotranspirative Cover Systems at Three Sites in the Semi-Arid and Arid Southwest U.S.," dissertation, U. Texas, Austin, Texas

Hadj-Hamou, T. and Kavazanjian, E. Jr., (2003) "Monitoring and Evaluation of Evapotranspirative Cover Performance," Proceedings of Sardinia '03 - 9th International Waste Management and Landfill Symposium, Environmental Sanitary Engineering Centre (CISA), University of Padua, Italy (on CD ROM).

Kavazanjian, E., Jr. (2001), "Design and Performance of Evapotranspirative Cover Systems for Arid Region Landfills," Proc., *36th Annual Engineering Geology and Geotechnical Engineering Symposium*, U. Nevada, Las Vegas, NV

Khire, M.V., Benson, C.H., and Bosscher, P.J. (1999). "Field Data from a Capillary Barrier and Model Predictions with UNSAT-H," *Journal of Geotechnical and Geoenvironmental Engineering*, Vol. 125, No. 6.

Mualem, Y. (1976). "A New Model for Predicting the Hydraulic Conductivity of Unsaturated Porous Media," *Water Resources Research*, Vol. 12, No. 3.

Roesler, A.C., Benson, C.H., and Albright, W.H. (2002). *"Field Hydrology and Model Predictions for Final Covers in the Alternative Assessment Program - 2002,"* Geo Engineering Report No. 02-08, Geo Engineering Program, University of Wisconsin-Madison, WI..

Scanlon, B.R., Christman, M.C., Reedy, R.C., Porro, I., Simunek, J., and Flerchinger, G.N. (2002). "Intercode Comparisons for Simulating Water Balance of Surficial Sediments in Semiarid Regions," *Water Resources Research*, Vol. 38, No. 12.

Stephens, D.B. (1992). "A Comparison of Calculated and Measured Unsaturated Hydraulic Conductivity of Two Uniform Soils in New Mexico", *Proceedings of the International Workshop on Indirect Methods for Estimating the Hydraulic Properties of Unsaturated Soils*, M.Th. van Genuchten, F.J. Leij, and L.J. Lund (eds), University of California at Riverside, Riverside, CA.

van Genuchten, R. (1980). "Closed-Form Equation for Predicting the Hydraulic Conductivity of Unsaturated Soils," *Soil Science Society of America Journal*, Vol. 44, No. 5.

Numerical Modeling of Artificial Soil as an Evapotranspirative Cover

A. Wayllace[1] and W. J. Likos[2]

[1]University of Missouri – Columbia, Department of Civil and Environmental Engineering, Columbia, MO, 65211; PH (573) 882-6269; FAX (573) 882-4784; email: awr39@mizzou.edu
[2]University of Missouri – Columbia, Department of Civil and Environmental Engineering, Columbia, MO, 65211; PH (573) 882-3345; FAX (573) 882-4784; email: likosw@missouri.edu

Abstract

An "artificial soil" created from industrial and municipal by-products is evaluated as an evapotranspirative (ET) cover via finite-difference based seepage modeling. Wetting front propagation is simulated under a series of long-term (sustained) and short-term (intense) precipitation events and compared with actual infiltration data obtained from an instrumented test section over a natural 24-day precipitation/evaporation sequence in Northeast Missouri. The predicted depth of the wetting front is 250 cm, which compares reasonably well with moisture data obtained from the field site and is less than the total thickness of the cover (425 cm). Complete breakthrough of the wetting front is predicted not to occur if cumulative precipitation remains less than 16 cm, which is equivalent to an event slightly larger than the 25-year 24-hour storm for Northeast Missouri (14.6 cm). Results indicate that the artificial soil acts as an effective ET cover system by restricting wetting front propagation and causing water to either evaporate or flow laterally. Design charts are developed that may be used to assist in making decisions regarding proposed modifications to the design of the cover system.

Introduction

Artificial soils engineered by blending industrial and municipal by-products (e.g., bio-solids, fly ash, blast furnace slag, cement kiln dust) have received increasing attention in recent years as a sustainable land reclamation and beneficial reuse strategy (e.g., Reynolds et al., 1999; Cox and Whelan, 2000; Chu et al., 2005). Evapotranspirative (ET) cover systems have also received considerable attention as

potential alternatives to conventional "resistive" barrier systems for waste containment applications, particularly in arid and semi-arid regions (e.g., Dwyer, 1998; Zornberg et al., 2003; Nyhan, 2005).

An innovative application using an artificial soil as an ET cover system was implemented for full-scale field evaluation in 2002 by a cement manufacturing plant in Hannibal Missouri. Municipal yard waste (e.g., grass clippings, wood chips) and bio-solids are blended and placed as an organic-rich O-horizon approximately 1.5-m-thick (5 ft) over a mineral-rich C-horizon approximately 3-m-thick (10 ft) and consisting of blended coal ash and cement kiln dust (CKD). As illustrated in Figure 1, the O- and C-horizons form a stratified sequence that simulates a natural residual soil column (i.e., mineral-rich at depth and organics-rich near the surface). This "artificial soil" layer is placed over an underlying CKD base and then seeded with native grass and tree species to begin the biological processes associated with naturally occurring Missouri soils. The system is intended to be an evapotranspirative barrier that limits percolation into the underlying CKD by storing and subsequently removing water under natural evaporation and transpiration processes. By July 2005, more than 90,000 tons (US) of artificial soil were placed and more than four acres of land have been reclaimed (Table 1).

This paper describes a numerical modeling effort conducted to assess the general effectiveness and behavior of artificial soil as an evapotranspirative barrier to fluid flow. A numerical seepage model is used to simulate infiltration through the layered system under a variety of long-term (sustained) and short-term (intense) precipitation events. Results from the simulations are compared with in-situ infiltration data obtained from an instrumented full-scale test section constructed at the Hannibal site. Finally, a series of design charts is developed that may be used to assist in making decisions regarding proposed modifications to the current design of the artificial soil profile.
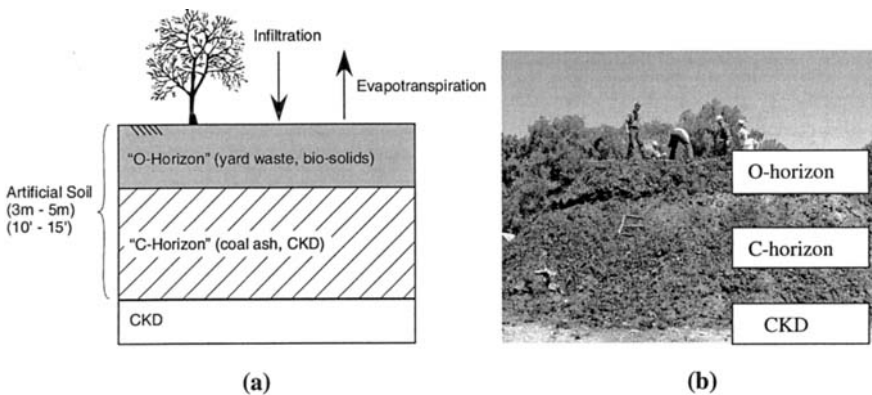
Figure 1. (a) Schematic of artificial soil profile; (b) photo of field test section.

Table 1. Summary of materials placed as artificial soil through July 2005.

Material	Source	Approx. US Tons Placed
Cement Kiln Dust	Continental Cement Company	32,000
Yard Waste	Cities of Quincy, IL, Hannibal, MO Paris, MO, Springfield, IL	28,000
Bio-solids	Metro Sewer District: Hannibal, MO St. Louis, MO.	20,000
Power Plant (Coal) Ash	University of Missouri – Columbia	14,000

Numerical Model

VS2D. Seepage modeling was conducted using the USGS finite-difference based code VS2DI described by Lappala et al (1987) and Healy (1990). VS2DI is a graphically-based software package that solves the Richards' equation for unsaturated fluid flow in one or two dimensions using either Cartesian or radial coordinate systems. Constitutive relations between suction head, water content, and hydraulic conductivity may be represented by the functions developed by van Genuchten, Brooks and Corey, Haverkamp et al., or by tabulation (see Lu and Likos, 2004). Initial conditions may be specified as static equilibrium above a specified water table (field capacity), specified pressure head, or specified moisture content. Boundary conditions include specified pressure or total head, specified flux, infiltration with ponding, evaporation, transpiration, and possible seepage faces. Seepage faces are boundaries along which liquid may leave the system and along which the total potential is equal to the elevation potential.

Modeling Domain and Material Properties. The modeling domain (Figure 2) was designed to simulate a full-scale test section constructed previously in the field at the Hannibal site (Figure 1b). The field test section was instrumented with moisture sensors, temperature sensors, lysimeters, and a surface weather station to quantify the rate and depth of moisture infiltration under natural precipitation events (Bobba et al., 2005). The section was monitored for one year to observe infiltration behavior over a full range of environmental extremes.

The 1000 cm × 600 cm modeling domain was sized to simulate the layered O-Horizon, C-Horizon, and CKD profile having layer depths of 125 cm, 300 cm, and 175 cm respectively (Figure 2). Boundary conditions were divided into six segments, three segments on top, two at the sides, and one at the bottom. Although the field test section was only about 500-cm wide, the model was selected with a width of 1000 cm to minimize end-effects on the sides of the system. Precipitation/evaporation fluxes were applied only to the top-middle segment, which has the width of the actual test section (500 cm). Observation points were embedded into the modeling mesh along the centerline below the top-middle boundary at depths corresponding approximately

to the locations of volumetric moisture content sensors installed in the field test section (at $z = 19, 59, 125, 228$, and 445 cm).
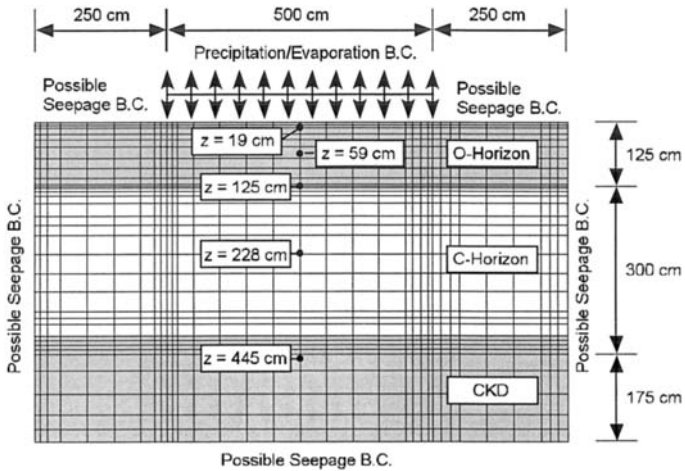
Figure 2. Schematic diagram of VS2D modeling domain.

Three textural classes were defined to model the three materials comprising the layered artificial soil system. Laboratory tests were conducted using representative samples of the O-Horizon, C-Horizon, and CKD materials to quantify relevant engineering properties, including moisture-density relationships, specific gravity, saturated hydraulic conductivity (k_{sat}), field capacity (θ_{fc}), and soil-water characteristic curves (SWCC). Material properties required by VS2DI include porosity (n), horizontal and vertical saturated hydraulic conductivities (k_x and k_z), and modeling constants (fitting parameters) that define the SWCC. General material properties and parameters selected for the modeling simulations are summarized in Table 2. Figure 3 shows SWCCs for the O-Horizon and C-Horizon materials determined using modified Tempe Cells (modified for large representative specimen sizes). Samples for these tests were reconstituted by compacting them close to in-situ densities measured in the field test section using a sand-cone apparatus (Table 2). SWCCs were modeled using the Brooks and Corey (1964) model:

$$\theta = \begin{cases} \theta_s & h < h_b \\ \theta_r + (\theta_s - \theta_r)\left(\dfrac{h_b}{h}\right)^{\lambda} & h \geq h_b \end{cases} \tag{1}$$

where θ_r is residual water content, θ_s is saturated water content ($\theta_s = n$), h is matric suction head (cm), h_b is the bubbling (air entry) head, and λ is a fitting parameter.

Table 2. Summary of material and modeling parameters.

Property	Units	O-Horizon	C-Horizon	CKD
Field cap., θ_{fc}	m³/m³	0.15	0.17	ND
In-situ moist.	m³/m³	0.21	0.20	0.26
Spec. grav., G_s	---	1.71	2.12	ND
In-situ Dens, γ	kN/m³ (pcf)	4.9 (31)	7.1 (45)	7.1 (45)
dry dens, γ_d	kN/m³ (pcf)	2.5 (16)	5.0 (32)	4.9 (31)
Proctor dens.	kN/m³ (pcf)	5.3 (34)	10.8 (69)	ND
Porosity, n	---	0.90	0.80	0.43
k_{sat}	cm/s	7×10^{-3}	8.5×10^{-3}	2.6×10^{-4}
@ dry dens.	kN/m³ (pcf)	2.6 (16.5)	6.1 (39)	ND
k_z/k_x	---	1.0	1.0	1.0
AE head, h_b	cm	4.00	0.95	100
RMC, θ_r	m³/m³	0.10	0.13	0.17
Brooks-Corey λ	---	1.50	0.80	2.00
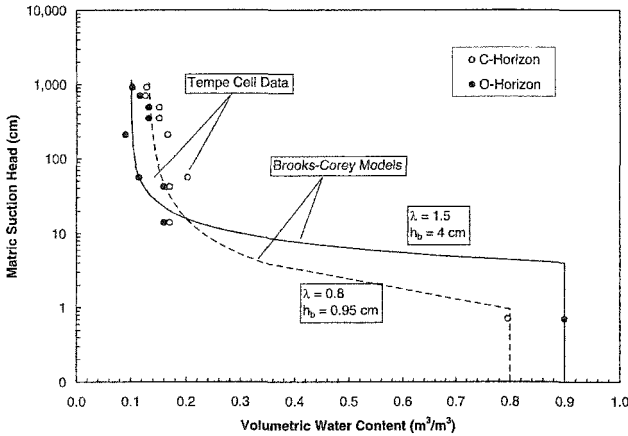
Figure 3. SWCCs and Brooks-Corey models for O- and C-Horizons.

Initial and Boundary Conditions. Initial conditions for the O- and C-Horizons were assigned as their measured in-situ moisture values of $\theta = 0.21$ and 0.20, respectively (measured as average over layer depth at the time of sensor installation). The measured in-situ volumetric water content ($\theta = 0.26$) was used for the CKD initial condition because it remained fairly constant in the field over a period of six months. For comparison, a second series of simulations was conducted using initial conditions set to the field capacities measured in the laboratory (Table 2).

Boundary conditions were specified by "recharge" periods. For each recharge period, the top-middle segment of the domain (Figure 2) was assigned with either a constant flux of precipitation or evaporation, while all the other segments were assigned a "possible seepage" condition. The complete 24-day simulation cycle is summarized in Table 3, which shows 11 recharge periods during which the top boundary was subject

to alternating precipitation and evaporative fluxes. This 11-cycle recharge period was designed to simulate actual precipitation conditions measured at the field test site during the Fall of 2004 when a cumulative precipitation of 14 cm occurred over a period of 24 days. An evaporative flux of 0.01 cm/h was used for each evaporation recharge cycle (National Oceanic and Atmospheric Administration electronic database for Hannibal, MO).

Table 3. Summary of recharge periods for 24-day (566 h) simulation.

Recharge Period	Top Boundary Condition*	Duration (h)	Cumulative Duration (h)	Flux (cm/h)	Cumulative Precip. (cm)
1	E	45.8	45.8	0.01	0
2	P	24.5	70.3	0.18	4.50
3	E	120.0	190.3	0.01	4.50
4	P	36.0	226.3	0.03	5.70
5	E	163.0	389.3	0.01	5.70
6	P	5.2	394.5	0.35	7.50
7	E	73.3	467.8	0.01	7.50
8	P	6.2	474.0	0.11	8.20
9	E	25.2	499.2	0.01	8.20
10	P	33.0	532.2	0.18	14.00
11	E	33.5	565.7	0.01	14.00

* E = Evaporation, P = Precipitation

Results and Discussion

Comparison of Modeled and Measured Behavior. Figure 4 shows time domain results from a VS2D simulation in the form of volumetric water content at various depths (i.e., the observation points at z = 19, 59, 125, 228, and 445 cm; Figure 2). The vertical dashed lines correspond to the beginning and end times for the 11 precipitation/evaporation recharge periods summarized on Table 3.
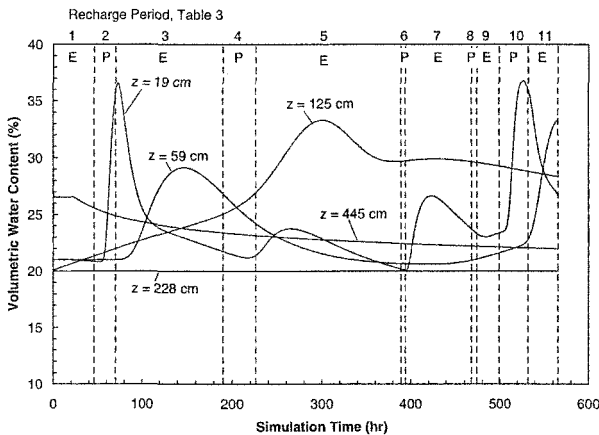
Figure 4. Water contents at various depths over 11-cycle simulation period.

It is readily apparent from Figure 4 that moisture content near the surface is highly sensitive to environmental loading. The volumetric moisture content at $z = 19$ cm below the ground surface approaches a maximum value of about 37% during or immediately following the relatively intense precipitation events of recharge periods 2, 6, and 10. The moisture content at $z = 59$ cm also increases as a result of these precipitation events, but the effect is significantly more attenuated and time lagged. The most significant increase in moisture content appears to occur at $z = 125$ cm, which is at the interface of the O- and C-Horizon. The C-Horizon material at $z = 228$ cm maintains its initial water content over the entire cycle. The CKD underlying the artificial soil cover ($z = 445$ cm) experiences a slow drying process, decreasing from an initial water content of 26% to a final value of about 22%. Each soil layer in the profile remains partially saturated (i.e., $\theta < n$) over the complete simulation cycle.

Figure 5 shows simulated moisture content profiles at various times during the simulation cycle. The predicted profiles are compared to upper and lower bounds of moisture content obtained from field measurements at the instrumented test section. Predicted values generally fall within the bounds defined by the experimental measurements. The largest range of moisture variation occurs in both the modeling results and the field measurements at locations at or above the interface of the O- and C-Horizons, indicating that downward water flow is restricted and results in ponding at the interface. The ponded water at the O-C interface either evaporates or flows laterally. The simulations suggest that the maximum depth of the wetting front over the 24-day cycle is about 250 cm from the surface, which compares reasonably well with the moisture data obtained from the field instrumentation. Infiltration for the analyzed precipitation and evaporation values did not reach the CKD layer either in the field test section or in the numerical modeling simulation.
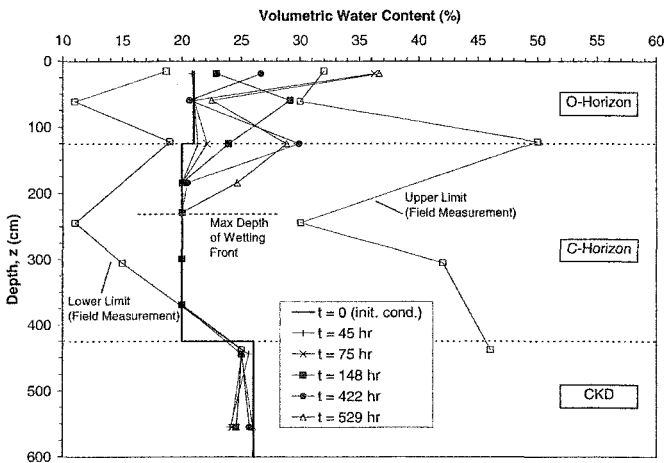
Figure 5. Water content profiles and experimental upper and lower bounds.

Parametric Analyses. Parametric analyses were conducted to simulate variations in precipitation rate, precipitation event duration, and soil-layer thickness. The first set of simulations was conducted to determine how different precipitation rates and durations affect the maximum depth of the wetting front and to predict combinations of rate and duration sufficient to cause the wetting front to break through the system. Boundary conditions applied for these analyses included a short-term precipitation event of specified flux, followed by 1000 hours of evaporation. The purpose of the second recharge period (evaporation) was to allow the water from the precipitation event to infiltrate to a quasi-equilibrium condition, thus allowing the maximum depth of the wetting front to be determined. Precipitation rates ranged from 0.033 cm/h to 10 cm/h (0.01 in/h to 3.9 in/h), where each was applied for 1, 2, 4, 5, 8, 12, and 24 hours. Cumulative precipitation for each event is the product of its rate and duration.

Figure 6a shows results in the form of maximum wetting front depth as a function of precipitation rate for various event durations (hours). Figure 6b shows the same data as a function of duration for various precipitation rates. Figure 6c compares maximum wetting front depths for models using initial conditions assigned as the in-situ water contents and using initial conditions as the field capacities.

At the lowest precipitation rate (0.033 cm/h), the wetting front (Fig. 6a & b) does not propagate past the organic (O) layer, even after 24 hours of rainfall. A cumulative precipitation of about 5 cm is necessary for the wetting front to break through the organic layer. For precipitation rates between 0.1 cm/hr to 0.5 cm/h, the wetting front advances faster during the first 5 hours, and slows down significantly while infiltrating through the less porous C-Horizon. All other precipitations (1 cm/hr to 10 cm/h) reach the C-Horizon in less than one hour. Complete breakthrough of the wetting front (i.e., propagation completely through the artificial soil layer and into the underlying CKD) does not occur for events that result in cumulative precipitation less than 16 cm (6.3in). This is equivalent to an event slightly larger than the 25-year 24-hour storm for Northeast Missouri (cumulative precipitation of about 14.6 cm (5.75 in)). The wetting front depth (Fig. 6c) for a given event intensity is not as deep using the lower (field capacity) initial conditions. Water is retained close to the surface for longer time, which allows more evaporation to occur, thus decreasing the maximum wetting front depth for a given precipitation event.

A second set of analyses was conducted to investigate the effect of increasing the C-Horizon thickness from the current design value of 300 cm. Five different thicknesses were considered: 300, 320, 340, 360, and 400 cm. Results were obtained in the form of "limiting" precipitation rate (i.e., the flux required to cause complete breakthrough) for event durations of 5, 12, and 24 hours. The relation between C-Horizon thickness and limiting precipitation rate is shown in Figure 7a. Figure 7b shows corresponding limiting cumulative precipitation as a function of C-Horizon thickness. Results indicate that the limiting cumulative precipitation increases linearly with increasing layer thickness. An increase of 100 cm in the thickness of the C-Horizon increases the limiting cumulative precipitation from 16 cm to about 27 cm.
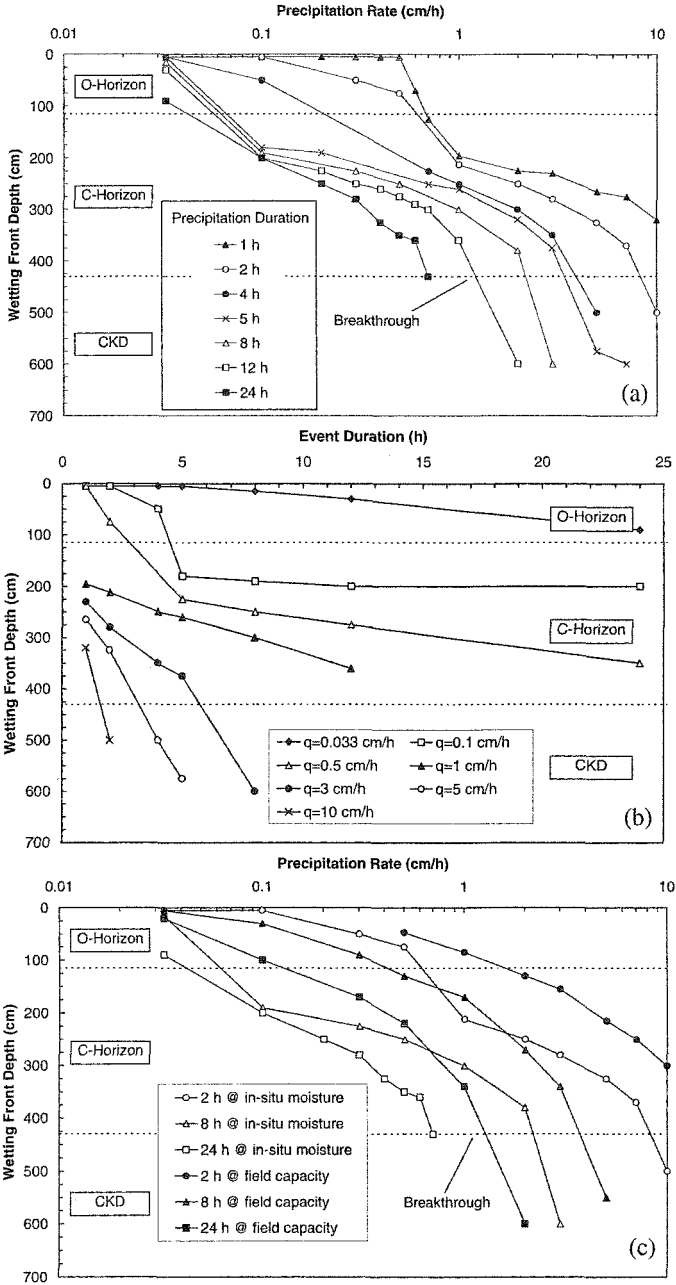
Figure 6. Depth of wetting front as function of (a) precipitation rate; (b) event duration; (c) precipitation rate for different initial conditions.

The sharp transition in the SWCCs (Figure 3) from residual to saturated conditions at relatively low suctions (~100 cm of water) suggests that the materials may become saturated relatively rapidly during infiltration. Further, the relatively high saturated conductivity of the materials indicates that water entering the soil should drain relatively rapidly. The numerical results indicate that the system remains partially saturated over the simulation period; however, this is may not be the case for extreme precipitation events. As such, the system is designed to maximize storage capacity by using a layer thickness (~15' – 20') that is significantly greater than that used in ET covers constructed from more "traditional" soils (~3'-6'). This is evident in the numerical parametric analysis of C-Horizon thickness summarized on Figure 7.
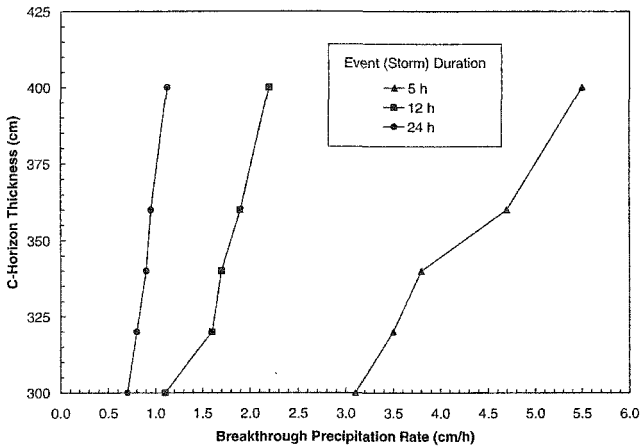
7(a)
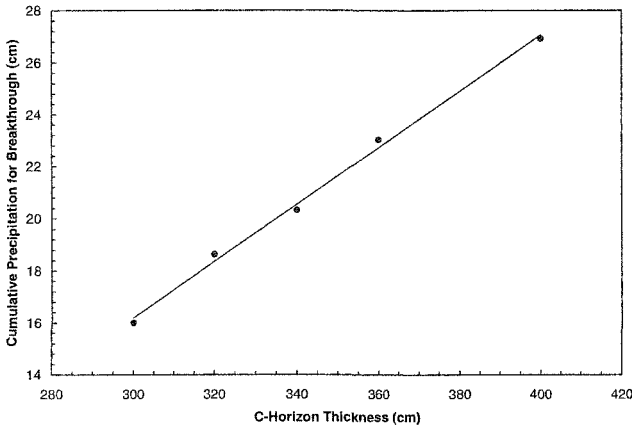
7(b)

Figure 7. Breakthrough precipitation rate (a) and cumulative precipitation (b) as a function of C-Horizon thickness.

Summary and Conclusions

Numerical seepage modeling has been conducted to assess the general effectiveness of an "artificial soil" created from industrial and municipal by-products as an evapotranspirative (ET) percolation barrier. The modeling domain was selected to represent dimensions of a full-scale instrumented test section installed at a field site. Model validation was performed by simulating a representative 24-day period of precipitation and evaporation field data and comparing the modeled and measured behavior. Results suggest that the maximum depth of wetting front propagation over the simulation period is about 250 cm and that complete breakthrough of the wetting front through the cover system does not occur. Modeling and field monitoring results show that the artificial soil is acting as an effective cover system by restricting wetting front propagation beyond the interface of the O- and C-horizons, causing water to be stored, evaporate, or flow laterally.

A series of parametric analyses was conducted to simulate variations in precipitation rate, precipitation event duration, and soil layer thickness. Simulations suggest that breakthrough of the wetting front does not occur for rainfall events that result in cumulative precipitation less than 16 cm, which is slightly greater than the 25-year 24-hour storm for Northeast Missouri. If the thickness of the C-Horizon is increased by 100 cm, the limiting cumulative precipitation increases from 16 cm to about 27 cm. The relation between layer thickness and limiting precipitation is linear.

Results may be used to optimize the geometry and design of similar artificial soil ET barrier systems under anticipated environmental conditions at other sites. The findings also provide data for assessing the general effectiveness of artificial soil for capping CKD deposits or other materials and reclaiming surface mined areas.

References

Bobba, R., Likos, W.J., Bowders, J.J., and Hammer, R.D. (2005). "Field and laboratory evaluation of artificial soil as an evapotranspirative barrier." *Proc. of 5th International Congress on Environmental Geotechnics*, ISSMGE, Cardiff, Wales, submitted.

Brooks, R.H. & Corey, A.T. (1964). "Hydraulic properties of porous media." Colorado State University, Hydrology Paper No. 3, March.

Chu, J., Goi, M.H., and Lim, T.T. (2005). "Consolidation of cement-treated sewage sludge using vertical drains." *Canadian Geotechnical Journal*, 42, 528-540.

Cox, J.A., and Whelan, R.J. (2000). "Soil development of an artificial soil mix: nutrient dynamics, plant growth, and initial physical changes." *Australian Journal of Soil Research*, 38, 465-477.

Dywer, S.F. (1998). "Alternative landfill covers pass the test." *Civil Engineering*, ASCE, 50-52.

Healy, R.W. (1990). "Simulation of solute transport in variably saturated porous media with supplemental information on modifications to the USGS Computer Program VS2D." *Water Resources Investigations Report 90-4025*.

Lappala, E.G., Healy, R.W. & Weeks, E.P. (1987). "Documentation of computer program VS2D to solve the equations of fluid flow in variably saturated porous media." *USGS Water Resources Investigations Report 83-4099*.

Lu, N. and Likos, W.J. (2004). *Unsaturated Soil Mechanics*, Wiley, Hoboken, NJ.

Nyhan, J.W. (2005). "A seven-year water balance study of an evapotranspiration landfill cover varying in slope for semiarid regions." *Vadose Zone Journal,* 4, 466-480.

Reynolds, K., Kruger, R., and Rethman, N. (1999). "The manufacture and evaluation of an artificial soil (SLASH) prepared from fly ash and sewage sludge." *1999 International Fly Ash Utilization Symposium*, Center for Applied Energy Research, University of Kentucky, Paper No. 1.

Zornberg, J.G., LaFountain, L., Caldwell, J.A. (2003). "Analysis and design of evapotranspirative cover for hazardous waste landfill." *Journal of Geotechnical and Geoenvironmental Engineering*, Vol. 129, No. 5, 427-438.

Numerical Modelling of Soil-Atmosphere Interaction for Unsaturated Surfaces

G. Gitirana Jr.[1], M.D. Fredlund[2], and D.G. Fredlund[3]

[1]School of Civil Engineering, University of Goiás, Goiânia, Brazil. Praça Universitária, s/n, Setor Universitário, Goiânia, GO, Brazil 74605-220; PH +55 (62) 3204-6099; FAX +55 (62) 3204-6099; email: gilsongj@eec.ufg.br
[2]SoilVision Systems Ltd., 2109 McKinnon Avenue S., Saskatoon, SK, Canada S7J 1N3; PH +1(306) 477-3324; FAX +1(306) 955-4575; email: murray@soilvision.com
[3]Department of Civil and Geological Engineering, University of Saskatchewan, 57 Campus Drive, Saskatoon, SK, Canada S7N 5A9; email: unsaturatedsoil@yahoo.com

Abstract: The computation of soil-atmosphere water fluxes such as infiltration, evapotranspiration, and runoff is required for the analysis of numerous problems in geotechnical, geoenvironmental engineering and hydrogeology. The soil-atmosphere interaction processes can be represented by a series of partial differential equations. This paper presents a PDE formulation that was developed for soil-atmosphere analysis and presents three cases demonstrating the application of the formulation developed to laboratory and fields conditions. Comparisons against experimental data show that evaporative fluxes can be successfully reproduced by theoretical models. The PDE solutions were used for the simulation of the fluxes through two soil cover configurations to exemplify the application of theoretical models to design. The results indicate that the manner how runoff is computed strongly affects the results. The numerical solutions appear robust and can be applied to the design of soil structures such as soil-cover systems, geo-hazard hazard quantification, and other unsaturated soil problems.

1.   INTRODUCTION

The computation of soil-atmosphere water fluxes (e.g., infiltration, evapotranspiration, and runoff) is required for the analysis of numerous problems in geotechnical, geoenvironmental engineering and hydrogeology. The design of earth covers, for instance, requires the prediction of water fluxes through the cover as a function of the soil properties and atmospheric forcing conditions.

The analysis of soil-atmosphere water fluxes problems can be undertaken within the framework of partial differential equation (PDE) solutions. This paper describes a PDE formulation that was developed for soil-atmosphere analysis and presents three cases demonstrating the application of the formulation developed to laboratory and fields conditions.

2.   THEORETICAL FRAMEWORK

Several physical processes are involved in the flow of soil moisture. Moisture moves through soils driven by gradients of total head of each of the moisture phases (i.e., liquid water and water vapour) and other gradients, such as heat and chemical gradients. In order to obtain the equations governing moisture transfer constitutive flow laws and water volume change constitutive laws are combined with conservation equations. Appropriate equations for the soil-atmosphere flux boundary conditions are also required.

2.1 Partial differential equations for water and heat flow

The two-dimensional PDEs presented herein are simplifications of the general equations presented by Fredlund and Gitirana Jr. (2005). Combining the equation of conservation of mass for the water phase, Darcy's law for the flow for liquid water, Fick's law for the flow of water vapor, and Lord Kelvin's relative humidity equation, the following PDE is obtained:

$$
\frac{\partial}{\partial x}\left[k^w \frac{\partial}{\partial x}\left(\frac{u_w}{\gamma_w}+y\right)+\frac{k^{vd}}{\gamma_w}\frac{\partial u_w}{\partial x}-\frac{k^{vd}}{\gamma_w}\frac{u_w}{(T+273.15)}\frac{\partial T}{\partial x}\right]
$$
$$
+\frac{\partial}{\partial y}\left[k^w \frac{\partial}{\partial y}\left(\frac{u_w}{\gamma_w}+y\right)+\frac{k^{vd}}{\gamma_w}\frac{\partial u_w}{\partial y}-\frac{k^{vd}}{\gamma_w}\frac{u_w}{(T+273.15)}\frac{\partial T}{\partial y}\right]=m_2^w\frac{d(u_a-u_w)}{dt}
$$

[1]

where k^w = hydraulic conductivity function; u_w = pore-water pressure; γ_w = unit weight of water; y = elevation; k^{vd} = vapour diffusivity; T = temperature; m_2^w = slope of the soil-water characteristic curve; and u_a = pore-air pressure.

A PDE governing heat flow must be solved along with Eq. 1 for the variables u_w and T. In order to obtain the heat flow PDE, the equation of conservation of heat must be combined with the heat flow laws (conduction and latent heat), and Lord Kelvin's equation. Furthermore, the total amount of heat within the R.E.V. must be written as a function of the volumetric specific heat of the soil. The following equation results:

$$
\frac{\partial}{\partial x}\left[\left(\lambda-L_V k^{vd}\frac{\rho_w}{\gamma_w}\frac{u_w}{T+273.15}\right)\frac{\partial T}{\partial x}+L_V k^{vd}\frac{\rho_w}{\gamma_w}\frac{\partial u_w}{\partial x}\right]
$$
$$
+\frac{\partial}{\partial y}\left[\left(\lambda-L_V k^{vd}\frac{\rho_w}{\gamma_w}\frac{u_w}{T+273.15}\right)\frac{\partial T}{\partial y}+L_V k^{vd}\frac{\rho_w}{\gamma_w}\frac{\partial u_w}{\partial y}\right]=\zeta\frac{\partial T}{\partial t}
$$

[2]

where λ = thermal conductivity of the soil; L_v = latent heat of vaporization; ρ_w = specific mass of water; and ζ = volumetric specific heat of the soil.

Equations 1 and 2 present five non-linear unsaturated soil property functions (i.e., k^w, k^{vd}, m_2^w, λ, and ζ) that render the equations non-linear. Equation 1 may be simplified

by neglecting temperature gradients and neglecting Eq. 2. This simplification will be employed in one of the computer codes presented in the next sections.

2.2 Soil-atmosphere coupling

The net soil-atmosphere moisture flux is a function of some of the key components of the hydrology cycle; namely, precipitation, actual evaporation, and run-off. The net soil-atmosphere flux may result in either infiltration (positive flux) or exfiltration (negative flux) as indicated by the following water balance equation:

$$NF = P \cos \alpha - AE - R \qquad [3]$$

where NF = the net moisture flux; P = precipitation; α = ground surface slope; AE = actual evaporation; R = runoff.

The terms in Eq. 3 are illustrated in Fig. 1. The net moisture flux, NF, corresponds to a natural (i.e., flux) boundary condition. The amount of precipitation, P, is a "known" input. The term $\cos \alpha$ is based on the assumption that precipitation falls in a vertical trajectory and is typically measured on a horizontal surface. The terms AE and R are a function of weather and the soil suction at the soil-atmosphere boundary.

Actual evaporation can be computed based on the potential evaporation and a limiting function (Wilson et al., 1997). Runoff must be computed in an interactive manner. If the embankment being analysed has an efficient drainage system, any runoff water will be removed from the ground surface. In this case, the amount of net moisture flux, NF, should not produce pore-water pressures higher than zero at ground surface. The following equations can be used to represent this condition (Gitirana Jr., 2005):

$$NF = \begin{cases} P \cos \alpha - AE & : \text{if } P \cos \alpha - AE > 0 \text{ and } u_{ws} < 0 \\ EF(0 - u_{ws}) & : \text{if } P \cos \alpha - AE > 0 \text{ and } u_{ws} \geq 0 \\ P \cos \alpha - AE & : \text{if } P \cos \alpha - AE \leq 0 \end{cases} \qquad [4]$$

where u_{ws} = pore-water pressure at the surface; EF = a large number.

If the multiplier EF tends to infinity, the area flux boundary condition $NF = EF(0 - u_{ws})$ becomes mathematically equivalent to an essential (i.e., node value) boundary condition, $u_w = 0$. Therefore, the boundary condition from Eq. 4 is an alternative to switching to an essential boundary condition when the pore-water pressure at the soil surface becomes positive.

The approach based on switching boundary conditions often results in numerical oscillations due to instantaneous changes on node values. These instantaneous u_w value changes do not represent real-world conditions. Instantaneous changes in node values require mesh refinements that should theoretically be infinitesimal (Gitirana Jr., 2005, Nelson, 2004). Equation 4 appears to impose a more realistic condition.
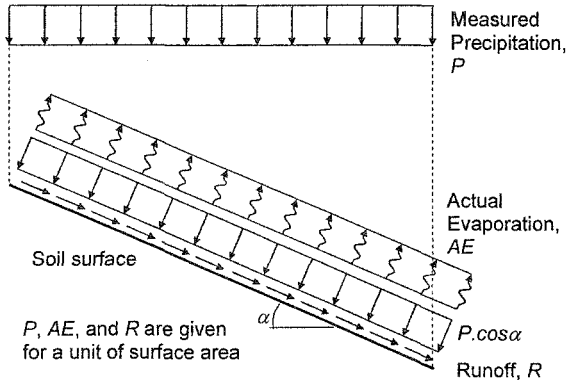
Figure 1   Soil-atmosphere moisture flux components.

3.   METHODOLOGY

Two software packages were used in this study; namely, SVFlux and Vadose/W. SVFlux (SoilVision Ltd., 2005) is a seepage analysis package capable of solving 1D, 2D, and 3D seepage problems under steady-state and transient conditions. SVFlux uses FlexPDE (PDE Solutions Inc., 2005) as a PDE solver engine. Liquid water and water vapour flow are considered in the PDEs adopted, according to the formulation presented in Gitirana Jr. (2005). Soil-atmosphere interaction is reproduced using Eq. 4. SVFlux makes use of an automatic adaptive mesh technique. The adaptive mesh refinement algorithm is tuned to be sensitive to high gradients in pore-water pressure, hydraulic conductivity, or any other variable that needs to be solved with a given desired accuracy.

Vadose/W (Geo-Slope International, 2005) is capable of solving seepage problems where soil-atmosphere interaction is of interest. Vadose/W is primarily a 2D package but can be used for 1D problems through the use of appropriate geometries and boundary conditions. Vadose/W has a special feature that allows the accumulation of runoff in surface depressions and subsequent infiltration. The mesh construction in Vadose/W is manual and the mesh remains fixed throughout the analysis.

Vadose/W uses a technique for computing infiltration and runoff were "natural" and "essential" boundary conditions are switched based on the soil conditions at the ground surface. The ground surface is treated as a "potential seepage surface". The instantaneous application of "essential" boundary conditions that are not continuous may result in numerical oscillations. However, small time steps are expected to minimize such oscillations.

Three problems were investigated as part of this study. First, the data from a laboratory evaporation test was reproduced. Significantly high gradients were expected in this problem, resulting in demanding computations. Next, two problems

are analyzed that involved alternating weather conditions. The fluxes past soil covers associated with the reclamation of mine sites are presented.

4.   ANALYSIS OF EVAPORATION FROM A SOIL COLUMN LABORATORY TEST

This verification example demonstrates the coupling between moisture and heat and the importance of the water vapour flow component during evaporation. The results of a sand column drying experiment performed by Wilson (1990) were selected. Both experimental and simulation results are available for comparison. The drying test was performed in the laboratory, under controlled temperature and relative humidity conditions. Measurements of actual evaporation and the distributions of temperature along the column depth were obtained, providing several measures that can be used for the verification of the theoretical and numerical model. Wilson (1990) presented also a one-dimensional finite difference numerical model called "Flux" for the simulation of the drying test. Reasonable results were obtained from the comparison of measured data and results computed using the Flux program. Both the measured and computed results from Wilson (1990) are compared against the result obtained using the numerical model presented herein.

Figure 2 presents the geometry of the drying column experiment and the initial and boundary conditions. Due to the problem geometry and boundary conditions, the flow is essentially one-dimensional. Therefore, the three-dimensional axisymmetric geometry was reduced to a one-dimensional problem. Boundary conditions forcing zero water and heat flow were applied at the bottom and lateral boundaries.

More complex boundary conditions were applied to the upper boundary, which is in contact with the atmosphere. The temperature boundary condition applied to the upper end of the column was the experimentally measured surface temperatures. The moisture flow boundary condition applied was Eq. 4 along with the actual evaporation equation proposed by Wilson et al. (1997). The values of potential evaporation required by the equation proposed by Wilson et al. (1997) were obtained during the drying column test; from measured values of evaporation from a water pan. Wilson (1990) presents additional variables required by the soil-atmosphere coupling boundary condition; namely, the relative humidity and the air temperature.

The soil selected by Wilson (1990) for the analyses was the Beaver Creek sand. Figure 3 presents the hydraulic soil properties of the soil used. The soil-water characteristic curve was obtained by Wilson (1990) using Tempe cell tests and desiccators. The hydraulic conductivity function was obtained from the saturated hydraulic conductivity obtained in the laboratory and using the Brooks and Corey equation. The moisture conductivity corresponding to the vapour diffusion coefficient is also presented in Fig. 3. A comparison of the functions k^w and k^{vd} provides an estimation of the range of soil suction and water content for which liquid water flow or water vapour flow dominate. For the Beaver Creek sand, vapour

diffusion takes over for values of soil suction higher than 20 kPa and degree of saturation lower than approximately 20%. The highly steep hydraulic conductivity function shown in Fig. 3 poses a considerable challenge for the numerical model.

Figure 4 presents the thermal property functions of the Beaver Creek sand. These functions were obtained using the formulations presented by de Vries (1963). According to the prediction equations, the thermal conductivity and the volumetric specific heat are function of the characteristics of the individual phases and are functions of the amount of water stored in the soil. The effect of the amount of water stored in the soil pores is shown by the decrease in thermal conductivity and volumetric specific heat, as soil suction increases.
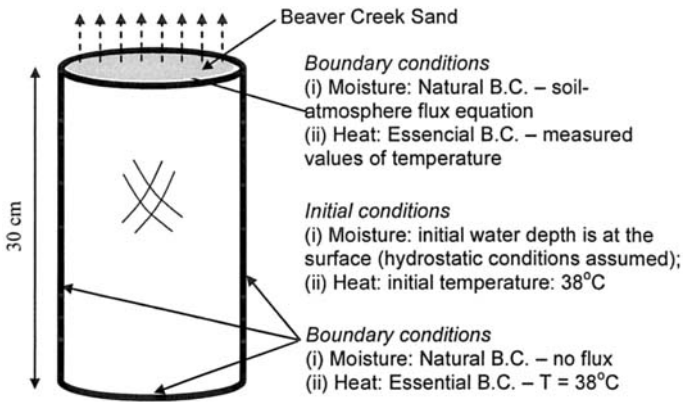
Figure 2   Numerical simulation of the drying column test – initial and boundary conditions (Wilson, 1990).
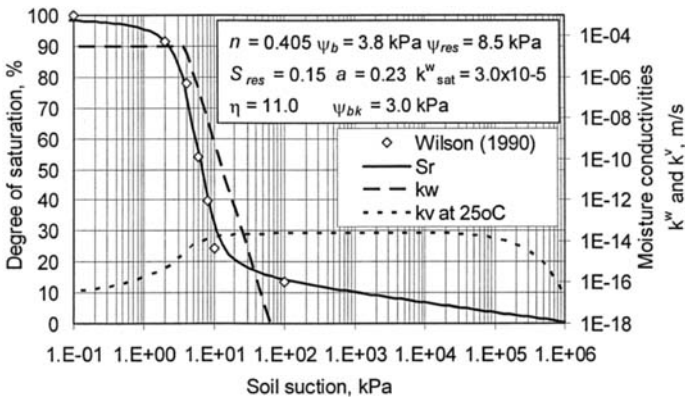
Figure 3   Hydraulic properties for the Beaver Creek sand.
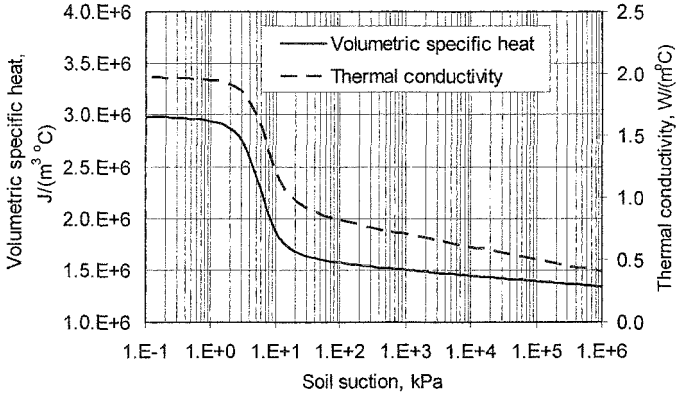
Figure 4   Thermal properties for the Beaver Creek sand.

The experiment and the numerical analyses were carried out for a period of 40 days. Figure 5 presents the actual evaporation values obtained experimentally, using the numerical model proposed by Wilson (1990), using a fully coupled solution presented by Gitirana Jr. (2005) and using a isothermal solution provided by SVFlux. Close agreement was observed between the all the results. The hydraulic property functions of the sand are extremely steep, and pose a numerical challenge. The automatic mesh and time refinement procedures were able to track the nonlinearities and ameliorate the numerical difficulties in solving the nonlinear system. The computing time required was approximately 20 hours on a Pentium 3 600MHz.
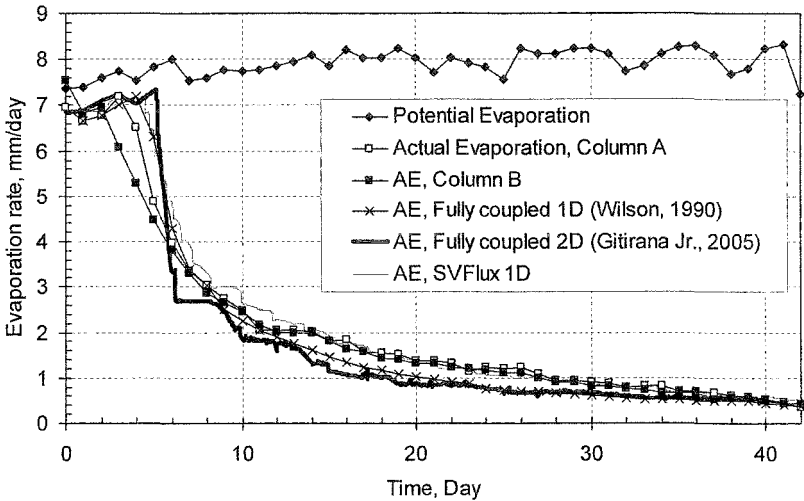
Figure 5   Verification of the coupled heat and moisture flow model: evaporation rates.

Figure 6 presents the pore-water pressure profiles for $t = 29$ days. Close agreement is observed between the experimental measurements, the results obtained using the numerical codes. A sharp drying front is observed. The pore-water pressure near the ground surface corresponds to a considerably dry condition, and approaches 1,000,000 kPa as time advances. The difficulty in computing extremely low hydraulic conductivities at the drying front were considered the cause of the small differences between computed and measured values.

Figure 7 presents the temperature profiles for $t = 1$ day, 6 days, and 12 days. Close agreement is once again observed between the experimental measurements and the computer code results. As the soil begins drying, the surface starts to cool, because of the latent heat of vaporization (see profile for day 1 in Fig. 7). The profiles for day 6 and 12 show that the cooling front follows the drying front, as expected.

5.   ANALYSIS OF TWO SOIL COVER CONFIGURATIONS

Analysis of infiltration past soil covers is a common type of analysis used in the long-term reclamation of mine sites. 1D or 2D finite element seepage software packages are typically used for this type of analysis. The final proposed design is often based on the results of the finite element analysis of the system. Calculation of actual evaporation rates and runoff becomes significant in the long-term fluxes through cover systems. Two soil column problems were used to illustrate the impact of varying methods of calculating runoff, infiltration, and evaporation on calculations performed over the course of one year. In the examples presented here the input data was kept as much the same as possible between the various computer codes.
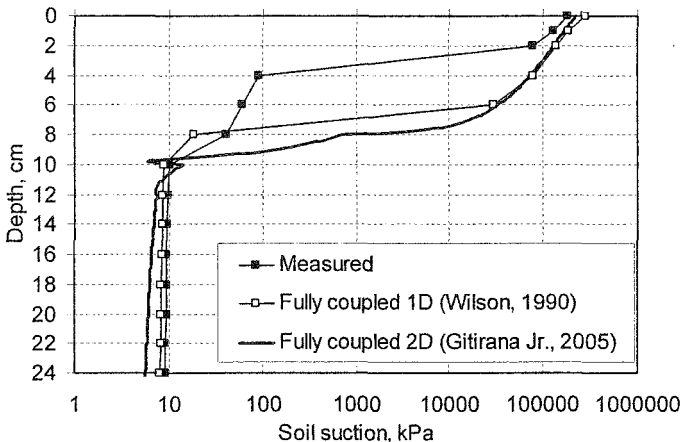
Figure 6   Verification of the coupled heat and moisture flow model: pore-water pressure distributions for $t = 29$ days.
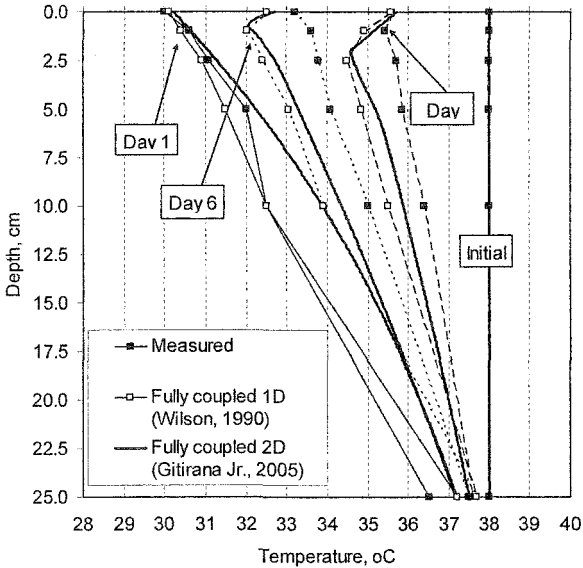
Figure 7   Verification of the coupled heat and moisture flow model: temperature distributions for several time steps.

Applied precipitation levels in the first 14 days of analysis are abnormally high due to the occurrence of snowmelt during this time. The daily precipitation values were assumed to be concentrated at a period of eight hours. The first soil column is comprised of a Till cover 1 m thick with k^w_{sat} = 9×10^{-2} m/day. The van Genuchten and Mualem representation of the unsaturated hydraulic conductivity curve was used for all soils. Beneath the cover there were two layers of tailings each 2.5 m thick with varying hydraulic parameters of 9×10^{-1} m/day and 9×10^{-2} m/day respectively.

Results of the analysis of column 1 are presented in Figure 8. From these results it can be seen that this scenario accentuates the differences in runoff calculation. Vadose/W overestimates runoff values. As a result, less water entered the system than what was predicted using SVFlux. The reduced amount of water entering the system results in higher soil suctions, thereby producing lower evaporation rates.

In the second column the same soil geometry was used but the conductivity of the top layer was decreased to 9×10^{-3} m/day. This should have the effect of increasing the total runoff calculation. The results for the second column may be seen in Figure 9. Significantly greater quantities of runoff were predicted using both software packages. It can also be seen that Vadose/W again presents higher runoff rates with the resulting decrease in actual evaporation.
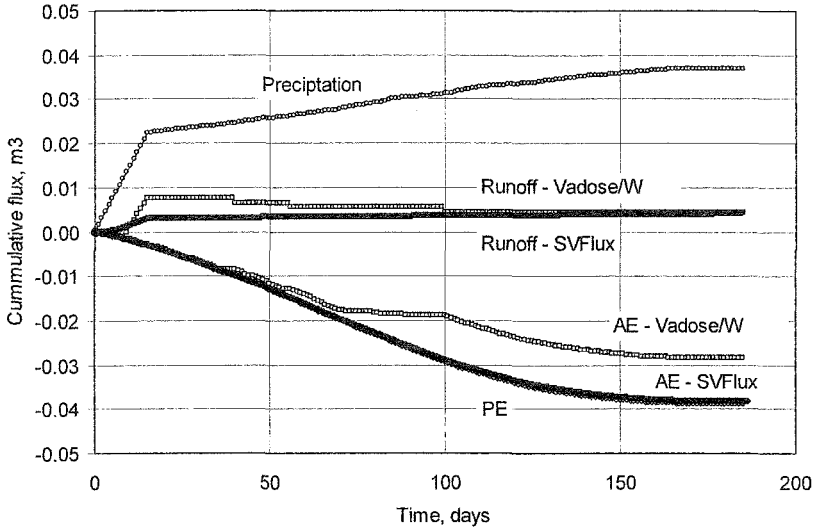
Figure 8   Runoff and AE predictions for column 1.
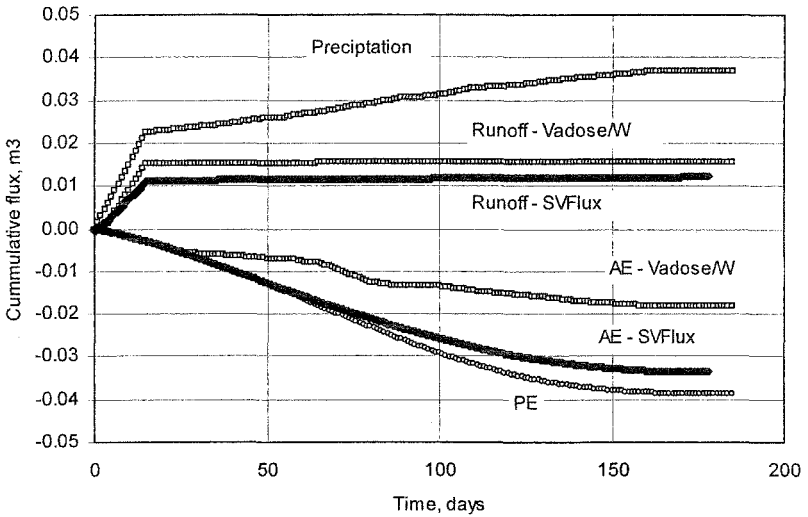
Figure 9   Runoff and AE predictions for column 2.

Mass balance checking was performed on all SVFlux runs and all scenarios solved with a total mass balance error of less than 5%. Figures 10 and 11 present a closer look at infiltration and runoff predictions using Vadose/W and SVFlux. The manner

how precipitation is represented by each package is somewhat different. Vadose/W uses a sinusoid whose total area is equal to the amount of daily precipitation. SVFlux uses a step-function that also corresponds to the daily amount of precipitation. As precipitation progresses, both packages predict high rates of infiltration, close to the total amount of precipitation. However, the amount of infiltration predicted by Vadose/W is slightly lower. The lower values of infiltration predicted by Vadose/W are in agreement with the overestimated runoff presented in column 1.

6.   CONCLUDING REMARKS

This paper presented a PDE formulation that was developed for soil-atmosphere analysis and presented three cases demonstrating the application of the formulation developed to laboratory and fields conditions. Comparisons against experimental data showed that evaporative fluxes can be successfully reproduced by theoretical models. The PDE solutions were used for the simulation of the fluxes through two soil cover configurations. The results indicate that the manner how runoff is computed strongly affects the results. The numerical solutions appear robust and can be applied to the design of soil structures such as soil-cover systems.

ACKNOWLEDGEMENTS
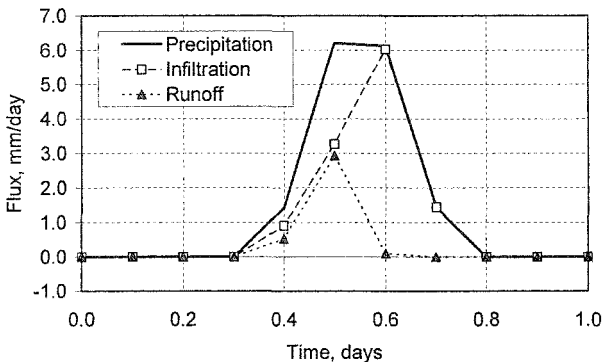
Figure 10   Vadose/W predictions for column 1, day 1.
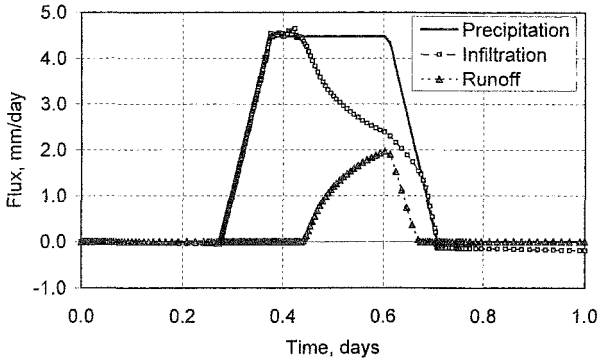
Figure 11   SVFlux predictions for column 1, day 1.

REFERENCES

de Vries, D.A. (1963). "Thermal properties of soils." *Physics of Plant Environment.* W.R. van Wijk (ed.), Amsterdam, New Holland, 382p.

Fredlund, D.G. and Gitirana Jr., G.F.N. (2005). Keynote Address: Unsaturated Soil Mechanics as a Series of Partial Differential Equations. *GEOPROB 2005.* Famagusta, Cypurs. 3-30.

Geo-Slope International Ltd. (2005). *"Vadose/W User's Manual, Version 1.10."* Copyright 1991-2005. Geo-Slope Ltd., Calgary, Alberta, Canada.

Gitirana Jr., G.F.N. (2005). "Weather-Related Geo-Hazard Assessment Model for Railway Embankment Stability". Ph.D. Thesis. University of Saskatchewan, Saskatoon, SK, Canada, 411p.

Nelson, R. (2004). *Personal Communication.* PDE Solutions Inc.

PDE Solutions Inc. (2005). *"FlexPDE 5.0 - Reference Manual."* Antioch, CA, USA.

SoilVision Systems Ltd. (2005). *"SVFlux User's and Theory Guide. Version 5.55."* Saskatoon, SK, Canada.

Wilson, G.W. (1990). *"Soil Evaporative Fluxes for Geotechnical Engineering Problems."* PhD Thesis, Department of Civil Engineering, University of Saskatchewan, Saskatoon, Canada, 464p.

Wilson, G.W., Fredlund, D.G., Barbour, S.L. (1997). The effect of soil suction on evaporative fluxes from soil surfaces. *Canadian Geotechnical Journal,* 34(4): 145-155.

The Impact Of Slope And Exposure On The Design Of Soil Covers In Three Dimensions

B. Weeks[1] and G.W. Wilson[2]

[1] Department of Mining Engineering, University of British Columbia, Room 506A, 6350 Stores Road, Vancouver, BC, Canada, V6T 1Z4; PH (604)-822-6717; FAX (604) 822-5599; email: bweeks@interchange.ubc.ca

[2] Department of Mining Engineering, University of British Columbia, Room 517, 6350 Stores Road, Vancouver, BC, Canada, V6T 1Z4; PH (604)-822-6781; FAX (604) 822-5599; email: gww@mining.ubc.ca

Abstract

The importance of climate and earth-atmosphere interactions for the design of soil covers is now well-established. Modeling tools have been developed to predict the performance of such covers, based on local climate data, and the flow of subsurface water and heat in either one or two dimensions. These tools are commonly used in the design of soil covers. The application of these design tools carries the assumption that climate will be relatively constant throughout the site under consideration. However, it has been well-established in the field of microclimatology that local climates can be significantly impacted by the topography at a site, particularly with respect to the direction faced by sloped ground surfaces, and the steepness of the ground slope.

Presented in this paper is a proposed approach for factoring the impact of slope and exposure into the design of a soil cover, incorporating established models for predicting actual evaporation with a recent model for net radiation on sloped surfaces

Introduction

It is now well established in unsaturated soil studies that tools for the prediction of flux boundary conditions through surface soils are very useful to have. Such tools have found their most ready application in the design of soil covers for waste disposal sites. At such sites, the engineer is typically concerned with predicting the performance of soil covers in terms of the water balance over the soil cover (infiltration, evaporation, etcetera), and in the water content that will be maintained in

the cover soils. Several powerful numerical tools have emerged for predicting the flux boundary conditions of surface soils, based on climatic conditions and soil properties at a given site. In particular, several codes are now available based on the coupled solution of the modified Penman Equation (Wilson, 1990), coupled with the solution of heat and water flow equations. These tools are now commonly used geotechnical practice for the design of soil covers.

When using either one or two dimensional flux boundary models, climate is normally assumed constant over the entire site. While this approximation is generally reasonable, it is well established that for sites with significant topographic variations, there can be large differences over the site in the local microclimate. For sites where there are steeply sloped portions of the cover that make up a large fraction of the site area, climate data collected at a weather station located on a horizontal surface may not be representative of climate conditions on a steep north-facing slope. In particular, the net radiation (Q_{net}, a major driving factor in evaporation) will be different on sloped surfaces of different slope and orientation in the same general area (Oke 1987), which may have a significant effect on evaporation (Raupach and Finnigan 1997, Sellers et al 1997). Slope may also affect evaporation by affecting moisture distribution along the slope (Sellers et al, 1997), a factor that can be modeled in existing two-dimensional formulations of flux boundary models. Slope may also affect wind over the site, with potential impacts on evaporation (Raupach and Finnigan 1997).

To quantify the effect that slope variations have on net radiation at a given site, a model has been developed to predict net radiation on a sloped surface, based on net radiation measured on a horizontal surface. Aspects of this model have been presented in Weeks and Wilson (2003) and Weeks and Wilson (2004). This model was designed specifically for integration with existing flux boundary models, to improve the accuracy of evaporation calculations on sloped surfaces in three dimensions. As will be shown in this paper, linking the net radiation model with the flux boundary model allows designs to be modified reflecting the differences in radiation receipt on different slopes.

Theoretical Background

The commonly used flux boundary models SoilCover (1993), SVFlux (2004) and Vadose/W (2003) are all based on the solution of the modified Penman Equation (Wilson, 1990), coupled with the solution of heat and mass transport equations, to calculate actual evaporation (AE). The modified Penman Equation is shown below:

$$AE = \frac{\Gamma Q_{net} + \nu E_a}{\Gamma + A \nu}$$

Where:

$\Gamma =$ slope of the saturation versus vapour pressure curve at the mean air temperature

$\nu =$ psychrometric constant

$E_a =$ $f(u)e_a(B_h-A)$

$f(u) =$ a wind mixing function

$e_a =$ vapour pressure of the air above the evaporating surface

$B_h =$ inverse of air relative humidity

$A =$ inverse of relative humidity at soil surface

As can be seen from the form of this equation, Q_{net} (the net radiation) is a major climatic control on the actual evaporation. In SoilCover (1993) the solution of this equation was coupled with the one-dimensional solution of the heat and water transfer equations, while in Vadose/W (2003), the solution of the modified Penman Equation (Wilson, 1990) was coupled with a two-dimensional equations for water and heat movement, permitting slope effects on moisture redistribution to be predicted and analyzed. In both models, climate is implicitly assumed to be constant over the entire surface modeled, regardless of orientation/location.

In the case of a one-dimensional model, the water table below the ground surface is necessarily modeled as being at a uniform depth, which is often reasonable for approximately horizontal soil surfaces. However, where soil surfaces are steeply sloped, there can be considerable variation along the slope in the depth to water table. This variation will affect the moisture distribution along the slope length, as will the gravity-driven flow of moisture downslope. Since the moisture content of the soil at any point along the soil slope will affect infiltration/runoff partitioning of runoff (as well as evaporation rates), it becomes important to consider the moisture distribution along the slope. The distribution of moisture throughout a soil slope follows certain typical patterns. In topographic lows, the water table is usually located closer to the ground surface, while at topographic highs the water table is deeper (Freeze and Cherry, 1979). Yang and Yanful (2002) demonstrated for both sand and silt soils that increasing the depth to the water table resulted in decreased evaporation rates by limiting the water supply at the ground surface. Two-dimensional models for actual evaporation provide a means to assess the magnitude of such effects over sloped topography.

Weeks and Wilson (2003, 2004) developed a net radiation model to be integrated with models such as SoilCover (1993) and Vadose/W (2003). The net radiation model uses information on the local topography (slope angle, directions of slope exposure, latitude and elevation) in combination with the climate data needed for the evaporative model (primarily net radiation on a horizontal surface, temperature and humidity data) to predict net radiation values for the slope. This is done by using the measured climate data to estimate the longwave and shortwave components of the net radiation data. These components are then modified to reflect the impact of the specified slope on the overall radiation receipt. The modified net radiation calculated can then be used as an input to the evaporative model. More detail on the theory of

the net radiation model is available Weeks and Wilson (2003), with aspects of the model verification and application illustrated in Weeks and Wilson (2004).

To demonstrate the coupling of the net radiation model with flux boundary models, a simple soil cover design is evaluated in this paper. The cover is evaluated with a two-dimensional flux boundary model, to demonstrate the impact of variable depths to water table on moisture content and evaporation rates. The cover is also evaluated with a one-dimensional model to illustrate a proposed design approach for soil covers.

Research Site Data

To illustrate the application of the coupled radiation and flux boundary models, data collected at an existing soil cover site was used to define soil properties, site geometry, and climatic conditions for an example cover. The data used was collected at Placer Dome's Equity Silver Mine Site in north-central British Columbia. The net radiation model of Weeks and Wilson (2003) has been thoroughly tested with data collected at this site (as well as with data collected at other sites in British Columbia and Australia).

Waste rock disposed of at the Equity Site was covered with an engineered soil cover. This cover consisted of a 0.5 m thick layer of compacted till, overlain by a 0.3 m thick layer of non-compacted till. Soil water characteristic curves for the tills are shown in Figure 1, with key soil properties summarized on Table 1 (after O'Kane, 1995). The soil cover had an areal extent of approximately 100 ha, with portions sloped as steeply as 2.5H:1V.
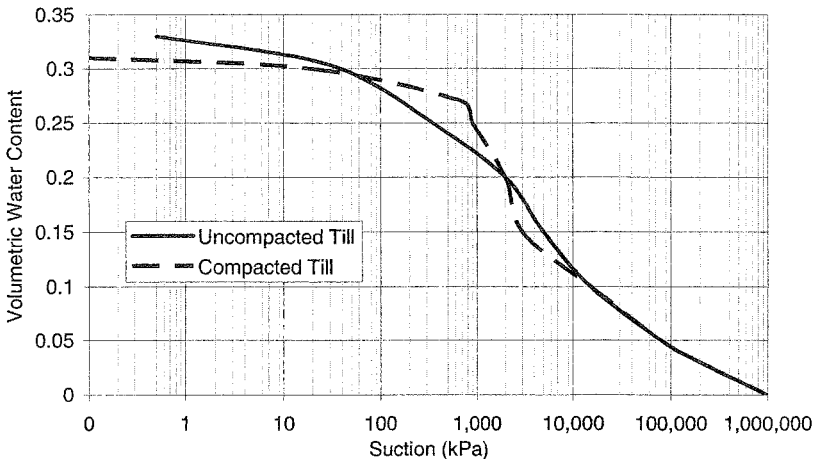
Figure 1: Soil Water Characteristic Curve for Equity cover till (after O'Kane, 1995).

Table 1: Characteristics of Till Cover Soils at Equity

Properties	Uncompacted	Compacted
K_{sat} (m/sec)	3×10^{-8}	5×10^{-10}
Porosity	0.33	0.31
Sg	2.77	2.77
Air Entry Value (kPa)	100	1000
Classification	SC-CL	SC-CL

The Equity Site is located in a humid alpine climate. The regional average annual total precipitation in the area was 710 mm. This precipitation (60% snow, 40% rain) exceeded the annual potential evaporation (500mm) at the site (Swanson et al. 2003). Average monthly temperatures at the site were below zero between November and March, with the majority of the snowmelt and runoff typically occurring in May. Climate data has been collected directly on the Equity cover with an automated weather station continuously since April 1993. The weather station was equipped to record key data such as temperature, windspeed, net radiation, humidity, and rainfall. For modeling purposes, a ten-year data set has been extracted from the weather data. This data set consists of averaged data for the 191-day period starting in mid-April, representing the portion of the year during which the majority of evaporation and flux movements through the surface soils will take place (that is, the portion of the year when there is no snow cover).

Comparative Slope Analysis

Coupling the net radiation model with a two-dimensional flux boundary models such as Vadose/W permits a pseudo-three dimensional analysis of slope effects on evaporation. By modifying net radiation input as a function of the direction faced by the slope and the steepness of the slope, the orientation of the surface in three-dimensional space can be at least partially accounted for, while the 2D solution of the heat and moisture transport equations accounts for factors such as variable moisture contents in the soil.

To illustrate this application, a simple monolayer cover has been analyzed. The cover used for this illustration consists of a single layer of the uncompacted Equity till, 80 cm thick. Note that this cover, lacking a compacted layer, would be expected to allow considerably more infiltration than the cover actually in place at the Equity site. As shown on the finite element mesh in Figure 2, the cover layer was modeled on a slope that is 2.5H:1V and had a horizontal length of 25 m with a height of 10 m. The water table was set as a boundary condition 1 m below the toe elevation of the slope. For initial moisture conditions in the model, an initial water table was set with negative porewater pressures above the water table limited to 12 kPa (the suction at residual water content in the waste rock). The 10-year averages for the Equity climate data set (1994-2003) were used as the climate boundary for the model.

Two slopes were analyzed – one facing due north, and one facing south. For each slope, the net radiation input to the finite element model was modified in the net radiation model, based on the slope angle, site latitude, and daily measured values of temperature and radiation. The results from this model showed that the south-facing slope had less total infiltration (approximately 72 mm) than the north-facing cover (approximately 84 mm per year).
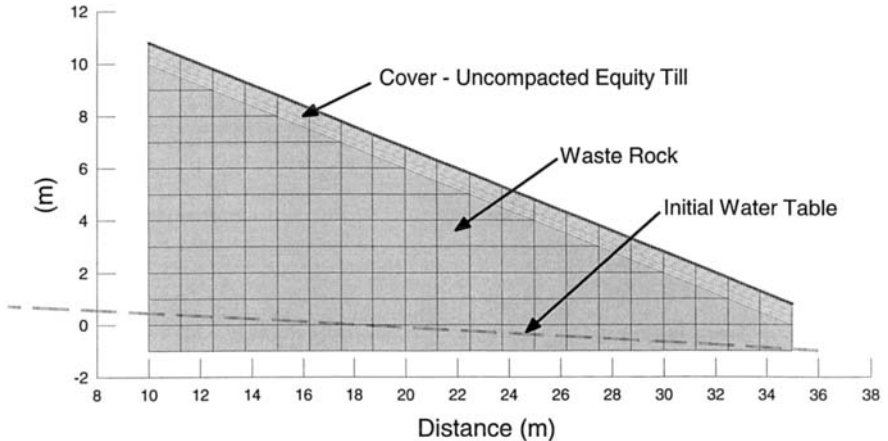
Figure 2: Finite element mesh use for the analysis of slope effects.

As expected, the calculated values of both potential and actual evaporation were higher on the south-facing slope. The potential evaporation rate on the south-facing slope was uniform at 505 mm per year, while potential evaporation on the north facing slope was 60 mm less (445 mm per year). Figure 3 shows the calculated annual actual evaporation rates on both slopes, including the variation of actual evaporation along the length of the slope. For comparison, the calculated actual evaporation is also shown for the case using the net radiation as measured on the horizontal as an input (as would be used when the net radiation model is not available).

The average rate of actual evaporation on the south-facing slope was 373 mm per year, 31 mm more than the 342 mm per year rate on the north-facing slope. As shown on Figure 3, the rate of actual evaporation tended to be slightly higher near the toe of the slope, where the moisture contents were higher. The difference between evaporation rates at the crest and at the toe were quite small for the cases modeled – for the south-facing slope the difference between evaporation rates at the crest and at the toe were 2.5 mm per year, while on the north face the difference was only 1.5 mm. This indicated that for this particular combination of site geometry, soils and boundary conditions that the differences in evaporation rate induced by the slope

direction (north versus south) were far greater than the differences induced by the position along the slope. This is not to say that slope direction will always be the more important factor, as there may be alternative configurations with different soils and different initial conditions where slope position is a more important factor.
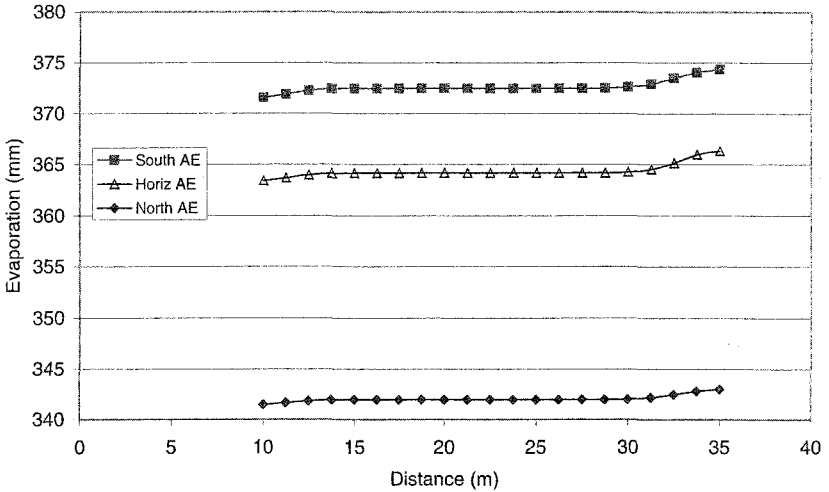
Figure 3: Actual evaporation rate along slope for base case (crest of slope located at distance = 10 m).

Design Information From Coupled Models

The previous example showed in a general way how the net radiation model could be coupled with a flux boundary model, to evaluate the impact of slope direction on evaporation. The following case shows a more design-oriented approach, to evaluate different cover thickness for obtaining equivalent cover performance.

Similar to the previous case, a simple monolayer cover is considered with the uncompacted Equity till placed over waste rock. For covers on sloped surfaces facing different directions, various cover thicknesses are compared, to identify cover configurations that will give comparable performance on opposing slopes.

When considering the performance of a cover for a design case, it is important to be clear on the design philosophy behind the cover. For a cover that is to act as a

moisture barrier, the most important design consideration is the total flux through the cover into the underlying waste (infiltration). For covers over potentially acid-generating waste rock that are designed to act as oxygen barriers (limiting acid generation), infiltration is a less important consideration that the degree of saturation that is maintained in the cover. In general terms, a high degree of saturation (at least 85%) needs to be maintained year-round through at least a portion of the cover profile, if the cover is to be an effective oxygen barrier. For both of these performance criteria, the actual evaporation that takes place from the cover is an important determinant of its behavior.

Alternative covers were evaluated with thicknesses that varied from 40 to 80 cm, with increments in thickness of 20 cm modeled. In this case, the program SoilCover (1993) was used for the analysis of a 1-D column of soil located on the slope. The underlying waste rock was modeled as a 2 m thick layer, with a lower boundary condition set to a constant soil suction (12 kPa), equivalent to the soil suction when the waste rock was at residual water content. Climate boundary conditions were taken from the ten-year average Equity weather data set previously discussed. Each case was modeled once with the original net radiation data from the data set, representing the horizontal case. The net radiation model was then used to transform the net radiation data to represent the cases of 2.5H:1V slopes to the north and the south.

Taking the case of a cover designed as an oxygen barrier, Figure 4 shows the average degree of saturation maintained in the lower 10 cm of the covers analyzed, as a function of the cover layer thickness. Trends shown on the graph show clearly that for this particular case, the north facing slope is better at maintaining saturation for a given thickness, and that the average degree of saturation maintained in the lower 10 cm of any cover increased with increased cover thickness.

Assuming a design criteria for the oxygen barrier cover that the lower 10 cm of the cover maintain an average degree of saturation of at least 90%, the results of the coupled models suggest that meeting this requirement would require that the cover be about 75 cm thick on the south-facing slope, while on the north-facing slope, a cover only 50 cm thick would be required to meet the same criteria. One can also see that the cover thickness needed on the horizontal portions of the cover would be comparable to the thickness required on the south slope.

That a thinner cover is needed on the north slope is a function of the fact that less evaporation takes place on the north slope. This is illustrated on Figure 5, which shows a comparison of the predicted evaporation rates on all slopes, again as a function of cover thickness. The rate of actual evaporation shown on Figure 5 varied considerably as a function of the direction faced by the slope, with the most evaporation on the south-facing slope. However, the thickness of the cover had a much less dramatic impact on evaporation rates. The slight increase in the predicted evaporation rate that did occur with thicker covers likely reflected the influence of increased moisture storage.
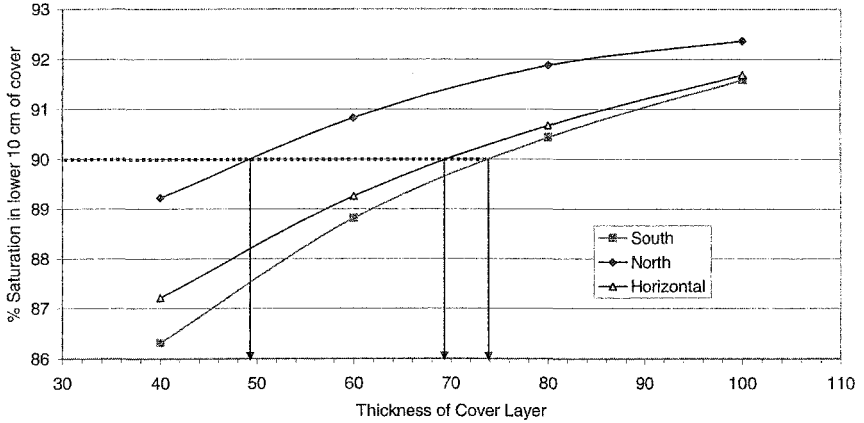
Figure 4: Average degree of saturation in the lower 10 cm of the uncompacted cover. (Arrows indicate thickness of cover required to maintain 90% saturation)
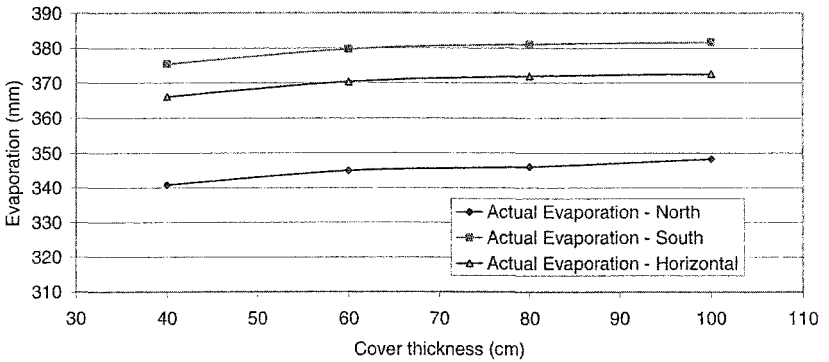
Figure 5: Effect of slope and cover thickness on actual evaporation from the uncompacted cover.

For the case of a cover designed as an infiltration barrier, Figure 6 shows the comparison of the performance of the various cover configurations in terms of moisture percolation through the cover into the underlying waste rock, as a function of cover thickness. Not surprisingly for a cover that consisted of a fairly permeable single soil layer, all of the profiles let through a significant portion of the annual precipitation – the values shown on Figure 6 range from 15 to 25% of the average annual precipitation at the site. However, to illustrate the design principal, a hypothetical design criteria is shown on Figure 6 for a maximum annual infiltration

through the cover of 100 mm. For this criteria, the south and horizontal faces would require a cover layer approximately 50 cm thick, while the north face would require a slightly thicker cover (62 cm thick) to obtain comparable performance. Interestingly, despite the differences in evaporation rate between the horizontal surface and the south-facing surfaces (shown on Figure 5), Figure 6 shows that in terms of percolation through the cover, the two cases perform almost identically.
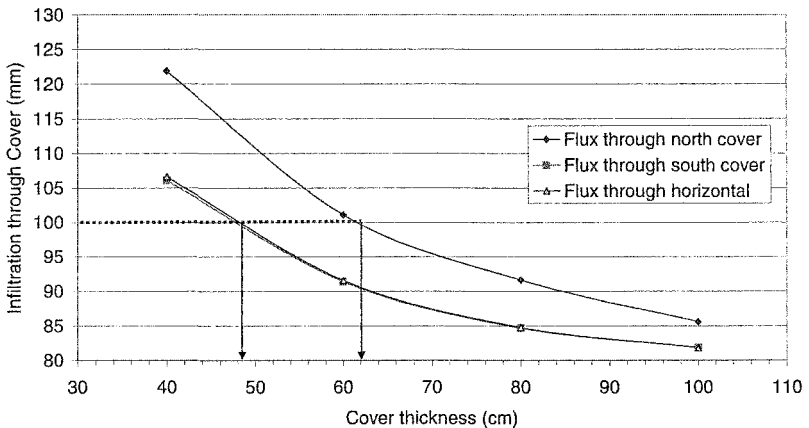
Figure 6: Effect of slope and cover thickness on annual infiltration through the uncompacted cover (Arrows indicate equivalent cover thicknesses for 100 mm infiltration limit).

These graphs illustrate a general approach that could be used for applying the net radiation model in conjunction with SoilCover to compare the performance of soil covers with different orientations at the same site. This type of approach could be used at any site and for any climate design.

Note that in evaluating the differences in cover thickness needed to obtain equivalent performance from covers facing different directions that the design criteria are key. For an oxygen barrier cover in this environment, a south-facing slope needs to be thicker than a north-facing slope to perform in an equivalent manner. Conversely, for a cover that is to act as an infiltration barrier, the north-facing slope would need to be thicker than the south-facing slope to obtain equivalent performance.

Summary

Finite element models such as SoilCover (1993) and Vadose/W (2003) have become well-established as tools used by engineers for the design and evaluation of soil covers on waste disposal sites. These tools allow the flux boundary conditions over unsaturated soils to be estimated, and used in the calculation of soil moisture conditions and infiltration for covers under a wide variety of environmental conditions. Using a model for the prediction of net radiation (Weeks and Wilson 2003) it has been demonstrated that the net radiation predictions for sloped surfaces can be incorporated to the boundary conditions of the finite element models, and used to predict the effect of slope orientation on flux boundary conditions.

Coupling the net radiation model with Vadose/W (2003), a simple sloped soil cover was analyzed for north and south facing slopes. For this particular case, it was apparent that the direction faced by the slope had a greater impact on the flux boundary conditions that the location considered along the slope. The same general approach can be used to evaluate the relationship between slope direction, angle, and location for evaporation and infiltration for any combination of climatic and soil conditions.

Coupling the net radiation model with SoilCover (1993) showed how the two models can be used to compare similar cover designs on different slopes, and to develop covers that perform in an equivalent manner despite differences in the local climate. Again, the approach illustrated would be applicable to a wide variety of soil and climate combinations.

References

Freeze, R. A. and Cherry, J. C. (1979). Groundwater, Prentice Hall, Englewood Cliffs, NJ.

O'Kane M.A. (1995) Instrumentation and monitoring of an engineered soil cover system for an acid generating mine waste. M.Sc. Thesis. (University of Saskatchewan, Saskatoon, Canada).

Oke, T. R. (1987). Boundary Layer Climates, Routledge, London and New York.

Raupach, M. R. and Finnigan, J. J. (1997). "The influence of topography on meteorological variables and surface-atmosphere interactions." Journal of Hydrology, 190, 182-213.

Sellers, P. J., Heiser, M. D., Hall, F. G., Verma, S. B., Desjardins, R. L., Schuepp, P. M., and MacPherson, J. I. (1997). "The impact of using area-averaged land surface properties - topography, vegetation conditions, soil wetness - in calculations of intermediate scale (approximately 10 km^2) surface-atmosphere heat and moisture fluxes." Journal of Hydrology, 190, 269-301.

SoilCover (1993) User's Manual.   Unsaturated Soils Group.   University of Saskatchewan. Saskatoon, Canda.

Swanson D.A., Barbour S.L., Wilson G.W., and O'Kane M. (2003). "Soil-atmosphere modelling of an engineered soil cover for acid generating mine waste in a humid, alpine climate." Canadian Geotechnical Journal, 40, 276-292.

SVflux (2004). SoilVison Systems Ltd., Saskatoon, Saskatchewan, Canada.

Weeks, B. and Wilson, G. W. (2004). "The Impact Of Slope And Aspect On Evaporation From Soils In Three Dimensions." 57th Canadian Geotechnical Conference, Session 2D:21-27.

Weeks, B. and Wilson, G. W. (2003). "The influence of solar radiation on evaporation for three-dimensional flux boundary modelling of soil cover systems on waste rock dumps." International Conference on Acid Rock Drainage (ICARD), 711-717.

Wilson, G. W. (1990). Soil Evaporative Fluxes for Geotechnical Engineering Problems. Doctoral Thesis. University of Saskatchewan.

Yang M. and Yanful E.K. (2002). "Water balance during evaporation and drainage in cover soils under different water table conditions." Advances in Environmental Research , 6, 505-521.

Vadose/W (2003) User's Manual. Geoslope International Ltd. Calgary, Canada.

DESIGNING ALTERNATIVE LANDFILL COVERS USING PARAMETRIC UNCERTAINTY ANALYSIS

Michael H. Young[1]*, William A. Albright[2], Karl F. Pohlmann[1], Greg M. Pohll[2], Walter H. Zachritz[3], Stephen Zitzer[4], David S. Shafer[5], Irene Nester[6], Layi Oyelowo[7]

[1]Division of Hydrologic Sciences, Desert Research Institute, 755 E. Flamingo Rd. Las Vegas, NV 89119-7363; PH (702) 862-5489; FAX (702) 862-5427; email: michael.young@dri.edu, karl.pohlmann@dri.edu.
[2]Division of Hydrologic Sciences, Desert Research Institute, 2215 Raggio Pkwy, Reno, NV 89512-1095; email: bill.albright@dri.edu, greg.pohll@dri.edu.
[3]National Park Service, Chesapeake Watershed CESU, 301 Braddock Road, Frostburg, MD 21532; email: Walter_Zachritz@nps.gov
[4]Division of Earth and Ecosystem Sciences, Desert Research Institute, 755 E. Flamingo Rd, Las Vegas, NV 89119-7363; email: stephen.zitzer@dri.edu.
[5]Center for Environmental Remediation and Monitoring, Desert Research Institute, 755 E. Flamingo Rd, Las Vegas, NV 89119-7363; email: david.shafer@dri.edu.
[6]Tybrin Corporation, 5 E. Popson Ave, Edwards AFB, CA 93524; email: irene.nester@edwards.af.mil.
[7]Environmental Management, 5 E. Popson Ave, Edwards Air Force Base, CA 93524; email: layi.oyelowo@edwards.af.mil.

ABSTRACT

This presentation describes a comprehensive effort to address landfill cover design using innovative numerical estimation methods with site-specific data. The sensitivity of predicted cover performance was evaluated while incrementally changing engineering variables including cover thickness, soil type, and percent plant cover. For each of the 72 different combinations of these variables, a Monte Carlo technique was used to vary soil hydraulic properties for 1000 simulations, with a statistical range determined by laboratory analyses of soil samples collected from the site. The multiple simulations represent a stochastic technique that allows for the variability of measurement results to be included in numerical predictions. Modeling results demonstrated that a minimum thickness for covers of all soil types and the presence of at least a minimum plant cover were necessary to prevent drainage of more than 0.5 cm/yr. Variations in both cover thickness and percent plant cover showed the presence of threshold values for each soil type tested, beyond which incremental additions added little to cover performance. The methods developed demonstrate innovative uses for numerical simulations, which can provide for cost effective cover designs and contribute to improved decision making by improving the technical basis for negotiating final cover systems with regulatory authorities.

INTRODUCTION

Landfill closure for most waste streams typically requires some means to predict final cover performance. Conventional designs that use a resistive barrier of low-conductivity materials (i.e., finer-grained soil and/or geomembranes) to impede drainage through the cover typically rely on specification of materials and methods and are not commonly subjected to a performance criterion such as a maximum drainage rate. In contrast, alternative cover designs, often called evapotranspiration (or ET covers), rely on development of a functioning system of soil, climate, and plants to maintain a favorable water balance and to minimize drainage. The site-specific nature of alternative cover designs requires a method to predict performance, given design variations, so that the results can be compared to regulatory standards. Furthermore, regulations for alternative designs for municipal waste under the Resource Conservation Recovery Act (RCRA) require demonstration of performance equal to or exceeding that of the minimum recommended (i.e. resistive barrier) design (USEPA, 1992). Numerous simulation codes are available that regard the landfill cover as an ecosystem with integrated components, and several have been used to predict performance of alternative cover designs. However, recent studies that compared simulated and field-measured drainage (i.e. the flow of water through the bottom of the simulated cover) have demonstrated the inconsistency of current codes and application methods to predict outcomes with the accuracy often desired for regulatory permitting activities (Albright et al., 2002; Scanlon et al., 2002). In some cases, the resulting uncertainty associated with simulated performance can exceed target performance standards. Debate among design engineers and regulatory analysts has touched on the role of simulation results in permitting activities and the question of how to incorporate uncertainty in the modeling approach.

One approach for capturing uncertainty in alternative cover design parameters (ITRC, 2003) is a "design sensitivity analysis" (DSA). DSA entails a pragmatic procedure whereby specific engineering design variables are systematically varied to allow evaluation of the resulting change in simulated performance. Deterministic evaluation of the trends in predicted performance, estimated as a function of one, two, or more important parameters (e.g., cover thickness, soil type, or plant cover), can provide a stronger basis for regulatory negotiation. There is also recognized variation of soil hydraulic properties within a soil type or borrow source that can influence cover performance, and this variation can be described in statistical terms. Despite the relatively small number of important hydraulic parameters, a substantial number of simulations is often required before the effect of these parameter distributions on predicted performance can be quantified.

Our technical analyses used for this study rely heavily on Monte Carlo simulation techniques to assess uncertainty in predicted performance. Monte Carlo simulation randomly varies model parameters within a statistical range of known characteristics (e.g., mean, variance and shape of the distribution) and leads to a related statistical distribution of outputs, described by the ensemble mean and variance. By varying an input parameter (i.e., soil hydraulic properties) the sensitivity of a dependent variable (i.e., drainage) can be evaluated in light of the statistical range of the parameter. In

this analysis, the soil hydraulic properties were treated as stochastic variables having known mean, variance, and distribution, and the soil type, percent plant cover, and cover thickness were treated as categories of known values. Unlike cover thickness, the soil hydraulic properties vary in a way that cannot be accounted for through typical engineering practices; therefore, varying this parameter around a mean with known variance accounts for the random nature of soil variability.

MATERIALS AND METHODS
Site Description

This research took place at Edward Air Force Base (EAFB), located northeast of Lancaster, California, USA, approximately 125 km north of Los Angeles in the western Mojave Desert, which is characterized by long, hot summers and short, mild winters. Average annual precipitation (P) since 1942 is 14.83 cm (5.84 in) and annual potential evapotranspiration (PET) is about 200 cm (78.7 in).

Site Characterization
Soil Material
Characterization of soil material required soil sampling and laboratory analysis of 13 available borrow sources at EAFB (nine existing and four proposed). Both saturated (saturated hydraulic conductivity, K_s) and unsaturated soil hydraulic properties (van Genuchten's α and n) were determined for each of the 39 soil samples (three samples from each of the thirteen borrow pits). Four soil types were described: an underlying layer of coarse partially decomposed granitic material (known as grus) and 3 different surface soils broadly classified as silty sands. Mean property values are found in Table 1.

Plant Communities
Mojave Desert plant communities were characterized by a combination of site visits and review of existing literature (e.g., Charlton, 1994). Native Mojave Desert plant communities consist of various proportions of evergreen shrubs, drought deciduous shrubs, perennial forbs and grasses, succulents, and winter annuals. Total perennial plant cover in Mojave Desert communities varies from 5 to 40 percent (Romney et al., 1973). For the systems at EAFB, a sustainable plant cover design could consist of a creosotebush-white bursage community with plant cover ranging from 15 to 20 percent; this study used a wider range of plant cover from 0 to 30 percent.

Climate
The precipitation data set chosen for the numerical simulations consists of daily values for a period of ten years. The daily precipitation records cover the period from 1974 through 1983, which had the highest 10-yr mean annual precipitation for any combination of ten consecutive years for the period of record (1942 through 2000). For the selected 10-yr period the mean annual precipitation was 20.46 cm (8.05 in) compared to the long-term average of 14.83 cm (5.84 in). The highest recorded

Table 1. Mean value of hydraulic properties determined from laboratory tests.							
	K_s		α	n	m	θ_s	θ_r
	cm/d	cm/s	1/cm	--	--	cm^3/cm^3	cm^3/cm^3
Surface soil #1	20.54	2.38E-04	0.028	1.441	0.306	0.033	0.396
Surface soil #2	84.62	9.79E-04	0.050	1.408	0.290	0.036	0.368
Surface soil #3	247.52	2.86E-03	0.022	1.690	0.408	0.032	0.386
Subsurface Grus	32.68	3.78E-04	0.024	1.363	0.266	0.041	0.383

annual total was 39.42 cm (15.51 in) in 1983, the lowest recorded annual total was 4.60 cm (1.81 in) in 1975 and precipitation during 8 of the 10 years was greater than the long-term mean.

Evaporation and Transpiration
The numerical approach requires input for potential transpiration (PT) and potential evaporation (PE). In this study we started with potential evapotranspiration (PET) and derived values for PT and PE as follows. Pan evaporation data were obtained from the Mojave, CA weather station between 1964 through 1978, located immediately northwest of EAFB, and were converted to average monthly values of PET by using a crop coefficient of 0.70 (Farnsworth and Thompson 1982). The average monthly values of PET were used for each year of the 10-yr simulations.

PET data were then partitioned into PE and PT values based on seasonal changes in PT, the degree of plant cover, and the uptake phenology of the plants that typically populate the southwestern Mojave Desert. Using a mixed canopy structure with fixed percentages of evergreen shrubs, drought deciduous shrubs, perennial forbs and grasses, and winter annuals, similar to that observed at EAFB, an aggregate of individual leaf area indexes, LAI, was calculated (Kemp et al., 1997). Four different % covers were used (0, 10, 20, and 30%). Total PET was partitioned into PT and PE using the method of Kemp et al. (1997) who partitioned the solar radiation component of the energy budget by canopy interception. Table 2 shows the partitioning.

Using the previous description of desert plant phenology, water uptake was assigned as percentages of PET to evergreen shrubs (25 percent PET), winter annuals (between 20 percent and 37 percent PET, depending on time of year and winter rainfall), and drought-deciduous shrubs (17 percent of PET, also depending on the time of year). Winter precipitation is important for seed germination, so uptake by winter annuals and drought-deciduous shrubs was reduced and zeroed, respectively, for those years when winter rainfall (between 1 November and 28 February) was less than 26.8 mm (~ 1 inch). Figure 1 illustrates how PT was distributed throughout each year of the 10-yr period for a plant cover scenario of 30 percent.
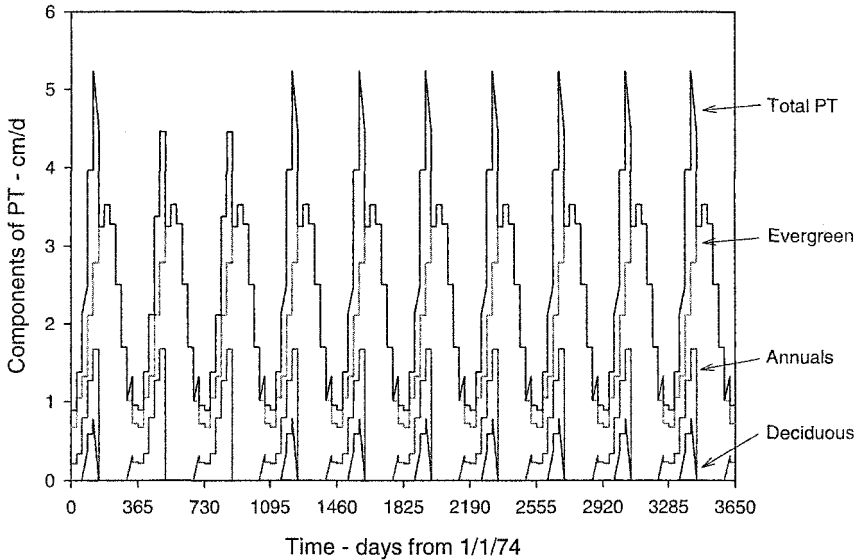
Figure 1. Time series of PT for 10-yr period, assuming 30 percent cover.

Numerical Implementation

Model and Dataset Descriptions

HYDRUS-2D (Šimunek et al., 1999), a finite element code which numerically solves Richards' equation for variably saturated porous media, was used for the design sensitivity analysis. The model was assigned a free drainage (unit gradient) bottom boundary condition that represents the base of the cover and the sides of the domain were assigned a no-flow condition. The atmospheric upper boundary includes the 10-yr precipitation record and the estimates of PET, partitioned into PE and PT. Daily values of precipitation were used and the precipitation was distributed evenly across each 24-hr time period. Root zone distributions were used to specify the location in the model of water loss due to transpiration and were calculated for each of the modeled geometries using the approach of Vrugt et al. (2001) to account for variations in the thickness of surface soil. Root zone distributions were limited to surface soil only, and prohibited from penetrating the subsurface (grus) layer. Actual transpiration is controlled in HYDRUS-2D by a stress response function with specified values for wilting point, anaerobiosis point, and pressure heads corresponding to optimal water uptake as defined by Feddes et al. (1978). Required soil hydraulic parameters include saturated hydraulic conductivity, saturated and residual water content, and the van Genuchten (1980) parameters (α and n). The van Genuchten-Mualem unsaturated hydraulic conductivity function was used. Initial conditions are specified as pressure head in the soil profile.

Table 2. Partitioning of potential evapotranspiration into components of plant transpiration and soil evaporation for a specific canopy structure.

Growth Form	% of Canopy	LAI Multiplier	Ground Cover			
			0%	10%	20%	30%
Evergreen	0.25	0.65	0	0.016	0.033	0.049
Annuals	0.20	1.17	0	0.023	0.047	0.070
Deciduous	0.35	5.70	0	0.200	0.399	0.599
Grass/forb	0.20	5.97	0	0.119	0.239	0.358
		Sum	0	0.359	0.717	1.076
		PT (canopy)	0%	20.1%	36.1%	48.9%
		PE (soil)	100%	79.9%	63.9%	51.1%

Table 3. Statistics for Monte Carlo simulations.

Distribution Parameters[†]				Factored Covariance Matrix			
m	A	B	Distribution		α	n	K_s
-3.71	---	---	Lognormal	α	0.522	---	---
1.42	---	---	Normal	n	-0.021	0.129	---
-1.10	1	100	Log ratio	K_s	0.192	0.148	0.600
Distribution Parameters				Factored Covariance Matrix			
m	A	B	Distribution		α	n	K_s
-3.00	---	---	Lognormal	α	0.251	---	---
1.43	---	---	Normal	n	-0.016	0.113	---
-1.00	25	250	Log ratio	K_s	0.514	0.232	0.210
Distribution Parameters				Factored Covariance Matrix			
m	A	B	Distribution		α	n	K_s
-2.95	---	---	Lognormal	α	0.381	---	---
1.65	---	---	Normal	n	-0.100	0.055	---
-0.50	100	500	Log ratio	K_s	0.591	0.271	0.047
Distribution Parameters				Factored Covariance Matrix			
m	A	B	Distribution		α	n	K_s
-3.70	---	---	Lognormal	α	0.765	---	---
1.51	---	---	Normal	n	0.022	0.201	---
-4.01	0.2	2000	Log ratio	K_s	1.843	0.194	1.701

[†] m, A, B are the mean, lower and upper limit of the lognormal distribution used for K_s.

Six 1-dimensional geometries were selected for the Monte Carlo simulations. Each geometry combined different thicknesses of the topsoil and underlying grus layer, with total thicknesses starting at 46 cm and increasing in thickness to 122 cm. The number of nodes used in the simulation increased with cover thickness, with an average element thickness of ~0.5 cm. A variable grid density was used so that the upper boundary had an element thickness of <1 mm and the bottom boundary had an element thickness of ~1 cm.

Monte Carlo Implementation

The DSA used an uncertainty approach to evaluate how slight changes in cover design and material properties might affect the long-term drainage (i.e. the flow of water across the bottom boundary of the model). Saturated hydraulic conductivity and the two shape parameters (α and n) were assumed to be uncertain in the stochastic analysis.

Parameter values for each of the four soils under study were obtained from the laboratory analyses. A mathematical transformation was then selected for each variable such that the transformed variable yielded a normal distribution function. For all soil types, a lognormal and log ratio transformation were used for alpha and saturated hydraulic conductivity, respectively. The van Genuchten shape parameter (n) did not require a transformation to yield a normal probability density function. After the appropriate transformation was established, the laboratory values were used to determine the mean and sample covariances among the transformed variables. Because each transformed variable is normally distributed, a multivariate normal distribution was selected to represent the joint probability density function for the uncertain variables. The required statistics for the Monte Carlo simulations are shown in Table 3. The multivariate normal distribution for the transformed variables yielded a partial correlation when the uncertain variables were randomly generated.

RESULTS AND DISCUSSION

Figure 2 shows the frequency distribution of the simulated K_s for the surface soils and underlying grus used in the Monte Carlo simulations. Differences in the mean K_s can be seen for each of the three surface soil types (Fig. 2a). We note that an insufficient number of samples for the surface soils were available to verify the log-normal distributions; however, for the purposes of illustrating the effects of different soil properties on drainage, we assumed that the samples followed a log-normal distribution and generated K_s values. As an example, the distribution of the grus soil (Fig. 2b) did show a more distinct log-normal-type distribution, with K_s results ranging from less than 10 cm/d (1.2×10^{-4} cm/s) to over 1800 cm/d (2.1×10^{-2} cm/s) (mean value = 36 cm/d, or 4.2×10^{-4} cm/s).

The results of the simulations are represented in three nomograms that show how drainage changes as a function of cover thickness and vegetative cover (Fig. 3). The general shapes of the nomograms are very similar, though some differences are apparent between soil types. A large percentage (75%) of the total combinations of cover thickness and percent plant cover led to drainages below 0.5 cm/yr, whereas
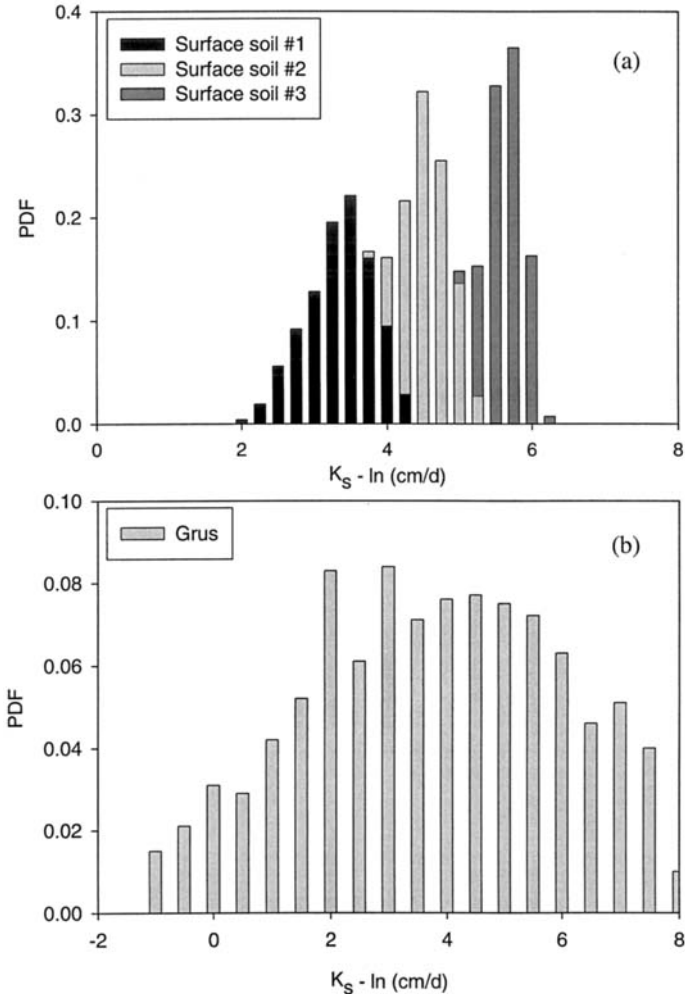
Figure 2. Statistical distributions of saturated hydraulic conductivities for surface soils (a) and underlying grus (b). Distributions were generated using results of laboratory analyses of field soil samples collected at EAFB borrow sources.

Surface soils #2 and #3 with higher K_s had fewer combinations yielding this low level of drainage (65% and 25% respectively). Each nomogram has specific regions where the ensemble average of the mean annual flux (MAF) is high (>1 cm/yr), and regions where the MAF is significantly reduced (i.e., below 0.5 cm/yr). The nomograms show clear trends toward decreasing MAF for thicker covers and those that have higher percent vegetative cover. Thicker covers clearly reduce drainage because the
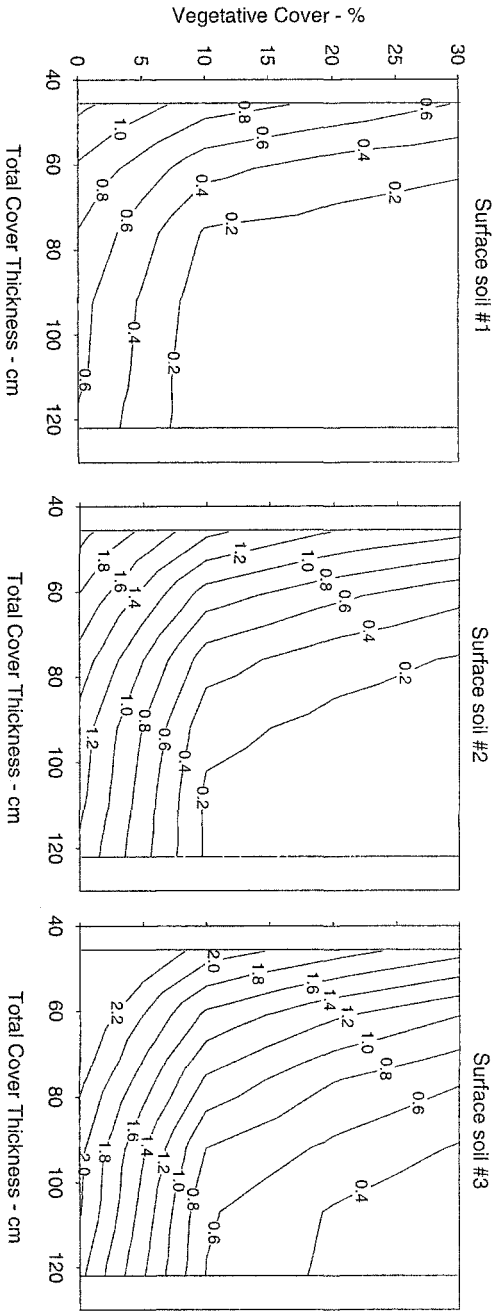
Figure 3. Nonogram showing average drainage for 10-yr simulations. Units are in cm/yr for all three nonograms.

water holding capacity of the thicker soil is higher, allowing the cover to act as a "store and release" feature that holds the water within the profile and makes it available for soil evaporation and/or plant transpiration. In very thin covers, like those at 46 cm, drainage is higher regardless of the presence or absence of plants, because the water percolates below the base of the cover before ET processes can act. As the covers thicken, the effect of the higher water holding capacity can be seen in every combination of percent vegetative cover and surface soil type. Adding soil to the cover and increasing the water holding capacity provides marginal improvements on cover performance when thickness reaches a certain threshold, between 70 cm and 85 cm depending on soil type.

A significant dependency on the presence of plants was observed, where no combination of soil type and thickness, tested without plants, reduced estimates of drainage below 0.5 cm/yr. Increasing percent plant cover from 0 to 10% significantly reduced drainage regardless of the cover thickness or the soil type, but additional increases in percent plant cover had less effect. Figure 4 shows this result for Surface soil #1. In this example, more intensive revegetation yields progressively fewer benefits when considered in terms only of drainage reduction; adding vegetation to the thinner cover systems reduced the drainage only marginally (from 1.25 cm/yr to 0.59 cm/yr). Thicker soil covers, for example 107 cm, experienced a more significant reduction in drainage as the percent plant cover was increased from 0 to 30% (from 0.59 cm/yr to 0.02 cm/yr).

CONCLUSIONS

In this project, on-site soil, climate and plant community data were included in a sensitivity analysis using a Monte Carlo-based numerical estimation scheme to estimate the performance of earthen landfill covers of various designs for a location in southeastern California. The Monte Carlo modeling approach systematically varied input parameters (soil type, cover thickness, plant cover) according to either their categorical range or statistical description. The results provide a range of potential drainages, and hence a means to directly compare the benefits or limitations of different designs. The nomograms used to present the results show clear trends toward decreasing mean annual drainage for covers that thicken and those that have higher vegetative cover. In the former case, thicker covers clearly reduce estimates of drainage, because the water holding capacity of the cover increases as it becomes thicker. As expected, a significant dependency on the presence of plants was observed and no combination of soil type and thickness tested without plants reduced estimates of drainage below 0.5 cm/yr. Increasing percent plant cover from 0 to 10% significantly reduced drainage; further increases in percent plant cover reduced the drainage, but at a slower rate. These observations show that reductions in drainage are maximized only by considering the interactions between soil hydraulic properties, cover thickness, and percent plant cover. It is apparent that relative benefits of adding more soil to a landfill cover will reduce drainage only to a point. Likewise, the effort needed to establish some vegetative cover at this arid site will significantly
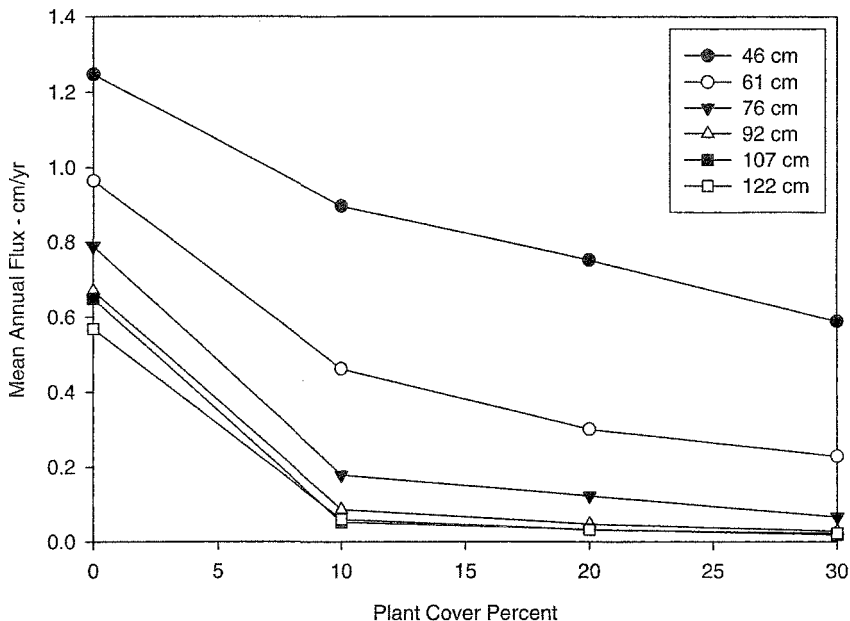
Figure 4. Drainage as functions of percent plant cover and cover thickness for Surface soil # 1.

reduce drainage, but marginal improvements in drainage reduction were seen after the percent plant cover was higher than 10%. By constructing a cover thick enough to store winter-dominated precipitation, and then establishing a plant canopy capable of removing that water, drainage can be minimized.

Results of the analyses presented here show more than predictions of performance; they explain the way design parameters and environmental stresses combine in the mechanisms that determine cover performance. The process of permitting an alternative final landfill cover properly addresses primarily questions of uncertainty and the approach taken here evaluated the uncertainties in design and environmental parameters that may affect cover performance, and yielded a series of analytical tools that allow rapid assessment of performance. The intent of this research was to develop and illustrate an approach for designing cost-effective covers, not to design any cover per se. These procedures could thus be used for any site where soil properties, plant community characteristics and climate are appropriate for ET covers, simply by identifying design parameters (material thickness, and plant cover), and then incorporating the material variability into the analyses.

REFERENCES
Albright, W. H., Gee. G. W., Wilson, G. V., and Fayer, M. J. (2002). "Alternative Cover Assessment Project, Phase I Report." *DRI Report No. 41183*. Desert Research Institute, Nevada System of Higher Education, Reno, NV.

Charlton, D. (1994). "Plant species of Edwards Air Force Base". *Letter of Technical Direction 17P4D0017*, completed under Contract F04611-92-C0045.

Farnsworth, R.K. and E.S. Thompson. (1982). "Mean monthly, seasonal, and annual pan evaporation for the United States". *NOAA Technical Report NWS 34*. Office of Hydrology, NOAA

Feddes, R.A., Kowalik, P.J., Azradny, H., (1978). "Simulation of field water use and crop yield". John Wiley and Sons, New York.

Interstate Technology & Regulatory Council. (2003). "Technical and Regulatory Guidance for Design, Installation, and Monitoring of Alternative Final Landfill Covers". Prepared by the Alternative Landfill Technologies Team.

Kemp, P.R., J.F. Reynolds, Y. Pachepsky,J-L Chen. (1997). "A comparative modeling study of soil water dynamics in a desert ecosystem". *Water Resources Research*. 33:73-90.

Romney, E. M., V.Q. Hale, A. Wallace, J.D. Childress, D. Kaaz, G.V. Alexander, J.E. Kinnear, and T.L. Ackerman. (1973). "Some Characteristics of Soil and Perennial Vegetation in the Northern Mojave Desert areas of the Nevada Test–Site". *Atomic Energy Commission Report AT (04-1)*.

Scanlon, B.R., M. Christman, R.C. Feedy, I. Porro, J. Šimunek, G.N. Flerchinger. (2002). "Intercode comparisons for simulating water balance of surficial sediments in semiarid regions". *Water Resources Research* 38 (12):1323-1339.

Šimunek, J., M. Šejna, and M. Th. van Genuchten. (1999). "HYDRUS-2D/MESHGEN-2D software for simulating water flow and solute transport in two-dimensional variably saturated media. Version 2.0". IGWMC-TPS–53C, International Ground Water Modeling Center, Colorado School of Mines, Golden, CO, 227 pp.

USEPA, (1992). "USEPA Subtitle D clarification. 40 CFR 257 and 258. EPA/OSW-FR-92-4146". *Fed. Regis.* 57:28626-28632.

van Genuchten, M.Th. 1980. A closed-form equation for predicting the hydraulic conductivity of unsaturated soils. Soil Sci. Soc. Am. J. 44: 892-898.

Vrugt, J. A., J. W. Hopmans, and J. Šimunek. (2001). "Calibration of a two-dimensional root water uptake model for a sprinkler-irrigated almond tree". *Soil Sci. Soc. Am. J.* 65 (4): 1027-1037.

Decision Analysis for Design of Evapotranspirative Landfill Covers

John S. McCartney[1] and Jorge G. Zornberg[1]

[1]Department of Civil, Architectural and Environmental Engineering, The University of Texas at Austin, 1 University Station, Austin, TX 78712-0280; PH (512) 232-3595; FAX (512) 471-6548; email: jmccartney@mail.utexas.edu

Abstract

A decision framework was developed to identify the optimal cover thickness, soil type, and soil density for an evapotranspirative landfill cover. A simplified model was used to consider the hydraulic performance of several cover alternatives during a design precipitation event, neglecting effects of interflow, surface water runoff, and moisture removal due to evapotranspiration. Monte Carlo simulation was used to estimate the probability of failure of each alternative given a selected failure criterion. Expected costs for each alternative were calculated using the probability of failure and the costs associated with implementation, compaction effort, and failure. The optimal alternative was identified as having the lowest expected cost.

Introduction

The management of waste generated by a growing population is an important topic for regulators and engineers. The current trend in waste management is the isolation of waste in protected containment facilities to minimize human and environmental contact. Accordingly, one of the key engineered components in municipal and hazardous waste containment systems is the cover system. The objective of a cover system is to prevent infiltration of water into the waste, which is often translated as a design that minimizes basal percolation. If water reaches the waste, it may mobilize contaminants that may eventually reach the groundwater.

One particular cover type, the evapotranspirative (ET) cover, is gaining popularity in arid climates (Dwyer 1998; Zornberg *et al.* 2003). Conceptually, an ET cover is a simple system that involves a monolithic soil layer with a vegetative cover. Evapotranspiration and moisture storage play significant roles in the performance of this system. An ET cover acts not as a barrier, but as a reservoir that stores moisture during precipitation events and subsequently returns it to the atmosphere as evapotranspiration. ET covers are generally constructed using low plasticity silts and

clays placed at different relative compactions to satisfy design values of moisture storage, saturated hydraulic conductivity, desiccation cracking potential, and ability to support vegetation. ET covers are relatively simple to construct, require low long-term maintenance, and may provide significant cost savings (Zornberg *et al.* 2003). As ET covers function with a reasonably broad range of soils, much of the cost savings result from constructing these covers using local soils.

A decision analysis is presented in this paper using experimental data obtained as part of the design process of a multi-acre ET landfill cover (Zornberg and McCartney 2003). A significant testing program was conducted for this site to characterize soil hydraulic properties for identification of appropriate borrow sources, and to characterize the site meteorology. Further, a field monitoring program was conducted at the site to evaluate the actual performance of several prototype covers with different soil types and cover thicknesses. For simplicity, this study focuses on cover design using the information available from the laboratory testing program (*i.e.*, a prior analysis), while the field monitoring results will be used in a future study to refine the design process (*i.e.*, a Bayesian posterior analysis). A decision framework is presented to objectively consider the optimal cover thickness, soil type, and soil-placement conditions given a design precipitation event (intensity and duration). A simple performance model for ET covers is used to evaluate the suitability of the framework for cover design. An example with a hypothetical set of construction and failure costs is used to evaluate different cover alternatives on a minimal cost basis.

Design of Evapotranspirative Cover Systems

The goal of an ET cover is to minimize basal percolation over a multi-acre area for the lowest cost possible. There are several tradeoffs between performance and cost that must be considered when selecting appropriate values of the relevant design variables. The primary design variables that must be considered include the cover geometry, soil hydraulic properties, vegetative cover properties, design precipitation event, and initial conditions (*e.g.*, the soil moisture storage at the time of the design precipitation event).

Cover geometry variables include the thickness of the cover T, as well as the cover slope angle β. As the performance of the cover soil depends on its capacity to store liquid, a thicker cover will have a higher moisture storage capacity. The slope of the cover will determine both its stability as well as the amount of surface water runoff during a precipitation event. The slope angle can be considerable in some covers such as the OII landfill in Pomona, California (Zornberg *et al.* 2003).

The soil hydraulic properties relevant to the performance of ET covers include the saturated hydraulic conductivity (K_{sat}), the soil-water retention curve (SWRC), and the K-function. The SWRC is the relationship between soil suction and moisture content, which can be used to determine the moisture storage capacity of the soil. The saturated hydraulic conductivity provides a measure of the minimum impedance to moisture flow through the cover, while the K-function provides a measure of the

increased impedance to moisture flow as the soil dries out (decreasing the available pathways for water flow). Determining the required soil hydraulic properties is perhaps the most challenging aspect of ET cover design. Target values of the hydraulic properties are typically selected based on the required cover performance under the expected precipitation conditions at the site. The target values can be obtained using numerical modeling or judgment, and are useful to identify acceptable soil types from local borrow areas. However, even when target values are selected, the methods used to evaluate hydraulic properties in the laboratory are highly sensitive to sample preparation and testing procedures. In particular, the relative compaction of the soil and its compaction moisture content will typically determine the soil's hydraulic properties. Finally, the hydraulic properties determined in the laboratory are often different from those in the field (Daniel *et al.* 1984). In addition to specimen preparation variability, the field hydraulic properties may change with time due to processes such as hysteresis (different behavior during wetting and drying), soil cracking, settlement, plant or animal intrusion, and erosion. Practically, hydraulic properties are typically selected at a site by characterizing soils from different local borrow sources placed at several densities, and comparing the experimental hydraulic properties with target values.

Vegetative cover properties are those that determine the amount of water that can be removed from the cover. Evapotranspirative covers should perform adequately without the assistance of plants for removal of water from the cover. This is especially relevant for locations that may suffer from prolonged droughts. Because this study considers the cover behavior during an infiltration event, this study does not consider the moisture removal properties of a vegetative cover.

As meteorological conditions are highly site specific, they are critical to the selection of the required cover thickness and soil properties. Design typically involves use of numerical models to determine the performance of the cover under the actual precipitation and evapotranspiration recorded at the site (Zornberg and McCartney 2005). For simplicity, this study considers only a design precipitation event and neglects moisture removal processes during this event.

Decision Analysis

Among the decisions to be made in the design of ET covers, the choice of the cover thickness may have the greatest impact on cover performance and cost. A thicker cover can store more water, but will increase costs due to greater soil requirements. This may also have implications on the selection of the particular borrow sources for cover soils. The decision process must also evaluate the tradeoffs between the hydraulic properties of the soils from the available borrow sources, which are often sensitive to the soil-placement conditions (density). Given a design precipitation event, the particular combinations of design variables will lead to cover success or failure. As the hydraulic properties for a given soil type and soil density were obtained from available test results, this study is classified as a prior analysis. A decision tree for an ET cover is shown in Figure 1. More information on the use of

decision trees may be obtained from Ang and Tang (1990). In this tree, the squares denote decision nodes, while the circles denote chance nodes. The tree is shown in collapsed form: starting from the left, each open-ended alternative is connected to the next set of branches. In other words, once the thickness is selected, the soil type must be selected, and then the density must be selected. For each combination of alternatives, a likelihood of success or performance can be calculated by assuming a performance model, a failure criterion, and an approach to consider uncertainty. This study uses a Monte Carlo analysis to consider uncertainty.
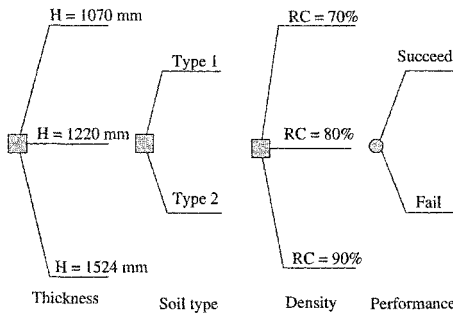
Figure 1: Decision tree for ET cover design

The decision framework can be evaluated on a minimum cost or maximum utility basis. As an example, this study assumes hypothetical values of costs for each alternative (*e.g.*, a cover with a given thickness, soil type, and density) to evaluate the framework on a minimum cost basis. Soil transportation costs of $120,000 and $100,000 per 1-m thickness were selected for soil types 1 and 2, as the borrow source for soil type 1 is further from the site. Soil compaction is assumed to cost $10,000 for 70% relative compaction, $20,000 for 80% relative compaction, and $40,000 for 90% relative compaction. These compaction costs were selected to incorporate construction costs as well as possible costs required to establish plant growth in denser soil. Failure criteria used for ET covers typically do not indicate catastrophic failure (McCartney and Zornberg, 2002). However, excessive percolation may require increased maintenance costs, such as addition of amendments to the soil or improvement of the vegetative cover health. Accordingly, the failure cost is assumed to be related to the probability of failure given from the performance model as $50,000$p_f$. In summary, the costs assumed for this example penalize thicker covers, longer soil transportation distances, denser cover soil, and cover soils that are not hydraulically suitable for a design precipitation event. The costs were arbitrarily assigned, and are used only to analyze the features of the decision framework.

Performance Model

Vertical flow of water through a soil layer under unsaturated conditions requires the numerical solution of Richards' equation, given by:

$$\frac{\partial \theta}{\partial \psi} \frac{\partial \psi}{\partial t} = \frac{\partial}{\partial z}\left[K(\psi)\left(1+\frac{\partial \psi}{\partial z}\right)\right] \tag{1}$$

where z is the depth from the surface of the cover, t is time, θ is the volumetric moisture content, ψ is the soil suction, $\delta\theta/\delta\psi$ is the slope of the SWRC, and $K(\psi)$ is the K-function. To avoid long computation times associated with solving Richards' equation for different hydraulic parameters simulated using Monte Carlo analysis, a simple load-capacity model was developed to estimate the hydraulic response of the landfill cover to a design precipitation event (described by intensity and duration). The field capacity is used as a measure of the moisture storage of the cover. The field capacity can be thought of as the moisture content at which water will drain from the soil under its own weight.   In other words, field capacity is reached during an infiltration process when the gravity potential of the water exceeds the pressure head potential of the water.   Water will want to flow downward instead of being held within the soil pores.   The field capacity is typically calculated as the moisture content corresponding to a suction of 33 kPa, calculated from the SWRC.   This rule-of-thumb is generally accepted to be representative of the field capacity in most soil types (sand, silt, clay).   The van Genuchten model (van Genuchten 1980) was used to characterize the SWRC for the different soils, given by:

$$\theta_{fc} = \theta_r + (\theta_s - \theta_r)\left[1 + \left(\alpha\psi_{fc}\right)^N\right]^{-\left(1-\frac{1}{N}\right)} \tag{2}$$

where θ_{fc} is the field capacity moisture content, ψ_{fc} is the suction at field capacity equal to 33 kPa, θ_r is the residual moisture content, θ_s is the saturated moisture content (equal to the porosity), and α and N are shape factors.

The moisture storage capacity (MSC) of the cover can be calculated using the thickness of the cover, the moisture content at field capacity, and the moisture content at the initiation of the design precipitation event θ_i, as follows:

$$\text{MSC} = (\theta_{fc} - \theta_i)T \tag{3}$$

In this simple model, the amount of moisture that infiltrates into the cover during a design precipitation event is assumed to depend both on the characteristics of the precipitation event and the impedance of the cover to moisture flow. The minimum impedance of the cover to moisture flow is the saturated hydraulic conductivity. For a precipitation event with an infiltration rate I and duration D, it is assumed that the amount of moisture that infiltrates into the cover during the event (M_{in}) is equal to:

$$M_{in} = \begin{cases} K_{sat}D \text{ if } I > K_{sat} \\ I D \text{ if } I < K_{sat} \end{cases} \tag{4}$$

This implies that if the infiltration rate is less than the saturated hydraulic conductivity of the soil, moisture will enter the soil at a rate equal to I. Otherwise moisture will enter at the saturated hydraulic conductivity. Eq. (4) assumes a unit gradient in the total head, representative of gravity-driven flow, and neglects surface ponding. However, water infiltration into the cover will occur at a higher rate due to matric suction gradients greater than unity corresponding to low suction at the soil surface and a higher suction corresponding to the initial moisture content. Accordingly, the assumption of a unit gradient may represent unconservative estimate of the moisture infiltrated into the cover. To account for this in the simplified model, the duration of precipitation was overestimated by 20%.

The failure criterion selected for this study is the event for which the amount of moisture entering the cover exceeds the MSC. Although this criterion indicates failure when percolation initiates, drainage from the soil will continue to occur after failure, resulting in significant percolation. Future research will incorporate different performance criteria proposed in the literature (McCartney and Zornberg 2002) using numerical solutions of Richards' equation for given atmospheric boundary conditions.

Statistical Evaluation of Model Parameters

Soil Properties. The saturated hydraulic conductivity and the van Genuchten parameters governing the shape of the SWRC parameters (α, N, θ_s, θ_r) were considered to be random variables in this analysis. Two soil types were identified at the site for hydraulic characterization, referred to as Soil type 1 and Soil type 2. Both soils have similar mineralogy, and are classified as clays of low plasticity (USCS type CL). Soil type 1 has a fines content ranging from 37 to 40%, while Soil type 2 has a fines content of 53 to 67%. A total of 4 specimens from different borrow sources and depths from the surface were identified as Soil type 1, while a total of 8 specimens from other borrow sources were identified as Soil type 2. K_{sat} and the SWRC were determined for specimens from each soil type placed at optimum water content at relative compactions of 70, 80, and 90% with respect to the maximum dry density obtained using the Standard Proctor compaction energy (for a total of 12 specimens from Soil type 1 and 24 specimens from Soil type 2). Flexible wall permeameter tests were used to define the K_{sat} values for specimens, while a combination of the pressure plate, hanging column, chilled mirror hygrometer, and thermocouple psychrometer were used to determine the drying path of the SWRC. This study uses the drying path SWRC to estimate the field capacity moisture storage during infiltration.

Figure 2(a) shows the variation in hydraulic conductivity with the actual relative compaction of each specimen (*i.e.*, not the target relative compactions). This figure indicates a decrease in saturated hydraulic conductivity of 7 orders of magnitude when RC increased from 65% to 95%. Figure 2(b) shows the variation in the mean hydraulic conductivity $E(K_{sat})$ for the two soil types with increasing relative compaction, with 95% confidence bounds. This figure replicates the increasing trend, and indicates that variability tends to increase with increasing relative compaction.
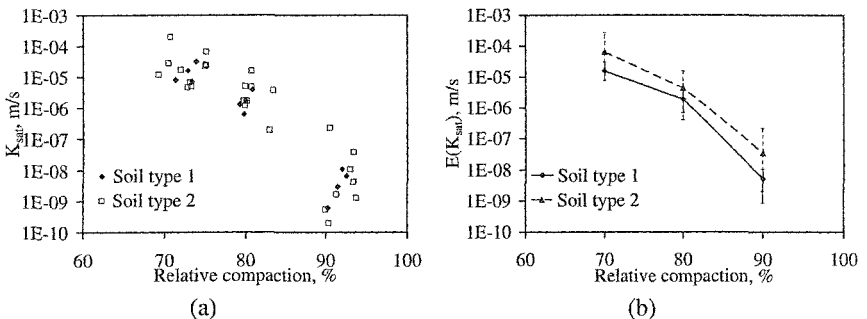
Figure 2: (a) Variation in K_{sat} with relative compaction; (b) $E(K_{sat})$

Table 1 summarizes the statistical descriptors for the saturated hydraulic conductivity values. Despite some scatter, the coefficient of variation (c.o.v.) increases with relative compaction for Soil types 1 and 2. This indicates that variability in hydraulic conductivity increases with increasing relative compaction. This is supported by the wide range in hydraulic conductivity values observed for specimens compacted at high densities in Figure 2(a). The cumulative density functions for the K_{sat} data indicates a lognormal distribution can be used to estimate its probability distribution.

Table 1: Statistical descriptors for the saturated hydraulic conductivity

Descriptor of K_{sat}	Soil type 1			Soil type 2		
	RC = 70%	RC = 80%	RC = 90%	RC = 70%	RC = 80%	RC = 90%
Mean (m/s)	1.56E-05	1.88E-06	5.33E-09	6.41E-05	4.32E-06	3.60E-08
St. dev. (m/s)	9.56E-06	1.23E-06	3.93E-09	9.14E-05	4.72E-06	7.43E-08
c.o.v.	0.61	0.65	0.74	1.43	1.09	2.06
Min. (m/s)	7.2E-06	6.2E-07	6.2E-10	4.7E-06	1.9E-07	2.0E-10
Max. (m/s)	3.1E-05	3.9E-06	1.1E-08	2.8E-04	1.6E-05	2.3E-07

Figures 3(a-c) show the SWRCs for the 12 different soil specimens (labeled 1A to 1D, and 2A to 2G) tested under relative compactions of 70, 80, and 90%. As a reference, the dashed vertical lines in Figures 3(a-c) denote the field capacity suction of 33 kPa. The field capacity varies between 12% and 40% for the soils tested.
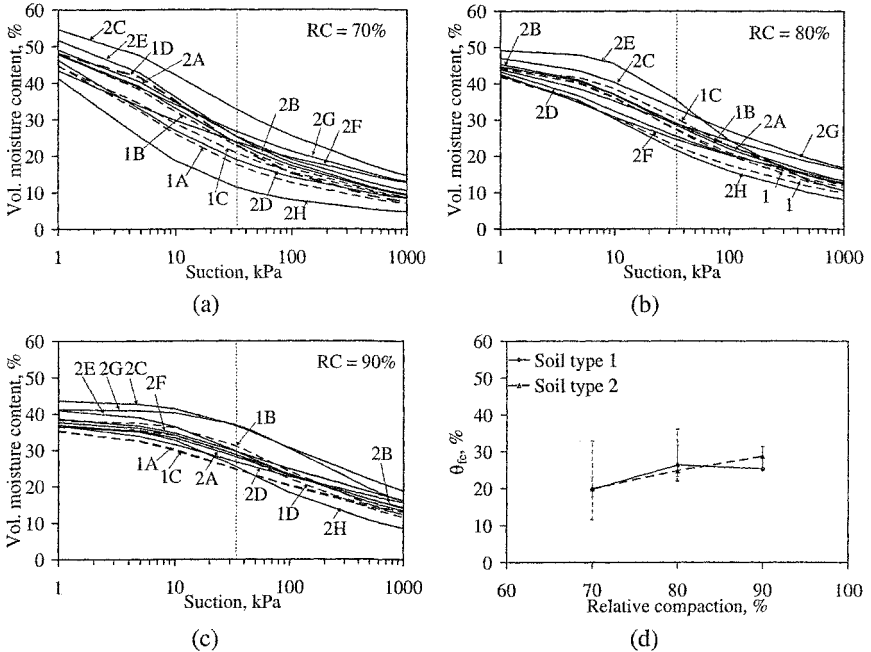
Figure 3: SWRC results: (a) 70% relative compaction; (b) 80% relative compaction; (c) 90% relative compaction; (d) Moisture content at field capacity

In general, the porosity (θ_s) decreases with increasing relative compaction, and the rate of decrease in moisture content with suction decreases with relative compaction (*i.e.*, the soil will hold more water at higher suctions for denser soils). Figure 3(d) shows the moisture contents at field capacity for the two soil types with increasing relative compaction, along with 95% confidence bounds. In general, the field capacity increases linearly with relative compaction, although the variability is higher at lower relative compactions. Table 2 shows the statistical descriptors of the SWRC parameters. In the Monte Carlo analysis, the SWRC parameters were modeled using lognormal distributions as they are strictly positive for soils, and because of the multiplicative combination of the parameters in the SWRC function [Eq. (2)].

Table 2: Statistical descriptors for the SWRC parameters

| Relative compaction (%)	Descriptor	Soil type 1					Soil type 2				
		α (kPa^{-1})	N	θ_s (%)	θ_r (%)	θ_{fc} (%)	α (kPa^{-1})	N	θ_s (%)	θ_r (%)	θ_{fc} (%)
70	Mean	0.004	1.38	49.59	2.83	39.07	0.007	1.32	52.46	1.99	37.58
	St. dev.	0.002	0.07	0.99	0.75	0.02	0.007	0.11	2.56	1.63	0.06
	c.o.v.	0.385	0.05	0.02	0.26	0.00	0.975	0.08	0.05	0.82	0.00
	Min.	0.002	1.31	48.67	2.06	17.71	0.003	1.18	47.56	0.00	11.53
	Max.	0.005	1.49	51.26	3.78	23.09	0.025	1.55	56.79	4.21	32.86
80	Mean	0.002	1.30	44.70	1.27	40.90	0.003	1.26	46.69	0.77	40.04
	St.dev.	0.001	0.02	0.55	0.26	0.03	0.003	0.10	1.48	1.31	0.05
	c.o.v.	0.502	0.01	0.01	0.21	0.00	0.821	0.08	0.03	1.70	0.00
	Min.	0.001	1.27	43.87	0.94	23.18	0.000	1.17	44.24	0.00	22.01
	Max.	0.003	1.32	45.35	1.67	30.77	0.009	1.52	49.41	4.13	36.10
90	Mean	0.001	1.28	36.67	1.35	34.99	0.001	1.261	39.39	1.16	37.94
	St.dev.	0.001	0.08	0.99	1.38	0.03	0.001	0.079	2.34	1.29	0.04
	c.o.v.	0.634	0.06	0.03	1.02	0.00	0.629	0.063	0.06	1.11	0.00
	Min.	0.000	1.19	35.75	0.00	24.84	0.000	1.163	36.85	0.00	24.84
	Max.	0.002	1.36	38.33	3.12	31.32	0.002	1.391	43.87	3.44	31.32

The correlation coefficients between the soil hydraulic properties calculated for the Soil types 1 and 2 are shown in Table 3. The parameters of the SWRC and K_{sat} have strong interrelationships because the soils have similarly shaped SWRCs, as shown in Figure 3. Further, soils with a smaller porosity have lower saturated hydraulic conductivity, which adds physical significance to the use of correlation coefficients. Accordingly, the correlation coefficients should be considered in the Monte Carlo analysis represent these inter-relationships. The correlation coefficients are used in the Monte Carlo analysis to transform independent standard normal variables to correlated random variables (Ang and Tang 1990).

Table 3: Correlation coefficients for the different soil types

Variable 1	Variable 2	Correlation coefficient $\rho_{1,2}$					
		Soil type 1			Soil type 2		
		RC = 70%	RC = 80%	RC = 90%	RC = 70%	RC = 80%	RC = 90%
K_{sat}	α	0.71	1.00	0.97	0.86	0.87	-0.15
K_{sat}	N	-0.60	-0.79	-0.92	-0.17	-0.29	0.60
K_{sat}	θ_s	-0.59	-0.69	-0.76	0.13	0.11	-0.47
K_{sat}	θ_r	-0.44	-0.27	-0.83	-0.02	-0.30	0.16
α	N	-0.75	-0.79	-0.99	-0.40	-0.56	-0.67
α	θ_s	-0.06	-0.69	-0.72	0.14	-0.08	-0.49
α	θ_r	-0.51	-0.27	-0.94	-0.40	-0.51	-0.52
N	θ_s	-0.30	0.33	0.71	-0.74	0.43	0.07
N	θ_r	0.95	0.79	0.98	0.83	0.97	0.82
θ_s	θ_r	-0.43	-0.05	0.58	-0.56	0.58	0.22

Design Precipitation Event. The precipitation intensity was determined by analyzing the precipitation history for the site for the period from July 1998 to May 2003. The site is located near Denver, Colorado and is in a relatively arid region. Figure 4(a) indicates that the cumulative seasonal precipitation is greatest in the spring or summer, while Figure 4(b) also indicates that the maximum seasonal precipitation intensities occur in the spring and summer. The maximum precipitation in the spring and summer months was modeled with a type I maximum value distribution with a mean of E(I) = 30.5 mm/day and a standard deviation of σ(I) = 9.9 mm/day.
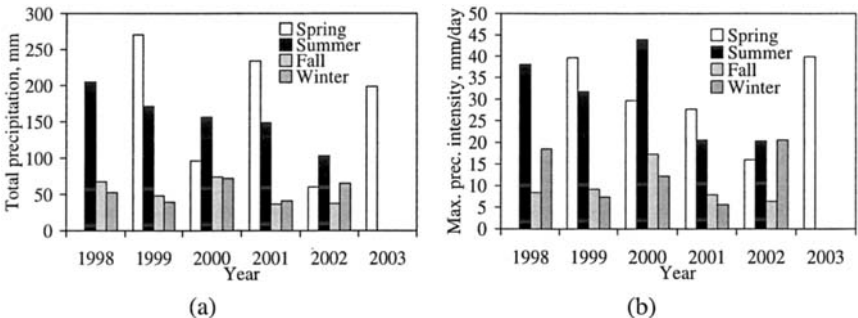
Figure 4: (a) Total seasonal precipitation; (b) Maximum precipitation intensity

To determine the duration of the precipitation event, precipitation records were analyzed to find the maximum number of subsequent days in which precipitation occurred. Table 4 indicates that during the spring months, when the number of precipitation events is the highest, 40% of the days in any period of time had precipitation. Accordingly, 4 sequential days of rain during a 10 day period was assumed as the worst case scenario. To account for the underestimation of the influx in Eq. (4), the duration was increased. The maximum duration was modeled with a type I maximum value distribution with a mean of E(D) = 5 days and a standard deviation of σ(D) = 2 days. A correlation coefficient of 0.6 between I and D was used to estimate a scenario in which a longer duration storm has high intensity.

Table 4: Duration analysis

L (days)	D = # of events in a period of L days		
	L = 20	L = 10	L = 5
Spring 1999	7	4	2
Spring 2000	9	5	2
Spring 2001	7	4	2
Spring 2002	6	3	2
Spring 2003	8	4	2
$E(D)$	7	4	2
$\sigma(D)$	1.31	0.65	0.35
$E(D)/L$	0.37	0.39	0.40

Initial Conditions. Eq. (3) indicates that the capacity of the soil depends on the initial moisture content in the soil. Investigation of the moisture content values in the instrumented ET test covers at the site indicates that the mean volumetric moisture content in the cover is approximately 0.15 (McCartney and Zornberg 2004). After periods of intense precipitation during which significant increases in moisture content were observed, the covers returned to the mean volumetric moisture content after 2 to 3 weeks. Accordingly, the initial moisture content θ_i was modeled using a lognormal distribution with a mean value of 0.15 and a standard deviation of 0.05. To account for the possibility that higher moisture contents are likely during periods of intense precipitation, positive correlation coefficients of 0.75 were assumed between the initial moisture content and the precipitation intensity and duration, respectively.

Monte Carlo Analysis

Monte Carlo analysis was used to simulate the variables in Eqs. (3) and (4) to determine the likelihood that the moisture applied to the soil during a precipitation event is greater than the moisture storage capacity of the soil. 10,000 realizations were used to estimate the probability of failure for each alternative using correlated non-normally random variables (Ang and Tang 1990). Each realization consisted of: (*i*) generating a uniformly distributed random number for each of the variables in the performance model, (*ii*) transforming the random numbers to a standard normal distribution, (*iii*) transforming the independent standard normal random numbers to correlated normal variables using the mean values and correlation coefficients defined from the laboratory testing program, (*iv*) transforming the correlated normal variables to the probability distribution selected for each variable, (*v*) calculating the MSC and moisture infiltrated from Eqs. (3) and (4) using the simulated variables, and (*vi*) checking if failure occurred for the realization. Estimates of the probabilities of failure for covers with different thicknesses constructed using Soil types 1 and 2, given the design precipitation event, are shown in Figures 5(a) and 5(b). The estimated probabilities of failure ranged from 1.4×10^{-4} to 0.8 except for Soil type 1 with RC = 90%, which had a probability of failure less than the precision of the Monte Carlo analysis (*i.e.*, less than 10^{-5}). The relatively high probabilities of failure are consistent with field observations by Zornberg and McCartney (2003), who report that test covers using these soils exceed field capacity approximately every two years.

(a)   (b)
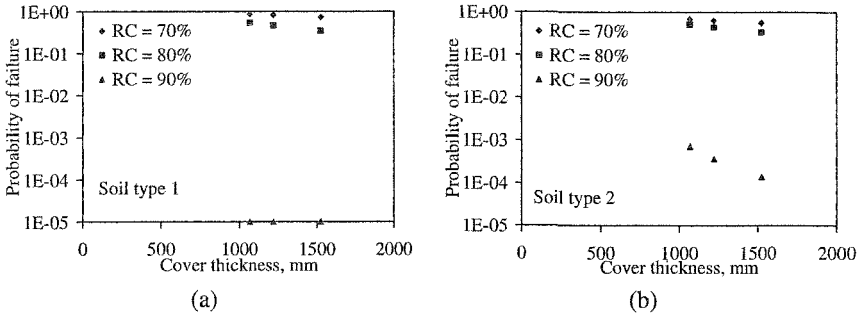
Figure 5: Simulation results: (a) p_f for Soil type 1; (b) p_f for Soil type 2

Results

Using the probability of failure values from the Monte Carlo simulations, the decision analysis was conducted for the example costs. The total alternative cost was calculated as the sum of the construction, densification, and the failure costs. As each alternative has a likelihood of successful or failure and will have different total costs based on the outcome of its performance, the probability of failure is used to calculate the expected cost for the alternative, as follows:

$$\text{Expected Cost} = p_f\left(\text{Cost of failed cover}\right) + (1-p_f)(\text{Cost of successful cover}) \qquad (5)$$

The expected costs for the different cover alternatives using the example costs given in the introduction are shown in Figure 6. For these example costs, the cover alternative with the minimum expected cost is a 1.067 m-thick cover constructed using Soil type 2 placed at 80% relative compaction. Although this cover had the lowest expected cost, is did not have the lowest cost of success. However, the expected cost allows the likelihood of success and failure to be balanced. Although this approach allows the optimal design alternative to be identified, the approach is undeniably sensitive to the example costs. However, the flexibility of assigning the costs allows a designer to customize the decision analysis to the goals of the parties interested in cover design.

Figure 6: Decision analysis for example costs with optimum alternative circled

Discussion

The decision analysis presented in this paper provides a simple yet objective means to select important design variables that affect the performance of ET covers while considering uncertai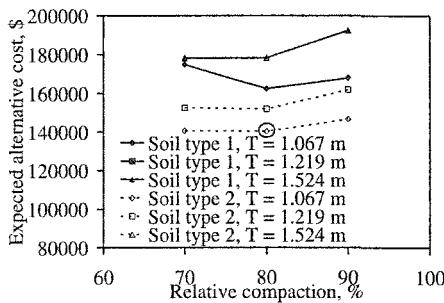nty in soil hydraulic properties and design precipitation events. This analysis may be extended by incorporating a rigorous solution of Richards' equation in response to atmospheric boundary conditions into the Monte Carlo analysis routine. Further, it may be extended by including moisture removal from the cover, which is an essential component to cover performance. Incorporating these features into a decision analysis may lead to a better quantification of the expected performance for each cover, but it will significantly increase the computation time. Although the technical features of the flow process may be improved, an appropriate failure criterion and alternative costs are still required to evaluate the analysis results. An important future component of this research will include comparison of the results of the prior decision analysis presented in this paper with the data from the field monitoring program for the ET covers at the site. As mentioned, field monitoring data is available from several prototype test covers, each with different cover thicknesses and soil types. Accordingly, the field data can be used to update the probabilities of failure calculated in this study using Bayesian analysis. This may help determine whether site-specific compliance testing is necessary, or if reliance on laboratory data and simplified analyses is sufficient.

References

Ang, A.H.S., and Tang, W.H. (1990). *Probability Concepts in Engineering Planning and Design: Volume II – Decision, Risk, and Reliability*. University of California, Irvine.

Daniel, D.E. (1984). "Predicting Hydraulic Conductivity of Clay Liners." *Journal of Geotechnical Engineering*. ASCE. 110(2), 285-300.

Dwyer, S. F. (1998). "Alternative Landfill Covers Pass the Test." *Civil Eng*. 50-52.

McCartney, J.S. and Zornberg, J.G. (2002). "Design and Performance Criteria for Evapotranspirative Cover Systems." *4th Int. Congress on Environmental Geotechnics*. Rio de Janeiro, Brazil.

McCartney, J.S. and Zornberg, J.G. (2004). "Use of Moisture Profiles and Lysimetry to Assess Evapotranspirative Cover Performance." *Proceedings of the 5th Annual PhD Symp. in Civil Eng*. T. Scarpas, ed. Delft, the Netherlands.

van Genuchten, M. (1980). "A Closed-Form Equation for Predicting the Hydraulic Conductivity of Unsaturated Soils." *Soil Sc. Soc. Am. Jour*. 44:892-898.

Zornberg, J.G., LaFountain, L., and Caldwell, J.A. (2003). "Analysis and Design of Evapotranspirative Covers for Hazardous Waste Landfill." *Journal of Geotechnical and Geoenvironmental Engineering*. 129(6):427-438.

Zornberg, J.G. and McCartney, J.S. (2003). *Analysis of Monitoring Data from the Evapotranspirative Test Covers at the Rocky Mountain Arsenal*. Geotechnical Research Report, USEPA, Region 8, December 2003, 227 pp.

Zornberg, J.G., and McCartney, J.S. (2005). "Evaluation of Evapotranspiration from Alternative Landfill Covers at the Rocky Mountain Arsenal." *Experus 2005*. June 26-29. Trento, Italy.

Evapotranspiration Landfill Cover Design: Characterization and Soil Environment

Pat McGuire [1], Jon Gumtow[2], and Ed Doyle[3]

[1]Earth Tech, 4135 Technology Parkway, Sheboygan, WI 53083; PH (920) 451-2572; FAX (920) 458-0550: email: pat.mcguire@earthtech.com
[2] Earth Tech, 1020 North Broadway, Milwaukee, WI 53202; PH (414) 225-5160; FAX (414) 225-5111; email:jon.gumtow@earthtech.com
[3] Environmental Information Logistics, 360 Prairie, Naperville, IL 60540; PH (630) 416-8742; FAX (630) 416-8743: email: ed.eil@sbcglobal.net

Abstract

Physical and chemical soil properties including soil particle size distribution, texture, soil water retention characteristics, hydraulic conductivity, and soil productivity influence potential evapotranspiration (ET) cover performance. Borrow source characterization is necessary to define the spatial variability of soil properties, the location(s) of suitable material, and a method to select material during excavation. Understanding the soil environment of a borrow source provides insight for site characterization including soil sampling design and data interpretation. The methods for soil characterization at three sites in the United States are discussed. Soil near Colorado Springs, Colorado developed predominantly from aeolian (loess) deposits and had distinct soil horizons with relatively uniform soil properties. The site soil sampling plan and data interpretation considered soil morphology and was based on collection of discrete soil samples from each soil horizon. Soil near Golden, Colorado developed from fluvial deposits. Horizons from soil forming factors were not present due to prior soil removal (quarry operation) and soils were spatially variable throughout the profile with interbedded fine and coarse-grained horizontal layers. A statistical approach was used to collect soil samples from this fluvial deposit. Composite soil samples were obtained from the vertical face of excavated pits that were randomly selected. Soil characterization was based on analysis of duplicate samples, composite samples that included fine-grained clay clods, and composite samples from which clay clods were removed by sieving. This evaluation was conducted to assess the potential variability of soil properties that impact ET cover performance. Soils for a site near Arlington, Oregon were located in facility stockpiles. Characterization of stockpiles is problematic, particularly if materials are

not segregated by soil type. Soil characterization considered the potential variability of site soil types that were excavated for stockpiles.

Introduction

Evaluations to determine site suitability and design thickness for an ET cover are typically based on site climatic conditions, borrow source soil characteristics, and capability of cover vegetation to affect the water balance (Albright et al., 2004; EPA, 2003, Hauser et al. 2001).

Characterization of the borrow source is critical because of the influence that soil physical, hydraulic, and chemical properties may have on ET cover performance.
Soil physical properties including particle size distribution (texture) and structure affect hydraulic conductivity, soil water retention characteristics, and water storage (Gurdal and Benson, 2003). Soil chemical properties including organic matter content, pH, and salinity parameters influence vegetation productivity (Brady and Weil, Chapters 9 & 12, 1999). Therefore, borrow source characterization is necessary to:

- Determine soil suitability
- Define the spatial variability of soil properties and the locations of suitable/unsuitable soil
- Determine the feasibility of segregating the most productive soils for topsoil use
- Design the cover thickness

Understanding the soil environment with reference to origin and soil forming processes, provides a basis for developing a sampling program and obtaining data for borrow source characterization. The methods that were used to characterize three borrow source areas are described. Soil from an undisturbed borrow source near Colorado Springs, Colorado originated from aeolian (loess) deposits and had distinct soil horizons with relatively uniform soil properties. Soil from a disturbed borrow source near Golden, Colorado, where developed soil horizons had been excavated, originated from fluvial deposits. Soils were spatially variable throughout the profile with interbedded fine and coarse-grained horizontal layers. Existing stockpiles of segregated soils that represent locally available materials were evaluated at a site near Arlington, Oregon.

Fort Carson

An ET cover was constructed in 2000 at Fort Carson, a U.S. Army Facility located near Colorado Springs, Colorado. Following a preliminary investigation, a borrow source was located 16 km (10 mi) south of the landfill site. The borrow source was about a 16+ ha (40 ac) area located on a flat plateau that was adjacent to an active sand & gravel quarry.

Based on the United States Department of Agriculture (USDA) El Paso County Soil Survey Report, the soils formed in mixed alluvial and aeolian (wind blown) materials and the predominant soil series (family of soils with distinct properties) mapped for the borrow area was the Fort Collins series (Larsen, 1981). The Fort Collins series is described as a deep soil with a soil profile texture that ranges from loam to clay loam based on the USDA Soil Classification System (USDASCS).

A field investigation was conducted to characterize soil types, soil properties, and spatial soil variability within the borrow area. The methods used for the field investigation considered soil morphology, since undisturbed surface soils typically develop horizons or soil layers with distinct properties. Soil profiles were described in the field and the data was used to select sample locations to characterize physical, hydraulic, and chemical (plant productivity potential) properties of soil horizons through laboratory analysis. Soil profile horizons were described at ten locations (quarry escarpment or test pits). Soil descriptions were based on USDA soil taxonomy nomenclature. Major soil horizons were defined including the A, B, and C-horizons. Typically A and B-horizons have properties that are most capable of supporting vegetation including enriched organic matter, microbial populations, and macronutrients (Brady and Wiel, Chapter 12, 1999). Field soil profile descriptions included the soil horizon designation and associated depth interval, estimated soil texture using a field method (Brady and Weil, Chapter 4, 1999), soil structure (granular, subangular blocky, prismatic etc.), consistence (friable, firm, hard etc.), moisture content (dry, moist), rock fragment (diameter, percentage), potential carbonate presence (salinity) based on hydrochloric acid reaction, and root quantity.

Following an evaluation of the soil field descriptions, soil core and bag samples were collected from five of the ten exposed soil profiles and submitted to the Colorado State University Soil and Plant Laboratory (CSU Lab) in Fort Collins. In-situ core samples (7.6 cm [3 in] diameter by 15 cm [6 in] length) sealed in plastic bags were analyzed for moisture content (ASTM D 2216), dry bulk density (Blake and Hartge, 1986), and saturated hydraulic conductivity based on the falling head method (Klute and Dirksen, 1986). Bag samples were analyzed for sand, silt, and clay fractions (Gee and Bauder, 1986), and soil moisture retention characteristics (Klute, 1986). The soil moisture retention characteristics (SMC's) were determined from samples remolded to a bulk density similar that of the borrow area (1.1 kg/m^3 [69 pcf]). Bag samples were also analyzed for soil chemistry parameters (plant productivity) including, pH (Thomas, 1996), electrical conductivity (Rhoades, 1996), sodium adsorption ratio which compares soil solution concentrations of Na$^+$ to that of Ca^{2+} and Mg^{2+}(Sumner and Miller, 1996), organic matter content (Nelson and Sommers, 1996), and macronutrients (nitrogen, phosphorus, and potassium).

Duplicate samples were collected at selected locations and submitted to Daniel B. Stephens Laboratory (DBS Lab) in Albuquerque, New Mexico. Bulk samples were analyzed for standard Proctor maximum dry density (ASTM D698). Following evaluation of in-situ soil bulk density data, saturated hydraulic conductivity (ASTM

D 2434) and SMC (ASTM D 2325; Klute, 1986) were determined from samples that were remolded to 75 and 85 percent of standard Proctor maximum dry densities.

Some in-situ soil horizon properties are provided in Table 1. As anticipated based on the soil field descriptions, the distribution of sand, silt, and clay is relatively uniform for soil profiles and horizons. The predominant USDASCS soil texture is clay loam, which is comparable to a lean clay or lean clay with sand using the Unified Soil

Table 1. SOIL IN-SITU HORIZON PROPERTIES
FORT CARSON, COLORADO SPRINGS.

Sample Description			Soil Properties							
Soil Profile No.	Depth Interval (cm)	USDA Soil Horizon	USDA Sand/Silt/Clay Particle Size (%)	USDA Soil Texture	Dry Bulk Density (kg/m³)	Volumetric Water Content (%)	Hydraulic Conductivity (m/s)	pH	Electrical Conductance dS/m	Sodium Adsorption Ratio	Organic Matter (%)
1	13-18	A	32/27/41	Clay	1.27	21	2.5×10^{-8}	6.3	0.5	1.3	1.7
	58-63	B	30/31/39	Clay Loam	1.25	12	4.0×10^{-9}	7.9	0.5	2.4	1.0
	140-145	C1	28/39/33	Clay Loam	1.18	11	6.9×10^{-5}	8.2	2.1	5.0	0.5
	259-267	C2	33/35/32	Clay Loam	1.17	9	9.0×10^{-6}	8.1	1.7	4.7	0.6
2	13-18	A	34/33/33	Clay Loam	1.16	10	4.6×10^{-6}	6.7	0.6	0.3	2.1
	43-48	B	29/30/41	Clay	1.25	10	5.6×10^{-8}	7.3	0.4	1.5	1.2
	155-157	C1	30/38/32	Clay Loam	1.17	12	1.4×10^{-7}	8.1	3.1	4.3	0.6
	282-287	C2	34/35/31	Clay Loam	1.16	9	1.2×10^{-5}	8.2	1.7	5.6	0.6
	366-371	C3	38/35/27	Clay Loam/Clay Loam	1.00	17	2.3×10^{-5}	8.1	2.1	4.6	0.5
3	13-18	A	37/21/42	Clay	1.25	22	2.1×10^{-5}	7	0.6	0.8	1.5
	48-53	B	40/27/33	Clay Loam	1.14	16	1.6×10^{-6}	7.9	0.4	1.1	0.6
	122-127	C1	46/23/31	Sandy Clay Loam	1.13	23	5.6×10^{-7}	8.1	0.5	2.2	0.4
	231-236	C2	37/33/30	Clay Loam	1.15	21	1.0×10^{-6}	8.3	0.9	6.1	0.5
	358-363	C3	51/18/31	Sandy Clay Loam	1.10	21	5.4×10^{-6}	8.1	2.3	5.1	0.6
5	18-23	B	42/21/37	Clay Loam	1.10	24	2.0×10^{-8}	7.1	0.4	0.4	1.3
	86-91	C1	36/34/30	Clay Loam	1.18	25	1.4×10^{-6}	8.2	0.4	0.5	0.4
	195-201	C2	40/31/29	Clay Loam	1.13	11	2.8×10^{-6}	8.5	0.8	11.1	0.4
	282-287	C3	46/20/34	Sandy Clay Loam	1.10	10	2.1×10^{5}	8.2	2.3	7.5	0.6
8	0-8	A	39/37/24	Loam	1.10	22	1.3×10^{-4}	6.8	0.5	0.4	3.4
	30-35	B	29/36/35	Clay Loam	1.18	14	1.1×10^{-7}	6.8	0.2	0.8	7.4
	99-104	C	33/38/29	Clay Loam	1.15	19	8.6×10^{-7}	8.3	0.7	4.8	0.7

NOTES:

Soil horizon designation, particle size, and texture are based on U.S. Department of Agriculture (USDA) nomenclature and classification.

Analysis by Colorado State University Soil, Water, and Plant Testing Lab.

Classification System (USCS). The dry bulk density values ranged from 1.0 kg/m^3 (62 pcf) to 1.27 kg/m^3 (79 pcf) with a median value of 1.16 kg/m^3 (72 pcf). The saturated hydraulic conductivity ranged from 2.0 x 10^{-8} m/s to 1.3 x 10^{-4} m/s with a median value of 1.0 x 10^{-6} m/s. The soil productivity parameter values from 25 samples did not indicate that any horizon was subject to diminished plant productivity due to salinity. Soils are considered normal (non-saline) if pH is less than 8.5, electrical conductance (EC) is less than 4 dS/m, and sodium adsorption ratio (SAR) is less than 13 (Brady and Weil, Chapter 10, 1999). The organic matter content ranged from 0.4 to 7.4 percent with higher values typically associated with the A and B-horizons.

The soil horizon properties of remolded/compacted soil samples are provided in Table 2. The soil bulk densities and most hydraulic parameter values from samples compacted to 75 percent of the standard Proctor are most comparable to in-situ borrow soils. The SMC's for selected soil horizon samples (A, B, C) remolded to 85 percent of their standard Proctor maximum dry densities are plotted in Figure 1.

Table 2. REMODELED SOIL SAMPLE PROPERTIES
FORT CARSON, COLORADO SPRINGS, COLORADO.

| Soil Profile No./USDA Horizon[1]	USDA Soil Texture	Sample Type[1]	Dry Bulk Density (kg/m³)	Residual Volumetric Water Content (m³/m³)	Saturated Volumetric Water Content (m³/m³)	van Genuchten Parameters[2] α (cm⁻¹)	n	Saturated Hydraulic Conductivity (m/s)
1/A	Clay	75% Proctor	1.21	0.00	0.52	0.137	1.18	2.4 x 10^{-5}
		85% Proctor	1.37	0.02	0.39	0.003	1.31	6.2 x 10^{-8}
8/B	Clay Loam	75% Proctor	1.18	0.00	0.56	0.124	1.16	1.1 x 10^{-5}
		85% Proctor	1.33	0.00	0.43	0.005	1.20	1.1 x 10^{-8}
8/C1	Clay Loam	75% Proctor	1.22	0.00	0.52	0.046	1.19	3.0 x 10^{-6}
		85% Proctor	1.38	0.00	0.45	0.008	1.21	2.1 x 10^{-8}
1/C2	Clay Loam	75% Proctor	1.24	0.00	0.56	0.030	1.22	8.8 x 10^{-6}
		85% Proctor	1.41	0.00	0.44	0.008	1.20	9.6 x 10^{-8}
3/C2	Clay Loam	75% Proctor	1.23	0.00	0.55	0.051	1.21	2.7 x 10^{-6}
		85% Proctor	1.39	0.00	0.45	0.010	1.21	2.1 x 10^{-7}
5/C3	Sandy Clay Loam	75% Proctor	1.32	0.01	0.50	0.045	1.22	3.3 x 10^{-6}
		85% Proctor	1.49	0.00	0.39	0.015	1.17	2.6 x 10^{-8}

NOTES:

[1] Soil horizon descriptions and texture are based on United States Department of Agriculture (USDA) nomenclature and soil classification.

Analysis by Daniel B. Stephens Lab.

Soil properties based on in-situ conditions and samples compacted to 75% and 85% of the standard Proctor maximum dry density.

[2] Soil hydraulic parameters for soil retention curves (van Genuchten, 1980).
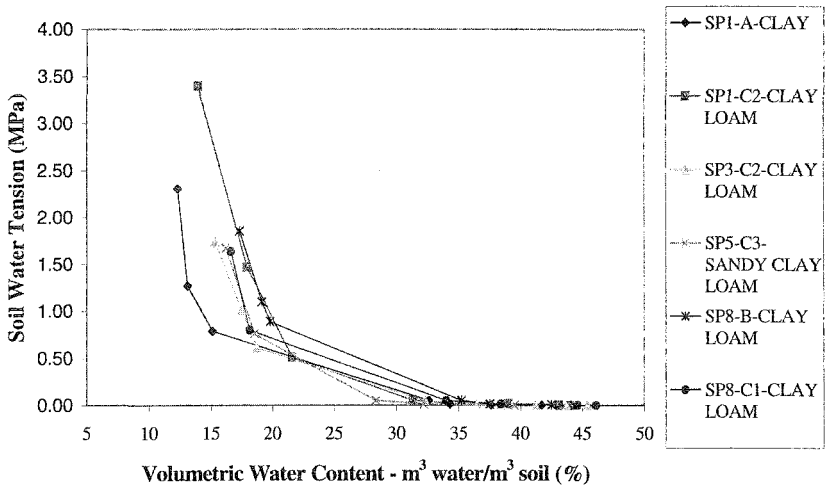
Figure 1. Soil water retention characteristics
Fort Carson, Colorado Springs, Colorado.

NOTES:
SP=Soil pit
Samples remolded to 85% of standard Proctor maximum dry density

The SMC's of these soils and other samples obtained from horizons at borrow area locations were similar, which is consistent with the field soil horizon descriptions and the relatively uniform particle size distributions within soil horizons (Table 1).

By considering the soil environment which included developed soil horizons that originated from a uniform loess deposit, it was possible to characterize the borrow source with limited number of discrete samples that were collected from soil profile horizons.

Rocky Flats

A borrow source investigation was conducted in fall 2002 to evaluate the potential for ET cover construction at a landfill within the Rocky Flats Environmental Technology Site (RFETS) located north of Golden, Colorado. The borrow source was on an active aggregate quarry property about 11.3 km (7 mi) northwest of the RFETS near Brighton and adjacent to the South Platte River. A preliminary field investigation based on descriptions of excavated pits showed that the soil deposits formed from fluvial deposits associated with the South Platte River floodplain. Developed soil horizons were absent because the surface soils were removed during past quarry

operations. The existing soil deposits included interbedded layers of sand and fine-grained soil (silt and clay) with randomly distributed pockets of sand and gravel.

Due to the spatial variability of the soils, a statistical approach was used for sampling. A grid system of 41 grid squares (27.3 m (90 ft)) was superimposed over a planimetric map of the 3.0 ha (7.5 ac) site. A random number generator was used to select 15 grid squares for trench excavation, soil description, and sampling. Duplicate composite samples were collected by using an excavator bucket to scrape soil from the face of an excavated trench. Samples were mixed, placed in plastic bags, and submitted to the CSU Lab for analysis. Samples were analyzed for sand, silt, and clay fractions (Gee and Bauder, 1986). Saturated hydraulic conductivities based on the falling head method (Klute and Dirksen, 1986) were conducted on samples remolded to 1.40 kg/m^3 (87 pcf). Soil chemistry parameters that were analyzed included pH (Thomas, 1996), electrical conductance (Rhoades, 1996), and SAR (Sumner and Miller, 1996).

The results of the composite sample lab analysis are provided in Table 3. The gravel content in samples ranged from 0 to 40 percent with five samples having gravel content greater than 15 percent. The USDASCS textures ranged from sandy loam to clay with most samples classified as clay loam (5) or sandy clay loam (6). The saturated hydraulic conductivities of samples ranged from 1.8 x 10^{-5} m/s to 1.3 x 10^{-7} m/s. The soil productivity parameter values did not indicate that soils were subject to diminished plant productivity due to salinity. The relatively high organic matter content in soils, which ranged from 1.7 to 3.8 percent, was attributed to organic matter associated with the fluvial deposits. Based on field descriptions and lab analysis, it was determined that field·inspection of borrow soil would be required during excavation to define significant gravel and/or coarse-grained soil pockets that do not have favorable water retention characteristics.

Many of the composite samples included aggregated clay clods from the fine-grained soil layers that were mixed with a coarser-grained soil matrix. Therefore, additional analyses were conducted on selected samples to determine if results were consistent between labs using similar methods and to evaluate the influence of the clay aggregates on the particle size distribution results. Duplicate samples were split and submitted to separate labs (CSU Lab and Geosystems Analysis, Inc. (Geosystems), Tucson, Arizona) for particle size analysis (Gee and Bauder, 1986). Hydraulic conductivities based on constant head (Klute and Dirksen, 1986) and SMC's (ASTM D 2325; Klute, 1986) analyses were conducted by Geosystems on samples that were remolded to 1.40 kg/m^3 (87 pcf). At each lab, selected samples were split and one sample was analyzed with clay aggregates and one sample was analyzed by removal of clay aggregates with a 19 mm (3/4 in) mesh sieve, prior to analysis.

The results of the particle size and hydraulic conductivity analysis are provided in Table 4. The reported particle size distributions for duplicate samples submitted to the labs were comparable. The particle size distributions and hydraulic conductivities of samples with and without clay aggregates were comparable. The SMC's for

Table 3. FLUVIAL COMPOSITE SAMPLE PROPERTIES
ROCKY FLATS, GOLDEN, COLORADO.

Sample Description							Soil Properties[1]					
							Physical/Hydraulic			Chemical		
Sample ID	Soil Pit No.	Composite Sample Depth Interval (m)	USDA Particle Size (%)				USDA Soil Texture	Hydraulic Conductivity[2] (m/s)	pH	Electrical Conductance (dS/m)	Sodium Adsorption Ratio	Organic Matter Content (%)
			Gravel	Sand	Silt	Clay						
1	1	0-3.0	31	52	4	44	Sandy Clay	4.6×10^{-6}	--	--	--	--
4	15	0-3.6	4	52	18	30	Sandy Clay Loam	--	7.5	1.2	2.5	2.5
7	2	0-4.3	0	40	26	34	Clay Loam	--	--	--	--	--
10	14	0-4.6	0	38	25	37	Clay Loam	3.7×10^{-7}	7.9	1.2	1.0	3.8
14	13	0-4.6	2	48	22	30	Sandy Clay Loam	--	--	--	--	--
18	12	0-5.5	21	54	20	26	Sandy Clay Loam	--	--	--	--	--
22	11	0-2.7	40	36	19	45	Clay	--	--	--	--	--
26	10	0-2.4	18	40	20	40	Clay/Clay Loam	1.3×10^{-7}	7.6	1.8	2.7	2.7
30	9	0-2.1	0	66	16	18	Sandy Loam	1.8×10^{-5}	7.6	0.6	1.8	1.7
34	7	0-3.0	0	48	26	26	Sandy Clay Loam	--	--	--	--	--
38	3	0-5.2	6	52	24	24	Sandy Clay Loam	--	--	--	--	--
42	8	0-3.6	3	26	30	44	Clay	--	--	--	--	--
46	6	0-4.6	1	41	24	35	Clay Loam	--	7.9	0.7	1.7	2.4
50	5	0-3.6	1	41	25	34	Clay Loam	--	--	--	--	--
54	4	0-1.8	22	52	18	30	Sandy Clay Loam	1.0×10^{-5}	7.6	2.4	2.6	2.7

NOTES:

[1] Analysis by Colorado State University Soil, Water, and Plant Testing Lab.

[2] Samples remolded to dry bulk density of 1.4 g/cm^3 (87 pcf).

Table 4. FLUVIAL COMPOSITE SOIL SAMPLE COMPARISONS
ROCKY FLATS, GOLDEN, COLORADO.

| Sample Description | | | USDA Particle Size Distribution and Texture Class | | | | | |
| Soil Pit No. | Composite Sample Depth Interval (m) | Type[1] | Gravel | Sand | Silt | Clay | USDA Texture | Saturated Hydraulic Conductivity[2] (m/s)[2] |
			Percent					
			Duplicate Samples					
4	0-1.8	CSU	22	52	18	30	Sandy Clay Loam	NA
		GA	11	56	18	26	Sandy Clay Loam	3×10^{-6}
10	0-2.4	CSU	18	40	20	40	Clay Loam	NA
		GA	6	26	38	36	Clay Loam	4×10^{-5}
14	0-4.6	CSU	0	38	25	37	Clay Loam	NA
		GA	0	40	23	37	Clay Loam	5×10^{-6}
			Soil Matrix With and Without Clay Inclusions					
6	0-4.6	M&I (CSU)	Screened from Sample	41	24	35	Clay Loam	NA
		M (GA)		56	18	26	Sandy Clay Loam	1×10^{-6}
9	0-2.1	M&I (CSU)	Screened from Sample	66	16	18	Sandy Loam	NA
		M&I (GA)		68	14	18	Sandy Loam	4×10^{-6}
		M (GA)		68	16	16	Sandy Loam	3×10^{-6}
15	0-1.8	M&I (CSU)	Screened from Sample	52	18	30	Sandy Clay Loam	NA
		M (GA)		60	15	25	Sandy Clay Loam	3×10^{-6}

NOTES:

[1] CSU = Colorado State University Soil, Water, & Plant Testing Lab.; GA = Geosystems Analysis, Inc. Lab.; M&I = Soil matrix with clay inclusions; M = Soil matrix without clay inclusions.

[2] Sample remolded to dry bulk density from 1.40 g/cm^3 (87 pcf) to 1.45 g/cm^3 (90 pcf); NA = Not Analyzed.

samples with and without clay aggregates are provided in Figure 2. The SMC for the sandy loam with clay aggregates indicated more water retention at higher tensions as compared to the soil without clay aggregates. Most of the other SMC's were comparable. The results indicate that the overall composite sampling was not biased by the clay aggregates that were included in samples.
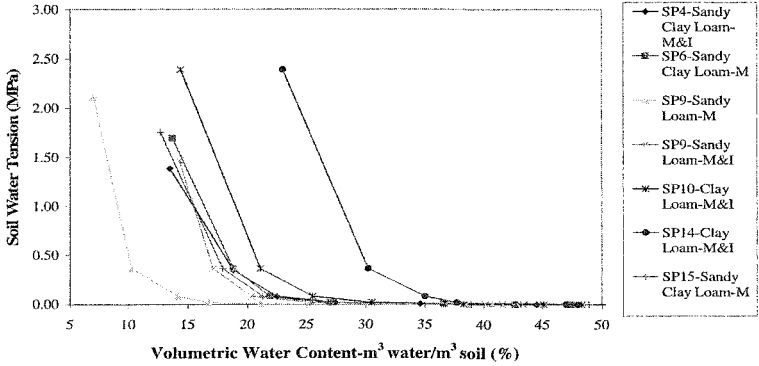

Figure 2. Soil water retention characteristics
Rocky Flats, Golden, Colorado.

NOTES:
SP=Soil pit
M&I =Soil matrix with clay inclusions
M=Soil matrix without clay inclusions
Samples remolded to dry bulk density from 1.4 g/cm3 (87 pcf) to 1.45 g/cm3 (90 pcf)

The random sampling and collection of composite samples was effective for characterizing the predominant soil matrix associated with fluvial deposits. Field soil descriptions indicate inspections during excavation would be required to define pockets of sand and gravel which do not have the water retention properties of the predominant soil matrix.

Columbia Ridge

A borrow source investigation was conducted in fall 2004 at the Columbia Ridge Landfill, which is located near Arlington, Oregon, to evaluate the potential for ET cover construction. The preliminary borrow source investigation was based on the analysis of 8 segregated soil stockpiles that were located on the facility. The stockpiles included the soil types that are locally available. Six of the stockpiles included soil that originated from bedrock or volcanic deposits and are defined locally as a buff claystone (2), pink claystone (1-volcanic), rattlesnake ridge claystone & sandstone (2-volcanic), and siltstone mixed soils (1). Two stockpile soils originated from loess (aeolian deposit) and based on the USDA soil survey are the most common surface soil for the area (Hosler, 1984).

Soil samples were collected from stockpiles and submitted to the CSU Lab for USDASCS particle size distribution (Gee and Bauder, 1986) and soil chemistry parameters including pH (Thomas, 1996), electrical conductance (Rhoades, 1996), and SAR (Sumner and Miller, 1996). Selected duplicate samples were submitted to the DBS Lab for USCS particle size distribution (ASTM D 422), standard Proctor maximum dry density (ASTM D 698), and Atterberg Limits (ASTM D 4318). Saturated hydraulic conductivities based on constant head (ASTM D 2434) and SMC's (ASTM D 2325; Klute, 1986) were determined from samples that were remolded to 85 to 100 percent of standard Proctor maximum dry densities to obtain densities that would not inhibit plant root development.

The results of the lab analysis are provided in Table 5. The USDASCS textures ranged from sandy loam to clay. The pink claystone and rattlesnake ridge claystone and sandstone (volcanic deposits) had relatively high liquid limits. Three of the soil samples were nonplastic. The soil productivity parameter values did not indicate that soils were subject to diminished plant productivity due to salinity. Organic matter content was low in the soils. The hydraulic properties of stockpile soils, developed from the SMC's, are variable as shown in Table 6.

Table 5. STOCKPILE SAMPLE SOIL PROPERTIES COLUMBIA RIDGE, ARLINGTON, OREGON.

Stockpile[1]		Soil Classification USDA (USCS)[2]	Atterberg Limits (LL/PL/PI)	pH (SU)	Electrical Conductance (dS/m)	Sodium Adsorption Ratio	Organic Matter (%)
Location	Source						
1	Buff Claystone	Clay	-	-	-	-	-
		Clay	-	7.6	0.6	1.9	0.1
2	Buff Claystone	Clay Loam	-	-	-	-	-
		Sandy Loam	-	7.4	0.4	1.7	0.2
5	Pink Claystone	Clay Loam	-	-	-	-	-
5		Sandy Clay Loam	-	7.3	0.2	1.4	0.2
5		Sandy Clay Loam	-	-	-	-	-
5[1]		Clay Loam (MH)	119/64/55	-	-	-	-
7	Surface Soil	Sandy Loam	-	8.3	0.4	5.2	0.5
7[1]	Loess	Silt Loam (ML)	NP	-	-	-	-
9[1]	Claystone & Sandstone	Sandy Loam (MH)	72/68/4	-	-	-	-
10	Claystone & Sandstone	Sandy Loam	-	-	-	-	-
10		Sandy Loam	-	7.5	0.4	2.3	0.4
10[1]		Sandy Loam (ML)	NP	-	-	-	-
12	Surface Soil	Sandy Loam	-	8.4	0.6	7.9	0.4
12[1]	Loess	Silt Loam (ML)	NP	-	-	-	-
13	Siltstone	Silt Loam	-	-	-	-	-

NOTES:

[1] Analysis by Colorado State University Soil, Water, and Plant Testing Laboratory, except denoted samples which were analyzed by Daniel. B. Stephens Lab.

[2] USDA = United States Department of Agriculture; USCS = Unified Soil Classification System.

[3] LL = Liquid Limit, PL = Plastic Limit, PI = Plasticity Index, NP = Non-Plastic.

Table 6. REMOLDED SOIL SAMPLE PROPERTIES
COLUMBIA RIDGE, ARLINGTON, OREGON.

Stockpile	USDA Soil Texture	Percent of Maximum Standard Proctor Density	Dry Bulk Density (kg/m³ [pcf])	Residual Volumetric Water Content (m³/m³)	Saturated Volumetric Water Content (m³/m³)	van Genuchten Parameters α (cm⁻¹)	n	Saturated Hydraulic Conductivity (m/s)
5	Clay Loam	100	0.83 (52)	0.00	0.66	0.000	1.43	2.9×10^{-10}
7	Silt Loam	90	1.43 (89)	0.22	0.48	0.008	1.41	6.7×10^{-7}
9	Sandy Loam	85	0.88 (55)	0.00	0.67	0.027	1.17	4.6×10^{-5}
10	Sandy Loam	100	1.32 (82)	0.00	0.47	0.001	1.23	2.4×10^{-9}
12	Silt Loam	90	1.48 (92)	0.003	0.41	0.006	1.33	1.6×10^{-8}

Conclusions

Soils are often heterogeneous which makes characterization challenging in terms of sample design, data interpretation, and cost. Understanding soil formation factors of a borrow source provides insight for site characterization method (s). Characterization of heterogeneous soils can often be accomplished more efficiently by considering soil characteristics of existing local soil types, depositional environment, and surface soil formation factors that influence horizon development. Soil horizon descriptions and discrete horizon samples were used to characterize a borrow source with developed surface horizons. Randomly selected sample locations and composite sampling were used to characterize a borrow source that originated from fluvial subsurface deposits that were variable and included pockets of sand and gravel. Samples were collected from segregated stockpiles that represented locally available soil types to characterize the range of soil conditions.

References

Albright, W. H., C.H. Benson, G.W. Gee, A.C. Roesler, T. Abichou, P. Apiwantragoon, B. Lyles, and S. Rock (2004). "Field Water Balance of Landfill Final Covers." *J. Environ. Qual.* 33:2317-2332.

Blake G. and K. Hartge (1986). "Bulk Density." p. 364-367. In A. Klute (ed.) *Methods of Soil Analysis.* Part 1. 2nd ed. Agron. Monogr. 9. ASA and SSSA, Madison, WI.

Brady, N.C. and R.R. Wiel (1999). "Chapter 1-The Soils Around Us, Chapter 4-Soil Architecture and Physical Properties, Chapter 10, Alkaline and Salt Affected Soils and Their Management, Chapter 12-Soil Organic Matter." The Nature and Properties of Soils. Prentice Hall, N.J.

Environmental Protection Agency (September 2003). "Evapotranspiration Landfill Cover Systems Fact Sheet." EPA 542-F-03-015, http://cluin.org.

Gee, G.W. and J.W. Bauder (1986). "Particle Size Analysis." p. 396-399. In A. Klute (ed.) *Methods of Soil Analysis*. Part 1. 2nd ed. Agron. Monogr. 9. ASA and SSSA, Madison, WI.

Gurdal T., C.H. Benson, and W.H. Albright (2003). "Hydrologic Properties of Final Cover Soils from the Alternative Cover Assessment Program." Geo Engineering Report No. 03-02, Geo Engineering Program, University of Wisconsin-Madison.

Hauser, V., B. Weand, and M. Gill (2001). "Natural Covers for Landfills and Buried Waste." *J. Environ. Eng.* 127:768-775.

Hosler, R. (1984). "Soil Survey of Gilliam County." United States Department of Agriculture-Soil Conservation Service, U.S. Govt. Printing Office, Washington, D.C. 172 pp.

Klute, A. (1986). "Water Retention: Laboratory Methods." In A. Klute (ed.) *Methods of Soil Analysis*. Part 1. 2nd ed. Agron. Monogr. 9. ASA and SSSA, Madison, WI. p. 641-656.

Klute, A. and C. Dirksen (1986). "Hydraulic Conductivity and Diffusivity: Laboratory Methods."." In A. Klute (ed.) *Methods of Soil Analysis*. Part 1. 2nd ed. Agron. Monogr. 9. ASA and SSSA, Madison, WI. p. 694-703.

Larsen, L (1981). "Soil Survey of El Paso County Area, Colorado." U.S. Department of Agriculture-Soil Conservation Service in cooperation with the Colorado Agricultural Experiment Station. U.S. Gov. Printing Office, Washington,D.C. 212 pp.

Nelson, D.W. and L.E. Sommers (1996). "Total Carbon, Organic Carbon, and Organic Matter." In D.L. Sparks (ed.) *Methods of Soil Analysis*. Part 3. Agron. Monogr. 5. ASA and SSSA, Madison, WI. p. 995-996.

Rhoades, J.D. (1996). "Salinity: Electrical Conductivity and Total Dissolved Solids." In D.L. Sparks (ed.) *Methods of Soil Analysis*. Part 3. Agron. Monogr. 5. ASA and SSSA, Madison, WI. p. 427-431.

Sumner, M.E. and W.P. Miller (1996). "Cation Exchange Capacity and Exchange Coefficients." In D.L. Sparks (ed.) *Methods of Soil Analysis*. Part 3. Agron. Monogr. 5. ASA and SSSA, Madison, WI. p. 1201-1229.

Thomas, G.W. (1996). "Soil pH and Soil Acidity." In D.L. Sparks (ed.*) Methods of Soil Analysis*. Part 3. Agron. Monogr. 5. ASA and SSSA, Madison, WI. p. 475-488.

van Genuchten, M. Th.(1980)."A closed form equation for Predicting the Hydraulic Conductivity of Unsaturated Soils." Soil Sci.Am. J., 44:892-898.

Coupled Environmental Processes in the Mojave Desert
and Implications for ET Covers as Stable Landforms

David S. Shafer[1*], Michael H. Young[1], Stephen F. Zitzer[2], Eric V. McDonald[3] and
Todd G. Caldwell[3]

[1]Division of Hydrologic Sciences, Desert Research Institute, 755 E. Flamingo Road,
Las Vegas, NV 89119; PH (702) 862-5564; FAX (702) 862-5427; email:
david.shafer@dri.edu; *Corresponding author
[2]Division of Earth and Ecosystem Sciences, Desert Research Institute, 755 E.
Flamingo Road, Las Vegas, NV 89119
[3]Division of Earth and Ecosystem Sciences, Desert Research Institute, 2215 Raggio
Parkway, Reno, NV 89512

Abstract

Monolayer evapotranspiration (ET) covers are the baseline method for closure
of disposal sites for low-level radioactive waste (LLW), mixed LLW, and transuranic
(TRU) waste at the Nevada Test Site (NTS). The regulatory timeline is typically
1,000 years for LLW and 10,000 years for TRU waste. Covers for such waste have
different technical considerations than those with shorter timelines because they are
subject to environmental change for longer periods of time, and because the
environmental processes are often coupled. To evaluate these changes, four analog
sites (approximately 30, 1,000 to 2,000, 7,000 to 12,500, and 125,000 years in age)
on the NTS were analyzed to address the early post-institutional control period (the
youngest site), the 1,000-year compliance period for disposal of LLW, and the
10,000-year period for TRU waste. Tests included soil texture, structure, and
morphology; surface soil infiltration and hydraulic conductivity; vegetation and
faunal surveys; and literature reviews. Separate measurements were made in plant
undercanopy and intercanopy areas. The results showed a progressive increase in silt
and clay content of surface soils with age. Changes in soil texture and structure led to
a fivefold decline in saturated hydraulic conductivity in intercanopy areas, but no
change in undercanopies, which were subject to bioturbation. These changes may
have been responsible for the reduction in total plant cover, most dramatically in
intercanopy areas, primarily because more precipitation either runs off the site or is
held nearer to the surface where plant roots are less common. The results suggest that
covers may evolve over longer timeframes to stable landforms that minimize the need
for active maintenance.

Introduction

Vegetated, evapotranspiration or "ET" covers are rapidly gaining acceptance at arid and semi-arid sites for waste site closure based on water-balance and related studies being conducted at sites such as those at Sandia National Laboratories, New Mexico (Dwyer, 2003), and the Hanford Nuclear Reservation, Washington (Gee *et al.*, 1997). In addition, at more than a dozen sites across the United States (U.S.) through the U.S. Environmental Protection Agency's Alternative Cover Assessment Program (http://www.dri.edu/Projects/EPA/boston-brochure2.html), ET components have been incorporated into alternative cover designs. Other facilities, such as the Edwards Air Force Base in California, are developing site-wide closure strategies for disposal sites using ET covers (Young *et al.*, 2004a). Evapotranspiration covers are a significant departure from traditional closure cover designs. Rather than attempting to restrict infiltration of water, the ET cover allows water to infiltrate into the cover material where natural processes of evapotranspiration and evaporation remove it. At the Nevada Test Site (NTS), monolayer ET covers have been selected as the baseline technology for closure of landfills being used for low-level radioactive waste (LLW), mixed LLW, as well as areas of shallow-land disposal of transuranic (TRU) and mixed TRU waste (Bechtel Nevada, 2001).

However, vegetated ET covers cannot be viewed as static features, but rather as features subject to natural processes of change, the same as any alluvial/colluvial landform, particularly after cover maintenance ends. These changes, and their subsequent effect on long-term cover performance, are difficult to capture in performance modeling because, in many cases, they are poorly understood. Among the most significant shortcomings is our understanding of the relationships between soil water dynamics, soil morphologic development, and plant ecology in arid regions (McDonald, 2002). Thus, the goals of this study were to identify a landform chronosequence at the NTS, describe the sites for soil morphologic, hydrologic, and biotic characteristics, and then analyze the characteristics for interrelationships that would indicate the coupling of environmental processes.

Materials And Methods

Site Description

The NTS, managed by the U.S. Department of Energy (DOE), is located 105 kilometers northwest of Las Vegas, Nevada (Figure 1). Yucca Flat, where the analog sites are located, is a structurally closed basin in the northeast quadrant of the NTS, encompassing an area of about 780 km^2. The Yucca Flat Playa, normally dry, is situated on the southern end of the basin. Average annual precipitation is about 16 cm based on a 1960 to 2003 summary of data

(http://www.sord.nv.doe.gov/home_climate_MEDA.htm). On average, 57 percent of annual precipitation on the NTS occurs between November and March.
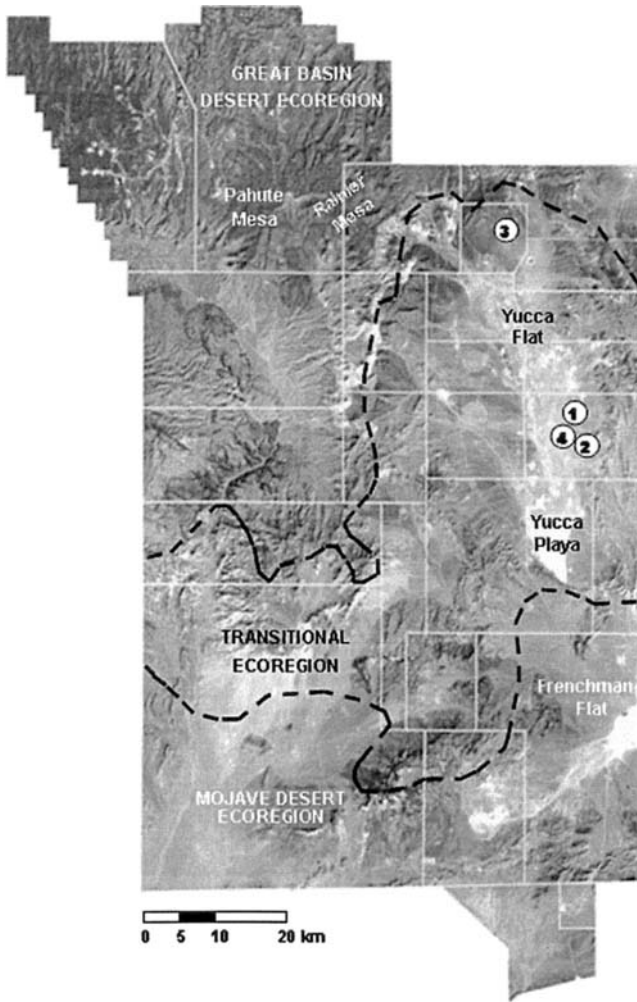
Figure 1. The Nevada Test Site, located 105 km northwest of Las Vegas, Nevada. Analog Sites 1, 2, and 4 are on the east side of Yucca Flat, while Site 3 is on the north end of the basin. The analog sites are in a transition zone between the Mojave and Great Basin desert ecoregions (Wills and Ostler, 2001).

Analysis of Analog Sites

Site Selection

The analog sites (Site 1: ~30 years; Site 2: 1,000 to 2,000 years; Site 3: 7,000 to 12,500 years; and Site 4: ~125,000 years in age) were selected to addresses changes in the early post-institutional control period (the youngest site), the 1,000-year compliance period for disposal of LLW and mixed LLW, and the 10,000-year compliance period for TRU waste sites. Analog sites were selected based on criteria that included 1) evidence that the sites had been isolated from recent alluvial, colluvial, and erosional processes that would not be expected to be agents on newly constructed ET covers; 2) low surface gradients, eliminating the need to consider processes such as sheet wash that a newly constructed cover would also be designed not to experience; 3) minimal anthropomorphic impacts, or, if present, their impacts were clearly distinguished from natural processes; and 4) that some means of obtaining age control could be established for the site (Shafer *et al.*, 2004). The four sites are located within an elevation range of 1,261 and 1,483 m in Yucca Flat, which lies within an ecosystem transition region between the Mojave Desert and the Great Basin (Wills and Ostler, 2001).

Biotic Surveys

At each site, a series of 5 x 10 m subplots were established in a 50-m-long belt transect in which all perennial plants had their rectangular coordinates and their canopy heights and widths measured (Zitzer *et al.*, 2004). Plant nomenclature was based on Hickman (1993). Winter annual plant diversities and density were measured in five paired subplots at each site. Annuals were noted as living in the undercanopy of perennial shrubs or, when at least 0.5 m from the shrub canopy edge, as being in the intercanopy area. The frequency and size of animal burrows were also measured and their distribution noted as being in undercanopy or intercanopy environments. The depth of animal burrows was noted in soil trenches constructed at Sites 1, 2, and 3. A literature review was conducted to determine possible burrowing vertebrate and invertebrate species at the sites, and their habits that would affect the depth and distribution of their burrows.

Soil Morphology

Soils were described from trenches constructed at Sites 1, 2, and 3. Trenches were dug to a depth at which the maximum fine rooting depth was observed. Representative bulk samples for laboratory analysis were collected from each horizon from paired undercanopy and intercanopy soil profiles. Soil characteristics were described in accordance with U.S. Natural Resources Conservation Service soil survey methods (USDA, 1999) as well as those of Birkeland (1999). Soils were analyzed for particle-size distribution using laser light scattering (Gee and Or, 2002), carbonate content using Chittick apparatus (Dreimanis, 1962; Machette, 1985), and electrical conductivity (Rhoades, 1996). Using methods from Birkeland (1999), particle-size distribution of the less than 2 mm fraction is shown as percent weight of each major fraction (sand, silt, clay) and weight percent of each subfraction (Table 1). Abbreviations used in soil morphology descriptions are from USDA (1999).

Table 1. Average ± standard deviation for textural components of material sampled at intercanopy and undercanopy areas. Gravel fraction is the weight percent of the entire sample >2 mm. The remaining textural analysis involves only the fine-earth fraction (<2 mm).

Intercanopy

Year	%Gravel[1]	%Sand[2]	%Silt[3]	%Clay[4]
30	49.3 ± 5.2	79.7 ± 6.0	14.5 ± 1.9	5.8 ± 2.5
1,000 to 2,000	35.8 ± 7.8	80.2 ± 3.0	14.2 ± 0.5	5.7 ± 2.4
7,000 to 12,500	55.6 ± 17.7	55.6 ± 6.0	28.3 ± 2.6	16.1 ± 1.9
125,000	31.6 ± 21.0	50.6 ± 3.9	34.1 ± 1.7	15.3 ± 3.8

Undercanopy

Year	%Gravel[1]	%Sand[2]	%Silt[3]	%Clay[4]
30	38.6 ± 7.8	84.1 ± 3.0	10.9 ± 1.1	5.0 ± 1.2
1,000 to 2,000	33.0 ± 13.4	80.7 ± 2.8	15.6 ± 1.1	3.7 ± 0.8
7,000 to 12,500	26.4 ± 7.9	65.1 ± 5.0	23.0 ± 1.6	11.9 ± 5.4
125,000	27.2 ± 12.6	70.4 ± 8.0	23.0 ± 2.8	6.6 ± 2.6

[1]%Gravel is representative of the total sample > 2 mm.
[2]%Sand of the fine-earth fraction ranging from 62.5 μm to 2,000 μm.
[3]%Silt of the fine-earth fraction ranging from 3 μm to 62.5 μm.
[4]%Clay of the fine-earth fraction < 2 μm.

Hydraulic Property Estimation

The tension infiltrometer (TI) method (Ankeny *et al.,* 1988; Reynolds and Elrick, 1991) was used for determining the soil hydraulic properties of the surface soil. Paired locations of undercanopy and intercanopy locations were identified in undisturbed areas adjacent to the biotic transects. Five paired locations were identified at each site, with the locations for the canopy area chosen to maximize the spacing between measurements. The locations for the intercanopy were chosen to be within one to two meters of the shrub used for canopy measurements. Triplicate measurements were taken whenever possible to account for spatial variability of hydraulic properties.

Measurements followed the procedures described by Casey and Derby (2002) and Young *et al.* (2004b), using four to five tension steps for each test, typically at levels -12, -9, -6, -3, and 0 (saturation) cm. At the conclusion of each test, a bulk density sample of the soil was collected for volumetric water content and particle-size distribution analysis. In total, 48 TI tests were conducted at the four sites, with at least three measurements for any particular treatment used to calculate the mean. Two analytical methods were used for solving for hydraulic conductivity (K_{sat}) (see Table 2). The semi-empirical, nonlinear least-squares regression routine for Wooding's Analysis was used to solve for two unknowns ($Ksat_w$ and α_w) by minimizing error through iterative solutions (Logsdon and Jaynes, 1993). A numerical inversion method using the HYDRUS-2D model (Simunek *et al.,* 1996) provided a complete set of hydraulic properties. The hydraulic properties refer to the soil water retention curve (van Genuchten, 1980), and the hydraulic conductivity equation derived by Mualem (1976) and modified by van Genuchten (1980). Results produced a series of

fitting parameters and physical properties of the soil that were cross-correlated to geomorphic and age setting and the hydraulic properties. Correlation tables were constructed to identify the most sensitive parameters affecting hydraulic properties.

Table 2. Results of field analyses of hydraulic properties at the four analog sites. K_{sat} and alpha parameters are represented as geometric mean. Other parameters are arithmetic mean.

Wooding's Analysis – Intercanopy

~ Age (years)	$Ksat_w$ (cm/d)	α_w (cm^{-1})	R^2
30	119.12	0.268	0.951
1,000 to 2,000	87.95	0.133	0.948
7,000 to 12,500	66.56	0.181	0.930
125,000	25.27	0.123	0.961

Wooding's Analysis – Undercanopy

~ Age (years)	$Ksat_w$ (cm/d)	α_w (cm^{-1})	R^2
30	75.01	0.313	0.961
1,000 to 2,000	147.18	0.260	0.940
7,000 to 12,500	55.13	0.180	0.887
125,000	81.01	0.251	0.950

HYDRUS-2D Analysis - Intercanopy

~ Age (years)	θs	α_{vg} (cm^{-1})	n	$Ksat_{vg}$ (cm/d)	$1/\alpha$ (cm)	R^2
30	0.262	0.137	1.495	280.02	7.29	0.997
1,000 to 2,000	0.269	0.060	2.522	86.98	16.58	0.999
7,000 to 12,500	0.304	0.086	1.753	109.10	11.59	0.999
125,000	0.215	0.064	2.454	27.95	15.56	0.998

HYDRUS-2D Analysis – Undercanopy

~ Age (years)	θs	α_{vg} (cm^{-1})	n	$Ksat_{vg}$ (cm/d)	$1/\alpha$ (cm)	R^2
30	0.318	0.204	1.378	392.74	4.90	0.997
1,000 to 2,000	0.397	0.182	1.471	131.16	5.50	0.997
7,000 to 12,500	0.316	0.127	1.586	275.88	7.87	0.998
125,000	0.341	0.102	1.713	398.77	9.82	0.999

Results And Discussion

Using the field methods described above, it was clear that the most significant soil-forming process observed at the sites was the development of an Av vesicular soil horizon, commonly found in desert soils in the southwest U.S. and formed from the long-term accumulation of aeolian silt and clay below the soil surface (McFadden *et al.*, 1998). Intercanopy development of Av horizons began at Site 2 (1,000 to 2,000 years old) with the development of Avj1 and Avj2 horizons. At Site 3, a well-developed and thick (10 cm) Av horizon developed (Figure 2a). The percent silt/clay is actually higher at Site 3 than Site 4, likely because it is situated at the north end of Yucca Flat, which contributes significant aeolian material. In contrast, soils in the undercanopy areas at all the sites exhibited abundant signs of faunal and floral bioturbation. The AC soil horizons at Sites 2 and 3 are largely composed of soil material excavated from below by animals. The excavated material forms circular and

conical mounds that extend slightly beyond the edge of the shrub canopy (Figure 2b). While an overall increase with time of aeolian-deposited material was observed, Av and Avj horizons were discontinuous and mixed due to bioturbation and have morphological properties similar to BC and BCk horizons.
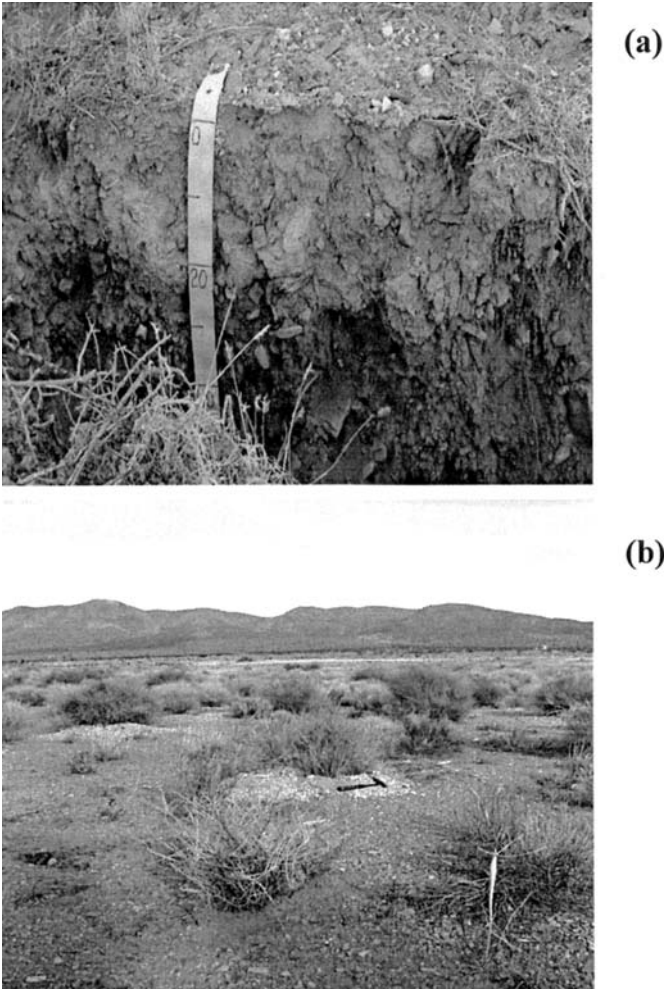
Figure 2. A well-developed Av horizon at 10 to 20 cm depth in a soil trench at the 7,000-12,500-year-old site (a), and conical mounds of lighter-toned soil formed by bioturbation in the undercanopy of shrubs at the 1,000- to 2,000-year-old sites (b).

Development of the near-surface, platy-structure Av horizon was found to restrict water infiltration into the soils profile, and thus water percolation to deeper horizons where plants roots are located. Coupled with the development of desert pavement at Site 3 by 10,000 yr BP, the pedogenic development of the Av horizon probably accounts for a significant decrease in K_{sat} in intercanopy areas over time. The decrease is most evident using the parameter estimation method, in which a fivefold decrease in K_{sat} in intercanopy areas over time was observed. Results of Wooding's Analysis also showed a decrease with increasing site age, although less consistently than with HYDRUS-2D (Figure 3). In contrast to the intercanopy areas, K_{sat} remains relatively constant in the undercanopy areas based on both Wooding's and parameter estimation analyses. We hypothesize that bioturbation in the undercanopy areas from small mammals as well as perennial plant rooting probably prevented the development of Av horizons, which was found (Young et al., 2004a) at other sites in the Mojave Desert to control water entry into soil.
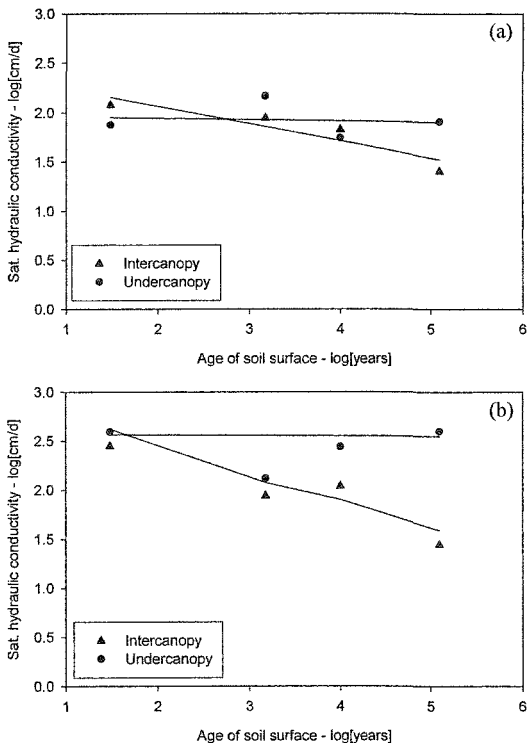
Figure 3. Geometric means of K_{sat} using the semi-empirical (a) Wooding's Analysis, and parameter estimation (b) based on HYDRUS-2D methods, for intercanopies and undercanopies. Regression models are shown as solid lines.

As site age increased, percent perennial plant cover increased to a maximum of 31 percent on Site 3 (7,000 to 12,500 years old), although it decrease to 23 percent at Site 4 (125,000 years old). For all sites, shrubs made up greater than 85 percent of total cover. However, a strong disconnect was observed between peaks in species richness and plant density versus percent cover (Figure 4). Total annual plant density peaked at 246 plants/m^2 at Site 1 (1,000 to 2,000 years old), declined by 55 percent on Site 3, and continued to decline by 83 percent at Site 3. In addition, the highest annual plant density occurred at Site 2 (1,000 to 2,000 years old), and may reflect the period of time when water balance was most affected by transpiration. With increasing age, the development of soil structure such as the Av horizon in the intercanopy areas and the resultant decrease in K_{sat} produced significant contrasts in vegetation density in the intercanopy and undercanopy environments. For example, when comparing annual plant densities at Sites 2 and 3, the undercanopy remained greater than 200 plants/m^2, while intercanopy density decreased by 73 percent. Thus, it appears that pedologic development, especially the surface features of the soil structure and Av horizons, could be reducing the amount of infiltration and/or increasing the water holding capacity of the surface soils, in both cases reducing the depth of wetting front penetration and hence the amount of plant-available water.
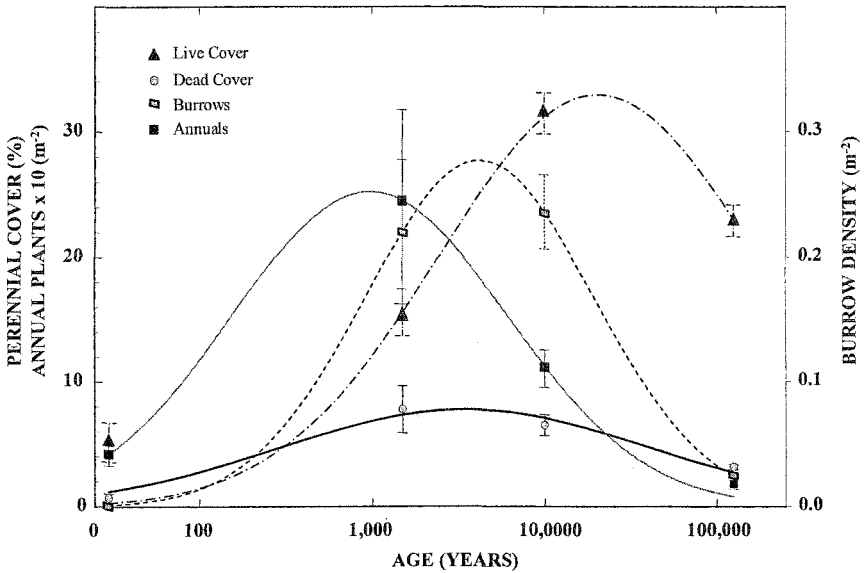
Figure 4. Age relationships between plant cover and winter annual and burrow densities at the four analog sites. Data are plotted at the midpoint of the age range for each site.

Conclusions

Results suggests the presence of complex interactions over time between pedogenic development, hydrology, and biotic activity, but that ET covers allowed to develop naturally may lead toward stable landforms that minimize the need for active maintenance. At any one time, both evapotranspiration and transpiration processes probably contribute to the success of ET covers. However, if the respective roles of "E" and "T" are partitioned over time, soil morphologic development dramatically increases the roles of transpiration over time in maintaining water balance for LLW and TRU covers.

While the study of analog sites suggests that ET covers can evolve naturally for effective performance, cover designs need to incorporate "ingredients" necessary for favorable natural processes to occur. Furthermore, some common cover "maintenance" activities may actually set back natural processes that promote the development of stable cover landforms. For example, the study sites suggest that bioturbation may actually initiate the process of desert pavement development. Surface disturbance outside of shrub canopies from small mammal activity, particularly early in the development of covers, may lead to higher vegetation cover from perennial shrubs and annuals during the period of time when transpiration plays a greater role in water balance for ET covers. While subsurface biological activity could be viewed as a threat to long-term cover performance, the maximum depth of active burrows and krotovina (older, filled-in burrows) coincided with the depth of larger roots, and decreased from a maximum of 0.70 m at Site 1 to 0.30 m at Site 3. Further, consideration of the burrowing characteristics of animals could be used to construct *de facto* barriers. For example, the only rodent species in the study region capable of excavating soil particles of 5 cm or larger is the Botta's pocket gopher (*Thomomys bottae*) (Winkel *et al.*, 1995). Mixed clast size in the biologically active zone of a cover could inhibit the development of macropores from burrows or krotovina.

A legitimate concern is whether the development of the Av horizon and desert pavement, and concomitant decrease in K_{sat}, could result in higher surface runoff that could damage the structural integrity of a cover. However, the lowest K_{sat} estimated was 25 to 81 cm/day, depending on the analytical approach, values still high enough to allow water entry from most storms that would affect the region.

Acknowledgements

References

Ankeny, M.D., T.C. Kaspar and R. Horton. 1988. Design for an automated tension infiltrometer. *Soil Science Society of America Journal* 52:893-896.

Bechtel Nevada. 2001. Integrated Closure and Monitoring Plan for the Area 3 and Area 5 Radioactive Waste Management Sites at the Nevada Test Site. DOE/NV/11718—449-Rev.1.

Birkeland, P.W. 1999. Soils and Geomorphology. Oxford Press, New York, 372 pp.

Casey, F.X.M. and N.E. Derby. 2002. Improved design for an automated tension infiltrometer. *Soil Science Society of America Journal* 66:64-67.

Dreimanis, A. 1962. Quantitative gasometric determinations of calcite and dolomite by using Chittick apparatus. *Journal of Sedimentary Petrology* 32:520-529.

Dwyer, S. 2003. Water Balance Measurements and Computer Simulations of Landfill Covers, Ph.D. Dissertation, University of New Mexico.

Gee, G.W. and D. Or. 2002. Particle-size analysis: *In* Dane, J.H. and G.C. Topp (eds.), Methods of Soil Analysis, Part 4. Physical Methods, Soil Science Society of America Book Series no. 5. p. 255-293.

Gee, G.W., A.L. Ward and M.J. Fayer. 1997. Surface barrier research at the Hanford site. *Land Contamination and Reclamation* 5(3): 233-238.

Hickman, J.C. 1993. The Jepson Manual-Higher Plants of California. University of California Press, Berkeley.

Logsdon, S.D. and D.B. Jaynes. 1993. Methodology for determining hydraulic conductivity with tension infiltrometers. *Soil Science Society of America Journal* 57:1426-1431.

Machette, M.N. 1985. Calcic soils of the southwestern United States. Geological Society of America Special Paper. 203. 1-21pp.

McDonald, E.V. 2002. Numerical simulations of soil water balance in support of revegetation of damaged military lands in arid regions. *Arid Land Research and Management* 16(3) 277-291.

McFadden, L.D., E.V. McDonald, S.G. Wells, K. Anderson, J. Quade and S.L. Forman. 1998. The vesicular layer of desert soils: Genesis and relationship to climate change and desert pavements based on numerical modeling, carbonate translocation behavior, and stable isotope and optical dating studies. *Geomorphology*, p. 101-145.

Mualem, Y. 1976. A new model for predicting the hydraulic conductivity of unsaturated porous media. *Water Resources Research* 12:513-522.

Reynolds, W.D. and D.E. Elrick. 1991. Determination of hydraulic conductivity using a tension infiltrometer. *Soil Science Society of America Journal* 55:633-639.

Rhoades, J.D. 1996. Salinity: electrical conductivity and total dissolved solids. *In*, Sparks, D.L. ed., "Methods of Soil Analysis, Part 3: Chemical Methods," Monograph No. 5. American Society of Agronomy, Madison, WI. Pp. 417-435.

Shafer, D.S., Young, M.H., Zitzer, S.F., McDonald, Eric and Todd Caldwell. 2004. Coupled environmental processes and long-term performance of landfill covers in the northern Mojave Desert. Desert Research Institute Publication No. 45203 for the DOE NNSA Nevada Site Office, DOE/NV/13609-32. 54pp.

Simunek, J., M. Sejna and M.T. van Genuchten. 1996. The HYDRUS-2D software package for simulating water flow and solute transport in two-dimensional variably saturated media. Version 1.0. IGWMC - TPS - 53, International Ground Water Modeling Center, Colorado School of Mines, Golden, CO.

U.S. Department of Agriculture (USDA). 1999. Examination and description of soils in the field, *in* Soil Survey Manual, USDA-Agriculture Research Service: U.S Government Printing Office, Washington D.C.

van Genuchten, M.T. 1980. A closed-form equation for predicting the hydraulic conductivity of unsaturated soils. *Soil Science Society of America Journal* 44:892-898.

Wills, C.A. and W.K. Ostler. 2001. Ecology of the Nevada Test Site: An Annotated Bibliography. Bechtel Nevada Ecological Services, DOE/NV/11718-594.

Winkel, V.K., J.P. Angerer, D.B. Hall, M.W. Fariss and K.R. Johnejack. 1995. Plant and Burrow Animal Characteristics; Integrated Closure Program for the Area 3 and Area 5 Radioactive Waste Management Sites Nevada Test Site. Prepared for U.S. Department of Energy, Nevada Operations Office. 41pp.

Young, Michael, Albright, William, Zachritz, Walter, Shafer, David, Pohlmann, Karl, Cablk, Mary, Zitzer, S.F. and E.V. McDonald. 2004a. Technical approach for designing alternative covers at Edwards Air Force Base, California. DRI Publication No. 41192 for the Environmental Management Directorate, Edwards Air Force Base, California. 58pp.

Young, M.H. E.V. McDonald, T.C. Caldwell, S.G. Benner, D.G. Meadows. 2004b. Hydraulic properties of a desert soil chronosequence in the Mojave Desert, USA. *Vadose Zone J.* 3:956-963.

Zitzer, S.F., D.S. Shafer, M.H.Young, Eric McDonald, and Todd Caldwell. 2004. Changes in diversity and density of northern Mojave plant communities resulting from desert pavement development on a 125,000-year-old chronosequence. Ecological Society of America, 2004 Annual Meeting, Portland.

Darcian Flux Estimations in Evapotranspiration Landfill Covers

James A. Kelsey[1], John T. Kay[2], Mark Ankeny[3], and Mitch Plummer[4]

[1]Daniel B. Stephens & Associates, Inc. 6020 Academy NE, Suite 100, Albuquerque, NM 87109; PH (505) 822-9400; FAX (505) 822-8877; jkelsey@dbstephens.com

[2]Daniel B. Stephens & Associates, Inc. 6020 Academy NE, Suite 100, Albuquerque, NM 87109; PH (505) 822-9400; FAX (505) 822-8877; jkay@dbstephens.com

[3]Idaho National Engineering and Environmental Laboratories. P.O. Box 1625, Mail Stop 2107, Idaho Falls, ID 83415-2107; PH (208) 526-5748; FAX (208) 526-0875; ankemd@inel.gov

[4]Idaho National Engineering and Environmental Laboratories. P.O. Box 1625, Mail Stop 2107, Idaho Falls, ID 83415-2107; PH (208) 526-5748; FAX (208) 526-0875; plumma@inel.gov

Abstract

Evapotranspiration (ET) landfill cover designs are increasingly being considered for use in the arid western United States, in place of standard regulatory designs that require impermeable layers or synthetic materials. Prior to regulatory approval, ET covers are often required to pass a field test designed to demonstrate adequate performance. Daniel B. Stephens & Associates, Inc. (DBS&A) has conducted field demonstrations of ET covers at several locations using a method that estimates flux in ET covers based on daily soil matric potential (ψ) values measured *in-situ*. The method uses heat dissipation sensors (HDSs), soil matric potential/soil moisture content (ψ/θ) relationships for site-specific soils, and Darcian flux calculations to estimate the rate, volume, and direction of soil moisture movement.

Results from two separate multiple-year flux monitoring studies—one where the method worked well and one where it did not—suggest that this method is valid for monitoring flux in covers where relatively low moisture conditions exist, but that it can be highly inaccurate under conditions approaching saturation or where extremely large gradients exist (across wetting fronts or near a capillary break or other impending layer). The uncertainty associated with these measurements is strongly dependent upon site-specific factors including soil properties, magnitude of the hydraulic gradient, and the rate of change of moisture content. These factors produce

inaccurate flux calculations that arise from limitations and assumptions of the Darcian flux calculation, rather than improper functioning of the HDS. These studies suggest that the Darcian flux method, although limited in its application, can provide accurate results when applied under the appropriate conditions, at a substantially lower cost than other methods.

Introduction

In semiarid environments, such as those that exist throughout much of the western United States, alternative or evapotranspiration (ET) landfill covers have been shown to equal the performance of prescriptive covers at substantially reduced costs (Wing and Gee, 1994; Morris and Stormont, 1997). ET covers generally consist of one or more soil layers and reduce infiltration through storage of soil moisture during wet periods and subsequent removal of moisture through evaporation and plant transpiration during dry periods.

Prior to approval of an ET cover by regulatory agencies, it is often desired (or required) that flux be monitored during a test period, to demonstrate that the ET cover meets or exceeds the performance requirements of a prescriptive cover or other regulatory flux criteria. The criteria for demonstrating equivalency have not been strictly or universally quantified; however, the U.S. Environmental Protection Agency's Alternative Cover Assessment Program has suggested that the equivalent performance of an ET cover compared to a soil cover in a semiarid region is 1.0 centimeters per year (cm/yr) flux and compared to a composite prescriptive cover, 0.3 cm/yr flux. In our experience, regulatory agencies have selected the 0.3-cm/yr value as the site-specific performance requirement for approval of an ET cover.

The demonstration of equivalence has typically focused on monitoring moisture conditions within the constructed cover or a test pad designed to mimic conditions of the final cover. A variety of instrumentation and methods for estimating moisture flux in alternative covers has been described and evaluated, including water content reflectometers, time domain reflectometry, heat dissipation sensors, tensiometers, psychrometers, and lysimeters (Gee and Hillel, 1988; Benson et al., 2001). Advantages and disadvantages have been noted for each method, and lysimeters are widely accepted as the most accurate, albeit the most expensive (Gee and Hillel, 1988; Benson et al., 2001). In many instances, however, the goals of a particular study do not require the kind of accuracy associated with lysimeters.

This paper presents the results from two separate field studies that were designed to estimate flux in landfill ET covers using a cost friendly method, referred to as the "Darcian flux calculations" method, that would satisfy regulatory review by providing flux estimates that were accurate enough to convincingly answer the question "is the flux less than or greater than 0.3 cm/yr" Monitoring results from the two studies are presented and used to evaluate the effectiveness of Darcian flux calculations in demonstrating compliance with this regulatory criterion. The effectiveness and limitations of the method, as well as site-specific conditions that contributed to inaccuracies, are discussed.

Site Descriptions and Method Description

Flux within ET covers at two separate landfill sites was estimated. The same methods were used at each site, with the exception of some site-specific differences (such as cover thickness) as described. One of the sites is located in southwest Idaho, the other in west Texas.

Site 1, Idaho
The Idaho site is located at a hazardous waste landfill in southwestern Idaho. Flux was estimated in a test pad constructed following the proposed design for a pending cover for the landfill. Based on a moisture flux modeling analysis conducted using UNSAT-H (Fayer and Jones, 1990), regulators agreed in 2000 to consider the substitution of an ET-type cover for a RCRA Subtitle C prescriptive cover. A 5-year demonstration project was required, with final approval of an ET cover dependent upon the collection of 5 years of moisture flux calculations indicating a cumulative flux of no greater than 0.3 cm/yr through the base of the test pad, at 5 feet below ground surface. The 5-year monitoring period was completed in October 2005.

The test-pad cover at the Idaho site was comprised of four separate soil materials (Figure 1). The subgrade material below the intermediate soil cover layer is not part of the actual cover design; it would be waste if the test pad was an actual landfill cover. When the instruments were installed, core samples of undisturbed soil were collected from each soil type for laboratory determination of hydraulic properties and grain size distribution. Soil physical properties used in the calculation of flux are presented in Table 1. The average monthly rainfall and potential ET at the Idaho site is presented in Figure 2.
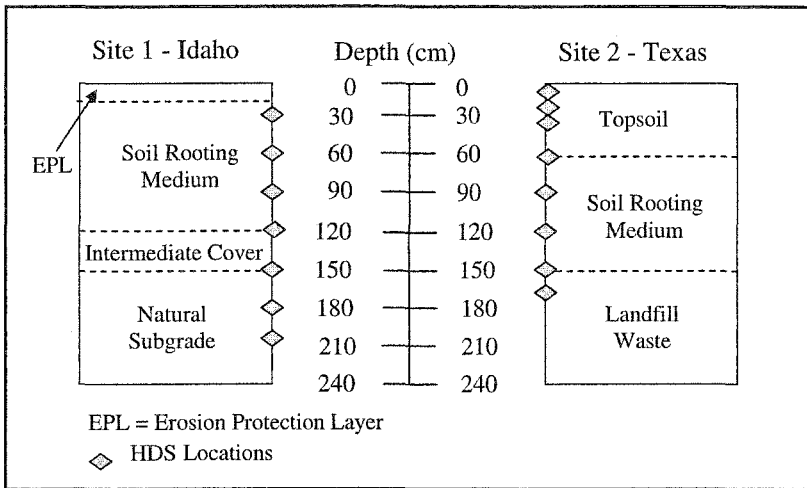
Figure 1: Soil profiles and heat dissipation sensor locations for the Idaho and Texas sites.

Table 1: Soil properties for the two field demonstration sites.

Soil Property	Site 1, Idaho			Site 2, Texas	
	SRM	ISC	Subgrade	Topsoil	SRM
ASTM classification	SM	GP-GM	GP-GM	SM	SC
Dry density (g/cm^3)	1.51	1.27	1.43	1.61	1.50
d_{10} (mm)	0.0080	0.061	0.038	0.0014	0.11
d_{60} (mm)	0.16	8.2	5.0	0.0028	0.14
Porosity (cm^3/cm^3)	0.430	0.520	0.410	0.394	0.435
K_{sat} (cm/s)	0.00085	0.00062	0.00021	0.00016	0.000093
θ_s (cm^3/cm^3)	0.4297	0.5360	0.3980	0.4010	0.4278
θ_r (cm^3/cm^3)	0.0346	0.0258	0.0264	0.0486	0.0176
α (1/cm)	0.0434	0.0615	0.0312	0.0204	0.0168
N	1.2801	1.1458	1.376	1.4750	1.2965

SRM = soil rooting material

ISC = intermediate soil cover
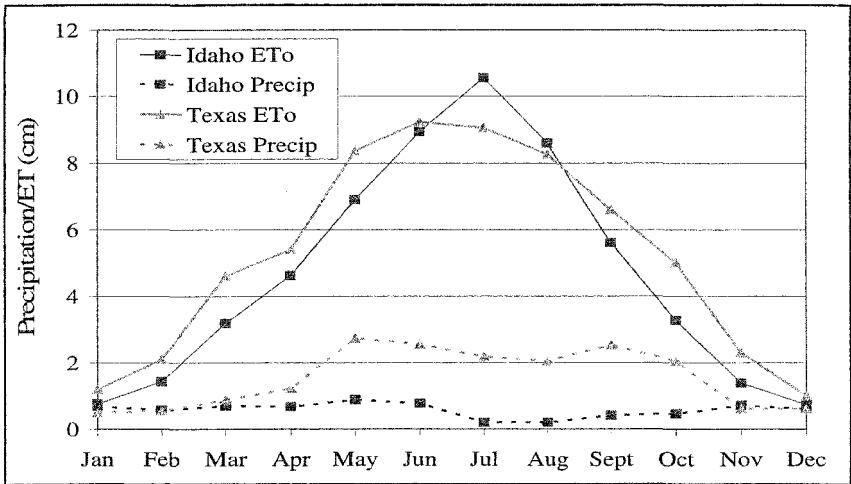
Figure 2: Monthly average precipitation and reference evapotranspiration (ETo) for Idaho and Texas sites, from the Western Regional Climate Center and West Texas Mesonet websites (www.wrcc.dri.edu/index.html; www.mesonet.ttu.edu).

When the cover was constructed in 2000, a seed mix was applied to the cover that included representative local grasses such as crested wheatgrass, siberian wheatgrass, and streambank wheatgrass. The seed mix was drilled in and fertilized over a 2-day period. Vegetative coverage on the test pad is seasonally dynamic, and over the 5-year test period, it has become similar in type and density to the surrounding landscape.

Site 2, Texas

The Texas site is located at a municipal waste landfill in western Texas. Flux calculations were made in three separate existing landfill covers built prior to implementation of Subtitle C requirements. Two of the covers are non-compacted soil covers, and one is a compacted soil cover. The objective of this project was to determine if the pre-Subtitle C covers could match the performance of a Subtitle C prescriptive cover. Monitoring at the Texas site was conducted continually for 30 months, starting in September 2002 and ending in February 2005. The demonstration period was initially intended to last for 5 years, but was cut short when it became apparent that the covers would not perform as well as a prescriptive cover.

The covers at the Texas site were constructed of two separate soil materials (Figure 1). Again, core samples of undisturbed soil were collected from each soil type at the time of instrumentation for laboratory determination of hydraulic properties and grain size distribution; the results of those analyses are presented in Table 1. Figure 2 shows the average monthly rainfall and potential ET for each month of the year at the Texas site. A seed mix of native grasses had been planted on the covers at the time of construction, and vegetation was fully established when the study began.

Instrumentation

Soil moisture potential readings were obtained using Campbell Scientific Model 229 heat dissipation sensors (HDSs) installed in a vertical profile in the subsurface (Figure 1). The HDSs consist of a porous ceramic body that surrounds a heating element and thermocouple. When the porous ceramic body is buried in the ground, it maintains equilibrium with the surrounding soil. HDSs measure the thermal conductivity of their ceramic body, which can be related to the moisture content and matric potential of the ceramic and surrounding soil using the methods described by Flint et al. (2002).

Installation of the sensors was done in vertical profiles, from near ground surface to the bottom of each cover (Figure 1). In Idaho, the sensors were emplaced during construction of the test pad cover. In Texas, the sensors were installed in a trench excavated into the existing covers (the trench was backfilled using the same material that existed prior to excavation). The sensors were installed at a minimum interval of 2 inches from the nearest adjacent probe and at a maximum interval of 12 inches from the nearest adjacent probe (Figure 1).

Flux Calculations

Flux calculations are based on the Darcy's equation for unsaturated flux (van Genuchten, 1980; van Genuchten et al., 1991):

$$q = K(\theta) \bullet \frac{dH}{dL} \quad \text{(L/T)} \qquad \text{(Equation 1)}$$

where: q   = Darcian Flux (L/T)
        $K(\theta)$ = unsaturated hydraulic conductivity (L/T)
        dH/dL = pressure gradient between two points (L/L)

The equation is one-dimensional, assuming that all movement of moisture is either in the upward or downward direction.   A positive flux indicates movement is downward; a negative flux indicates movement is upward. The unsaturated hydraulic conductivity was determined from characteristic curves for the soils in which each sensor was emplaced, using the soil matric potentials measured by the HDSs. Gradients were determined by computing the difference in hydraulic head for adjacent probes.

In its expanded form, equation 1 takes the following form:

$$q = \frac{K(\theta_2) + K(\theta_1)}{2} \bullet \frac{(Z_2 + \psi_2) - (Z_1 + \psi_1)}{Z_2 - Z_1} \text{ (cm/yr)} \qquad \text{(Equation 2)}$$

where: $K(\theta_1)$ = hydraulic conductivity at lower HDS location (cm/yr)
        $K(\theta_2)$ = hydraulic conductivity at higher HDS location (cm/yr)
        ψ_i = soil matric potential at HDS location i (–cm)
        Z_i = elevation head at HDS location i (cm)

Flux was calculated daily for each coupled pair of adjacent HDSs. Cumulative flux was determined by summing the daily fluxes.

Results

The fluxes determined for the two sites show strikingly different types of behavior. While the Idaho site produced what appear to be very reasonable and consistent flux results, the Texas site produced erroneous flux results that were much greater than could be reasonably expected. The difference in the quality of results obtained from the two sites appears to be related to climatic conditions, particularly the rate and time of year that precipitation occurs and the rate of wetting front progression to the subsurface.

Site 1, Idaho

During the 5 years of monitoring at the Idaho site, precipitation was very near normal; two years had slightly greater than and three years had slightly less than the annual average of 23 cm. Typically, the greatest precipitation occurred during March and April, and the least precipitation occurred from July through October. Moisture

potentials near the surface were influenced by climatic conditions to a much greater extent than those at greater depths. While the near-surface potentials (at 30 cm deep) fluctuated seasonally between approximately –500 cm and –750,000 cm, the potentials near the base of the cover remained between approximately –10,000 cm and –100,000 cm at all times (Figure 3). The change in potentials below 60 cm was muted in comparison to the changes at 30 and 60 cm; that is, although some seasonal response was evident throughout the cover, the majority of moisture infiltration into the cover was limited to the top 60 cm.
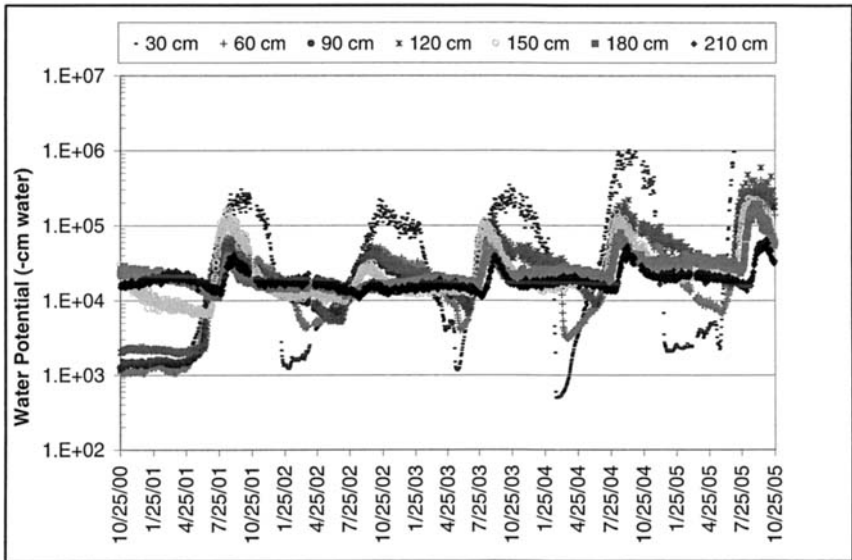
Figure 3: Daily heat dissipation sensor data from the Idaho site.

Figure 4 depicts the daily fluxes calculated using the Darcian flux method. Between 30 and 60 cm, downward flux in response to periods of precipitation, as well as upward flux in response to periods of dry heat, are pronounced. Below 60 cm, fluxes still show some seasonal trends; however, they are much smaller in magnitude compared to the near-surface flux. The average annual flux at the base of the cover (150 cm) was calculated to be 1.72×10^{-4} cm in the downward direction (Table 2). The fluxes determined at the other depths within the cover are all relatively consistent, with the exception of the fluxes in the subgrade material (150 to 210 cm), which were calculated to be in the upward direction. This change in direction is likely due to water removal that occurred during the summer months, which caused increased drying at depths up to 150 cm, relative to depths 180 and 210 cm.
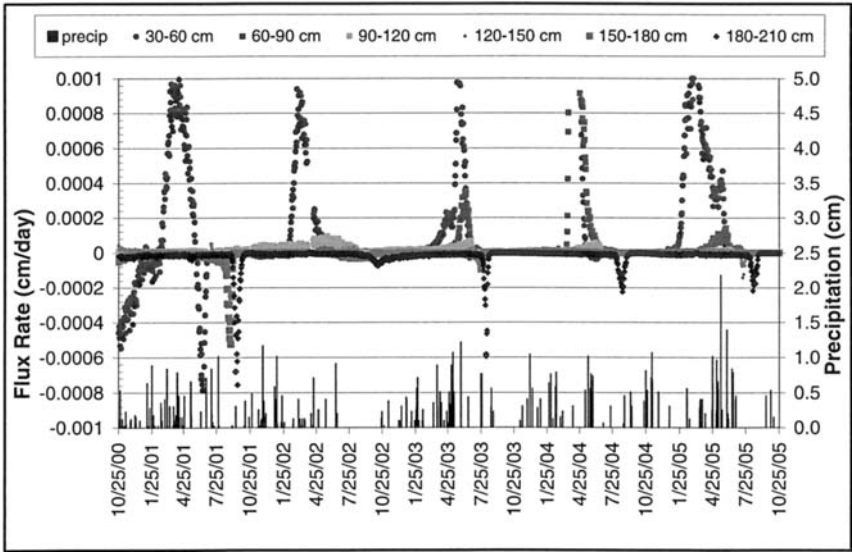
Figure 4: Daily flux at the Idaho site. Positive flux values indicate flux in the downward direction; negative values indicate flux in the upward direction.

Table 2: Calculated average annual flux at each monitoring depth. Negative values indicate flux in the upward direction.

Site 1, Idaho		Site 2, Texas	
Depth	Flux (cm/yr)	Depth	Flux (cm/yr)
--	--	5-10 cm	7,375
--	--	10-30 cm	2.4
30-60 cm	6.58×10^{-4}	30-60 cm	-263
60-90 cm	4.30×10^{-5}	60-90 cm	123,170
90-120 cm	4.96×10^{-5}	90-120 cm	160
120-150 cm	1.72×10^{-4}	120-150 cm	7397
150-180 cm	-8.07×10^{-6}	--	--
180-210 cm	-2.00×10^{-5}	--	--

Site 2, Texas

Conditions at the Texas site contrasted sharply to those at the Idaho site. Rather than receiving numerous small (<1 cm) precipitation events and very few large (>2 cm) precipitation events, the Lubbock site regularly received multiple large precipitation events in rapid succession. During the summer months, when the air was warm and

vegetation was most active, infiltration was limited to the uppermost 60 cm; however, during the fall and winter months, precipitation infiltrated through the entire cover. Figure 5 shows how on several occasions the moisture conditions throughout the entire cover profile shifted quickly from very dry conditions (approximately −10,000 cm) to near saturation.
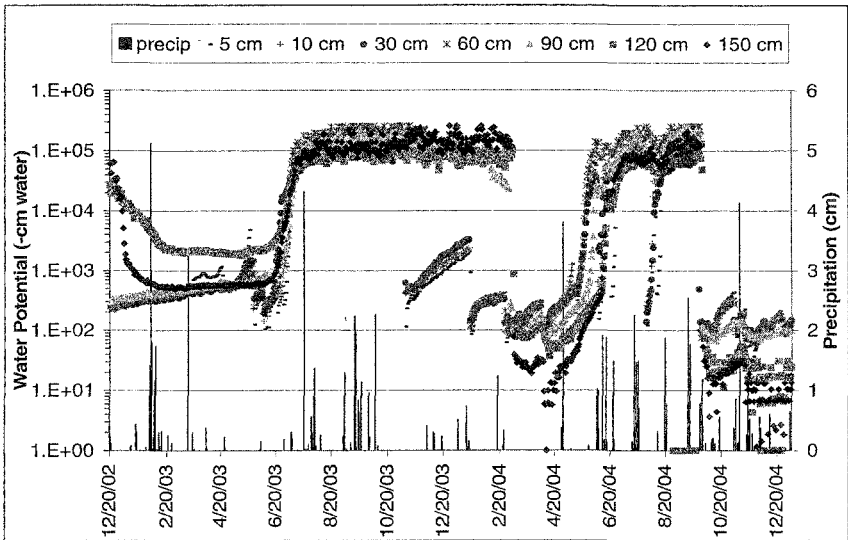
Figure 5: Soil moisture potential data obtained from Texas site.

When these large-scale shifts occurred, extremely large gradients developed between adjacent probes. Although these gradients typically only lasted for several days, the magnitude of the gradient, sometimes in excess of 100,000 cm, resulted in the calculation of impossibly large fluxes (Figure 6). These extremely large fluxes were determined for both the upward and the downward directions. The effect of the large gradients on the flux calculations is magnified with increasing moisture content, because the hydraulic conductivity becomes substantially greater as well.

Efforts to correct for the anomalous flux calculations by assuming a unit gradient of one during the periods of rapid change were attempted, but they were ultimately abandoned because they were too subjective and not rooted in any particular scientific basis. For the purposes of the study, it was determined that a cover with a saturated hydraulic conductivity of approximately 10^{-5} cm/s that remained at or very near saturation for more than 60 consecutive days was certainly allowing more than 0.3 cm of moisture to pass through it.
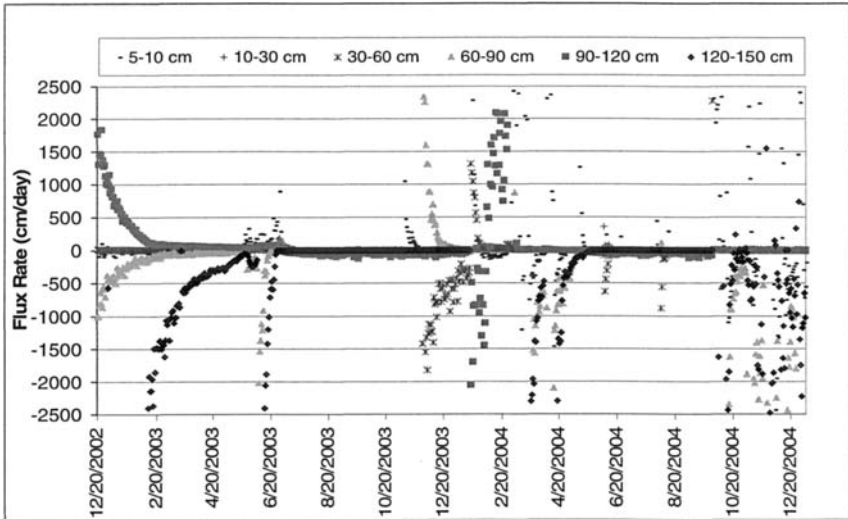
Figure 6: Calculated fluxes for Texas site.

Discussion and Conclusions

The results of the two studies presented in this paper seem to support previous observations regarding the accuracy of Darcian flux calculations. Specifically, Darcian flux measurements are subject to large potential errors, orders of magnitude in some cases, and are not a good alternative to lysimeters when very accurate quantification is necessary (Gee and Hillel, 1988; Benson et al., 2001). Monitoring the matrix material of a cover is vital to confirm proper performance of an ET cover and to confirm that predicted cover storage, thickness, and hydraulic properties were achieved during construction. Our experience suggests that the Darcian flux methods described in this paper can be successfully used to estimate flux within the unsaturated zone present in many ET covers. However, the method is better suited to environments with consistently dry conditions and where sharp wetting fronts never, or infrequently, reach the plane of compliance (usually the base of the cover). In an environment where a low equivalency percolation rate, such as 0.3 cm/yr, truly has a potential of being realized, the base of a cover that has been conservatively modeled, designed and constructed and that uses material of well defined hydrological properties should meet these assumptions.

In locations where Darcian calculations are not suitable to determining flux, the matric potential data obtained from HDSs can be useful in guiding the design or modification of ET covers to provide adequate storage capacity. For example, data from the Texas site suggest that, even though gradients are very high, causing unrealistic predictions of moisture movement, conditions exist that cause large amounts of moisture to move both in and out of the cover. Specifically, conditions

indicate that moisture is removed from the cover during the summer months to the maximum depth of the cover at 150 cm below ground surface. Perhaps by increasing the storage capacity of the cover, either by use of a capillary barrier or increasing soil thickness, an ET cover may still be a viable alternative for this site.

The use of HDSs is a valid means of obtaining matric potential at depth at these and other similar sites; however a more robust model than the Darcian flux is required to enable meaningful flux calculations under conditions of high or rapidly changing moisture content. Such a model would need to (1) consider textural effects that greatly influence soil/water interactions and (2) limit calculated flux by invoking mass balance accounting.

References

Benson, C., Abichou, T., Albright, W., Gee, G., and Roesler, A. 2001.   Field Evaluation of Alternative Earthen Final Covers. Int. J. Phytoremediation, 3(1), 105-127.

Fayer, M.J., and Jones, T.L. 1990. *UNSAT-H version 2.0: Unsaturated soil water and heat flow model*, PNL-6779, Pacific Northwest Laboratory, Richland, Washington.

Flint, A.L., Campbell, G.S., Ellett, K.M., and Calissendorff, C. 2002. Calibration and temperature correction of heat dissipation matric potential sensors. *Soil Science Society of America Journal* 66: 1439-1445.

Gee, Glendon W. and Hillel, Daniel. 1988. Groundwater Recharge in Arid Regions: Review and Critique of estimation Methods. *J. Hydrolog. Proc.* Vol 2, 255-266.

Morris C. and J. Stormont. 1997 Capillary barriers and subtitle D covers: Estimating equivalency. *J Envir. Engng.,* ASCE 123(1), 3-10.

van Genuchten, M.T. 1980. A closed-form equation for predicting the hydraulic conductivity of unsaturated soils. *Soil Science Society of America Journal* 44, 892-898.

van Genuchten, M.T., Leij, F.J., and Yates, S.R. 1991. *The RETC code for quantifying the hydraulic functions of unsaturated soils.* Robert S. Kerr Environmental Research Laboratory, Office of Research and Development, U.S. Environmental Protection Agency, Ada, Oklahoma. EPA/600/2091/065. December 1991.

Wing, N and G. Gee. 1994. Quest for the perfect cap. *Civil Eng.* 64(10), 38-41.

Lysimeters versus Water-Content Sensors for Performance Monitoring of Alternative Earthen Final Covers

Michael A. Malusis[1] and Craig H. Benson[2]

[1]Department of Civil and Environmental Engineering, Bucknell University, Lewisburg, PA 17837, USA; PH: (570) 577-1683; FAX: (570) 577-3415; email: mam028@bucknell.edu
[2]Department of Civil and Environmental Engineering, University of Wisconsin-Madison, Madison, WI 53706, USA; PH: (608) 262-7242; FAX: (608) 263-2453; email: benson@engr.wisc.edu

Abstract

This paper reviews the relative merits of two approaches for performance monitoring of alternative earthen final covers (AEFCs): (1) direct measurement of percolation via large-scale pan lysimetry and (2) indirect assessment using data from water-content sensors. Large-scale lysimeters account for spatial variability and preferential flow and can resolve percolation rates on the order of 0.1 mm/yr, which is at least ten times lower than typical percolation criteria applied in practice (1-3 mm/yr). However, factors such as the capillary break effect, thermal water fluxes, and leaks can affect the accuracy of percolation rates measured with lysimeters. Lysimeters are also expensive and difficult to install. In contrast, water-content sensors are relatively inexpensive and are relatively simple to install, permitting multiple monitoring points within a cover at relatively low cost. However, demonstrating compliance using water content data is confounded by several factors, particularly spatial variability, scale effects, pedogenesis, and preferential flow. An analysis conducted using Monte Carlo simulation shows that estimates of percolation rate from water content data can vary by as much as six orders of magnitude due to spatial variability alone. For sites where a percolation criterion has been established, the best approach is to combine lysimetry and water-content sensors. Percolation rates measured with the lysimeter can be used for compliance monitoring and water-content data can be used for interpreting the lysimeter data and to assess reliability and representativeness.

Introduction

Alternative earthen final covers (AEFCs) are earthen covers for waste containment systems that rely on water balance principles to limit the rate of percolation into the underlying waste. An AEFC generally is used as an *alternative* to a conventional cover that relies on a resistive barrier (i.e., a compacted clay or geomembrane-clay composite barrier) to limit percolation. In many applications, the AEFC is required to be *equivalent* to the conventional cover, which usually means that the percolation rate from the AEFC must be no more than the percolation rate expected for the conventional cover.

AEFCs function by storing water that infiltrates during periods of elevated precipitation and minimal evapotranspiration and subsequently transmitting the stored water back to the atmosphere via evapotranspiration during drier periods (Stormont and Morris 1998, Khire et al. 2000). AEFCs are effective when the cover profile has sufficient storage capacity and sufficient evapotranspirative demand exists to remove the stored water. When an AEFC performs satisfactorily, water contents within the AEFC rise and fall on a seasonal basis in response to infiltration and evapotranspiration. Provided the cover has adequate storage capacity and functions properly, percolation rates from AEFCs can be very low (< 1 mm/yr) (Albright et al. 2004).

Because AEFCs are a relatively new technology, monitoring often is required to demonstrate that the cover is satisfying a percolation criterion. Two approaches currently are used to monitor the percolation rate: (i) direct measurements using large-scale pan lysimeters or flux meters and (ii) indirect measurements using water-content sensors. The objective of this paper is to assess the viability of both monitoring approaches and to discuss conditions under which the methods are applicable. Limitations of each approach are discussed and potential sources of uncertainty are identified. A combined approach is discussed that benefits from the merits of both techniques.

Lysimeters

Two devices are available for obtaining direct measurements of percolation: pan lysimeters and flux meters (Gee and Hillel 1988, Benson et al. 2001, Gee et al. 2002). Schematics of both are shown in Figure 1. Pan lysimeters typically are used for measuring percolation over a relatively large area, whereas flux meters are used for point measurements of percolation. Spatial variability (i.e., heterogeneity in hydraulic and vegetation properties) and preferential flow through macrofeatures (i.e., cracks, holes, etc.) are key factors that affect the rate at which percolation is transmitted, and accounting for these factors requires a measurement large enough to reliably represent the pathways conducting flow. Because the properties of engineered soils are correlated over distances of 1-3 m (Benson 1991), an area with dimensions of 10 m x 10 m or larger is needed to adequately account for spatial variability and preferential flow (Benson et al. 2001). For this reason, percolation measurements made with large-scale pan lysimeters are considered to be more representative than those with flux meters. Modern pan lysimeters that are carefully designed can be used to resolve percolation rates as low as 0.1 mm/yr (Benson et al. 2001).
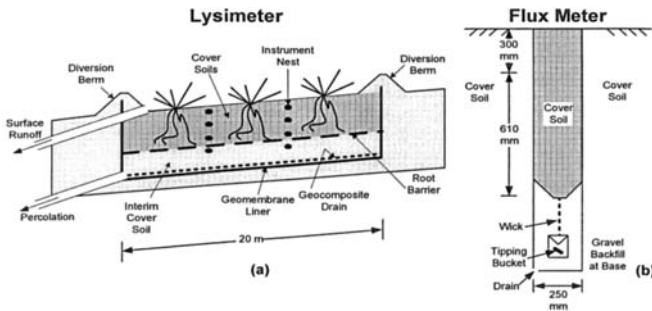
Figure 1. Schematics of (a) a pan lysimeter and (b) a flux meter. Adapted from Benson et al. (2001) and Gee et al. (2002).

Although pan lysimeters provide a simple large-scale measurement of percolation, they also have several drawbacks that affect the accuracy with which percolation can be measured. The three most significant technical drawbacks are (i) the capillary break effect at the interface between the drainage material at the base of the cover and the overlying cover soil, (ii) the barrier to vapor diffusion caused by the collection pan, and (iii) the possibility of leaks or a malfunction that prevents water from being collected. Lysimeters also are difficult and costly to install, which limits the number of points that can be monitored.

Capillary Break Effect

The capillary break effect is caused by the contrast in hydraulic properties at the interface between the base of the cover and the drainage layer. The capillary break formed at this interface impedes the flow of water into the drainage collection system until the soil immediately above the interface is nearly saturated.   This impedance can result in underestimation of the percolation rate relative to that which might occur in the actual cover. An example of the capillary break effect is illustrated by field data obtained from a lysimeter at the Rocky Mountain Arsenal (RMA) that was used to evaluate one of four AEFC designs proposed for the site. The cover profile consisted of a 1.07-m-thick layer of clayey sand with a field capacity (defined as the water content at a matric suction head of 3.3 m) ranging from 15 to 30 % (average field capacity $\approx$ 23 %) (TTFW 2005b). Percolation from the base of the cover was collected in a geocomposite drainage net (GDN) underlain by a geomembrane (GM). The lysimeter was similar to that shown in Figure 1a, except there was no root barrier, interim cover soil, or sidewalls.   Moderate-frequency (MHz range) time domain reflectometry (TDR) sensors were installed within the perimeter of the lysimeter at six different depths to record temporal and spatial variations in volumetric water content.

Water contents measured during the Spring and Summer of 1999 are shown in Figure 2. Near the base of the cover, the water contents exceed the average field capacity in May and June. However, no percolation was recorded in May or June 1999, or for the remainder of the summer. The absence of percolation when the water content at the base is above field capacity is indicative of a capillary barrier effect.

Laboratory tests were conducted by Tetra Tech FW, Inc. (TTFW 2005a) to determine if a similar capillary barrier effect could be reproduced in the laboratory using borrow soil that exhibits similar texture and has been approved for full-scale AEFC construction at RMA. Soil water characteristics curves (SWCCs) were measured for the GDN and the borrow soil and column tests were conducted that simulated infiltration into the cover profile.   The SWCC data are shown in Figure 3 along with smooth curves corresponding to the van Genuchten function (van Genuchten 1980).   The suction (ψ_b) and water content (θ_b) corresponding to imminent breakthrough across the capillary break, as defined by Khire et al. (2000), are also shown in Figure 3.   According to the theory in Khire et al. (2000), breakthrough across the interface between the cover soil and GDN will occur when the suction drops below 0.01 m.   At this suction, the water content of the cover soil at the interface will be approximately 43%, which is nearly the same water content reached at the base of the test cover in June 1999 (Figure 2). Thus, percolation into the GDN of the lysimeter underlying the test cover probably was imminent in June 1999. If the capillary break had not been present, the additional water stored at the base of the cover (i.e., $\geq$ 22 mm for $\theta_{fc} \leq 30\%$) may have been transmitted as percolation.
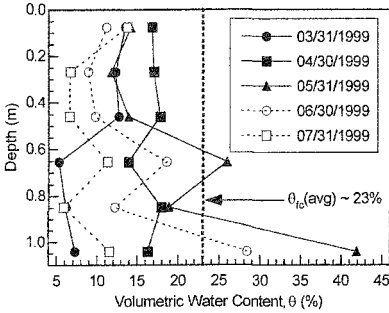
Figure 2. Water content profiles from lysimeter at RMA. Base of the cover is at 1.07 m.
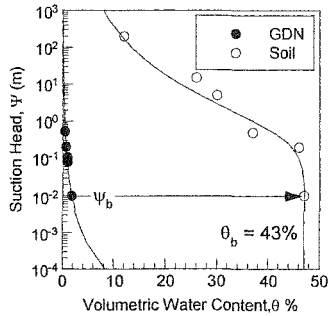
Figure 3. SWCCs for RMA geocomposite drainage net (GDN) and cover soil.

The column testing apparatus used by Tetra Tech FW, Inc. was similar to that used by Stormont and Anderson (1998). A schematic of the column is shown in Figure 4a. The column consisted of a 202-mm-diameter plastic cylinder containing a 500-mm-thick layer of clayey sand underlain by the GDN and a layer of gravel (TTFW 2005a). Tensiometers were installed in the fine soil at depth increments of 100 mm, except for the lowermost tensiometer, which was installed at a depth of 490 mm (10 mm above the interface between the cover soil and the overlying GDN). Inflow into the column was controlled by a peristaltic pump and outflow was measured with a tipping bucket. Data collected from the column test are shown in Figure 4b. Breakthrough occurs when the suction at the lowermost tensiometer is between 0.013 and 0.020 m, which corresponds to suctions ranging between 0.003-0.010 m at the interface between the fine soil and the GDN. This suction is in close agreement with ψ_b estimated using the theory in Khire et al. (2000) and the data in Figure 3.

Capillary break effects caused by the presence of a lysimeter are negligible if the soil overlying the drainage layer is coarse-grained or if a similar capillary break is expected to occur at the base of the cover profile in areas outside the lysimeter. Cases where this might occur include covers underlain by a coarse-grained biota barrier (e.g., crushed rock) or covers placed on municipal solid waste, which has air entry suction on the order of 0.01-0.03 m (Benson and Wang 1998).

If a capillary break will not exist outside the boundaries of the lysimeter, some means of minimizing the capillary effect is needed to more appropriately simulate the lower boundary in the cover. One approach is to place a geosynthetic root barrier and a layer of fine-textured interim cover soil between the base of the cover and the surface of the drainage layer, as shown in Figure 1a. The root barrier prevents roots from entering the interim cover soil, and therefore precludes root water uptake from the interim soil layer. Consequently, once the interim cover soil is wetted for the first time, the soil will remain wet due to the capillary effect from below and the lack of root-water uptake. Sensors such as TDR probes may be used to verify that the root barrier and interim cover soil are functioning as intended. However, inclusion of an interim cover soil layer adds complexity to the lysimeter design.
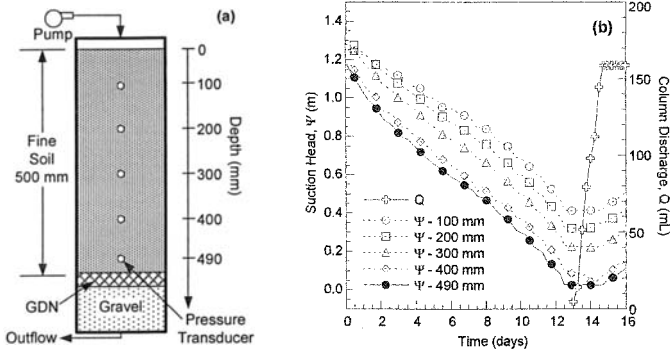
Figure 4. (a) Schematic of column test conducted by Tetra Tech FW, Inc. for evaluating capillary barrier effect and (b) data collected from column test (graphed using data from TTFW 2005a).

Another approach is to use an automated equilibrium tension lysimeter (AETL), where the water status at the base of the profile is continuously adjusted so conditions inside and outside the lysimeter are the same (Masarik et al. 2004). However, AETLs have only been applied in agricultural applications in humid regions. Thus, their effectiveness is unknown in drier climates (where AEFCs are common) and in cover monitoring programs, where very low percolation rates need to be measured.

Vapor Barrier Effect

The barrier to thermally driven vapor flow caused by the base of the lysimeter results in a conservative error in percolation rate. Water flowing downward in response to thermal gradients in the summer months is blocked at the bottom of the lysimeter and collected in the lysimeter pan, whereas water that flows upward in the winter is blocked but not collected. In effect, the lysimeter pan behaves as a hydraulic rectifier, and too much water can be collected in the lysimeter.
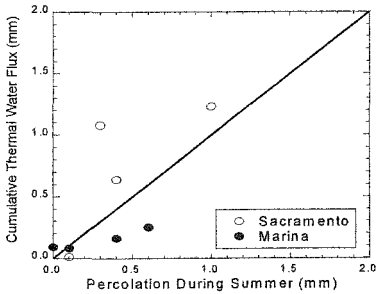
Figure 5. Computed thermal flux and measured percolation for lysimeters in Marina and Sacramento, CA, USA during the summer months of 2001-2004.

An example of this effect is shown in Figure 5 where computed cumulative thermally-driven water fluxes are compared with percolation measured in lysimeters for AEFCs in Marina, CA, USA and Sacramento, CA, USA as part of USEPA's Alternative Cover Assessment Program (ACAP). Soil temperatures for the thermal flux calculations were measured during the summer months of 2001 through 2004. The method in Globus and Gee (1995) was used to compute the thermal water fluxes.

At both sites, hydraulically driven flows are expected to be negligible during the summer months because precipitation is nil and the soil-water storage is depleted. Nevertheless,

percolation trickled into the lysimeter during the summer months at both sites, as shown in Figure 5. The computed cumulative thermal water fluxes shown in Figure 5 agree reasonably well with the percolation data, suggesting that the percolation collected in the lysimeter during the summer months was largely due to thermal effects. More importantly, the thermal fluxes can be as large as 1 mm over a three-month period, which is large enough to cause non-compliance at sites where the maximum percolation rate is 1 mm/yr or less.

Leaks and Malfunctions

The potential for leaks or malfunctions exists whenever flows are being monitored. In lysimeters, these effects can be evaluated by including a test pipe in the lysimeter and incorporating regular lysimeter tests in the monitoring program (Benson et al. 2001). The inlet to the test pipe is above ground and the outlet is in the lysimeter sump. A known quantity of water is introduced into the test pipe, followed by monitoring of the discharge from the percolation collection system.

Water-Content Sensors

Water-content sensors have been used for qualitative and quantitative monitoring of AEFCs. Qualitative applications consist of monitoring the temporal variation in soil-water storage or water content over time to verify that storage and removal of water are occurring, or verifying that a wetting front is not reaching the base of the cover. Quantitative applications include comparisons against a "threshold" water content or soil-water storage above which cover performance is considered unsatisfactory, or using water-content data to calculate percolation for comparison against a percolation criterion. Both of these quantitative approaches are similar, because Darcy's law provides the linkage between water content and percolation.

Hydraulic properties of the cover soil are needed to calculate percolation rates from water content data or to define a threshold water content using Darcy's law. Hydraulic properties typically are measured in the laboratory and include the SWCC (i.e., van Genuchten parameters) and the saturated hydraulic conductivity. A theoretical model then is used to define the unsaturated hydraulic conductivity function. These computations are straightforward and simple but are prone to appreciable error due to factors such as spatial variability, scale effects, pedogenesis, preferential flow, and inaccuracies in the hydraulic conductivity model. Ambiguities in the hydraulic gradient and drift in instrument calibrations also confound the computations and lead to uncertainty.

Spatial Variability

The following example illustrates how spatial variability in soil properties can confound a compliance assessment based on water-content measurements. Consider a monolithic cover where the hydraulic properties of the cover soil are free of spatial variability and are known with certainty. Assume that the saturated hydraulic conductivity of the cover soil is 10^{-5} cm/s, the porosity is 0.45, the residual water content is zero, and the van Genuchten parameters α and n are 2.2 m^{-1} and 1.3. Field capacity for these conditions corresponds to a water content of 0.24. The percolation rate corresponding to field capacity of this cover soil is 1.3 mm/yr if a unit downward gradient condition is assumed (i.e., the worst case condition).

Although the cover soils in this example were assumed to be free of variability, actual cover soils exhibit considerable variability in hydraulic properties due to spatial variations in characteristics such as density, placement method, and soil composition (Gurdal et al. 2003). To illustrate the effect of spatial variability, the cover soils cited in the above example were assumed to exhibit low, moderate, or high spatial variability using statistical data from ACAP reported by Gurdal et al. (2003). Monte Carlo simulation was used to compute percolation rates by applying Darcy's law and assuming unit gradient downward flow. The saturated hydraulic conductivity (K_s) and van Genuchten's α parameter were assumed to be log-normally distributed, and van Genuchten's n parameter was assumed to be normally distributed. In all cases, the residual water content was assumed to be zero, the saturated water content was fixed at 0.45, and all parameters were assumed to be uncorrelated. The input parameters used for the simulations are given in Table 1. For each Monte Carlo realization, the percolation rate was computed for a water content of 0.24 (i.e., the water content corresponding to field capacity with no spatial variability). A uniformly distributed error of ±0.02 in water content was included to account for the uncertainty associated with water contents measured with conventional TDR probes (Benson and Bosscher 1999, Gee and Ward 1999).

Table 1. Hydraulic properties used in Monte Carlo simulation.

Parameter	Data from Alternative Cover Assessment Program			RMA Data[1]
	Low Variability	Typical Variability	High Variability	
Standard deviation in $\ln K_s$	0.12	1.35	4.32	3.4
Standard deviation in α	0.05	0.67	2.20	1.4
Standard deviation in n	0.01	0.18	1.24	0.19

[1]RMA = Rocky Mountain Arsenal (computed using data from TTFW 2005b).

Percolation rates computed using this approach are summarized in Table 2. When spatial variability is low, the calculated percolation rates range between 0.15 and 1.8 mm/yr, which is reasonably close to the percolation rate obtained without considering spatial variability (1.3 mm/yr). However, when typical (i.e., moderate) variability exists, the calculated percolation rate corresponding to a water content of 0.24 can range between 0.001 and 242 mm/yr (approximately five orders of magnitude). Based on this level of variability, a water content of 0.24 would correspond to an actual percolation rate in excess of 1.3 mm/yr only 35 % of the time. In practical terms, this means that percolation can, at best, be predicted with a potential error of as much as five orders of magnitude and a false positive rate of 65 % for cover soils that exhibit typical variability. An even larger range of percolation rates (up to six orders of magnitude) is possible for a cover with high variability. Based on the results of this analysis, percolation rates computed based on water content data can be highly unreliable.

Computations of percolation rate also were made using statistical parameters describing the variability in the hydraulic properties of cover soils anticipated for use in the full-scale AEFCs at the Rocky Mountain Arsenal (RMA). These parameters were computed based on hydraulic properties measured on more than 40 samples that met the requirements for construction of full-scale covers at RMA. The statistical parameters used as input are summarized in Table 1. The original test data are summarized in TTFW (2005b). Percolation rates computed using the statistical data from RMA are summarized in Table 2.

For the level of spatial variability expected in the full-scale covers at RMA, percolation rates ranging between 0.0001 and 14,400 mm/yr can be computed for a water content of 0.24.

Table 2. Effect of variability in hydraulic properties on percolation at field capacity.

Percolation Statistic	Flux Under Unit Gradient (mm/yr)			
	Low Variability	Typical Variability	High Variability	RMA Conditions
Min. Percolation (mm/yr)	0.15	0.001	0.0001	0.0001
Max. Percolation (mm/yr)	1.8	242	350	14,400
% Exceeding 1.3 mm/yr	2	35	43	30
% Below 1.3 mm/yr	98	65	57	70

Scale Effects

Laboratory specimens typically are too small to adequately represent the network of pores controlling flow in the field. As a result, differences may exist between hydraulic properties measured in the laboratory on small specimens and hydraulic properties operative at field scale. Because specimen size is a key factor contributing to the difference in hydraulic properties, this phenomenon is referred to as the scale effect.

An example of a scale effect is shown in Figure 6, which shows annual percolation rates measured in lysimeters by ACAP as a function of the annual peak soil-water storage normalized by the soil water storage corresponding to field capacity. Soil-water storage was obtained by spatially integrating water contents measured with moderate frequency TDR probes installed in the lysimeters. Soil-water storage at field capacity was computed using the water content at field capacity and the thickness of each layer in the profile. Field capacity was defined as the water content at a matric suction head of 3.3 m and was obtained from SWCCs measured in the laboratory on undisturbed specimens collected during construction. In principle, non-zero percolation rates should correspond to cases where the ratio of peak soil-water storage to field capacity storage (S_p/S_c) exceeds 1.0. However, percolation is transmitted when S_p/S_c is as low as 0.69 because, in some cases, the storage capacity operative in the field is lower than that computed from laboratory data.
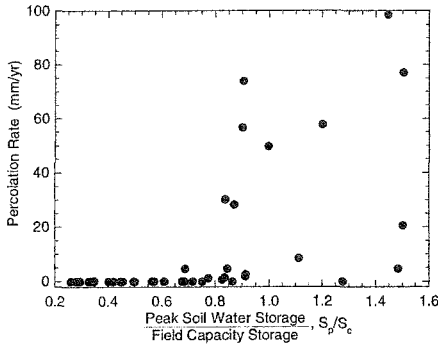
Figure 6. Annual percolation rates versus peak soil-water storage normalized by storage at field capacity for sites in the Alternative Cover Assessment Program (adapted from Albright et al. 2004).

Scale effects confound performance assessments based on water content monitoring because the magnitude of scale effects is not known *a priori*. As a result, an appropriate threshold water content or storage capacity cannot be defined reliably. An exception would be if large-scale testing is conducted to define field-scale hydraulic properties, but such tests are not

common and the appropriate size needed to represent field-scale conditions has not been determined for AEFCs. The potential for error is apparent when the data in Figure 6 are considered. For example, a performance requirement stipulating that S_p (computed using water content data) must be less than S_c could correspond to percolation rates either as low as zero or more than 50 mm/yr.

Pedogenesis

Time-dependent changes in cover soil properties caused by pedogenesis (changes in soil structure due to processes such as weathering and biota intrusion) confound quantitative assessments based on water-content measurements. For example, data collected by ACAP show that, within five years from the end of construction, the saturated hydraulic conductivity of cover soils can increase by a factor of more than 1000 and van Genuchten's α parameter can increase by a factor of 100 (Benson et al. 2005). Changes of this magnitude can have a large effect on interpretations based on water contents unless a new threshold water content is regularly defined in accordance with the level of pedogenesis that has occurred. An appropriate method to redefine this threshold water content over time is unclear. However, at a minimum, periodic collection and re-testing of large-scale undisturbed samples from the cover soils would be necessary to evaluate potential changes in hydraulic properties.

Preferential Flow

One of the most important deficiencies in monitoring cover performance with water-content sensors is the inability to detect preferential flow. Data from water-content sensors are characteristic of conditions within the soil matrix at the location of the sensor and not along cracks, fissures, or macropores. Moreover, even if sensors could detect preferential flow, placement of sensors along preferential flow paths is nearly impossible since locations of these paths are not known *a priori*. Consequently, water content data can provide a false impression regarding the effectiveness of a cover.

Khire et al. (1997) provide an example of preferential flow in a 0.8-m-thick monolithic cover instrumented with water-content sensors and a lysimeter. Data collected during the winter of 1995 (Figure 7) show that percolation was transmitted even though the water-content sensors suggested that water had not passed through the cover. Pulses of percolation transmitted through preferential flow paths were regularly collected in the lysimeter shortly after precipitation events (Figure 7a), but two months before the deepest sensors indicated that water was reaching the base of the cover (Figure 7b).

Combined Approach

Any performance monitoring program for an environmental technology should be developed in conjunction with an appropriate set of data quality objectives that define the type, quality, and quantity of data needed to make reliable inferences regarding performance of the technology (USEPA 2000). An AEFC is a technology that is intended to perform equivalently to (or better than) a prescribed conventional cover. Thus, data must be collected to reliably demonstrate that an AEFC is providing equivalent performance throughout the intended service life. If equivalent performance is defined in terms of a maximum percolation rate, the monitoring method must be able to provide a reasonably accurate assessment of percolation rate. Given the uncertainties associated with
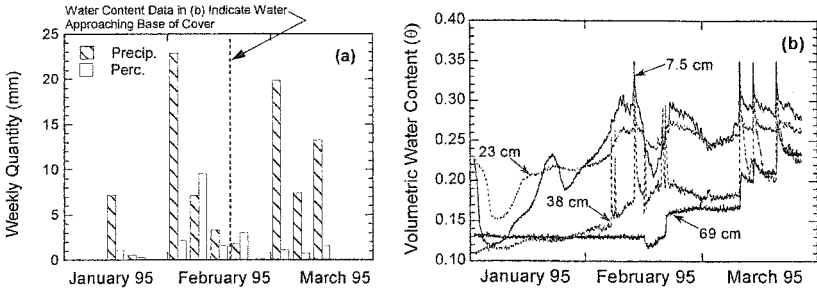
Figure 7. Data from Khire et al. (1997) showing (a) close correspondence between precipitation and percolation measured with a lysimeter during January-March 1995 and (b) water-content data suggesting that water did not reach the base of the cover until late February 1995.

percolation rates inferred from lysimeters and water content sensors, lysimetry is more suitable for monitoring percolation rate with less potential for decision error. However, water-content sensors can play a valuable role, because water-content data can be used to satisfy other objectives such as ensuring reliability or assessing the impact of corrective actions on hydrologic processes that affect percolation (e.g., storage water storage or root water uptake). Moreover, secondary data are essential for testing hypotheses regarding mechanisms that may be responsible for non-compliance of an AEFC (e.g., excessive percolation rates). Also, multiple nests of water-content sensors can be installed inside and outside a lysimeter to assess boundary effects and to obtain a quality understanding of site-wide spatial variations.

An example is shown in Figure 8, where data from water-content sensors were used to understand why percolation rates transmitted by an AEFC in Sacramento (cited previously in the discussion of Figure 5) were much higher than expected. The AEFC was designed to transmit no more than 3 mm/yr of percolation. However, during Water Years 2001-02 (July 1, 2001 to June 30, 2002) and 2003-04 (July 1, 2003 to June 30, 2004), approximately 100 mm of percolation was transmitted (Figure 8a). The reason for the high percolation rate became evident when the water-content data were evaluated, either as soil-water storage (Figure 8a) or water contents at various depths (Figure 8b). During the Summers of 2001 and 2003, water stored during the pervious winter was not completely removed (Figure 8a). As a result, the cover had inadequate soil water storage capacity the following winters, which resulted in the two large percolation events.

The data in Figure 8b provide some clues regarding the unexpected behavior. Water contents within the upper 600 mm of the cover decreased during spring and summer 2001, but not to the extent that had occurred in 2000 or in 2002, and very little depletion in water content occurred at depths greater than 600 mm in 2001. This suggests that the vegetation was not functioning as intended in 2001, with the portion of the root zone deeper than 600 mm being nearly inactive. The water-content data from summer 2003 show a different phenomenon. The entire depth of the root zone was active in summer 2003, but water removal ceased when the water content reached approximately 0.15, whereas water was removed until the water content reached 0.10-0.12 during the summers of 2001 or 2003. Reasons for this unexpected behavior currently are being studied.
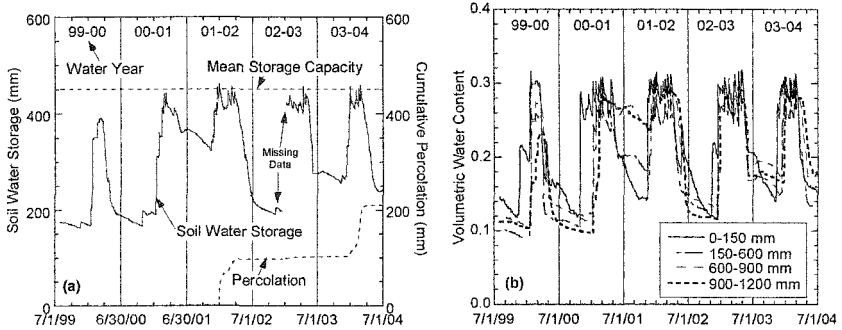
Figure 8. Temporal record between July 1999 and July 2004 for an AEFC in Sacramento, CA, USA: (a) soil-water storage and percolation; (b) water contents at four depths.

Summary and Conclusions

Lysimetry and water-content sensors are two methods commonly used for performance monitoring of alternative earthen final covers (AEFCs). The data presented in this paper illustrate that lysimetry appears to be the best practical means currently available to monitor percolation transmitted from final covers provided that the lysimeter is sufficiently large, is properly designed to minimize the impacts of capillary breaks, and is tested regularly to ensure leakage is not occurring. Inferences regarding percolation rates can be made with water content data, but these inferences are prone to considerable uncertainty due to spatial variability of soil properties, scale effects, and pedogenesis. However, water-content sensors are useful as a secondary monitoring tool to verify the reliability of lysimeters, evaluate potential causes of excessive percolation rates, and assess the effectiveness of corrective action on hydrologic processes that affect percolation.

Acknowledgments

References

Albright, W. H, Benson, C. H., Gee, G. W., Roesler, A. C., Abichou, T., Apiwantragoon, P., Lyles, B. F., and Rock, S. A. (2004), Field Water Balance of Landfill Covers, *J. of Env. Qual.*, 33(6), 2317-2332.

Benson, C. (1991), Predicting Excursions Beyond Regulatory Thresholds of Hydraulic Conductivity Using Quality Control Measurements, *Proc. First Canadian Conf. on Environ. Geotechnics*, Canadian Geotech. Society,, 447-454.

Benson, C., Abichou, T., Albright, W., Gee, G., and Roesler, A. (2001), Field Evaluation of Alternative Earthen Final Covers, *International J. of Phytoremediation*, 3(1), 1-21.

Benson, C. and Wang, X. (1998), Soil Water Characteristic Curves for Solid Waste, Environmental Geotechnics Report 98-13, Dept. of Civil and Environmental Engineering, University of Wisconsin-Madison.

Benson, C. and Bosscher, P. (1999), Time-Domain Reflectometry in Geotechnics: A Review, *Nondestructive and Automated Testing for Soil and Rock Properties*, STP 1350, ASTM, W. Marr and C. Fairhurst, Eds., 113-136.

Benson, C., Bohnhoff, G., Ogorzalek, A., Shackelford, C., Apiwantragoon, P., and Albright, W. (2005), Field Data and Model Predictions for an Alternative Cover, *Waste Containment and Remediation*, GSP No. 142, A. Alshawabkeh et al., eds., ASCE, Reston, VA, 1-12.

Gee, G. and Hillel, D. (1988), Groundwater Recharge in Arid Regions: Review and Critique of Estimation Methods, *J. of Hydrological Processes*, 2, 255-266.

Gee, G. and Ward, A. (1999), Innovations in Two-Phase Measurements of Soil Hydraulic Properties, in *Proc. International Workshop on Characterization and Measurement of the Hydraulic Properties of Unsaturated Porous Media*, M. Th. Van Genuchten, F. J. Leij, and L. Wu (Eds.), U. C. Riverside Press, Riverside, CA, 241-269.

Gee, G., Ward, A., Caldwell, T., and Ritter, J. (2002), A Vadose Zone Water Fluxmeter with Divergence Control, *Water Resources Research*, 38(8), 16:1-7.

Globus, A. and Gee, G. (1995), Method to Estimate Diffusivity and Hydraulic Conductivity of Moderately Dry Soil, *Soil Sci. Soc. Am. J.*, 59, 684-689.

Gurdal, T., Benson, C., and Albright, W. (2003), Hydrologic Properties of Final Cover Soils from the Alternative Cover Assessment Program, Geo Engineering Report 03-02, Geo Engineering Program, University of Wisconsin-Madison.

Khire, M., Benson, C., and Bosscher, P. (1997), Water Balance Modeling of Earthen Landfill Covers, *J. of Geotech. and Geoenvironmental Eng.*, 123(8), 744-754.

Khire, M., Benson, C., and Bosscher, P. (2000), Capillary Barriers: Design Variables and Water Balance, *J. of Geotech. and Geoenvironmental Eng.*, 126(8), 695-708.

Masarik, K., Norman, J., Brye, K., and Baker, J. (2004), Improvements to Measuring Water Flux in the Vadose Zone, *J. of Env. Qual.*, 33, 1152-1158.

Stormont, J. and Morris, C. (1998), Method to Estimate Water Storage Capacity of Capillary Barriers, *J. of Geotech. and Geoenviron. Eng.*, 124(4), 297-302.

Stormont, J. and Anderson, C. (1998), Capillary Barrier Effect from Underlying Coarser Layer, *J. of Geotech. and Geoenvir. Eng.*, 125(8), 641-648.

TTFW (2005a), Final Capillary Break Test Report, Prepared by Tetra Tech FW, Inc., Rocky Mountain Arsenal, Commerce City, CO, USA.

TTFW (2005b), Final Summary Report for Acceptance Zone Development and Density Requirements for RCRA-Equivalent Cover Soils, Prepared by Tetra Tech FW, Inc., Rocky Mountain Arsenal, Commerce City, CO, USA.

USEPA (2000), Guidance for the Data Quality Objectives Process, Report *EPA QA/G-4*, United States Environmental Protection Agency, Washington, DC.

van Genuchten, M. Th. (1980), A Closed Form Equation for Predicting the Hydraulic Conductivity of Unsaturated Soils, *Soil Sci. Amer. J.*, 44, 892-898.

The infiltrate-stabilize-evapotranspire or ISE landfill cover

Geoffrey E Blight[1]

[1]Professor Emeritus, Civil and Environmental Engineering, University of the Witwatersrand, Johannesburg. Private Bag 3, Wits, 2050, South Africa. PH/FAX: -- 27 11 476 8759; email: blight@civil.wits.ac.za

Abstract

Concern at the long period required for landfilled municipal solid waste to decompose and stabilize in water-deficient climates has led to an extension of the concept of the evapotranspirative or ET cover. The ET cover is designed to store all rain infiltration and re-evapotranspire it during dry weather, but prevent infiltration from entering the waste. With the ISE (Infiltrate-Stabilize-Evapotranspire) cover, rain infiltration during wet weather is stored in the cover and any excess is permitted to enter the underlying waste. This acts to accelerate the decomposition and stabilization process. Excess infiltration is then removed from both waste and cover by evaporation during dry weather.

The construction and performance of a set of experimental ISE covers of various thicknesses in a summer rainfall water-deficient climate is described. Field observations of rainfall, soil evaporation and water stored in the covers has allowed water balances to be constructed for the covers of various thicknesses (so far, for a period of 18 months). These observations show that the ISE concept is viable. In the limit, when there is insufficient rainfall to exit the cover and infiltrate the waste, an ISE cover operates as an ET cover.

Introduction

The soil cover layer of a landfill is designed to separate the landfilled waste from its surface environment, preventing exposure of the waste by, for example, sheet or gully erosion caused by wind and water, or burrows dug by animals, and at the same time controlling and even eliminating infiltration of rainfall. The cover should also allow landfill gas to percolate out of the waste and oxidize as it passes through the soil (e.g. Figueroa, 1993, Bergman, et al, 1993), to disperse relatively harmlessly into the surrounding air.
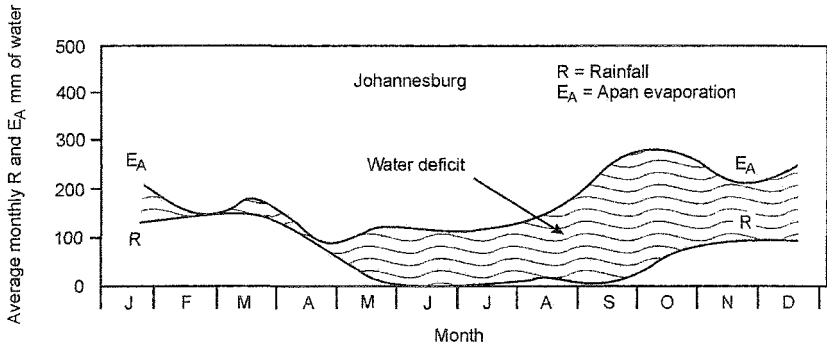
Figure 1: Average monthly rainfall ® and A-pan evaporation (E_A) for Johannesburg,
        South Africa

Over as much as 65% of the earth's land surface the climate is water-deficient with clearly divided rainy and dry seasons and with potential annual evaporation or evapotranspiration exceeding rainfall. As an example, Figure 1 shows the monthly average rainfall (R) and American Standard evaporation pan (A pan) evaporation (E_A) for a South African city, Johannesburg, which is located in a water-deficient climatic zone with warm rainy summers and cool dry winters. Figure 1 shows that on average, Johannesburg has a perennial water deficit, i.e. on average, monthly potential evaporation always exceeds rainfall. In a climate like this, there is the potential for infiltration occurring into a landfill during the wet season to be completely re-evaporated during the ensuing dry season, so that net accumulation of water in a landfill over a period of years could be zero, or could fluctuate about zero. This may sound like a desirable situation, since pollution of surface and ground water by the emission of leachate by the landfill is then unlikely to occur. However, if kept completely dry, the waste will never decompose and stabilize and will maintain its potential to pollute if it is ever exposed in the future.

Many authors, e.g. Barlaz et al (1990) and Baldwin et al (1998) have also emphasized the importance of moisture in decomposing and ultimately stabilizing waste. The role of moisture in stabilizing waste is very well summed up by El-Fadel and Al-Rashed (1998), as follows: "Moisture content appears to be the variable that is associated with the greatest effect on biodegradation processes because it provides an aqueous environment that facilitates the transport of nutrients and microbes within the landfill. This transport mechanism dilutes the concentration of inhibitors and enhances micro-organisms' access to their substrates and hence improves gas generation and stabilization." The advantages of encouraging biological degradation in landfills now appears to be generally accepted. To quote a recent text book

(Vesilind, et.al., 2002): "The rate of stabilization in 'dry' landfills may require many years, thereby extending the acid formation and methane fermentation phases of waste stabilization over long periods of time...... In contrast, leachate re-circulation may be used....... This option offers more rapid development of active anaerobic microbial populations and increases reaction rates .... The time required for stabilization of the readily available organic constituents can be compressed to .... Two to three years rather than the 15- to 20- year period" [expected for a dry landfill].

In water-deficient zones, however, insufficient leachate is generated to operate a wet system by leachate re-circulation. It seems logical, therefore, to maximize the waste stabilizing effect of the rain that does fall, by allowing it to be absorbed by the landfill cover (as with the evapotranspirative or ET cover, Benson et al, 2002), to penetrate in a controlled way into the waste, and then to re-evaporate after seasonally or periodically accelerating the process of stabilization of the waste. This is the rationale for the Infiltrate-Stabilize-Evapotranspire or ISE landfill cover, as well as how it is intended to function. Even with an annual or periodic infusion of rain infiltration, stabilization times will still be very long. Rohrs et al (2001) have estimated, for example, that at least 1.6 pore volumes of infiltration must pass through landfilled waste before chloride concentrations in the leachate will reach acceptable levels of about 100 mg/litre, and the landfill can be regarded as having reached stability. Even with a steady annual through-flow of leachate of 200 mm, this could take 300 to 500 years, which emphasizes the needs for long term aftercare of closed landfills and for covers to be designed to remain effective for centuries rather than decades.

Evaporation from a landfill surface

There is a common misconception that if water penetrates a landfill to deeper than 1 m or so, the water will move beyond the influence of evaporative forces, and will continue to migrate downwards to exit at the base of the waste body as leachate. This has been disproved in a number of experiments on landfills in water-deficient climates. Blight et al (1992) presented water content profiles measured at the ends of the wet and dry seasons in landfills situated in both Cape Town and Johannesburg. The Cape Town landfill was temporarily capped with 300 mm of clean beach sand, while the Johannesburg landfill was temporarily capped with 300 mm of a pervious silty sand residual from the decomposition of granite. The water content measurements showed that in Cape Town, waste seasonally dried by evaporation to a depth of 7.5 m (the full depth of the waste). In Johannesburg similar profiles showed seasonal drying to a depth of 16 m. In a separate experiment, (originally set up to test the results of the water content profile observations), Roussev (1995, quoted by Blight, 1997) constructed two pairs of identical lysimeters in a landfill in Johannesburg. Each lysimeter measured 4.5 m square in plan, one pair of lysimeters was 3 m deep, the other 5.5 m deep. The 4 sides and the base of each lysimeter were sealed by means of sheets of geomembrane welded to form an impervious box. Each lysimeter was equipped with a drainage layer at the base and a 100 mm diameter

observation well and was filled with compacted waste. The top surfaces of two of the lysimeters (3 m and 5.5 m deep) were then sealed with a geomembrane, while the surfaces of the other two lysimeters were left open to the atmosphere. All four lysimeters were brought to their water storage capacity by irrigating their surfaces until leachate appeared in the observation wells. By lowering a submersible pump down each observation well, the leachate was then pumped out until no more collected. At this stage the waste in the lysimeters was at its water storage capacity. The lysimeters were then left for a period of 4 months and measured quantities of water were then slowly added at the surface until leachate again appeared in each observation well. The difference between the water added to the open-topped and closed-topped lysimeters was then taken to be the evaporative water loss from the open-topped lysimeters. The experiment was then repeated over a period of 6 months. It was found that the 3 m deep lysimeter lost an average of 0.17 mm per m depth of waste per day while the 5.5 m deep one lost 0.22 mm $m^{-1}d^{-1}$. This was taken as a demonstration that evaporative losses can occur from waste at least to depths of 5.5 m and supported the evidence of the earlier water content profiles.

Further evidence that little or no leachate ever exits the base of a landfill in a semi-arid climate was advanced by Fourie, et al (1999). They investigated six long-established unlined landfills in South Africa that are situated in both water-deficient and marginally water surplus climatic zones. The results of soil sampling around the landfills showed that very little leachate had exited any of them, even those located in marginally water-surplus climates.
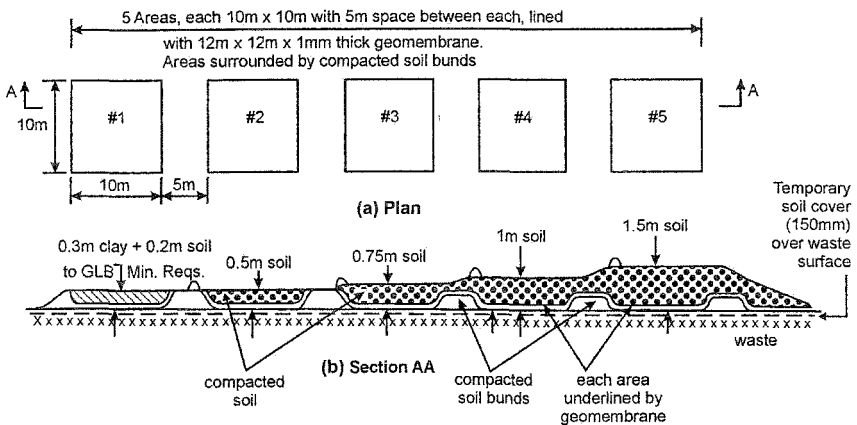
Figure 2: Layout of experimental landfill covers at Simmer and Jack landfill, Johannesburg

Description of experimental ISE covers

To explore the concept of the ISE cover, a large-scale experiment was set up in Johannesburg.

The objectives of the experiment were as follows:

- to record rainfall and evaporation from the cover surfaces (by energy balance methods, Blight, 1997, 2002);
- to sample and record variations in pore water stored by capillarity in covers of various thicknesses throughout the seasons, and thus
- to construct a water balance for each experimental cover; and
- to observe any other aspects of cover performance (e.g. surface cracking and wind and water erosion); and hence
- to assess the potential for practical implementation of the ISE cover, including required thickness for the combination of local soil properties and climate.

Five large test covers were constructed at the Simmer & Jack landfill near Johannesburg. The plan and longitudinal section of the experimental covers are shown in Figure 2.

The geomembrane lining mentioned in Figure 2 (plan) defines the base of each trial cover. Any infiltration in excess of the water storage capacity of the soil will be intercepted and trapped by the geomembrane basin where it can be detected and measured, but will still be available to evaporate out through the soil at a later time. This gives an indication of the quantity of water available to infiltrate the underlying waste. The first cover (#1 on the left of Figure 2) consists of a 300 mm clay layer covered by 200 mm of soil. This satisfies the South African statutory Minimum Requirements' (1998) specification for a GLB⁻ landfill (i.e. a Large landfill receiving General waste and located in a B⁻ (water-deficient) climate and allows the behaviour of a cover incorporating a clay layer to be studied. Thicknesses of compacted soil cover (silty sand) increasing from 0.5 to 0.75, to 1.0 to 1.5 m were provided in covers 2 to 5. Each cover area is separated from its neighbours by a 0.5 m high compacted soil bund, square in plan, within which the geomembrane forms an impervious basin. The possible accumulation of excess free water within each basin can be detected and measured by means of four perforated vertical standpipes built into each basin. Bunds, 0.3m high, were constructed to prevent run-on of water from the 1.5m-thick cover to the 1m cover and the 1m cover to the 0.75m cover.

Construction of these facilities was completed by mid 2001. Monitoring was not started until October 2002, as it was considered preferable to monitor covers that had first been through a full seasonal cycle to show up any obvious defects.

Because of the presence of scavengers on the landfill, it was not possible to expose or incorporate anything scavengeable into the experiment, and no instrumentation, not even a rain-gauge, could be left *in situ*. Rainfall measurements were made in the

garden of a sympathetic householder across the road running along the boundary of the landfill.

The cover surfaces were not vegetated, as it was decided to see if, and what type of volunteer vegetation would establish itself. By the end of 2003 only a sparse scattering of perennial grasses and annual weeds had invaded the set of covers. Thus any losses of infiltrated water from the trial covers have resulted from evaporation from the soil, with a negligible component of transpiration from the grass and weeds.

Properties of soil used in the covers

Two soils were available at Simmer and Jack, one is a silty sand residual from the decomposition of quartzites, and the other a more clayey material residual from the decomposition of diabase intrusions into the quartzites. The decomposed quartzite was used as the main material of the covers while the residual diabase was used to construct cover [#]1, the "Minimum Requirements" cover. Figure 3(a) shows the particle size analyses of the residual quartzite soil and the residual diabase. Figure 3(b) shows the suction-water content curves for the compacted residual quartzite and diabase both of which have little hysteresis between wetting and drying cycles.

Index properties of the residual quartzite are: Liquid Limit: 21%, Plasticity Index: 4%, Linear Shrinkage: 2%. For the residual diabase they are: Liquid Limit 33%, Plasticity Index 14%, Linear Shrinkage 8%. In situ permeabilities measured by means of ring infiltrometer tests were 35 mm/h for the residual quartzite and 6 mm/h for the residual diabase. Thus a residual quartzite surface can be expected to promote infiltration.

Performance of covers

Because the soil contained occasional boulders of residual rock, it proved impossible to auger holes to recover samples for water content measurements. Instead, 1mx1m sampling pits had to be hand excavated to obtain water content samples. The sampling pits were carefully backfilled in 0.1m compacted layers, but the area occupied by each pit (1% of the cover area) limited the number of times each cover could be sampled.

Figure 4 shows the wettest and driest conditions encountered up to the beginning of 2004 in the experimental covers. Even under the wettest condition of March 2004, no free water was encountered on any of the geomembrane liners. Comparing the water contents for the wettest condition (Figure 4a) with the suction-water content curves shown in Figure 3b, it will be seen that caps [#]1, 2, 3 and 4 were about to change their function from ET caps to ISE caps. There appeared to be a small wave of moisture moving down through cap [#]5, but the cap as a whole had not yet reached its field moisture storage capacity.
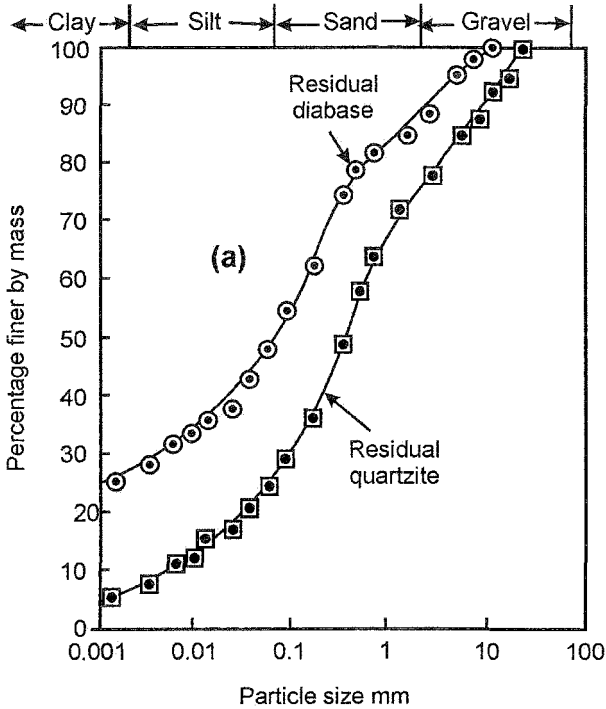
Figure 3a: Particle size analyses for soils used in Simmer and Jack experimental covers.

Figure 5 shows the water balance for the experimental covers. The water balance can be expressed as

$$R - RO = I = \Delta S + E \tag{1}$$

Where R = rainfall, RO = runoff, I = infiltration, ΔS = change in soil water storage, and E = evaporation from surface.

Figure 5 shows the cumulative rainfall, ΣR, evaporation rates found by solar energy balance measurements on the landfill surface, $\dot{E}_B$, and the storage in the five covers, S, expressed in mm of water. The energy balance method used to measure $\dot{E}_B$ has been fully described by Blight (1997, 2002), and is also described by Blight (2006) in these proceedings. The figure shows the results of every set of measurements made in the first 18 months of the experiment. The numbers on the curves of storage, S,
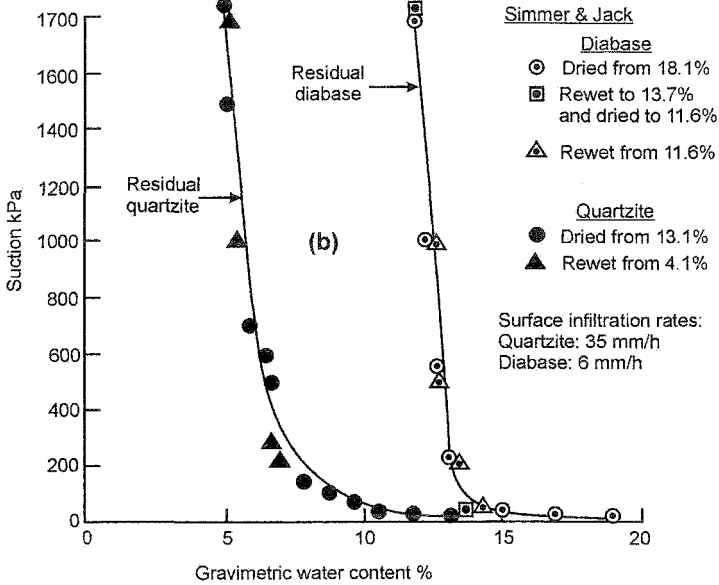
Figure 3b: Section: water content relationships for soils used in Simmer and Jack experimental covers.

cumulative rain, ΣR, and cumulative evaporation, ΣE_B, indicate when each measurement was made. The upper diagram in Figure 5 (which is on the same time scale as the rest of the figure) shows rates of evaporation measured in situ on the landfill between December 2002 and October 2003. For periods in which there is either very little rain, or for which runoff can be regarded as negligible, the water balance equation can be rearranged as

$$E = R - \Delta S$$
(1a)

and actual evaporation rates in mm/d can be estimated ($\dot{E}$ in Figure 5).

The calculated $\dot{E}$ values are considerably less than those measured on the adjacent landfill, which was temporarily capped with a random mixture of residual quartzite and diabase. The difference is probably accounted for by the presence of the geomembranes which limited the availability for evaporation of water in the experimental covers whereas there was no such limitation for the landfill itself. As a matter of interest, the A-pan evaporation rate for the site over a year varies from 3.7 mm/d in June to 8.3 mm/d in October and averages 6.1 mm/d. Thus actual evaporation from the landfill surface is slightly more than one third of A-pan evaporation. It should be noted in Figure 5 that the October to October rainfall in
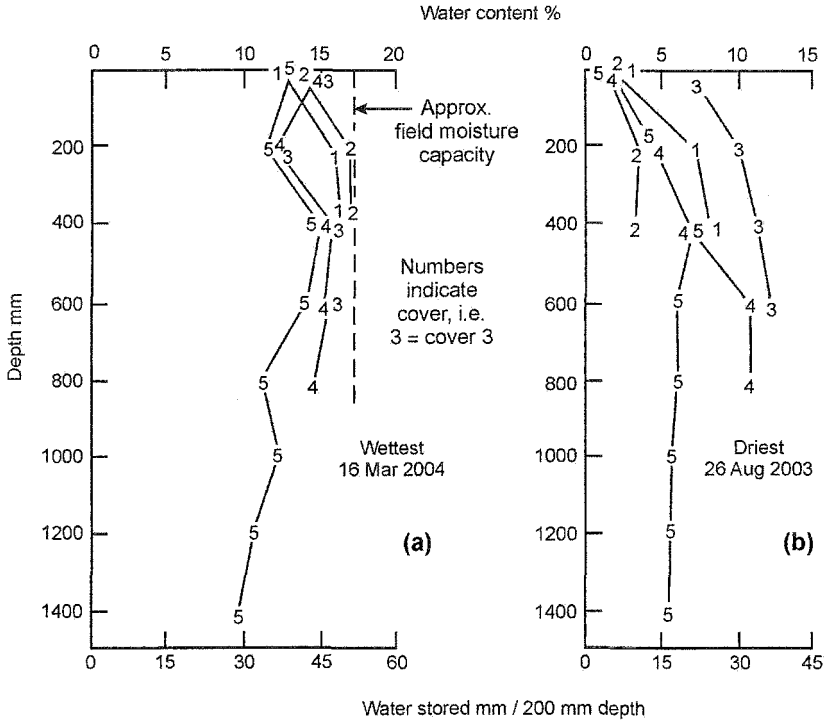
Figure 4: Water content-depth profiles for Simmer and Jack experimental covers:
          (a) Wettest condition.
          (b) Driest condition.

2002/2003 was only 379 mm whereas the long-term average rainfall is 750 mm. Thus this period was abnormally dry. Because of the relatively permeable nature of the residual quartzite, it had been assumed, in the early stages of the experiment, that no run-off was occurring and that all rainfall infiltrated. When after the five month wet spell from mid-October 2003 to mid-March 2004, it was found that no free water had accumulated on any of the geomembranes underlying the caps, it was at first thought that run-off was the reason for this. However, as the calculations on Figure 5 show (assuming that evaporation was occurring in accordance with measured $\dot{E}_B$) run-off either did not occur (negative figures for RO) or was very small (19 mm for cover [#]1 and 2 mm for cover [#]4). It then became apparent that evaporation from the surface must have almost been keeping pace with rainfall. For this 150 day period, evaporation measured by solar
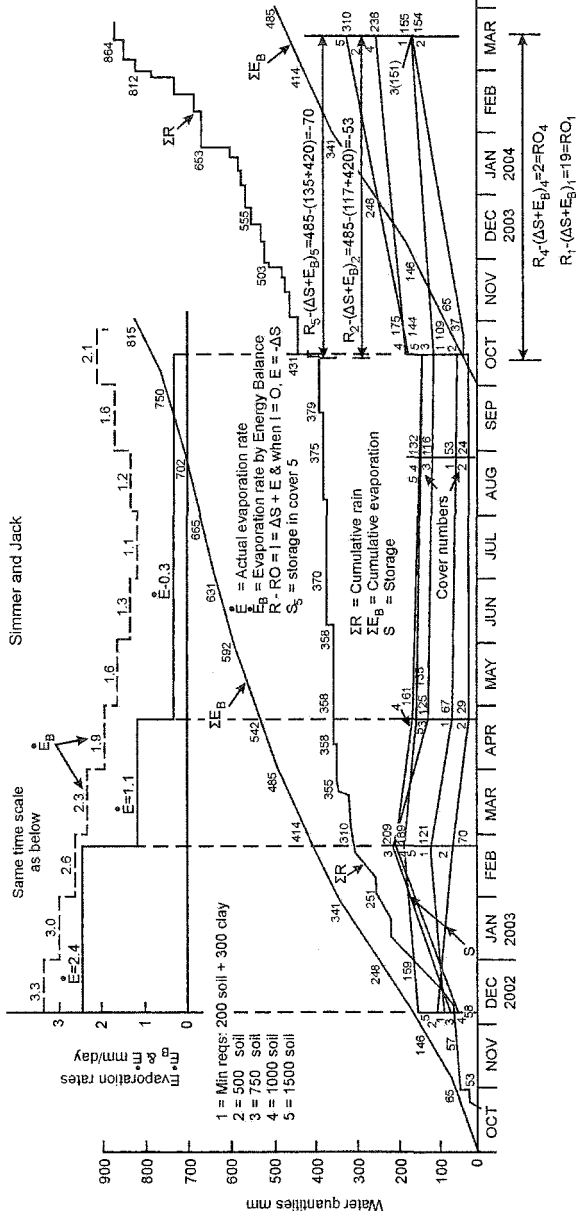
Figure 5: Water balance data for Simmer and Jack experimental covers:
October 2002 to March 2004.

radiation balance (ΣE_B) amounted to 420 mm (2.8 mm/d), whereas rainfall (ΣR) was 485 mm (3.2 mm/d). The difference ($\Sigma R - \Sigma E_B$) was absorbed by the cover layers, and any discrepancies in the figures can be explained by differences between actual evaporation and evaporation predicted by solar energy balance. Figure 5 also shows that a cover thickness of 750 to 1000 mm (covers [#]3 and [#]4) would probably be adequate to function as an ISE cover. However, an allowance for annual erosion would have to be added to these figures. As erosion rates for silty sand soils in the area can be as much as 50 Tons/ha/year (3 mm/y or 300 mm/century) (Amponsah-Da Costa and Blight, 2003) the above cover thicknesses would have to be considerably increased to allow for erosion.

Concluding discussion

1. Evapotranspirative (ET) landfill covers are designed to exclude infiltration into the landfilled waste by maximizing run-off and storing any infiltration within the soil layers of the cover pending its re-evaporation or transpiration. Any infiltration into the waste body is regarded as a leakage, and therefore a short-coming of the cover.
2. Recognizing that decomposition and stabilization of the waste requires water to be available to promote bacteriological activity, and knowing that stabilization of the waste is likely to be extremely slow if the water content of the waste is not supplemented, the ISE cover is designed to encourage limited infiltration into the waste during the wet season. This is aimed at promoting decomposition and stabilization, without causing leachate to reach the base of the waste body, and then allowing any excess infiltration to be re-evaporated during the ensuing dry season.

3. The experimental covers have demonstrated that the ISE concept will work in semi-arid climates with summer rainfall. They have also demonstrated that in drier years, an ISE cover will function as an ET cover, storing all infiltration into the cover and attenuating infiltration before it reaches the waste. In wetter years, or during exceptionally wet periods, the ISE cover will function as designed.

References

Amponsah-Da Costa, F. and Blight, G.E. (2003). "A quest for long-term erosion resistant tailings dam slopes". *International Erosion Control Association, Annual Conference*, Steamboat Springs, Co, USA, 1-12.

Baldwin, T.D., Stinson, J. and Ham, R.K. (1998). "Decomposition of specific materials buried within sanitary landfills". *ASCE Journal of Environmental Engineering,* 124(12), 1193-1202.

Barlaz, M.A., Ham, R.K. and Schaefer, D.M. (1990). "Methane production from municipal refuse: a review of enhancement techniques and microbial dynamics". *Critical Reviews in Environmental Control*, 19(6), 557-584.

Benson, C.H., Albright, W.H., Roesler, A.C. and Abichou, T. (2002). *WM'02 Conference,* Tuscon, Arizona, USA, 1-18.

Bergman, H., Jacobsson, A. and Lagerkvist, A. (1993). "Investigations regarding biofilters for methane oxidation in landfill top covers". *4th International Landfill Symposium*, Cagliari, Italy,1, 717-728.

Blight, G.E. (1997). "Interactions between the atmosphere and the earth". *Geotechnique*, 47(4), 715-767.

Blight, G.E. (2002). "Measuring evaporation from soil surfaces for environmental and geotechnical purposes". *Water S.A.*,28(4), 381-394.

Blight, G.E. (2003). "The vadose zone soil-water balance and transpiration rates of vegetation". *Geotechnique*, 53(1), 55-64.

Blight, G.E. (2006). "Measuring evaporation from grassed surfaces and trees by energy balance". *4th International Conference on Unsaturated Soils. This Conference.*

Blight, G.E., Ball, J.M. and Blight, J.J. (1992). "Moisture and suction in sanitary landfills in semi-arid areas". *Journal of Environmental Engineering, A.S.C.E.*, 118(6), 865-877.

El-Fadel, M. and Al-Rashed, H. (1998). "Settlement in municipal solid waste landfills. 1. Field scale experiments". *Journal of Solid Waste Technology and Management*, 25, 89-98.

Figueroa, R.A. (1993). "Methane oxidation in landfills top soils". *4th International Landfill Symposium*, Cagliari, Italy, 1, 701-716.

Fourie, A.B., Blight, G.E. and Pinheiro, J. (1999). "Subsurface contamination by leachate at six unlined landfill sites in South Africa". *7th International Waste Management and Landfill Symposium.* Cagliari, Italy, 133-140.

Rohrs, L.H., Fourie, A.B. and Blight, G.E. (2001). "Modelling landfill leachate quality to determine long-term pollution potential of landfills". *8th International Waste Management and Landfill Symposium*, Cagliari, Italy, 1, 169-178.

Roussev, K.I. (1995). *Evaluating components of the water balance for waste deposits.* Ph.D Thesis, University of the Witwatersrand, Johannesburg, South Africa.

South African Department of Water Affairs and Forestry (1998). "Minimum Requirements for Waste Disposal by Landfill, 2nd Edition", *Department of Water Affairs and Forestry*, Pretoria, South Africa.

Vesilind, P.A., Worrell, W. and Reinhart, D. (2002). *Solid waste engineering,* Brooks/Cole, Pacific Grove, California, USA.

Long-Term Performance of a "Store/Release" Cover Over Potentially Acid Forming Waste Rock in a Semi-Arid Climate

D.J. Williams[1], D.J. Stolberg[2] and N.A. Currey[3]

[1]Department of Civil Engineering, The University of Queensland, QLD 4072, AUSTRALIA; PH +61-7-3365-3642; FAX +61-7-3365-4599; email: D.Williams@uq.edu.au
[2]Department of Civil Engineering, The University of Queensland, QLD 4072, AUSTRALIA; PH +61-7-3365-3745; FAX +61-7-3365-4599; email: D.Stolberg@uq.edu.au
[3]Placer Dome Australia Limited, Level 2, 189 Coronation Drive, MILTON QLD 4064, AUSTRALIA; PH +61-7-3510-6713; FAX +61-7-3510-6744; email: Nick_Currey@placerdome.com

Abstract

The reclamation of potentially acid forming waste rock is site specific, being a function, among other factors, of the rock types, the dumping and storage method employed and, importantly, the climatic setting. The "store/release" cover developed to manage acid rock drainage from mineralised waste rock dumps at Kidston Gold Mines' open pit operations in the semi-arid, seasonal, sub-tropical climate of North Queensland, Australia, has been monitored for up to 9 years. The paper describes the philosophy behind the store/release cover design and its adaptation over time to suit Kidston's conditions. The results of monitoring of the store/release cover system over 9 years are presented, and estimates are made of the water balance of the store/release cover for a range of annual rainfall totals and of the overall water balance of the waste rock dumps. The Kidston story is a valuable case study of a successful approach to remediating an identified source of acid rock drainage in a semi-arid climate, which has actively engaged all Stakeholders.

Site Setting

Kidston Gold Mines are located in North Queensland, Australia, approximately 360 km south west of Cairns (Kidston Gold Mines Limited, 2000). The

elevation of the site is about 540 m Australian Height Datum (AHD). The climatic setting of Kidston Gold Mines is semi-arid, sub-tropical, with pronounced wet and dry seasons. On average, 82% of the annual rainfall falls between November and April, with high intensity storms being common. The annual rainfall averages about 700 mm, but it can range from a low of about 400 mm/year to a high of about 1,500 mm/year. The average pan evaporation is about 2,800 mm, four times the average annual rainfall. Average daily winter temperatures range between a minimum of -2 C and a maximum of 22 C. Average daily summer temperatures range between a minimum of 23 C and a maximum of 36 C. The prevailing wind direction is from the east to south east.

The topography of the site is generally gently sloping, with rocky "knolls" rising about 50 m above the surrounding topography. The site vegetation is an altered open woodland, comprising native grasses, ironbark trees and Gilbert river boxes, supporting semi-domestic cattle, wild pigs, native animals and a prolific bird life.

Overview of Mining and Milling Operations

Kidston Gold Mines' low grade phorphyry gold deposit was mined by two open pits using truck and shovel methods, commencing in 1984, with the first gold poured in April 1985. Wises Hill Pit was mined out to a depth of about 240 m in 1996, when the surface area reached 52 ha. The adjacent Eldridge Pit was mined out to a depth of typically 270 m in June 2001, when the surface area reached 55 ha. Milling and conventional carbon-in-pulp (cyanide) processing was carried out at an average throughput of 750 tph, and ceased in July 2001. Over 3.5 million ounces (about 100 t) of gold was produced. A total mass of about 250 Mt (about 93 Mm^3) of rock was excavated from the open pits, comprising about 155 Mt (about 86 Mm^3) of waste rock and about 95 Mt (about 59 Mm^3) of tailings. The total area disturbed by mining and milling operations was about 830 ha.

Overview of Surface Waste Rock Disposal

The waste rock included oxide (weathered) waste rock, fresh (inert) barren waste rock, and mineralised waste rock. The waste rock from Wises Hill Pit was truck dumped in surface engineered dumps surrounding the pit. The 20 Mt (about one sixth of the total waste rock placed in surface dumps) of mineralised waste rock excavated from Wises Hill Pit was placed in the South and North Dumps on a pad of fresh barren waste rock, with a wide encapsulation (up to 60 m horizontally) of fresh barren waste rock. The waste rock dumps were typically constructed to a height of about 36 m by end-dumping over the crest of the dump. The waste rock types were selectively placed, based on their identified geology and inferred acid rock drainage potential. All of mineralised waste rock excavated from Eldridge Pit was dumped into the mined out Wises Hill Pit, along with thickened tailings. The final surface waste rock dump footprint covered about 340 ha and the dumps contain about 120 Mt of waste rock.

Geochemical Characterisation of Mineralised Waste Rock

The sub-economic mineralised waste rock is potentially acid forming. It has a gold content in the range from 0.55 to 0.7 g/t, a typical total sulphur content of 0.9%, an Acid Neutralisation Capacity (ANC) of 54 kg of $CaCO_3$ per t of material, a Net Acid Producing Potential of -24 kg of $CaCO_3$ per t of material, and an ANC/MPA (MPA = Maximum Potential Acidity) of 1.8. The potential for the mineralised waste rock to produce acidity was realised when the pH of the seepage emanating from the South (mineralised waste rock) Dump dropped suddenly during the extreme 1990/91 wet season from about 7.5 to about 4.5, about 4 years after the construction of the dump.

Philosophy Behind Store/Release Cover System

The mineralised waste rock that comprised about one sixth of the total waste rock stored in surface dumps at Kidston was placed on a pad of fresh barren waste rock and encapsulated laterally by fresh barren waste rock. It was required to construct a cover over the mineralised waste rock and fresh barren waste rock lateral encapsulation to limit the percolation of rainfall into the dump and hence limit any acid drainage, with any reduction in oxygen ingress being a bonus. It was recognised that in Kidston's highly seasonal and variable semi-arid climate, a rainfall-shedding cover would not be a sustainable means of minimising rainfall percolation into the mineralised waste rock. During the long dry season, the oxide waste rock available for cover construction would desiccate leading to vegetation die-back. The subsequent summer storms would then erode the desiccated, poorly vegetated surface, with the likelihood of breaking through the cover.

Instead, a store/release cover system was developed for Kidston (Williams *et al.*, 1997), which recognised the need to avoid desiccation and the eroding effects of rainfall runoff, and relied on storage within the cover of rainfall infiltration during the short wet season and its release during the long subsequent dry season through evapotranspiration.

The store/release cover system had the following aims.
- To provide a cover with sufficient water storage capacity to "store" the bulk of the 3-month summer wet season rainfall, without causing saturated breakthrough into the underlying mineralised waste rock, limiting rainfall percolation through the cover to < 5% of annual rainfall.
- To "release" the stored water through evapotranspiration during the 9-month dry season, while maintaining the compacted clayey layer at the base of the cover moist to preserve its integrity. The vegetative cover plays a key role in ensuring that this aim is met.
- To provide a cover system that cycles annually between wet and dry states, without progressively wetting up or drying out.

South Dump Store/Release Cover Trial

A scaled schematic of the original store/release cover system used for the 23 ha South Dump trial cover is shown on Figure 1. Prior to the construction of the store/release cover, the top of the dump was sloped to prevent the ponding of any water that penetrates the cover. A near-saturated 0.5-m-thick compacted clayey (fine-grained oxide waste rock) layer was then placed, overlain by a loose rocky soil mulch (coarse-grained oxide waste rock) layer a minimum 1.5-m-thick, which serves as the store/release layer and protects the underlying compacted clayey layer.
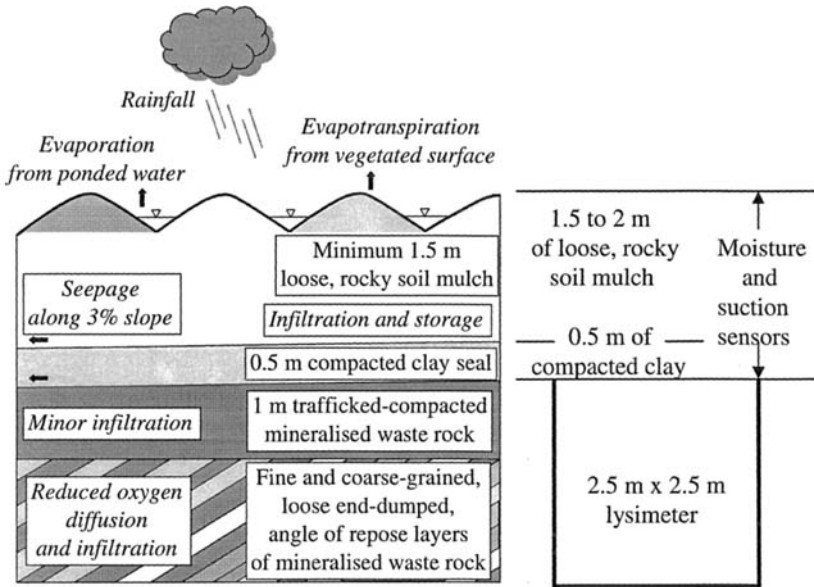
Figure 1. Schematic of original store/release cover system used for South Dump cover trial.

The rocky soil mulch layer was placed by paddock dumping from haul trucks, forming a hummocked surface profile that prevented rainfall runoff, which would erode the cover. The surface was vegetated to ensure sufficient transpiration to just remove the stored water without excessively drying out the cover. The store/release cover extended over both the mineralised waste rock and the fresh barren waste rock lateral encapsulation, to avoid rainfall infiltration through the side slopes of the dump intercepting mineralised waste rock. The dump side slopes were left at the angle of repose of the fresh barren waste rock, ensuring both adequate geotechnical and erosional stability. Oxide waste rock was over-dumped from the crest and the slope aerially grass seeded and fertilised.

The geotechnical parameters of the cover materials are summarised in Table 1. Rocky soil mulch with between 25% and 45% passing 2 mm provides reasonable erosion resistance without adversely affecting its revegetation potential. The loose dumping of the rocky soil mulch ensured an average porosity of about 0.4. Assuming that a porosity of at least 0.25 is available to store rainfall infiltration (given that some of the porosity will be taken up by entrained moisture and that full saturation is unlikely), a minimum 1.5-m-thick mulch layer could store up to 350 mm of infiltration (about half the average annual rainfall). Any excess water will serve to maintain the sealing layer near-saturated and may pond between the hummocks. Provided the sealing layer remains near-saturated, it will limit the diffusion of oxygen into the underlying potentially acid forming waste rock. The cover surface was fertilised and seeded with pasture grasses and native trees.

Table 1. Geotechnical parameters of cover materials.

Geotechnical parameter	Compacted clay	Rocky soil mulch
% gravel-sized and coarser	30	72
% sand-sized	35	26
% silt-sized	15	2
% clay-sized	10	-
Specific gravity	2.65	2.65
Liquid limit (%)	41	Non-plastic
Plasticity Index (%)	21	Non-plastic
Unified Soil Classification	GM/GC	GW
Standard Maximum Dry Density (t/m^3)	1.81 - 1.97	-
Standard Optimum Moisture Content (%)	15.6 - 10.3	
Nominal placed porosity	0.3 *	0.4
Saturated hydraulic conductivity (m/s):		
Laboratory falling head	$5 \times 10^{-10} - 2 \times 10^{-8}$	-
Field permeameter #	$\sim 10^{-8}$	$\sim 2 \times 10^{-6}$

*   This was the target based on laboratory compaction testing, but was not achieved in the field.
#   CSIRO ring and Guelph permeameters.

Figure 2 shows the placement of the rocky soil mulch layer by loose paddock dumping on the compacted clayey layer on the South Dump. The revegetation comprised grasses planted from seed, plus planted acacias and eucalypts, and volunteer acacias. Two years after planting, the shallow-rooted grass growth was somewhat diminished due to the consumption of the initial fertiliser application and the lack of a continuous moisture supply close to the surface of the cover, and acacias were the only other species that survived. More fertiliser was subsequently added to ensure sufficient ongoing consumption of water stored within the cover through transpiration, so avoiding the gradual wetting up of the cover over time. However, this additional fertiliser was also exhausted over time and the state of the vegetative cover was further diminished by the prevailing extended dry conditions. While the dry

conditions would limit the potential for percolation through the cover, the lack of a good vegetative cover could also limit the release of infiltration stored in the cover should a wetter than average period occur.

Performance Monitoring of South Dump Trial Store/Release Cover

Instrumentation of the South Dump trial store/release cover comprised a full weather station established on the top of the dump, five large size (2.5 m diameter and height) lysimeters located in the waste rock just under the cover, and Campbell Scientific TDR-based volumetric water content and thermal conductivity-based matric suction sensors within the cover (see Figure 1). The lysimeters were formed from HDPE water tanks with the tops removed. Their 2.5 m wall height ensured that they were non-wicking, and they were periodically pumped out from a small sump in the base to determine rainfall percolation through the cover. The plan dimension of the lysimeters ensured that they were overlain both by cover hummocks and troughs, thus providing a representative estimate of percolation.

Figure 2. Placement of rocky soil mulch layer on South Dump cover trial.

The climatic data were used as input to the computer program SoilCover (Unsaturated Soils Group, 1997) to predict the performance of the cover. Calculations using SoilCover (Durham *et al.*, 2000) indicated that the average annual rainfall would produce about 1% percolation, while twice the average annual rainfall could produce percolation of 5% of incident rainfall.

The lysimeter data have shown that percolation through the trial store and release cover into the South Dump mineralised waste rock has averaged less than 0.25% of incident rainfall, with a maximum recorded percolation of 1.1% of incident rainfall. However, readings of the lysimeters have been sporadic, and were discontinued in late 2001 when rehabilitation of the site was completed. A percolation of 1% of the

average annual rainfall or 7 mm/year, which is equivalent to an unsaturated hydraulic conductivity of 2.2×10^{-10} m/s, is comparable to the low unsaturated natural deep drainage rate of the area.

The cumulative annual rainfall (together with the annual totals) recorded on the top of the South Dump is shown on Figure 3. All but the 2000/01 annual rainfall totals were significantly below the average annual rainfall of 700 mm. Ponding of water between the hummocks has been observed during the wet season, and no significant cracking of the surface has been observed during the dry season.

Annual Totals	
96/97	524 mm
97/98	623 mm
98/99	475 mm
99/00	522 mm
00/01	713 mm
01/02	523 mm
02/03	423 mm
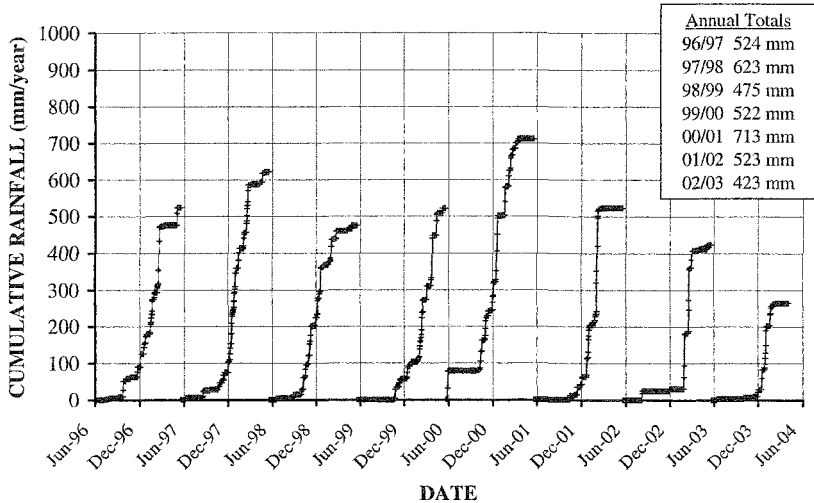
Figure 3. Cumulative annual rainfall recorded on top of South Dump.

As shown on Figure 4, the store/release cover undergoes wetting up during each wet season, followed by drying during each succeeding dry season, with the dried-out states at each depth showing little net change over time. Wetting up of the cover occurred within about 1 month, implying an infiltration rate of about 8×10^{-7} m/s. This suggests preferred pathways, the dominant ones being the interfaces formed on successive paddock dumping of the rocky soil mulch. The release of the stored rainfall infiltration through evapotranspiration is more gradual.

After each dry season, the volumetric water content of the upper rocky mulch layer drops to a minimum of about 0.10 (degree of saturation S of 0.2 and gravimetric moisture content w of 5%, for a porosity of 0.4), while after the wet season the average volumetric water content of the cover rises to about 0.35 (S ~ 0.7 and w ~ 20%). The slight increase in the volumetric water content in the winter dry seasons of 1998 and 1999 was related to a diminished vegetative cover, which was corrected by refertilising. The subsequent increase in the volumetric water content in the winters of 2001 and 2002 was related to a further diminished vegetative cover, caused by

extended dry weather, but this was addressed by refertilising and tree seeding with eucalypts.
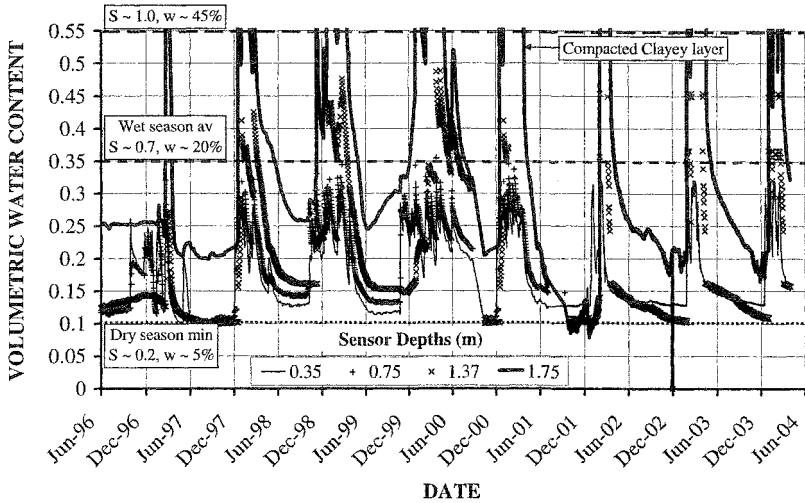
Figure 4. Wetting and drying cycles of South Dump trial store/release cover.

Laboratory and Field Soil Water Characteristic Data for South Dump Trial Cover

Figure 5 shows Soil Water Characteristic Curves (SWCCs) fitted (using the method of Fredlund *et al.* (1997) and the program SoilVision) to the data measured within the South Dump trial store/release cover, and average laboratory fitted SWCCs for the compacted clayey and rocky soil mulch layers. The saturated volumetric water contents for each of the field curves were based on measured field data at each sensor level, and indicate generally increasing porosity with depth. While the range of porosity is larger than would be expected, it may be explained by the ravelling of coarse-grained particles towards the base of rocky soil mulch layer forming a loose matrix, the hanging up of fines towards the top of the mulch layer, the compaction of the near surface materials by wetting and drying cycles, and inadequate compaction of the base clay layer. According to Campbell Scientific, the thermal conductivity matric suction sensors are most reliable over the suction range 10 to 1,000 kPa. The recorded matric suctions ranged from 3 to over 10,000 kPa. Over range from 10 to 10,000 kPa, Figure 5 shows that the field SWCC for the compacted clay (at 1.77 m depth) is higher than the compacted clay laboratory curve, indicating that the field porosity was than that tested in the laboratory. The three field curves for the rocky soil mulch layer over the suction range from 10 to 1,000 kPa plot lower than the laboratory curve, indicating that the field porosity was lower than that tested in the laboratory.

Figure 6 shows the laboratory and field unsaturated hydraulic conductivity functions derived using the method of Fredlund *et al.* (1994) from the fitted SWCCs and

measured saturated hydraulic conductivities for the South Dump trial store/release cover materials. Over the recorded matric suction range, the compacted clay layer remained unsaturated with an unsaturated hydraulic conductivity of lower than about 2×10^{-9} m/s, and an average annual value of about 2×10^{-10} m/s, as suggested by the lysimeter results. The rocky soil mulch layer was more permeable and was also likely to have preferred seepage paths.
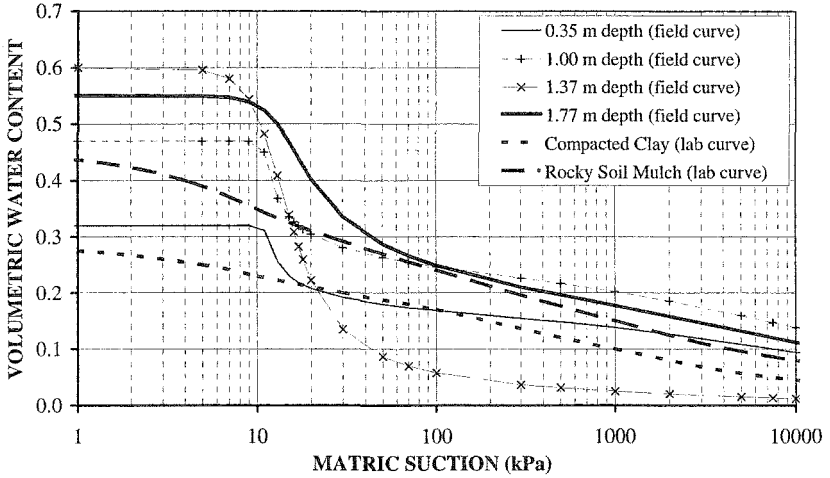
Figure 5. Fitted laboratory and field SWCCs for South Dump trial cover.
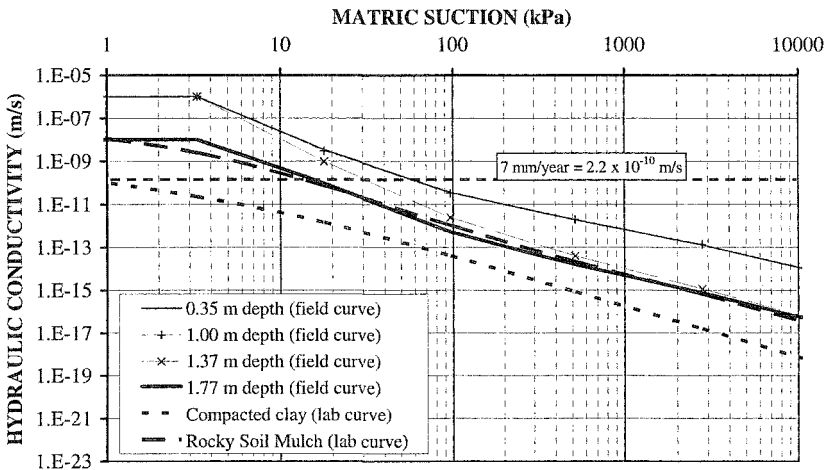
Figure 6. Laboratory and field unsaturated hydraulic conductivity functions.

Water Balance for South Dump Trial Cover

Figure 7 shows the estimated response of the South Dump trial cover to a range of annual rainfall totals ranging from 400 to 1,500 mm, as a function of annual rainfall. The estimated response was based on the following assumptions.

- Percolation increasing linearly from zero for 400 mm annual rainfall to 1% of annual rainfall for the average annual rainfall of 700 mm, and again increasing linearly to 5% of annual rainfall for 1,500 mm annual rainfall, as predicted using SoilCover.
- The water storage of the cover assumed to increase linearly from 350 mm for 400 mm annual rainfall to 525 mm for the average annual rainfall, and again increase linearly to full saturation of 605 mm for 1,500 mm annual average rainfall (assuming that this will be extracted via evapotranspiration following heavy rainfall events, making additional storage available for subsequent rainfall events).
- An evaporation rate assumed to increase linearly from 50 mm for 400 mm annual rainfall to 240 mm for 1,500 mm annual rainfall.
- Effective transpiration, by eucalypt trees in particular (which can remove the equivalent of between 2 mm/day and 20 mm/day, compared with maximum extraction rates of 4 mm/day for acacias and grasses, and evaporation rates off ponded water of up to 10 mm/day), to take up any excess water during wet periods.
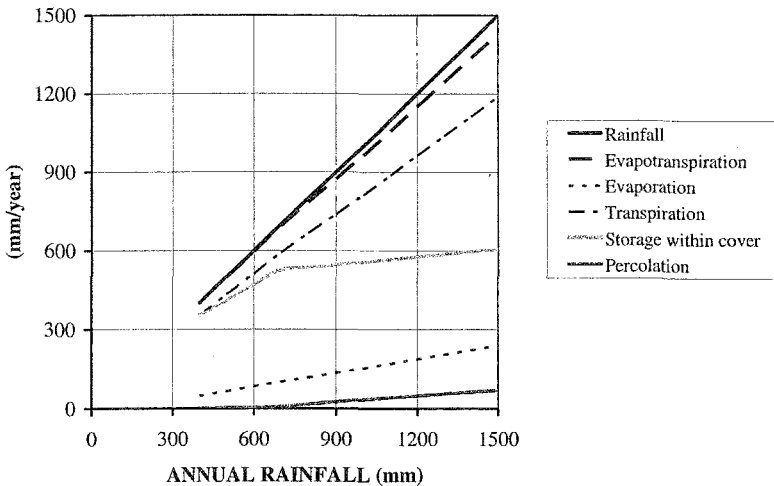
Figure 7. Estimated evaporation, transpiration, storage within cover and percolation as a function of annual rainfall for South Dump trial cover.

Overall Water Balance for Waste Rock Dumps

The waste rock dumps receive ongoing incident rainfall from their 340 ha catchment averaging 2.4 Mm^3/year. An estimated 0.4 Mm^3/year of incident rainfall would fall above mineralised waste rock, which comprises about 17% of the total volume of the waste rock dumps. During dump construction, perhaps half of the incident rainfall would have infiltrated the dumps, some going into storage and some going to seepage. Over the 10 years that acidic conditions prevailed, prior to covering the dumps, perhaps 10 Mm^3 of moderately acidic seepage would have been generated, some of which will continue to seep from the dumps over time.

Infiltration will continue into the side slopes, which comprise 10 to 15% of the surface area of the dumps, contributing to ongoing relatively clean seepage at a rate of perhaps 0.15 Mm^3/year. This will reduce due to transpiration by the grasses planted in the oxide waste rock dumped over the slope crest and with the gradual generation of further fines through weathering, which will add water storage capacity and increase runoff. With the establishment of the vegetated store/release covers, perhaps only 0.001 Mm^3/year on average will intercept mineralised waste rock. A further source of seepage is flow through the dump along buried natural drainage channels. To date, the quantity of seepage emanating from the dumps has declined by a factor of about five from that experienced prior to the cover being placed, and is continuing to decline. The seepage water quality is improving and is expected to improve further over time.

Modifications to Store/Release Cover System and North Dump Cover

For subsequent covers, the hummocked surface was smoothed by a single pass of a low bearing pressure dozer, to disrupt possible preferred seepage paths at the interface between successive paddock dumps, and to enhance revegetation while retaining high porosity. The revegetation approach was also modified, with fertilising and native tree-seeding carried out in the first year, followed by refertilising and grass-seeding in the second year. This allows the deeper-rooted native trees to become established, rather than be choked out by grasses. Instrumentation of the North Dump store/release cover, which was constructed in December 2001 using the modifications described above, showed a similar pattern of seasonal variation in volumetric water content to that observed for the South Dump trial cover (Figure 4), but with somewhat slower wetting up of the cover following rainfall due to the smoothing of the hummocks.

Conclusion

The key elements of the Kidston dump design are a base pad of fresh barren waste rock, with a wide encapsulation (up to 60 m horizontally) of fresh barren waste rock, leaving the side slope at the angle of repose of the material, and end-dumping a partial cover of oxide waste rock from the crest to facilitate revegetation. The key elements of the store/release cover system developed for Kidston are a 0.5-m-thick

compacted layer, overlain by a minimum 1.5-m-thick rocky soil mulch layer with a dozed mounded surface that is revegetated. Reducing the amplitude of the hummocks by means of a single dozer pass helps to seal off possible preferred seepage paths at the interface between successive paddock dumps, and enhances revegetation while retaining high porosity. The choice of appropriate vegetation to transpire excess stored water from the rocky mulch layer is vital to maintaining the function of the store/release cover system. Trees are best planted in the first year of revegetation, with grasses seeded the second year. A eucalypt tree cover represents the only sustainable means of achieving sufficient transpiration in the long-term.

Over the 9 years of monitoring, the maximum recorded percolation through the trial store/release cover has been 1.1% of incident rainfall, although most of these years have experienced below average annual rainfall. The compacted clay layer at the base of the store/release cover is key to limiting percolation, since the rocky soil mulch layer permits preferred flow. The vegetative cover is key to ensuring the release of the stored rainfall infiltration. The instrumented store/release covers have undergone annual cycles of wetting up during each wet season, followed by drying during each succeeding dry season, with the dried-out states at each depth within the cover showing little net change over time.

Acknowledgements

References

Durham, A.J.P., Wilson, G.W., Bews, B.E. and Currey, N.A. (2000). Evaluation of a low flux cover system for mine waste rock in an arid climate. *Proceedings of 6th International Conference on Acid Rock Drainage, Denver, Colorado, USA, 21-24 May 2000*, 2, 1319-1326. Society for Mining, Metallurgy and Exploration Inc.

Fredlund, M.D., Fredlund, D.G. and Wilson, G.W. (1997). Prediction of the soil water characteristic curve from grain size distribution and volume mass properties. *Proceedings of 3rd Brazilian Symposium on Unsaturated Soils, Rio de Janeiro, Brazil, 22-25 April 1997*, 12 pp.

Unsaturated Soils Group. (1997). *SoilCover, User's Manual, Version 4.0*. Unsaturated Soils Group, University of Saskatchewan, Saskatoon, Canada.

Williams, D.J., Wilson, G.W. and Currey, N.A. (1997). A cover system for a potentially acid forming waste rock dump in a dry climate. *Proceedings 4th International Conference on Tailings and Mine Waste '97, Fort Collins, Colorado, USA, 13-17 January 1997*, 231-235. A.A. Balkema, Rotterdam.

Field Performance of Capillary Break Covers Over Hypersaline Tailings in an Arid Climate

D.J. Williams[1] and D.J. Stolberg[2]

[1]Department of Civil Engineering, The University of Queensland, QLD 4072, AUSTRALIA; PH +61-7-3365-3642; FAX +61-7-3365-4599; email: D.Williams@uq.edu.au
[2]Department of Civil Engineering, The University of Queensland, QLD 4072, AUSTRALIA; PH +61-7-3365-3745; FAX +61-7-3365-4599; email: D.Stolberg@uq.edu.au

Abstract

As part of research investigating cover systems on hypersaline tailings deposits in the arid climate of the Eastern Goldfields region in Western Australia, different cover trials have been monitored for salinity up-take into the cover. Among the parameters monitored were moisture content, suction, salinity and pH in the covers and underlying hypersaline tailings, and the success of revegetation. The performance of a large (60 m by 60 m) conventional "continuous" cover has been compared with the performance of small (nominally 10 m in dimension) "discontinuous" cover mounds. The trial covers comprised a 400-mm-thick capillary break layer above the hypersaline tailings, overlain by a minimum 200 mm thickness of growth medium ("topsoil"). Four different capillary break materials were investigated, including coarse quarry rock, hard pit rock, caprock and oxide waste rock. Since the construction of the cover trials, there has been a gradual increase in salinity in each of the cover systems, due to the evaporative (matric suction) and osmotic suction-induced upward migration of salt from the underlying hypersaline tailings. The hard pit rock performed best as a capillary break layer, remaining drier than the other materials used for this purpose, but salt still breached this layer and migrated into the overlying growth medium. Perhaps counter-intuitively, the salinity levels were found to be much higher in the small cover mounds than in the large cover, due to the lateral migration of salts into the small cover mounds from beneath the surface of the surrounding tailings, via the growth medium overlapping the sides of the mounds. Salt uptake into the cover system potentially limits revegetation, as is

the case for a natural saltpan. The low regional rainfall further challenges revegetation. The greater salt uptake into the small cover mounds makes their revegetation even more of a challenge.

Introduction

The Eastern Goldfields region of Western Australia has an arid climate, with an average annual rainfall of 257 mm, and significant variations due to periodic droughts and heavy rainfall associated with occasional cyclonic influences to the north. While the rainfall is well distributed throughout the year, it occurs mainly in intense events of short duration. The Eastern Goldfields region experiences average maximum and minimum temperatures of 25°C and 11°C, respectively, and an average annual pan evaporation of 2,400 mm, with actual evapotranspiration taking up most of the annual rainfall.

The Eastern Goldfields region is underlain by hypersaline groundwater, with total dissolved salt concentrations of up to 250,000 ppm which, due to the shortage of good quality water in the region, is used for processing the ore. As a result, the tailings formed have highly saline pore water. The high salt content of the tailings has a number of effects. The formation of a salt crust on the surface of the tailings on evaporative desiccation tends to close off further desiccation, while at the same time limiting dusting. However, the salt crust also makes revegetation problematic. Hypersaline tailings are analogous to the natural saltpans that exist in the region.

Where tailings contain highly saline pore water, a conventional continuous cover will require a capillary break to prevent saline water rising to the vegetation root zone within the cover. An alternative is a discontinuous cover system comprising small cover mounds. Apart from being a much cheaper option than placing a continuous cover, the discrete cover mounds could serve as "dams" to spread the rainfall runoff over a larger evaporative surface area, and would potentially act as island sanctuaries for vegetation with bare tailings salt pans between, mimicking a natural saltpan. The performance of the discontinuous cover system is discussed herein, and compared with that of a conventional continuous cover system.

Trial Cover Design

The trial covers were constructed in February 2001 on Cell 2 of Tailings Storage Facility 1 at Mount Keith Nickel Operation, located about 350 km north of Kalgoorlie in Western Australia. On the western side of the central decant access way of the facility, a 60 m x 60 m "continuous" main pad was constructed. This main pad was split up into four quadrants, each 30-m square. This was done so that four different capillary break materials could be investigated simultaneously. On the eastern side of the central decant access way, two series of discrete small pads, each pad measuring a nominal 10 m in dimension and a nominal 10 m apart, were constructed. The two trial cover systems are illustrated in Figure 1, which shows

limited revegetation of the trial covers with salt-tolerant species, although these proved very difficult to establish, requiring several attempts. The almost bare bottom right quadrant of the main pad is underlain by the hard pit rock capillary break material, and proved almost impossible to revegetate due to the inability of the relatively coarse-grained growth medium layer to hold water above the free-draining hard pit rock.
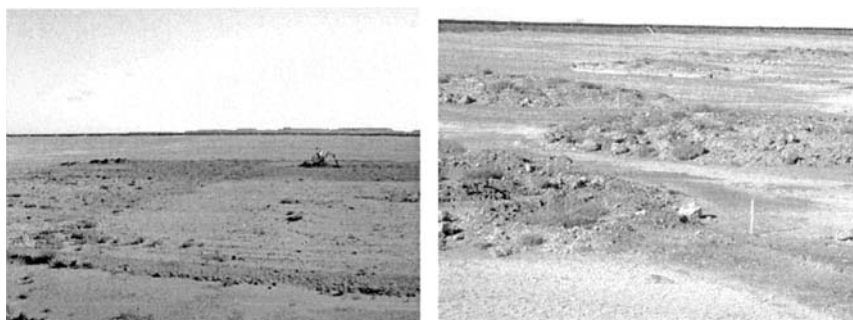
Figure 1. Continuous (left) and discontinuous (right) trial cover systems at Mount Keith Nickel Operation (June 2004).

The trial cover profile (for both continuous and discontinuous covers) is shown in Figure 2. It comprised a 400-mm-thick capillary break layer above the hypersaline tailings, overlain by a minimum 200-mm thickness of growth medium ("topsoil"). The growth medium contained typically 17 to 31% gravel-sized (2 to 60 mm), 81 to 67% sand-sized (0.06 to 2 mm) and 2% silt-sized particles (0.002 to 0.06 mm), and overlapped the sides of the trial covers to some extent. The air entry suction of the growth medium (about 1.2 kPa) gives it a capillary rise of only about 120 mm, making it unable to hold much water to establish and sustain vegetation. Four different capillary break materials were investigated.

- Coarse quarry rock, containing about 62% gravel-sized, 26% sand-sized and 2% silt-sized particles.
- Hard pit rock, containing about 75% gravel-sized or coarser, 23% sand-sized and 2% silt-sized particles.
- Caprock, containing 53% gravel-sized, 45% sand-sized and 2% silt-sized particles.
- Oxide waste rock, containing 27% gravel-sized, 60% sand-sized and 13% silt-sized particles, which is a similar particle size distribution to the growth medium.

For all of the capillary break materials investigated, the 400-mm-thickness of the capillary break layer is far greater than the theoretical height to which water could rise under the effects of capillary action (ranging from 40 to 150 mm for the materials investigated). The capillary break layer must be much thicker than is theoretically

required, to prevent it from being rendered ineffective by the infiltration of fines from the overlying growth medium. Alternatively, a graded filter and/or geotextile would be required, involving considerable cost.
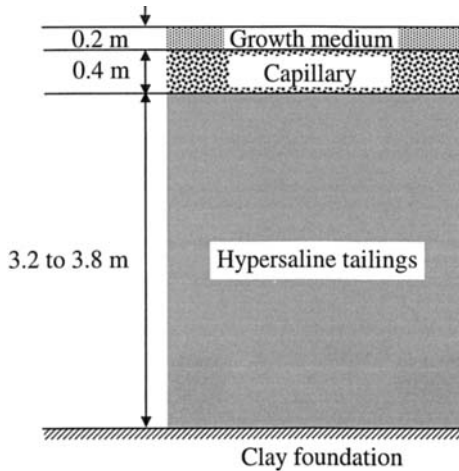
Figure 2. Trial cover profile overlying hypersaline tailings.

Sampling and Testing Methods

The trial cover testing was carried out in November 2001 (9 months after the construction of the trial covers), May and November 2002, October 2003 and June 2004. Moisture, pH (not reported herein), suction and salinity (reported indirectly herein as osmotic suction) profiling with depth was carried out during each investigation, for covered areas as well as beneath exposed tailings. The testing involved sampling of the cover materials from the sides of test pits and hand augering through the tailings, to obtain closely-spaced samples. The gravimetric moisture content (mass of water/mass of dry solids, expressed as a percentage) of the recovered samples was determined in the mine site laboratory (using AS 1289.2.1.1, 1994), and selected samples were subjected to total suction, pH, electrical conductivity (EC) and salinity (total dissolved solids, TDS) testing. The pH, EC and TDS determinations were carried out on a paste formed by adding distilled water to the moist sample in a nominal water (distilled water plus pore water) to dry solids mass ratio of about 5 to 1, as recommended by Hunt and Gilkes (1992). The distilled water had a neutral pH of 7 and as a result the pH was not affected by the addition of distilled water.

EC and TDS were determined on a solids dry mass basis. The amount of distilled water added was sufficient to ensure that all soluble salts on the tailings particles were dissolved (Hunt and Gilkes, 1992). The EC values in µS/cm were approximately twice the numerical TDS values in mg/L. A portable psychrometer (HR-33 Dew Point

Microvoltmeter, manufactured by Westcor Inc. of Logan, Utah, USA) was used to determine the total suction, which is the (combined effect of the salts in the pore water, giving rise to osmotic suction, and matric suction, which develops on desaturation of the material. Osmotic suction is useful when looking at the stress states of unsaturated materials and may be derived from the EC using the logarithmic relationship presented in Figure 3 (reproduced from USDA, 1954). Osmotic suction values are plotted herein as a representation of salinity within the different cover profiles. Subtracting the estimated osmotic suction values from the corresponding measured total suction values gave the matric suction values.
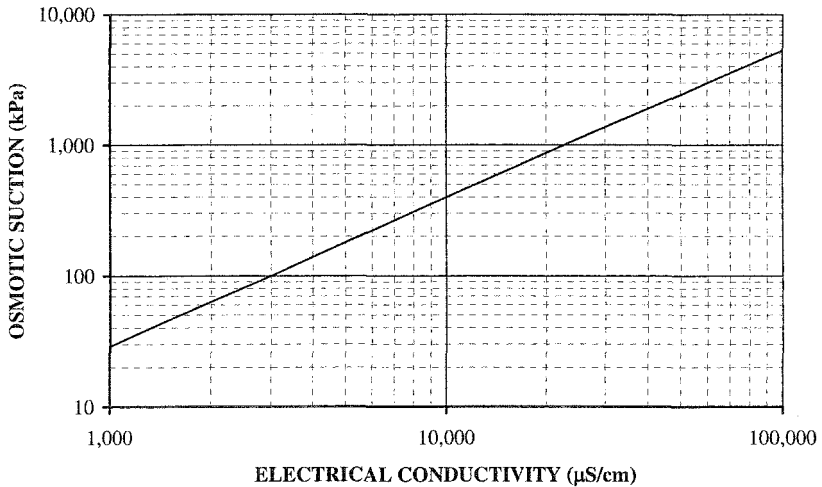
Figure 3. Logarithmic relationship between osmotic suction and electrical conductivity (after USDA, 1954).

Results of Monitoring

Since the construction of the cover trials, there has been a gradual increase in salinity (osmotic suction) in each, due to the evaporative (matric suction) and osmotic suction-induced upward migration of salt from the underlying tailings. The hard pit rock performed best as a capillary break layer, but remained drier than the other materials used for this purpose. Perhaps counter-intuitively, the osmotic suctions were found to be much higher in the small cover mounds (discontinuous cover) than in the large (continuous) cover and, as a result, this finding is the key focus of the paper. The performance of the continuous and discontinuous trial covers were studied during the October 2003 and June 2004 site visits, with moisture content, osmotic suction and matric suction profiles with depth being generated for the different capillary break materials. This enabled a comparison to be made between the continuous and discontinuous cover systems.

In October 2003, the performances of the main pad and small cover mound incorporating caprock as the capillary break were compared. Figure 4 shows the profile obtained for the main pad incorporating caprock as the capillary break. Also shown on Figure 4 is the osmotic suction profile with depth obtained at the centre of the small cover mound incorporating caprock as the capillary break. The discontinuous cover developed much higher osmotic suctions, particularly at the cover surface, than the continuous cover. This indicates that there has been substantially more migration of salts into the small cover mound, which initially had low salt levels (corresponding to less than 100 kPa osmotic suction).
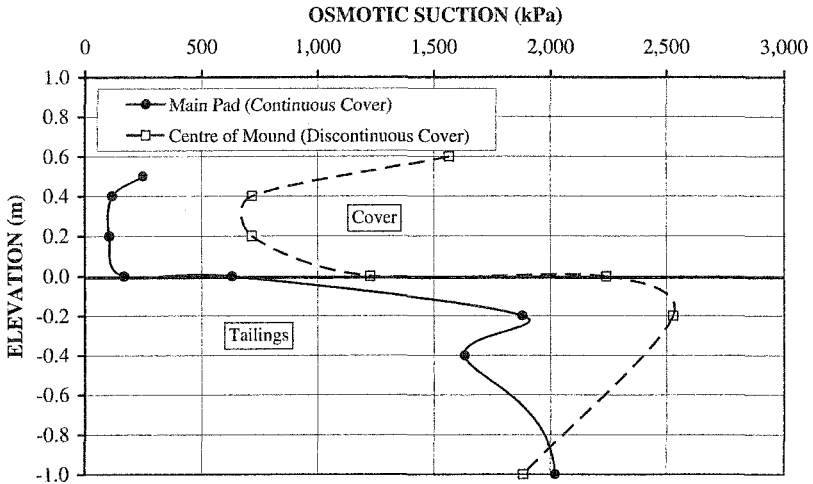
Figure 4. Comparison of continuous and discontinuous covers incorporating caprock as a capillary break (October 2003).

To confirm the apparent greater accumulation of salts in the small cover mounds compared with the main pad, all four capillary break materials were investigated during a site visit in June 2004. The osmotic suction profiles with depth obtained in June 2004 showed greater salt uptake into the discontinuous cover than the continuous cover, for all capillary break materials.

Also, during the June 2004 investigation, each of the four cover mounds was sampled with depth at a range of offsets from the toe of the mound. The mound surface salinity, measured in the growth medium, was found to generally increase towards the toe of the mound, due to a combination of a progressively decreasing thickness of capillary break material towards the toe and a surface covering of growth medium fines, either placed during the construction of the mounds or eroded since, that facilitated the upward migration of salts from the uncovered tailings surrounding the mound.

Figure 5 shows the osmotic suctions measured on the sloping surface of the mounds for each of the underlying capillary break materials. There is a general trend of very high osmotic suctions (corresponding to very high salt concentrations) at and near the toe of the mound, which decrease up the mound at a rate somewhat proportional to the relative effectiveness of the underlying capillary break material. The finer-grained oxide waste rock capillary break, being the least effective, facilitated the greatest accumulation of salts at the surface, both at the toe and up the mound. The caprock and coarse quarry rock capillary breaks produced slightly lower but comparable osmotic suctions at the toe, with more rapid dropping off of osmotic suction up the mound than for the oxide waste rock capillary break. The coarse-grained nature of the hard pit rock not only prevents capillary rise but also facilitates the leaching of salts with rainfall infiltration. This may well account for the very much reduced osmotic suction at the toe of the mound underlain by hard pit rock, when compared with the other capillary break materials. The osmotic suction up the mound underlain by hard pit rock is also reduced.
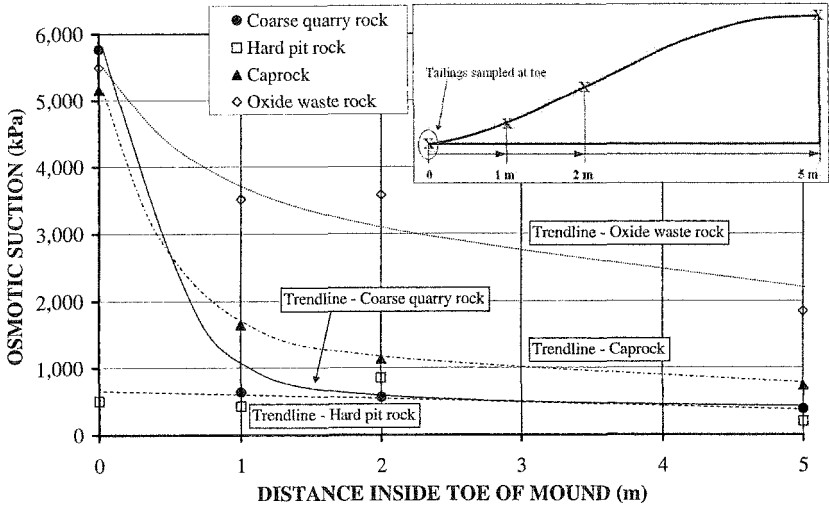
Figure 5. Mound surface osmotic suctions for all capillary break materials.

The monitoring times and average osmotic suctions in the growth medium are superimposed on the daily rainfall data on Figure 6. Of particular note are the low amount of rainfall and relative absence of high daily rainfalls recorded between May and November 2002. These two factors are reflected by the higher osmotic suctions measured during this period.

Surficial gravimetric moisture contents and matric suctions were also measured up the mounds during the June 2004 investigation, as shown on Figures 7 and 8, respectively. The moisture content trendlines are not consistent. For the oxide waste

rock and coarse quarry rock capillary breaks, the moisture content was significantly higher at the toe and dropped off considerably with increasing elevation up the mound. The high toe moisture contents may have been due to an accumulation of fines and rainfall runoff at the toe. For the hard pit rock and caprock capillary breaks, there was little change in moisture content with elevation up the mound.
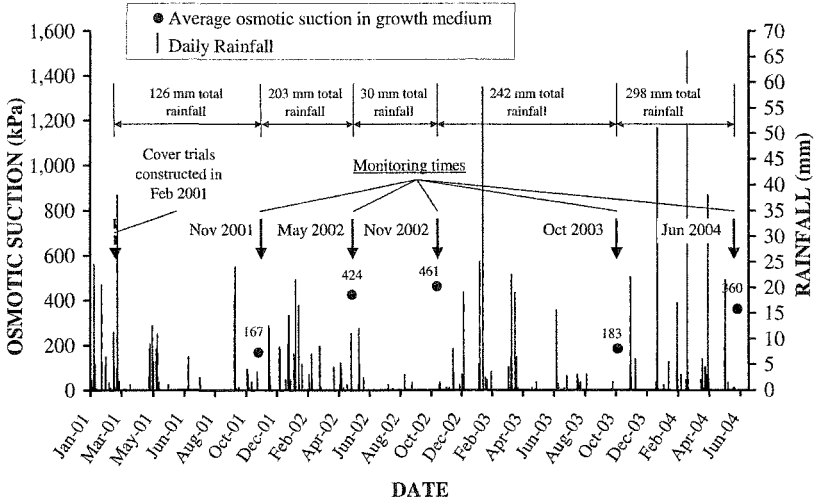
Figure 6. Monitoring times and average growth medium osmotic suctions superimposed on daily rainfall data.
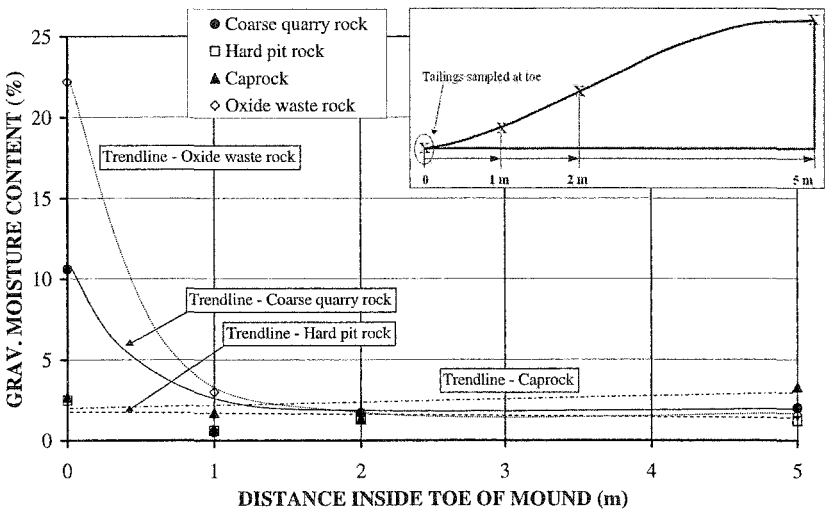
Figure 7. Mound surface moisture contents for all capillary break materials.

The matric suction trendlines showed relatively little variation with elevation up the mound, with the highest value being measured at the toe of the hard pit rock capillary break mound, and the lowest values being measured for the caprock and oxide `waste rock capillary breaks.
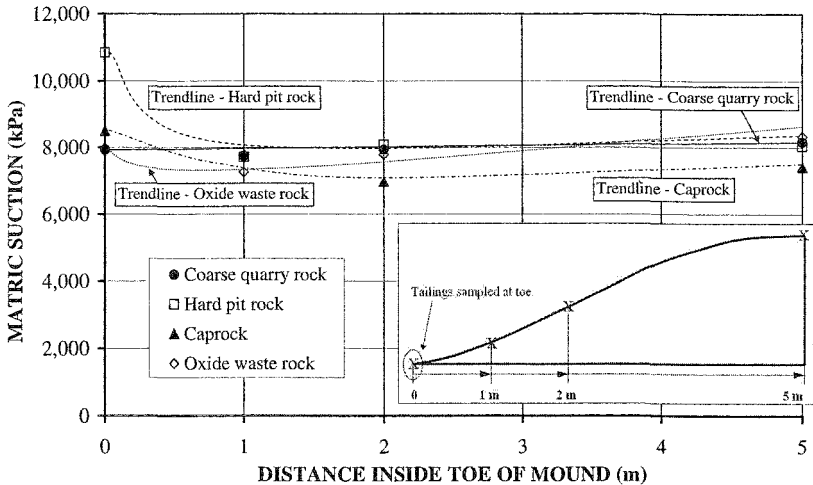
Figure 8. Mound surface matric suctions for all capillary break materials.

A number of simultaneous processes (depicted on Figure 9) explain the higher salt accumulation in the small discontinuous cover mounds.

- Evaporation drives salts from the underlying tailings into both the main pad and small cover mound, but the high total suction of the tailings salt crust underlying the covers (> 7,000 kPa) and the thickness of the cover limits this process.
- The cover itself undergoes significant evaporative drying, concentrating the salts migrating from the underlying tailings, although this process reduces as the total suction and salt accumulation rise within the cover.
- The growth medium layer was allowed to overlap the sides of the small cover mounds during construction, and further fines are added due to the erosion of fines downslope, providing a pathway for salt migration that renders the capillary break layer less effective. Salt is drawn up from below the tailings crust beyond the cover mound and into the growth medium via this layer of fines. The spillover of fines on the sides of the much larger main pad at Mount Keith does not significantly affect its performance, and this effect would not exist for a completely continuous cover.
- The tailings underlying the surface crust have a gravimetric moisture content of about 30%, much wetter than the tailings crust and adjacent capillary break materials (in the range from 4 to 8%), which are in turn generally much wetter

than the surface of the mound (in the range from 2 to 4%, except at the toe in some cases). Thorpe and Barbour (1991) found that, for a given water flux, the velocity of advective salt transport increases as the moisture content decreases. The low moisture content of the growth medium results in the rapid transport of salts to the evaporative front at the mound surface, where they are concentrated as a result of evaporation.

Implications of Results

Covers for tailing storage facilities are intended to limit the infiltration of rainfall into potentially contaminating tailings, and so limit the potential for contaminated seepage through the walls of the facility or into the foundation. The conventional approach is to attempt a continuous, vegetated cover that sheds rainfall runoff by concentrating it in engineered drains over the sides of the facility. In an arid climate, it may not be necessary to shed rainfall incident on a tailings storage facility, and indeed rainfall shedding will may it even more difficult to establish and sustain a vegetative cover, and may lead to excessive erosion. Incident rainfall may be removed by evaporation or evapotranspiration without inducing excessive seepage through the walls of the facility or into the foundation, and without causing erosion. Hypersaline tailings make it difficult to prevent salt migration from the tailings into the cover, and hence make revegetation problematic.

The results of the trial cover monitoring bring into question the effectiveness of a discontinuous cover system for hypersaline tailings in an arid climate. However, even a continuous cover system with an ineffective capillary break and/or one having a growth medium that is too coarse-grained to hold water will be unable to establish and sustain vegetation in an arid climate.

A discontinuous cover system is very attractive from the point of view of its reduced cost compared with a continuous cover and may be a cost-effective option under certain circumstances.

- In situations where revegetation of the tailings storage facility is not the aim (or is impossible to achieve due to low rainfall and poor soils), discrete mounds may be shaped and located to serve as dams to spread rainfall runoff over the surface of the tailings to facilitate its removal by evaporation.
- The revegetation of a discontinuous cover system may be possible where the tailings contain manageable levels of salinity, or where salt leaching of coarse-grained tailings occurs by means of regular rainfall.
- A revegetated discontinuous cover system may be possible even for hypersaline tailings where particular attention is paid to the design, material selection and construction of a capillary break under the mound, and to the placement of a fine-grained growth medium.
- This could involve constructing a lip of capillary break material around the perimeter of the mound to contain the growth medium material on top of the

mound and prevent the spreading and erosion of fines down the mound slopes, as illustrated in Figure 10.

Evaporation-driven migration
of salts from below the tailings
crust through outer layer of fines

Evaporation-driven
concentration of salts

Growth medium

Capillary break

Hypersaline tailings

Limited osmotic suction-driven
migration of salts from covered
(non-crusting) tailings surface
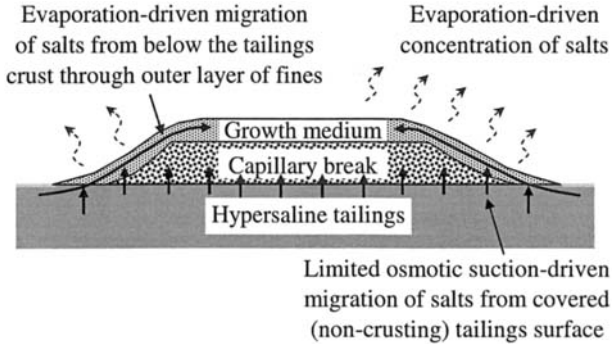
Figure 9. Main processes driving salt migration in trial cover mounds at Mount Keith.

Growth medium

Capillary break

Hypersaline tailings
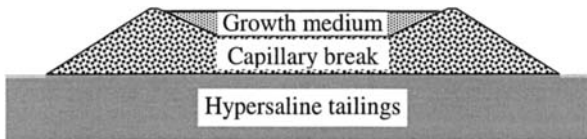
Figure 10. Alternative mound construction to prevent salt from migrating up sides of mound.

Conclusion

Continuous and discontinuous cover systems, incorporating various capillary break materials with an overlying growth medium, have been investigated for hypersaline tailings at the Mount Keith Nickel Operation in the arid Eastern Goldfields region of Western Australia. This region is underlain by hypersaline groundwater which, due to the shortage of good quality water in the region, is used to process the ore. As a result, the tailings formed have highly saline pore water. The effectiveness of covers constructed on these tailings therefore hinges almost entirely on their resistance to the upward migration of salt from the hypersaline tailings, together with their ability to retain moisture to establish and sustain vegetation, if this is to form part of the final rehabilitation plan.

The parameters monitored as part of the cover studies were moisture content, suction, salinity (reported indirectly herein as osmotic suction) and pH (not reported herein), within the covers and underlying hypersaline tailings. The performance of a large conventional continuous cover was compared with the performance of small discontinuous cover mounds. The trial covers comprised a 400-mm-thick capillary

break layer above the hypersaline tailings, overlain by a minimum 200-mm thickness of growth medium ("topsoil"). Four different capillary break materials were investigated, including caprock, hard pit rock, coarse quarry rock, and oxide waste rock. Since the construction of the cover trials, there has been a gradual increase in salinity in each of the cover systems, due to the evaporative (matric suction) and osmotic suction-induced upward migration of salt from the underlying tailings. The hard pit rock performed best as a capillary break layer, but remained drier than the other capillary break materials.

Perhaps counter-intuitively, the osmotic suctions were found to be much higher in the small cover mounds than in the large cover. This was due to a combination of the lateral movement of salts from beneath the salt-crusted tailings surrounding the small cover mounds as they undergo evaporation, and the presence of a thin outer layer of fines covering the capillary break material providing a route for advective salt transport. This effect could be overcome by fully encapsulating the growth medium by an effective capillary break material.

Acknowledgements

References

AS 1289.2.1.1 (1994). *Australian Standard - Method 2.1.1: Soil moisture content tests - Determination of the moisture content of a soil - Oven drying method (standard method)*. Standards Australia.

Hunt, N. and Gilkes, B. (1992). *Farm Monitoring Handbook*. The University of Western Australia, Nedlands, WA.

Thorpe, M.B. and Barbour, S.L. (1991). Key factors affecting the movement of sodium into surface amendments used to reclaim saline land. *Proceedings of 44th Canadian Geotechnical Conference, Calgary, Canada, 29 September to 2 October 1991*, 2, 65-1 to 65-9. Canadian Geotechnical Society.

USDA (1954). *Agricultural Handbook No. 60, Diagnosis and Improvement of Saline and Alkali Soils*. L.A. Richards (ed.). United States Department of Agriculture.

Case History and Regulatory Aspects of a Final Cover Performance Evaluation Involving Conventional and Evapotranspirative Cover Designs

Stockdill, D.[1], Jorgenson, R. R.[2], and Obermeyer, J. E.[3]

[1]Great River Energy, Coal Creek Station, 2875 3rd Street Southwest, Underwood, ND 58576; PH (701) 442-7012; FAX (701) 442-7212; email: dstockdill@grenergy.com
[2]Golder Associates Inc., 44 Union Boulevard, Suite 300, Lakewood, CO 80228; PH (303) 980-0540; FAX (303) 985-2080; email: rjorgenson@golder.com
[3]Golder Associates Inc., 44 Union Boulevard, Suite 300, Lakewood, CO 80228; PH (303) 980-0540; FAX (303) 985-2080; email: jobermeyer@golder.com

Abstract

In May 2004, lysimeters were constructed at Great River Energy's Coal Creek Station to allow a comparative field-scale evaluation of the environmental performance of three earthen final cover designs. Two of the cover profiles use conventional compacted clay hydraulic barriers to limit percolation, while the third profile is designed to store and release water via evapotranspiration. Although a considerable amount of progress has been made in modeling and understanding both types of cover systems in recent years, less attention has been devoted to the challenges introduced when attempting to obtain regulatory acceptance of an alternative final cover system. In this paper, the authors present a case history of the project, with an emphasis on permitting challenges associated with alternative final cover equivalency demonstrations. Cover system field performance to date is also discussed.

Introduction

A final cover is constructed after closure of a waste containment facility (or a portion of a waste containment facility) primarily for the purpose of limiting the infiltration of water into the waste mass below. A conventional earthen cover design generally includes a compacted low-permeability soil (LPS) layer to provide a barrier against flow through the cover system. However, evapotranspiration (ET) covers have been employed with increasing frequency in recent years as alternative final cover (AFC) designs (Benson et al. 2005). These covers rely on the capability of cover soils to store water and the ability of native vegetation and evaporation to remove the water from the soil before it has a chance to infiltrate into the waste.

A significant amount of modeling has been performed to predict conventional cover and ET cover performance (e.g. Roesler et al. 2002, Khire et al. 1997). Additionally, numerous investigations have been conducted to evaluate the actual field performances of conventional and ET covers in a range of climatic environments (e.g. Albright et al. 2004, ITRC 2003a). Considerable progress has been made in modeling and understanding both types of cover systems, helping designers develop more efficient and cost-effective AFC designs for equivalent protection of the environment. In a number of situations, however, a serious challenge to implementing these innovative designs still exists. Reluctance on the part of regulatory bodies to accept or approve newer technologies implicit in the design of an AFC is an issue still faced by many designers.

This paper presents the case history of a project designed by Golder Associates Inc. (Golder) to obtain regulatory approval of an AFC design for coal combustion product (CCP) disposal facilities at a site near Underwood, North Dakota. The first phase of the project consisted of a modeling effort designed to estimate the percolation rate through two conventional cover designs and one ET cover design over time. The second phase of the project involves an ongoing field-scale evaluation of the performances of three earthen cover designs using lysimetry. Results of both the modeling and the field-scale evaluation to date are presented, and permitting challenges and other regulatory aspects of the project are emphasized.

Background

The project is being conducted at Coal Creek Station (CCS), an 1,100-megawatt coal-fired power plant site owned and operated by Great River Energy (GRE). Located approximately 80 km (50 mi) northwest of Bismarck, North Dakota, CCS is North Dakota's largest electrical generation facility. Ground was broken for construction of the facility in 1974, and CCS became fully operational in 1981.

Approximately 6.8 million tonnes of lignite are burned annually at CCS, generating as by-products approximately 460,000 tonnes of fly ash, 280,000 tonnes of bottom ash, 25,000 tonnes of economizer ash, 10,000 tonnes of pulverizer rejects, and 110,000 tonnes of flue gas desulfurization sludge. The high quality of CCS fly ash allows for more than half of the fly ash to be sold into the cement market, and a portion of the bottom ash is also used beneficially on site. The unused CCPs are disposed on site in one of two surface impoundments or at one of four landfills. Each of these disposal facilities will require final cover upon closure. The surface area of the facilities to be closed is approximately 110 hectares (270 acres).

Disposal of CCPs is regulated by the North Dakota Department of Health under the category of special waste. Special waste disposal facilities in North Dakota require a minimum final cover thickness of 1.5 m (5 ft), of which 0.61 m (2 ft) must be LPS material having a hydraulic conductivity of 1×10^{-7} cm/s or less. This cover thickness is conservative with respect to thickness requirements in the surrounding states. Prescriptive final cover requirements for CCP disposal facilities in North Dakota and its neighboring states are presented in Table 1.

Table 1. Final cover requirements for North Dakota and surrounding states.

| State | LPS Layer | | Subsoil Layer | Erosion Layer | Total |
	Thickness mm (in)	Hydraulic Conductivity cm/s	Thickness mm (in)	Thickness mm (in)	Thickness mm (in)
Montana	457 (18)	1×10^{-5}	None	152 (6)	610 (24)
Nebraska	None	None	610 (24)	None	610 (24)
South Dakota	None	None	610 (24)	None	610 (24)
Minnesota	610 (24)	None	None	None	610 (24)
Wyoming	None	None	610 (24)	152 (6)	762 (30)
Iowa	610 (24)	None	305 (12)	None	914 (36)
North Dakota	610 (24)	1×10^{-7}	762 (30)	152 (6)	1,524 (60)

Based on the information presented in Table 1, closure of the six disposal facilities at CCS will require between 688,000 and 994,000 m^3 (900,000 and 1,300,000 yd^3) more material than would be required in any of the surrounding states for the same facilities. The conservative cover requirements in North Dakota introduce additional costs and environmental impacts associated with:

- locating and stockpiling additional borrow materials;

- disturbing larger areas to obtain additional borrow materials;

- processing, hauling, placing, and compacting additional final cover materials;

- performing construction quality control and construction quality assurance on a larger volume of final cover materials;

- making less efficient use of available airspace; and

- permitting, constructing, monitoring, and closing additional disposal facilities needed due to the airspace forfeited to additional final cover materials.

More than 27 million tonnes of coal are burned by North Dakota's power producers annually, making the coal-fired power industry one of the most important components of the state's economy. The objective of the project at CCS is to investigate the viability of an AFC design that will reduce costs associated with the closure of disposal facilities for North Dakota's power producers, make more efficient use of North Dakota's soil resources, and provide equivalent or superior environmental performance relative to the prescriptive cover design.

Cover Designs

The cover designs can be described as follows (Figure 1):

- CC5 – a 1.5-m (5-ft) soil cover having a 0.61-m (2-ft) compacted LPS layer, this is the prescriptive cover for special waste disposal sites in North Dakota.

- CC3 – a 0.91-m (3-ft) soil cover having a 0.46-m (1.5-ft) compacted LPS layer, this is the prescriptive cover for municipal solid waste (MSW) disposal sites in North Dakota.

- ETC – a 0.91-m (3-ft) ET cover, this design relies on principles of water balance, specifically the capability of soil to store water and native vegetation and evaporation to remove water from the soil cover.

The third design, an ET cover, should be of particular interest to those who study the behavior of unsaturated soils, since the objective is to design the cover system such that the soil is prevented from reaching its field capacity. Therefore, modeling and design of ET cover systems require careful consideration of the unsaturated flow characteristics of the cover soils.
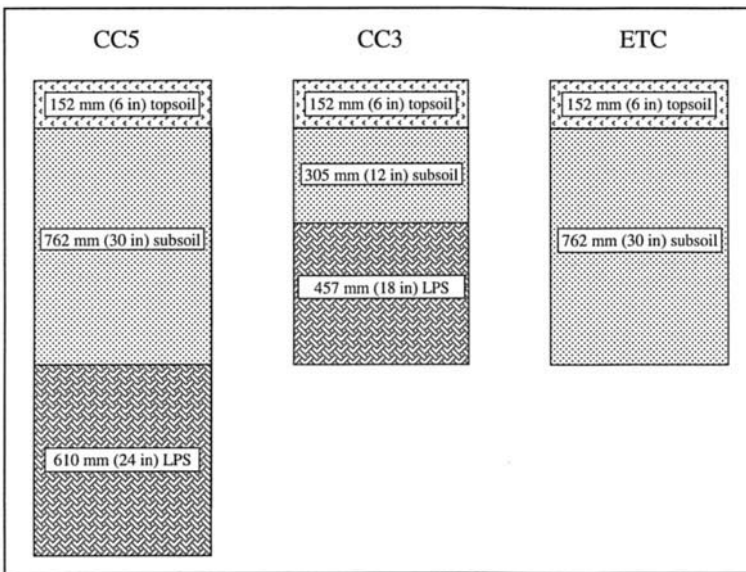
Figure 1. Cover designs.

Evapotranspiration covers can provide advantages over conventional covers, depending on the local climate and the engineering properties of available soils. They are especially viable in semi-arid climates similar to that of central North Dakota. Potential advantages of ET covers include the following (ITRC 2003a):

- a wider range of soil types may be used to construct an ET cover than can be used to construct a conventional cover,

- construction of an ET cover generally requires less soil conditioning and processing than construction of a conventional cover,

- construction quality control and construction quality assurance are generally less complex for an ET cover than for a conventional cover, and

- long-term cover performance and integrity may be better for an ET cover than for a conventional cover.

Cover Performance Modeling

In 2002, Golder used the Hydrologic Evaluation of Landfill Performance (HELP) model (Schroeder et al. 1994) and the Unsaturated Soil Water and Heat Flow (UNSAT-H) model (Fayer 2000) to compare the predicted performances of the CC3 and CC5 conventional cover designs. Khire et al. (1997) evaluated the relative accuracy of these two programs and concluded that UNSAT-H was more accurate, although the errors made by HELP in predicting percolation were conservative. The HELP model was used due to regulatory familiarity and ease of use, and UNSAT-H was used to simulate cover performance more accurately.

The HELP model predicted average annual percolation rates of 3.3 mm/yr for the CC3 cover design and 12.4 mm/yr for the CC5 cover design. The disparity in the predicted cover performances is related to the predicted average hydraulic head exerted on the barrier layer. For the 0.91-m (3-ft) cover design, the average hydraulic head was estimated to be 7.6 mm, whereas the predicted value for the 1.5-m (5-ft) cover design was 40.6 mm. Presumably, the model predicts that at some depth in the 1.5-m (5-ft) cover design, water can no longer be removed via ET and eventually percolates into the waste. The results from the HELP model were shown to be sensitive to an order-of-magnitude increase in the barrier layer hydraulic conductivity for the CC3 cover design (average annual percolation rate of 13.7 mm), but not for the CC5 cover design (average annual percolation rate of 12.4 mm).

The UNSAT-H modeling indicated that only nominal amounts of percolation would be allowed by either cover design. The percolation rate was shown to be insensitive to an order-of-magnitude increase in the hydraulic conductivity of the barrier layer for both cover designs.

The initial modeling results were considered by the regulators to be an insufficient basis for approval of the CC3 cover design for the special waste disposal facilities at CCS (ironically, this cover design is prescribed for MSW facilities in North Dakota). Consequently, GRE elected to proceed with a comparative field-scale evaluation of the CC5 and CC3 cover designs, along with the ETC cover design.

For the ETC cover design, UNSAT-H modeling was used to help select an appropriate cover thickness to store water that infiltrates without allowing excessive percolation during wet periods. The modeling indicated that a 0.91-m (3-ft) ET cover would allow negligible percolation, even if the wettest year of the last ten years was repeated ten times consecutively. This thickness is generally consistent with recommendations by Benson and Chen (2003) using the unit storage capacity approach for the Bismarck site and the site-specific soil data shown in Figure 2 (Benson and Wang 2004).

The chart shows Matric Suction (kPa) on the y-axis ranging from 1.0E-03 to 1.0E+06, and Volumetric Water Content on the x-axis ranging from 0 to 0.5. Legend shows Fitted (line) and Measured (squares). Parameters box shows: $\alpha = 0.0017$, $n = 1.219$, $\theta_r = 0.00$, $\theta_s = 0.42$.
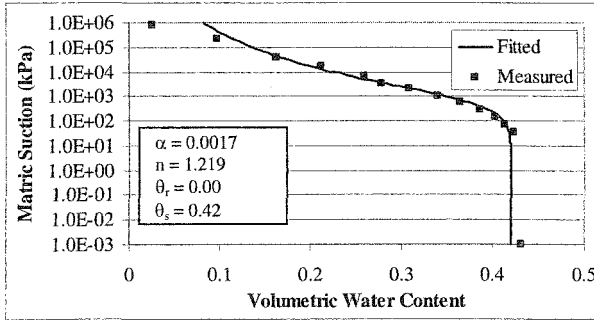
Figure 2. Soil-water characteristic curve for CCS subsoil.

Field-Scale Evaluation

In May and June of 2004, three lysimeters measuring 20 m by 10 m (66 ft by 33 ft) were constructed, side by side, to allow a comparative evaluation of CC5, CC3, and ETC cover performance over a three-year time span (Figure 3). Design and installation of the lysimeters were modeled after the United States Environmental Protection Agency's (EPA's) Alternative Cover Assessment Program (ACAP), as discussed by Bolen et al. (2001).

The floor and sidewalls of the lysimeters consist of high-density polyethylene (HDPE) geomembrane. A drainage geocomposite was placed on the floor of each lysimeter to allow for transmission of collected percolation to the sump. A 150-mm (6-in) layer of bottom ash (similar to a poorly graded sand) was then placed to provide a cushion against damage to the geomembrane and geocomposite during compaction of the overlying soils. A biota barrier (geotextile with embedded trifluralin nodules) was installed in each lysimeter just above the bottom ash layer to protect the geocomposite from damage due to root intrusion. The respective soil cover profile was then constructed in each lysimeter using similar techniques to those used during large-scale cover construction.

Low-permeability soil layers were constructed within the CC5 and CC3 lysimeters with the intent of achieving hydraulic conductivity values less than or equal to 1×10^{-7} cm/s. Construction quality assurance included moisture-density testing of the compacted soils using a nuclear density gauge and a sand-cone device, as well as flexible-wall permeability testing on Shelby tube samples. As specified, moisture-density test results generally plotted near the line of optimums at relative compaction values between 96 and 100 percent (based on standard compaction testing). The geometric mean hydraulic conductivity value for four LPS samples was 5.6×10^{-8} cm/s. This value compares well with the results of hydraulic conductivity tests from full-scale projects at Coal Creek Station involving the construction of LPS layers.

The subsoil material (sandy clay) was selected based on its abundance on the site and proximity to the site's disposal facilities. Subsoil materials were placed in all three

lysimeters with the intent of achieving an average relative compaction value consistent with that obtained with typical construction haul traffic (based on a pre-construction test fill). Construction quality assurance included moisture-density testing of the soils using a nuclear density gauge and a sand-cone device, as well as flexible-wall permeability testing on Shelby tube samples. Moisture-density testing indicated that the subsoil's natural moisture content was higher than was desired (near or slightly above optimum moisture content), resulting in average relative compaction values near 90 percent and lower hydraulic conductivity values than were intended or would be expected for a water storage layer. The geometric mean hydraulic conductivity value for six subsoil samples was 3.0×10^{-7} cm/s. The use of a sandier material or looser placement would likely have resulted in superior water storage performance for the subsoil layers and less chance of desiccation cracking.

Figure 3. Lysimeters during construction (project trailer is on the right).

Instrumentation was installed to allow continuous measurement of climate and soil conditions, as well as runoff and percolation from all three lysimeters and lateral flow from the CC3 and CC5 lysimeters. Climatic parameters being measured include air temperature, relative humidity, precipitation, wind speed, wind direction, and solar radiation. Each lysimeter contains three nests of soil sensors, which include time-domain reflectometers to allow computation of soil moisture content and heat dissipation units to allow computation of soil matric suction. A trailer was installed to house collection basins for measurement of surface water runoff, percolation, and lateral flow volumes.

The heated and air-conditioned trailer represents an improvement over ACAP's typical subsurface collection basin installation, particularly in an environment where frost depths would necessitate a cover soil thickness of a meter or more over the collection basins. Pressure transducers and dose floats provide redundant measurements of flow into the collection basins. The percolation collection basins are fitted with rain gauges to allow an additional means for flow measurement.

Data Summary

Data collection began in June 2004 and will likely continue through December 2006. A summary of water balance data from January 1, 2005, to

December 31, 2005, is contained in Table 2. Data from June 2004 through December 2004 are not included since this was an equilibration period during which water stored in the cover soils as a result of precipitation received during construction drained from the lysimeters and was measured as percolation. The data in Table 2 indicate similar performance for the three cover designs to date.

For the time period indicated, surface runoff accounted for a larger percentage of the water balance than was observed at any of the sites described by Albright et al. (2004). Most of the runoff occurred following two particularly intense precipitation events (on the order of 40 mm/d) in May and June of 2005. The large amounts of runoff may be attributed to the relatively low subsoil permeability.

Only a small amount of lateral flow along the LPS layers was measured for both conventional covers. This observation is consistent with the findings at many of the sites described by Albright et al. (2004).

The amount of percolation measured represents a small percentage of the total precipitation for all three cover designs. While the project is primarily a comparative evaluation of the cover designs, the small amount of percolation transmitted from all three lysimeters indicates that each cover design is likely appropriate for disposal facilities at CCS.

Table 2. Water balance data from January 1, 2005, to December 31, 2005.

Cover Design	Runoff mm	Lateral Flow mm	Percolation mm	Precipitation mm
CC5	45.8	1.6	2.7	
CC3	44.3	1.1	1.8	449.8
ETC	35.9	N/A	4.6	

The 449.8 mm of precipitation measured at the National Weather Service station in Underwood, North Dakota, from January 1, 2005, to December 31, 2005, represents a value slightly higher than the annual average precipitation (446.0 mm). The ET cover design has been put to the test early, and so far it has performed well, especially given that the vegetation has only had a year to mature (point-frame testing in June 2005 indicated about 70 percent vegetative coverage for all three lysimeters).

Regulatory and Permitting Challenges

The challenges often faced when attempting to obtain regulatory approval of an AFC design are stated well in a guidance document issued by the Interstate Technology and Regulatory Council (ITRC 2003b):

> *"[Regulators] may or may not be well-versed in the various disciplines required to evaluate the flexibility imbued in the regulations they are implementing and interpreting. If regulators are applying regulations for which they do not have substantive*

background or training, then they may tend toward a conservative application of the regulations without fully appreciating the regulators' inherent options. Some agencies tend to be overly conservative in their approach to interpreting their regulations and the flexibility built into the regulations. This is demonstrated by a degree of unwillingness on the part of some regulators and/or agencies to deviate from the regulation-derived conventional covers."

Waste containment facility operators and designers attempting to obtain regulatory approval of AFC designs will likely encounter regulatory agencies of varying technical sophistication and experience with AFC designs. This disparity, coupled with the current lack of consistent performance criteria for AFC designs, create an environment where the effort to obtain – and the likelihood of obtaining – regulatory approval of an AFC design can vary greatly. Furthermore, the idea behind AFCs is to move away from prescriptive designs and toward site-specific design processes, involving a shift in design philosophies that some regulators don't understand or feel comfortable making (Albright 2003).

In Golder's experience of designing and permitting AFCs, the following issues have tended to arise most frequently as regulatory objections to proposed designs:

1. *Modeling approach.* Depending on the sophistication of the program used to predict percolation rates, a large number of input parameters may be required. Consistent with Benson and Chen (2003), the modeling approach should be discussed with the regulators and ideally agreed to prior to executing the model. The importance of this recommendation increases with model complexity and execution time. Furthermore, a literature review or preliminary sensitivity analysis may help identify the most important input variables for the specific program, potentially accelerating and simplifying the modeling approach agreement. The climatic period to be modeled (e.g. wettest year repeated, wettest consecutive 30-year span) may represent the most debatable input parameter. In some instances, regulators will require a field demonstration to confirm the results of a modeling effort.

2. *Lysimetry.* A challenge associated with using lysimetry to measure percolation rates in the field involves the potential for capillary barrier effects to exist in the lysimeter's drainage layers and possibly influence the measured percolation rates. Albright et al. (2004) contend that the inclusion of a root barrier at a sufficient depth prevents the removal of water from a perched saturated zone above the drainage layer. The advantage of comparative evaluations, such as the one at CCS, is that, from a practical standpoint, the quantitative measure of percolation rates may be less important than the relative performance of the cover designs, all of which are subject to the same potential for capillary barrier effects.

3. *Acceptable percolation rates.* Given the scarcity of available field data for actual performance of final covers, it is difficult to quantify typical

percolation rates for conventional or prescriptive designs with much certainty. Therefore, establishing an acceptable percolation rate for an AFC design is problematic. Several authors (e.g. Albright et al. 2004) have suggested values in this regard, but additional performance data for conventional covers and a consistent set of performance criteria that account for liner design, waste characteristics, and climate are needed before these values can be applied as more than simply guidance. The problem of defining acceptable percolation rates has given rise to the concept of equivalency for both modeling and field demonstration exercises.

4. *Equivalency.* Conceptually, equivalency is straight-forward. The performance of an AFC design must be demonstrated to be equivalent to or superior to that of the prescriptive cover design. The difficulty arises in attempting to quantify uncertainty in model predictions or field demonstration results. For modeling exercises, uncertainty is introduced with each input parameter that is not precisely known. The three most important sources of uncertainty for field demonstrations are typically measurement accuracy, temporal variability, and spatial variability (Benson 2003). The concept of equivalency should include provisions to account for uncertainty in the predicted or observed percolation rates for both prescriptive cover and AFC designs.

Typically, equivalency may be demonstrated by an AFC design allowing an average annual percolation rate within some tolerance of the prescriptive cover's average annual percolation rate. For field demonstrations, guidance for quantifying uncertainty due to temporal variability and spatial variability may be available in the literature (e.g. Albright and Benson 2002, Gurdal et al. 2003). Measurement accuracy errors can typically be quantified by the specific measurement device manufacturer. For modeling scenarios, the literature may also provide some guidance, depending on the program that is being used. In the case of the field-scale demonstration at CCS, equivalency will be achieved by an alternative cover design (CC3 or ETC) if its average annual percolation rate in Years 2 and 3 of the demonstration is equal to or less than the average annual percolation rate from the CC5 lysimeter for the same years, with an allowance of 2.4 mm/yr to account for uncertainty in the percolation rates.

5. *Duration of field-scale demonstrations.* Field-scale demonstrations are particularly useful when regulators are hesitant to approve an AFC design on the basis of modeling alone. The usefulness of a field-scale demonstration diminishes, however, if the duration of the evaluation precludes a relatively swift decision regarding the approval of an AFC design. For the period during which a field-scale demonstration is conducted, the best possible information regarding actual cover performance should be obtained. In most cases, the information from such demonstrations represents a much better basis for design decisions than otherwise exists (Albright 2003).

At the ACAP test sites, as well as for the demonstration at CCS, a duration of three years was considered appropriate for evaluation of relative cover performance. While every climatic condition and soil process cannot possibly occur during such a time span, sufficient data can be collected to calibrate models based on observed percolation rates and extrapolate the trends for a range of scenarios. Data from ACAP suggest that changes in the hydraulic properties of the soils, particularly changes due to desiccation of LPS layers, are typically observed within a three-year timeframe (Albright 2003).

In general, regulatory familiarity with AFC designs and the issues they present is increasing nationwide, due in large part to ACAP. The field-scale demonstration at CCS will add a data point to the existing information regarding ET cover performance in semi-arid regions. With this and other information being presented in the literature, the goal of geoenvironmental engineering practice should be to pave the way for a consistent regulatory framework for evaluating and approving AFCs. Regulatory agencies have the opportunity to follow the EPA's lead and partner with designers to elevate and advance the state of the practice with respect to cover design.

Conclusions

A case study describing a field-scale final cover demonstration at GRE's CCS has been presented. The preliminary modeling effort and the installation of three ACAP-style lysimeters have been described, and the results of the field-scale demonstration to date have been summarized. The ET cover design has been emphasized due to its relevance to the topic of unsaturated soil behavior. To date, the percolation rates through CC3 and ETC have been similar to that through CC5. The performance of the ETC cover is anticipated to improve as the vegetation matures.

The case study has also been used to introduce a discussion of the current regulatory environment related to the permitting of AFC designs. Common regulatory objections to AFC evaluations have been presented, along with recommendations for finding common ground in negotiations with regulators. Most importantly, both designers and regulators are working toward the goal of providing appropriately engineered final covers that perform effectively. Thus, a common vision and a partnership to provide a more consistent regulatory framework for evaluating and permitting AFCs should be pursued.

Acknowlegements

References

Albright, W. H. (2003). Personal communication, January 25, 2003.

Albright, W. H. and Benson, C. H. (2002). "Alternative Cover Assessment Program 2002 annual report." Publication 41182, Desert Research Institute, Reno, NV.

Albright, W. H., Benson, C. H., Gee, G. W., Roesler, A. C., Abichou, T., Apiwantragoon, P., Lyles, B. F., and Rock, S. A. (2004). "Field water balance of landfill final covers." *Journal of Environmental Quality*, 33(6), 2317-2332.

Benson, C. H. (2003). Personal communication, March 10, 2003.

Benson, C. H., Bohnhoff, G. L., Ogorzalek, A. S., Shackelford, C. D., Apiwantragoon, P., and Albright, W. H. (2005). "Field data and model predictions for a monolithic alternative cover." *Waste Containment and Remediation*, GSP No. 142, ASCE, 1-12.

Benson, C. H. and Chen, C. (2003). "Selecting the thickness of monolithic earthen covers for waste containment." *Soil and Rock America 2003*, Verlag Gluck auf GMBH, Essen, Germany, 1397-1404.

Benson, C. H. and Wang. X. (2004). "Soil water characteristic curves for specimens from the GRE final cover test sections, Underwood, North Dakota." Geo Engineering Report 04-10, University of Wisconsin-Madison, Madison, WI.

Bolen, M. M., Roesler, A. C., Benson, C. H., and Albright, W. H. (2001). "Alternative Cover Assessment Program: Phase II report." Geo Engineering Report 01-10, University of Wisconsin-Madison, Madison, WI.

Fayer, M. J. (2000). "UNSAT-H Version 3.0: Unsaturated Soil and Heat Flow Model – theory, user manual, and examples." Report No. PNNL-13249, Pacific Northwest National Laboratory, Richland, WA.

Gurdal, T., Benson, C. H., and Albright, W. H. (2003). "Hydraulic properties of final cover soils from the Alternative Cover Assessment Program." Geo Engineering Report 03-02, University of Wisconsin-Madison, Madison, WI.

Interstate Technology and Regulatory Council (ITRC). (2003a). "Technology overview using case studies of alternative landfill technologies and associated regulatory topics." March 2003.

Interstate Technology and Regulatory Council (ITRC). (2003b). "Technical and regulatory guidance for design, installation, and monitoring of alternative final landfill covers." December 2003.

Khire, M. V., Benson, C. H., and Bosscher, P. J. (1997). "Water balance modeling of earthen landfill covers." *Journal of Geotechnical and Geoenvironmental Engineering,* ASCE, 123(8), 744-754.

Roesler, A. C., Benson, C. H., and Albright, W. H. (2002). "Field hydrology and model predictions for final covers in the alternative cover assessment program – 2002." Geo Engineering Report 02-08, University of Wisconsin-Madison, Madison, WI.

Schroeder, P. R., Dozier, T. S., Zappi, P. A., McEnroe, B. M., Sjostrom, J. S., and Peyton, R. L. (1994). "The Hydrologic Evaluation of Landfill Performance (HELP) model: Engineering documentation for Version 3." EPA/600/R-94/168b, United States Environmental Protection Agency, National Risk Reduction Engineering Laboratory, Cincinnati, OH.

Lysimeter Tests for an ET Cover Design at Monticello, Utah

W. J. Waugh[1], P. S. Mushovic[2], and A. W. Kleinrath[3]

[1]Environmental Sciences Laboratory*, 2597 B ¾ Road, Grand Junction, CO 81503; PH (907) 248-6431; email: jody.waugh@gjo.doe.gov
[2]U.S. Environmental Protection Agency, 999 18th Street, Denver Place, Denver, CO 80202; PH (303) 312-6662; email: mushovic.paul@epamail.epa.gov
[3]U.S. Department of Energy, 2597 B ¾ Road, Grand Junction, CO 81503; PH (907) 248-6037; email: art.kleinrath@gjo.doe.gov

*Operated by S.M. Stoller Corporation for the U.S. Department of Energy Office of Legacy Management under DOE contract number DE–AC01–02GJ79491.

Abstract

The U.S. Department of Energy (DOE) and the U.S. Environmental Protection Agency (EPA) collaborated on the design of an alternative cover for a uranium mill tailings disposal cell at Monticello, Utah. The Monticello design relies on the water storage capacity of a thick, fine-textured soil layer overlying a sand-and-gravel capillary barrier to store precipitation while plants are dormant, and on evapotranspiration (ET) to remove stored water during the growing season. A series of field lysimeter studies were conducted to help design and then monitor the performance of the Monticello cover. Initially, small weighing lysimeters containing mature native vegetation growing in intact monoliths of undisturbed soil provided evidence that an ET cover was a reasonable option even at Monticello, which has an annual average precipitation of 390 mm and a relatively short growing season. Favorable results led to installation of 15 additional small weighing lysimeters to compare water-storage capacities and drainage from different borrow soil types and layer thicknesses. Loam and clay loam soils had the highest water storage capacities. Drainage was less than 3 mm/yr for all treatments during an 8-yr period. Two caisson lysimeters (3-m diameter) were installed adjacent to the construction site to mimic and monitor the range of conditions as built in the actual cover. A loam topsoil compacted to 1.45 g/cm, installed in one lysimeter, had a 40% greater water storage capacity than a gravely clay loam subsoil compacted to 1.65 g/cm^2 installed in the other lysimeter. Only 0.1 mm of drainage occurred in both lysimeters, an amount well below the EPA target of <3.0 mm/yr.

Introduction

The U.S. Department of Energy and the U.S. Environmental Protection Agency collaborated on the design and construction of a disposal cell to contain uranium mill tailings at Monticello, Utah. The Monticello mill, built in 1942, processed nearly 1.0 million tons of uranium ore and produced more than 2.5 million m^3 of tailings before its closure in the early 1960s. The disposal cell design was subject to both (1) minimum technology guidance for hazardous waste disposal facilities (USEPA 1989) under subtitle C of the Resource Conservation and Recovery Act of 1976 (RCRA) and (2) design guidance for radon attenuation and 1,000-yr longevity (USDOE 1989) under the Uranium Mill Tailings Radiation Control Act of 1978 (UMTRCA).

At semiarid sites such as Monticello, relatively low precipitation (P), high potential evapotranspiration (PET), and thick unsaturated soils favor long-term hydrologic isolation of buried waste (Winograd 1981). However, simple P/PET relationships inadequately predict recharge in semiarid regions (Gee and Tyler 1994). Recharge can be minimized using covers designed with thick, fine-textured soil layers that store precipitation, and evapotranspiration (ET) to seasonally remove water (Anderson et al. 1993). Capillary barriers consisting of coarse-textured sand and gravel placed below this soil "sponge" can enhance water storage and limit unsaturated flow (Nyhan et al. 1990, Ward and Gee 1997).

Weighing and drainage lysimeters offer the most direct and reliable means for evaluating soil-water balance of alternative cover designs (Gee and Hillel 1988). Lysimeters have been used for many years to evaluate irrigation needs and, more recently to test the hydrologic performance of landfill covers (Sackschewsky et al. 1995, Ward and Gee 1997, Albright et al. 2004). This paper reviews a case study consisting of a series of field lysimeter experiments conducted at Monticello beginning in 1990 to help design and then monitor the performance of a disposal cell cover that relies in part on soil water storage and ET to limit infiltration and leaching of contaminants from tailings.

Monticello Climate, Soils, and Vegetation

Monticello is semiarid with cold, windy winters and mild summers. The 30-yr average (1961–1990) annual precipitation is 390 mm. Three seasons occur with respect to soil-water balance: November through March, the season of deep infiltration and moisture accumulation in soils (precipitation averages 160 mm); April through June, a moisture-depletion period when plants are most active (precipitation averages 60 mm); and July through October, a season of shallow moisture accumulation and depletion resulting from monsoonal convection storms (precipitation averages 170 mm).

The clay loam to sandy loam soils within the footprint of the Monticello disposal cell, *Monticello very fine sandy loam*, formed in Pleistocene loess (USDA, 1945). The

natural vegetation consists primarily of Western wheatgrass, Sandberg bluegrass, blue grama, mountain big sagebrush, and rubber rabbitbrush with a canopy coverage of 50 to 60%.

Monticello Cover Design

The Monticello cover (Figure 1) is fundamentally an ET cover with a capillary barrier. It consists of a 163-cm fine-textured soil sponge layer overlying a 38-cm sand layer. A gravel admixture controls erosion (Ligotke 1994, Finley et al. 1985) and, functioning as a mulch, enhances seedling emergence and plant growth (Waugh et al. 1994). The soil depth is more than adequate to protect underlying RCRA components (CSL and geomembrane) from frost damage (Smith and Reger 2002). The soil sponge thickness is the primary biointrusion deterrent. Water retention in the soil sponge limits deep root penetration, and the layer exceeds the depth of most burrowing vertebrates in the area. A layer of cobble-size rock 30.5 cm above the capillary barrier is an added deterrent should deeper burrowers, such as prairie dogs, move into the area in response to climate change. Fine-textured soil fills the interstices of the cobble layer. The topsoil layer has physical and hydraulic properties similar to the rest of the soil sponge, but also contains available nutrients, propagules, and microorganisms needed to establish a sustainable plant community.
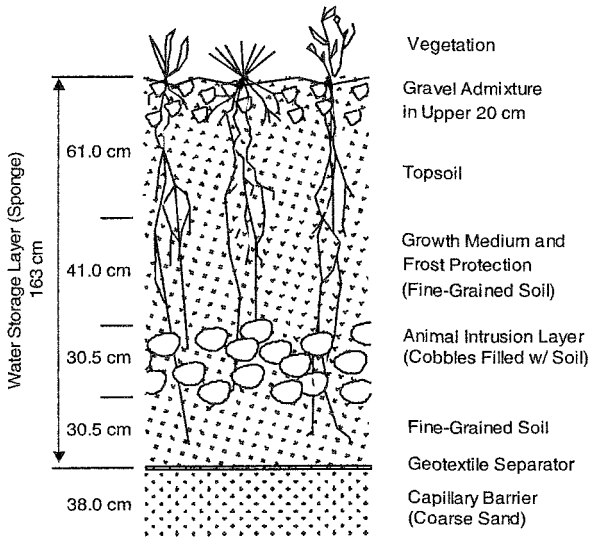
Figure 1. Monticello cover design.

Small Monolith Lysimeters

Monolith lysimeters were installed to evaluate plant water relations in small lysimeters and their adequacy for screening tests of ET cover designs at Monticello,

and were used to measure the soil-water balance of a simple cover design containing mature vegetation and a well-developed soil. Small weighing lysimeters have previously been used for agronomic applications (Shawcroft and Gardner 1983, Martin et al. 1985), to study solute and contaminant transport (Bowman et al. 1994, Corwin et al. 1994), and to test effects of various erosion control practices on soil-water balance (Waugh et al. 1991). Potential drawbacks of small weighing lysimeters include restriction of rooting volume, accentuation of diurnal temperature fluctuations, insufficient volume to adequately encompass soil macropore variability, creation of an artificial lower boundary in the soil profile, and greater edge flow effects (Dugas et al. 1985).

Five monolith lysimeters installed in 1991 consisted of a 102-cm length of 30-cm (i.d.) PVC pipe fitted with lifting rings and a PVC end cap. A sloping PVC plate in the bottom of the end cap directed drainage water to a sampling port. Installation of monolith lysimeters involved excavating an intact soil pedestal slightly larger than the lysimeter pipe, fitting the pipe down over the pedestal, detaching this encased soil monolith, placing pea gravel and a geofabric separator in the end cap, sealing the end cap to the bottom of the pipe, and then lowering the complete lysimeter into a 38-cm (i.d.) PVC sleeve that had been placed in the excavation. Moneliths lysimeters were installed in a thick clay loam loess supporting native Western wheatgrass. The soil monolith lysimeters preserved, as well as possible, native soil structure and plant root distribution as might develop in a cover over the long-term.

Comparisons of water relations of plants growing in and adjacent to lysimeters show the effects of isolating the soil monoliths. Confining undisturbed soil profiles in the small lysimeters had no observable effect on plant species composition but did alter plant abundance and increased water stress. Wheatgrass plants confined in lysimeters had 25% lower leaf area compared with plants adjacent to lysimeters. Western wheatgrass is rhizomatous (spreads via underground roots). Cutting connecting roots during lysimeter construction prevented transfer of photosynthates, nitrogen, water, and hormones from the larger wheatgrass clone outside the lysimeters (Bazzaz 1996) perhaps causing the reduction in leaf area inside the lysimeters.

Predawn leaf water potential (ψ_l) values, measured using a pressure chamber technique (Scholander et al. 1965), suggest that the reduction in wheatgrass leaf area was an adaptation to greater water stress during the mid-summer season of soil moisture depletion, and indicate that soils were drier inside the lysimeters. Correlations between predawn ψ_l and soil water potential values have been observed for both C4 and C3 grasses, although the correlation weakens as phenological development becomes more advanced (Link et al. 1990). Porometry data confirm that the physiological responses of Western wheatgrass to confinement are related to water stress. Shoots within lysimeters were deprived of water from rhizomes and roots of neighboring plants. Slightly lower stomatal conductance and transpiration rates as measured with a steady-state porometer were consistent with ψ_l data. One would expect water-stressed grasses in the lysimeters to transpire less water than grasses in

the undisturbed population. Diurnal porometry data suggest that transpiration rates continued lower on than adjacent to the lysimeters for the entire period between June and late August when ψ_l values remained more negative. Predawn ψ_l values can be a strong determinant of conductance and transpiration, independent of other diurnal variables (Link et al. 1990).

Small Lysimeter Array

An array of small weighing lysimeters was installed to evaluate the water storage capacity of a range of soil types and sponge layer depths. Unless the water content of the soil sponge layer becomes elevated above its storage capacity, in accordance with Richards effect (Richards 1950), downward water movement into the coarse sand layer should be inconsequential. Water-storage capacity has been defined as the difference between the amount of water retained in a soil at field capacity, the *drained upper limit,* and the amount of water remaining when the soil dries to the permanent wilting point, the *lower limit of extraction* (Ritchie 1981). At the permanent wilting point, soil water tensions become too high for plants to remove any more water. The water-storage capacity is greater for a fine-textured soil layer if placed over a coarse-textured capillary barrier. Water-storage capacity was measured as the difference between the drained upper limit and the lower limit of extraction by plants.

The treatment structure compared three soil types (clay, clay loam, loam) and three soil layer thicknesses (100, 150, and 200 cm) overlying a 15-cm pea gravel capillary barrier. The soil types encompassed the range of textural classes within in the footprint of the disposal cell. The lysimeter array consisted of five rows of weighing lysimeters with three lysimeters in each row. Thirty PVC pipes, 38 cm diameter by 230 cm long placed in a trench, served as sleeves within which the lysimeters were raised and lowered. Lysimeters end caps had an interior PVC ring welded to the bottom plate and two drainage ports, one inside the ring to measure drainage through the soil mass and the other outside the ring to measure preferential drainage along the sidewall. Lysimeters were filled by hand in 15-cm lifts placed relatively dry (10 vol.% water) and compacted to a dry-weight bulk density of about 1.4 g/cm^3, simulating the native soil bulk density.

Water-storage changes were estimated from weight changes measured by suspending lysimeters from a load cell anchored to a ½-ton gantry. The load cell had a resolution of about 1.4-mm water equivalent. Initial water storage in the soil sponge was calculated from volumetric moisture samples taken for each lift. Precipitation, water storage, and drainage were measured biweekly from April through September 1995 and again monthly from September 1999 to July 2001. ET was calculated as the mass balance, and water balance data were recorded as millimeters of water.

For all treatments (soil types and layer depths), drainage was well below the EPA standard of 3.0 mm/yr. The highest mean drainage over the 7-yr period (1.56 mm) occurred in the 200-cm clay loam treatment, most of it during the exceptionally wet

winter and spring of 1995. Drainage values were not significantly different among treatments (mean = 0.44 mm; $p < 0.05$). A drop in mean drainage for all treatments from 0.29 mm/yr in 1995 to less than 0.01 mm/yr by 1999 can be attributed to plant root development and increasing ET (annual precipitation remained above the 50-yr average from 1997 through 2001). Higher drainage in the 200-cm clay loam in 1995 suggests that the shallow, immature roots allowed moisture content to reach saturation at the capillary barrier interface. By 2000, roots were likely deep enough in all treatments to prevent saturation at the capillary barrier interface.
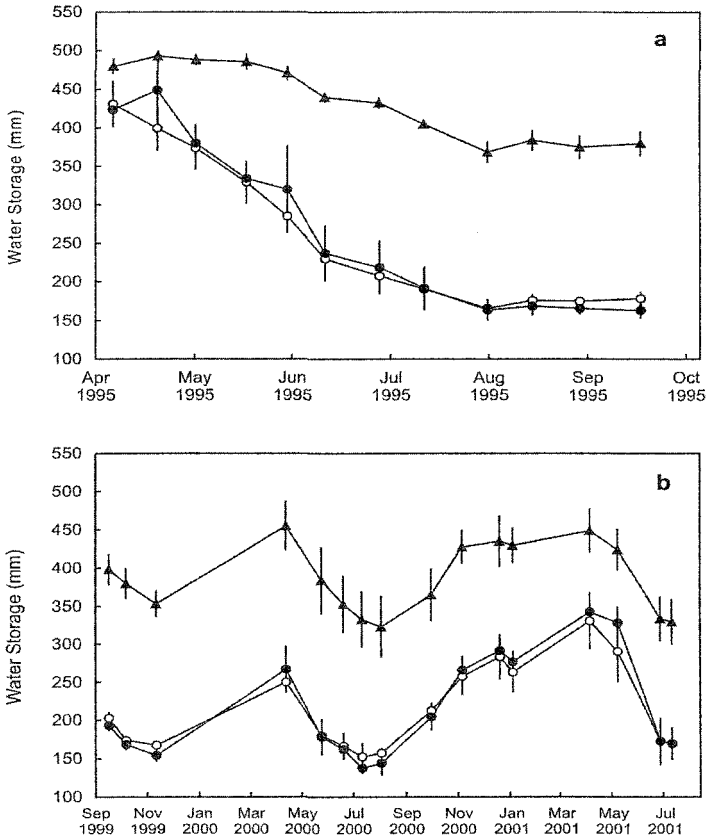
Figure 2. Seasonal water-storage changes for alternative covers with 150-cm soil layers consisting of loam (open circles), clay loam (closed circles), and clay (triangles): (a) during the 1995 growing season and (b) from September 1999 to July 2001. Bars are 2 standard error of the mean, $n = 3$.

Time series of soil-water storage are displayed as millimeters of water in Figure 2. For all treatments, yearly high and low water storage occurred in mid-to-late spring

and mid-summer to mid-fall, respectively. Timing depended on precipitation seasonality and amount, and vegetation maturity. In 1995 and again in 2000, when Monticello received close to normal summer rainfall (124 mm in 1995 and 137 mm in 2000; 50-yr average is 125 mm), the low occurred in mid-July and early August. In 1999, the low was delayed until November because of higher than normal summer rainfall (274 mm). For all monitoring periods, mean water-storage values for loam and clay loam treatments were not significantly different ($p < 0.05$).

The highest water-storage levels occurred in 1995 when grasses planted in the lysimeters were still immature. Because drainage occurred for all treatments storage, values were assumed to be the drained upper limit (Table 1). After the grasses matured (1999–2001), peak storage values ranged from 8% (clay treatment) to 42% (loam and clay loam treatments) below the drained upper limit. Although the drained upper limit was highest for the clay soil (150 cm), the water-storage capacities were 64% to 83% higher for the loam and clay loam soils.

Table 1. Drained upper storage limit and water-storage capacity for combinations of soil sponge layer depths and soil type treatments. The drained upper limit is the water storage measurement when drainage occurred in 1995. Means followed by the same letter are not significantly different ($p < 0.05$).

Treatment Layer Depth (cm)	Soil Type	Drained Upper Limit (mm water)	Water-Storage Capacity (mm water)
150	Loam	431 ± 30 c	279 b
150	Clay	493 ± 7 b	170 d
150	Clay loam	449 ± 45 bc	311 b
100	Clay loam	321 ± 3 d	214 c
200	Clay loam	593 ± 30 a	368 a

Caisson Drainage Lysimeters

Two large drainage lysimeters were installed to evaluate the range of as-built conditions in the actual Monticello cover (Figure 3). Lysimeter 1 closely matched conditions as built during the latter stages of construction (loam topsoil compacted to 1.45 g/cm^2), and lysimeter 2 matched less desirable conditions as built during the early stages (clay loam subsoil compacted to 1.65 g/cm^2). Corrugated steel culverts (3.05 m in diameter by 2.75 m in depth) formed the lysimeter walls. Instrumentation was accessed through a smaller caisson (1.52 m in diameter by 3.66 m in depth) placed between the lysimeters. Culverts were lined with 40-mil HDPE and leak tested using a manometer. HDPE drainage tubes were inserted through ports between the access and lysimeter caissons. Cover layers consisted of stockpiled soils tamped in lifts to achieve bulk-density specifications. Bulk density was monitored with a nuclear density gauge.

Revegetation of the caisson lysimeters matched the specifications and methods used

for the adjacent tailings disposal cell (Kastens and Waugh, 2002). Lysimeters were seeded in September 2000 with a mixture of grasses, forbs, and shrubs in an attempt to
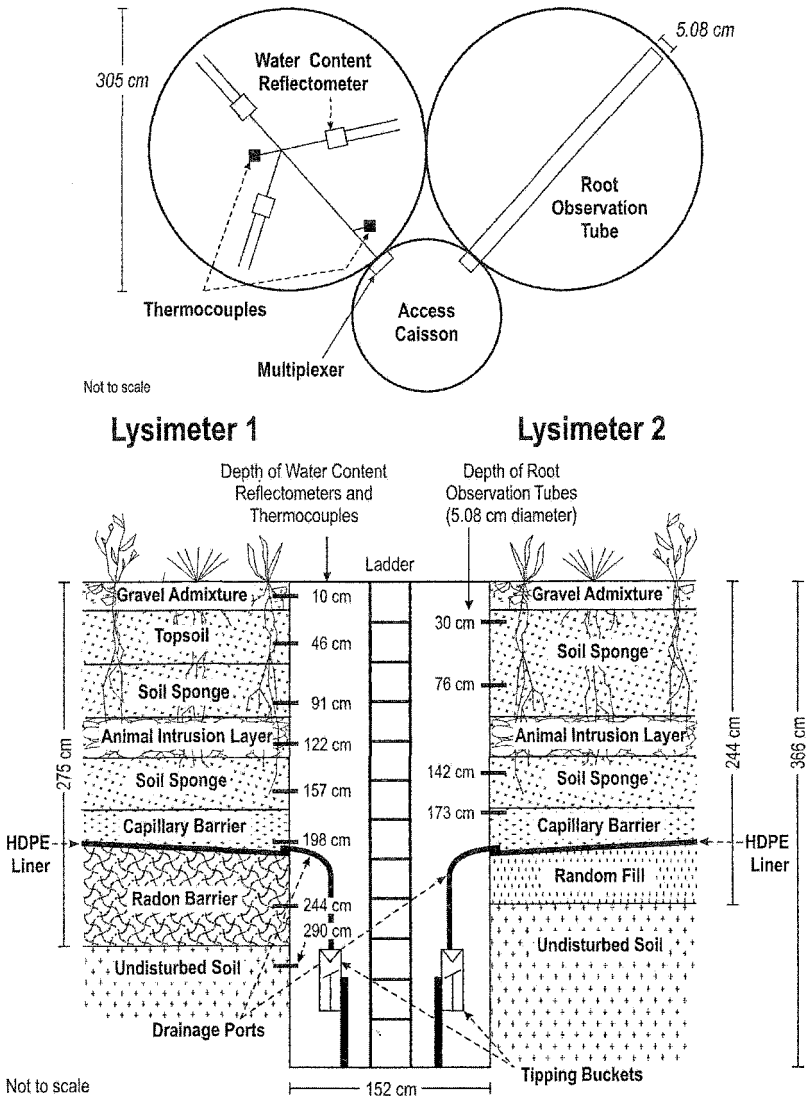
Figure 3. Plan view (top) and cross section (bottom) of instrumentation in the lysimeter and access caissons. Water Content Reflectometers, thermocouples, and root observations tubes, shown separately for purposes of illustrating layouts and depths, were all installed in both lysimeters.

mimic the potential natural vegetation of the borrow soils and local climate. Monitoring instrumentation and methods focused on the components of the soil-water balance (precipitation, water storage, drainage, and evapotranspiration) and on plant community composition and relative abundance.

Soil Water Balance

Caisson lysimeter surfaces were isolated from runoff and runon, hence ET was estimated using a simplified water balance equation:

$$ET = P - D - \Delta S,$$

where *ET*, *P* (precipitation), and ΔS (soil water storage changes) were recorded as mm of water. Precipitation, drainage, and water storage were monitored, and ET was estimated by difference. Total annual precipitation was less than the 30-yr average (39 cm). The 2002 growing season was particularly dry, with winter and spring precipitation about 50% and 15% of normal, respectively. Precipitation was 57% of normal between November 2000 and June 2002, the critical period for plant establishment. Soil moisture and water storage were monitored with water content reflectometers. Drainage was monitored with tipping bucket rain gauges.

Time series of water storage changes show conspicuous seasonal variability and an overall drying trend (Figure 4). As with the small lysimeters, seasonal high and low water storage occurred in mid-to-late spring and mid-to-late fall, respectively, depending on amount and seasonality of precipitation, soil type and compaction, and vegetation maturity. Maximum storage and the only drainage occurred in spring 2000 before plants became established (drainage did not exceed 0.1 mm/yr, well below the EPA target of <3.0 mm/yr). Water storage reached about 440 mm in Lysimeter 1 and 400 mm in Lysimeter 2. The lower value for Lysimeter 2 may be attributable to a lower porosity in the more compacted clay loam. Once vegetation established during the dry years, the seasonal peak storage did not approach the maximum limit.

Differences in seasonal low water-storage levels may be attributable to differences in ET. In 2000 before plants established, the seasonal low was about 280 for both lysimeters. After plants became established, water storage in the less compacted loam (Lysimeter 1) dropped below 200 mm, about 30 mm below levels in the compacted clay loam (Lysimeter 2). Therefore, water storage capacity was about 40% greater in the less-compacted loam soil (about 250 mm) than in the more-compacted clay loam (about 175 mm).

Plant Abundance

The hydrologic performance of the Monticello cover relies on the establishment and resilience of a diverse plant community. Species composition, leaf area index (LAI),

productivity, and percent canopy cover were measured on the caisson lysimeters near
the end of the 2002 and 2003 growing seasons and compared with revegetation
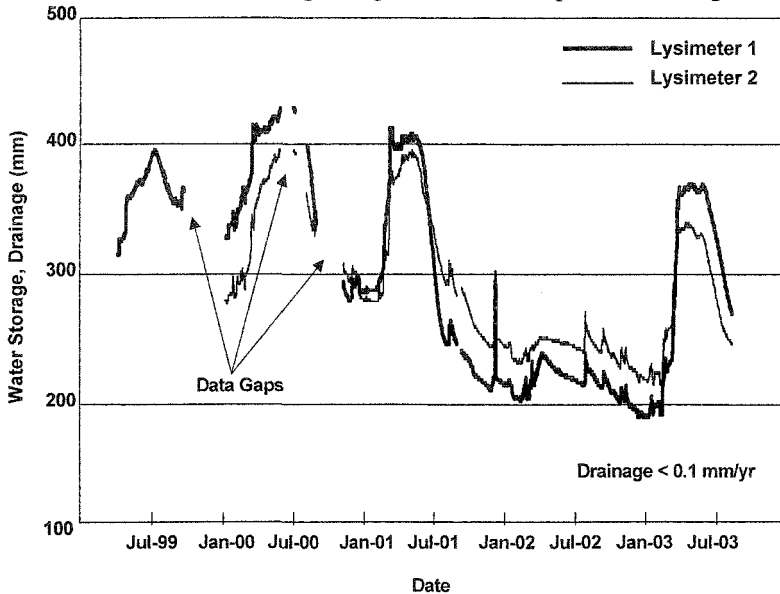
Figure 4.   Soil-water storage time series in Lysimeter 1 (less compacted loam
soil sponge) and Lysimeter 2 (more compacted clay loam soil sponge) between
July 1999 and August 2003.

criteria. The surface was divided into 50-by 100-cm quadrats. All plant species in
each quadrat were recorded and canopy cover was measured using an ocular point-
intercept sampling method (Floyd and Anderson, 1982).   LAI and productivity of
current year's growth were sampled in half of the quadrats by harvesting and running
green leaf material through an electronic area meter. Total percent cover for all plants
growing in lysimeters, when averaged over years and lysimeters (37.1%, S.E.=0.6%,
n = 4), was close to the minimum 40% canopy cover criterion (Kastens and Waugh,
2002). However, as much as 21% (56% relative cover) consisted of undesirable
plants. Only 17% cover consisted of permissible species, well below the requirement.
Total plant cover remained consistent between lysimeters and years. Green LAI, a
better indicator of the transpiration potential than percent cover, was significantly
greater in 2002 on the less compacted loam (Lysimeter 1) than on the overly
compacted clay loam (Lysimeter 2). Greater transpiration loss may partially explain
the seasonally lower water storage values and consistently greater water storage
capacity of the less compacted loam.

Conclusions

Results of lysimeter studies supported construction of an ET cover at the Monticello, Utah, Superfund site. Plant-water relations data indicated that small weighing lysimeters moderately underestimated ET. However, for initial screening tests of the hydrologic performance of cover designs, results support the use of the small lysimeters as a reasonable alternative to large, expensive, agronomic-type lysimeters, particularly for factorial experiments requiring multiple treatments and replication.

Two caisson lysimeters installed adjacent to the disposal cell were used to evaluate the range of conditions as constructed in the actual cover. When plants were immature, a loam topsoil compacted to 1.45 g/cm^3, representing a later phase of construction, had a 40% greater water storage capacity than a gravely clay loam compacted to 1.65 g/cm^3, representing an earlier phase of construction. The difference may be attributable in part to higher green leaf area and water extraction by young plants in the loam soil. Once plants became well established, drainage was minimized for both conditions.

References

Albright, W.C., C.H. Benson, G.W. Gee, A.C. Roesler, T. Abichou, P. Apiwantragoon, B.F. Lyles, and S.A. Rock. (2004) "Field water balance of landfill final covers." *Journal of Environmental Quality* 33, 2317-2332.

Anderson, J.E., R.S. Nowak, T.D. Ratzlaff, and O.D. Markham. (1993) "Managing soil moisture on waste burial sites in arid regions." *Journal of Environmental Quality* 22, 62–69.

Bazzaz, F.A. (1996) "Plants in changing Environments: Linking physiological, population, and community ecology." Cambridge University Press.

Bowman, B.T, R.R. Burnke, W.D. Reynolds, and G.J. Wall (1994) "Rainfall simulator-grid lysimeter system for solute transport studies using large, intact soil blocks." *Journal of Environmental Quality* 23, 815–822.

Corwin, D.L., and R.D. Lemert. (1994) "Construction and evaluation of an inexpensive weighing lysimeter for studying contaminant transport." *Journal of Contaminant Hydrology* 15, 107–123.

Dugas, W.A. W.L. Bland, and G.F. Arkin. (1985) "Evapotranspiration measurements from different-sized lysimeters." In: *Advances in Evapotranspiration*, Proceedings of the National Conference, Chicago, Illinois. December 16–17, 1985, American Society of Agricultural Engineers, St. Joseph, MO.

Finley, J.B., M.D. Harvey, and C.C. Watson. (1985) "Experimental study: erosion of overburden cap material protected by rock mulch," pp. 273–282. In: *Proceedings of Seventh Symposium on Management of Uranium Mill Tailings, Low-Level Waste, and Hazardous Waste*, Colorado State University, Ft. Collins, CO.

Floyd, D.A., and J. E. Anderson. (1982) "A new point interception frame for estimating cover of vegetation." *Vegetatio* 50, 185–186.

Gee, G.W., and D. Hillel. (1988) "Groundwater recharge in arid regions: Review and critique of estimation methods." *Hydrological Processes* 2, 255–266.

Gee, G.W., and S.W. Tyler (eds.). (1994) "Symposium: Recharge in arid and semiarid regions." *Soil Science Society of America Journal* 58, 5–72.

Kastens, M., and J. Waugh. (2002) "Methodology for determining revegetation success at the Monticello repository." GJO-2002-325-TAR, U.S. Department of Energy, Grand Junction, CO.

Ligotke, M.W. (1994) "Control of eolian soil erosion from waste-site surface barriers." pp. 545–559. In: G.W. Gee and N.R. Wing (eds.), *In-Situ Remediation: Scientific Basis for Current and Future Technologies*. Battelle Press, Columbus, OH.

Link, S.O. G.W. Gee, and J.L. Downs. (1990) "The effect of water stress on phenological and ecophysiological characteristics of cheatgrass and sandberg's bluegrass." *Journal of Range Management* 43, 506–513.

Martin, D.L., N.L. Klocke, and D.L. Dehaan, (1985) "Measuring evaporation using mini lysimeters." In: *Advances in Evapotranspiration*, Proceedings of the National Conference, Chicago, Illinois, December 16–17, 1985, American Society of Agricultural Engineers, St. Joseph, MO.

Nyhan, J., T. Hakonson, and B. Drennon, (1990) "A water balance study of landfill cover designs for semiarid regions." *J. Envir. Quality* 19, 281-288.

Richards, L.A. (1950) "Laws of soil moisture." *Trans. Am. Geophys. Union* 31, 750–756.

Ritche, J.T. (1981) "Soil Water Availability." Plant soil, 58, 327–338.

Sachschewsky, M.R., C.J. Kemp, S.O. Link, and W.J. Waugh. (1995) "Soil water balance changes in engineered soil surfaces." *Journal of Environmental Quality* 24, 352–359.

Scholander, P.F., H.T. Hammel, E.D. Bradstreet, and E.A. Hemmingsen, "Sap pressure in vascular plants." Science 148, 339–346.

Shawcroft, R.W. and W.H. Gardner. (1983) "Direct evaporation from soil under a row crop canopy." *Agricultural Meteorology* 28, 229–238.

Smith, G.M. and R.E. Reger. (2002) "Protective layer design in landfill covers based on frost protection," *Journal of Geotechnical and Geoenvironmental Engineering* 128, 794–799.

U.S. Department of Agriculture. (1945) "Soil Survey: San Juan Area, Utah," Series 1945, No. 3, Soil Conservation Service, Washington, DC.

U.S. Department of Energy. (1989) *Technical approach document, revision II.* UMTRA–DOE/ AL 050425.0002, U.S. Department of Energy, Albuquerque, NM.

U.S. Environmental Protection Agency. (1989) *Technical guidance document, final covers on hazardous waste landfills and surface impoundments.* EPA/530–SW–89–047, Washington, DC.

Ward, A., and G. Gee. (1997) " Performance evaluation of a field-scale surface barrier." *Journal of Environmental Quality* 26, 694–705.

Waugh, W.J., M.E. Thiede, D.J. Bates, L.L. Cadwell, G.W. Gee, and C.J. Kemp. (1994) "Plant cover and water balance in gravel admixtures at an arid waste burial site." *Journal of Environmental Quality* 23, 676–685.

Waugh, W.J., M.E. Thiede, L.L. Cadwell, G.W. Gee, H.D. Freeman, M.R. Sackshewsky, and J.F. Relyea. (1991) "Small lysimeters for documenting arid soil water balance." In: R.G. Allen, T.A. Howell, W.O. Pruitt, I.A. Walter, and M.E. Johnson (eds.), *Lysimeters for Evapotranspiration and Environmental Measurements*, American Society of Civil Engineering, New York.

Winograd, I.J. (1981) "Radioactive waste storage in thick unsaturated zones." *Science* 212, 1457–1464.

Long-term Performance of a Reclamation Cover: the Evolution of Hydraulic Properties and Hydrologic Response

C.J. Kelln[1], S.L. Barbour[2], A. Elshorbagy[3], and C. Qualizza[4]

[1]Chris Kelln, Department of Civil and Geological Engineering, University of Saskatchewan, Saskatoon, Canada, S7N 5A9; PH (306) 343-6808; FAX (306) 966-5427; email: cjk123@mail.usask.ca
[2]S. Lee Barbour, Department of Civil and Geological Engineering, University of Saskatchewan, Saskatoon, Saskatchewan, Canada, S7N 5A9; PH (306) 966-5369; FAX (306) 966-5427; email: slb727@mail.usask.ca
[3]Amin Elshorbagy, Department of Civil and Geological Engineering, University of Saskatchewan, Saskatoon, Saskatchewan, Canada, S7N 5A9; PH (306) 966-5414; FAX (306) 966-5427; email: amin.elshorbagy@mail.usask.ca
[4]Clara Qualizza, Syncrude Canada Limited, Fort McMurray, Alberta, Canada; PH (780) 790-5216; email: qualizza.clara@syncrude.com

Abstract

The performance of a prototype reclamation cover constructed over saline-sodic shale overburden was tracked over a six-year period. The test cover, constructed on a 5H:1V slope, was comprised of a thin layer (~20 cm) of a peat-mineral soil mixture overlying a thicker layer (~80 cm) of 'secondary' (glacial lacustrine or till). The primary objective of the cover design was to provide sufficient moisture storage for vegetation while mitigating the upward diffusion of salts from the underlying pyritic shale. *In situ* measurements of saturated hydraulic conductivity were conducted using a Guelph permeameter. Hydrologic measurements included soil moisture, matric suction, soil temperature, surface runoff, and interflow. The major ion chemistry of both surface runoff and interflow waters were measured. *In situ* measurements of hydraulic conductivity over the six-year period demonstrated that the cover developed secondary structure within four years of placement, likely due to repeated freeze/thaw and wet/dry cycles. The hydrologic response data and interflow chemistry suggests that the mechanisms responsible for the rapid delivery of precipitation to the base of the cover during spring melt are controlled by interactions between soil conditions and climate. Preferential flow occurs when a threshold wetting is achieved and when the ground is either frozen or the matric suctions are low. It also appears that the relative contribution of 'event' and 'pre-event' water evolves as interflow proceeds. Lateral interflow appears to be an important mechanism for mitigating the upward diffusion of salts into the cover.

Introduction

Syncrude Canada Ltd. (SCL) utilizes moisture soil covers to reclaim large tracts of mine waste at their Mildred Lake operation. Soil covers have been used in reclamation and decommissioning for a variety of mining and waste disposal facilities (e.g. Aubertin *et al.*, 1996). The primary purpose of many of these covers is to mitigate infiltration into the waste while restricting oxygen ingress (Nicholson *et al.*, 1989; O'Kane *et al.*, 1998). The reclamation covers at SCL are placed with the primary goal of supporting a sustainable boreal forest ecosystem by providing the required hydrologic, geochemical, and biological functions. The hydrologic functions are the focus of this paper and include moisture and salt management.

There are many factors that affect the performance of a soil cover including climatic conditions, vegetation, geometry (thickness and topography) and material properties. Soil covers are subjected to a number of physical, chemical, and biological processes that can alter performance over time including freeze/thaw and wet/dry cycling, erosion, root penetration, and bioturbation (MEND, 2004). These processes ultimately affect key cover properties such as the hydraulic conductivity and moisture retention characteristics.

This paper presents a case study on the long-term hydrologic performance of a reclamation cover in a cold, semi-arid environment. The objectives of the study are to: (1) track the long-term evolution of a moisture store-and-release cover; (2) evaluate the impact of cover evolution on the hydrologic response; and, (3) discuss the potential implications for the salt and water balance of the covers.

Background

The study site is located at the SCL Mildred Lake mine, 40 km north of Fort McMurray, Alberta. An 'instrumented watershed' was developed on the Southwest 30 waste dump (SW30) in 1999 by SCL and the University of Saskatchewan to track the long-term performance of reclamation covers constructed over sodic/saline overburden. A central focus of this research was to define the 'trajectory' of cover evolution to determine if current reclamation practices will provide appropriate conditions from which a healthy and sustainable ecosystem can evolve (Qualizza *et al.*, 2004). SCL is reconstructing entire landscapes and watersheds are the 'building blocks' of these landscapes. Interactions of the hydrologic, geochemical and biologic systems at a landscape scale control the performance of these systems and as such, studies to understand these components and their interactions must be conducted at this scale.

Three prototype test covers of varying thickness (35, 50, and 100 cm) were constructed over a pyritic saline-sodic shale overburden. Each cover is approximately 1 ha (200 m by 50 m) and constructed on a 5H:1V slope. The 100 cm cover has a thickness mandated by environmental regulations and is the focus of this paper. It was comprised of approximately 20 cm of a peat-mineral mixture overlying a thicker layer (~ 80 cm) of 'secondary' (glacial lacustrine or till soil), referred to in this paper

as till. The covers are designed to provide sufficient moisture for vegetation while mitigating the upward diffusion of salts from the underlying pyritic shale.

Field Instrumentation and Methodology

The evolution of the saturated hydraulic conductivity (K_s) of the cover materials and underlying shale was tracked from 2000 to present using a Guelph permeameter (Meiers *et al.*, 2003). Guelph testing (Reynolds, 1993) involves measuring the steady state infiltration through an uncased, cylindrical auger hole under a constant water depth. Approximately 30 measurements were made on the covers each year at depths of 15 cm, 30 cm, 40 cm, and 60 cm. Soil instrumentation stations were installed on each cover to monitor soil moisture (TDR), temperature (Campbell Scientific model 107F thermister), and matric suction (Campbell Scientific model 229 thermal conductivity) throughout the cover profile (Figure 1). A meteorological station (MET) was used to collect data on wind speed/direction, temperature, precipitation, and relative humidity. Meteorological data was used to calculate the potential evaporation (PET) from the covers using the FAO method (Allen *et al.*, 1998). PET values were compared to actual evapotranspiration (AET) values estimated using a system dynamic watershed (SDW) model developed by Elshorbagy (2005).
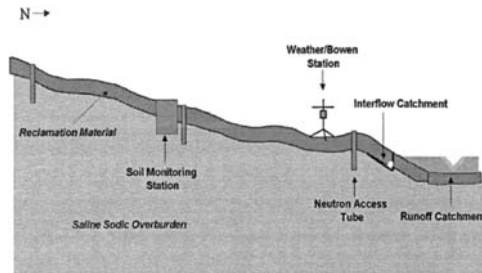
Figure 1. Schematic of instrumented test section (from Boese, 2003).

Surface runoff was measured using v-notch weirs and interflow along the till-shale interface was measured using a collection system constructed at the toe of the slope upstream of the runoff ditch. The interflow collection system consisted of a geo-membrane cutoff containing a sand filter and drainage pipe leading to collection barrels. Water samples from the surface runoff and interflow collection systems were tested for major ions and isotopes. Two rows of shallow monitoring wells were installed upslope of the interflow collection system to monitor the development of a perched water table over the shale. Soil cover geochemistry was quantified from soil samples obtained using a hand auger. Soil salinity analyses were conducted on the samples as per the methods outlined in McKeague (1978).

Results and Discussion

Climate and Evapotranspiration

The Mildred Lake site receives an average of 442 mm of precipitation annually (1955 to 2000). The average annual PET exceeds precipitation and the climate is classified as semi-arid based on the Thornthwaite (1948) classification. Approximately 30% of the annual precipitation occurs as snow. The annual precipitation on the covers was below average between 1999 and 2004.

The values of AET and PET presented in Figure 2 for the 100 cm cover demonstrate that AET begins to increase in the middle of May when the average daily air temperature is above 0°C, the ground is thawed, and seeds begin to germinate. AET increases rapidly to around 2 mm/day in June as the air temperature rises and vegetation begins to flourish and peaks at between 2 and 4 mm/day in the middle of July. It begins to decrease in August as moisture depletion in the covers limits plant moisture uptake and by September/October the AET has decreased to less than 1 mm/day due to colder temperatures and killing frosts.
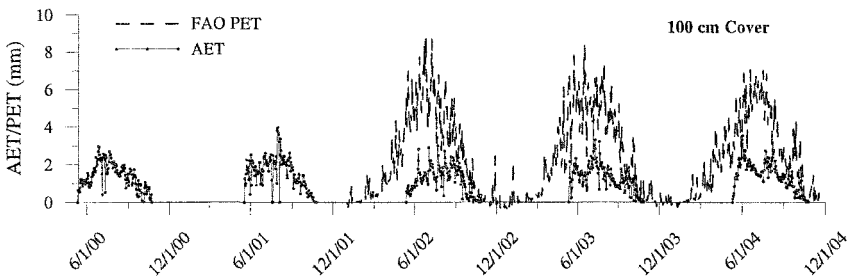
Figure 2. Actual evapotranspiration (AET; not calculated for 2000 and 2001) and potential evapotranspiration (PET).

In situ Hydraulic Conductivity

The average *in situ* saturated hydraulic conductivity (K_s) of the shale overburden, till, and peat is presented in Figure 3. The Guelph permeameter provides a more realistic estimate of bulk hydraulic conductivity than laboratory derived K_s because it tests a larger soil volume, thereby capturing macro-scale features such as fractures. The K_s of the shale overburden was initially 1×10^{-9} m/s and increased by about one order of magnitude by 2002. The till experienced the largest increase in K_s, from around 1×10^{-8} m/s to 1×10^{-6} m/s. The peat K_s increased by approximately half an order of magnitude. In all cases, K_s increased over the four years after placement. In subsequent years, the K_s either remained constant or, in the case of the till, decreased marginally. The decrease may be a result of borehole smearing due to elevated moisture conditions during testing.
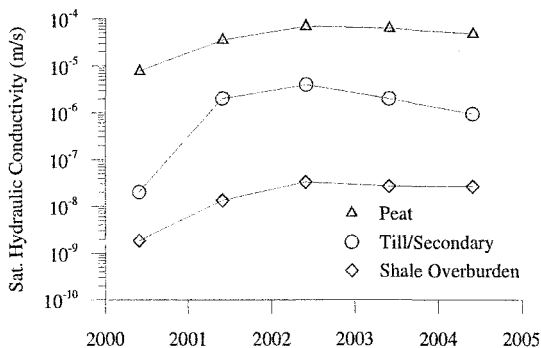
Figure 3. *In situ* **saturated hydraulic conductivity (after Meiers *et al.*, 2003).**

The increase in K_s in the first four years after placement is likely the result of the development of macrostructure or preferential flow paths. Macrostructure develops because of bio-physical and/or chemical processes such as freeze/thaw effects, wet/dry cycles, osmotic consolidation, root penetration, and bioturbation (MEND, 2004). Biological processes such as root penetration likely played a negligible role in altering the hydraulic properties of the till because vegetation first began to flourish in 2001. Furthermore, the vegetation on the covers was initially dominated by green foxtail (*Setaria viridis*), which has a shallow root biomass concentrated in the top 15 cm of the cover. Most of the *in situ* measurements, except for those in peat, were conducted below this depth. The peat was least susceptible to changes in hydraulic properties because it contains less clay fraction.

Meiers (2003) suggested that freeze-thaw effects were likely responsible for the evolution of hydraulic conductivity. The till is comprised of 25% to 40% clay with average plastic and liquid limits of 28% and 44%, respectively. Numerous laboratory and field studies have demonstrated that freeze/thaw cycles can cause increases in K_s in clay-rich materials (Benson *et al.*, 1995; Benson and Othman, 1993; Chamberlain *et al.*, 1995). These authors report increases in hydraulic conductivity as result of two mechanisms: water migration towards the freezing front causing desiccation cracking, and the formation of ice lenses which alter soil structure (Othman and Benson, 1993). *In situ* monitoring confirmed that the full cover depth freezes annually. Soil desiccation due to wet/dry cycling can cause a similar change in structure due to desiccation cracking. Suction sensors indicated that suction often exceeded 1500 kPa during the driest months.

Cover Geochemistry

Figure 4 illustrates typical sulphate concentrations through the cover and shale on the top of the SW30 waste dump. Samples were collected in October 2004 at a location where the cover-shale interface was at a depth of approximately 85 cm. It is noted (data not presented) that all of the major pore water ions in the till exceed background levels, including calcium, magnesium, potassium, sodium, chloride,

nitrate, and bicarbonate. The sulphate concentration above the till-shale interface varied from approximately 2500 mg/L to 4000 mg/L. The shape of the profile in Figure 4 suggests that the primary transport mechanism is upward diffusion from the shale. Consequently, lateral interflow along the cover-shale interface could potentially 'flush' the system and attenuate the upward diffusion of salts into the cover. Observations suggest that the interflow is a combination of matrix-dominated and preferential flow. Matrix dominated interflow would be the most effective in providing uniform flushing of salts from above the till-shale interface.
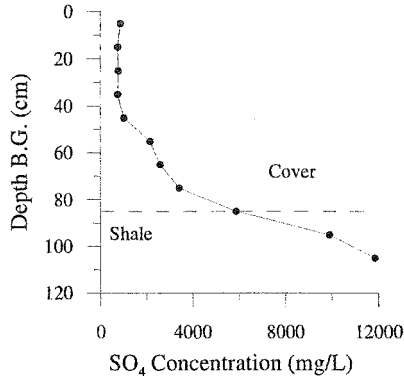
Figure 4. Profile of pore water sulphate concentrations in the till and shale.

Interflow

Table 1 and Figure 5 highlight interflow volumes and sulphate concentrations between 2000 and 2005 along with the average measured snow pack depth in the area. The volume of water collected in the first year that the interflow system was installed (2000) is an estimate because of flow rate measurement problems. Interflow volumes ranged from 965 litres in 2001 to over 60,000 litres in 2005. Nearly all of the interflow water was collected during the spring melt with the exception of 1700 litres in 2000, a number of small summer interflow events in 2002, and 4000 litres collected during the fall of 2003.

Table 1. Summary of annual interflow volumes, maximum SO$_4$ concentration, and snow depth in equivalent mm of water (SWE).

Year	Volume (L)	Volume (mm)	Max. SO$_4$ (mg/L)	SWE (mm)
2000	1700	0.17	-	40
2001	965	0.01	-	44
2002	1513	0.15	2370	77
2003	12341	1.2	2530	23
2004	17518	1.8	2490	67
2005	60000	5.9	-	81
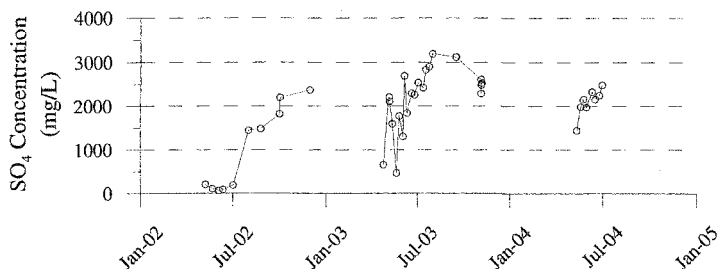
Figure 5. Measured SO₄ concentration of interflow water.

The concentrations in the interflow during the spring snow melt provide the most convincing evidence that secondary structure developed in the covers by 2001. The sulphate concentrations (Figure 5) demonstrate that the mechanism for lateral saturated flow along the till-shale interface changes from preferential flow to matrix driven groundwater flow. The sulphate concentration increases from near 0 mg/L at the start of spring melt to values similar to concentrations near the interface (~2500-3000 mg/L). This suggests that 'event' water in the macrostructure nearest the interflow pipe drains into the interflow collection system almost immediately. As the fractures near the interflow pipe drain and a perched water table develops upslope of the pipe, 'pre-event' or matrix water (i.e. connate) is displaced down slope. The time to transition from 'event' to 'pre-event' water would depend on the upslope continuity and connectivity of preferential flow paths and the volume of water stored in the macrostructure.

These observations are supported by other studies where preferential flow generates transient perched water tables at the interface of a lower K_s unit, creating a saturated and highly mobile zone of water that can move laterally down slope (Burns et al., 2001; Hinton et al., 1994; Jardine et al., 1990; Newman et al., 2004; Peters et al., 1995). Macrostructure produces vertical preferential flow paths that transmit water rapidly to depth when the precipitation intensity exceeds the ability of the matrix to absorb water, thereby inducing overflow of soil water from the matrix into the macropores. Uchida et al. (2004) and Tromp van Meerveld and McDonnel (2004) have shown that lateral flow is highly threshold dependent and largely via discontinuities at the soil-impervious layer interface. The water that moves down slope can be predominantly connate or 'pre-event' water displaced from the soil matrix or some mixture of 'pre-event' and 'event' water, depending on the relative contribution of lateral preferential flow.

Although the volume of interflow increased significantly between 2000 and 2005, there does not appear to be a direct correlation between the amount of water collected and the increase in hydraulic conductivity. For example, the most dramatic increase in K_s occurred between 2000 and 2001, but the amount of interflow decreased between those years. This lack of correlation is likely due to differences in autumn climatic conditions and subtle differences in the heat and mass transfer

dynamics of the system. The connate water stored in the cover prior to spring melt would have originated from the previous fall. As a result, the amount of precipitation and infiltration prior to freeze-up will exert a direct control on the volume of saturated lateral flow collected in spring.

The hydrologic and geochemical response of the cover in 2004 is presented in Figure 6 to highlight the mechanisms that control preferential and lateral saturated flow. The figure includes matric suction at a depth of 55 cm, the approximate thickness of the perched water table near the interflow pipe and 20 m upslope, interflow SO_4 concentrations, cover temperature at depths of 55 cm and 90 cm, and annual precipitation. This data suggests that preferential flow is governed by ground temperatures, antecedent moisture conditions (i.e. matric suction), and the intensity of the precipitation event. Saturated lateral groundwater flow began on May 8, 2004 and terminated on June 19, 2004. Similarly, a perched water table develops around the initiation of interflow and recedes by the end of June. It is interesting to note, however, that the peak flow rate through the weir (data not presented), which is indicative of the timing of snow melt, occurred nearly 1.5 months earlier when the average daily air temperatures were above 0°C. This offset of over one month between snow melt and interflow indicates that vertical preferential flow via the macrostructure occurs when the ground is frozen and the matrix hydraulic conductivity is very low. Numerous studies on snowmelt infiltration have found that fractures can provide vertical pathways in otherwise frozen soil (Baker and Spaans, 1997; Derby and Knighton, 2001; Sharratt and Goldsmith, 1997). Once the ground thaws, water stored in the preferential flow paths migrates into the soil matrix, mixing with 'old' water and creating a perched water table on the till-shale interface.

The cessation of interflow coincides with the increase of AET in the middle of June and the subsequent rise of matric suction in the till (Figure 6). This indicates that interflow is highly dependent on soil moisture conditions. It is well known that antecedent soil moisture is the most important parameter controlling moisture movement in the vadose zone. Soils with negative pore-water pressures will have reduced hydraulic conductivity and therefore limited potential for lateral moisture translocation during precipitation events. It is evident in Figure 6 that interflow does not occur in July through August when matric suctions exceed the wilting point suction (1500 kPa), despite precipitation events of over 20 mm/day. In contrast, the cover responded instantaneously to two precipitation events in May and early June 2004 when matric suctions were low. These events were marked by a sharp reduction in the SO_4 concentration of the interflow water, indicating the greater contribution of preferential flow paths to interflow during the 'wet' conditions.
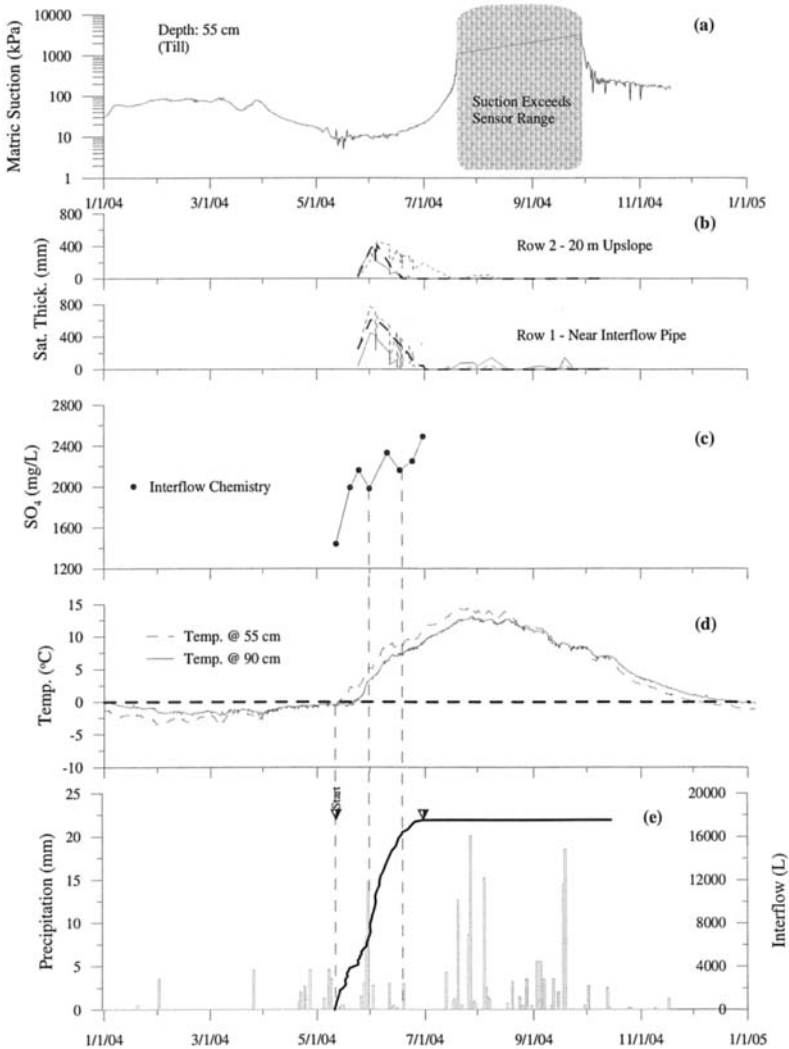
Figure 6. Hydrologic and soil station data from 2004. (a) Matric suction (b) Saturated thickness (c) SO₄ concentration (d) Soil temperature (e) Interflow volume and precipitation.

The influence of vertical preferential flow paths on groundwater flow will be reduced during periods when AET is high and matric suctions are elevated. High matric suction increases the available water storage and encourages flow into the matrix during infiltration events. Vertical moisture dynamics continue to dominate even during high intensity rainfalls when the AET demand is high. These processes

are evident in the 100 cm cover interflow data. The only post-spring interflow events were recorded during the summer of 2002 and in the fall of October 2003. Wet conditions throughout the summer of 2002 caused the interflow to continue from July to September. In 2003, frequent precipitation events in September and October increased antecedent moisture conditions in the cover (reducing matric suction), making the cover more responsive to subsequent precipitation events and eventually leading to interflow.

In summary, the spring snow melt is the most dominant hydrologic event of the year and thus plays a major role in cover performance. The occurrence of interflow, triggered by vertical preferential flow into the macrostructure during snowmelt, has implications for the salt balance in the reclamation cover. It is likely that the upward diffusion of salt from the underlying shale will be attenuated by flushing during the spring snowmelt. The 'event' water that generates the perched water table mixes with salt rich 'pre-event' pore water near the cover-shale interface and eventually displaces 'pre-event' water down slope toward the interflow collection system. The effectiveness of this flushing mechanism will depend on the relative contribution of matrix-dominated and preferential groundwater flow and therefore evolves over time each year.

Summary and Conclusions

This study investigated the long-term performance of a reclamation soil cover constructed of peat and till. Measurements of *in situ* hydraulic conductivity demonstrated that that the K_s of the cover evolved within four years after placement. The evolution of hydraulic properties corresponded to a change in the hydrologic response of the cover during snowmelt events and wet conditions. Hydrologic and geochemical monitoring data suggest that preferential flow is controlled by the timing of snowmelt, ground temperatures, antecedent moisture conditions, and the duration and intensity of the precipitation event. In general, preferential flow occurs when the ground is either frozen or matric suctions are low, and a high intensity precipitation event occurs that exceeds the infiltration capacity of the soil matrix. If the matric suctions are relatively low and the ET demands do not reverse the wetting trend, a perched water table will develop and interflow will commence. The interflow water is initially 'event' water that drains from the macrostructure. Eventually, the 'event' water begins to displace 'pre-event' water down slope towards the collection pipe. This process results in an increase in the concentration of the interflow as salt rich matrix pore water is displaced. The flushing of salts through this mechanism acts to mitigate the upward salt transport into the covers by diffusion and will be critical to the long-term performance of the reclamation covers.

References

Allen, R. G., Pereira, L. S., Raes, D., and Smith, M. (1998). "Crop evapotranspiration - Guidelines for computing crop water requirements - FAO Irrigation and drainage paper 56." FAO - Food and Agricultural Organization of the United Nations Rome.

Aubertin, M., Bussiere, B., Chapuis, R. P., and Barbera, J. "Construction of Experimental Cells with Covers on Acid Producing Tailings." *Proceedings of the 49th Annual Canadian Geotechnical Conference*, St. John's, Newfoundland, 655-662.

Baker, J. M., and Spaans, E. J. A. "Mechanics of meltwater movement above and within frozen soil." *International Symposium on Physics, Chemistry, and Ecology of Seasonally Frozen Soils*, US Army Cold Regions Research Engineering Laboratory, Fairbanks, AK, 31-36.

Benson, C., Abichou, T., Olson, M., and Bosscher, P. J. (1995). "Winter effects on the hydraulic conductivity of a compacted clay." *Journal of Geotechnical Engineering*, 121(1), 69-79.

Benson, C., and Othman, M. (1993). "Hydraulic conductivity of compacted clay frozen and thawed insitu." *Journal of Geotechnical and Environmental Engineering*, 119(2), 276-294.

Burns, D. A., McDonnell, J. J., Hooper, R. P., Peters, N. E., Freer, J. E., Kendall, C., and Beven, K. J. (2001). "Quantifying contributions to storm runoff through end-member mixing analysis and hydrologic measurements at the Panola Mountain Research Watershed, Georgia, USA." *Hydrological Processes*, 15, 1903-1924.

Chamberlain, E., Erickson, A., and Benson, C. (1995). "Effects of frost action on compacted clay barriers." Geoenvironment 2000, ASCE, New York, 702-717.

Derby, N. E., and Knighton, R. E. (2001). "Field-scale preferential transport of water and chloride tracer by depression-focussed recharge." *Journal of Environmental Quality*, 30, 194-199.

Elshorbagy, A., Jutla, A., Barbour, S. L., and Kells, J. (2005). "System dynamics approach to assess the sustainability of reclamation of disturbed watersheds." *Canadian Journal of Civil Engineering*, 35(1), 144-158.

Hinton, M. J., Schiff, S. L., and English, M. C. (1994). "Examining the contributions of glacial till water to storm runoff using two- and three-component hydrograph separations." *Water Resources Research*, 30(4), 983-993.

Jardine, P. M., Wilson, G. W., and Luxmoore, R. J. (1990). "Unsaturated solute transport through a forest soil during rain storm events." *Geoderma*, 46, 103-118.

McKeague, J. A. (1978). "Manual on sampling and methods of analysis." Canadian Society of Soil Science, Ottawa, ON.

Meiers, G. P., Barbour, S. L., and Meiers, M. K. (2003). "The use of field measurements of hydraulic conductivity to characterize the performance of reclamation soil covers with time." 6th ICARD, Cairns, Australia.

MEND. (2004). "Report 2.21.4: Design, Construction, and Performance Monitoring of Cover Systems for Waste Rock and Tailings." O'Kane Consultants Inc., ed., 93.

Newman, B. D., Wilcox, B. P., and Graham, R. C. (2004). "Snowmelt-driven macropore flow and soil saturation in a semiarid forest." *Hydrological Processes*, 18, 1035-1042.

Nicholson, R. V., Gillham, R. W., Cherry, J. A., and Reardon, E. J. (1989). "Reduction of acid generation in mine tailings through the use of moisture-

retaining cover layers as oxygen barriers." *Canadian Geotechnical Journal*, 26, 1-8.

O'Kane, M., Wilson, G. W., and Barbour, S. L. (1998). "Instrumentation and monitoring of an engineered soil cover system for mine waste rock." *Canadian Geotechnical Journal*, 35, 828-846.

Othman, M., and Benson, C. (1993). "Effect of freeze-thaw on the hydraulic conductivity and morphology of compacted clay." *Canadian Geotechnical Journal*, 30(2), 236-246.

Peters, D. L., Buttle, J. M., Taylor, C. H., and LaZerte, B. D. (1995). "Runoff production in a forested, shallow soil, Canadian Shield basin." *Water Resources Research*, 31(5), 1291-1304.

Qualizza, C., Chapman, D., Barbour, S. L., and Purdy, B. "Reclamation research at Syncrude Canada's Mining Operation in Alberta's Athabasca Oil Sands Region." *16th International Conference, Society for Ecological Restoration*, Victoria, Canada.

Reynolds, W. D. (1993). "Saturated hydraulic conductivity field measurements." Soil Sampling and Methods of Analysis, M. R. Carter, ed., 599-605.

Sharratt, B. S., and Goldsmith, R. S. (1997). "Field study of spatial variability in unsaturated flow beneath and adjacent to playas." *Water Resources Research*, 33, 2239-2252.

Thornthwaite, C. W. (1948). "An approach toward a rational classification of climate." *Geographical Review*, 38, 55-94.

Tromp van Meerveld, I., and McDonnell, J. J. (2004). "Measured non-linearities in subsurface flow: a 147 storm analysis of the Panola hillslope trench." *Water Resources Research*, accepted.

Uchida, T., Asano, Y., Mizuyama, T., and McDonnell, J. (2004). "Role of upslope soil pore pressure on lateral subsurface storm flow dynamics." *Water Resources Research*, 40, W12401.

INFLUENCE OF MATRIC SUCTION ON THE VOLUME CHANGE BEHAVIOUR OF A COMPACTED CLAYEY SOIL

Nubia A. González[1] and Julio E. Colmenares[2]

[1] Research student at Technical University of Catalonia, Barcelona, Spain. Formerly at the National University of Colombia, Bogotá D.C; Street Jordi Girona, 31; 08034; Building D2 305, Barcelona; +34934017411; nubia.aurora.gonzalez@upc.edu.
[2] Associate Professor National University of Colombia, Bogotá D.C., Ciudad Universitaria, Av. Carrera30#45-03, Building IEI (406)- 201; +5713165182; jecolmenaresm@unal.edu.co.

ABSTRACT: Estimation of volume changes in compacted soils is an important aspect for the analysis, design and performance of geotechnical works. It has been observed that several stability problems, involving those materials, are due to water content changes and therefore to matric suction changes that occur periodically in nature. This paper shows the results of an experimental programme carried out to study the volume change behaviour due to wetting processes on compacted kaolin samples. The influence of the dry density, compaction water content and the stress conditions prior to wetting, on the collapsible and expansive behaviour, is discussed paying special attention to the influence of suction. The experimental programme used conventional oedometer and suction controlled oedometer testing. Different wetting stress paths were followed verifying the applicability of an elastoplastic constitutive model for the volume change behaviour of compacted soil.
KEYWORDS: Volume change, suction, collapse, expansion, compacted kaolin.

1. INTRODUCTION

The soils used as construction materials, after compaction present unsaturated conditions due to the presence of air and water in some pores of the soil. The compaction conditions do not guarantee the volumetric stability of soils against water content changes (or suction changes). When a compacted soil is wetted, it may experience volume reduction (collapse), volume increase (swelling) or no significant volume change. The extent and type of volumetric change depends on the soil type, fabric and structure, the initial soil density, the stress state (total stresses and pore water pressure) and the amount of wetting that takes place (i.e. the reduction in suction) (Jennings and Burland, 1962). However, some conditions have been associated with collapse and other conditions have been associated with swelling.

A laboratory investigation has been undertaken to study the volume change behaviour and the importance of the water content (or suction), dry density and vertical stress on the collapse or swelling potential of compacted kaolin after wetting. The relationships between dry density, compaction water content and suction for compacted kaolin samples were established.

A conventional oedometer was used to establish the volume change potential of compacted samples when flooded under constant vertical stress. The influence of the applied vertical stress prior to wetting is also discussed. Additional testing to study in detail the soil behaviour under controlled conditions (i.e. controlled wetting to reduce the suction) was carried out in the suction controlled oedometer. The oedometer uses the osmotic technique as presented by Dineen and Burland (1995), Dineen (1997) and Colmenares (2002), in order to control the matric suction. The experimental programme carried out using suction controlled oedometer included testing of low initial dry density materials (i.e. materials likely to collapse). The analysis of results and discussion of the applicability of constitutive models (Alonso et al., 1987, Alonso, et al., 1990) for the prediction of volumetric behaviour of compacted soils is presented.

2. DESCRIPTION AND COMPACTION-SUCTION CHARACTERISTICS OF THE MATERIAL

The material used in this study was commercial Kaolin. The basic characteristics of the material are shown in Table 1. An analysis of X-ray diffraction was done to identify the principal components of the material. It was found that most abundant mineral is Kaolinita with a proportion of 40%, followed by Illite in a proportion ranging between 3 and 10%.

Table 1. Summary of the characterization and classification tests for the material

Type of test	Value
Liquid Limit (ASTM D-4318)	81 %
Plastic Limit (ASTM D-427)	48 %
Plasticity Index:	34 %
Skempton's Activity:	0.47 (Inactive clay)
Percent of fractions < 2μ: (ASTM D-422)	72 %
Specific Gravity: (ASTM D-854)	2.61

2.1   Compaction Procedure

Two compaction methods have been used: dynamic compaction and static compaction. The dynamic compaction is the most commonly used method, and the procedures followed ASTM D698-70 and D1557-70, for the Standard and Modified Compaction Energy respectively. Using the standard compaction energy a maximum dry density of 1.24 Mg/m^3, at an optimum water content of 34% were found, whereas for modified compaction energy, a maximum dry density of 1.41 Mg/m^3 at an optimum water content of 24% were obtained. In the static compaction method, the soil is compacted by a gradually applied monotonic force. The soil is confined in a container and compaction is achieved by the movement of a piston. The tests performed in this work follow the procedure described by Venkatarama Reddy and

Jagadish (1993), in which a static force is gradually applied until a specific final thickness (volume) is achieved.

2.2 *Dry density-compaction water content and suction relationships*

For both dynamically and statically compacted samples under different dry density and water content, the equilibrium matric suction was measured using the filter paper technique. Contours of constant suction where then drawn by interpolating in a rational way within the experimental values (see Figure 1). The suction contours are in general nearly vertical at low dry densities and tend to curve to the left at relatively high densities. On the other hand, above the optimum water content of the standard energy, the contours curve becomes asymptotic to the 100% degree of saturation line. Therefore it is apparent that the suction depends more on the water content, with some influence of dry density, than on the compaction technique (i.e., static or dynamic).

Figure 2 shows the variation in the matric suction with the as-compacted degree of saturation for compacted samples with different dry densities. The dry density is expressed as a percent of the maximum dry density attained with the standard compaction energy. This percent is named relative compaction. It is observed that at any relative compaction, an increment in the as-compacted degree of saturation markedly reduces the matric suction of the compacted soils. Additionally, the relation between the matric suction and the degree of saturation is distinctly affected by the relative compaction of the samples. So at a given degree of saturation, the smaller pores of denser samples produce higher matric suction.
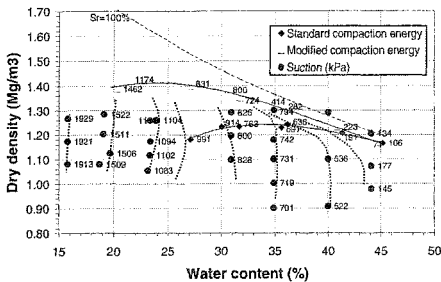
Figure 1. Contours of constant suction (Herrera, 2004)
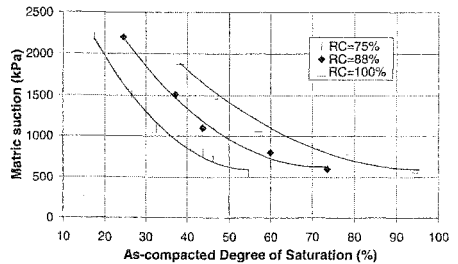
Figure 2 Matric suction – As-compacted Degree of Saturation for compacted samples

3. INVESTIGATION INTO THE VOLUME CHANGE BEHAVIOUR DURING WETTING BY INUNDATION

This section presents the results of volumetric change behaviour of compacted samples with different initial conditions flooded under constant vertical stress. Specimens of statically compacted kaolin were prepared directly into a conventional oedometer ring. Evaporation during loading was prevented by using a latex membrane to seal the gap between the top cap and the clamping ring. The samples were loaded to constant vertical stresses of 50, 100 and 200 kPa and when they reached equilibrium (defined by no further vertical deformation), flooding was

allowed through a porous stone placed in the bottom of the oedometer. When no further volume change was recorded, any excess of water from the top was mopped up and the access to water from the bottom was prevented, the sample was then unloaded.

3.1   Contours of equal volume change

Figure 3 shows the measured volumetric changes of compacted kaolin samples after wetting at a constant vertical stress of 50 kPa. The points (with numbers to their left) represent the dry density and water content after loading and just before wetting. The number represents the % of volume change. Collapse deformations are represented as positive and swelling deformations are presented as negative.

It follows from Figure 3 that, the amount of collapse increases as both the initial dry density and the compaction water content reduces. Alternatively, the swelling potential increases as the dry density increases and the compaction water content decreases. There is a zone (in general close to the optimum compaction conditions for the standard compaction energy) where compacted materials may exhibit negligible volume changes after wetting. This is represented in Figure 3 as a stable zone and it is located closer to 90% of the maximum dry density, the zone is narrow and expands at higher water contents. This zone corresponds to a transition from collapse to swelling deformations after wetting, as the dry density increases at constant water content. Also it is observed that the dry density for which the volume change is negligible seems to be no very much influenced by the water content.
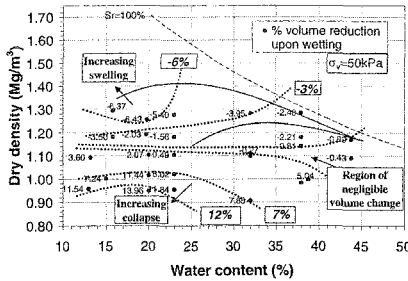
Figure 3. Contours of equal volume change following wetting under a constant vertical stress of 50 kPa.

It can be seen in Figure 3 that a strong collapse or expansion potential is observed in compacted samples on the dry side of optimum, while on the wet side of optimum the deformations are smaller. Studies of the microstructure of soils based in SEM observations and porosimetry studies presented by Alonso, et al., (1987), have shown that on the dry side of optimum the fabric is composed by aggregates of clay particles like granular materials with several dominant pores sizes, whereas on the wet side of the optimum, the structure is more homogeneous with one dominant pore size. A consequence of this observations, is that for the dry side of the optimum the structure is more open and then more susceptible to collapse and for the wet side of optimum the structure is uniform with smaller size pores and then less susceptible to collapse.

3.2   *Variation of the collapse and swelling potential in terms of the initial water content and dry density*

Figure 4 shows the volumetric change potential after wetting by inundation of compacted samples at dry side (water content of 25%) and wet side (water content of 38%) of optimum water content of the standard energy. Several researchers have suggested that soils compacted at water contents higher than the optimum for the standard energy do not collapse. This concept is not strictly valid because it does not consider either the prewetting density (and, hence, degree of saturation) of the soil or the possibility for postcompaction drying of the soil. Samples compacted 4% wet of optimum with relative compactions (RC) of 75% (ρ_d=1.10 Mg/m^3) and 100% (ρ_d =1.24 Mg/m^3) are shown in Figure 4. It is observed that the compacted sample with RC of 75% presents a maximum collapse potential of 11%, while the compacted sample with RC of 100% shows an almost negligible volume change. Although the effect of the denser dry density of the sample with RC=100% is an important factor in the collapse potential decrease, probably is the higher degree of saturation of the sample with RC=100% (Sr= 87%) compared with the degree of saturation of the sample with RC=75% (Sr=46%), the predominant factor for the negligible collapse potential. This big difference in the collapse potential of samples compacted at the same water content emphasize on the wrong assumption that if the material is compacted wet of optimum it does not collapse.
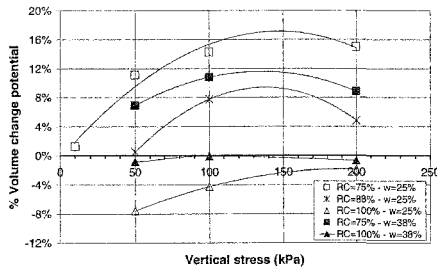
Figure 4. Variation of the collapse and swelling potential with the compaction conditions.

It is also shown in Figure 4 that, as the vertical stress increases, the amount of collapse experimented by the soil reaches a maximum and then decreases, for both compacted samples of dry and wet of optimum. This reduction in the collapse potential is due to the increase in both the density and the degree of saturation produced by the increment in the vertical stress.

In Figure 4 it is observed that the samples compacted at a water content of 25% (9% dry of optimum) exhibit a higher collapse potential at lower dry density and for a given dry density (expressed as relative compaction), the collapse potential increases as the water content decreases. On the other hand it is suggested that the swelling potential decreases with the vertical stress and is bigger for samples compacted on the dry side of the optimum. In addition, the effect of having higher dry densities not only reduces the collapse potential but also the applied stress needed to produce this collapse is higher. So, the sample compacted at a water content of 25% and RC of 75% shows a collapse potential of 8% at a vertical stress of 40kPa, whereas the same

collapse potential is presented at vertical stress of 100 kPa for the compacted sample at RC of 88%.

3.3   Influence of matric suction on the volumetric change potential

Figure 5 shows the variation of volumetric change potential with the initial matric suction for compacted samples flooded at 50 kPa and 100 kPa. The variations in matric suction are due to changes in the compaction water content of samples with the same relative compaction. It is observed in Figure 5 that for the looser sample (RC=75%), a rise in the matric suction produces an increase in the collapse potential whereas the volumetric change potential of the denser samples is less affected by the variations in the initial matric suction. Apparently, there is a maximum value of the matric suction such that, for values above this, the collapse or swelling potential does not change.
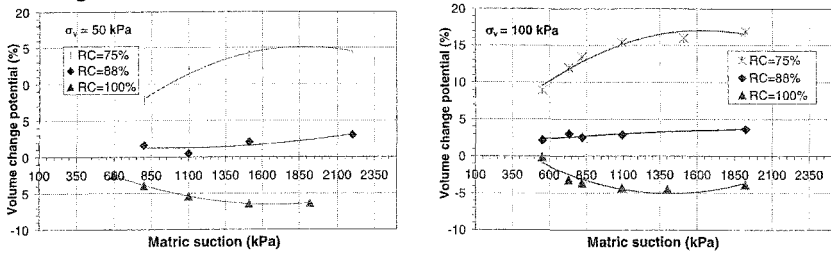
Figure 5. Influence of Matric suction on volumetric change potential of samples with constant relative compaction (RC). a) Vertical stress of 50 kPa. b) Vertical stress of 100 kPa

In general it was found that the collapse and swell potential are function of the initial suction, the fabric constructed by the compaction process and the vertical stress applied. Assuming that the behaviour of the net mean stress corresponds to the vertical stresses applied, the behaviour observed can be described by the framework proposed by Alonso, Gens and Hight (1987) for a collapsible material. Experimental evidence suggests the existence of a region in terms of void ratio (or dry density), suction (or water content) and applied vertical stress (prior to wetting), such that samples compacted within this region will undergo negligible volume changes after wetting. Samples compacted above this region will collapse after wetting, whereas samples compacted below this region will swell after wetting (see Figure 6).
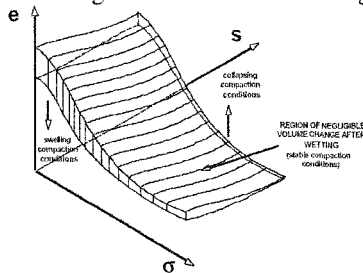
Figure 6. Region of negligible volume change after inundation in a void ratio, vertical stress and suction space (Colmenares, 2002)

4. INVESTIGATION INTO THE VOLUME CHANGE BEHAVIOUR DURING CONTROLLED WETTING

The behaviour of the compacted kaolin and its relation with the principal variables of compaction has been studied through conventional oedometric test without suction control. In these tests the water content is maintained constant during loading and the suction continuously changes with the progress of deformations. Additional testing using the oedometer with suction control was carried out to study in more detail the changes of volume, water content and suction during the wetting process.

4.1 Description of the oedometer with suction control

The oedometer developed at the Soil Mechanics Laboratory of the National University of Colombia, utilized the osmotic technique to control the matric suction in eodometer testing under atmospheric conditions, and is based in the oedometer originally developed by Dineen and Burland (1995) and Dineen (1997). The suction in the specimen is controlled via a semi-permeable membrane that is located below the oedometer ring. A salt solution with a high osmotic potential (in this case Polyethylene Glycol, PEG) is circulated through a reservoir below the membrane (Figure 7). PEG of 6000 molecular weight and one poly-ether sulphanate ultra filtration membrane of 5000 molecular weight cut off (MWCO) were used for the osmotic system.
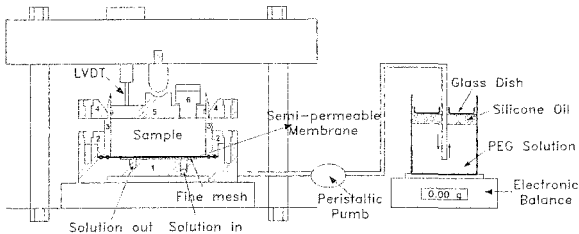
Figure 7. Schematic view of the suction controlled oedometer (González, 2005)

If the osmotic potential of the solution is greater than the suction in the specimen then water is drawn from the soil into the solution, increasing the suction in the specimen. However, water will be drawn into the soil decreasing the suction, if the osmotic potential of the solution is lower than the suction in the soil (for example when circulating distilled water instead of salt solution). Changes in the water content of the specimen are estimated by measuring the change in mass of the circulating solution. This is undertaken by placing the stock solution on an electronic balance. Evaporation from the surface of the solution is minimised by placing a layer of silicone oil and a glass dish on the exposed surface (Figure 7). A calibration of the evaporation losses was made (González, 2005), and it is used to correct the mass of the solution recorded from the balance. The PEG solution is circulated from the stock container to the base of the oedometer using a peristaltic pump. The system of load application is the same used by the conventional oedometer, in which the load is applied on the top cap through a piston and a load frame operated by a lever system.

4.2   *Experimental programme*

Two tests were carried out on specimens of compacted kaolin in static way, these tests were performed under similar initial conditions of dry density and water content (dry side of the optimum). A summary of the initial conditions of the samples tested is presented in Table 2. The stress paths followed in the tests are shown in Figure 8. Small increments of load were applied (usually of 10 kPa) with the purpose of avoiding important changes of suction, which can take place due to the system of load application as was established by Cui and Delage (1996) and Dineen (1997).

Table 2. General characteristics of the samples tested

Test No.	Dry density (Mg/m3)	Void ratio	Water content (%)	Degree of Saturation (%)	Matric Suction (kPa)
1	0.97	1.58	26	43.2	1050
2	1.01	1.57	24.5	40.7	1000
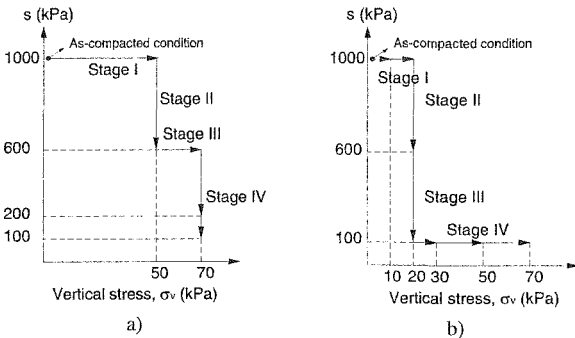
Figure 8. Stress paths followed. a) Test 1. b) Test 2

4.3   *Test 1*

Test 1 follows a load path at constant suction and then reduces the suction at constant vertical stress (see Figure 8a). Figure 9a) show the variation of void ratio with the time from the start of the test and Figure 9b) show the variation of the water exchange between the sample and the PEG stock solution during the test. A PEG solution with an osmotic potential of 1000 kPa equivalent to the initial suction of the sample, was initially circulated beneath the semi-permeable membrane. During the stage I, two increments of load were applied up to vertical stress of 50 kPa, then the osmotic potential of the PEG solution was changed from 1000 kPa to 600 kPa in order to reduce the suction (stage II). In the stage III additional load was applied up to 70 kPa, the PEG solution was unchanged of 600 kPa. The osmotic potential of PEG was again changed (stage IV), first from 600 kPa to 200 kPa and then from 200 kPa to 100 kPa.

The results of this test can be interpreted by using the elasto-elastic model proposed by Alonso, Gens & Hight (1987) to describe the behaviour of partly saturated collapsible soils. The model suggests that there is a yield line (LC) as shown in the Figure 10a). When the stress path crosses this yield line, irreversible volumetric

strains may occur. A reduction in suction may generate collapse strains (C), and an increase in load may generate loading strains (L).

(a)   (b)
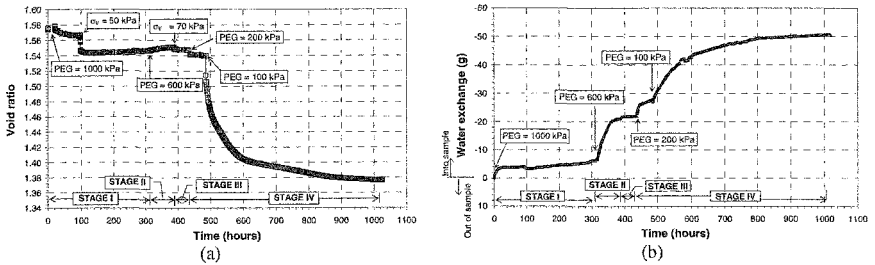
Figure 9. Test No. 2. Void ratio and water exchange vs. time relationship for different PEG solutions circulated.

The loading-collapse curve shown in Figure 10a) had been drawn given a value of preconsolidation stress in saturated condition (Po*) of 35 kPa, this value was obtained through a one-dimensional consolidation test on a sample with similar compaction characteristics. It was also considered that the yield stress for a sample loaded at constant initial suction of 1000 kPa is equivalent to the maximum compaction pressure applied to the sample that in this case was about 100 kPa. The last assumption is supported by Honda, M. et al., (2003), who found that in compacted samples the inflexion point of compression curves at constant suction almost coincide with the compaction pressure.

(a)   (b)   (c)
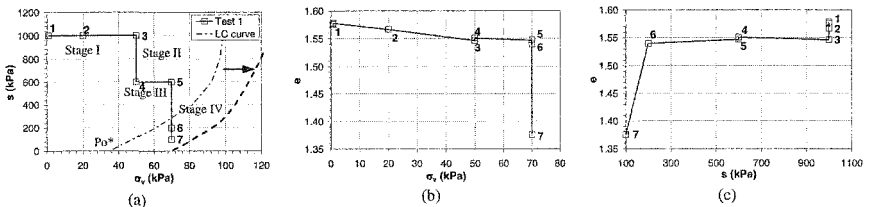
Figure 10 Test No. 1. a) Loading – Collapse line LC. b) Variation of void ratio with the vertical stress c) Variation of the void ratio with the matric suction.

During the reduction of suction from 600 to 200 kPa (stage IV) it is observed that the wetting path crosses the LC curve around 200 kPa, this explains the little collapse observed (see Figure 10c). During the reduction of suction from 200 to 100 kPa, an important decrease in the void ratio was recorded (see Figure 10c), this deformation occurred under the LC curve and this explains the high collapse produced. The collapse generated by the reduction of suction in this test, produces plastic volumetric strains and the movement associated of the LC curve, as it is shown in Figure 10a).

The results show in Figure 10, indicate that the net collapse or swell is function of the suction of the sample and the volume change generated by a reduction of suction at a given vertical stress, can change the sign throughout the wetting path. So, during

the reduction of suction from 600 to 200 kPa, initially an increased of volume and then a decreased of volume were recorded. If the reduction of suction had been carried out in a gradual way, the exact value of the suction for which the transition of swell to collapse deformations occurs would have been detected. On the other hand it was found that during the last reduction of suction (from 200 to 100 kPa), the amount of water entering the sample was important, filling the interaggregates spaces (macroporosity). This leads to an important reorganization of the material structure producing high collapse deformations.

4.4   Test 2

Test 2 first follows a wetting path at low vertical stress and then a loading path at low constant suction (see Figure 8b). A PEG solution with an osmotic potential of 1000 kPa was initially circulated beneath the semi-permeable membrane (see Figure 11). During the initial load stage to 20 kPa (stage I), water entered into the sample and a reduction in the void ratio was recorded. During stage II (reduction of suction to 600 kPa) an important amount of water entering the sample generated an increase in the volume of the sample (see Figure 11). It took a long time to get the equilibrium (about 13 days). This was due to a reduction of the suction at low vertical stress which generates a big swell in the material and therefore more time is required to reach equilibrium. The third stage involved a reduction of suction from 600 to 100 kPa. An additional increase in volume was observed while some water entered moderately into the sample. Stage IV consisted in the gradual application of load keeping a constant suction of 100 kPa, in this case vertical stresses of 30, 40, 50, 60 and 70 kPa, were applied. The water exchange registered a permanent variation during the application of load and it hardly got equilibrium.

(a)   (b)
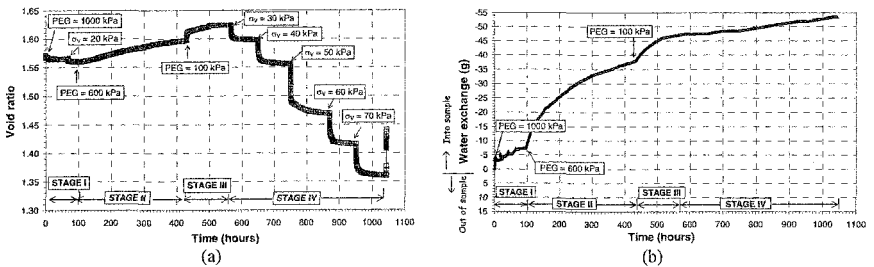
Figure 11. Test No. 2. Void ratio and water exchange vs. time relationship for different PEG solutions circulated.

When the test was finished, some evidence of the presence of PEG solution in the sample was observed, however, the membrane did not show signs of break and then possibly a chemical breakdown occurred. This phenomenon was explained by Tarantino & Mongiovi (2000). According to Figure 11, apparently this decomposition started in stage III where it was noticed that water entered permanently into the sample. Colmenares (2002) studied the stability in long-term of the control suction system in mixtures of sand-bentonite. He found that after

approximately 2 weeks the stability of the system can not be guaranteed completely, due to a gradual pass of a small amount of PEG molecules through the membrane.
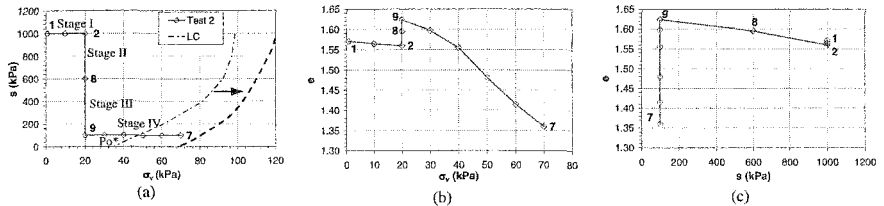
Figure 12. Test No. 2. a) Loading – Collapse line LC. b) Variation of void ratio with the vertical stress. c) Variation of the void ratio with the matric suction

4.5   Comparison between tests 1 and 2

Figure 13 displays a comparison of the results obtained in tests 1 and 2. The final volumetric deformation induced were similar in both cases and therefore it can be concluded that whatever the origin of the strains, they have a similar effect on the structure of the material as represented by the movement of the LC yield curve, this proved the uniqueness of the LC curve, as proposed by Alonso, Gens y Hight (1987). This implies that given an initial structure of the soil, a state more compressed for the soil under either a loading path or wetting path can be reached.
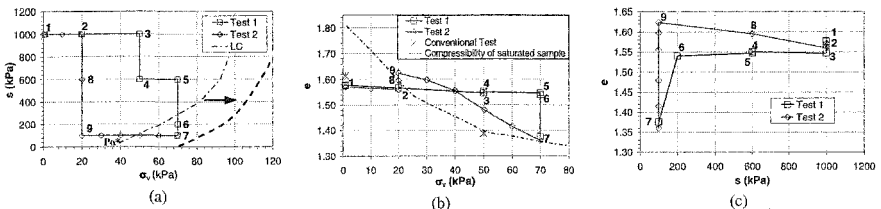
Figure 13. Comparison between Tests 1 and 2. a) Loading – Collapse line LC. b) Variation of void ratio with the vertical stress. c) Variation of the void ratio with the matric suction.

5.   CONCLUSIONS

- The matric suction of the kaolin compacted samples depends principally on the water content, with some influence of dry density and the compaction technique (i.e., static or dynamic) in less extent.
- The relationship between the matric suction and the degree of saturation is affected in different way according to the dry density. Such that, at a given degree of saturation, the smaller pores of denser samples produce higher matric suction.
- For the material used in this study, the region of negligible volume change is located at about 90% of the maximum dry density of the standard compaction energy.
- Microstructures of samples compacted wet of optimum are less susceptible to volume changes than the microstructures of samples compacted dry of optimum, however, this factor is secondary when compared with the initial dry density and possible suction variations.

- The looser samples show an increase in the collapse potential as the initial matric suction increases, whereas the volumetric change potential of denser samples is less affected by variations in the initial matric suction. Apparently, there is a maximum value of the matric suction such that, for values above this, the collapse or swell potential does not change.
- The results of tests performed with the osmotic oedometer have been successful in reproducing the mechanical behaviour of compacted soils found by previous research. However, there is some evidence of the instability of the system with the time due to the chemical breakdown of the semi permeable membrane.
- Most of the collapse of the material happened during the last stage of reduction of suction. An important amount of water entered into the sample at low suctions filling the inter aggregates spaces (macroporosity). This leads to an important reorganization of the material structure producing high collapse deformations.
- The volumetric behaviour of the material is fitted with the constitutive model. It was possible to assume an LC curve for the compaction conditions studied. On the other hand it was verified that independent of the origin of the strains (ie. loading or wetting), they have a similar effect on the structure of the material as represented by the movement of the LC yield curve and this proved the uniqueness of the LC curve, as proposed in the constitutive model.

REFERENCES

Alonso, E.E., Gens A. and Hight D.W., (1987). *Special problems soils*. General report, proc. 9th. Eur. Conf. Soil Mechanics, Dublin, Vol.3. pp.1087-1144.

Alonso E.E., Gens, A. and Josa, A (1990). *A constitutive model for partially saturated soils*. Geotechnique 40, No.3, pp. 405-430.

Colmenares M., J.E. (2002). *Suction and volume changes of compacted sand-bentonite mixtures*. PhD Thesis. University of London.

Cui, Y.J. and Delage, P (1996). *Yielding and plastic behaviour of an unsaturated silt*. Geotechnique 46, No.2, pp. 291-311.

Dineen, K. and Burland, J.B. (1995). *A new approach to osmotically controlled oedometer testing*. Proceedings of the First International Conference on Unsaturated Soils. Alonso, E.E. and Delage, P. Editors. Vol. 2, pp. 459-465. Paris. Balkema.

Dineen, Kieran (1997). The influence of soil suction on compressibility and swelling. PhD Thesis. University of London.

González, Nubia (2005). *Influencia de la succión en el comportamiento volumétrico de suelos compactados*. Tesis para optar al título de Magíster en Geotecnia. Universidad Nacional. Bogotá.

Herrera, Felipe (2004). *Estudio experimental del comportamiento volumétrico de muestras de caolín compactadas, sometidas a procesos de humedecimiento*. Tesis para optar al título de Ing. Civil. Universidad Nacional. Bogotá.

Honda,M., Seguchi,H., Kim,E., Kawai,K., Iizuka, A. y Karube,D. (2003). *A study of the relation between volume change characteristics of compacted soil and the condition of compaction*. Proc. of 2nd Asian Conference on Unsaturated Soils, pp.177-170, 2003.

Jennings, J.E.B. and Burland, J.B. (1962) *Limitations to the use of effective stresses in partly saturated soils*. Géotechnique 12 (2), pp 125-144.

Tarantino A. and Mongiovi, L. (2000). *A study the efficiency of semi-permeable membranes in controlling soil matrix suction using the osmotic technique*. Proceedings of the second international conference on Unsaturated Soils. Toll & Leong editors, pp. 303-308. Asia.

Venkatarama, Reddy B.V. and Jagadish, K.S. (1993). *The static compactation of soils. Geotechnique*. Vol. 43, No. 2, pp 337-341.

An evaluation method for the volume change characteristics of compacted soil

M. Honda[1], A. Iizuka[2], S. Ohno[3], K. Kawai[4], and W. Wang[5]

[1] Nikken Sekkei Civil Engineering Ltd, Technical Development Department, 102-8117, Iidabashi 2-18-3, Chiyoda-ku, Tokyo; PH +81-3(5226)-3070; FAX +81-3(5226)-3075; email: hondam@nikken.co.jp
[2] Kobe University, Center of Urban Safety and Security
[3] Tokyo Institute of Technology, Department of International Development Engineering
[4] Kobe University, Department of Civil Engineering
[5] Nikken Soil Research Ltd, Technical Department

Abstract

This paper discusses the volume change characteristics of compacted soil based on oedometer test results. After making specimens with different water contents and under different compaction loads, compression tests are conducted under both saturated and unsaturated conditions. The effects of the compaction conditions on the compression curves are discussed. It is confirmed that the yield stress and the water content are important factors when evaluating a compression curve, while dry density and suction are important factors when evaluating the yield stress.

Introduction

Recently, a shift from specification-based design schemes to performance-based design schemes has been attempted. In order to apply the concept of a performance-based design scheme to earth structures such as embankments, it is necessary to clarify the relationship between the required quality of a compacted ground after the fill operation and the quality control value of the soil compaction during the fill operation. This paper studies volume change characteristics as one type of mechanical characteristic, and the relationship between the compaction curves and the compression curves of compacted specimens is examined through oedometer tests results.

Test Procedure

Oedometer tests were conducted on two types of soil. The physical properties are shown in Table 1. Samples of the powder condition were adjusted by spray to obtain the required water contents, and then compaction was applied to make the specimens.

· Series I

Specimens were compacted under two static loads, namely, 156.8 kPa and 313.6 kPa, for samples adjusted at three different water content. Then, oedometer tests were conducted on the six specimens. The test apparatus is shown in Figure 1. The suction of the specimens was measured soon after compaction, and the suction during the oedometer tests was controlled in order to maintain the measured value. In addition, oedometer tests were conducted on initially soaked specimens with a standard consolidation test apparatus. The specimens were compacted at 313 kPa for samples adjusted at five different water content.

· Series II

Specimens were compacted at 313.6 kPa for samples adjusted at three different water content. The test apparatus was the same as that used in Series I (Figure 1). The suction during the tests was controlled in order to maintain the values of 73.5 kPa and

Table 1   Physical properties of the soils

	ρ_s (g/cm^3)	w_p (%)	w_L (%)	Ip
Series I	2.70	29.6	43.0	13.4
Series II	2.71	20.3	33.5	13.2

Figure 1. Test apparatus

(a) Series I   (b) Series II

Figure 2. Compaction curves

(a) Series I   (b) Series II
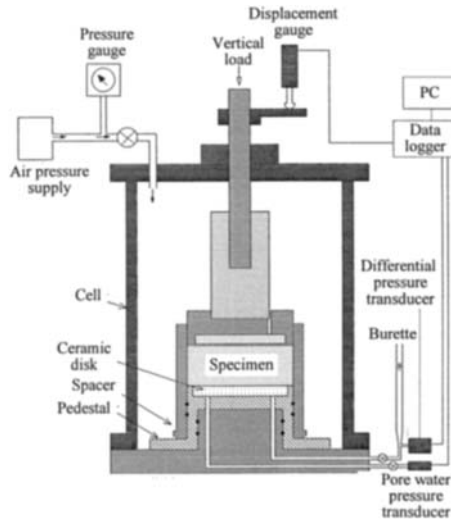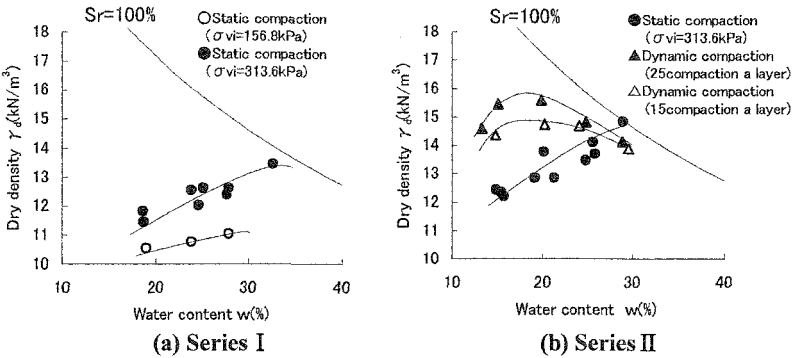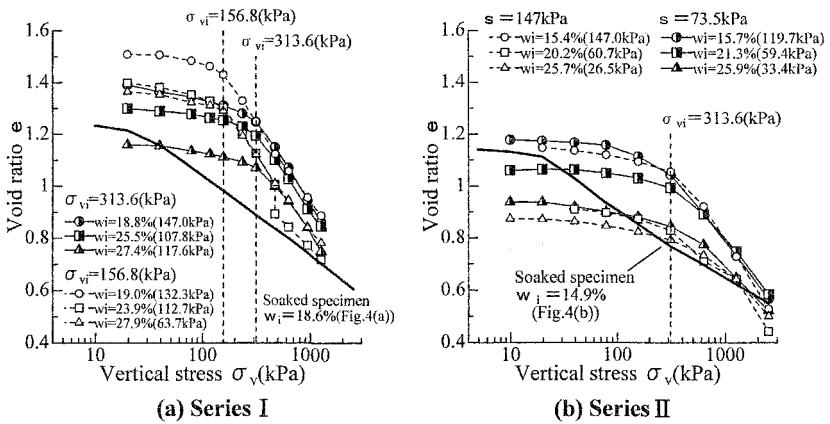
Figure 3. Oedometer test results (unsaturated specimens, static compaction)
*In Figures (a) and (b), the numerical values shown after the initial water content
indicate the suction measured after compaction (kPa)

(a) Series I   (b) Series II
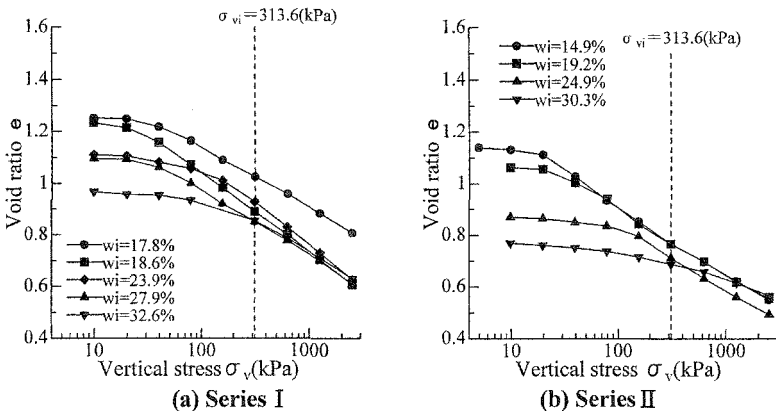
Figure 4. Oedometer test results (soaked specimens, static compaction)
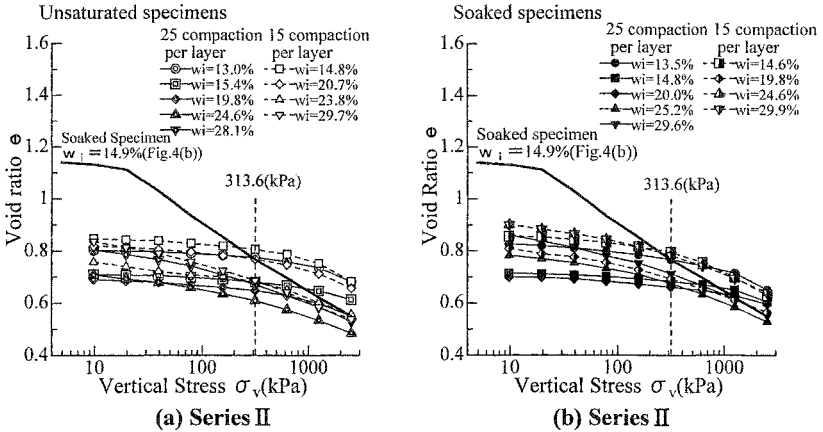
Figure 5. Oedometer test results (dynamic compaction)

147 kPa. Oedometer tests were conducted on a total of six specimens. The controlled suction during the tests was different from the measured value taken after compaction. Oedometer tests on initially soaked specimens were conducted by the same method and with the same apparatus as those used in Series I . The initially soaked specimens were compacted at 313.6 kPa for samples adjusted at four different water content. In addition to static compaction tests, oedometer tests were conducted for dynamic compaction specimens. The samples were compacted by method JIS A 1210 A-c. The mold was 10 cm in diameter and 12.73 cm in height. A standard consolidation test apparatus was used for the dynamic compaction specimens, as it had been for the initially soaked specimens. The samples were separated into three layers and then compacted by a 2.5 kg rammer. The compaction was carried out according to two methods. One method applied 25 times the compaction per layer and the other method applied 15 times the compaction per layer. These dynamic compaction specimens were in an unsaturated condition, but a soaked condition was also used. The suction during the oedometer tests on the dynamic compaction specimens was not controlled.

Test Results

Figure 2(a) shows the compaction curves for Series I . The dry density of the specimens compacted at 313.6 kPa is higher than that of the specimens compacted at 156.8 kPa. The dry density decreased with a decrease in the water content, and all the specimens were on the dry side of the optimum water content.

Figure 2(b) shows the compaction curves for Series II . The dry density of the dynamic compaction specimens is higher than that of the static compaction specimens. Although the static compaction specimens were on the dry side of the optimum water content, some of the dynamic compaction specimens were on the wet side of the optimum, and the dry density decreased with an increase in the water content.

Changes in the void ratio in the oedometer tests are shown in Figures 3(a) and (b). Figure 3(a) shows the results for Series I , in which the maximum curvature points of the compression curves almost coincide with the compaction stress. Figure 3(b) shows the results for Series II, in which the maximum curvature points of the compression curves do not coincide with the compaction stress. The suction of the specimens in Series II was controlled at a different value from the measured value taken soon after compaction. The difference between the maximum curvature points and the compaction stress occurred due to the suction. The maximum curvature points of the compression curves are interpreted as the preconsolidation stress levels of the specimens, but this stress was influenced by the suction during the unsaturated state.

Figures 4(a) and (b) show the results for the saturated specimens. The maximum curvature points of all the specimens are less than the compaction stress of 313.6 kPa. This can be interpreted as an effect of the reduction in the stiffness of the soil skeleton caused by a reduction in the meniscus force of the interparticles. The initial void ratio, calculated directly from the dry density, decreased with an increase in the compaction water content because all the specimens were on the dry side of the optimum. The maximum curvature points increased with an increase in the water content during the compaction, and the compression curves tended to converge into

(a) Series I   (b) Series II
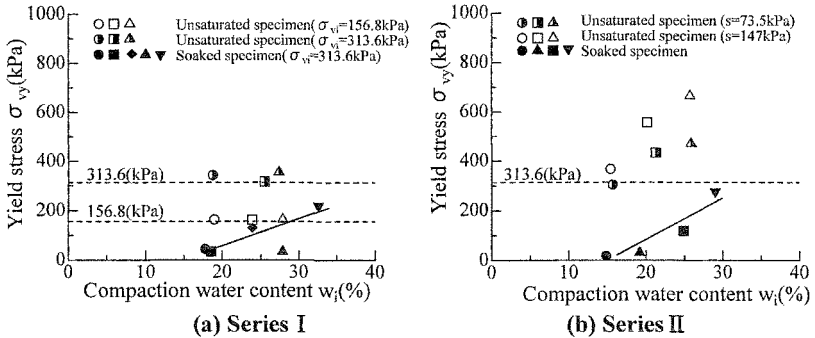
Figure 6. Yield stress ～ water content relationship(static compaction)
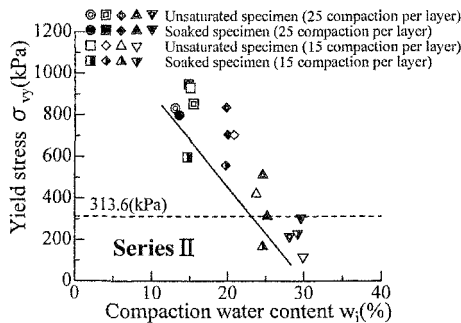
Figure 7. Yield stress ～ water content relationship(dynamic compaction)

(a) Series I   (b) Series II
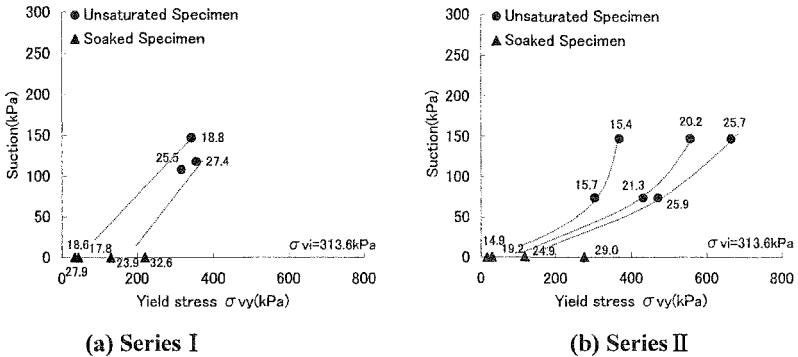
Figure 8. Yield stress ~ Suction relationship
*Numerical value in the figure indicates the compaction water content wi(%)

one line in the region where the stress exceeded the maximum curvature points.

The compression curve composed by the white square symbols in Figure 3(a) indicates the specimen of initial water content wi = 23.9% and was soaked at 470.4 kPa. The compression curve after saturation tends to coincide with the initially saturated specimens. The compression curve after saturation was not affected by the compaction stress, the water content, or the suction history. In the samples used in the present paper, it is thought that the yield stress of the specimens in the saturated condition is determined by the structure of the soil skeleton which is reflected by the void ratio.

Edahiro et al. (2002) confirmed that the normal consolidation line for a saturated specimen is not affected by the compaction conditions; they studied the quality control value of the backfill of a retaining wall for a collapse settlement using a compression curve and the overburden pressure. The compression curve of the saturated specimen showed various behaviors according to the soil type. More studies are required to clarify the compression characteristics. However, it is thought that the number of soils which have only a normal consolidation line under a soaked condition is not few.

Figures 5(a) and 5(b) show the compression curves for the dynamic compaction specimens in Series II. Since the dry density is high, the void ratio is smaller than for the static compaction specimens and the stress of the maximum curvature points increases.

Yield Stress of the Compacted Soil

Figures 6 and 7 show the yield stress determined by the Casagrande method; it is plotted for the water content at compaction. Under a saturated condition, the yield stress of the dynamic compaction specimens increased with a decrease in the water content at compaction, although the yield stress of the static compaction specimens increased with an increase in the water content at compaction. The specimens on the wet side of the optimum water content were included in the dynamic compaction

specimens, while all of the static compaction specimens were on the dry side of the optimum, and the dry density decreased with an increase in the water content at compaction. Just as for the static compaction specimens, it is thought that the yield stress of the dynamic compaction specimens in a saturated condition is also determined by the structure of the soil skeleton which in turn is reflected by the void ratio.

Figure 8 shows the relationship between suction and the yield stress. The yield stress increased with suction, and a yield locus exists for each level of water content at compaction. Although the yield stress of the saturated specimens is only dependent on the dry density, the suction also affects the unsaturated specimens.

Compression Curves for Compacted Soil

Figures 9 and 10 show the change in the equivalent void ratio proposed by Toll (1995). For comparison, the void ratio are also plotted in the same figures and are expressed with the same type of plots. The equivalent void ratio is defined by the following equation:
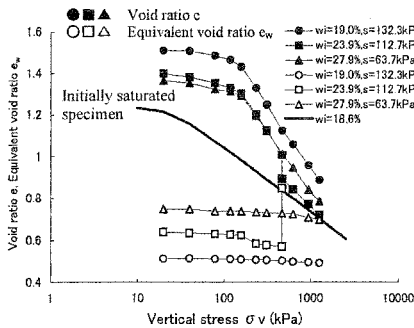
(a) σ_{vi}=156.8kPa
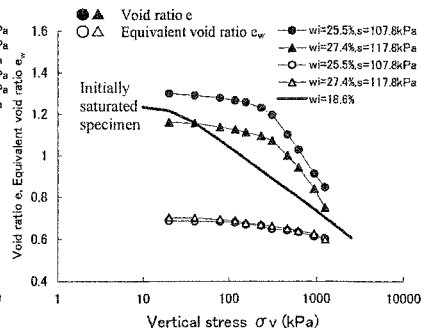
(b) σ_{vi}=313.6kPa

Figure 9. Void ratio and Equivalent void ratio (Series I)
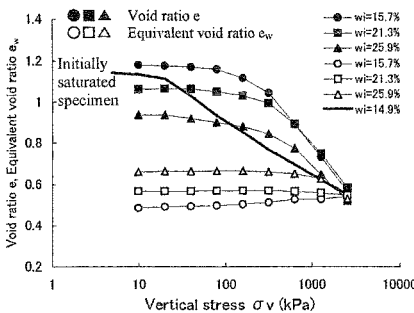
(a) σ_{vi} =313.6kPa, s=73.5kPa
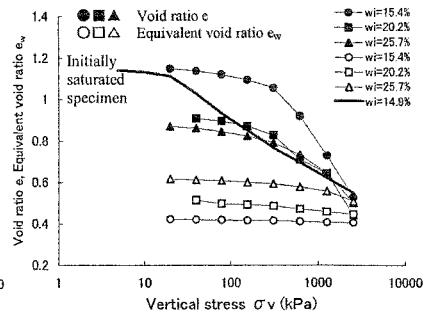
(b) σ_{vi} =313.6kPa, s=147kPa

Figure 10. Void ratio and Equivalent void ratio (Series II)

$$e_w = Gs \cdot w = e \cdot Sr \qquad (1)$$

where e_w is the equivalent void ratio, Gs is the specific gravity, e is the void ratio and S_r is the degree of saturation. The equivalent void ratio tends to approach the void ratio with the progress of compression. Changes in the equivalent void ratio are smaller than those for the void ratio, and the degree of saturation increases with compression. As shown in equation (1), the equivalent void ratio is expressed by the product of the void ratio and the degree of saturation, and the equivalent void ratio is equal to the void ratio at the state of saturation. For reference, the compression curves for the initially saturated specimens are shown in the same figures. The equivalent void ratio tends to coincide with the void ratio on the compression curves for the initially saturated specimens. These results can easily be understood by considering the test results shown in Figures 4(a) and (b) in which the normal consolidation curves for the saturated specimens are not affected by the compaction condition and they tend to be expressed only by lines.

In the case of specimens with a high degree of saturation, the action of suction is almost equal to the effective stress of the saturated soil, and an increase in suction leads to an increase in the confining stress and a decrease in the void ratio. The point of convergence between the void ratio and the equivalent void ratio may be shifted from the compression curve of the initially saturated specimens on the graph expressed by the axis of the void ratio and the effective stress without considering the effect of suction. This is because the action of suction and the effective stress are about the same. In the case of the present test results, however, the difference from the compression curve of the saturated specimens is not remarkable.

Evaluation Methods for the Compression Characteristics of Compacted Soil

The evaluation methods for the compression characteristics of compacted soil are studied in this chapter based on the above-mentioned test results. The results of the tests conducted in this study are summarized in the following.

1) The yield stress of saturated specimens only depends on the dry density. The dry density is affected by the water content at compaction, the compaction load, and the compaction method (e.g., static or dynamic). The suction also affects the yield stress of unsaturated specimens. Although the yield stress increases with an increase in suction, the rate of increase in the yield stress with suction shows various trends, even in the case of the same samples. These trends might be influenced by the stress history and so on.

Matyas et al.(1968) confirmed that the existence of a contour line for the void ratio in the plane consists of a horizontal axis of applied stress and a vertical axis of suction. The contour line in the figure inclines to the right with a decrease in the void ratio, i.e., the rate of increase in yield stress with suction increases with a decrease in the void ratio. This is caused by the evolution of the structure of the soil skeleton; Karube (1997) expressed this characteristic in the constitutive equation.

A detailed study is required to prove this mechanism concerning the evolution of the structure of the soil skeleton during compaction and compression. It is also necessary to study the influence of suction on the evolution of the structure of the soil skeleton. Although the amount of suction applied to the specimens is 100 to 150 kPa in Figure 6, the yield stress is higher (200 to 500 kPa) than that in the saturated state. It is interesting to note that the increments in yield stress are larger than the suction applied to the specimens. Bishop et al. (1960) proposed an effective stress for the unsaturated state, but it is inapplicable to these test results even if parameter χ equals 1.

The static compacted specimens are on the dry side of the optimum and most of the pore water is distributed to the interparticles as meniscus water. The increments in yield stress are caused by the effect whereby suction prevents interparticle slips. The cone index on specimens in a mold is often encountered or CBR tests on specimens in a mold often show a sharp rise with a decrease in the water content. The effect of an increase in the deformation resistance by suction might be large when the interparticle slips are prevented. This is because most soil deformations are caused by interparticle slips.

2) The yield stress of the static specimens and the compaction stress are about the same if the suction is controlled at the value measured after compaction. There is a possibility that the yield stress will differ from the compaction stress even if the suction is controlled. The reasons are as follows:

· During compaction, changes in the degrees of saturation and suction lead to changes in the stress transmitted to the structure of the soil skeleton.

· The yield stress is affected by the history of the stress transmitted to the structure of the soil skeleton by the applied stress and suction.

The relationship between the yield stress and the compaction stress must be studied further. When the degree of saturation of a specimen is high, an increase in the suction leads to the compression of the structure of the soil skeleton, because the action of suction is similar to that of effective stress for saturated soil. If the suction measured during compaction is higher than that measured after compaction, a possibility exists that the yield stress will be higher than the compaction stress even if the suction is controlled at the value measured after compaction. This is because the stress history is given to the structure of a soil skeleton by suction. When the degree of saturation of a specimen is low, however, an increase in suction leads to an increase in the stiffness of the soil skeleton without compression, while a decrease in suction leads to the compression of the structure of the soil skeleton due to a decrease in stiffness. In the present paper, it is interpreted that the stress history is not given by suction to the structure of the soil skeleton during compaction for the following reasons:

· Pore water exists at the interparticles as meniscus water, because samples in the powder condition were adjusted by spray before compaction for the required water content.

(a) Compaction curve   (b) Compression curve   (c) Water characteristic
                                                              curve
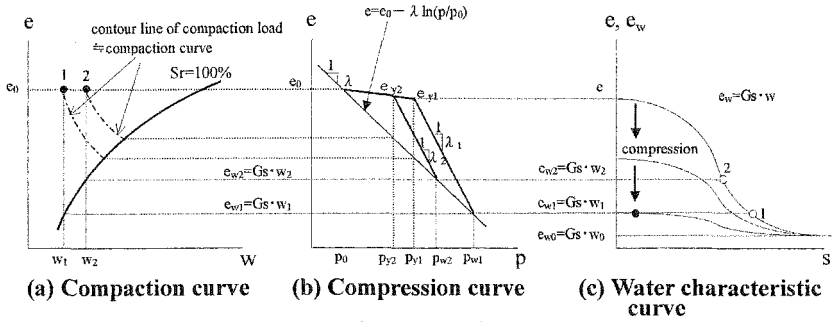
**Figure 11. Relationship in conception among the compaction curve,
the compression curve, and the water characteristic curve**

*For comparison, the compaction curve of Figure(a) is drawn by the void ratio which is
equivalent to the dry density. (e =Gs/ γ d - 1 Gs is the specific gravity)

· In the first half of compaction, the degree of saturation was low and the suction of the specimens was increased, because the number of interparticle points increased due to the compression which lead to a lack of pore water.

· In the latter half of compaction, the degree of saturation was high, the pore water pressure increased, and the suction decreased due to the compression of the structure of the soil skeleton. This is because pore water existed within the soil skeleton as bulk water.

3) For the static compaction specimens, the normal consolidation lines in a saturated condition are expressed only by lines. Although the compression curves for the dynamic compaction specimens vary, the unevenness of the compressive curves in the saturated condition is smaller than that for the unsaturated specimens. These results imply that the differences in the structures of the soil skeletons formed due to the differences in compaction conditions tend to disappear with saturation. In addition to this, the degree of saturation increases due to compression, results in saturation, and finally becomes normal consolidation lines for the unsaturated specimens towards the points on the normal consolidation lines for the saturated specimens. The void ratio of the convergence points is evaluated by the product of the specific gravity and the water content.

Figures 11(a) and (b) show the relationship in conception between the compaction curves and the compressive curves. The compaction curves in Figure 11(a) are expressed by the void ratio calculated from the dry density and the specific gravity. Two types of specimens are expressed in the figure as a concept. The water content of specimen 2 is higher than that of specimen 1, but the void ratios are equal. As shown in Figure 11(b), the yield stress of specimen 2 is smaller than that of specimen 1, because the water content is high and the suction is low. Although the compression curves after the yield approach the points of those of the saturated specimens, the void ratio of the convergence point in specimen 1 is smaller than that

of specimen 2, because the void ratio of the convergence point is evaluated by the product of the specific gravity and the water content.

The compression curves in the unsaturated condition are determined by assuming that the shape of the normal consolidation lines in the e-log p plane are linear if the yield stress is known before the design. However, it is difficult to estimate the yield stress from the compaction load of a compactor. This is because the vertical stress changes with the depth of wheels sinking into a compacted ground, in the case of a rubber-tired roller, although it is easy in case of a bulldozer, because the area which makes contact with the ground does not change and the vertical stress is clear.

As shown in Figure 11(a), the compaction stress is estimated from the void ratio on the saturation curve in the compaction curves by assuming the compaction curves as contour lines of the compaction stress. However, it is hard to estimate the stress accurately. The accumulation of data is required for the relationship between the compaction stress of the compactor and the yield stress.

Although the above-mentioned attempts are based on the assumption that the water content does not change, the effects of changes in the water content and in suction should be taken into consideration and the water retention curve should be determined in order to accurately predict the mechanical behavior. The water retention curve expressed by the equivalent void ratio is shown in Figure 11(c). As Kawai et al. (2000) has proposed, the effect of the void ratio should be taken into account when determining the suction-water content relationship to predict the behavior accurately.

Conclusion

The relationship between the compaction curves and the compression curves of compacted soil has been studied in this paper. Based on the oedometer test results, the effects of the compaction conditions on the compression curves have been discussed. The compression curves of compacted soil have been evaluated by the yield stress and the convergence point to the normal consolidation line of saturated specimens. Because the changes in the water content has been smaller than those for the void ratio during compression and the degree of saturation has been increased with the progress of compression. The convergence point has been evaluated by the equivalent void ratio proposed by Toll and derived by the product of the specific gravity by the water content. The yield stress has been directly determined by the dry density in a soaked condition, but the suction is also affected by the unsaturated condition. The water content, the dry density, and the suction are the important factors when evaluating the compression curves of compacted soil.

References

Bishop, A. W., Alpan, I., Blight, G. E. and Donald, I. B. (1960). "Factors controlling the strength of partly saturated cohesive soils" Proc. Colorado Conf., 503-532

Edahiro, T., Honda, M., Ochiai, F., and Hata, K. (2002). "An examination of the quality control value for compacted soil by using compression curve", Proc. 47th Geotechnical Engineering Symposium, 309-314 (in Japanese)

Honda, M., Iizuka, A., Ohno, S., Kawai, K., Wang, W. (2005). "A study of the evaluation method for deformation characteristic of compacted soil" J. of Geotechnical Engineering, JSCE, No.806/3-73, in printing (in Japanese)

Karube, D. (1997). "Stress analysis of unsaturated soil based on 'driest curve'" Proc. 14th ICSMFE, 333-336

Kawai, K., Karube, D. and Kato, S. (2000). "The model of water retention curve considering effects of void ratio" Proc. Asian Conf. on Unsaturated soils, 329-334

Matyas, E. L. and Radhakrishna, H. S. (1968). "Volume change characteristics of partially saturated soils" Geotechnique Vol. 18 No. 4, 432-448

Toll, D. G. (1995). "A conceptual model for the drying and wetting of soil" Proc. 1st Int. Conf. on Unsaturated Soils Vol. 2, 805-810

Suction Controlled Laboratory Tests on Undisturbed Pyroclastic Soil: Stiffnesses and Volumetric Deformations.

Eduardo Bilotta[1*], Vito Foresta[2*], and Giancarlo Migliaro[3*]

[1]Professor[*], PH (+39) 089-964120; email:e.bilotta@unisa.it
[2]Engineer[*], PH (+39) 089-963410; email:vforesta@unisa.it
[3]Ph.D Student[*], PH (+39) 089-964172; email:gmigliaro@unisa.it
[*] Department of Civil Engineering, University of Salerno, Ponte Don Melillo, 84084 Fisciano (SA), Italy

Abstract

This paper summarizes the preliminary results of a study on the effects of suction on stiffness and compressibility of ashy layers which cover the Pizzo d'Alvano relief (Sarno-Southern Italy). These soils, similarly to other pyroclastic soils, show some peculiar characteristics, as a remarkable secondary settlement, a metastable structure and a limited range of suction variation.

At first, the influence of secondary settlement on the long-term deformability is presented. The influence of suction on the apparent preconsolidation stress and, in general, on the stress-strain behaviour of such soils is also shown by means of suction controlled tests. Finally, the metastable structure of these soil is investigated by means of a suction controlled oedometer apparatus.

Results show that a reduced time of load permanence, in oedometer tests, is suitable to determine both the entity of primary settlements and the law of variation of secondary settlements of solid phase. More time is needed for the complete measure of the water content variation. The effect of suction is evident on the apparent preconsolidation stress value and on both the primary compressive index (C_t) and the creep coefficient (C_α). The influence of suction on the deformability parameters of the solid skeleton seems to vanish at high stress levels. Isotropic triaxial tests show a general anisotropic behaviour of the soil within the apparent preconsolidation range although a not so clear influence of suction on this behaviour is observed. Comparing the collapse tests on undisturbed and remoulded specimens, it is possible to identify a metastable structure in the first ones and, on the contrary, a lacking of collapse in the others.

Introduction

On May 1998, a catastrophic event, causing huge damages to buildings and people, occurred in the district of Salerno (Southern Italy). Several flowslides triggered from Pizzo d'Alvano mountain and involved several villages (Bracigliano, Quindici, Sarno and Siano) located at the toe of the massif. Following the hydrogeological disaster, the working Unit n. 2.38 of the National Group for the Prevention from Hydrogeological disasters (G.N.D.C.I.) at University of Salerno, started to coordinate a number of studies aimed at providing primary interventions to face the emergency. At a first stage, the attention was focused on the flowslides triggering mechanism which occurred on the slopes and on the early defensive stabilization measures.

The pyroclastic cover of the Pizzo d'Alvano Massif, originated from the explosive phases of Somma-Vesuvius volcanic activity (Campania Region, South Italy), generally comprises by a sequence of ashy and pumiceous layers (Bilotta et al., 2005). Undisturbed samples were collected using cylindrical samplers 0.10 m wide and 0.30 m long. Sampling was performed by hand or with the help of a hydraulic jack in suitable pits.

Laboratory tests were performed to determine the physical properties and the influence of the matric suction on the soil shear strength. Results on these issues have been already reported (Bilotta and Foresta, 2002). The above mentioned laboratory tests were carried out on intact specimens obtained by manual sampling and the results indicated that the soils, formed of a relatively homogeneous material (Bilotta et al., 2005), are generally partially saturated with a suction value not exceeding 65kPa (Cascini and Sorbino, 2002).

In order to increase the knowledge on the mechanical behaviour of these soils and to assure the correct design of new works, the results obtained by studying the influence of the suction on the stress-strain behaviour are reported in this paper. The ashy soil used in this study is a relatively undisturbed homogeneous material, composed of 60 % to 50 % silt and 40 % to 50 % sand (Bilotta and Foresta, 2002). The saturated hydraulic conductivity is $5.0 \cdot 10^{-6}$ m/s. (Sorbino and Foresta, 2002). This soil is characterized, as most of the soils of analogous origin, by very low values of dry unit weight (γ_d) and by high values of void ratio (e). In particular (γ_d) values range from 6.3 kN/m^3 to 8.2 kN/m^3 while (e) values range from 1.90 to 2.78. The mean specific gravity of the soil grains is 2.45.

In order to investigate the stress-strain relationships of such a pyroclastic soil, three different laboratory equipments have been used, i.e. conventional Casagrande-type oedometer, a suction controlled oedometer and a suction controlled triaxial, all respectively referred to as ED, SCO and USP in this paper. The layout of suction controlled apparatuses (SCO and USP) is reported in Rampino (1997) and Nicotera (1998). In these equipments, suction values are imposed on specimens via the axis translation technique (Richards, 1941; Hilf, 1956) by changing the value of air pressure (u_a) or water pressure (u_w) in the pores, while suction changes are given by the difference between them ($s = u_a - u_w$).

Volumetric strains of the specimen (only for USP) and its water volume variations ΔV_w (both for USP and SCO) have been measured by means of two

differential pressure transducers both linked to two reference burettes. In particular, volumetric strains have been computed by measuring the water volume changes occurring in a distilled water chamber surrounding the specimen. Along the line of water drainage a peristaltic pump provides flushing of diffused air through the HAEV porous stone with an air entry value of 100 kPa and 300 kPa.

As far as the oedometer tests are concerned, specimens with 50 mm and 56 mm diameter and 20 mm height have been used, respectively in ED and SCO apparatuses. The load has been applied either suddenly, in multiple steps, or with a controlled rate of 7 kPa/h. The latter procedure has been founded to be adequate in performing fully drained tests (constant suction). Load values ranging from 5 kPa to 4020 kPa were adopted. The former stress value corresponds to the minimum value allowed by the apparatus used. Collapse tests have been performed on specimens in which the suction was gradually reduced, in multiple steps, from the initial value of 50 kPa to 0 kPa. Oedometer tests on remoulded specimens have been also performed. The adopted remoulding technique was already reported by Bilotta and Foresta (2002).

Triaxial tests have been carried out on specimens with 68 mm and 70 mm diameter and 136 mm and 140 mm height. Three different suction values of 10 kPa, 20 kPa and 50 kPa have been imposed to the specimens. Two different types of triaxial tests, IRL (isotropic loading with a controlled rate of 2.5 kPa/h) and F (shear test with a strain controlled rate of 0.1 % /h), have been carried out.

Compressibility and stiffness measured with oedometer tests on nearly saturated specimens.

After the catastrophic event, as mentioned before, a preliminary characterization of the ashy soils with conventional laboratory equipments was requested to the Department of Civil Engineering of the University of Salerno. Due to the urgent need of estimating the compressibility of these soils and considered their grain size distribution and saturated hydraulic conductivity, a series of oedometer tests was performed with 2 hours load permanence ($\Delta t=2h$).

Figure 1 shows axial deformations versus time for each load increment with the indication of its vertical net stress (σ_v-u_a) applied. The primary settlement ends in less than 10 minutes, as it is shown in Figure 1a. A notable viscous effect is evident with a trend of secondary settlement fully defined within two hours after the load application. Then, it was decided to perform tests with a 24 hour load permanence to emphasize possible differences on the stress-strain behaviour of the specimens (see Figure 1b). In this section the results of ED tests, on water submerged samples, and SCO tests, with a null imposed suction, are examined. In the next section, the effect of suction on the deformability parameters is shown. The main physical properties of the tested specimens and the type of performed tests in SCO are listed in Table 1.

In Figure 2 are reported the apparent preconsolidation stress (σ_c) - obtained by the Casagrande's construction - plotted against the void ratio (e) in the conventional tests and in the null suction tests. The diagrams show an influence of the load permanence time on σ_c caused by the viscous behaviour of the material, while it seems that there is no difference between ED and SCO tests.
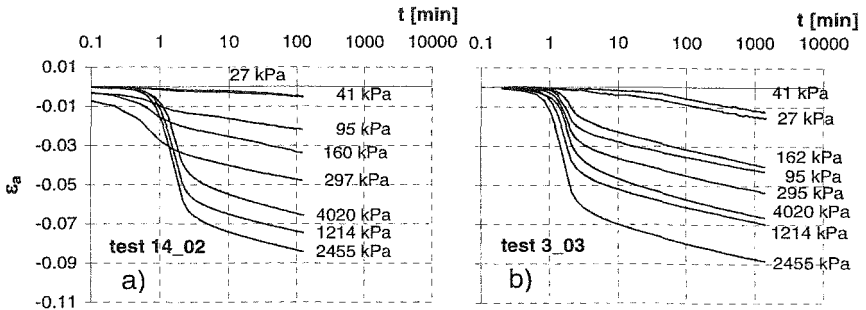
Figure 1. Vertical deformation ε_a against time in logarithmic scale: (a) $\Delta t = 2h$ load permanence; (b) $\Delta t = 24h$ load permanence.

In Figure 3 the values of the creep coefficient C_α (i.e. the ratio between the secondary settlement and its logarithmic time interval) in tests with null suction (by ED and SCO) are plotted against the vertical net stress at two different values of Δt.

Table 1. Soil specimen physical properties and tests type in SCO apparatus.

Specimen	Sr_{in}	γ kN/m^3	γ_d kN/m^3	e	test type	s_{in} kPa	s_{appl} kPa
3_03	0.851	11.56	7.15	2.565	A	8	0
7_03	0.772	12.63	6.89	2.698	A	16	0
14_03	0.583	11.65	7.45	2.410	A	19	0
14_02	0.706	12.30	7.27	2.497	B	9	0
4_03	0.671	12.07	7.16	2.549	A	2	10
3_04	0.861	13.65	7.68	2.122	C + A	10	10
12_04	0.855	13.38	7.51	2.196	C + A	2	10
5_03	0.728	12.67	7.41	2.427	A	16	20
5_04	0.852	13.62	7.63	2.218	C +A	4	20
13_04	0.824	13.24	7.54	2.241	C +A	-	20
14_04	0.800	12.76	7.08	2.453	A	-	20
16_02	0.728	12.69	7.58	2.350	B	18	20
2_03	0.834	13.77	7.93	2.206	A	16	50
9_03	0.653	11.87	7.16	2.416	A + D	31	50
11_03	0.540	10.89	6.87	2.596	A + D	29	50
12_03	0.500	10.08	6.33	2.776	A + D	25	50
13_03	0.531	10.60	6.66	2.673	A + D	28	50
4_04	0.819	13.17	7.32	2.341	C + D	2	50
6_04	0.904	14.11	8.05	2.037	C + D	1	50
10_04	0.819	13.09	7.20	2.397	C + D	1	50
11_04	0.819	13.23	7.41	2.300	C + D	5	50
15_04	0.833	13.07	7.19	2.402	C + D	4	50
8_04	0.797	12.96	7.24	2.376	C + A	4	50
17_02	0.900	13.30	6.88	2.489	B	8	50
8_03	0.651	11.73	7.01	2.624	B	8	50

Notes: test A (24h load steps); test B (2h load steps); test C (controlled load rate); test D (reduction of applied suction up to null value); Sr_{in} (initial saturation degree); s_{in} (initial matric suction); s_{appl} (matric suction applied).
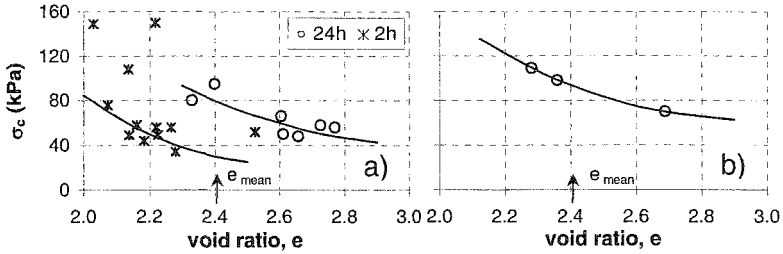
Figure 2. Apparent preconsolidation stress σ_c from oedometer tests with load permanence of 24h and 2h: (a) ED; (b) SCO with null suction.

Figure 3a shows that the values calculated from conventional tests with a Δt=2h are similar to those calculated with Δt=24h. Moreover the figure shows that C_α increases with (σ_v-u_a) in the preconsolidation field and it is almost constant and equal to 0.013 cm/min for a vertical net stress higher than σ_c. For this last stress field the secondary settlement is so evident that the deferred settlement δ_{def} (secondary settlement conventionally calculated at 28 days according to Pellegrino, 1967) has the same order of magnitude of the immediate one (δ_{im}). Since the deferred settlement at 28 days is larger than the 80% viscous settlement occurred in 10 years, in Figure 4 the total modulus [$E_{tot}=E_{im}*E_{def}/(E_{im}+E_{def})$], as calculated by the tests with Δt=2h and Δt=24h, is reported. The expression of E_{tot} is obtained considering that: (δ_{tot})$_{28days}$=δ_{im}+δ_{def} in which (δ_{tot})$_{28days}$ is the total settlement referred to 28 days. The figure shows similar results for two types of tests.

Effect of suction on stiffness and volumetric compressibility measured with oedometer tests.

To study the effects of suction on apparent preconsolidation stress, stiffness and volumetric compressibility, compression tests have been performed with suction controlled equipments using the axis translation technique. The effects of suction on these parameters have been shown in Figure 5. Figure 5a shows a trend of σ_c decreasing with increasing of void ratio and increasing with suction. At a void ratio equal to 2.40 the apparent preconsolidation stress increases its value to around 90
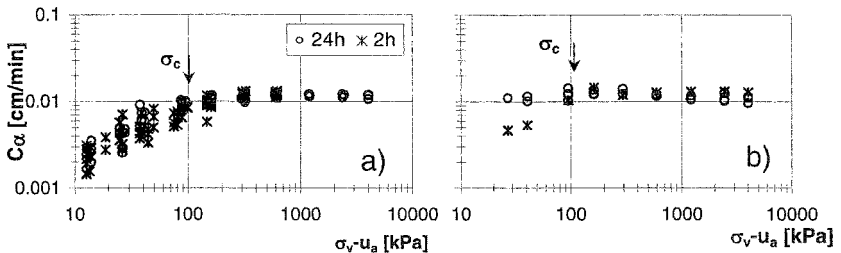
Figure 3. Values of creep coefficient C_α from oedometer tests with load permanence of 24h and 2h: (a) ED; (b) SCO with null suction.
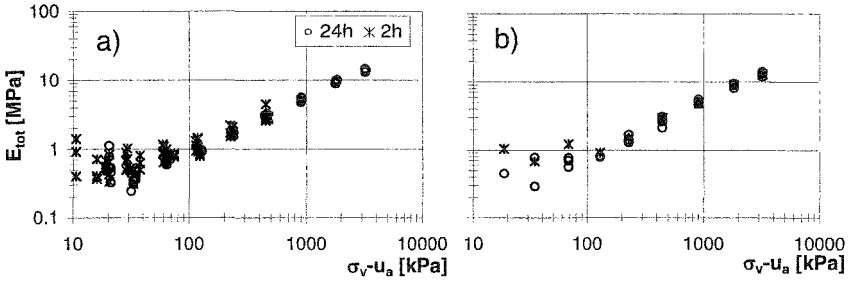
Figure 4. Total oedometer moduli from tests with load permanence of 24h and 2h: (a) ED; (b) SCO with null suction.

kPa as suction increases from 0 kPa to 50 kPa. The distribution of the creep coefficient C_α against the vertical net stress for the suction values of 0 kPa and 50 kPa is plotted in Figure 5b. In the preconsolidation field the values of C_α for null
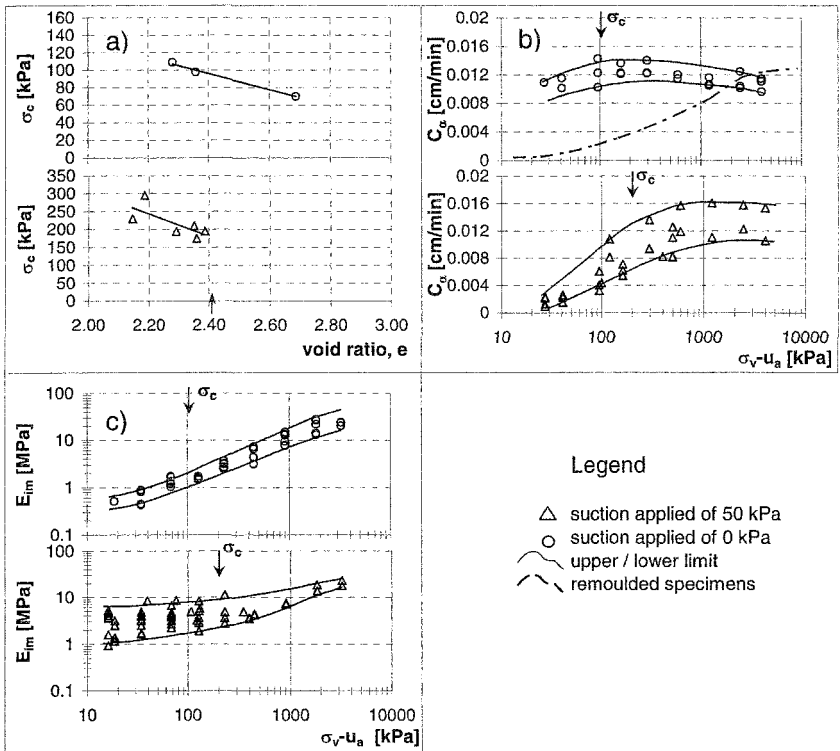
Figure 5. SCO tests with applied suction of 0 kPa and 50 kPa for $\Delta t=24h$ load permanence: (a) σ_c against initial void ratio (e_0); (b) C_α against (σ_v-u_a); (c) immediate modulus (E_{im}) against (σ_v-u_a).

suction are higher than those for suction equal to 50 kPa, although an increasing trend with the vertical net stress is shown for both. From the upper limit of C_α distribution and for $(\sigma_v$-$u_a)>\sigma_c$, values of 0.014 cm/min and 0.016 cm/min are reached respectively for suction equal to 0 kPa and 50 kPa. This figure also shows, with a dash-dot line, the mean distribution of the creep coefficient C_α for remoulded samples. This curve will be useful to explain the metastable structure in a following section dedicated to the soil behaviour at collapse. The immediate modulus (see Figure 5c) notably increases its value with the suction applied in the preconsolidation field. For high values of the vertical net stress $(\sigma_v$-$u_a)>\sigma_c$ E_{im} moduli are almost the same for both investigated suctions.

To analyze the settlement of the structure built in these soils after 28 days of constant load, the total modulus against the net vertical stress is reported in Figure 6. This figure shows a trend of E_{tot} similar to the immediate modulus (see Figure 5c), but obviously, with smaller values.

In Figure 7 the compressive index C_t is reported against the vertical net stress. This index represents the variation of void ratio with the logarithmic vertical net stress increment (Fredlund and Rahardjio, 1993). The absolute value of C_t increases with the stress for all explored values of suction, but with different gradients. In fact, for s = 0 kPa the gradient decreases monotonically with the vertical net stress, while for s = 50 kPa a similar behaviour is shown only for a stress higher than σ_c. There is a rapid variation of this gradient in correspondence of $(\sigma_v$-$u_a) = \sigma_c$, with a smaller gradient in the preconsolidation field.

The water content index D_t against the vertical net stress is reported in Figure 8. This index represents the variation of water content (ΔW) with the logarithmic vertical net stress increment (Fredlund and Rahardjio, 1993). The figure shows that the variation of D_t is limited for stress levels smaller than σ_c for both the suction values. Obviously, the water content variation is more evident for the lowest suction.

Effect of suction on stiffness measured with triaxial tests.

Conventional direct shear tests and suction controlled triaxial tests were performed on undisturbed pyroclastic samples to study the shear strength and the influence of suction on it (Bilotta et al. 2005). The data collected during the triaxial
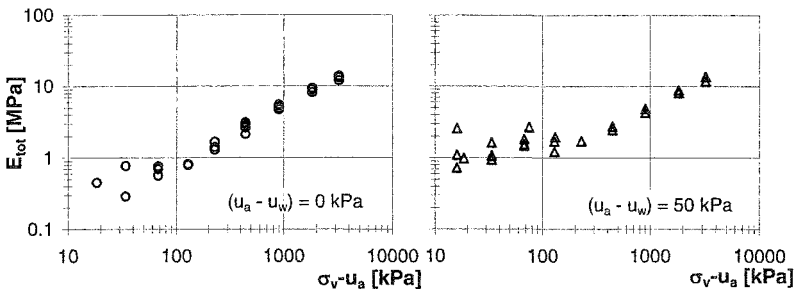
Figure 6. Suction effect on total oedometer moduli.
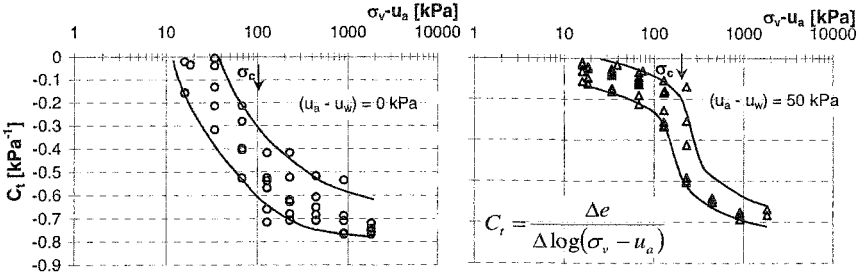
Figure 7. Trend of the C_t index with (σ_v-u_a) at 0 kPa and 50 kPa suction applied.

shear tests and some isotropic compression tests are used for a preliminary study on the volumetric compressibility and stiffness of these soils. The initial physical properties of the tested specimens and the kind of tests performed are reported in Table 2. These tests have been essentially carried out to calibrate a constitutive model on these soils in unsaturated conditions, as it will be shown in a future paper. The isotropic tests are only used to examine the influence of suction on the deformability parameters even if such parameters are also influenced by the initial void ratio. These tests have shown, in the preconsolidation field, an anisotropic behaviour of the material with values of $\Delta\varepsilon_r/\Delta\varepsilon_a$ ranging from 6 to 1 although an influence of suction is not evident. The soil exhibits an isotropic behaviour for high values of mean net stress.

To examine the stress-strain behaviour of these soils, with reference to F type triaxial tests (see Table 2), all the following pieces of information are taken: measurement of the initial suction; volumetric variation of the pore water ε_w and of the solid phase ε_v during all the test stages (equalization under imposed suction, consolidation and shear). The value of ε_w is defined by $\Delta V_w/V$, where ΔV_w is the water volume variation and V is the initial specimen volume.

The equalization of the imposed suction was attained after at least one week. The values of the volumetric variation of the pore water phase are clearly higher than those of the solid phase (ε_w=5-10% while ε_v=0.1-0.9%). During the consolidation stage, the volumetric variation of the solid phase is always larger than that of the water phase. The values of the creep coefficient are of the same order than those calculated from the oedometer tests at corresponding stress levels.
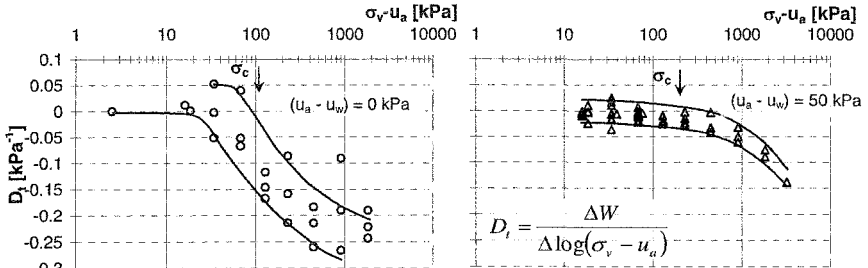
Figure 8. Trend of the D_t index with (σ_v-u_a) at 0 kPa and 50 kPa suction applied.

Table 2. Soil specimen physical properties and test type.

Specimen	Sr_{in}	γ kN/m^3	γ_d kN/m^3	e	test type	s_{in} kPa	s_{appl} kPa
10RMC	0.650	11.76	7.29	2.240	F	34	10
11RMC	0.500	11.13	7.70	2.180	F	56	10
12RMC	0.690	12.31	7.54	2.240	F	14	10
13RMC	0.813	12.81	7.08	2.389	F	5	10
14RMC	0.840	13.10	7.22	2.323	F	5	10
5R	0.830	12.97	7.15	2.400	F	4	10
8RMC	0.650	12.46	8.18	1.910	F	13	20
9RMC	0.630	12.22	8.02	1.970	F	14	20
17RMC	0.807	12.71	6.99	2.432	F	4	20
4R	0.730	12.86	7.91	2.100	F	9	50
6RMC	0.650	12.38	8.13	1.930	F	4	50
7RMC	0.710	12.37	7.39	2.310	F	10	50
b8	0.901	13.26	7.28	2.357	IRL	-	0
b9	0.838	12.84	6.93	2.528	IRL	-	0
4i	0.806	12.80	7.14	2.363	IRL	4	10
7i	0.780	12.63	7.09	2.447	IRL	4	10
5i	0.858	13.46	7.59	2.162	IRL	2	20
6i	0.822	13.00	7.28	2.298	IRL	3	20
8i	0.551	10.86	6.90	2.542	IRL	32	50

Shear tests were performed with a deformation rate of 0.1%/h. In this stage the material exhibits a contractive behaviour for all values of the suction applied (s = 10, 20, 50 kPa) with an isotropic consolidation net stress of 30 kPa and 50kPa; instead, for an isotropic consolidation net stress of 10 kPa the soil has a dilatant behaviour which increases with suction. At failure, the volumetric deformation of contractive specimens does not exceed 5-10%, while ε_w is significantly lower. From these tests and in particular from the $(q-\varepsilon_a)$ graphs of the shear stage, the values of E_{50} moduli were obtained. This quantity represents the secant modulus at 50% of the failure deviatoric stress (q_f). The variation of E_{50} with suction is represented in Figure 9a. Since the consolidation pressure is lower than the apparent preconsolidation stress and the number of tests is limited, in this figure all the values of E_{50}, referred to an isotropic consolidation net stress of 30 kPa and 50 kPa, are globally interpolated. Secant oedometer moduli are reported in Figure 9b. These moduli are calculated from oedometer tests with various suction applied and they refer to the stress range $[(\sigma_v-u_a)_i \,; (\sigma_v-u_a)_f]$.

In order to compare the triaxial modulus E_{50} and the oedometer modulus E_{ed}, the value $(\sigma_v-u_a)_i$ on the oedometer path (point 1 in Figure 9c) corresponds to the mean net stress $[(p-u_a)=p_{con}$ with q=0] of the triaxial test (point 2) and the value $(\sigma_v-u_a)_f$ (point 3) corresponds to the mean net stress on the triaxial path with a deviatoric stress equal to half of failure value $[(p-u_a)=p_{50}$ with $q=q_f/2]$ (point 4). Hence

$$\left(p-u_a\right)_{con;50} = \frac{1+2K_0}{3}\left(\sigma_v-u_a\right)_{i;f} \Rightarrow \left(\sigma_v-u_a\right)_{i;f} = \frac{3\left(p-u_a\right)_{con;50}}{1+2K_0}$$

K_0 value was obtained by $K_0=1-\sin\varphi'$, with an effective friction angle equal to 34°
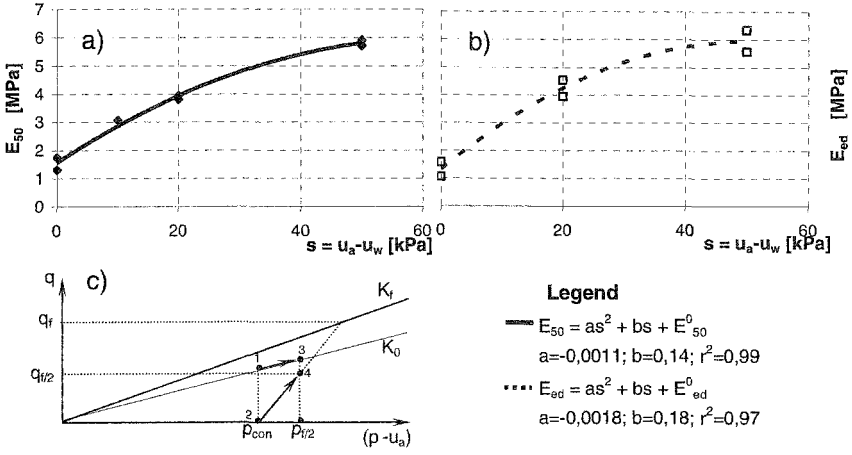
Figure 9. Suction effect on the stiffness: (a) triaxial modulus E_{50}; (b) oedometer modulus E_{ed}; (c) vertical net stress range kept on oedometer curve by calculate the secant modulus.

(Bilotta et al., 2005). Its value has been verified by performing a drained triaxial anisotropic compression test on a saturated sample using a Bishop apparatus. In this test the recorded radial deformation was always null. The E_{50} moduli increse with suction, similarly to the oedometer moduli, although the latter are slightly higher.

Collapse

The open structure of such soils induces a metastable behaviour (collapse) when the suction is reduced (wetting). Oedometer suction controlled tests have been performed to investigate the variation of the collapse settlement with the intensity of net vertical stress applied. The collapse also occurs when the vertical net stress is very low. An initial slight swelling, always followed by collapse, has been recorded only for values of net vertical stress lower than 30 kPa in correspondence of null suction values (s = 0 kPa).

In Figure 10 the variation of the height of the specimens (h) against the net vertical stress is reported in logarithmic scale. Test number 1 was performed on a submerged specimen (null suction) while test number 2 was performed on a specimen with a constant suction of 50 kPa for all load steps. Tests from number 3 to number 5 were performed on specimens with an initial suction of 50 kPa decreasing until s= 0 kPa under a load of 41 kPa, 120 kPa and 500 kPa respectively. The figure shows decreasing collapse settlement with increasing vertical net stress. The time reported in the figure (t_{collap}) refers to a complete development of the collapse settlement, while Δh_{collap} represents the entity of collapse. t_{collap} is the time needed to attain the equalization of the imposed suction when an HAEV porous stone is used. Really, the collapse occurs instantaneously when the suction is set to zero. This last circumstance is confirmed by tests performed on specimens in which suction has been suddenly set to zero, by submerging them with distilled water (data not
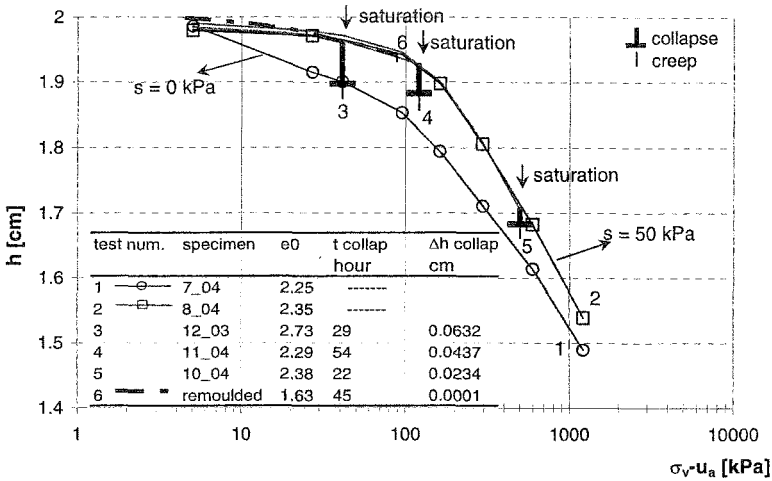
Figure 10. Collapse values at various net vertical stress and for intact and remoulded specimens.

reported).

The result obtained on a remoulded specimen, which has been loaded to 90 kPa under a constant suction of 50 kPa, is also reported in the same figure with a dash-dot line. At vertical net stress of 90 kPa the suction has been annulled, but any collapse occurred. In this stage, the only recorded settlement is a creep settlement, developed in the equalization time, according to the creep coefficient for remoulded specimens (see Figure 5b).

Conclusions

The pyroclastic soils covering Pizzo d'Alvano massif are usually in partially saturated condition and are characterized by viscous properties and by an open structure. The aim of this study is to increase the knowledge on the mechanical behaviour of these soils. In this paper the preliminary findings of the influence of suction on the stress-strain behaviour are reported and here summarized:

- The primary settlement occurs in a short time and since no substantial differences between the oedometer tests carried out with a time load of 2h and 24h have been observed, it can be assumed that 2 hours are satisfactory to analyze the deformability and viscous properties of these soils;
- The primary settlements are of the same magnitude of the deferred settlements calculated for a load application time of 28 days. The total settlement at 28 days represents a considerable amount of the settlement which occurs during the lifetime of the works performed on this soil;
- As suction increases, the apparent preconsolidation stress increases; in the preconsolidation range, primary and deferred settlements reduce as well as the volumetric deformations of the solid phase and the variation of the water content;
- The number of isotropic triaxial tests performed is not sufficient to provide

indications about the suction effect on the stress-strain behaviour. The soil behaviour is anisotropic only for stress lower than the apparent preconsolidation stress, but the suction effect is not well defined.
- The immediate oedometer modulus (E_{im}) and the triaxial modulus referred to 50% of the failure deviatoric stress (E_{50}) can be expressed, in the low stress range analyzed, by a polynomial function like $E = a \cdot s^2 + b \cdot s + E_0$;
- For high stress levels, all the deformability parameters of the solid phase are not influenced by suction;
- Finally, by observing the collapse phenomenon on undisturbed and remoulded specimens it is possible to assess a metastable structure in the first ones and, on the contrary, a lacking of collapse in the others.

References

Bilotta, E., and Foresta, V. (2001) *Sulla resistenza a taglio di alcune piroclastiti dei monti di Sarno*, Report n. 20, Dept. of Civil Engineering, University of Salerno, 26 pages. (in Italian).

Bilotta, E., and Foresta, V. (2002) On the measured shear strength of some pyroclastic soils of Sarno mountains, in *Proc. of the 3rd International Conference on Unsaturated Soils,* Recife, Balkema, Rotterdam, Vol 2, pp. 495-500.

Bilotta, E., Cascini, L., Foresta, V., and Sorbino, G. (2005) Geotechnical characterisation of pyroclastic soils involved in huge flowslide, *Geotechnical and Geological Engineering* **23**, 365-402.

Cascini, L. and Sorbino, G. (2002) Soil suction measurement over large areas: a case study, in *Proc. of the 3rd Int. Conf. on Unsaturated Soils,* Recife, Balkema, Rotterdam, Vol 2, pp. 829-834.

Fredlund, D.J. and Rahardjio, H. (1993) *Soil mechanics for unsaturated soils.* John Wiley & Sons Inc, New York.

Hilf, J.W. (1956) *An investigation of pore-water pressure in compacted cohesive soil*, Ph. D. Dissertation, Tech. Mem. Dept. of the Interior, Bureau of Reclamation, Design and Construction Div., Denver, CO., U.S..

Nicotera, M.V. (1998) *Effetti del grado di saturazione sul comportamento meccanico di una pozzolana del napoletano,* Ph.D. Thesis, University of Naples, 1998. (in Italian).

Pellegrino, A. (1967) Proprietà fisico-meccaniche dei terreni vulcanici del Napoletano *Proc. of VIII Conv. Italiano di Geotecnica, Cagliari,* **3**, 113-146. (in Italian).

Rampino, C. (1997) *Comportamento meccanico di una sabbia limosa ed argillosa costipata parzialmente satura,* Ph.D. Thesis, University of Naples, 1997. (in Italian).

Richards, L.A. (1941) A pressure membrane extraction apparatus for soil suction, *Soil Science* **51**, 377-386.

Sorbino, G. and Foresta, V. (2002) Unsaturated hydraulic characteristics of pyroclastic soils, in *Proc. of the 3rd International Conference on Unsaturated Soils,* Recife, Balkema, Rotterdam, Vol 1, pp. 405-410.

A microstructural model for the volume changes of unsaturated clayey soils due to wetting

V. Ferber[1], J.C Auriol[1], J.P. Magnan[1], Y.J. Cui[2], E. De Laure[2], C. Gerente[3]

1: LCPC, France, E-mail : ferber@lcpc.fr, auriol@lcpc.fr, magnan@lcpc.fr
2 : ENPC-Paris, E-mail : cui@cermes.enpc.fr, delaure@cermes.enpc.fr
3 : Ecole des Mines de Nantes, E-mail : gerente@emn.fr

Abstract
Soil microstructure is a key parameter of the swelling behaviour of fine-grained soils, but the detailed mechanisms of its role are still insufficiently described and understood. The paper proposes a novel microstructural model which permits to quantitatively describe the evolution of aggregate and inter-aggregate void ratios of plastic compacted clays upon wetting. The interpretation of wetting tests on the basis of this microstructural model shows that the macroscopic swelling due to wetting is resulted from an increase of aggregate void ratio and a decrease of inter-aggregate void ratio. Moreover, the inter-aggregate void ratio decrease seems to be proportional to the inter-aggregate void ratio before wetting. Mercury intrusion porosimetry tests performed on samples before and after wetting confirm the relevance of the microstructural model and the wetting tests interpretation.

1 Introduction

Soil microstructure is defined as the arrangement of particles and voids (Collins and McGown, 1974), which involves particles size and shape, particles orientation and position, pore size distribution and particles cementation, etc. The implication of microstructure in the wetting-induced volume change has been mentioned by many authors and some experimental results clearly suggest that particles organization controls part of the volume change (Gens *et al.*, 1995). However, the influence of microstructure on wetting behaviour has not been clearly demonstrated and quantified until now. Two main reasons could explain this situation :

- the description and quantification of parameters related to microstructure requires special devices and methods as electron microscopy, porosimetry, X-ray diffraction etc., with generally special sample preparation techniques. This does not allow extensive tests. Moreover, all existing preparation procedures disturb the microstructure, thus affecting the results quality (Delage *et al.*, 1996) ;

- a large number of parameters control wetting volume change since both initial conditions (water content, void ratio) and soil nature (Holtz and Gibbs, 1956 ; Seed *et al.*, 1962) can play an important role. Since in most cases the effects of all these parameters appear at the same time, it is difficult to distinguish the specific effect of each parameter.

In this paper, a method aiming at establishing the link between microstructure and wetting behaviour is proposed and evaluated. The target solution is to define a simple but quantitative microstructural model which accounts for the relationships between initial conditions and microstructural parameters, on the basis of current knowledge and specific microscopic observations. Wetting tests performed on a plastic clay are interpreted using this model and the results of this interpretation are confronted to mercury intrusion porosimetry tests.

2   A new quantitative microstructural model

The proposed microstructural model has not the ambition to take into account all the microstructural parameters involved in volume change behaviour, but only focuses on voids distributions. This is mainly for two reasons :

- it has been observed that these parameters are sufficient to establish a link between microstructure and macroscopic behaviour;
- the microstructural parameters defined can be easily quantified using simple conventional parameters;

This does not mean that no other parameters could bring more information to the understanding of the links between microstructure and macroscopic behaviour. The proposed model should be considered only as a new step that must be complemented by further studies, taking into account more microstructural parameters if necessary.

In the following, the assumptions made in the model will be first presented on the basis of microscopic observations and then a presentation of the model formulation will be made.

2.1   Basic observations

During the last forty years, various researchs on soil microstructure brought numerous results and observations concerning the organization of particles in elementary levels (Bennet and Hulbert, 1986). The mineralogical nature of clay particles, their proportion, moisture content and dry density have been found to be chief parameters affecting the microstructure. In order to have a general model, it is interesting to underline the common points of different soils microstructures.

The first common point is the major difference between clay and non clay particles. The former have a distinctive flat shape, large specific surfaces, high cation exchange capacities and, more generally, a specific physico-chemical activity and then a strong affinity for water. On the contrary, non clay particles have almost no physico-chemical activity and their affinity for water is much lower. Consequently, in fine-grained soils, the clay particles proportion is a chief parameter, which

determine whether the clay fraction will control the whole soil behaviour, or whether the macroscopic behaviour will be partly affected by clay activity and partly by non clay particles mechanical interactions.

The second common point deals with clay particles organization. All microscopic observations show that, whatever the mineralogical nature of clay particles (kaolinite, illite, smectite etc.), all these active particles are within an aggregate-like organization. Moreover, the smallest aggregates are gathered in big aggregates, which themselves are gathered in bigger aggregates, leading to a fractal organization of aggregates and voids (Moore and Donaldson, 1995 ; Gimenez *et al.*, 1997). This organization leads to define two types of voids (Alonso *et al.*, 1999) :

- intra-aggregate voids, which are located in clay aggregates ;
- inter-aggregate voids, which are located between clay aggregates.

The third common point concerns the place of water in an unsaturated compacted soil as compacted soil. A formal answer to this point can be brought by simple considerations on suction, since water is located where suction is the highest. In a fine-grained soil, the highest suction component is due to adsorption forces at the contact of clay particles. A lower component is the capillary suction, which increases when pore size decreases, according to the Jurin-Laplace law. Since the smallest pores are intra-aggregate pores, the suction of the soil is supposed to be predominantly defined by intra-aggregate pores. Consequently, the water should be preferentially attracted by intra-aggregate pores and should fill in inter-aggregate pores only when the adsorption and capillary suction in aggregates are compensated. Thus, the fact that all water is located in aggregates suggests there is no water in the inter-aggregate voids of an unsaturated fine-grained soil. In the proposed model, it will also be assumed that aggregates are fully saturated and there is no air in the intra-aggregate voids.

These theoretical considerations can be confronted to reality thanks to the Environmental Scanning Electron Microscope (ESEM), which gives the opportunity to observe wet samples without any special preparation. It's possible to wet a compacted sample inside the microscope and to see where the water is preferentially attracted. This was performed in this study on the clay fraction of a silty soil (Figure 1). It is observed that the first wetting stage leads to a saturation of aggregates (Figure 1-B) and that filling of large inter-aggregate pores occurs only in a second time (Figure 1-C).

Observations made using Mercury Intrusion Porosimety (MIP) showed that void ratio decrease leads to a reduction of inter-aggregate voids volume only, and to almost no variation of intra-aggregate void volume. This means that the compaction process has a direct effect on the inter-aggregate volumes but does not affect the intra-aggregate pores (Wan *et al.*, 1995 ; Delage *et al.*, 1996).
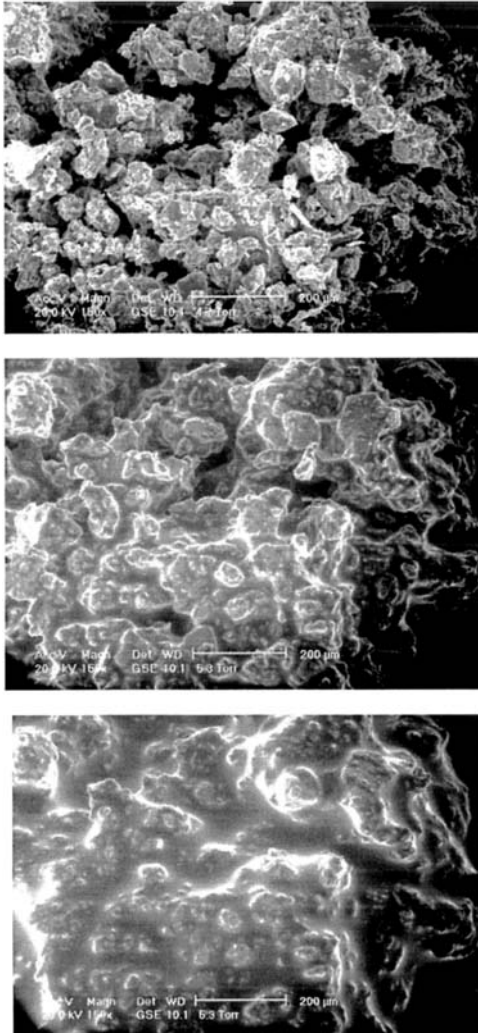
Figure 1. ESEM observation of clay particles at different stages of wetting (A : before wetting ; B : after aggregates filling is completed ; C : after inter-aggregate filling is completed).

2.2   Model formulation

Based on the previous observations and assumptions, a quantification of intra-aggregate and inter-aggregate void ratio can be undertaken. This constitutes a microstructural model, supposed to be relevant for unsaturated soils.

Firstly, the intra-aggregate void ratio, noted e_{ag}, will be defined as the ratio between the intra-aggregate voids volume, V_{ag}, and the solid volume, V_s. It must be noted that the solid volume is the volume of all particles, independently of their nature (clay or non clay particles). On the contrary, the intra-aggregate voids volume is the volume of voids in clay aggregates. According to the previous discussions, all water is located within aggregates and all aggregates are supposed to be fully saturated. This leads to write the intra-aggregate void ratio as the ratio between water volume, V_w, and solid volume and, consequently, as the product between massic water content, w, and specific density of particles, ρ_s, divided by the density of water assumed to be equal to 1 Mg/m³ (Equation 1).

$$ e_{ag} = \frac{V_w}{V_s} = \frac{w\rho_s}{\rho_w} \tag{1} $$

This equation reflects a linear relationship between water content and intra-aggregate void ratio (Figure 2).
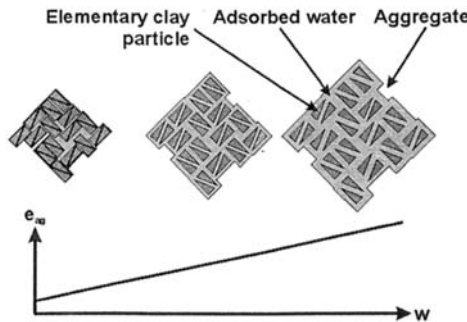
Figure 2. Schematic representation of the effect of water content, w, on aggregate void ratio, e_{ag}.

Secondly, since all air is in inter-aggregate voids and all water is in the intra-aggregate voids, the inter-aggregate voids volume is equal to the air volume, and therefore, the inter-aggregate void ratio, $e_{i\text{-}ag}$, is equal to the difference between the global void ratio, e, and the intra-aggregate void ratio, e_{ag} (Equation 2).

$$ e_{i-ag} = e_{air} = e - e_{ag} = e - \frac{w\rho_s}{\rho_w} \tag{2} $$

Figure 3 illustrates schematically the implication of this equation on the microstructure of an unsaturated soil and shows the combined effect of water content and dry density on microstructure.
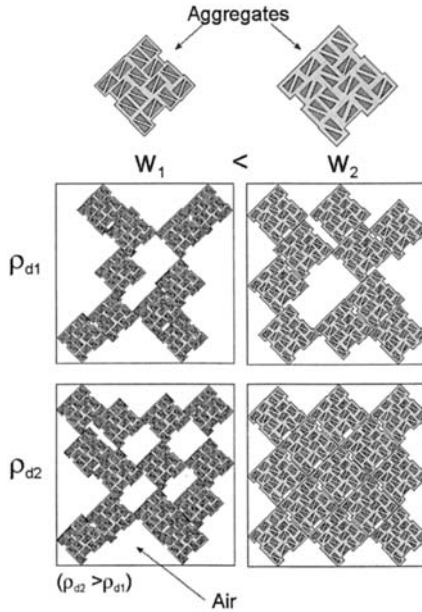
Figure 3. Schematic representation of the combined influence of dry density and water content on microstructure.

The formulation of the model is quite simple with only two microstructural parameters. The parameters determination can be done using conventional geotechnical parameters as water content, dry density and specific density of particles. It can be noticed that the clay content is not useful in the model, since the clay intra-aggregate volume is controlled by water content.

3 Materials and experimental procedure

All the tests presented here were done on a high plasticity clay from northern France. This soil contains 66% of clay particles ($C_{2\mu m}$) consisting of 60% smectite and 40% illite. This leads to a high liquid limit w_L, plasticity index I_P, methylene blue value V_{bs}, standard Proctor optimum water content w_{OPN} and cation exchange capacity CEC (Table I).

Table I. Geotechnical properties of A34 clay.

w_L (%)	I_P	$C_{2\mu m}$ (%)	ρ_s (Mg/m^3)	w_{OPN} (%)	$\rho_{d,OPN}$ (Mg/m^3)	Methylene blue value (g/100 g)	CEC (cmol+/kg)
98.1	61	66	2.71	28	1.45	10.66	41.2

The soil was air-dried and sieved through a 2 mm sieve. It was then wetted at different water contents and left in sealed bags for at least one day. The samples were prepared by compaction using a mini-hammer (Figure 4). Six different initial water contents (Figure 5) and, for each water content, six different dry densities are considered.

Moving mass : 1,039 kg
Drop height : 50 mm
Hammer diameter : 23 mm
Thickness of compacted soil : ~ 25mm
Sample diameter : 70 mm
Number of blows by layer : 56
Volumic energy ~ 593 kN.m/m^3

B – Main characteristics

A – The mini hammer

C – Distribution of the blows in the oedometric mold
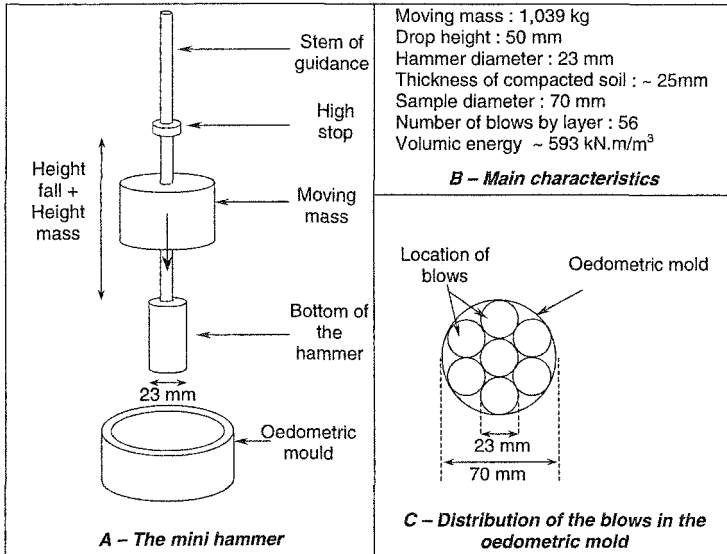
Figure 4 : Characteristics of the mini-hammer

Wetting tests (or free swell tests) were performed in conventional oedometers, Unsaturated compacted samples were loaded under 3 kPa vertical stress and left until mechanical equilibrium. Then, the oedometer cells were filled with de-ionised water and settlement was recorded until a new equilibrium was observed. The main result of the test is the void ratio at equilibrium states.

4 Wetting tests results

The presentation and interpretation of the tests will aim at describing the effects of initial inter-aggregate void ratio, $e_{i\text{-ag}}$, on the global void ratio, e, at the main stages (after compaction, after inundation). As a matter of fact, we do think that the evolution of inter-aggregate volume under hydro-mechanical effects is a capital phenomenon. In this regard, some discussions have already been made by different authors on whether this evolution is positive or negative (Alonso et al., 1999). It seems interesting to refer to the microstructural model in these discussions.

4.1   Experimental results

The results of wetting tests are presented in a graph were the global void ratio after swelling is reported versus the inter-aggregate void ratio before swelling. The results (Figure 5) indicate that there is a linear relationship between these two parameters. This relationship means that the higher the inter-aggregate void ratio before swelling,
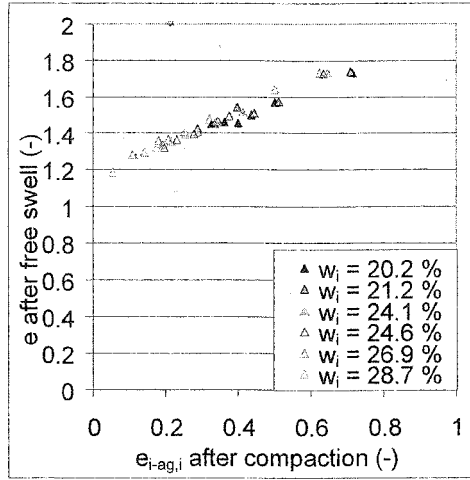
Figure 5. Influence of initial inter-aggregate void ratio, e_{i-ag}, on the global void ratio, e, after free swell.
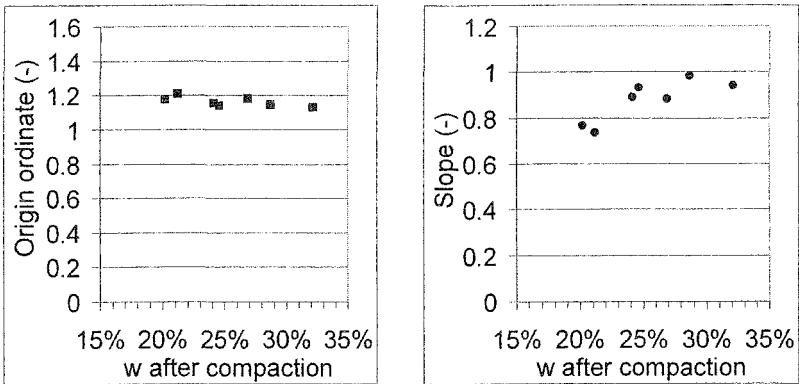
Figure 6. Influence of the molding water content on the origin ordinate and slope of linear relationship between inter-aggregate void ratio, e_{i-ag}, and global void ratio, e, after free swell.

the higher the global void ratio after swelling. Moreover, the relationship can be easily described using the intercept point and slope calculated by a linear regression (Figure 6).

It can be observed that the intercept point is almost not sensitive to the molding water content (Figure 6), showing only small erratic variations around a mean value of 1.16. On the contrary, the slope is clearly influenced by the molding water content and the trend shows that the lower the molding water content, the smaller the slope.

4.2   Microstructural interpretation

According to the microstructural model, the origin ordinate would correspond to the void ratio after swelling of a sample containing no inter-aggregate volume. Thus, the behaviour of such a sample would represent the behaviour of aggregates alone. In others words, the origin ordinate could be considered as the void ratio of aggregates after swelling, and it seems to be independent of the molding water content and dry density.

A microstructural interpretation of the slope can be made on the basis of a simple mathematical approach :

-   before wetting (Equation 3), the global void ratio, e_i, is the sum of inter-aggregate and intra-aggregate void ratio, respectively $e_{i-ag,i}$ and $e_{ag,i}$, as defined by the model;

$$e_i = e_{i-ag,i} + e_{ag,i} \qquad (3)$$

-   after swelling, a similar equation can be written (Equation 4). Because experimental results also indicate a linear relationship between void ratio after swelling, e_f, and inter-aggregate void ratio before swelling, therefore equation 5 can be given, where α and β are repectively the slope and the origin ordinate of the relationship. If it is assumed that aggregate void ratio after swelling $e_{ag,f}$ is a constant (equal to β here), equations 4 and 5 lead to a new expression (Equation 6). This equation suggests that the slope is the ratio of inter-aggregate void ratio after swelling, $e_{i-ag,f}$, to inter-aggregate void ratio before swelling $e_{i-ag,i}$. Thus, the lower the slope, the higher the inter-aggregate volume loss due to swelling.

$$e_f = e_{i-ag,f} + e_{ag,f} \qquad (4)$$

$$e_f = \alpha \cdot e_{i-ag,i} + \beta \qquad (5)$$

$$\alpha = \frac{e_{i-ag,f}}{e_{i-ag,i}} \qquad (6)$$

In conclusion, the experimental results interpretation using the microstructural model has shown that macroscopic swelling is the result of two opposite microscopic phenomena, namely an aggregate void ratio increase, due to water adsorption, and an inter-aggregate void ratio decrease, probably due to the re-organization of aggregates during the wetting process. The microstructural model enables a quantification of these phenomena.

The linear relationship between the global void ratio after swelling and the inter-aggregate void ratio before wetting suggests that the inter-aggregate void ratio after swelling is proportional to the inter-aggregate void ratio before wetting.

5   *Porosimetry results*

In order to evaluate the previous interpretations, MIP observations were performed on samples before and after swelling. The samples tested were all compacted at a molding water content of 22%, at three different void ratios. They were then dried by lyophilisation allowing satisfactory microstructure preservation.

The MIP results on samples before swelling (Figure 7) show that:

- samples are characterized by a double structure of voids, with a micropores family (from 0.01 to 1 μm diameter), and a macropores family (> 10 μm diameter);

- micropores seem to be insensitive to compaction and can be assimilated to intra-aggregate pores ;

- macropores are highly affected by the compaction process; both mean diameter and global volume are reduced.

The MIP results on samples after swelling (Figure 8) show that :

- the double-pores families structure is not altered by the swelling phenomena in this clay ;

- the micropores family shifted towards larger pores, but the pore size distribution of this family is not affected by the molding void ratio. This observation supports our assumption about the independency of the aggregate void ratio after swelling on initial conditions ;

- macropores volumes decreased for all samples. This decrease is particularly noticeable for the high molding void ratio sample, showing the decrease of both macropores mean diameter and volume.

A comparison between microstructural parameters calculated from experimental results and from MIP results was performed (not presented here). It showed that the trends suggested by the model are well illustrated by MIP results (influence of inter-aggregate void ratio before wetting, for example). However, some non negligible discrepancies were also observed. They could be partly the consequence of microstructure modifications due to dessiccation, in spite of the particular attention paid to the lyophilisation process (Delage *et al.*, 1996), and partly the result of the bad representation of the small size samples used in MIP tests.
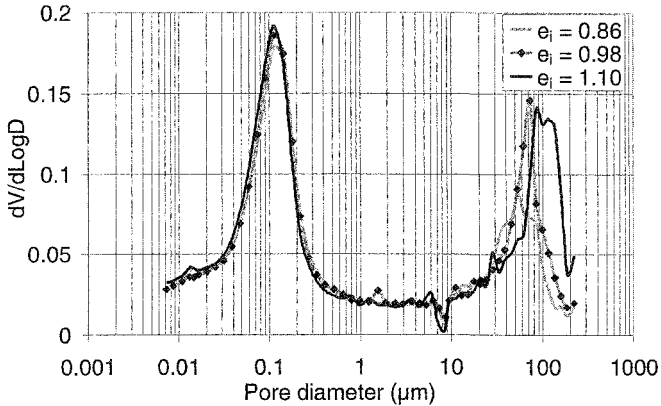
Figure 7. Influence of molding void ratio on pore size distribution after compaction.
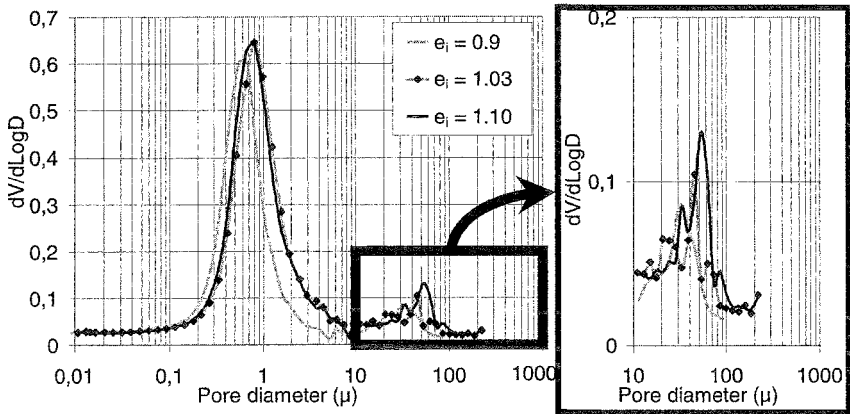
Figure 8. Influence of molding void ratio on pore size distribution after wetting tests (left-hand : all pores ; right-hand : macropores).

6   Conclusions

The microstructural model and the experimental results presented in this paper suggest a new approach to analyse wetting tests, on the basis of a quite simple quantification of microstructural parameters. This approach indicates that a macroscopic swell is the result of both an aggregate void ratio increase and an inter-aggregate void ratio decrease. This was supported by MIP observation. This

approach was applied to wetting tests under vertical stress and drying tests, showing its relevance in describing the volume change behaviour of unsaturated soils upon wetting.

Regarding the results and their interpretation, the main conclusions concerning the microstructure influence on swelling behaviour are as follows :

- the inter-aggregate volume variation due to wetting seems to be systematically a volume decrease, and no inter-aggregate volume increase has been described using the proposed approach. More experiments, in particular cyclic suction controlled tests, are necessary to confirm these observations;
- the inter-aggregate volume variation is proportional to inter-aggregate volume before wetting, which was a useful by a little surprising finding that would require more explanations and verifications ;
- as previously suggested by other authors (Alonso *et al.*, 1999), the irreversible behaviour of soils could be associated to inter-aggregate volume variations, whereas intra-aggregate volume is supposed to be reversible by the microstructural model.

Finally, the application of this approach to wetting tests on various soils showed that a relationship was also observed between aggregate void ratio after swelling and the liquid limit, confirming the intrinsic behaviour of aggregates in fine-grained soils.

7   References

Alonso E.E., Vaunat J., Gens A. (1999). Modelling the mechanical behaviour of expansive clays, *Engineering Geology*, vol. 54, n°2 pp. 173-183.

Benett R.H., Hulbert M.H. (1986). *Clay microstructure*, International human resources development corportation, Boston, 161 p.

Collins K., McGown A. (1974). The form and function of microfabric features in a variety of natural soils, *Géotechnique*, vol. 24, n°2, pp. 223-254.

Delage P., Audiguier M., Cui Y.J., Howat M.D. (1996). Microstructure of a compacted silt, *Canadian Geotechnical Journal*, vol. 33, n°1, pp. 150-158.

Gens A., Alonso E.E., Suriol J. (1995). Effect of structure on the volumetric behaviour of a compacted soil, *First int. conf. on unsaturated soils, UNSAT'95*, Paris, France, 6-8 sept 1995, pp. 83-88.

Gimenez D., Allmaras R.R., Nater E.A., Huggins D.R. (1997). Fractal dimensions for volume and surface of interaggregate pores - scale effects, *Geoderma*, vol. 77, n°1, pp. 19-38.

Seed H.B., Woodward R.J., Lundgren R. (1962a). Prediction of swelling potential for compacted clays, *Journal of the soil mechanics and foundation division, ASCE*, SM3, pp. 53-87.

Wan A.W., Gray M.N., Graham J. (1995). On the relations of suction, moisture content and soils structure in compacted clays, *First int. conf. on unsaturated soils, UNSAT'95*, Paris, France, 6-8 sept 1995, pp. 215-222.

Water Retention Properties and Volume Change Behaviour of Natural Romainville Clay

Yu-Jun Cui[1], Altin-Théodor Mantho[1], Kai Cui[2], Martine Audiguier[3]

1 : ENPC-Paris, fax : +33 1 64 15 35 62, E-mail : cui@cermes.enpc.fr, mantho@cermes.enpc.fr
2 : Institut National de la Recherche Agronomique, Unité d'agronomie de Laon-Péronne, E-mail : kai.cui@laon.inra.fr
3 : Ecole Nationale Supérieure des Mines de Paris, CGI, E-Mail : audiguier@cgi.ensmp.fr

Abstract

A good understanding of the water retention properties and volume change behaviour of swelling clays is important for the analysis of hazards related to clays swelling upon wetting or clays shrinking upon drying. In this paper, the results of Romainville clay from the basin of Paris are presented and discussed. The retention curve was determined together with the corresponding volume change behaviour. Two suction control methods were used: the osmotic method for low suction range (1 – 6.1 MPa) and the vapor equilibrium technique for high suction range (6.1 to 216 MPa). Both wetting and drying paths were followed. At each suction, when equilibrium was reached (which is characterized by weight stabilization), soil samples are weighed and their volume determined by using a mercury immersion system. The obtained results showed a good repeatability of the tests, attesting a satisfactory homogeneity of the studied soil. The air entry value 13.1 MPa which is quite high. Significant hysterisis was observed either on water content changes or on void ratio changes. But it clearly appears that this hysteresis only occurs at suctions lower than 131 MPa, beyond this value the soil behavior has been found to be recoverable. This observation confirms that at high suction only recoverable physico-chemical phenomena are involved.

Introduction

Hazards caused by drought have become more and more important over the world. In France, the extensive drought from 1989 to 1990 affected shallowly founded buildings of 216 communes in 17 departments (Vandangeon 1992). In the decree of 11.01.05 (French Official Journal 1.2), more than 870 communes were considered affected by the drought in 2003. Economically, the cost of damages related to the shrinkage/swelling phenomenon is enormous in France: for the period 1989-2002, 3.3 billion € was paid in compensation for drought-related damage, which represents

about 40% of all natural-disaster compensation. This does not account for the cost of the 2003 drought that is particularly high. From the point of view of unsaturated soil mechanics, theses hazards are related to the differential settlement or uprising resulting from soil shrinkage upon drying or soil swelling upon wetting. In this regard, understanding the water retention properties and volume change behaviour of the subject soil is important for hazards analysis.

In the region of Paris, the problematic soil is Romainville clay which is a swelling clay and usually named "Romainville green clay". In the present work, its water retention properties and volume change behavior were studied. The results show a satisfactory homogeneity of the studied soil. Significant hysterisis at suctions lower than 131 MPa; in the higher suction range the soil behavior has been found recoverable showing that only recoverable physico-chemical phenomena are involved.

Materials

Romainville clay was taken in blocks during a building construction project in the East of Paris; its initial water content was 38%. Initial suction was measured using a tensiometer; it is about 40 kPa. Grain size distribution analysis using sieving and sedimentation techniques showed that fine grains smaller than 80 µm is 92% and clay fraction (< 2 µm) represents 68%. The liquid limit is 95%, the plastic limit is 41%, defining a plasticity index of 54. According to Casagrande criterion Romainville clay is classified as highly plastic clay. The carbonates content in this clay is 13%, which is significant. The mineralogy analysis by X-ray diffraction showed that the clay fraction is composed of illite and smectite. Analysis in methylene blue gave a methylene blue value of 14.3 which corresponds to a specific surface of 340 m^2/g. Table 1 summarises the main geotechnical properties of Romainville clay.

Table 1. Main geotechnical properties of Romainville clay

Property	Romainville clay
Natural water content (%)	38
Liquid limit (%)	95
Plastic limit (%)	41
Plasticity index	54
In-situ suction (kPa)	40
Clay fraction (% < 2 µm)	68
Clay composition	Illite and smectite
Carbonates content (%)	13
Specific surface area, S (m^2/g)	340

Testing equipment and experimental procedure

The osmotic technique was used for suction control in the range from 1 to 6.1 MPa. This technique was initially developed by biologists (Lagerwerff et al. 1961), and later adopted by soil scientists (Zur 1966). It was introduced in geotechnical engineering by Kassiff & Benshalom (1971) and Delage et al. (1987). In this

technique, losses or uptake of water are caused by osmosis process. The soil sample is placed in contact with a semi-permeable membrane behind which is an aqueous solution of large sized polyethyleneglycol (PEG) molecules. Since water molecules can cross the membrane whereas PEG molecules cannot, an osmotic suction that increases with the PEG concentration is applied to the soil through the semi-membrane. Because water transfer takes place in the liquid phase and ions can cross the semi-membrane freely, the osmotic technique controls the matric suction of soil, and not the osmotic suction.

The relationship between osmotic pressure and PEG concentration is well known for two molecular weights (PEG 6 000 and 20 000). Williams and Shaykewich (1969) found a good agreement between different calibrations performed by various authors either by direct pressure measurement or by controlling the relative humidity induced by PEG solutions. The suction ranged from 0 to 1.5 MPa. Delage et al. (1998) extended this calibration up to 10 MPa. In this study, Delage et al's calibration curve was used and two PEG molecular weights were employed: PEG 20 000 for low suction (1 MPa) and PEG 6 000 for higher suction (2, 4 and 6.1 MPa). Special attention was paid to the sensitivity of semi-permeable membrane to bacteria attacks by adding penicillin drops to PEG solutions.

In the test, the soil sample is placed in a tube-shaped semi-permeable membrane and immersed in a PEG solution which is stirred by a magnetic stirrer to maintain its homogeneity. Detailed procedure was described in Cui & Delage (1996). The samples were prepared by coring into the natural soil bloc. Their dimension is about 25 mm in diameter and 40 mm high.

The vapor equilibrium technique was used to control the suction ranging from 6.1 to 216 MPa. This technique was described in Tessier (1984), Delage et al. (1998), Tang and Cui 2005). A common practice of this technique is to place soil samples on a rigid grid above a saline solution inside a desiccator. The saline solution imposes a relative humidity to the air. The soil suction is controlled due to the water vapour exchange between soil and the ambient air. Marcial et al. (2002) proposed using air circulation ensured by a pump in order to significantly reduce the equilibrium time, from 6 months down to 2 – 4 weeks.

In the test, small cubic samples (15 to 20 mm dimension) were prepared by trimming from the natural soil block. Some samples were subjected to drying processes only by following the suction change: 6.1, 13.1, 24.9, 82, 113, 136, 216 MPa; others were subjected to a suction cycle: 82, 113, 136, 216, 113, 24.9, 6.9 MPa. The salts used are summarised in Table 2. An air circulation technique was used to shorten the equilibrium time.

The volume change of specimens was monitored after each suction imposition using the vapour equilibrium technique. The soil samples were first weighed in air, then immersed in mercury, weighed again using a balance of 1/2000 accuracy. The obtained weights allowed the volume to be determined. In practice, it was necessary to calibrate the measurement device by performing a test without soil specimen.

Table 2. Salts used and their corresponding suction and relative humidity at 20°C temperature

Salt	Suction (MPa)	Relative humidity (%)
$CuSO_4.5H_2O$	6.1	95.7
$Na_2SO_3.7H_2O$	13.1	90.9
$(NH_4)SO_4$	24.9	83.5
$Mg(NO_3)_2$	82	55
K_2CO_3	113	44
$MgCl_2$	136	33
LiCl	262	15

Experimental Results

Figure 1 presents the water retention curve obtained using the osmotic technique in the low suction range. Continuous water content decrease is observed with increasing suction: the relationship is almost linear. Because no volume monitoring was carried out, it was not possible to draw any conclusions regarding the soil saturation state.
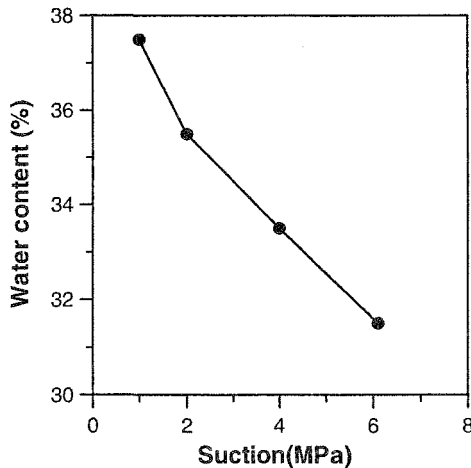
Figure 1. Water retention curve obtained using the osmotic technique (low suctions)

Figure 2 presents changes in water content, void ratio and degree of saturation with increasing suction applied using the vapour equilibrium technique. The zero suction state was also considered. The results obtained using the osmotic technique was not taken into account for lack of volume monitoring. Two specimens from the same soil block were tested. It was observed that

i)   the two samples show a similar response to suction change in terms of water content and void ratio, showing a good repeatability of the test on one hand and a satisfactory homogeneity of the soil on the other hand;

ii)   water content change is at three different rates: for 0 – 6.1 MPa suction a high rate was recorded and the water content goes down sharply from 38 to 18%; for 6.1 – 82 MPa suction, a moderate transition rate was recorded with a water content change from 18 to 10%; for 82 – 216 MPa suction a linear small change was recorded, from 10 to 4%;

iii)   as water content changes, void ratio change also occurs at three distinct rates: for 0 - 6.1 MPa suction the void ratio change is significant, from 1 to 0.6; for 6.1 – 82 MPa suction the change is smaller, from 0.6 to 0.37; for 82 – 216 MPa suction a linear relationship was obtained with a small slope, the void ratio change being from 0.37 to 0.34.

iv)   regarding the degree of saturation S_r, for suctions lower than 13.1 MPa, S_r is equal to 100%; when applying higher suctions, S_r starts to decrease. This clearly defines the air entry value of Romainville clay: 13.1 MPa; at 216 MPa suction, S_r is far from zero, equal to 30%, showing that this clay is quite plastic, in agreement with its high plasticity index (54); 30% must be close to the value of residual degree of saturation.

Figure 3 presents the changes in water content and void ratio when applying suction cycle using vapour equilibrium technique. As before, the zero suction state is also considered. Three samples were used in this test. It was observed that

i)   the three samples give almost the same response, reinforcing the excellent repeatability of the test and a good homogeneity of the tested material;

ii)   upon drying, the soil shows a significant water content change when the imposed suction is lower than 113 MPa, beyond that the change is slowed down with a linear relationship defined by a small slope;

iii)   upon wetting the soil shows a linear water content change with decreasing suction, the slope being the same as that during drying process in high suction range. This implies water change reversibility for high suctions (> 113 MPa) and significant irreversibility in the low suction range. This observation is consistent with that made by Fleureau et al (1993) who worked on kaolinite slurry;

iv)   regarding void ratio changes, the soil upon drying shows a significant volume change when suction was increased to 113 MPa and a linear change for higher suction application;

v)   upon wetting the soil shows a small linear change in almost the full working suction range; however, a trend of acceleration can be observed at suctions lower than 30 MPa: the void ratio increase seems to be speeded.

vi)   volume change reversibility is also observed in the suction range from 113 to 216 MPa and irreversibility is obtained in lower suction range.
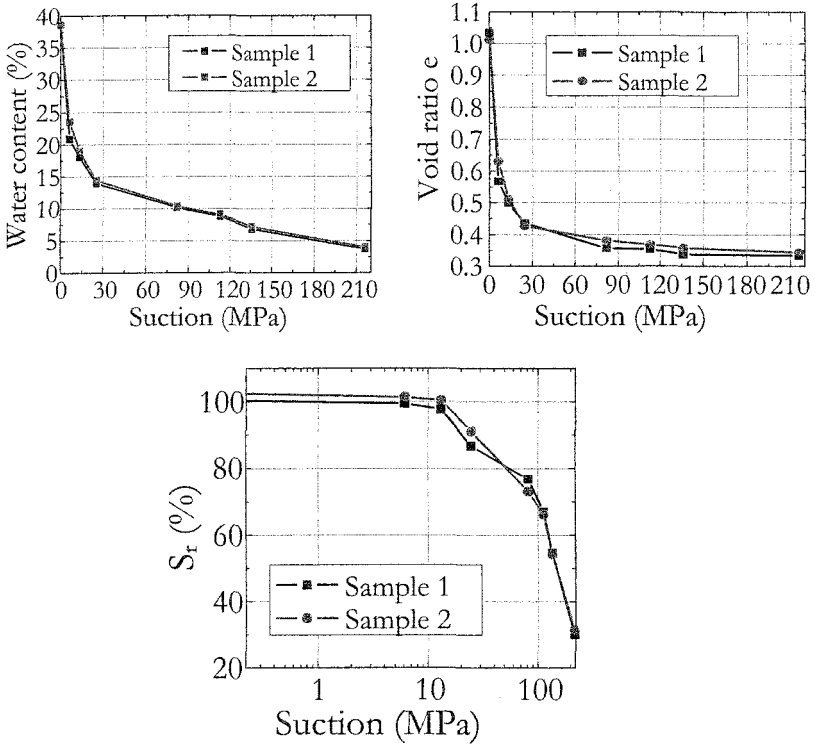
Figure 2. Changes in water content, void ratio and degree of saturation with increasing suction (vapor equilibrium technique)
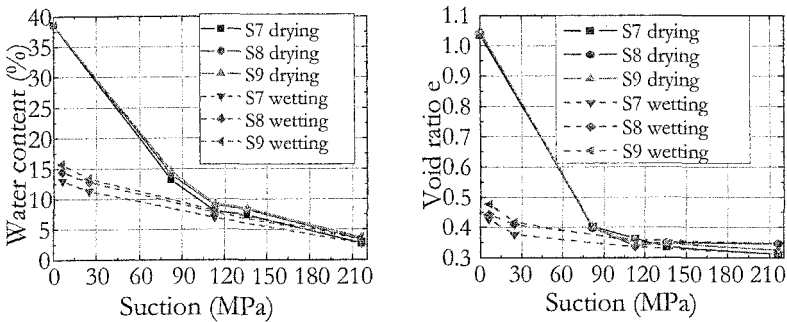
Figure 3. Changes in water content and void ratio when applying suction cycle (vapour equilibrium technique)

Discussion

The experimental results presented above show significant irreversible water content and volume change when applying suction from 0.04 MPa (natural state) to 216 MPa. The soil response to wetting paths showed however reversible changes in water content and void ratio in suction range from 113 MPa to 216 MPa. This observation can be explained by the mechanism defined by Olson and Mesri (1970) and Cui et al. (2002). This mechanism considers the main parameters involved in the volume change process when changing the suction in a swelling soil.

From a mechanical point of view, three parameters are considered.

i)   Clay particle shape, defined by the ratio d/e (diameter / thickness). The smaller is the d/e ratio, the more the material is rigid. Clays as kaolinite and illite have a small d/e ratio therefore a rigid behaviour; on the contrary smectite has a large d/e, presenting a flexible behaviour.

ii)   The geometric arrangement of particles, defined by the contact angle α between particles. The mechanical effect is more pronounced when α is large.

iii)   The surface friction, defined by the coefficient of friction μ. Mechanical effects are more important when μ is larger.

From a physicochemical point of view, there are also three parameters to be considered.

i)   The shape of clay particles: physicochemical effects are more significant with wide, flat (large d/e) and smooth particles.

ii)   The geometric arrangement of clay particles: when the contact angle α is small, i.e. the particles have almost a parallel arrangement, physicochemical interactions are more significant.

iii)   The other chemical variables considered are the surface charge density, the valence of adsorbed cations, the dielectric constant, the permittivity, the concentration of electrolyte and other less important factors.

The physicochemical effect only takes place in micro-pores between clays particles. For compacted soils, Delage et al. (1996) showed a microstructure defined by aggregates with inter-aggregate macro-pores. Clay particles are located in the aggregates. For these soils, Li (1995) and Romero (1999) observed that at low saturation degree, increasing soil density did not affect the soil. This observation showed that at low saturation degree, pore water is located within aggregates and the soil suction is totally defined by the suction in aggregates. Because mechanical compression does not modify the aggregates structure, the overall suction does not change. From a physicochemical point of view, because clay particles are not compressed by the mechanical effect, the distance between them does not change, therefore the corresponding suction does not change.

For a given swelling clay, the mechanism presented above shows that the contact angle is the only parameter to govern its volume change behaviour. In a macroscopic level this angle is represented by soil density or void ratio. Romainville clay in natural state has a quite low density (e = 1), its microstructure must be defined by a

dominating face to edge particle arrangement, with a large contact angle value. This is mainly due to the electrical charges of clay minerals. When suction is increased, water is expelled from the soil, giving rise to collapse of the face-edge structure and rendering clays particles more and more oriented (face to face structure). This microstructure collapse corresponds at a macroscopic level to irrecoverable volume change and water content change. When the contact angle becomes small enough, the microstructure becomes stable with respect to suction increases and the transition from face to edge structure to face to face structure ends, physicochemical effect prevails on mechanical effect. Further suction increase only affects the face to face distance, leading to small changes in void ratio and water content. This physicochemical effect is reversible.

The observed accelerated soil swell when suction is decreased to lower than 30 MPa is consistent with the results obtained on others soils. Cui et al. (2002) made a microstructure observation on compacted Kunigel V1 clay and Hostun sand mixture (70%/30% by mass) using mercury intrusion technique and scanning electron microscopy. They observed that when decreasing the soil suction from 57 MPa to zero, the microstructure change takes place significantly only when the suction is lowered down to 1 MPa. Figure 4 presents the soil microstructure at 57 MPa and zero suction. It appears that at 57 MPa suction, the soil aggregates and inter-aggregates pores are apparent. On the contrary, at zero suction the initial structure is completely destroyed and a relatively homogeneous microstructure is observed.

(a)   (b)
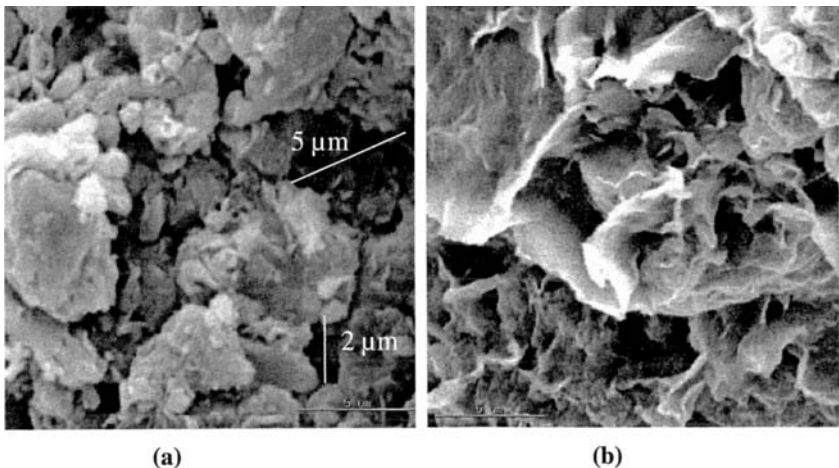
Figure 4. Microstructure of Kunigel V1 clay at different suction: (a) s = 57 MPa, (b) s = 0

Based on this observation, Cui (2002) proposed an idealised scheme for clay particle swelling: when the suction is low enough, the initially well oriented clay particles can go back to the face to edge arrangement, giving rise to significant swell. This is particularly the case for free swell condition.

Conclusion

In order to make an evaluation of the hazards caused by drought in the region of Paris, Romainville clay was studied in terms of changes in water content and void ratio. According to Casagrande criterion this soil is classified as highly plastic clay.

Both osmotic technique and vapor equilibrium technique were used for suction control in the range from 1 to 216 MPa. The volume change of samples was monitored by weighing in mercury after each suction imposition using vapour equilibrium technique.

The obtained results showed a good repeatability of the test and a satisfactory homogeneity of the soil. Significant irreversible change in water content and void ratio was observed when applying suction from 0.04 MPa (natural state) to 216 MPa.; the soil behaviour is nevertheless reversible in the high suction range (113 – 216 MPa). Interpretation was made by using an idealised mechanical and physicochemical scheme. The observed speeded soil swell when suction is decreased to lower than 30 MPa is consistent with the results obtained on others soils and can be explained by a microstructure change from face to face scheme to face to edge scheme due to repulsion force between clay particles.

References

Cui Y.J. & Delage P. 1996. Yielding and plastic behaviour of an unsaturated compacted silt. Géotechnique 46 (2), 291-311.

Cui Y.J. 2002. Experimental unsaturated soil mechanics (swelling, collapsible and compacted soils) : evaluation report. 3rd Int. Conf. on Unsaturated Soils, Recife, vol 3.

Cui Y.J., Loiseau C. and Delage P. 2002. Microstructure changes of a confined swelling soil due to suction controlled hydration. Proc. of the Third Inter. Conf. on Unsaturated Soils UNSAT2002, Recife, vol. 2, 593-598.

Cui, Y.J., Yahia-Aissa, M., Delage, P. 2002. A model for the volume change behaviour of heavily compacted swelling clays. Engineering Geology, 64(2-3): 233-250.

Delage P., Suraj De Silva G.P.R. & De Laure E. 1987. Un nouvel appareil triaxial pour les sols non saturés. Comptes-rendus de la 9ème Conf. Européenne de Mécanique des Sols et des Travaux de Fondations, Dublin, vol. 1, 26-28.

Delage P., Audiguier M., Cui Y. J. & Howat M. 1996. Microstructure of a compacted silty clay. Canadian Geotechnical Journal, Vol. 33, 150-158.

Delage P., Howat M. & Cui Y.J. 1998. The relationship between suction and swelling properties in a heavily compacted unsaturated clay. Engineering Geology, 50 (1-2), 31-48.

Fleureau J.M., Kheirbek-Saoud S., Soemitro R. & Taïbi S. 1993. Behaviour of clayey soils on drying-wetting paths. Canadian Geotechnical Journal 30 (2), 287-296.

Kassiff G. and Benshalom A. 1971. Experimental relationship between swell pressure and suction. Géotechnique 21: 245-255.

Lagerwerff J.V., Ogata G. & Eagle H.E. 1961. Control of osmotic pressure of culture
    solutions with polyethylene glycol. Science 133, 1486-1487.
Li Z.M. 1995. Compressibility and collapsibility of compacted unsaturated loessial
    soils. Proc. 1st Int. Conf on Unsaturated Soils UNSAT' 95 1, 139-144,
    Paris, Balkema, Rotterdam.
Marcial, D., Delage, P., and Cui, Y.J. (2002) « On the high stress compression of
    bentonites. » *Candadian Geotechnical Journal*, 39, 812-820.
Olson R. O. et Mesri G. 1970. Mechanisms controlling compressibilty of clays.
    Journal of Soil Mechanics and Foundation Division, Proceeding of the
    American Society of Civil Engineers. SM6, 1863-1878.
Romero E., Gens A. & Lloret A. 1999. Water permeability, water retention and
    microstructure of unsaturated compacted Boom clay. Engineering
    Geology. 54, 117-127.
Tang, A.-M. and Cui, Y.-J. 2005. Controlling suction by the vapour equilibrium
    technique at different temperatures and its application in determining the
    water retention properties of MX80 clay. Canadian Geotechnical Journal.
    42: 287-296.
Tessier, D. 1984. Étude expérimentale de l'organisation des matériaux argileux :
    hydratation, gonflement et structuration au cours de la dessiccation et de
    la réhumectation. Ph.D. thesis, Université de Paris VII, Paris, France.
Vandangeon P. 1992. Exemple de sinistres en région parisienne. Revue Française de
    Géotechnique, n°58, 7-14.
Williams J. & Shaykewich C. F. 1969. An evaluation of polyethylene glycol PEG
    6000 and PEG 20000 in the osmotic control of soil water matric
    potential. Can. J. Soil Science 102 (6): 394-398.
Zur B. 1966. Osmotic control the matric soil water potential. Soil Science 102, 394-
    398.

Unsaturated Properties of Mixtures of Waste Rock and Tailings

B.E. Wickland[1], G.W. Wilson[1], D.G. Fredlund[2], and D. Wijewickreme[3]

[1]Mining Engineering Department, University of British Columbia, 6350 Stores Road, Vancouver BC, V6T 1Z4; PH (604)-822-6781; FAX (604)-822-5599; website: http://www.wilson.mining.ubc.ca/

[2] Department of Civil and Geological Engineering, University of Saskatchewan, Saskatoon, S7N 5A9, Canada, PH (306) 261-8629; email: unsaturatedsoil@yahoo.com

[3]Department of Civil Engineering, University of British Columbia, 6250 Applied Science Lane, Vancouver, BC, Canada V6T 1Z4; PH (604) 822-5112; FAX (604) 822-6901; e-mail: dwije@civil.ubc.ca

Abstract:

Mixtures of mine waste rock and tailings, tailings alone, and waste rock alone were examined for soil-water characteristic curves (SWCC's) along the drying path. Laboratory data were compared with matric suction measurements and observations from a two year meso-scale column study of self-weight consolidation under free drainage. Waste rock alone had a near zero air-entry value and reached residual water content at low matric suctions. The mixture remained saturated relative to waste rock alone, a finding that was attributed to the presence of a fine-grained tailings matrix. The tailings had a high air-entry value, but also had significant volume change with increasing matric suction. The mixture had less total volume change than tailings for a given change in matric suction. The lower total volume change of mixtures was attributed to the presence of an internal "waste rock skeleton." Both the mixture, and tailings alone had SWCC's with a change in slope that was dominated by changes in volume, rather than a distinct air entry value (AEV), and a volume change correction was required to accurately determine the SWCC. Under prolonged drainage and/or high matric suctions, the mixture developed cracks within the tailings matrix. In general, the results indicate that mixtures can remain tension saturated for long periods of time relative to waste rock alone. Mixing for disposal therefore has the potential to limit the rate of acid rock drainage, particularly for wet climates.

Introduction
Problems associated with conventional methods of mine waste disposal have lead to an increasing interest in alternative disposal methods. Conventional disposal methods involve end dumping of waste rock in large piles and the impoundment of slurried tailings. The porous, open structure of waste rock piles allows convective flow of oxygen and has resulted in the problem of acid rock drainage (ARD). The semi-fluid structure of tailings in impoundments has, in combination with the upstream method of construction, resulted in catastrophic failures involving loss of life and environmental damages. Both ARD and potential for liquefaction failure are long term liabilities.

Mixing mine waste rock and tailings is an alternative disposal practice with the potential to limit the production of acid rock drainage (ARD) by maintaining a water saturated void space. This paper compares the soil-water characteristic curves (SWCC's) of a mixture of waste rock and tailings with waste rock alone, and with tailings alone. The laboratory derived SWCC's are also compared with results from a meso-scale column test described in Wickland and Wilson (2005).

Methods
Soil-water characteristic curves (SWCCs) for specimens of Carbon in Pulp (CIP) tailings and for a mixture of waste rock and tailings were obtained by Tempe Cell test. The mixture material was sampled during construction of a field scale experiment described by Wickland and Wilson (2005), and tested in a 150 mm diameter Tempe cell, shown in Figure 1.
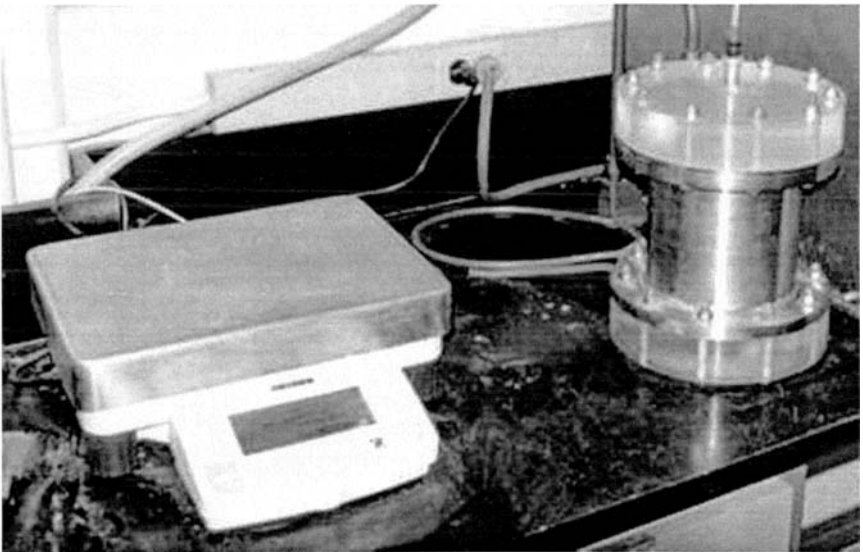
Figure 1. Large diameter Tempe cell with scale.

The tailings were taken from a mill circuit, thickened using a flocculant, and then tested in a standard Tempe cell ring. For both tests, specimen dimensions were measured to determine specimen volumes at the end of each pressure interval. The mixture specimen was constructed using altered sedimentary waste rock and tailings slurry. The SWCC of the altered sedimentary waste rock was not tested in this study but the SWCC for a similar rock type, a black sedimentary waste rock, was previously determined and is included for comparison purposes. Both rock types were taken from the same open pit and had similar particle size distributions. It is noted that the altered sedimentary waste rock was slightly more competent and less friable than the black sedimentary rock.

Particle size distribution was determined for a duplicate specimen of the mixture material by using a washed sieve analysis and for a tailings specimen by hydrometer and wet sieve analysis. The tailings were tested for liquid and plastic limits following ASTM D4318-84. The shrinkage limit of the tailings was also determined by placing tailings in a metal ring, drying at room temperature and in an oven, then coating the specimen in wax to determine final dried volume.

Results

Particle Size Distributions
Particle size distributions of the mixture, source materials, and the black sedimentary rock, are shown in Figure 2.
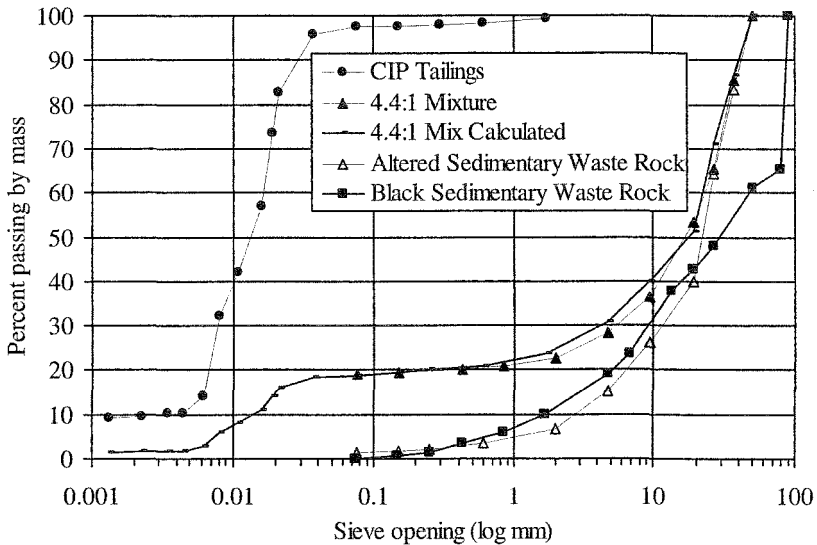
Figure 2. Particle size distributions.

The mixture ratio for the mixed specimen was 4.4:1 waste rock to tailings by dry mass. The mixture was constructed with the same CIP tailings. The tailings, mixture and waste rock specimens had 97%, 19%, and less than 2% passing the 75μm sieve, respectively. The tailings are considered to be fine-grained relative to other types of tailings. The particle size distribution of the black sedimentary rock was similar to the altered sedimentary waste rock used as a source for the 4.4:1 mixture, shown in Figure 2. On the basis of similar particle size distributions, the SWCC's for the black sedimentary waste rock and altered sedimentary waste rock used to construct the mixture are also expected to be similar.

Soil-Water Characteristic Curves
SWCC's for the mixture, tailings, and black sedimentary rock are shown in Figure 3. Data for the mixture and tailings are corrected for volume change and waste rock data are uncorrected for volume change. Values of volumetric water content for the oven-dried condition are assumed to be zero corresponding to a matric suction of 1,000,000 kPa.
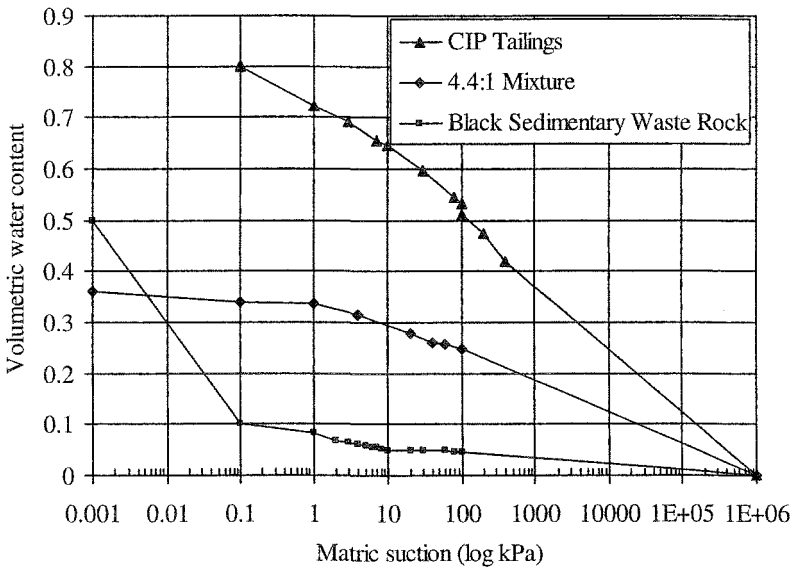
Figure 3. SWCC for tailings, mixture, and waste rock.

The data in Figure 3 indicate the tailings, mixture, and waste rock had initial volumetric water contents of 0.8, 0.36, and 0.50, respectively. At matric suctions greater than approximately 0.1 kPa, the mixture had slightly less than half the volumetric water content of the tailings and more than three times that of the waste rock.

The waste rock had an air entry value (AEV) of less than 1 kPa matric suction with a residual volumetric water content of approximately 0.05 (or 5%) at 10 kPa. The values of AEV for the mixture and tailings are not immediately apparent from Figure 3 because most of the change in volumetric water content was due to volume change or specimen shrinkage rather than de-saturation. According to measurements of specimen volume, the data presented in Figure 3 do not define an AEV or residual water contents for the waste rock, or for the tailings. The difficulty in determining AEV and residual suction is partly due to the limited range of suctions tested, but also due to shrinkage of specimens during the test.

The SWCC data for the tailings and mixture in Figure 3 are corrected for changes in volume during the test as recommended by Fredlund (1999). The volumetric water content corresponding to each applied matric suction during the Tempe cell test was calculated using:

1) $\theta(\psi) = [w(\psi)G_s] / [1+e(w(\psi))]$, where

θ is volumetric water content, ψ is matric suction, w gravimetric water content, G_s is specific gravity, and e is void ratio (Fredlund 1999). More simply, the specimen volume was determined at the end of each matric suction increment in order to calculate volumetric water content. Specimen volumes were calculated with the assumption that the mixture and tailings specimens remained saturated for the duration of the test (excluding the 1,000,000 kPa matric suction – oven dry condition). The assumption that the specimens remained saturated is valid for suctions to at least 40 kPa, and was made on the basis of shrinkage curve data. The value of G_s of the tailings was taken as 2.89

Shrinkage Curves
The specimen dimensions of mixture and tailings specimens were recorded at the end of each matric suction interval during the Tempe cell test. The tailings changed in volume by 53% for an increase in matric suction of 0 kPa to 100 kPa. The mixture changed in volume by 15% for an increase in matric suction of 0 kPa to 100 kPa. Changes in waste rock volume were not measured, but were quite small. Specimen volumes and void ratios were determined from specimen dimensions for the mixture and tailings specimens and are plotted as shrinkage curves in Figures 4 and 5, respectively.
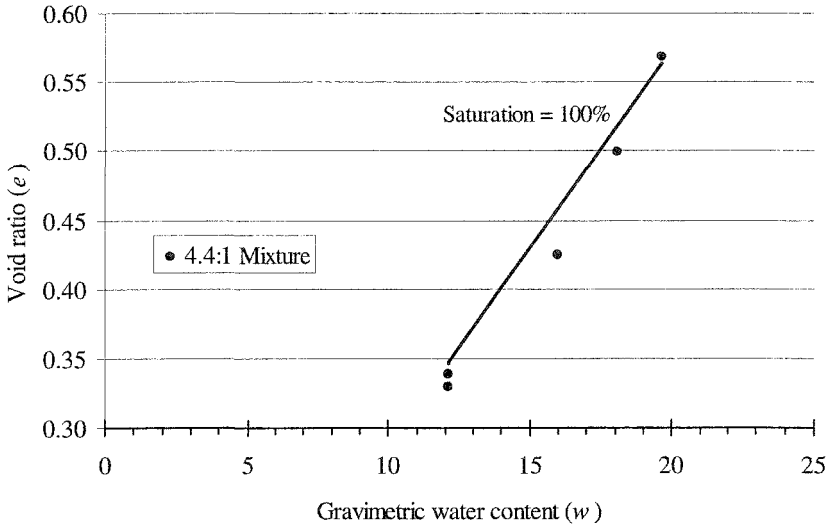
Figure 4. Shrinkage Curve for 4.4:1 Mixture.
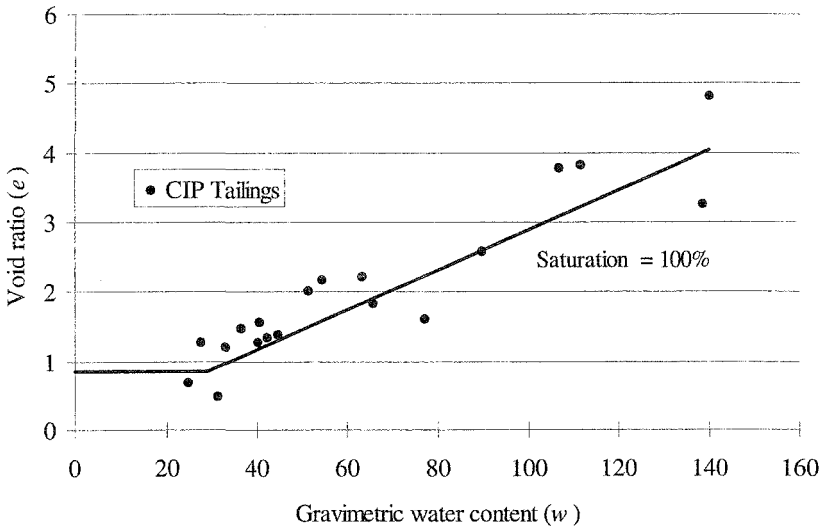
Figure 5. Shrinkage Curve for CIP Tailings.

The data in Figure 4 fall near the 100% saturation line, suggesting that the maximum applied matric suction of near 100 kPa (excluding the oven-dried condition of 1,000,000 kPa) did not exceed the AEV of the material. Small cracks were observed on the surface of the mixture specimen during tests at matric suctions greater than 40 kPa, corresponding to a gravimetric water content of 12%. The assumption that the specimens remained 100% saturated during the test is subject to interpretation. There is the possibility that there was some error in accurately determining specimen volume from dimensional measurements, particularly after the development of cracks. However, the assumption does not significantly change the shape of the SWCC, and provides a more accurate representation of behaviour than the assumption of zero volume change during the test.

The data presented in Figure 5 do not indicate a defined AEV for the tailings. The scatter in the data is attributed to errors in measuring specimen volume. Fredlund (1999) suggested using a correction for volume change based on the shrinkage limit. A shrinkage test was performed to determine final specimen volume for the oven-dried condition and results are illustrated in Figure 5 and included in Table 1. The measured shrinkage limit of 29% corresponds to a void ratio of 0.85, as illustrated in Figure 5. The shrinkage limit was also estimated from the Plasticity Index, and is included in Table 1.

Atterberg Limits
The liquid and plastic limits of the tailings were determined from laboratory testing, and are presented in Table 1. The shrinkage limit presented in Table 1 was estimated from the equation:

2) $SL = 20 +- \Delta PI$, where

SL is the shrinkage limit, and ΔPI is the distance between the plasticity index and the A-line.

Table 1 Atterberg Limits for CIP Tailings.

CIP Tailings	Gravimetric Water Content (%)
Liquid Limit	50.2
Plastic Limit	33.2
Plasticity Index	17.0
Shrinkage Limit	
- measured	29.3
- estimated	25.0

Holtz and Kovacs (1981) provided a more detailed explanation of the method of estimation, and noted that the accuracy of such estimates is similar to the accuracy for actual laboratory shrinkage tests. The initial gravimetric water content of the slurry was near 110%.

Meso-Scale Column Study Results

Data from a meso-scale column study of the mixture material are presented here for comparison with laboratory results. The column study was described by Wickland and Wilson (2005), and involved loading three mixtures of waste rock and tailings into columns of 1 m diameter and 6 m in height, then monitoring for drainage, settlement, and pore water pressure response. A fourth column was loaded with waste rock only as a control. The columns were equipped with base drains and fitted with lids that allowed air flow but prevented influx of rainfall. Matric suctions measured for the mixture in Column 1, (a specimen of the same mixture is labelled "4.4:1 mixture" in this paper), are presented in Figure 6. Figure 6 includes measurements taken 125 days after column loading. A curve representing hydrostatic conditions with a water table at the base of the profile and matric suction measurements taken just prior to deconstruction are labelled "final."
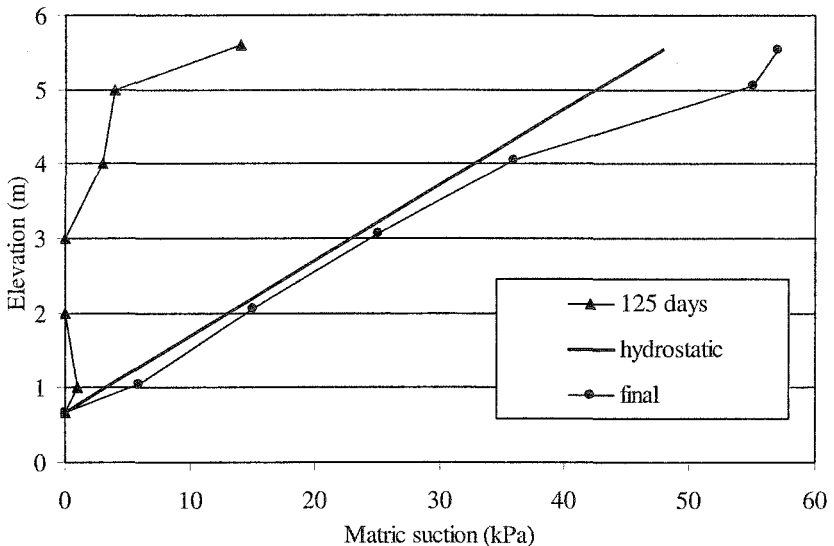
Figure 6. Mixture matric suction measurements from Meso-scale column study.

Immediately after placement of the fill the mixture profile was observed to undergo a phase of double drainage and ponding followed by a phase of single drainage with the development of negative pore-water pressures from the top down. Water exiting the surface of the specimen during the double drainage phase remained ponded on the surface of the profile until approximately 85 days after placement, leaving approximately 40 days of free drainage to develop the matric suction profile labelled "125 days" in Figure 6.

The column study was run for approximately two years and then dismantled. The profile was flooded six months prior to deconstruction, and then allowed to drain to the condition marked "final" in Figure 6. The final condition was close to the

hydrostatic case with slightly higher matric suctions near surface. The maximum measured matric suction was 57 kPa. During final excavation and sampling of the Column 1 profile it was observed that mixture was drier near the surface, with the material becoming wetter with depth. Cracks and fissures were observed within the tailings matrix of the mixture above 4 m elevation. Material below the 3.5 m elevation was cohesive.

Analysis and Discussion
Analysis and discussion of results is divided into interpretation of laboratory results and relationship of laboratory testing results to the matric suction measurements and observations from the meso-scale column study.

Laboratory
Analysis of laboratory derived SWCC's for tailings, waste rock, and mixtures indicated the following:

1) Mixtures maintained water saturation upon application of matric suctions relative to waste rock alone due to the presence of a fine-grained tailings matrix. The air-entry values and residual matric suctions of the mixture and tailings specimens were not apparent from the range of matric suctions tested.

2) The waste rock had an air-entry value less than 1 kPa and reached residual water content at low matric suctions (near 10 kPa).

3) The tailings underwent a large volume change or shrinkage during the Tempe Cell test. From 0 kPa to 100 kPa matric suctions in the tailings specimen shrank by slightly more than 50% and the mixture shrank by 15%. The large degree of volume change was anticipated for slurried tailings. The volume change of the waste rock during the test was not measured but was quite small.

4) The limited volume change of the mixtures was attributed to the presence of a "waste rock skeleton." Tailings within the void space of the skeleton were observed to shrink and crack at higher suctions but the total volume of the mixture specimen did not change significantly. The phenomenon described is related to the construction of a mixture using tailings slurry with high water content.

5) Significant volume changes during de-saturation must be accounted for to accurately determine the SWCC; a finding which supports the conclusion of Fredlund (1999). Otherwise, the interpretation of the air-entry value for the SWCC will be inaccurate. Specimen volumes must be determined at the end of each matric suction interval and used to calculate volumetric water content, as in Equation 1. For the mixture and tailings specimens tested, the curved shapes of the SWCC's were due almost entirely to volume change associated with water loss from a saturated specimen rather than entry of air into the pore space.

6) Cracking upon de-saturation is, in some cases, more important than the air-entry value. The air-entry value (AEV) is defined as "...the matric suction value that must be exceeded before air recedes into the soil pores..." (Fredlund and Rahardjo 1993). If a saturated porous soil matrix is continuous,

then the movement of air through the specimen will be limited to diffusive flow. If cracking occurs while the pores of the soil remain tension saturated, then there can be a significant increase in the air coefficient of permeability at matric suctions below the AEV. Air may flow through the cracks of the specimen while the pore space remains saturated. Air permeability will become a function of the size and connectivity of cracks dividing the saturated portions of the specimen.

Field Study

Comparison of laboratory SWCC's with matric suction measurements from a meso-scale column study indicated:

1. The column mixture profile maintained water saturation for prolonged periods of free drainage without access to water. The maximum matric suction measured in the column profile at 125 days after construction was near 15 kPa. The SWCC data indicated that the laboratory specimen was saturated, at 15 kPa. The laboratory test data and field observations imply that the column profile was saturated after 125 days of free drainage without access to water.

2. After a six-month period of free drainage without access to water, the maximum final measured matric suction was near hydrostatic with a maximum measured matric suction of near 60 kPa at the surface of the profile. The laboratory mixture specimen shrank and developed fine cracks within the tailings matrix at suctions greater than 40 kPa. During deconstruction of the column experiment, cracks and fissures were observed in the upper 1.5 m to 2 m of the column mixture profile, corresponding to measured matric suctions of greater than 40 kPa.

3. The control column with a waste rock only profile was initially unsaturated following construction, and remained unsaturated until flooded at day 13 of the test.

Summary and Conclusions

The soil-water characteristic curves, SWCCs, of tailings, waste rock, and a mixture of tailings and waste rock were presented and compared to results from a meso-scale column study. Key findings included:

1. Mixtures of waste rock and tailings remained saturated for significantly longer periods of time and at higher matric suctions than waste rock alone. The maintenance of saturation was attributed to the presence of a fine-grained tailings matrix. The result indicates that mixing waste rock and tailings for disposal has the potential to limit the production of acid rock drainage (ARD).

2. Mixtures had less volume change than tailings alone, a finding that was attributed to the presence of an internal "waste rock skeleton." Slurried tailings were observed to undergo a large degree of volume change or shrinkage upon application of matric suction. The large change in volume of the tailings was attributed to the high initial water content.

3. Under prolonged drainage without access to water the mixture material was observed to develop cracks through the tailings matrix. However, the mixture material was less prone to volume change and shrinkage upon drying than tailings alone. Instead, shrinkage cracking was observed within the tailings matrix while the total volume of the specimen was maintained. If mixtures are used as a mine waste disposal technique, then extreme drought and dry conditions have the potential to cause cracking and an increase in air and water coefficients of permeability. Consequently, the climate of a site and rainfall in particular should be considered in the application of mixing for disposal.
4. The findings of this study re-enforce the need to account for volume change when determining the soil-water characteristic curve, particularly for slurried specimens such as the tailings examined herein.

Acknowledgements

References

Fredlund, D.G., and Rahardjo, H. (1993). *Soil Mechanics for Unsaturated Soils*. John Wiley and Sons Inc. New York.

Fredlund, M.D. (1999). The Role of Unsaturated Soil Property Functions in the Practice of Unsaturated Soil Mechanics, Ph.D. Thesis, University of Saskatchewan.

Holtz, R.D., and Kovacs, P.E. (1981). *An Introduction to Geotechnical Engineering*, Prentice-Hall, N.J.

Wickland, B.E., and Wilson, G.W. (2005). Self-weight consolidation of mixtures of mine waste rock and tailings. *Canadian Geotechnical Journal*, 42(2), 327-339.

The Effect of Vertical Pressure on the Deformation and Strength of Expansive Soil during Cyclic Wetting and Drying

Rui Zhang[1]   Heping Yang[2]   Jianglong Zheng[3]

[1]PhD candidate, School of Highway Engineering, Changsha University of Science and Technology, P.O. Box 410076, Changsha, Chiling Road 45#, China.; PH (86) 731-2300823; FAX (86) 731-2309581; email: mikezr@126.com
[2]Professor, School of Highway Engineering, Changsha University of Science and Technology; PH (86) 731-2309581; FAX (86) 731-2309581; email: cscuyang@126.com
[3]Professor, President, PhD supervisor, Changsha University of Science and Technology; PH (86) 731-2309080; FAX (86) 731-2309080; email: jlzheng@126.com

Abstract:

A test on the effect of vertical pressure on the deformation and strength characteristics of undisturbed expansive soil obtained from Ningming (a city in southern Guangxi, China) was conducted during wetting and drying cycles. In addition, the expansion and shrinkage were measured. The testing data indicated that the swelling and shrinking of expansive soil were not completely reversible, and upon repeated wetting and drying, the soil showed signs of fatigue after every cycle resulting in decreased swelling ability. Furthermore, it was noted that the first cycle causes the most reduction in swelling-shrinking potential. As the number of cycles increased, additional reduction was observed until a state of equilibrium was reached. For the Ningming expansive soil, the equilibrium cycle ranged between 3 and 4. Moreover, the vertical pressure in certain range had effects to restrain the swelling-shrinking deformation and the attenuation of shear strength. The higher the vertical pressure, the more obvious the effect was. Therefore, in order to acquire the parameters in accord with the engineering practice, the vertical pressure must be taken into account in the wet-dry cycling test of expansive soils.

Introduction

The swelling-shrinking and strength characteristics of expansive soils during cyclic wetting and drying have been investigated by many Chinese researchers, such as Liu T.H. (1997), Xu Y. F(2000), Liu S.Y(1999), Lu Z.H.(2002). Moreover, they

have achieved many significant results. Nevertheless, in previous tests on wetting and drying cycles of expansive soils, the water content varied between saturation and shrinkage limits without vertical pressure while in engineering practice soils were always located in a certain depth or undergo certain loads. Therefore, such kind of testing condition was out of accord with the practice. Available observation data, C.W.W. Ng (2002), shows that the variety of water content in a 1m depth of slope surface layer was great, but it was stable under the depth of 1m, (in the range of 4% or 5%). Therefore, in order to acquire the experimental parameters and indices in accordance with the engineering practice, it is necessary to consider the effect of vertical pressure in the tests on the deformation and strength characteristics of expansive soils during cyclic wetting and drying.

A 14 km long region, continuously distributing Ningming expansive soil, was found during the construction of Nangning to YouyiGuan expressway (NY expressway) as it crossed the edge of Ningming basin. The Ningming soil is eluvial expansive soil with moderate-strong swelling potential, and its material source is from the weathering of early Tertiary Nadu formation shale. Nearly all cut slopes, during the construction of NY expressway, slide in different scales (Yang, 2005). Therefore, how to effectively treat cut slopes to prevent landslides became the most challenging technical problem in the engineering construction. A research group, set up by the Changsha University of Science and Technology, adopted a flexible supporting measure to treat expansive soil slopes and achieved great success. This measure was to use reinforced structure with enough thickness to apply upper pressure to the expansive soil in the slope, and to resist swelling pressure of the side slope and prevent, or decrease, the adverse effects of wetting and drying cycles due to weather (Zheng, 2004). In order to study the working principle of a flexible supporting measure quantificationally, as well as provide parameters for the designing method of protecting and supporting expansive soil cut slope, the authors studied the effect of vertical pressure on the deformation and strength of expansive soils during cyclic wetting and drying, based on an analysis of similar earlier studies.

Testing Design and Procedure

Testing design. The testing apparatus used to simulate the cycle of wetting and drying is shown in Photo 1. The cycles and shearing were both conducted in a direct shear apparatus. Four specimens were arranged as a group and put into four cells of the direct shear apparatus, and the initial moisture content of each sample was natural moisture content. They were then subjected to one, two, three, and four cycles of wetting and drying respectively under the same vertical pressure. To accelerate the testing process, illumination of four high-power bulbs were used to simulate sun light on desiccate specimens to control moisture content range. It had been validated by a test that illumination of 96 hours, with an indoor temperature of 20 ℃, could decrease the specimens' moisture content by 5% to 6%, to the required minimum moisture content in the test. During the cycles, the height of each specimen was observed; unfortunately the moisture content could be measured only at the start and end of each cycle. When a cycle was completed, the specimen was quickly sheared.

For each group, the vertical pressure on specimens was held constant at 25kPa, 50kPa, and 100kPa respectively, which represents a typical pressure range, when expansive behavior is a concern. Thus, the change of deformation and strength of specimens, along with wet dry cycles and vertical pressures, could be obtained. The testing results can be used to study the effect of vertical pressure on the deformation and strength of expansive soils during cyclic wetting and drying.
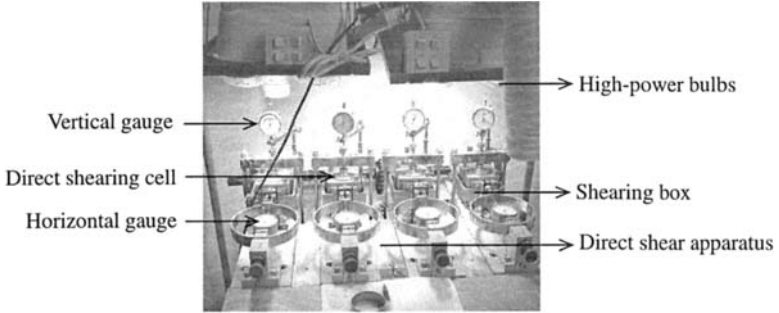
Photo 1. The testing apparatus

Test soil and preparation.   Tests was performed on undisturbed, weathered samples of light-gray expansive soil from K134+080 of Nan-You expressway, Guangxi China. The sample was obtained from a depth of 2m. Its physical properties are shown in Table 1. From Table 1 the swell potential of the soil can be classified as moderate-strong. The sample was trimmed into 23 specimens by fixed-ring consolidation cells (height of 20mm and diameter of 61.8 mm), and 12 of them (the density difference between being less than $30kg/m^3$) were selected as testing specimens, whose average dry density was $1500kg/m^3$. In addition, the 12 specimens were classified into four groups, each of which was used in tests under three different vertical pressures. Because the whole testing time was very long, the specimens were sealed in airtight plastic bags, and stored in a container maintained at 100% relative humidity to keep the change of undisturbed water content at a minimum.

Table 1. Soil Properties of Test Specimen

w_L (%)	w_p (%)	I_P (%)	f_S (%)	w_s (%)	PS $\leq 2\mu$ (%)	Clayey Mineral	w_0 (%)	G_s
55.9	28.2	27.7	68	15.50	52.13	Illite/Montmorillonite	27.5	2.74

Note: w_L=liquid limit, w_p=plasticity limit, I_P=plasticity index, w_s=shrinkage limit, PS= particle size(mm), f_S = free swelling ratio, w_0=natural moisture content, G_s =Specific gravity

Test procedure.   To describe the experimental procedure, the test on cyclic wetting and drying under vertical pressure of 25 kPa, is used as an example:

Step 1: Arrange four specimens as a group, put them into shearing cells of the direct shear apparatus respectively, and label the boxes No.1-4. Then exert a vertical pressure of 25kPa on each of them. Put wet washrags on the top of the cells to maintain the initial moisture content of each specimen.

Step 2: Install vertical gauges on the top of each specimen (They are used to observe the change of the specimens' height in the processes of consolidation, cyclic wetting and drying) respectively. When the consolidation, under 25kPa, is completed, record the height of specimens at their initial height of wet dry cycles, but the moisture content can not be measured.

Step 3: Evenly illuminate the four boxes with high-power bulbs. The temperature at the top of cells will be steady at 50°C after a few minutes. Continue illuminating for 96 hours. Then turn off the bulbs and maintain this state (with wet washrags on the top of cells keeping moisture content) for 24 hours to ensure the outer and inner water content and temperature of the specimens remains consistent. Record the reading of the clock gauges.

Step 4: Add water into shearing boxes until the specimens are inundated. Observe the changes in the vertical deformation of inundated specimens. Be sure that the soaking time is 24 hours to let the specimens swell fully. Record the reading at the swell height of the first cycle.

Step 5: Quickly shear the No.1 box under 25kPa. This way the change of the shear strain along with stress can be obtained. Let the peak stress be the shear strength. Collect the soil on the shearing surface to measure the water content of failure specimens, which is regarded as swelling water content after inundation and the other specimens' initial water content of the next cycle.

Step 6: Continue the same procedure for the other three specimens according to Step 3-5, so that the deformation and shear strength of the second, the third and the fourth cycle, as well as the water content after shearing, can be obtained.

Process of cyclic wetting and drying under a vertical pressure is shown in Figure 1.
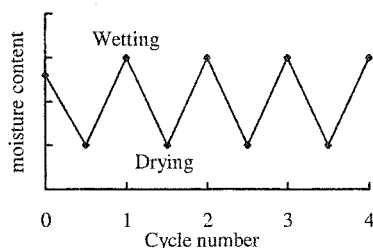
Figure 1. Process of cyclic wetting and drying

Testing Results and Analysis

Testing results. The reading of clock gauges and the changes of specimens' height

during four wet dry cycles under three vertical pressures are shown in Table 2. Moreover, variation of specimens' height along with cycles is shown in Figure 2.

Table 2. The Reading of Vertical Gauge and Specimens' Height During Wet and Dry Cycles Under Three Vertical Pressures

Vertical Pressure	25 kPa		50 kPa		100 kPa	
	Reading (0.01mm)	Height (mm)	Reading (0.01mm)	Height (mm)	Reading (0.01mm)	Height (mm)
Initial state	620	20.0	540	20.0	650	20.0
Post-consolidation	516	19.0	392	18.5	484	18.3
The 1st drying	301	16.8	241	17.0	370	17.2
The 1st wetting	690	20.7	503	19.6	573	19.2
The 2nd drying	315	17.0	247	17.1	379	17.3
The 2nd wetting	670	20.5	490	19.5	569	19.2
The 3rd drying	377	17.6	269	17.3	401	17.5
The 3rd wetting	612	19.9	474	19.3	547	19.0
The 4th drying	373	17.5	263	17.2	390	17.4
The 4th wetting	593	19.7	470	19.3	541	18.9
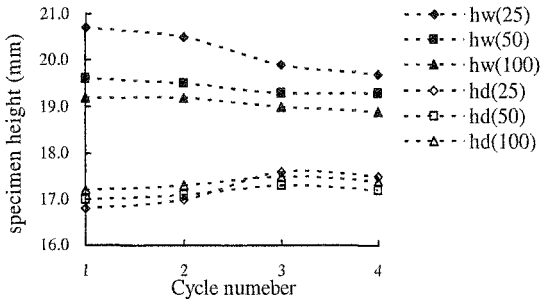
Note: $h_w(25)$=The height after wetting under 25kPa
$h_d(25)$=The height after drying under 25kPa

Figure 2. Change of specimens' height with cycle number

When a specimen completed a wetting and drying cycle under a vertical pressure and soaked to reach the maximum swelling height, it was quickly sheared under the same pressure at a rate of 0.8mm/min (Standard for Civil Engineering Experiment of Highway Project, 1999). The reading of horizontal gauge beside load cell was recorded every 15 seconds and the maximum shear stress was shear strength. The results of direct shear tests are shown in Table 3 and Figure 3.

Table 3. Shear Strength under Different Vertical Pressures after Wet Dry Cycles

Shear strength (Kpa)		Cycle number			
		1	2	3	4
Vertical pressure (Kpa)	25	64.41	48.39	37.33	35.09
	50	76.28	61.47	55.18	57.10
	100	93.23	84.90	79.20	78.47
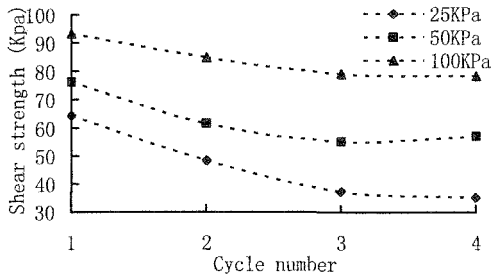
Figure 3. Change of shear strength with cycle number

Analysis of results. Figure 2 has shown that the swelling and shrinking of specimens all decreased with cycle number under the three vertical pressures. The swelling due to wetting, and the shrinking due to drying, during the former two cycles changed greatly in a larger range, but changes were insignificant during the latter. The swelling and shrinking deformation of expansive soil was not reversible.

In order to quantitatively study the effect of vertical pressure on the deformation of expansive soils during cyclic wetting, the absolute and the relative swelling and shrinking ratios were defined respectively (in light of figure 1) to describe the changing tendency and degree of swelling and shrinking.

η_{wi} stands for the absolute swelling ratio and η_{di} stands for the absolute shrinking ratio. These were used to quantify the deformation of specimens in the whole process.

$$\eta_{wi} = \frac{|h_{wi} - h_0|}{h_0} \tag{1}$$

$$\eta_{di} = \frac{|h_{di} - h_0|}{h_0} \tag{2}$$

Where h_{wi} is the swelling height in cycle of number i, h_{di} is the shrinking height in cycle of number i after a specimen is dried for 4 days, h_0 is the height after a specimen is consolidated under some vertical pressure, i is the cycle number.

Meanwhile, the relative expansion ratio δ_{wi} and relative shrinking ratio δ_{di} were used to quantify the deformation of specimens in a certain cycle.

$$\delta_{wi} = \frac{\left|h_{wi} - h_{di}\right|}{h_{di}} \qquad (3)$$

$$\delta_{di} = \frac{\left|h_{di} - h_{w(i-1)}\right|}{h_{w(i-1)}} \qquad (4)$$

Where $h_{w(i-1)}$ is the swelling height in cycle of number i-1

The absolute and relative ratio of swelling and shrinking under different vertical pressures were calculated according to Formula 1, 2, 3 and 4. The calculated results are presented in Table 4.

Table 4. Swelling Ratio and Expansion Water Content during Cycles Under Different Vertical Pressures

Vertical Pressure	Cycle number	η_d	η_w	δ_d	δ_w	w
25 kPa	1	11.53%	8.92%	—	23.11%	31.6%
	2	10.78%	7.89%	18.09%	20.93%	30.5%
	3	7.55%	4.82%	14.31%	13.37%	31.4%
	4	7.89%	3.69%	12.13%	12.58%	30.2%
50 kPa	1	8.04%	6.11%	—	15.38%	30.6%
	2	7.71%	5.41%	13.02%	14.21%	30.5%
	3	6.53%	4.54%	11.32%	11.84%	29.7%
	4	6.89%	4.32%	10.94%	12.05%	31.0%
100 kPa	1	6.01%	5.05%	—	11.77%	29.8%
	2	5.54%	4.84%	10.08%	10.99%	29.2%
	3	4.33%	3.68%	8.75%	8.37%	28.5%
	4	4.92%	3.33%	8.29%	8.68%	28.7%
Note:	The relative shrinking ratio (δ_d) of the first cycle was not available because the cycle began at the natural water content, not the saturated water content.					

Change of absolute swelling and shrinking ratio with the cycle and vertical pressure. Figure 4 and Figure 5 present the absolute swelling and shrinking ratio change with cycle numbers when specimens were under different vertical pressures. The absolute swelling and shrinking ratio decreased with the increase of the cycle number, and the initial absolute swelling and shrinking were significantly higher than that at the fourth cycle. Furthermore, there were only minor differences between the third and the fourth cycle.
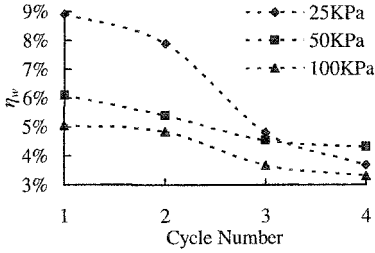
Figure 4. Change of absolute swelling ratio with cycle number
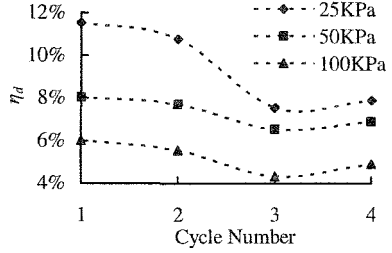
Figure 5. Change of absolute shrinking ratio with cycle number

Figure 6 and Figure 7 show that the absolute swelling and shrinking ratios varied with vertical pressures when specimens underwent different cycles of wetting and drying. The absolute swelling and shrinking ratios all decreased with the increase of vertical pressure at the same cycle. In addition, at the first and second cycle, the vertical pressure of 50kPa had an obvious effect on the decrease of swelling and shrinking capabilities of expansive soil, while under the vertical pressure of 100kPa, the swelling potential tended to be steady and the changeable range of shrinking ratio was smaller than under 50kPa. The changes at the third and fourth cycle were different from the former cycles, but with the increase of vertical pressure, the swelling and shrinking ratio tended to be at a minimum.
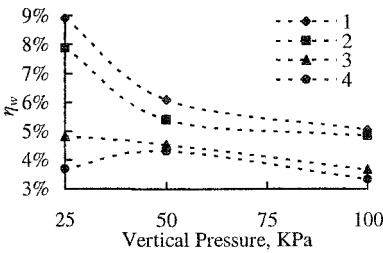
Figure 6. Change of absolute swelling ratio with vertical pressure
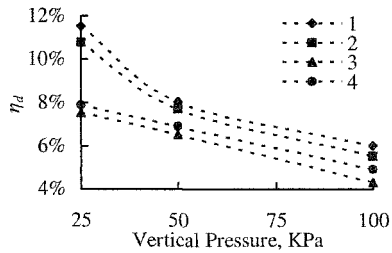
Figure 7. Change of absolute shrinking ratio with vertical pressure

Change of relative swelling and shrinking ratio with the cycle and vertical pressure. Figure 8 and Figure 9 clearly show that the relative swelling and shrinking ratios changed with cycle numbers when specimens were under different vertical pressures. This indicates the difference between the swelling and shrinking potential among the cycles. The relative swelling and shrinking ratio also decreased with the increase of cycle numbers, while the specimens had higher swelling and shrinking ratios at the first and second cycle, thus indicating that the specimens showed signs of fatigue after every cycle, resulting in decreased swell-shrink ability.

After the third and fourth cycle, the effect of vertical pressure on the change of specimen's deformation was not obvious.
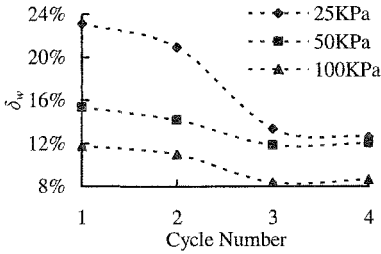
Figure 8. Change of relative swelling ratiowith cycle number
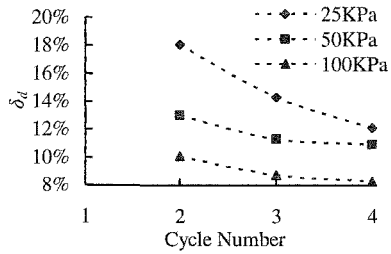
Figure 9. Change of relative shrinking ratio with cycle number

Figure 10 and Figure 11 indicate that the relative swelling and shrinking ratio varied with vertical pressures when specimens underwent different cycles of wetting and drying. There were similar rules to the absolute ratio. The vertical pressure has the effect of restraining swell-shrink deformation of expansive soil in its wetting and drying cycles.
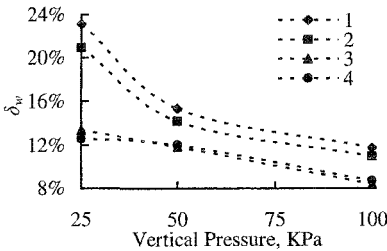
Figure 10. Change of relative swelling ratio with vertical pressure
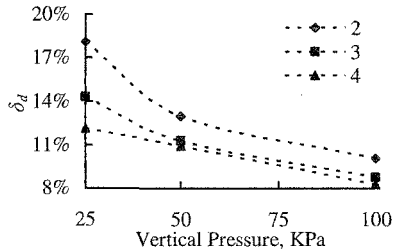
Figure 11. Change of relative shrinking ratio with vertical pressure

Change of shear strength with the cycle number and vertical pressure. From the results of the direct shear test, it can be found that at the same cycle of wetting and drying, the shear strength increased with the vertical pressure. Nevertheless, under the same vertical pressure the strength decreased with the increase of cycle numbers (shown in Figure 2). In order to compare the attenuation degree of shear strength, the attenuation ratio $\beta_{\tau i}$ at the cycle of number i was defined.

$$\beta_{\tau i} = \frac{\tau_1 - \tau_i}{\tau_1} \times 100\% \tag{5}$$

Where τ_1 is the shear strength at the first wetting and drying cycle. τ_i is the shear

strength at the cycle of number i.

From Figure 2, the range of shear strength attenuation decreased with the increase of vertical pressure, and under 25Kpa, 50Kpa and 100Kpa, the β_{r4} is 46%, 25% and 16% respectively, which means the vertical pressure has the effect to inhibit the attenuation of shear strength due to cyclic wetting and drying. Moreover, the attenuation ratio at the 2nd cycle, under any pressure, was always the maximum.

Reasons for Changes of Deformation and Strength of Expansive Soil in the Test

In the test, for the specimens under the same vertical pressure, the highest swelling and shrinking all happened at the first wetting and drying cycle, and decreased with the increase of cycles (in agreement with the findings of Ai-Homoud (1995), Lu (2002)). The decrease in swelling and shrinking characteristics on repeated wetting and drying is consistent with the reconstruction of the clay microstructure. The original structure of expansive soil was broken after the first or second cycle. The repeating shrinking and expansion caused the aggregation and arrangement of soil mass, the small interparticle separation generated significant capillary stress during air-drying that drew particles intimately and permitted development of Vander Waals bonds, which were not easily reversed. In addition, the resultant particle aggregation reduces the available surface for interaction with water and, hence, a reduction in clay content, specific surface area and plasticity. In addition, the structural element orientation is relatively low and becomes even lower due to the integration of structure along the bedding resulting in correspondingly lower water absorption. At the fourth cycle, the microstructure becomes even more uniform in nature thus ensuring lesser water absorption resulting in lesser swell. This inevitably caused a reduction in the amount of swelling and shrinking, which was obvious at the second cycle, as the number of cycles increase up to a point where steady or equilibrium state was reached. This may explain the fact that the first or second cycle of wetting and drying contributed to a large reduction in maximum swell and shrinkage, and lower swelling-shrinking ability was produced alone with increase of wetting-drying cycles.

Meanwhile, because of particle aggregation during cycles, void ratio and permeability increased, and the structure bond force between soil mass became weak resulting in a correspondingly lower swelling pressure. When three specimens under the same vertical stress underwent the same cycles of wetting and drying, the vertical pressure counteracted a part of the swelling force, hence, caused a reduction in swelling ratio. As the number of cycles increased, the swelling force decreased. Therefore, the vertical pressure can produce obvious effects on the deformation and strength characteristics, which are shown in Figures 6, 7, 10 and 11.

The increase of wet and dry cycle readily causes the growth of cracks, along with changes to the microstructure mentioned above. This causes the shear strength to be lowered. However, because of the stress state, the attenuation degree of shear

strength was not different. The higher the vertical pressure acts on the specimen, the less the swelling-shrinking deformation will be, and the fewer cracks will grow. Thus, the attenuation degree of shear strength under 100Kpa is much less than that under 25Kpa.

Conclusions

Based on the analysis of the experimental results presented in this study, the following conclusions are given.

In order to discover the changes of strength and deformation of expansive soil with cycles of drying and wetting in accord with the field-condition, the effect of vertical pressure should be considered when a test is carried out to simulate cycles of wetting and drying.

The obtained data clarified the fact that under vertical pressure, the shrink-swell deformation was not reversible. Upon repeated wetting and drying, both the absolute and the relative swelling and shrinking ratios decreased. The first or second cycle causes the most reduction in swelling-shrinking potential. As the number of cycles increased, further reduction was observed until a state of equilibrium was reached in which the swelling-shrinking potential seemed to level off. For the three groups of specimens, the equilibrium cycle ranged between 3 and 4. This means that the soils show signs of fatigue after each cycle, and this resulted in decreased swelling-shrinking ability. Meanwhile the shear strength decreased primarily at the first cycle, and leveled off after the third cycle.

The effect of vertical pressure will cause the fabric change of expansive soil during cycles of wetting and drying. This consequently influences the characteristics of shrink-swell deformation and shear strength. When undergoing the same cycle of wetting and drying, the higher vertical pressure acted on the specimen, while the lower the swelling-shrinking ability was, the less the attenuation of the shear strength was. The vertical pressure has the effect of restraining the deformation and the strength attenuation of expansive soil during cyclic wetting and drying. Therefore, the flexible support method has the effect of stabilizing the expansive cut slope.

Finally, the testing results can be applied to determine the thickness of the reinforcing body and provide a reference to the stabilization analyses of reinforced slopes, when the flexible support method is adopted to treat the landslides in expansive soil cut slopes.

References

A. S. Ai-Homoud, (1995). "Cyclic swelling behavior of clays." *Journal of geotechnical engineering,* July, 562-566.

C.W.W. NG, (2002) "Performance of an unsaturated expansive soil slope subjected to artificial rainfall infiltration". *Geotechnique,* 143-157.

Liu T.H., (1997). "The problems of expansive soil in engineering projects". *Architecture Industry Press,* Beijing China, 43-44.

Liu S.Y., (1999). "Approach to cyclic swelling behavior of compacted expansive clays." *Chinese Journal of Geotechnical Engineering*, 21(1), 9-13.

Lu Z.H., Chen Z.H., (2002). "A CT study on the crack evolution of expansive soil during drying and wetting cycles." *Rock and Soil Mechanics,* 23(4), 417-412.

Research Institute of Highway of Ministry of Communications, (1999). "Standard for Civil Engineering Experiment of Highway Project." *The People's communication Press*, Beijing, China, pp.121.

Yang H.P., Qu Y.X., Zheng J.L.,(2005). "New development in studies on Ningming expansive soils". *Chinese Journal of Geotechnical Engineering*.17(9), 981-987.

Xu Y.F., (2000). "The strength theory of unsaturated soil and its application to engineering". *Dong Nan Univ. Press,* Nanjing, China, 185-186.

Zheng J.L., Yang H.P., (2004). "The treatment theory, techniques and practice of expansive soils." *The People's communication Press*, Beijing, China, 18-19.

Volume change behavior of a fissured expansive clay containing anhydrous calcium sulfate

Shahid Azam[1] and G. Ward Wilson[2]

Department of Mining Engineering, University of British Columbia, 6350 Stores Road, Vancouver, B.C., V6T 1Z4, Canada; [1]PH (604) 822-0073; FAX (604) 822-5599; email: azam@mining.ubc.ca; [2]PH (604) 822-6781; FAX (604) 822-5599; email: gww@mining.ubc.ca

Abstract

Expansive clays in eastern Saudi Arabia are generally fissured and contain high quantities of anhydrous calcium sulfate. Similar to clay minerals, this secondary mineral causes swelling when hydrated and forms gypsum that, in turn, dehydrates and transfers back to anhydrite during compression. The main objective of this paper was to understand the volume change behavior of a local expansive clay containing 50% anhydrous calcium sulfate. Swelling and consolidation tests were conducted on undisturbed field samples according to the constant volume method. A conventional oedometer sample was used to determine the maximum possible volume change. Likewise, a large-scale oedometer sample was used to capture the influence of fissuring on volume change. The large-scale sample was thoroughly instrumented to determine both the vertical and the lateral swelling pressure. Results indicated a two-fold increase in swelling pressure of the desiccated clay when corrections were applied to account for sample disturbance. The corrected vertical swelling pressure of the clay was 320 kPa for the conventional sample and 245 kPa for the large-scale sample. The lateral swelling pressure was 40% of the vertical swelling pressure and the swelling index was one-third of the compression index for the investigated soil.

Introduction

Expansive clays in eastern Saudi Arabia are invariably fissured due to desiccation in the prevalent arid climate (Abduljauwad 1994). In addition to clay mineral species such as smectite and illite, most local soil deposits contain high quantities of diagenetically developed anhydrous calcium sulfate ($CaSO_4$). Hydration of this secondary mineral to form gypsum ($CaSO_4.2H_2O$) can cause up to 60% swelling whereas gypsum dehydration and a reversal back to anhydrite can result in a maximum compressibility of 40% (Zanbak and Arthur 1986). These distinctive features govern the behavior of indigenous expansive clays and influence the nature and extent of the resulting geotechnical engineering problems.

Volume change tribulations encountered in eastern Saudi Arabia occur in both vertical and horizontal directions (Azam and Abduljauwad 2000). Typical problems due to vertical soil deformation include differential movements in residential units, undulating water supply and sewerage lines, massive uplift in pavement embankments, and settlement in multi-storey buildings. Several housing and commercial complexes in the area suffer structural distress in the form of cracks in masonry walls, grade beams, and members of reinforced concrete. Horizontal distress is observable in numerous abutments of road drainage structures and in retaining walls constructed for stabilizing slopes.

Geotechnical problems in the area are primarily attributed to human activity such as lawn watering and utility leakages in constructed facilities as well as excessive water curing of poured concrete and masonry bricks during construction. Lightly loaded structures are particularly vulnerable to damages when the subsoils are periodically and/or differentially wetted and dried. In a newly constructed 600 unit housing compound, 40 residential units had to be demolished for unserviceability. The main reason for this loss was an incomprehensive investigation of the underlying expansive clays that lead to inadequate design (Abduljauwad 1994).

The objective of this paper was to understand the volume change behavior of a local expansive clay containing 50% anhydrous calcium sulfate. Swelling and consolidation tests were conducted on undisturbed field samples according to the constant volume method. A conventional oedometer sample was used to determine the maximum possible volume change and a large-scale oedometer sample was used to capture the influence of fissuring on volume change. The latter sample was thoroughly instrumented to determine the vertical and the lateral swelling pressure.

Soil Development

Eastern Saudi Arabia is part of a rectangular depression, representing a buried basement configuration, that rises at a rate of approximately 1 m/km westward and northward from the Persian Gulf (Al-Amoudi and Abduljauwad 1995). The surface soils include argillaceous shale and calcareous materials such as dolomitic limestone, marl, and chert in several formations of the Phanerozoic succession (Slater 1983). These materials weathered to the present-day expansive clays in the Gulf basin that restrained water mobility. An abundance of Na^+, K^+, Ca^{2+}, Mg^{2+}, Cl^-, and SO_4^{2-} in regional waters catalyzed such chemical weathering (Mitchell and Soga 2005).

Calcium sulfate developed within the calcareous expansive clays due to extensive dolomitization. This diagenesis was initiated in the host aragonite-rich clays when Mg^{2+} replaced Ca^{2+} in the crystal lattice of aragonite. The displaced Ca^{2+} combined with SO_4^{2-} from the pore water to precipitate as gypsum that, in turn, dehydrated to form anhydrite (Blyth and deFreitas 1984). Given the limited water mobility, these reactions mainly occurred in isolated pockets thereby leading to the formation of granular calcium sulfate (Azam and Abduljauwad 2000). Reworking during the sequential geological cycle of deposition, burial, uplift, and erosion imparted soil heterogeneity. The present-day clay deposits of Al-Qatif, Al-Hassa, and Ummus Sahik contain anhydrous calcium sulfate as granular inclusions in their profiles (Azam et al. 1998).

The eastern part of the Arabian Peninsula falls within the Hot Dry (B) climate according to the Köppen Climate Classification. The average annual rainfall and evaporation are 50 mm and 1250 mm, respectively (Al-Amoudi and Abduljauwad 1995). The region does not receive any appreciable precipitation for at least eight months of the year, that is, from April through November. During these months, the average temperature ranges from 15°C to 45°C and can reach up to 50°C, remaining high for several successive days in the summer. This harsh climate renders local expansive clays desiccated to the extent that calcium sulfate loses its structural water and occurs in an anhydrous form. According to Wilson et al. (1997), unsaturated soils undergo cracking because of a net upward flux that is associated with an increase in soil suction. The exposed surface layers of local clay deposits observe this generalization and invariably exhibit extensive fissuring (Abduljauwad 1994).

Laboratory Investigations

The laboratory investigations were conducted on a fissured expansive clay containing 50% anhydrous calcium sulfate. Undisturbed block samples were obtained from a 3 m deep and 4 m x 4 m test pit near Al-Qatif, Saudi Arabia (latitude 26°30′ N and longitude 50°00′ E). After excavation with a Poclain Series 90 backhoe, the floor of the test pit was leveled and stainless steel boxes were slowly inserted into the ground to retrieve individual samples. The soil around the boxes was dug out to isolate the samples from the parent soil. Stainless steel plates were fastened to the boxes and the latter were carefully inverted. To preserve the in situ moisture, the samples were wrapped with cheesecloth and painted with molten wax. All samples were stored at 25°C in a humidity chamber.

The amount of anhydrite in the expansive clay was determined by the $BaSO_4$ method (Nelson 1982). The index properties were determined according to standard ASTM test methods. Likewise, the volume change behavior of the field samples was determined using the constant volume method as per the ASTM Standard Test Methods for One-Dimensional Swell or Settlement Potential of Cohesive Soils (D4546-96). Both conventional and large-scale oedometers were used. The design, fabrication, and calibration of the large-scale oedometer and the large-scale sample mold was described earlier by Azam et al. (2000).

Figure 1 gives the spatial arrangement of ENTRAN (EPN-300-100) pressure transducers in the large-scale sample. Three surface transducers were installed radially at an equal separation distance and three mid-depth transducers were installed circumferentially 120° apart in the circular sample. The surface and mid-depth transducers measured the vertical swelling pressure (p_{vs}) and the lateral swelling pressure (p_{ls}), respectively.

During the entire process, the samples were carefully handled to minimize disturbance. Despite precautions, some disturbance was unavoidable and may have occurred during sample retrieval and transportation as well as during transducer installation and oedometer mounting. According to Fredlund et al. (1980), disturbance increases soil compressibility and prevents the sample to return to the field stress state at the in situ void ratio. To account for sample disturbance, the measured swelling pressure was corrected.
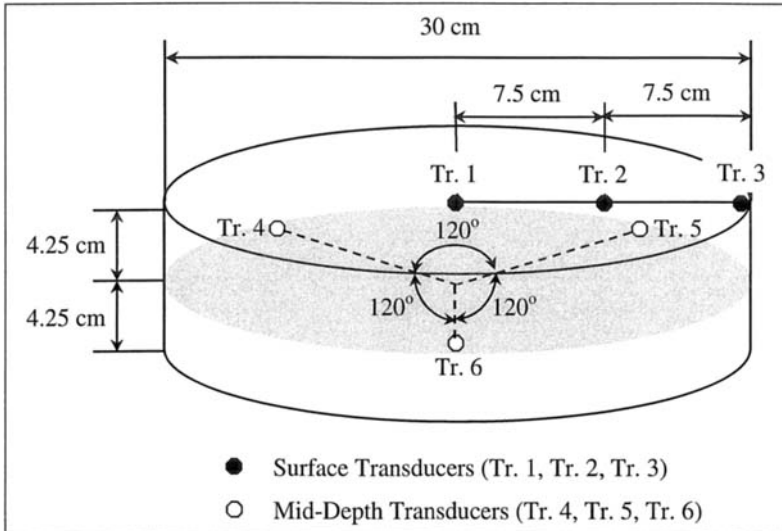
Figure 1: Transducer arrangement in large-scale sample

Results and Discussion

Table 1 summarizes the index properties of the investigated clay. The exposed strata at the sampling site constituted brown clay with calcium sulfate intercalation up to a depth of 3 m. The measured water content (w) for the top 1 m to 3 m of the deposit averaged 28%. Likewise, the specific gravity (G_s) and the dry unit weight (γ_d) of the clay measured 2.85 and 1.37 g/cm^3, respectively. From knowledge of γ_d, the in situ soil void ratio (e_i) was determined to be 1.1. With a degree of saturation (S) of 75%, the surface layer appeared desiccated and exhibited soil discontinuities. A visual survey of the exposed cutting showed extensive variation in the dip angles of fissures with respect to the horizontal. The high values of liquid limit (w_l) and plastic limit (w_p) indicated the high water intake and water holding capacity of the investigated clay (Mitchell and Soga 2005).

Table 1: Index Properties of the investigated clay

Property	ASTM Standard	Value
Water Content, w (%)	D 2216 – 98	28
Specific Gravity, G_s	D 854 – 00	2.85
Dry Unit Weight, γ_d (g/cm^3)	D 5030 – 04	1.37
In Situ Void Ratio, e_i*		1.1
Degree of Saturation, S (%)[†]		75
Liquid Limit, w_l (%)	D 4318 – 00	115
Plastic Limit, w_p (%)		55

* $e_i = (G_s/\gamma_d) - 1$
[†] $S = w\, G_s/e_i$

Figure 2 gives the constant volume test results in the form of void ratio versus applied pressure for the conventional sample. The data depicted herein represents actual soil deflections minus apparatus compressibility (apparatus calibration data is not given in this paper). The sample was initially subjected to a seating pressure of 7 kPa and immediately inundated with water. Permeation of the soil sample was initiated at the bottom and water was allowed to move upwards. The oedometer was equipped with a pneumatic loading system to prevent vertical expansion of the specimen due to water addition. A load cell connected to a data logger measured the pressure required to prevent expansion. After the swelling pressure was fully developed, the submerged specimen was loaded and unloaded incrementally. Volume changes during consolidation were recorded by a Linear Variable Displacement Transducer (LVDT) connected to a data logger that, in turn, was linked to a portable computer.

The measured swelling pressure, pertaining to the maximum value on the initial straight-line portion of the curve, was corrected to account for sample disturbance. Horizontal, tangential, and bisector lines were drawn through the point of maximum curvature on the compression branch of the curve. The intersection of the compression line with the bisector line represented the corrected swelling pressure (Fredlund and Rahardjo 1993). The corrected vertical swelling pressure for the investigated clay was found to be 320 kPa, which was more than twice the measured value. As mentioned earlier, disturbance increased soil compressibility and prevented the sample to return to the field stress state at the in situ void ratio.
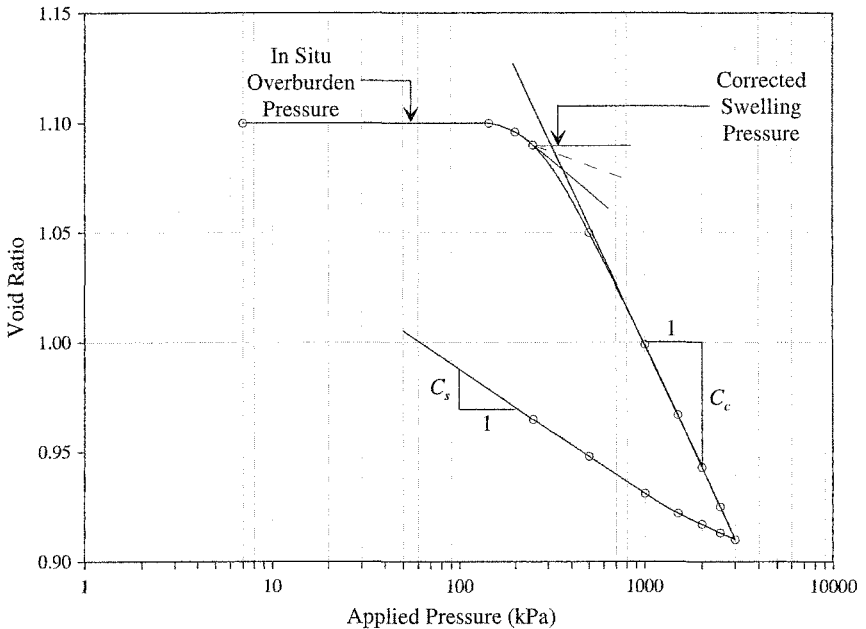
Figure 2: Void ratio – applied pressure for conventional sample

The compression index (C_c) and the swelling index (C_s) of the soil were 0.189 and 0.057, respectively. The C_c fell within the range typical of inorganic silty clays, which is between 0.15 and 0.3 (Mitchell and Soga 2005). The high C_s (about one-third of the C_c) is attributed to the infilling of soil discontinuities with expanded clay and calcium sulfate particles. The sample rebounded when unloaded because the preceding loading mainly removed the pore water. Much of the adsorbed clay water and the structural calcium sulfate water remained in the sample (Azam et al. 2000).

Figure 3 plots the measured vertical swelling pressure versus elapsed time for the conventional sample. The data depicted herein represents the initial straight-line portion of Figure 2. The S-shaped vertical swelling pressure curve shows that water moved through the desiccated sample in a typical manner. According to Barbour et al. (1992), water flow through an unsaturated soil takes place under a hydraulic gradient set up by negative pore water pressure within the sample relative to free water, that is, soil suction. The swelling pressure curve comprised of initial, primary, and secondary stages. The low swelling rate during the initial stage is attributed to the low unsaturated hydraulic conductivity of the sample. Once water mobility was initiated, both the clay and anhydrous calcium sulfate particles were readily hydrated thereby resulting in a high rate of primary swelling. The gradual reduction in the swelling rate during the primary and secondary stages and the eventual cessation of the vertical swelling pressure in the latter stage is attributed to increasing sample saturation due to water migration. A higher degree of saturation is associated with a lower soil suction that translates to a lower soil affinity for water adsorption.
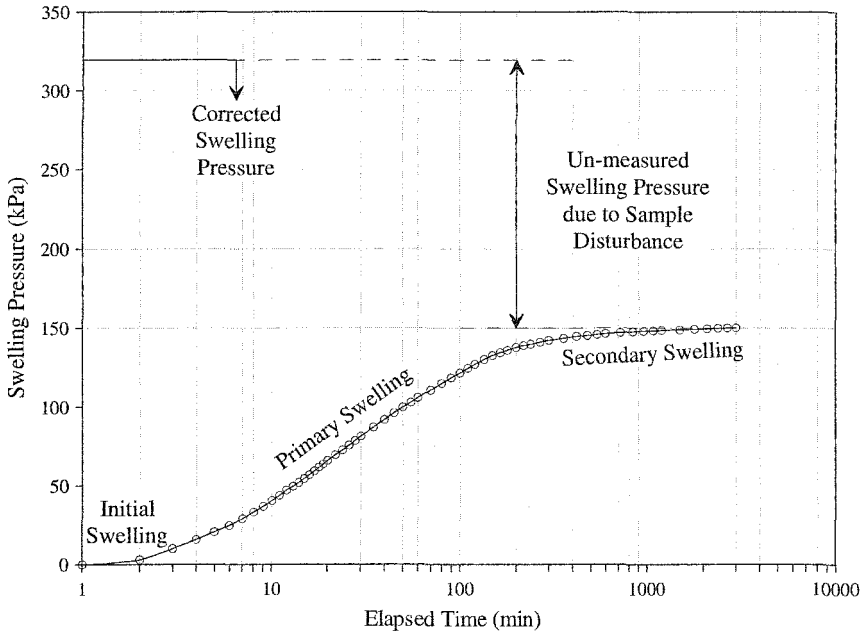
Figure 3: Measured swelling pressure – time for conventional sample

The surface layer of the clay deposit experiences 54 kPa overburden pressure and the measured swelling pressure of 150 kPa misrepresented the soil as one with low swelling capability. The corrected swelling pressure of 320 kPa was more than twice the measured value and this observation was typical of desiccated clays. Fredlund et al. (1980) reported more than 300% increase in swelling pressure for a similar clay deposit from Regina, Canada. Correction to the measured swelling pressure was the prerequisite for an adequate soil characterization. The conventional sample gave an upper bound swelling pressure because of an incomprehensive capture of a key feature of the local clay deposit, namely; soil fissuring.

Figure 4 gives the constant volume test results in the form of void ratio versus applied pressure for the large-scale sample. The test was conducted as before and the data were corrected for apparatus compressibility. The corrected vertical swelling pressure was found to be 245 kPa. This amounted to a reduction of about 25% over the conventional sample and is attributed to the large sample size that contained numerous soil fissures. These discontinuities adsorbed part of the deformation during expansion of both clay and calcium sulfate particles.

The C_c of the soil in the large-scale sample was 0.15. This reduction was due to the 20 times higher wall contact area of the large-scale sample (800 cm^2) compared to the conventional sample (40 cm^2). The deforming soil was offered a greater frictional resistance that allowed a smaller change in void ratio under a given load. The unaltered C_s confirmed the removal of only the pore water, and not the adsorbed clay water or the structural calcium sulfate water, during consolidation.
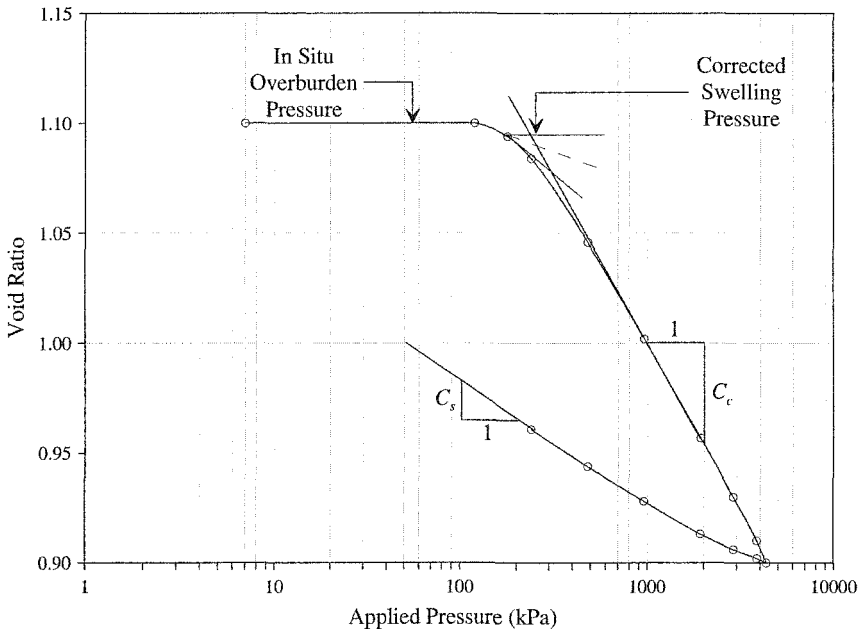
Figure 4: Void ratio – applied pressure for large-scale sample

Figure 5 gives the development of the measured swelling pressure as a function of time for the large-scale sample. Both the vertical swelling pressure and the lateral swelling pressure plotted as S-shaped curves indicating the typical water movement through the unsaturated soil, as described earlier. The time required for the three swelling stages was higher (and the rate of water mobility was lower) than the conventional sample because water traversed much longer paths in the large-scale sample. Due to an abundance of soil discontinuities in the latter sample, water initially moved favorably into these paths of least resistance. However, soil particles expanded into the void spaces thereby closing the flow channels; subsequent water flow occurred through the regular soil matrix (Barbour et al. 1992). This internal assimilation of soil expansion in the large-scale sample resulted in slower swelling pressure development when compared with the conventional sample.

The corrected vertical swelling pressure of 245 kPa was approximately twice the measured value of 120 kPa. The vertical swelling pressure of the investigated clay measured by the load cell closely matched the average vertical swelling pressure obtained from the three surface transducers. The vertical swelling pressure recorded by the surface transducers gradually increased away from the center and reached a maximum of 134 kPa along the wall. This trend was analogous to the contact pressure distribution of rigid footings on clays and can be confirmed using the theory of elasticity. Given an initially leveled sample surface, the non-uniform vertical swelling pressure distribution is partially related to the inhomogeneity of the investigated clay and to sample disturbance.
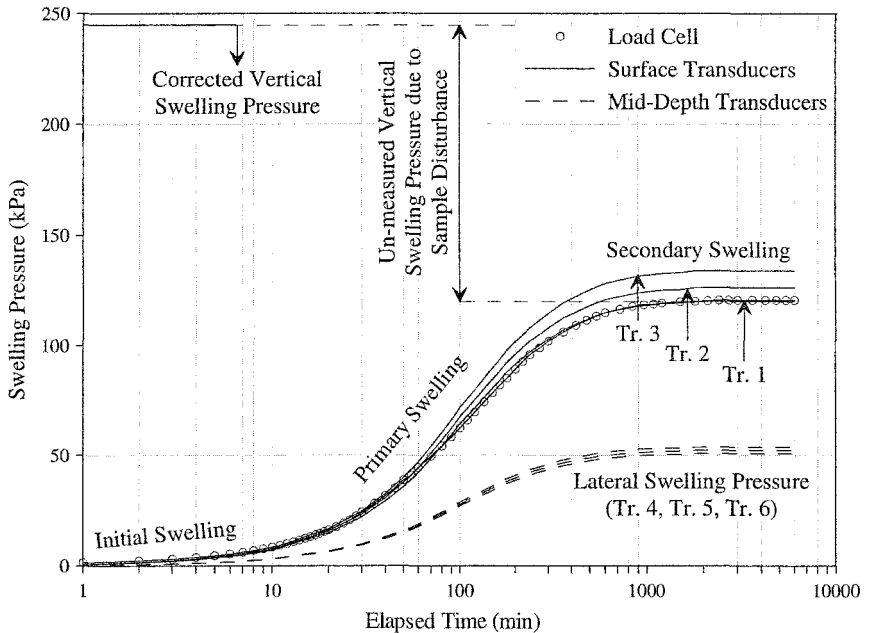
Figure 5: Measured swelling pressure – time for large-scale sample

The average lateral swelling pressure measured 51 kPa, which equated to 40% of the average measured p_{vs}. This reduction is attributed to the predominantly horizontal clay particle stacking in the deposit with localized randomly oriented anhydrous calcium sulfate (Azam et al. 1998). Water was adsorbed between the stacked clay platelets causing the latter to push in the direction normal to the layering. Vertical swelling pressure developed when this expansive movement of the clay particles was restrained by the top and bottom plates. Due to this confinement, the sample laterally redistributed part of the clay expansion (Edil and Alanazy 1992). Volume increase due to calcium sulfate hydration was randomly redirected.

Table 2 summarizes the volume change characteristics of the investigated clay. Heave (ΔH) in the surface layer of the deposit was predicted using the following equation (Fredlund and Rahardjo 1993):

$$\Delta H = H \frac{C_s}{1 + e_i} \log \frac{p_{vs}}{\sigma_{vf} - u_{wf}} \tag{1}$$

where, H was the thickness of the swelling soil, σ_{vf} was the total vertical overburden pressure and u_{wf} was the final pore water pressure. For a constant vertical swelling pressure in the soil layer and $u_{wf} = 0$, the estimated heave was 62.9 mm from the conventional sample and 53.5 mm from the large-scale sample. The table indicates that the former sample provided an upper bound of volume change. The large-scale sample better represented field conditions due to an effective capture of soil fissuring.

Table 2: Summary of volume change characteristics of the investigated clay

Parameter	Conventional Sample	Large-Scale Sample
Vertical Swelling Pressure, p_{vs} (kPa)		
Measured	150	120
Corrected	320	245
Lateral Swelling Pressure, p_{ls} (kPa)*	----------	51
Compression Index, C_c	0.189	0.150
Swelling Index, C_s	0.057	0.057
Estimated Heave, ΔH (mm)	62.9	53.5

* Measured Average of Tr. 4, Tr. 5, and Tr.6

Conclusions

1. Geology and climate govern the development and behavior of expansive clays in eastern Saudi Arabia. Local clay deposits are invariably fissured and contain high quantities of anhydrous calcium sulfate.

2. Due to an effective capture of soil fissuring, the large-scale sample provided better volume change estimates. The discontinuities partly consumed the expansive movement of the soil during hydration.

3. Correction yielded a two-fold increase in measured swelling pressure of the desiccated clay. The corrected vertical swelling pressure of the clay was 320 kPa for the conventional sample and 245 kPa for the large-scale sample.

4. The measured lateral swelling pressure was about 40% of the measured vertical swelling pressure. Likewise, the swelling index was one-third of the compression index for the investigated soil.

Acknowledgments

References

Abduljauwad, S.N. (1994). Swelling behavior of calcareous clays from the Eastern Province of Saudi Arabia. *Quarterly Journal of Engineering Geology*. 27: 333-351.

Al-Amoudi, O.S.B. and Abduljauwad, S.N. (1995). Compressibility and collapse potential of an arid, saline sabkha soil. *Engineering Geology*. 39(3):185-202.

Azam, S. and Abduljauwad, S.N., (2000). Influence of gypsification on engineering behavior of expansive clay. *Journal of Geotechnical & Geoenvironmental Engineering*. 126(6):538-542.

Azam, S., Abduljauwad, S.N., Al-Shayea, N.A., and Al-Amoudi, O.S.B. (2000). Effects of calcium sulfate on swelling potential of an expansive clay. *Geotechnical Testing Journal*. 23(4):389-403.

Azam, S., Abduljauwad, S.N., Al-Shayea, N.A., and Al-Amoudi, O.S.B. (1998). Expansive characteristics of gypsiferous/anhydritic soil formations. *Engineering Geology*. 51(2):89-107.

Barbour, S.L., Fredlund, D.G., Gan, J.K-M., and Wilson, G.W. (1992). Prediction of moisture movement in highway subgrade soils. *Proceedings, 45th Canadian Geotechnical Conference*. Toronto, ON, Canada. 41(A):1-13.

Blyth, F.G.H., and deFrietas, M.H. (1984). *A Geology for Engineers*. 7th ed., Butler and Tanner, London, UK.

Edil, T.B. and Alanazy, A.S. (1992). Lateral swelling pressures. *Proceedings, 7th International Conference on Expansive Soils*, Dallas, TX, USA. 1: 227-232.

Fredlund, D.G. and Rahardjo, H. (1993). *Soil Mechanics for Unsaturated Soils*. John Wiley and Sons, Inc. NY, USA.

Fredlund, D.G., Krahn, J., and Hasan, J.U. (1980). Variability of an expansive clay deposit. *Proceedings, 4th International Conference on Expansive Soils*. Denver, CO, USA. 1:322-338.

Mitchell, J.K. and Soga, K. (2005). *Fundamentals of Soil Behavior*. 3rd ed. John Wiley and Sons, Inc. NY, USA.

Nelson, R.E. (1982). Carbonate and Gypsum. *Methods of Soil Analysis*. 2nd ed., American Society of Agronomy, Madison, Wisconsin. 29(2):181-197.

Slater, D.E. (1983). Potential expansive soils in Arabian Peninsula. *Journal of Geotechnical Engineering*. 109(5):744-746.

Wilson, G.W., Fredlund D.G., and Barbour, S.L. (1997). The effect of soil suction on evaporative fluxes from soil surfaces. *Canadian Geotechnical Journal*. 34(1):145-155.

Zanbak, C. and Arthur, R.C. (1986). Geochemical and engineering aspects of anhydrite/gypsum phase transitions. *Bulletin of the International Association of Engineering Geologists*. 23(4):419-433.

Analysis of the Volume Change Behavior of Expansive Compacted Soils

C. L. Velosa[1] and J. E. Colmenares[2]

[1]School of Engineering. National University of Colombia – Bogotá. 30th Avenue # 45-03, Building 406, Room 208; Phone: +(57)-1-3165000 ext. 13312; Fax: +(57)-1-3165459; e-mail: clvelozag@unal.edu.co
[1]School of Engineering. National University of Colombia – Bogotá. 30th Avenue # 45-03, Building 401, Dean Office; Phone: +(57)-1-3165000 ext. 13552; Fax: +(57)-1-3165184; e-mail: jecolmenaresm@unal.edu.co

Abstract

Compacted mixtures of sand-bentonite (commonly named Bentonite Enhanced Sand, BES) are widely used to control the movement or migration of hazardous substances from the disposal site to the surrounding environment. Barriers built with those materials exhibit high strength and low compressibility with a very low permeability. Those characteristics can be reached by using mixtures with enough sand (to ensure good stability of the compacted mixture) and bentonite (to fill the voids between the sand particles). This paper shows the results of an experimental study of the volumetric behavior of compacted mixtures of sand-bentonite following wetting under constant vertical stress. The influence of initial compaction conditions, the applied vertical stress and the bentonite content were studied. The experimental program included a series of odometer tests performed with samples compacted at different densities and water contents. The results indicate that the development of swelling deformations with time is highly dependent on the compaction conditions of the BES and the confining stress.

Introduction

Compacted mixtures of sand-bentonite have been used in the construction of barriers to isolate the disposal of toxic waste due to its excellent structural stability and low hydraulic conductivity. Even though the behavior of those soils had been studied by numerous authors (Chapuis, 1990; Bradley et al., 1998; Alawaji, 1999; Komine et al., 1994, 1999; Colmenares, 2002 and Stewart et al., 2003), it is necessary to continue the study of such materials in order to understand their behavior so that rational methods of engineering liner design can be implemented.

Compacted barriers of BES exhibit a condition of partial saturation. Therefore, the study of compacted BES needs to take into account the recent developments in unsaturated soil mechanics. This document includes the results of an experimental investigation on the volume change behavior of compacted, unsaturated BES. The influence of the applied vertical stress, the initial dry density, the compaction water content and the bentonite content was studied. The results suggest that a combination of initial conditions such as low confining stresses, high dry densities and low compaction water contents result in swelling deformations when the water content of the soil is subsequently increased. On the other hand, high confining stresses, low initial dry densities and low compaction water contents contribute to the occurrence of collapse deformations when the sample is wetted.

Materials and Sample Preparation

Materials. A mixture of thirty percent of sodium bentonite (30%) and seventy percent of sand (70%), by dry weight, was used. The index properties and the chemical analysis of the bentonite used are shown in Table 1.

Table 1. Index Properties and Chemical Analysis of Bentonite

INDEX PROPERTIES		CHEMICAL ANALYSIS (%)	
Type	sodium bentonite	CaO	0.69
Specific gravity	2.925	SiO_2	56.59
Liquid Limit	470 %	Al_2O_3	18.71
Plastic Limit	38 %	Fe_2O_3	7.44
Plasticity Index	432 %	MgO	2.32
clay content ($< 2\mu$)	93 %	Na_2O	2.16
Activity	4.6	K_2O	0.16

The used sand corresponds to a well graded sand composed of silica. The index properties and the chemical analysis of sand are listed in Table 2. Table 3 shows the particle size distribution of the sand.

Table 2. Index Properties and Chemical Analysis of Sand

INDEX PROPERTIES		CHEMICAL ANALYSIS (%)	
Type	silica sand	milky quartz	97.2
Specific gravity	2.640	pink quartz	0.9
Uniformity coefficient	3.5	smoked quartz	1
Curvature coefficient	1.14		

Table 3. Gradation of Sand

Diameter (mm)	Percentage passing
2.000	100
1.190	48.34
0.600	18.53
0.425	11.44
0.300	7.02
0.250	5.44
0.150	2.66
0.075	1.01

A parametric study to identify the influence of the hydration time on the values of Atterberg limits was carried out. The Atterberg limits were evaluated for different hydration times (1, 7, 21 and 28 days) with the ASTM D 4318-00 standard (using the fraction smaller than 0.425 mm by dry method). Because the behavior of the fraction smaller than 0.425 mm may not be a good indicator of the behavior of the entire compacted BES, Atterberg Limits were also obtained for the entire un-graded specimen. The results are shown in Table 4 which represents the average values obtained with three tests. The specific gravity was also obtained for the entire un-graded specimen.

The difference in Atterberg Limits obtained with both methods was contributed to the effective bentonite content of the tested material, where the effective bentonite content was found to be 80% with the ASTM procedure and 30% with the second method. For the whole fraction, the granular material reduces significantly the plasticity of the sample. On the other hand, the variation of the Atterberg Limits measured at different hydration times is an indication of the importance of physical-chemical phenomena occurring at the micro-structural level over the mechanical behavior of clay materials. Gens and Alonso (1992) considered that the behavior of partly saturated soils is highly influenced by different processes occurring at the particle level; therefore, for the formulation of their constitutive model for partly saturated expansive soils (Barcelona Expansive Model, Gens et al,, 1992), a distinction is made between structural levels: a micro-structural level containing all the chemically active minerals and a macro-structural level resulting from the aggregation of the elementary particles of clay.

Table 4 illustrates that Liquid Limit, *LL*, is highly dependent of hydration time and the Plastic Limit, *PL*, is relatively constant. Casagrande (1932) found LL is nearly equal to the water content at which a soil has shear strength of about 2.5 kPa. Russell and Mickle (1970), Wroth and Word (1979) and Whyte (1982) indicated that LL for fine-grained soils corresponds to shearing resistance between 1.7 and 2.0 kPa. This means that the decrease of LL with time could be associated with any increase of the material strength. In this way, the water content necessary to satisfy the strength

conditions at LL is smaller. That behavior could be related with a combination of two different phenomena: Syneresis and Thixotropy of the clay minerals.

When materials are at rest (e.g. hydration is occurring), if the repulsion forces after mixing are bigger than the attraction forces, there will be a tendency towards flocculation of particles and particle groups; therefore a reorganization of the water-cation structure, to a lower energy state, will occur. This process is time dependent and is known as Thixotropic hardening. Simultaneously, it is possible that some kind of bonding between clay particles is developing. It may cause the contraction of the soil structure and the expulsion of liquid from its pores. This contributes to the stiffening of the soil and the increase of the shearing resistance. This phenomenon is also time dependent and is named Syneresis. (Mitchell J, 1996 and Forero C, 1998).

Table 4. Atterberg Limits of Mixtures (BES)

	ASTM D 423-66 and 424-59				whole sample			
	hydration times				hydration times			
	1	7	14	28	1	7	14	28
Liquid Limit (%)	248	228	214	202	71	68	56	55
Plastic Limit (%)	28	29	30	30	15	15	16	16
Plasticity Index	220	199	184	172	56	53	40	39
Specific gravity	2.720							

Sample Preparation. The sand and the air dry bentonite were mixed initially by hand to obtain an uniform mixture. Then water was added slowly while mixing continued ensuring a uniform distribution of the water. The material was stored in plastic bags in a closed environment for a period of minimum 28 days before compaction. This allowed enough hydration time and a uniform water distribution within the mixture. Samples of 64 mm diameter and 28 mm height were statically compacted. After compaction, the degree of saturation, void ratio and initial density were recorded. Controlled laboratory environmental conditions were guaranteed. A temperature of 18° C $\pm$ 0.5° C and a relative humidity of $75\% \pm 0.5\%$ were monitored.

Experimental Program

In order to study the influence of initial water content and dry density over volume change behavior of BES, samples were compacted statically at different initial dry densities (ranging from 1.13 Mg/m^3 to 1.76 Mg/m^3), and at different initial water contents (ranging between 6.96% and 13.93%). The samples were loaded to a constant vertical stress in a standard odometer, recording the vertical strains. In order to study the influence of the applied vertical stress, 42.5 kPa, 85 kPa and 170 kPa pressures were used. When no more vertical deformation was observed, the samples were soaked.

Experimental Results

Volume Changes. Figure 1 shows the potential of volume change of compacted BES, on a compaction plot, for different initial dry densities and water contents after a wetting process under a constant vertical stress of 42.5 kPa. The potential of volume change was evaluated as:

$$\varepsilon = \frac{\Delta h}{H_o} * 100\% \qquad (1)$$

where ε is the potential of volume change (swelling/collapse) or volumetric strain, Δh is the change in height of the sample, and H_o is the initial height of the sample. Two mechanisms of volume change were identified during the wetting stages: swelling (increase in volume) and collapse (reduction in volume). A combination of conditions such as relatively high densities and low compaction water contents (related to with the standard compaction characteristics, $\rho_{d\max} = 1.79 \, Mg/m^3$ and $w_{opt} = 16.5\%$), contribute to the generation of swelling, when the material is soaked. This behavior is related to the size of the macro-structural pores resulting from the compaction process. Under those conditions the bentonite has less space to swell within the macro-structure and therefore results in a general increase of the sample volume. Additionally, for a given volume, a sample with a higher density contains more solids than a sample with a low density and therefore more clay particles are involved in the swelling process.

On the other hand, low dry densities and low compaction water contents contribute to the occurrence of collapse deformations. In this case, the sand particles are in a loose condition and their temporal stability is associated to capillary forces and the effect of clay bridges between the particle contacts (Dineen et al., 1999 and Colmenares, 2002). When the soil under those conditions is wetted, the capillary forces are reduced, the clay bridges tend to get softer and therefore, because of the vertical stress applied the sand particles tend to slide producing a denser arrangement.

A region of negligible volume change can also be identified in Figure 1. That region is located at densities close to 78% of the optimum compaction conditions. The region is almost parallel to the water content axis and becomes bigger as the water content increases.
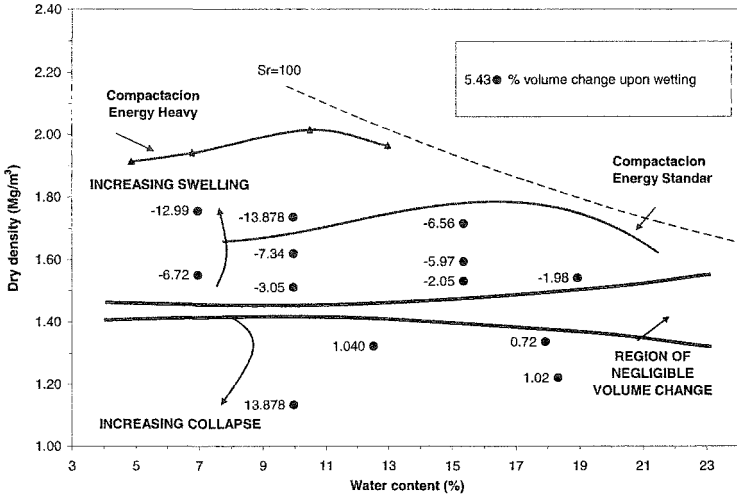
Figure 1. Volumetric Change upon Wetting under Constant Vertical Stress of 42.5 kPa

Figures 2 and 3 show the contours of equal volume change potential for constant vertical stresses of 85 kPa and 170 kPa, respectively. A vertical movement of the negligible volume change region can be seen. Additionally, a reduction of the swelling deformations and an increase of the collapse deformations can be observed with the increase of the confining stresses. The lowest swelling potential of the soil is associated with the highest confining stresses. For a given density, this behaviour is due to a reduction in the swelling pressure of bentonite, and therefore the volume change is minor.
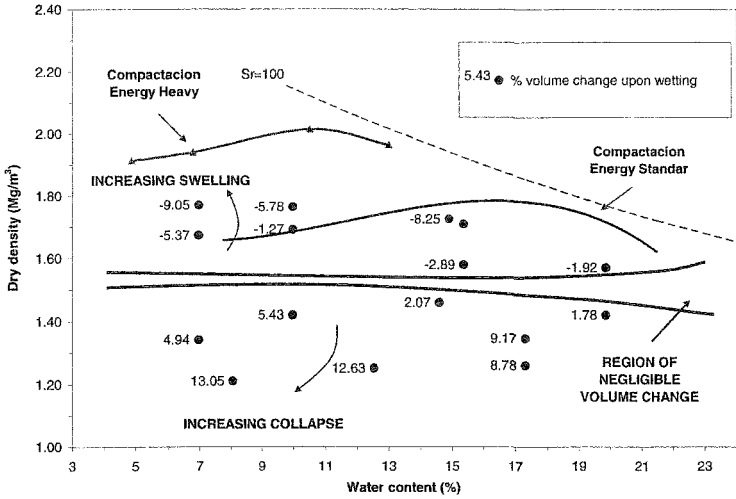
Figure 2. Volumetric Change upon Wetting under Vertical Stress of 85 kPa
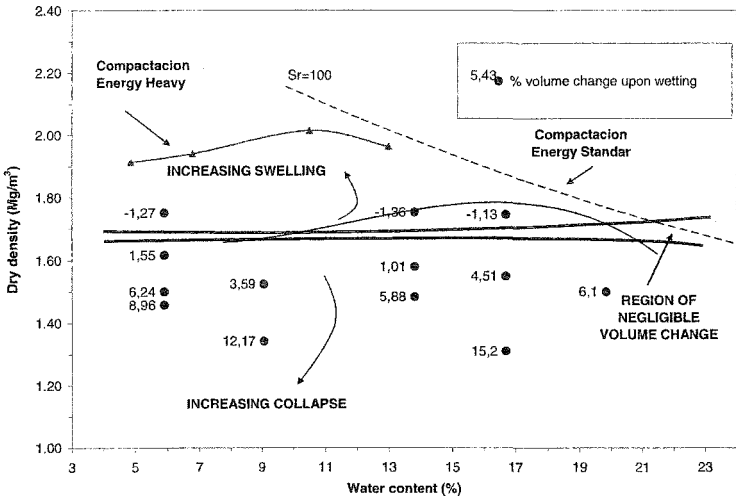
Figure 3. Volumetric Change upon Wetting under Vertical Stress of 170 kPa

Influence of Betonite Content. Figure 4 shows the relationship between the maximum swelling or collapse volumetric strain (after soaking) and the compaction dry density of samples of BES with different bentonite contents under a constant vertical stress of 85 kPa. The information shows the experimental results presented by Colmenares (2002) and those obtained during this investigation. It is observed that an increase in bentonite content corresponds to a smaller density for the condition of zero volume change. The increase of clay particles associated with a higher bentonite content means that more physico-chemical activity is occurring at a particle level during the wetting stage. Therefore, the swelling potential increases as the bentonite content increases.
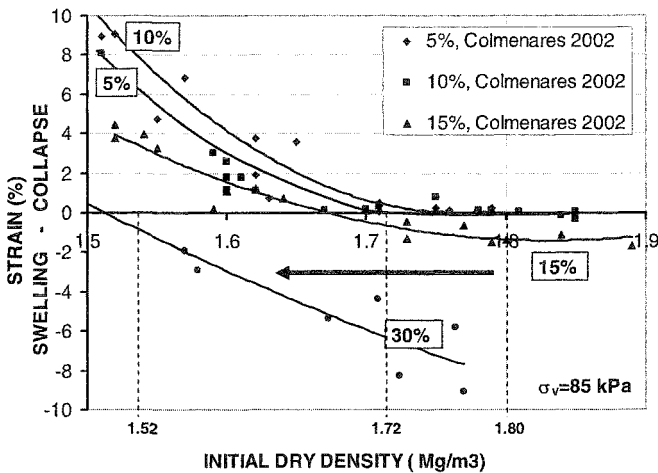
Figure 4. Strain vs. Dry Density per Varying Betonite Content

Swelling Deformations of BES. Figure 5 shows the results of a wetting test on compacted BES with low initial water content (9.97%) at different initial dry densities. The samples were wetted under a constant vertical stress of 42.5 kPa and 85 kPa. The development of swelling deformations with time can be appreciated. The rate of deformation is higher for the denser sample. The maximum swelling deformations are exhibited by the densest sample under low vertical stresses. Therefore, volumetric deformations are dependent on the initial dry density and on the confining stress.
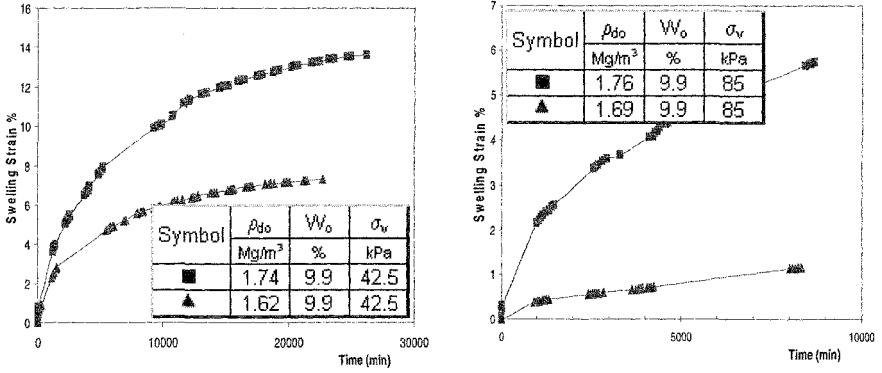
Figure 5. Evolution of the Swelling Strain with time at Lower Water Content. a) Vertical Stress of 42.5 kPa, b) Vertical Stress of 85 kPa

Figure 6 shows similar results but this time for samples compacted at higher water contents. For low confining stresses the initial rate of deformation is bigger for low density samples. However, denser samples exhibit higher final deformations.
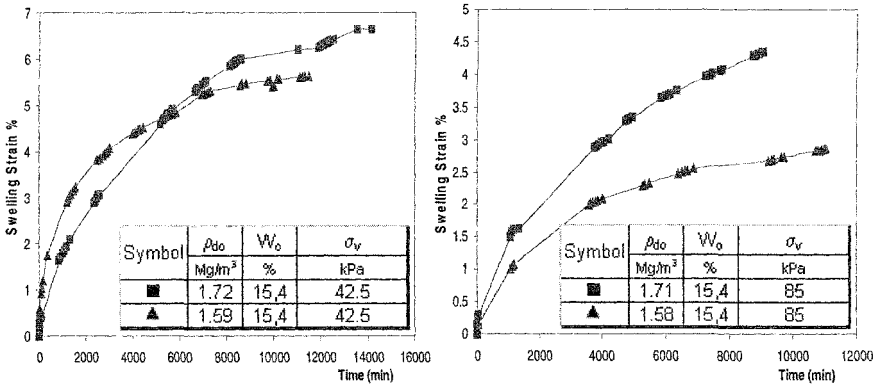
Figure 6. Evolution of the Swelling Strain with Time at Higher Water Content. a) Vertical Stress of 42.5 kPa, b) Vertical Stress of 85 kPa

Figures 7 and 8 show the evolution of deformation with time (following wetting) for samples compacted at a similar dry density but different initial water content under the same relatively low confining stress. The results suggest that for low initial dry densities, the development of swelling strains is initially independent of the compaction water content, however the final overall higher swelling is associated with the sample compacted at a lower water content. For high compaction dry

densities, the sample with lower compaction water content also exhibits the higher final swelling deformations and in this case the development of swelling deformations shows a higher rate for the sample compacted at a lower initial water content.

Symbol	ρ_{do} Mg/m^3	w_o % %	σ_v kPa
■	1,59	15,36	42,5
▲	1,62	9,97	42,5
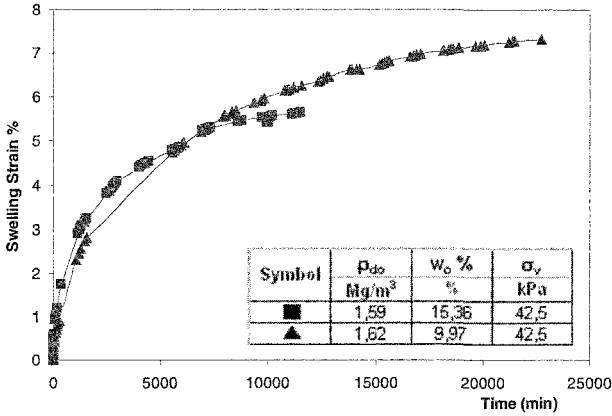
Figure 7. Evolution of the Swelling Strain with Time at Lower Dry Density and Different Water Content

Symbol	ρ_{do} Mg/m^3	w_o %	σ_v kPa
■	1,72	15,36	42,5
▲	1,74	9,97	42,5
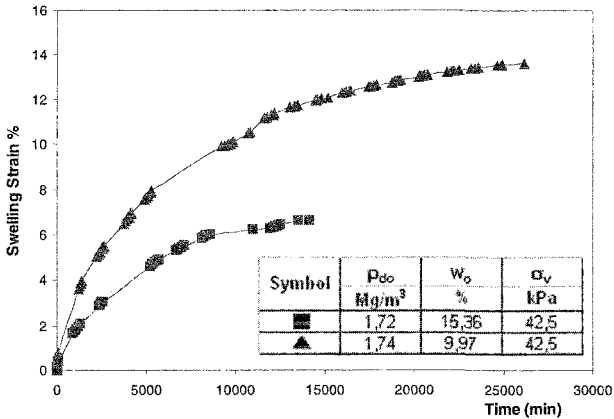
Figure 8. Evolution of the Swelling Strain with Time at Higher Dry Density and Different Water Content

The previous results indicate that the relationship between volumetric swelling deformations and time (during wetting) are highly dependent of the compaction conditions of the BES and the confining stress.

Conclusions

1. In materials of special behavior such as BES, determination of the index properties following standards developed for common soils may not lead to properly characterise the expected soil behaviour.

2. The differences found between the Atterberg limits determined at different hydration times are an indication of the importance that the physico-chemical behavior of the elementary particles may have on the soil behavior. Therefore, it is important to understand and to take into account such phenomena for the modelling and prediction of the behavior of engineered barriers built with those materials.

3. A combination of initial conditions such as low confining stresses, high dry densities and low compaction water contents result in swelling deformations, when the water content of the soil is subsequently increased. On the other hand, high confining stresses, low initial dry densities and low compaction water contents contribute to the occurrence of collapse deformations when the sample is wetted.

4. The magnitude of the confining stress that is applied before wetting influences the size and position of the region of negligible volume change and the magnitude of the volumetric strains (i.e. swelling or collapse). For higher bentonite content lower densities of the samples will exhibit negligible volume change.

5. The development of swelling deformations with time is highly dependent on the compaction conditions and of the confining stress. The maximum swelling deformations are exhibited by the densest samples under low vertical stresses. Therefore, volumetric deformations are dependent on the initial dry density and the confining stress. For low initial dry densities, at low confining stresses, the initial rate of deformation is independent on the initial compaction water content. However, higher final swelling deformations are exhibited by samples compacted at lower initial water contents. For higher initial dry densities and higher confining stresses the development of swelling deformations is highly dependent of the compaction water content. Samples with higher compaction water contents exhibit smaller final swelling deformations.

References

Alawaji, H.A. (1999). "Swell and compressibility characteristics of sand-bentonite mixtures inundated with liquids." *Applied clay Science*, 15, 411-430.
American Society of Testing and Materials. (2000). D 4318 – 00.
Bradley, W., Graham, J., Tang, G.X., and Dixon D. (1998). "Influence of pressure, saturation, and temperature on the behavior of unsaturated sand-bentonite." *Canadian Geotechnical Journal,* 35, 194-205.
Casagrande, A. (1932). "Research on the Atterberg limits of soils." Publics Roads, October.

Chapuis, R.P. (1990). "Sand-bentonite liners: predicting permeability from laboratory tests." Canadian Geotechnical Journal, 27, 47-57.

Colmenares, J.E. (2002). "Suction and volume changes of compacted sand-bentonite mixtures." *PhD Thesis. University of London.*

Dineen, K., Colmenares, J.E., Ridley, A.M. and Burland, J.B. (1999). "Suction and Volume Changes of a bentonite-enriched sand." *Geotechnical Engineering. Proceedings of The Institution of Civil Engineers*, 137(4), 197-201.

Forero, C (1998). "Characterization of a silica-gel as a geotechnical cement." *PhD Thesis. University of London.*

Gens, A., and Alonso, E.E. (1992). "A framework for the behavior of unsaturated expansive clays." *Canadian Geotechnical Journal*, 33, 11-22.

Komine, H., and Ogata, N. (1994). "Experimental study on swelling characteristics of compacted bentonite." *Canadian Geotechnical Journal*, 31, 478-490.

Komine, H., and Ogata, N. (1999). "Experimental study on swelling characteristics of sand-bentonite mixture for nuclear waste disposal." *Soils and Foundations,* 39(2), 83-97.

Mitchell, J.K. (1993). "Fundamentals of Soil Behavior." *Second Edition*, John Wiley and Sons, Inc, New York.

Stewart, D.I., Studds, P.G., and Cousens, T.W. (2003). "The factors controlling the engineering properties of bentonite-enhanced sand." *Applied clay Science*, 23, 97-110.

Russell, E.R., and Mickle, J.L. (1970). "Liquid limit values of soil moisture tension" *Journal of Soil Mechanics and Foundations Division.*, ASCE, 96, 967-987.

Whyte, I.L. (1982) "Soil plasticity and strength – a new approach using extrusion." *Ground Engineering*, 15(1), 16-24.

Wroth, C.P., and Wood, D.W. (1978). "The correlation of index properties with some basic engineering properties of soils." *Canadian Geotechnical Journal*, 15(2), 137-145.

Application of vertical strain control to measure swelling pressure of clayey soils

D. Marcial [1], P. Delage [2] and Y. J. Cui [2]

[1] Instituto de Materiales y Modelos Estructurales, Facultad de Ingeniería, Universidad Central de Venezuela, Apartado 50.361, Caracas 1050-A, Venezuela; PH (212) 605-1743; FAX (212) 605-3135; e-mail: marciald@ucv.ve

[2] Centre d'Enseignement et de Recherche en Mécanique des Sols, Ecole Nationale des Ponts et Chausées, 6-8 Av. B.Pascal, 77455 Marne la Vallée, Cedex 2, Paris, France ; PH (1) 64153544 ; FAX (1) 64153562 ; e-mail : delage@cermes.enpa.fr

Abstract
Since the use of bentonite based engineered barriers has been considered for nuclear waste disposal facilities, swelling pressure measurement techniques have been improved. However, some experimental evidence shows that vertical strain control plays an important role on such measurements. In this paper, some results are presented to show that strain control is a key aspect to be considered when measuring swelling pressure.

Introduction
Since swelling clayey soils have occasioned important economical losses due to induced damage to man made structures, measuring swelling properties on these materials has been a common practice in soil mechanics for decades. To do so, practitioners have traditionally used classical load step oedometer testing, as actually prescribed by international standards (e.g. ASTM). Although, this type of test requires continuous supervision of the technical staff, implicating higher costs as the soil is more impervious and swelling takes longer time periods.

More recently, with the development of nuclear waste repositories (NWR) based on engineered clay barriers (ECB), the determination of swelling properties on highly compacted swelling clays have encouraged researchers to improve on laboratory techniques. This is especially due to the very low permeability and high swelling pressures developed by ECB materials.

Classically, for the characterization of swelling properties of clayey soils, one is interested on the maximal strain the material can develop while soaking under a certain stress level. More precisely, the definition of swelling pressure is the

maximum stress developed by the soil when soaked and kept at constant volume, from a particular initial condition in terms of water content and dry density.

In the case of ECB materials, the confining conditions are nearly constant volume conditions and the swelling pressure becomes an important parameter to be determined. Additionally, in the context of a NWR the ECB will be unsaturated during different periods of the possible evolution scenarios of the system. For that reason, one is also interested in the suction – stress couplings at constant volume conditions.

Actually, the laboratory experimental setup for determining swelling pressure tends basically to be composed by a reaction frame, an oedometer cell and a load cell permitting the continuous monitoring of swelling pressure changes during soaking. This, of course, accompanied by a complete data acquisition system permitting to follow vertical stress changes with a minimum of human supervision. An example of this configuration is shown in Figure 1, as presented by Komine & Ogata (1994).

(1) Reaction frame
(2) Load cell
(3) Oedometer ring
(4) Piston
(5) Base
(6) Porous stone
(7) Sample
$\phi = 60$ mm; h = 5 mm
(8) Water inflow
(9) Drainage
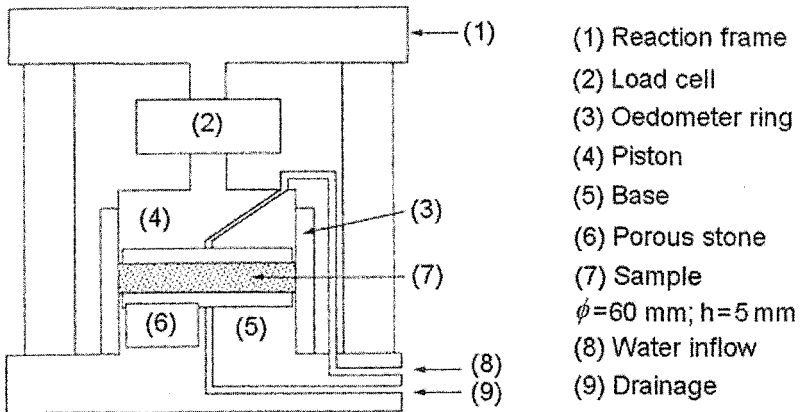
Figure 1. Schematic representation of experimental set-up to determine swelling pressure on ECB materials (Komine & Ogata 1994)

Due to the very low permeability of ECB materials the soil specimens are often very thin ones. To illustrate this, one may point out that Komine & Ogata (1994) have fixed, for the study of swelling properties of Japanese ECB materials (Kunigel VI bentonite/sand mixtures), a thickness of 5 mm, indicating that the deflection δ_v of the reaction frame (see item 1 on Figure 1) was negligible in relation to the size of the specimens ($\delta_v < 0.01$ mm for a 3 MPa swelling pressure).

However, working with a 70/30 Kunigel VI/sand bentonite mixture, Loiseau (2001) obtained a strong dependency between the swelling pressure and the specimen size, by using an experimental set-up similar to that used by Komine & Ogata (1994). Figure 2 shows how the influence of the height h of the specimens reduces as h increases.

One thinks that this dependency is due to the deformation of the system presented in Figure 1, rather than a property of the ECB material. Even if the reaction frame (see item 1 in Figure 1) is rigid enough, its deflection is not the only element to be taken into account within the δ_v value, because all elements contribute to permit in some extent a partial swelling of the specimen. For instance, we have observed in the lab that a commercial 5 Ton load cell (see item 2 in Figure 1) contributes with about 0.25 mm to the δ_v value, when submitted to a 1 T load (about 5.1 MPa for a specimen of 50 mm in diameter). For this stress level, one estimates that the whole system allows for a δ_v value of about 0.5 mm. In the case of 5 mm thick specimens, this strain represents 10 % of its total volume, reducing dramatically the dry density and thus the swelling pressure. For a specimen having h = 5 mm and ρ_d = 1.7 Mg/m^3, a vertical strain of 0.1 induces a density variation of 0.15 Mg/m^3.
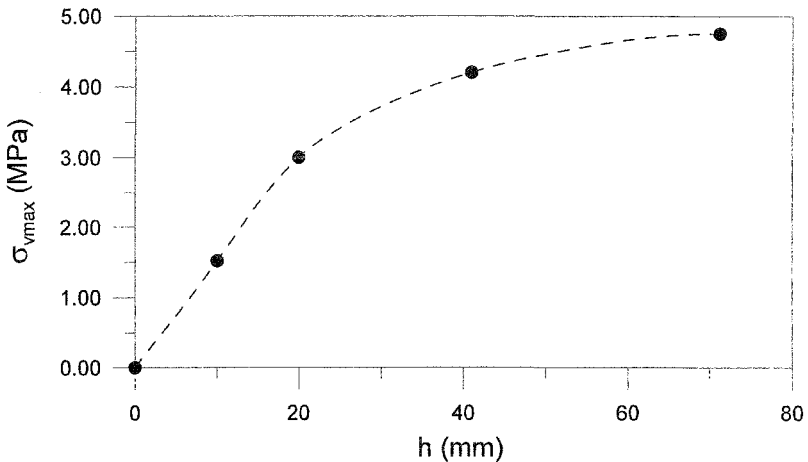
Figure 2. Changes in swelling pressure with the height h for a 70/30 Kunigel VI / sand mixture, for a dry density of about 2 Mg/m^3 (Loiseau 2001).

If one refers now to Figure 3 and verifies the variation of swelling pressure with dry density, one may verify the influence of the δ_v/h rate when measuring swelling pressure. It is easy to deduce that results from Loiseau (Figure 2) do not show a real dependency of swelling pressure on the specimen height, but a consequence of a diminution of dry density due to a partial swelling of the specimen allowed by the experimental set-up. It is obvious that, with the increase of the specimen height, the δ_v/h rate diminishes and also the reduction of swelling pressure.

Figure 3 shows, among others, the results obtained by Komine & Ogata (1994) for Kunigel VI bentonite with 5 mm thick specimens. It is interesting to compare these results with those obtained by Loiseau (2001). Because results presented in Figure 3 correspond to pure Kunigel VI bentonite and those presented in Figure 2 correspond to a 70/30 Kunigel VI bentonite/sand mixture, a direct comparison of results is not possible. Considering that sand particles do not contribute to the generation of

swelling pressure, it is necessary to reduce the corresponding weight and volume of the sand fraction from the bentonite/sand mixture, considering ρ_{sand} = 2.65 Mg/m^3. Then, one estimates the dry density of the clay fraction in the mixture with the remaining weight and volume. This procedure permits to determine the effective clay dry density ρ_c (Dixon et al. 1996) being 1.81 Mg/m^3. This is the density of the bentonite fraction, in the mixture used by Loiseau, which contributes to generate the swelling pressure reported in Figure 2 and to be compared with Figure 3. For the same dry density, the swelling pressure obtained by Komine & Ogata (1994) is of about 1.3 MPa. However, Figure 2 shows that the swelling pressure for this material goes to 5 MPa for this density. Moreover, the differences observed in Figure 3 for MX-80 bentonite, when comparing the results by Pusch (1982) and Gray et al (1984) may be due to differences within the specimen sizes and the rigidity of the corresponding experimental set-ups.

In this paper, we deal with the influence of strain control during swelling pressure determination. Some results show that strain control is an aspect of major interest in this matter.
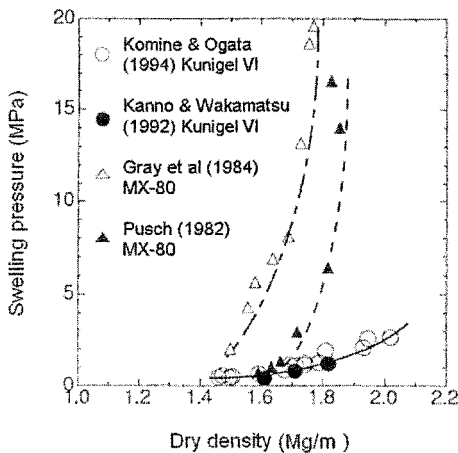
Figure 3. Changes in swelling pressure with dry density on ECB materials, Kunigel VI and MX-80 (Komine & Ogata 1994)

Experimental Set-up
To reduce the influence of the δ_v/h rate on measured swelling pressure, one may act in two different ways. One can either fix a high h value, or use a system that really allows for negligible deformations on the soil specimen. The first option is easy to apply, but duration of tests would be long. Loiseau (2001) shows that, for an h value of about 7 cm, the duration of a swelling pressure test may go beyond 2 months. Such a specimen height seems to be necessary to obtain a negligible influence of the δ_v/h rate, when using an experimental set-up similar to that shown in Figure 1.

In order to avoid using large height specimens and thus to have long duration tests, an experimental set-up as presented in Figure 4 can be used, permitting to compensate the height variations of the soil specimen during hydration (soaking or suction controlled). As one can see, this set-up is similar to that shown in Figure 1, with addition of a vertical strain control system. To do so, the piston is simply instrumented with a digital displacement gauge, with a precision of 0.001 mm that permits the continuous monitoring of the vertical strain of the soil specimen. Elsewhere, the thickness of the oedometer ring must be large enough to avoid lateral strain to affect the measurement of swelling pressure. In this case, the thickness of the ring was fixed to 10 mm; what was considered large enough for the range of swelling pressures to be measured in this study, of about 10 MPa. The set-up was based on the use of a digitally controlled 50 kN electromechanical press. The press platen can be piloted at controlled speed, commanded by a computer to compensate the displacements measured by the digital gauge, and oedometer rings were specially designed to incorporate the measure of lateral stresses.
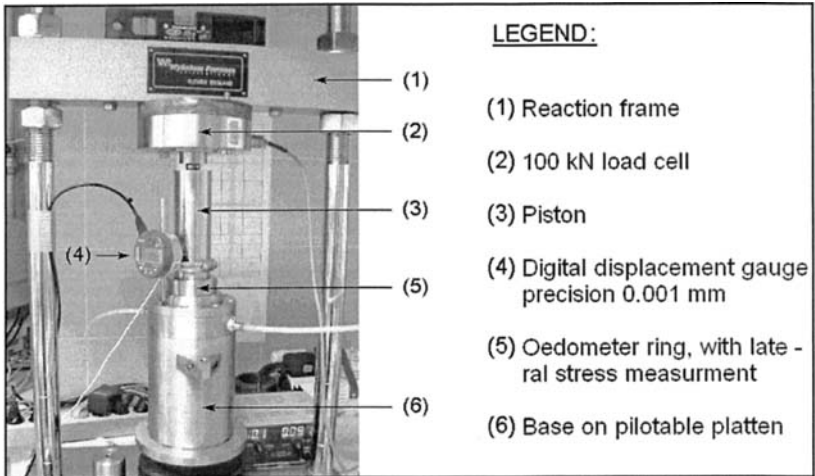
Figure 4. Experimental set-up for the study of suction – stress couplings at constant volume conditions.

Experimental program and results discussion

For this study, the MX-80 bentonite clay was used, which is international referenced swelling clay. The identification parameters of this material are summarized in Table 1.

The clay, provided in a fine granulated form, was equilibrated to a suction of about 103 MPa by using the vapor phase technique, with a K_2NO_3 saturated saline solution, and them compacted to a target dry density of $1.7 \, Mg/m^3$. The water content corresponding to equilibrium with the 103 MPa suction was about 8.2 %. The soil

specimens were compacted in a rigid mould, with a diameter of 49.95 mm, slightly lower than the 50 mm oedometer ring diameter. This was done to account for specimens rebound after pushing them off the rigid mould. After Marcial (2003), a direct compaction of the specimens into the oedometer ring introduces undesirable residual lateral stresses, giving rise to friction effects that significantly influence oedometer test results. By reducing the rigid mould diameter of 0.05 mm for 50 mm specimens, they can be pushed into the oedometer ring with a slight pressure (about 25 kPa), immediately after compaction. This is just enough to ensure the contact between the oedometer ring walls and the compacted specimen, before starting with hydration. A thin silicon grease layer was spreaded on the ring walls, before pushing in the samples, to reduce friction effects.

Table 1. Identification parameters of the used MX-80 bentonite clay.

Mineralogy	82 % montmorillonite (Na/Ca=5,5) [1]
C.E.C (meq/100g)	69,6 [1]
w_L (%)	520
w_P (%)	42
ρ_s (Mg/m^3)	2,65 [1]
Skempton's activity	5,8
S (m^2/g)	800 [2]

[1] Sauzeat et al. (2000) [2] Pusch (1982)

A series of tests, summarized in Figure 5 were conducted in order to verify the effect of controlling δ_v and h values, and the hydration mode (liquid or vapor phase) to reach zero suction conditions (s = 0). The first test was conducted by soaking without strain control, but measuring the δ_v value. The height and the dry density of the specimen were respectively 10.11 mm and 1.68 Mg/m^3. The result is represented by the dashed line in Figure 5, the vertical stress σ_v stabilized on 4.59 MPa after about 5 days. The measured lateral stress σ_h at the end of the test was 7.09 MPa, giving rise to $k_o = \sigma_h/\sigma_v = 1.55$. Additionally, δ_v of 0.257 mm was recorded, which implies a drop of the dry density to $\rho_d = 1.64$ Mg/m^3.

A second test was also conducted by soaking, for similar specimen dimensions and density ($h = 10.27$ mm and $\rho_d = 1.67$ Mg/m^3), but introducing the vertical strain control. In this case, the stresses σ_v and σ_h stabilized at 8.90 and 4.01 MPa respectively, giving rise to $k_o = 0.54$. When comparing with previous test, one observes two main differences. First, the measured vertical stress at stabilization increased from 4.59 to 8.90 MPa by introducing strain control and avoiding the 0.257 mm vertical strain measured in the first test. Second, the lateral stress reduced from 7.09 to 4.01 MPa, changing the final k_o value from 1.55 to 0.45.

One thinks the condition $\sigma_h > \sigma_v$ is logic in the first test, considering that vertical strain was relatively important while lateral strain remained restricted. Thus, a relaxation of vertical stress is consequently obtained. Elsewhere, the condition $\sigma_h < \sigma_v$ is also logic in the second test considering that having a real constant volume condition, due to the vertical strain control, the response of the specimen in terms of stresses would be conditioned by its stress path history (compaction + unmoulding + constant volume hydration).
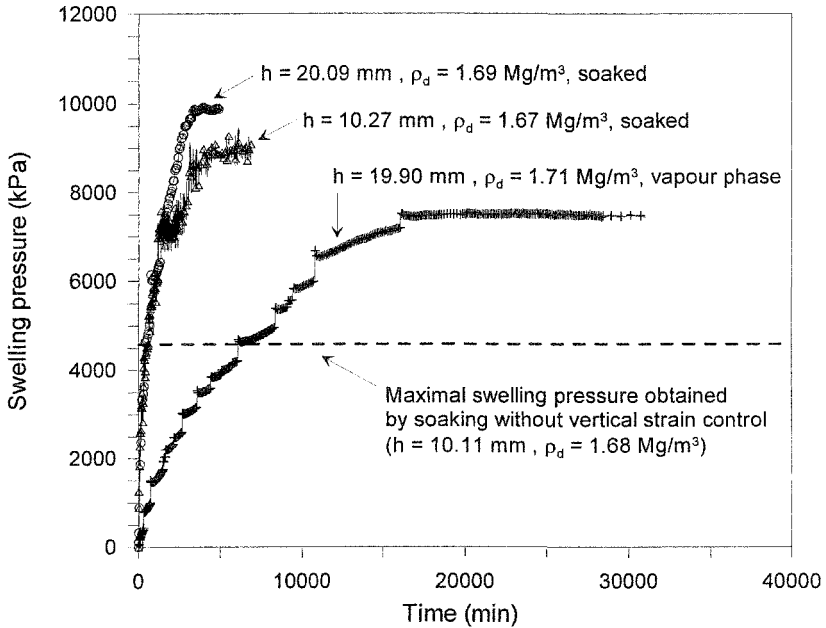
Figure 5. Changes on swelling pressure with time for specimens hydrated to s = 0, by liquid phase (soaking) and vapor phase (100 % relative humidity).

To better understand this behavior, it is necessary to follow the k_o changes with time during the second test, as shown in Figure 6. One may see that initially, k_o increases rapidly (1.35) and then decreases and stabilizes on 0.45. The initially observed k_o maximum is due to the initial deformation of the confining system. When hydrating by soaking, the soil swells very fast as compared with the response of the system that is relatively slow. For the different tests, an initial δ_v value was measured to be between 0.01 and 0.02 mm. This vertical strain is further gradually compensated, and the δ_v value stabilizes around 0.001 mm, that is the precision of the digital displacement gauge. Note that the initial k_o value (1.35) measured for the second test is comparable with the k_o value measured for the first test (1.55) without vertical strain control.
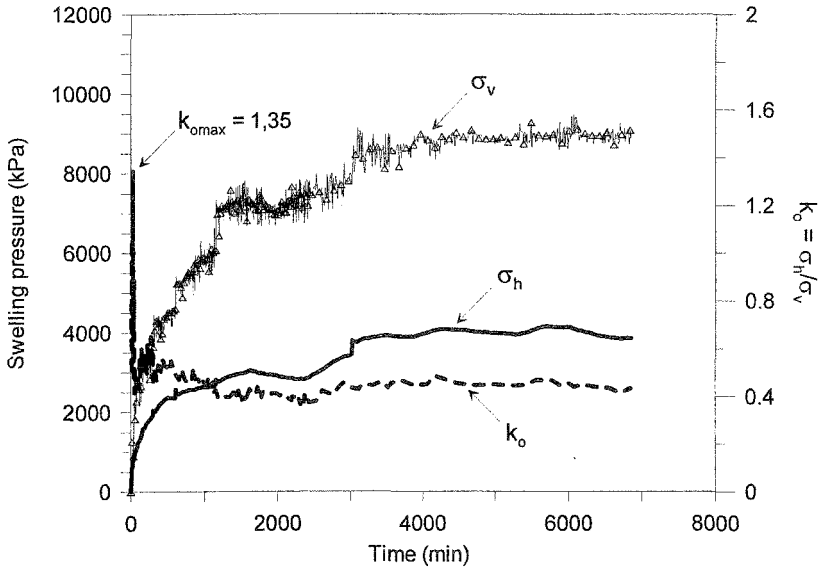
Figure 6. Changes on swelling pressure with time for a specimen hydrated by soaking (s = 0) at constant volume ($h = 10.11$ mm et $\rho_d = 1.67$ Mg/m^3)

Additionally, one may notice two maximums for swelling pressures. A first one (7.36 and 3.04 MPa for σ_v and σ_h respectively) is observed at the time $t = 1600$ min. Then, the swelling pressure drops slightly and continues increasing to stabilize on a second and higher maximum. This two maximum trend has been observed by Pusch (1982) on compacted MX-80 clay. Pusch indicates that first maximum is due to the softening of clay aggregates, induced by the hydration of clay particles that further reorganize from an aggregated structure to a more stable one. Then, a second maximum is reached when full hydration is reached. This is relatively compatible with observations made by Marcial (2003) on the changes of porosity during hydration of aggregated ECB materials at constant volume conditions. One thinks that first maximum indicates the beginning of mobilization of microporosity into macroporosity, corresponding to the softening of clay aggregates noticed by Pusch. When macroporosity becomes fully reduced, the reorganization of porosity from microporosity to macroporosity cannot continue and swelling pressure begins again to increase to reach the second maximum.

To study the effect of h on swelling pressure, we have doubled the height of the soil specimen ($h = 20.09$ mm and $\rho_d = 1.69$ Mg/m^3), and a new test was conducted by soaking with vertical strain control (Figure 7). For this test, the two maximum trend was not observed for σ_v that stabilizes on 9.92 MPa at about 3500 min. However, for σ_h one observes again a two maximum behavior. A first maximum ($\sigma_h = 3.77$ MPa), better defined than the previous test, is observed at $t = 1000$ min. After the maximum,

σ_h drops to 1.99 MPa ($t = 2800$ min), when σ_h begins again to increase. At the end of the test (5126 min) σ_h had reached to 2.99 MPa but it had not been yet stabilized on the second maximum. Concerning k_o, one observes a maximum (1.59) at the beginning of the test, due to the initial deformation of the system. After that, the changes on k_o are controlled by the behavior of σ_h, one observes a minimum of 0.21 at $t = 2800$ min and at the end of the test k_o value reaches 0.30 with an increasing trend.
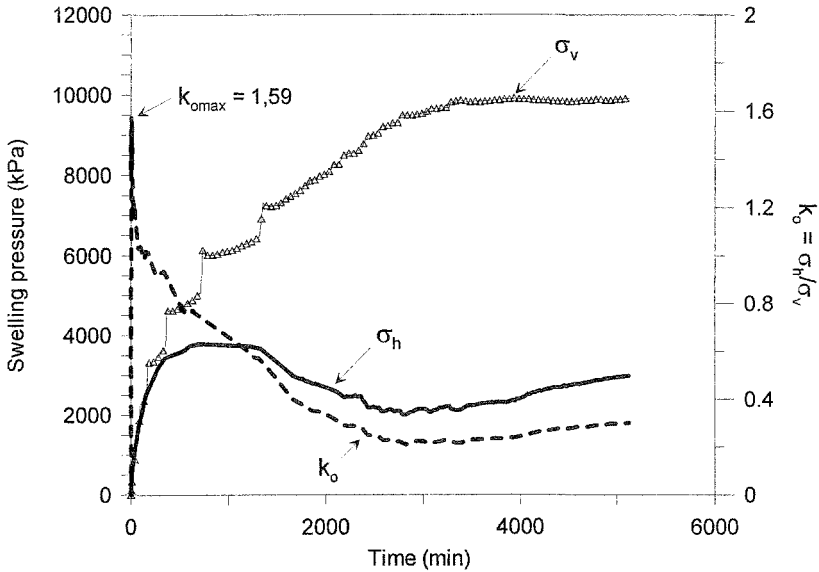
Figure 7. Changes on swelling pressure with time for a specimen hydrated by soaking (s = 0) at constant volume ($h = 20.09$ mm et $\rho_d = 1.69$ Mg/m^3)

Comparing the results obtained with specimens having different heights and tested in similar conditions, one note an increase of σ_v from 8.90 to 9.92 MPa for h values of 10.27 and 20.09 mm respectively. Considering the slight difference in terms of density between these two test (1.67 and 1.69 Mg/m^3), as well as the high influence of density on swelling pressure (see Figure 3), these results show that swelling pressure does not depend on the height of the specimens. Note also, when comparing the results shown on Figure 5 a difference of 100 % is observed on swelling pressure for specimen heights of 10 and 20 mm. The figure shows that σ_v values, obtained without vertical strain control, are 1.5 and 3.0 MPa respectively.

A last test was conducted (Figure 8) to see the difference between the hydration to zero suction condition (s = 0) by soaking and vapor phase. In this case, the specimen characteristics were $h = 19.90$ mm and $\rho_d = 1.71$ Mg/m^3. It is important to point out

that differences on density, obtained for the various tested specimens, are maybe due to slight variations on the initial water content of clay powder, considering that compaction stress (39 MPa) was kept constant for all cases.
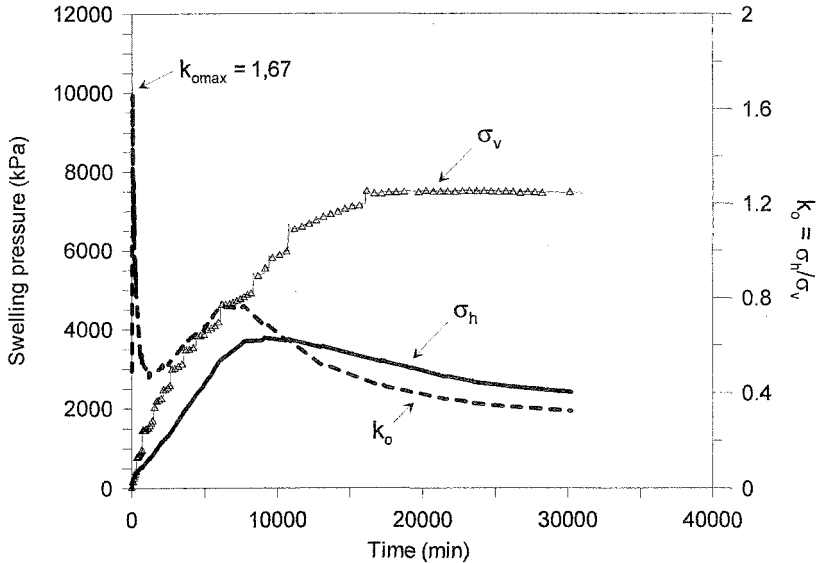
Figure 8. Changes on swelling pressure with time for a specimen hydrated by vapor phase (s = 0) at constant volume (h = 19.90 mm et ρ_d = 1.71 Mg/m³)

In contrast with previous test, conducted by soaking, the hydration kinetics of this test is much slower (see Figure 5) and σ_v stabilizes at t = 20000 min. For a similar h (about 20 mm) the stabilization of σ_v takes a time period that is 5 times longer. Additionally, the σ_v value obtained by vapor phase (7.55 MPa) is lower than the one obtained by soaking, even if density is slightly higher. In this case, σ_v continuously increases without showing a two maximum behavior. However, σ_h shows a maximum (3.78 MPa) at t = 10000 min, then diminishes progressively and seems to stabilize toward the end of the test at 2.41 MPa. As observed with previous test, k_o shows a trend that is controlled by the behavior of σ_h. A maximum of 0.77 is observed at t = 7650 min, followed by a progressive drop, and at the end of the test k_o stabilizes at 0.32. Also, σ_h does not seem to stabilize at the end of the test. One thinks that, for a longer time period, σ_h could show a two maximum behavior where the second maximum is a higher one, as observed on Figure 6.

In relation to σ_v, one observes a drop of about 1.86 MPa when comparing the obtained value (7.55 MPa) with the mean value obtained by soaking. This difference in terms of vertical stress with the hydration mode was also observed by Loiseau (2001). He obtained a σ_v drop from 4.75 to 3.75 MPa with a clay / sand mixture.

Marcial et al. (2002) indicate that double layer effects on bentonite clays have an influence on stress – strain couplings on a range of stresses up to 1 - 2 MPa. Since double layer phenomena do not develop without a liquid phase, the results obtained with last test are reasonable.

Conclusions

Hydration tests conducted with vertical strain control, and thus at real constant volume conditions, permitted to verify that swelling pressure does not depend on the height of tested specimens. Important differences in swelling pressures, obtained by various authors on similar materials, might be linked to differences on experimental set-ups and specimen sizes. The influence of experimental set-ups becomes less important as the height of the specimens increases.

For different tests, the swelling pressure behavior shows two maxima. The first one corresponds to the softening of compacted clay aggregates. After softening, a redistribution of porosity is accompanied by a drop on swelling stresses. As microstructure reorganizes and becomes more stable, swelling stresses increase again to reach a second and higher maximum.

Results presented here show that compacted bentonite clays have a complex hydromechanical behavior, strongly coupled with microstructure.

References

ASTM Standard D 2435. Test method for one dimensional consolidation properties of soils. *Annual Book of ASTM Standards.* Vol. 04.08.

Dixon D. A. Gray M. N. and Graham J., 1996. Swelling and hydraulic properties of bentonites from Japan, Canada and the USA. *Environmental Geotechnics* 1, 43-48.

Komine H. & Ogata N. 1994. Experimental study on swelling characteristics of compacted bentonite. *Canadian geotechnical journal.* Vol. 31, *pp.* 478-490.

Loiseau C. (2001). Transferts d'eau et couplages hydromécaniques dans les barrières ouvragées. Thèse de doctorat. Ecole Nationale des Ponts et Chausées. Paris, France.

Marcial D. (2003). Comportement hydromécanique et microstructural des matériaux de barrière ouvragée. Thèse de doctorat. Ecole Nationale des Ponts et Chausées. Paris, France.

Marcial D., Delage P. & Cui Y. J. (2002). On the high stress compression of bentonites. *Canadian Geotechnical Journal* 39, 1-9.

Pusch R., 1982. Mineral-water interactions and their influence on the physical behavior of highly compacted Na bentonite. *Canadian Geotechnical Journal.* 19, 381-387.

Sauzeat E., Villiéras T. F., François M., Pelletier M., Barrés O., Yvon J., Guillaume D., Dubbessy J., Pfeiffert C., Ruck R. and Cathelineau M., 2000. *Caractérisation minéralogique, cristallochimique et texturale de l'argile MX-80.* LEM-CREGU. ANDRA Technical Report. France.

Results of Long-Term Infiltration Tests on Unsaturated Swelling Clay

G. A. Siemens[1], J. A. Blatz[1] and D. G. Priyanto[1]

[1]Department of Civil Engineering, University of Manitoba, Winnipeg, MB, R3T 5V6; PH: (204) 474-8072; FAX: (204) 474-7513; Email: umsieme7@cc.umanitoba.ca

Abstract

Results of two long-term infiltration tests conducted in a triaxial cell are presented. Results of the testing are examined to assess mechanical and hydraulic behavior of an unsaturated swelling clay. In one test, radial flow is enforced with water pressure applied at the perimeter and drainage is allowed at the center of the specimen. In the second long-term test, vertical flow is applied with water pressure at the base and drainage is allowed out the top of the specimen. In both cases water flow into specimens and air flow at the downstream side is measured along with volume changes. Suction at the center of the specimen is measured in the vertical flow test using an embedded sensor. Water flow, volume change and suction responses are discussed to assess how flow and boundary conditions affect behavior. Differences in behavior during infiltration are noted due to anisotropy in the compacted specimens. Final distributions of water content, bulk density, dry density and degree of saturation are presented and discussed. Results show that these infiltration tests are important for understanding the physical movement of water through unsaturated swelling clay materials.

Introduction

Measuring hydraulic conductivity of high plastic unsaturated soils is a lengthy process. During laboratory tests, changes in water content, density, volume and saturation may occur. Measuring and or controlling these variables must be performed to ensure proper interpretation of test results. Performing hydraulic conductivity tests in a triaxial cell with volume measurement allows control or measurement of the stress and volume states.

Many test apparati have been developed for measuring the hydraulic conductivity of clay materials. Apparati and procedures range in form from rigid (Dixon et *al.* 1999) to flexible cells (ASTM D5084) with constant gradients to constant flow conditions

939

imposed. Vertical and radial flow paths (Leroueil et *al.* 1990) have also been applied to test the variation of hydraulic conductivity with respect to direction of flow. In saturated soils testing, the flexible membrane hydraulic conductivity test (ASTM D5084) is used most often for fine-grained materials. In unsaturated soils testing no standard method exists to determine hydraulic conductivity.

This paper presents results from two long-term water infiltration tests on an unsaturated high plastic soil. One test applies radial flow while the other test imposes vertical flow. The soil being tested is an expansive sand-bentonite mixture. Volume, mean stress, suction, inflow and outflow are measured during testing. After removal, final spatial distribution of gravimetric water content and bulk density are measured to calculate saturation and dry density. Test results and post-test measurements are discussed and compared. The radial flow test is shown to achieve flow and volume equilibration sooner than the vertical flow test due to the shorter flow path.

Test Apparati

The radial and vertical flow apparati are incorporated in the High Temperature High Pressure (HITEP) triaxial cells at the University of Manitoba. Both systems include electronic measurement of volume change and water inflow using five Linear Variable Displacement Transformers (LVDTs – 4 radial strain / 1 axial strain) and Differential Pressure Transducers (DPTs) connected to burettes. A custom data acquisition / control system is used in both apparati (Blatz et *al.* 2003, Siemens 2004).

One apparatus applies radial flow from the perimeter to center while the second apparatus imposes vertical flow from the bottom to top of specimen. Both apparati are described in this section.

Radial flow apparatus. The new radial flow apparatus (Figure 1) is similar to one described by Siemens and Blatz (2005) except that prior to installation a 0.47 mm hole is drilled through the entire length of the triaxial specimen and a wire mesh inserted. In the previously described apparatus a suction sensor is compacted at the center of the specimen. The specimen is surrounded with a non-woven geotextile (Amoco Propex 4553) to apply water pressure to the entire periphery. Lucite discs are located above and below the triaxial specimen to prevent axial flow. Plastic wrap is attached to the Lucite discs with grease to reduce friction between the specimen and discs. Filter stones and filter paper are placed on the opposite side (from the specimen) of the Lucite discs to provide direct hydraulic connection to the burettes. The arrangement from pedestal base to top cap is filter paper, filter stone, Lucite disc, plastic wrap, triaxial specimen, plastic wrap, Lucite disc, filter stone and filter paper. To allow drainage along the center of the specimen and out of the triaxial cell, a hole is drilled through the pedestal base. A copper pipe inserted which extends through holes in the base, bottom filter paper, filter stone and Lucite disc to approximately 35 mm inside the mesh at the center of the specimen. During installation the annulus between the Lucite disc and copper pipe is sealed with quick drying glue. The copper

pipe is connected to a bubbler to measure downstream flow from the center of the specimen. Four (4) LVDTs are placed around the perimeter of the specimen at mid-height to measure radial displacements. These along with one (1) axial LVDT are used to measure point displacements in order to calculate volume strains.

As shown in Figure 1 the apparatus applies radial flow to triaxial specimens. Flow paths are therefore approximately symmetric about the specimen's center axis. Axial flow is not applied in order to provide a consistent flow regime throughout specimens.
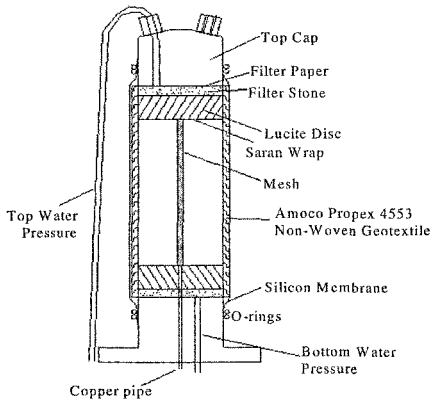
Figure 1. Radial flow apparatus

Vertical flow apparatus. The vertical flow apparatus is similar to the traditional flexible-walled permeameter (ASTM D5084) with water pressure applied at the specimen base and flow out the top cap measured with a bubbler. In addition, a suction sensor is compacted at the center of the specimen. Two (2) radial LVDTs are placed at both one-third and two-thirds height of the specimen. These along with the axial LVDT are used to measure point displacements during testing.

Post-test measurements. Following all tests, specimens are removed and spatial distributions of gravimetric water content and bulk density are measured to calculate dry density and degree of saturation. Bulk density is measured using Archimedes' Principle by surrounding the samples with wax and then determining the volume of soil and wax. Volume of wax is then subtracted from the total volume measured since its density and mass are known.

Specimens are cut along compacted layers and then divided into three radial sections using two (2) cutting tools. Two samples from each of the outer two rings and one sample from the center region are used for water content and bulk density measurements. The average is reported for each region. In the radial flow test, flow

paths are symmetric about the center axis of the specimen. Therefore regional measurements from each layer should be equal within measurement error. In the vertical flow test, average measurement from each layer is reported.

Test procedure. Both the radial and vertical flow apparati use similar test procedures. They begin with a phase which applies only hydrostatic pressure (no additional cell pressure) to allow the suction sensor (vertical test) to reach equilibrium with the specimen. A similar equilibration time is allowed for in the radial test to ensure results are comparable. The isotropic compression phase then begins with cell pressure increasing incrementally to the desired mean stress level. This stress level is maintained within ±15 kPa for the rest of the test. Following 24 hours of isotropic compression, the hydraulic conductivity phase begins by filling the plumbing with water. In the radial flow test this is performed by flowing water from the bottom burette through the plumbing and geotextile until the top pressure cavity is filled. Then the top and bottom burettes are pressurized. In the vertical flow test, the bottom pressure cavity is filled and then the bottom burette is pressurized to the selected pressure level. Hydraulic conductivity tests continue until volume, suction, inflow rate and outflow rate equilibrate. Tests reported here last approximately 150 days.

Materials and Specimen Preparation

Test specimens used in this study are composed of a 50:50 mixture (by weight) of clay and sand. The clay is a sodium rich bentonite with w_L = 590-610% and I_L = 550-570 (Blatz et al. 2005). The sand is well-graded angular silica sand. Sand-bentonite specimen preparation procedure was originally described by Yarachewski (1993). Equal parts of clay and sand are combined with distilled de-aired water to 19.4% gravimetric water content. Following 72 hours equilibration in a sealed bag specimens are statically compacted in five layers to 1.67 Mg/m^3 dry density which gives a degree of saturation approximately 85%.

Results

Results are presented from one radial and one vertical flow test performed on sand-bentonite specimens. The two flow tests were conducted at 500 kPa mean stress to allow for comparison with previous radial infiltration tests where no drainage was provided at the center (Siemens and Blatz 2005).

500 kPa radial flow test results. Results from the 500 kPa radial flow test are shown in Figure 2. Volume strain, water added to specimen and downstream flow are plotted *versus* time for the entire test. The overnight equilibration phase is followed by an isotropic compression phase where cell pressure (mean stress) is raised to 500 kPa in a single increment. The specimen compresses in response (positive volume strain). The isotropic compression phase lasts 24 hours allowing for suction and volume equilibration (Blatz and Graham 2000, 2003). Radial flow is applied to the specimen at about 1.8 days. Flow rate in and out of the specimen decrease

throughout the test until they reach a relatively constant value. Due to increasing water content, the clay component of the triaxial specimen expands (negative volume strain). Relatively rapid expansion is observed for the first 15 days and then a significantly reduced rate of volume change is noted. This corresponds with water flow being observed out the center of the specimen. The radial flow test is completed after 150 days with 46 mL of total inflow (water), 22 mL total outflow (air and water) and specimen expansion to -9.3% volume strain.
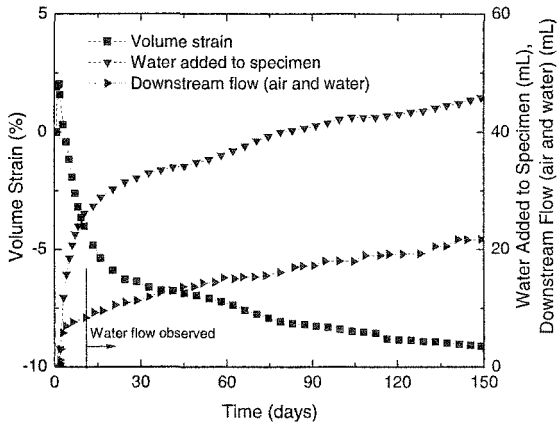
Figure 2. Radial flow test results (GS-051)

500 kPa vertical flow test results. Results from the 500 kPa vertical flow test are shown in Figure 3. Volume strain, suction, water added to the specimen and downstream flow are plotted *versus* time. The test begins with equilibration and isotropic compression as in the radial flow test. In this case, the specimen compresses in response and suction decreases due to compression of the air component (Blatz and Graham 2000 and 2003, Blatz et *al.* 2003). Vertical water flow begins at about two (2) days. Water flow rate into the specimen becomes constant at approximately 30 days. Conversely, downstream air flow rate is relatively higher at the beginning of the test. Air outflow then levels off at about 60 days and no further outflow is observed for the remainder of the test. Volume change observed during infiltration is slight compression at the beginning followed by expansion. Suction initially stays at the isotropic compression level, then slightly increases and then decreases. At approximately 45 days suction measurement drops below zero. Since the Xeritron sensor is a relative humidity device and cannot measure positive pore pressure, this is not meaningful and as such suction readings are ignored for the rest of the test. Suction is assumed to be approximately 0.5-1.0 MPa for the remainder of the test as this is the calculated osmotic suction in a sand-bentonite material (Wan 1996) with the same preparation procedure but uses Avonlea bentonite instead of Wyoming. The two types of bentonite were shown to behave similarly at higher

suctions (lower water contents) under drying paths, isotropic compression and shear (Blatz et *al.* 2005). Their comparative suction behavior at lower suctions is not known at this time and 0.5-1.0 MPa is considered a best estimate. The vertical flow test was considered complete with 20 mL of inflow (water), 56 mL outflow (air only observed) and specimen expansion to 2.7% volume strain. From the final post-test measurements the specimen had not reached overall equilibrium however since the radial and vertical test lengths are equal results are valuable for comparison.
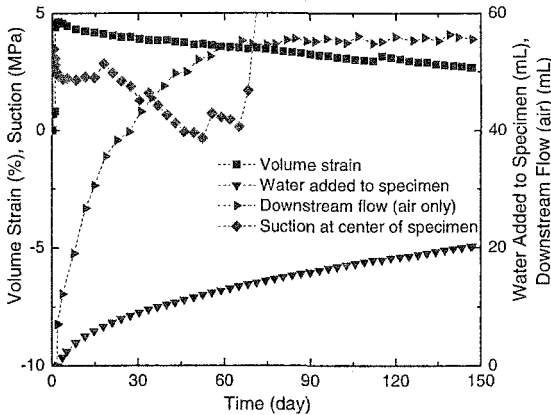
Figure 3. Vertical flow test results (GS-052)

Post-test measurements. Average post-test measurements for the radial and vertical specimens are plotted in Figure 4a-4d. Average gravimetric water content, bulk density, degree of saturation and dry density are plotted *versus* normalized distance. Distance is normalized from the outflow to the inflow end of the specimen. In the radial test this corresponds to the distance from the wire mesh to the perimeter while in the vertical test this is the final height of the specimen. Also shown on the plots are the estimated as-compacted and pre-infiltration values of each measurement. These are calculated from quality control specimens examined immediately following compaction combined with volume change measurements during the tests.

Measuring the spatial distribution of phase properties, including gravimetric water content and bulk density, following hydraulic conductivity tests provides valuable insight regarding internal material changes that occurred during the test. Since the soil being tested is an unsaturated swelling clay mixture, changes in water content, bulk density, dry density and saturation are anticipated.

a. water content

b. bulk density

c. saturation

d. dry density
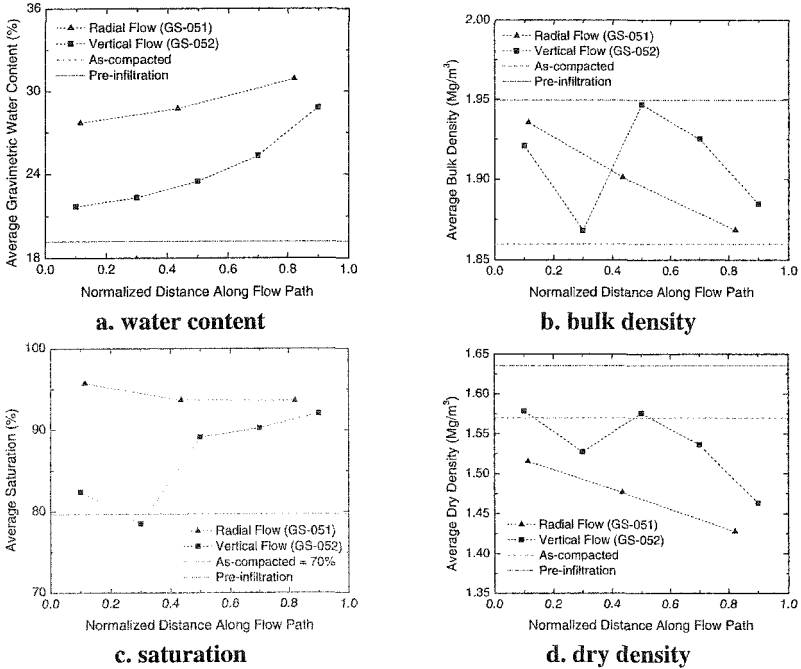
Figure 4. Average post-test phase relationship distributions

Water content is greatest near the source and decreases along the flow path for both tests (Figure 4a). Measurements are consistently higher in the radial flow test compared to vertical flow test. Bulk density increases from the perimeter to center in the radial flow test (Figure 4b). In the vertical flow test bulk density increases from the upstream end, unexpectedly decreases and then increases again. Saturation in the radial flow specimen (Figure 4c) is constant for the outside two measurements and then increases towards the center. The vertical flow specimen shows an overall increase in saturation from top to bottom however the second measurement shows a decrease. This is likely an erroneous measurement as noted with the sharp change of bulk density at the same level. From Figure 4d, both specimens show a trend of decrease in dry density from downstream to upstream. The second measurement in the vertical flow specimen shows some variation as discussed.

Results Comparison

Flow. Inflow and outflow results from the radial and vertical flow test specimens show both similar and distinctive behavior (Figure 2 and Figure 3). Both specimens show decreasing inflow rate which eventually reduces to a relatively constant value. The radial flow specimen's final average flow rate is approximately 0.11 mL/day over

the last 100 days. The vertical specimen shows lower inflow rate throughout the test. At the end of the test, inflow rate is approximately 0.08 mL/day and it is still slowly reducing. Both tests use the same water pressure at the upstream end of 200 kPa but the gradient across the vertical specimen is half of the radial flow specimen due to the flow regime imposed during testing. Also, anisotropic conductivity is anticipated in these specimens due to preparation procedure of static compaction. Greater water content and lower dry density of the radial flow specimen compared with the vertical (Figure 4a and Figure 4d) will also affect the flow rate. The result is a total of 46 mL of inflow in the radial test compared with only 20 mL into the vertical specimen.

Outflow results (air and water) show distinctive behavior compared with inflow. In the radial specimen, until day 11 air flow was observed and following that timeframe only water flowed out of the specimen. In the vertical specimen the same general trend is observed for outflow as inflow with a high initial rate that reduces to an average of 0.08 mL/day over the last 100 days of the test. Only air was observed flowing out the top of the vertical specimen. In this case there was a higher initial flow rate which dropped to essentially zero for the final 80 days of the test.

From this comparison the radial flow test appears to attain flow equilibrium sooner than the vertical flow test since inflow and outflow are equal on average over the last 100 days of the test. Also, as anticipated for equilibrium, water is flowing in and out of the radial flow specimen. In the vertical flow test, water outflow was not observed. Although some water vapor likely exited the specimen this was not measured. Total outflow volume in the vertical specimen was over twice that of the radial specimen (56 and 22 mL respectively). Air outflow stopped after approximately 60 days in the vertical test while water outflow approached a constant rate in the radial test.

Determination of hydraulic conductivity is possible in the radial flow specimen as both in-test and post-test measurements show equilibrium is reached. Due to the radial flow field imposed during the test, conductivity can be expressed as

$$k = \frac{Q\rho g \ln\left(\dfrac{r_e}{r_w}\right)}{2\pi h(P_e - P_w)}$$

where:
k = hydraulic conductivity
Q = equilibrium flow rate
ρ = density of fluid (water)
r_e = outside radius of specimen
r_w = inside radius of specimen
h = height of specimen
P_e = pressure applied at perimeter of specimen
P_w = pressure applied at inside radius of specimen

Using values obtained from the radial flow test gives a hydraulic conductivity of 4×10^{-13} m/s. This agrees with previously published data obtained from rigid-cell conductivity tests on a similar material (Dixon et al. 1999).

Understanding the vertical flow test requires interpretation of the location of the water-air interface which is outside the scope of this publication. This could be achieved through back analysis using a finite element program or using a solution similar to one provided by Buckley and Leverett (1942) which is based on water-air frontal advance theory. Alternatively, to achieve equilibrium in a reasonable time an increased gradient could be applied. Applying the same pressure differential, as in tests reported here, across a 50 mm long specimen would allow for comparison with the radial flow test. Reducing specimen length is anticipated to decrease equilibration time; however the radial test would likely still be shorter as the total volume of material is less. This will be considered in future testing.

Volume. Volume change during the test begins with the isotropic compression phase. The two specimens were prepared, compacted and installed using the same procedure except for slight inclusion differences as noted previously. Therefore following isotropic compression at 500 kPa, they are assumed to be at the same volume and stress state. From test data (Figure 2 and Figure 3) the vertical flow specimen shows larger volume strain during this phase. This is likely due to compliance in the volume measurement system (LVDTs). During the hydraulic conductivity phase the radial flow specimen expands (negative volume strain) at a significantly greater rate than the vertical flow specimen. At the end of the radial test, volume change had essentially finished and volume equilibrium is interpreted to have taken place. In the vertical flow test, volume change occurs at a slower rate and only 1.9% volume expansion was observed compared to 11.3% in the radial test during water flow.

One important point is that the four radial LVDTs placed at the mid-height perimeter of the radial flow specimen and are considered representative of the entire specimen due to the axi-symmetric nature of the test. In the vertical flow test, two LVDTs each are placed at one-third and two-thirds height of the specimen. These point measurements cannot capture the non-uniform volume changes which occur at other heights and this is recognized as a limitation of the vertical flow apparatus. Following removal of the vertical flow specimen, lower layers were observed to have a larger diameter than the top layers due to the amount of water taken up by the soil.

The radial flow test shows faster volume equilibration times during infiltration. In addition, the four radial LVDTs placed at mid-height of the specimen give a better representation of volume change throughout testing as the flow paths are approximately symmetric about the specimen's center axis.

Suction. Results discussed here are only for the vertical flow specimen since suction was not measured in the radial flow test. During isotropic compression, suction measurement at the center of triaxial specimens is representative of the entire

specimen (Blatz and Graham 2000). Following installation, suction equilibrates to 3.1 MPa. During the 500 kPa isotropic compression phase suction decreased to 2.4 MPa. This response is anticipated due to reduction is due to compression of the air phase (Blatz and Graham 2000 and 2003, Blatz et *al.* 2003).

During water infiltration, the sensor measures suction at a point along the flow path. As water infiltration begins, little change in suction is noted until day 18 when a small jump is noted followed by decrease in suction. Suction continues to decrease until the reading drops below zero. As discussed earlier a final suction value of between 0.5-1.0 MPa is assumed for the remainder of the test.

Post-test measurements. Comparing post-test measurements shows the same overall trends occur in both tests with the radial flow test approaches equilibrium sooner than the vertical flow test. Assuming that both specimens would eventually have the same distribution of phase relationships given enough time, in each case the radial flow specimen is closer to this equilibrium state when testing is complete.

Figure 4a shows consistently higher gravimetric water contents for radial flow compared to vertical flow. Trends are the same with increasing gravimetric water content from downstream to upstream. Also, extrapolating to the upstream end shows both specimens trending towards approximately 32% gravimetric water content.

Bulk density comparisons are difficult to make as they incorporate changes in water content and density. Figure 4b shows overall decrease in bulk density from downstream to upstream. Also upstream end measurements trend to similar values.

Saturation measurements (Figure 4c) show interesting results as the radial flow test shows essentially constant degree of saturation along the flow path at 93% with some variation at the center. The vertical flow specimen shows increasing overall saturation from downstream to upstream. Extrapolating the measurements to the upstream end shows they trend towards the same 93% observed in the radial specimen. Passing enough pore volumes through the specimen, it is expected to reach 100% saturation but even after 150 days this was not measured in either specimen. Some saturation decrease could be caused due to specimen expansion during removal.

During constant pressure infiltration tests, higher water contents are anticipated with lower dry densities. This is observed in Figure 4d for both test specimens. The radial flow test shows a linear change in dry density while in the vertical specimen a strongly non-linear distribution of dry density is observed. Both distributions tend to approach 1.40 Mg/m^3 at the upstream end.

Proposed Models

Capturing the hydraulic behavior of a swelling soil subjected to water imbibition is a complicated task. As has been shown above, the testing reported is

long-term, transient and spatial changes of density and water content occur. Models for these soils need to incorporate these mechanical and hydraulic behaviors.

To understand the hydraulic behavior a capillary tube model that incorporates changes in tube diameter with time has been developed (Siemens et *al.* 2005). As water flows along the length of the tube, it decreases in diameter to represent the swelling nature of the bentonite. Swell rate can be controlled by the input parameters. Tube geometry is selected based on Mercury Intrusion Porosimetry tests and hydraulic conductivity tests reported. Results show that it captures behavior observed during these tests.

For mechanical behavior a constitutive model which incorporates swelling nature such as Alonso et *al.* (1999) could be used. Another alternative is to build on the framework presented by Blatz and Graham (2003). Their current model is based on tests using a similar sand-bentonite material under drying conditions. This would be expanded to incorporate increases in water content (decreasing suction).

Conclusions

Two long-term hydraulic conductivity test apparati developed for high plastic clays are presented. In one apparatus radial flow is imposed from perimeter to center while in the other vertical flow from bottom to top is applied. Test results are compared along with spatial distribution of phase properties. The radial test shows faster equilibration due to the shorter flow path. Internal changes in water content and density show that both test specimens trend towards the same final values.

Acknowledgements

References

Alonso, E.E., Vaunat, J. and Gens, A. 1999. Modelling the mechanical behaviour of expansive clays. Engineering Geology, 54, 173-183.

ASTM D5084, 2003, Standard test method for measurement of hydraulic conductivity of saturated porous materials using a flexible wall permeameter ASTM, Philadelphia, Pennsylvania, USA.

Blatz, J.A., Anderson, D.E.S. and Siemens, G.A. 2005. Evaluation of the yielding behaviour of two unsaturated bentonite mixtures. Canadian Geotechnical Journal. *In Review.*

Blatz, J.A. and Graham, J. 2000. A system for controlled suction in triaxial tests. Géotechnique, 50, No. 4, 465-478.

Blatz, J.A., and Graham, J. 2003. Elastic plastic modelling of unsaturated high-plastic clay using results from a new triaxial test with controlled suction. Géotechnique Special Symposium in Print on Unsaturated Soils, Géotechnique, 53, No. 1, 113-122.

Blatz, J.A., Anderson D.E.S., Graham J., and Siemens G.A. 2003. Evaluation of Yielding in Unsaturated Clays Using an Automated Triaxial Apparatus with Controlled Suction. Invited Lecture. International Conference From Experimental Methods Towards Numerical Modeling of Unsaturated Soils, Bauhaus-Universität, Weimar, Germany, September 2003.

Buckley, S.E. and Leverett, M.C. 1942. Mechanism of fluid displacement in sands. American Institute of Mining and Metallurgical Engineers -- Transactions -- Petroleum Development and Technology Division, 146, 107-116.

Dixon, D.A., Graham, J. and Gray, M.N. 1999. Hydraulic conductivity of clays in confined tests under low hydraulic gradients. Canadian Geotechnical Journal, 36, 815-825.

Leroueil, S., Bouclin, G., Tavenas, F., Bergeron, L. and Rochelle, P.LA. 1990. Permeability anisotropy of natural clays as a function of strain. Canadian Geotechnical Journal, 27, 568-579.

Siemens, G.A. 2004. Importance of stress path control in soils testing. 2004. Proceedings of the 1st Canadian Young Geotechnical Engineers and Geoscientists Conference (cYGEGC), Quebec City, Quebec, Canada. 27-30 October 2004.

Siemens, G.A. and J.A. Blatz. 2005. A triaxial apparatus for applying liquid infiltration under controlled boundary conditions with internal suction measurement. ASCE Geotechnical Journal of Geotechnical and Geoenvironmental Engineering to be considered for publication. *In Review.*

Siemens, G.A., Blatz, J.A. and Ruth, D. Development of a capillary tube model for swelling soil. *In Preparation* to be submitted to Canadian Geotechnical Journal.

Wan, A.W.L. 1996. The use of thermocouple psychrometers to measure in-situ suctions and water contents in compacted clays. Ph.D. Thesis, Department of Civil and Geological Engineering, University of Manitoba, (Winnipeg, Manitoba).

Yarechewski, D.S., Constant mean effective stress tests on sand-bentonite specimens at elevated temperature. M.Sc. Thesis, Department of Civil Engineering, University of Manitoba, Winnipeg, Manitoba, 1993.

Parameters for Heave Prediction by Oedometer Tests

John D. Nelson, Ph.D., P.E., F.ASCE[1], Diane K. Reichler[2],
Jason M. Cumbers, P.E., M.ASCE[3]

[1] Professor, Colorado State University, Fort Collins, Colorado, 80521 USA, Corporate Consultant, MFG, Inc., 3801 Automation Way, Suite 100, Fort Collins, Colorado 80525 USA, 970-223-9600
[2] Former Graduate Assistant, Colorado State University
[3] Senior Staff Geotechnical Engineer, MFG, Inc., 3801 Automation Way, Suite 100, Fort Collins, Colorado 80525 USA, 970-223-9600

Abstract

This paper describes a methodology to determine the constitutive parameters needed for prediction of heave using oedometer test data. Heave prediction using an effective stress based approach utilizes data from the oedometer test. An important constitutive parameter used in that method is the heave index, C_H. The parameter C_H is the ratio of the percent swell observed in the oedometer test to the vertical stress applied to the sample when it was inundated, i.e. the inundation pressure. This paper outlines methodology for determination of C_H using oedometer test results obtained using reconstituted Pierre shale samples from both consolidation-swell (CS) tests, performed according to the ASTM D 4546 Method A procedure, and constant volume (CV) tests, performed according to the ASTM D 4546 Method C procedure. Most commonly, however, test result data from only one type of test is available, usually the CS test. Therefore, it is useful to establish a relationship between the parameters determined in the CS test and the CV test so that data from only one type of test is necessary. This paper outlines a proposed methodology for correlating test results from CS and CV tests and presents results of a laboratory investigation to assess values of parameters needed in the relationship between swelling pressure from consolidation swell tests and constant volume oedometer tests.

Introduction

The prediction of free-field heave at expansive soils sites generally follows an effective stress based approach utilizing data from oedometer methods of testing. This approach is mechanistic and considers the soil as a continuum. The constitutive

parameters for each soil will depend on their physicochemical characteristics, necessitating a careful test program at each site.

Methodology for predicting heave using an effective stress-based approach has been published previously. (See for example, Fredlund (1983), Nelson and Miller (1992) or Fredlund and Rahardjo (1993).) Different procedures have been suggested for determining the value of the constitutive parameter in the heave equation. This paper presents a rigorous, and relatively simple, method for determining that parameter based solely on test results from consolidation-swell test data. Experimental results from a laboratory investigation are presented to aid in assessing appropriate values for parameters used in the relationship. The reasonableness of the proposed approach is discussed and the general accuracy of the methodology is assessed in terms of practical experience.

Oedometer Test Stress Paths

Two different oedometer test procedures will be considered. The first procedure commonly termed the "consolidation-swell" test, ASTM Test Method D 4546 Method A, is outlined in Nelson and Miller (1992). The second is commonly referred to as the "controlled strain" or "constant volume" test. This test method is also described in Nelson & Miller (1992) and in ASTM Test Method D 4546 Method C.

The stress state variables used in this paper include $(\sigma - u_a)$ and $(u_a - u_w)$ where σ is the total stress, u_a and u_w are pore air and pore water pressure respectively. The term $(\sigma - u_a)$ is a form of the effective stress utilizing pore air pressure instead of pore water pressure as would be the case for saturated soils. This term will be simply termed the "net normal stress", and the symbol $\sigma' = \sigma - u_a$ will be used. The term $(u_a - u_w)$ is the matric suction in the soil. Stress state variables for unsaturated soils are discussed in detail in Fredlund and Rahardjo (1993) and in Nelson and Miller (1992).

In both oedometer tests the soil samples are placed in an oedometer, and subjected to an inundation stress; the sample is inundated, and the swelling characteristics are determined. In Colorado, the inundation pressure that is used is sometimes equal to the in situ overburden pressure, but more commonly it is an arbitrary value, commonly 1,000 psf. In the consolidation-swell test, the practice along the Front Range of Colorado is to subject the sample to an inundation stress, σ'_i, until it comes into equilibrium with that stress. Water is then added and the sample is allowed to swell until swelling has been completed. Additional load is added to the sample until it has been compressed to its initial height or less. The sample is then unloaded if desired.

In the constant volume test the sample is loaded to the inundation pressure, σ_i', and is then confined so that no volume change occurs during the inundation phase. The applied stress required to prevent the sample from swelling is noted, and the sample is then either loaded further or unloaded as desired.

Figure 1 shows the constitutive surface for one-dimensional vertical strain, ε_v, as a function of the two stress state variables $(\sigma - u_a)$ and $(u_a - u_w)$. The vertical strain is termed "percent swell" for applications related to expansive soil and the symbol % S will be used here. For purposes of illustration the constitutive surface shown in Figure 1 will be considered to be planar. This constitutive surface is discussed in detail in Fredlund and Rahardjo (1993). Figure 1 also shows the stress paths followed in each oedometer test. Similar stress paths are discussed in Nelson and Miller (1992) in a somewhat different form.

After a soil sample has been placed in an oedometer the net normal stress is initially zero and the matric suction in the soil is equal to $(u_a - u_w)_o$. This stress state is represented by point N in Figure 1. In a consolidation-swell test, as the sample is subjected to an inundation stress, σ_i', the stress follows the line NO. Along this line,
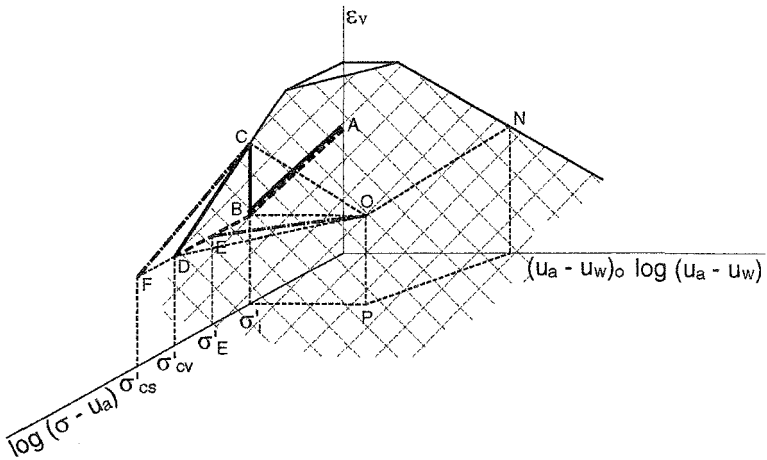
Figure 1 – Oedometer Test Stress Paths

there will be some compression of the sample, and the matric suction may decrease due to the applied load. When the sample is inundated the soil imbibes water to the point that the matric suction is decreased to zero. The stress path for this part of the test follows the constitutive surface and traces out the line OC. The loading portion of the test, follows the line CF to the point where the sample was compressed to its

original height. If soil disturbance was not an issue, the stress path would follow the line CD. It can be noted that ε_v is the same value at points O, D and F.

In a constant volume test the sample follows the same stress path NO as for the consolidation-swell test. However, when it is inundated the volumetric strain does not change; and the stress path will follow the line OD. In an ideal, reversible system the net normal stress at point D, i.e., the swell pressure, should be the same for both types of oedometer tests.

In the constant volume test, sample disturbance will cause the sample not to develop the full swell pressure, and the stress path will follow line OE. Methods for correcting constant volume oedometer test data to determine point D more accurately are presented in Nelson and Miller (1992) and Fredlund and Rahardjo (1993). With the correction applied, point D can be determined from the constant volume test. In further discussion in this paper the constant volume swell pressure will be termed σ'_{cv} and this will be understood to be the corrected swell pressure corresponding to point D.

In the consolidation-swell test the soil sample does not behave as an ideal, reversible system. Some of the water that is imbibed in following the stress path, OC goes into water of hydration with the absorbed cations in the soil. That water is difficult to remove by mechanical means. Also, due to other factors influencing the physicochemical aspects, it requires more work to expel the water that has been imbibed than would be required to prevent the water from entering the soil as in the constant volume test. Consequently, during the reloading portion of the test, the stress path follows the line CF instead of the line CD. Thus, point F corresponds to the swell pressure for the consolidation-swell test. This swell pressure will be termed σ'_{cs}.

When oedometer test data is plotted in a two dimensional format, the entire stress path is projected onto the plane defined by the $(\sigma - u_a)$ and ε_v axes. The consolidation-swell test data follows the projected path ABCF, whereas the constant volume test data follows the projected stress path ABD. Example test data is shown in Figure 2.

The slope of the loading portion of the curve shown in Figure 2 is the compression index C_c, and that of the rebound portion of the curve is the rebound index C_s. The volumetric strain experienced during inundation is the percent swell, % S.

Figure 3 shows the vertical overburden stress states at three different depths in a soil profile with similar soil throughout. At all points all samples are in a condition of zero lateral strain with a vertical overburden stress equal to σ'_{vo}. If a consolidation-swell test is conducted on a sample identical to that at depth, Z_A, at an inundation stress, $(\sigma'_i)_A = (\sigma'_{vo})_A$, the sample will swell by an amount % S_A as shown in

Figure 4. Similarly for a sample at depth Z_B, the sample would be subjected to an inundation stress, $(\sigma_i')_B = (\sigma_{vo}')_B$, and the sample would swell by an amount % S_B.
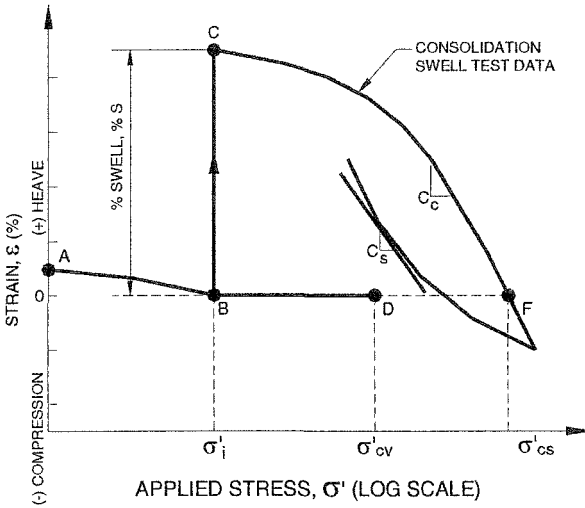
Figure 2 – Terminology and Notation for Oedometer Tests
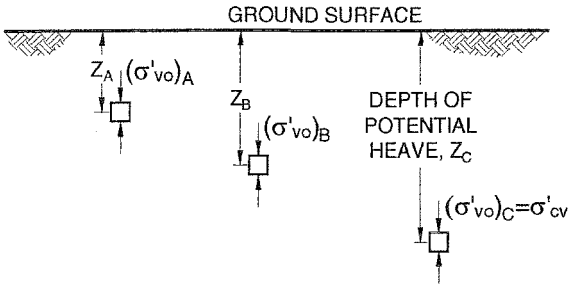
Figure 3 – Vertical Stress States in Soil Profile

Heave Prediction Equation

The general equation for predicting heave or settlement in a soil stratum of thickness Δz is

$$\rho = \frac{\Delta e}{1 + e_o} \cdot \Delta z \qquad \text{(Eq. 1)}$$

APPLIED STRESS (LOG SCALE)
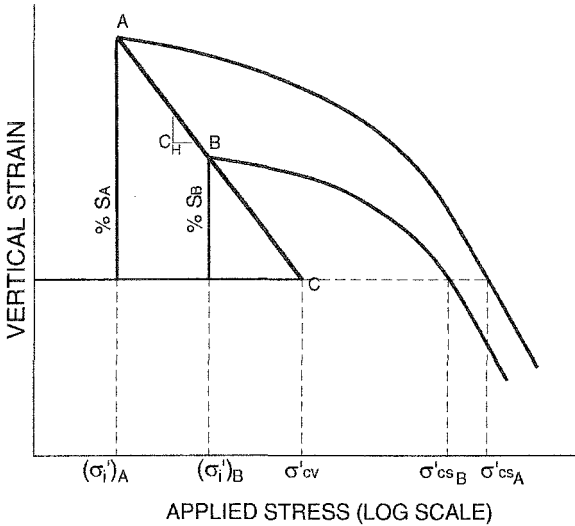
Figure 4 – Hypothetical Oedometer Test Results for Stress States Shown in Figure 3

where ρ is the change in height of the soil stratum. For purposes of this paper ρ will be considered to be heave, e_o is the initial void ratio of the soil and Δe is the change in void ratio of the soil in the stratum.

For uniform vertical strain throughout the stratum the strain is equal to

$$\varepsilon_V = \frac{\Delta e}{1 + e_o} \qquad \text{(Eq. 2)}$$

Noting that in the oedometer test, the vertical strain is % S and substituting Equation (2) into Equation (1),

$$\rho = \varepsilon_V \cdot \Delta z = \%S \cdot \Delta z \qquad \text{(Eq. 3)}$$

It is desired to develop an equation for the strain in a layer of soil using oedometer test results. At some depth the overburden pressure will equal the swelling pressure of the soil. At that depth, the sample will not swell upon wetting. If a consolidation-swell test is performed on the sample at an inundation pressure of that magnitude, no swell will occur and this is tantamount to a constant volume test.

Thus, at any depth in the soil the percent swell that will occur will fall along the line ABC. For all practical purposes that line can be defined by a straight line connecting point A (the point defined by the percent swell in a consolidation-swell test) and point

C (the point corresponding to the constant volume swell pressure, σ'_{cv}. The slope of that line is denoted by the heave index, C_H where

$$C_H = \frac{\%S_A}{\log\sigma'_{cv} - \log(\sigma'_i)_A} = \frac{\%S_A}{\log\left[\dfrac{\sigma'_{cv}}{(\sigma'_i)_A}\right]}$$
(Eq. 4)

If values of C_H and σ'_{cv} are known, the vertical strain, or percent swell, that will occur during inundation at any depth z in a soil profile can be determined from Equation 4. In rewriting Equation 4 as Equation 5, when the soil at depth z is inundated, the stress on the soil is the overburden stress, $(\sigma'_{vo})_z$. This value is therefore used for the inundation stress, σ'_i, in Equation 5.

$$(\varepsilon_v)_z = \%S_z = C_H \log\left[\frac{\sigma'_{cv}}{(\sigma'_{vo})_z}\right]$$
(Eq. 5)

Therefore, for a layer of soil of thickness Δz that exists at a depth z to its midpoint, the maximum heave that will occur due to expansion of that stratum during complete inundation would be obtained by substituting Equation 5 into Equation 3. Thus,

$$\rho = C_H \cdot \Delta z \log\left[\frac{\sigma'_{cv}}{(\sigma'_{vo})_z}\right]$$
(Eq. 6)

In actual application of Equation 6 a soil profile will be divided into layers of thickness, Δz, the value of heave for each layer will be computed, and the incremental values will be added to determine the total heave. It should be noted that the value of $(\sigma'_{vo})_z$ to be used in Equation 6 is the stress at the midpoint of the layer at depth z.

The line ABC in Figure 4 and the heave index C_H can be determined by conducting consolidation-swell and constant volume oedometer tests on samples of the same soil and connecting point A obtained from the consolidation-swell test with point C obtained from the constant volume test. However, to do so is generally not practical. Even if the additional cost and time to perform two tests were not an issue, which is usually not the case, it is almost impossible to obtain two identical samples from the field. For that reason a relationship between σ'_{cv} and σ'_{cs} will be proposed so that the value of the heave index can be determined from a single consolidation-swell test. In this way a better characterization of the soil can be accomplished without performing two oedometer tests on each soil sample.

Relationship Between σ_{cv}' and σ_{cs}'

A relationship between σ_{cv}' and σ_{cs}' exists that is of the form

$$\sigma_{cv}' = \sigma_i' + \lambda(\sigma_{cs}' - \sigma_i') \qquad \text{(Eq. 7)}$$

The rationale behind this equation follows from the stress paths that were presented in Figure 1. The value of σ_i' must be less than σ_{cv}' otherwise heave would not have occurred. Also as noted previously, it is reasonable to expect that σ_{cv}' will be less than σ_{cs}' based on the irreversibility of the system and on experimental results. Equation 7 proposes that the value of σ_{cv}' falls between σ_i' and σ_{cs}' by the proportionality defined by the value of λ. The results of a laboratory investigation to evaluate the values of λ will be discussed.

Laboratory Investigation

The details of the laboratory investigation are presented in detail in Reichler (1997). The soil used in the laboratory investigation was Pierre Shale taken from the Expansive Soils Field Test Site on the Colorado State University campus. The soils at this test site have been described in detail by Abshire, Durkee and Nelson (1998). The Pierre Shale is a marine shale containing highly-expansive bentonite beds that are typically 1 to 3 inches thick. Categorized as a sedimentary rock, the composition of the Pierre Shale often contains various amounts of glass and volcanic ash which have been weathered to montmorillonite (Chen, 1988). Carroll and Crawford (2000) states that the Pierre Formation has a high potential for shrink-swell and heaving bedrock problems due to presence of smectitic claystone and bentonite beds.

The Plastic Limit and Liquid Limit of the soil were 22 % and 56 %, respectively. This corresponds to a USCS classification of a high plasticity clay (CH). The results of several consolidation-swell tests from the investigation are presented in Figure 5.

In this investigation, Pierre shale cuttings were mixed, pulverized, sieved though a #10 sieve and then compacted at air-dried moisture contents ranging from 4 to 6 % into an oedometer ring to achieve an initial void-ratio between 0.60 and 0.62. Significant variation from this occurred in the first samples. Therefore only those samples with an initial void-ratio between 0.60 and 0.62 were selected for analyses in this paper. The results of the oedometer tests for these samples are presented in Table 1, which includes the data for two constant volume tests. The swell pressures for the constant volume tests include the correction for sample disturbance performed according to the procedure outlined in Nelson and Miller (1992).

The data shown in Figure 5 illustrates an important point with regard to the swell pressure, σ_{cs}'. In general, the samples that exhibited the greatest percent swell
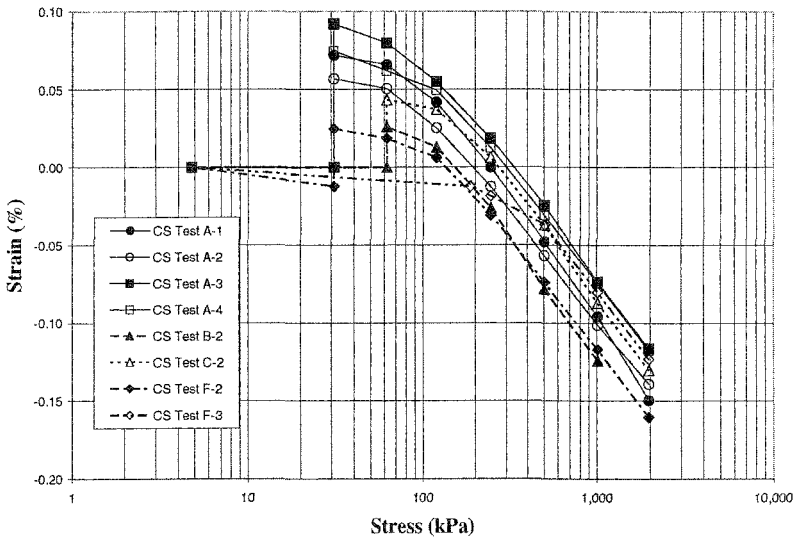
Figure 5 – Oedometer Test Results

exhibited the greatest swell pressure. Also notable is that the compression curves (after inundation) follow parallel lines. If the constant volume test curves had been plotted, they too would approach a parallel line after sufficient loading. The constant volume test exhibits a swell pressure, σ_{cv}', which is close to the value of σ_{cs}' at low swell percentages.

Table 1 – Samples Used for Oedometer Tests

Test ID	Type	%Swell	Swell Pressure (kPa)	Inundation Pressure (kPa)	Initial Void Ratio
A-4	CS	6.85	330	31	0.606
C-2	CS	3.73	282	62	0.61
D-2	CV	0.00	201	31	0.616
D-3	CV	0.00	201	31	0.612
F-2	CS	3.78	177	31	0.616
F-3	CS	0.00	187	187	0.617

The results for tests F-2 and F-3 are somewhat anomalous. Test F-2 exhibited a swell pressure less than that for the constant volume tests. This is an anomalous result, and therefore, these test results are not used in the analysis. Test F-3 actually turned out to be a constant volume test because the sample did not exhibit swell at its inundation

pressure. The value of swell pressure (and inundation pressure) is very close in value to that for tests D-2 and D-3.

If the data presented in Table 1 are used to compute the value of λ the values of λ shown in Table 2 are obtained. For those computations σ'_{cv} was taken to be equal to 201 kPa from tests D-2 and D-3.

Table 2 -- Values of λ Computed from CS and CV Tests

Test ID	λ
A-4	0.57
C-2	0.63

For Test F-3 the value of λ is not defined because the sample was inundated at its swelling pressure. Test F-2 gives anomalous results because the value of σ'_{cv} should not be greater than σ'_{cs}. Therefore, considering the data for Tests A-4 and C-2 a value of λ of about 0.6 appears to be reasonable.

Alternatively, the value of σ'_{cv} was computed from the consolidation-swell test data for different values of λ and compared to the value of σ'_{cv} measured in Tests D-2 and D-3. The results are shown in Figure 6. The value of σ'_{cs} in test F-2 is equal to σ'_{cv} for that test since the percent swell was zero. That value of σ'_{cv} is also plotted in Figure 6. The average values of σ'_{cv} computed from the data for all four consolidation-swell tests listed in Table 1 are also plotted in Figure 6 along with the averages for only Tests A-4 and C-2 which were very close in value. Again considering the data shown in Figure 6 it is apparent that a value of 0.6 for λ is quite reasonable. Furthermore, from Figure 6 it is evident that an appropriate value for λ is in the general range of 0.5 to 0.7.
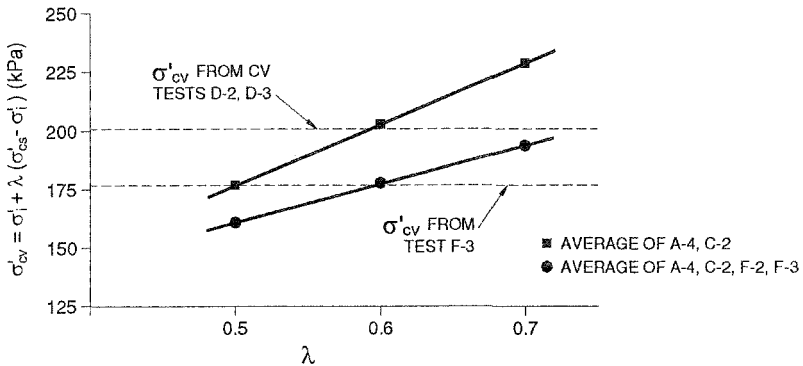
Figure 6 – Variation of Computed Value of σ'_{cv} with λ

Discussion and Conclusions

A rational method for heave prediction utilizing data from both consolidation-swell (CS) and constant volume (CV) oedometer tests was presented. The heave index was defined as the slope of the line between the point representing percent swell and the point representing the constant volume swell pressure, σ'_{cv}. Typically, budgetary concerns do not allow for both CS and CV tests to be performed. Therefore, a procedure to determine the value of σ'_{cv} through a relationship with the inundation pressure and the consolidation-swell test swelling pressure σ'_{cs} was developed. This relationship eliminates the need for the constant volume test. The value for the parameter λ to be used in the equation for σ'_{cv} was evaluated on the basis of laboratory experiments. In that laboratory investigation a total of 22 oedometer tests were performed. Because of the variability from sample to sample only 6 tests were utilized to evaluate a value for λ. This variability underscores the need to eliminate the requirement for two identical field samples in order to determine the heave index because obtaining two identical field samples is virtually impossible.

This proposed method for determination of the heave index is considered to be practical and rational but the actual value of λ to be used for different soils should be investigated on a case by case basis. The first and third authors of this paper have used a value of 0.6 which has been shown to provide reasonably accurate values of predicted heave in a case where actual measurements were possible. The form of the equation used to correlate swell pressures from CV and CS tests is considered to be reasonable and useful.

References

Abshire, M.S., Durkee, D.B., and Nelson, J.D. 1998. "Case History: A Field Investigation of Moisture Migration and Heave of Simulated Slabs-on-Grade." Proceedings of the Second International Conference on Unsaturated Soils – Beijing, China. Vol.1. pp 303-308. August 27-30. International Academic Publishers.

Carroll, C.J. and Crawford, T.A. 2000. *Geologic Map of the Colorado Springs Quadrangle, El Paso County, Colorado.* Colorado Geological Survey Open File Map 00-3 SR. 1:24,000-scale.

Chen, F.H. 1988. *Foundations on Expansive Soils.* Elsevier Science Publishers B.V. Amsterdam.

Fredlund, D. G. (1983). "Prediction of Ground Movements in Swelling Clays." 31st Annual Soil Mech. Found. Eng. Conf., University of Minnesota, Minneapolis.

Fredlund, D.G., and Rahardjo, S. 1993. *Soil Mechanics for Unsaturated Soils.* John Wiley & Sons, Inc., New York.

Nelson, J.D. and Miller, D.J. 1992. *Expansive Soils: Problems and Practice in Foundation and Pavement Engineering.* John Wiley & Sons, Inc., New York.

Reichler, D.K. 1997. *Investigation of variation in swelling pressure values for an expansive soil.* Thesis (M.S.)--Colorado State University.

Influence of Water Chemistry on the Swelling Capacity of a High-Density Bentonite

Ernesto Castellanos[1], Antonio Gens[2], Antonio Lloret[2] & Enrique Romero[3]

[1]PhD Student, Universitat Politècnica de Catalunya, 08034, Barcelona, Spain.(34) 93 401 16 97, (34) 93 401 72 51, jose.ernesto.castellanos@upc.edu
[2]Professor of Civil Engineering, Universitat Politècnica de Catalunya, 08034, Barcelona, Spain. antonio.gens@upc.edu and antonio.lloret@upc.edu
[3]Head of Geotechnical Laboratory, Universitat Politècnica de Catalunya, 08034, Barcelona, Spain. enrique.romero-morales@upc.edu

Abstract

The paper presents the results of a systematic experimental investigation under oedometer conditions aimed at understanding the chemical influence of the water chemistry on the swelling capacity of a statically compacted Ca-bentonite. Specimens were soaked under constant stress (0.02, 0.5 and 2.0 MPa) using distilled water, and NaCl and $CaCl_2$ aqueous solutions with concentrations of 0.5, 2.0 and 5.5 M. test results showed important mechanical changes induced by the effect of the hydration fluids. The swelling strains of compacted samples on soaking were systematically reduced with increasing solute concentrations. This observation had an important consequence on the development of swelling pressures, which are a key design parameter of the engineered barrier system.

1. Introduction

The hydro-mechanical properties of expansive soils are of significant importance in geotechnical and geoenvironmental engineering. Swelling due to wetting processes can originate failures and therefore economic losses when associated with pavements and buildings, while enhances the sealing potential when these materials are used as barriers in radioactive waste disposal.

The swelling potential and hydraulic conductivity of bentonites depend on the density of the sample and on the salinity of pore water (Karnland 1998; Dixon 2000). Changes in the concentration of pore water on clays may cause cation exchange, variations in the electrochemical forces and in the osmotic pressures (Van Olphen 1977; Mitchell 1993).

During the operational period of clay barriers that are part of radioactive waste disposal schemes, solute transport and thermal gradients may alter the solute concentrations of pore water. These changes may have important consequences on hydro-mechanical properties and microstructural alterations (mineral composition and pore size distribution changes) of the clay barrier. Chemically induced changes originated by different imbibition fluids and soil mineral compositions have been a subject with a long research tradition (e.g. Bolt 1956; Mesri and Olson, 1971; Sridharan 1986; Di Maio 1996; Musso *et al.* 2003; Di Maio 2004). These authors have been mainly focused on the behaviour of reconstituted soils starting from slurry and saturated with saline solutions at elevated concentrations, where hydro-mechanical changes are clearly detected. In contrast, available information concerning the response of high-density compacted clays under partially saturated conditions and subjected to chemically induced actions with a wide range of pore solution concentrations is limited in spite of its practical relevance to environmental geotechnics. This situation has been caused, at least in part, by the difficulties of identifying significant hydro-mechanical changes when clays with low water storage capacity have been used. Nevertheless, this paper will demonstrate that even in the case of high density fabrics, considerable changes can be observed when high activity clays (bentonites) are hydrated with pore fluids of different composition.

2. Materials

2.1. Bentonite

The FEBEX Ca-bentonite was used in this investigation. The bentonite was obtained from the Cortijo de Archidona deposit, Almería, South-eastern Spain. The material presents a content of montmorillonite equal to 92%, remaining minerals being small quantities of quartz, plagioclase, cristobalite, K-feldspars, trydimite and calcite. Furthermore, the material has a liquid limit of 102%, plastic limit of 49%, specific gravity of soil particles of 2.70, total specific surface of 725 m²/g using Keeling hygroscopicity method, and a cation exchange capacity of 112 meq/100g - 38% Ca^{+2}, 23% Na^{+} exchangeable cations - (ENRESA 2000).

2.2. Solutions

The solutions used in the experimental programme were distilled water and solutions of sodium chloride (NaCl) and calcium chloride (CaCl$_2$) with concentrations of 0.5, 2.0 and 5.5 M.

3. Experimental procedure

The hydro-mechanical behavior of the bentonite is heavily related to the initial structure of the clay and to the changes in the microstructure undergone by the material due to loading, hydration or chemical actions. In order to characterize the

microstructure of the different samples and to provide information about factors influencing their microstructural changes, pore size distribution determinations and environmental scanning electron (ESEM) photomicrographs were used. The pore size distribution was quantitatively obtained using mercury intrusion porosimetry technique (Webb and Orr 1977). To avoid excessive shrinkage, a freeze drying process was used to prepare the dehydrated samples required by MIP tests (Delage *et al.* 1982; Delage *et al.* 1996). Although the ESEM observations mainly provide qualitative information, the use of this technique is of interest to enhance the knowledge of the structure changes.

The artificially prepared samples were statically compacted to a dry density of 1.65 Mg/m³ at a water content of 13.7%, (hygroscopic water content). Compaction was carried out under oedometer conditions at a vertical displacement rate of 0.2 mm/min and at a maximum vertical stress of 23.0 MPa. Specimens were 10.5 mm high and 50 mm in diameter. Once compacted, the samples were loaded in steps at constant water content up to the vertical stress of the flooding stages (0.02, 0.5 or 2.0 MPa). During the loading stage the volume changes were small, since the applied load was lower than the compaction stress previously indicated and the samples remained in an overconsolidated state. Specimens were soaked under load using distilled water, and NaCl and $CaCl_2$ aqueous solutions with concentrations of 0.5, 2.0 and 5.5 M. In the soaking stages, the time necessary to reach the stabilization of vertical displacements was about 5 days, but the whole stage was extended to two weeks. After soaking, the saturated bentonite was loaded in steps under oedometer conditions up to 2.0 MPa. The unloading stage was performed in two steps. The stress paths followed for the artificially prepared samples are sketched in Figure 1.

4. Tests results and interpretation

4.1. Study of the microstructure

The effect of the type of sample preparation can be readily observed in Figure 2, where the differences between a consolidated slurry and a compacted sample are presented. The compacted sample, shows dense aggregations separated by pores of greater dimensions (inter-aggregate pores), the dominant sizes are 20 □m corresponding to the inter-aggregate pores and 15 nm to the pores inside aggregations (intra-aggregate porosity). The consolidated slurry, which has a dry density of 1.15 Mg/m³, displays a uniform and homogeneous structure (matrix structure), in which peds are not clearly distinguished. The pore size distribution of the slurry presents a clear mode at an entrance pore size of 0.42 µm and a depressed mode at a pore size of 15 nm.

The microstructural changes observed on soaking with distilled water and 0.5 M NaCl saline solution of the compacted bentonite are shown in Figure 3. In the photomicrographs, the invasion of the macroporosity is clearly observed, in which the initially aggregated structure tends to a matrix structure typical of the slurry samples. In the sample flooded with saline solution, a lower invasion of the

macroporosity appears to be observed. In addition, the emerging pore size is slightly lower than that of the sample saturated with distilled water. This emerging pore size can be probably associated with the progressive splitting of the original structure of the pseudomorphs, which are purely smectitic piles (Villar 2000). The progressive subdivision originates the increase in the number of reactive surfaces and the emerging pore size (Musso *et al.* 2003, Romero *et al.* 2003, Lloret *et al.* 2004). Lloret *et al* (2004) presented a complete study of the structural changes observed and undergone by a compacted bentonite on progressive wetting with suction control
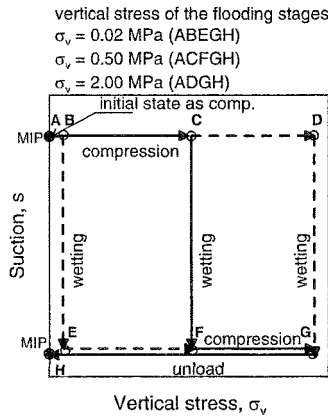
Figure 1. Stress paths followed under oedometer conditions

4.2. Liquid limit

The determination of the liquid limit provides a qualitative measure of the remoulded properties of the material. In this study, the liquid limit was obtained by mixing the FEBEX bentonite powder with distilled water, as well as with solutions of varying concentrations of NaCl and $CaCl_2$ (0.1 to 5.5 M). The variation of the solid mass with increasing salinity was considered.

Figure 4 shows that the liquid limit considerably diminishes when the concentration of the solution increases. The above-mentioned observation is consistent with the results obtained by several authors (Mesri and Olson 1971, Barbour and Young 1993, Di Maio 1996, Gleason *et al.* 1997, Alawaji 1999, Di Maio *et al.* 2004) with samples of bentonite and sand-bentonite mixtures. It can be appreciated that for the same molar concentration the values of liquid limit obtained from samples saturated with solutions of $CaCl_2$ are smaller than those obtained with samples saturated with solutions of NaCl. This shall depend on the fact that calcium ions are bivalent while sodium ions are monovalent, so that at the same concentration the ionic strength of calcium solutions is higher. According to classical models of colloid chemistry, the double layer thickness should reduce more, and with it the repulsive forces acting between single platelets.
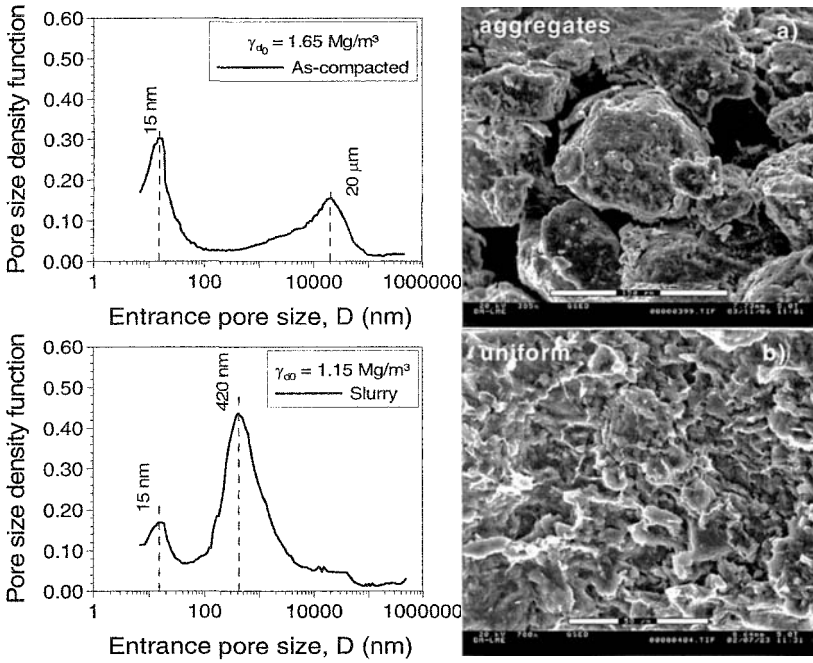
Figure 2. Pores size distributions and ESEM photomicrographs: (a) compacted sample, and (b) remoulded sample (slurry)

4.3. Effect of salinity on swelling strains

The time evolution of volumetric strains during wetting of the compacted samples is presented in Figure 5. Negative volumetric strains correspond to swelling. When high vertical stresses are applied (2.0 MPa) all samples experienced an initial collapse associated with the rearrangement of the macrostructure. Afterwards, the hydration of the microstructural level induced an important swelling. In the same figure, it can be observed that an increase in the saline concentration reduces the value of the final swelling strain. The elapsed time to start and finish the swelling process appears to be approximately the same for the samples loaded at 0.02 MPa and soaked with different NaCl solutions (around 10 min after flooding for the initiation of the process and around 2000 min for the end of the process). However, in samples flooded with $CaCl_2$ solutions at the same stress, the swelling ending time appears to increase with increasing concentration, despite some opposite trend of the soaked sample with 2.0 M. Loading at 2.0 MPa slightly increased the starting time of the different soaked samples. Again, a larger lasting process is detected when soaking at 2.0 MPa with 5.5 M $CaCl_2$ solution.
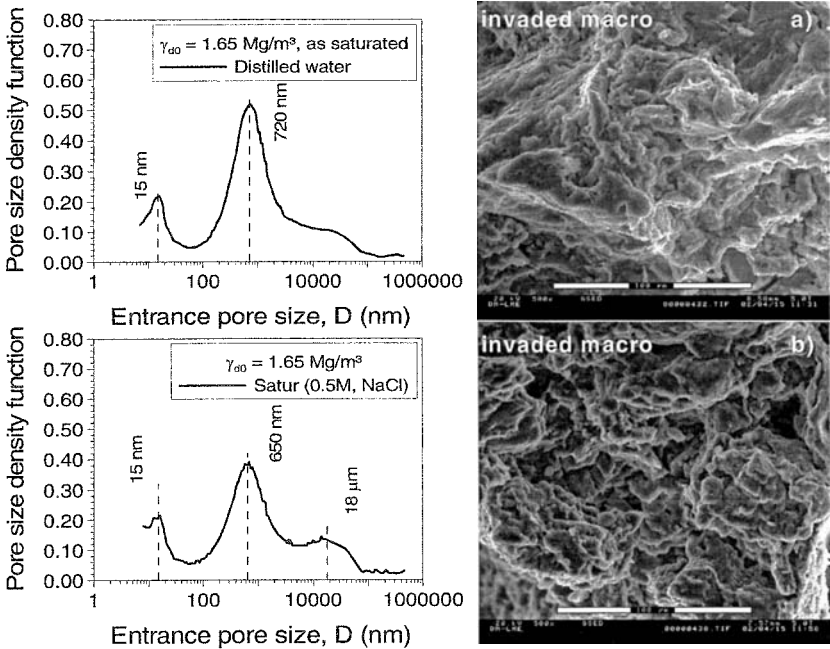
Figure 3. Pore size distributions and ESEM photomicrographs of saturated samples: (a) saturated with distilled water, and (b) saturated with 0.5 M of NaCl solution
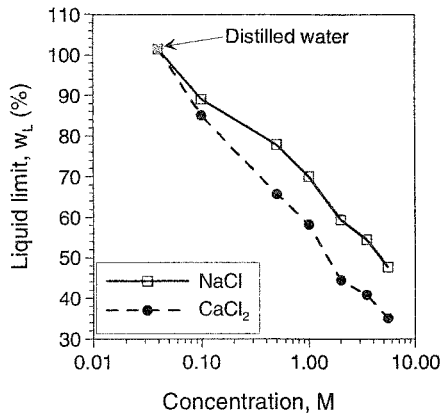
Figure 4. Influence of solute concentration on liquid limit

Very interestingly, the amount of collapse strains induced on highly loaded samples seems to be influenced by the type of cationic specie and not much by concentration. Specimens saturated with distilled water and $CaCl_2$ showed larger strains, the ones occurring with NaCl solutions being about the half. Collapse, as a consequence of the redistribution of soil aggregates due to reduced suctions, is quicker as is occurs at macrostructural scale. Chemical swelling, as a consequence of the increase in the repulsion forces acting inside the aggregates, emerges over longer times as smaller pores are inundated later.

Figures 6 show, respectively, the effects of the applied vertical stress and the concentration of the saline solution on the final swelling strains undergone by the compacted samples on soaking. It can be observed that the swelling capacity decreases significantly with salinity and that the differences in the swelling strains tend to be smaller when increasing the vertical stress. On the other hand, samples soaked with both $CaCl_2$ and NaCl solutions presented similar swelling strains.
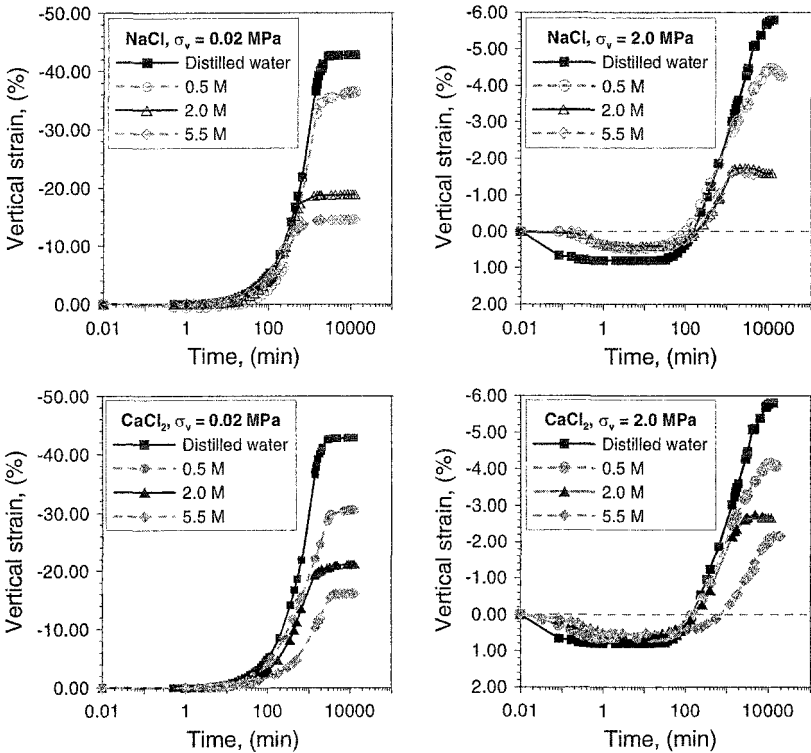
Figure 5. Time evolution of volumetric strains undergone by the compacted samples on soaking with different salt solutions and under different vertical stresses

The reduction of the swelling strains at increasing concentrations of the flooding solution can be explained by the increase of the electrolyte concentration near the clay particle surfaces that reduces the thickness of the double layer. In addition, high saline concentrations may also induce cation exchange phenomena that also affect the thickness of the double layers.

4.4 Water permeability results

Using the Terzaghi's 1D consolidation theory it is possible to obtain the coefficient of consolidation (c_v), the oedometer modulus (E_m) and the water permeability (k_w). In Figure 7, the variation of c_v and E_m with the concentration of both saline solutions is presented. The increase with salinity of the consolidation coefficient, water permeability and stiffness, cannot be solely attributed to solute effects. In fact, the void ratio changes undergone by the samples during the previous saturation path also play a significant role in the value of these parameters. It is not easy to separate the effects of chemical induced changes and void ratio changes undergone on the previous paths, since both are dependent variables. Isolating the influence of void ratio from the contribution of chemical effects requires advanced constitutive frameworks.
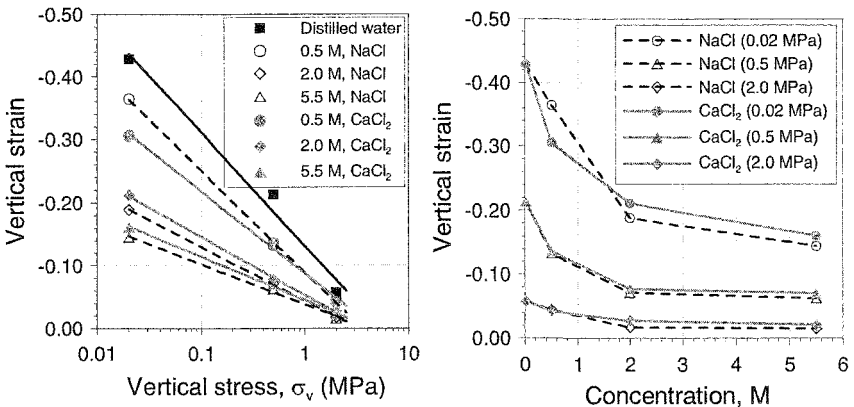
Figure 6. Swelling strains against vertical stresses and concentration of NaCl and CaCl$_2$ saline solutions for compacted samples in soaking under load tests

Figure 8 presents the variation of water permeability with void ratio for both saline solutions at different concentrations. It is clearly observed that the permeability increases with increasing concentration of saline solutions. However, no clear trend is detected regarding the type of solute used. The increase of the permeability with concentration can be explained based on the photomicrographs shown in Figure 3. As observed in this figure, when imbibed with saline solution the aggregates are still distinguishable leaving some macroporosity between them, which explains the increase of the permeability.
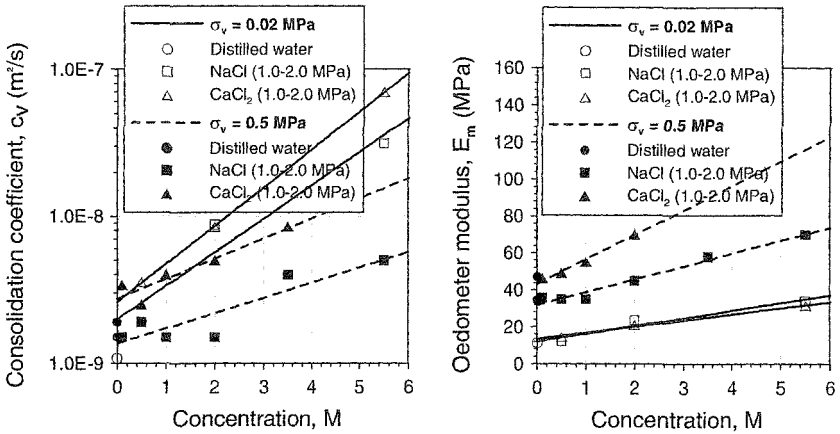
Figure 7. Consolidation coefficient (c_v) and oedometer modulus (E_m) of compacted samples for different NaCl and $CaCl_2$ concentrations
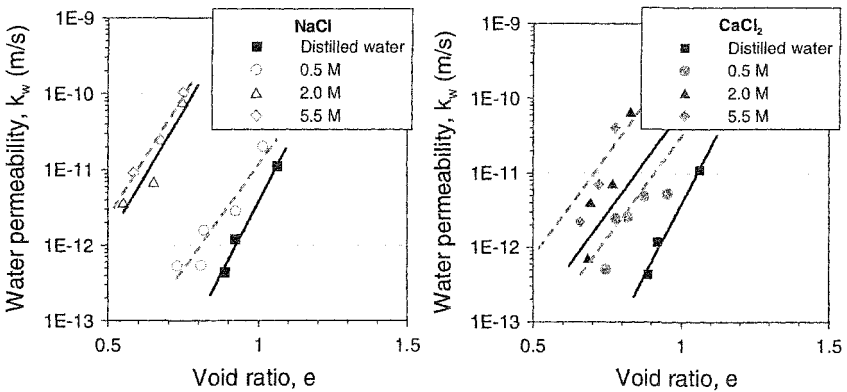
Figure 8. Water permeability as a function of void ratio and pore fluid concentration

5. Summary and conclusions

Experimental results were reported to extend the knowledge of chemical induced changes on soil expansivity, compressibility on loading and water permeability. A systematic testing programme under oedometer conditions was performed on bentonite samples compacted at 1.65 Mg/m³ dry density. Compacted samples, displaying an aggregated structure with two contrasting pore sizes, were initially soaked at constant stress with different concentrations of NaCl and $CaCl_2$ salt solutions, and thereafter loaded and unloaded under saturated conditions.

Significant reductions of swelling strains were observed on soaking with increasing saline concentrations, whereas the effect of the type of cation was not remarkable. The reduction of the swelling capacity at increasing concentrations was explained by the increase of the electrolyte concentration near the clay particles and the depletion of the double layer thickness. In addition, high saline concentrations may also induce cation exchange phenomena that also affect the thickness of the double layers. Higher water permeability values and oedometer moduli were systematically observed at higher concentrations on artificially prepared structures.

Mercury intrusion porosimetry tests and environmental scanning photomicrographs were also reported to characterize the porosity network of the artificially prepared bentonites under different chemical and hydro-mechanical states. The observations at microstructural level provided complementary insights into the understanding of chemical effects on the hydraulic response.

Acknowledgments

References

Alawaji, H. (1999). Swell and compressibility characteristics of sand-bentonite mixtures inundated with liquids. *Applied Clay Science*, 15: 411-430.

Barbour, S.L. & Yang, N. (1993). A review of the influence of clay-brine interactions on the geotechnical properties of Ca-montmorillonitic clayey soils from western Canada. *Can. Geotech. J.*, 30: 920-934.

Bolt, G.H. (1956). Physico-chemical analysis of the compressibility of pure clays. *Géotechnique*, 6(2): 86-93.

Delage, P., Tessier, D. & Audiguier, M.M. (1982). Use of the cryoscan apparatus for observation of freeze-fractured planes of a sensitive Quebec clay in scanning electron microscopy. *Can. Geotech. J.*, 19: 111-114.

Delage, P., Audiguier, M., Cui, Y.-J. & Howat, D. (1996). Microstructure of a compacted silt. *Can. Geotech. J.*, 33: 150-158.

Di Maio, C. (1996). Exposure of bentonite to salt solution: osmotic and mechanical effects. *Géotechnique*, 46(4): 695-707.

Di Maio, C., Santoli, L. & Schiavone, P. (2004). Volume change behaviour of clays: the influence of mineral composition, pore fluid composition and stress state. *Mechanics of Materials*, 36: 435-451.

Dixon, A.D. (2000). Porewater salinity and the development of swelling pressure in bentonite-based buffer and backfill materials. Posiva Oy Report, POSIVA 2000-04. Helsinki.

ENRESA. (2000). FEBEX Project. Full-scale engineered barriers experiment for a deep geological repository for high level radioactive waste in crystalline host rock. Final Report. Technical Publication ENRESA 1/2000. Madrid.

Gleason, M.H., Daniel, D.E. & Eykholt, G.R. (1997). Calcium and sodium bentonite for hydraulic containment applications. *J. Geotech. Geoenviron. Eng.*, ASCE 123(5): 438-445.

Karnland, O. (1998). Bentonite swelling pressure in strong NaCl solutions. Posiva Oy Report, POSIVA 98-01. Helsinki.

Lloret, A.; Villar, M.V. & Romero, E. (2004): Final report on thermo-hydro-mechanical laboratory tests. Internal report CIEMAT/DIAE/54520/3/04. FEBEX report 70-UPC-L-7-13 rev 0.0. Barcelona.

Mitchell, J.K. (1993). Fundamentals of Soil Behaviour. John Wiley& Sons. Inc., New York, 2nd ed.

Mesri, G. & Olson, R.E. (1971). Consolidation characteristics of montmorillonite. *Géotechnique*, 21(4): 341-352

Musso, G., Romero, E., Gens, A. & Castellanos, E. (2003). The role of structure in the chemically induced deformations of FEBEX bentonite. *Applied Clay Science*, 23: 229-237.

Romero, E., Hoffmann, C., Castellanos, E., Suriol, J. & Lloret, A. (2003). Microstructural changes of compacted bentonite induced by hydro-mechanical actions. Large Scale Field Tests in Granite. Backfill and plug, FEBEX, Prototype, TBT. Sitges, Spain.

Sridharan, A.; Rao, S.M. & Murthy, N.S. (1986). Compressibility behaviour of homoionized bentonites. *Géotechnique*, 36 (4): 551-564.

Studds, P.G., Stewart, D.I. & Cousens, T.W. (1998). The effects of salt solutions on the properties of bentonite-sand mixtures. *Clay Minerals*, 33: 651-660.

Van Olphen H. (1977). An introduction to clay colloid chemistry, Wiley Interscience, New York

Villar, M.V. (2000). Caracterización termo-hidro-mecánica de una bentonita de Cabo de Gata. *PhD Thesis*. Universidad Complutense de Madrid. Madrid. (In Spanish).

Webb, P.A. & Orr, C. (1997). Analytical methods in fine particle technology. Micromeritics Instrument Corp., Norcross.

Hydro-mechanical small-scale tests on compacted bentonite

C. Hoffmann[2,1], E. Romero[1] and E.E. Alonso[1]

[1]Department of Geotechnical Engineering and Geosciences, Universitat Politècnica de Catalunya, c/Jordi Girona 1-3, Building D2, 08034 Barcelona, Spain; PH +34 934016888; FAX +34 934017251; email: enrique.romero-morales@upc.edu, eduardo.alonso@upc.edu. The first author formerly PhD student at Universitat Politècnica de Catalunya.
[2]Dipartimento di Ingegneria Meccanica e Strutturale, Università degli Studi di Trento, Via Mesiano 77, 38050 Trento-Povo, Italy; PH +39 0461 882551; FAX +39 0461 882599; e-mail: christian.hoffmann@ing.unitn.it

Abstract

Artificially prepared bentonite-based granular mixtures at very low water content have been proposed as possible candidate materials for the construction of engineered barriers for radioactive waste disposal. This material, which is capable of being emplaced by auger technique, improves the emplacement operations and minimizes air gaps of engineered barriers in horizontal drifts installed in competent clay formations. An extensive laboratory test program was performed to characterize this partially saturated material at nearly emplacement scale and at a low emplacement dry density (around 1.4 Mg/m^3) using a small-scale hydration equipment. A constant volume hydration column 70-mm in diameter and 200 mm high was used to simulate different hydration conditions. One of the aims of this paper is to describe the small-scale equipment by detailing its capabilities and presenting selected test results. Sample preparation techniques and main properties of the mixture are also presented.

Introduction

Artificially prepared expansive clays are widely proposed as possible materials for the construction of engineered barriers for radioactive waste disposal. Within the 5th Framework of the European Union Research Projects, the Engineered Barrier Emplacement Experiment (AITEMIN 2001) demonstrated a new concept to improve the emplacement operations and to minimize air gaps of engineered barriers in horizontal drifts installed in competent clay formations. This concept was based on the use of bentonite-based granular mixtures at very low initial water content capable of being emplaced by auger technique. The low water content was required to achieve an elevated dry density of the granules, which compensated the low dry density of the

emplaced mixture and ensured an adequate swelling pressure on wetting. One of the objectives of this project was to characterize at laboratory scale the hydro-mechanical response of this artificially aggregated material with 15-mm maximum size along a hydration process and under constant volume (isochoric) conditions.

An extensive laboratory test program was performed to characterize this partially saturated material at nearly emplacement scale and at a low emplacement dry density (around 1.4 Mg/m^3) using a small-scale hydration equipment. A constant volume hydration column 70-mm in diameter and 200 mm high was used to simulate the different hydration conditions of the in situ test. Both pressure and volume rate conditions of water injection were applied using a pressure / volume controller driven by a stepper motor. The evolution of lateral stresses on wetting was monitored by means of three total pressure cells located at different heights. The evolution of axial stress on hydration was also registered with an external load cell.

One of the aims of this paper was to describe the small-scale equipment by detailing its capabilities and presenting selected test results. Sample preparation techniques, and main properties of the mixture were also reported. Test results showed the important consequences on the hydro-mechanical response of the material when different injection boundary conditions were applied. The following phenomena were clearly detected on wetting: occlusion of the large inter-granular porosity due to the swelling of the bentonite pellets, local collapses that occurred on initial imbibition of the inter-grain porosity, and the progressive erasure of the initial anisotropy that was induced on 1D sample preparation. Another objective of the paper was focused on the interpretation of the results within the framework of a suction-dependent double porosity model (Hoffmann 2005).

Small-scale hydration column

A constant volume hydration column (70 mm in diameter and 200 mm high) was constructed to test the partially saturated mixtures under different water injection conditions applied on the top and bottom boundaries. Both water pressure and volume rate controlled injections were applied at the bottom boundary, whereas the top boundary was maintained at atmospheric conditions. An automatic pressure / volume controller driven by a stepper motor (GDS Instruments Ltd.) was used to control water injection. Total vertical stress was monitored with an external load cell installed at the base plate (Figure 1). Total horizontal stresses were registered by three total stress cells installed at different locations throughout the sample height. Data was automatically logged. In this way, the time evolution of swelling pressure on hydration could be monitored. A photograph of the column and a cross-section scheme of the infiltration test are shown in Figure 1. Location of the water injection plate and the different transducers are also indicated. Table 1 summarizes the main properties of the transducers.

Figure 2 shows the calibration results of the different transducers. Total stress and load cells were calibrated with water pressure. Increasing / decreasing water pressure cycles were applied at a maximum value of 1 MPa. A linear response is observed with no significant hysteresis.
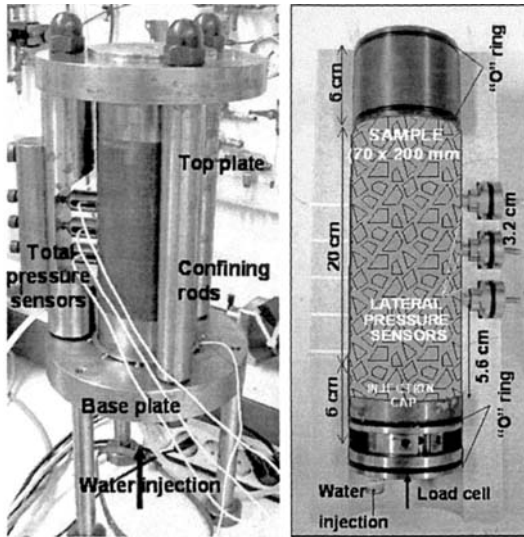
Figure 1. a) Small-scale hydration column. b) Cross-section scheme.
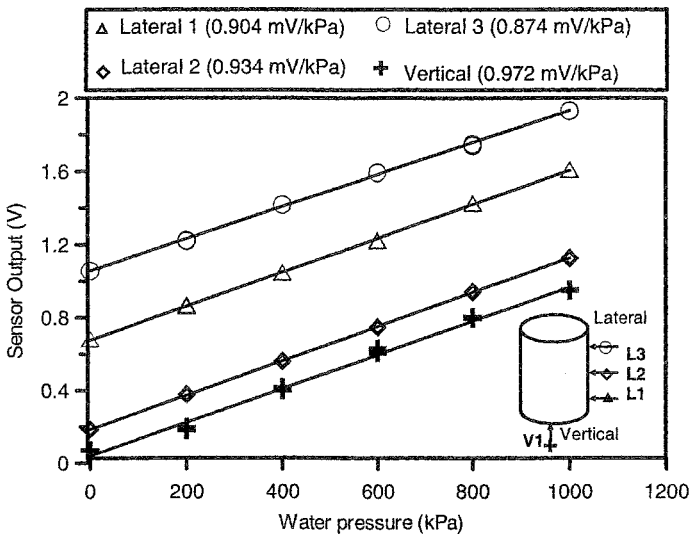
Figure 2. Calibration of the different transducers by water backpressure.

Table 1. Properties of the transducers and water injection system.

Properties	Load cell	Total stress cell	Water injection
Model	Sensotec LFH-71	GS Sensors XMR10	GDS press./ vol. controller
Range	5 kN	1 MPa	2 MPa / 200000 mm³
Accuracy; resolution	± 0.7% FS	± 0.6% FS	press. 0.25% FS; ± 1 mm³/± 1 kPa

Tested material and sample preparation

Clay pellets were prepared from FEBEX bentonite powder (Almería, Spain). Bentonite properties are summarized in Table 2. Further details on this material can be found in ENRESA (2000). The following procedure, which is described in Figure 3a, was followed to fabricate the pellet-based material. Naturally-aggregated bentonite was compacted using a roller press. In order to facilitate this operation, the bentonite powder was pre-heated to 120°C. As a result of this process, granules with a dry density of around 1.95 Mg/m^3 and reduced water content of 3-4% were obtained. Finally, the fraction of granules with sizes larger than 10 mm was used as the basic material for the production of pellets with a jaw crusher. Afterwards, these pellets were sorted, sieved and mixed to arrive to the optimal grain size distribution. Pellet properties are also indicated in Table 2. Laboratory tests were performed on mixtures with a maximum pellet size D_{max} = 10 mm. A minimum pellet size of D_{min} = 0.4 mm was selected to avoid the tendency towards segregation of the finer particles. The distribution curve follows a modified form of the Fuller curve, to allow for a minimum diameter cut-off, D_{min}, given by

$$p = 100 \frac{\sqrt{D/D_{max}} - \sqrt{D_{min}/D_{max}}}{1 - \sqrt{D_{min}/D_{max}}}$$

where p represents the percentage passing, referred to the total dry mass and D the pellet size. Figure 3b shows the pellet size distribution curve. Further properties of this pellet-based material are presented in Hoffmann (2005).

Table 2. Material properties. FEBEX bentonite and clay pellets.

FEBEX bentonite (montmorillonite content higher than 90%)			
ρ_s (Mg/m^3)	$w_P(\%)$	$w_L(\%)$	% of particles < 2 μm
2.7	47 - 56	93 - 106	64 - 70
Pellets			
ρ_d (Mg/m^3)	e_0	w (%)	Initial suction (MPa)
1.95	0.38	3 - 4	250-300
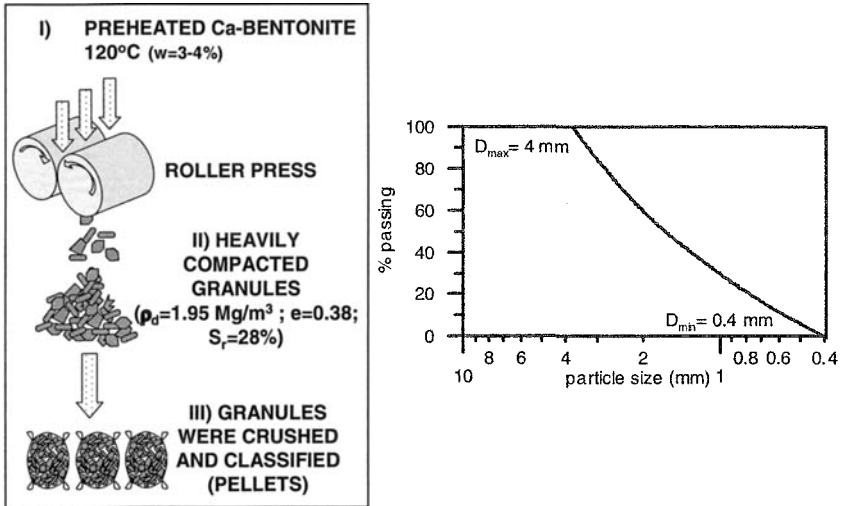
Figure 3. a) Fabrication process of artificially-prepared pellets. b) Particle size distribution of the tested material.

As the overall dry density of the emplaced material was reported as 1.36 Mg/m^3 (NAGRA 2003), tests were performed on samples prepared at a dry density of 1.4 Mg/m^3. Samples 70-mm in diameter and 180 mm high were prepared using one-dimensional static compaction at constant deformation rate (0.2 mm/min) in three layers of 60-mm. Vertical load and lateral stress were measured during compaction and stress paths in terms of vertical and horizontal stresses were deduced. Stress paths corresponding to the third layer are presented in Figure 4. During this compaction stage, sensors 2 and 3 are in contact with the previously compacted material, whereas sensor 1 is measuring the stress evolution of the material being compacted. Some collapses are observed in the stress path corresponding to sensor 1 due to granule breakage and rearrangements.

Test description and results

Two tests were performed on identical samples but using different hydration boundary conditions to simulate different wetting situations existing in the real scale test. In TEST 1, a constant water injection rate of 375 mm^3/s was applied during the initial part of the test but as the injection pressure increases, and a medium value of 200 kPa was reached, injection pressure was set constant to 200 kPa until the end of the test (Figure 5a). In TEST 2, a pressure controlled injection was used. The pressure was linearly increased from zero to a target value of 200 kPa during the first minute

of the test. After this initial ramp the injection pressure was maintained constant at 200 kPa until the end of the test. The evolution of the water injection pressure, the injected volume and the rate of water injection for both tests are shown in Figure 5. When comparing the evolutions of the different variables during the initial part of both tests it can be observed that when a volume rate controlled injection is used (TEST 1) a large amount of water is injected. In addition, it is observed that in TEST 2, the injection system could not increase the injection pressure according to the applied ramp (Figure 5b) due to the very high initial permeability of the granular material. As the hydration progresses, the bentonite pellets expand filling the large intergranular pores and inducing the water permeability to decrease. Under this condition a constant injection pressure of 200 kPa could be maintained.

In both tests, the hydration stage was maintained until an overall degree of saturation of around 80 % was reached. Once this stage was finished the sample was extruded, cut into slices and the water content and dry density of each slice measured using the paraffin wax method.
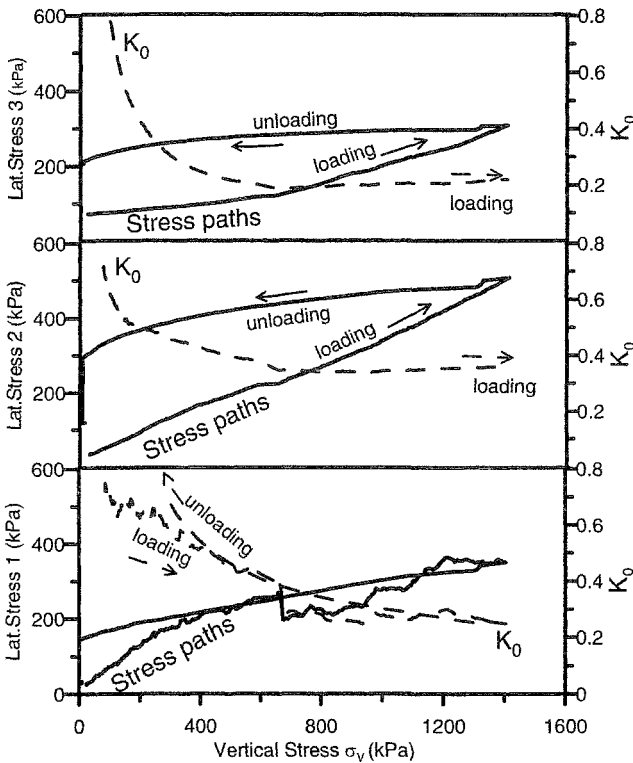
Figure 4. Stress path and coefficient of earth pressure (K_0) obtained during sample static compaction.
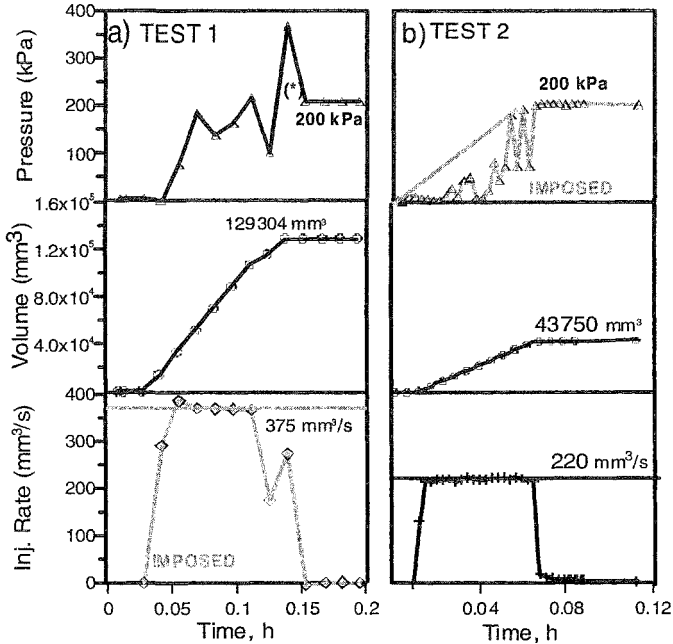
Figure 5. Water injection at the bottom boundary for both tests.

The evolution of the different variables during the hydration stage of TEST 2 is shown in Figure 6. It can be observed that after 4200 hours of hydration, an overall degree of saturation of 0.82 was reached and the load cell and total pressure sensors are measuring almost the same total swelling pressure value of 800 kPa. This indicates that as the hydration progress the expansive granular mixture evolves to an almost isotropic state of stress erasing the initial anisotropy introduced during the sample fabrication process. In addition, some intermediate collapses are observed in the lateral stress as the swelling progresses. These collapses, which were also observed in the real scale test, could be explained due to the occurrence of two different volume change mechanisms. The first mechanism is associated with the volume change characteristics of the granular arrangements of pellets. When the water goes into the sample filling the large macropores, the intergranular forces holding the granular packing stable are reduced or evenly destroyed and the structural collapse of the specimen is susceptible to occur. This collapse depends not only on suction but also on the stress level acting in the granular packing (Alonso et al. 1990). The second volume change mechanism is associated with the expansive behaviour of the high-density bentonite pellets. Expanding pellets hydrates

exchanging water with the macropores and progressively swell filling the intergranular pores. Considering the existence of these two mechanisms implies the assumption that two different water potentials exist at a given time in the same elementary volume of the specimen. The water filling the macropores has a macro potential, not necessarily in equilibrium with the water potential inside the aggregates. The overall behavior of the sample will depend not only on the properties of the material but also on the water injection conditions. Micro and macro volume change mechanisms on wetting of this pellet-based material are discussed in detail in Hoffmann (2005) and Hoffmann et al. (2006).
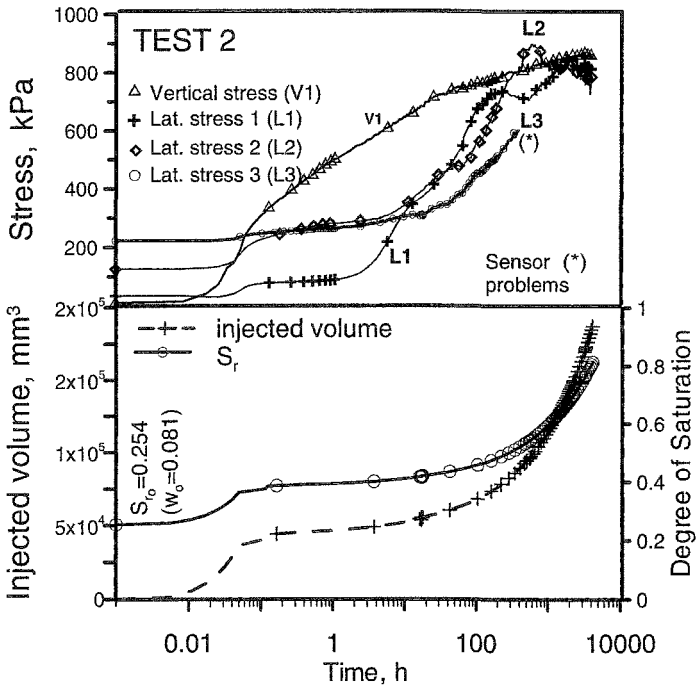
Figure 6. Evolution of stresses, degree of saturation and injected water volume during TEST 2.

A major improvement of the small-scale test equipment is that the total stress state can be monitored along the different stages: sample compaction and the subsequent hydration phase. Stress paths were deduced considering the vertical stress and the three lateral stresses. Figure 7 shows the stress paths followed in terms of vertical and horizontal total stresses. All paths display an initial phase that follow K_0 conditions, similar to the loading / unloading paths. After this initial phase, the stress paths change and move towards an almost isotropic stress state. This behavior can be

explained because during this initial phase of the test, the injected water is stored in the bottom part of the sample and the material located far from the injection cap remains almost dry. As the bottom part of the sample swells, the material located just above is vertically compressed and evolves according to the elastic properties of the as compacted material. As the hydration progresses and wetting involves the material located in contact with the lateral sensors, the stress path change its slope indicating that some swelling is occurring in this part of the sample and the material evolves to an isotropic state of stress.
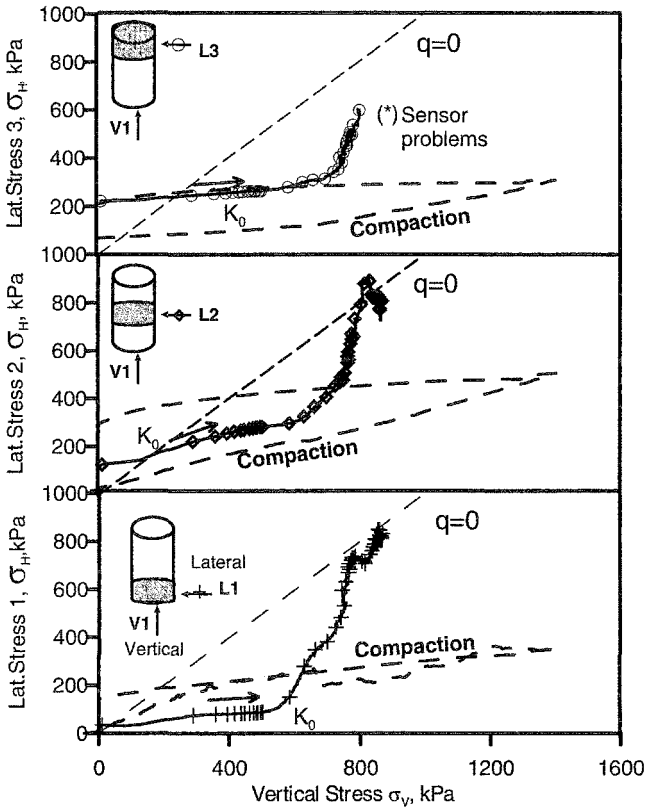
Figure 7. Stress paths followed according to the different transducers.

Once the hydration phase was finished, the sample was extruded, and the water content and dry density distributions measured. The material evolved from an initial granular structure to a more homogeneous structure on saturation. During hydration, the expanding pellets progressively fill the intergranular voids. The water content,

degree of saturation and dry density distributions corresponding to the end of TEST 2 are shown in Figure 8. Analyzing the dry density distribution, it can be observed that the bottom part of the sample has decreased its dry density due to swelling, while the upper part of the sample has been compressed. During the initial part of the test, the lower material swells while the upper part remains dry. At the final hydration stage, the upper material begins to swell compressing the lower part of the sample (almost saturated), but some structural collapses occur compensating for the swelling effect of the high-density granules.
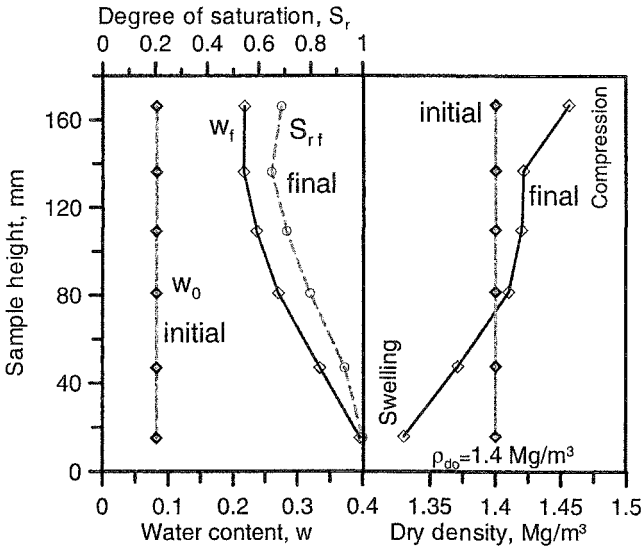
Figure 8. Water content, degree of saturation and dry density distributions at the end of the hydration phase (TEST 2).

Summary and conclusions

Within the context of the Engineering Barrier Emplacement Experiment (AITEMIN 2001), a material made of bentonite pellets has been suggested as a suitable alternative for the construction of isolating barriers in deep radioactive waste repositories. A series of hydro-mechanical small-scale tests were performed to study the response of this bentonite pellet-based mixture on hydration. New testing equipment were designed and constructed, in which different boundary conditions could be applied using either pressure controlled or volume rate controlled water injections. Different transducers were included to monitor the evolution of total vertical and horizontal stresses at different locations on the sample.

The tested material was defined based on the conditions of the emplaced material. Samples were prepared using one dimensional static compaction at a dry density of 1.4 Mg/m^3. Two tests were performed considering different hydration conditions. Based on the results obtained some important aspects of the hydro-mechanical response of the material were identified. The following features have been observed:

- As the hydration evolved the stress state progressed to an isotropic stress state erasing the initial anisotropy induced during the sample fabrication process.
- Some collapse was observed associated with the reduction of the intergranular forces holding the granular packing stable and the increase in the stress level induced by the expanding pellets.
- Results were conceptually interpreted considering two different volume change mechanisms acting at different structural levels. The existence of two water potentials coexisting in the same elementary volume inside the sample was proposed. One associated with the water stored in the intergranular pores, and another associated with the water stored inside the high-density pellets.

References

AITEMIN (2001). *The EB Experiment Engineered Barrier Emplacement in Opalinus Clay*. Test Plan, version 3.0. NAGRA, Wettingen.

Alonso, E.E, Gens, A. and Josa, A. (1990). *A constitutive model for partially saturated soils*. Géotechnique 40(3), 405-430.

ENRESA (2000). *FEBEX Project. Full-scale engineered barriers experiment for a deep geological repository for high level radioactive waste in crystalline host rock*. Final report. Publicación Técnica ENRESA 1/2000, Madrid.

Hoffmann, C. (2005). *Caracterización hidromecánica de mezclas de pellets de bentonite. Estudio experimental y constitutivo*. PhD Thesis. Universitat Politècnica de Catalunya, Spain.

Hoffmann, C., Alonso, E.E. & Romero, E. (2006). *Fabric changes of a pellet-based bentonite buffer material and its effect on mechanical behavior.* Accepted for publication in 4th Int. Conf. on Unsaturated Soils, Carefree, Arizona.

NAGRA (2003). *Engineer Barrier Emplacement Experiment in Opalinus Clay (EB). Granular material emplacement.* QA Report with Emplacement Description. Deliverable D12.NAGRA, Wettingen.

Evaluation of Two Constitutive Models to Simulate Behavior during Constant Volume Infiltration on a Swelling Clay Soil

D. G. Priyanto[1], G. A. Siemens[1], and J. A. Blatz[1]

[1]Department of Civil Engineering, University of Manitoba, Winnipeg, MB, R3T 5V6
PH: (204)474-8072; FAX: (204)474-7513; email: umpriyan@cc.umanitoba.ca

Abstract

The Parameter Evaluation Method (PEM, Priyanto et al. 2004) algorithm is applied to determine parameters of the Barcelona Basic Model (BBM, Alonso et al. 1990) and the Blatz and Graham Model (BGM, Blatz and Graham 2003) for a constant volume infiltration test on an unsaturated swelling clay soil. The limitations of both constitutive models to simulate the stress path for this example are indicated. The recommendation to incorporate different swelling induced pressure for drying and wetting stress paths may be made by introducing parameter $\kappa_{rat} = \kappa/\kappa_s$, which represents the degree of the swelling induced pressure. The numerical modeling of this test is also accomplished using finite difference analysis (FLAC, Itasca 2001) incorporating fluid-mechanical interaction. It shows that the hydraulic constitutive models (soil water characteristic curve (SWCC) and permeability laws) play a significant role for this type of analysis. The future application of the PEM algorithm (Priyanto et al. 2005) combined with triaxial tests with controlled and measured suction (Blatz and Graham 2000, Siemens and Blatz 2005) can reduce the necessity of independent permeability testing to establish hydraulic parameters. The PEM can also be used to create a 'parameter generator' to characterize the behavior of unsaturated high plastic clay. Consequently, the number of parameters used in the constitutive model is independent of the difficulty associated with calibrating the parameters using physical measurements.

Introduction

In comparison with other engineering materials, unsaturated soils are notably difficult to characterize (Lade 2005). Characterization of unsaturated high plastic clay can be done by means of laboratory testing combined with numerical modeling. Numerical modeling of unsaturated high plastic clay itself provides many challenges (Priyanto et al. 2005). Due to the complexity of unsaturated clay behavior, a simple constitutive model may not be adequate to describe the general response to all possible stress paths. Consequently, more comprehensive constitutive models (such as those referred to as critical state models) are required. Unlike critical state soil mechanics (Roscoe and Burland 1968) for saturated clay, a widely accepted constitutive model for unsaturated high plastic clay is not clearly established at this time. There are many constitutive models proposed that are developed for various types of clay materials, using different laboratory test methods, and for varying stress state and environmental conditions. Selection of the most suitable constitutive model to simulate a particular type of material forms a considerable challenge.

It is also possible that a specific constitutive model is only adequate to simulate a specific clay mineral or soil type. When such a constitutive model is applied to different types of material and conditions, modifications of the model are required. The Basic Barcelona Model (BBM) (Alonso et al. 1990) was originally calibrated based on clay with low-to-medium plasticity. Additional features are required to capture the swelling behavior when used for high plastic clay as outlined in Alonso et al. 1999. Consequently assessment of the capability of existing constitutive models is important. In this discussion, the BBM (Alonso et al. 1990) and BGM (Blatz and Graham 2003) are selected in the analysis based on the following reasons. The BBM is the first critical state soil model for unsaturated clay, while the BGM is developed based on the laboratory test results using a similar clay material as this paper. It is important to note that the BGM model was developed on the foundation of the BBM and simply adds some new features of behavior for the specific clay and preparation procedure used.

Assessment of the capability of various constitutive models can be done with application of the Parameter Evaluation Method (PEM) algorithm (Priyanto et al. 2004). In this paper, the PEM algorithm is applied to results from laboratory testing along stress paths from the constant volume infiltration triaxial test. Based on this analysis, the limitations of both constitutive models to simulate the stress path examined for this material is evaluated. A recommendation to incorporate different swelling pressure relationships for drying and wetting stress paths is provided by introducing that parameter κ_{rat} (= κ/κ_s), which represents the degree of the swelling induced pressure.

Numerical modeling of unsaturated clays does not only require mechanical constitutive models (stress-volume relationship), but also hydraulic constitutive models (soil water characteristic curve (SWCC) and permeability laws). Fluid-

mechanical interaction behavior of the constant volume infiltration triaxial test is modeled in this paper using FLAC (Itasca 2001). The results show that the hydraulic constitutive models are an important feature of the model in terms of being able to capture the behaviour of the specimen in the constant volume infiltration triaxial test.

Constitutive models based on critical state soil mechanics (Roscoe and Burland 1968, Alonso et al. 1990, Alonso et al. 1999, Blatz and Graham, 2003) require more parameters than traditional linear elasticity and linear elastic-perfectly plastic models that use the Mohr-coulomb failure criteria (Terzaghi 1936, Fredlund and Rahardjo 1993) since they capture more features of material behavior. There is a general sense that the more complex the constitutive model, the more parameters that will be required. This is then considered to require more laboratory testing that results in more time and money required for the use of more advanced models. In addition to time and costs considerable effort is required to calibrate parameters for more comprehensive constitutive models. Consequently models with less parameters are generally more widely used in typical engineering applications.

The paper introduces the future proposed application of the PEM algorithm (Priyanto et al. 2004) combined with controlled and measured suction triaxial testing results (Blatz and Graham 2000, Siemens and Blatz 2005) to characterize a compacted unsaturated bentonite clay. The ability to determine both mechanical (stress-strain relationship) and hydraulic constitutive models (SWCC and permeability laws) simultaneously may reduce the necessity of independent permeability testing that can be inaccurate (variations in order of magnitude). This is intended to reduce the impact of the number of parameters on the selection of a constitutive model. Instead, when parameters of a constitutive model are proven to be independent of the stress-paths, initial and boundary conditions, it can reduce the number of laboratory test results required which means reduced time and costs for calibration. This future application also shows promise as a 'parameter generator', such that a more rationale approach is defined to determine parameters used in the constitutive model. However, the largest challenge faced in implementing this approach in numerical modeling is how to apply the more comprehensive constitutive models for analysis of engineered structures which is a topic beyond the scope of this discussion.

The Parameter Evaluation Method (PEM)

The Parameter Evaluation Method (PEM) algorithm proposed by Priyanto et al. (2004) provides an alternative approach to determine parameters of a constitutive model. The PEM is developed based on the following assumptions: the numerical model must be calibrated from laboratory results; when such a constitutive model is representative to simulate the behavior of particular material, its parameters are independent of stress path or environmental conditions applied to the material.

The PEM (Priyanto et al. 2004) provides a statistical interpretation of laboratory results to obtain constitutive model parameters and to assess the capabilities of the

constitutive model to simulate the behavior of high plastic clay materials. The ability of the PEM algorithm for various constitutive models demonstrates that it can be used as a tool to select a constitutive model by providing a measure of comparison between the model predicted stress paths and measured stress paths from experimental testing. The ability of the application of the PEM algorithm to capture limitations of a constitutive model results in a measure of how to modify existing constitutive models to provide better predictions of general soil behavior. This concept was explored in the application of the PEM algorithm for two specimens subjected to isotropic stress paths in Priyanto et al. 2005.

The PEM algorithm is based on an iterative back-fitting process that compares laboratory test results and numerical simulations based on three PEM criteria. These three criteria include: 1) the difference between results from the model simulation and the experiment; 2) the location of the yield surface; and 3) the variation of parameters generated using different selected stress paths. These additional criteria make the PEM somewhat different from a traditional back-fitting analysis.

Generally back-fitting analysis is conducted by altering parameters when numerical modeling results are different from the laboratory results. This is done with a specific fit in mind in terms of one aspect of behavior related to the application of interest. In the PEM algorithm, the back-fitting for various stress paths is used to assess the capability of constitutive models, since the existing constitutive models have not been proven to be independent of stress path, initial and boundary conditions for such a material.

The overall process used to apply the PEM algorithm is illustrated in Figure 1. Three stress states variables are used in this paper to describe the stress path of the specimen, which are: mean stress (p), deviatoric stress (q), and suction (s) (Fredlund and Rahardjo 1993). The stress-strain relationships were measured in triaxial tests as plotted in p-s space and p-v space in Figure 1 (where v is the specific volume). The suction and mean stress relationship (p-s space) measured in the laboratory test is discretized and used as the input function in the numerical simulation program. Initial parameters are selected based on reasonable ranges from past experience. The numerical simulation program then uses a finite difference formulation with a selected interval (up to 250 points are used in the analysis presented). The numerical simulation with initial parameters generates a stress-volume (p-v space) response that is likely different from the laboratory test results as a first approximation. The laboratory results are then used as the target. The difference between the target and the numerical simulation in p-v space is minimized by iteration of the input parameters for the constitutive model. After minimization is completed within a pre-selected tolerance the parameters of the constitutive model are recorded. This process is repeated for a particular constitutive model using different stress paths available from experimental testing. If the PEM criteria are not satisfied then one can infer that the constitutive model being used is not able to represent the soil over the stress paths being examined. An alternate constitutive model can then be tested or modifications

to the existing constitutive model can be examined. This allows the evaluation of the PEM criteria for existing constitutive models to be used as a basis to give direction on what modifications can be made to specific constitutive models to better represent the behavior measured in the laboratory. When the PEM criteria are satisfied for a given model and set of stress paths, it indicates that the parameters of the constitutive models are stress path independent.
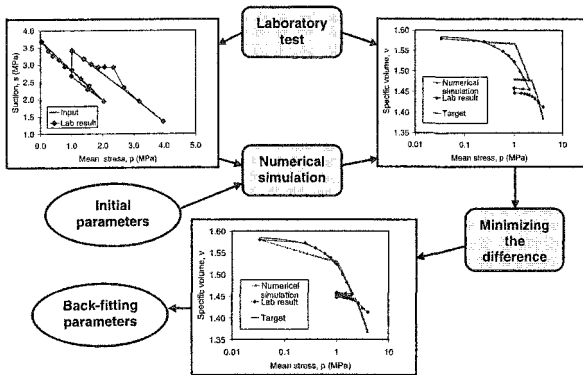
Figure 1. Fitting process used in the Parameter Evaluation Method (PEM)

Application of PEM for Two Mechanical Constitutive Models

Two mechanical constitutive models. In this study two constitutive models based on general critical state soil mechanics principles are used in the simulations. The Basic Barcelona Model (BBM) (Alonso et al. 1990) and Blatz and Graham Model (BGM) (Blatz and Graham 2003) are chosen for the following reasons. The BBM is the first critical state soil model for unsaturated clay and is widely accepted in the geotechnical community. The BGM model is based on the BBM model and was developed for the specific material used in the experimental work reported in this paper. The BGM model is also based on the original BBM model as the foundation for its development. Details of both constitutive models are described in the original publications.

Stress paths. Laboratory results used in this paper include results of triaxial tests with controlled and measured suctions (Blatz and Graham 2000 and Siemens and Blatz 2005). Figure 2 illustrates the stress path GS041 (Siemens and Blatz 2005) and JB104 (Blatz and Graham 2003). Both specimens consisted of a 50:50 mixture (by weight) of a well graded sand and bentonite. All specimens have an initial 'as-compacted' suction of approximately 3 to 4 MPa. Although specimen JB104 used Avonlea bentonite while the specimen GS041 used Wyoming bentonite, comparisons of both specimens selected are considered reasonable within experimental accuracy (Anderson et al. 2002, Priyanto et al. 2004).

Specimen GS041 (Siemens and Blatz 2005) was subjected to constant volume infiltration in the triaxial cell (Siemens and Blatz 2005). It follows stress path f-g in p-s space as indicated in Figure 2a. Specimen GS041 was initially loaded isotropically (q = 0) to 0.5 MPa. It was then given access to water (wetting) under controlled constant volume boundary conditions until equilibrium. The constant volume boundary condition was achieved by an automated cell pressure controller.

a.   b.
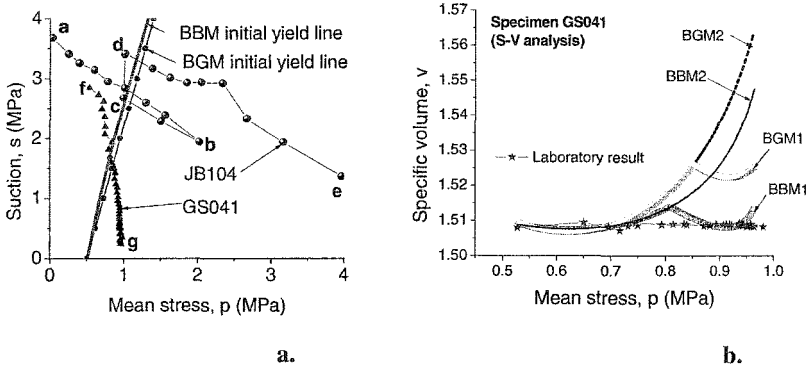
Figure 2. a. Laboratory stress paths of specimens JB104 and GS041 plotted in p-s space with the initial yield lines; b. Results of S-V analysis for specimen GS041 plotted in v-p space with the laboratory test results.

Specimen JB104 (Blatz and Graham 2003) (Figure 2a) follows stress path a-b-c-d-e in p-s space. This specimen was loaded isotropically (q = 0) along a-b until yielding was observed, indicating that the loading yield line had been reached (Figure 2a). Figure 2a shows that increasing mean stress is accompanied by a decrease in suction. The results are consistent with those reported by Tang et al. (2002). After yielding occurred, specimens were unloaded from b-c to achieve an overconsolidation ratio of approximately 2.0. The specimen was then dried while still under constant pressure in the triaxial cell to a target suction value. This produced increasing suction from c to d. Once suction equilibrium was achieved, the specimen was again isotropically loaded (d-e) to measure its compressibility and suction response to re-loading.

Stress to volume (S-V) analysis. The PEM algorithm uses the laboratory test as an input and target to obtain the best-fit parameters. The PEM is implemented using stress variables (suction, s or mean stress, p) as an input in the numerical simulation to calculate the resulting specific volume (v). This type of analysis is referred to as S-V analysis in this paper. Priyanto et al. (2004, 2005) used this form of analysis to simulate stress paths from triaxial testing with controlled and measured suction (Blatz and Graham 2000, Anderson et al. 2002, Siemens and Blatz 2005).

Priyanto et al. (2005) used the two stress paths including the one from specimen JB104 (Figure 2a) as an input in the simulations for both selected constitutive models (BBM and BGM). After application of the PEM algorithm in Figure 1, the best fitted parameters for the specimens are obtained. These parameters as well as all parameters used in this paper are tabulated in Table 1. The results of this analysis shows reasonable agreement with the laboratory test (Priyanto et al. 2005). The results also demonstrated that using both constitutive models with a similar set of stress paths, the parameters only varied slightly for suctions up to 10 MPa.

The same parameters determined by the PEM with the two constitutive models using specimen JB104 stress paths are applied in the numerical simulation of specimen GS041. This analysis is made to examine the dependence of the parameters of both constitutive models (BBM and BGM) on the predicted stress paths. The specific volume responses for both constitutive models are illustrated in Figure 2b as BBM1 and BGM1. The initial yield lines produced by the parameters BBM1 and BGM1 (Table 1) are plotted in Figure 2a. Based on the set of parameters, the stress path GS041 experiences yield such that a notable transition exists in the specific volume v for both constitutive models (BBM1 and BGM1) as illustrated in Figure 2b.

Table 1. Parameters used in the numerical simulation

BGM (Blatz and Graham 2003)				BBM (Alonso et al. 1990)			
Parameter	JB104 BGM1	BGM2 BGM3	BGM4	Parameter	JB104 BBM1	BBM2 BBM3	BBM4
λ	0.11	0.11	-	$\lambda(0)$	0.13	0.13	-
κ	0.021	0.021	0.010	κ	0.012	0.012	0.010
κ_s	0.067	0.067	0.052	κ_s	0.018	0.018	0.052
p_o (MPa)	0.50	1.00	-	p_o^*(MPa)	0.50	1.00	-
r	0.23	0.23	-	p^c (MPa)	0.014	0.014	-
				r	0.70	0.70	-
				β (MPa^{-1})	0.23	0.23	-
$\kappa_{rat} = \kappa/\kappa_s$	0.31	0.31	0.19		0.67	0.67	0.19

The laboratory test results in p-s space and p-v space (Figures 2a and 2b) for specimen GS041 do not indicate that yielding occurs for this specimen. This is likely due to the controlled boundary condition environment and the difference in the stress path. One could assume that the stress path of specimen GS041 is in the elastic range at all times along this stress path. The yield line can be shifted by setting the parameters p_o and p_o^* equal to one for BBM2 and BGM2 (Table 1), so that the specimen GS041 does not experience yield. The specific volume (v) in this case is illustrated in Figure 2b as BBM2 and BGM2. The comparison of the specific volume of all four cases (BBM1, BBM2, BGM1 and BGM2) is shown in Figure 2b and the laboratory results indicate that constant volume conditions cannot be obtained by either constitutive model.

Volume to Stress (V-S) Analysis. The second form of control with the analysis is to input the specific volume into the numerical simulation to calculate the stress path (termed V-S analysis in this paper). The analysis was conducted using the parameters previously discussed (BBM2 and BGM2 in Table 1) again assuming that yield does not occur for specimens GS041. The specific volume versus suction (v-s), which shows that specific volume v is controlled to be constant for the test duration, is used as an input in V-S analysis. The stress paths in p-s space generated in this V-S analysis for both constitutive models are illustrated in Figure 3 as BBM3 and BGM3. Both constitutive models highly overestimate the mean stress (p) compared with the laboratory results (Figure 3). Application of the algorithm in Figure 1 to reduce the difference of the laboratory results and the numerical simulations by iteration of the related parameters (κ and κ_s in Table 1) generates the parameters shown in Table 1 as BBM4 and BGM4. The stress paths generated from this analysis are illustrated in Figure 3 as BBM-BGM4. The results are the same for both constitutive models because the coefficients of compressibility (κ_s and κ) are constant in the elastic range for both constitutive models. Although, the BBM-BGM4 stress path (Figure 3) is close to the laboratory test results, the limitation of both constitutive models to capture the behavior of specimen GS041 is still indicated by the dependency of the parameters of both constitutive models on the stress path as noted in Table 1. For different stress paths, the parameters required to fit the model to the experiments are different. As an example, both coefficients of compressibility κ and κ_s for specimen GS041 are much greater than those for specimen JB104 (Table1). Secondly, the different shape of BBM-BGM4 compared with the laboratory results is illustrated in Figure 3.
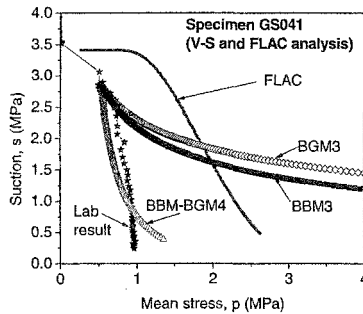
Figure 3. Stress paths calculated from the V-S analysis and stress path generated from FLAC.

Modification of both constitutive models (BBM and BGM) to capture this behavior can be made by introducing a parameter κ_{rat}. The value of κ_{rat} is introduced and shown in Table 1. It is the ratio of coefficient of compressibility for the change of mean stress to that of suction (κ/κ_s). The greater the value of κ_{rat}, the greater the swelling induced

pressure. This value is greater for stress paths involving wetting (BBM4 and BGM4) than for stress paths involving drying (specimen JB104). The value of κ_{rat} can be used as an additional parameter to modify both constitutive models to be able to more accurately capture the behavior of specimen GS041. Further investigation of the rationale for this parameter is required. The following section will demonstrate that the introduction of the hydraulic constitutive model can aid in addressing the lack of fit for the swelling induced pressures.

Modeling the Constant Volume Infiltration Triaxial Test

Finite difference analysis using FLAC-2D (Itasca, 2001) has been used to model the constant volume infiltration tests discussed in the previous sections. Two-phase flow and fluid-mechanical interaction is utilized in the analysis to incorporate the soil water characteristic curve (SWCC) and permeability function. The SWCC and permeability function is defined using the van Genuchten (1980) model, with parameters a = 0.20, b=0.50, c=0.50, P_o = 2.0 x 10^6 Pa, and residual saturation S_r = 0.01. These parameters are obtained from best-fitting laboratory results from Blatz (2000). The saturated hydraulic conductivity k_h = 5 x 10^{-12} m/s (Graham et al. 1997), that has been used by Thomas et al. (2003) to model the buffer material. The mechanical behavior is described by means of a linear-elastic constitutive model with bulk modulus (K) of 42 MPa and shear modulus (G) of 34 MPa used by Chandler (2000) for the same material. The input and output are shown in Figure 4.
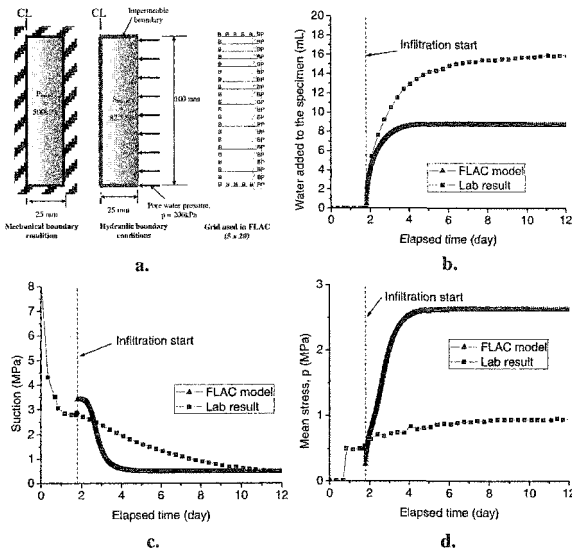
Figure 4. a. Mechanical and hydraulic initial and boundary conditions b. water added to specimen, c. suction, and d. mean stress vs. time.

The mechanical and hydraulic boundaries, initial condition and the grid used in the FLAC analysis are illustrated in Figure 4a. The model used is axisymmetric with 5x20 elements (Figure 4a). The initial means stress of 500 kPa and degree of saturation of 82.5% are applied as initial conditions (Figure 4a). The porosity n of 0.38 is assumed as a constant in the FLAC analysis (Itasca 2001); it is taken from the laboratory measurement (Siemens and Blatz 2005). Fixed displacement boundaries in the x and y directions are applied along the boundaries (Figure 4a). Once the model is started, the pore water pressure of 200 kPa is applied along the perimeter boundary, while impermeable boundary conditions are applied at the top, bottom, and the center line (Figure 4a).

Figures 4b, 4c, and 4d illustrate the time history response of FLAC compared with the laboratory test results. Figure 4b shows that the FLAC analysis underestimates the volume of water added to the specimen but it overestimates the mean stress as shown in Figure 4d. The FLAC analysis underestimates the laboratory results after 3 days as illustrated in Figure 4c. Figures 4b to 4d indicate that FLAC analysis in this paper reaches equilibrium in day 4, which is much faster than that of the laboratory test which tool 12 days. Improvement in the approximation of parameters is required for this analysis. Development of porosity and permeability functions depending on the stress level is expected to improve these results of this analysis. In the modeling presented the porosity and permeability are independent of stress level. The estimation of these relationships as well as the improvement of the parameter approximation for this analysis is a topic currently being investigated.

Although a simple linear-elastic model is used in this analysis, the FLAC results in p-s space (Figure 3) indicate the improvement in the shape compared to the laboratory test results. Compared with previous analyses (BBM1-4, BGM1-4 in Figures 2 and 3) that consider the mechanical constitutive model independently, the FLAC analysis (Figure 3) indicates considerable improvement in magnitude and shape. This demonstrates that the hydraulic constitutive models (SWCC and permeability laws) are very important for determining the behavior of specimen GS041.

Conclusions

Application of the PEM algorithm for two mechanical constitutive models (Alonso et al. 1990, Blatz and Graham 2003) for constant volume infiltration triaxial stress paths (specimen GS041) indicates the limitation of both models for this particular stress path for this material. The recommendation to introduce the parameter κ_{rat} ($= \kappa/\kappa_s$) may improve the ability of both constitutive models to capture the measured behavior. The hydraulic constitutive models (SWCC and permeability laws) play important roles in modeling this stress path. Future applications of the combination of the triaxial test with controlled and measured suction (Blatz and Graham 2000, Siemens and Blatz 2005) and the PEM algorithm (Priyanto et al. 2004) can reduce the necessity of independent permeability testing to characterize unsaturated clay soil subjected to wetting conditions.

Acknowledgements

References

Alonso, E.E., Gens, A., and Josa, A. (1990) "A constitutive model for partially saturated soils." *Géotechnique*, 40(3): 405-430.

Alonso, E.E., Vaunat, J., and Gens, A. (1999) "Modelling the mechanical behaviour of expansive clays." *Engineering Geology* 54: 173-183.

Anderson, D, Blatz, J., Graham, J., and Chandler, N. (2002). "Yielding behaviour of unsaturated and compacted bentonite." *Proceedings of the 55th Canadian Geotechnical and 3rd Joint IAH-CNC and CGS Groundwater Specialty Conferences*, Niagara Falls, Ontario, October 20-23, 2002, Vol. 2, pp.1255-1260.

Blatz, J.A. (2000) *Elastic-plastic modelling of unsaturated high-plastic clay using results from a new triaxial test with controlled suction.* Ph.D Thesis, Department of Civil Engineering, University of Manitoba, Winnipeg, MB, Canada.

Blatz, J.A. and Graham, J. (2000) "A system for controlled suction in triaxial tests." *Géotechnique*, 50(4): 465-478.

Blatz, J.A., and Graham, J. (2003) "Elastic plastic modelling of unsaturated high-plastic clay using results from a new triaxial test with controlled suction." *Géotechnique* 53(1): 113-122.

Chandler, N.A. (2000) *Water Inflow Calculations for the Isothermal Buffer-Rock-Concrete Plug Interaction Test. Atomic Energy of Canada Ltd.* Report No: 06819-REP-01200-10046-R0.

Cross, H. (1949). "Analysis of Continuous Frames by Distributing Fixed-End Moments." *In Numerical Methods of Analysis in Engineering.* Successive Corrections. L B. Grinter, ed. New York.

Fredlund, D.G and Rahardjo, H. (1993) *Soil mechanics for unsaturated soils.* New York: John Wiley and Sons.

Graham, J., Chandler, N. A., Dixon, D. A., Roach, P.J., To, T. & Wan, A. W. L. (1997). *The Buffer/Container Experiment: Results, synthesis, issue.* Report AECL-11746, COG-97-46-I. Atomic Energy Canada Limited, Ontario.

Itasca Consulting Group, Inc. (2001) *FLAC Fast Lagrangian Analysis of Continua, Fluid-Mechanical Interaction.* Itasca Consulting Group, Inc. Minneapolis, Minnesota.

Lade, P. V. (2005). Overview of constitutive models for soils. Keynote lecture at the G-I Geo-Frontiers 2005 conference in Hilton Austin Convention Center, Austin, Texas, January 23-27, 2005.

Priyanto, D. G., Blatz, J.A., Siemens, G. A., and Graham, J. (2004). "The parameter evaluation method (PEM) of elastic-plastic model properties for unsaturated high-plastic clay." *The 57th Annual Canadian Geotechnical Conference,* Quebec City, October 24-27, 2004.

Priyanto, D. G., Blatz, J.A., and Siemens, G. A. (2005). "Comparison of two constitutive models to simulate the behaviour of unsaturated swelling clay." *The 58th Annual Canadian Geotechnical Conference,* Saskatoon, Saskatchewan, September 18-21, 2005.

Roscoe, K. H., and Burland,J.B. (1968) "On the generalized stress-strain behaviour of 'wet' clay." *Engineering Plasticity, J.* Heyman and F. Leckie (eds.). Cambridge University Press, Cambridge, : 535-609.

Siemens, G.A. and J.A. Blatz. (2005). "A triaxial apparatus for applying liquid infiltration under controlled boundary conditions with internal suction measurement." *Manuscript in preparation to be submitted to ASCE Journal of Geotechnical and Geoenvironmental Engineering, August 2005.*

Tang, G.X, Graham, J., Blatz, J., Gray, M., and Rajapakse, R.K.N.D. (2002). "Suctions, stresses and strengths in unsaturated sand-bentonite." *Engineering Geology,* Vol. 64, pp.147-156.

Terzaghi, K. (1936) "The shear resistance of saturated soils," in Proc. 1st Int. Conf. Soil Mech. Found. Eng. (Cambridge, MA), vol. 1, pp. 54-56.

Thomas, H. R., Cleall, P.J., Chandler, N., Dixon, D., & Mitchell, H. P. (2003). "Water infiltration into a large-scale in-situ experiment in an underground research laboratory." *Geotechnique* 53, No. 2, 207-224.

van Genuchten, M. Th. (1980). "A Closed Form Equation for Predicting the Hydraulic Conductivity of Unsaturated Soils." *Soil Sc. Soc. Am. J.,* Vol. 44, pp.892-898.

Soil-water Characteristic Curve of Remolded Expansive Soils

Linchang Miao[1], Fei Jing[2] and Sandra L. Houston[3]

[1] Institute of Geotechnical Engineering, Southeast University, Nanjing, 210096, China, PH (86) 25 83795836, FAX (86) 25 83795836, email: Lc.miao@seu.edu.cn

[2] Institute of Geotechnical Engineering, Southeast University, Nanjing, 210096, China, PH (86) 25 83795029, FAX (86) 25 83795836, email: jingfei9212@sohu.com

[3] Department of Civil & Environmental Engineering, Arizona State University, AZ 58287, USA, PH (480) 965 3589, FAX (480) 965 0557, email: Sandra.Houston@asu.edu

Abstract

The state behavior of unsaturated soils is controlled in part by the soil-water characteristic curve (SWCC) and unsaturated permeability. Both these soil properties are dependent on pore geometry. The SWCC exhibits hysteresis, so the wetting and drying curves of the SWCC are different. In this paper, SWCCs of remolded Guangxi and Hefei expansive soils of varying dry densities have been measured and studied. The research shows that the shape of SWCC depends on the dry density of soil samples. The slope of soil-water characteristic curves between the air entry value point and residual water content point will be steeper when the dry density increases. The slope of the soil-water characteristic curve fluctuates for low dry density soil samples and it is stable for higher dry density soil samples. The air entry value of the soil-water characteristic curve increases with the dry density, but the variation of the residual water content is small over the dry density range considered. The SWCC characteristics are correlated to the pore structure. The authors present the volumetric water content (which is defined as the ratio of the volume of water in sample to the total volume of sample) in the sample as a parameter, normalizing a single variable

for plotting the soil-water characteristic curves of expansive soil. The volumetric water content can embody the effect of water content, degree of saturation and void ratio of sample.

Introduction

Determination of unsaturated soil parameters using experimental procedures is time consuming and difficult. In recent years, the soil–water characteristic curve (SWCC) has become an important tool in the interpretation of the engineering behavior of unsaturated soils. The indirect determination of these parameters may be justified not only by the difficulties involved in such tests but also by the costs associated with determinations of these parameters (e.g., Fredlund 1998). The proliferation of SWCC use for indirect determination of unsaturated soil properties is natural and in some cases desirable for implementation of unsaturated soil theory. The volume change with increased suction will depend on the initial void ratio and/or the stress history and wetting or drying states. The shape of the SWCC reflects the influence of stress history on the soil as well as soil plasticity (Miao et al. 2002; Marinho, 2005). The shape of the SWCC depends on the pore size distribution and compressibility of the soil in relation to suction. Thus, the characteristics of porous materials, including SWCC, are affected by the initial water content, soil structure, mineralogy, and the stress history (e.g., Lapierre et al. 1990; Vanapalli et al. 1999). Most SWCCs are S shaped and the curve shapes are primarily affected by the pore size distribution of the material. Though models used for predicting unsaturated soil parameters of SWCC should consider the influence of all factors. For practical engineering, there seems to be difficulties to take into account the multi-factors, so the emphasis is a gradation.

For determination of hydraulic conductivity, the SWCC may be measured in the laboratory, from which a pore-size distribution (PSD) is inferred and used, together with measured saturated conductivity, to derive the corresponding unsaturated hydraulic conductivity function. Two assumptions are used: (a) The PSD is constant during the SWCC tests. (b) Pore geometry is characterized as a series of capillary tubes (Marinho, 2005). It has been previously shown that the effective PSD changes significantly during drying. Many researchers have shown that the SWCC is strongly influenced by pore connectivity. Therefore neither the SWCC nor the hydraulic conductivity function is a unique function of PSD. Clay soils typically have non-uniform grain size and pore size distributions (e.g., Delage and Lefebvre 1984). As a consequence, linear and less steeply sloping SWCCs (using a semilog plot) are normally obtained for clays. Clays may experience shrinkage that reduces pore size. Fine-grained soils with a liquid limit greater than 25% typically exhibit significant shrinkage characteristics when dried. Shrinkage phenomena in clays due to increased

suction can play an important role in shaping the SWCC. During shrinkage the emptying of pores is accompanied by reduction in pore size, which keeps the spaces filled with water and increases the air entry value.

In this paper, SWCCs of remolded Guangxi and Hefei expansive soils of varying dry densities have been measured and studied. Taking into account the influence factors of the pore structure, pore size and pore connectivity, the authors present the volumetric water content in the sample as normalizing parameter, which can serve to unify the soil-water characteristic curves of expansive soils for different densities. The volumetric water content can embody the effect of water content, degree of saturation and void ratio of the sample.

Soil-water Characteristic Curve Measurements

In this study, soil-water characteristic curves of Guangxi and Hefei expansive soils are measured using a pressure plate made by Soilmiosture Equipment Corporation of Canada. The specimens were prepared by the static compaction. The physical properties of Guangxi and Hefei expansive soils are summarized in Tables 1 and 2, respectively. The soil mineralogy, which was assessed by X-ray diffraction, is summarized in Tables 3 and 4, respectively. For specimen preparation, the expansive soils were crushed to pass the 2 mm sieve, were dried at 108°C for 8 hr. in an oven, mixed with appropriate amount of distilled water in a glass-jar mixer, and allowed to equilibrate in an air-tight plastic bag at constant room temperature (20±0.5°C) for 24hr. The samples are compacted by static compaction in steel rings to achieve a particular dry density. The compacted samples were saturated with assistance of vacuum to facilitate introduction of water into the pores. The samples were prepared at three dry densities, $1.42g/cm^3$, $1.48g/cm^3$ and $1.54g/cm^3$.

Table 1 Physical properties of Guangxi expansive soils

G_s	W_L (%)	W_P (%)	I_p	Free sweling (%)	Gradation (%)		
					>0.05mm	0.05~0.005mm	<0.005mm
2.70	61.4	30.3	31.1	45.0	10.6	39.5	49.9

Table 2 Physical properties of Hefei expansive soils

G_s	W_L (%)	W_P (%)	I_p (%)	Free sweling (%)	Gradation (%)		
					>0.05mm	0.05~0.005mm	<0.005mm
2.72	58.6	26.4	32.2	57.5	3.8	46.6	49.6

Table 3 Mineral composition of Guangxi expansive soils

Smectite	Illite	Quartz	Feldspar	Other
8~10%	15-25%	20-30%	5~10%	15-20%

Table 4 Mineral composition of Hefei expansive soils

Smectite	Illite	Quartz	Feldspar	Other
13~18%	15-25%	25-35%	5~15%	5-10%

The SWCCs for Guangxi and Hefei expansive soils are shown in Figures 1 and 2. The air entry value of the soil–water characteristic curve increases as dry density of the soil sample increases. The residual water content point is essentially stable for different dry density samples. The key values of the SWCC are summarized in Table 5. When pore air pressure is larger than the air entry value, the matric suction will nearly linearly increase as water content decreases. The slope of the soil-water characteristic curves between the air entry value point and residual water content point will be steeper in slope as the dry density increases. The slope of soil-water characteristic curve varies for low dry density soil samples. The SWCC behaviors are related to the pore structure, pore size and pore connectivity.

Table 5 The key values of SWCCs of Guangxi and Hefei expansive soil

Dry density, g/cm^3		1.42	1.48	1.54
Guangxi expansive soil	Air entry value (kPa)	10.0	33.0	45.0
	Residual water content (%)	6.35	6.66	6.92
Hefei expansive soil	Air enter value (kPa)	21.0	82.0	98.0
	Residual water content (%)	8.24	8.64	9.02
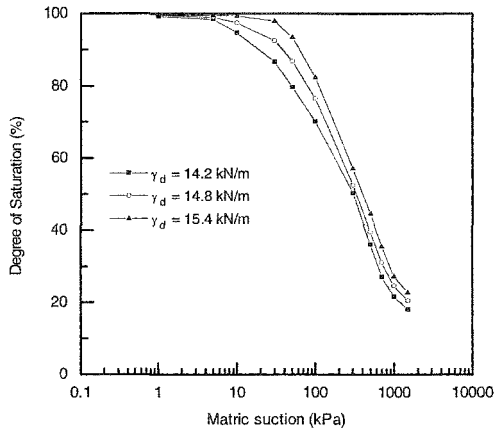
Fig. 1 Soil-water characteristic curves for various dry densities of Guangxi expansive soils (drying curves).
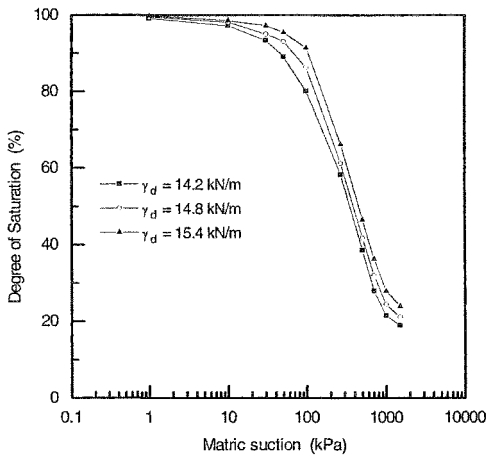
Fig. 2 Soil-water characteristic curves for various dry densities of Hefei expansive soils (drying curves)

Discussion

Soil-water characteristic curves have been measured on remolded samples of Guangxi and Hefei expansive soils. The investigations demonstrate that the shapes of soil-water characteristic curves of expansive soils are correlated to dry density, void ratio and pore structure. The shapes of SWCCs are related to the volumetric water content in the soil sample. It is apparent that the air–void ratio has a definite influence on expansive soils. It is suggested that the air–water distribution state of expansive soils be taken into account and that it is useful for the SWCCs to be presented in terms of volumetric water content. The volumetric water content can embody the effect of water content, degree of saturation and void ratio of sample bringing together the different density SWCCs. Figures 3 and 4 are the matric suction–volumetric water content curves of Guangxi and Hefei expansive soils, respectively, showing the normalizing effect of volumetric water content. A mathematical fitting formula can be used to denote the influence of dry density, pore size and pore structure on the shape of soil-water characteristic curve. The relationship between the matric suction and the volumetric water content of Guangxi and Hefei expansive soil can be expressed as follows:

$$u_s = 7588.4e^{-0.1534\theta}, R^2 = 0.868 \quad \text{(Guangxi expansive soils)} \qquad (1)$$

$$u_s = 6558.3e^{-0.1387\theta}, R^2 = 0.799 \quad \text{(Hefei expansive soils)} \qquad (2)$$

where u_s is the matric suction of the expansive soil, θ is the volumetric water content of the expansive soil.
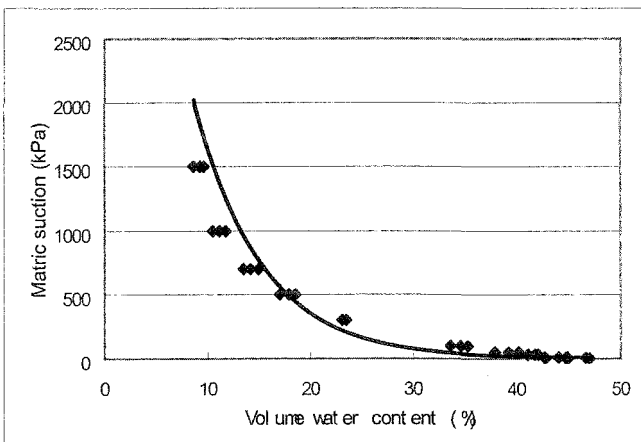
Fig. 3   Matric suction-volumetric water content of Guangxi expansive soil.
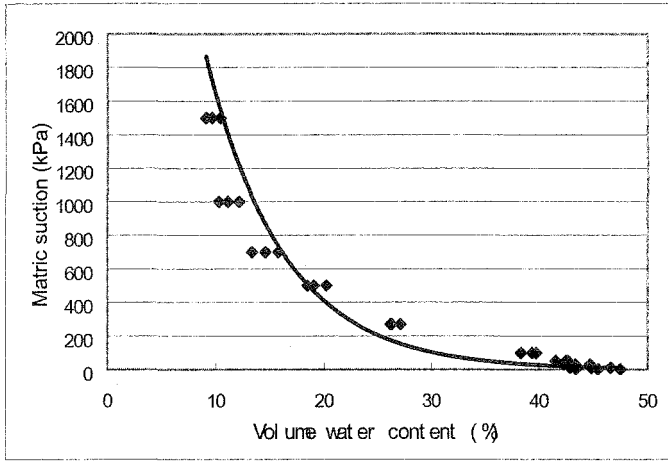
Fig. 4 Matric suction-volumetric water content of Hefei expansive soil.

Conclusion

In this paper, the soil-water characteristic curves of remolded Guangxi and Hefei expansive soils of varying dry densities have been investigated. The studies show that the shapes of soil-water characteristic curves are correlated to dry density, pore size and pore structure. The authors suggest using the volumetric water content of the sample for presenting the SWCC to denote the effect of dry density, pore size and pore structure. The volumetric water content embodies the effect of water content, degree of saturation and void ratio of expansive soil sample resulting in normalization the SWCC. A mathematical fitting formula for the SWCC can be used to denote the effect of dry density, pore size and pore structure to compute the relationship between matric suction and volumetric water content.

Acknowledgments

References

Delage, P., and Lefebvre, G. (1984). Study of the structure of a sensitive Champlain clay and of its evolution during consolidation. Can. Geotech. J., 21, 21–35.

Fredlund, M. D. (1998). Unsaturated seepage modeling made easy. Geotech. News, June, 52–59.

Lapierre, C., Leroueil, S., and Locat, J. (1990). Mercury intrusion and permeability of Louiseville clay. Can. Geotech. J., 27, 761–773.

Miao, L.C., Liu, S.Y. and Lai, Y. M. (2002). Research of soil-water characteristics and shear strength features of Nanyang expansive soil, Engineering Geology, 2002(65), No.4, pp261-267.

Marinho, F. A. M. (2005). Nature of soil-water characteristic curve for plastic soils. J. Geotech. Geoenviron. Eng., 131(5), 654–661.

Vanapalli, S. K., Fredlund, D. G., and Pufahl, D. E. (1999). The influence of soil structure and stress history on the soil-water characteristics of a compacted till. Geotechnique, 49(2), 143–159.

Behavior of bentonite-sand mixtures subjected to cyclic drying and wetting paths

E. Romero[1], E.E. Alonso[1] and C. Hoffmann[2,1]

[1]Department of Geotechnical Engineering and Geosciences, Universitat Politècnica de Catalunya, c/Jordi Girona 1-3, Building D2, 08034 Barcelona, Spain; PH +34 934016888; FAX +34 934017251; email: enrique.romero-morales@upc.edu, eduardo.alonso@upc.edu. The first author formerly PhD student at Universitat Politècnica de Catalunya.
[2]Dipartimento di Ingegneria Meccanica e Strutturale, Università degli Studi di Trento, Via Mesiano 77, 38050 Trento-Povo, Italy; PH +39 0461 882551; FAX +39 0461 882599; e-mail: christian.hoffmann@ing.unitn.it

Abstract

Soils are naturally subjected to cyclic and strong drying and wetting paths due to atmospheric conditions. Clayey soils subjected to these processes develop swelling and shrinkage deformations, which give rise to the accumulation of expansion or compression strains during suction cycles. In order to study the main features of these processes, a systematic experimental programme was performed on an artificially prepared bentonite-sand mixture using an oedometer cell. Several controlled-suction wetting-drying cycles with suction ranging between 130 MPa and 4 MPa were applied using vapour equilibrium technique. Tests were performed at different vertical net stresses. Along the successive cycles, the tested samples showed cumulative shrinkage strains at increasing vertical net stresses. Test results were interpreted and simulated using the suction-dependent elastoplastic model proposed by Alonso et al. (1999).

Introduction

Soils are commonly subjected to strong drying and wetting cycles due to natural environmental fluctuations. Clayey soils undergo swelling during water uptake and experience shrinkage on water removal, which give rise to the accumulation of irreversible compression or expansion strains during suction cycles.

Several studies were undertaken in the past; however, few of them have been reported in the literature using controlled-suction techniques by vapour transfer. Vapour migration plays a major role in liners or engineered barriers, in which thermal

gradients are expected to occur. Experimental results describing the volume change response of expansive soils exposed to cyclic wetting and drying have been reported by Dif and Bluemel (1991) and Al-Homoud et al. (1995), who detected 'fatigue' of swelling (shrinkage accumulation) that increases at higher vertical stresses. This behaviour was explained in terms of a continuous rearrangement of soil particles, leading to a less active microstructure. On the contrary, Pousada (1984) observed that the amount of swelling increased with the number of cycles. Day (1994) and Basma et al. (1996) reported cumulative shrinkage or swelling, depending on the suction reached during the drying paths.

A systematic laboratory test program was performed on a compacted Ca-bentonite - sand mixture to study these cyclic processes and to identify the relevant features characterizing soil behaviour. Results were interpreted and simulated within the context of the elastoplastic model proposed by Alonso et al. (1999).

Experimental Program

Tested material
        Tests were performed on statically compacted bentonite-sand mixture. Ca-bentonite was mixed with silica sand to achieve a dry mass ratio of 80% bentonite and 20% sand. The bentonite has a liquid limit $w_L = 93\%$, a plastic limit $w_P = 47\%$, a density of solid particles of 2.7 Mg/m^3, and 45% of particles less than 2 μm. The sand presents a uniformity coefficient $C_u = 2$ and an effective size $D_{10} = 0.21$ mm. This material was selected due to the following favourable properties: significant swelling-shrinkage potential and acceptable water permeability, which allowed the equalisation time to be kept within reasonable bounds.

The mixture was allowed to equilibrate at an average relative humidity of 55% (suction of $s = 80$ MPa). Soil specimens were then statically compacted at constant water content $w = 10.5\%$ to a target dry density of 1.5 Mg/m^3. The initial degree of saturation was 35%. Further details of the mixture are presented in Alonso et al. (2005).

Experimental technique and equipment
        Suction was applied by controlling the relative humidity of a closed system in contact with the soil. In order to speed up the process, a forced convection system with an air pump was used to transfer the vapour. The relative humidity of the system was controlled by varying the chemical potential of two types of aqueous solutions. $CuSO_4$ was used under saturated conditions of dissolution, which allowed attaining suctions between 4 and 6 MPa. This solution was used during the wetting paths. H_2SO_4 solutions were used in the drying paths, achieving a target relative humidity of 40% ($s = 130$ MPa).

The tests were performed under oedometer conditions. Each wetting or drying step was maintained for more than 10 days until the rate of straining had reduced to an

axial strain rate of 0.1%/day. Alonso et al. (2005) presented a detailed description of the experimental techniques and equipment used.

Stress paths followed

The different stress paths followed are shown in Figure 1, where tests are indicated in the vertical net stress (σ_v): suction (s) plane. A swelling pressure test starting from the as-compacted state and a loading-unloading cycle at constant $s = 80$ MPa were initially performed. Based on these preliminary results, the position of the loading-collapse LC yield surface for the as-compacted state was determined. This LC yield locus, which is shown in Figure 1, represents the increase of the preconsolidation stress with suction (Alonso et al. 1990).

The drying-wetting paths at constant vertical stress were selected taking into account the position mapped for the LC curve. Applied σ_v were lower than the yield stress for saturated conditions σ_{vo}^*. The reason for this selection was to investigate the behaviour of the soil in the 'swelling region' at elevated overconsolidation ratios and far from the collapse mechanism described by the LC curve. Three cyclic drying-wetting tests were performed at $\sigma_v = 100$, 200 and 400 kPa. Alonso et al. (2005) presented a detailed description of all the tests performed.
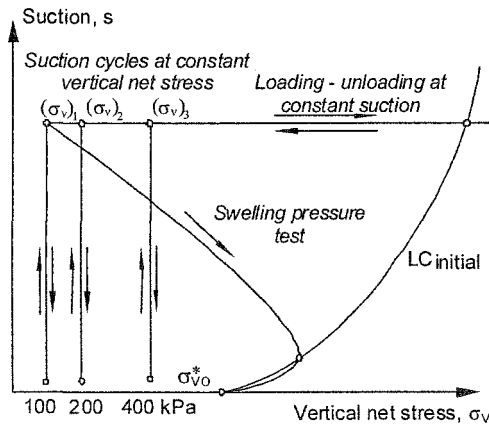
Figure 1: Stress paths followed. LC yield locus for the as-compacted state.

Test Results

Figure 2a shows the loading-unloading path at $s = 80$ MPa. Clear pre and post-yield responses are identified, showing a preconsolidation stress on the LC curve of the as-compacted state at $\sigma_v = 5$ MPa. Figure 2b presents the time evolution of vertical net stress and degree of saturation on wetting of the path for the swelling

pressure test. Different patterns of behaviour are observed in this path. The swelling pressure increases in the early transient stage to compensate for the swelling strain caused by wetting, but eventually the sample yields (activation of the LC curve at $\sigma_v^* = 1.05$ MPa –point A in Figure 2b). From this point on, the collapse tendency is compensated for by the vertical stress reduction to maintain the constant volume condition (the path follows approximately the LC yield locus towards the saturated vertical preconsolidation stress $\sigma_{vo}^* = 0.65$ MPa -point B in Figure 2b). The yield point A is reached at an approximate degree of saturation of 70% (Figure 2b), which corresponds to a suction $s = 10$ MPa that was measured on a duplicate sample by psychrometric technique. Based on this information, the LC yield locus is qualitatively depicted in Figure 1.
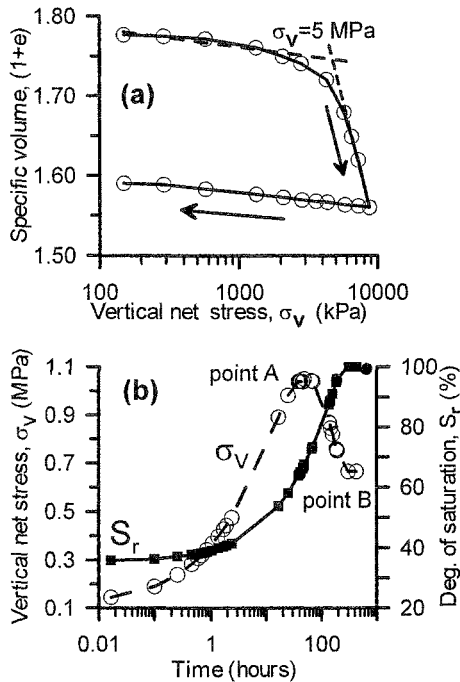
Figure 2: (a) Loading-unloading test at $s = 80$ MPa on the as-compacted sample. (b) Swelling pressure test.

The variation of volumetric strain ε_v (+ in compression) with cycles of suction at different vertical stresses is shown in Figure 3. The first wetting path results in all cases in sample expansion. However, as the subsequent drying-wetting cycles are applied there is a net accumulation of sample compression, which is clearly observed at intermediate and high stresses. As the number of cycles increases the difference

between two successive wetting-drying paths becomes smaller. Clearly, the soil tends towards an 'elastic' (reversible) state. This trend is better appreciated when the volumetric strains are plotted with the evolution of cycles, which is shown in Figure 4 for the test series with $\sigma_v = 200$ kPa. The difference –a net compression- tends to zero with increasing number of cycles. This limiting value of volumetric strains, which is not strictly reached for the number of cycles applied in these experiments, marks a stable elastic state that may be approximately taken as the state for the last suction change applied.
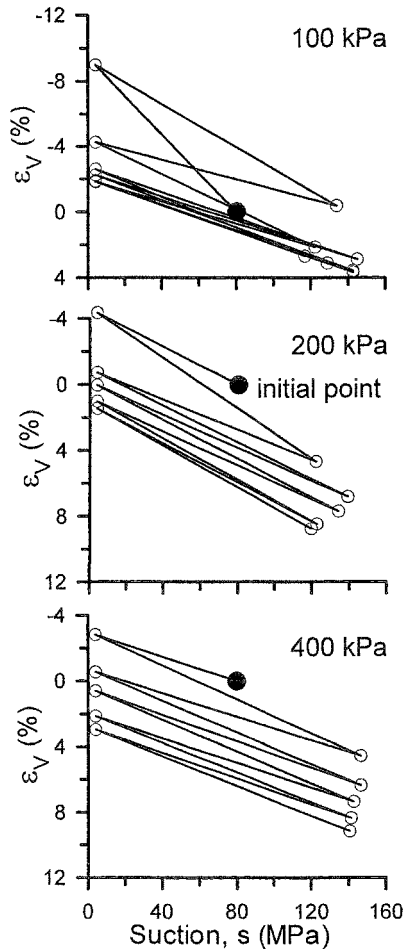
Figure 3: Volumetric strains in cyclic controlled-suction paths at constant vertical stress.
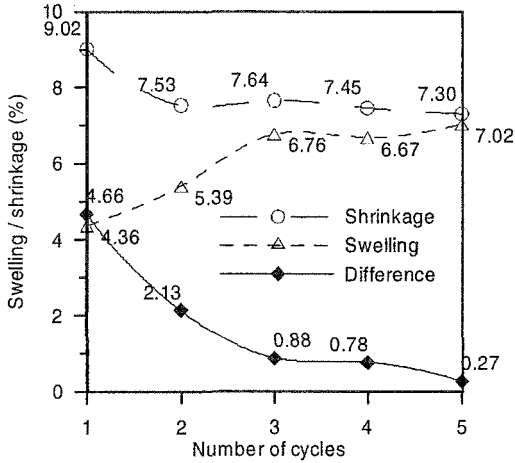
Figure 4: Evolution of swelling and shrinkage with the number of controlled-suction cycles for $\sigma_v = 200$ kPa.

The results presented and their interpretations given above provide data to investigate the capability of the theoretical framework, described in the next section, to model the soil behaviour against suction cycles.

Modelling Test Results

Description of the model

Using concepts of hardening plasticity a double-porosity model was proposed by Alonso et al. (1999) to simulate expansive soil behaviour. The model considers two structural levels and a coupling between them. The microstructural level - associated with the response of the bentonite fabric- is considered to be appropriately described by an elastic model. The macrostructural level -associated with the skeleton and responsible for major structural rearrangements- is described by the Barcelona Basic Model BBM for unsaturated soils (Alonso et al. 1990). Coupling between micro and macrostructure results in the build-up of macrostructural irreversible strains when microstructural reversible strains develop. Further details are described in Alonso et al. (2005).

a) Microstructural level

As previously indicated, bentonite fabric is assumed to react in a pure volumetric and elastic way against changes in stress and suction. The microstructural volumetric strain is expressed by

$$d\varepsilon^e_{vm} = \frac{d\hat{p}}{K_m} \tag{1}$$

where K_m is a rigidity coefficient and $\hat{p}$ is a microstructural effective stress, defined as

$$\hat{p} = p + S_{r\,mic}^{\alpha}\, s \tag{2}$$

where p is the mean net stress, s is the suction, $S_{r\,mic}$ is the degree of saturation at the microstructural level (which depends on s), and α is a model parameter.

The coefficient K_m is not constant. It depends on the confining stress. A suitable expression can be derived from the widely used logarithmic law of void ratio reduction for increasing stress

$$K_m = \frac{(1+e_m)\hat{p}}{\kappa_m} \tag{3}$$

where κ_m is the compressibility index and e_m is the void ratio of the microstructure.

b) Macrostructural level

Macrostructural volumetric elastic strain is given by

$$d\varepsilon^e_{VM} = \frac{dp}{K_p} + \frac{ds}{K_s} \tag{4}$$

where

$$K_p = \frac{(1+e_M)p}{\kappa} \; ; \; K_s = \frac{(1+e_M)(s+p_{atm})}{\kappa_s} \tag{5}$$

and e_M, κ, κ_s are (macro) void ratio and compressibility indexes for mean net stress and suction changes, respectively.

The variation of preconsolidation stress with suction is given by the LC yield surface (Figure 5)

$$p_0 = p_c \left(\frac{p_o^*}{p_c} \right)^{\frac{\lambda(0)-\kappa}{\lambda(s)-\kappa}} \; ; \; \lambda(s) = \lambda(0)\left[r + (1-r)e^{-\beta s} \right] \tag{6}$$

where p_o^* is the saturated preconsolidation stress, p_c is a reference stress, $\lambda(0)$ is the slope of the saturated virgin compression line and (r, β) are model parameters.

The model describes the plastic straining by means of two additional yield curves –SI and SD associated with suction increase and suction decrease, respectively (Figure 5). These yield curves are defined by the expressions $\hat{p} - s_I = 0$ for the SI yield curve

and $\hat{p} - s_D = 0$ for the SD yield curve; s_I, s_D being the hardening parameters. When SI and SD yield curves are activated, plastic strains are induced, which are given by the following expressions

$$d\varepsilon_{vM}^p = f_I \, d\varepsilon_{vm}^e \; ; \; d\varepsilon_{vM}^p = f_D \, d\varepsilon_{vm}^e \tag{7}$$

where f_I and f_D are micro-macrostructural interaction functions that are made dependent on p/p_0, p_0 being the current preconsolidation stress at the current value of suction, as given by the LC yield curve.

SI and SD hardening is governed by $d\alpha_1 = d\varepsilon_{vSI}^p + d\varepsilon_{vSD}^p$, where ε_{vSI}^p and ε_{vSD}^p are the volumetric plastic strains due to the activation of SI and SD, respectively (plastic strains are given by Equation (7)). LC hardening is assumed to depend on $d\alpha_2 = d\varepsilon_{vSI}^p + d\varepsilon_{vSD}^p + d\varepsilon_{vLC}^p$, where ε_{vLC}^p is the volumetric plastic strain due to the activation of LC (Alonso et al. 1990). Hardening laws are defined as follows

$$ds_I = \frac{K_m d\alpha_1}{f} = ds_D \; ; \; \frac{dp_0^*}{p_0^*} = \frac{(1+e_M)d\alpha_2}{\lambda(0) - \kappa} \tag{8}$$

The function f corresponds to the micro-macrostructural interaction function in use, either f_I or f_D depending on whether yielding is occurring on the SI or SD curve.

Figure 5 shows the different yield surfaces (LC, SI and SD) used by the model.
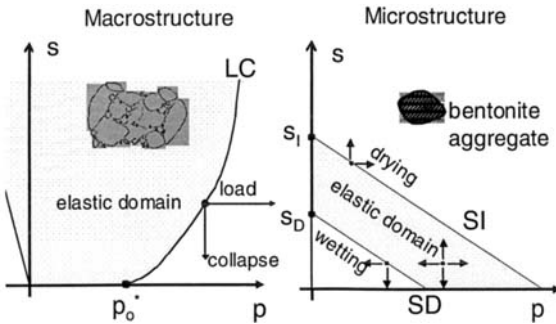
Figure 5: Yield surfaces LC, SI and SD.

Determination of parameters

Since the model is formulated in differential terms, the stress paths followed should ideally be performed in small increments. However, in view of the long time required to equalise, the suggested procedure would be unpractical. On the other hand, the large suction changes make it difficult to apply in a direct manner the constitutive relations presented before. In order to derive model parameters in a

systematic way some hypotheses and simplifications were assumed, even if some model capabilities were reduced:

- Since horizontal stresses were not measured, the mean net stress p in the model was replaced by the vertical net stress σ_v. Such a replacement introduces an error – p varies along the stress paths due to the variation of the horizontal stress, whereas σ_v is kept constant.
- Microstructural strains are governed by changes in effective stress. This assumption means setting $\alpha = 0$ in Equation (2), which eliminates the need to introduce the microstructural water retention curve.
- Suction induced elastic strains are considered only as microstructural deformations ($K_s \rightarrow \infty$ in Equation (4)).
- SI and SD yield surfaces are always activated as suction changes during the application of drying-wetting cycles –the elastic region bounded by SI and SD is assumed to be negligible $s_D = s_I$ in Figure 5.

The determination of the micro-macrostructural interaction functions (Equation (7)) is done following this procedure:
- The microstructural elastic parameter κ_m was first derived from the final (quasi-reversible) suction cycle applied, assuming that irreversible swelling and shrinkage strains were negligible.
- Plastic strains were then computed for each suction cycle by subtracting elastic strains from total strains.
- Values of σ_v / σ_{vo}^* were derived for each cycle, where σ_{vo}^* was initially taken from the swelling pressure test. Subsequent changes in σ_{vo}^* were determined from Equation (8).
- The ratio of the increments of strains $\varepsilon_{vM}^p / \varepsilon_{vm}^e$ was plotted for the different σ_v / σ_{vo}^* attained during the suction cycles. The experimental micro-macrostructural interaction functions were derived by fitting these values to the following sigmoidal functions

$$f_I = \frac{f_{I1} - f_{I2}}{\pi} \tan^{-1}\left[K_I\left(\frac{\sigma_v}{\sigma_{vo}^*} - X_I\right)\right] + \frac{f_{I1} + f_{I2}}{2}$$

$$f_D = \frac{f_{D1} - f_{D2}}{\pi} \tan^{-1}\left[K_D\left(\frac{\sigma_v}{\sigma_{vo}^*} - X_D\right)\right] + \frac{f_{D1} + f_{D2}}{2}$$

$$(9)$$

Table 1 shows the common set of parameters adopted to simulate the results.

Simulation of suction cycles

Figures 6 and 7 show the comparison of measured strains with model simulations, as well as the measured and predicted evolution of the ratio of the increments of strains $\varepsilon_{vM}^p / \varepsilon_{vm}^e$ for the tests performed at $\sigma_v = 200$ and 400 kPa, respectively. As observed, the correspondence obtained between measured and

predicted deformations is reasonably good. These figures also show the progressive evolution of the sample state towards the crossing point of the interaction functions (refer to the bottom graphs). This tendency towards the left implies a soil densification with an increasing value of the preconsolidation stress –LC moves to the right enlarging the elastic domain (Figure 5). Soil achieves a higher density at the end of the cycles as a consequence of the higher values of f_I compared to f_D -zone at the right of the crossing point in which irreversible shrinkage predominates over the plastic straining during wetting. As the cycles evolve, the soil reaches a new point, in which the net shrinkage at the end of the new cycle is lower than in the previous one. Finally, after a large number of cycles the ratio σ_v / σ_{vo}^* ends at the equilibrium point –i.e. intersection point of the interaction functions. At this point, macrostructural plastic strains still develop, but they compensate themselves without net predominant phenomenon.
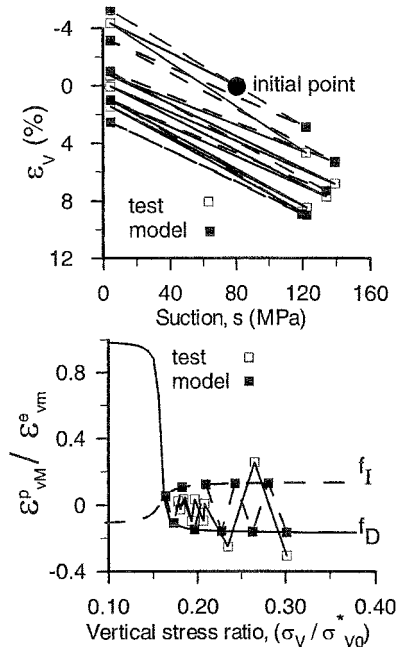
Figure 6: Model prediction and test results ($\sigma_v = 200$ kPa).

Table 1: Material parameters used in the simulation.

Macrostructure	$\lambda(0) = 0.25; r = 0.85; \beta = 0.05$ MPa^{-1};
	$\kappa = 0.008;\ p_0^* = 650$ kPa; $p_c = 0.008$ kPa
Microstructure	$\kappa_m = 0.09$
Interaction functions	$f_{I1} = -0.12; f_{I2} = 0.14; K_I = 100; X_I = 0.158$
	$f_{D1} = 1.0; f_{D2} = -0.17; K_D = 400; X_D = 0.158$
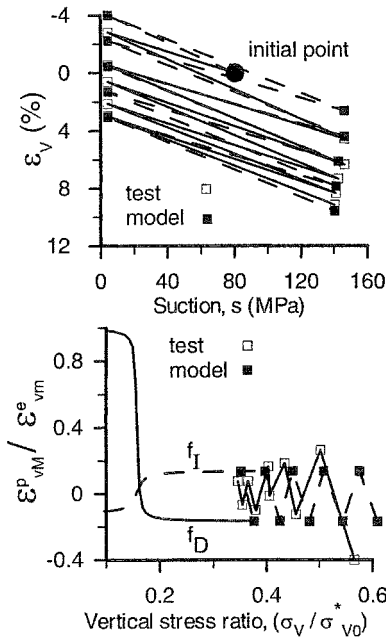
Figure 7: Model prediction and test results ($\sigma_v = 400$ kPa).

Conclusions

The effect of applying wetting-drying cycles on a bentonite-sand (80/20) compacted mixture has been investigated. Suction cycles with a large amplitude between $s = 130$ MPa and 4 MPa were applied by vapour equilibrium technique in an oedometer cell at different constant vertical stresses.

Samples experienced progressive shrinkage as the suction cycles accumulate, which was larger at higher stresses. Eventually a quasi-reversible response was approached. This progressive shrinkage led to an increase of the overconsolidation ratio.

Test results have been interpreted within the framework of a suction-dependent elastoplastic constitutive model (Alonso et al. 1999, 2005), which uses a double structure approach and is briefly outlined in the paper. A systematic procedure to derive model parameters has been proposed. The model has captured the essential features of observed behaviour.

Acknowledgements

References

Al-Homoud, A.S., Basma, A.A., Husein Malkawi, A.I. and Al-Bashabsheh, M.A. (1995). Cyclic swelling behaviour of clays. *J. Geotech. Engrg.*, ASCE, 121 (7), 562-565.

Alonso, E.E, Gens, A. and Josa, A. (1990). A constitutive model for partially saturated soils. *Géotechnique*, 40, 405-430.

Alonso, E.E., J Vaunat and A Gens (1999) Modelling the mechanical behaviour of expansive clays. *Engineering Geology*, 54, 173-183.

Alonso, E.E., Romero, E., Hoffmann, C. and García-Escudero, E. (2005). Expansive bentonite–sand mixtures in cyclic controlled-suction drying and wetting. *Engineering Geology*, 81, 213-226.

Basma, A.A., Al-Homoud, A.S., Husein Malkawi, A.I. and Al-Bashabsheh, M.A. (1996). Swelling-shrinkage behavior of natural expansive clays. *Applied Clay Science*, 11 (2-4), 211-227.

Day, R.W. (1994). Swell-shrink behavior of compacted clay. *J. Geotech. Engrg.*, ASCE, 120 (3), 618-623.

Dif, A.E. and Bluemel, W.F. (1991). Expansive soils under cyclic drying and wetting. Technical note. *Geotechnical Testing Journal*, GTJODJ, 14 (1), 96-102.

Pousada, E. (1984). *Deformabilidad de arcillas expansivas bajo succión controlada*. Doctoral Thesis. Universidad Politécnica de Madrid, Spain.

Preliminary Observation on Volumetric Behavior of Unsaturated Collapsible Loess

Radhey S. Sharma[1] and Sonal Singhal[2]

[1]Department of Civil and Environmental Engineering, Suite 3505 CEBA Building, Louisiana State University, Baton Rouge, LA 70803, USA; Email: rsharma@iastate.edu
[2]Formerly Graduate Student, Department of Civil, Construction, and Environmental Engineering, Iowa State University, Ames, IA, USA.

Abstract

Collapsible soils have porous structure, high void ratios, and relatively low dry unit weights in dry conditions. These soils consist mainly of wind-blown silt. Collapsible soils are moisture sensitive and susceptible to large reductions in volume primarily, with increase in moisture content. In this investigation, a commonly found collapsible soil, known as loess was tested on the laboratory compacted specimens to study its volume change behavior. The collapse tests were conducted using conventional oedometer. The collapse potential of loess was found to be dependent on the initial water content, initial dry unit weight and flooding stress (vertical stress at inundation).

Introduction

Occurrence of problematic soils such as expansive and collapsible is common. Design and construction of foundations and other geoinfrastructure in problematic soils is unavoidable in many cases, and therefore, it is important to understand the behavior of these soils. Most soils are sensitive to seasonal changes in moisture regime. The soils which respond quickly to changes in moisture regime may lead to deleterious consequences (e.g. Chen, 1988, Gallipoli et al., 2003, Sharma 2003, and Wheeler et al., 2003) such as swell, collapse, or loss of strength upon wetting. The problem of wetting may arise from a variety of sources, such as changes in surface and ground water regimes. It has been found that compacted soils are susceptible to compression upon wetting (Houston et al. 2001). The response of compacted soils to inundation depends on

the type of the soil, compactive effort, compaction water content and stress level at the time of inundation (Lutenegger and Saber, 1988 and Houston and Houston, 1997).

Identification of collapsible soils is achieved by testing soil specimens compacted at different values of water content and dry unit weight and over a range of stress levels expected in the field. Appropriate compaction specifications and construction controls leading to minimization of collapse can be achieved by identifying the conditions leading to collapse of a soil in the laboratory. The laboratory test data on collapse of soil on inundation, which corresponds to complete saturation, can be used in estimating the *in situ* collapse settlement of a soil deposit expected on full wetting corresponding to a high degree of saturation. This paper deals with a study on collapsible soil, loess obtained from Turin, Western Iowa. The main objectives of this study were to investigate the volume change behavior of loess under controlled and uncontrolled flooding conditions.

Experimental Program

Soil and Test Program

The loess soil used in the test program was obtained from Turin in Monona County, Western Iowa. This loess cliff is located along the north of Larpenteur Memorial road in Turin. The soil is a non-plastic, light-brown, silty soil. It was slightly moist, and had a natural water content of 9%. It lost moisture quickly on being exposed to atmosphere. The index properties of the soil are summarized in Table 1. Based on the index properties and gradation analysis, soil is classified as a ML (ASTM D2487).

Table 1 - Index properties of western Iowa loess.

Property		Standard designation	Value
Specific gravity, G_s		ASTM D854 – 02	2.62
Natural water content, $w_n(\%)$		ASTM D4318 – 00	9.0
Liquid limit (%)		ASTM D4318 – 00	29
Plastic limit (%)		ASTM D4318 – 00	23
Plasticity index (%)		ASTM D4318 – 00	6
Grain	Gravel (%) (>6.20 – 4.75	ASTM 98 D422 – 63	0.04
	Sand (%) (4.75 – 0.075	ASTM 98 D422 – 63	3.16
	Silt (%) (0.075 – 0.002	ASTM 98 D422 – 63	91.43
	Clay (%) (<0.002 mm)	ASTM 98 D422 – 63	5.37

The experimental program was a parametrical study aimed at studying the effect of important placement conditions of soil such as initial water content, initial dry unit weight and flooding stress (namely, the vertical compressive stress at which the soil is inundated with water) on collapse potential and other important volume change characteristics (e.g. compression index and swelling index). These placement conditions were chosen because of their role in the collapse of a soil. The investigation comprised of three series of collapse tests. In this paper only a few results are presented to highlight the main features of volumetric response of loess.

Sample Preparation

Various techniques of compaction are available such as dynamic compaction, static compaction and kneading compaction. Of these available methods static compaction method was chosen for the sample preparation to ensure uniformity and repeatability. The dynamic compaction method was not used as it is recognized as an effective technique for improving the engineering behavior of collapsible soils. For the sample preparation soil was initially oven-dried at $110^{\circ}C$ for 24 hours to remove all of the hygroscopic moisture. The soil was allowed to cool down to room temperature in a flat pan and sieved through a 425 micron sieve. A calculated amount of water was mixed with soil to achieve desired water content. The soil was kept in plastic bags for preventing moisture loss and for moisture homogenization for one hour. The soil was statically compacted directly into the consolidation ring in three layers. The surface of each layer was scarified before adding the material for the next layer. Each layer of the soil specimen was statically compacted. A constant displacement rate of 7.4 mm/min was maintained to achieve the required static compaction stress. The reason for choosing such a high value of displacement rate was to minimize the changes in water content during compaction. The sample was trimmed on both sides after compaction. Test water content was checked.

Testing Procedure

The collapse tests for all the three series of tests were conducted in a conventional oedometer in which the accurate displacement readings were recorded by an automated data logging system using linear variable displacement transducers (LVDTs) of 0 to 10 mm range. In each test, porous stones were placed at each end of the sample prepared for the testing to ensure double drainage. The consolidation ring was covered with plastic wrap to minimize moisture loss. Vertical compressive loads were applied on the specimen starting from 6 kPa. The load was increased as 12, 25, 50, 100, 200, 400, 800 and 1600 kPa. Each load increment was applied on the specimen for two hours during the unsaturated condition. However, time duration of 24 hours was allowed for the specimen to consolidate under the applied loads after flooding.

After the applied load reached the predetermined flooding stress, specimen was allowed to be compressed for two hours at that particular vertical compressive stress. On the specimen reaching the equilibrium void ratio at the flooding stress in the unsaturated condition, the sample was inundated. The sample was compressed for duration of 24 hours under each load higher than the flooding load also. When the stress level reached 1600 kPa, the sample was gradually unloaded to 400, 100, 25 and 6 kPa, each decrement being maintained for 24 hours.

Test Results and Discussion

Figure 1 shows three parts of the e versus log σ_v curve, namely A, B and C which are considered as separate stages for the test results obtained in this study to facilitate the presentation and discussion. The variation in void ratio, e with vertical stress, σ_v prior to inundation is shown by Part A. In this curve the sample is in unsaturated condition with the same water content as the placement water content. While, Part B and Part C of the e - log σ_v curve show the variation of void ratio at constant flooding stress, σ_{fl} and subsequent loading and unloading of sample at and after σ_{fl}, respectively.
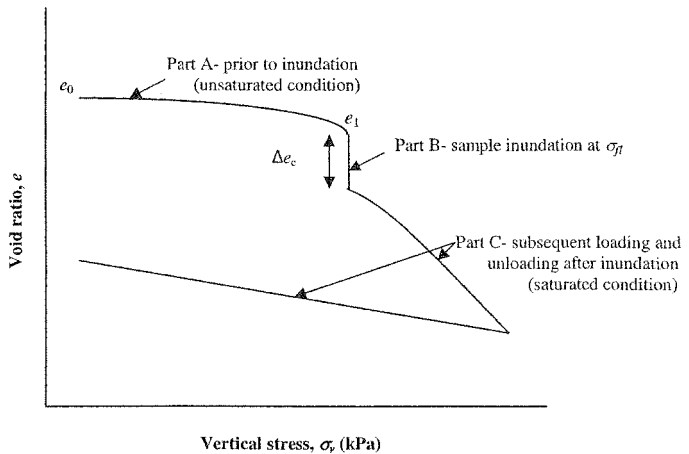
Figure 1 – Stages of a typical e versus log σ_v curve in an oedometer collapse test.

The tests were carried out at constant water content of 6% and by varying flooding stress and static compaction stress values. The results for the following set of variables are presented in this paper:

Constants: *Initial water content* $w_i = 6\%$;
Static Compaction Stress SCS = 100 kPa;
Variables: Vertical stress at which the sample was flooded (σ_{fl}) = 6 kPa, 12 kPa, 25 kPa, 55 kPa, 100 kPa, 200 kPa, and 400 kPa.

Figure 2 shows the results corresponding to Part A (see Figure 1) of 7 tests. From Figure 2, the maximum decrease in void ratio from initial void ratio, e_0 (at 6 kPa) on loading to
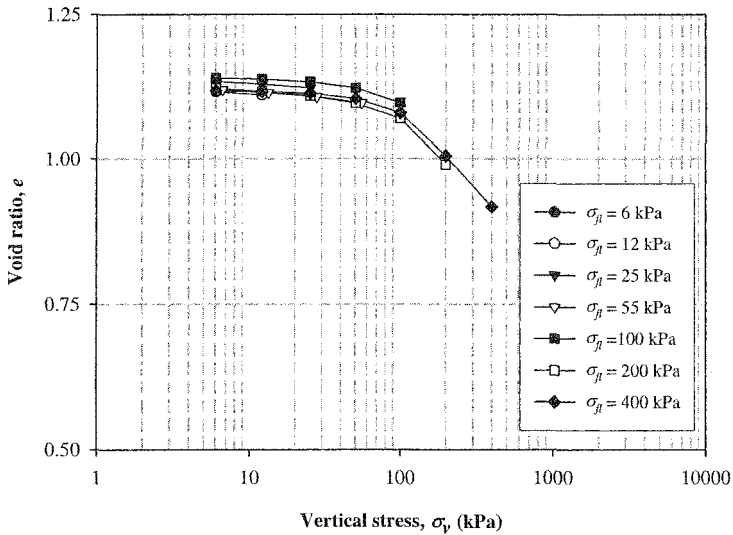
Figure 2 – Results for Part A of e versus log σ_v curve (SCS = 100 kPa; w_i = 6%).

100 kPa is found to be 0.043, which is a relatively small value. However, there is a significant decrease in the void ratio on increasing the vertical stress beyond 100 kPa. The maximum decrease in void ratio on loading from 100 kPa to 400 kPa was 0.20. Using Casagrande's graphic construction to determine the preconsolidation pressure, the preconsolidation pressure, σ_{uc} from unsaturated portion of the e-log σ_v curve is

approximately 120 kPa as shown in Figure 3. It seems that the samples started yielding beyond preconsolidation pressure, σ_{uc}.

An estimate of collapse potential values at various flooding stresses, σ_{fl} can be made from Figure 4, which shows an increase in collapse potential values with increasing σ_{fl} values from 6 kPa to 55 kPa. Between 55 kPa and 200 kPa the soil collapsed to the maximum extent. After 200 kPa σ_{fl}, however, the collapse potential started decreasing. Hence, 55 kPa can be said to be the critical value of collapse potential for the soil used for the given placement conditions ($w_i = 6\%$ and $SCS = 100$ kPa). It is worth noting that, with increasing vertical stress in unsaturated condition followed by flooding, the collapse potential decreased after a certain value of vertical stress. This phenomenon suggests that the soil was already compressed to a large degree in the unsaturated condition prior to flooding. This means that the higher the values of overburden pressures (vertical stress) lower the value of collapse potential. Table 2 summarizes the values of collapse potential at varying flooding stresses.
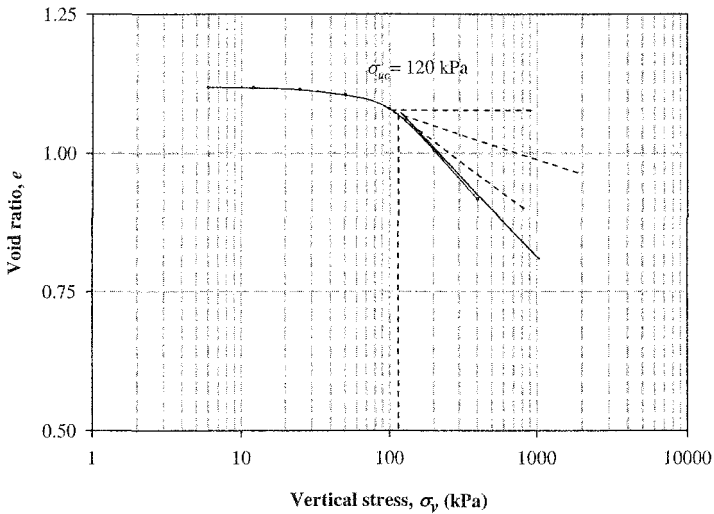
Figure 3 – Results of Part A of e versus log σ_v curve ($SCS = 100$ kPa; $w_i = 6\%$; $\sigma_{fl} = 400$ kPa).
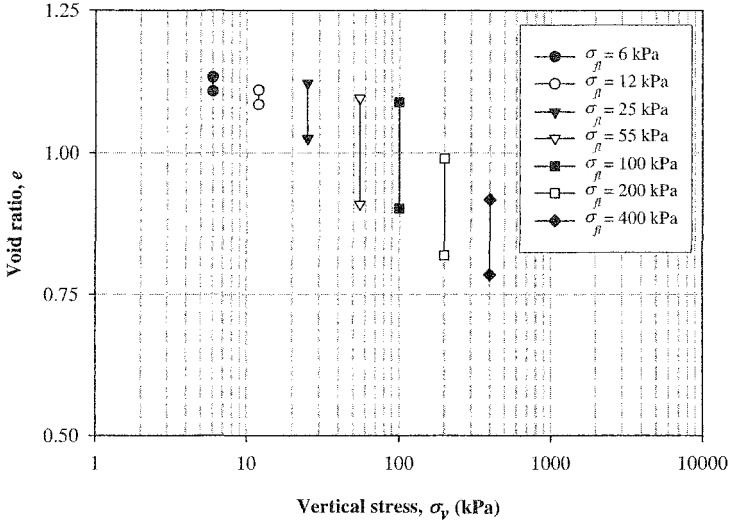
Figure 4 - Part B of e versus log σ_v curve ($SCS = 100$ kPa; $w_i = 6\%$).

Table 2 - Collapse potential values at different vertical stresses at inundation ($w_i = 6\%$; $SCS = 100$ kPa).

Flooding stress, σ_{fl} (kPa)	Collapse potential, CP (%)
6	1.11
12	1.21
25	4.60
55	8.96
100	8.98
200	8.59
400	6.90

Inspection of Table 2 shows that collapse potential is a function of stress which the flooding of the soil sample commences. It has important implications for response of geoinfrastructure involving collapsible unsaturated soils. Moreover, it seems that the

collapse behavior of loess is similar to the wetting-induced collapse of other types of unsaturated soils. Based on the preliminary data, it looks feasible that the elato-pastic framework developed for unsaturated soils in recent past can be used to provide new insight.

Conclusions

An experimental investigation was carried out to understand the volumetric response of unsaturated collapsible soil from Western Iowa, US. Conclusions based on the experimental results can be summarized as follows:

- Loess is sensitive to variations in moisture content.
- The amount of collapse noticed was a function of the vertical stress at which the flooding started.
- Based on preliminary observations, it seems feasible to interpret the behavior of unsaturated soils in terms of the elasto-plastic constitutive framework developed for unsaturated soils.

References

Chen, F. H. (1988). *Foundations on Expansive Soils*, Elsevier Science, Amsterdam, The Netherlands.

Gallipoli, D., Gens, A., Sharma, R. and Vaumat, J. 2003. An elasto-plastic model for unsaturated soil incorporating the effects of suction and degree of saturation on mechanical behavior. Geotechnique 53(1):123-135.

Houston, S. L., and Houston, W. N. (1997). "Collapsible soil engineering," Unsaturated Soil Engineering Practice, Geotechnical Special Publication, 68, 199-232.

Houston, S. L., Houston, W. N., and Zapata, C. E. (2001). "Geotechnical engineering practice for collapsible soils," Geotechnical and Geological Engineering, 19(34), 333-355.

Lutenegger, A. J., and Saber, R. T. (1988). "Determination of collapse potential of soils," *Geotechnical Testing Journal*, 111(3), 173-178.

Sharma R. S. (2003). "Mechanical behavior of Unsaturated Expansive and Collapsible Soils". CD ROM Proceedings of 11th Annual Great Lakes Geotechnical/Geoenvironmental Conference (GLGGC), Purdue University, West Lafayette, IN.

Wheeler, S.J., Sharma, R.S. and Buisson, M.S.R. 2003. Coupling of hydraulic hysteresis and stress-strain behavior in unsaturated soils. Geotechnique 53, (1):41-54.

Relationship between Collapse and Soil-Water Retention Curve of a Sandy Soil

R. A. Rodrigues[1] and O. M. Vilar[2]

[1]Graduate Student; University of São Paulo, Brazil; E-mail: rogerar@sc.usp.br

[2] Professor; University of São Paulo, Brazil; E-mail: orencio@sc.usp.br

Abstract

Volume decrease associated to an increase of water content of a soil, at almost constant total stress has been termed collapse. Some evidences from laboratory tests and field observation indicate that soil collapse can arise from moisture variation or, more appropriately, from suction variation conditions that are far from saturation or far from zero suction. This paper deals with the influence of soil-water characteristic curve of an undisturbed sandy soil on collapse deformation. The results analyzed come from suction controlled oedometer tests and soil-water retention curves. The results show some features of the gradual collapse behavior of the tested soil and its relationship with the form and parameters of soil-water retention curve and presents an empirical equation able to calculate the collapse potential development under matric suction variations using the parameters of the soil water retention curve.

Introduction

Some soils under constant stress show volume decrease related to an increase of water content. This wetting-induced deformation or soil collapse is a typical behavior of the so called collapsible soils which are characterized by an unstable structure (Dudley, 1970). Current studies about collapsible soils usually rest on the measurement of collapse deformation when soil approach saturation in conventional oedometer tests. However, some evidence from laboratory tests and field observation indicate that soil collapse can arise from moisture variation or, more appropriately, from suction variation conditions that are far from saturation or far from zero suction (Escario and Saez, 1973; Vilar, 1995). Thus, in light of current concepts of unsaturated soils, a better representation of collapse deformation should consider the stress state variable, net normal stress, $\sigma - u_a$ and matric suction, u_a-u_w, as they are recognized to be useful to the process of collapse. The suction controlled oedometer tests are useful for this purpose as they can provide such facilities.

1025

The soil water retention curve (SWRC) has been recognized to be of paramount importance in the description of unsaturated soil behavior. Besides dealing with the water retention in a soil it has been largely used to forecast some soil properties, such as unsaturated hydraulic conductivity (van Genuchten, 1980) and unsaturated shear strength (Fredlund et al., 1995). Many attempts have been performed in order to mathematically represent the SWRC. They comprise of simple empirical curve fitting and more sophisticated models that take into account some physical characteristic of soil, such as the pore distribution. Amongst the many propositions, those of van Genuchten (1980) and of Fredlund and Xing (1994) have been largely used in Geotechnical Engineering.

Although the SWRC has been much applied to predict some soil properties, there are very few attempts to relate it to the collapse mechanism of soils.

This paper deals with some features of collapse behavior of an undisturbed sandy soil. The gradual collapse development observed in suction controlled oedometer tests is analyzed and related to the soil water retention curve.

The Soil Studied

The soil used in this study is a typical collapsible soil from the Northwest of Sao Paulo State, Brazil. Large areas of this region are covered by sandy soils that are of colluvial nature and reach depths of about 10 meters. These soils present low units weights and low degree of saturation. The main characteristics of the studied soil are: specific gravity, $G_s = 2.63$; dry density, $\rho_d = 1.44$ Mg/m^3; water content, $w = 7.2$ %; void ratio, $e = 0.845$; porosity, $n = 46$ %; liquid limit, $w_L = 18$ %; plastic limit, $w_P = 11$ %; clay fraction = 15 %; silt fraction = 6 % and sand fraction = 79 %.

Experimental Program

Laboratory tests with undisturbed samples were performed to characterize the water retention and the gradual collapse of the soil. The characteristics of the tests performed are as follow.

Suction controlled oedometer tests

These tests were performed using the axis translating technique in a cell similar to that developed by Escario and Saez (1973). Specimen dimensions were 70 mm in diameter and 20 mm in height.

The samples were first wetted to release suction and then submitted to an initial suction of 200 kPa, following a drainage path. After equilibrium, they were loaded under net normal stress ($\sigma - u_a$) of 50, 100, 200 and 400 kPa allowing for the equilibrium of deformation under load. Then the suction was gradually reduced to 100, 50, 25, 10 and finally to 0 kPa and the corresponding collapse strains and volume of water that entered the soil were registered.

In some samples, cycles of loading and unloading were applied and other tests were stopped after total collapse strain has been completed. These later

specimens, after ceasing the volume reduction were released from the loading and tested in a drainage path to know their SWRC.

The wetting-induced or collapse deformations (CP) were calculated by Equation 1:

$$CP = \frac{\Delta H_i}{H_{ai}} \cdot 100\%$$ (1)

Where, ΔH_i: height variation of the sample after collapse; H_{ai}: height of the sample before the wetting (or suction reduction).

Soil-Water Retention Curve

The soil-water retention curves were obtained with axis translating technique proposed for Hilf (1956) following two suction paths:

Drainage path

In the drainage path the sample was first saturated and then gradually drained by increasing the air pressure in the chamber. In these tests, undisturbed specimens and specimens from the oedometer tests after completion of the tests were used.

Wetting path

The soil water retention curve under a wetting path was obtained using the suction controlled oedometer tests. As this test allows the measurement of the amount of water that enters the soil, under a known suction, it is capable of yielding the soil water retention under some known load acting in the soil.

The samples with net normal stress of 50 and 400 kPa were chosen for discussion of results, because these are the high and small studied wetting stress. The sample with net normal stress of 100 kPa was also analyzed because it had shown the largest collapse potential.

Test Results

Volume Change and Collapse

Figure 1 shows the oedometer compression curves of samples with initial suction of 200 kPa and wetted under net normal stress of 50, 100, 200 and 400 kPa.

The collapse strains refer to the total collapse after suction reduction from 200 kPa to zero. The largest collapse was associated to the load of 100 kPa, that is collapse strains increase with load up to a maximum and then decrease with load, which is a typical behavior of many Brazilian collapsible soils.

The total collapse strains showed in Figure 1 are the result of the gradual strains that arise upon suction reduction. Figure 2 show the collapse potential related to each value of suction.
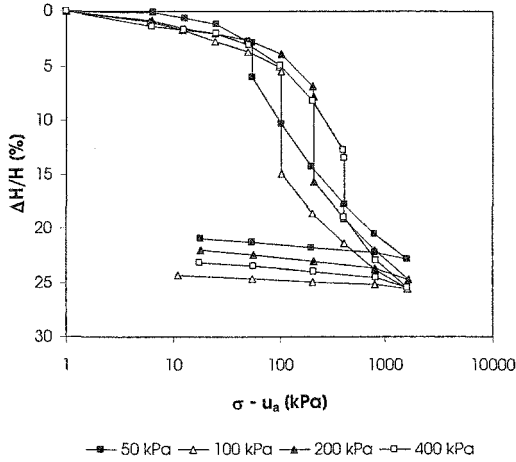
Figure 1. Oedometer compression curves of samples under initial suction of 200 kPa and collapse strains.
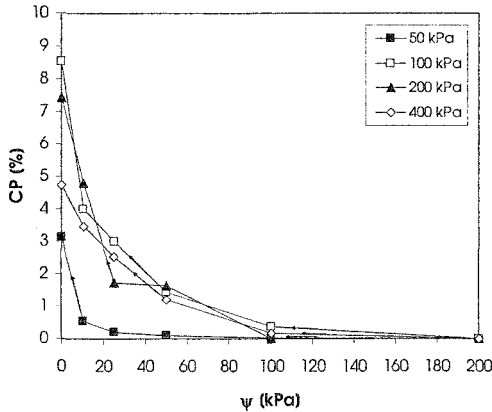
Figure 2. Collapse potential under gradual suction reduction.

The sample tested under $(\sigma - u_a)$ of 50 kPa presented an almost negligible collapse potential when suction was decreased from 200 to 25 kPa. The largest part of collapse developed when the suction was reduced from 25 to 0 kPa. On the other extreme, a rather different behavior is observed. For the sample tested under $(\sigma - u_a)$ of 400 kPa, appreciable collapse potential begins to develop for suction lower than 100 kPa.

Thus, the soil is capable of supporting the suction reduction until a limit value, from which the collapse strains begin to develop more intensively. This

behavior should be related to the associated water retention characteristics of the soil as explained in the next item.

Soil-Water Retention Curves

Figure 3 sketches a SWRC for a sandy soil, as the one studied here. In the desaturation zone, a low suction variation implies large water content variation.

Thus, the collapse will increase when the wetting occurs in the desaturation zone of the retention curve, because a large water amount will be necessary to change the suction.
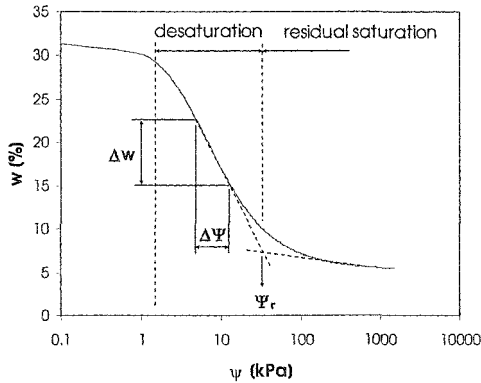
Figure 3. Soil-water retention curve of sandy soil.

In the tests reported in this paper, the collapse strains did not behave equally with the suction variation in each net normal stress. The differences can be associated to the change in the retention characteristics of the soil, as each specimen experienced volume variations after loading and subsequent wetting.

The grain and pore size distributions, as well as the stress state are examples of factors that influence the form of the soil-water retention curve (Yamada and Kondou, 2002; Zhou and Yu, 2005). When the soil is compressed and later wetted, the volume change takes place in the macro-pores and affects the SWRC.

Figure 4 shows soil-water retention curves of undisturbed soil and loaded-wetted-unloaded samples that have come from the oedometer tests after collapse strains have ceased. Table 1 presents the adjusted parameters using the Van Genuchten's equation expressed as:

$$w = w_r + (w_s - w_r)\left\{ \frac{1}{\left[1+(\alpha\psi)^n\right]^m} \right\} \qquad (2)$$

Where, w_r: residual water content; w_s: saturation water content; α, m e n: fitting parameters.

■ 0 kPa   × 50 kPa   △ 100 kPa   ● 400 kPa
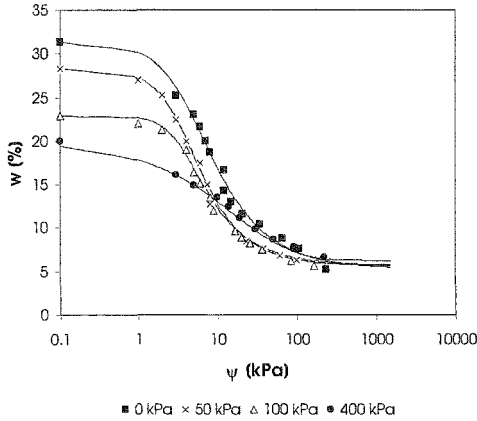
Figure 4. Soil-water retention curves (drainage path). Natural soil (0 kPa) and curves determined on samples after compression in the oedometer tests.

Table 1. Adjusted parameters of Van Genuchten Model.

$\sigma - u_a$ [kPa]	α [cm^{-1}]	m	n	w_r [%]	w_s [%]	r^2
-	0.2250	0.5232	1.5941	5.24	31.33	0.988
50	0.2836	0.5255	1.9556	5.58	28.26	0.997
100	0.2796	0.3584	2.4907	5.60	22.90	0.966
400	0.0016	10.0261	0.6358	6.20	19.94	0.998

As can be seen, the initial portion of the curves changes reflecting the effect of volume variation that took place after loading and wetting, while the remaining of the curves are more or less similar.

Table 2 shows percent collapse potential, PCP, the relationship between collapse potential at any suction and total collapse versus suction reduction. It was considered that the collapse potential for $\Psi = 0$ kPa corresponds to 100 % of collapse. Now, the results plotted in the Figure 2 follow a similar pattern, as the wetting-induced deformation not only have the same origin, but also converge to the same point. Figure 5 shows percent collapse potential versus suction.

In the sample wetted under 50 kPa of net normal stress, the suction reduction from 200 to 25 kPa caused 6.5 % of total collapse. As suction is reduced from to 10 to 0 kPa, the accumulated collapse potential raises from 17.5 % to 100 %. For 400 kPa of net stress, the steps of suction reduction induced more or less similar collapse strains.

The results also show that collapse strains start to increase at a faster rate for suction values lower than a critical value. As shown in Figure 3, larger collapse seems to be associated with the desaturation zone of SWRC, thus it is reasonable to suppose that this critical value is associated to the residual suction that depends on

the load applied to the sample. The few data provided in this study were not enough to clarify this question and more data are needed to confirm this feature.

Table 2. Collapse potential, CP, and percent collapse potential, PCP, during suction reduction. Specimens under net normal stress of 50, 100 e 400 kPa.

Ψ [kPa] reduction	$\sigma - u_a = 50$ kPa		$\sigma - u_a = 100$ kPa		$\sigma - u_a = 400$ kPa	
	CP [%]	PCP [%]	CP [%]	PCP [%]	CP [%]	PCP [%]
200	0.00	0.0	0.00	0.0	0.00	0.0
$200 \rightarrow 100$	0.02	0.7	0.37	4.3	0.18	3.7
$100 \rightarrow 050$	0.09	2.8	1.42	16.6	1.19	25.1
$050 \rightarrow 025$	0.20	6.5	2.99	35.1	2.54	53.7
$025 \rightarrow 010$	0.55	17.5	3.99	46.9	3.48	73.6
$010 \rightarrow 000$	3.12	100	8.52	100	4.73	100
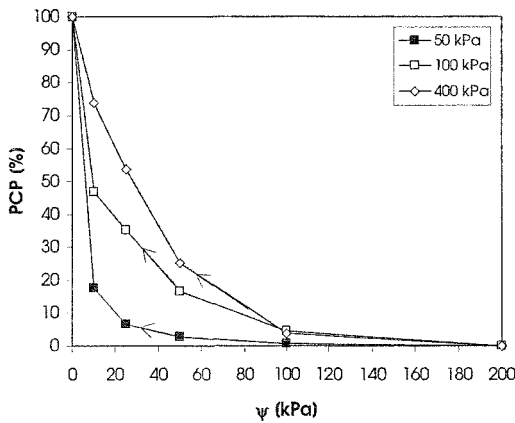
Figure 5. Percent Collapse Potential versus matric suction.

Evaluation of Collapse Strains

As can be seen in the test results, the gradual collapse that develops upon wetting (or suction reduction) is function of the amount of water that is allowed to reach the sample. As it is obvious this amount is commanded by matric suction or by the soil water retention characteristics. So, besides allowing measuring the collapse strains, the suction controlled oedometer cell allows to measure the water retention of the specimen, which is under some known load.

The analysis of collapse strains pattern suggests that it follows the same pattern observed in the SWRC. Thus, an obvious suggestion of these observations is

try to empirically model the collapse strain with an equation similar to that used to model the SWRC. As the van Genuchten (1980) equation (eq. 2), was used to mathematically fit the SWRC, an equation analogous to (eq. 2) was proposed to represent the accumulated percent collapse potential (PCP) with suction, as follows:

$$PCP = 100 \left\{ \frac{1}{\left[1 + (\alpha\psi)^n \right]^m} \right\}$$

(3)

Table 3 shows the fitting parameters of Equation (3) when applied to the experimental data of collapse potential. The high coefficient of determination shows that the proposed equation is capable of adequately reproducing the variation of PCP with suction, what can be confirmed in Figures 7, 8 and 9, considering the curves named T.

This finding and the possibility of obtaining the fitting parameters, α, m and n, from other sources makes Equation (3) very useful to forecast CP. Although it was deduced from empirical observation, it encompass the two state variables that command the amount of soil collapse, that is, the net normal stress and the matric suction. Some alternatives to find the fitting parameters are outlined in order to ease the calculus of CP.

Table 3. Adjustments parameters of Equation 3.

$\sigma - u_a$ [kPa]	α [cm^{-1}]	m	n	r^2
50	0.0422	3.837	0.6011	1.000
100	0.0014	10.2988	0.6256	0.998
400	0.0021	15.8412	1.0533	0.999

Alternative 1 (A-1)

This alternative considers the soil water retention curve obtained from the measurement of matric suction and moisture content in the controlled suction oedometer test. Figure 6 shows the SWRC from these tests and the experimental data was fitted with Equation (2). The fitting parameters α, m and n are summarized in Table 4 and the resulting curves using these parameters in eq. (3) are plotted in Figures 7 to 9 and identified under name A – 1.

Table 4. Fitting parameters of Equation (2).

$\sigma - u_a$ [kPa]	α [cm^{-1}]	m	n	w_r [%]	w_s [%]
50	0.8057	0.4642	1.8663	5.8	25.7
100	1.1427	0.3078	1.4446	5.4	20.7
400	0.0847	0.3704	2.5022	5.6	16,1
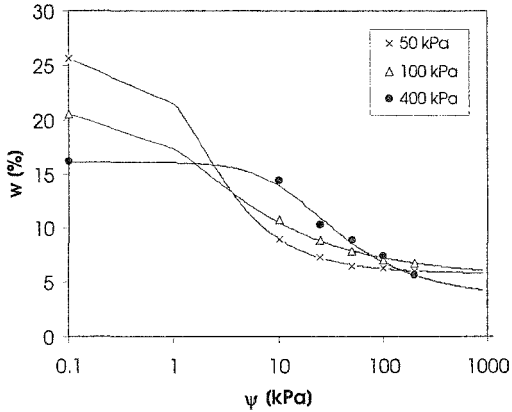
Figure 6. Soil-water retention curves (wetting path) from oedometer tests. Specimens wetted under 50, 100 and 400 kPa of net normal stress.

Alternative 2 (A-2)

In this case, the SWRC obtained using drainage path after the specimen had been compressed under a known load is considered. The experimental data and adjusted curves were already shown in Figure 4, together with the curve of a specimen tested without any load and the fitting data were summarized in Table 1.

The adjusted curves are also plotted in the same Figures 7 to 9 and identified as A-2.

Alternative 3 (A–3)

Other option is to consider the SWRC determined for the soil without any loading in a drainage path. This is the more common way of measuring the retention properties of a soil and the idea is to test if this option can yield at least a rough estimative of collapse potential. This curve is in Fig. 4 (0 kPa) and the adjusted parameters are in Table 1. The resulting curve using eq. (3) is plotted in Figs. 7 to 9, curves A-3.

The curves T represented in Figures 7 to 9 shows the nice fitting of Equation (3) to the experimental data, when they were directly adjusted to the results of percent collapse potential.

Alternatives 1 and 2 tend to approach the experimental data, however with some deviation for Alternative 2. Reasons for these deviations should rest on the peculiar features presented during water retention measurement used in alternatives 1 and 2. For instance, the SWRC used in Alternative 2 was obtained in a drainage path. Besides, that the sample after loading was released and tested without any overburden stress. Alternative 3 tends to approach the measured results for the net

normal stresses of 100 kPa, however it overestimates the results for 50 kPa and underestimates the collapse potential for the net stress of 400 kPa. Obviously, this deviation should be expected considering the difference in the drainage paths and in the net normal stresses used in the oedometer tests and in the SWRC.
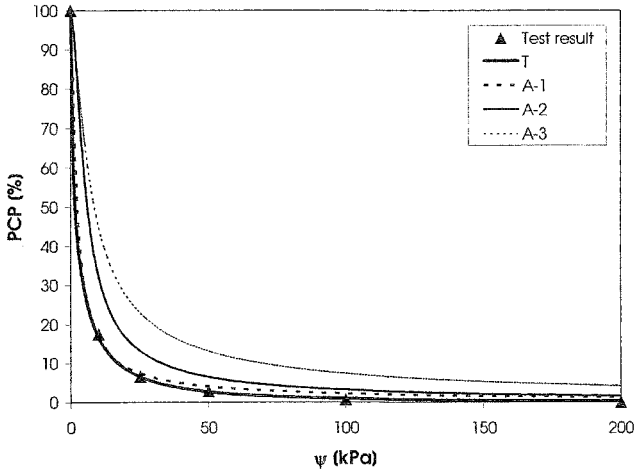
Figure 7. Percent collapse potential versus matric suction and fitting curves. Specimen under net normal stress of 50 kPa.
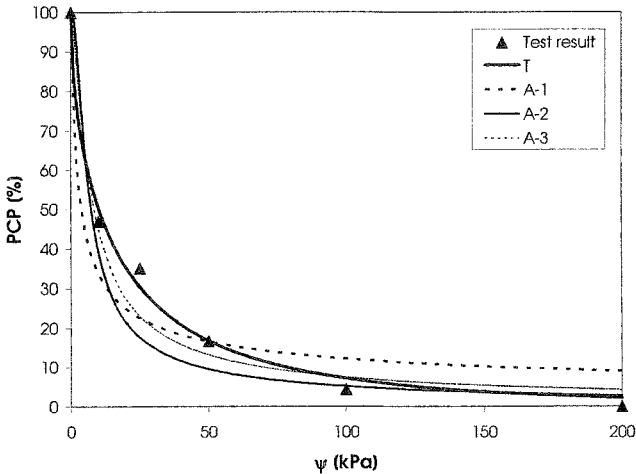
Figure 8. Percent collapse potential versus matric suction and fitting curves. Specimen under net normal stress of 100 kPa.
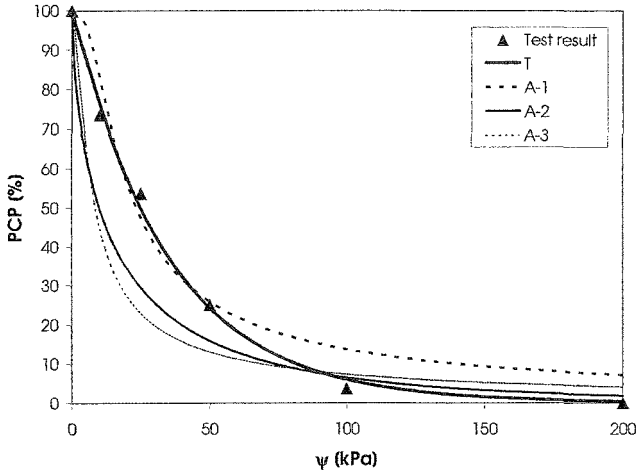
Figure 9. Percent collapse potential versus matric suction and fitting curves. Specimen under net normal stress of 400 kPa.

The many alternatives analyzed encourage further studies on this subject dealing specially with the improvement in the measurement of the SWRC. This should duplicate drainage and load path expected in the problem under analysis. In addition, other soils should be tested in order to confirm the behavior reported here. If this behavior is confirmed, other use for the SWRC will be available, that is the prevision of collapse strains.

Conclusion

The sandy soil studied showed gradual collapse strains after matric suction reduction. The collapse strains tended to increase as suction decreased and reached their largest value for zero suction. The accumulated collapse strains could be related to matric suction according to an equation analogous to the Van Genuchten (1980) equation for the soil-water retention curve. Some alternatives to obtain the fitting parameters for the proposed equation were presented and discussed and have shown the possibility of using the SWRC to calculate the accumulated collapse potential of soils.

Acknowledgements

References

Dudley, J.H. (1970). "Review of Collapsing Soils". *Journal of the Soil Mechanics and Foundation Division*, v. 96, n. SM3, p. 925-947.

Escario, V. and Saez, J. (1973). "Gradual collapse of soils originated by a suction decrease". *In: International Conference on Soils Mechanics and Foundation Engineering, 8,* Moscow, Proceedings, v. 4.2, p. 123-124.

Fredlund, D.G., Vanapalli, S.K., Xing, A. and Pufahl, D.E. (1995). "Predicting the shear strength function for unsaturated soils using the soil-water characteristic curve". *Proc. 1rd Int. Conf. on Unsaturated Soils*, France, v1, p. 63-69.

Fredlund, D.G. and Xing, A. (1994). "Equations for the soil-water characteristic curve". *Canadian Geotechnical Journal*, 31, p.521-532.

Hilf, J.W. (1956). An investigation of pore-water pressure in compacted cohesive soils. Denver, 109p. (Thesis, Faculty of Graduate School of the University of Colorado).

van Genuchten, M.T. (1980). "A closed form equation for predicting the hydraulic conductivity of unsaturated soils". *Soil Science Society of America Journal*, Madison, v.44, p.892-898.

Vilar, O.M. (1995). "Suction controlled oedometer tests on compacted clay". *Proc. 1rd Int. Conf. on Unsaturated Soils*, France, vol.1, p. 201-206.

Yamada, K. and Kondou, T. (2002). "Relationship between soil-water characteristic curve and void ratio, Unsaturated Soils". *Proc. 3rd Int. Conf. on Unsaturated Soils*, Brazil v1, p. 209-214.

Zhou, J. and Yu, J.L. (2005). "Influences affecting the soil-water characteristic curve". *Journal of Zhejiang University Science*, 6A (8), p.797-804.

An Empirical Relationship for Predicting Soil Collapsibility due to Soaking under Compression and Shear

N. Yasufuku[1], H. Ochiai[2] and D. Hormdee[3]

[1]Geotechnical Laboratory, Department of Civil Engineering, Kyushu University, P.O. Box 812-8581, Fukuoka, Japan, PH (81) 92-642-3284; FAX (81) 92-642-3285; email: yasufuku@civil.kyushu-u.ac.jp
[2]Geotechnical Laboratory, Department of Civil Engineering, Kyushu University, P.O. Box 812-8581, Fukuoka, Japan, PH (81) 92-642-3283; FAX (81) 92-642-3285; email: ochiai@civil.kyushu-u.ac.jp
[3]Department of Civil Engineering, Khon Kaen University, P.O. Box 40002, Khon Kaen, Thailand, PH (66) 43-202846-7; FAX (66) 43-202846-7 Ext. 102; email: dolhor@kku.ac.th

Abstract

Collapse and direct shear box tests on an unsaturated compacted soil with suction and water content measurements due to soaking are first presented. The compressibility, strength and dilatancy characteristics are discussed on the basis of the experimental results, paying attention to the initial water contents and the normal stresses. Then, a simplified relationship for rationally predicting the collapse settlement under one-dimensional compression condition is presented based on the experimental considerations. The applicability of the empirical relationship presented is finally discussed by comparison with the experimental data obtained by one-dimensional compression tests.

Introduction

One of the most problematic unsaturated soils is the collapsible soil, which is a common geotechnical concern in arid regions. Although these relatively high void-ratio soils exhibit a significant strength and low compressibility at their natural, in-situ water content, they collapse significantly upon wetting under load. The decrease in soil suction and weakening of bonds associated with accidental or intentional wetting triggers the collapse. Most often, the damage to constructions results from differential deformations, which had not been anticipated at the design and construction stages. Therefore, the estimation of the collapse settlements which linked with the collapse potential and shear strength become major components in the moisture-sensitive soil sites. A laboratory or field test is commonly used for structuring the model to estimate the collapsible potential settlements of soils under a certain rainfall condition. Many researches have already carried out the studies on the collapsible behaviors of unsaturated soils from theoretical and practical points of view (e.g., Chen, et al., 1999; El-Ehwany and Houston, 1990; Fredlund and Rahardjo, 1993; Habibagahi and Mokhberi, 1998; Nishimura, et al., 1998; Tadepalli and Fredlund, 1991).

The objective of the study presented here is first briefly introduce an new direct box shear apparatus with measurements of volumetric water contents and also to investigate the strength and deformation characteristics of the compacted soil during infiltration, with reference to the effects of loading history and shear level for soaking. In addition, an experimental based model, which can simply estimate the collapsible strains and/or settlements of the compacted soil during infiltration, is presented. The empirical relationship is mainly considered to reflect the characteristics of collapse settlement during soaking under one-dimensional compression conditions. The applicability of the empirical relationship is verified using the experimental data.

Sample and Test Apparatus used

A non-plastic volcanic sandy soil, Shirasu, less than 0.85 mm in the particle size is used in this study (see Hormdee et al., 2004) to show the compressibility, strength and dilatancy characteristics of the soils with different initial water contents and also to demonstrate the effect of soaking on those characteristics. The fundamental properties of Shirasu soil used are shown in Table 1, where the collapse indices of Shirasu soils are in the range from moderate to severe condition, but depending on the differences of relative density and initial water content condition that means for the specimen at air-dry water content, collapse index is upto 6%

Table 1 Index properties of volcanic ash sandy "Shirasu" soil.

Property	Shirasu soil
Specific gravity	2.54
Grain size distribution	
Sand: Silt: Clay	85 : 13 : 2
Air dried water content	0.6-1.2 %
OMC	8.1 %
γ_{dmin}	0.954 g/cm^3
γ_{dmax}	1.44 g/cm^3

(Hormdee et al., 2004). Shirasu soils are widely distributed in the region of southern part of Kyushu island, Japan. Samples were prepared in 'identical' fashion by controlling initial water content and dry density. An innovative adaptation to the direct shear apparatus is shown in Figure 1. Shear forces were induced by displacing the upper portion of the shear box. They were measured by a load cell installed on the lateral surface of the upper portion of the shear box. Note that these processes were done at a constant confining pressure applied by the air cylinder. It should be mentioned here that the response of the upper load cell reduces the applied confining pressure to the specimen due to the effect of side friction in consolidation process.

Figure 1 The modified direct shear
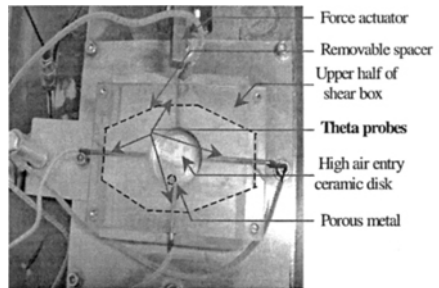
Figure 2 The modified shear box for measured pore-water pressure and water content during shear

To determine the changing in water content during testing, Theta probes based on dielectric methods with time domain reflectometry (TDR) have been installed, located on the upper half of the shear box near the shearing zone as shown in Figure 2. These probes consist of four stainless shafts. One of them receives the signal from the others to transducer. It senses the volumetric water content (θ_w) by means of evaluating the changing of apparent dielectric constant (ε). The θ_w is represented as the ratio of volume of water (V_w) to the total volume (V). For a completely dry sample θ_w is 0 and θ_w is equal to 1.0 (which is pure water). Soil specimens have a diameter of 60 mm and a height of 21 mm (including spacing of 1 mm). A one-dimensional, static compaction was applied to prepare the soil specimens by controlling the compaction water content about 1% or 8%. The soil was compacted into the direct shear box with 65% of relative density. Pore air pressure was kept as atmospheric pressure and also pore water pressure was measured by a transducer through a ceramic base plate. Normal stresses, where the maximum pressure was 160kPa, were applied to the soil specimens for a period of time sufficient to reach equilibrium of settlement and pore pressure. Each specimen, therefore, was subjected to net normal stress of 10kPa to make identical then applied a constant net vertical stress of 20, 80 or 160 kPa throughout the test.

Figure 3 Typical degree of saturation measured in compression, soaking and shearing stages

During shearing of the specimens, the pore-air pressure and vertical stress were maintained at constant level. The shear rate in all the test was 0.2 mm/min. Vertical load (P_v), shear force (T), vertical displacement (ΔV_D), horizontal displacement (Δh), suction values (s_u) and changes of water contents (Δw) mainly under soaking were automatically measured by an upper load cell, load cell for shear, vertical and horizontal dial gauges, pore water pressure transducer through ceramic disk and theta probe transducer, respectively, as shown in Figures 1 and 2. Figure 3 shows a typical result for changes of volumetric water contents and suction values under the process of compression, soaking and shearing related to the elapsed time. We can see that the apparatus can measure the changes of volumetric water contents during testing.

Compressible Characteristics

Figure 4 shows the results of one-dimensional compression curves of Shirasu specimen in medium dense state with initial water contents of 1%, 8% and 40% at normal stress of 10kPa for making specimen identical. The results are compared using three kinds of diagrams, in which the v-log σ_n, log v-log σ_n, and log ε_v-log σ_n, relationships are depicted in Figures 4 (a), (b) and (c), respectively. Note that v is defined as specific volume which equals to (1+e) and ε_v is defined as natural volumetric strain, thus, a natural volumetric strain ε_v (compression positive) is given as a function of the specific volume such that:

$$\varepsilon_v = \int_{\varepsilon_{v0}}^{\varepsilon_v} (d\varepsilon_v) = -\int_{v_0}^{v} (dv/v) = -\ln(v/v_0) \quad (1)$$

with v_0 as strain origin. It should be emphasized that ε_v is directly related to the specific volume in Eq. (1).

It can be seen from these figures that both plots of the v-log σ_n and the log v-log σ_n relationships do not appear as a straight line irrespective of water contents, but the log ε_v-log σ_n, relationships for the specimen with different water contents can be regarded as straight lines. These straight relationships will be one of the key relationships in the empirical relationship of collapsible volumetric strains mentioned below. When focusing on the differences in water contents, the corresponding specific volume at a fixed normal stress becomes smaller as water content increases, and also the differences in specific volume tend to become smaller as normal stresses increase.

Strength and Dilatancy Characteristics

Based on the τ-Δh and ΔV_D-Δh relationships of Shirasu sandy soil used, Figures 5 and 6 are depicted by Hormdee et al. (2005a and 2005b). Figure 5 shows the relationships between normal stresses and shear stresses at peak state of the soil with three kinds of water contents. Then, Figure 6 shows the shear stresses at peak state normalized by the corresponding normal stress against the dilatancy index defined by $-(\Delta V_D/V_D)/(\Delta h/V_D)=-(\Delta V_D/\Delta h)$. From these figures, even though the failure envelope defined by the peak shear stresses

Figure 4 One-dimensional compression tests results with different initial water contents

is strongly dependent on the initial water contents as shown in Figure 5, the normalized failure shear stresses shown in Figure 6 is uniquely determined by the dilatancy index, irrespective of the initial water contents and normal stresses. Therefore, we can say that such unique relationship is effective and essential not only in the case of saturated specimen, but also in the case of unsaturated ones. Figure 7 shows the stress-dilatancy

Figure 5 Relationship between net normal stress and strength for compacted specimens with Dr = 65%
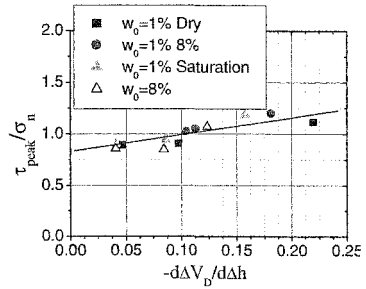
Figure 6 Relationship between dilatancy index and normalized peak strength

relationships of Shirasu sandy soil with different normal stresses, in which the normalized shear stresses, τ/σ_n, divided by the corresponding normalized stresses at peak state, τ_{peak}/σ_n, are used as a vertical axis. It should be emphasized that although there exists some scatter especially at low normalized stress ration, the normalized stress ratio, $(\tau/\sigma_n)/(\tau_{peak}/\sigma_n)$, against the dilatancy index, $-(\Delta V_d/\Delta h)$, is explained by a unique line, irrespective of normal stresses.

Empirical Relationship for Collapse Volumetric Strains

Basic idea for estimating compression curves. Volumetric strains ε_v under one-dimensional compressions for the Shirasu sandy soils with various initial water contents are simply assumed as a function of initial water contents, w_0, and normal stresses, σ_n, such that:
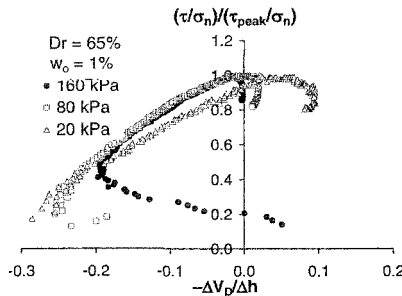
Figure 7 $(\tau/\sigma_n)/(\tau_{peak}/\sigma_n)$-$dV_D/dh$ relationships under various water contents and confining pressures

$$\varepsilon_v = f_1\!\left(\sigma_n, \; w_o\right) \tag{2}$$

Then, taking ε_v as the natural strain, a natural volumetric strain increment, $d\varepsilon_v$, is expressed as:

$$d\varepsilon_v = \frac{\partial f_1}{\partial \sigma_n} d\sigma_n + \frac{\partial f_1}{\partial w_0} dw_0 \tag{3}$$

When considering the compression curve without changes in water contents, that is, $dw_0=0$, Eq.3 becomes as follows:

$$d\varepsilon_v = \frac{\partial f_1}{\partial \sigma_n} d\sigma_n \tag{4}$$

In order to find a concrete function of f_1, the log ε_v-log σ_n, relationship is assumed to be linear as shown in Figure 4(c). Thus, based on such linear relationships, f_1 is derived as:

$$f_1 = k_a\!\left(\frac{\sigma_n}{\sigma_{n0}}\right)^l \tag{5}$$

where, k_a and l are defined as ε_v at $\sigma_n = \sigma_{n0}$, and the slope in log ε_v-log σ_n linear relationship, respectively, in which both parameters are clearly dependent on the water contents of soils. When introducing Eq.5 into Eq.4, $d\varepsilon_v$, is given by,

$$d\varepsilon_v = lk_a\!\left(\frac{\sigma_n}{\sigma_{n0}}\right)^l \frac{d\sigma_n}{\sigma_n} \tag{6}$$

which is a basic equation for estimating the natural volumetric strain increments under virgin loading process, where, l and k_a may be constant when at least initial water contents are constant. The effectiveness of this relationship for saturated sandy soils over
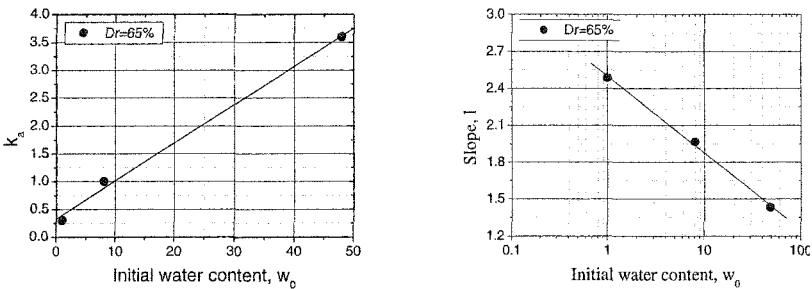
Figure 8 Characteristics of parameters needed; a) Parameter k_a-w_o relationships in the case of Dr = 65%, b) Parameter between slope l of log ε_v-log σ_n curves and w_o in the case of Dr = 65%
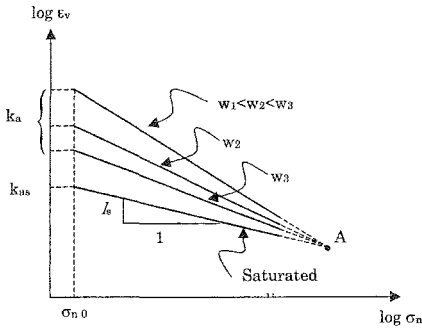
Figure 9 The schematic one-dimensiona compression curves

a wide stress region has been already reported by Yasufuku et al.,(1991). When the experimental parameters l and k_a are properly determined, Eq.6 seems to be effective in predicting the volumetric strains due to compression for sandy soils.

Estimation of collapse volumetric strain changes under one-dimensional condition. The experimental parameters l and k_a in Eq.6 are linked with the water

Figure 10 Effect of shear level of infiltration process; a) τ-dh relationships, b) dV_D–dh relationships , c) ε_v–dh relationships

content. Figures 8(a) and (b) show a typical k_a-w_0 and a l-logw_0 relationships of the Shirasu sandy soil used, respectively, which are obtained from the results in Figure 4(c). It is clear that both relationships indicate a good linearity. From these results, l and k_a are assumed to be expressed as a function of initial water contents such that;

$$l = l_0 + b \ln w_0 \tag{7}$$

$$k_a = k_{as}\left(\frac{k_{a0}}{k_{as}}\right)^{\frac{l_s-\{l_0+b\ln w_0\}}{l_s-l_0}} \tag{8}$$

where, w_0 is the initial water contents, k_{a0} is the value of k_a when w_0 becomes unit water contents, in this case, 1% was used, k_{as} is the value of k_a at saturated condition, l_0 is the value of l at unit value of w_0 in %, that is 1%, l_s is the value of l at saturated condition and also parameter b is a slope of l-ln w_0 linear relationship. It is important to explain that when Eq.8 is derived, the following assumption is used, that is, all the compression

curves for unsaturated specimen converge to the saturated compression curve, and also all the curves touch at a same normal stress, irrespective of the difference in water contents as shown in Figure 9. Actually, Figure 4 supports this idea. Then, introducing Eqs.7 and 8 into Eqs.5 and 6, f_1 and $d\varepsilon_v$ can be rewritten as:

$$f_1 = k_a \left(\frac{\sigma_n}{\sigma_{n0}} \right)^{(l_0 + b \ln w_0)} \tag{9}$$

$$d\varepsilon_v = (l_0 + b \ln w_0)(k_a) \left(\frac{\sigma_n}{\sigma_{n0}} \right)^{(l_0 + b \ln w_0)} \frac{d\sigma_n}{\sigma_n} \tag{10}$$

where, Eq. 8 is used in Eqs. 9 and 10. It is important to point out that Eq.10 may be useful in estimating one-dimensional compression curves not only for Shirasu soils with various initial water contents but also for the different kinds of sandy soils. In Eq.3, the collapsible volumetric strain increments due to soaking, which causes the changes of initial water contents, at constant normal stress is given by

$$d\varepsilon_v = \frac{\partial f_1}{\partial w_0} dw_0 \tag{11}$$

Introducing Eq.8 into Eq.10 and then after some calculations, the collapsible volumetric strain increment is given by the following equation.

$$d\varepsilon_v = \ln \left(\frac{\sigma_n}{\sigma_{n0}} \times \left(\frac{k_{a0}}{k_{as}} \right)^{\frac{l}{l_s - l_0}} \right)^{k_a \frac{b}{w_0}} \left(\frac{\sigma_n}{\sigma_{n0}} \right)^{(l_0 + b \ln w_0)} dw_0 \tag{12}$$

where, k_u is estimated by Eq.8. It should be emphasized that when a change of initial
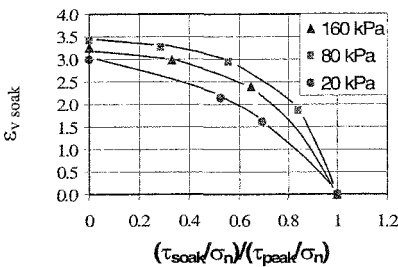
Figure 11 Relationship between $\varepsilon_{v\,soak}$ during soaking and normalized shear stress level $(\tau_{soak}/\sigma_n)/(\tau_{peak}/\sigma_n)$ at soaking
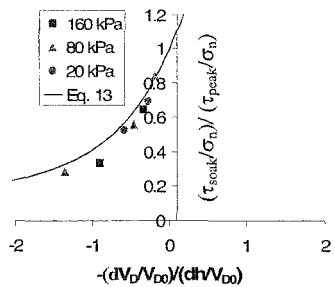
Figure 12 Relationship between $(\tau_{soak}/\sigma_n)/(\tau_{peak}/\sigma_n)$ and $-(dV_D/V_{D0})/(dh/V_{D0})$ during soaking process

water content is clearly known, Eq.12 is useful to estimate the collapse volumetric strain increment due to soaking. Note that Eq.12 may also have a limitation on the applicable normal stresses for predicting the collapse volumetric strains of unsaturated sandy soils. The applicability is limited within a normal stress in which the compression curves for unsaturated specimen touch with the curve for saturated ones as expected from the results shown in Figure 4(c). Thus, beyond such a limited normal stress, one-dimensional compression curves follow the saturated one, and thus, no collapsible volumetric strain is considered to occur in such stress region.

Effect of shear level at soaking on collapse volumetric changes. Figure 10 shows the effect of shear stress level under infiltration process on the collapse volumetric changes, in which; τ-δh relationships, ΔV_D-Δh relationships and -($\Delta V_D/V_{D0}$)- Δh relationships are depicted in Figures 10(a), (b) and (c), respectively. In this study, -($\Delta V_D/V_{D0}$) is assumed to be roughly equivalent as the volumetric strain during shear process. Thus for simplicity, term ε_v is used instead of term -($\Delta V_D/V_{D0}$) named as normalized vertical displacement. In these figures, the behaviors at soaking processes are indicated as the plots of marks. It is clear that the volumetric changes at soaking decreases with increasing shear stress level. On the other hand, the horizontal displacements increase with the increasing stress level at soaking. Where, shear stresses during soaking were always kept constant by automatically controlling a stepping motor shown in Figure 1. Figure 11 shows the relationship between $\varepsilon_{v\,soak}$ during soaking and the corresponding normalized shear stress level (τ_{soak}/σ_n)/(τ_{peak}/σ_n) with normal stresses of 20kPa, 80kPa and 160kPa. It can be seen that the incremental normalized collapsible vertical displacements non-linearly decrease with the increasing normalized shear stress level during soaking and also depend on the applied normal stresses. If such tendency could be properly expressed as a simple function for practical use, it must be effective in evaluating the collapse volumetric strains under an arbitrary shear stress level. Such trial will be considered as a next step.

Estimation of dilatancy properties at soaking without any stress changes. The dilatancy property at soaking process is shown in Figure 12, which is indicated as the relationship between the dilatancy index -$d(\Delta V_D/V_{D0})/d(\Delta h/\Delta V_D)$ at soaking and the normalized stress ratio defined by (τ_{soak}/σ_n)/(τ_{peak}/σ_n), where τ_{soak} is a shear stress τ at soaking. It should be noted that the dilatancy index at soaking is determined by assuming that the ΔV_D-Δh relationship at soaking process in Figure 12 can be approximated by a unique straight line. Therefore, one value of -$d(\Delta V_D/V_{D0})/d(\Delta h/\Delta V_D)$ under soaking process is obtained at a fixed stress level. It can be seen from this figure that the dilatancy index has a roughly unique relationship with the normalized stress ratio, irrespective of the applied normal stresses and the initial water contents.

Verification of Empirical Relationship Presented

Figure 13 shows the relationship between predicted and measured normalized collapse vertical displacements, which is equivalent to collapse volumetric strains, due to soaking at various σ_n under one-dimensional compression and the initial water contents. The experimental parameters used here in predictions are summarized in Table 2. It is found that the predicted results follow the experimental tendency that the normalized collapse vertical displacements decrease with the increasing initial water contents, and also the model can roughly predict the effect of the normal stresses on the collapsibility.

Conclusions

The main conclusions obtained are summarized as follows:
1) A direct shear box test apparatus with water content measurements due to probe equipments. It senses the volumetric water content by means of evaluating the changing of apparent dielectric constant. It has been found that the volumetric water content obtained for calibration process with this application is quite good.
2) The relationship between the natural volumetric strains and normal stresses in log scale at one dimensional compression of Shirasu sandy soils with different initial water contents are expressed as a linear relationship, which become a key characteristic for prediction of collapse volumetric strains. In this study, the collapse volumetric strains were considered to be equivalent to normalized collapse vertical displacement.
3) An empirical relationship for predicting the collapse volumetric strains at soaking for sandy soils under different normal stresses is derived on the basis of experimental data obtained. The model can rationally predict the collapse incremental volumetric strains with the changes of water contents and normal stresses.
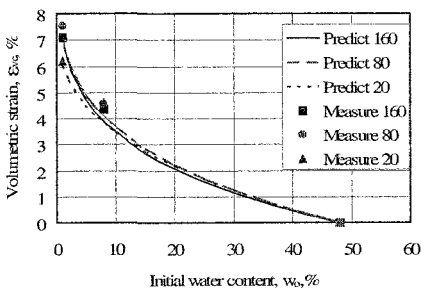
Figure 13 Comparison of predicted and experimental normalized collapse vertical displacement

Table 2 Summery of experimental parameters used

Parameter	Value
l_0	0.595
l_s	0.266
b	-0.085
k_{a0}	3.62%
k_{as}	0.268% at 1kPa
σ_{no}	kPa
w_{sat}	48%

4) The effects of shear stress level at soaking on the corresponding collapse volumetric strainare experimentally made clear. The collapse volumetric strains decrease with increasing shear stress level at soaking.

5) The dilatancy property at soaking is expressed as a unique relationship with the normalized stress ratio, irrespective of the applied normal stresses and the initial water contents. It is concluded that the relationship is effective in relating the collapse volumetric strains with the corresponding collapse shear displacement or strains under soaking process.

References

Chen, Z.-H. Fredlund, D.G. & Gan, J.K.-M. 1999 "Overall volume change, water volume change, and yield associated with an unsaturated compacted loess." *Can. Geotech. Journal,* 36: 321-329.

Designation: D5333-92(1996): "Standard Test Method for Measurement of Collapse Potential of Soils." *Annual Book of ASTM Standards,* Vol 04.08

El-Ehwany, M. & Houston, S.L. 1990 "Settlement and moisture movement in collapsible soils." *Jr. of Geotech. Division,* ASCE, 116(10): 1521-1535.

Fredlund, D.G., Morgenstern, N.R. & Widger, R.A. 1978 . "Shear strength of unsaturated soils." *Can. Geotech. Journal,* 15(3): 521-532.

Fredlund, D.G. & Rahardjo, R. 1993 *Soil Mechanics for Unsaturated Soils,* John Wiley & Sons, Inc., New York.

Fredlund, D.G. & Rahardjo, R. 1993 "The rule of unsaturated soil behaviour in geotechnical engineering practice." *11th SEAGC in Singapore* 37-49

Habibagahi, G. & Mokhberi, M. 1998 "A hyperbolic model for volume change behavior of collapsible soils." *Can. Geotech. Journal,* 35: 264-272.

Han, K.K. 1997 *"Effect of hysteresis, infiltration and tensile stress on the strength of unsaturated soil"* Ph.D.Thesis, School of Civil and Structural Eng., Nangyang Technological Univ., Singapore.

Hormdee, D., Ochiai, H. and Yasufuku, N. 2004 *"Influence of Stress History and Soaking Pressure on Collapsibility of Shirasu Soil" 15th SEAGC in Thailand* 31-36

Hormdee, D. Ochiai, H. and Yasufuku, N. 2005 *"Advance direct shear testing for collapsible soils with water content and matric suction measurement" Geo-Frontriers 2005 Conference in Texas*

Hormdee, D., Ochiai, H. & Yasufuku, N. 2005b. *"Direct shear and compression behaviors for an unsaturated compacted soil with water content and matric suction measurement" EXPRUS Conference in Trento (to be submitted).*

JGS 0561-2000 *"Method for consolidated constant pressure direct box shear test on soils"* Method and description of soil testing, Japan Geotechnical Society: 569-574

Nishimura, T. Hieabayashi, Y., Fredlund, D.G. & Gan, J.K.-M. 1998. "Influence of stress history on strength parameters of an unsaturated statically compacted soil." *Can.Geotec. Journal,* 36: 251-261.

Rampino, C., Mancuso, C. & Vinale, F. 1999 "Laboratory testing on an unsaturated soil: equipment, procedure, and first experimental results." *Can. Geotech. Journal,* 36: 1-12.

Tadepalli, R. & Fredlund, D.G. 1991 "The collapse behavior of a compacted soil during inundation." *Can. Geotech. Journa,l* 28: 477-488.

Yasufuku,N., Murata, H., Hyodo, M, and Hyde, A.F.L. 1991. "A stress-strain relationship for anisotropically consolidated sand over a wide stress region. "*Soils and Foundations,* 31, 4, 75-488.

Study of the Infiltration of Water Through Collapsible Soil

F.M.Abdrabbo and T.M.Abdelaziz

Structural Engineering Department, Faculty of Engineering, Alexandria University, Egypt, 21544

Abstract

Laboratory infiltration tests have been performed to predict the extent of wetting zone within a collapsible soil. During these tests, the rainfall water was simulated in laboratory to investigate the infiltration of rain water around and beneath a footing model resting on collapsible soil. Distribution of soil water content beneath and around the footing model was assessed. Consequently, accurate details of the progression of wetting zone front were also measured. The effect of the relative density of the formed soil, the initial water content of soil, and the intensity of induced water are studied. A relationship between depth of wetting zone and time was established, and a proposed mathematical formula for predicting the optimum depth of wetting zone is presented.

Introduction

Collapsible soils are covering vast areas of many arid and semi-arid countries. Particularly in Egypt, they are widely distributed throughout the Egyptian western desert. Predicting of collapse settlement forms an important aspect of engineering practice. El-Ehwany and Houston (1990) reported that high-quality prediction of collapse settlement depends strongly on an accurate estimate of the depth of the wetting zone. So, the attentions of many researches were given to that depth. In fact, several studies have been conducted to determine the depth of wetting zone. Mohamed, 1998 and Reznik (1992) quoted that Gardner and Widtsoe (1921) reported a parabolic relationship between the moisture movement (infiltration) in soils and the time. They reported that the depth of the wetting zone (d) depends on the initial water content of soil. Also, Mohamed, 1998 and Reznik (1992) reported that Ostashev (1939) proposed a relationship to describe the advancement of the wetting zone in soil. Later, Houston (1992) quoted that El-Ehwany and Houston (1990) reported that the combined influence of suction and gravity gradient causes

the water infiltration through the soil. El-Ehwany and Houston (1990) developed laboratory one-dimensional infiltration tests to determine the partially saturated flow characteristics through collapsible soils.

Walsh et al (1993) developed suction contours for a site to evaluate the extent of soil wetting. The underlying soils at the site were highly variable in fine content. A method of producing suction values from the geotechnical testing results was reported. They reported that the most important aspects in wetting sensitive soil are the source of water and the extent of wetting. Sources can be quantified from records. But the extent of wetting can be measured rather predicted.

The paper presents the outcome results from a part of a testing program set-up to investigate the depth of the wetting zone due to infiltration of rainfall water, i.e due to limited source of water, through a collapsible soil. Accurate description of the wetting zone, with time, beneath and around an existing unloaded footing was obtained through the distribution of soil water content and suction with depth. The achieved test results were used to study the effect of soil properties such as relative density, initial water content of soil, and the intensity of rainfall on the depth of wetting zone front. Also, the depth of the wetting zone front versus time relationship was explored.

Testing Set-up and Material

The testing set-up, shown in figure (1), consists of soil bin, elevated water tank, plastic pipes, water distribution steel grid, nonwoven geotextile and footing model. The soil bin was made of transparent walls machined from perspex and stiffened by steel angles. The bin walls of thickness 6 mm were braced laterally with rolled section of steel angles. The bin base was machined from prespex of 12 mm thickness. The water tank was machined from stainless steel plates of 1 mm thickness. The tank's base was adjusted perfectly in a horizontal position and thirty six copper nozzles of 3 mm internal diameter were fixed to the water tank base. In order to simulate rainfall water, the nozzles were connected to thirty-six flexible plastic pipes of 6 mm inner diameter and had the same length and the pipes were attached at the other ends to thirty-six copper nozzles fixed to the water distribution steel grid, resting on top edges of the soil bin.

During tests, the steel grid was placed horizontally on top edges of the soil bin. A square steel plate of dimensions 80×80 mm and 10 mm thickness, which used as a footing model, was placed accurately at the center of soil bin. The footing model was not subjected to any loads. The collapsible soil had a natural water content of 2.1% and was classified as CL based on the Unified Soil Classification System , and as A-6 according to AASHTO soil classification system. The soil, which is collapsible in nature (Mohamed ,1990), was imported from Borg-Elarab city,60 kms. South-West of Alexandria city, in the Egyptian western desert. The grain size distribution curve of the soil was constructed and from which; $D_{10\%}$ = 0.0015 mm, % of fine (passing sieve No. 200) = 67.8 % , uniformity coefficient (c_u) = 42.06 ,

and coefficient of curvature (c_c) = 4.48. Atterberg's limits were also determined, w_L = 30.0 % , w_P= 18.0 % , and P.I. = 12.0 % . These tests were carried out following ASTM standard D422 and D4318. To form the soil in the soil bin, the required weight of oven dried soil assigned for the required relative density was determined, using a balance of 5 gm accuracy. The soil was mixed with the required amount of water to achieve the desired initial water content. The soil was placed in soil bin in six layers each of 50 mm thickness and compacted using a steel tamper weighing 20 N to achieve the desired relative density. The upper surface of soil was adjusted in an accurate horizontal level using a spirit level. The levelling of soil surface is very important to get a uniform distribution of water when allowed to seep. Two sheets of nonwoven geotextile (A301) of 2.5 mm thickness were placed on the soil surface during tests to act as filter and distributor when water was supplied from source to the soil and to prevent any possible erosion in soil surface. The geotextile sheets had a coefficient of permeability of 2.5 mm/sec and transmissivity of 170 L /m/h.
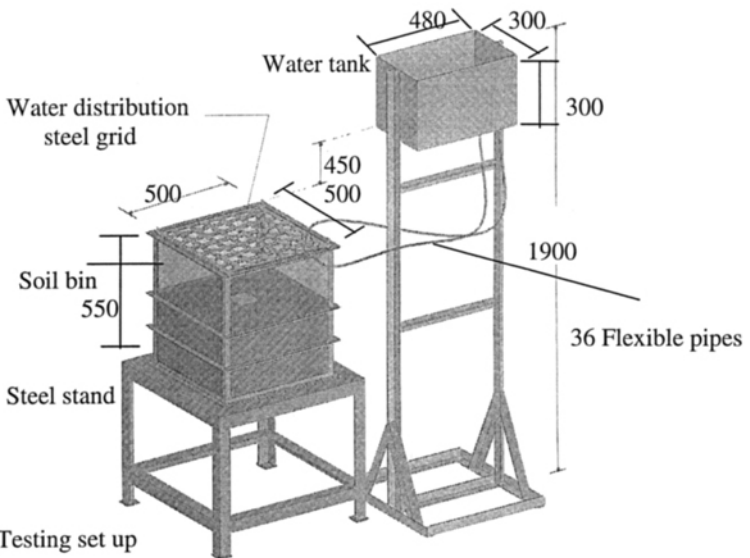
Figure 1. Testing set up

Testing Procedure

Forty two tests were conducted to investigate the effects of initial water content of soil, relative density and amount of induced surface water on soil suction and the progression of wetting zone front. In each test, the soil was formed at the required properties and the footing model was placed accurately at the center of soil bin. The required amount of water was allowed to seep on the soil surface via the flexible pipes. As the soil surface was below the top edges of the soil bin by 250 mm, the water flowing from water tank, via the plastic pipes, was sprinkled uniformly on soil surface simulating rainfall. The uniformity of sprinkling water on soil surface was ensured by , equal length and diameter of the flexible pipes

connecting the inlet and outlet nozzles, equal diameter of inlet and outlet nozzles , uniform distribution of outlet nozzles on soil surface , and finally placing tow nonwoven geotextile sheets on soil surface. The sheets of nonwoven geotextile were immersed in distilled water for two hours until saturation, and then placed on the soil surface. To avoid water evaporation during the running of test, the soil was covered by an impermeable plastic sheet. But during the time of inducing water onto soil surface, the evaporation effect was neglected because this process took a very short time (about 1 minute for most tests). The required amount of induced water was prepared by weighing the water using a balance with accuracy of 5 g, considering the unit weight of water equals 1.0 g /cm^3 and neglecting the correction factor of temperature. The amount of water placed in water tank was completely induced to the soil. For each test, the water was allowed to seep through the soil to a specified elapsed time. For each studied parameter, six tests were carried out for elapsed time of 30 mins, 1 hr., 24 hrs., 48 hrs., 120 hrs. (5 days), and 336 hrs. (14 days). After an elapsed time from allowing the water to seep through the soil, that is to say from the commencement of test, the footing model was taken out and a vertical cut was made just below the center-line of the footing model through the total thickness of the formed soil using a trowel and a spirit level to adjust the verticality of the cut. Then, soil samples were taken for water content determination from different locations along the vertical cut to assess the distribution of water content. The locations of soil samples were measured using a stainless steel scale of accuracy 1 mm.

In order to determine the soil water content, special home-made samplers were used. The samplers were machined from copper and had a height of 15 mm, 8 mm inner diameter and 10 mm outer diameter. Twenty six samplers were used to recover soil samples in order to decrease the time of sampling. So, the ambient temperature effect was minimized on soil water content. Nevertheless, the tests were carried out in relatively humid room. The samplers were pushed horizontally in the vertical cut to a depth of 15 mm to recover soil samples. The samplers were pushed immediately after the cut was formed. The process of recovering soil samples was last for about 3 to 7 minutes, then; the samplers were pulled out with the retained soil. The recovered samples had a weight varied from 1.0 g to 7.0 g. Standard method for water content determination was implemented using a balance of 0.01 g accuracy for weighing the soil samples. It was noticed that there was no water head above the soil surface when the amount of induced water equals 0.0025 m^3, but in case of 0.005 m^3 induced water, there was a head of 8 mm and decreased gradually to zero within 4 minutes. Also, in case of 0.0075 m^3 induced water, there was a head of 18 mm and decreased gradually to zero within 11 minutes. So, it can be reported that for all performed tests, the amount of water induced from source was limited. Soil samples were, also, taken using the oedometer cutter ring for the determination of the soil suction at different depths. Measurements of both total and matric suction were done using the filter paper method following ASTM D5298-94. The same procedure was implemented by Sivakumar et al (2005). Filter papers used in the performed tests were Whatman No.42 with diameter of 90 mm. The obtained values of water content and corresponding values of soil suction were used to construct the soil-water characteristic curve (SWCC) of the studied cases.

Test Results

Details of wetting zone. Figures (2) and (3) illustrate the test results of a group of six tests where the initial dry unit weight of soil 13.57 kN/m^3 , relative density 43.55% and amount of induced water equal to 0.0025 m^3. Figure (2) shows that the wetting zone front was not horizontal in the early stage of infiltration due to the existence of footing model. The induced water seeps downward under the effect of gravity and suction potential while seeps horizontally under the effect of suction gradient only. This stage of combined seepage, horizontally and vertically, took a limiting time up to 48 hrs. to get a uniform horizontal water front. The limiting time and the rate of wetting zone front progression depend on the void ratio of soil, the intensity of induced water (Qw), and the suction gradient. To interpret the achieved test results, it is useful to review the rules governing the water flow through unsaturated soil. In homogeneous, isotropic soil, water flows through unsaturated soil if there is water content gradient, matric suction gradient, or hydraulic head gradient. These gradients may be considered as driving potential causes flow (Fredlund and Rahardjo, 1997). Thus, water flows from a point of higher water content to a point of lower water content. Also, a matric suction gradient has sometimes been considered to be the driving potential for water flow. But these two concepts sometimes are not valid. In unsaturated soil, water flow can be defined more appropriately in terms of a hydraulic head gradient (i.e, pressure head and elevation head). In the special case, where the air pressure gradient is zero and this is the common situation in nature (Fredlund and Rahardjo, 1997), the matric suction gradient is numerically equal to the pressure gradient in the water.

The flow of water in a saturated soil is commonly described using Darcy's law. For saturated soil, the coefficient of permeability (Ks) is constant. Fredlund and Rahardjo (1997) quoted that (Buckingham, 1907; Richared , 1931; Childs and Collis George,1950) reported that Darcy's law also could be applied for the flow of water through an unsaturated soil.

As the coefficient of permeability in unsaturated soil (k$_w$) is mainly function of water content, the matric suction, and void ratio of soil, the coefficient (k$_w$) can not be assumed constant. Fredlund and Rahardjo (1997) quoted that El-zeftawy and Cartwright (1981) mentioned that the coefficient of permeability in an unsaturated soil (K$_w$) is directly proportional to the water content of soil and subsequently is *inversely proportional to the matric suction of soil. It is noticed from figure (2) that* the rate of infiltration was initially rapid and gradually decreased. This is because the quantity of induced water is constant, then the magnitude of water content and the water content gradient decreased as the wetting zone front went deeper into the soil. Also, it should be realized that as the wetting zone front went deeper into the soil, the gravitational head acting at a point on wetting zone front decreased. In addition, the pore-water pressure decreased as the water content decreased. As a result, the energy driving the water in wetting zone decreased and consequently the water velocity decreased. It was noticed that at early stage of infiltration, the water

content gradient just above the wetting zone front was too high compared to the later stage of the test. Also, the gradient of water content versus depth lines reflected the water velocity which decreased with the elapsed time from commencement of test (Abdelaziz, 2006). Figure (3) indicates that at a point within the soil above the wetting zone front, the matric suction increased with the elapsed time, while reflected a decrease in pore-water pressure as the water content decreased. Also, the figure confirmed that the suction gradient decreased with the elapsed time which reflected the decrease in water infiltration velocity with time. Figure (3) indicates that at early stage of tests, up to 48 hrs., there is a transition zone near the wetting zone front where the gradient in water content and matric suction is very high. Thus, the infiltration process was characterized by relatively sharp fronts of water movement. This finding confirmed previous results reported by El-Ehwany and Houston (1990).
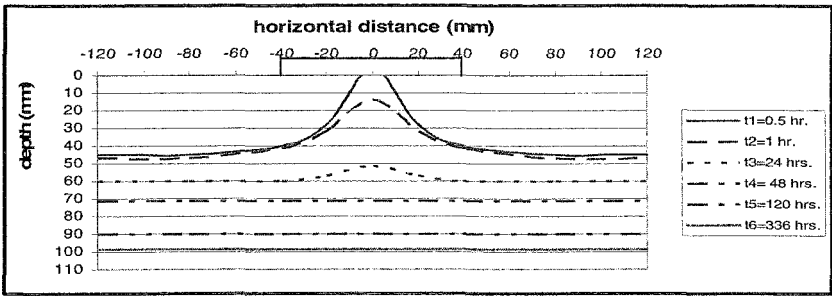
Figure 2. Progression of wetting zone front with time
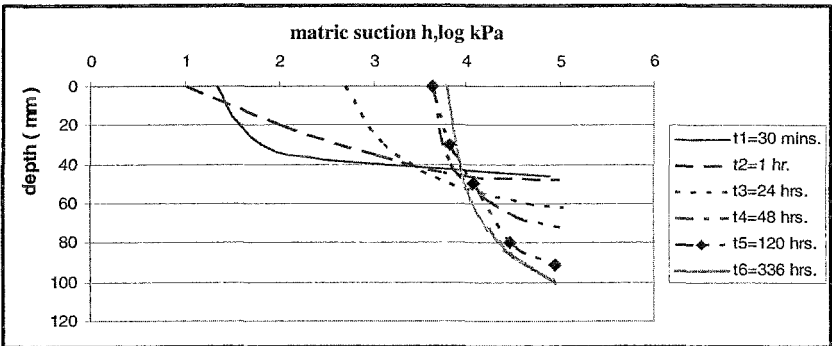
Figure 3. Values of matric suction versus depth at different elapsed times

Figure (4) demonstrates the effect of relative density of soil on the rate of water infiltration through soil, in which, the figure presents the matric suction of soil at early stage and later stage of test. The shown results confirmed that the matric suction of soil decreased as the relative density of soil decreased. But it is interesting to note that the infiltration velocity of water at wetting zone front decreased as the relative density of soil increased. The reason may be due to that the suction gradient which governs the movement of water at wetting zone front was increasing with the

decrease of relative density of soil. In figure (5), the effect of induced surface water intensity is clear in a way that the larger amount of induced water results in a faster infiltration of water. It is expected that as the amount of induced surface water increased, the degree of saturation of the top portion of soil increased. Thus, it is expected a higher infiltration velocity of wetting zone front at early stage and later stage of infiltration test. Also, as the water content increased, the matric suction decreased. One can observe from figure (5) that as the amount of induced water increased, the inundated volume of soil didn't increase by the same rate. As a result, the volumetric water content increased but not in a linear function as the induced amount of water increased. So, it is expected, also, that the pore-water pressure increased. As a result, the matric suction gradient across the wetting zone front increased as the amount of induced water increased and consequently an increase in infiltration velocity at wetting front. Figure (5) indicates that as the amount of induced water increased from 0.0025 m^3 to 0.0075 m^3, the volume of wetting zone increased 2.5 times the value corresponding to the case of 0.0025 m^3. So, the pore-water pressure in soil increased but not linearly with the amount of induced water due to water adhering with soil particles. As a result, the velocity of water infiltration at wetting zone front increased with the increase of the amount of induced water but with a decreasing rate.
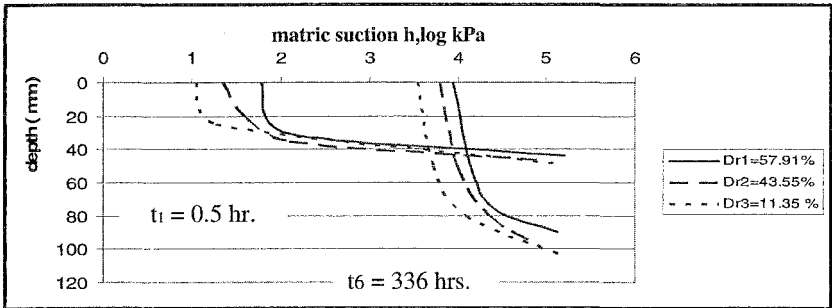
Figure 4. Distribution of matric suction with depth
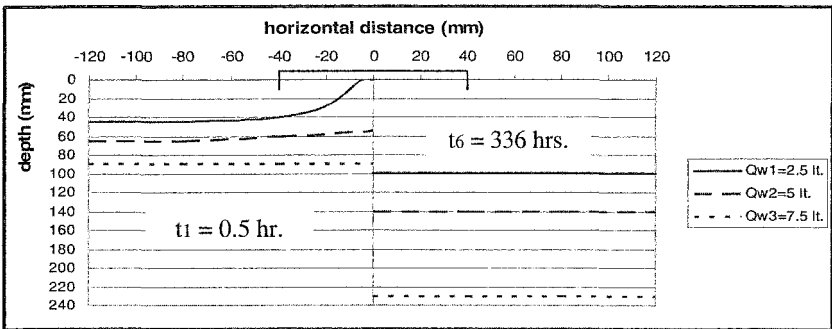
Figure 5. Effect of the intensity of induced water (Qw) on the progression of wetting zone front

The effect of initial water content of soil is shown in figure (6). The depth of wetting zone front increased with the increase of the initial water content of soil. This can be explained as the initial water content increased the amount of air in soil pores decreased and then, the coefficient of permeability increased. In an unsaturated soil, the coefficient of permeability is significantly affected by combined changes in the void ratio and the degree of saturation of soil. Fredlund and Rahardjo (1997) quoted that Brooks and Corey (1964) reported that in an unsaturated soil, the coefficient of permeability (K_w) can be predicted from the matric suction versus degree of saturation curves as follows:

$$K_w = K_s.(S_e)^\delta \qquad\qquad (1)$$

where:

δ = an empirical constant related to the pore size distribution ,

S_e = the effective degree of saturation which can be determined from the matric suction versus degree of saturation curve.

So, it is expected that water infiltrates the soil faster in case of higher initial water content. The figure indicates that the matric suction decreased as the initial water content increased. It was established that the increase in water content results in an increase in pore-water pressure (u_w) and a decrease in matric suction (Fredlund and Rahardjo, 1997). Also, as the water content increased, an increase in the coefficient of permeability is observed. The result is an increase in water infiltration velocity. So, the gradient in matric suction along the wetting zone front increased as the initial water content decreased.
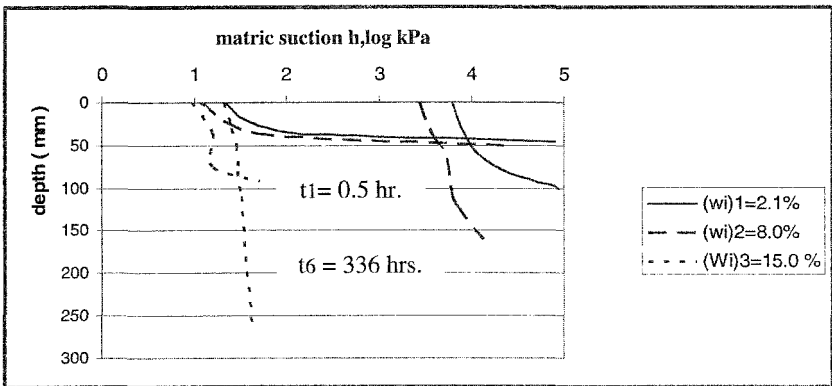
Figure 6. Distribution of matric suction with depth

Relationship between (d_{max}) and time . To achieve the optimum inundation depth of soil (d $_{opt.}$), which is corresponding to an equilibrium condition of water content along the inundated depth , a long time is required for running the infiltration test. Herein a procedure for the determination of (d $_{opt.}$). From test results, the maximum depth of the wetting zone front, measured away from the footing, was recorded after elapsed time of (0.5, 1, 24, 48,120,336 hrs.) while there was no head of water above soil surface. Relationships between time (t) versus (d_{max}) are constructed for all test

results. Figure (7) shows an example of these relationships. The mathematical relationship between (t) versus (d_{max}) was assumed hyperbolic. In other words, the relationship between (t/d_{max}) versus (t) is linear. It's worth mentioning that El-Ehwany and Houston (1990) proposed a parabolic function to relate between time and depth of wetting zone front in case of ponded water (i.e. water head above soil surface was existed) .

The hyperbolic relationship between (t) and (d_{max}) has a limiting horizontal line corresponding to a value of the optimum depth of wetting zone (d $_{opt.}$) which can be determined as:

$$d_{opt.} = 1 / \tan \theta \qquad (2)$$

where:

$d_{opt.}$ = the optimum depth of wetting zone .

$\tan \theta$ = the slope of straight line which relates (t) versus (t/d_{max}) .
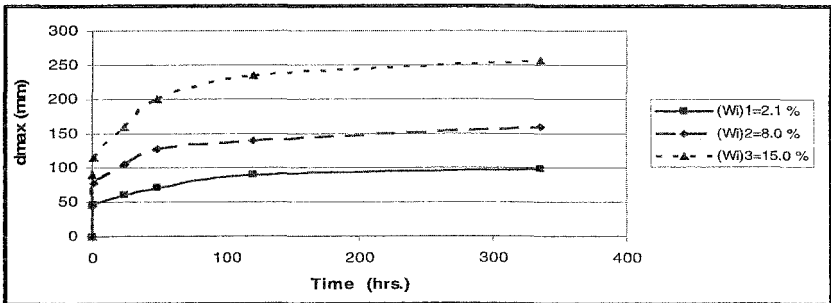
Figure 7. Relationship between (dmax) and (t) for different values of initial water content of soil

The straight line relationships between (t) versus (t/d_{max}) were constructed, figure (8). For the best fitting, the relationship may be consisted of two intersecting straight lines. The slope ($\tan \theta$) of the upper part of the relationship appears to be more accurate for determining ($d_{opt.}$).
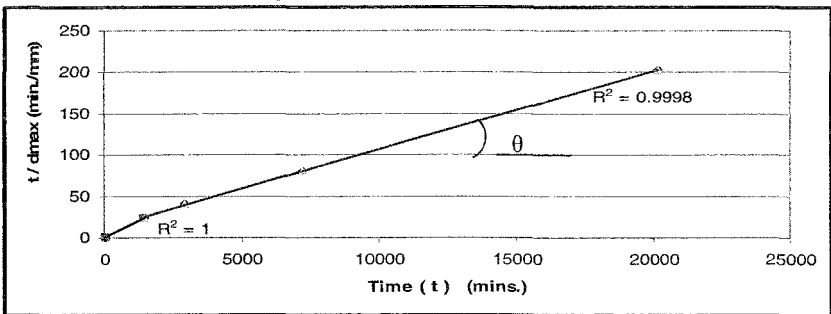
Figure 8. Relationship between (t) versus (t/d max)

In this case, the mathematical relationship between (t) and (t/d_{max}) for the upper part can be written as:

$$t = A (d_{max}) / [1 - \tan \theta (d_{max})] \qquad (3)$$

A   a fictitious value represents the interception of the straight line with t/d_{max} axis and was found to be equal to 11.572 min./mm

Theoretically, the time (t) corresponding to ($d_{opt.}$) is infinity, but time (t) corresponding to (0.99 $d_{opt.}$) may be obtained from equation (3) by substituting d_{max} equals to (0.99) of ($d_{opt.}$).

Calculation of ($d_{opt.}$). The predicted value of ($d_{opt.}$) was found to be directly proportional to the intensity of induced surface water (Q_w) and the initial water content of soil (w_i) and inversely proportional to the initial dry unit weight of soil ($\gamma_{d.in}$) (Abdelaziz , 2006). Consequently, the optimum inundation depth may be expressed as:

$$d_{opt.} = \alpha (e)^{\beta.X} \qquad (4)$$

in which:

$$X = [(\sqrt{w_i}) . (Q_w)] / (\gamma_{d.in})$$

where:

$d_{opt.}$ = the expected optimum depth of wetting zone in (mm), e = the natural log base, wi = the initial water content of soil (%) , $\gamma_{d.in}$ = the initial dry unit weight of soil (kN/m^3) , Qw = the intensity of induced surface water (cm/unit area) , and α , β constants depend on the initial dry unit weight of soil, initial water content of soil and the intensity of induced surface water.

For all studied cases, the relationship between ($d_{opt.}$) and (X) was drawn, figure (9). A unique relationship was found and then the values of α, β were obtained and found to be equal to (61.607) and (4.6516) respectively. The optimum inundated depth may depend upon the percentage of fine in soil and this point is under studying.
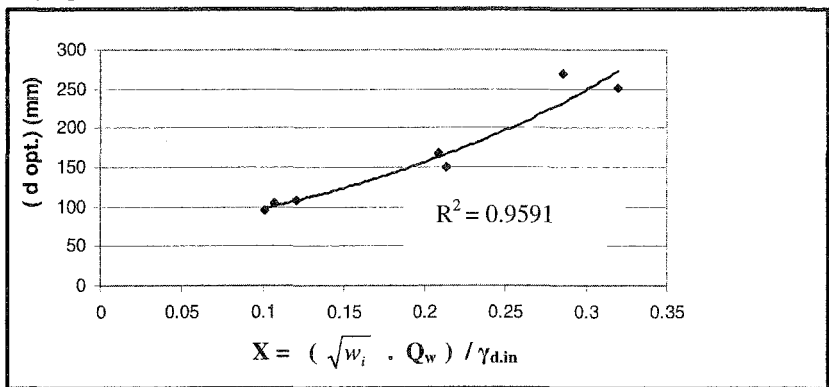
Figure 9. Relationship between predicted (d opt.) and the initial water content of soil, initial dry unit weight of soil ,and intensity of induced water

To evaluate the accuracy of the proposed formula, the values of (α, β, wi, $\gamma_{d.in}$, Qw) of all cases were used to calculate the values of ($d_{opt.}$) for the studied cases. A comparison between the predicted values of ($d_{opt.}$), equation (2), which are based on the experimental results and the calculated values which are based on the proposed formula, equation (4), was made, table (1). The ratio (R) between the two values varies form (0.862) to (1.108).

Table 1. Values of predicted and calculated ($d_{opt.}$) and the ratio (R).

Test group No.	1	2	3	4	5	6	7
Calculated value of ($d_{opt.}$) (mm)	98.35	101.24	108.04	162.44	232.38	166.38	273.42
Predicted value of ($d_{opt.}$) (mm)	95.5	104.9	108.8	167.2	269.2	150.2	250.6
R	1.029	0.965	0.993	0.972	0.862	1.108	1.091

Conclusions

The main conclusions drawn from the reported study are given below:

The wetting zone front beneath and around an existing footing during the early stage of infiltration is not horizontal. After a limiting time from the commencement of infiltration test, the wetting zone front becomes horizontal. The limiting time of the early stage of infiltration depends upon the soil properties and may be on the footing size.

The progression rate of the wetting zone front is directly proportional to the intensity of induced water (Q_w) and the initial water content of soil (w_i), and inversely proportional to the relative density of soil (D_r).

In case of induced water, simulated to a rainfall, the relationship between maximum depth of wetting zone front (d_{max}), away from the footing, and time (t) may be a hyperbolic and the optimum depth of wetting zone front equals to ($1/\tan\theta$) where ($\tan\theta$) is the slope of the straight line relating (t) versus (t/d_{max}).

The optimum inundated depth ($d_{opt.}$) is directly proportional to the intensity of induced water (Q_w) and the initial water content of soil (w_i), and inversely proportional to the relative density of soil (D_r).The authors proposed a mathematical formula to calculate the value of (d_{opt}).

The matric suction gradient at the wetting zone front is directly proportional to the intensity of induced water (Q_w) and inversely proportional to the relative density of soil (D_r) and the initial water content of soil (w_i).

References

Abdelaziz, T.M. (2006). Response of shallow foundations resting on collapsible soil, forthcoming Ph.D. dissertation, Alexandria University .

ASTM Standard D422-94: Standard Test Method for Particle-Size Analysis of Soils, Annual Book of ASTM Standards, ASTM International.

ASTM Standard D4318-94: Standard Test Method for Liquid Limit, Plastic Limit, and Plasticity Index of Soils, Annual Book of ASTM Standards, ASTM International.

ASTM Standard D5298-94: Method for Measurement of soil Potential (suction) Using Filter Paper, Annual Book of ASTM Standards, ASTM International.

El-Ehwany, M. & Houston, S.L. (1990). Settlement and moisture movement in collapsible soils, Journal of Geotechnical Engineering, vol.116, No.10 pp.1521-1535.

Fredlund, D.G. & Rahardjo, H. (1997). Soil mechanics for unsaturated soils, A Wiley- Interscience publication .

Houston , S.L. (1992) .Partial wetting collapse prediction ,7th Int. conference on expansive soils, vol.1 ,pp. 302-306.

Houston , S.L. & Hisham H.H. Mahmoud & William N. Houston (1995). Down-Hole collapse test system , Journal of Geotechnical Engineering , vol.121, No.4 ,pp.341-349.

Mohamed,K.M. (1998). Response of foundation on collapsible soil, A thesis submitted to Alexandria University in partial fulfillment of requirements for the M.SC.

Reznik, Y.M. (1992). Discussion on "Settlement and moisture movement in collapsible soils", Journal of Geotechnical Engineering, vol.118, No.4 ,pp.656-658.

Sivakumar Babu, G.L. & Peter, J. & Mukesh, M.D. & Gartung, E. (2005). Significance of Soil Suction and Soil Water Characteristic Curve Parameters, Geotechnical Testing Journal, Vol.28, No.1,pp.1-6.

Walsh, K.D & Houston W.N. & Houston S.L.(1993). Evaluation of in-place wetting using soil suction measurements, Journal of Geotechnical Engineering, vol.119, No.5 ,pp. 862-873.

Pavement Engineering Parameters for Thai Collapsible Soil

D. A. Cameron[1] and R. Nuntasarn[2]

[1]Senior Lecturer, School of Natural and Built Environments, University of South Australia, Mawson Lakes, SA 5095; PH (61) 8 8302 3128; FAX (61) 8 8302 5082; email:Donald.Cameron@unisa.edu.au
[2] Ph.D. student, School of Natural and Built Environments, University of South Australia, Mawson Lakes, SA 5095; PH (61) 8 8302 3453; email: Ratamanee.Nuntasarn@postgrads.unisa.edu.au

Abstract

This paper presents an investigation of the potential of collapsing soil or loess from Thailand for possible use as a pavement material or subbase. Earlier studies indicated high CBR values for well-compacted material. The collapsing soil is classified as silty sand, with a slight to moderate degree of collapse index. Thai collapsible soil samples were tested generally in the compacted condition (Modified compaction) at optimum moisture content and maximum dry density. Consolidated Isotropic Undrained (CIU) triaxial testing with pore water pressure monitoring was performed on back-saturated samples to quantify the permissible stress states for resilient modulus testing. The resilient modulus of the soil was found to be stress dependent and trends agreed reasonably well with the current AASHTO empirical equation for the resilient modulus of sand.

Introduction

Khon Kaen is a province of North-Eastern Thailand, which is on a high plateau (the Khorat), 100 to 200 m above mean sea level. Khon Kaen is an inland province, which is surrounded by Udon-Thani, Loei and Nong-Bua-Lam-Phu in the north, Nakhon-Rachasima and Buri-Ram in the south, Kalasin and Maha-Sarakham in the east, and Chaiyaphum and Phetchabun in the west. The Phetchabun and Phu-kra-deung mountain ranges are on the western side of Khon Kaen, while a river basin

is located on the eastern and south-eastern sides. The climate of Khon Kaen is Tropical Savannah. The average temperature, rainfall and water evaporation intensity between 1971 and 2000 were approximately 26.8°C, 1210 mm and 1802 mm, respectively (Meteorological Department 2004). Collapsible soil behavior is common in Khon Kaen in deposits of Aeolian (wind-blown), either yellow or red, silty sand.

The strength of undisturbed Khon Kaen loess has been evaluated by Udomchoke (1991) based on unconsolidated undrained (UU) triaxial testing. The results revealed that both the apparent cohesion and internal friction angle of the soil decreased upon wetting, as shown in Figures 1 and 2. The trendlines indicate that the soil at 5% moisture content has a friction angle greater than 25° and an apparent cohesion above 30 kPa. However if the soil is wetted to moisture content of 15% or more, the friction angle is likely to be between 5 and 10°, while the cohesion will drop below 10 kPa.

Udomchoke (1991) also determined the collapse index of red and yellow Khon Kaen loess from double oedometer testing; the collapse index, I_c, is the differential settlement between the wet and dry samples at a vertical pressure of 200 kPa. The average of his oedometer results indicated a severe degree of collapse for dry red loess (collapse index of 18 % at 2.4% moisture content and dry density of 14.8 kN/m^3), and a moderately severe degree of collapse for yellow loess (collapse index of 8.7% at 2.6% moisture content and 15.7 kN/m^3 dry density). Udomchoke investigated the influence of initial moisture content on collapse index. As expected the collapse index decreased as the initial moisture content increased, as shown in Figure 3 (the initial dry density was kept constant).
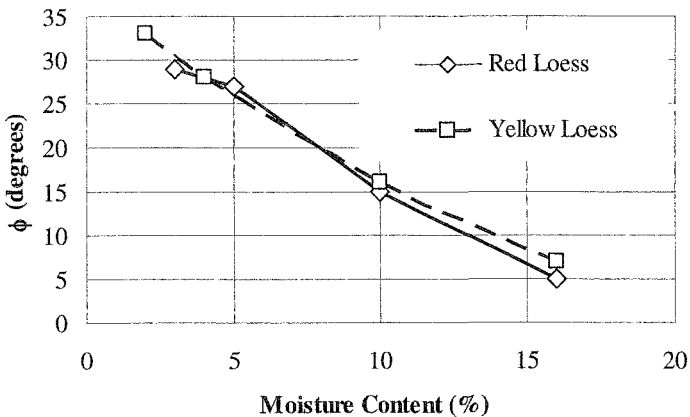
Figure 1. Variation of the friction angle of Khon Kaen loess with moisture content (Udomchoke 1991)
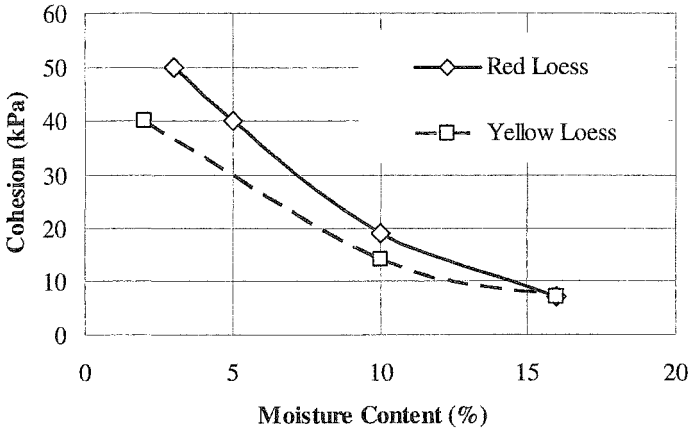
Figure 2. Variation of the cohesion of Khon Kaen loess with moisture content (Udomchoke 1991)
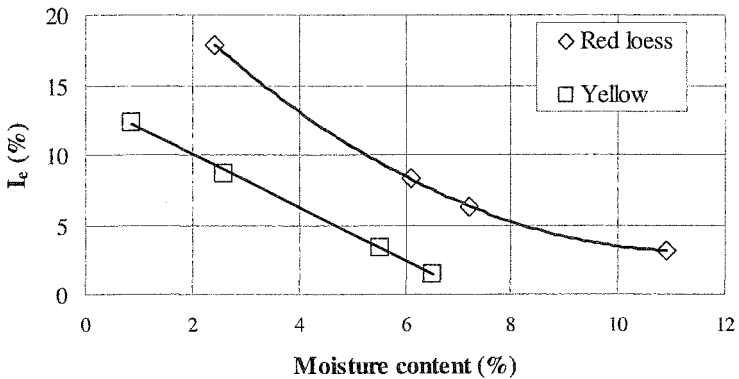
Figure 3. Variation of collapse index of Khon Kaen loess with initial moisture content (Udomchoke 1991)

Basic properties

The basic properties of the red Khon Kaen loess sample in this research program are presented in this section, in terms of soil particle size distribution, specific gravity, calcium carbonate content, salinity and pH. The soil particle size distribution of red Khon Kaen loess was determined by wet sieve analysis and hydrometer testing. Dry sieving was found to significantly under-predict the fines content of the soil.

The wet sieve analysis indicated a composition of 17% clay, 29% silt and 52% sand. Subsequently this collapsible soil can be classified as a sandy loam after USDA, or silty sand (SM) after ASTM.

The liquid limit and plastic index of the fines were 13.4% and 0.0%, respectively. The specific gravity of Khon Kaen loess is 2.65.

Unlike South Australian collapsing sands, there was no calcium carbonate present in the soil ($CaCO_3$) (Cameron, Nuntasarn and Gasaluck 2005). The calcium carbonate contents were tested by measuring the pressure of carbon dioxide (CO_2), generated from the reaction between hydrochloric acid (HCl) and calcium carbonate ($CaCO_3$) (ASTM D4373-96).

The degree of salinity of Khon Kaen loess was evaluated by testing the electrical conductivity of 1:5 soil-water suspensions ($EC_{1:5}$). Typically, the degree of salinity of a soil is based on the electrical conductivity of saturated paste (EC_e). The conversion factors of Northcote (1979) were used to estimate EC_e from $EC_{1:5}$, based on the soil texture. A conversion factor of 13.8 was selected. Since $EC_{1:5}$ was 0.11 ds/m, the estimated value of EC_e was 1.5 ds/m. This level of conductivity indicates a non-saline soil.

The results of evaluations of both the $CaCO_3$ and soil salinity were in agreement with the pH value of 6, which was in the moderately acid range.

Engineering properties

Samples were tested to determine engineering properties, which included pressure plate testing to evaluate the gravimetric soil moisture characteristic, double oedometer testing for collapse potential, consolidated-undrained triaxial tests on back-saturated specimens for shear strength evaluation, California bearing ratio and resilient modulus testing. Unless otherwise specified, all samples were compacted with Modified compactive effort, at optimum moisture content (8.5%) and maximum dry density (2.09 t/m^3).

Pressure plate. The drying soil water characteristic curve (SWCC) of compacted Khon Kaen loess was determined in a 1500 kPa pressure plate device (ASTM D2325-98). The available pressure system was capable of achieving soil matric suctions between 25 and 1000 kPa.

Two samples of compacted Khon Kaen loess were constrained by sample rings and filter paper was placed under each sample to catch loose soil grains. The initial density and moisture content of each sample were determined. Prior to applying air pressure in the chamber above the plate, samples were soaked for 3 days, and were weighed thereafter. The samples were then conditioned or desaturated by applying an air pressure of 25 kPa within the chamber. The mass of each sample was measured until the mass change was considered negligible, indicating equilibrium between the

soil and the imposed equivalent matric suction of 25 kPa. The process was repeated with an increased air pressure level until the final matric suction of approximately 1 MPa was reached. Once the test was completed, the final moisture content of both the samples and the filter papers were determined to back-calculate the water content of the soil specimen at all other values of matric suction.

Soil mass changes were derived from the total change in mass of filter paper and soil and the moisture content - matric suction relationship for the filter paper. The results are provided in Figure 4. The plot assumes a matric suction of 1 kPa for the saturated state for convenience for plotting the SWCC on a log suction scale. The rate of change of moisture content was found to be almost negligible as matric suction was increased above 50 kPa.
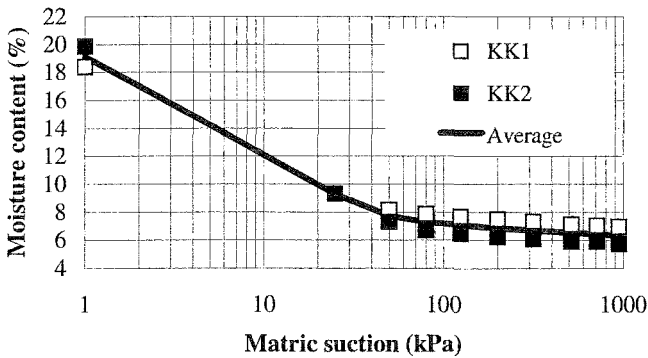
Figure 4. Drying soil water characteristic curve of compacted Khon Kaen loess

Oedometer test. The double oedometer method of Jennings and Knight (1957) was adopted. The procedure employs two companion samples, one wetted after applying a small seating load and an "as prepared" moisture condition sample (for undisturbed soils the sample is prepared at the field moisture content). Both samples are then progressively loaded as in a normal consolidation test. The difference in vertical strain between the wet and dry samples at an applied pressure of 200 kPa is referred to as the collapse index (I_e) in accordance with ASTM D5333-92 (ASTM 1992). The wet sample was used to find the typical consolidation characteristics of the soil, such as pre-consolidation pressure (p_c), compression index (C_c) and swell index (C_s).

All the results from the double oedometer testing are presented in Table 1 and Figures 5 and 6. The degree of collapse was evaluated as "slight", suggesting that Modified compaction effectively breaks down the weak cementation between soil grains.

Table 1. Double oedometer results of compacted Khon Kaen loess.

Property	Value
Pre-consolidation pressure, p_c	73.5 kPa
Compression index, C_c	0.082
Swell index, C_s	0.008
Collapse index, I_e (%)	1.2%
Degree of collapse	Slight
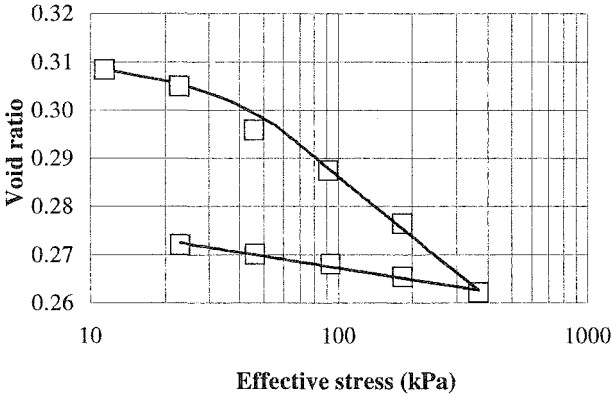
Figure 5. Consolidation curve of compacted and wetted Khon Kaen loess
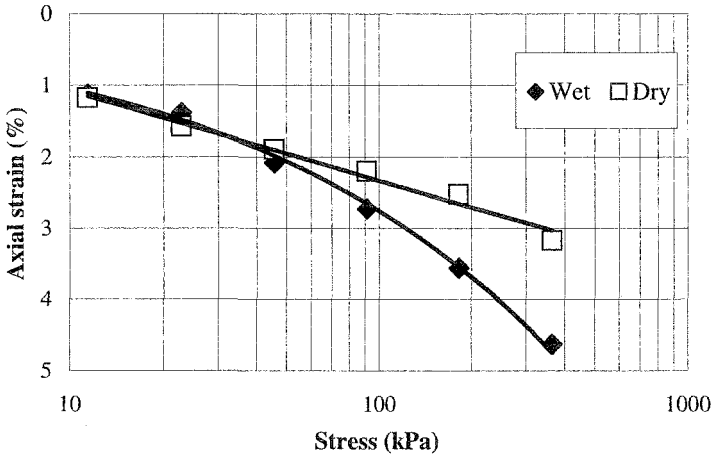
Figure 6. Wet and dry soil settlement curves from double oedometer tests

California Bearing Ratio. Soils can be tested in either the unsoaked or soaked condition, according to the expected moisture conditions that the pavement will be subjected to in its life. For the soaked condition, the soil sample must be soaked for at least 4 days after compaction (AS1289.6.1.1-1998).

The CBR-values of soaked and unsoaked samples were 19 and 34%, respectively. Therefore soaking caused a 44% reduction in the CBR value, despite the relatively low collapse potential of this soil.

Shear Strength. Three samples of compacted Khon Kaen loess, 50 mm in diameter and 100 mm high, were each saturated by applying a back-pressure lower than the confining pressure of 20 kPa, prior to isotropic consolidation. Saturation was checked by increasing the confining pressure with the drains closed. Saturation was assumed for values of the "B" pore water pressure parameter greater than 98%. Then an undrained test at a confining pressure of approximately 50, 100 or 200 kPa was conducted. Each sample was sheared at an axial strain rate of 0.1 % and pore water pressures were monitored.

The stress - strain curves of compacted Khon Kaen loess are presented in Figure 7. The peak shear strengths varied between 470 and 1400 kPa. Pore water pressures developed during shear were almost negligible, as shown in Figure 8, and so had minor impact on the effective shear strength parameters. The Mohr's circles and failure envelope for effective stress from the triaxial testing are presented in Figure 9. The friction angles and apparent cohesions were 47° and 25 kPa, and 45° and 52 kPa, for total and effective stress, respectively. The total stress residual shear strength parameters, measured at approximately 20% of strain, were high; the residual friction angle was 33° while the cohesion was 19 kPa.

The secant Young's modulus was estimated from the stress - strain curves for deviator stress up to one half of the peak stress; modulus values were 45 and 145 MPa for confining pressures of 53 and 200 kPa, respectively.

Resilient Modulus. To determine resilient modulus, design stress levels were chosen from consideration of the total stress failure envelope determined from CIU testing. Stress paths were chosen to avoid failure as indicated in Figure 10. Pavement material will be compacted during construction and loaded in the undrained state by traffic.

Three Khon Kaen samples were statically compacted in two equal layers, to a diameter of 72 mm and a height of 152 mm. The samples were prepared, as for the CIU test, at OMC (8.5%) and maximum dry density (2.09 kN/m^3). Each sample was sealed in a membrane then three linear variable differential transformers were attached longitudinally to the sample to measure displacement over the middle third of the sample. One thousand cycles of preconditioning were used to bed the end caps into the specimen and to stabilize the soil. After preconditioning, the first pre-

selected confining pressure was achieved and each level of deviator stress was applied over 100 cycles to measure the resilient modulus.

The average resilient moduli were determined from the three samples over the range of applied stress states. Subsequently a relationship between resilient modulus and deviator stress was determined, which is illustrated in Figure 11.
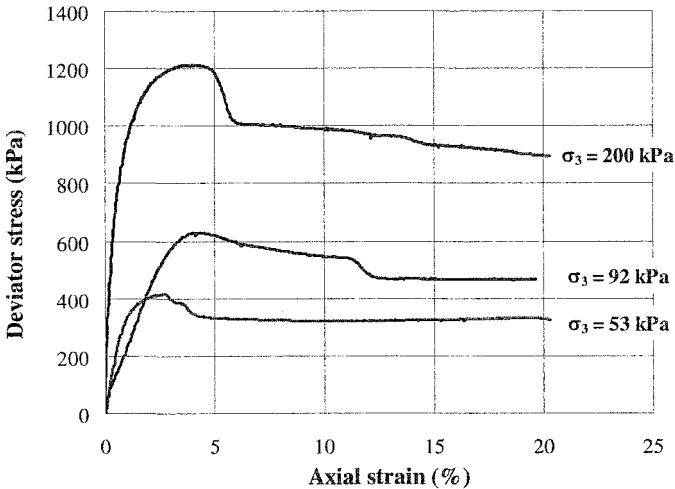
Figure 7. Stress - strain curves from CIU test of compacted loess
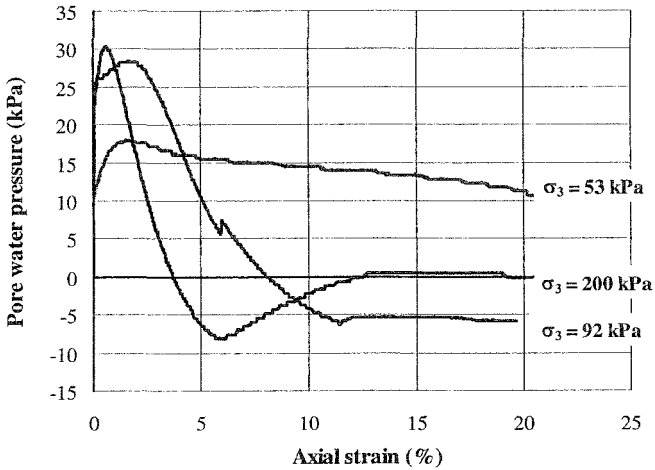
Figure 8. Pore water pressure during shearing from CIU test of compacted loess
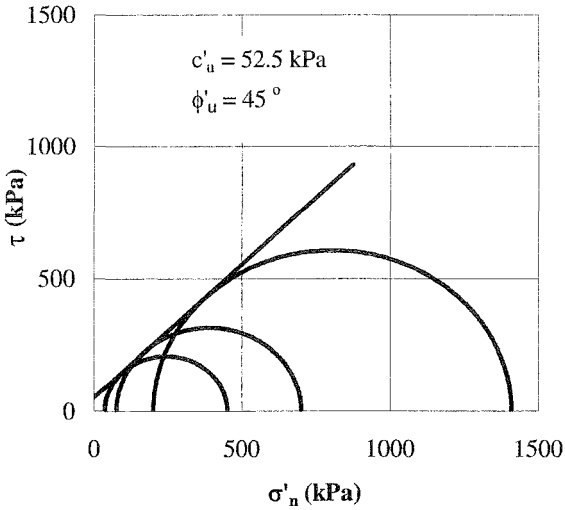
Figure 9. Effective stress shear strength parameters from CIU test of compacted Khon Kaen loess
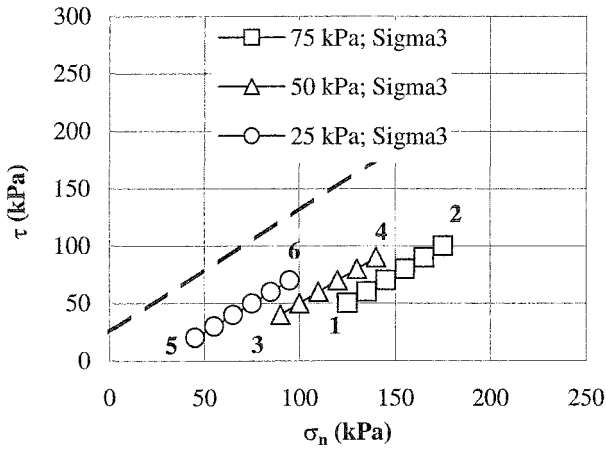
Figure 10. Design stress levels for resilient modulus tests based on CIU testing
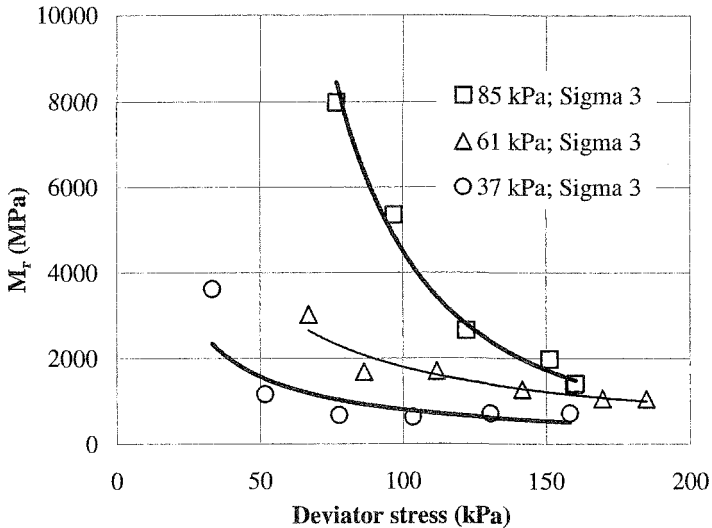
Figure 11. The relationship between resilient modulus and deviator stress

Discussions and Conclusion

The soil water characteristic curve (SWCC) of compacted Khon Kaen loess showed a large decrease of moisture content from the initial gravimetric moisture content of 19% to 8% moisture content at a matric suction of 50 kPa. Thereafter the moisture content decreased at a much slower rate.

The wet and dry double oedometer testing indicated that the collapsible behaviour of Khon Kaen loess was improved greatly by compaction. In earlier work on this same soil (Cameron, Nuntasarn and Gasaluck 2005), poorly compacted Khon Kaen loess was tested. The dry density and moisture content ratio of the soil were just 76 and 74.5% of maximum dry density and OMC (Modified compaction), respectively. Under these conditions, the collapse index was 19%, a severe degree of collapse.

As expected, the frictional shear strength of compacted Khon Kaen loess from CIU testing was higher than the UU test value for undisturbed soil reported by Udomchoke (1991). Interestingly the apparent cohesion of the compacted soil at OMC was practically the same as that found by Udomchoke for undisturbed soil at the same moisture state.

The effective stress parameters from the CIU testing of compacted Khon Kaen loess were almost identical to the total stress strength parameters indicating a free-draining soil, with little pore water pressure build-up during shearing.

The possible application of compacted loess as a pavement material appears promising as indicated by the resilient modulus test results. The resilient modulus values generally exceeded 500 MPa for the stress levels considered. The matric suction of the resilient modulus samples can be estimated from the SWCC in Figure 4 to be 33 kPa. However saturation may cause significant loss of stiffness as evidenced by the soaked CBR tests, which gave values that would be considered unacceptable for a subbase.

Finally, the 2002 AASHTO Pavement Design Guide provides empirical equations for the estimation of resilient modulus (M_r) at any stress state, based on the shear strength and basic properties of the soil, including moisture content and dry density of the sample. The equation for coarse-grained sand soil was used to predict the value of M_r. These estimates have been plotted against test observations in Figure 12. Reasonable and generally conservative estimates of resilient modulus were obtained, which would be useful for the design of pavements.
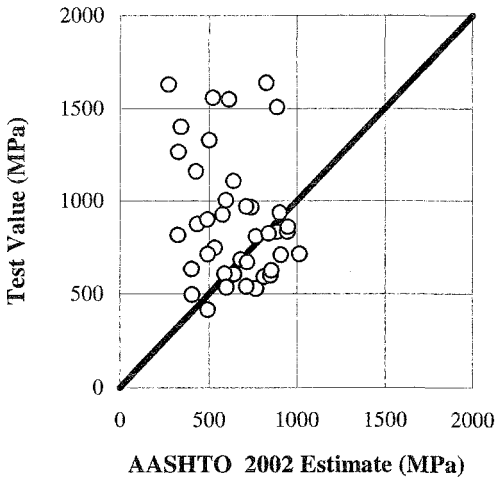
Figure 12. Comparison of observed and predicted (AASHTO 2002) resilient modulus

References

AASHTO. (2002). *Guide for the Design of New and Rehabilitated Pavement Structures*, National Cooperative Highway Research Program, Project 1-37A.

ASTM (1992). "Standard test method for measurement of collapse potential of soil." *American Society for Testing Material*, D5333-92, ASTM, Ann Arbor, MI.

ASTM (1996). "Standard test method for calcium carbonate content of soils." *American Society for Testing Material*, D4373-96, ASTM, Ann Arbor, MI.

ASTM (1998). "Standard test method for capillary-moisture relationships for coarse- and medium-textured soils by porous-plate apparatus." *American Society for Testing Material*, D2325-98, ASTM, Ann Arbor, MI.

Cameron, D. A., Nuntasarn, R. and Gasaluck, W., (2005). "A comparison of collapsing soil from Australia and Thailand." *Proc. Int. Conf. on Problematic Soils*, Eastern Mediterranean University, Famagusta, N. Cyprus, pp 705-713.

Jennings, J.E., and Knight, K. (1956). "Recent experience with the consolidation test as a means of identifying conditions of heaving of collapse on foundations of partially saturated soil". *Transactions, South African Instn. Civil Eng.,*V8, No. 8

Meteorological Department Ministry of Information and Communications Technology. viewed 6 May 2004. < http://www.tmd.go.th/~rwcne/ >.

Northcote, K.H. (1979). "A factual key for the recognition of Australian soils." *CSIRO*. (Rellim Technical Publications: Adelaide.)

Standards Australia. (1998) "Method 6.1.1: Soil strength and consolidation tests- Determination of the California Bearing Ratio of a soil - Standard laboratory method for a remoulded specimen." *AS 1289.6.1.1*, viewed 13 Oct 2003. < http://online.standards.com.au/online/>.

Udomchoke, V. (1991). "Origin and engineering characteristics of the problem soil a in the Khorat basin, Northeastern Thailand." *Ph.D. dissertation*. Asian Institute of Technology, Bangkok, Thailand.

EXPERIMENTAL STUDY OF DESICCATION OF SOIL

H. Péron[1], L. Laloui[1], T. Hueckel[2] and L. Hu[2]

[1]Soil Mechanics Laboratory, Ecole Polytechnique Fédérale de Lausanne (EPFL), Station 18, CH-1015 Lausanne, Switzerland. Email: herve.peron@epfl.ch, lyesse.laloui@epfl.ch.
[2]Department of Civil and Environmental Engineering, Duke University, Durham, N.C. 27708, U.S.A. Email: hueckel@duke.edu; lh19@duke.edu.

ABSTRACT:

Basic phenomena involved in crack generation during drying, and the ways to control or avoid it, are still elusive. Mechanisms of shrinkage and cracking are addressed, and especially the critical role in crack onset during drying of boundary constraints and induced tensile stresses. Two kinds of experimental tests were carried out on samples of fine-grained soil under controlled conditions: free desiccation tests and constrained desiccation tests. Measurements of strains, gravimetric water content and suction allow the drawing of some conclusions about the influence and the evolution of these tensile stresses during drying.

Introduction

Drying of soils and the ensuing cracking are of utmost importance in earth works as it entails degradation of many soil properties. Drying fractures strongly affect permeability and may compromise such structures as clay buffers for nuclear waste isolation, barriers such as landfill liners, top covers, etc. Hydraulic conductivity of clay liners material may increase from 1×10^{-9} m.s^{-1} for wet and intact soil, to 1×10^{-6} m.s^{-1} for the material after cracking, (Albrecht and Benson 2001). Compressibility increases substantially in the presence of desiccation cracks in soils (Yesiller et al. 2000) while its rate of consolidation decreases (Morris et al. 1992). Cracking is the cause of substantial damage in foundation supported structures. Cracks are also a possible precursor for inception of failure surface at the top of dams and embankments (Cooling and Marsland 1953).
Cracks form in soils due to a number of mechanical and environmental circumstances. The scope of this paper is limited to cracks due to drying. Desiccation cracks have been investigated for many years (see Corte and Higashi, 1960, Abu-Hejleh 1993, Konrad and Ayad 1997). Nevertheless, the understanding of

their initiation mechanisms and the links between them and soil parameters are still elusive.

Desiccation is the continuous process of pore water loss from a soil exposed to a drier and/or warmer environment. In response to drying, soil water volume decreases and, and in consequence the soil shrinks (Kleppe and Olson 1985, Miller et al. 1998). Desiccation macrocracks are likely to occur if the shrinkage is constrained and/or if tensile stresses are generated in the soil, which reaches its tensile strength (Corte and Higashi 1960). Typically, these constraints can arise from different causes (Hueckel 1992): (i) a frictional or any other traction or displacement boundary conditions, (ii) any eigen-stress concentrations within the soil sample, and (iii) intrinsic factors, such as soil texture (existence of large particles, Towner 1988) and soil structure (solid network formed by soil particles, Scherer 1997). In the field, (i) can arise from any restraining structure, and (ii) from soil moisture gradients which do not respect the compatibility equation. It must be pointed out that many studies, when performing desiccation crack tests, do not clearly distinguish among these phenomena.

In this article we intend to elucidate a potential link between the drying process and strain evolution of a fine-grained soil sample, and to investigate the special role of boundary constraints in desiccation crack initiation. For this purpose, two sets of tests will be examined: free desiccation tests for which no boundary constraints are imposed and constrained desiccation tests.

Experimental set up

Soil properties and preparation

The soil used in this study is a sandy silt from Bioley (Switzerland), from which particles greater than 90 μm (sandy fraction) have been removed (to avoid any effect of large rigid inclusions). The grain size distribution curve of the material is given in Figure 1. The clay fraction is 27 %. The liquid limit is $w_L = 31.8$ %, the plastic limit $w_P = 16.9$ %, and the unit weight of solid particles is $\gamma_s = 27.1$ kN/m^3.

The dry crushed soil was mixed with de-aired and demineralized water at a gravimetric water content of 1.5 times the liquid limit. The resulting slurry was then vigorously mixed and vibrated for two minutes to remove air bubbles. Such a preparation guaranties an initially saturated state. After being prepared and before use, the soil was left to settle for at least one day to ensure homogenisation. The water content of the slurry was approximately 49 %. This preparation enables the soil to be as close as possible to a virgin mechanical and saturation state. Moreover, it prevents formation of any initial soil structure such as particle aggregates.

Hydric characteristics of soil

To determine the hydro-mechanical behaviour of the slurry, void ratio (e), saturation degree (S_r) and gravimetric water content (w) are determined for various values of suction (s) under zero mechanical stress. For this purpose, tests in a

Richards cell were performed. Suction was applied to the slurry by the air over-pressure technique. To minimize friction and adhesion between the soil and the ring surrounding it, Teflon rings were used with their surface treated with a hydrophobic substance. During drying, detachment of the specimen from the ring was observed. At equilibrium, w was measured, and e and S_r were deduced from a volume measurement procedure taking into account sample detachment (Péron et al. 2006). Both drying (from the initial slurry to various suction stages) and wetting (from 100 kPa to 50 kPa) have been tested. An air entry value of about 100 kPa and a shrinkage limit at about 200 kPa were determined. Suction – water content (s-w) and suction induced strains curves (s-e) are shown in Figure 2. Suction induced strains curve for drying path is very close for suction below 100 kPa, to the normal consolidation line (slope C_c), as determined in isotropic triaxial tests. A marked hysteresis onset is observed on wetting path between 100 kPa and 50 kPa. Strains are large and irreversible (plastic) during the virgin drying of the soil: rewetting of the soil produces only slight swelling.
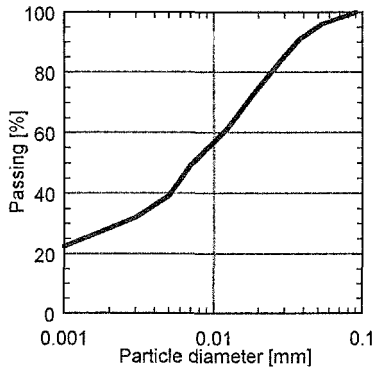
Figure 1. Grain size distribution of Bioley silt.
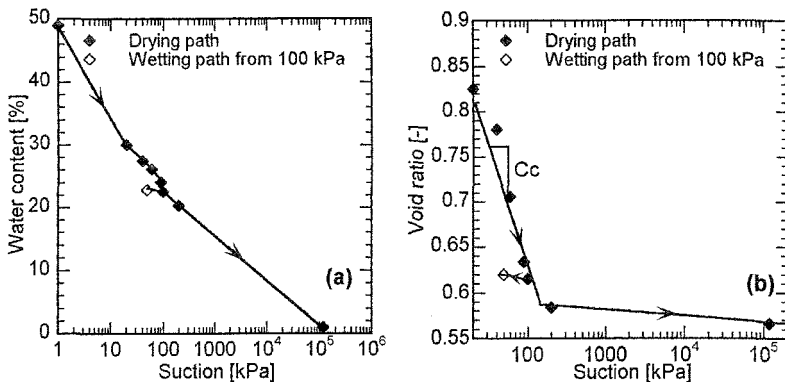
*Figure 2. Hydro-mechanical behaviour of Bioley silt: suction – water content (a)
and suction induced strains (b).*

Desiccation tests procedure

Strain variation in time and space, mass water content (w), and crack form were investigated during the continuous air-drying of a bar-shaped soil cake. Limited suction measurements were performed. Two extreme cases with different mechanical boundary conditions were studied: free desiccation tests and constrained desiccation tests.

Free desiccation tests

Sample preparation and drying conditions
Free desiccation tests were conducted, avoiding any mechanical constraints at the boundaries due to cohesive-frictional effects during shrinkage as much as possible. So, the drying was undertaken on a Teflon support treated with a hydrophobic substance. The prepared slurry was poured in a 300 mm x 50 mm, by 12 mm high, sliding mould, immediately removed, in order to obtain regular and reproducible bar-shaped slurry cakes (Figure 3). All the tests were performed in a climate chamber with controlled relative humidity and temperature, fixed at 40 % and 18 °C, respectively.

Water content measurements
Average gravimetric water content of the whole cake was recorded with respect to time by continually weighing the drying cake. Local water content was also measured at different drying times by rapidly retrieving fragments from reference samples drying at the same conditions.

Strain measurement
A difficulty arose in measuring strains because of the very low consistency of the slurry at the early stages of drying. Evolution of axial and vertical strains with time was measured with callipers, which were fixed on the Teflon support. The calliper accuracy was 1/50 mm. A needle, fixed to the calliper sliding base, was regularly and carefully put in contact with the soil. The measurement system is shown in Figure 3. Strains in all three directions were measured using this method.
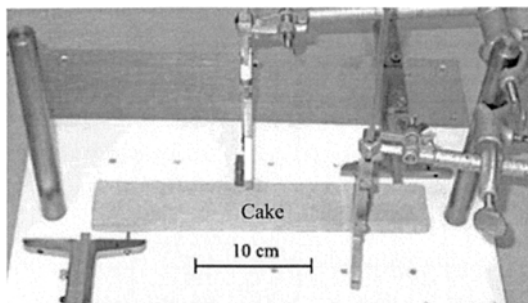
Figure 3. Set up for vertical and transversal strains.

Constrained desiccation tests

Sample preparation and drying conditions
    For these tests, during shrinkage, a constraint was created at the bottom surface in the longitudinal direction, by using a substrate with thin parallel notches. Slurry cakes were prepared in the same way as for free desiccation tests and dried in the same conditions.

Water content and suction measurements
    During the desiccation, total water content evolution with time was recorded by continuous weighing. For each sample, as soon as a crack appeared, a small piece of cake (about 2 cm wide) containing the crack was retrieved in order to measure water content in the crack's vicinity. The remaining cake material was then used for a total moisture content measurement. In the same way, suction was measured by inserting a minitensiometer UMS T5 (UMS 2001) in the neighboring of a newly formed crack. The probe's components were carefully saturated. Air entry value of the probe's ceramic tip was 500 kPa.

Strain measurements
    Strains were measured in the same way as for free tests. In addition, photographs of the cake were periodically taken during drying and cracking with a digital camera, and crack openings were measured using an image analysis software, Winanalyse® (Winanalyse 1998).

Desiccation test results

Free desiccation tests

Gravimetric water content-strain relationships
    It appeared that drying rate was constant and equal to about 0.025 %.min^{-1} before decreasing at about water content values of 20 %. For all of the free desiccation tests, none of the cakes experienced cracking.
Local water content values and strain measurements performed at various drying time showed that the sample dries faster at the extremities than at the centre. Below $w = 25$ %, this heterogeneity disappeared and water content was constant on average.
Below a gravimetric water content of about 23 %, the cake experienced a slightly upward curling at its extremities. At the very end of the drying process, the two extremities had risen about 2 mm. Consequently, the strain measurements below $w = 23$ % were less accurate.
The comparison between axial and vertical strains versus gravimetric water content shows that the cake shrank in the vertical direction rather than in the horizontal one, up to $w = 32$ % (which corresponds to the liquid limit value). From this value on, the horizontal shrinkage increased noticeably. Various hypotheses may be advanced about the reasons for this disparity. One possible explanation suggests that before reaching the liquid limit value, soil is in a liquid state, and exhibits settlement

(vertical strains are greater than horizontal ones). In such a state, the possibly constraint induced stresses are negligible and cannot lead to cracking. This behaviour has been seen in slurries undergoing desiccation (Kodikara et al. 1999). Also Corte and Higashi (1960) observed the disparity and attributed it to the adhesive role of the water film between the sample and the substrate despite application of a repellent coating. Consequently, the behavior below water content of w = 32 %, corresponding to the liquid limit value is considered as uninhibited drying shrinkage, which is linear and isotropic. Shrinkage in this phase only will be considered in what follows, as presented in Figure 4. Further experiments are required to clarify the mechanisms developing above the liquid limit.

Comparison of free desiccation tests with Richards cell tests
      In Figure 5, the void ratio values against average gravimetric water content are shown for free desiccation tests as well as for the Richards cell tests. It is clear that in both tests the moisture loss below 21-23% has little effect on volumetric strain. The difference between the two methods can be linked to the loss of accuracy of caliper measurements when a tip curling developed above w = 25 %.

Constrained desiccation tests

General observations
After 16 hours drying time, a series of 6 to 8 cracks always appeared in the direction parallel to the notches of the support. A few photographs of the obtained crack patterns are shown in Figure 6. In all of the tests, no more than 1.5 hour would generally elapse between the first and the last crack. Once these cracks were formed, diffused cracking occurred between the soil in the notches and the rest of the soil mass, and each soil cell between two neighboring cracks exhibited a slight upward curling. Actually, after cracking, caliper measurement were not representative of strains anymore and were stopped.
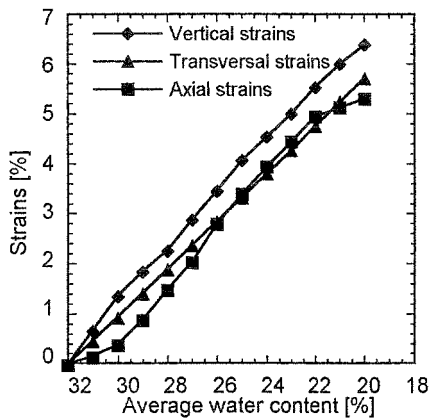
Figure 4. Strains evolution versus average water content from liquid limit value to shrinkage limit value for free desiccation tests.
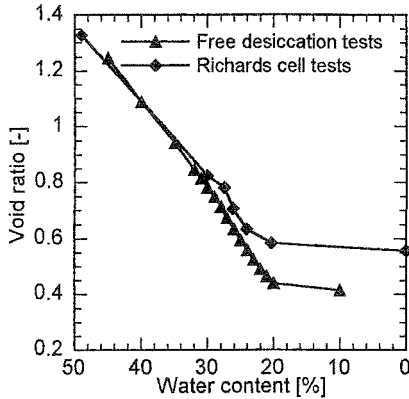
Figure 5. Comparison of free desiccation tests and Richards Cell tests results.
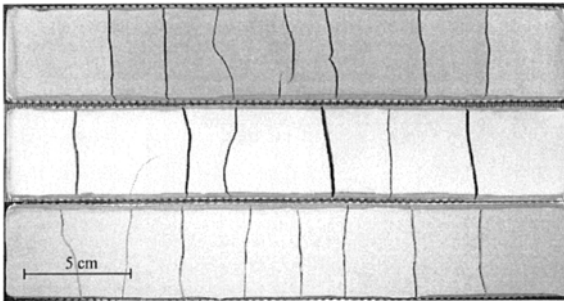
Figure 6. Examples of final crack patterns.

Cracking water content and suction

The first crack appeared on average at a water content of about 24 %, and the last crack never appeared below w = 22 %, which is a notably narrow range. In addition, local water contents, measured in the vicinity of each newly formed crack, were always remarkably close to 22 % for all the cracks, irrespective of their order of appearance. The local value of suction measured by the tensiometer, still in the vicinity of the cracks, was equal to 90 kPa/100 kPa, which corresponds to water content values comprised between 22 and 24% in Figure 2 (a).

Gravimetric water content-strain relationships

Strain evolutions with respect to average water content below the liquid limit value are plotted in Figure 7. The parallel notches noticeably decreased the value of axial strains (they did not overcome 0.5 % at the onset of cracking) compared to unconstrained case. As the support was not in Teflon, a slight friction was also created in the transversal direction: strains in this direction are lower than in the free desiccation tests for the same water content value. In turn, still for the same water content, vertical strains were larger than those observed in free desiccation tests.

Crack openings

It appeared that cracks were fully developed about 20 minutes after the crack appearance, and that crack opening evolved slowly after this time, in relation with a residual shrinkage, and curling. Opening of all the cracks, measured once each crack was fully developed, are compiled in Figure 8. As the phenomenon is subjected to a certain variability from one test to another, mean value and standard deviation are given. Nevertheless, a marked tendency for successive crack openings to decrease is observed.

Analysis of the results

Origin of cracks

It is assumed that the desiccation induced stress increment $d\sigma_{ij}$ may be expressed by:

$$d\sigma_{ij} = E_{ijkl}d\varepsilon_{kl}^{m} = E_{ijkl}(d\varepsilon_{kl} - d\varepsilon_{kl}^{h}) \tag{1}$$

where E_{ijkl} is an incremental stiffness tensor, $d\varepsilon_{kl}^{m}$ refers to the mechanical strain responsible for stress generation, $d\varepsilon_{kl}$ is the observed total strain rate, $d\varepsilon_{kl}^{h}$ is a free desiccation strain rate (the only one occurring if desiccation is not constrained).
Drying process may induce a significant increase in soil stiffness. Thus, tensile stress in a soil undergoing desiccation depends on two factors: constraint induced strains ($d\varepsilon_{kl} - d\varepsilon_{kl}^{0}$), and change in incremental soil stiffness (E_{ijkl}). For the discussed experimental setup, during constrained desiccation tests, constraint induced stress may arise due to: (a) boundary constraints, (b) strain proportional to a vertical and horizontal water content gradients, which do not necessarily satisfy compatibility conditions.
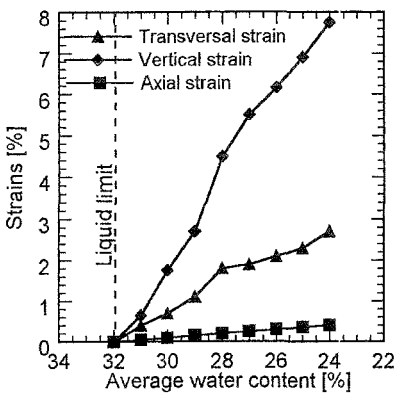
Figure 7. Strains evolution versus average water content for constrained desiccation tests.
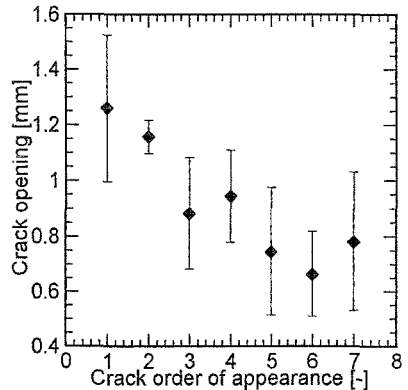
Figure 8. Crack opening with respect to the order of the crack appearance.

Given that a succession of cracks parallel to the notches have been observed, the axial boundary constraint created by notches ((a) type), is clearly responsible for cracking. In this direction, the sample experiences tensile stresses (in Equation 1, $d\varepsilon_{kl} << d\varepsilon^h_{kl}$), which may reach tensile failure criterion. Only a slight water content gradient have been measured along the axial direction (lower than 2% on the cake length), which disappeared below w = 25 %. The possible horizontal (axial) gradient induced stresses ((b) type) would create cracks parallel to the cake axis. Vertical moisture gradients were also very limited, and often below the resolution of our capability of a reliable sampling.

Parameters controlling desiccation induced stresses

Total mechanical strains (ε^m_{kl})
         In Figure 9, mechanical strains (assumed to be equal to the difference between observed constrained desiccation strain and free desiccation strain) are plotted versus average water content, up to first crack appearance, at w = 24 %. As the sample looses water, it experiences a measurable mechanical strain (negative in tension): for the tested material, the strain threshold value, above which cracking occurs, can be estimated to - 3.5 % in the axial direction. All strains are average total strains assuming their uniformity along the sample.
While the sample experiences traction in both horizontal directions, a vertical contraction is observed. Let us assume an elastic behaviour, and a null vertical desiccation stress (which is in accordance with the top boundary conditions). The latter condition implies that vertical mechanical strains ε^m_{11} are then given by:

$$\varepsilon^m_{11} = -\nu \frac{\varepsilon^m_{22} + \varepsilon^m_{33}}{(1-\nu)} \qquad (2)$$

where ν is the Poisson ratio, and ε^m_{22} and ε^m_{33} respectively the transversal and axial strains.
The values of ε^m_{22} and ε^m_{33} can be calculated as a difference between the observed constrained desiccation strain and free desiccation strain from the two kinds of tests reported above. These strain components are the most accurate, since they are deduced from transversal and axial displacements, much larger than the vertical ones. Thus, using the values of ε^m_{22} and ε^m_{33} calculated as the strain difference in Equation 2, a calculated value of 2.5 % for ε^m_{11} is obtained at the onset of the first crack. This value is finally in agreement with the 3.2 % calculated again from the strain difference between the two test types as presented in Figure 9.
It needs to be reminded that the above considerations regard total strains across the sample. That implies that the strains are uniformly distributed across the sample. While the measured variations are limited (Péron et al. 2005), the effect of edges predicted theoretically (Hu et al. 2006) does affect only less than 1/8 of the nearby soil.
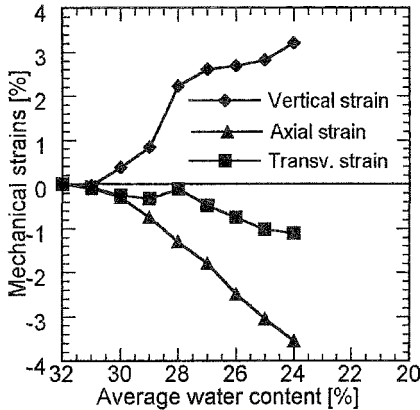
Figure 9. Difference between strains observed in free and constrained tests.

Hydric strains (ε^{h}_{kl})

The building up of mechanical strains ε^{m}_{kl} calculated in the previous paragraph is governed by the nature of the constraint, and by the amount of free desiccation strains experienced by the cake (in Equation 1). These strains are large and plastic during the first drying of the soil (this behaviour is underlined in Figure 3). In consequence, desiccation stress building up can be seen as being largely determined by the nature of suction induced strains. Large plastic strains are believed to be one of the cause of stress generation and subsequent cracking.

Parameters controlling failure criterion

For all the cracks, local water content and suction values in the vicinity of the crack at its onset was remarkably close, irrespective of the crack order of appearance. At the same time, cracking starts for a higher total water content, always close to 24 %. These observations suggest that while total mechanical (constrained) strains control desiccation stress generation, desiccation crack initiation is rather linked to local soil state. As cracking local suction and water content values are very close to air entry value, air entry value influence on crack initiation can be inferred. Several studies show the key role of air filled pores in crack initiation (Snyder and Miller 1985). It has been shown that air entry value is close to shrinkage limit (see Fleureau et al. 2002), therefore, Bioley silt at crack onset is also close to its shrinkage limit.

Stress release

Still assuming an elastic behaviour, a theoretical crack opening displacement for the first crack can be calculated. Desiccation induced stresses in the transversal direction are neglected (although it exists a measurable negative mechanical strain) and a total stress release at the first crack appearance is

assumed. With these hypotheses, a 4.7 mm first crack opening value is obtained, which is significantly higher than the measured value (1.3 mm, see Figure 8). This could mean that the stress release is not total when the first crack is created, and that subsequent cracks release some residual stresses. These cracks, as they are appearing at lower total water content, should also release a subsequent rebuild-up of stresses due to subsequent partially constrained desiccation.

Conclusion

Strains, crack forms, water content and suction were investigated during free and constrained desiccation of a bar shaped silt sample. The tests have allowed to underline the key role of boundary constraints and suction induced strains in crack initiation, and the drawing of some conclusions about the evolution of desiccation induced stresses during drying. Further investigations will be focused on tensile stress behaviour quantitatively with respect to hydration state.

Acknowledgements

References

Abu Hejleh, A. N. M. (1993). *Desiccation theory for soft cohesive soils, PhD Thesis, University of Colorado*, Boulder, Colorado.
Albrecht, B.A. and Benson, C.H. 2001. "Effect of desiccation on compacted natural clay." *Journal of Geotechnical and Geoenvironmental Engineering* 127(1), 67-75.
Cooling, L.F and Marsland, A. (1953). "Soil Mechanics of Failures in the Sea Defence Banks of Essex and Kent." *ICE Conference on the North Sea Floods of 31 January / 1 February*.
Corte, A. and Higashi, A. (1960). *Experimental Research on Desiccation Cracks in Soil, Research Report 66: U.S. Army Snow Ice and Permafrost Research Establishment*, Wilmette, Illinois.
Fleureau, J.M., Verbrugge, J.C., Huergo, P.J., Gomes Correia, A. and Kheirbek-Saoud, S. (2002). "Aspects of the behaviour of compacted clayey soils on drying and wetting paths." *Canadian Geotechnical Journal* 39, 1341-1357.
Hu, L., Péron, H., Hueckel, T. and Laloui, L. (2006). "Numerical and phenomenological study of desiccation of soil." *Proceedings of GeoShangai, International Geotechnical Conference*, submitted.
Hueckel, T. (1992). "Water-mineral interaction in hygro-mechanics of clays exposed to environmental loads: a mixture approach." *Canadian Geotechnical Journal* 29, 1071-1086.
Kleppe, J.H. and Olson, R.E. (1985). "Desiccation cracking of soil barrier." *Hydraulic Barrier in Soil and Rock, STP 874, ASTM, 263-275.*

Kodikara, J., Barbour, S.L. and Fredlund, D.G. (1999). "Changes in clay structure and behaviour due to wetting and drying.". *Proceedings of the eighth Australia New Zealand Conference on Geomechanics*, Hobart, 1, 179-185.

Konrad, J.M. and Ayad, R. (1997). "An idealized framework for the analysis of cohesive soils undergoing desiccation." *Canadian Geotechnical Journal* 34, 477-488.

Miller, C.J., Mi H. and Yesiller, N. (1998). "Experimental analysis of desiccation crack propagation in clay liners." *Journal of the American Water Resources Association* 34(3), 677-686.

Morris, P.H., Graham, J. and Williams, D.J. (1992). "Cracking in drying soils." *Canadian Geotechnical Journal* 29, 262-277.

Péron, H., Laloui, L., and Hueckel, T. (2005). "An experimental evidence in desiccation cracking in sandy silt." *Advanced Experimental Unsaturated Soil Mechanics,* Tarantino et al eds., Taylor, & Francis Group, London, 475–481.

Péron, H., Hueckel, T. and Laloui, L. (2006). "A note on the volume measurement in determining soil water retention curve." *Geotechnical Testing Journal,* submitted.

Scherer, G.W. (1997). "Stress for re-immersion of partially dried gel." *Journal of Non-crystalline Solids* 212, 268-280.

Snyder, V.A. and Miller, R.D. (1985). "Tensile strength of unsaturated soils." *Soil Science Society of America Journal* 49, 58-65.

Towner, G.D. (1988). "The influence of sand and silt size particles on the cracking during drying of small clay-dominated aggregates." *Journal of Soil Science* 39, 347-356.

UMS GmbH (2001). User manual T5 Miniature Pressure Pore Transducer version 1.8. Muenchen.

Winanalyse Automatic Motion Analysis Version 1.4 (1998). *Manual,* Micromak GmbH.

Yesiller, N., Miller, C.J., Inci, G. and Yaldo, K. (2000). "Desiccation and cracking behaviour of three compacted landfill liner soils." *Engineering Geology* 57, 105-121.

Prediction of the Limiting Void Ratio of Clayey Soils after Drying

M. E. Bardanis[1] and M. J. Kavvadas[2]

[1]Doctoral student, Department of Civil Engineering, National Technical University, 9 Iroon Polytechniou st., Athens 157 73, Greece; PH (+30) 210 772 3434; FAX (+30) 210 772 3428; e-mail: bardanis@mail.ntua.gr
[2]Associate Professor, Department of Civil Engineering, National Technical University, 9 Iroon Polytechniou st., Athens 157 73, Greece; PH (+30) 210 772 3434; FAX (+30) 210 772 3428; e-mail: kavvadas@central.ntua.gr

Abstract

Samples of two clays and two marls consolidated or reconstituted to various initial void ratios were left to dry to constant volume and the limiting lower value of the void ratio at that state, e_r, was measured. Drying of the initially fully saturated samples of each soil was achieved by leaving the samples under atmospheric conditions. The data presented suggest, at first glance, that limiting lower void ratio after drying, e_r, for each soil increases as the initial void ratio of the soil increases. Normalizing e_r by the initial void ratio results in the ratio e_r/e_o increasing as the initial void ratio decreases. Plotting the ratio e_r/e_o for all soils against initial void ratio normalized by the void ratio at the liquid limit e_L ($= w_L \cdot G_s$) shows that the results from all soils lie very close to a unique line, which passes through point [$e_o/e_L=0$, $e_r/e_o =1$] and has a very high correlation coefficient. This linear relation appears valid for values of e_o/e_L between 0.6 and 1.7. Using the relation between e_r/e_o and e_o/e_L the limiting lower void ratio after drying can be predicted when the initial void ratio of the soil e_o (expressing the initial state of the soil) and its liquid limit w_L and specific gravity G_s (expressing the nature of the soil) are known. Also, according to this relation, e_r exhibits a maximum value as e_o increases and then starts to decrease again as e_o increases further.

The empirical relation derived may be used for the prediction of a mechanical parameter of use to modern constitutive modeling of unsaturated soils such as the limiting lower void ratio after drying. It may also be used as a means to study unsaturated soil behavior as far as the evolution of e_r with initial void ratio and physical properties of soils is concerned.

Introduction

Prediction of the expected volume change during changes in suction is an essential part of the mechanics of unsaturated soils. Models proposed for the prediction of volume change due to suction changes, predict volume changes by using the stiffness parameters κ_s and λ_s, which correspond respectively to elastic and plastic regions of deformation caused by changes in suction (Alonso et al, 1990, Wheeler & Sivakumar, 1995 etc.). Until recently however they failed to predict a limit of the anticipated volume change as well established experimentally by shrinkage limit determination tests (e.g. Fredlund & Rahardjo, 1993, Fredlund et al., 2002). More recently, models have been proposed which have a parameter limiting volume change due to suction increase either at zero or significant net pressure (e.g. Kohgo, 2004). This has been a very useful development in constitutive modeling of unsaturated soils, which, however, adds the need to carry out specific tests to measure the limiting value of a property such as void ratio, the change of which expresses volume change. In order to cope with this problem the limiting lower void ratio after drying, e_r, of two clays and two marls was measured and then correlated to initial void ratio and physical properties. This paper presents the experimental results used for this correlation.

The soils tested

The soils used in the experimental program undertaken were two clays and two marls. The two clays were Chania clay and Speswhite Kaolin and the two marls were Corinth marl and Kifissia marl. Chania clay is a relatively recent (Holocene) low plasticity alluvium clay found around the city of Chania in Crete. Marly layers can be found intercalating with the clayey ones and both types of material are characterized by the large percentage of silicate minerals, even in the fraction passing through sieve No 200 (all of the material remaining on the No 200 sieve is of silicate nature). Speswhite kaolin contains more than 80% kaolinite and is procured in the form of dry powder. Corinth marl is a highly cemented, low- to medium-plasticity marl found in the greater area of the city of Corinth and the Corinth Canal (regarding the cementation and the engineering behavior of the Corinth marl, see Kavvadas et al. 1993, 2002). Kifissia marl is a medium-plasticity marl found in north-western Athens in layers intercalating with the medium-plasticity clay found in the same area. All of the soils tested (except for Speswhite kaolin) were acquired in the form of undisturbed or disturbed samples from boreholes or slope faces. Given that the research at this point focused on the properties of reconstituted soils in order to find out if a trend exists, the disturbance of the samples acquired did not play any role. The index properties of the soils tested are presented in Table 1, while the clay, silt and sand contents are presented in Table 2. Table 3 presents the major minerals contained in the four soils as identified from the combination of results from quantitative x-ray diffraction and methylene blue methods performed on the fraction of the soils passing through Sieve No 200 (data for Speswhite Kaolin from Dineen, 1997). The fraction of the soils remaining on Sieve No 200 is of silicate nature. As shown in Figure 1, Chania clay is a low plasticity clay (CL), Speswhite kaolin is a

Table 1. Index properties of the soils tested.

Soil	w_l (%)	w_p (%)	I_p	G_s	Clay Fraction (%)	Activity
Chania Clay	24	15	9	2.68	18.1	0.50
Speswhite Kaolin	64	32	32	2.61	68.3	0.47
Plastic Corinth Marl	34	22	12	2.67	10.7	1.07
Kifissia Marl	31	16	16	2.66	24.9	0.62

Table 2. Grain size distribution properties of the soils tested.

Soil	Clay fraction (%)	Silt fraction (%)	Sand fraction				Gravel fraction (%)
			Fine (%)	Medium (%)	Coarse (%)	Total (%)	
Chania Clay	18.1	49.8	28.8	2.9	0.4	32.1	-
Speswhite Kaolin	68.3	31.7	-	-	-	0	-
Plastic Corinth Marl	10.7	86.1	3.2	-	-	3.2	-
Kifissia Marl	24.9	68.1	5.9	0.8	0.2	7.0	0.1

Table 3. Minerals detected in the soils tested (fraction passing through Sieve No 200).

Mineral Groups	Minerals	Chania clay (%)	Speswhite Kaolin (%)	Plastic Corinth Marl (%)	Kifissia Marl (%)
Silicate	Quartz	60	-	16	18
	Albite	3	-	3	2
	Total	**63**	**0**	**19**	**20**
Carbonate	Calcite	3	-	60	52
	Dolomite	-	-	2	-
	Total	**3**	**0**	**62**	**52**
Clay	Halloysite	10	-	-	-
	Kaolinite	-	82	-	-
	Illite	3	5	7	5
	Muscovite	5	-	1	3
	Serpentine	-	-	1.5	-
	Chlorite	3	4	1.5	2
	Montmorillonite	9	8	7	17
	Total	**30**	**99**	**18**	**27**
Other minerals		4	1	1	1
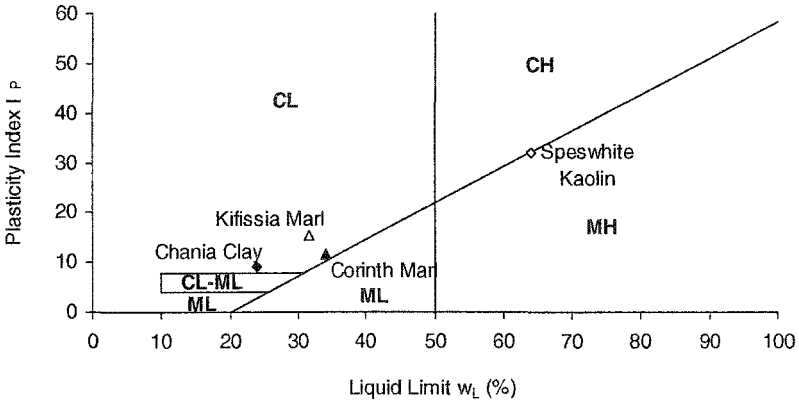
Figure 1. Casagrande's Plasticity Chart with Atterberg Limit values of the soils tested.

high plasticity clay lying practically on the A-Line on Casagrande's Plasticity Chart (CH), while Corinth and Kifissia marls are both characterized as low plasticity clays.

Experimental method

Samples of the four soils were reconstituted to an initial water content of approximately 1.5 times their liquid limit using distilled, deaired water. The slurries produced were left for sufficient time for hydration to take place, with occasional measurement of the water content over that time (and addition of water if needed) and stirring to ensure that settlement of heavier particles would not take place, causing inhomogeneity of the slurry. Measurement of the water content of the slurry was made by taking spoonful sized samples on a daily basis during hydration and measuring their water content. Once hydration was achieved, material from each slurry was poured into oedometer cells and consolidated one-dimensionally to various void ratio values. When consolidation was completed, the samples prepared were taken out of the cells and left to dry under atmospheric conditions. Similar sized and shaped samples of the slurries were prepared by pouring material into an oedometer ring fixed on a glass plate. The weight of each sample was monitored until its stabilization, which corresponds to the residual water content of the soil. Measuring the water content at the end of the test allowed back calculation of the water content values over the period of drying (from total weight measurements during that time). In order to ensure that total weight -and therefore water content- stabilization corresponded to volume stabilization after shrinking, except for samples monitored until stabilization of their weight, other samples were left to dry until a shorter time. Both these samples and the samples left to dry completely were cut diametrically in halves, one of which was placed in the oven for water content measurement and the other was dipped in melted paraffin wax in order for its total volume to be measured and thus its void ratio to be calculated. As a result water

content w and void ratio e during drying of samples prepared at the same initial conditions were measured, allowing thus the full shrinkage curve (e-w) to be determined and thus the shrinkage limit w_s and the void ratio at it, e_s, to be determined for each soil and each initial void ratio. The procedure used is not the standard procedure but it allows the measurement of the limiting lower void ratio e_r of each soil, after which there is no further decrease of void ratio. Figure 2a shows water content vs time curves from two samples of Chania clay after they were consolidated to 100 and 1600 kPa. The degree of saturation vs time curves for the same samples are shown in Figure 2b, with the void ratio vs time curves shown in Figure 2c and the shrinkage curves (void ratio-water content) shown in Figure 2d. As can be seen from Figure 2 a complete shrinkage curve was obtained and the void ratio reached its limiting value during drying over the time the samples were left to dry (approximately 7 days).
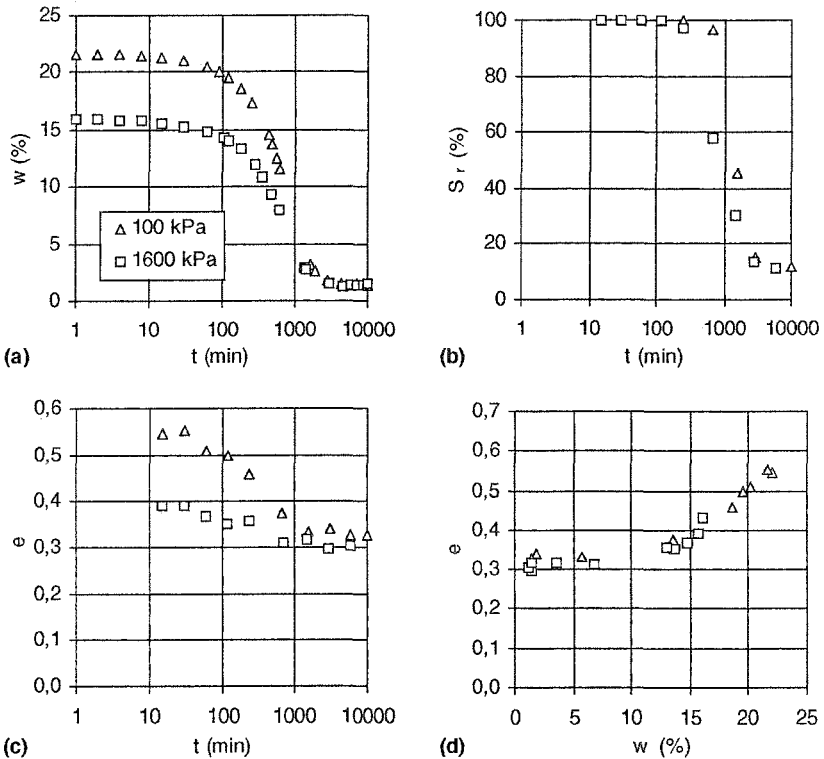
Figure 2. (a) Water content w, (b) degree of saturation S_r, (c) void ratio e of samples of reconstituted Chania clay consolidated to 100 and 1600 kPa during drying with time and (d) shrinkage curve for the same samples.

The limitations of the experimental procedure are the need to be able to produce similar samples of reconstituted soil at given initial void ratio values before drying commences, the accuracy of the measurement of void ratio using the paraffin wax method and the non uniform water content of the samples, especially at short times after drying has begun (which is not the case if a corresponding suction is applied using one of the methods developed for that purpose). Yet, if care is taken in the preparation of slurries (in the case of reconstituted soils) or the selection of relatively uniform samples (in the case of undisturbed samples of soils) and in the consolidation to specific initial void ratios by careful oedometer testing, practically identical soil samples may be reproduced and used for the measurement of both w and e at specific times after drying. Careful application of the paraffin wax method and swift movements when working with the samples which have been left to dry only for a few minutes can ensure accurate measurement of the total volume, and thus accurate calculation of the void ratio, without the need to use mercury (either TRRL or ASTM method) as proposed for the determination of shrinkage curves by Fredlund & Rahardjo (1993) and described in detail by Head (1984). Finally, given that for small time intervals after the beginning of drying the water content is not uniform throughout the sample, the sample needs to be sealed in an air-tight, plastic bag without any air in it, and placed in a dry, dark place until water content uniformity is achieved throughout the sample. Obviously, swiftness of movements both when placing the sample in the bag and when taking it out for water content and total volume measurements, is critical.

Results and discussion

The limiting lower void ratio after drying, e_r, was anticipated to be a function of both the physical properties of the soils and their initial state at the beginning of drying. In order for this to be demonstrated, e_r was initially plotted against the initial void ratio e_o (Figure 3). It appears that for a given soil, as initial void ratio increases, e_r increases too. This, as will be shown, is misleading. Normalising e_r by initial void ratio e_o as shown in Figure 4 yields that the opposite trend is true, i.e. as initial void ratio of a given soil increases, the ratio of e_r/e_o decreases, with curves for the same soil having a tendency to pass through point [$e_o=0$, $e_r/e_o=1$]. This may have been expected, given that a soil with greater initial void ratio at the start of drying, and therefore a more open structure, would naturally tend to shrink more under the influence of the suction developed during drying, and stop at a relatively smaller limiting value of void ratio in comparison with a soil with initially smaller void ratio. At the end, for a practically solid soil sample (e_o close to zero) one would expect no volume decrease and therefore the ratio e_r/e_o would lie close to unity.

Given the establishment of the trend existing between normalized e_r and e_o, the need for a normalization with physical properties was anticipated. Initial void ratio of a soil at the beginning of drying can express the structure of that soil (in the case of reconstituted soils consolidated to a specific pressure and then unloaded without any other form of structure-generating factors allowed to interfere). When

comparing results from soils with different physical properties there is a need to normalize the initial void ratio with the parameter expressing these properties.
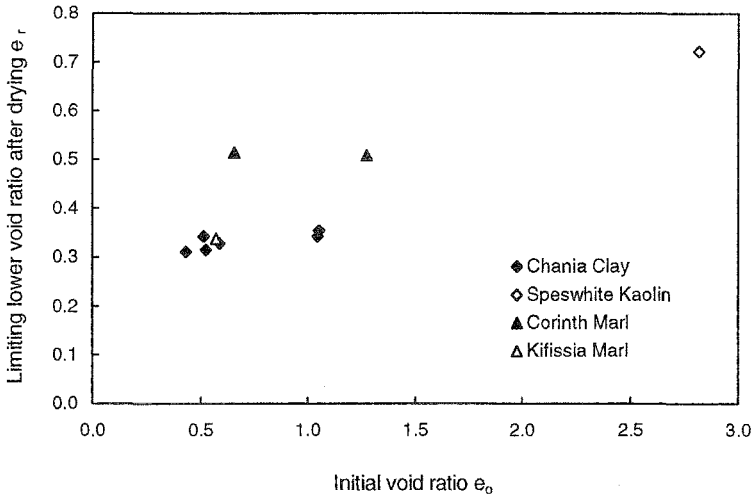
Figure 3. Limiting lower void ratio after drying e_r vs initial void ratio at the beginning of drying.
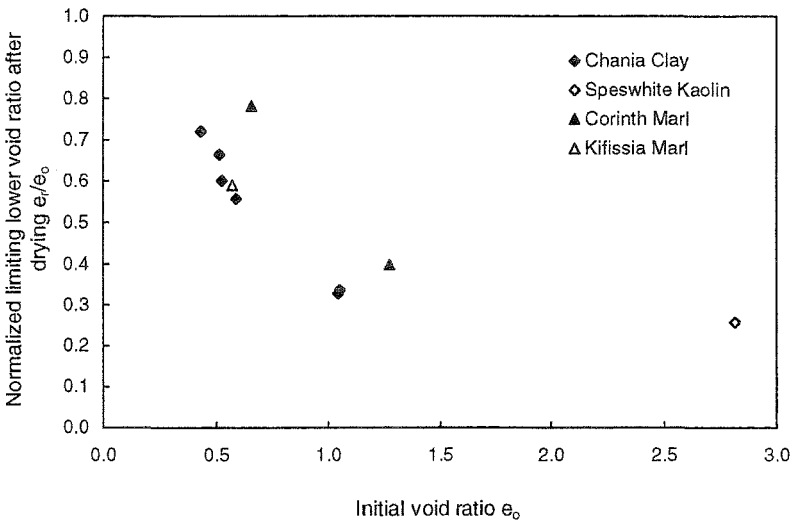
Figure 4. Normalized limiting lower void ratio after drying e_r/e_o vs initial void ratio at the beginning of drying.

The void ratio at liquid limit, e_L (= $w_L . G_s$, where w_L is the liquid limit and G_s the specific gravity), was selected as such a parameter, and the ratio of e_r/e_o was plotted against the ratio of e_o/e_L (Figure 5). As shown in Figure 5, all points tend to lie along a unique line, consistent with the aforementioned expected trend; the line practically passes through point [e_o/e_L=0, e_r/e_o=1], and is expressed by Equation 1 with a 90% degree of correlation.

$$\frac{e_r}{e_o} = 1 - m \cdot \frac{e_o}{e_L}$$

[1]

where e_r is the limiting lower void ratio after drying, e_o the initial void ratio at the beginning of drying, e_L the void ratio at the liquid limit and m is an empirical constant with value, obtained on the basis of the test results presented in this paper, 0.43. Rearranging Equation 1 by multiplying both sides by e_o and substituting e_L by $w_L \cdot G_s$, Equation 2 is obtained:

$$e_r = e_o \left(1 - \frac{m}{w_L \cdot G_s} \cdot e_o \right)$$

[2]

Equation 2 predicts the limiting lower void ratio after drying of reconstituted clayey soils on the basis of initial state, as expressed by initial void ratio e_o, the physical properties, as expressed by the liquid limit w_L and the specific gravity G_s, and an empirical constant m, found equal to 0.43 from the test results presented herein. The importance of Equation 2 in understanding unsaturated soil behavior is shown further by its incorporation into Figure 3. In Figure 6 e_r is plotted against initial void ratio e_o as in Figure 3, but with contours of e_r for constant liquid limit w_L as predicted from Equation 2 for w_L between 20 and 100% at intervals of 10% (G_s was taken to be a constant, equal to 2.65; obviously if such curves are to be determined for a particular soil the actual value of G_s should be used). These contours are convex, passing through point [e_o=0,e_r=0] predicting an increase of e_r as e_o increases until a maximum value of e_r is achieved and then e_r starts decreasing with increasing e_o until it is predicted close to 0 for very large values of e_o. Taking the first derivative of e_r from Equation 2 yields Equation 3:

$$e_r' = 1 - 2 \cdot \frac{m}{w_L \cdot G_s} \cdot e_o$$

[3]

Which, if set equal to 0, predicts the value of initial void ratio at which e_r becomes maximum for a given soil, i.e. for a given combination of liquid limit and specific gravity (Equation 4):

$$e_o(e_r \rightarrow \max) = \frac{w_L \cdot G_s}{2 \cdot m} = \frac{e_L}{2 \cdot m}$$

[4]

The lower or greater than $e_L/2m$ the initial void ratio e_o becomes, the lower becomes e_r. Also, substituting Equation 4 into Equation 2, Equation 5 is derived which describes the line shown in Figure 6 connecting the points of maximum e_r for each w_L contour:

$$e_{r,\max} = \frac{e_L}{4 \cdot m} \qquad [5]$$

Investigating the limits of application of Equation 2, e_o values at which e_r becomes 0 were examined. These are easily found to be $e_o=0$ and $e_o=e_L/m$. The case of $e_o=0$, although unachievable, is the mathematical limit of the logical assumption that the lower the initial void ratio, the lower will be the limiting void ratio after drying. For the case $e_o=e_L/m$, i.e. $e_o= \sim2.3e_L$ and given that we examine the properties of initially fully saturated soils, $w_o= \sim2.3w_L$, caution should be exercised. The maximum initial water content of slurries examined relative to liquid limit was only 1.7 times the liquid limit. Although a trend has been established, according to which, as the initial water content of the slurry increases the limiting value of void ratio after drying relative to initial void ratio should decrease, it seems unlikely that e_r/e_o will actually become 0, especially at such a low value of w_o/w_L as 2.3. The validity of Equation 2 therefore should be limited to w_o/w_L values between 1.7 and 2, at least until further tests on liquid slurries are conducted. Until then, a curve like that shown indicatively as a dashed curved line in Figure 5 should be expected to follow the linear portion of the relation between e_r/e_o and e_o/e_L expressed by Equation 2.
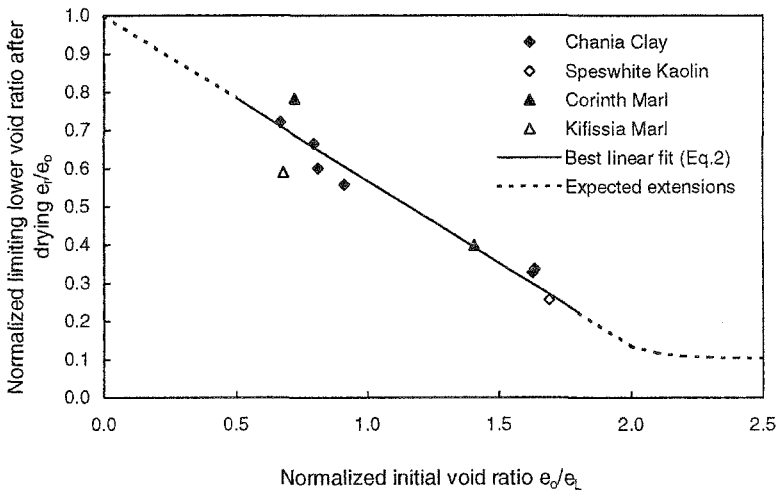
Figure 5. Normalized limiting lower void ratio after drying e_r/e_o vs normalized initial void ratio (e_o/e_L) at the beginning of drying with best linear fit and expected extensions of the relation established.
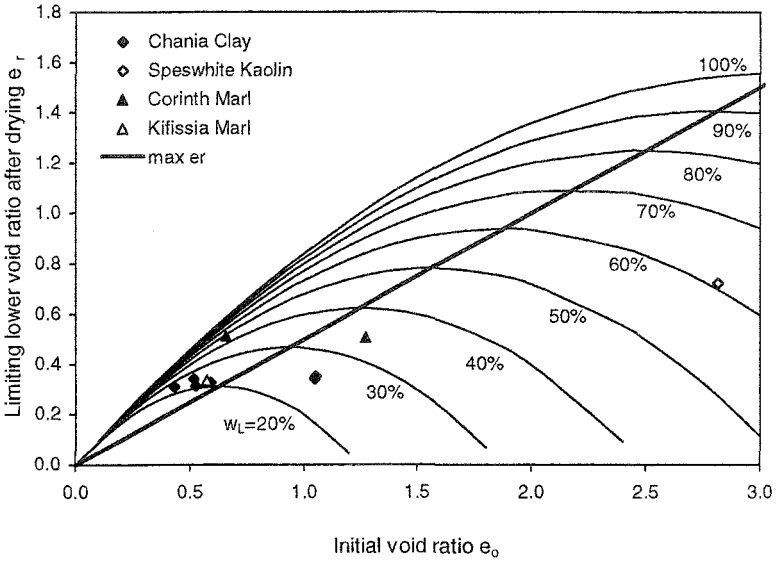
Figure 6. Limiting lower void ratio e_r after drying vs initial void ratio at the beginning of drying with contours of c_r for constant liquid limit values.

Conclusions

The limiting lower void ratio after drying of two clays and two marls, reconstituted to slurry form and then left to dry immediately or after consolidation to various initial void ratios, were measured. The ratio of the limiting lower void ratio after drying to initial void ratio at the beginning of drying, e_r/e_o, was found to decrease with increasing e_o for a given soil. The same ratio e_r/e_o was found to decrease with increasing values of the ratio e_o/e_L, with results for all soils lying very close to a unique line bearing a very high degree of correlation (90%). This relation (Equation 2) allows prediction of the limiting lower void ratio after drying of reconstituted clayey soils on the basis of initial state, as expressed by initial void ratio e_o, the physical properties, as expressed by liquid limit w_L and specific gravity G_s, and an empirical constant m, found equal to 0.43 on the basis of the test results presented.

Apart from the usefulness of such an empirical relation to predict e_r, especially in the context of constitutive modeling of unsaturated soils, and the need in that field to predict a limit to the volume change induced by suction, its importance in understanding unsaturated soil behavior was shown by predicting the maximum value of c_r that may be expected for a given clayey soil without structure

caused by natural agents. This is achieved at a value of e_o equal to $e_L/2m$ and becomes $e_L/4m$. Clayey soils with void ratio at the beginning of drying lower or greater than this value will have a lower value of e_r. The empirical relation predicting e_r should be limited to low to medium plasticity reconstituted soils in the form of slurries or consolidated to lower void ratios corresponding to w_o/w_L ratios at the beginning of drying between 0.6 and 1.7.

Further testing is needed for soils with higher plasticity and w_o/w_L ratios outside the aforementioned range, especially towards higher values, in order to investigate the extents of linearity of the empirical equation derived. The final step would be the incorporation of test results on natural, structured soils with the most intriguing aspect of the process being the need to introduce a parameter expressing structure in the relation.

Acknowledgments

References

Alonso, E. E., Gens, A., Josa, A. (1990). "A constitutive model for partially saturated soils", *Géotechnique*, **40**, 3, 405-430.

Dineen, K. (1997). *The influence of soil suction on compressibility and swelling*, PhD Thesis, Imperial College of Science, Technology and Medicine, University of London.

Fredlund, D. G., Rahardjo, H. (1993). *Soil Mechanics for Unsaturated Soils*, John Wiley & Sons, Inc., New York.

Fredlund, M. D., Wilson, G . W., Fredlund, D. G. (2002). "Reprersentation and estimation of the shrinkage curve" Juca, de Campos & Marinho (eds), Proc. 3rd Int. Conf. on Unsaturated Soils, UNSAT 2002, 10-13 March 2002, Recife, Brazil, Swets & Zeitlinger, Lisse, 1, 145-149.

Head, K. H. (1984). *Manual of Soil Laboratory Testing*, Vol. 1: Soil Classification and Classification Tests, ELE International Ltd, Pentech Press Ltd, London.

Kavvadas, M. J., Anagnostopoulos, A. G., Georgiannou, V. N., Bardanis, M. E. (2002). "Characterisation and engineering properties of the cemented Corinth marl." Tan et al (eds), Proc. Int. Workshop *'Characterisation and Engineering Properties of Natural Soils'*, AA Balkema Publishers, 2, 1435-1459.

Kavvadas, M. J., Anagnostopoulos, A. G., Kalteziotis, N. (1993). "A framework for the mechanical behavior of the cemented Corinth marl." Proc. Int. Symp. on Hard Soils – Soft Rocks, AA Balkema Publishers, 577-583.

Kohgo, Y. (2004). "Elastoplastic models for unsaturated soils with two suction effects and unsaturated soil behavior". Jucá et al (eds), Proc. 3rd Int. Conf. Unsaturated Soils, Swets & Zeitlinger, Lisse, 905-915.

Wheeler, S. J., Sivakumar, V. (1995). "An elasto-plastic critical state framework for unsaturated soil", *Géotechnique*, **45**, 1, 35-53.

Shrinkage of Clays

Amy B. Cerato[1] and Alan J. Lutenegger[2]

[1]Assistant Professor, University of Oklahoma, Department of Civil Engineering and Environmental Science, 202 W. Boyd St., Rm. 334, Norman, OK 73019; PH (405) 325-5625; FAX (405) 325-4217; email: acerato@ou.edu
[2]Professor, University of Massachusetts, Department of Civil and Environmental Engineering, 27 Marston Hall, Amherst, MA 01003; PH (413) 545-2508; FAX (413) 545-4525; email: lutenegg@ecs.umass.edu

Abstract

In many parts of the world the shrink-swell characteristics of fine-grained material is of considerable importance and of potential economic significance. Expansive soils cause significant damage to structures and roadways by cyclically shrinking and swelling within the active zone, which is defined as the depth in a soil to which periodic changes of moisture occurs. In the U.S., expansive soils cover large parts of Texas, Oklahoma and the upper Missouri Valley, and are typically montmorillonitic in nature. Traditionally there are two ways to identify the shrink-swell potential of the clay deposit: measure the shrinkage characteristics or measure the swelling characteristics. This paper discusses the shrinkage characteristics of fine-grained soils.

Four natural and pure clays were tested to determine shrinkage characteristics and the respective shrinkage curves are presented and discussed. The direct measurement of the limit of shrinkage from the shrinkage curves of the Linear Shrinkage and Shrinkage Limit tests are discussed and compared to the calculated Shrinkage Limit from the ASTM D-427 Shrinkage Limit test. It is shown that the Linear Shrinkage and the Shrinkage Limit tests produce similar shrinkage curves and a consistent Limit of Shrinkage. The calculated Shrinkage Limit from the Shrinkage Limit test underpredicts the limit of shrinkage for the soils tested and is extremely operator dependent.

Introduction

Measuring the shrinkage characteristics of a soil can help to delineate clay mineralogy (montmorillinitic-illitic-kaolinitic) and shrink/swell potential of a

geologic deposit. Two laboratory test methods of measuring the shrinkage properties of fine-grained soil are the Shrinkage Limit (Transport and Road Research Laboratory Method (TRRL), Head (1994) and ASTM D-427:04) and the Linear Shrinkage (BS-1377:90). The Shrinkage Limit test calculates the volumetric shrinkage and the Linear Shrinkage test is used to calculate one-dimensional shrinkage, although the volumetric shrinkage may be calculated. The linear shrinkage is a measure of the average oven dry length of the sample after shrinkage to the original length which occurs at an initial water content at or above the Liquid Limit. The Shrinkage Limit of a soil is defined as the water content at which no further volume decrease occurs, but where the degree of saturation is still essentially 100 % (Holtz and Kovacs 1981) (Figure 1). This curve can be reproduced in the laboratory by weighing and measuring the sample as it dries slowly over several days (TRRL Method, Head 1994). The distinct break in the curve where water content continues to decrease but volume remains constant is a direct, and the truest, measure of the limit of shrinkage. This direct measurement of the limit of shrinkage was performed in this study to have a basis to compare to the calculated Shrinkage Limit test results.
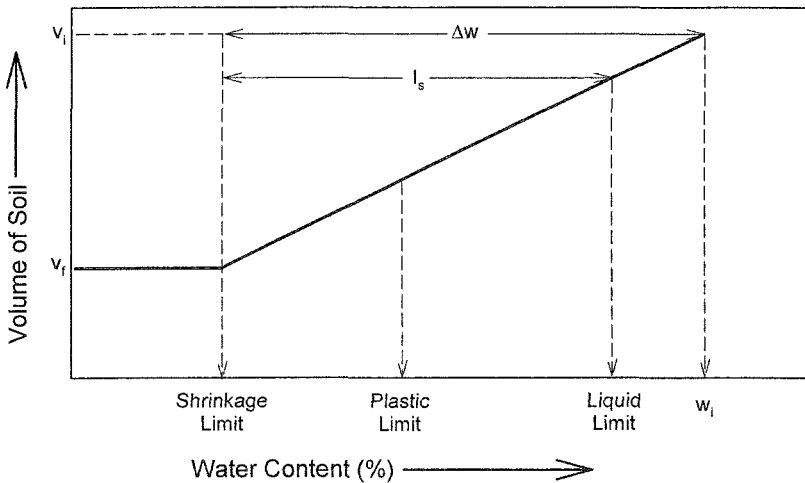
Figure 1. Definition of Shrinkage Limit.

In most cases, the shrinkage curve shown in Figure 1 is not actually determined and the Shrinkage Limit is obtained by calculation per ASTM D-427 which provides a simple point observation.

Four natural and pure clays will be tested to determine shrinkage characteristics. The direct measurement of the limit of shrinkage from the shrinkage curves of the Linear Shrinkage and Shrinkage Limit tests are discussed and compared to the calculated limit of shrinkage from the Shrinkage Limit test. It is shown that the Linear Shrinkage and the Shrinkage Limit tests produce similar shrinkage curves and that the Linear Shrinkage test, because of its ease and reproducibility is an acceptable

substitute for the operator dependent and somewhat material intensive (use of Mercury) Shrinkage Limit test.

Investigation

Three general approaches have been used to determine limits of shrinkage in clays; (1) The measurement of volumetric shrinkage of clays using mercury performed in general accordance with the British Standard (BS-1377:1990 Test 6.3) using the TRRL Method (a multi-point method that determines the shrinkage limit by measuring volumetric shrinkage using mercury while slowly drying the sample over several days to create a shrinkage curve), (2) the measurement of volumetric shrinkage of clays using mercury performed in general accordance with American Society for Testing and Materials (ASTM) D 427-04 Standard Test Method for *Shrinkage Factors of Soils by the Mercury Method* (ASTM 2005), and (3) the measurement of linear shrinkage of clays performed in general accordance with the British Standard (BS 1377:1990, Test 5). The Linear Shrinkage Test may be an attractive alternative to the Shrinkage Limit Test (ASTM D 427) which requires the use of mercury in determining the final volume of the soil pat after oven drying. The test only describes the change in length of the sample even though three-dimensional shrinkage occurs. The three dimensional shrinkage can be calculated by assuming that shrinkage is uniform in all directions.

In this study, both a direct measurement of the limit of shrinkage, which is the true measure, and a calculated shrinkage limit were determined. The direct measurement of the limit of shrinkage was determined from shrinkage curves, which were created by allowing soil in both tests to dry slowly in room temperature conditions over several days while taking frequent readings of water content and length/diameter changes. Measuring the length/diameter changes over time eliminates the need for mercury to measure the volumetric shrinkage over time, as proposed in the TRRL Method. The limit of shrinkage was determined at the water content below which there was no further decrease in volume. This direct measurement of the limit of shrinkage was compared to the calculated shrinkage limit which was determined by ASTM D-427 using the volumetric displacement of mercury.

Calculated Shrinkage Limit
An aluminum shrinkage dish was coated with petroleum jelly to prevent the soil from sticking to the dish and forming cracks when drying. The dish was filled in three layers by placing approximately one-third of the amount of wet soil to fill the dish and tapping the dish on a firm base until no apparent air bubbles remained. This step was repeated with the second and third layers and the soil was smoothed across the top of the dish with a spatula. The mass of the soil and dish was recorded. The dish and soil were air dried for a few hours until the soil turned a lighter color and then oven dry the soil at $110°$ C to constant mass. The dried dish was removed from the oven and weighed.

The volume of the shrinkage dish was found by filling the dish to slightly overflowing with mercury and pressing the glass plate down on the mercury surface to remove the excess. The mass of the dish and the mercury was obtained and the volume of the "wet soil" pat was computed by divided the mass of the mercury by the unit weight of mercury, which is 13.55 g/cm^3. The volume of the "dry soil" pat was found by filling a glass cup with mercury, using the glass plate with three prongs to remove any excess. The glass cup was placed in an evaporating dish of known mass and the dried soil from the shrinkage dish was removed and placed on the mercury surface (it floats). Using the glass plate with the three prongs, the soil pat was immersed in the mercury until the glass plate rested firmly on the glass cup with no air trapped between the mercury and the plate. The dispersed mercury was measured and the volume of the dry pat was recorded. The shrinkage limit was determined by the following equation:

$$SL = w - \left(\frac{V - V_0}{M_0} \rho_w \right) \times 100 \tag{1}$$

where:

w = Initial water content of the soil as a percentage of the dry mass (%)

$$w = \left[\frac{(M - M_0)}{M_0} \right] \times 100 \tag{2}$$

where:

M = initial wet soil mass (g)
M_0 = dry soil mass (g)
ρ_w = approximate density of water equal to 1.0 g/cm^3
V = volume of the wet soil pat or mercury in shrinkage dish (cm^3)
V_0 = volume of the dry soil pat (cm^3)

Linear Shrinkage

The Linear Shrinkage Test appears to have been first introduced by the Texas Highway Department in 1932 (Heidema 1957) and is currently described as a standard test procedure in British Standard BS 1377:1990. The bar linear shrinkage test was found to be the most reliable calcrete soil constant in road construction (Netterberg 1978) and most significant indicator of plasticity/cohesion for a gravel wearing course material (Paige-Green 1989). Haupt (1980) and Emery (1985) performed studies to determine subgrade moisture prediction models and indicated that the inclusion of the bar linear shrinkage produced as good, if not better, prediction models than the inclusion of any of the other Atterberg Limit results. Paige-Green and Ventura (1999) conclude from their evaluations of various bar linear

shrinkage tests performed that the bar linear shrinkage test is a more effective test to indicate material performance than the more traditional Atterberg limits.

The Linear Shrinkage Limit test was performed with one hundred and fifty grams of soil mixed with tap water until reaching a consistency of 15 blows in the Casagrande cup. A third of the soil was placed in a greased brass mold approximately 140 mm long and 25 mm in diameter. The soil was placed in the mold in three layers and tapped against a flat surface in between the layering to remove air bubbles from the soil. The sample was allowed to air dry for four hours. Then the soil sample was placed in an oven at 105°C for 18 hours.

After the soil was dry, the mold was removed from the oven and allowed to cool. The length of the soil sample was measured three times with digital calipers and the average was used to calculate linear shrinkage using the equation:

$$LS = \left(1 - \frac{L_{avg}}{L_o}\right) \times 100 \tag{3}$$

where:

LS = Linear Shrinkage (%)
L_{avg} = Average Length (mm)
L_o = Original Length of Brass mold (mm)

The Linear Shrinkage test potentially has a number of advantages over other tests, including:

1. The test is simple to perform
2. The test is essentially independent of operator and therefore may be subject to less variability.
3. The equipment is simple and inexpensive.
4. The test does not require use of toxic materials.
5. The test can be used for soils of low plasticity, such as silts, as well as for clays.
6. The test directly measures the desired behavior; i.e., shrinkage.

To calculate the volumetric shrinkage from a linear shrinkage test, uniform 3-D shrinkage is assumed and the volumetric shrinkage is calculated as:

$$VS = 1 - \frac{V_f}{V_o} \times 100\% . \tag{4}$$

where:

VS = Volumetric Shrinkage (%)
$V_f = 0.5 L_f \pi r_f^2$ = final volume (mm^3) $\tag{5}$

where:

L_f = final measured length (mm)
π = constant = 3.14
r_f = final calculated radius assuming constant 3D shrinkage (mm)
$V_o = 0.5 L_o \pi r_o^2$ = initial volume (mm^3)   [6]

where:

L_0 = original measured inside length of mold (mm)
r_0 = initial measured inside radius of mold (mm)

This volumetric shrinkage calculation may be related to the shrinkage index, I_s, which is the difference between LL and SL.

Tests were performed on one pure clay and three natural clays from different geologic regions: 1. Kaolinite – Georgia, 2. Residual Deposit – White Marsh, Maryland, 3. Loess Deposit – Nebraska, 4. Iowa Clay Paleosol – Highly weathered glacial till, ABE 9-7. In addition to the Shrinkage Limits and Linear Shrinkage tests, other laboratory characterization tests included Atterberg LL and PL, total specific surface area (SSA), Cation Exchange Capacity (CEC), and hydrometer analysis to determine the clay fraction (CF) (< 0.002 mm).

Results

Table 1 provides the data from the tests performed.

	Total SSA (m^2/g)	CF (%)	CEC (meq/100 g)	LL %	PL %	Calculated SL %	Direct Measure SL %	I_s	LS %
Georgia White Dirt	13	29.3	2.0	42.7	30.0	24.0	28.0	18.8	7.1
White Marsh, MD	54	33.0	7.6	35.9	20.8	11.2	18.0	24.7	10.3
Nebraska Loess	115	19.5	18.7	42.0	25.1	16.0	21.0	26.1	11.8
Clay Paleosol	298	52.2	27.0	56.5	24.1	2.4	9.0	54.1	18.9

The soils tested are arranged in order of increasing total surface area, from kaolinite to a natural soil containing montmorillonite (SSA = 13 to 298 m^2/g).

Shrinkage Curves from Shrinkage Limit Dish and Linear Shrinkage Mold
        The shrinkage curves for the four soils from both the Linear Shrinkage and Shrinkage Limit Tests are presented in Figure 2 through Figure 9. The limit of shrinkage is determined at the point at which there is no further change in specimen

dimensions. It can be seen that the shrinkage curves from the two tests are very similar and show the same limit of shrinkage value. The calculated Shrinkage Limit values from the mercury method are shown on the figures and are 2.5 to 6.8 % lower than the limit of shrinkage determined from the shrinkage curves, depending on the soil tested. Figure 2 presents typical data from both procedures for Georgia White Dirt and Figure 3 presents the same data normalized by the respective original length or diameters to show that the shrinkage curves are almost identical from both tests.
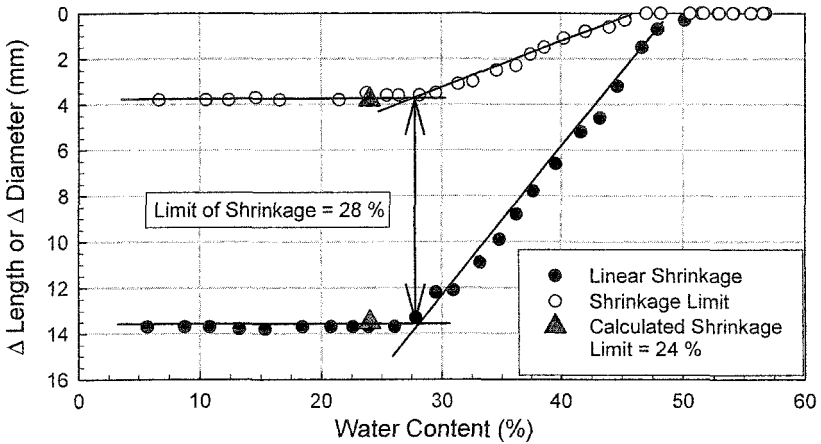
Figure 2. Georgia White Dirt Kaolinite Shrinkage Curves from Linear Shrinkage and Shrinkage Limit Tests.
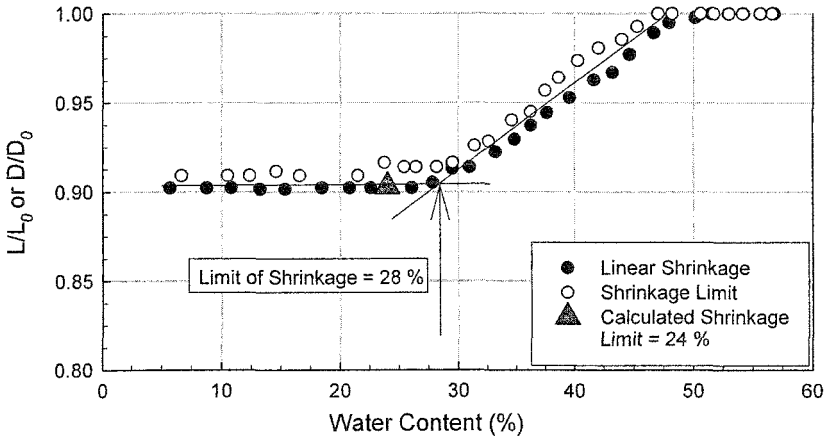
Figure 3. Georgia White Dirt Kaolinite Normalized Shrinkage Curves from Linear Shrinkage and Shrinkage Limit Tests.
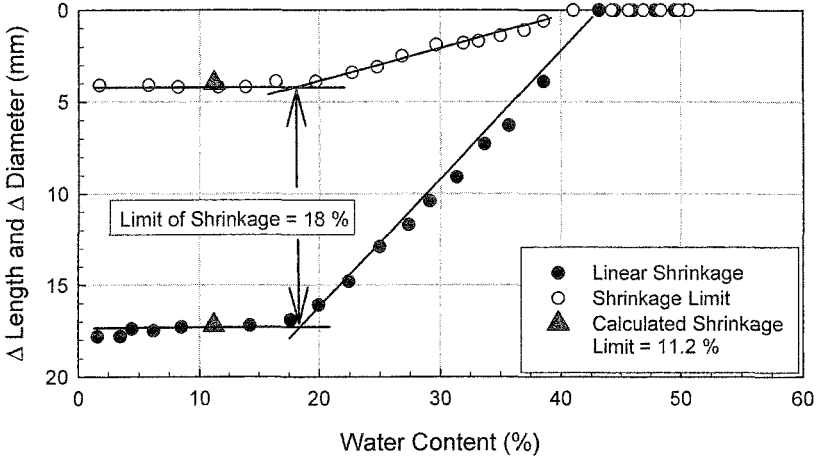
Figure 4. White Marsh Residual Soil Shrinkage Curves from Linear Shrinkage and Shrinkage Limit Tests.
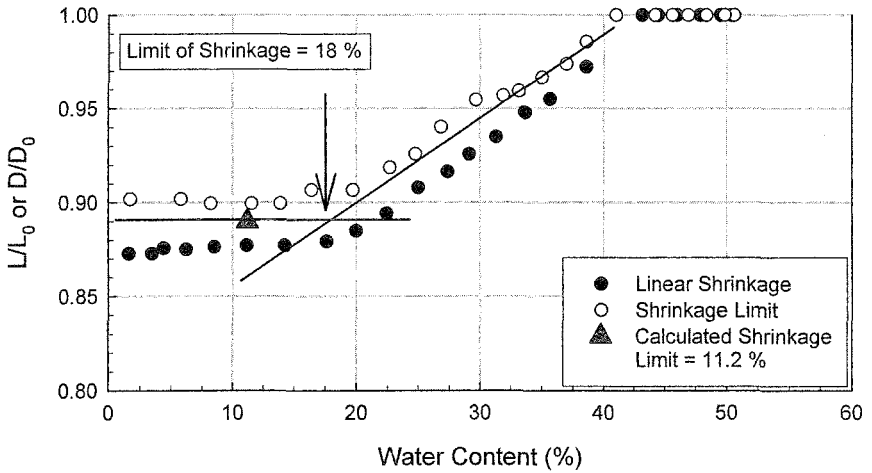
Figure 5. White Marsh Residual Soil Normalized Shrinkage Curves from Linear Shrinkage and Shrinkage Limit Tests.
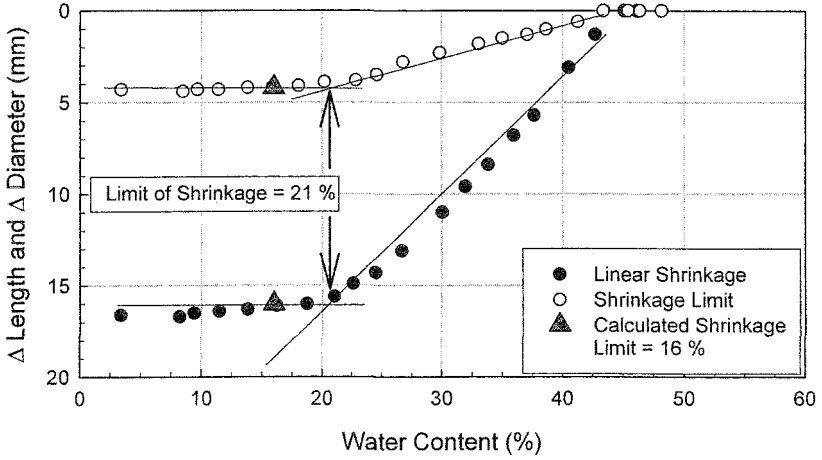
Figure 6. Nebraska Loess Shrinkage Curves from Linear Shrinkage and Shrinkage Limit Tests.
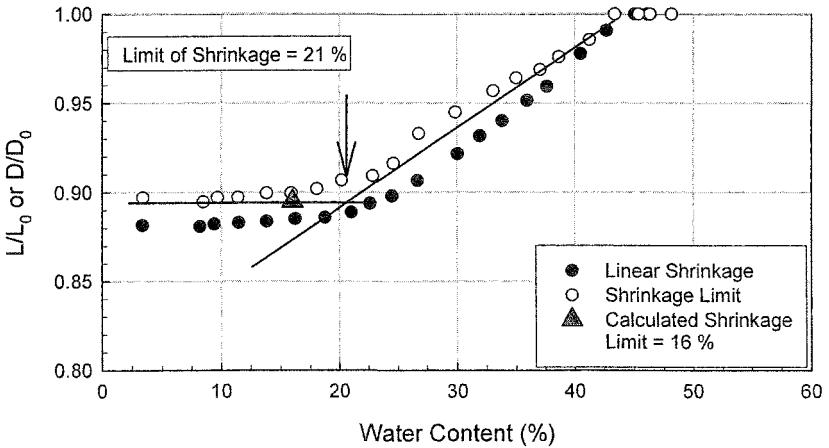
Figure 7. Nebraska Loess Shrinkage Curves from Linear Shrinkage and Shrinkage Limit Tests.

Discussion

The shrinkage limit curves, produced by measuring both the weight and length or diameter as the soil slowly dried, show a linear drying portion between length and diameter change and water content and then a distinct break at which water content

keeps decreasing but no more volume change occurs. This point is called the limit of shrinkage and occurs at the same water content for the shrinkage curves from both the shrinkage limit and linear shrinkage tests. It is the true measure of the limit of shrinkage. However, the calculated shrinkage limit using ASTM D-427 is lower than the direct measurement of the limit of shrinkage for all four soils; in one case by almost 8%. Directly measuring the limit of shrinkage by creating a shrinkage curve is the most accurate method. However, it is time consuming (> 1 week for highly expansive soils) and requires multiple measurements and care so that the soil does not dry too quickly. Therefore, although the direct measurement of the limit of shrinkage is the most accurate method, it would be preferable to obtain the shrinkage limit of a soil by making one measurement as in ASTM D-427 or BS 1377:1990.

However, performing a shrinkage limit test following the ASTM D 427-04 standard using the mercury method is extremely operator dependent, as is the newer ASTM D4943-02 Standard Test Method for Shrinkage Factors of Soil by the Wax Method, although the latter does not use a toxic material to measure shrinkage. Mercury is extremely dense and therefore, one extra or one missing drop of mercury in the displacement calculation or a crack or chip in the soil pat can change the shrinkage limit result by a few percent. Even repeat experimental tests performed by the same operator with the same soil pat can result in slightly different shrinkage limit results.

The linear shrinkage test, while easier and less operator dependent also has a few problems with repeatability, such as cracking and bowing, variations in drying, lubrication of the troughs and filling the troughs, as identified in Sampson et al. 1992. For highly expansive clays, the soil tends to bow upward during drying, therefore making a "linear" measurement extremely difficult. The use of a slot rather than a trough in order to eliminate or at least reduce bowing was first described by Wall (1959) and subsequently evaluated by Newill (1961) and Sampson et al. (1992). This slot allows material being tested to dry from two sides and makes the drying process more even. However, even with the aforementioned problems, the linear shrinkage test has been found to be repeatable to better than 1% (Wall 1959) and less than 2 % (Heidema 1957), which is considerably better than the results of the LL, PL and PI results which have been shown to be operator dependent and have large variability (Shook and Fang 1961).

It is recommended when possible, the limit of shrinkage be obtained from a shrinkage curve because that method produces the most accurate limit of shrinkage. However, when time does not permit, we recommend using the Linear Shrinkage test in lieu of the ASTM D-427 mercury method because it is very repeatable and not influenced by operator experience. If the SL is desired, the volumetric shrinkage should be calculated from the linear shrinkage test as described in Equation 4 and be related to the shrinkage ratio, I_s, which is the difference between the LL and the SL as shown in Figure 1. The volumetric shrinkage calculated from the linear shrinkage test may be higher than the I_s value because the calculated volumetric shrinkage is taken from the initial water content, which is usually higher than the LL, to the oven-dry weight, where I_s is the difference between LL and SL.
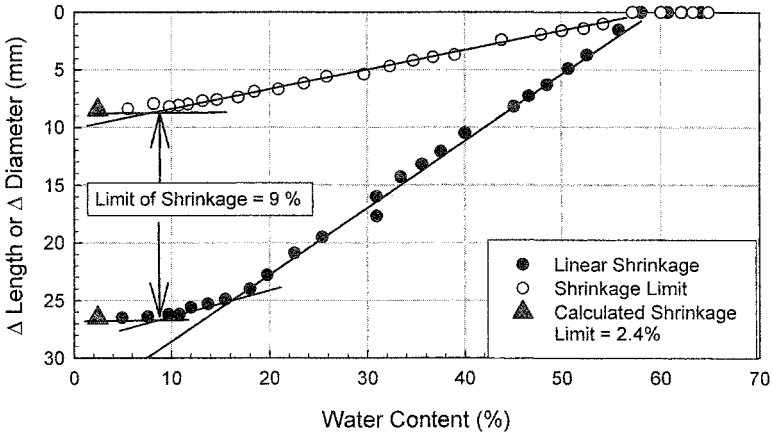
Figure 8. Iowa Paleosol Shrinkage Curves from Linear Shrinkage and Shrinkage Limit Tests.
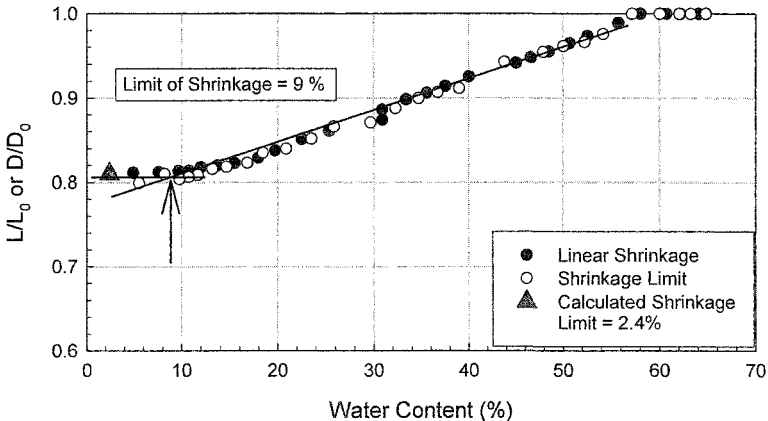
Figure 9. Iowa Paleosol Normalized Shrinkage Curves from Linear Shrinkage and Shrinkage Limit Tests.

Conclusions

After comparing the results of the calculated Shrinkage Limit test to the direct measurement of the limit of shrinkage using a shrinkage curve, it was found that the calculated Shrinkage Limit value from ASTM D-427 consistently underpredicted the limit of shrinkage directly determined from the shrinkage curve and was difficult to obtain repeatable results. Therefore, we recommend determining the limit of shrinkage by creating a partial shrinkage curve using either the Shrinkage Limit or Linear Shrinkage test procedure for sample preparation and measuring the change in

length or diameter over time. The length of time to construct a shrinkage curve may be reduced to one to two days if a few points were measured initially to construct the linear drying portion of the shrinkage curve, and then the sample was oven dried to get the final point on the horizontal line where no additional volume change takes place. The intersection of these two lines will be the limit of shrinkage. This procedure produces the most repeatable and accurate method of determining the limit of shrinkage of a soil.

References

Emery, S.J. (1985). Prediction of moisture content for use in pavement design. Ph.D. Thesis, University of Witwatersrand, Johannesburg.

Haupt, F.J. (1980). Moisture conditions associated with pavements in Southern Africa. MSc Thesis, University of Witwatersrand, Johannesburg.

Head, K.H. (1994). Manual of Soil Laboratory Testing. Soil Classification and Compaction Tests. 2nd Edition. Vol 2. pp. 99-104.

Heidema, P.B. (1957). The Bar-Shrinkage Test and the Practical Importance of Bar-Linear Shrinkage as an Identifier of Soils. Proceedings of the 4th International Conference on Soil Mechanics and Foundation Engineering, Vol. 1, pp. 44-48.

Holtz, R.D. and Kovacs, W.D. (1981). An Introduction to Geotechnical Engineering. Prentice-Hall. Ed. Newmark, N.M. and Hall, W.J.

Paige-Green, P. (1989). The influence of geotechnical properties on the performance of gravel wearing course materials. Ph.D. Thesis, University of Pretoria, Pretoria.

Paige-Green, P. and Ventura, D. (1999). The bar linear shrinkage test – More useful than we think!. 12th Regional Conference of the Geotechnics for Developing Africa. Ed. Blight and Fourie, Vol. 12, pp. 379-387.

Netterberg, F. (1978). Calcrete wearing courses for unpaved roads. The Civil Engineer in South Africa, Vol. 20, No. 6, pp. 129-138.

Newill, D. (1961). An investigation of the linear shrinkage test applied to tropical soils and its relation to the plasticity index. Crowthorne: Road Research Laboratory, Research Note RN/4106/DN.

Sampson, L.R., Ventura, D.F.C. and Kalombo, D.K. (1992). The linear shrinkage test: justification for its reintroduction as a standard South African test method. Pretoria: South African Roads Board. Research Report 91/189.

Shook, J.F. and Fang, H.Y. (1961). A Study of Operator Variability in the Determination of Liquid and Plastic Limits of Soil. HRB Highway Research Abstracts, Vol. 31, No. 9, pp. 26-28.

Wall, G.D. (1959). Observations of the use of lineal shrinkage from the liquid limit as an aid to control in the field. Proceedings of the 2nd Regional Conference for Africa on Soil Mechanics and Foundation Engineering. pp. 175-180.

Stress-strain-suction behaviour of two clayey materials under unconfined conditions

Jubert A. Pineda[1,2] and Julio E. Colmenares[2]

[1]Department of Geotechnical Engineering and Geosciences, Technical University of Catalonia, Barcelona, Spain, Jordi Girona 1-3, Building D-2, room 214; PH (+34) 646-160-736; email: jubert.pineda@upc.edu.
[2]Departament of Civil and Agricultural Engineering, National University of Colombia, Bogotá, Colombia, Ciudad Universitaria, Building 406, room 208; PH (+57) 1-3165000 ext.13312; email: jecolmenaresm@unal.edu.co

ABSTRACT: A series of unconfined undrained triaxial tests were performed, on compacted and reconstituted samples of clayey soils, at different degrees of saturation. Pore water pressure changes were recorded. Stress-strain-suction relationships were studied and analyzed. The soil water retention curve (SWRC) or any scanning curve exhibit an S-inverted shape. At low suctions the curve has a small gradient which increases and tends to be constant at intermediate suctions. Two different stress-strain-suction behaviour patterns were identified depending on the initial position (before shearing) of the soil sample on the SWRC. Samples initially located in the zone of small gradient, of the SWRC, exhibited a stress-strain-suction behaviour which is similar to that of normally consolidated samples (i.e. strain hardening), whereas samples initially in the higher gradient zone, of the SWRC, exhibited a similar behaviour to that of over-consolidated samples (i.e. dilatancy occurred). On shearing, the behaviour of the soil at peak conditions was not dependant of the initial fabric. There was no influence of the suction history of the sample before shearing.

1 INTRODUCTION

The engineering properties of an unsaturated soil can be studied by using the Soil Water Retention Curve (SWRC) which relates the suction with the gravimetric water content (w), the volumetric water content (θ) or the degree of saturation. The shape of the SWRC is related to the pore size distribution and the compressibility of the soil in relation to the suction. These two characteristics are affected by the initial water content, soil structure, mineralogy and stress history (Lapierre et al, 1990; Vanapalli et al, 1999; Marinho, 2005). Fine-grained soils typically have two levels of structure: a macro-level structure and a micro-level structure. The soil microstructure is described by the elementary particle associations within the soil, whereas the arrangement of the soil aggregates is referred to as the macrostructure (Mitchell, 1993). The resulting macrostructure of specimens prepared at different initial water contents is different in spite of their identical mineralogy, texture and method of preparation (Vanapalli et al, 1999).

Croney & Coleman (1954) stated that the moisture content held at any suction is clearly a function of the state of disturbance of the soil. If the soil is disturbed without change in moisture content, irrespective of its initial suction, it will assume a suction given by a line termed *Continuously Disturbed Line (CDL)* which has been identified as a *Critical State Line (CSL)* for the *SWRC* (e.g., Croney & Coleman, 1954; Brady, 1988). If the suction-moisture content relationship of the soil is represented by a point above this line, disturbance will cause a decrease in suction to the value given by this line at the moisture content of the sample. Similarly, if the initial suction is represented by a point below this, disturbance will be accompanied by an increase of suction until reach this curve (Croney & Coleman, 1954).

This paper shows the stress-strain behaviour of two clayey soils subjected to drying processes. Moreover, results of unconfined compression test on both soils are analyzed. The analysis of results clearly indicates that the soil fabric plays an important role on the response of soils during drying and shearing. At ultimate conditions, the behaviour of the soil is independent of the soil fabric. Finally, a relationship to evaluate the volumetric conditions under unconfined conditions is presented.

2 SOILS USED AND TEST PROCEDURE

Table 1 shows the index properties of two soils used in this research. The first material was an artificial soil composed of fine quartz silt (70%), Speswhite kaolin (20%) and London Clay (10%). The second material used was Commercial Kaolin originated from volcanic ash. The X Ray Diffraction Test indicates that the soil is mainly composed by kaolin (more that 40%). In addition, the fraction analysis of soil oxides indicated that there is silicon ($SiO_2 > 47\%$) and alumminium ($Al_2O_3 > 31\%$). The pore size distribution showed that the clay content was higher than 70%.

Clayey silt samples were reconstituted from slurry at a water content of 1.5 times the liquid limit and consolidated in an oedometer up to a total vertical stress of 200 kPa (Colmenares, 1997). Statically compacted kaolin samples were prepared at a water content of 32% and a dry density of 1.22Mg/m^3 (Pineda, 2004). The total vertical stress was equal to 400 kPa. Details of sample preparation for both soils are presented in Colmenares & Ridley (2002), and Pineda & Colmenares (2005a & 2005b).

Table 1. Index properties of Clayey silt and Commercial kaolin

	Clayey silt	Commercial kaolin
LL (%)	28.3	84
PL (%)	17.6	46
I_P (%)	10.7	38
Gs	2.64	2.61

2.1 Determination of the Soil Water Retention Curve (SWRC) on drying

The suction-water content relationships under drying for both reconstituted and compacted samples were obtained using the filter paper method. In this method the matric suction of the soil can be related to the water content of the filter paper using the calibration proposed by Chandler et al (1992). At the same time, the samples were weighed, and measured to determine its volume. The final weight was used to establish the moisture content and the void ratio of the sample at each stage of the test.

2.2 *Unconfined compression test*

Both soils were tested under unconfined conditions measuring the changes in pore water pressure. Two different techniques were used: the IC tensiometer (Ridley & Burland, 1993) and the axis translation technique (Hilf, 1956). The reconstituted samples were subjected to drying until they reached a pre-determined and different water content (matric suction) before shearing. Compacted samples were subjected to wetting until they reached pre-determined values of matric suction before shearing. Details of testing procedures can be seen in Colmenares & Ridley (2002) and Pineda & Colmenares (2005a).

3 EXPERIMENTAL RESULTS

3.1 *Soil Water Retention Curve on drying*

Figure 1 shows the gravimetric water content-matric suction relationship for reconstituted clayey silt and compacted Commercial kaolin obtained during the drying process. Additionally, the SWRC of reconstituted Commercial kaolin (consolidated to a total vertical stress of 200 kPa) obtained by Pineda-Jaimes (2003) is included. It can be seen that the drying curve for the compacted Commercial kaolin lies below that of the reconstituted kaolin but is more or less parallel up to a suction of about 1000 kPa. For a suction value of 1500 kPa the reconstituted kaolin curve merges the compacted curve and for higher suctions both follow a similar path. The differences between both curves can be explained by the different fabrics obtained by the preparation process. Reconstituted soils consist of a uniform arrangement of soil particles compressed forming a single mass. Compacted soils consist of a large number of densely packed soil "clods" with a relatively uniform arrangement of particle sizes, which is termed *the microfabric*. Those "clods" are packed together in a random arrangement, which is termed *the macrofabric* (Ridley, 1995). Although the SWRC behaviour at low suction values is heavily influenced by the macrofabric of the soil, for high values of suction (near to the residual water content) the behaviour of the soil is dependent of the microfabric (Vanapalli et al 1999). This means that for the reconstituted and compacted kaolin samples, although the macrofabrics are considerably different, the microfabrics are probably similar. Romero & Vaunat (2000) showed that for deformable clayey soils in the low range of water content (high range of suction) the behaviour of the SWRC is determined by the *specific surface*. They pointed out that the main wetting and drying paths in terms of water ratio (volume of water to volume of solids) indicate a delimiting zone in the water retention curve of an aggregated clayey fabric separating a region of intra-aggregate porosity from an inter-aggregate porosity adjoining area. In the intra-aggregate region, water is not dependent on void ratio and retention curve parameters are mainly dependent on *specific surface*. However, in the inter-aggregate region, water ratio is dependent on void ratio and strongly coupled to mechanical actions.

On the other hand, the soil water retention curves presented in figure 1 showed the same S-inverted shape. The shape of the SWRC for reconstituted clayey silt shows a more gradual reduction in water content as suction increases (which is reflected in the low slope) compared with kaolin samples. The reconstituted clayey silt presents different pore size distribution because it is composed by 3 different materials (quartz

silt, kaolin and London Clay). This result in a non-uniform grain size and pore size distributions (e.g., Delage & Lefebvre, 1983, Marinho, 2005). As a consequence, linear and less steep slope of the SWRCs (using a semi-log plot) are obtained for the clayey silt. Moreover, the clayey silt exhibits smaller suctions for the same value of water content. This is related to the clay content of the clayey silt (30%) with respect to the kaolin (more than 70%). The water storage capacity of a soil will be influenced by the macrofabric (at low suction levels) and the specific surface (at high suction levels) (Romero & Vaunat, 2000). Therefore, the suction developed for two clayey soils (with the same specific surface) will depend on the clay content of each.
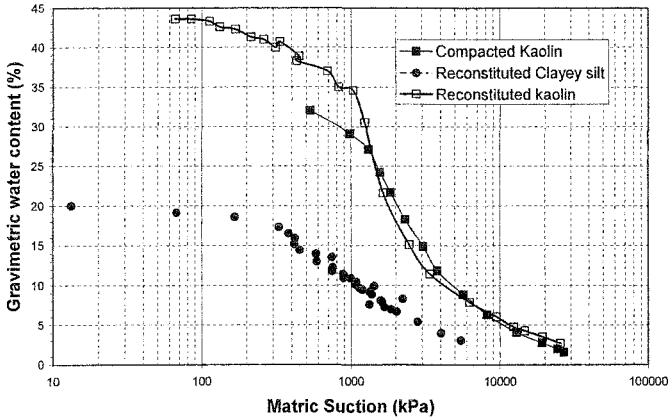
Figure 1.Water Retention Curves under drying for Reconstituted clayey silt and Reconstituted and compacted kaolin

Figure 2 shows the void ratio-gravimetric water content relationships for both the reconstituted clayey silt and the compacted Commercial kaolin. The values of gravimetric water content for which no further shrinkage occurs were obtained from figure 2. This value was defined by Dineen (2000) as the limit of volumetric shrinkage (LVS). For compacted kaolin the LVS was close to 25% (figure 3) and was equal to the value obtained by Herrera (2004) and Mendoza et al (2005). For clayey silt the LVS was close to 15.5%. The differences in LVS's values are due to different fabrics and mineralogical components.

Figure 3 shows the initial suction-gravimetric water content values for the unconfined compression test, together with the drying SWRC from figure 1. The wetting path for the compacted kaolin samples correspond to a scanning curve. Because the samples started the wetting process at relatively high water contents, the wetting path would never join the main wetting curve. Due to the hysteretic behaviour of this process, the main wetting curve will be located below the main drying curve. The hysteretic nature of this process for this material was reported by Pineda-Jaimes (2003).

On the other hand, the initial suction-gravimetric water content conditions for the clayey silt lie below the reconstituted drying line. This reduction in suction (between sample preparation and the shearing) will be the cause of an overconsolidated behaviour.
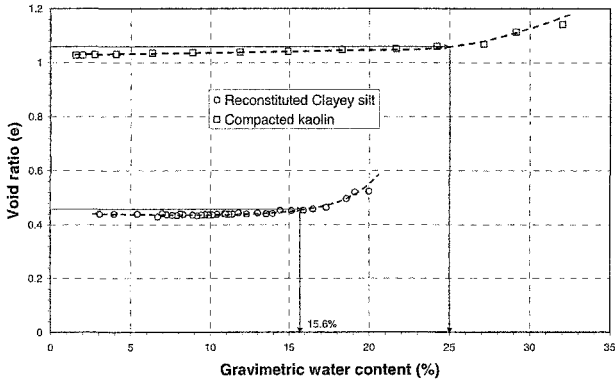
Figure 2.Variation of void ratio with the gravimetric water content for reconstituted clayey silt and compacted Commercial kaolin under drying
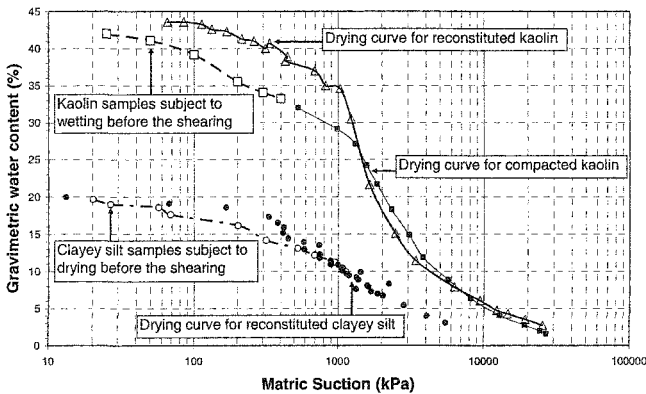
Figure 3.Initial water content-suction characteristics of unconfined compression samples

3.2 Stress-strain-suction behaviour

Figures 4 and 5 show the relationship between deviatoric stress and axial strain for the unconfined compression test obtained on reconstituted clayey silt and compacted Commercial kaolin. Those curves were presented by Colmenares & Ridley (2002) for the clayey silt and Pineda & Colmenares (2005) for the compacted kaolin. The specimens tested where also shown in figure 3 (open circles and open squares). Table 2 shows for each material, the initial water content (w/c), the degree of saturation (S_r) and suction (S), together with the maximum deviator stress (q) and the suction recorded at peak deviatoric stress. It can be seen that both clayey silt and compacted kaolin exhibit an increase in shear strength and stiffness as suction increases (degree of saturation decreases). Moreover, the axial strain at peak decreases as the initial suction increases. In both cases, this is due to the more rigid structure produced by an increase in matric suction (independent of the soil fabric).
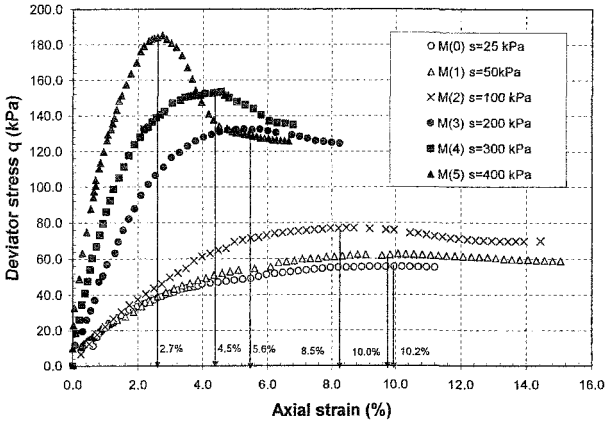
Figure 4.Stress-strain curves for compacted Kaolin samples (Pineda & Colmenares, 2005)

(a)
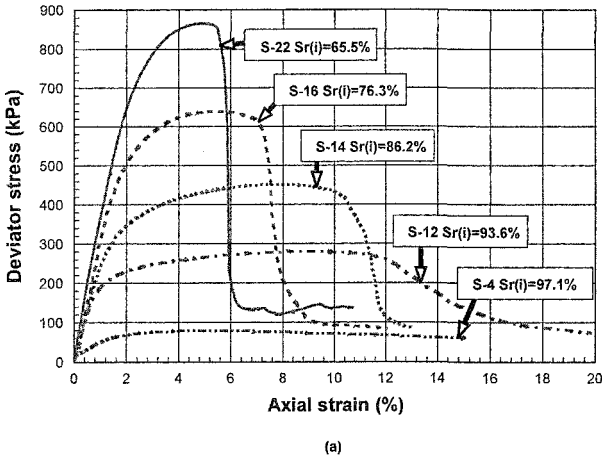
Figure 5.Stress-strain curves for compacted Kaolin samples (Colmenares & Ridley, 2002)

For a similar degree of saturation, the shear strength at peak developed for reconstituted clayey silt was much higher in comparison with results obtained on compacted kaolin. This is due mainly to two characteristics (independently of the different mineral content): (1) the more homogeneous fabric obtained in reconstituted samples which produce a uniform arrangement of soil particles compressed into a single mass; and (2) the low void ratio of reconstituted clayey silt (0.51 for clayey silt, and 1.22 for compacted kaolin). This confirms the influence of the macrofabric on the shear strength on these materials. Similar results were presented by Ridley et al (1995) on reconstituted and compacted Speswhite kaolin.

For compacted Commercial kaolin, samples with initial degree of saturation smaller than 85% showed contractant behaviour. In contrast, samples with initial de-

gree of saturation higher than this value showed a dilatant behaviour (Pineda & Colmenares, 2005). Reconstituted clayey silt shows the same behaviour but the limit value between contractant-dilatant responses was registered for a degree of saturation of about 95% (Colmenares & Ridley, 2002). However, there are some differences in the behaviour of each soil due to the wetting process (compacted kaolin samples) and the drying process (reconstituted clayey silt) before shearing. The brittle response was much more marked in samples subjected to previous drying than in those samples subjected to previous wetting (figure 3).

Table 2. Test results for compacted kaolin and reconstituted clayey silt (from Pineda & Colmenares (2005) and Colmenares & Ridley (2002)).

Sample No.	w/c (%)	Sr (%)	S_i (kPa)	S_f (kPa)	q_{peak} kPa
M0	42.00	90.10	25	40	56.0
M1	41.10	88.90	50	58	62.9
M2	39.20	84.9	100	90	77.3
M3	35.51	80.00	200	195	131.5
M4	34.07	77.10	300	283.5	153.6
M5	33.20	75.10	400	383	185
S-2	19.67	100	20.15	32.99	65.92
S-4	19.02	97.11	26.57	42.15	80.30
S-6	18.61	98.02	56.81	59.57	109.91
S-8	17.65	96.64	68.74	77.91	151.79
S-12	16.16	93.59	200.75	122.84	281.00
S-14	14.20	86.18	314.43	214.59	453.27
S-24	13.11	82.33	527.13	313.53	595.63
S-16	12.18	76.29	690.30	377.69	640.83
S-28	11.25	70.30	944.23	520.71	778.95
S-22	10.42	65.54	1060.7	692.15	865.93
S-20	9.94	62.02	1127.6	793.90	925.34

M = Compacted Kaolin   S = Reconstituted clayey silt

3.3 Gravimetric water content-suction relationships during shearing

Colmenares (1997) proposed an equation to represent the relationship between the water content and the suction at peak deviator stress (equation 1):

$$w = w_{100} - \lambda \ln\left[\frac{S_{peak}}{100}\right] \qquad (1)$$

where w_{100} is the corresponding value of water content for a suction value equal to 100 kPa, λ is the slope of the line water content versus natural log of the suction at peak, and S_{peak} is the value of suction at peak deviator stress. Pineda (2004) found that this equation can also be used for compacted kaolin under unconfined conditions. Figure 6 shows values of water content, initial suction and suction at peak for the reconstituted clayey silt and compacted Commercial kaolin together with values presented by Ridley (1995) for reconstituted and compacted Speswhite kaolin. The slope of the linear relationship for peak conditions is smaller for the clayey silt compared with that of the compacted Commercial kaolin which exhibits a different pore size distribution (different fabric).
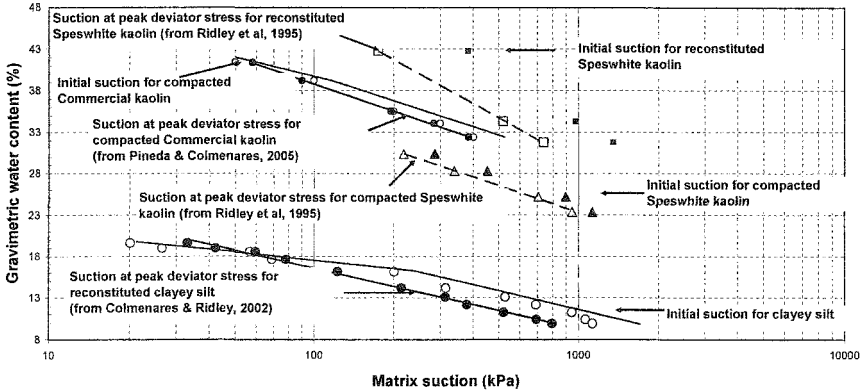
Figure 6.Initial suction and suction at peak deviatoric stress for unconfined compression test (including data of Speswhite kaolin from Ridley, 1995)

It can be seen that the final conditions for Speswhite kaolin both reconstituted and compacted showed the same linear tendency indicating that equation (1) can be used if the water content for a matric suction of 100 kPa is known. With this evidence it is clear that the relationship between gravimetric water content and suction at peak can be represented by equation (1) both for reconstituted and compacted soils tested under unconfined conditions independently of the fabric of the soil. This has been proved experimentally for suction values between 25 kPa and 1500 kPa (figure 6).

3.4 Volumetric conditions

Using equation (1) and having into account that the specific water volume is defined as $\upsilon_w = 1 + S_r e = 1 + wG_s$, a relationship between the specific water volume and the suction at peak conditions can be obtained (equation 2):

$$\upsilon_w = 1 + \left[\frac{w_{100} - \lambda \ln\left(\dfrac{S_{peak}}{100}\right)}{100} \right] G_s \tag{2}$$

where w_{100} is the corresponding value of water content for a suction value equal to 100 kPa, λ is the slope of the water content versus natural log of the suction at peak, S_{peak} is the value of suction at peak deviator stress, and G_s is the specific gravity of the soil particles. Equation (2) can be re-written as

$$\upsilon_w = \left(1 + \frac{w_{100}G_s}{100}\right) - \left[\frac{\lambda \ln\left(\dfrac{S_{peak}}{100}\right)}{100} \right] G_s \tag{3}$$

If the Air Entry Value (AEV) of the soil is higher than 100 kPa (which is true for most fine soils), the SWRC is more or less flat in this zone, and the water content

w_{100} is reasonably closer to w in saturated conditions. Thus, the first term, between brackets, in equation (3) becomes equal to the specific volume υ in saturated conditions and this relationship will take the form

$$\upsilon_w = \upsilon - f(\mu_a - \mu_w) \tag{4}$$

where the last term is a function of suction. Replacing the values of w_{100}, λ and G_s obtained for each material by Pineda & Colmenares (2005) (for compacted kaolin) and Colmenares & Ridley (2002) (for reconstituted clayey silt) in equation (3), the equations for specific water volume for the compacted kaolin (eq. 5) and reconstituted clayey silt (eq. 6) are obtained:

$$\upsilon_w = 2.02 - 0.122 \ln\left(\frac{S_{peak}}{100}\right) \tag{5}$$

$$\upsilon_w = 1.44 - 0.089 \ln\left(\frac{S_{peak}}{100}\right) \tag{6}$$

Figure 7 shows the specific water volume-suction relationships for both clayey silt and compacted Commercial kaolin calculated using the experimental data from water content and the conventional equation of specific water volume ($\upsilon_w = 1 + S_r e = 1 + wG_s$) (circles), and values of this parameter using equations (5) and (6) (lines).
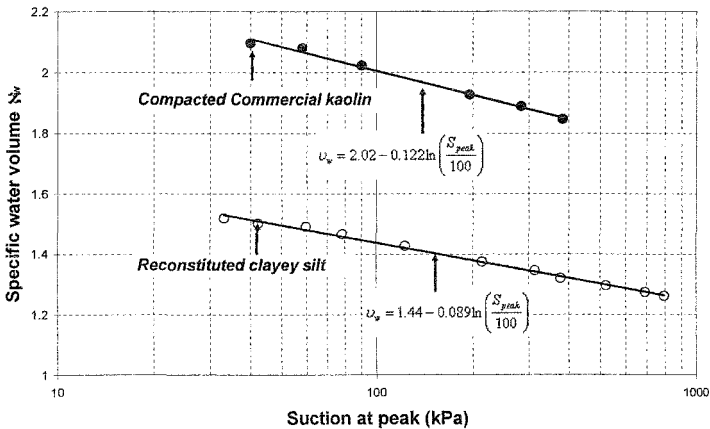
Figure 7. Specific water volume-suction relationship at peak for reconstituted clayey silt and Commercial compacted kaolin obtained using equations (5) and (6)

Values obtained using equations (5) and (6) correspond very well with experimental data. For both soils the specific water volume reduces as suction increases due to the de-saturation process (reduction in water content). In equation (5) it can be noted that the values of specific volume ($\upsilon = 2.02$) and coefficient 0.122 for compacted Commercial kaolin are very similar to values of the intercept and the slope of the critical state line (CSL) for saturated kaolin (Γ) and (λ^*) respectively. These values were obtained by Wheeler & Sivakumar (1995) on compacted Speswhite kaolin (2.011 and 0.128 respectively). Thus, equations (5) and (6) can be written in a more general form as

$$\upsilon_w = \Gamma - \lambda^* \ln\left(\frac{S_{peak}}{100}\right) \tag{7}$$

expressed in terms of critical state parameters of saturated soils (Γ) and (λ^*). A similar approach was presented by Wheeler (1991) assuming that the state variables (p-u_a) and (u_a-u_w) can be uncoupled. Moreover, the critical state parameter (λ^*) can be determined as (comparing equations (7) and (3)):

$$\lambda^* = \frac{\lambda G_s}{100} \tag{8}$$

In this expression λ^* is the critical state parameter and λ is the slope defined in equation (1). Using values of critical state parameters of Speswhite kaolin presented by Wheeler & Sivakumar (1995) the expression obtained in this paper for the specific water volume was evaluated. Specific water volume values were obtained using equation (7) and compared with values obtained from experimental data ($\upsilon_w=1+S_re=1+wGs$). The maximum error in the predicted values of υ_w was 1.5% showing the good prediction of equation (7). In the case of reconstituted kaolin this variation can not be determined because the critical state parameters are not available. However, it is assumed that for this material equation (7) can also be used. Therefore, the variation of specific water volume can be evaluated using both equations (3) in terms of parameters obtained from equation proposed by Colmenares (1997), or using the equation (7) in terms of critical state soil parameters in saturated conditions. Obviously, the test presented here are insufficient and the problem must be investigated further for different soil fabrics.

3.5 *Critical State and Continuously Disturbed State*

Figure 8 shows the form of the gravimetric water content-suction relationship for the unconfined compression test on reconstituted clayey silt and compacted Commercial kaolin together with results presented by Ridley (1995) on reconstituted and compacted samples of Speswhite kaolin. Reconstituted kaolin samples tested by Ridley fall close to the critical state line (CSL) for saturated reconstituted Speswhite kaolin. Compacted Speswhite kaolin formed a single relationship similar to the continuously disturbed line (CDL), that appears to be independent of the initial macrofabric but lies below and approximately parallel to the CSL for saturated reconstituted Speswhite kaolin (Ridley, 1995). In the case of compacted Commercial kaolin it can be seen that the gravimetric water content-suction values at failure lie between the CSL and the CDL for Speswhite kaolin.

Following Croney & Coleman (1954), the relationship obtained for Commercial kaolin can be defined as the Continuously Disturbed Line (CDL) for this soil which represents the water content-suction conditions at failure. CDL obtained for Speswhite kaolin differ of CDL obtained for Commercial kaolin due to differences in minerals content, represented by the different liquid limit (64% for Speswhite kaolin and 84% for Commercial kaolin). Differences in liquid limit are directly related with different *specific surfaces* and different water storage capacity (equal to *suction capacity* defined by Marinho & Chandler, 1993; Romero & Vaunat, 2000; Marinho,

2005). The curve obtained for reconstituted clayey silt showed the same tendency that CSL and CDL for Speswhite kaolin and the CDL for Commercial kaolin. Further testing is needed to state if the relationship presented in this paper is the CSL or the CDL for this material.
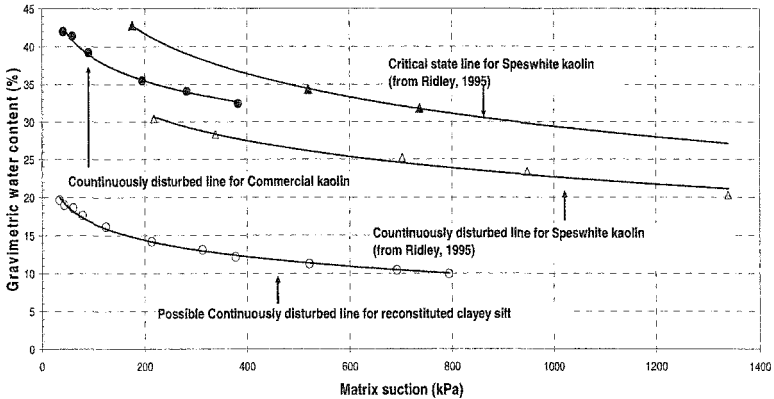
Figure 8.Critical state and Continuously Disturbed State for reconstituted clayey silt and Commercial and Speswhite kaolin (values of Speswhite kaolin Ridley, 1995).

4 CONCLUSIONS

The gravimetric water content-suction relationships of Commercial kaolin and the reconstituted clayey silt are dependent on the initial fabric of the soil. The initial position of the drying curve is controlled by the macrofabric whereas the behaviour to high suction values is controlled by the microfabric (specific surface). Results of unconfined compression test on both clayey silt and compacted Commercial kaolin showed that an increase in suction leads to an increase in both shear strength and the brittleness. Moreover, the shear strength-suction relationships are highly dependent on the macrofabric. The relationship between the gravimetric water content and the suction at peak proposed by Colmenares (1997) (eq. 1) showed to be independent of the soil fabric. Therefore, this equation can be used to represent the Critical state line (CSL) and the Continuously Disturbed Line (CDL) obtained from constant water content shear test in the range of suction between 25 to 1500 kPa (experimentally proved by the authors). Using the equation proposed by Colmenares (1997) two approaches to establish the volumetric conditions in terms of specific water volume υ_w have been presented. The first use the same parameters that are proposed in equation (3) in terms of water content. The second approach is a modification of equation (3) and it is expressed in terms of the critical state parameters for saturated soil (Γ) and (λ^*) (equation 7). Additionally, a relationship between the critical state parameter (λ^*) and the slope of the water content versus natural log of the matrix suction at peak (λ) is proposed (equation 8). The Continuously Disturbed Line (CDL) was obtained for Commercial kaolin using concepts presented by Croney & Coleman (1954). This curve is parallel to the CSL and CDL obtained by Ridley (1995) on Speswhite kaolin. This may be due to differences in the specific surface for both soils.

5 REFERENCES

Brady, K. C. (1988) Soil suction and the critical state. Geotechnique 38, No 1, pp. 117-120.

Chandler, R.J., Crilly, M.S. & Montgomery-Smith (1992) A low-cost method of assessing clay desiccation for low-rise buildings. Proc. Instn. Civ. Engng, 92;2; 82-89.

Colmenares J.E. (1997) A Comparison of Predicted and Measured Values of Shear Strength in Partly Saturated Materials. MSc Dissertation, Imperial College, University of London.

Colmenares J.E. & Ridley, A. (2002) Stress-strain and strength relationships for a reconstituted clayey silt. UNSAT 2002 (Brazil), Juca, de Campos & Marinho Edit., pp 481-484

Croney, D. & Coleman, J.D.(1954) Soil structure in relation to soil suction (pF) J.Soil Sci,5(1),75-84.

Delage, P. & Lafebvre, G. (1983) Study of the structure of a sensitive Champlain clay and of its evolution during consolidation. Can. Geotechnical Journal, 21, pp 21-35.

Dineen, K. (2000) Soil-Water Characteristic Curves. The importance of soil Suction-Short Course Notes. Junio 20-22 de 2000. London.

Herrera A.F. (2004) Estudio experimental del comportamiento volumétrico de muestras de caolín compactadas sometidas a humedecimiento. Bachelor thesis, National University of Colombia.

Hilf, J.W. (1956) An investigation of pore water pressure in compacted cohesive soils. U.S. Dept. Interior Bur. Reclamation tech. Memorandum 654.

Lapierre, C., Leroueil, S. & Locat, J. (1990) Mercury intrusion and permeability of Louiseville clay. Can Geotechnical Journal, 27, pp 761-773.

Marinho, F. (2005) Nature of Soil-Water Characteristic Curve for plastic soils. J of Geotech. And Geoenv. Eng., 131 (5), pp 654-661.

Marinho, F. & Chandler, R. J. (1993) Aspects of the behaviour of clays on drying. Unsaturated Soils, ASCE Geotechnical Special Publication No 39, ASCE, New York, 77-90.

Mendoza, C. E., Colmenares, J. E. & Merchán, V. E. (2005) Stiffness of an Unsaturated Compacted Clayey Soil at Very Small Strains. Proc. Int. Symposium Advanced Experimental Unsaturated Soil Mechanics EXPERUS2005, pp 199-204. Balkema.

Mitchell, P. W.. (1993) Fundamentals of Soil Behavior. New-York: Wiley.

Pineda, J.A. (2004) Influence of matric suction on the shear strength of a compacted soil (in Spanish). MSc Thesis in Soil Mechanics, National University of Colombia, Bogotá.

Pineda, J. A. & Colmenares, J. E. (2005) Influence of suction on shear strength of a compacted soil under unconfined condition. Part 1: Experimental results. Proc. Int. Symposium Advanced Experimental Unsaturated Soil Mechanics EXPERUS2005, pp 215-220. Balkema.

Pineda, J. A. & Colmenares, J. E. (2005) Influence of suction on shear strength of a compacted soil under unconfined condition. Part 2: Shear strength prediction. Proc. Int. Symposium Advanced Experimental Unsaturated Soil Mechanics EXPERUS2005, pp 221-226. Balkema.

Pineda-Jaimes J.A. (2003) An Experimental study of the volumetric behavior of a shallow clay from Bogotá basin following a drying path (in Spanish). MSc Thesis in Soil Mechanics, National University of Colombia, Bogotá.

Ridley, A.M., & Burland, J.B. (1993) A new instrument for the measurement of soil moisture suction. Geotechnique 43(2), pp 321-324.

Ridley, A.M (1995) Strength-suction-moisture content relationships for kaolin under normal atmospheric conditions. UNSAT 1995, Vol 2, pp 645-651. Paris.

Romero, E. & Vaunat, J. (2000) Retention curves of deformable clays. Proc. Int. Workshop on Unsaturated Soils: Experimental Evidence and Theoretical Approaches in Unsaturated Soils, Balkema, Rotterdam, The Netherlands, 91-106.

Vanapalli, S. K., Fredlund, D. G. & Pufahl, D. E. (1999) The influence of soil structure and stress history on the soil-water characteristics of a compacted till. Geotechnique, 49(2), pp 143-159

Wheeler S.J. (1991) An alternative framework for unsaturated soil behaviour. Technical note Geotechnique. Vol. 41, No. 2, pp 257-261.

Wheeler S. J & Sivakumar V. (1995) An elasto-plastic critical state framework for unsaturated soil. Geotechnique. Vol. 45, No. 1, pp 35-53.

Small-Strain Stiffness Behavior of Unsaturated Compacted Subgrade

A. Sawangsuriya[1], T. B. Edil[2], P. J. Bosscher[2], and X. Wang[3]

[1]Ph.D. Student; email: sawangsuriya@wisc.edu
[2]Professor; email: edil@engr.wisc.edu, bosscher@engr.wisc.edu
[3]Laboratory Manager; email: wang1@cae.wisc.edu
Department of Civil and Environmental Engineering, University of Wisconsin-Madison, 2226 Engineering Hall, 1415 Engineering Drive, Madison, WI 53705; PH (608) 262-3225; FAX (608) 263-2453

Abstract

This paper presents an experimental investigation of the small-strain stiffness behavior of an unsaturated compacted subgrade soil. The small-strain stiffness tests were performed under two testing schemes, namely as-compacted state (at the initial compaction condition during construction) and post-compacted state (service life after construction when subject to moisture regime changes). A non-destructive elastic wave propagation technique using bender elements was utilized to monitor and to evaluate the shear wave velocity and corresponding small-strain shear modulus (G_o) of the compacted soil specimens. A new test apparatus was designed to control two stress state variables, the net confining pressure and the matric suction, during the G_o measurements. Finally, a model was proposed for the small-strain stiffness behavior of unsaturated compacted subgrade soil.

Introduction

Compacted soils used in earthen structures are often in unsaturated state. Their mechanical behavior under unsaturated conditions has been rarely explored. In particular, very limited research has been conducted to investigate the small-strain stiffness behavior of unsaturated compacted soils. The small-strain stiffness of soils is routinely measured in earthquake engineering. In pavement engineering, the application of the small-strain stiffness tests to assess the stiffness of pavement materials and structural uniformity has been increasing (Kim and Stokoe 1992, Souto et al. 1994, Kim et al. 1997, Chen et al. 1999, Yesiller et al. 2000, Zeng et al. 2002, Nazarian et al. 2003). The main advantage of small-strain stiffness tests is the ability to non-invasively and non-destructively assess the stiffness of pavement materials at

the surface or under a free-field condition (i.e., zero or small confining pressure). Laboratory test methods are also available for measuring small-strain stiffness that can reproduce similar results to those measured in the field.

In pavement subgrade, the mean stress level (i.e., confinement effect) within the subgrade is relatively low. The vertical stress at the top of the subgrade under a properly designed pavement may be only one tenth of the tire pressure applied at the surface of the pavement since the purpose of the pavement is to limit long-term deformations of the subgrade by reducing stress (Briaud 2001). Thompson and Robnett (1979) also indicated that the confining pressure that exists in the upper regions of the subgrade of a flexible pavement system is typically small, normally less than 34.5 kPa. Furthermore, typical strain levels are also expected to be relatively small at the top of the subgrade. At small strains, the subgrade soil behaves as a linear elastic material and hence the measurement of small-strain stiffness might be considered as an appropriate parameter for characterizing pavement subgrade.

This paper presents the experimental investigation on the small-strain stiffness behavior of an unsaturated compacted subgrade soil under two testing schemes, namely as-compacted state (corresponding to the initial compaction condition during construction) and post-compacted state (corresponding to service state after construction subject to moisture regime changes). Finally, a model is also proposed for the small-strain stiffness of unsaturated compacted subgrade soil.

Properties of Test Soil

A common subgrade soil, classified as clayey sand (SC) and A-2-4(0) according to the Unified Soil Classification System (USCS) and American Association of State Highway and Transportation Officials (AASHTO), respectively, was selected for this study. This soil consists of 59% sand, 23% silt, and 18% clay with the specific gravity of approximately 2.70. The maximum dry unit weight and optimum water content are 18.5 kN/m^3 and 13.5%, respectively based on the standard Proctor effort (ASTM D 698).

Testing Program

In this study, the influence of moisture and suction variations on the small-strain stiffness of subgrade soils are explored under two testing schemes: (1) as-compacted state (at the initial compaction condition during construction) and (2) post-compacted state (service state after construction subject to moisture regime changes). The testing program for each scheme is described as follows.

As-compacted state
In the first testing scheme, the stiffness behavior is examined at the initial compaction condition. The relationship of the compaction (molding) moisture content and matric suction with the stiffness of compacted subgrade soil was investigated along the well-established dry unit weight versus moisture content relationship. The SC soil was

prepared in a 150-mm diameter standard Proctor mold using standard Proctor compactive effort (ASTM D 698). Five specimens were prepared at varying compaction moisture contents: 4 percent dry of optimum (Opt-4%), 2 percent dry of optimum (Opt-2%), 2 percent wet of optimum (Opt+2%), 4 percent wet of optimum (Opt+4%), and at optimum (Opt). The bender element test was performed to determine the small-strain shear moduli of these specimens immediately after compaction. A pair of bender elements was mounted to the sides and at the mid-height of the specimen in diametrically opposite positions. In this setup, the shear wave propagating in horizontal (diametrical) direction with soil particles vibrating in a horizontal plane (S_{hh}) was monitored and the travel time of S_{hh}-wave ($t_{s,hh}$) was measured across the diameter of the specimen (in the horizontal plane). The velocity of S_{hh}-wave is computed as $V_{s,hh} = L/t_{s,hh}$, where L is a tip-to-tip distance between source and receiver. Knowing $V_{s,hh}$ and total mass (bulk) density of the specimen (ρ), the corresponding small-strain shear modulus from S_{hh}-wave ($G_{o,hh}$) can be determined as $G_{o,hh} = \rho V_{s,hh}^2$.

The matric suctions corresponding to these specified compaction moisture contents were measured using the filter paper method (ASTM D 5298). This method was selected because of its simplicity and capability to evaluate suction in a wide range of interest (i.e., 10 kPa to 10 MPa). Moreover, it has been commonly used in geotechnical engineering applications (Fredlund and Rahardjo 1993). The filter paper used was Whatman No. 42.

Post-compacted service state
In the second testing scheme, the stiffness behavior of compacted subgrade soil subjected to the moisture regime changes subsequent to construction is examined. The stiffness of the compacted SC soil specimens prepared in the first stage was explored along the soil moisture characteristic curve. Three specimens compacted at Opt-4%, Opt, and Opt+4% were trimmed to 73-mm diameter and 25-mm height specimens. These specimens were first saturated and then subjected to a drying cycle. A new test apparatus was developed to incorporate two stress state variables, the net confining pressure (σ_o-u_a) and the matric suction (u_a-u_w), during the small-strain shear modulus measurements. Figure 1 illustrates a schematic diagram of the unsaturated small-strain stiffness test. The test apparatus comprises two major components: (1) bender element testing system and (2) triaxial cell that allows an external stress to be applied to the soil specimen and that takes into account two stress state variables. With this test setup, the horizontally polarized shear wave (S_{hh}) was measured across the diameter of the specimen (in the horizontal plane).

A desorption (drying) test was initiated by first increasing the cell pressure (σ_o) to induce a net confining pressure of 34.5 kPa while maintaining the matric suction at zero (i.e., no air pressure, u_a, is applied) and then recording the location of the air-water interface in the horizontal capillary tube. Location of the air-water interface was monitored periodically after applying σ_o and after applying each increment of u_a to establish equilibrium (i.e., the movement of air-water interface ceases). Then the travel time of S_{hh}-wave ($t_{s,hh}$) was measured across the diameter of the specimen. The

small-strain shear modulus in the horizontal plane from S_{hh}-wave ($G_{o,hh}$) was computed as aforementioned. The suction was increased successively while keeping net confining pressure constant at 34.5 kPa until the maximum suction (~1,000 kPa) was achieved.
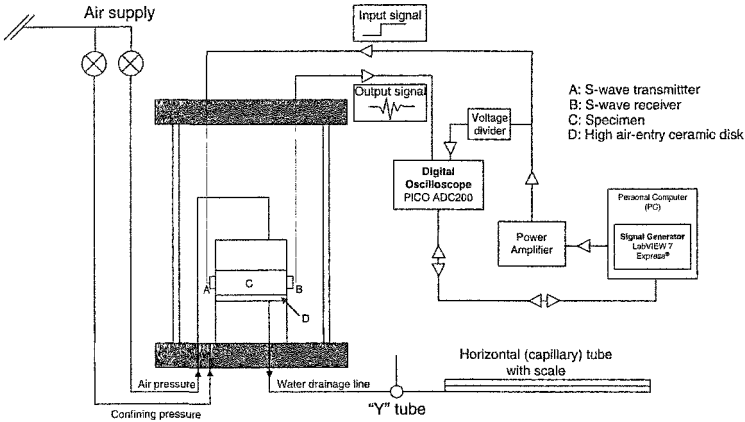
Figure 1. Schematic diagram of the unsaturated small-strain stiffness test.

Results and Discussion

Results for the as-compacted state are presented in terms of the small-strain shear modulus-matric suction-compaction moisture content-dry unit weight relationships in Figure 2. Typical variation of dry unit weight with compaction moisture content (bell-shaped compaction curve) of the SC soil is shown in Figure 2(a). The plot of small-strain shear modulus versus dry unit weight is presented in Figure 2(b). No particular trend was observed between small-strain shear modulus and dry unit weight. Moreover, the maximum small-strain shear modulus did not correspond to the maximum dry unit weight. Similar observation was also reported by Yuan and Nazarian (2003). The compaction moisture content-matric suction relationship is illustrated in Figure 2(c).

As shown in Figure 2(c), although the correlation exhibits the same trend as the soil water characteristic curve (SWCC), it does not form the SWCC but consists of a series of points corresponding to different microstructures (Graham et al. 2001). Specimens compacted at varying moisture contents are considered as points on a series of separate SWCCs that are unique for each compaction moisture content (Wan et al. 1995). Each compaction moisture content generates a unique soil structure that in turn has its own SWCC. As a result, the point for a given compaction moisture content would represent one point on the SWCC for a given initial condition. The variations of small-strain shear modulus with matric suction and compaction moisture content are presented in Figure 2(d) and Figure 2(e), respectively. In general, the small-strain shear modulus increases with increasing matric suction and decreasing

compaction moisture content. The small-strain shear modulus correlates well with both matric suction and compaction moisture content and their correlation is also better than the small-strain shear modulus-dry unit weight correlation. Furthermore, no peak in the small-strain shear modulus was observed in this range of compaction moisture contents and the maximum small-strain shear modulus was not at the optimum compaction moisture content. The small-strain shear modulus is expected to reach a peak value as the soil continues to dry for this SC soil (see Nazarian et al. 2003).
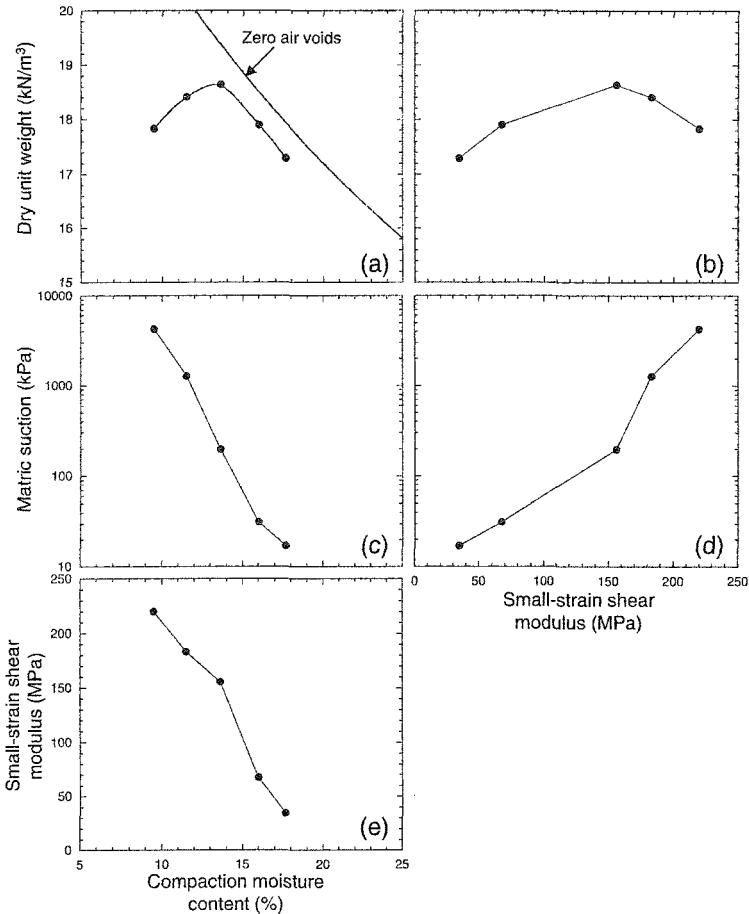
Figure 2. Small-strain shear modulus-matric suction-compaction moisture content-dry unit weight relationship for the SC soils.

Results for the post-compacted service state are presented in terms of the small-strain shear modulus and SWCC relationships. The SWCCs (matric suction versus volumetric water content) of the compacted SC soil as determined from the new test apparatus under a constant net confining pressure are shown in Figure 3. In addition, a few more data points at the very dry end of the SWCC were obtained from the chilled mirror hygrometer test since it can be assumed that no appreciable effect of the net confining pressure on the SWCC at very high matric suction (>1,000 kPa). The SWCCs were modeled by fitting the van Genuchten (1980) equation using a least-squared optimization algorithm. The van Genuchten equation was selected in this study because it has been widely used and provides a sigmoid shape of the SWCC applicable to most natural soils. The optimization algorithm results in a set of parameters, i.e., θ_s = saturated volumetric moisture content, θ_r = residual volumetric moisture content, and the van Genuchten curve-fitting parameters (α, n, and m), which provide the best fit of the measured data points. A summary of the fitted parameters for the SC soil compacted at three compaction moisture contents (Opt-4%, Opt, and Opt+4%) using standard Proctor effort are presented in Table 1. Figure 3 shows the SWCCs of the SC soil compacted at three levels of compaction moisture contents. The compaction moisture content has a considerable influence on the SWCC. The wet-of-optimum specimen had the highest air-entry suction and its SWCC lies above that of the specimens compacted at optimum and dry of optimum moisture contents. The SWCC of the specimen compacted at optimum lies in between the specimens compacted dry and wet of optimum moisture contents. The effect of compaction moisture contents is more significant at low suctions where capillary forces dominate and in predominantly fine-grained soils for which the differences in pore structure are especially important (Edil and Motan 1979, Tinjum et al. 1997).

Table 1. van Genuchten parameters for compacted clayey sand (SC).

Parameter	Opt-4%	Opt	Opt+4%
θ_s	0.308	0.261	0.320
θ_r	0.000	0.000	0.000
α (kPa^{-1})	0.253	0.007	0.004
n	1.185	1.321	1.395
m	0.156	0.243	0.283

The relationships between small-strain shear modulus and matric suction for the specimens compacted at Opt-4%, Opt, and Opt+4% are shown in Figure 4. The small-strain shear modulus increases with increasing matric suction for the range of matric suction measured. Results also agree well with previous studies (Edil and Motan 1979, Edil et al. 1981, Motan and Edil 1982). The small-strain shear modulus of the SC specimen compacted dry of optimum is greater than that of the specimen compacted at optimum and the small-strain shear modulus of the specimen compacted wet of optimum is lower than that of the specimen compacted at optimum. The relationships between the small-strain shear modulus and the volumetric water content of the specimens compacted at Opt-4%, Opt, and Opt+4% are illustrated in
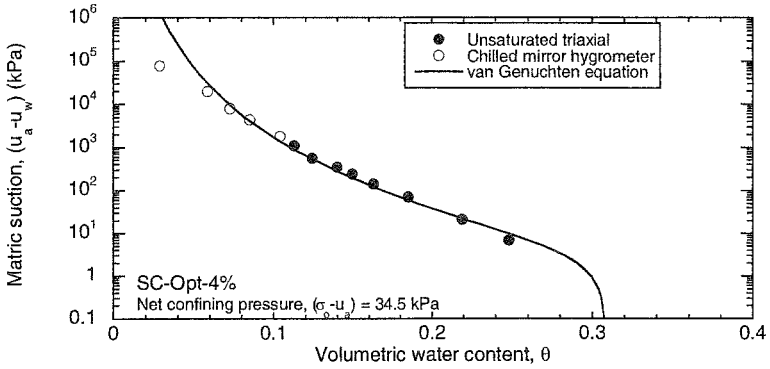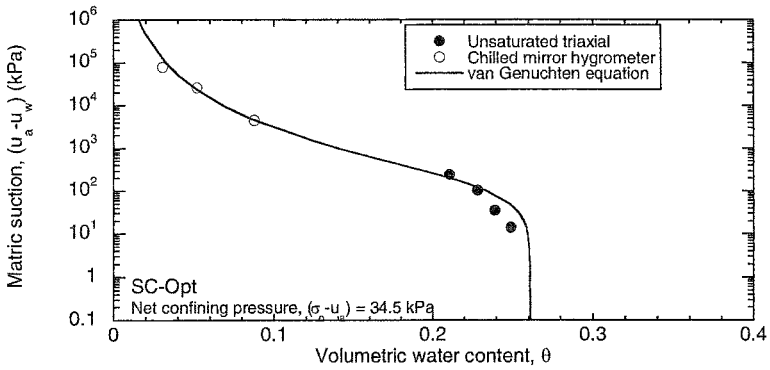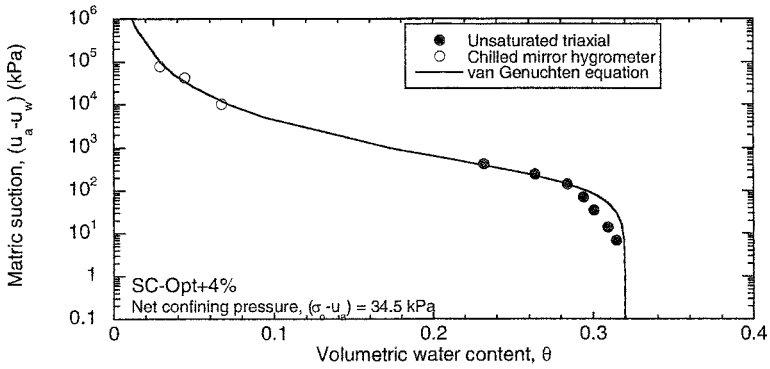
Figure 3. Soil water characteristic curves of the SC soils compacted at three compaction moisture contents.
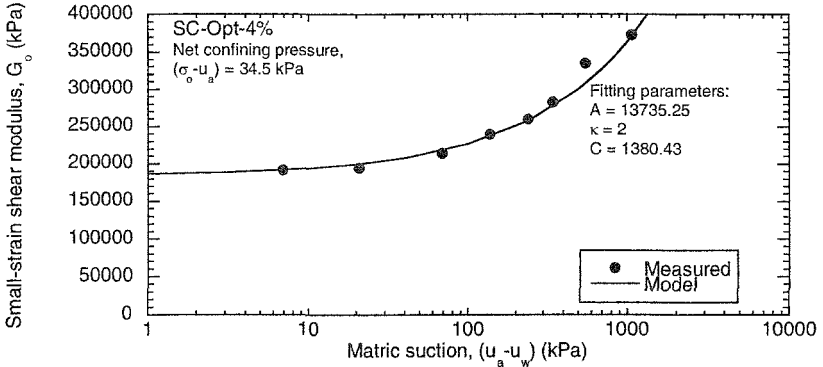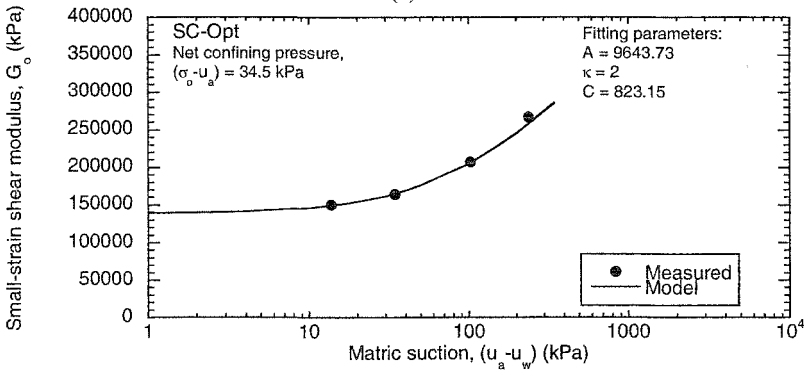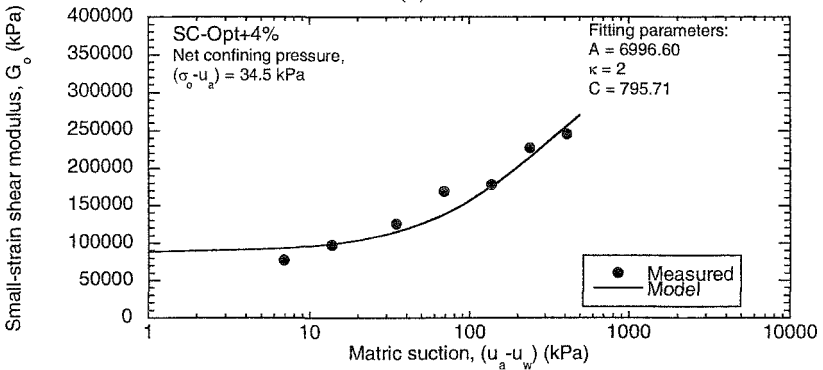
Figure 4. Small-strain shear modulus as function matric suction for the SC soils compacted at three compaction moisture contents.

Figure 5. In general, the small-strain shear modulus increases as the volumetric water content decreases for the range of volumetric water content measured. Consistent trends were also observed by Edil and Motan (1979). Similar to small-strain shear modulus-matric suction relationship, the small-strain shear modulus of the specimen compacted dry of optimum is the highest; whereas that of the specimen compacted wet of optimum compaction water content is the lowest.

Model for Small-Strain Stiffness of Unsaturated Soils

To incorporate the two stress state variables (i.e., net normal stress and matric suction terms) for describing the behavior of unsaturated small-strain shear modulus, a model is proposed. For a saturated or dry reconstituted soil, the small-strain shear modulus (G_o) can be estimated on the basis of the current state of the soil, which is presented in terms of void ratio (e) and mean effective principle stress or confining pressure (σ_o'). For the small-strain shear modulus of unsaturated soils, the dependency of modulus on the net normal stress variable and the matric suction variable must be expressed. The proposed equation for unsaturated small-strain shear modulus in the horizontal plane from S_{hh}-wave ($G_{us,hh}$) is therefore expressed as:

$$(G_{us})_{hh} = A f(e)(\sigma_o - u_a)^n + B(u_a - u_w) \tag{1}$$

where A is a material constant which is associated with soil microstructure or fabric, f(e) is a void ratio function, n is a stress exponent which is approximately 0.5 at small strains, ($\sigma_o - u_a$) is the net confining pressure, and B is a new parameter introduced in the proposed model so as to define the rate of change of G_{us} with matric suction ($u_a - u_w$). The parameter B is similar in definition to $\tan\phi^b$ for the case of shear strength of unsaturated soils (Fredlund et al. 1978) and k_s for the case of resilient modulus of unsaturated soils (Oloo and Fredlund 1998). To provide a theoretical basis for the use of the SWCC in predicting G_{us}, the normalized volumetric water content (Θ), which is expressed as $\dfrac{\theta - \theta_r}{\theta_s - \theta_r}$, is included in the model to reflect the amount of water in the soil from the saturated to the dry condition as suggested by Vanapalli et al. (1996). In the case of the shear strength of unsaturated soils, Vanapalli et al. (1996) related a parameter $\tan\phi^b$ with $\Theta^\kappa \tan\phi'$. This implies a simple linear relationship between $\tan\phi^b$ and Θ^κ by having $\tan\phi'$ as a linear fitting coefficient. Since the contribution of matric suction on the shear modulus is similar to that on the shear strength (i.e., increase or decrease the particle contact points). By having a constant C as a linear fitting coefficient, the parameter B can be rewritten as:

$$B = C\Theta^\kappa \tag{2}$$

Finally, by inserting Eq. (2) in Eq. (1), G_{us} is rewritten in the form of:

$$(G_{us})_{hh} = A f(e)(\sigma_o - u_a)^n + C\left(\frac{\theta - \theta_r}{\theta_s - \theta_r}\right)^\kappa (u_a - u_w) \tag{3}$$
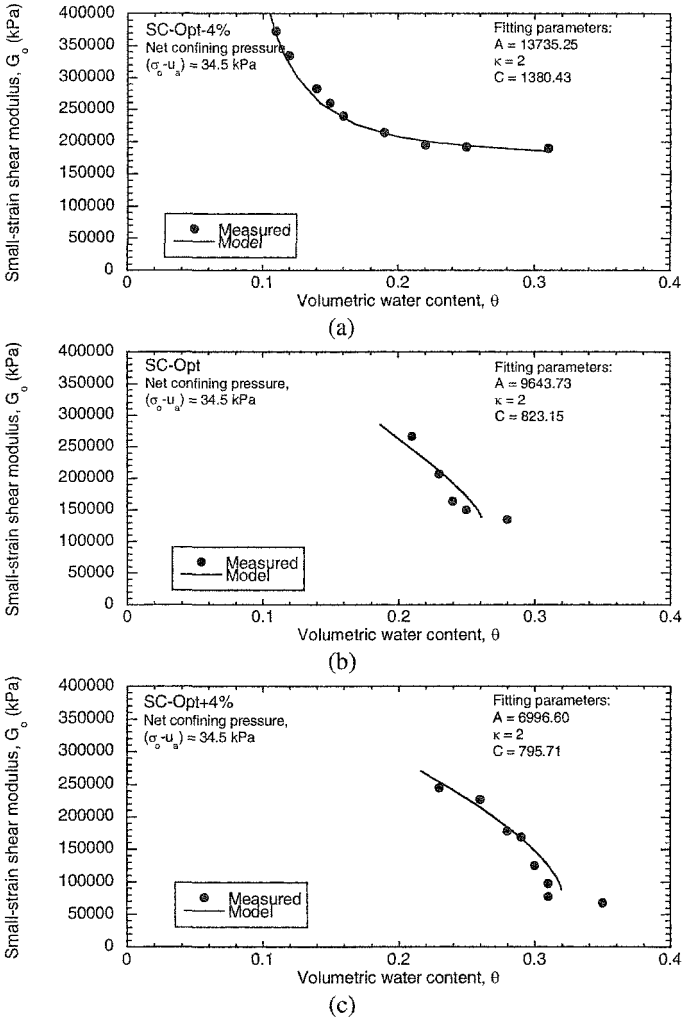
Figure 5. Small-strain shear modulus as function volumetric water content for the SC soils compacted at three compaction moisture contents.

where A, C, and κ are fitting parameters used for obtaining a best-fit between the measured and predicted values. For this model, the parameter f(e) used is given by Hardin (1978) for sands and clays as $\dfrac{1}{0.3 + 0.7e^2}$. This void ratio function has been previously employed by several investigators (Acar and El-Tahir 1986, Hardin and Blandford 1989, Inci et al. 2003). The stress exponent n used is 0.5. Note that no appreciable change in volume was observed in this study.

The proposed model was validated by fitting Eq. (3) to the experimental data obtained from the laboratory unsaturated small-strain stiffness test on three SC soil specimens prepared at Opt-4%, Opt, and Opt+4%. Figure 4 and Figure 5 illustrate the proposed model fitted with three sets of experimental data. The three fitting parameters obtained for each specimen using a least-squared optimization procedure are also provided in Figure 4 and Figure 5. To further evaluate and validate the proposed model, additional tests on other soil types are underway. In addition, to make the model more robust, future studies will include the correlation of the fitting parameters A, C and κ with the basic soil properties such as void ratio, plasticity index, and compaction moisture content.

Summary

The behavior of small-strain stiffness of an unsaturated compacted clayey sand subgrade soil has been investigated under two testing schemes, namely as-compacted state (at the initial compaction condition during construction) and post-compacted state (service life after construction subject to moisture regime changes). A new test apparatus has been developed for investigating the unsaturated small-strain stiffness behavior in such a way that it can incorporate two stress state variables, the net confining pressure and the matric suction and allow continuous small-strain shear modulus measurements. Finally, a model has been proposed for the small-strain shear modulus of unsaturated compacted subgrade.

References

Acar, Y. B., and EL-Tahir, E. A. (1986). "Low strain dynamic properties of artificially cemented sand." *J. of Geotech. Engr.*, 112(11), 1001-1015.

Briaud, J.-L. (2001). "Introduction to soil moduli." *Geotechnical News*, 19(2), 54-58.

Chen, D.-H., Wu, W., He, R., Bilyeu, J., and Arrelano, M. (1999). "Evaluation of in-situ resilient modulus testing techniques." *Recent Advances in the Characterization of Transportation Geo-Materials*, GSP 86, Reston, VA.,1-11.

Edil, T. B., and Motan, S. E. (1979). "Soil-water potential and resilient behavior of subgrade soils." *Trans. Res. Rec.* 705, 54-63.

Edil, T. B., Motan, S. E., and Toha, F. X. (1981). "Mechanical behavior and testing methods of unsaturated soils." *Laboratory Shear Strength of Soil, ASTM STP 740*, West Conshohocken, PA, 114-129.

Fredlund, D. G., Morgernstern, N. R., and Widger, R. A. (1978). "The shear strength of unsaturated soils." *Can. Geotech. J.,* 15(3), 316-321.

Fredlund, D. G., and Rahardjo, H. (1993). *Soil mechanics for unsaturated soils*, John Wiley & Sons, Inc., New York, NY.

Graham, J., Blatz, J. A., Alfaro, M. C., and Sivakumar, V. (2001). "Behavioral influence of specimen preparation methods for unsaturated plastic compacted clays." *Proc. of the 15th Int. Conf. on Soil Mech. and Geotech. Engr.*" Istanbul, Turkey, 633-638.

Hardin, B. O. (1978), "The nature of stress-strain behavior of soils." *Proc. of the Geotech. Engr. Div. Specialty Conf. on Earthquake Engr. and Soil Dynamics*, Pasadena, CA, 1-90.

Hardin, B. O., and Blandford, G. E. (1989). "Elasticity of particulate materials." *J. of Geotech. Engr.*, 115(6), 788-805.

Inci, G., Yesiller, N., and Kagawa, T. (2003). "Experimental investigation of dynamic response of compacted clayey soils." *Geotech. Testing J.*, 26(2), 125-141.

Kim, D.-S., and Stokoe, K. H., II (1992). "Characterization of resilient modulus of compacted subgrade soils using resonant column and torsional shear tests." *Trans. Res. Rec.*1369, 83-91.

Kim, D.-S., Kweon, G.-C., and Lee, K.-H. (1997). "Alternative method of determining resilient modulus of compacted subgrade soils using free-free resonant column test." *Trans. Res. Rec.*1577, 62-69.

Motan, S. E., and Edil, T. B. (1982). "Repetitive-load behavior of unsaturated soils." *Trans. Res. Rec.* 872, 41-48.

Nazarian, S., Yuan, D., and Williams, R. R. (2003). "A simple method for determining modulus of base and subgrade materials." *Resilient Modulus Testing for Pavement Components, ASTM STP 1437*, West Conshohocken, PA, 153-164.

Oloo, S. Y., and Fredlund, D. G. (1998). "The application of unsaturated soil mechanics theory to the design of pavements." *Proc. of the Fifth International Conference on the Bearing Capacity of Roads and Airfields*, Trondheim, Norway, 1419-1428.

Souto, A., Hartikainen, J., and Özüdoğru, K. (1994). "Measurement of dynamic parameters of road pavement materials by the bender element and resonant column tests." *Geotechnique*, 44(3), 519-526.

Tinjum, J. M., Benson, C. H., and Blotz, L. R. (1997). "Soil-water characteristic curves for compacted clays." *J. of Geotech. and Geoenvi. Engr.*, 123(11), 1060-1069.

Thompson, M. R., and Robnett, Q. L. (1979). "Resilient properties of subgrade soils." *Trans. Engr. J.*, 105(TE1), 71-89.

van Genuchten, M. (1980), "A closed-form equation predicting the hydraulic conductivity of unsaturated soils." *Soil Sci. Soc. Am. J.*, 44, 892-898.

Vanapalli, S. K., Fredlund, D. G., Pufahl, D. E., and Clifton, A. W. (1996). "Model for the prediction of shear strength with respect to soil suction." *Can. Geotech. J.*, 33(3), 379-392.

Wan, A. W.-L., Gray, M. N., and Graham, J. (1995). "On the relations of suction moisture content and soil structure in compacted clays." *Proc. of the 1st Int. Conf. on Unsaturated Soils*, Paris, France, 215-222.

Yesiller, N., Inci, G., and Miller, C. J. (2000). "Ultrasonic testing for compacted clayey soils." *Proc. of Sessions of Geo-Denver 2000, Advances in Unsaturated Geotechnics*, GSP 99, Denver, CO, 54-68.

Yuan, D., and Nazarian, S. (2003). "Variation in moduli of base and subgrade with moisture." *Trans. Res. Board 82nd Annual Meeting*, Washington, D.C. (CD-ROM)

Zeng, X., Figueroa, J. L., and Fu, L. (2002). "Measurement of base and subgrade layer stiffness using bender element technique." *Proc. of the 15th ASCE Engr. Mech. Conf.*, New York, NY, 1-10.

Cyclic shear behavior of unsaturated volcanic sandy soil under various suction conditions

T. Unno[1], M. Kazama[2], N. Sento[3] and R. Uzuoka[4]

[1]Geotechnical Engineering Laboratory, Department of Civil Engineering, Graduate School of Engineering, Tohoku University, Aoba 6-6-06, Aramaki, Aoba-ku, Sendai, Miyagi, JPN 980-8579; PH +81-22-795-7438; FAX +81-22-795-7435; email: unno@soil1.civil.tohoku.ac.jp
[2]ditto; email: m-kazama@civil.tohoku.ac.jp
[3]ditto; email: nsento@civil.tohoku.ac.jp
[4]ditto; email: uzuoka@civil.tohoku.ac.jp

Abstract

Mudflow type failure of a gentle fill slope occurred at Dateshita in Tsukidate town during the 2003 Sanriku-Minami earthquake in Japan. The flowed fill material was pyroclastic sediment that was classified as a volcanic sandy soil with pumice. This study reports the results of cyclic shear triaxial tests of unsaturated volcanic sandy soil considering suction. Tests were conducted for specimens with different initial suctions and the same dry density under undrained conditions for both air and water. Volcanic sandy soil specimens lost their effective stress under cyclic shear loading even if the degree of saturation is about 70%. If the initial suction is lower than the air entry value (AEV) of the soil-water characteristic curve, the effective stress of the specimens became zero or an extremely small value, and stiffness decreased. On the other hand, stiffness did not decrease in cases where the initial suction was higher than the AEV of the soil-water characteristic curve. It is considered that the variation of air distribution pattern in specimens below under the AEV and above the AEV causes the apparent difference in cyclic behaviors.

Introduction

Mudflow type failure of a gentle fill slope composed of volcanic sandy soil occurred at Dateshita in Tsukidate town during the 2003 Sanriku-Minami earthquake in Japan. Several investigative groups have reported failure details. Based on eyewitnesses' accounts, the slope failed suddenly during the earthquake and the flowed soils contained much water. Those facts indicate that the interstitial pore water plays an important role in the phase transformation from a static condition, as a

solid phase, to a fluid-like phase after shaking. On the other hand, it was also reported that rain didn't fall for a week before the date of the earthquake and that the ground surface was unsaturated. Because of the peculiar moist nature of volcanic sandy soil with pumice, the soil contained much water in its natural condition before the earthquake. Furthermore, seismic motion triggered the failure. Therefore, it has been considered necessary to study the cyclic shear behavior of unsaturated soils to clarify the mudflow type failure mechanism. The mechanical behavior of unsaturated soil is known to be influenced by soil suction. A preliminary study conducted by the author applied a shaking disturbance to unsaturated volcanic sandy soil using a shaking table test, the soil suction changed. The objective of this study is to evaluate the cyclic shear behavior of unsaturated volcanic sandy soil.

Tsukidate volcanic sand
Physical properties of volcanic sandy soil with pumice

The flowed fill material was volcanic sand with pumice, which originated from pyroclastic sediments about 800,000–1,000,000 years ago. Materials used in this study are called "Tsukidate volcanic sand". Table 1 shows physical properties of Tsukidate volcanic sand that was sampled from the remaining fill at the failure site. The listed values show representative results for several investigation points. The remaining fill was very loose: its dry density was about 1.120 g/cm^3. Measured natural water contents of 28% were found very high for sandy soils. Photograph 1 shows a scanning electron microscope (SEM) image with magnifications of x1000. Photograph 1 indicates the gravel (i.e. pumice) surface. Numerous microcavities are visible in the soil particle surface. High water content and low specific gravity are

Table 1. Physical properties of Tsukidate volcanic sand

Soil smple	Specific gravity G_s	Grain size (mm)	Fine-content $F_c(\%)$
Soil of in-situ conditon	2.478	0.000-20.00	30.0
Tsukidate volcanic sand A	2.514	0.000-2.000	35.5
Tsukidate volcanic sand B	2.523	0.075-2.000	0
Toyoura sand	2.643	0.075-0.425	0
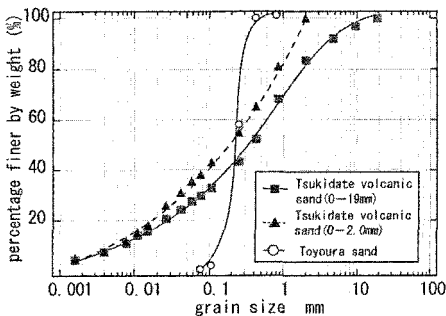
Figure 1. Grain size distribution of Tsukidate volcanic sand
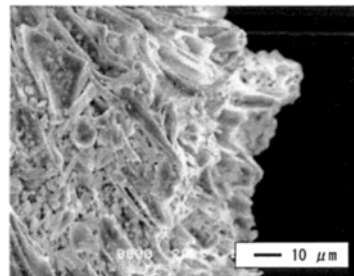
Photo 1. Pumice of Tsukidate volcanic sand

considered to be attributable to the porous microstructure of pumice. In fact, the specific gravity was 2.478. This value is smaller than that of ordinary Tayoura sand, shown in Table 1 for comparison. Figure 1 shows the grain size distributions of the Tsukidate volcanic sand that was used in this study. That of Toyoura sand is also shown for comparison. It is representative of fine clean sand in Japan. Tsukidate volcanic sand consists of about 20% gravel, 50% sand, 20% silt, and 10% clay. Series of triaxial tests were conducted for two different grain size ranges of Tsukidate volcanic sand A: 0–2.0 mm and Tsukidate volcanic sand B: 0.075–2.0 mm. Tsukidate volcanic sand B fine contents were removed by water washing.

Soil-water characteristic curves under static condition

The relationship between suction and the degree of saturation (i.e. soil-water characteristic curves) of Tsukidate Volcanic sand was studied using on two different methods.

· Water retention test (JGS standard, 1990) using axis translation technique.

· Relationship between suction and degree of saturation of consolidated unsaturated samples, which are initial conditions for triaxial tests.
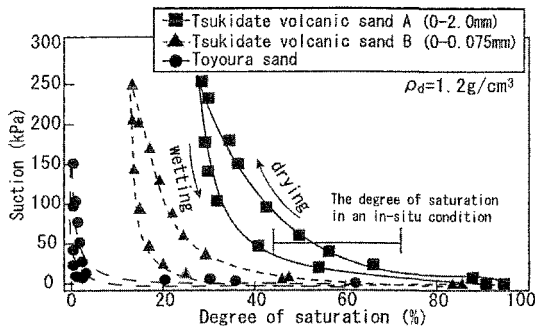
Figure 2. Soil-water characteristic curves from water retention tests
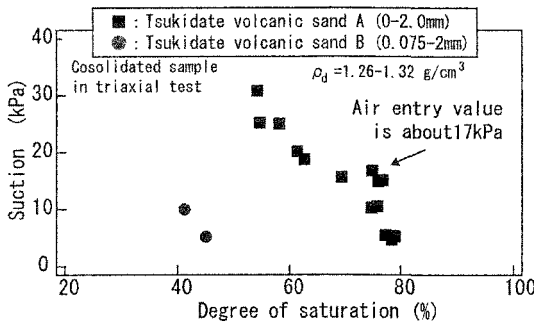
Figure 3. Relationship between Suction and Degree of saturation as an initial condition for triaxial tests

Figure 2 shows soil-water characteristic curves (SWCC) of Tsukidate volcanic sand and Toyoura sand obtained from water retention tests. Soil specimens of Tsukidate volcanic sand were adjusted to a dry density of about 1.2 g/cm^3, which is considered to resemble the in-situ condition. The curves were obtained from a stage test for the drying process and the subsequent wetting process. That is, from a full saturation condition with atmospheric pressure under a drained condition, the prescribed pore air pressure was applied and left for 24 h until the pore air pressure reached an equilibrium condition. Maximum suction of 260 kPa was applied to Tsukidate volcanic sand to find the air entry value (AEV) capacity of ceramic discs. Subsequently, the applied pore air pressure decreased gradually; suction under the

Figure 5. Example of the time history of cell pressure and pore air pressure during consolidation process
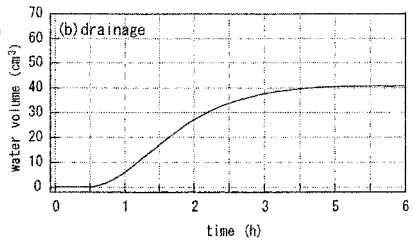
Figure 6. Example of the time history of drained water volume during consolidation process

Figure 4. Configuration of equipment of the unsaturated triaxial test system
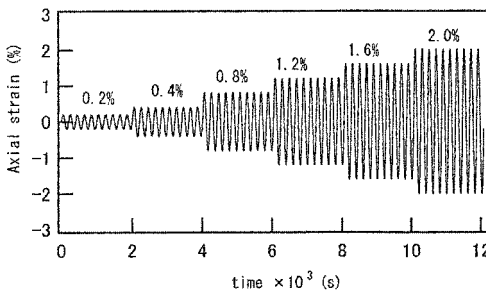
Figure 7. Time history of axial strain during cyclic loading process

following wetting process was observed. Tsukidate volcanic sand has higher water content than Toyoura sand at the same suction. This similarity implies that Tsukidate volcanic sand has a high water-retention capacity.

Figure 3 illustrates the relationship between suction and degree of saturation following a drying path of Tsukidate volcanic sand as initial conditions for cyclic triaxial tests. Suction during the tests was controlled using the axis translation technique. It is likely that the AEV of Tsukidate volcanic sand A is about 17 kPa.

Testing system and test conditions
Unsaturated cyclic shear triaxial tests

Figure 4 shows the systematic diagram of the strain-controlled unsaturated triaxial setup. In that test, pore water pressure and pore air pressure were measured to obtain the soil suction. The air entry value (AEV) capacity of ceramic discs was used as 200 kPa. The volumetric strain was measured directly using inner cell and the maximum measured volumetric strain was 25%.

Test conditions and test series

Two kinds of test series were conducted – series A and series B. Tsukidate volcanic sand A (0.00–2.00 mm) and Tsukidate volcanic sand B (0.075–2.00 mm) were used respectively as series A and series B. All test specimens with 5.0 cm diameter and 10.0 cm height were used in triaxial tests. Soil specimens were adjusted to initial dry densities of 1.20 g/cm^3 in both series of tests and initial water contents of 35% in series-A and 38% in series-B.

It is noteworthy that the soil was in a slurry condition in that situation. Then, soil specimens were consolidated under net stress (σ_{net}) of 20 kPa. Table 2 shows initial suction data for different test cases: s = 0, 5, 10, 15, 17, 20, 25, 60 kPa. The degree of saturation of these cases was 60–100%. It is noteworthy that the consolidation process of this test series was regarded as the SWCC drying process since both air and water pressures were imposed. Figure 5 and Figure 6 respectively show exemplary time histories of cell pressure and pore air pressure, and the drained water volume change during consolidation process.

Table 2. Initial properties of specimens after consolidation process

Sample	Test No	Inital Cell press σ_c (kPa)	Inital Net stress σ_{net}(kPa)	Inital w w_o(%)	Inital u_{a0} (kPa)	Inital u_{w0}(kPa)	Inital Sr Sr_0(%)	Inital volume of air V_{a0} (cm^3)	Inital void ratio e_0	Inital Dry density ρ_{d0}(g/cm^3)	Inital mean effective prinitpal stress ※ $\sigma_{m0}{}'$ (kPa)
	a–1	121.4※2	–	39.2	–	100 ※2	100	–	0.98	1.27	21.1
	a–2	27.2	21.9	28.5	5.3	0.0	78.8	18.1	0.91	1.32	26.1
Tsukidate	a–3	31.4	21.7	27.7	9.7	0.0	75.0	20.9	0.93	1.30	28.8
volcanic	a–4	35.3	19.6	28.4	15.7	0.0	76.8	18.5	0.93	1.30	32.2
sand A	a–5	36.8	20.0	27.2	16.8	0.0	75.2	22.0	0.91	1.32	33.6
(0 – 2.0mm)	a–6	38.0	20.8	25.0	17.2	0.0	69.1	25.9	0.91	1.31	31.6
	a–7	40.0	20.4	22.4	19.6	0.0	62.0	32.6	0.91	1.31	31.7
series A	a–8	44.3	19.6	19.7	24.7	0.0	54.4	38.3	0.91	1.31	33.2
	a–9	79.3	19.2	14.6	60.1	0.0	40.2	50.2	0.91	1.32	43.8
Tsukidate volcanic sand B (0.075 – 2.0mm) series B	b–1	25.1	20.0	18.2	5.1	0.0	45.8	75.6	1.00	1.26	21.4
	b–2	30.1	20.2	16.9	9.9	0.0	41.3	73.6	1.03	1.28	23.4

※ Effective stress of Unsaturated soil based on Bishop's law.
    parameter of suction χ represents the degree of saturation.
※2 Sample was saturated with back pressure of 100kPa.

Figure 7 shows that sinusoidal cyclic loading was used with a frequency of 0.005 Hz. The loading rate was sufficiently slow for achieving the equilibrium condition between air and water pressure. During cyclic shear, the migration of pore water and pore air to the outside was prevented (i.e. undrained). Table 2 depicts the initial condition of triaxial tests after the consolidation process.

Definition of pore air pressure during undrained cyclic loading process

Air pressure was measured using a pressure gauge during the consolidation process under a drained condition (i.e. during consolidation, the migration of pore water and pore air to the outside were allowed). However, during the undrained cyclic shear loading process, the measured pore air pressure was inaccurate because of the triaxial test system in this study. In this test system, the inner volume of the air pressure measuring tube, which connects between the two-way valve and top of the specimen in Figure 4, is 7.5 cm^3. During the cyclic loading process, the pressure gauge, which measured air pressure, was influenced by the length of the air pressure measuring-tube.

The air pressure during cyclic loading was determined using the following approach. During cyclic loading, the volumetric strain of specimen was measured from the volume change of inner cell directly because the variation of volumetric strain of air is much larger than that of soil particles and water. Therefore, volumetric strain is the amount of volumetric shrinkage of pore air. Pore air pressure during cyclic loading is obtainable using the Boyle-Charles' law (fixed temperature). The air pressure is defined by the following equation:

$$(V_c + V_{a0})u_{a0} = V_c u_{a,mes} + (V_{a0} + \Delta V_a)u_{a,soil},$$ (1)
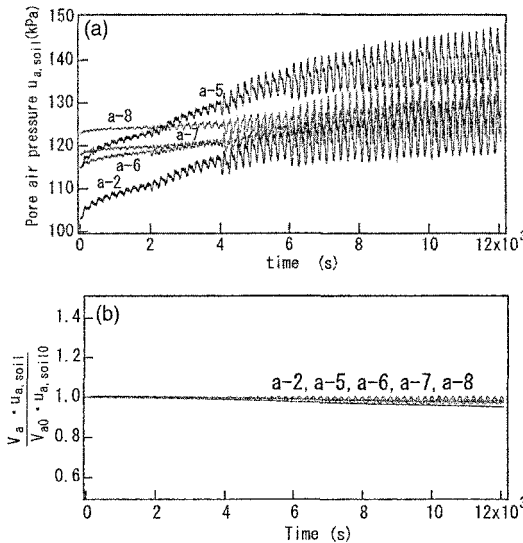
Figure 8. Time history of pore air pressure $u_{a,soil}$ and u_a*V_a
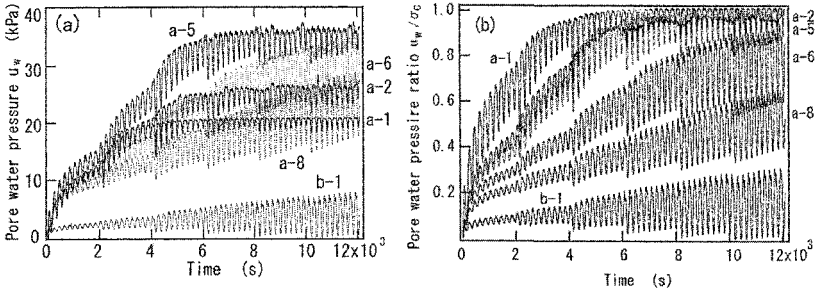
Figure 9. Pore water pressure and the pore water pressure ratio
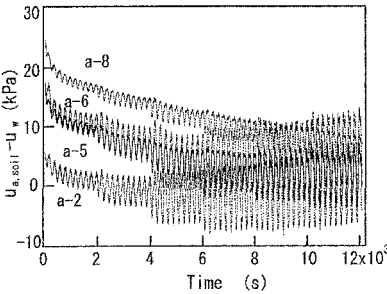
**Figure 10. Time history of
suction during cyclic loading**
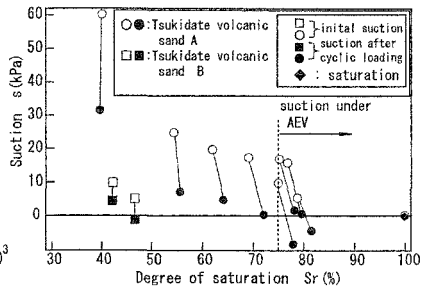
**Figure 11. Changes of suction
and the degree of saturation
between before and after cyclic
shear**

where V_c represents the volume of air pressure measuring tube (7.5 cm^3) and V_{a0} is the initial volume of pore air, u_{a0} is the initial air pressure, $u_{a,mes}$ is the measured air pressure using the pressure gauge (i.e. air pressure in the measuring tube), and $u_{a,soil}$ is the assessed pore air pressure finally, ΔV_a is assumed equal to the volumetric change of the specimen. Figure 8(a) depicts for some tests the time history of the assessed pore air pressure $u_{a,soil}$ and Figure 8(b) illustrates the time history of $V_a u_{a,soil}$ during cyclic loading, where $V_a (= V_{a0} + \Delta V_a)$ is the pore air volume. This value was normalized by $V_{a0} u_{a,soil0}$, where V_{a0} and $u_{a,soil0}$ respectively represent the initial pore air volume and the initially assessed pore air pressure. The assessed pore air pressure $u_{a,soil}$ increased with time in all test cases. On the other hand, the normalized value of $V_a u_{a,soil}$ is almost unity, implying that the assessed pore air pressure was reasonable. Therefore, in this research study, $u_{a,soil}$ was used to represent the pore air pressure of soil during cyclic loading.

Test results of cyclic shear test
Pore water pressure and suction behavior

Figure 9(a) and Figure 9(b) respectively indicate the time histories of pore water pressure, and pore water pressure ratio. Pore water pressure ratios were obtained by normalizing the pore water pressure by its initial effective principal stress, similarly to the liquefaction test. Figure 9(a) shows that the pore water pressure increased under cyclic loading. Ultimately, each specimen's pore water pressure increased and approached the cell pressure (i.e. total stress). Figure 9(b) shows that the pore water pressure ratio of specimens with initial suction under AEV increased to near 1.0.

Figure 10 shows suction behavior during cyclic loading of Series-A. Suction was obtained by subtracting pore water pressure from the assessed pore air pressure. Suction decreased during cyclic loading because pore water pressure and pore air pressure increased and the final suction of some specimens became less than zero (i.e. under atmospheric pressure). Figure 11 illustrates the change of relationship between suction and the degree of saturation before and after the cyclic loading process. The degree of saturation increased with cyclic loading because of the development of volumetric strain. The degree of saturation of the samples' initial suction under AEV (i.e. 17 kPa) reached zero or less than zero. For that reason, the degree of saturation increased if the initial suction was less than the AEV. Table 3 shows test results after cyclic shear loading.

Definition of effective stress

Equation (2) shows the effective stress of unsaturated soil as defined based on Bishop's proposal (1963).

$$\sigma' = (\sigma - u_a) + \chi(u_a - u_w) \tag{2}$$

In that equation, u_a, u_w and χ respectively represent the pore air pressure, pore water pressure, and the material parameter. Several definitions have been proposed by authors for parameter χ (Bishop et al., 1963; Karube et al., 1996; Gallipoli et al., 2002). In this study, parameter χ is defined as the degree of saturation.

Stress-strain relationships and effective stress paths

Figure 12 shows exemplary test results. Figure 12(a) depicts stress-strain relationships here as Figure. 12(b) depicts the effective stress paths during cyclic loading for several cases.

In the saturated soil specimen, the stiffness decreased during cyclic loading and the mean effective principal stress reached zero. That soil specimen liquefied. In this case, the effective stress is definable using Terzaghi's definition.

Results of unsaturated specimens No. a-2 (u_{a0}=5.3 kPa, Sr_0=78.8%) and No. a-5 (u_{a0}=16.8 kPa, Sr_0=75.2%) indicate that the peak of the deviator stress decreased with increasing strain amplitude and that the stiffness decreased in each cycle loading. Consequently, the mean effective principal stress became zero. This test case had initial suction that was lower than AEV. On the other hand, the result of No. a-6 (u_{a0}=17.2 kPa, Sr_0=69.1%) and that of a-8 (u_{a0}=24.7 kPa, Sr_0=54.4%) show different

behaviors from those of Nos. a-2 and a-5. The peak of the deviator stress of Nos. a-6 and a-8 did not decrease with increasing strain amplitude, even though the stiffness decreased in each cycle loading. In these cases, the mean effective principal stress decreased during cyclic loading. However, it did not reach zero. The result of a-8 illustrates that the mean effective principal stress became about 50% of its initial value and was not zero.

The result of b-1, which had the same initial suction of a-2, resembled the result of a-8. In other words, the peak of the deviator stress did not decrease, whereas strain amplitude developed and the mean effective principal stress decreased, but did not become zero.

These results demonstrate that, if the initial suction is lower than AEV, the effective stress of the specimens becomes zero or an extremely small value, and stiffness decreased. In contrast, if the initial suction is higher than the AEV of soil-water characteristic curve, then stiffness does not decrease. It is believed that the variation of air distribution patterns in specimens below the AEV and above the AEV causes the apparent differences in cyclic behavior. Note that suction values lower than the AEV also correspond to high degree of water saturation and reduced mobility of the air phase and water phase inside the pore space. Thus, it seems likely that Bishop's effective stress decrease is mainly due to both pore air pressure and pore water pressure (Figure 8 and 9).

Dissipation energy

Stress-strain loops were obtained based on time histories of stress and strain. The dissipation energy was estimated as a function of time by integrating the area covered by the stress-strain loops and calculated as follows.

$$\Delta W(t) = \oint \tau(\gamma) d\gamma = \int_0^t \tau(\gamma) \dot{\gamma}(t) dt \tag{3}$$

In those equations, $\Delta W(t)$ represents the dissipation energy accumulated by time t, $\tau(\gamma)$ is the shear stress in terms of shear strain, and $\dot{\gamma}(t)$ is the rate of shear strain, where shear stress was obtained as half the deviator stress and shear strain was obtained as 1.5 times the value of axial strain.

The accumulated dissipation energies during the cyclic loading process for different test cases are shown in Figure. 13. The accumulated dissipation energy was normalized with respect to its initial effective principal stress. Normalization by the initial effective stress derives from the same concept as the current evaluation method of liquefaction potential using undrained cyclic shear strength curve.

Differences in the behavior of cases a-1 – a-5 and case a-6 are apparent in Figure 13. The normalized dissipation energy of the saturated specimen and unsaturated specimens with initial suction less than 17 kPa (i.e. under AEV) were low. However, the normalized dissipation energy of unsaturated specimens with initial suction over AEV is remarkable.
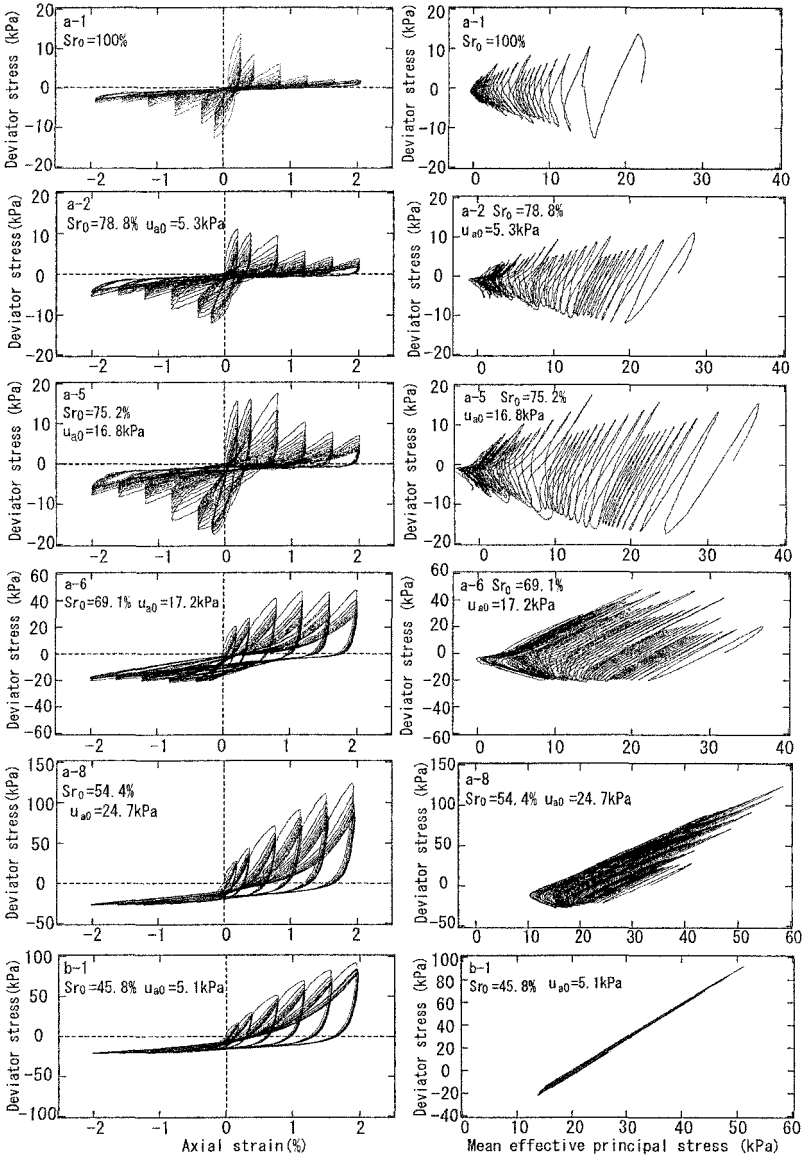
(a) Stress vs. Strain relations (b) Effective stress path
Figure 12. Test results of unsaturated cyclic shear triaxial tests
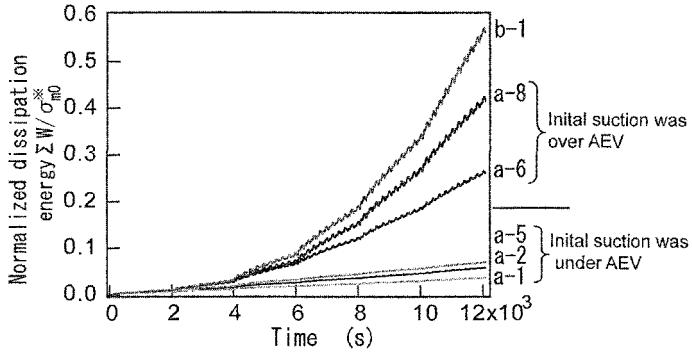
Figure 13. Time history of normalized dissipation energy

Table 3. Test results

Test sample	Case No	Volume change pore air ΔV_a (cm^3)	Measured pore air press $u_{a,mes}$ (kPa)	Degree of saturation S_r (%)	Pore water press u_w (kPa)	Pore air press Boyle-Charles' law $u_{a,soil}$ (kPa)	Suction $u_{a,soil} - u_w$ (kPa)	MEPS* σ_m^* (kPa)	Normalized dissipation energy $\Sigma W / \sigma_{m0}^*$ -
Tsukidate volcanic sand A (0-2.0mm)	a-1	-	-	100	21.4	-	-	-0.1	0.036
	a-2	3.4	17.2	81.6	27.4	22.8	-4.6	0.4	0.056
	a-3	3.2	23.9	77.9	32.1	23.5	-8.6	0.9	0.075
	a-4	3.2	21.5	79.7	34.8	35.3	0.5	0.0	0.035
	a-5	3.9	25.1	78.2	36.8	38.4	1.6	-0.7	0.066
	a-6	3.7	29.0	72.2	32.9	32.8	-0.1	3.7	0.249
	a-7	-1.7	29.9	64.2	26.6	31.3	4.7	10.4	0.284
	a-8	-1.0	31.5	55.7	23.2	30.3	7.1	14.8	0.367
	a-9	-1.1	57.8	39.7	26.0	57.4	31.4	29.0	0.338
Tsukidate volcanic sabd B (0.075-2.0mm)	b-1	-1.5	8.6	46.7	5.3	4.1	-1.2	17.1	0.563
	b-2	-1.9	13.2	42.2	8.8	13.3	4.5	15.4	0.623

MEPS* – mean effective principal stress using bishop's law

Conclusion

The authors conducted cyclic shear triaxial tests under an unsaturated condition using volcanic sandy soil, which was the fill material of slope that failed during the Sanriku-minami earthquake in 2003. Conclusions obtained from this study are summarized as follows:

1) Tsukidate volcanic sand has high water retention capacity and an air entry value (AEV) of 17 kPa.

2) The suction of unsaturated specimens decreased during cyclic loading. The grade of the decline of soil suction depended on the initial degrees of saturation.

3) In the initial suction lower than the AEV of soil-water characteristic curve, the effective stress of the specimens became zero or an extremely small value, and stiffness decreased. On the other hand, stiffness did not decrease in the initial suction higher than the AEV of soil-water characteristic curve.

4) It is considered that the variation of air distribution patterns in specimens under the AEV and over the AEV cause the apparent difference in cyclic shear behavior.

References

Joint Delegation Team with Japan Society of Civil Engineers and The Japanese Geotechnical Society (2003). "Reconnaissance report on the May 26, 2003 Miyagiken-Oki Earthquake." *JSCE*, (in Japanese).

Fukuoka, H., Wang, G., Sassa, K., Wang, F., and Matsumoto, T. (2004). "Earthquake-induced rapid long-traveling flow phenomenon: May 2003 Tsukidate landslide in Japan." *Landslides,* 2, pp.151–155.

Uzuoka, R., Sento, N., Kazama M., and Unno, T. (2005). "Landslides during the earthquakes on May 26 and July 26, 2003 in Miyagi." *Soils and Foundations*, Vol.45, No.4, pp.149–163.

Kazama M., Uzuoka, R. Sento, N., and Unno, T. (2004). "Soil-water characteristic curve of volcanic sandy soil which caused mudflow type failure during the 2003 Sanriku-minami earthquake, *Taiwan-Japan Joint Workshop on Geotechnical Hazards from Large Earthquakes and Heavy Rainfall*, Taipei, Taiwan.

Kazama M., Unno, T., Sento, N., and Uzuoka, R. (2005). "Mudflow type failure of artificial fill with volcanic sandy soil during the earthquake on May 26, 2003 in Japan." *International Geotechnical Symposium on Geotechnical Aspects of Natural and Man-made Disasters*, Astana, Kazakhstan, pp.31–36.

Unno, T., Kazama M., Uzuoka, R., and Sento, N. (2004). "Change of moisture and suction properties of volcanic sand induced by shaking disturbance." *Soils and Foundations*, (submitted in 2004).

Japanese Geotechnical Standards No. T151, (1990).

Bishop, A.W. and Blight, G.E. (1963). "Some aspects of effective stress in saturated and partly saturated soils." *Geotechnique,* Vol.13, No.3, pp.177–197.

Gallipoli, D., Gens, A., Vanet, J. and Romero, E. (2002) "Role of degree of saturation on the normally consolidated behavior of unsaturated soils." *Proc. of 3rd Int. Conf. on Unsaturated Soils*, pp.115–120.

Karube, D., Kato, S., Hamada, K., and Honda, M. (1996) "The relationship between mechanical behavior and the state of pore water in unsaturated soil." *JSCE, Journal of Geotechnical Engineering*, No.535/ III-34, pp.83–92 (in Japanese).

Effects of stress-strain history on the initial shear stiffness of an unsaturated compacted silt

R. Vassallo[1] C. Mancuso[2] and F. Vinale[3]

[1]Dipartimento di Strutture, Geotecnica, Geologia – Università della Basilicata, 85100 Potenza, Italy; PH (+39) 0971-205390; FAX (+39) 0971-205070; rvassall@unibas.it
[2]Dipartimento di Ingegneria Geotecnica – Università di Napoli Federico II, 80125 Napoli, Italy; PH (+39) 081-7683894; FAX (+39) 081-7683481; mancuso@unina.it
[3]Dipartimento di Ingegneria Geotecnica – Università di Napoli Federico II, 80125 Napoli, Italy; PH (+39) 081-7683469; FAX (+39) 081-7683481; vinale@unina.it

Abstract

This paper is focused on the results of an experimental study of the effects of mean net stress $(p-u_a)$ and suction (u_a-u_w) history on the initial shear stiffness G_0 of a compacted silt. Isotropic tests were performed using two suction controlled devices, a triaxial cell and a Resonant Column Torsional Shear (RCTS) cell, so as to investigate the volumetric behavior of this material. In addition, by using the RCTS cell, initial shear stiffness was measured almost continuously along different isotropic stress paths in the plane $(p-u_a):(u_a-u_w)$, including constant suction- compressions and single stages or cycles of drying and wetting.

The obtained results show a strong dependency of G_0 on mean net stress and suction. Cycles of suction, in particular increasing suction beyond the past maximum value, induce significant accumulation of irreversible strains and increase of stiffness, confirming that G_0 is not univocally linked to the stress state expressed in terms of $(p-u_a)$ and (u_a-u_w).

The influence that mean net stress - suction history has on initial shear stiffness is analyzed and ascribed to the accumulation of irreversible volumetric strains. A model able to predict the observed behavior is proposed.

Introduction

This paper deals with the small strain behavior of an unsaturated soil used as construction material. This study is part of a broader project still in process at the University of Naples Federico II (Italy), which aims to analyze the effects of suction

and compaction variables on soils' mechanical response. Two main reasons inspired this investigation. On one hand, it seemed relevant to go deeper into a topic of theoretical and practical interest for which, up to today, the contributions available in the literature are still few and often divergent. On the other hand, the goal was to strengthen the link between the behavior of saturated soils at small strains and that of unsaturated soils at medium-high strains. The issue of small strain behavior under unsaturated conditions is also important for engineering applications as it offers the possibility of keeping into account the influence of these conditions on those parameters (shear stiffness, damping) which, under static and dynamic conditions, affect the performance of geostructures, with regards to deformations.

Tested soil, experimental devices, program and procedures

The tested soil is a clayey - slightly sandy silt representative of the materials used for constructing embankments on the Po river (Italy). It has a liquid limit (w_L) of 50.4% and a plasticity index (IP) equal to 17.9%. The soil was compacted at the optimum water content using the standard Proctor procedure (ASTM D691-91). On average, w=23.12% and γ_d=15.60 kN/m^3 were obtained.

The triaxial apparatus used for this experimentation is a stress path triaxial cell working under unsaturated conditions (Rampino et al. 1999). Suction is controlled via the axis translation technique and separated systems for measuring volume and water content changes are included.

The Resonant Column Torsional Shear (RCTS) device allows to independently control cell, water and air pore pressures. Suction is imposed by the axis translation technique and can reach a maximum of 500 kPa. Both water- and air-pore pressures are applied through the base pedestal, obtaining a fixed-free torsional restraint condition. Axial displacements are measured by an LVDT coaxial to the specimen, while radial displacements are obtained by monitoring the change in the water level of a bath surrounding the sample, using a differential pressure transducer DPT. Water content changes are measured through a system of two double-walled burettes connected to another DPT (Mancuso et al. 2002, Vassallo 2003).

Fifteen suction controlled tests were performed using the triaxial cell. The condition of saturation and the suction levels 50, 100, 200 and 400 kPa were studied.

Twelve suction controlled tests were carried out using the RCTS cell. During seven of them, after a preliminary equalization stage, an isotropic compression was carried out (in three cases both loading and unloading) measuring almost continuously the initial stiffness. The remaining five tests included stages of compression and stages of drying and wetting at constant (p-u_a), again with a continuous measure of stiffness. The test notation system used henceforward (mp00RC, mp01RC, ...) simply reproduces the chronological order followed during this experimental study. In several tests, during compression stages, the maximum (p-u_a) achievable by this apparatus was reached in order to investigate normally consolidated conditions. Overall, three levels of suction (100, 200 and 400 kPa) and mean net stresses ranging from 25 to 700 kPa were investigated.

The procedures used to apply a certain suction level (equalization) and a certain mean net stress (compression) are similar for triaxial and RCTS tests.

At first, the desired suction is applied at the specimen boundary and then kept constant, under a mean net stress $(p-u_a)$ of about 10 kPa. The final condition of equilibrium is inferred by the stabilization of volume and weight.

Isotropic compression is performed by linearly increasing $(p-u_a)$ up to a final target value. A loading rate of 4 kPa/h on 76 mm high specimens (triaxial cell) and 72 mm high specimens (RCTS cell) proved to be slow enough to ensure drained (i.e. constant suction) conditions. This rate was considered appropriate after theoretical calculations and after checking that, by suspending the compression, no further significant changes in volume and water volume still occurred (Vassallo 2003).

When additional wetting or drying stages are scheduled, they are carried out at constant mean net stress, applying the required suction at the specimen boundary in a relatively short time and waiting for the achievement of equilibrium. For the tested soil this occurred always within about a week.

During compression in the RCTS cell, initial stiffness G_o is measured at set time intervals through resonant column tests at very small shear strain level. As clarified above, compression is a constantly-drained process (i.e., constant u_a-u_w all over the specimen while continuously changing total stresses). Thus, each measured G_o can be ascribed to the current $p-u_a$ and u_a-u_w. Conversely, during wetting or drying G_o is still measured at fixed time intervals, but only the final stiffness, achieved at the equilibrium, can be attributed to the $p-u_a$ and u_a-u_w acting at the specimen boundary.

The aspects of damping and non-linear behavior of the tested soil were also thoroughly examined by Vassallo (2003) but are not analyzed here.

Experimental results

Equalizations and compressions

Figure 1 reports the variation of water content observed in equalization stages performed both with the triaxial and with the RCTS cell at different suction levels. Changes in w are all positive at suction 50 kPa and all negative at suction 200 kPa. The different value of water content changes for equalizations performed at a certain suction level can be justified by the small differences in moisture - dry unit weights of compacted samples from target standard Proctor optimum values. For equalizations at 100 kPa these changes induce a final water content that always falls above (in two cases around) the Proctor optimum 23.0%. Overall, as a consequence of these observations, the after compaction suction $(u_a-u_w)_o$ of the samples was estimated greater than 100 kPa and lower than 200 kPa, and in average was assumed equal to 140 kPa. Data here not reported indicate contractile variations of specific volume, independently of the suction applied during equalization. For suction levels of 50 and 100 kPa the magnitude of these volume changes and the behavior observed in the subsequent compression stages (similar to that of a saturated overconsolidated soil) would suggest a moderate "re-arrangement" of the soil skeleton resulting from anisotropic strain: swelling in axial direction and contracting in radial direction, rather than collapse (Vassallo 2003).
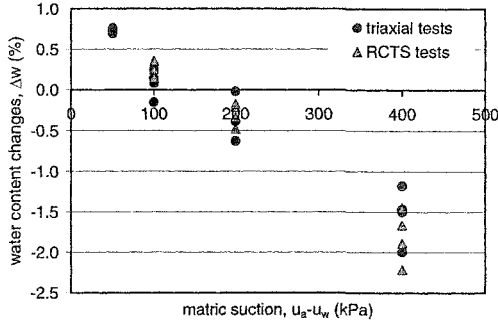
Figure 1. Water content changes observed during equalization stages.
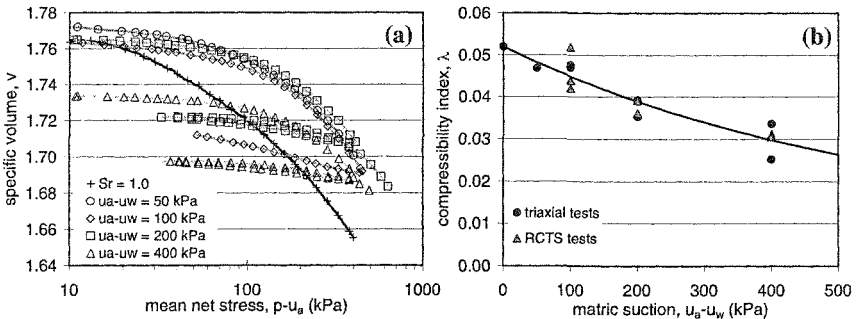
Figure 2. (a) Results in the plane log(p-u_a):v of isotropic compression tests. (b) Suction influence on compressibility index λ of the normally consolidated soil.

Figure 2a exemplifies the influence of suction on compressibility by showing some results of isotropic compression stages on saturated and unsaturated samples. The whole set of data pertaining to compressibility, obtained by using the two apparatuses, permits to define virgin compression lines for each suction value. Since the compression lines show a non negligible curvature, the compressibility index λ is here introduced with the meaning of local slope in the plane ln(p-u_a):v and fitting of experimental data is always limited to the range 10 – 400 kPa of (p-u_a). As suction increases, a gradual decrease in the compressibility index is observed (see Fig. 2b), but λ does not stabilize at all in the investigated range, suggesting that the possible minimum could be achieved at suctions significantly greater than 400 kPa.

Despite the change in slope of the v:log(p-u_a) curves is quite gradual, an increase in the apparent overconsolidation pressures (p-u_a)$_o$ as (u_a-u_w) increases can also be observed. As it will be illustrated, these pressures can be interpreted as yield stresses and, taking into account the possible hardening caused by drying stages towards suctions greater than the after-compaction one, can be used to predict Loading Collapse (LC) and Suction Increase (SI) yield loci active after equalization.

In order to stress out the irreversibility of strains that in some cases have been observed on drying, Figure 3 reports the results of tests mp05RC and mp07RC. In
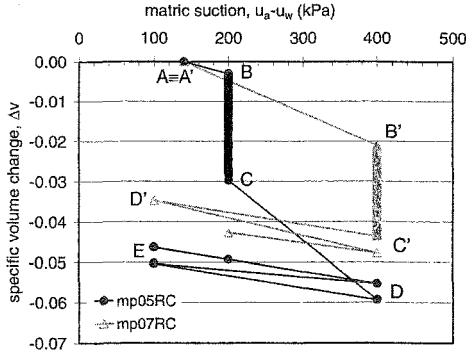
Figure 3. Specific volume changes during cycles of drying and wetting.

these tests, after equalization at suction of 200 kPa and 400 kPa, respectively, and compression to (p-u$_a$)=200 kPa (ABC and A'B'C'), suction cycles at constant mean net stress were performed, beginning with drying CD in test mp05RC and with wetting C'D' in the test mp07RC. These data clearly show that volume changes are irreversible during the first drying at 400 kPa suction (CD and A'B') while substantially reversible along the subsequent cycles of suction (DE and C'D').

Initial stiffness measurements during compression

After the preliminary equalization stage, each of the twelve tests carried out by the RCTS cell has been followed by an isotropic stress path in the plane (p-u$_a$):(u$_a$-u$_w$), along which the initial shear stiffness G$_o$ has been measured. Seven tests have been carried out at constant suction (100, 200 or 400 kPa). The other five have included one or more wetting and/or drying stages at constant (p-u$_a$).

Three tests consisted of a preliminary wetting stage at suction 100 kPa and (p-u$_a$)=10 kPa. The obtained results are plotted in Figures 4a for initial stiffness and 4b for specific volume changes (where Δv=0 corresponds to the as-compacted state). In
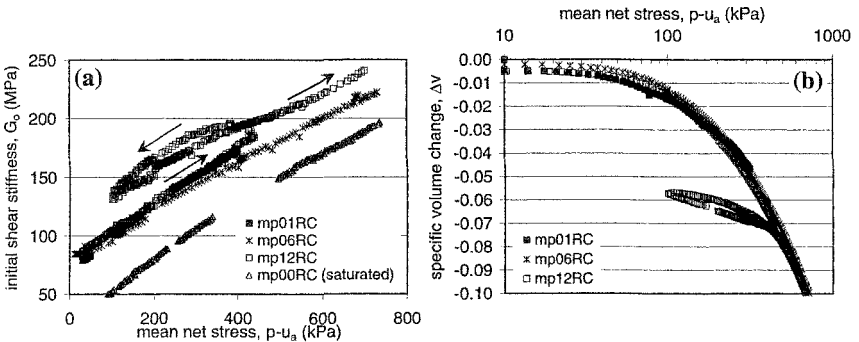
Figure 4. Results of tests carried out at constant suction 100 kPa: (a) initial shear stiffness; (b) specific volume changes.

tests mp01RC and mp06RC the specimens were then compressed up to a (p-u_a) of 400 kPa and 700 kPa, respectively. In the test mp12RC the soil was first compressed to (p-u_a)=430 kPa, then unloaded to 100 kPa and finally re-loaded to 700 kPa. The observed behavior is similar to that of saturated soils: in first loading, as (p-u_a) increases the shear modulus increases almost linearly; during the unloading and re-loading the shear modulus attains greater values than those of the previous monotonic compression and shows some hysteresis. Beyond the maximum mean net stress previously applied the curve G_o:(p-u_a) seems to join the prolongation of the first loading branch. In the same figure the curve stiffness: mean effective stress pertaining to the saturated material (test mp00RC) is also represented for comparison. The repeatability of the results is satisfactory, for G_o as well as for Δv.

Trends similar to those examined above for stiffness measurements in normally consolidated and overconsolidated states have been detected in tests mp11RC and mp10RC referring to compression performed at constant suction of 200 kPa and 400 kPa, respectively. In addition, trends similar to those obtained at 100 kPa are obtained for groups of tests pertaining to 200 and 400 kPa constant suction.

Initial stiffness measurements during wetting and drying

Stages of wetting and drying were performed at constant mean net stress, applying the required suction in relatively short time and waiting for the achievement of equilibrium. In this section, the results of two out of the five tests including wetting or drying stages (besides equalization) are considered and compared to those of "less complex" equalization + compression- tests. The paths relevant to the tests mp05RC, mp07RC, mp10RC and mp11RC are illustrated in Figure 5.

The tests mp05RC includes compression at (u_a-u_w)=200 kPa up to a mean net stress of 200 kPa and drying/wetting cycles with suction varying between 400 kPa and 100 kPa. Figure 6 shows stiffness and volume change measurements, reported together with the data pertaining to the tests mp10RC and mp11RC, i.e. constant suction loading and unloading at (u_a-u_w) of 400 kPa and 200 kPa, respectively. The results of these tests highlight that the stage of drying CD caused hardening of the
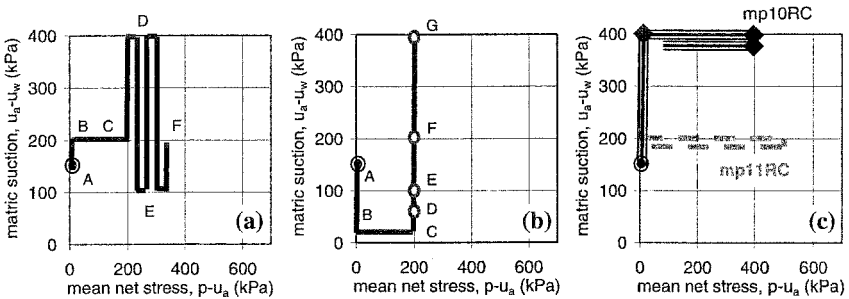
Figure 5. Stress paths of tests mp-: (a) 05RC; (b) 08RC; (c) 10RC, 11RC.
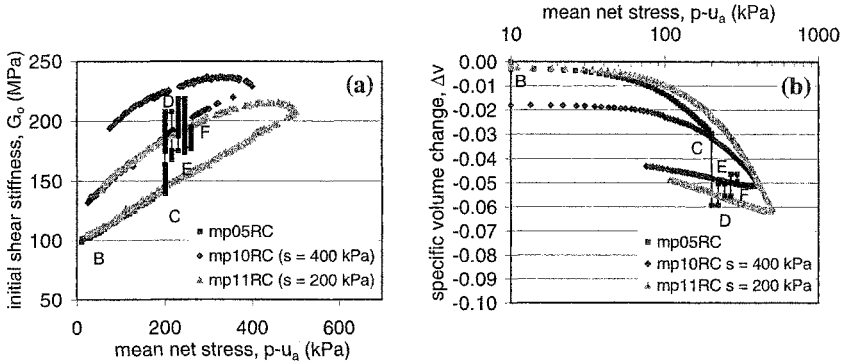
Figure 6. Results of tests mp05RC, mp10RC, mp11RC: (a) initial shear stiffness; (b) specific volume changes.
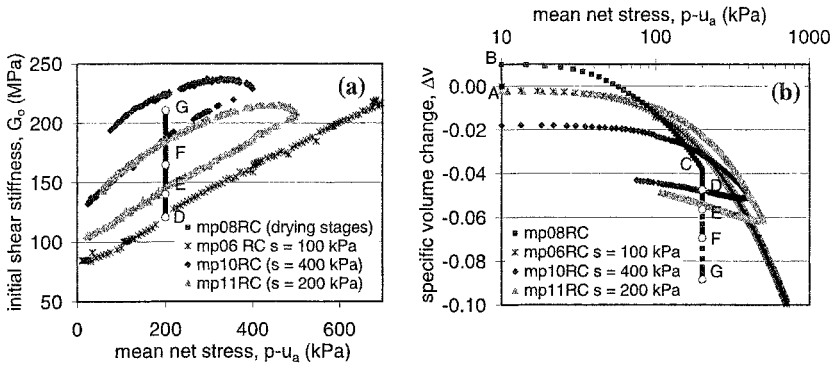
Figure 7. Results of tests mp08RC, mp06RC, mp10RC, mp11RC: (a) initial shear stiffness; (b) specific volume changes.

material. As a matter of fact, the stiffness at the end of first drying CD for the test mp05RC is significantly greater than that pertaining to the test mp10RC at equal (p-u_a), i.e. to the first loading G_o:(p-u_a) curve at suction 400 kPa. Plastic hardening is also revealed by the relatively large decrease in specific volume that occurred during the first drying. As a matter of fact, the final point (p-u_a, Δv) lies below the unloading branch of the test mp10RC. This suggests that the increase in stiffness can be related to the expansion of the yield surface caused by drying at 400 kPa.

The results obtained during the subsequent suction cycles of the test mp05RC confirm the irreversible nature of the volumetric changes due to the first drying. As a matter of fact, during the subsequent cycles smaller variations in G_o and v occur. The material never recovers its initial state: at the end of the test, going back to the same stress state as the end of compression (p-u_a=200 kPa, u_a-u_w=200 kPa, point F), the specific volume appears permanently lower. All the above influences significantly the stiffness: the values achieved at (u_a-u_w)=100 kPa and 400 kPa are still greater than

those pertaining to first loading stages and "stable" enough. The relatively slight increase in G_o along suction cycles can be ascribed to the long duration of the tests and to the consequent weight of creep.

Figure 7 shows the results of the test mp08RC. During this test a preliminary saturation at constant volume (AB in Figg. 5b and 7b) was performed inside a constant volume- saturation device. Actually, even if the water content has significantly increased with respect to the after compaction state, a complete saturation was not achieved. Thus, during the following equalization in the RCTS cell at 20 kPa, the soil swelled (see point B in Fig. 7b) and absorbed water. Starting from this condition, $(p-u_a)$ was increased up to 200 kPa (BC), and four stages with suction increase up to 50 kPa, 100 kPa, 200 kPa and 400 kPa were carried out (CG). Again, the stiffness values reached at the equilibrium during the aforementioned stages of drying are greater than those pertaining to first loading curves at equal suction and significant volume changes come with stiffness changes due to drying.

Modeling initial shear stiffness measured during compression stages

First, it is relevant to analyze the stiffness measurements observed during constant suction monotonic compression stages. In Figure 8 the results of these stages are grouped according to constant suction levels and compared with measurements performed on the saturated material. The modulus G_o is normalized with respect to the atmospheric pressure and the void ratio function f(e) proposed by Hardin and Black (1968):

$$[1] \qquad f(e) = \frac{(2.973 - e)^2}{1 + e}$$

Fundamentally, this choice is conventional, and pursues the idea of showing data of the unsaturated soil in the same way often used for saturated materials. The function f(e) alone is not capable of clearing out stress history effects from the stiffness measurements, since it does not allow for a single relationship $G_o:(p-u_a):(u_a-u_w)$ for normally- and over-consolidated conditions. On the other hand, however, the normalization allows for the reduction of some scattering due to the lack of homogeneity in the after compaction void ratio (Vassallo 2003).

A significant effect of suction on shear stiffness can be observed: the groups of curves $G_o:(p-u_a)$ pertaining to the various suction levels have average slopes quite similar, but shift upwards as suction increases. Given that for each level of suction the overconsolidation pressure $(p-u_a)_o$ is known [as indicated by compression $v:\log(p-u_a)$ curves], it is also possible to make out on each stiffness: mean net stress-curve the points characterized by $OCR=(p-u_a)_o/(p-u_a)$ equal to one.

In Figure 8, data of the saturated normally consolidated soil are fitted by:

$$[2] \qquad \frac{G_o}{f(e) \cdot p_{atm}} = S \left(\frac{p'}{p_{atm}} \right)^n$$

with S=194.7 and n=0.547.

If one replaces p' with $(p-u_a)$, the same function, shifted upwards of an
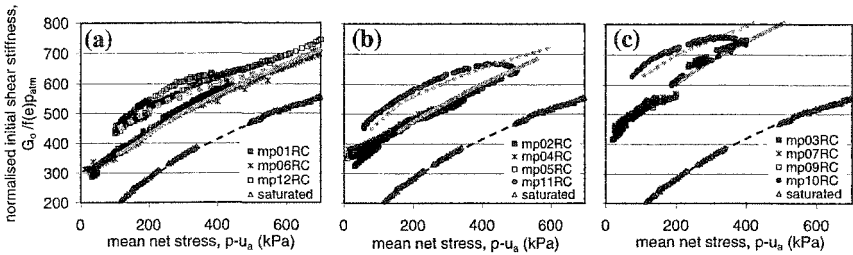
Figure 8. Modeling the results of compression stages carried out at suction: (a) 100 kPa;(b) 200 kPa;(c) 400 kPa.

amount dependent on suction, can also fit the data pertaining to unsaturated conditions with very good approximation. In other words, the following expression was found valid in normally consolidated conditions (OCR=1):

$$[3] \qquad \frac{G_o}{f(e) \cdot p_{atm}} = S \left(\frac{p - u_a}{p_{atm}} \right)^n + F(u_a - u_w)$$

The function $F(u_a - u_w)$ increases as $(u_a - u_w)$ increases and, thus, expresses soil stiffening due to suction. For the tested soil, it varies less than linearly with suction and does not tend to a threshold in the studied $(u_a - u_w)$ range (Vassallo et al. 2005b).

The solid grey lines in Figure 8 represent the G_o values predicted with the procedure so far described. A generally good agreement between the model predictions and the experimental data pertaining to OCR=1 is observed.

As an effect of the overconsolidation induced by $(p - u_a)$, the stiffness achieves values greater than those of normally consolidated samples in tests mp10RC, mp11RC and mp12RC. The Equation:

$$[4] \qquad \frac{G_o}{f(e) \cdot p_{atm}} = S \left(\frac{p - u_a}{p_{atm}} \right)^n OCR^m + F(u_a - u_w)$$

is appropriate to fit the results of all suction levels with m=0.207, as it is shown in Figure 8 by dashed grey lines [despite some minor problems related to creep and hysteresis (Vassallo et al. 2005a,b)].

Therefore, the introduction of $F(u_a - u_w)$ and the use $(p - u_a)$ in place of p' permit to generalize typical G_o:p':OCR relations for saturated soils to the unsaturated case, also allowing to predict the increase in stiffness generated by a cycle of $(p - u_a)$.

Modeling initial shear stiffness measured during drying and wetting stages

According to the model proposed by Alonso et al. (1990) and those deriving from it, irreversible strains correspond to a phenomenon of hardening represented by the expansion of the yield locus, consisting of LC and SI lines. Of course, this hardening may be linked to the "overconsolidation state" of an unsaturated soil and therefore, like in saturated soil mechanics, can affect its stiffness. Because of that, it was necessary to focus on modeling the volumetric behavior of the tested material, so

as to facilitate, then, to rationally represent the effects of stress history in tests with "complex" stress paths including mean net stress and suction changes.

The yield loci of the tested soil and their evolution due to the applied stress paths are deduced by Vassallo et al. (2005b) by modeling the observed volumetric behavior. Here it is worth recalling that plotting data with reference to the variables $(p-u_a),(u_a-u_w)$ and Δv, where $\Delta v=0$ indicates the beginning of the equalization stage, permitted to clear out some scattering among after-compaction specific volumes.

The shape of the LC line is inferred by the yield points detected by isotropic compressions. This requires to take into account the yielding on the SI during equalizations at suction 400 kPa and the consequent coupled displacement of the LC. An expression obtained by slightly modifying that originally proposed by Wheeler and Sivakumar (1995) is used by Vassallo et al (2005b) including the variable Δv.

The yield locus is completed by the SI, for the sake of simplicity assumed as a horizontal line $(u_a-u_w)=(u_a-u_w)_0$ in the plane $(p-u_a):(u_a-u_w)$, as proposed by Alonso et al. (1990). The same authors suggest that the position of the LC can change not only due to stress paths that intercept it, but also because of yielding on the SI. In order to model this latter phenomenon, Vassallo et al. (2005b) predict the shift of the LC associated to displacements of the SI along drying paths by linking this shift to the observed irreversible volume changes as predicted by the Alonso et al. (1990) model:

$$[5] \qquad \ln\frac{[(p-u_a)_o^*]_f}{[(p-u_a)_o^*]_i} = -\frac{\Delta v_P}{(\lambda(0)-k)}$$

where $[(p-u_a)^*_o]_i$ and $[(p-u_a)^*_o]_f$ are the initial and the final yield stresses of the saturated soil, respectively, Δv_P is the observed irreversible specific volume changes, $\lambda(0)$ and k are the compressibility indexes of the saturated soil under normally consolidated and overconsolidated conditions, respectively.

On the other hand, it is assumed that yielding on the LC does not cause significant displacement of the SI, as suggested by the whole experimental data and verified by using the proposed model and finding a good accord with measurements.

In Figure 9 the predicted evolution of yield locus and stiffness due to the path followed during the test mp05RC is represented. The after-compaction locus is the curve indicated as Y.L.(A), passing through point A, with coordinates $(p-u_a)=10$ kPa and $(u_a-u_w)=140$ kPa, which are respectively the mean net stress during the equalization and the suction induced by compaction. In the equalization stage AB, the SI moves causing a slight expansion of the LC. In the following compression stage the LC is intercepted in point B' and then dragged up to point C. The stage of drying CD induces further yielding and subsequent expansion of the LC. The resulting yield locus is now indicated as Y.L.(D). In point D the material is overconsolidated and its OCR can be obtained comparing $(p-u_a)$ in points D and P.

The evolution of the initial shear stiffness during the test is still quite well predicted by Equation 4, previously obtained only considering overconsolidation due to a decrease in $(p-u_a)$, i.e. fitting results of tests mp10RC, mp11RC and mp12RC.

The yielding caused by the drying stage CD, expanding the yield locus up to the line indicated as Y.L.(D), justifies the relatively large values of stiffness measured in points D, E, F, G, H, since the material has become overconsolidated as an effect of
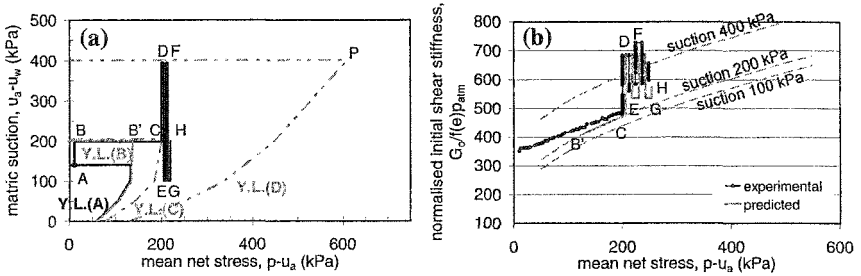
Figure 9. Predictions of the proposed model for test mp05RC: (a) yield loci; (b) normalized stiffness, compared to experimental values.
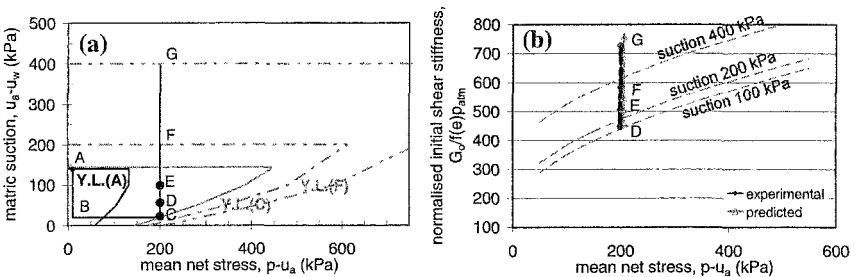
Figure 10. Predictions of the proposed model for test mp08RC: (a) yield loci; (b) normalized stiffness, compared to experimental values.

suction increase. In points E, G, H there is a twofold effect: indeed, the stress state is far from both the LC and the SI. In order to keep this into account Vassallo (2003) proposed a further extension of Equation 4:

$$[6] \qquad \frac{G_o}{f(e) \cdot p_{atm}} = S \left(\frac{p'}{p_{atm}} \right)^n \cdot OCR^m \cdot H \left[\frac{(u_a - u_w)_o}{u_a - u_w} \right] + F(u_a - u_w)$$

introducing H, function of the ratio between the maximum past suction $(u_a-u_w)_o$ and the current one (u_a-u_w), ranging between one, when $(u_a-u_w)_o$, is equal to (u_a-u_w), and a parametric value r^* greater than one, when $(u_a-u_w)_o$ is much greater than (u_a-u_w).

The interpretation of test mp08RC is represented in Figure 10. The compression BC, carried out at 20 kPa suction, moves the LC up to C. In the following drying stages CDEFG, the overconsolidation ratio is progressively increasing. Going from 100 kPa to 200 kPa of suction (EF) and then from 200 kPa to 400 kPa (FG) the SI is intercepted and dragged, also causing further shift of the LC.

In all the illustrated cases, as well as for other tests not reported here (Vassallo et al. 2005a,b), Equation 6 permits to evaluate quite accurately the effects of the stress history on the initial shear stiffness. Some slight discrepancies between predictions and experimental data are due to phenomena (like creep) that the model does not take into account. As an effect of the long confining time creep strains occur, causing an increase in G_o under constant stress state. Therefore, in test

mp05RC the stiffness measured after a suction cycle, in point F, is greater than that measured in point D (see again Fig. 7b). Of course, the model does not predict any difference between the two cases. Other minor incongruities are due to some experimental scattering of the curves G_o:(p-u_a) obtained under the same level of suction (Vassallo 2003). Despite of this, the proposed strategy of interpretation may be quite useful, since it proves very helpful at a qualitative level to summarize in a single representation the variations of overconsolidation state and to figure out the variation in stiffness that can be logically expected.

Conclusions

This paper illustrated some experimental results featuring simultaneous measurements of volume change and initial shear stiffness along various isotropic stress paths. A model able to predict the observed behavior and based on elasto-plastic formulations for unsaturated soils has been proposed, linking the influence of stress history on initial shear stiffness to the accumulation of irreversible volumetric strains. This interpretation also appears helpful from a theoretical point of view, since it allows to obtain a single and effective representation for the changes in overconsolidation state caused by non-elementary stress paths and to predict the variation in stiffness that these paths may induce.

References

Alonso, E.E., Gens, A., and Josa, A. (1990). A constitutive model for partially saturated soils. *Géotechnique*, 40(3): 405-430.

ASTM D698-91. Test method for laboratory compaction characteristics of soil using standard effort (12,400 ft·lbf/ft3 (600 kN·m/m3)), Philadelphia, USA.

Hardin, B.O., and Black, W.L. (1968). Vibration modulus of normally consolidated clay. *Journal of Geotechnical Engineering ASCE*, 94(2): 353-369.

Mancuso, C., Vassallo, R., and d'Onofrio, A. (2002). Small strain behavior of a silty sand in controlled-suction resonant column – torsional shear tests. *Canadian Geotechnical Journal*, 39: 22-31.

Rampino, C., Mancuso, C., and Vinale, F. (1999). Laboratory testing on a partially saturated soil: equipment, procedures and first experimental results. *Canadian Geotechnical Journal*, 36(1): 1-12.

Vassallo, R. (2003). Comportamento di terreni costipati non saturi a piccole, medie e grandi deformazioni. Ph.D. Thesis, University of Naples Federico II, Italy.

Vassallo, R., C. Mancuso, and Vinale, F. (2005a). Effects of net stress and suction history on the small strain stiffness of a compacted clayey silt. Submitted to *Canadian Geotechnical Journal*.

Vassallo, R., C. Mancuso, and Vinale, F. (2005b). Modelling the influence of stress-strain history on the initial shear stiffness of an unsaturated compacted silt. Submitted to *Canadian Geotechnical Journal*.

Wheeler, S.J., and Sivakumar, V. (1995). An elasto-plastic critical state framework for unsaturated soil. *Géotechnique*, 45(1): 35-53.

Effect of Cement and Saturation on the Stress-Strain Behavior of a Silty Clay

Víctor A. Rinaldi [1] and Julio A. Capdevila [2]

[1] Associate Professor, Geotechnical Laboratory, Department of Civil Engineering, National University of Córdoba, 5009, Córdoba, Argentina. Researcher CONICET. E-mail: vrinaldi@com.uncor.edu
[2] Graduate Student, Geotechnical Laboratory, Department of Civil Engineering, National University of Córdoba, 5009, Córdoba, Argentina, CONICET Fellow. E-mail: jcapdevila@com.uncor.edu

Abstract

Matric suction and cementation together have significant influence on the stress-strain behavior of many lightly cemented soils. The combined effects of suction and cementation during soil formation may stabilize the fabric of the soil at a very high void ratio. This is the case of wind-blown loess of the Pampas formation in Argentina. The scope of this work is to present some fundamental aspects related to the unsaturated stress-strain behavior of lightly cemented silty clay. Triaxial test were performed in laboratory and strains were monitored by means of local displacement transducers. Undisturbed structured specimens as well as remolded unstructured specimens were tested both in saturated and unsaturated condition. It was observed that cementation and unsaturation cause an increase in yielding stress and shear strength, decrease in volume contraction during loading, and a higher propensity to stress localization. These effects are mainly controlled by water content and confining pressure. At low confinements, the unsaturated and cemented specimens behave more brittle as compared to the uncemented specimens due to the much lower deformation threshold required to break cementing bonds than menisci. A bilinear model is proposed to model the fragile behavior of cemented specimens.

Introduction

Most natural soil deposits have some degree of cementation arising from post-depositional processes such as thermal cyclic loading, high past-pressures, chemical

binding and cement precipitation (Mitchell 1993). Loess deposits cover a wide area of the central region of Argentina with thickness from 20 to 60 meters. Loess is a wind-blown formation composed mainly of platy shape silt particles (40% and 60 %) and sand (5 % to 20 %) from volcanic origin. The clay fraction (20 % to 35 %) is usually Illite and Montmorillonite. The combined effect of particle shape, origin and particle gradation, render poorly accommodated and open fabric with clay minerals bonding particles together (Rinaldi et al. 2001). Usually loess presents some degree of weak cementation given by soluble salts, silica amorphous, calcium carbonate, gypsum and iron oxide. Upon wetting clay particles hydrate, suction decrease and the soil structure colapses in front of moderate loads and even under the self weight of the soil. The strengthening of soil structure due to cementing agents are sometimes difficult perceive since most of them weakens in front of water. However, cemented soils usually exhibit elastoplastic stress-strain behavior and the stress level at which yielding occurs is usually termed as collapse. Beyond the yielding stress, significant plastic strains occur, whereas within the yield locus strains are relatively small and recoverable (Vatsala et al. 2001).

Iron oxide, silica amorphous and carbonates are usually the most stable cementing materials. Water acidity has a significant effect on cement stability. Highly acidic leachate (eg. organic acids) dissolves carbonates while alkaline waters promote the development of silica bonding in prescence of hydroxides. Large amount of cementing agents fully disseminated in the soil and precipitated at particle contacts, increase significantly the shear strength of loess which may behaves as a true sedimentary rock locally known as "tosca" (Rocca 1985, Rinaldi 1994). Additionally, cementation may be found localized forming nodules and aggregates. In this case, loess behaves as a soil of larger particle size and its stress-strain behavior is controlled mainly by the size and distribution of the aggregates in the soil mass, strain level and confining pressure.

This work presents some fundamental results and conclusions of an experimental study developed to address the effect of suction and cementation on the stress-strain behavior of loess. A series of laboratory triaxial tests were performed on undisturbed (structured) specimens and remolded (unstructured) specimens, both in saturated and unsaturated condition. Local displacement transducers were implemented in the triaxial cell which allows us to reduce soil-cap contact effects and to measure strains below 10^4. Grain size distribution curves were obtained for undisturbed specimens by washing and sieving without application of energy to avoid the degradation of weakly cemented aggregates. The grain size distribution curves were used to evaluate the evolution of soil structure at different strain levels. A simple constitutive model was calibrated to fit the soil stress-strain response.

Soil Description and Testing Program

Block samples of Loess were obtained at the campus of the National University of Córdoba from a 4 meters deep open trench. Table 1 shows the most significant physical parameters of the soil tested (undisturbed and remolded samples).

Undisturbed (structured) and remolded (unstructured) specimens saturated and unsaturated (at natural water content) were prepared for testing in the triaxial cell. Triaxial specimens were 50 mm in diameter and 100 mm in height.

Table 1: Geotechnical relevant parameters of the loess tested in this work.

Sample	Soil Unified Clasification	Average Natural Water Content (%)	Plasticity Index	Dry Unit Weight [kN/m³]	Initial Degree of Saturation	Percent Passing Sieve N° 200	Natural Matric Suction [kPa]
Undisturbed	ML	18.0	3.6 %	12.5	42 %	92.4 %	75
Remolded	ML	16.9	3.6 %	12.8	41 %	92.4 %	77

The undisturbed specimens were obtained by triming while the remolded specimens were moisturized and prepared by manual tamping to the desired density. The soil used to prepare the remolded specimens was air dryed and sieved through the sieve number 40 prior to compaction in order to guarantee the complete destructuration of aggregates. Triaxial test were performed in consolidated drained condition. Table 2 display the soil parameters and testing conditions of the different specimens prepared here. The triaxial cell allows the measurement of strains by means of three local displacement transducers (LDTs) placed on the specimen under test. An additional displacement transducer was attached at the center of the sample to determine the local radial strains by measuring changes in specimen diameter. The LDTs used here are similar to those described by Goto et al. (1991) (see Figure 1).
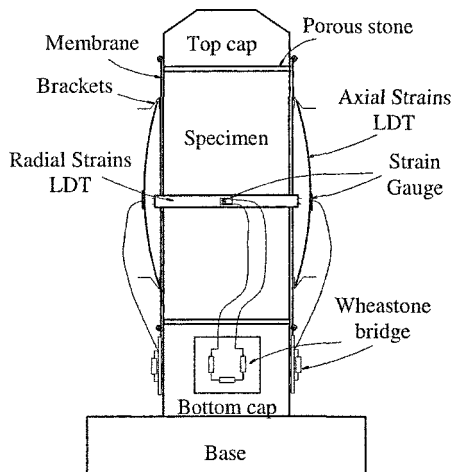
Figure 1: Location of the LDT sensors inside the triaxial cell

Table 2: Soil parameters and testing conditions of the prepared soil specimens.

Specimen	Testing Condition	Confining Pressure [kPa]	Dry Unit Weight [kN/m³]	Moisture Content [%]
U1	Unsaturated and Undisturbed	10	13.0	17.47
		20	12.8	16.13
		40	12.9	17.57
		80	12.6	17.18
U2	Saturated and Undisturbed	10	12.4	43.20
		20	12.4	43.20
		40	12.2	44.50
		80	12.6	41.90
R1	Unsaturated and Remolded	10	12.4	16.90
		20	12.3	16.90
		40	12.4	16.90
		80	12.4	16.90
R2	Saturated and Remolded	10	12.2	44.50
		20	12.3	43.80
		40	12.6	41.90
		80	12.5	42.50

A water tensiometer was used to evaluate soil matric suction of the different block samples obtained from the site. The tensiometer was placed inside an open borehole trimmed in the block and sealed with a paraffine resine. The average value of suction determined in this test is presented in the same Table 1.

The grain size distribution curve of the structured specimens were obtained by sieving analysis, following the convetional sieving test (ASTM D 422) but here, a block of the structured sample was placed on the coarsest sieve of the series and gently washed until the water extracted from last sieve N° 200 become clear indicating the absence of fine particles detached form the agregates retained in the upper sieves. No energy (eg. vibration, rotation) was applied to the soil during the test. The distribution curve corresponding to the distructured specimen was obtained in a similar fashion but the aggregates in this case were broken manually.

Test Results

Stress-Strain

Figure 2 shows the stress-strain results of triaxial compression tests corresponding to the loess samples performed in unsaturated and saturated conditions. Readings were obtained by means of the local LDT transducers up to the 8 % strain level.
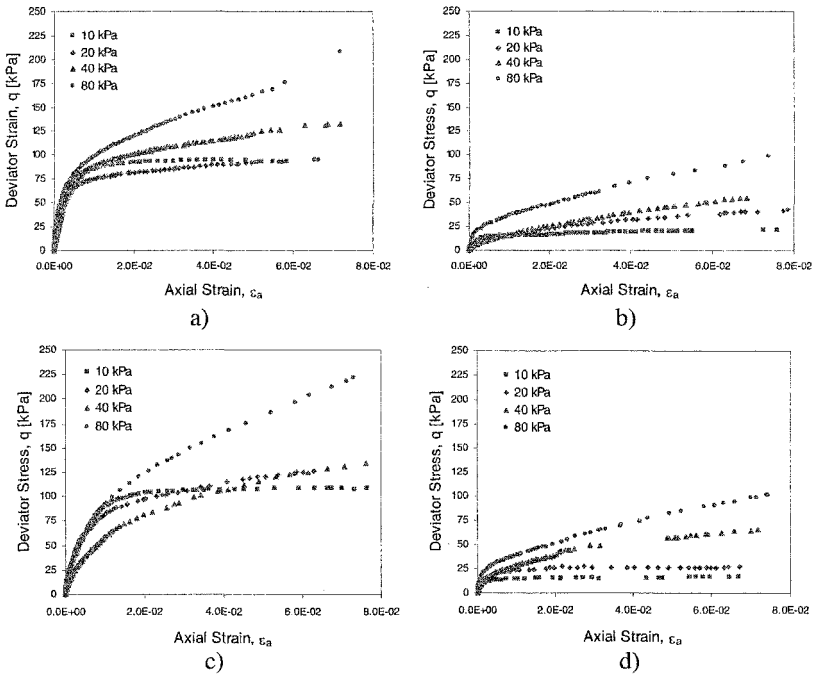
Figure 2: Stress-strain curves of undisturbed and remolded loess specimens tested at different confining pressure and moisture conditions measured in triaxial cell by means of LDT. (a) Undisturbed and tested at natural moisture content. (b) Undisturbed and tested saturated. (c) Remolded and tested at natural moisture content and (d) Remolded and tested saturated.

Test results show that unsaturated samples develop much higher deviatoric stresses respect to the specimens tested in saturated conditions. In general, it is observed at strain levels larger than 6 % that the higher the confining pressure the higher is the deviator stress. At strain levels less than 1 %, the effect of confining pressure on soil strength is not clearly defined and some of the undisturbed samples tested show higher shear strength at lower confining pressures. The saturated specimen tested at the lowest confining pressure, develops strain softening. At higher confining pressure all samples develop strain hardening behavior. The higher the confining pressure, the higher is the increment rate of hardening. Undisturbed and saturated samples show a clear yielding locus which indicates a britle behavior. Oppositely, unsaturated specimens and the remolded specimens develop a more ductile behavior and the yielding locus in the stress-strain is not clearly identified. It is important to mention, that the unsaturated specimens tested at the low confining pressures develop shear bands (stress localization) at failure while the other specimens bulged when loaded to failure. Here, stress yielding and brittle behavior can be related to stress localization.

Figure 3 displays the variation of the volumetric strain respect to the axial strain for the different specimens tested. The observed relationship is almost linear up the yielding locus. All samples contract during loading and there is a tendency to increase contraction with increasing confining pressure.
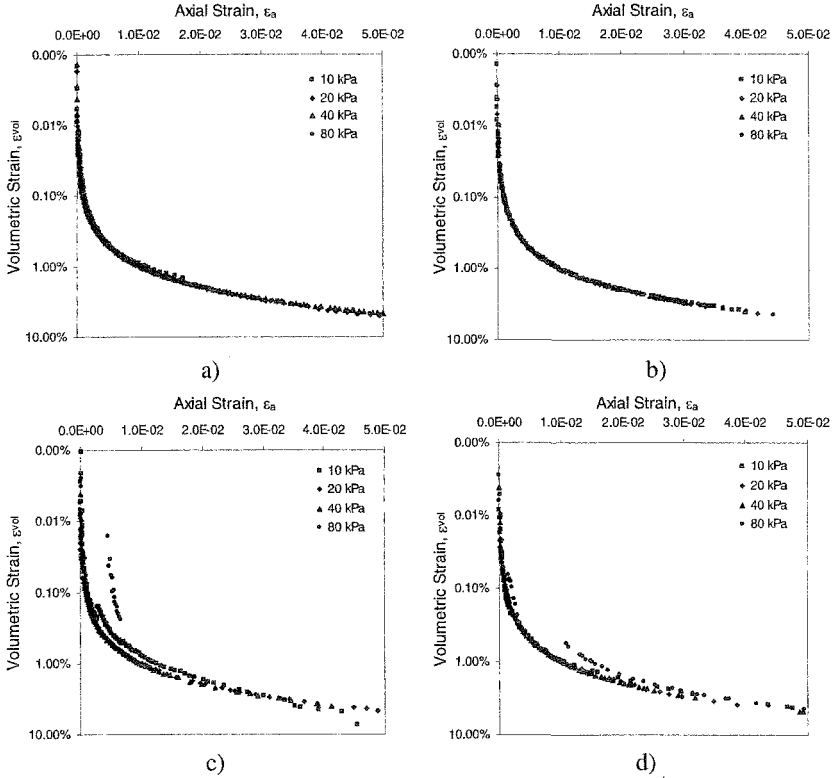
Figure 3: Volumetric strain variation of undisturbed and remolded loess specimens tested at different confining pressure and moisture conditions measured in triaxial cell by means of LDT. (a) Undisturbed and tested at natural moisture content. (b) Undisturbed and tested saturated. (c) Remolded and tested at natural moisture content and (d) Remolded and tested saturated.

Shear Strength Envelops

Figure 4 compares the failure envelops corresponding to the CD triaxial test for the undisturbed and the remolded specimens tested in the saturate condition and at similar dry unit weight (data from Figure 2b and 2d). The Mohr circles plotted here correspond to a deviator stress determined at the 6 % strain level. Figure 4 clearly shows the slightly higher shear strength values of the undisturbed specimen at the

lower confining pressures. The difference between both envelops reduces as the confining pressure increases. The envelope corresponding to the undisturbed specimen shows a true cohesion intercept at zero confining pressure.

Figure 5 displays the failure envelops of the undisturbed and remolded specimens tested at natural moisture content at the same unit weight (data from Figure 2a and 2c). Similarly, the Mohr circles plotted here correspond to a deviator stress determined at 6 % strain level. The remolded specimens show slightly higher strength values and both envelopes show cohesion intercept. The result highlights that in the unsaturated condition, shear strength is mainly governed by water menisci since the structured sample (assumed as cemented) develops similar shear envelope than that of the unstructured sample (remolded).
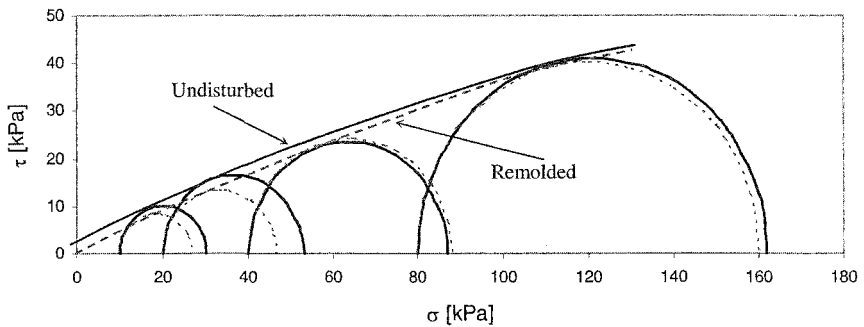
Figure 4: Mohr-Coulomb failure envelops corresponding to the undisturbed and remolded samples tested in drained (CD) and saturated conditions. Shear strength corresponds to the 6 % strain level (data from Figure 2b and 2d).
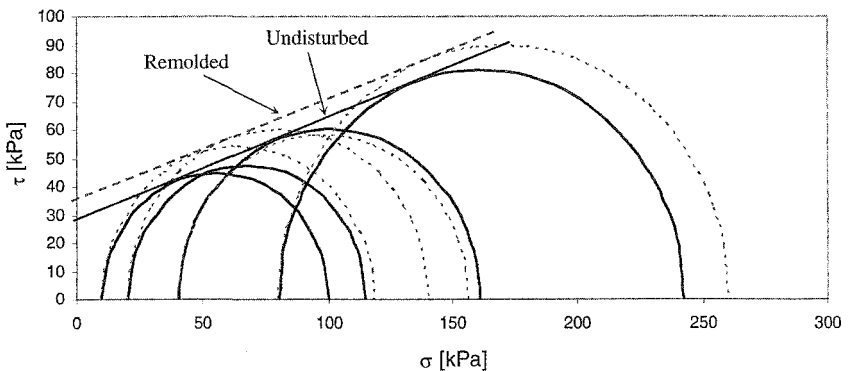
Figure 5: Mohr-Coulomb failure envelops corresponding to the undisturbed and remolded samples tested in drained (CD) and unsaturated conditions. Shear strength corresponds to the 6 % strain level (data from Figure 2a and 2c).

Evolution of Fabric

The grain size distribution curve corresponding to the undisturbed (structured) and the fully remolded (unstructured) samples are compared in Figure 6. The grain size distribution curves obtained for three specimens tested in the triaxial cell at natural water content and at the same confining pressure of 40 kPa, but sheared to different strain levels are superimposed in the same figure. This result clearly shows that the size of the cemented aggregates develops little evolution after shearing up to the 6 % strain level reached in this test. The complete destruction of aggregates described by the curve corresponding to the fully unstructured loess seems difficult to be reached at this confining pressure. Probably at much higher confining pressures evolution of fabric could be more significant than that observed here.
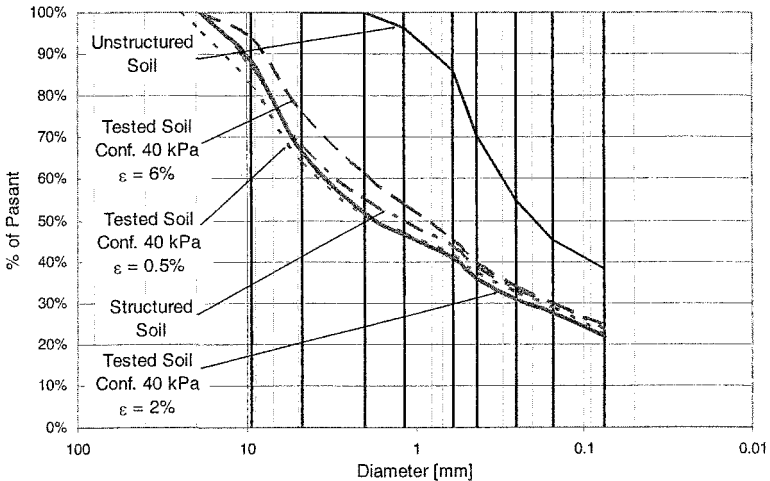
Figure 6: Grain size distribution curves of undisturbed (structured) and the fully remolded (unstructured) samples of loess (full lines). Dashed lines display the grain size distribution curves of undisturbed specimens at natural moisture content sheared to different strain levels and at the same confining pressure (40 kPa) in the triaxial test.

Interpretation of Test Results and Modeling

The stress-strain behavior of loess can be interpreted in terms of the interplay among water content, strain level, confining pressure and degree of cementation.

Below yielding, stress-strain behavior of the unsaturated specimens corresponds to a cemented material with a linear relationship between volumetric and axial strain (Airey and Fahey 1991). Here, no plastic strains are developed and stiffness, at a given confining pressure, is controlled initially by the cemented bonds and thereafter by water menisci since larger strain is required to overcome capillary forces (Cho

and Santamarina 2001 and Fernandez and Santamarina 2001). As the sample becomes saturated, cement weakens, capillary forces disappear and stiffness is mainly controlled by cement type and amount.

In saturated samples yielding occurs as a consequence of decementation and the degree of debonding is controlled by cement type and amount and confining pressure (Saxena and Lastrico, 1978). The weakly cemented loess specimens require very low strain levels for yielding (usually less than 0.5 %). Partial decementation may also take place solely by the application of high confining pressures prior to the application of deviatoric stresses (Rinaldi et al, 2001). In this case, shear stress at yielding may be lower that that corresponding to a similar specimen tested at lower confining pressures. In unsaturated samples, yielding occurs progressively and is controlled by the rate of decementation and capillary forces.

After yielding, shear strength may be mainly of a frictional or cohesive nature depending on cement strength, capillary forces and confining stresses. High degree of cementation, high suction forces and low confining pressures produce a blocky structure after yielding (Lambe, 1960) and friction is governed by the size distribution and shape of the aggregates. At high confining pressures, decementation of unsaturated specimens occurs progressively even at strain levels beyond the yielding locus. In saturated condition, post-yielding strength of loess is mainly of a frictional nature and cohesion may become important only at low confining pressures.

The stress-strain behavior of the remolded specimens at the natural unit weight shows similar behavior than normally consolidated soils. At a given constant unit weight, shear strength is mainly determined by water content and confining pressure. In the unsaturated condition, remolded and structured specimens show similar strength envelopes. This effect highlights that suction governs the shear strength behavior of loess and cementation is of little significance at the natural moisture content. The authors consider that the slightly higher strength of the remolded specimens compared to the undisturbed specimens (see Figure 5) may be attributed to the slightly higher suction of the remolded specimen prepared at natural water content (see Table 1). Further research efforts that include aging and water menisci development and distribution around particles are required to obtain a conclusive answer.

A bilinear constitutive model is considered here to approximate stress strain curves of the undisturbed loess. The required expressions can be written as:

$$\sigma = E \cdot \varepsilon \qquad \qquad \text{for} \quad \varepsilon < \varepsilon_y \qquad \qquad (1)$$

$$\sigma = \sigma_y + \left(\varepsilon - \frac{\sigma_y}{E} \right) \cdot K \qquad \text{for} \quad \varepsilon > \varepsilon_y \qquad (2)$$

Where E is the elastic modulus and K the elastoplastic modulus, and σ_y and ε_y are the yielding stress and strain respectively. Elastic modulus, E, depends on the confining stress as follow:

$$E = E_0 \left(\frac{\sigma_{conf}}{p_a} \right)^n \tag{3}$$

Where E_0 is a constant value, σ_{conf} is the confining stress, p_a is a reference pressure and n an constant exponent.

Figures 7 and 8 display the fitting of the model to the measure data corresponding to the undisturbed sample in the saturated and unsaturated condition. The model shows a good agreement for the unsaturated condition of the soil but it is poor for the saturated sample at the medium confining pressures used herein.
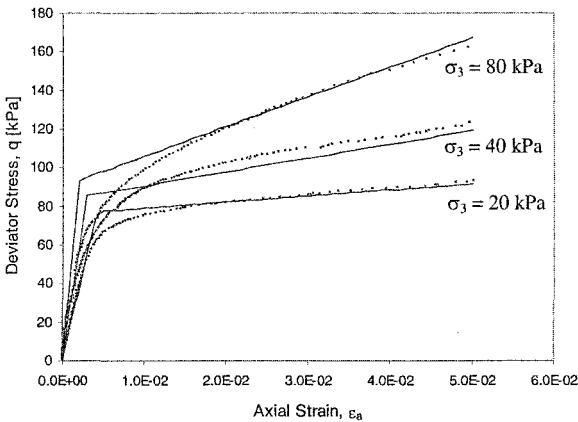
Figure 7: Agreement of the bilinear model to the stress-strain triaxial curves of the undisturbed and unsaturated loess at different confining pressure.
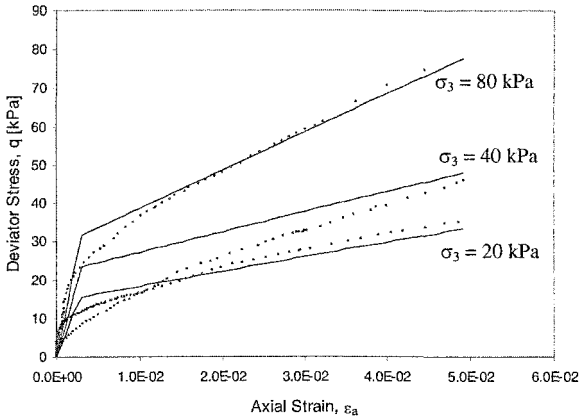
Figure 8: Agreement of the bilinear model to the stress-strain triaxial curves of the undisturbed and saturated loess at different confining pressure.

Conclusions

From the results and analysis presented in this work, the following conclusions can be summarized:

a. Below the yielding locus, behavior of saturated samples is controlled by cemented aggregates. Beyond the yielding locus, shear strength is mainly of a frictional nature. Shear strength difference between remolded and structured specimens decreases with confining pressure revealing that the effect of cementation becomes less significant. At low confining pressure cementation increases shear strength and true cohesion is developed in the structured specimens.

b. Water menisci increases shear strength of unsaturated specimens and yielding is gradually developed. Both, remolded and structured unsaturated specimens developed similar strength envelopes which reveals that cementation has little influence on shear strength.

c. Shearing the soil up to the 6 % strain level used here is not enough to break the cemented aggregates of unsaturated specimens under triaxial loads.

d. Undisturbed specimens present clear elastic to elastoplastic yielding locus, while remolded specimens show a hyperbolic stress-strain behavior. The proposed bilinear stress-strain model fit adequately the stress-strain results for unsaturated structured specimens, making it an excellent simple tool to predict the loess load-deformation behavior.

Acknowledgement

References

AIREY D. W. and FAHEY M., 1991. "Cyclic Response of Calcareous Soil from the North-West Shelf of Australia". *Geotechnique*, Vol. 41, No 1, pp. 101 - 121

CHO G. C. and SANTAMARINA J. C., 2001. "Unsaturated Particulate Materials – Particle-Level Studies". *Journal of Geotechnical and Geoenviromental Engineering*, Volume 127, No. 1 , pp. 84 – 96.

FERNANDEZ A. L. and SANTAMARINA J. C., 2001. "Effect of Cementation on the Small-Strain Parameters of Sand". *Canadian Geotechnical Journal.* Vol. 38 No 1, pp. 191 – 199.

GOTO S., TATSUOKA F., SHIBUYA S., KIM Y. S. Y SATO T., 1991. "A Simple Gauge for Local Small Strain Measurements in the Laboratory". *Soils and Foundations.* Volume 31, No 1, pp. 169 – 180.

LAMBE T. W., 1960. "A Mechanistic Picture of Shear Strength in Clay". *Res. Conf. on Shear Strength of Cohesive Soils.* ASCE. Pp. 555 – 580.

MITCHELL J. K., 1993. "Fundamentals of Soil Behavior". 2nd Edition, Wiley, New York

RINALDI V. A., CLARIA J. J. and SANTAMARINA J. C., 2001. "The Small-Strain Shear Modulus (Gmax) of Argentinean Loess". *XV International Conference on Soil Mechanics and Geotechnical Engineering.* Istanbul, Turkey, Vol. 1, pp. 495 – 499.

RINALDI V. A., 1994. "Propiedades Dieléctricas del Loess del Centro de Argentina". Tesis Doctoral presentada en la Universidad Nacional de Córdoba.

ROCCA R., 1985. "Review of Properties of Loess Soils". *CE 299* Report. Ms. Thesis. University of California, Berkeley, USA.

SAXENA S. K. and LASTRICO R. M., 1978. "Static Properties of Lightly Cemented Sands". *Journal of Geotechnical Engineering Division*, ASCE. Vol. 104, No 12, pp. 1449 – 1464.

VATSALA A., NOVA R. y SRINIVASA MURTHY B. R., 2001. "Elastoplastic Model for Cemented Soils". *Journal of Geotechnical and Geoenviromental Engineering*, Vol. 127, No 8, pp. 679 – 687.

Stiffness of a Compacted Residual Soil

E.C. Leong, J. Cahyadi and H. Rahardjo

School of Civil & Environmental Engineering, Nanyang Technological University, Blk N1, 50 Nanyang Avenue, Singapore 639798; email: cecleong@ntu.edu.sg, cjcahyadi@ntu.edu.sg and chrahardjo@ntu.edu.sg, respectively

Abstract

Compacted soils are often used in engineering structures such as pavement, backfills and embankments. The stiffness of the compacted soils is affected by dry density, degree of saturation and applied strain. This paper describes the stiffness-strain relationships of a compacted residual soil from undrained triaxial compression tests. The triaxial apparatus is equipped with load transducer, bender elements, local displacement transducers, linear variable differential transducer and proximity transducers. Therefore, stiffness from very small strain to large strain can be measured. The small strain stiffness is important in pavements where deformations in the subgrade can be small whereas the larger strain stiffness is applicable to retaining walls and foundations. The effects of initial matric suction and confining pressure on the stiffness-strain relationships are examined in the paper. Both initial matric suction and confining pressure affect the very small strain stiffness, G_{max}. However, only initial matric suction affects the entire stiffness-strain relationship of the compacted residual soil.

Introduction

Residual soils are commonly found in Singapore, occupying approximately two-thirds of the land area. Residual soils are an important source of borrow materials that is commonly transported from one construction site to another construction site for backfill purposes. Soils used in backfills are usually compacted. Compacted residual soils are also used in the construction of pavements and embankments. Deformation characteristics of the compacted soils are important for engineering calculations and one important parameter is stiffness. The stiffness of a compacted soil is affected by dry density, degree of saturation and applied strain. Recently, it has been widely recognized that the stiffness of soils are highly non-linear and soil stiffness decreases

with strain (Jardine et al. 1999, Atkinson 2000, Tatsuoka 2000). It is important to establish the stiffness-strain relationships of soils as deformation of geotechnical structures depends on the applied loading and the stiffness of the soil (Mair 1993) which in turns depends on the mobilized strain as shown in Figure 1. The availability of high accuracy deformation sensors such as local displacement transducer coupled with the usual linear variable differential transducer makes it possible to measure soil stiffness from very small strain to large strain in the laboratory. The purpose of this paper is to examine the stiffness-strain relationships of compacted residual soils as affected by initial matric suction and confining pressure using a triaxial apparatus equipped with local displacement transducers.
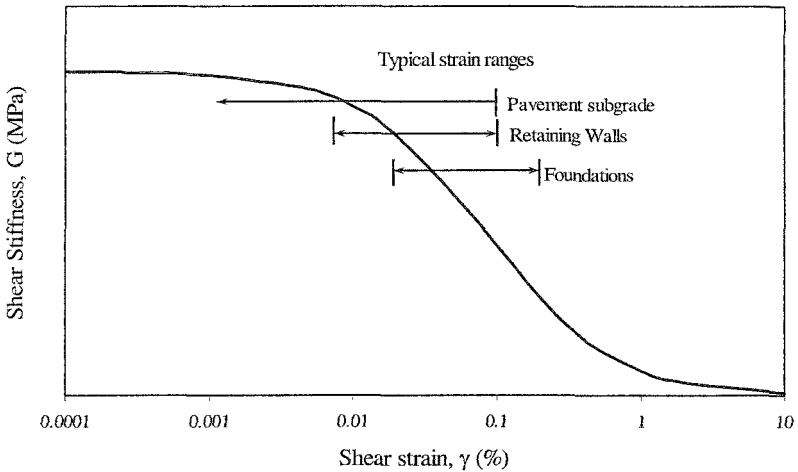
Figure 1. Characteristic stiffness-strain behaviour of soil with typical strain ranges for geotechnical structures.

Test Program

Residual soils from the Bukit Timah Granite formation were collected from a site in the Mandai area, central Singapore. The residual soils were air-dried and broken up. The grain size distribution of the residual soil is shown in Figure 2. The basic properties of the residual soil are summarized in Table 1. The standard Proctor compaction curve of the residual soil obtained in accordance to ASTM D698-91 (1998a) is shown in Figure 3. For this study, a number of soil samples were prepared using the standard Proctor method at a water content of 18.5% corresponding to 90% degree of saturation. The compacted conditions of these soil samples are also indicated in Figure 3. It was assumed that the differences of the compacted soil samples were negligible. The soil samples were then trimmed to dimensions of 50 mm diameter and 100 mm height using a soil lathe and placed in pressure plate apparatus to equilibrate at various matric suctions (30, 60, 120 and 240 kPa). At equilibrium, the soil specimens were transferred to the triaxial apparatus and sheared

under undrained condition. Confining pressures of 50, 100, 200, 400 kPa were applied. The test results of 10 soil specimens as indicated in Table 2 are reported in this paper to investigate the effects of matric suction and confining pressure on the stress-strain behavior of the compacted soil. The test number sXcY in Table 2 denotes test done on a soil specimen with initial matric suction of X kPa at a confining pressure of Y kPa.
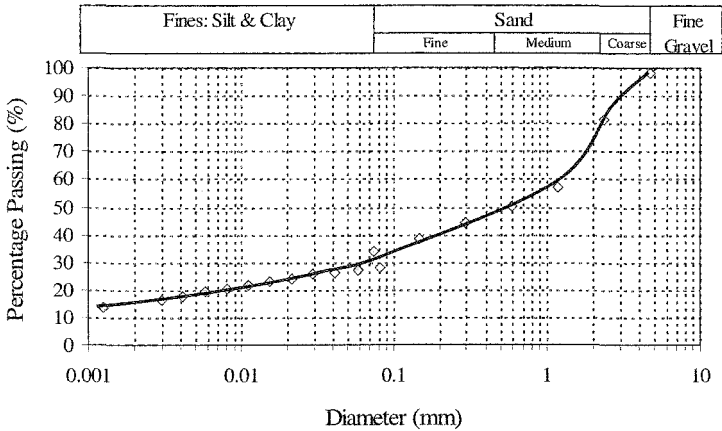
Figure 2. Grain size distribution of Bukit Timah Granite residual soil.
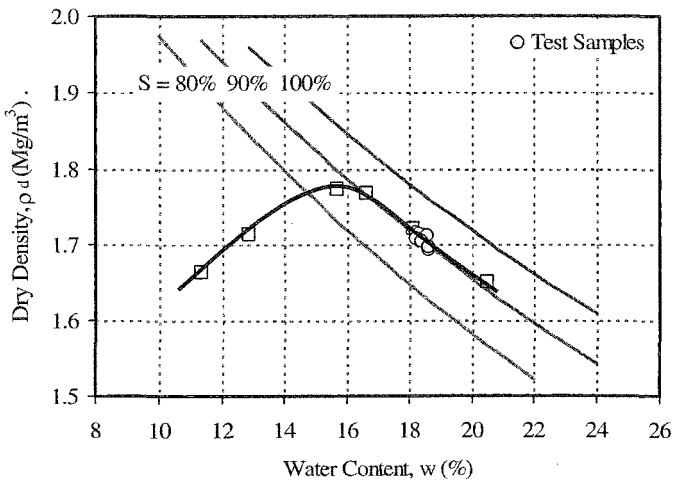
Figure 3. Standard Proctor compaction curve of Bukit Timah Granite residual soil.

Table 1. Basic properties of Bukit Timah Granite residual soil.

Properties	Values
Specific Gravity, G_s	2.62
Liquid Limit, LL (%)	62
Plastic Limit, PL (%)	29
Plasticity Index, PI (%)	33
Grain size distribution (%)	
- Sand	70
- Silt & Clay	30
USCS	SC (clayey sand)

Table 2. Illustrated soil tests.

Initial matric suction, $(u_a - u_w)$ (kPa)	Confining pressure, $(\sigma_3 - ua)$ (kPa)			
	50	100	200	400
30	s30c50	Not reported		
60	s60c50			
120	s120c50	s120c100	s120c200	s120c400
240	s240c50	s240c100	s240c200	s240c400

Soil-water Characteristic Curve

Pressure plate apparatuses with a 5-bar high air entry ceramic plate were used to induce various matric suction values on the soil specimens. The pressure plate test was done in accordance to ASTM D2325-68 (1998b). The air pressure, u_a, was increased incrementally from 30 kPa to 60 kPa, 120 kPa and eventually 240 kPa while water pressure u_w, was maintained at atmospheric condition. At each matric suction, the weights of the soil specimens were measured daily until the change in weight is negligible. After equilibration at each matric suction, the dimensions of the soil specimens were measured and its total volume determined. The time to equilibration at each suction ranged from 7 to 12 days. One or more soil specimens was then removed from the pressure plate apparatus and transferred to the triaxial apparatus for compression test. At the end of the triaxial compression test, the soil specimen was removed and oven dried to determine its water content. Using this water content and the change in weight during the pressure plate test, the volumetric water content of the soil specimen at each matric suctions can be determined. Collectively, the volumetric water contents of all the soil specimens can be used to determine an "average" soil-water characteristic curve as shown in Figure 4. The variation in volumetric water content between soil specimens is about ±1%, partly due to error in water content determination and partly due to the slight differences in sample condition. The average soil-water characteristic curve was determined by fitting the data to the Fredlund and Xing equation using correction factor of 1 as recommended by Leong and Rahardjo (1997). The equation of the average soil-water characteristic curve is given by:

$$\theta_w = \cfrac{\theta_s}{\left[\ln\left\{e + \left(\cfrac{u_a - u_w}{24.3\text{kPa}}\right)^{1.68}\right\}\right]^{0.11}} \tag{1}$$

where θ_w is the volumetric water content, θ_s is the saturated volumetric water content, e is natural base of logarithms and $(u_a - u_w)$ is matric suction.
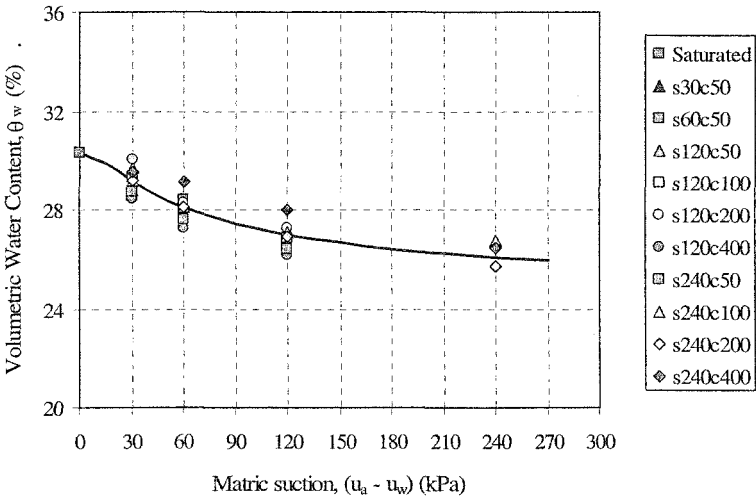
Figure 4. Soil-water characteristic curve of compacted Bukit Timah Granite residual soil.

Undrained Triaxial Compression Test

The triaxial cell was custom built to have internal tie rods and an external cell for ease of setting up the test specimen and attaching the on-specimen instrumentation. Eight ports were provided in the base of the triaxial cell to provide passage for the signal cables of the instrumentation on the test specimen. A pneumatic actuator provides the axial loading. The triaxial apparatus is equipped with the following instrumentations:

(1) A 5 kN submersible load cell for measurement of axial load.
(2) A pair of local displacement transducers (LDTs) for measurement of local axial strain. The LDTs were fabricated in-house following Goto et al. (1991).
(3) A pair of proximity transducers to measure radial strains. The proximity transducers are mounted diametrically opposite and a piece of thin aluminum foil is used as a target for each proximity transducer. The aluminum foil is attached to the rubber membrane at the center portion of the test specimen, by means of silicon grease.

(4) A submersible linear variable differential transducer (LVDT) is attached to one of the internal tie rods with its spindle resting on the load cell.

(5) A pair of bender elements for measurement of shear wave velocity. For this purpose, the top cap and bottom platen were specially designed to enable the installation of the bender elements.

All of the instruments were connected to a control and data acquisition system (CDAS) and a personal computer (PC). A schematic drawing of the test set-up is shown in Figure 5. In the triaxial compression tests, the soil specimens were loaded in the undrained condition at an axial strain rate of 0.017%/s.
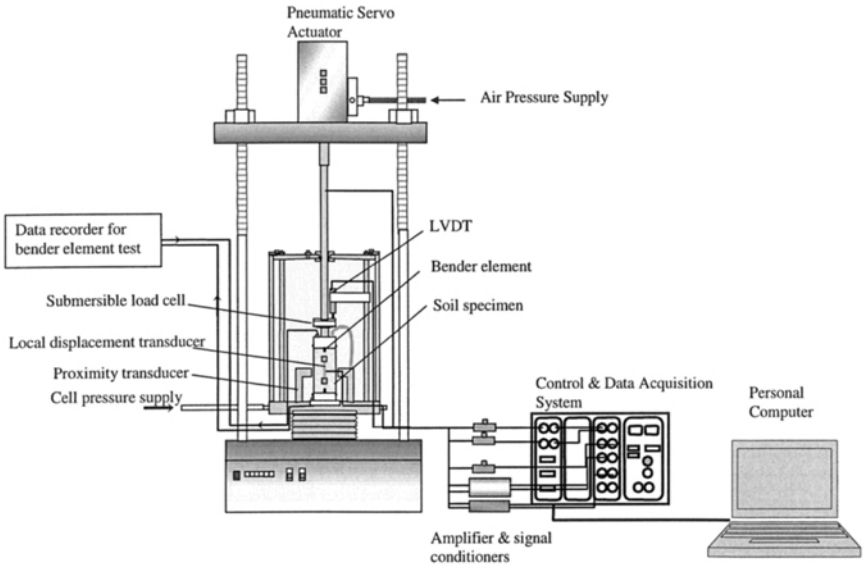
Figure 5. Schematic drawing of triaxial test set-up.

Shear Wave Velocity and Small Strain Stiffness

The shear wave velocity, V_s, is obtained from the bender element test by measuring the travel time of the shear wave from the transmitter bender element to the receiver bender element. The shear wave velocity is a function of the void ratio, e, and confining pressure, σ_3. Shear wave velocity, V_s, is related to the small-strain shear stiffness, G_{max}, as follows:

$$G_{max} = \rho V_s^2 \tag{2}$$

where ρ is the bulk density. The effect of confining pressure, σ_3, and the effect of initial matric suction, $(u_a - u_w)$, on the small strain shear modulus, G_{max}, are summarized in Figures 6 and 7, respectively.

Hardin and Black (1968) suggested the following empirical relation for G_{max} of sands:

$$G_{max} = f(e)\sigma_3^n \tag{3}$$

where $f(e)$ is a function of void ratio and n is an empirical constant. The exponent, n, was found to be 0.5. Mendoza et al. (2005) investigated the small strain stiffness of an unsaturated clayey soil and suggested that G_{max} is related to matric suction by the following empirical relation:

$$G_{max} = f'(e)[\ln(u_a - u_w)]^m \tag{4}$$

where $f'(e)$ is a function of void ratio and m is an empirical constant. The exponent, m, was found to be 1.35. For the present study, it is suggested that the effects of σ_3 and $(u_a - u_w)$ on G_{max} can be accounted for in a single equation as follows:

$$G_{max} = (G_{max})_0 \left[1 + \left(\frac{\sigma_3}{p_a}\right)^n\right]\left[1 + \left\{\ln\left(1 + \frac{u_a - u_w}{p_a}\right)\right\}^m\right] \tag{5}$$

where $(G_{max})_0$ is the G_{max} of the compacted soil at a confining pressure of 0 kPa and a matric suction of 0 kPa, p_a is atmospheric pressure (= 100 kPa) introduced for units consistency and, n and m are empirical constants. The values of $(G_{max})_0$, n and m were determined through curve fitting to be 38 MPa, 0.5 and 1.0, respectively. The curves given by Equation 5 are shown in Figures 6 and 7.
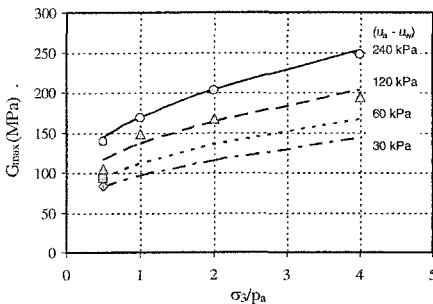
Figure 6. Effect of confining pressure on small strain shear modulus.
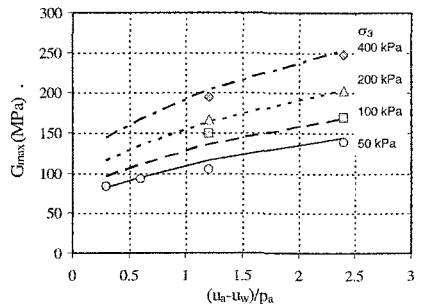
Figure 7. Effect of initial matric suction on small strain shear modulus.

Stress-Strain Behavior

The stress-strain curves of soil specimens at a confining pressure of 50 kPa and various initial matric suctions and for initial matric suctions of 120 kPa and 240 kPa at various confining pressures are shown in Figures 8a, 8b and 8c, respectively. The LDT measurements are indicated by markers whereas the LVDT measurements are indicated by a solid line. The ranges of LDT and LVDT measurements are indicated in Figure 8. From the figures, it may be seen that the range of measurement for LDT is up to 1% axial strain. Combining the axial strain measurement with the radial strain measurement from the proximity transducer reading, the Poisson's ratio of the soil specimen can be estimated. The value of Poisson's ratio ranges between 0.15 to 0.5 depending on the confining pressure and initial matric suction of the soil specimen. Using the stress-strain curve and the Poisson's ratio, the secant shear moduli at various strains can be estimated as shown in Figure 9. The shear moduli obtained from LDT and LVDT measurements show good agreement in the overlapped strain range of 0.01% to 1%.

Stiffness-Strain Relationship

Combining the shear moduli determined from the bender element tests and the triaxial compression tests with local strain measurements, the shear stiffness, G, of the compacted residual soil from very small strain to large strain can be obtained. Hardin and Drnevich (1972) suggested the following equation to describe the stress-strain relationship of soil:

$$\frac{G}{G_{max}} = \frac{1}{1 + \frac{\gamma}{\gamma_r}} \tag{6}$$

where γ is the shear strain and γ_r is the reference shear strain. A more general stress-strain relationship was suggested by Borden et al. (1996):

$$\frac{G}{G_{max}} = \frac{1}{\left(1 + a\gamma^b\right)^c} \tag{7}$$

where a, b and c are constants. Borden et al. (1996) found Equation 7 to fit the normalised shear modulus data for Piedmont residual soils reasonably well. Leong et al. (2003) found Equation 7 with $c = 1$ to fit the stress-strain relationships of undisturbed samples of sedimentary Jurong Formation residual soils well. Equation 7 was used to curve fit the stiffness-strain relationships for the compacted Bukit Timah Granite residual soils and shown in Figure 9 as the solid curves. The value of G_{max} for the compacted soil in the curve fitting exercise was estimated from Equation 5 and it was found that the best-fit curves were obtained for $c = 1$.
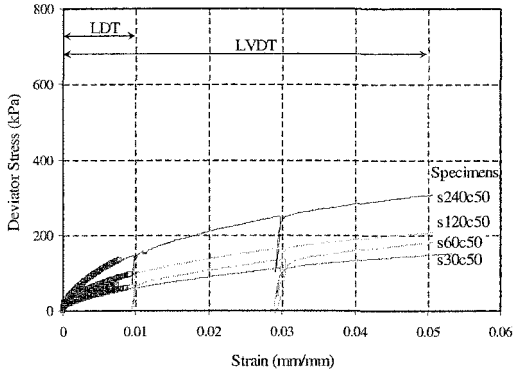
(a) At confining pressure of 50 kPa
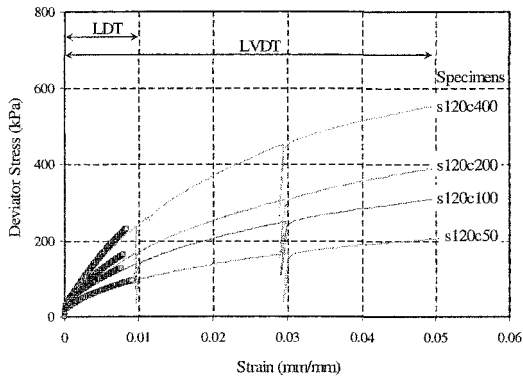
(b) At initial matric suction of 120 kPa
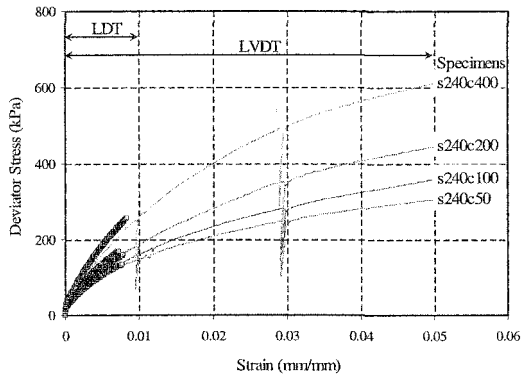
(c) At initial matric suction of 240 kPa

Figure 8. Effects of initial matric suction and confining pressure on stress-strain curves.
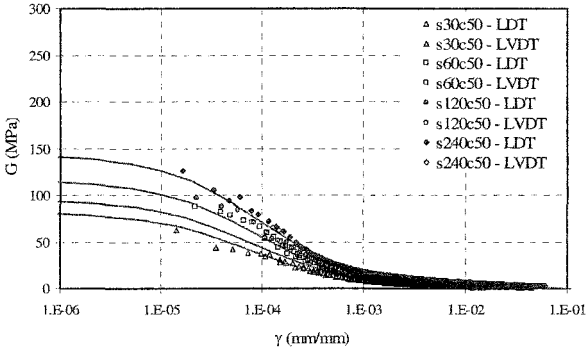
(a) At confining pressure of 50 kPa
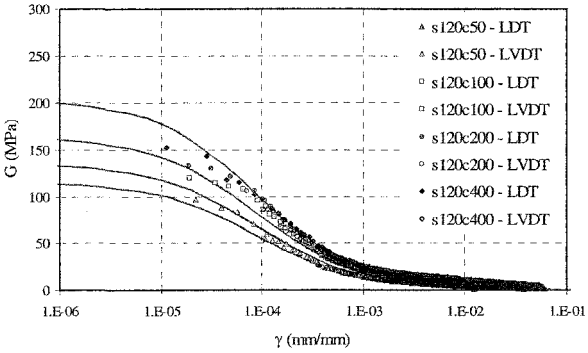
(b) At initial matric suction of 120 kPa
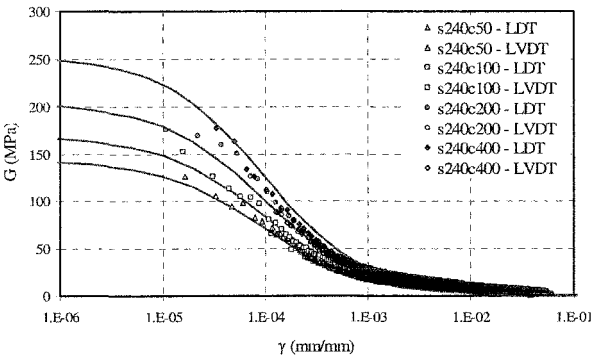
(c) At initial matric suction of 240 kPa

Figure 9. Effects of initial matric suction and confining pressure on stiffness-strain relationships.

The values of a and b for the best-fit curves are summarized in Table 3. Table 3 indicates that G_{max} estimated from Equation 5 was sufficient to account for the effect of confining pressure as shown in Figures 9b and 9c, and therefore the values of a and b do not change. However G_{max} estimated from Equation 5 was insufficient to account for the changes in stiffness-strain relationships due to changes in initial matric suction as shown in Figure 9a. The value of a decreases as initial matric suction of the soil specimen increases whereas b remains unchanged. Comparing Equations 6 and 7, a change in a is equivalent to a change in γ_r. As the value of a decreases, the value of γ_r increases indicating a greater structural change in the soil matrix than that due to an increased confining pressure and hence affecting the entire stiffness-strain relationship.

Table 3. Summary of best-fit constants a and b

Initial matric suction, $(u_a - u_w)$ (kPa)	Confining pressure, σ_3 (kPa)			
	50	100	200	400
30	s30c50 a =3800 b = 0.87	Not reported		
60	s60c50 a = 3500 b = 0.87			
120	s120c50 a = 3300 b = 0.87	s120c100 a = 3300 b = 0.87	s120c200 a = 3300 b = 0.87	s120c400 a = 3300 b = 0.87
240	s240c50 a = 3100 b = 0.87	s240c100 a = 3100 b = 0.87	s240c200 a = 3100 b = 0.87	s240c400 a = 3100 b = 0.87

Conclusion

The effects of initial matric suction and confining pressure on the stiffness-strain relationship of a compacted residual soil were investigated using undrained triaxial compression test together with bender element tests and local strain displacement measurements. Both initial matric suction and confining pressure affect the very small strain shear stiffness, G_{max}. An equation accounting for the effects of initial matric suction and confining pressure was proposed to estimate G_{max}. Initial matric suction has a more significant effect on the entire stiffness-strain relationship whereas the effect of confining pressure on the stiffness-strain relation was fully accounted for in the changes in G_{max}. More extensive tests are needed to fully generalize the effects of initial matric suction on the stiffness-strain relationship of compacted soils.

Acknowledgement

References

ASTM (1998a). "D698-91: Standard test method for laboratory compaction characteristics of soil using standard effort (12400 ft-lbf/ft3 (600 kN-m/m3))." *1998 Annual Book of ASTM Standards*, 04.09, Soil and Rock (II), American Society for Testing and Materials, West Conshohocken, PA, 77-84.

ASTM (1998b). "D2325 – 68: Standard test method for capillary-moisture relationships for coarse and medium textured soils by porous plate apparatus." *1998 Annual Book of ASTM Standards*, Vol. 04.08, Soils and Rock (I), American Society for Testing and Materials, West Conshohocken, PA, 195-201.

Atkinson, J. H. (2000). "Non-linear soil stiffness in routine design." *Géotechnique*, 48(5), 487-508.

Borden, R.H., Shao, L. and Gupta, A. (1996). "Dynamic properties of Piedmont residual soils." *J. of Geotech. Engrg*, ASCE, 122(10), 813-821.

Goto, S., Tatsuoka, F., and Shibuya, S. (1991). "A simple gauge for local strain measurements in the laboratory." *Soils and Foundations*, 31(1): 169-180.

Hardin, B.O. and Black, W.L. (1968). "Vibration modulus of normally consolidated clays." *J. of Soil Mech. And Found. Engrg.*, ASCE, 94(SM2), 353-369.

Hardin, B.O. and Drnevich, V.P. (1972). "Shear modulus and damping in soils: Design equations and curves." *J. of Soil Mech. And Found. Engrg.*, ASCE, 98(SM7), 667-692.

Jardine, R.J.; Kuwano, R.; Zdravkovic, L.; Thornton, C. (1999). "Some fundamental aspects of the pre-failure behaviour of granular soils." *Proc. of the Second International Symposium on Pre-failure Deformation Characteristics of Geomaterials*, Sep 28-30 1999, Torino, Italy, A.A. Balkema, 1077-1111.

Leong, E.C. and Rahardjo, H. 1997. "A review on soil-water characteristic curve equations." Journal of Geotechnical and Geoenvironmental Engineering, 123(12), 1106 - 1117.

Leong, E.C., Rahardjo, H., Cheong, H.K. (2003). "Stiffness-strain relationship of Singapore residual soils." *Proc. 7th Pacific Conference on Earthquake Engineering*, Christchurch, New Zealand, 13-15 February 2003, Paper No. 160.

Mair, R. J. (1993). "Developments in geotechnical engineering research: application to tunnels and deep excavations." Unwin Memorial Lecture 1992, *Proc. Inst. of Civil Engineers*, Civil Engineering, 93, 27-41.

Mendoza, C.E., Colmenares, J.E., and Merchán, V.E. (2005). "Stiffness of unsaturated compacted clayey soils at very small strains." *Proc. International Symp. On Advanced Experimental Unsaturated Soil Mechanics*, Trento, Italy, 27-29 June, 199-204.

Tatsuoka,F. (2000). "Impacts on geotechnical engineering of several recent findings from laboratory stress-strain tests on geomaterials." *2000 Burmister Lecture*, Columbia University, N.Y.

Determination of the shear strength parameters of two unsaturated colluvium soils using the direct shear test

C. Feuerharmel; A. Pereira; W. Y. Y. Gehling and A. V. D. Bica

Geotechnology Laboratory, Department of Civil Engineering, Federal University of Rio Grande do Sul, Oswaldo Aranha Ave. (99), Porto Alegre, CEP 90035-190; PH (55-51) 3316-3462; FAX (55-51) 3316-3999; email: carolina071078@yahoo.com.br; alvarop@pop.com.br ; gehling@vortex.ufrgs.br ; avdbica@vortex.ufrgs.br

Abstract

The shear strength of two colluvium soils, situated at the Serra Geral Formation scarp in Southern Brazil, was determined with conventional and suction-controlled direct shear tests. One investigated colluvium soil was originated from the weathering of a volcanic rock (Sample RO) and the other, possibly from the degradation of intertrapp sandstone layers (Sample AV). A study of matric suction influence on the shear strength of undisturbed samples of both soils is presented in this paper. Suction-controlled direct shear tests showed that shear strength envelopes are linear for matric suctions between 0 and 150 kPa. Further direct shear tests, carried out with air-dried samples, showed that those shear strength envelopes tend to become bilinear for higher suctions. In addition, the experimental data indicated that for both soils the internal friction angle (ϕ') seems to increase with matric suction and ϕ^b values are higher than corresponding ϕ' values.

Introduction

The interest in the study of unsaturated soils has been recognized since the establishment of Soil Mechanics as an engineering science. However, the principles of Classic Soil Mechanics had been developed with emphasis on saturated soils (pores filled with water) or dry soils (pores filled with air). For those two extreme conditions existing theories have been applied successfully for the description of soil mechanical behavior.

The theoretical background of Unsaturated Soil Mechanics has been developed mainly in last four decades. The study of unsaturated soils is extremely important, because those materials are found in all continents, particularly in arid and semiarid

regions (i.e. more than 60% of countries in the world). In tropical countries with long dry seasons, such as Brazil, the occurrence of unsaturated soils is also very frequent. For those soils the determination of shear strength and its variation with suction are of fundamental importance for a large number of geotechnical and geoenviroment problems. This knowledge allows a more faithful modeling of the real condition in which the soil is submitted in the field.

This paper presents results of conventional and suction-controlled direct shear tests carried out with two colluvium soils from Serra Geral Formation. Those data allowed the determination of shear strength parameters for the saturated condition – c' (cohesion intercept) and ϕ' (internal friction angle) – and as well as for the unsaturated condition - ϕ^b [(angle that quantifies the shear strength increase as a function of suction change (Fredlund and Rahardjo, 1993)]. The investigated colluvium soils showed shear strength envelopes initially linear (for matric suctions between 0 and 150 kPa) with ϕ^b values higher than ϕ'. This observation does not agree with some shear strength concepts currently accepted for unsaturated soils, where ϕ^b must be equal to ϕ' for suctions lower than the air-entry value and ϕ^b should decrease with increasing suction until the residual condition is reached (Vanapalli et al., 1996). Further direct shear tests were carried out using air-dried samples; all were tested under constant water content. The shear strength continued to increase with suction until high suctions were reached. Regarding ϕ', its value was shown to increase with increasing suction.

Background

The first studies related to the shear strength of unsaturated soils involved the concept of effective stress. Since the fifties, several empirical equations have been proposed for evaluating the shear strength of unsaturated soils. Common to all those equations is the incorporation of a soil parameter and the use of one or more stress state variables to represent the total stress and the suction contribution to the effective stress (Fredlund, 1979). Among those equations, the best known is due to Bishop (1959) (Equation 1). The χ value is equal to one, for saturated soils, and zero, for dry soils. Intermediate values of χ depend on the degree of saturation, wetting and drying cycles, soil structure and composition, stress history and followed stress path. Many authors later questioned the concept of effective stress proposed by Bishop (Jennings and Burland, 1962; Bishop and Blight, 1963; and Matyas and Radharkishna, 1968).

$$\tau = c' + \left[(\sigma - u_a) + \chi(u_a - u_w) \right] \tan \phi' \qquad \text{(Equation 1)}$$

By the end of the sixties, other researchers already noted the limitations and difficulties regarding the use of Bishop's equation and the need for using independent stress state variables to describe unsaturated soil behavior. Fredlund et al. (1978) proposed that the shear strength of an unsaturated soil be a function of two independent stress variables: the net normal stress ($\sigma-u_a$) and the matric suction (u_a-u_w). They suggested Equation 2 for describing of shear strength, where c' and ϕ' are saturated shear strength parameters and ϕ^b is the angle of friction with respect to suction u_a-u_w.

$$\tau = c' + (\sigma - u_a) \tan \phi' + (u_a - u_w). \tan \phi^b \qquad \text{(Equation 2)}$$

The shear strength envelope for unsaturated soils given by equation 2 was originally proposed as a planar surface, where both ϕ' and ϕ^b were assumed to be constant. Experimental evidence questioned this equation in some aspects. First, Escário and Sãez (1986), Gan et al. (1988), Abramento and Carvalho (1989) and Campos and Carrillo (1995) showed further data where the relationship between shear strength and suction was nonlinear. The non-linearity of the shear strength envelope is now well established, and there is a consensus that ϕ^b is not constant. Current knowledge assumes $\phi^b \approx \phi'$, for matric suctions lower than the soil air-entry value, and $\phi^b < \phi'$, as the value of suction increases. Second, the variation of ϕ' with suction also was verified by many authors (Drumright and Nelson, 1995; Röhm and Vilar, 1995; Wheeler and Sivakumar, 1995). This variation of ϕ' can be related to structural changes caused by a suction increase; those structural changes would then increase grain interlocking independently of applied stresses (Campos, 1997). Third, other studies observed that the amount of suction contribution to the shear strength can be limited depending on the interval of applied net normal stress. The strength envelopes of some soils obtained at different suction ranges can converge towards a unique point, thus indicating that there is no effect of suction for net normal stresses in excess of a given value (Delage et al., 1987; Maâtouk et al., 1995). Finally, ϕ^b values higher than ϕ' were found for some Brazilian undisturbed residual and colluvium soils (Abramento and Carvalho, 1989; Röhm and Vilar, 1995).

As a result, the failure criterion proposed by Fredlund et al. (1978) can be used for those unsaturated soils within some limited ranges of suction and net normal stress. However, some aspects need to be further discussed such as the influence of suction on the internal friction angle (ϕ') and the experimental observation that some soils present $\phi^b > \phi'$.

Investigated soils

The sampled colluvium soils may be described as unconsolidated clastic sediments originated from local Botucatu (Sample AV) and Serra Geral (Sample RO) formations. The investigated area is situated at the border between the states of Rio Grande do Sul and Santa Catarina, in Southern Brazil. Sample AV was taken from a colluvium layer situated near the bottom of the Serra Geral scarp; it possibly originated from the weathering of an intertrapp sandstone layer. Sample RO was taken from a colluvium layer situated near the middle of the scarp; it possibly originated from the weathering of a volcanic rock (basalt). Table 1 presents the basic physical and mineralogical characteristics of those soils. Particle size analyses showed that both soils are essentially clayey. However, visual inspection suggests that both soils are composed in their natural condition by silt or sand-sized aggregates of clay particles.

The soil-water characteristic curves (SWCC) of both soils are shown in Figure 1. Those curves were determined using both the filter-paper technique (for suctions between 10kPa and 30,000kPa) and the suction-plate technique (for lower suctions). More details about these testing techniques can be found in Feuerharmel (2003). The shape of both curves suggests that those soils have a bimodal distribution of pore sizes: macropores, between clay aggregates, and micropores, inside those aggregates.

This type of curve, known as "double S", shows an intermediate behavior between sandy and clayey soils, suggesting the existence of two air-entry values and the possible division of each curve into three desaturation zones (Feuerharmel et al., 2005). The desaturation is controlled by the macropores for low suctions (< 10kPa), and by the micropores, for higher suctions (> 3000kPa). For intermediate values of suction, removal of water does not occur probably because of the absence of intermediate pore sizes. Soil-water characteristic curves with this shape have been observed for some Brazilian sedimentary and residual soils (Bastos, 1999; Bortoli, 1999, Futai et al., 2004).

Table 1. Physical and mineralogical characterization data.

Soil Property	Sample AV	Sample RO
γ_s, kN/m³	28	28.6
Water content *, %	30	47.2
Degree of saturation *, %	84.4	81.3
Void ratio *	1.1	1.7
Liquid limit, %	56	74
Plastic limit, %	34	57
Plasticity index, %	22	17
Clay fraction, %	53	53
Silt fraction, %	15	34
Sand fraction, %	32	13
Main minerals	Kaolinite and quartz	Kaolinite, quartz and gibbsite

* average values.
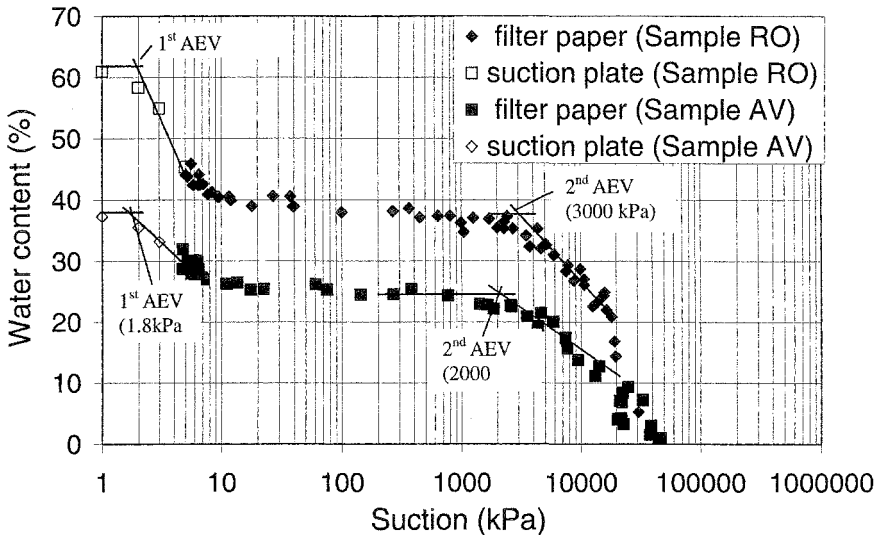
Figure 1 - Soil-water characteristic curve of undisturbed samples of colluvium soils.

Experimental Program

The experimental program included different types of direct shear tests: (i) with saturated specimens (suction of 0 kPa); (ii) suction-controlled tests with unsaturated specimens (matric suctions of 50, 100 and 150 kPa), and (iii) constant water content tests (with air-dried specimens). Those tests were carried out using undisturbed specimens with net normal stress of 25, 50, 100 and 150 kPa. Results of these tests allowed the determination of shear strength envelopes in the τ x $(\sigma-u_a)$ and τ x (u_a-u_w) planes, as well as the evaluation of shear strength parameters c', ϕ' and ϕ^b.

The shear strength tests for the saturated condition and the constant water content condition were carried out using a conventional direct shear testing equipment. These tests were carried out using undisturbed cylindrical specimens (60-mm diameter and 20-mm high) at the shear speed of 0.036mm/min (Pinheiro et al., 1997). The shear force was measured with a 2-kN load cell. The vertical and horizontal displacements were measured with a pair of 10-mm displacement traducers. All transducers were connected to a data acquisition equipment, controlled by a microcomputer. These tests followed the British Standard BS 1377-90 (BSI 1990). Tests for the saturated condition were carried out with soaked specimens and, for the constant water content tests, the shear box was involved with a plastic bag, to minimize loss of moisture in the specimen. The probable suction of the air-dried specimens was estimated on the basis of SWCC.

The unsaturated shear strength was determined with suction-controlled direct shear tests using an equipment developed by Bastos (1999), based on the model proposed by Gan and Fredlund (1988). In this equipment, an air-pressurized chamber allows, by the axis translation technique, the application of matric suction to the specimen during the equalization and shearing phases. The matric suction is imposed by the difference between the air pressure, applied to the top of the specimen, and the water pressure, applied by a water column (burette) to a high air-entry disk (3 bar) situated in the base. Vertical loading, applied with weights, was transmitted to the specimen by a top cap. The applied shear speed was 2.03 x 10^{-4}mm/s (Bastos, 1999) and the suction equalization time was of approximately 7 days. The shear force was measured using a 2-kN load cell, the horizontal and vertical displacements were monitored with 10-mm displacement traducers and the air pressure was measured with a 700-kPa pressure transducer. All transducers were connected to the same data acquisition equipment used for conventional direct shear testing.

Results

Results of conventional and suction-controlled direct shear tests obtained for the studied colluvium soils are presented in Figures 2 and 3, for Sample AV, and in Figures 4 and 5, for Sample RO. The projections of corresponding shear strength envelopes on planes τ x $(\sigma-u_a)$, shown in Figures 2 and 4, are approximately linear for net normal stresses between 25 and 150 kPa. The declivity of those envelopes, represented by ϕ', tends to increase with increasing matric suction. Table 2 presents values of ϕ' for different suctions levels. It can be observed that ϕ' seems to increase

when the matric suction varies from 0 to 150 kPa. For suctions higher than 150 kPa (air-dried specimens), values of ϕ' are still increasing. This behavior can be associated with some dispersion in the test or in the undisturbed samples. The suction for air-dried specimens, measure with filter paper, was around 6000 kPa, for Sample AV, and 7000 kPa, for Sample RO.
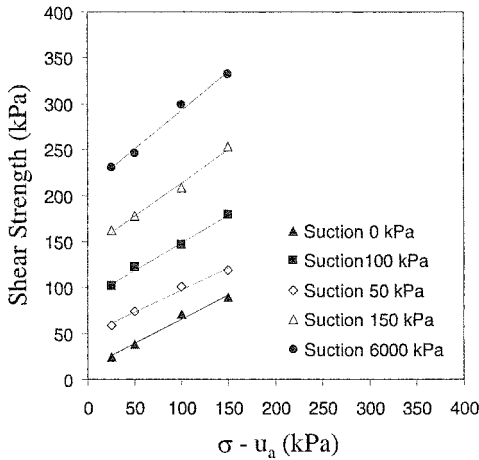
Figure 2 - Shear strength envelope projection on plane τ x (σ-u_a) -Sample AV.
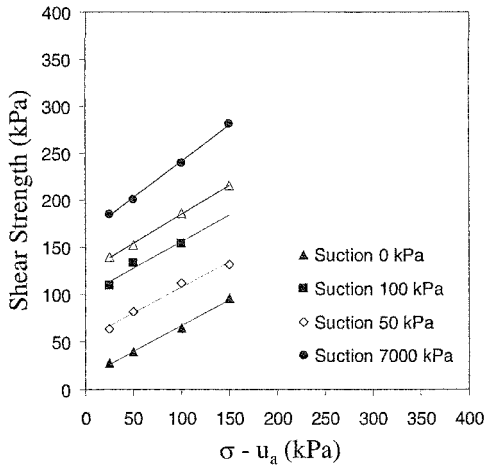
Figure 3 - Shear strength envelope projection on plane τ x (σ-u_a) –Sample RO.
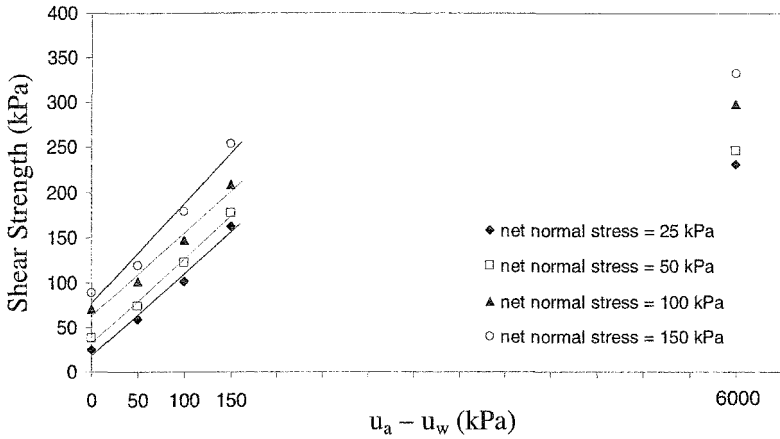
Figure 4 - Shear strength envelope projection on plane τ x $(u_a\text{-}u_w)$ –Sample AV.
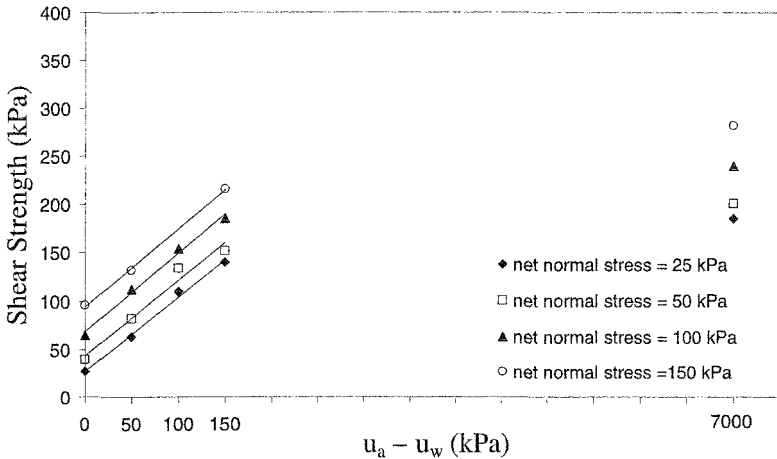
Figure 5 - Shear strength envelope projection on plane τ x $(u_a\text{-}u_w)$ –Sample RO.

The projections of those shear strength envelopes on planes τ x $(u_a\text{-}u_w)$, shown in Figures 4 and 5, are linear for matric suctions between 0 and 150 kPa. This behavior was observed for all net normal stress tested. Shear strength values of air-dried specimens were higher than those corresponding to the matric suction of 150 kPa, indicating that a suction contribution to the shear strength can be still observed even for high suctions. Those results also evidenced that the shear strength envelopes tend to become bilinear for higher suctions. The values of ϕ^b are shown in Table 3. The obtained average ϕ^b is 44°, for Sample AV, and 38.3°, for Sample RO. Such values of ϕ^b are higher than ϕ'.

Another interesting observation is that the applied matric suctions of 50, 100 and 150 kPa are situated along the horizontal plateau of the SWCC. This means that these suctions correspond to the same water content, but their shear strengths are different. This suggests that the shear strength of those soils is not governed by the water area nor by the amount of water inside the soil voids, but instead by the energy acting in pore-water (suction).

Table 2. Variation of ϕ' with matric suction.

Sample/Matric suction	0 (kPa)	50 (kPa)	100 (kPa)	150 (kPa)	Dry soil
AV	25.8 °	28.0 °	30.9 °	35.9 °	40.1 °
RO	28.5 °	28.6 °	29.6 °	31.7 °	37.9 °

Table 3. Variation of ϕ^b with net normal stress for matric suctions between 0 and 150 kPa.

Sample/Normal stress	25 (kPa)	50 (kPa)	100 (kPa)	150 (kPa)	ϕ^b average
AV	42.4 °	43.0 °	42.5 °	47.9 °	44.0 °
RO	37.5 °	37.9 °	39.0 °	38.8°	38.3°

Conclusions

This study presents shear strength parameters obtained for two undisturbed colluvium soils from Southern Brazil. These parameters were determined with saturated, suction-controlled and constant water content direct shear tests. Shear strength data indicated a possible increase of the internal friction angle (ϕ') with increasing matric suction, a phenomenon probably related to structural changes caused by this suction increase. The shear strength envelopes of those soils presented a linear relationship between matric suction and shear strength until a value of suction of 150 kPa is reached. For higher suctions, those envelopes became bilinear. In addition, values of ϕ^b are higher than corresponding ϕ', suggesting that an increase of suction causes an increase of shear strength more significant than that due to an increase of net normal stress. This observation does not agree with some currently accepted shear strength concepts and suggests the need for further investigation about the subject.

Acknowledgements

References

Abramento, M. and Carvalho, C. S. (1989). "Geotechnical parameters for study of natural slopes instabilization at Serra do Mar, Brazil". *Proc. 12th Intern. Conf. On Soil Mech and Found. Engn*, v.2: 1599-1602. Rio de Janeiro: Balkema.

Bastos, C. A. (1999). *"A geotechnical study on the erodibility of unsaturated residual soils"*. D.Sc. thesis, Federal University of Rio Grande do Sul, Porto Alegre, RS, Brazil [in Portuguese].

Bishop, A. W. (1959). "The principle of effective stress". Tecknisk Ukeblad, 106 (39): 859-863.

Bishop, A. W. and Blight, G. E. (1963). "Some aspects of effective stress in saturated and partly saturated soils". *Géotechnique* 13: 177-197.

Bortoli, C. R. (1999). *"Numerical-experimental study of saturated/unsaturated hydraulic conductivity of a structured unsaturated soil"*. M.Sc. dissertation, Federal University of Rio Grande do Sul, Porto Alegre, RS, Brazil [in Portuguese].

B.S.I. (1990). British Standard BS1377-90. Part 8: shear strength test (effective stress). London: British Standards Institution.

Campos, T. M. P. and Carrilo, C.W. (1995). "Direct shear testing on an unsaturated soil from Rio de Janeiro". Unsaturated Soils, ed. Alonso and Delage., *Proc. 1st Intern. Conf. on Unsaturated Soils*, v.1: 31-38 Paris: Balkema.

Campos, T. M P. (1997). "Shearing strength of unsaturated soils". *3° Simpósio Brasileiro de Solos Não Saturados*, v.2: 399-417, Rio de Janeiro, Brazil [in Portuguese].

Delage P.; Silva, G. P. R. S. and De Laure, E. (1987). "A new triaxial apparatus for non-saturated soils". *Proc. 9th Eur. Conf. Soil Mech*, v.1: 25-28. Dublin.

Drumright, E. E. and Nelson, J. D. (1995). "The shear strength of unsaturated tailings sand". Unsaturated Soils, ed. Alonso and Delage., *Proc. 1st Intern. Conf. on Unsaturated Soils*, v.1: 189-193 Paris: Balkema.

Escário, V. and Sáez, J. (1986). "The shear strength of partly saturated soils". *Géotechnique*, 36 (3):453-456.

Feuerharmel, C. (2003). *"Aspects of the unsaturated behavior of two colluvium soils -- Bolivia-Brazil gas pipeline"*. M.Sc. dissertation, Federal University of Rio Grande do Sul, Porto Alegre, RS, Brazil [in Portuguese].

Feuerharmel, C.; Gehling, W. Y. Y. and Bica, A. V. D. (2005). "Determination of the soil-water characteristic curve of undisturbed colluvium soils". *Proc.Int. Symp. Advanced Experimental Unsaturated Soil Mechanics*. Trento, Italy. v.1: 345-349.

Fredlund, D. G.; Morgenstern, N. R. and Widger, R. A. (1978). "The shear strength of unsaturated soils". *Canadian Geotechnical Journal* 15(3): 313-321.

Fredlund, D. G. (1979). "Appropriate concepts and technology for unsaturated soils". *Canadian Geotechnical Journal* 16(1): 121-139.

Fredlund, D. G. and Rahardjo, H. (1993). *"Soil Mechanics for Unsaturated Soils"*. John Wiley & Sons, Inc., 517 p.

Futai, M. M.; Almeida, M. S. S. and Lacerda, W. A. (2004). "Shear strength of unsaturated tropical soils". *5° Simpósio Brasileiro de Solos Não Saturados*, v. 1: 43-54, São Carlos, Brazil [in Portuguese].

Gan, J. K. M. and Fredlund, D. G. (1988). "Multistage direct shear testing of unsaturated soils". *Geotechnical Testing Journal* ASTM, 11(2): 132-138.

Jennings, J. E. B. and Burland, J. B. (1962). "Limitations to the use of effective stresses in partly saturated soils". *Géotechnique* 12: 125-144.

Maâtouk, A.; Leroueil, S. and La Rochelle, P. (1995). "Yielding and critical state of a collapsible unsaturated silty soil". *Géotechnique* 45 (3): 465-477.

Matyas, E. L. and Radhakrishnan, H. S. (1968). "Volume change characteristic of partially saturated soil". *Géotechnique* 18 (4): 432-448.

Pinheiro, R. J. B. (1997). *"Study of some slope instability cases at Serra Geral in the state of Rio Grande do Sul"*. D.Sc. thesis, Federal University of Rio Grande do Sul, Porto Alegre, RS, Brazil [in Portuguese].

Rohm, S. A. and Vilar, O. M. (1995). "Shear strength of an unsaturated sandy soil". Unsaturated Soils, ed. Alonso and Delage., *Proc. 1ˢᵗ Intern. Conf. on Unsaturated Soils*, v.1: 189-193 Paris: Balkema.

Vanapalli, D. G.; Fredlund, D. G.; Pufahl, D. E. and Clifton, A. W. (1996). "Model for the prediction of shear strength with respect to soil suction". *Canadian Geotechnical Journal* 33(3): 379-392.

Wheeler, S. J. and Sivakumar, V. (1995). "An elasto-plastic critical state framework for unsaturated soil". *Géotechnique* 45 (1): 35-53.

A study on the shear strength envelope of an unsaturated colluvium soil

A. Pereira; C. Feuerharmel; W. Y. Y. Gehling and A. V. D. Bica

Geotechnology Laboratory, Department of Civil Engineering, Federal University of Rio Grande do Sul, Oswaldo Aranha Ave. (99), Porto Alegre, CEP 90035-190; PH (55-51) 3316-3462; FAX (55-51) 3316-3449; email: engalvaro@gmail.com; carolina071078@yahoo.com.br; gehling@vortex.ufrgs.br ; avdbica@vortex.ufrgs.br

Abstract

A conventional triaxial equipment, originally used for testing soil specimens in the saturated condition, was modified in order to allow the testing of specimens in the unsaturated drained condition. In this device, the axis-translation technique is used to avoid cavitation in the pressure measuring system. The volume change in the specimen is determined from the measurement of changes in the volume of the triaxial cell confining fluid. Those tests were carried out using specimens of a colluvium soil of sandstone both in the saturated condition (drained and undrained tests) and in the unsaturated condition. The observed behavior was (i) an increase of shear strength with an increment of matric suction and (ii) the non-linearity of the shear strength envelope after the application of a higher value of matric suction.

Introduction

The objectives of this research were the evaluation of the unsaturated shear strength - including the determination of the three-dimensional Mohr-Coulumb shear strength envelope - of a colluvium soil of sandstone from Southern Brazil. Corresponding shear strength parameters were determined from the interpretation of results of saturated and unsaturated triaxial tests. Saturated tests were carried out both under drained and undrained conditions, although the unsaturated tests were carried out only in the drained condition. The triaxial equipment used for the unsaturated tests was modified from a conventional triaxial equipment; it was based on design concepts presented by Bishop and Henkel (1962), Ho and Fredlund (1982), and Fredlund et al. (1993). This equipment will be briefly described in the sequence.

Fredlund *et al.* (1978) proposed the shear strength equation (Equation 1) that was adopted for evaluating the unsaturated shear strength envelope of this colluvium soil. It considers (σ - ua) and (ua – uw) as stress variables. The advantage of selecting those variables is that only one is affected when a change of pore water pressure occurs.

$$\tau = c' + (\sigma - u_a).\tan\phi' + (u_a - u_w).\tan\phi^b \qquad \text{(Equation 1)}$$

Where τ = shear stress on the failure plane;

c' = cohesion intercept;

ϕ' = angle of internal friction;

$(\sigma - u_a)$ = net normal stress;

ϕ^b = angle indicating the rate of change in shear strength to changes in matric suction;

$(u_a - u_w)$ = matric suction.

Equation (1) considers the shear strength envelope as a planar surface in order to model the increase of the shear strength with suction. The validation of equation (1), as described by Fredlund *et al.* (1978), was made through the analysis of experimental data presented by other authors. The assumption of a planar shear strength envelope was however questioned by Escario and Saez (1986). Those authors presented non-linear shear strength envelopes obtained for different soils with suction-controlled direct shear tests. Fredlund *et al.* (1987) re-evaluated these data concluding that there are types of soils that may show some non-linearity in their shear strength envelopes for low suction values, i.e. when the soil still keeps a high saturation level. For this case, ϕ^b has almost the same value as ϕ'. For suctions higher than the air-entry value, ϕb starts to reduce and the shear strength envelope can be considered as bilinear. Abramento and Carvalho (1989), Campos and Carrilo (1995) and Bastos (1999) showed non-linear unsaturated shear strength envelopes for some Brazilian colluvium soils.

Characterization of the studied soil

The material used for those triaxial tests is a colluvium soil of sandstone denoted as Sample AV. The colluvium is situated at an altitude close to 150 m on the hillsides of the Serra Geral Formation, near the border between the states of Santa Catarina (SC) and Rio Grande do Sul (RS), in Southern Brazil. The physical characterization of this material was made with grain size analyses, specific gravity tests and Atterberg limits tests (Feuerharmel, 2003). Those data are presented in Figure 1 and Tables 1 and 2.

Table 1 - Physical characterization of Sample AV (Feuerharmel, 2003).

Material	γ_s (kN/m³)	Liquid Limit	Plastic Limit	Plasticity index
Sample AV	28	56%	34%	22%

Table 2 - Summary of the grain size analysis of Sample AV (Feuerharmel, 2003).

Grain size (%)	
Clay	53
Silt	15
Sand	32
Gravel	0
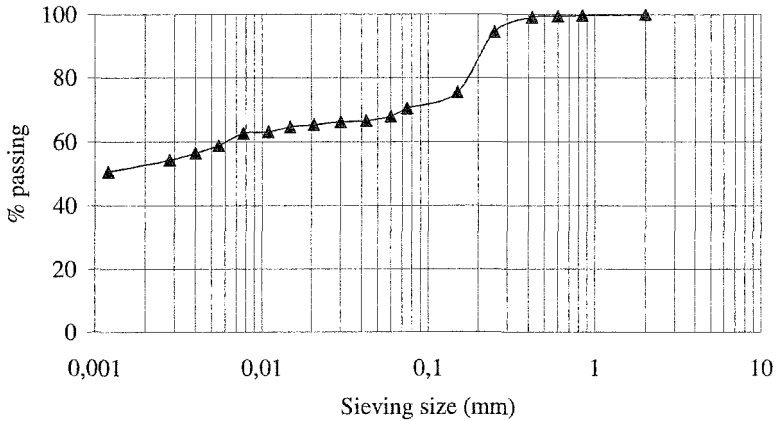
Figure 1 – Grain size curve of the tested soil

Apparatus

The triaxial equipment used to carried out those tests was manufactured by *Wille Geotechnik*. This equipment is provided with an automatic data acquisition system and a microcomputer that controls all phases of the triaxial test for both the saturated and unsaturated conditions. The original equipment was conceived for triaxial tests with saturated specimens only. Suction-controlled tests have been carried out with unsaturated specimens after some adaptations were made in the original equipment based on the experience of other authors (Bishop and Henkel, 1962; Ho and Fredlund, 1982; Fredlund *et al*, 1993 and Bucio, 2002). The main modifications introduced in the equipment are:

- adoption of the axis translation technique: the application of a positive pore air pressure and a positive pore water pressure within the specimen allowed the application of suctions higher than 101 kPa.

- installation of bubble flushing devices [for the interception of air bubbles, as described by Bucio (2002): the objective of these devices was to minimize the

presence of diffuse air bubbles. Two of them have been fitted in this triaxial equipment: one is located in the pore water pressure line and the other, in the confining pressure line (where volume change is measured).

- installation of a modified cell base: the modified design was based on that presented by Fredlund *et al.* (1993) and Rampino *et al.* (1999). This cell base allows the application of confining pressure, pore air and pore water pressure, together with the installation of a transducer for measuring pore water pressure. A high air-entry value porous stone was cemented to the pedestal of this cell base. Below the porous stone, grooves have been machined on the pedestal in order to allow the circulation of freshly de-aired water.

- installation of a high air-entry value porous stone: the 300-kPa air-entry value porous stone was cemented to the pedestal. It has a diameter of 41.5 mm and a height of 7 mm.

- measurement of volume change [following Bishop and Henkel, 1962; Lade, 1988; Fredlund *et al.*, 1993; Geiser *et al.*, 2000; Ng *et al.*, 2002 and Leong *et al.*, 2004): the volume change of unsaturated specimens was determined from the measurement of the change of volume of cell fluid during testing. According to those authors, this is one of the simplest methods available for measuring volume change, although it is very susceptible to errors. To reduce such errors, the following precautions and measurement corrections were taken: (i) the use of de-aired water; (ii) control of laboratory temperature [to keep it within $23°C \pm 2°C$]; (iii) frequent flushing of air bubbles in order to reduce the presence of diffuse air inside pressure lines; (iv) some fiberglass straps were cemented around the cell acrylic wall in order to reduce its deformation under pressure; (v) a previous calibration of the cell, pipes and connections elastic deformation under pressure was carried out, together with evaluation of water absorption by the acrylic wall; and (vi) a previous creep testing of those components was also carried out. The apparent volume change due to the penetration of the loading piston inside the triaxial cell during testing was also corrected.

Description of triaxial tests

The triaxial tests were carried out using 50-mm diameter and 100-mm high undisturbed specimens of the colluvium soil. For unsaturated tests the specimens were placed inside the triaxial cell at similar initial water contents. Specimens having water contents different than 24.5 % had been corrected for this value. Table 3 presents initial values of void ratio (e_i) and water content (w_i) for both saturated and unsaturated specimens used in this research.

For the saturated triaxial tests, all specimens were saturated by applying backpressure and then consolidated to the initial effective stress defined for each test. For the unsaturated triaxial tests, the consolidation phase corresponded to the equalization

phase of both air and water pressures that defined the applied suction. According to Fredlund *et al.* (1993), the balance is reached when the water change of the sample becomes null. Feuerharmel (2003) used, for low suction values, the equalization time of four days in order to determine the soil-water characteristic curve of this soil. For the triaxial tests described by Bucio (2002), the adopted equalization time was from three to four days. The equalization time used in this research was about four days, except for one specimen that was sheared after three days of balance, since it didn't show a significant water change.

Table 3 – Initial void ratios and water contents of unsaturated specimens

Specimen	$(\sigma - u_a)$ or $(\sigma - u_w)$ (kPa)	$(u_a - u_w)$ (kPa)	e	w_i (%)
Usat_t50_s25	50	25	0.76	25*
Usat_t50_s50	50	50	0.92	24.1
Usat_t50_s100	50	100	0.87	24.1
Usat_t50_s150	50	150	0.96	25.4
Usat_t100_s50	100	50	0.97	24.5*
Usat_t100_s100	100	100	1.07	24.5*
Usat_t100_s150	100	150	1.23	24.2
Und_t50	50	0	0.91	24.2
Und_t150	150	0	0.88	23
Und_t500	500	0	0.91	24
Drai_t50	50	0	0.82	24.5
Drai_t100	100	0	1.13	37
Drai_t350	350	0	0.89	23.8

* Corrected values of water content

The shear speed used in the drained unsaturated triaxial tests was 0.013 mm/min, which was defined according to the method suggested by Fredlund *et al.* (1993). The same speed was used for the drained saturated triaxial test specimens. The speed used for the undrained saturated specimens was 0.045 mm/min. The specimens were sheared until reaching a minimum axial strain of 15%.

Results and discussion

The measured volume change of cell fluid was corrected from the corresponding cell elastic and creep deformations and also from the loading piston penetration. Those corrections were applied while processing acquired triaxial testing data. The specimen area was corrected during shearing according to the formula proposed by La Rochelle *et al.* (1988). The equalization time of four days was found to be sufficient for allowing the equalization of suction, not being observed further water change inside the specimen after the third day. The method of determination of the

test speed presented by Fredlund *et al.* (1993) did not result in the development of excess pore water pressure during shearing.

The saturated shear strength parameters c′ and ϕ' were determined from the analysis of three consolidated drained and three consolidated undrained triaxial tests. The initial effective stresses of the drained tests were 50, 100 and 350 kPa. The initial effective stresses of the undrained tests were 50, 150 and 500 kPa. As shown by Figure 2, the resulting shear strength envelope corresponds to an angle of internal friction equal to 29.9° and to a cohesive intercept equal to 16.6 kPa.

The evaluation of unsaturated shear strength was performed using results obtained from triaxial tests carried out at net normal stresses (σ - ua) of 50 and 100 kPa. For the tests with the net normal stress of 50 kPa, applied suctions were 25, 50, 100 and 150 kPa. For the net normal stress of 100 kPa, applied suctions were 50, 100 and 150 kPa.

Figure 2 shows the effective stress paths in terms of q x (p-uw) or (p-ua) for all saturated and unsaturated triaxial tests. It is possible to observe that when the value of confining stress increases (effective stress and net normal stress), the shear strength also increases. In this figure $p' = (\sigma_1 + \sigma_3)/2 - u_w$ and $q = (\sigma_1 - \sigma_3)/2$.

The influence of suction on the shear strength can be observed in the q x (ua – uw) graph shown in Figure 3. The observed behavior is an increment of strength with an increase of suction. Contrasting with equation (1), the shear strength relationship appears to be non-linear. This type of behavior has been described by several authors (Escario and Saez, 1986; Fredlund *et al.*, 1987; Abramento and Carvalho, 1995; Rohm and Vilar, 1995). For the unsaturated shear strength envelope corresponding to the net normal stress of 50 kPa, the initial rate of shear strength increase is comparatively large until a value of suction equal to 50 kPa is reached. For suctions higher than 50 kPa this rate decreases.

As for the unsaturated shear strength envelope determined for the net normal stress of 50 kPa, the envelope corresponding to the net normal stress of 100 kPa shows a similar behavior until the suction of 50 kPa is reached. However, for suctions higher than 50 kPa, a loss of shear strength can be observed while suction still increases.

Contrasting with the behavior previously observed by Escario and Saez (1986), Fredlund *et al* (1987) and Fredlund *et al* (1993), Figure 3 implies that ϕ^b must be higher than ϕ' for low values of suction. For suctions higher than 50 kPa, ϕ^b becomes progressively lower. This type of behavior has been reported by Abramento and Carvalho (1989) and Röhm and Vilar (1995). Feuerharmel *et al* (2006) present unsaturated shear strength data obtained with direct shear tests carried out using this same colluvium soil. Their data also showed that ϕ^b is higher than ϕ'.
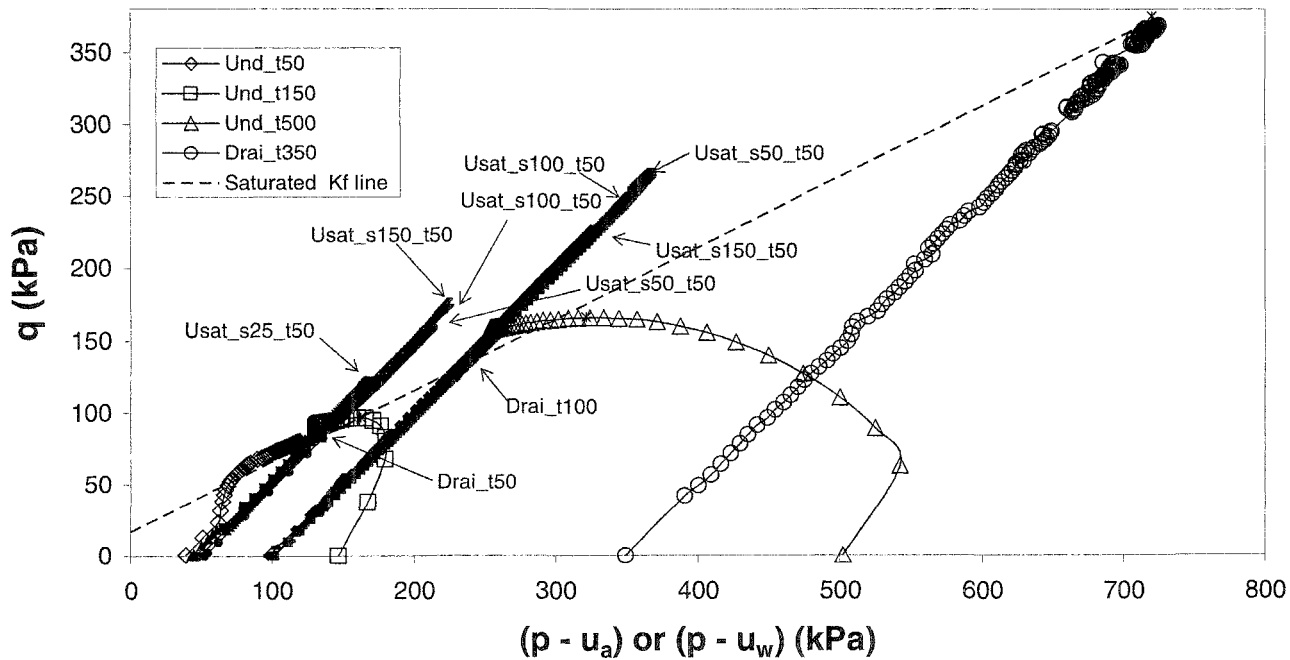
Figure 2 – p' x q curves for the saturated and unsaturated triaxial tests
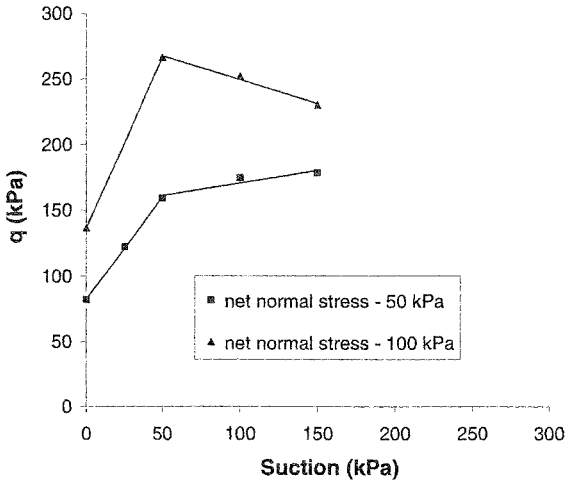
Figura 3 – q x (u_a – u_w) for unsaturated triaxial tests with two net normal stress values.

Conclusions

The different behavior of the unsaturated shear strength envelopes shown in Figure 3, for net normal stresses of 100 and 50 kPa, can be explained by considering the influence of the confining pressure (net normal stress) on suction for values of applied suction higher that 50 kPa. For suctions above 50 kPa, the confining pressure (net normal stress) appears to have more influence on the shear strength than the applied suction. For the net normal stress of 50 kPa, suction still has more influence on the shear strength than the confining pressure, but this influence is less intense. However, for the net normal stress of 100 kPa, the applied suction has less effect, even reducing the shear strength for values of suction higher that 50 kPa.

The behavior observed in Figure 3, where of ϕ^b values is higher than corresponding ϕ' values, is nowadays the subject of deeply study. Actually, believe that the microstructure present in those soils can influence their shear strength. Additionally the influence of deformation level used to obtain in the unsaturated shear strength envelope and adjustment in the results must be investigated.

Acknowledgements

References

Abramento, M. and Carvalho, C. S. (1989). "Geotechnical parameters for study of natural slopes instabilization at Serra do Mar, Brazil". *Proc. 12th Intern. Conf. On Soil Mech and Found. Engn*, v.2: 1599-1602. Rio de Janeiro: Balkema.

Bastos, C. A. (1999). *"A geotechnical study on the erodibility of unsaturated residual soils"*. D.Sc. thesis, Federal University of Rio Grande do Sul, Porto Alegre, RS, Brazil [in Portuguese].

Bishop, A. W. and Henkel, D. J. (1962). *"The measurement of soil properties in the triaxial test"*. 2nd ed. London: Edward Arnold, 227pp.

Bucio, M. B. (2002). *"Estudio experimental del comportamiento hidro-mecanico de suelos colapsables"*. D.Sc. thesis, Politechnical University of Catalunya, Barcelona, Spain [in Spanish].

Campos, T. M. P. and Carrilo, C. W. (1995). "Direct shear testing on an unsaturated soil from Rio de Janeiro". Unsaturated Soils, ed. Alonso and Delage., *Proc. 1st Intern. Conf. on Unsaturated Soils*, v.1: 31-38 Paris: Balkema.

Escário, V. and Sáez, J. (1986). "The shear strength of partly saturated soils". *Géotechnique*, 36 (3):453-456.

Feuerharmel, C. (2003). *"Aspects of the unsaturated behavior of two colluvium soils – Bolivia-Brazil gas pipeline"*. M.Sc. dissertation, Federal University of Rio Grande do Sul, Porto Alegre, RS, Brazil [in Portuguese].

Feuerharmel, C.; Pereira, A.; Gehling, W. Y. Y. and Bica, A. V. D. (2006)."Determination of the shear strength parameters of two unsaturated colluvium soils using the direct shear test". Submitted in this conference.

Fredlund, D. G.; Morgenstern, N. R. and Widger, R. A. (1978). "The shear strength of unsaturated soils". *Canadian Geotechnical Journal*, 15(3): 313-321.

Fredlund, D. G.; Rahardjo, H. and Gan, J. K. M. (1987). "Non-linearity of strength envelope for unsaturated soils". *Proc. 6th Intern. Conf. on Expansive Soils*. v. 1 pp 49-59. New Delhi.

Fredlund, D. G. and Rahardjo, H. (1993). *"Soil mechanics for unsaturated soils"*. John Wiley & Sons, Inc., 517 p.

Geiser, F.; Laloui, L. and Vulliet, L. (2000). "On the volume measurement in unsaturated triaxial test". *Asian Conference on Unsaturated Soils – UNSAT-ASIA 2000*. pp 669-674. Singapore.

Ho, D. Y. F. and Fredlund, D. G. (1982). "A multistage triaxial test for unsaturated soil". *Geotechnical Testing Journal*, 5(1/2):18-25.

Lade, P. V. (1988). "Automatic volume change and pressure measurement devices for triaxial testing of soils". *Geotechnical Testing Journal*, 11 (4): 263-268.

La Rochelle, P.; Leroueil, S.; Track, B. Blais-Leoux, L. and Tavenas, F. (1988). "Observational approach to membrane and area corrections in triaxial tests". *Advanced Triaxial Testing of Soil and Rock, ASTM STP 977*, Robert T. Donaghe, Ronald C. Chaney and Marsahll L. Silver, Eds. American Society for Testing and Materials, Philadelphia, pp. 715-731.

Leong, E. C.; Agus, S. S. and Rahardjo, H. (2004). "Volume change measurement of soil specimen in triaxial test". *Geotechnical Testing Journal*, 27 (1): 1-9.

Ng, C. W. W.; Zhan, L. T. and Cui, Y. J. (2002)."A new simple system for measuring volume changes in unsaturated soils". *Canadian Geotechical Journal* 36 (1): 1-12.

Rampino, C; Mancuso, C. and Vinale, F. (1999). "Laboratory testing on an unsaturated soil: equipment, procedures, and first experimental results". *Canadian Geotechnical Journal* 39: 757-764.

Rohm, S. A. and Vilar, O. M. (1995). "Shear strength of an unsaturated sandy soil". Unsaturated Soils, ed. Alonso and Delage., *Proc. 1st Intern. Conf. on Unsaturated Soils*, v.1: 189-193 Paris: Balkema.

The Shear Strength of Unsaturated Tropical Soils in Ouro Preto, Brazil

M.M.Futai[1] , M.S.S.Almeida[2] and W. A. Lacerda [2]

[1] Polytechnic School of the University of São Paulo, Av. Prof. Almeida Prado, Travessa 2, Department of Structures and Foundations, CEP 05508-900 São Paulo (SP), Telephone (011) 3091-5679, email: futai@usp.br
[2] COPPE-UFRJ, Cid. Univ., CT - B, Sala B-101, Ilha do Fundão - Caixa Postal 68506, RJ, email: almeida@coppe.ufrj.br and willyl@globo.com

Abstract

The shear strength of unsaturated soils is a subject which has received a lot of interest recently. Experimental results have been used to define mathematical formulations, but the data available on tropical soils is quite scarce. This paper presents the results of triaxial tests on unsaturated lateritic and saprolitic soils with the same rock mother. The variation of shear strength parameters with suction was analyzed. Air dried specimens tested with constant water content were used to define the maximum shear strength.

Introduction

Although the shear strength of unsaturated soils is of important use in geotechnical engineering, few construction projects are designed or analyzed using this concept. The consideration of the unsaturated condition of the soil in these projects can create savings and also avoid problems when the soil is inundated (in the case of ruptures, expansions, or collapses, for example). The distance between academic knowledge of unsaturated soils and the engineering practice occurs probably because there is still no consensus about the concepts of unsaturated soil mechanics.

In saturated soils shear strength can be easily interpreted physically. In a simplified form, the parameters of shear strength (c' and ϕ') can be obtained from a linear interpolation of the experimental strength results. The choice of the level of stress in laboratory tests is simple and easily related to the practical cases. In the case of unsaturated soils, suction is a third variable that needs to be defined. However, what

1200

suction values should be used for the laboratory tests? For the same type of construction work suction can vary considerably. For example, it can be low in humid areas (the south and southeast regions of Brazil) or extremely high in dry regions (semi-arid).

This paper will present experimental results obtained from tropical soils collected in Santo Antônio de Leite in Ouro Preto. The results will be used to discuss the shear strength of unsaturated soils.

Shear strength of unsaturated soils

The first equation proposed to represent the shear strength of unsaturated soils was that of Bishop et al (1960), though that of Fredlund et al (1978) is the best known. If parameter χ is taken to vary in a non-linear form with suction, Bishop's expression appears to be capable of predicting that the variation in apparent cohesion would be non-linear. Despite having different conceptual formulations, it can be admitted that Fredlund et al's proposal (1978) simplified Bishop's expression in such a way that tg $\phi^b = \chi$ tg ϕ', taking χ to be constant.

Fredlund et al.'s (1978) proposal to shear strength was widely diffused due to its simplicity. Experimental results from Escário (1980), Escário and Sãez (1986, 1987), Escário and Jucá (1989), indicate that resistance varies in a non-linear form with suction. Since then there has been a consensus in the geotechnic area that the value of ϕ^b is not constant. Until the value of the entry of air into the soil complies Terzaghi's principle of effective stress, however, ϕ^b must be equal to ϕ'.

De Campos (1997) verified the variation of ϕ^b / ϕ' in various Brazilian tropical soils, as can be seen in Figure 1. The results shown in Figure 1(a) present the expected behavior, since the values of ϕ^b / ϕ' start at 1 for the saturated condition until the air entry value, and then start to decrease until they stabilize. To the contrary, the values of ϕ^b / ϕ' for low suctions, as shown in Figure 1(b), are greater than 1, for which De Campo (1997) did not manage to find any physical justification. Pinto (2004) explained that the results obtained by Abramento and Pinto (1993) in which ϕ^b was higher than ϕ' occurred due to the value of the friction angle adopted, since the use of adequate values leads to more satisfactory results.

The variation of the friction angle with suction is a subject that is rarely discussed. Some authors, such as Escário (1980), Escário and Sãez (1986), Drumigh & Nelson (1995), and Wheeler and Sivakumar (1995) have presented experimental results in which there was no variation in the friction angle with suction; however no explanations were given for this variation.

The friction angle depends on the type of mineral that makes up the soil, particle arrangements, grain break-up, dilation, and the level of particle interpenetration. Little is known of the effects of this phenomena on unsaturated soils. Some hypotheses can

be advanced, such as the increase in interlacing caused by retraction due to drying, or an increase in dilation because of an increase in flow tension. Other comments will be made later based on the experimental results that will be presented.

There exist two possibilities for obtaining unsaturated shear strength parameters. One is to obtain them experimentally and the other is to use estimate models based on retention curves or other soil characteristics. Using retention curves for estimating shear strength has many advantages, including the avoidance of having to carry out shear strength tests with controlled suction, which as well as being very slow requires specific equipment. There are few tests for unsaturated soils and even less for tropical soils that can guarantee the validity of these estimates.

The forecasting of the shear strength of soil is almost always made based on the water retention curve (Oberg & Sallfors, 1995 and 1997; Vanapalli et al, 1996). De Campos (1997), Machado & Vilar (1998) and Oliveira & Marinho (2002) have evaluated the use of different functions for the forecasting of shear strength in tropical Brazilian soils. These analyses showed that shear strength could be conserved or overestimated. Various proposals for mathematical adjustments exist. Some take the friction angle to be constant and the cohesion variation to be apparent with suction (Fredlund et al, 1978; Abramento and Carvalho, 1989; Alonso et al, 1990; Röhm, 1992; Teixeira, 1996; Machado and Vilar, 1998). Other authors propose the variation of the two parameters with suction (Wheeler & Sivakumar, 1995; Silva Filho, 1998; Futai, 2002). The commonly used functions are: linear, linear per section, potency, hyperbolic, etc.

It can be said that cohesion will increase with matric suction. However, an analogous physical interpretation cannot be made for the variation of the friction angle with suction. A number of important works, such as Hom & Deer (1962) and Skinner (1969), discuss the difference of the friction angle in saturated and dry conditions and show that there could be an increase in the friction coefficient when the soil is dried. Based on these works, it is to be expected that, depending on mineralogical composition, the friction angle will vary with suction.

Material and methods

Various types of triaxial tests were carried out: saturated; with suction control; and with constant humidity (in air dried samples), (Futai, 2002). Triaxial equipment with automatic strain control and stress path control capacity was used.

Suction was controlled for axis translation. A porous stone with a high air entry value was installed in the base and air was applied via the top through a controlled servo valve. The variation of the volume in the test body and the volume of water drained were monitored with automatic volume meters. The stabilization of the initial suction was achieved through the control of water content, a suction equilibrium chamber

(axis translation) and further stabilization after the transfer of the specimen to the triaxial chamber.

The soils samples analyzed were collected for a study of the cave-in process. This involves a geotechnic profile composed of two very distinctive chambers. The surface soil is a lateritic clay and the underlying soil is a saprolitic gneiss soil. This paper shall present tests of samples collected between a depth of 1 m and 5 m in lateritic and saprolitic soils respectively. The main characteristics of these soils are given in Table 1.
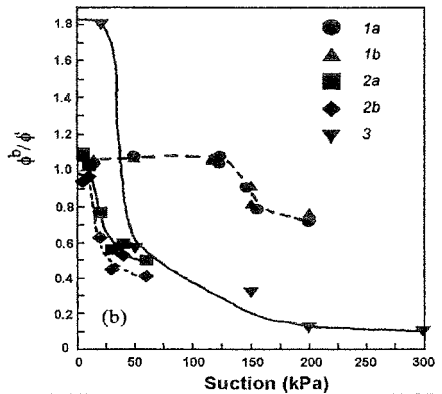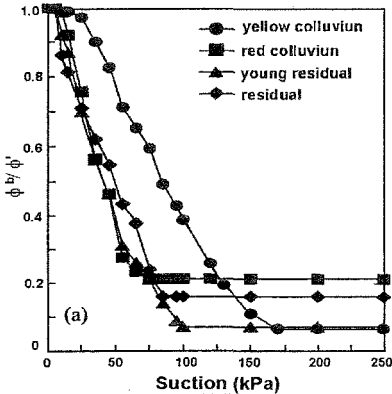
(a) Biotite-gneiss soils (from De Campos & Carrillo, 1995)

(b) 1a - Colluvial (Abramento and Carvalho, 1989);1b - Residual soil (Abramento and Carvalho, 1989); 2a – Saprolitic gneiss soil (Fonseca, 1991); 2b - Saprolitic gneiss soil (Fonseca, 1991); 3 - Lateritic sedimentary soil (Rohm & Vilar, 1995)

Figure 1 – Variation of ϕ^b / ϕ'with suction (from De Campos, 1997)

The water retention curves of the lateritic (1 m) and saprolitic soils (5 m) studied are quite distinctive, as can be seen in Figure 2. Although lateritic soil is much more clayey than saprolitic soil, the latter has a much lower air entry value (1 kPa) than saprolitic soil (10kPa). This occurs because of the structure and the distribution of pores in the soil, which can be visualized in the SEM shown in Figure 3.

After the air entry value the 1 m deep soil presents a rapid fall in the volumetric water content with the increase in suction until 20kPa, when it levels out due to the absence of the pores that command this suction band. The water content falls again after 2000kPa matric suction. The saprolitic soil contains various changes in gradient, which allows an average adjustment with a more conventional format than lateritic soil. After 100kPa matric suction the 1 m deep soil starts to retain more water than the 5 m soil.

Results of triaxial tests

The triaxial tests were carried out with controlled matric suction (100kPa and 300kPa) and with constant water content in air dried samples. The other tests can be consulted in Futai (2002), Futai et al (2004) and Futai & Almeida (2005).

Table 1 – Soil Characteristics

Characteristics	1 m	5 m
Sand (%)	44	38
Silt (%)	9	54
Clay (%)	46	8
w_L (%)	57	42
I_P (%)	29	19
Void ratio	1.3-1.5	0.8-1.0
Particle density	2.64	2.68
Kaolinite (%)	23	42
Quartz (%)	50	44
Oxides, hydroxides and amorphous (%)	19	6
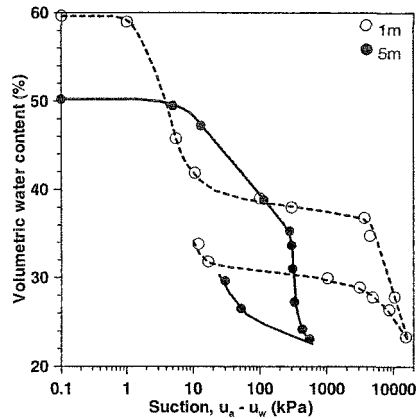
Figure 2 – Soil water retention curves
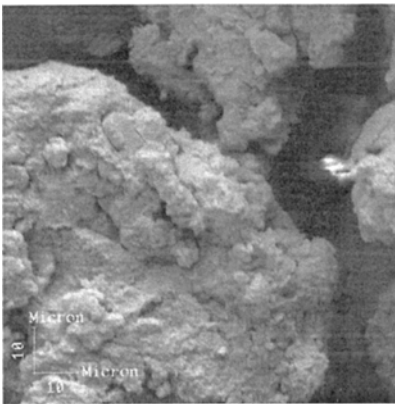
(a) 1 m   (b) 5 m

Figure 3 – Scanning electron microscopy of 1 m deep and 5 m deep soils

The deviator stress and volumetric strain against axial strain curves are contained in Figures 4 and 5 for 1 m and 5 m deep soils respectively. Figures 4 and 5 show a clear increase in shear strength and an increase in rigidity with the increase of suction. This comparison is much more striking if carried out with the saturated soils presented by Futai (2002), in which the 1 m deep soil has no dilation for the same levels of stress treated.

The strength envelopes of lateritic soil are given in Figure 6. The envelopes rise increase rapidly from saturated condition to the stage corresponding to 100 kPa matric suction. However, comparing the 100kPa and 300kPa suction envelopes, it can be seen that the difference in strength between them is small. This can be easily explained and interpreted by the water retention curve given in Figure 2. The plateau formed close to 38% volumetric water content is responsible for the large variation in suction with a small variation in water content.

The results of the retention curve are confirmed in the strength envelope, shown in Figure 6, in which the air dried soil presented a significant increase in strength in relation to the samples tested with a matric suction of 300kPa because the suction level surpassed the plateau formed in the retention curve. The envelopes are not parallel, there is an increase both in the cohesion and the friction angle with matric suction. The friction angle adopted to obtain the best adjustment was equal to 31.3°, nevertheless this value does not correspond to the friction angle of the soil in the saturated state. The (ϕ' constant) simplification causes greater differences in the adjustment of the lower stress levels ($\sigma_3 - u_a < 200$kPa), where the real envelope is a curve.

The strength envelopes of the 5 m deep soil (Figure 7) has different peculiarities from the 1 m deep soil. There is a difference of 48kPa in the apparent cohesion intercept and 5.8° in the friction angle between the air dried and saturated conditions.

Adjustment of Strength Parameters

The estimation of the shear strength of unsaturated soils based on saturated soil parameters and on a water retention curve does not produce good results. However, some envelopes with different suction values are necessary to define the best friction angle value. This eliminates the main advantage of prediction models, which is to dispense with the need for unsaturated tests. For this reason, only adjustments of the results obtained will be made. In this work the adjustment was made in two forms: taking the friction angle as either constant or variable with suction.

The hyperbolic adjustment was made according to the proposal made by Futai (2002) in which the function makes the parameter vary between the saturated condition and suction value tending to the infinite (extremely dry). The following expression is used:

$$c_{(s)} = c' + \left(c_{(u_a - u_w = \infty)} - c' \right) \left(1 - 10^{a(u_a - u_w)} \right) \tag{1}$$

where: $c_{(s)}$ - apparent cohesion intercept; c' - effective cohesion for soil in saturated condition; $c_{(u_a - u_w = \infty)}$ - maximum soil cohesion; a - apparent cohesion adjustment parameter.

This expression can only be used for soils with cohesion that always increases with suction. It is not valid, for example, to represent the entire variation in the apparent cohesion of pure sands. The value of $c_{(u_a-u_w=\infty)}$ can be obtained from tests with air dried specimens as shown in this work.
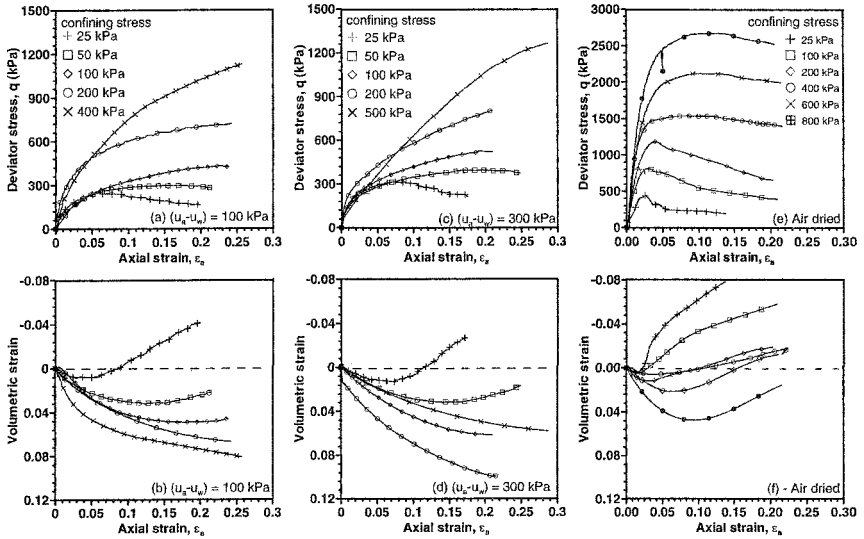
Figure 4 – Constant suction triaxial tests performed in 1.0 m specimens.
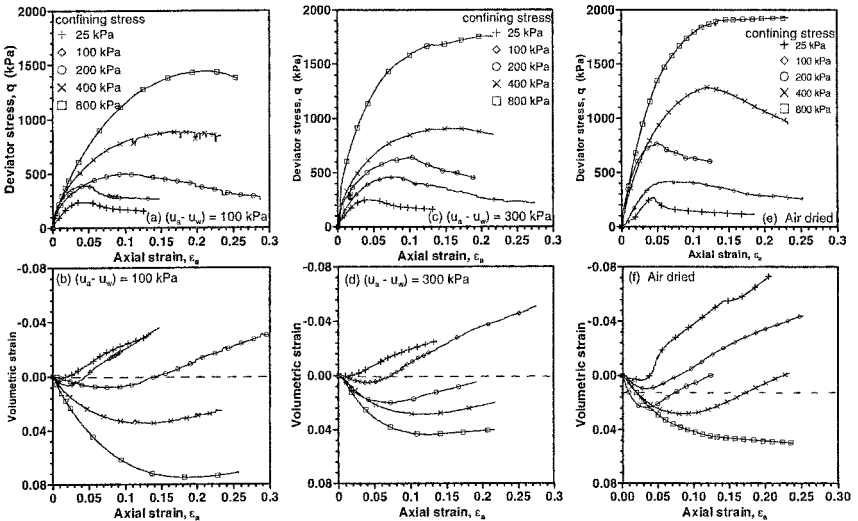
Figure 5 – Constant suction triaxial tests performed in 5.0 m specimens
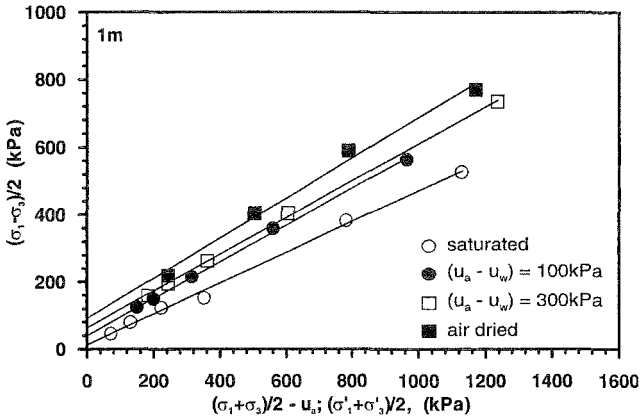
Figure 6 – Strength envelops for 1 m deep soil
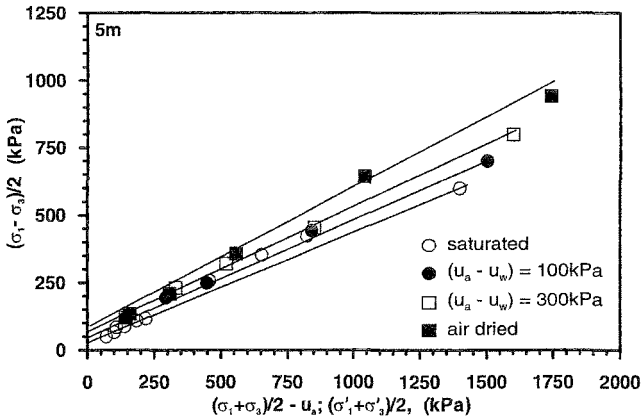
Figure 7 –Strength envelops for 5 m deep soil

The experimental results of the apparent cohesion intercepts using a constant friction angle and the adjustments made in accordance with expression (1) are shown in Figure 8. The cohesion intercept in the saturated condition for soil with a depth of 5 m is greater than for 1 m. However, after matric suction of 100kPa lateritic soil starts to present apparent cohesion intercepts that are much higher than for saprolitic soil. After a suction of 300kPa the curves were extrapolated without experimental results until the maximum cohesion expected was achieved (represented by the soil in the air dried condition). The adjustment shown in Figure 8 appears to present a good result. It should be noted that this adjustment is made with the cohesion values obtained from a linear regression, therefore, it is an adjustment of an adjustment.

The experimental results show that, for the soils studied with the characteristics presented in Table 1, the value of the friction angle varies with matric suction. Since the trend in the friction angle variation always increased with suction, the same type of function used to adjust cohesion was used:

$$\phi(s) = \phi' + \left(\phi_{(u_a-u_w=\infty)} - \phi'\right)\left(1 - 10^{b(u_a-u_w)}\right) \tag{2}$$

where: $\phi_{(s)}$ - variation of friction angle with suction; ϕ' - effective friction angle for soil in the saturated condition; $\phi_{(u_a-u_w=\infty)}$ - maximum value of the soil friction angle; b - friction angle adjustment parameter.

The adjustments made by expressions (1) and (2) for the 1 m and 5 m deep soils are shown in Figure 9. Good results were obtained from these functions and the use of the variation of the two parameters with suction guarantees better adjustments for the strength envelopes. Despite the fact that there are no experimental results above 300kPa matric suction, it is to be expected that the behavior will be similar to that presented by the adjustment, which rises to a maximum value and then stabilizes.

Using ϕ' constant the value of ϕ^b / ϕ' for the 1 m deep soil is equal to 1.16 in the suction interval between 0 and 100kPa of matric suction. When the friction angle varies with suction (Figure 9-b) the value of ϕ^b / ϕ' is equal to 0.87 ($0 < u_a-u_w < 100$kPa).

$$c(s) = 166(1-10^{-.00012(u_a-u_w)}) \quad \text{(a) 1m}$$

$$c(s) = 35 + 93(1-10^{-.0001(u_a-u_w)}) \quad \text{(b) 5m}$$
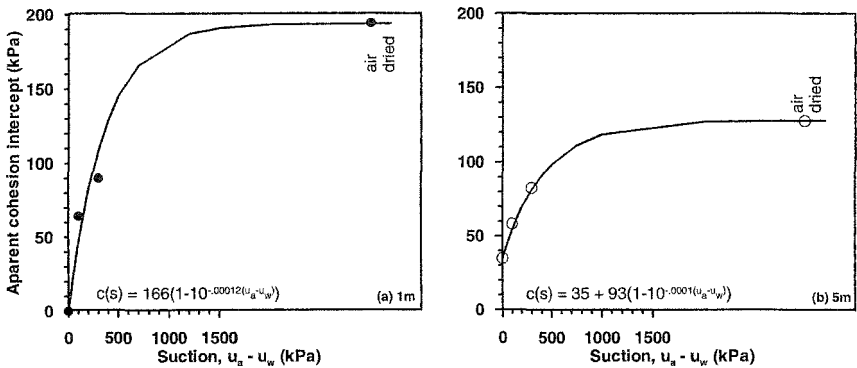
Figure 8 – Adjustment of the apparent cohesion intercept (ϕ constant)

(a) 1m

$\phi(s) = 28 + 7,5(1\text{-}10^{\text{-}.0025(u_a\text{-}u_w)})$

(c) 5m

$\phi(s) = 24,2 + 5,8(1\text{-}10^{\text{-}.0015(u_a\text{-}u_w)})$

(b) 1m

$c(s) = 8 + 115(1\text{-}10^{\text{-}.0017(u_a\text{-}u_w)})$

(d) 5m

$c(s) = 44 + 43(1\text{-}10^{\text{-}.0028(u_a\text{-}u_w)})$
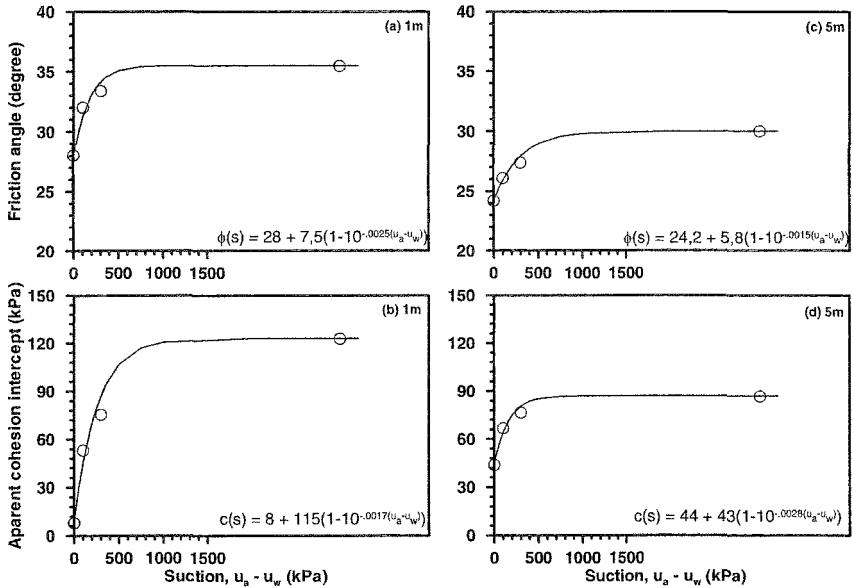
Figure 9 – Adjustment of the c and ϕ

Conclusions

This paper presented the results of the triaxial tests of specimens from two soils with the same origin, one of which was lateritic and the other saprolitic. As well as the saturated tests, tests were also carried out with controlled suction and with constant volumetric water content (air dried). The strength envelopes showed the known behavior of increased strength with increased suction. The behavior of cohesion was discussed and it was shown that, for the soils studied, the apparent cohesion increases with suction, with a trend to stabilize above a given suction value. The experimental results showed that the friction angle also increases with suction.

Variation of the friction angle with suction has important practical consequences. All the models for estimating strength use the hypothesis that the friction angle is independent of suction. This simplification can result in discrepancies when the friction angle variation is significant. In the same way, performing multiple tests with a single stress and suction variation level can be inadequate for estimating unsaturated strength when the envelopes are not parallel.

It is necessary to investigate the causes of friction angle variation with suction and to incorporate this in prediction models. Above all, though, caution is needed in the use of these models. A greater number of tests are needed, especially in tropical soils, to conclude when there is (or is not) friction angle variation and why this occurs.

The proposal to perform tests with constant volumetric water content in air dried specimens can be used as an indication of the maximum resistance that the soil can obtain, as well as the friction angle variation. The advantage of this type of test is that it does not require special equipment. However, this methodology is only valid for soils that have resistance that increases monotonically with suction.

Acknowledgements

References

Abramento, M & Pinto, C., (1993) Shear strength of unsaturated colluvium of Serra do Mar natural slopes. Solos e Rocha, vol. 16(3), 145-158. (in portugues)

Abramento, M. & Carvalho, C.S. (1989). Geotechnical parameters for the study of natural slopes instability in Serra do Mar, Brazil. Proc. 12th Int. Conf on Soil Mech. and Found. Engn, Rio de Janeiro. Balkema, V. 2, pp. 1599 - 1602.

Alonso, E. E., Gens, A. & Josa, A., 1990, A Constitutive Model For Partially Saturated Soils. Géotechnique, Vol. 40, N. 3, 405 - 430.

Bishop, A. W., Alpan, I., Blight,G.E. & Donald, I.B. (1960) Factors controlling the shear strength of party saturated cohesive soils. Conf. on Shear Strength of Cohesive Soils. Univ. of Colorado, 503-532.

De Campos, T.M.P. (1997) Shear strength of unsaturated soils. III Brazilian symp. Of ustaturated soils, vol.2, 399-417. (in portugues)

De Campos, T.M.P. & Carrillo, C. W. (1995). Direct shear testing on an unsaturated soil from Rio de Janeiro. Unsaturated Soils, ed. Alonso and Delage, Proc. lst Int. Conf on Unsaturated Soils, Paris, Balkema, Vol. 1, pp. 31-38.

Drumright, E.E. & Nelson, J.D. (1995). The shear strength of unsaturated tailings sand. Unsaturated Soils, ed. Alonso and Delage, Proc. lst Int. Conf on Unsaturated Soils, Paris, Balkema, Vol. 1, pp. 45 - 50.

Escário, V. & Jucá, J.F.T. (1989) "Strength and Deformation of Partly Saturated Soils", In: Proc. of the XII Int. Conf. on Soil Mech. Found. Eng., Rio de Janeiro.

Escário, V. & Sãez, J. (1986). The strength of partly saturated Geotechnique, 36 (3): 453 - 456.

Escário, V. & Sãez, J. (1987). Shear strength of partially saturated soils. Int. Conf. On Expansive soils. New Deli, 602-605

Escário, V. (1980) Suction controlled penetration and shear tests, Proc.4th Int. Conf. Expansive soils, Denver, ASCE, vol. 2 (781-797)

Fonseca, E.C. (1991) Direct shear strength with suction control in unsaturated soils. Masters Thesis, PUC-Rio. (in portugues)

Fredlund, D. G., Morgenstern, N. R. & Widger, R. S. (1978) The Shear Strength Of Unsaturated Soils. Can. Geotech. J., 15(3), 313-321.

Futai, M.M. (2002) Theoretical and experimental study of unsaturated tropical soil behavior: applied to a gully case. PhD Dissertation. COPPE-Federal University of Rio de Janeiro. 559p (in Portuguese)

Futai, M. M, Almeida, M. S. S, and Lacerda, W. A (2004) Yield, Strength and Critical State Conditions of a Tropical Saturated Soil. Journal of Geotechnical and Geoenvironmental Engineering (in print)

Futai, M.M. and Almeida, M.S.S. (2004) The behaviour of a gneiss residual soil under controlled suction, Geotechnique (in print)

Hom, H.M. & Deere, D.U. (1962). Frictional characteristics of minerals. Géotechnique 12:3 19-335.

Machado S.L. & Vilar, O.M. (1998) Unsaturated shear strength: laboratory tests and predictions , In: Soil and Rock, vol. 21(2), pp. 65-78, São Paulo. (in portugues)

Oberg, A. & Sallfors, G. (1997) Determination of Shear Strength of Unsaturated Silt and Sand Based on the Water Reflection Curve, Geotch. Testing Jnl., , Vol. 20(1), 40-48.

Öberg, A.L. & Sällfors, G.A. (1995) "Determination of the Shear Strength Parameters of Unsaturated Silts and Sands based on the Water Characteristica Cuve. Geotch. Test.Journal, vol. 20(1), pp. 40-48.

Oliveira, O.M. & Marinho, F.A.M (2002). Unsaturated shear strength of compacted residual soil by unconfined compression. XII COBRANSEG. Vol. 1, 507-518. (in portugues)

Pinto, C.S. (2004) Personal comunication

Rohm, S. A. (1992) Shear strength of lateritical sandy soil from. São Carlos-Sp, PhD thesis, São Carlos. (in Portugues)

Rohm, S.A. and Vilar, O.M. (1995). Shear strength of an unsaturated sandy soil. Unsaturated Soils, ed. Alonso and Delage., Proc. 1st Int. Conf on Unsaturated Soils, Paris, Balkema, Vol. 1, pp. 189 - 193.

Silva Filho, F. C. (1998) Numerical analysis of unsaturated soils, PhD thesis, COPPE/ UFRJ, Rio de Janeiro. (in Portugues)

Skinner , A. E. (1969) A note on the influence of interparticle friction on the shear strength of a random assembly of spherical particles. Géotechnique vol 19, 105-157.

Teixeira, R.S. (1996) Resistência ao Cisalhamento de um Solo Arenoso Compactado Não Saturado, MSc. Thesis, EESC/USP, São Carlos.

Vanapalli, D.G., Fredlund, D.G., Pufahl, D.E. & Clifton (1996) Model for the prediction of shear strength with respect to soil suction. Canadian Geotech. J. vol. 33, 379-392

Wheeler, S. J. & Sivakumar, V. (1995) An Elasto-Plastic Critical State Framework For Unsatureted Soil. Géotechnique, Vol. 45, N. 1, 35 - 53.

Effects of Hysteresis on Shear Strength Envelopes from Constant Water Content and Consolidated Drained Triaxial Tests

Trinh Minh Thu[1], Harianto Rahardjo[2] and Eng-Choon Leong[3]

[1]Research Scholar, School of Civil & Environmental Engineering, Nanyang Technological University, Block N1, B4b-06, Nanyang Avenue, Singapore 639798; PH (65) 67906442; email: minhthu@pmail.ntu.edu.sg

[2]Professor and Vice Dean, School of Civil & Environmental Engineering, Nanyang Technological University, Block N1, 01a-02, Nanyang Avenue, Singapore 639798; PH (65) 67904104; FAX (65) 67910676; email: chrahardjo@ntu.edu.sg

[3]Associate Professor, School of Civil & Environmental Engineering, Nanyang Technological University, Block N1, 01c-80, Nanyang Avenue, Singapore 639798; PH (65) 67904774; email: cecleong@ntu.edu.sg

Abstract:

Shear strength of unsaturated soil is commonly obtained from Consolidated Drained (CD) or Constant Water content (CW) triaxial tests. A series of CD and CW tests was carried out on statically compacted silt specimens. The results indicate that the effective angles of internal friction, ϕ', and the effective cohesions, c', of the compacted silt as obtained from both the CD and CW tests are identical. The ϕ^b angles from the CD and CW triaxial tests are essentially identical at matric suctions lower than the air-entry value. This could be attributed to the fact that the soil specimens remain saturated at matric suctions lower than the air-entry value in both the CD and CW tests. Similarly the ϕ^b angles from both tests are the same at matric suctions higher than the residual matric suction when the soil is at a relatively dry condition. However, the ϕ^b angles from the CD and CW tests are different at matric suctions between the air-entry value and the residual matric suction value. The difference is due to the lower failure envelope with respect to matric suction from the CW tests as compared to the failure envelope from the CD tests. This difference can be attributed to the hysteretic behavior of soil-water characteristic curve of the soil which will be explained in detail in the paper.

1212

Introduction

Consolidated Drained (CD) or Constant Water (CW) triaxial tests are commonly performed for obtaining shear strength of unsaturated soils. The objective of this paper is to compare the results obtained from a series of CD and CW triaxial tests carried out on statically compacted silt specimens.

Fredlund et al. (1978) proposed a shear strength equation using two stress state variables (i.e., net normal stress, $(\sigma - u_a)$ and matric suction, $(u_a - u_w)$) as follows:

$$\tau_{ff} = c' + \left(\sigma_f - u_a\right)_f \tan \phi' + \left(u_a - u_w\right)_f \tan \phi^b \qquad [1]$$

where:

τ_{ff}	=	shear stress on the failure plane at failure,
c'	=	intercept of the "extended" Mohr-Coulomb failure envelope on the shear stress axis when the net normal stress and the matric suction at failure are equal to zero. It is also referred to as the "effective cohesion",
$\left(\sigma_f - u_a\right)_f$	=	net normal stress on the failure plane at failure,
σ_f	=	total normal stress on the failure plane at failure,
u_a	=	pore-air pressure at failure,
ϕ'	=	angle of internal friction associated with the net normal stress state variable, $\left(\sigma_f - u_a\right)$,
$\left(u_a - u_w\right)_f$	=	matric suction at failure,
u_w	=	pore-water pressure at failure, and
ϕ^b	=	angle indicating the rate of change in shear strength relative to changes in matric suction, $\left(u_a - u_w\right)_f$.

Results of several shear strength tests on unsaturated soils have indicated some non-linearity of ϕ^b over a large range of matric suction (Escario and Saez, 1986; Gan, 1986; Fredlund et al., 1987; Gan et al., 1988). Generally, the tangent of ϕ^b is less than or equal to ϕ'. However, some other researchers (Gan, 1986; Escario and Saez, 1986) found that ϕ^b can be greater than ϕ' angle.

Gan (1986) conducted multistage direct shear tests on an unsaturated glacial till. The result showed non-linearity of the failure envelope on the shear stress versus matric suction. The angle of the failure envelope, ϕ^b, is 25.5^0 at low matric suctions and decreases to 5^0 - 7^0 at high matric suctions.

Fredlund et al. (1987) reanalyzed the shear strength data presented by Satija (1978). A re-evaluation was performed by assuming a curved failure envelope with respect to matric suction. The curved failure envelope have a slope angle, ϕ^b, equal to, ϕ',

starting at zero matric suction. The ϕ^b angle begins to decrease significantly at matric suction values greater than 50 kPa.

Soil Properties

The soil used in this study was coarse kaolin. Basic soil properties of the kaolin were tested following the ASTM (1997) standards. The index properties of the kaolin are presented in Table 1. The coarse kaolin is classified as silt with high plasticity (MH) according to the Unified Soil Classification System (ASTM D 2487 – 93, 1997).

Table 1. Index properties of the statically compacted kaolin specimen.

Soil Properties	Value
Specific gravity , G_s	2.65
Liquid limit, LL (%)	51
Plastic limit, PL (%)	36
Plastic index, PI (%)	15
Silt (%)	85
Clay (%)	15
Unified Soil Classification System (USCS)	MH (silt of high plasticity)
Maximum dry unit weight, $\rho_{d\max}$ (Mg/m^3)	1.35
Optimum water content, w_{opt} (%)	22.0
Coefficient of permeability with respect to water phase at saturation, k_s, (m/s)	6.4×10^{-8}

Procedure and Testing Program

The modified triaxial apparatus for the CD and CW tests was similar to the modified triaxial apparatus described by Fredlund and Rahardjo (1993). The modified triaxial apparatus allows the control of both pore-air and pore-water pressures using the axis-translation technique (Hilf, 1956). Identical specimens were obtained by compacting kaolin or silt at the maximum dry density of 1.35 Mg/m^3 and the optimum water content of 22%. The specimen was statically compacted in 10 layers of 10 mm thickness. The height and diameter of the specimens were 100 mm and 50 mm, respectively. Soil-water characteristic curve (SWCC) was also conducted on the statically compacted silt specimen using the modified triaxial apparatus as described in Thu (2005).

Saturation Stage

The soil specimen was initially saturated in all the tests in order to obtain consistent initial water content and degree of saturation. During the saturation process, the specimen was saturated by applying a cell pressure, σ_3, and a back

pressure, u_w, until the pore-water pressure parameter, B, was close to 1. Full saturation was assumed to have been achieved when the B value was greater than 0.97 (Head 1986). Each specimen required about four days for the saturation process to be completed.

Consolidation and Matric Suction Equalization Stages

During the consolidation stage, the specimen was allowed to consolidate under a specific isotropic net confining stress, $(\sigma_3 - u_w)$. The amount of water that drained out from the soil specimen during equalization was recorded by the digital pressure volume controller (DPVC). The consolidation was assumed to have been completed when the water volume change levelled off and the excess pore-water pressure had dissipated. Each specimen required about an hour for the consolidation stage to be completed.

Once the consolidation stage had been completed, the matric suction equalization stage was carried out. In order to apply matric suction, the water pressure line connected to the top loading cap was disconnected from the water pressure line and reconnected to the air pressure line. The specimen was allowed to consolidate under an isotropic confining pressure, a pore-air pressure, and a pore-water pressure. The amount of water that drained out from the soil specimen during equalization was recorded by the DPVC. The equalization was also assumed to have been completed when the water volume change levelled off. Each specimen required about three to five days for the matric suction equalization stage to be completed.

Shearing Stage

Rahardjo et al. (2004) used the strain rates of 0.009 mm/min and 0.0009 mm/min, respectively for the CD and CW triaxial tests on the compacted residual soil from the sedimentary Jurong Formation. In this study, strain rates of 0.009 mm/min and 0.0009 mm/min for the CD and CW triaxial tests were also used, respectively as the silt had similar properties (i.e., plasticity index, coefficient of permeability) to the the residual soil from the sedimentary Jurong Formation. Shearing was terminated when the deviator stress, $q = \dfrac{(\sigma_1 - \sigma_3)}{2}$, reached a constant value or a distinct shear plane in the specimen had been observed. The maximum axial strain was set at 20%. Each specimen required about one to two days for the shearing stage to be completed.

Shearing Stage for the CW

The soil specimen was sheared under drained conditions for the pore-air phase and undrained conditions for the pore-water phase. In this case, the valve for the air pressure line was opened and controlled at a required pressure while the valve for the water pressure line was closed during shearing. During the shearing stage, the pore-air pressure, u_a, was maintained at the same magnitude as that obtained at the end of the equalization stage. The pore-water pressure, u_w, increased or decreased

depending on the volume change of the soil specimen. The difference between the pore-air pressure, u_a and the pore-water pressure, u_w, gives the matric suction, $(u_a - u_w)$.

Shearing Stage for the CD

In the CD triaxial test, the soil specimen was sheared under drained conditions for the pore-air and pore-water phases. This means that during shearing the valves for the air pressure and water pressure lines were opened and controlled at the required pressures. In this shearing stage, the pore-air pressure, u_a, and pore-water pressure, u_w, were maintained at the same magnitudes as those obtained at the end of the equalization stage.

Tests for Obtaining Soil-water Characteristics Curve

The pressure plate was used to obtain the soil-water characteristics curve. The compacted soil specimens used were 20 mm in thickness and 50 mm in diameter. The specimens used for testing soil-water characteristics curve were compacted in the same compaction mould and the same process with the compaction soil specimen for triaxial tests in two layers. The specimens were put into the pressure plate and a matric suction of 20 kPa was then applied to the specimen by increasing air pressure in the pressure extractor to 20 kPa and leaving the burette line opened to atmospheric pressure (i.e., $u_a = 20$ kPa and $u_w = 0$ kPa). Due to the application of matric suction to the soil specimens, the pore-water in the specimens would be drained out through the ceramic disk. The mass of each specimen was recorded at 24 hour of interval until the specimens reached equilibrium. The same procedure was repeated in order to increase the matric suction to 50 kPa, 100 kPa, 200 kPa, 400 kPa and 700 kPa incrementally. Meanwhile for the wetting stage, matric suction was decreased to 500 kPa, 300 kPa, 200 kPa, 100 kPa, 70 kPa, 40 kPa, 20 kPa and 0 kPa.

Test Results and Discussions

A series of the CW triaxial tests were conducted on compacted silt specimens. The specimens were tested in the modified triaxial apparatus under net confining stresses of 25 kPa, 50 kPa, 100 kPa, 150 kPa 200 kPa, 250 kPa, 300 kPa and 350 kPa with different initial matric suctions (i.e., matric suctions of 0 kPa, 100 kPa, 150 kPa, 200 kPa and 300 kPa). Meanwhile, a series of the CD triaxial tests were also conducted on compacted silt specimens.

A naming convention for the tested soil specimens was adopted using a designation of CWx-y and CDx-y. The term x-y in CWx-y and CDx-y means that the test was conducted under a net confining pressure of x kPa and an initial matric suction of y kPa.

Mohr-- Coulomb Failure Envelope for CW and CD tests

The shear stresses at failure for the specimens used in the construction of the Mohr circles for the CW and CD triaxial tests were determined using the peak deviator stresses obtained from the stress strain curves. The typical Mohr–Coulomb failure envelope for the saturated specimens for the CW and CD triaxial tests with different net confining stresses are shown in Figure 1 and 2, respectively. Identical effective angle of internal friction, ϕ', of 32^0 and effective cohesion, c', of 0 kPa were obtained from Figures 1 and 2.
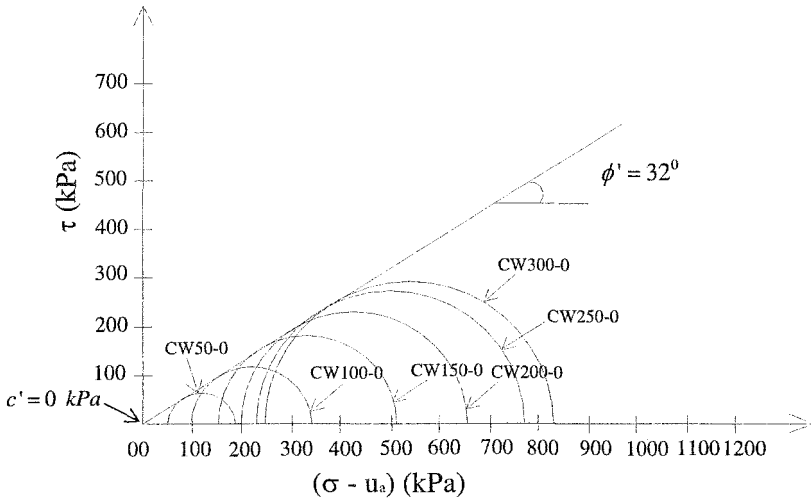
Figure 1. Mohr – Coulomb failure envelope for the compacted silt specimen under the CW triaxial tests at zero matric suction.

The extended Mohr – Coulomb failure envelopes can be constructed for different matric suction planes but at the same net confining stress by assuming that $\phi' = 32^0$ is applicable to all matric suction planes. The cohesion intercepts, c, from the CW and CD triaxial tests were determined by drawing the Mohr-Coulomb failure envelopes tangentially to the Mohr circles at failure as obtained from each CW and CD triaxial tests using a constant ϕ' of 32^0. Figure 3 indicates that the angle of the shear strength envelope with respect to matric suction had an average value, ϕ^b of 32^0 (i.e., equal to ϕ' of 32^0) at low matric suctions when the soil remained saturated. The ϕ^b angle began to decrease significantly at matric suction values between 55 and 75 kPa and reached an essentially constant value of 12^0 when matric suction exceeded 150 kPa. Figure 4 shows the nonlinearity of ϕ^b angle with respect to matric suction for compacted silt as obtained from the CW and CD triaxial tests.

Nonlinearity of ϕ^b angle with respect to matric suction was in agreement with data reported by Satija (1978), Fredlund et al. (1987) and Gan et al. (1988).
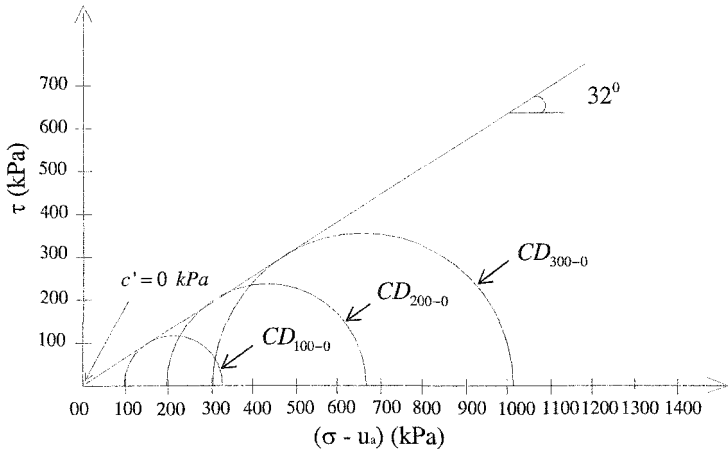
Figure 2. Extended Mohr – Coulomb failure envelope for the CD triaxial tests at zero matric suction
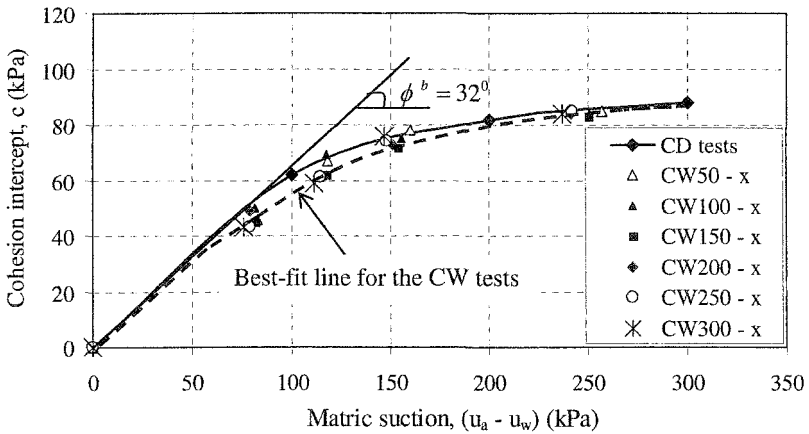
Figure 3. Cohesion intercepts of the failure envelopes on the zero net confining stress $((\sigma_3 - u_a) = 0)$ plane for the CD and CW triaxial tests
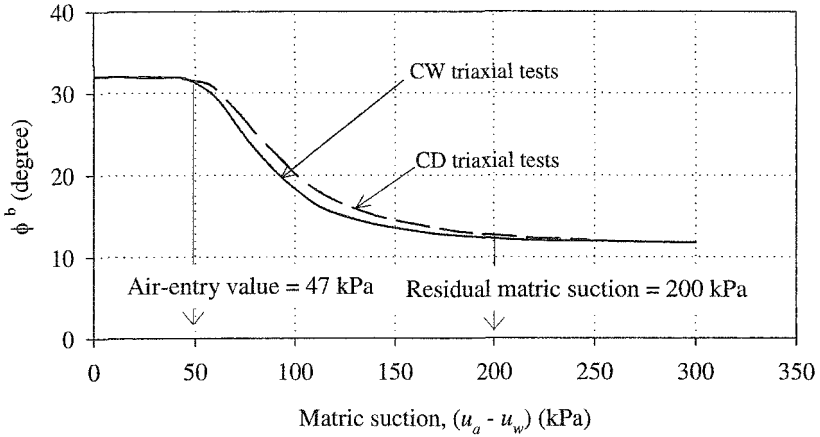
Figure 4. Nonlinear relationship between ϕ^b **and matric suction of the compacted silt specimen**

Figure 5 presents the SWCC for the compacted silt specimen. As indicated in Figure 5 the air-entry value of the statically compacted silt specimen was 47 kPa. It was also shown that the residual matric suction of the statically compacted silt was about 200 kPa.
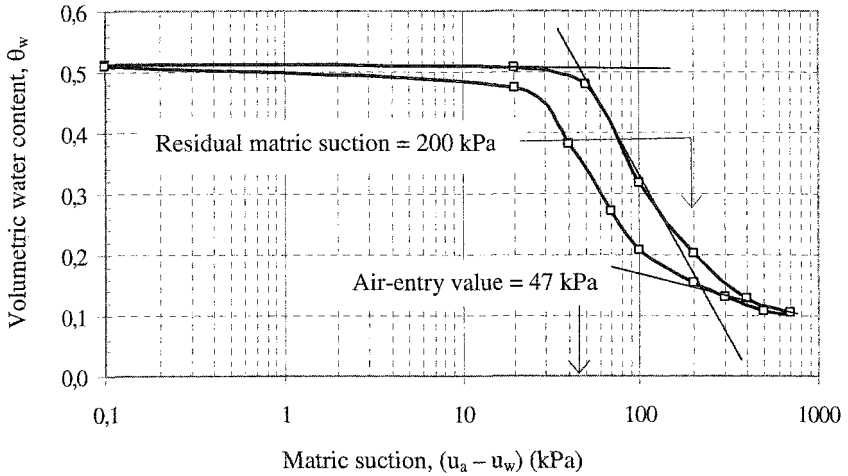
Figure 5. Air – entry value and residual matric suction of the compacted silt specimen

Comparisons of the Shear Strength for the CW and CD Triaxial Tests

The values of the shear strength parameters (i.e., ϕ', ϕ^b and c) obtained from the CW triaxial tests are compared with the shear strength parameters that were obtained from the CD triaxial tests. Figure 3 shows the cohesion intercepts of the failure envelopes on the zero net confining stress (($\sigma_3 - u_a$) = 0) plane for the CD and CW triaxial tests. The cohesion intercepts from the CW triaxial tests are close to the cohesion intercept line that was obtained from the CD triaxial tests indicating that uniqueness of the failure surface exists for the compacted silt specimens tested in the CD and CW triaxial tests. Figure 3 indicates a similar pattern of the increase in the cohesion intercept with an increase in the matric suction for both the CD and CW triaxial tests. The effective cohesion intercept, c' were found to be 0 kPa from both the CD and CW triaxial tests under the saturated condition. Figure 4 shows the nonlinear relationship between ϕ^b and matric suction for the CW and CD triaxial tests.

Rahardjo et al. (2004) explained that the degree of saturation of the specimen reflects the area of the pore-water in contact with the soil particles, which is responsible for the increase in the shear strength of the soils. It is noted that different degrees of saturation can exist in an unsaturated soil when subjected to the same matric suction. For matric suctions less than 47 kPa, the soil specimens would remain saturated (Figure 5) and the cohesion intercepts are the same for both CD and CW tests (Figure 3). However, for matric suctions ranging from 47 kPa to 200 kPa, the cohesion intercepts obtained from the CD triaxial tests were slightly higher than the cohesion intercepts obtained from the CW triaxial tests. The deviation of the cohesion intercepts of the CW triaxial tests from the cohesion intercepts of the CD triaxial tests can be explained by the differing degrees of saturation attained by the specimens at the end of shearing in the CW and CD triaxial tests. This difference in the cohesion intercepts at failure under the same matric suction can be attributed to the hysteresis observed in the soil-water characteristic of the soil (see Figure 5). Han et al. (1995) also reported hysteresis in shear strength where an unsaturated soil at drying exhibited a higher shear strength than the shear strength of the same soil at wetting, even though the stress conditions during shearing were exactly the same for both states (i.e., drying and wetting). The difference in shear strength could be contributed to the fact that the degree of saturation of the soil on the drying path (i.e., as in the CD triaxial tests) was higher than the degree of saturation of the soil on the wetting path (i.e., as in the CW triaxial tests). As a result, the cohesion intercept from the CD triaxial tests was higher than the cohesion intercept of the CW triaxial tests (see Figure 3). Meanwhile, the ϕ^b angle remained essentially constant at 12^0 for both CW and CD triaxial tests for matric suctions greater than 200 kPa. This could be explained by the fact that at the high matric suction range (i.e., matric suction higher than residual matric suction) hysteresis would become negligible as shown in Figure 5. As a result, the cohesion intercept seems to converge to the same value for both the CW and CD tests.

Conclusions

The conclusions from this study can be summarized as follows:

The results indicated that the effective angles of internal friction, ϕ', and the effective cohesions, c', of the compacted silt as obtained from both the CW and CD tests were identical. The results of the CW and CD triaxial tests showed that the effective angle of internal friction, ϕ', and effective cohesion, c', of the compacted silt were 32^0 and 0 kPa, respectively. Non-linearity was observed in the relationship between ϕ^b and matric suction from the CW and CD triaxial tests for the compacted silt. The ϕ^b angle was found to be the same as the effective angle of internal friction, ϕ' (i.e., 32^0) at low matric suctions (i.e., matric suctions lower than the air-entry value). The ϕ^b angle decreased to a magnitude as low as 12^0 at high matric suctions (i.e., matric suctions higher than the residual matric suction). However, the ϕ^b angles from the CW and CD tests were different at matric suctions between the air-entry value and the residual matric suction value. The difference was due to the lower failure envelope with respect to matric suction from the CW tests as compared to the failure envelope from the CD tests within this range of matric suction. This difference could be attributed to the hysteretic behavior of the soil-water characteristic curve.

Acknowledgment

References

ASTM D 2487 – 93. (1997). Standard Classification of Soils for Engineering Purposes (Unified Soil Classification System), 1993 *Annual Books of ASTM Standards*. 1. 04.08, Section 4, Philadenphia, P.A., 217-227.

Fredlund, D.G. and Morgenstern, N.R. (1977). "Stress State Variables for Unsaturated Soils". *Journal of the Geotechnical Engineering Division*, ASCE., 103 (GT5), 447-466.

Fredlund, D.G., Morgenstern, N.R., and Widger, R.A. (1978). "The Shear Strength of Unsaturated Soils". *Canadian Geotechnical Journal*. Vol. 15 (3), 313-321.

Fredlund, D.G., Rahardjo, H. and Gan, J. (1987). "Nonlinearity of Strength Envelope for Unsaturated soils". In proceeding of the 6th *International Conference Expansive Soils*. New Delhi, India, 1, 49-54.

Fredlund, D.G. and Rahardjo, H. (1993). *Soil Mechanics for Unsaturated Soils*. John Wiley and Sons Inc., New York.

Gan, J., Fredlund, D.G., and Rahardjo, H. (1988). "Determination of the Shear Strength Parameters of an Saturated Soil using the Direct Shear test". *Canadian Geotechical Journal*, 25 (3), 277-283.

Head, K.H. (1986). *Manual of Soil Laboratory Testing*. John Wiley and Sons, Inc., 3, 942-945.

Hilf, J.W. (1956). *An Investigation of Pore-water Pressure in Compacted Cohesive Soils.* Ph.D. Dissertation. Tech. Memo. No. 654, U.S. Dep. of the Interior, Bureau of Reclamation, Design and Construction Div., Denver, C.O.

Rahardjo, H., Heng, O.B., and Leong, E.C. (2004). "Shear Strength of a Compacted Residual Soil from Consolidated Drained and the Constant Water Content Triaxial Tests". *Canadian Geotechnical Journal,* 41, 1-16.

Satija, B.S. (1978). *Shear Behaviour of Partly Saturated Soil.* PhD. thesis, Indian Institute of Technology, Delhi, India.

Thu, M. T. (2005). *The Shear Strength and Volume Change Relationship for an Unsaturated Soil..* PhD. Dissertation, Nanyang Technological University, Singapore.

Effects of Drainage Conditions on the Shear Strength of Unsaturated Soil

M. Shimizu[1], S. Sakamoto[2] and T. Nishioka[3]

[1] Member of ISSMGE; Associate professor, Department of Civil Engineering, Faculty of Engineering, Tottori University, Koyama, Tottori City, Japan, 680-8552, PH [81] (857) 31-5290; FAX [81] (857) 28-7899; email: mshimizu@cv.tottori-u.ac.jp
[2] Student, Graduate School of Engineering, Tottori University, Tottori City, Japan, 680-8552, PH [81] (857) 31-5291; FAX [81] (857) 28-7899, email: sakamoto@geotec.cv.tottori-u.ac.jp
[3] Student, Graduate School of Engineering, Tottori University, Koyama, Tottori City, Japan, 680-8552, PH [81] (857) 31-5291; FAX [81] (857) 28-7899, email: nisioka@geotec.cv.tottori-u.ac.jp

Abstract

Aiming at the examination whether two factors of the net normal stress and the suction can express the shear strength of unsaturated soil under different conditions of drainage, triaxial tests were conducted on unsaturated specimens of a clayey silt under drained and undrained conditions. In drained tests with the pore-air pressure u_a and the suction s held constant (D-tests), the volume contraction occurred as well as the draining of the pore water. Two kinds of undrained tests were conducted with u_a regulated. In undrained tests with u_a constant (Ua-tests), s decreased during shear and the shear strengths became lower those in D-tests. Another kind of undrained tests in which u_a was regulated in order to keep s constant (Us-tests) resulted in simultaneous increases in u_a and u_w, and the state of stresses reached one corresponding to the unconfined compression. Shear strengths from Us-tests were much lower than those from D- and Ua-tests. Measured shear strengths were analyzed using an expression for the shear strength as a linear function of s and the net mean normal stress; results showed that, although the expression would be satisfactorily accepted, the effects of the difference of the testing conditions were detected.

Introduction

An ultimate objective of this study is to establish a rational way of assessing the stability of unsaturated soil-ground or soil-structures when external loads apply on them. For saturated soil, such a way has been established based on the principle of effective stress: for example, the short-term stability of saturated soft-ground can be rationally assessed by the unconsolidated and undrained shear strength.

A current objective is to examine whether it is two factors of the net normal stress σ_{net} and the suction s that control the shear strength of unsaturated soil. Fredlund et al. (1978) proposed an expression for the shear strength of unsaturated soil as a linear function of σ_{net} and s. Their expression seems to be widely accepted for understanding the shear strength; the verification, however, was made on the basis of shear strengths determined under usual conditions, i.e., drained tests in which the pore-air and pore-water pressures are kept constant, or undrained tests in which the pore-air pressure is held constant with the pore-water pressure varying.

In this study triaxial tests were conducted on unsaturated specimens of a clayey silt under drained and undrained conditions. Drained tests are usual ones as mentioned above. Undrained tests were conducted, under the conditions of constant water content with the pore-air pressure regulated, in two ways: in one way the pore air pressure (u_a) was held constant with the measurement of the pore water pressure (u_w) that varies during shear, and in the other way u_a was controlled so that the suction s, defined as $s=u_a-u_w$, would be held constant. Tests of the last kind are not for any practical purpose but they were designed to examine whether or not the shear strength depends on the path along which p_{net} and s vary.

In this paper, results from these three kinds of tests will be presented; the behavior of shear stress and volume change will be investigated, as well as the behavior of s or u_w in undrained tests. Measured shear strengths will be analyzed using the expression proposed by Fredlund et al. (1978), and the applicability of the expression will be discussed.

Sample and method

Sample

A clayey silt available on the market was used (see Figure 1). The sample is non plastic; in fact, the consistency limits could not be determined. It was thoroughly remolded with the water content of 60%. This value was determined because a preliminary test showed that the slurry was homogeneous with the water content of nearly 60%. The density of soil particles is 2.697 Mg/m³.
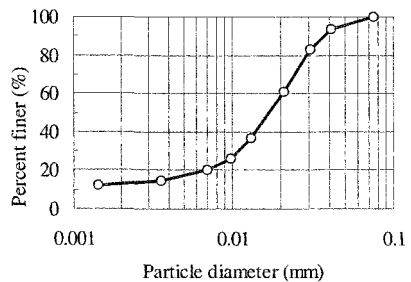
Figure 1. Particle size distribution curve of the sample used.

Preparation of unsaturated specimens

Unsaturated specimens were prepared in the triaxial cell of which details will be shown in the following section. At first, the slurry, almost fully saturated, was one-dimensionally consolidated in a cylindrical mold. The mold was temporarily installed to mount the pedestal in the triaxial cell. The vertical pressure was applied by increments up to 49kPa. After the consolidation, the vertical pressure was reduced to 6 kPa and, at the same time, the suction of 30 kPa was applied, which caused further the drainage of pore water. After the completion of the drainage, the mold was removed leaving the sample on the pedestal. The application of the suction made specimens unsaturated and also made them keep the shape; the degree of saturation decreased to 95 to 97%.

Apparatus for triaxial tests

Figure 2 shows the apparatus used for triaxial tests; it was developed by changing some parts of an apparatus originally designed for saturated soil. A ceramic plate (denoted by **g** in the figure) was installed on the pedestal (**h**); a tube was connected to the

a: load cell, b: displacement transducer, c: inner cell, d: outer cell, e: loading cap, f: specimen, g: ceramic plate, h: pedestal, i: pressure transducer, j: circle-seal valve, k: pressure difference transducer, *l*: double tube burette, u_a: pore-air pressure, u_c: cell pressure ($=\sigma_3$), u_b: back pressure.

Figure 2. Apparatus for triaxial tests.

loading cap (**e**) to apply the pore-air pressure through it. A part, designated as "inner cell" (**c**), was fixed inside the outer cell (**d**) to facilitate the measurement of the volume change.

The alteration is thus simple, but the altered apparatus has a problem. The inside volume of the outer cell can change when the cell pressure σ_3 changes; the change will make the water level in the inner cell vary; and therefore the measurement of specimen's volume will be inaccurate. To fix the problem, σ_3 was not changed throughout every triaxial test; the net confining stress σ_{3net} ($=\sigma_3 - u_a$) was controlled by changing u_a.

The drainage of pore air was always allowed. The drainage of pore water was controlled by the valve (**j**). In this paper the water pressure measured with the pressure transducer (**i**) is regarded as the pore-water pressure u_w.

Triaxial tests

Three kinds of triaxial tests were conducted:
- the consolidated and drained tests (D-tests),
- the consolidated and undrained tests with the pore-air pressure held constant (Ua-tests), and

Table 1. Testing conditions and some results.

	At the end of consolidation[a].					When maximum shear stress mobilized[b].					
	σ_{3net0} [c,d]	s_0	w_0	e_0	S_{r0}	s_f	w_f	e_f	S_{rf}	q_f	p_{netf}
	kPa	kPa	%		%	kPa	%		%	kPa	kPa
D-tests	99	68	14.3	0.910	43		11.7	0.890	36	255	354
	199	37	30.0	0.900	90	$=s_0$	27.6	0.830	90	353	553
	200	47	24.0	1.060	61		19.9	1.005	53	337	537
	200	67	13.3	0.920	39		11.3	0.883	35	326	527
Ua-tests	100	66	14.4	0.940	42	46		0.931	42	245	345
	201	26	34.3	0.840	100	-2		0.831	100	277	478
	200	37	29.9	0.956	84	6	$=w_0$	0.908	89	252	452
	201	45	21.3	0.920	62	31		0.853	67	315	516
	200	54	16.0	0.925	47	37		0.866	50	312	512
	199	67	13.5	0.870	42	47		0.862	42	312	511
Us-tests[e]	98	62	13.9	0.868	43	49		0.945	40	60	61
	100	66	14.7	0.954	42	52	$=w_0$	1.019	39	53	53
	199	67	13.3	0.877	41	66		0.871	41	56	58

a: subscript "0" is used for this state, b: subscript "f" is used for this state, c: $\sigma_{3net0}=p_{net0}$, d: values will be rounded up or down to group tests in some figures, e: the reason why s_f is different from s_0 will be explained in the *Results* section.

- the consolidated undrained tests with the suction held constant (Us-tests).
The undrained tests are those in which the drainage of pore water was not allowed but that of pore air was done; namely, not those in which both pore air and pore water are undrained (Fredlund and Rahardjo, 1993).

In all the tests, specimens were isotropically consolidated prior to the shearing. The drainage of both pore air and pore water was allowed. The net confining stress σ_{3net} was applied by increments up to 100 or 200 kPa with the suction s kept constant at a specified value in the range of 26 to 68 kPa. Table 1 presents the conditions applied for the consolidation and those having resulted from it; the table also includes some results from the shearing.

The degree of saturation S_{r0} decreased with an increase in the applied suction s_0 as shown in Figure 3. The subscript "0" stands for the final state in the consolidation stage or the initial state for the shearing stage; this notation will be adopted through the paper. The figure shows there is no specimen exhibiting peculiar behavior, at least in cases when the net confining stress σ_{3net0} was 200 kPa, which implies that the method of preparing specimens is effective to reproduce the initial conditions for the shearing.

Additionally, Figure 3 provides information about the moisture
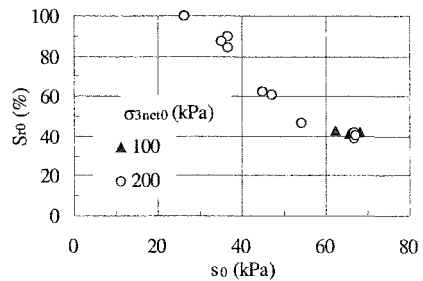
Figure 3. The degree of saturation (S_{r0}) and the suction (s_0) at the end of consolidation.

retention characteristics of the sample. The air entry value of the sample can be estimated between 26 and 37 kPa with σ_{3net} of 200 kPa.

Specimens were sheared under the drained or undrained conditions as mentioned above. For D-tests the drainage of both pore air and pore water was allowed with u_a and u_w held constant, and therefore with s ($=u_a\text{-}u_w$) held constant. For Ua-tests, the drainage of pore water was not allowed and u_a was held constant; u_w changed as well as s. For Us-tests, the drainage of pore water was not allowed as in Ua-tests, but u_a was regulated in order to keep s constant.

Shearing was conducted with a constant rate of axial strain: 0.0051 %/minute for D-tests and 0.0244 %/minute for Ua- and Us-tests.

Results

Stress and strain parameters

The following parameters for stresses are used:

$$p = \frac{\sigma_1 + \sigma_3}{2}, \quad p_{net} = \frac{\sigma_1 + \sigma_3}{2} - u_a \quad \text{and}$$

$$q = \frac{\sigma_1 - \sigma_3}{2},$$

where σ_1 and σ_3 are the axial stress and the cell pressure, respectively. The axial and total volumetric strains, denoted by ε_1 and ε_v, respectively, are defined as nominal strains taking positive values with compression.

D-tests

Results from D-tests are shown in Figures 4(a) and (b). In these figures, and also in some figures that will be presented later, some marks are used to distinguish a curve from others, and their locations have no meaning.

Figure 4(a) shows how the shear stress q and the volumetric strain ε_v vary with the axial strain ε_1. Higher maximum values of q are mobilized with higher p_{net0}; their dependency on the suction s is not clear in this figure. Relationships of the shear strength with p_{net} and s will be discussed in detail later. The axial strain at which q reaches the peak is larger with higher
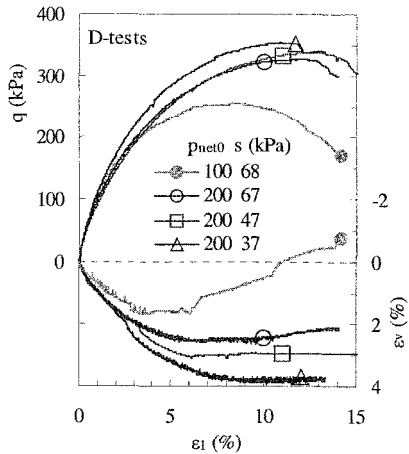
(a) Relationships of q and ε_v with ε_1.
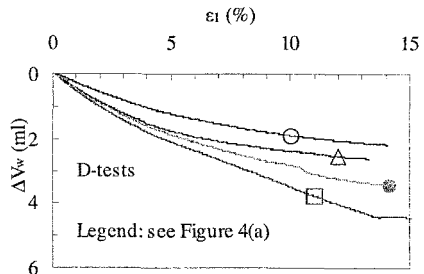
(b) Relationship between the drained volume of pore water, ΔV_w, and ε_1.

Figure 4. Results from D-tests.

p_{net0} and it seems not to depend on s.

The volume contracted as the shear stress developed (Figure 4(a)); however, when ε_1 reached certain levels, the contraction stopped, and in the test with p_{net0} of 100 kPa the volume changed to expand. There seems to be an effect of the suction on the volume change behavior: the amount of the contraction is larger when lower suctions are applied.

In D-tests, pore water drained as shown in Figure 4(b), in which the drained volume of pore water, ΔV_w is plotted against ε_1. Even limiting to the tests with p_{net0} of 200 kPa, effects of the suction on the drained volume cannot clearly be seen. But, it is interesting that the drainage continued after the volume contraction stopped or eventually the volume expansion occurred.

Ua-tests

The relationships of q and ε_v with ε_1 resulting from Ua-tests, shown in Figure 5(a), are similar to those in D-tests already shown in Figure 4(a). However, the dependence of the maximum shear stress on the initial suction, s_0, is clearer in Ua-tests than in D-tests. The maximum shear stresses mobilized in two tests with $s_0=37$ and 26 kPa and $p_{net0}=200$ kPa are obviously lower than others; they are comparable to that in the test with $p_{net0}=100$ kPa. The reason will be understood by considering the behavior of pore-water pressure.

The pore-water pressure increased in all the specimens for Ua-tests as shown in Figure 5(b), in which the excess pore-water pressure Δu_w, defined as $\Delta u_w=u_w-u_{w0}$, is plotted against ε_1. The increase in Δu_w is
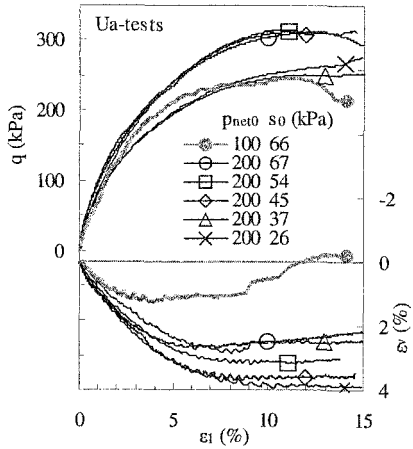
(a) Variations of q and ε_v with ε_1.
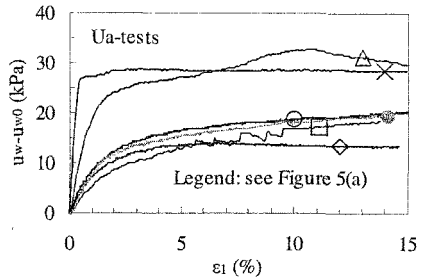
(b) Variations of excess pore water pressure, u_w-u_{w0} with ε_1.

Figure 5. Results from Ua-tests.
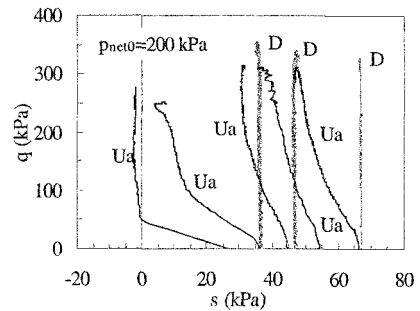
Figure 6. Relationships of q and s for Ua- and D-tests.

remarkably larger for two tests with s_0=26 and 37 kPa than for others.

The increase in the pore-water pressure means the decrease in the suction. Figure 6 shows how the suction varied with the shear stress in Ua-tests, including results from D-tests for comparison. We see that the suction reduced nearly to be zero or negative in two tests with s_0=26 and 37 kPa as the shear stress developed. This behavior is closely related to the fact that the degree of saturation was high in the specimens for these two tests (see Table 1). The results of these two tests will be used later to estimate the shear strength parameters for saturated states.
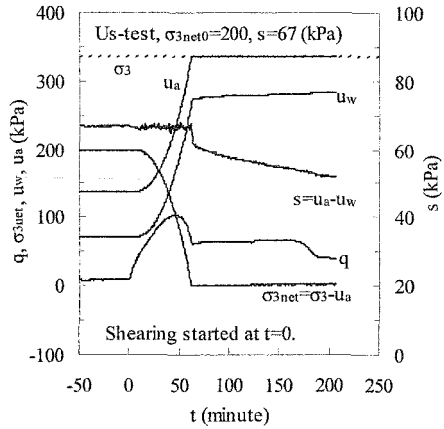
Figure 7. Variations of some quantities with time in a Us-test.

Us-tests

Using an example presented in Figure 7, it is explained how the suction was controlled in Us-tests. The pore-water pressure u_w increased in Us-tests as in Ua-tests. In order to keep the suction constant, the pore-air pressure u_a was increased by the same quantity as u_w increased. In this example, when 67 minutes passed, u_a became equal to σ_3. Once u_a became equal to σ_3, the regulation of u_a was stopped, which caused the decrease in s. In this test, the net confining stress σ_{3net} decreased from an initial value, 200 kPa in this example, to null. The decrease in σ_{3net}, or in p_{net}, affected the behavior of the shear stress q.
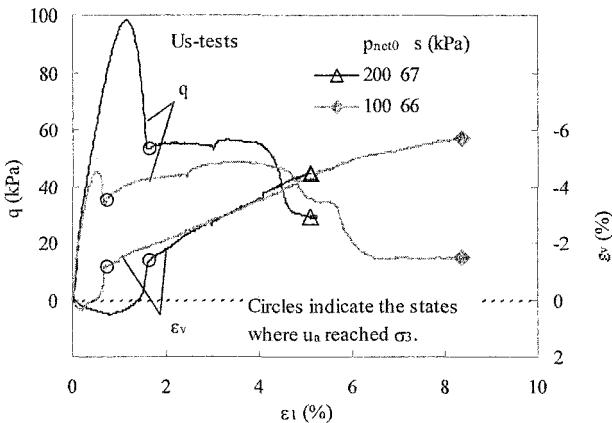
Figure 8. Results from Us-tests.

The behavior of the shear stress and volumetric strain in Us-tests is quite different from those in D- and Ua-tests (Figure 8). The shear stress increased early in the shearing, but began to steeply fall after showing its peak. Later, the shear stress tended to moderately increase and exhibited a peak again. The volume also changed in a complicated manner; the volume contracted a little at the very beginning of shear, and changed to continuously expand.
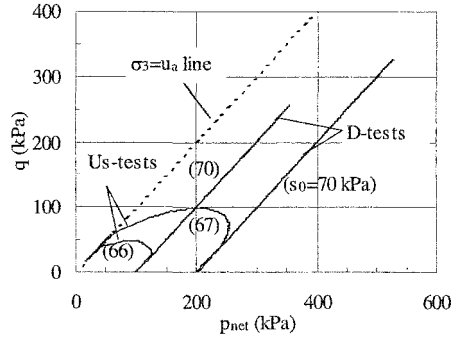
Figure 9. The p_{net}-q diagram for D- and Us-tests.

To see how q varied with p_{net}, the state paths in the p_{net}-q diagram are shown in Figure 9, including those for D-tests for comparison. The states moved to the $\sigma_3=u_a$ line and reached the failure mobilizing low shear strengths.

Figure 10(a) compares the state paths in the q-s diagram between D-, Ua- and Us-tests, all of which were sheared from the same initial state. The path for the Us-test is enlarged in Figure 10(b).

These figures show that the suction decreased in the Us-test. The decrease was caused by the unsuccessful regulation after u_a reached σ_3, but it was maintained as a level higher than that in the Ua-test. Although the suction is in a certain level, the
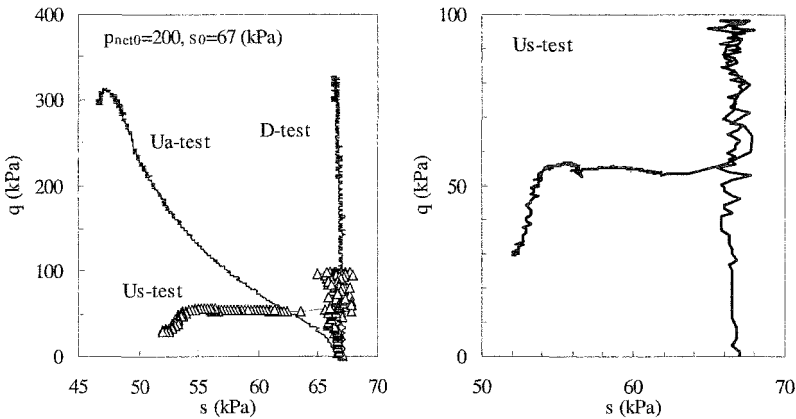
(a) Comparison of three tests.   (b) Enlargement for Us-test.
Figure 10. The s-q diagram for D-, Ua- and Us-tests.

shear strength is much lower than in the Ua-test. Such low shear strength resulted from the decrease in p_{net} as was explained in Figure 9.

Shear strength

Three different kinds of triaxial tests were conducted in this study. In this section it is examined whether the shear strengths measured in those tests can be explained as a function of two variables: the net mean normal stress p_{net} and the suction s. The shear strength is defined as the maximum shear stress; the subscript "f" is used to denote the state in which the shear strength is mobilized.

Effects of the net normal stress

In Figure 11, the shear strength q_f and the suction at failure s_f are plotted against the mean net normal stress at failure p_{netf} for all the tests conducted in this study. The shear strengths can be determined without problem for D- and Ua-tests; for Us-tests, however, the shear stress q reached a peak twice as was explained in the preceding section. Based on the visual observation that the shear band clearly developed after the second peak, the second peak was regarded as the failure. Two straight dashed-lines are drawn; what the lines mean will be explained in the following section.

The effects of p_{netf} are obvious in the figure: higher p_{netf} is, higher q_f is. On the other hand the effects of the suction s_f are not so clear because of the limited range of the suction applied in this study and also because of the variation of data resulting from the limited accuracy of experiments. But it will be seen at least that the suction plays a role of increasing the shear strength. Suction's effects will be discussed using another diagram later.
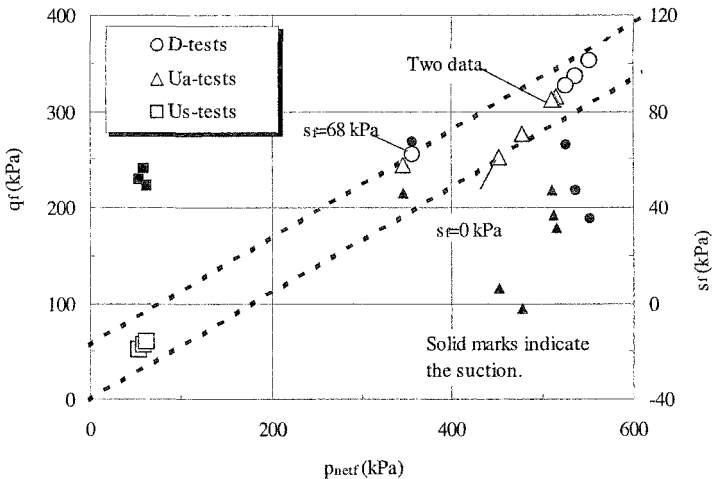
Figure 11. States of stresses at failure for all the tests conducted in this study.

Theoretical consideration

Fredlund et al. (1978) proposed the following expression for the shear strength τ_f

$$\tau_f = c' + \sigma_{netf} \tan \phi' + s_f \tan \phi^b, \tag{1}$$

where $\sigma_{net} = \sigma - u_a$. Using triaxial parameters, p_{net} and q, Equation (1) is written as

$$q_f = m \, p_{netf} + b(s_f) \tag{2}$$

with

$$m = \sin \phi' \tag{3}$$

$$b(s_f) = c' \cos \phi' + s_f \cos \phi' \tan \phi^b \tag{4}$$

Returning to Figure 11, the lower line was drawn so as to pass through the origin and two points obtained from the Ua-tests in which the suction became nearly equal to zero at failure. The upper line was drawn so as to have the same slope as the lower line and to envelope two plots corresponding to the tests conducted with the suction of 68 or 67 kPa, which is in the highest level of suction applied in this study.

On the lower line, s_f is assumed to be 0 as explained above and $b(s_f)=0$ because it passes through the origin (see Equation (2)). Therefore, the lower line leads to the assumption of $c'=0$ (see Equation (4)). The gradient of this line enables us to determine the value of m because $b(s_f=0)=0$, and therefore the value of ϕ' (see Equation (3)), in fact it was determined as 33.9°. The assumption that $c'=0$ could be validated considering that those two plots on the lower line correspond to specimens of high degree of saturation, and that all the shear tests were conducted from the normally consolidated state with respect to p_{net}.
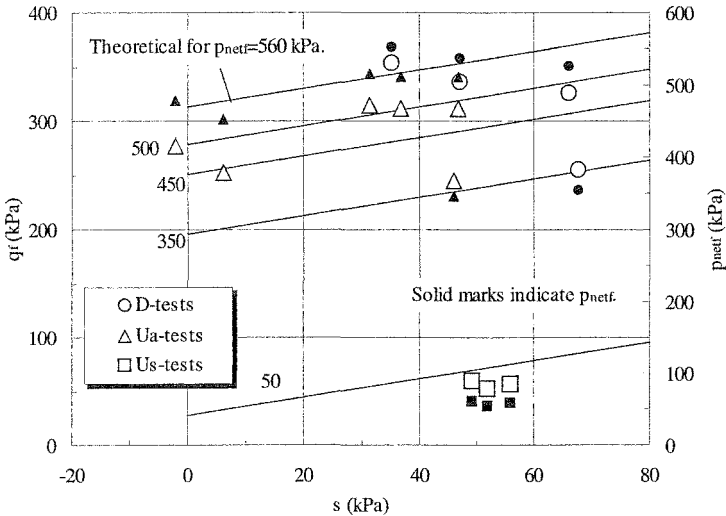
Figure 12. Predicted and measured effects of the suction on the shear strength.

The gradient of the upper line was set to m by assuming that ϕ' is constant, independently of testing conditions. The intercept of this line with the q_f axis gives the value of $b(s_f=68$ kPa). Now inserting values of c', ϕ', $b(s_f=68$ kPa) and $s_f=68$ kPa in Equation (4), ϕ^b can be determined: it is 35.3°.

Figure 12 was prepared to more directly observe the effects of suction on the shear strength, in which q_f and p_{netf} are plotted against s_f. The straight solid lines were drawn based on the calculation with parameters' values determined above. Calculation was made for some representative values of p_{netf}; they were selected so as to be possibly near the values measured in experiments.

For each level of p_{netf}, the theory seems to well predict the behavior of the shear strength. In particular, the assumptions that the function $b(s_f)$ is linear and that ϕ' is constant seem to be accepted for the results obtained in this study, although they are yet controversy (Gan et al., 1988; Vanapalli et al., 1996). As a reason for the acceptability, we may cite that the tests were conducted with the suction in a limited range in this study. Additionally, we should recall that ϕ^b is so high as 35.3° although the gradient of lines is not emphasized in the diagram; this value would be lower with higher suctions (Vanapalli et al., 1996).

Figure 13 compares the calculated strengths based on parameters' values determined above with the measured ones. The dashed lines bound the region inside which the difference between the calculated and measured strengths is less than 10%.

In the preceding discussion, the results from Us-tests were never distinguished from others. The figure, however, demonstrates the effects of the difference in the testing conditions upon the applicability of the theory: the calculation overestimates the shear strengths from Us-tests more than those from D- and Ua-tests. In the Us-tests, the states reached the line of $\sigma_{3net}=0$ at failure as was shown in Figure 9, in
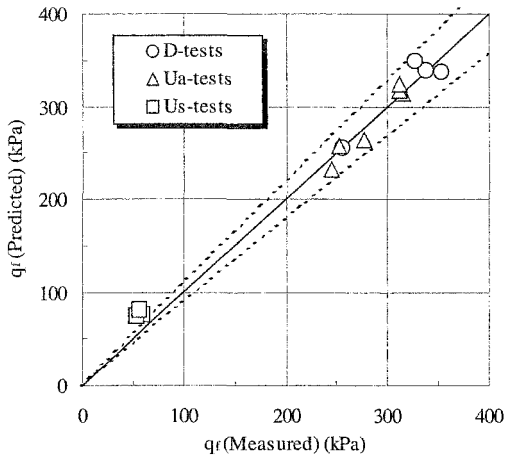
Figure 13. Comparison of predicted and measured shear strengths.

other words in these tests the failure occurred in a very low level of p_{net}. As Gan et al. (1988) discusses, the assumption that ϕ' is constant independently of the net normal stress might not be accepted a priori.

Conclusions

In the drained tests the volume contraction occurred as well as the draining of the pore water. In the undrained tests with u_a held constant, u_a and therefore the suction s decreased during shear. The shear strength in these tests was lower than that in the drained tests. The decrease in shear strength can be explained by the decrease in s in the undrained conditions.

Another kind of undrained tests in which s was regulated to be constant resulted in an increase in u_a with an increase in u_w. As a result, the net mean normal stress drastically decreased in the early stage of shearing and finally the states of stresses reached the line of $\sigma_{3net}=0$. The state of $\sigma_{3net}=0$ corresponds to the state for the unconfined compression test. The shear strength from this kind of undrained tests was much lower than the shear strength from the drained tests and the undrained tests with u_a constant under the same initial conditions for the shearing.

The expression proposed by Fredlund et al. (1978) was satisfactorily accepted. However, an effect of the difference of the testing conditions were detected. The assumption of constant ϕ' caused the effect.

Based on these observations we would say that:

(1) The short-term stability of unsaturated soil-ground or soil-structure of which the volume contraction and the drainage of pore water will occur due to external loads could be assessed by the shear strength to be determined from the undrained tests in which the pore-air pressure is constant.

(2) The manner in which the net normal stress and the suction affect the shear strength would depend on the path along which these factors pass.

References

Fredlund, D. G., Morgenstern, N. R., and Widger, R. A. (1978) "The shear strength of unsaturated soils." *Can. Geotech. J.* 15, 313-321.

Fredlund, D. G. and Rahardjo, H. (1993) *Soil mechanics for unsaturated soils,* John Wiley & Sons, Inc.

Gan, J. K. M., Fredlund, D. G. and Rahardjo, H. (1988) "Determination of the shear strength parameters of an unsaturated soil using the direct shear test." *Can. Geotech. J.* 25, 500-510.

Vanapalli, S. K., Fredlund, D. G., Pufahl, D. E. and Clifton, A. W. (1996) "Model for the prediction of shear strength with respect to soil suction." *Can. Geotech. J.* 33, 379-392.

Suction and its Effects on Shear Strength of Unsaturated Undisturbed Samples of a Volcanic Pumiceous Soil

M. Shimizu[1], D. Yamamoto[2] and Y. Tahara[3]

[1] Member of ISSMGE; Associate professor, Department of Civil Engineering, Faculty of Engineering, Tottori University, Koyama-Minami, Tottori City, Japan, 680-8552, PH [81] (857) 31-5290; FAX [81] (857) 28-7899; email: mshimizu@cv.tottori-u.ac.jp
[2] Student, Graduate School of Engineering, Tottori University, Koyama-Minami, Tottori City, Japan, 680-8552, PH [81] (857) 31-5290; FAX [81] (857) 28-7899; email: yamamoto@ geotec.cv. tottori-u.ac.jp
[3] Student, Graduate School of Engineering, Tottori University, Koyama-Minami, Tottori City, Japan, 680-8552, PH [81] (857) 31-5290; FAX [81] (857) 28-7899; email: tahara@geotec. cv.tottori-u.ac.jp

Abstract

This paper is concerned with the shear strength of undisturbed natural samples of volcanic pumiceous soil. The shear strength varies in a complicated manner with the normal stress lower than the consolidation yield stress p_c. Considering the suction as a factor affecting the shear strength characteristics, direct shear box tests were conducted after the consolidation during which the suction was measured and regulated. When consolidation pressures higher than p_c were applied, the suction decreased, eventually, to null with almost full degree of saturation; the shear strength with such high normal stresses obeyed the Mohr Coulomb criterion. To some specimens the suction was regulated with a normal stress lower than p_c; they mobilized shear strengths exhibiting a good correlation with the suction. Conclusions emphasize that the suction should be measured for unsaturated specimens even if they have so high degree of saturation as 80% or more, and that the suction will be effective for interpreting the variation of the shear strength, especially determined with relatively low normal stresses, of undisturbed natural samples.

Introduction

Volcanic soils cover wide areas such as Central America, South-Eastern Asia and Far-Eastern Asia, including Japan. They are inhomogeneous and usually unsaturated, and their stress histories are ambiguous. These features make it difficult to assess their strength characteristics by applying saturated-soil mechanics. Especially,

1235

weathered soils of pumiceous pyroclastic having been deposited in the Late Quaternary have caused serious engineering problems in Japan (Shimizu, 1998). Although they are classified as cohesive soils, they exhibit physical properties and mechanical behavior quite different from sedimentary cohesive soils in alluvial plains.

This paper is concerned with a soil of this type, particularly with undisturbed samples of which the degree of saturation is rather high as about 80% in natural conditions. Previous studies (e.g. Shimizu and Nishida, 1998; Shimizu, 2004) investigated shear strengths of samples of the same kind as those used in this study and analyzed them based on conventional saturated-soil mechanics. They showed that shear strengths could not be explained in terms of effective stress, and eventually, quite different strengths were determined even under an effective stress. It was also shown that the void ratio, which is one of factors explaining the shear strength of saturated soil, would not be effective in assessing such a variation of strengths.

One of purposes of this study is to try to explain the shear strength characteristics based on unsaturated-soil mechanics. The matric suction and water content are considered as factors for analyzing measured shear strengths.

The suction is one of major factors controlling the shear strength of unsaturated soil, which was foreseen theoretically (e.g. Bishop, 1955) and has been demonstrated experimentally in many literatures (e.g. Fredlund et al., 1978; Vanapalli et al., 1996).

In this study, direct shear tests were conducted. But, a direct shear box testing machine in which the suction can be measured was not available. To cover this disadvantage, for several specimens, the consolidation preceding the shear was made in a one-dimensional consolidation apparatus developed for unsaturated soil.

There are many researches using direct shear box tests with the measurement of suction (e.g. Escario and Saez, 1986; Gan et al. 1988; Vanapalli et al., 1996). There seems, however, no literature on the shear strength of undisturbed natural sample, in particular, of volcanic soils as treated in this study.

It was examined how the suction varied as the consolidation proceeded with time and as the consolidation pressure changed. Considering the behavior of suction, the shear strength dependency on the normal stress will be discussed in this paper.

Conclusions will say that the suction should be measured for unsaturated specimens even if they have the degree of saturation as high as 80% or more, and that the suction will be effective for interpreting the variation of the shear strength, especially determined under relatively low normal stresses, of undisturbed natural samples.

Sample

Samples were taken from the layer of Daisen Kurayoshi Pumice, called DKP in tephrochronology, which is one of representative tephras in Japan. The DKP was generated by the eruptions, in the Late Quaternary, of Mt. Daisen locating in western Japan. The DKP forms a part of thick layer of volcanic soils as more than 20 m even in the area 100 km distant from the mountain; the layer of DKP itself is about 3 m in thickness in that area.

The undisturbed sample tested in this study is called DKP3, which will be

distinguished from the sample (DKP2) used in a previous study (Shimizu, 2004). DKP2 and DKP3 were taken at different sites about 10 km distant from each other.

Undisturbed blocks of the sample were taken by two methods: the block sampling method (B) and the thin-wall-tube installation method (T). A block taken by the former method is a rectangular cylinder of 15x15x20 (cm); one by the latter method a circular cylinder of 8 cm in diameter and 25 cm in height. Specimens for mechanical tests were prepared by trimming those blocks; several specimens were prepared from one block. A block was named by the sampling method, B or T and a number following B or T, for example, as No.B6 or No.T4. A specimen is identified by the name of the block from which it was prepared and a number following it, as No.B6-1 or No.T4-1. The detail of the sampling and trimming methods were described in a literature (Shimizu, 2004).

Figure 1 shows the initial conditions of the sample DKP3, including the data for the sample DKP2 for information. Each plot corresponds to one specimen used for a mechanical test. The sample is so porous the void ratio exceeds 7 and so wet the water content reaches more than 200%. The degree of saturation varies from 70 to 90% except for some DKP2 specimens that were artificially saturated by vacuum in the previous study.

Another point we should pay attention to in Figure 1 is that the sample is so inhomogeneous that the indices widely vary between specimens prepared from a same block.

The sample is fragile, but it is rather stiff: we can trim it with a sharp-edged knife with little disturbing. However, once remolded, it easily becomes liquid as shown in Figure 2. We can understand that it is called "water soil" or "fermented soy-been paste soil" in the local area where it was taken.

Figure 1. The initial conditions of samples. Solid marks indicate samples artificially saturated.

The sample contains sand to clay fractions, as shown in Figure 3. The content of particles finer than 0.075 mm is more than 50%. Because of the high fine content, sieving and hydrometer tests have to be carefully conducted: drying will yield aggregation, and inhomogeneous moisture will result in an incorrect estimate for the total dry mass. Such difficulty was avoided by sieving in

Figure 2. The sample remolded at natural water content.

water and by directly measuring the dry mass.

The sample can be featured by its high values of consistency limits (Table 1). Considering that drying affects the determination of consistency limits for volcanic cohesive soils, consistency limit tests were done after moderately drying the sample in the air so that it could be pasted. Although the sample was not extremely air-dried, consistency limits determined in a wetting process were higher than those in a drying process: 10 to 20% for the liquid limit and 30% for the plastic limit (Shimizu and Yamamoto, 2004). The values shown in Table 1 are averaged ones.

The density of soil particles of the sample is a little higher than the common silicate soil particles (Table 1). The sample contains course particles of amphibole of which the density is higher than that of common silicate particles, and therefore the deviation of contents of such particles will yield some deviation in determining the soil particle density. To avoid the problem the sample was thoroughly remolded. The value presented in Table 1 is the average of 16 measurements.

Figure 3. Particle size distribution curves for the sample.

Table 1. Physical properties.

Liquid limit	131 %
Plastic limit	77 %
Soil particle density	2.783 Mg/m^3

Methods

Preparation of specimens

Specimens for mechanical tests were prepared according to the same method as in the previous studies. First, a block was cut into some pieces by an electric wire saw. Next, a piece was carefully trimmed with a sharp and thin straight edge by hand to be a cylindrical specimen of 2 cm in height and 6 cm in diameter.

Apparatuses

Some specimens were tested at first in a consolidation apparatus, and subsequently they were removed to a direct shear testing machine to be sheared. For other specimens, direct shear tests were conducted without procedure in the consolidation apparatus.

The consolidation apparatus, which had been developed for testing unsaturated soil (Shimizu and Nambu, 2003), consists of a pressure cell with an oedometer inside and the pressure regulation system (Figure 4). The loading plate or cap is perforated so that the cell pressure applies as the pore-air pressure u_a. The pore-water pressure u_w is measured or regulated below a ceramic plate installed in the base of the

oedometer. The suction s is defined as u_a-u_w. A ceramic plate of the air entry value of 500 kPa was used in this study.

The direct shear testing machine used in this study is an improved type developed by Mikasa (1960), which enables to hold the direction for the vertical loading during shear. This machine, however, does not enable the suction to be measured or regulated. It is, of course, desirable to use a direct shear box in which the suction can be regulated as in Escario and Suez (1986), or Gan et al. (1988), unfortunately, however, such a machine was not yet available in this study.

Measurement of initial suction and soil-water characteristic curve

a: Air compressor.   b: Air pressure regulator.
c: Differential pressure regulator.
d: Displacement sensor.   e: Loading ram.
f: Pressure cell.   g: Oedometer ring.
h: Ceramic plate.   i: Porous stone.
j: Differential pressure transducer.
k: Double tube burette.

Figure 4. Apparatus for consolidation tests with the measurement of suction (Shimizu and Nambu, 2003)

In the consolidation pressure cell, the cell pressure (=the pore-air pressure u_a) of 150 kPa was applied without net consolidation pressure under the undrained condition at the specimen's bottom. The pore-water pressure u_w was measured with time. When the change in u_w ceased, the difference between u_a and u_w was determined as the initial suction of the specimen.

In order to obtain the soil-water characteristics curve (s. w. c. c.) of the sample, the suction was cyclically changed after the measurement of the initial suction for one specimen. The suction was decreased to 13 kPa at first, increased up to 200 kPa next, and again decreased to 11 kPa.

Consolidation prior to shearing

After the measurement of the initial suction, the net consolidation pressure, denoted by p, was applied by increments. The drainage of pore air and pore water from the upper surface of the specimen was always allowed. The drainage from the specimen's bottom was not allowed during all the stages of consolidation other than at the final stage of consolidation. At each stage, the vertical displacement and u_w were measured with time. When the change in u_w was judged to have stopped, the next stage of consolidation was started.

The net consolidation pressure p was applied up to 80 kPa for all the specimens other than one specimen, No.T4-1. For the specimen No.T4-1, p of 640 kPa was applied at maximum then p was decreased to 80 kPa, which means that this specimen

was over-consolidated. The value of 80 kPa was adopted as a value lower than the consolidation yield stress, p_c, and that of 640 kPa as one sufficiently higher than p_c. The value of p_c was preliminarily estimated to be about 150 kPa based on previous studies; the estimate was validated from the compression curves obtained in this study as shown later.

In this study the term of the maximum pre-consolidation stress is not used but the consolidation yield stress is used because it is well known that the usual method of determining p_c such as the Casagrande's method overestimates the maximum pre-consolidation stress for volcanic soils, at least, in Japan.

At the final stage of consolidation, the drainage at the specimen's bottom was allowed so as to apply the suction of a specified magnitude. This process aims to examine suction's effects upon the shear strength. The suction applied at this stage is called the suction at the end of consolidation.

Direct shear tests

After the final stage of consolidation, the specimen was removed from the consolidation cell and set in the direct shear box. Direct shear box tests were conducted under the constant normal stress of 80 kPa, which is equal to the net consolidation pressure applied at the final stage of consolidation. The shear speed is 0.05mm per minute.

Dummy test

The suction at the end of consolidation of a specimen will differ from the suction that the specimen would exhibit at the beginning of the direct shear test. In order to discuss suction's effects on the shear strength we should measure the suction at the shear, or at least estimate it. From this point of view, a dummy test was conducted so as to estimate the change in suction that would occur during the process of removing the specimen from the consolidation cell to the shear box. In the dummy test, the specimen was installed not in the shear box test but in the consolidation ring again and the suction was measured. The dummy test proceeded according to the same sequence as ordinary tests with respect to the net consolidation pressure and the time taken for the transition from the consolidation ring to the shear box.

Results and Discussion

Compression curves

Figure 5 shows the compression curves resulting from the consolidation stages prior to direct shear tests; p is the net consolidation pressure and e is the void ratio. Results for specimens of which initial suctions were not measured are also included. Specimens prepared from three blocks are presented. Curves are different between specimens even if
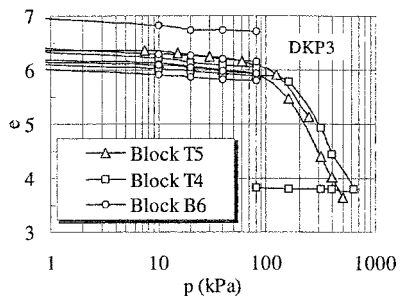
Figure 5. Compression curves.

they were prepared from the same block. The difference in the void ratio reaches nearly one at maximum, which is to be expected because the initial void ratio varied in a wide range as was shown in Figure 1.

The consolidation yield stress p_c was determined as 130 to 160 kPa according to the Casagrande's method. The determined values of p_c are similar to that estimated before tests as already mentioned. In general, shear strength characteristics depend on whether the normal stress is higher than p_c or not. In this meaning, the values of p_c are important; in fact they were taken into account for selecting the normal stress to apply in direct shear tests.

Measurement of initial suction

Figure 6 shows an example of the measurement of the initial suction, where the pore-air pressure u_a and the pore-water pressure u_w are plotted against time. At the moment u_a was applied, u_w started to rise, and reached the state of equilibrium in 50 minutes in this case. The difference of u_a and u_w at this state is the initial suction of the specimen.
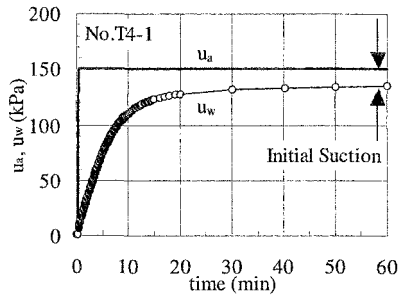
Soil-water characteristic curve

Figures 7(a) and (b) show the relationships of the water content w and the suction s for the soil-water characteristic curve, at the initial state and at the end of consolidation.

The initial suction varied in the range of 10 to 50 kPa depending on

Figure 6. An example of the measurement of the initial suction; variations of u_w and u_a with time.
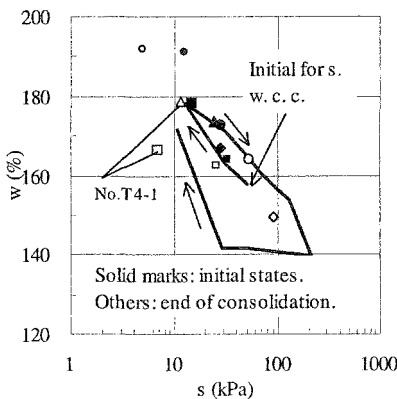
(a). Relationship of w and s. (b) Relationship of S_r and s.
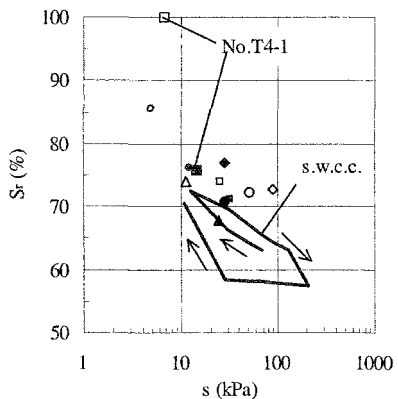
Figure 7. Relationships of the water content w and the degree of saturation Sr with the suction s.

specimens as shown in the figure. However, all the initial states in this diagram locate near the soil-water characteristic curve. The initial suction on the soil-water characteristic curve is higher than others; as a reason for this, the test for the curve was conducted most recently, and somewhat drying had proceeded.

In the consolidation, w and s changed. At the end of consolidation, s was regulated so that each specimen would be subjected to a magnitude different from others.

Behavior of u_w in consolidation

By exemplifying results from the test on the specimen No. T4-1, we see how the pore-water pressure u_w, or the suction s changed in the consolidation.

Figure 8(a) shows the variations of u_a, u_w and the displacement d with time when the net consolidation pressure p was changed from 20 kPa to 40 kPa. Figure 8(b) shows those when p was changed from 160 kPa to 320 kPa.

When p=40 kPa was applied, u_w increased to a certain level and it gradually decreased almost to the original level. The increase in u_w was less than 20% of the increase in p, i.e., B-value was less than 0.2. In this case, pore water was not found drained from the specimen.

On the other hand, when the higher pressure of p=320 kPa was applied, u_w increased much more than the case of p=40 kPa. In fact, it exceeded u_a although B-value was less than 0.2, too. It was observed that the pore water drained through the top platen on the specimen; as pore water drained, u_w gradually dissipated to the level of u_a. The drained volume of water could not be measured. The state of almost full degree of saturation was reached.

The vertical displacement occurred rapidly after the vertical consolidation pressure changed. Such rapid compression is due to the instantaneous drainage of pore air, and the subsequent migration or drainage of pore water.

Suction change due to reposition of a specimen

Figure 9 shows the results from the dummy test. We can see how the pore-water
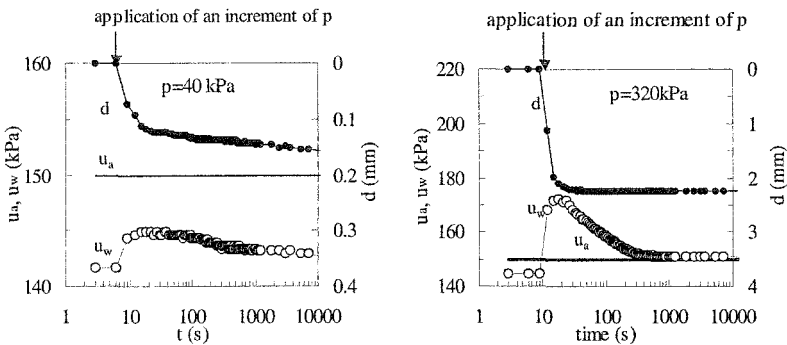
(a) p=40kPa from 20kPa.   (b) p=320kPa from 160kPa.

Figure 8. Behavior of u_w due to loading.

pressure u_w responded to the changes in the pore-air pressure u_a and the vertical pressure p.

At the final stage of consolidation (1634<t<4022 minutes), the suction of 90 kPa was applied under p=80 kPa. After the specimen was reinstalled into the consolidation ring (t>4039 minutes), the suction recovered to 78 kPa under p=80 kPa, which indicates that about 87% of the applied suction recovered, or about 13 % decreased. This decrease in the suction seems to

Figure 9. The change of the suction and applied loading sequence in the dummy test.

be caused by some inevitable disturbance of the specimen during the operation of the removal from and reinstallation into the consolidation ring.

The decrease of the suction was found to be so small as about 10%. Based on this result, it will be discussed the effects of suction on the shear strength using the suction at the end of consolidation in place of the suction at the beginning of the shear.

The discussion above is based on the results from one test, which will be the limitation of the approach in this study. As was stated in the section of "Apparatuses" it is preferred to use a direct shear testing system in which the suction can be measured or regulated.

Shear strength

The shear strength τ_f was plotted against the normal stress σ in Figure 10. The results obtained in the previous study (Shimziu, 2004) were also included for comparison. The solid marks indicate the results for the specimens that had been over-consolidated in an artificial manner as for the specimen No.T4-1 tested in this study. The shear strength τ_f is defined as the maximum value of the shear stress τ.

From this figure we can summarize the shear strength characteristics of the sample as follows. Shear strengths under high normal stresses can be well expressed by the Mohr-Coulomb failure criterion. On the other hand, shear strengths mobilized under low normal stresses, as lower than 150kPa, tend to vary non-linearly with normal stresses.

Strengths of specimens to which the suction was intentionally regulated ("DKP3 s measured" in the figure) are different from each other although they were tested under the same normal

Figure 10. Relationships between the shear strength τ_f and the normal stress σ.

stress of σ=80 kPa. This is due to hidden effects of the suction.

Recalling that the consolidation yield stress p_c of these samples was 130 to 160 kPa, as pointed out when referring to Figure 5, we might say that the shear strength of this sample could not be expressed as a function of one variable of σ if σ is lower than p_c.

In the following, it will be discussed about the effects of the void ratio, the water content and the suction. The discussion will be made based on the results from tests conducted under σ=80 kPa on the sample DKP3, because the suction was not measured on the DKP3 specimens tested with σ other than 80 kPa and on the sample DKP2.

Figure 11 shows the relationships between the shear strength τ_f and the void ratio, where the void ratios in two states are considered: e_c is the void ratio at the end of consolidation and e_f at the failure, i.e., when $\tau=\tau_f$. They were determined from the whole volume and the dry mass of specimens, and therefore they are not the void ratio at the shear zone.

A clear tendency for effects of e_c or e_f on τ_f can not be seen, if the plots for the artificial over-consolidation are excluded considering that the artificially over-consolidated specimen experienced a quite different stress history from ones that other specimens experienced.

The artificial over-consolidation reduces the void ratio and results in high strength; however, it is not assured that the shear strength increases by the amount to be estimated from the decrease in void ratio (Shimizu, 2004).

Figure 12 shows relationships between the shear strength τ_f and the water content at the end of consolidation, w_c. Except for the result for the over-consolidated
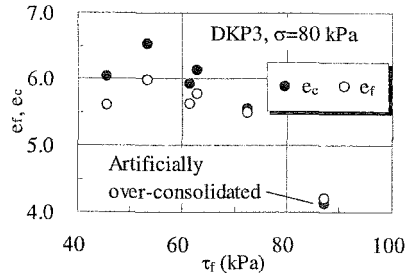
Figure 11. Relationships between the void ratio and the shear strength.
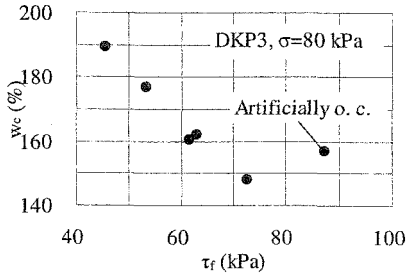
Figure 12. Relationships between the water content w_c at the end of consolidation and the shear strength τ_f.
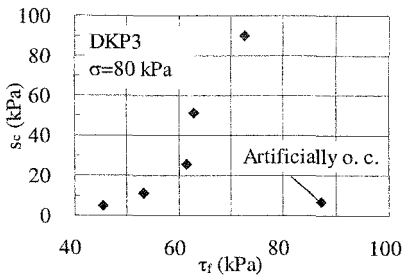
Figure 13. Relationships between the suction at the end of consolidation s_c and the shear strength τ_f.

specimen, a clear tendency can be found that τ_f becomes higher as w_c becomes lower. But, two data locating near the point (τ_f=60kPa, w_c=160%) deviates from the tendency.

As was shown in Figure 7, the water content is strongly correlated with the suction for the sample used in this study as usually observed for unsaturated soils, although a histeresis appeared depending on the process of drying or wetting. This fact makes us expect that the suction will be also correlated with the shear strength if the results in Figure 12 are considered.

In fact, Figure 13 validates the prediction above. A strong correlation exists: higher the suction is, higher the strength is. It should be noted that a little discrepancy found in Figure 12 has disappeared.

We can see that there is non-linearity between the suction and the shear strength. The linearity is assumed, e.g. in the expression proposed by Fredlund et al. (1978); a model to explain the non-linear relationship was studied by Vanapalli et al. (1996). It seems that the non-linearity is yet controversy.

Conclusions

Shear strengths determined under a normal stress lower than the consolidation yield stress p_c widely varied specimen by specimen. They were found clearly correlated with the suction measured at the end of the consolidation prior to shearing. Under normal stresses higher than p_c, shear strengths well obeyed the Mohr-Coulomb criterion for the shear failure; this can be explained by an experimental fact that high normal stresses made the suction disappear and the state of almost full degree of saturation was reached.

These observations will yield the followings as conclusions:
(1) The suction is effective for interpreting the reason why the shear strength of undisturbed natural samples of pumiceous soil varies even under a constant normal stress if it is lower than the consolidation yield stress.
(2) The suction should be measured for unsaturated specimens even if they have the degree of saturation as high as 80% or more.

In this study the correlation of the shear strength with the suction was discussed using the suction at the end of consolidation, neither at the beginning of the shearing nor at failure. Although the difference between the suction at the end of consolidation and that at the beginning of shearing was estimated, the estimation was based on the results from one test. This will be the limitation of the approach in this study. As was repeatedly stated in the paper, it is preferred to use a direct shear testing system in which the suction can be measured or regulated.

References

Bishop, A. W. (1955) "The principle of effective stress." *Teknisk Ukeblad*, 39, 859-863.

Escario, V. and Saez, J. (1986) "The shear strength of partially saturated soils." *Geotechnique* 36, 453-456.

Fredlund, D. G., Morgenstern, N. R., and Widger, R. A. (1978) "The shear strength of unsaturated soils." *Can. Geotech. J.* 15, 313-321.

Gan, J. K. M., Fredlund, D. G. and Rahardjo, H. (1988) "Determination of the shear strength parameters of an unsaturated soil using the direct shear test." *Can. Geotech. J.* 25, 500-510.

Mikasa, M. (1960) "A new type of direct shear box testing machine." *Proc. of the 15th Annual Conference on Civil Engineering*, Japan Society of Civil Engineers, 45-48 (in Japanese).

Shimizu, M. (1998) "Geotechnical features of volcanic-ash soils in Japan." Special Report B, *Proc. Int. Sym. on Problematic Soils, IS-Tohoku'98*, Japanese Geotechnical Society, 2, 907-927.

Shimizu, M. and Nishida, N. (1998). "Undrained shear strength of undisturbed weathered-pumice soil." *Proc. Int. Sym. on Problematic Soils, IS-Tohoku'98*, Japanese Geotechnical Society, 1, 169-173.

Shimizu, M. and Nambu, K. (2003) "One-dimensional consolidation of unsaturated soils and problems in experiments." *Proc. of the 2nd Asian Conference on Unsaturated Soils* (UNSAT-ASIA 2003), Japanese Society of Geotechnical Engineering, 117-122.

Shimizu, M. (2004) "Shear strength of undisturbed samples of weathered pumice soils." *Advances in Geotechnical Engineering: the Skempton Conference*, ICE, UK, 1, 618-629.

Shimizu, M. and Yamamoto, D. (2004) "Physical properties of Daisen Kurayoshi Pumice: effects of measuring methods." *Research Report of Faculty of Engineering*, Tottori University, 35, 31-34 (in Japanese).

Vanapalli, S. K., Fredlund, D. G., Pufahl, D. E. and Clifton, A. W. (1996) "Model for the prediction of shear strength with respect to soil suction." *Can. Geotech. J.* 33, 379-392.

Effects of wetting and drying on the unsaturated shear strength of a silty sand under low suction

Chaminda Pathma Kumara Gallage[1] and Taro Uchimura[2]

[1]Geotechnical Laboratory, Department of Civil Engineering, University of Tokyo, 7-3-1, Bunkyo-ku, Hongo, Tokyo, Japan 113-8656; PH +81-3-5841-6123; FAX +81-3-5841-8504; e-mail: chaminda@geot.t.u-tokyo.ac.jp
[2]Geotechnical Laboratory, Department of Civil Engineering, University of Tokyo, 7-3-1, Bunkyo-ku, Hongo, Tokyo, Japan 113-8656; PH +81-3-5841-6120; FAX +81-3-5841-8504; e-mail: uchimura@geot.t.u-tokyo.ac.jp

Abstract

Shear strength properties of unsaturated soils are important in evaluating the stability of geotechnical structures such as natural slopes, embankments, retaining walls, excavations, and footings. This importance is more in countries, where intense rainfalls cause the instability of natural and man-made slopes.

An unsaturated soil behaves differently at wetting and drying and this difference in behavior is referred to as hysteresis. Hysteresis is often exhibited in soil-water characteristic curves of unsaturated soils. The hysteresis in the shear strength behavior of unsaturated soil under wetting and drying has not been fully investigated. Shear strength tests on unsaturated soils have usually been conducted following the drying process. For example, in a multi-stage shear test, the soil is subjected to increasing matric suctions at subsequent stages. Very few studies have been conducted on the unsaturated shear strength parameters on wetting process by which slopes become more unstable.

Re-compacted soil specimens of silt-sand were tested in a modified triaxial apparatus to examine the effects of wetting and drying on shear strength. Identical soil specimens were tested at wetting and drying under controlled air and water pressures. The study was conducted for low suction range, (i.e. 0 ~50 kPa). The soil at the drying had lower shear strength as compared to the soil at the wetting under the same matric suction. Furthermore, the study was extended to investigate the effects of suction and the hysteresis of SWCC on shear strength parameters such as effective friction angle, ϕ', and the apparent cohesion, c. Results exhibited no significant effects of suction and the hysteresis of SWCC on the effective friction angle. It was observed that the apparent cohesion at the wetting was higher than that was obtained at the drying under the same suction. The c increases as the suction increase with the decreasing rate at wetting.

Itroduction

A number of shallow-depth slope failures have taken place during or just after rainfall in regions experiencing high seasonal rainfalls (Brand et at. 1984). Some of these failures seem to be caused   not only by an increase of positive pore water pressure in soils resulting from a rise in the ground water level but also by the degradation of soil strength forming the slopes. In order to predict the stability of slopes induced by rainfalls, it is important to investigate the change of the shear strength of soils due to the infiltration of rain water or in other word due to the reduction of negative pore-water pressure.

A significant amount of research has been conducted on the shear behavior of unsaturated soils (Fredlund et al. 1978; Ho et al. 1982a, b; Fredlund et al. 1987; Gan et al. 1988; Gan et al. 1996; Blatz et al. 2002). Most of investigations focused on unsaturated shear strength of soils in relation to the magnitude of the matric suction which was often achieved by following the drying path of soil-water retention curves due to less time consumption for a test. They found that the higher the matric suction the soil possesses the larger the shear strength will be. Han et al. 1995 studied the hysteresis effect of wetting and drying on the shear strength of residual soils employing a direct shear apparatus. The results indicated that the shear strength of residual soils at the wetting was lower than at the drying.

(Fredlund et al.1978) proposed an equation to interpret the shear strength of unsaturated soils in terms of two stress state variables,

$$\tau = (\sigma_n - u_a) \tan \phi' + c \tag{1}$$

$$c = c' + (u_a - u_w) \tan \phi^b$$

where τ = shear strength of unsaturated soil; c = apparent cohesion; c' = effective cohesion of saturated soil; ϕ' = the shearing resistance angle which is assumed to be constant for all values of matric suction and is equal to saturate condition; ϕ^b = the angle of shearing resistance with respect to suction; σ_n = the total normal stress on the plane of failure; u_a = air pressure in the soil mass; u_w = pore water pressure; (u_a-u_w) = the matric suction of the soil in the failure plane.

In this interpretation, the relationship between τ and (u_a-u_w) is assumed to be linear. However, (Escario & Saez 1986) determined that this relationship is actually non-liear. Later several other researchers observed the non-linear relation between apparent cohesion and matric suction (Fredlund et al. 1987; Wheeler 1991; Ridley 1995; Ridley et al. 1995).

It is critically importance to acquire good awareness on unsaturated shear strength parameters at low net normal stress and low matric suction because most of rainfall-induced slope failures are shallow and occur at the high degree of saturation (low matric suction). Also the effects of wetting-drying hysteresis on unsaturated shear strength parameters can cause slopes to be unstable during and after rain.

This paper describes the results of a series of drained shear tests conducted on unsaturated re-compacted silty sand employing a modified triaxial apparatus aiming to investigate the followings:

(1) effects of the low matric suction and the wetting-drying hysteresis behavior on shearing resistance angle (ϕ').

(2) Effects of the wetting-drying hysteresis on the relationship between the apparent cohesion and the matric suction.

Tested Material

Edosaki sand which contains 16.4 % of non-plastic fines (particles smaller than 75 micron) was used as the testing material. The material was excavated from a natural slope in Edosaki area, Japan. The index properties of the sand determined by laboratory tests according to Japanese standards are summarized in Table 1. Figure 1 depicts the soil-water characteristic curves (SWCCs) of the tested material obtained from Tempe pressure cell employing the axis-translation technique.

Table 1. Index properties of the tested material

D_{50} [mm]	C_u	C_c	e_{max}	e_{min}	G_s	Optimum water content [%]	$\rho_{d\,(max)}$ [g/cm^3]
0.228	16.67	4.71	1.588	1.011	2.75	16.5	1.725
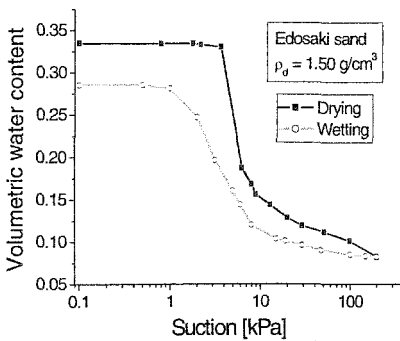
Figure 1. Laboratory obtained SWCCs of testing material
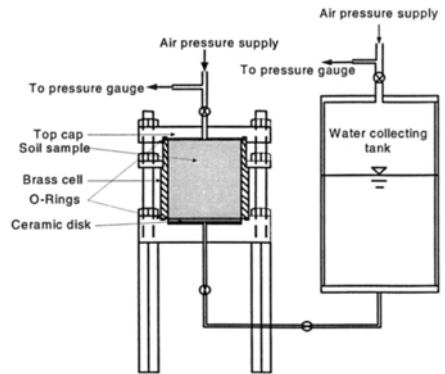
Figure 2. The schematic diagram of Tempe pressure cell

Apparatus

Tempe pressure cell

The schematic diagram of the Tempe pressure cell which was used to obtain laboratory soil-water characteristic curves is shown in Figure 2. This apparatus

consists of a brass cylinder with diameter of 50 mm and height of 60 mm, a high air-entry (300 kPa) ceramic disk embedded in the base plate, and a top cap.

A test was started by saturating the high air-entry ceramic disk and associated system (the compartment between ceramic disk and the base plate and an outlet tube connected to the base plate). Then the cylindrical brass cell was mounted and the specimen was prepared on the ceramic disk. After saturating the specimen, excess water was removed from the cell. The top plate was then mounted and tightened into place and the weight of the assembly was measured. To obtain the drying curve, air pressure was supplied through the inlet tube on the top plate and the outlet tube located at the base plate allowed water to drain out to a water tank, which was opened to atmospheric pressure and the water level was maintained equal to the middle height of the soil specimen. Once the air pressure was applied, water started draining from the specimen through the high air-entry disk until equilibrium was reached. The equilibrium was ensured when the assembly had constant weight and the value was noted. During the weight measurement, both inlet and outlet tubes were closed. The procedure was then repeated at higher applied air pressure (i.e. higher matric suction). The apparatus was used for matric suction up to 200 kPa (applied air pressure 200 kPa).

The wetting process was simulated by increasing the water pressure while keeping the air pressure at constant value of 200 kPa. Once the water pressure was increased, water flowed into the cell through the disk until the equilibrium was reached. The weight of the assembly was noted when it reached equilibrium. This procedure was repeated at higher water pressure (i. e. lower matric suction).
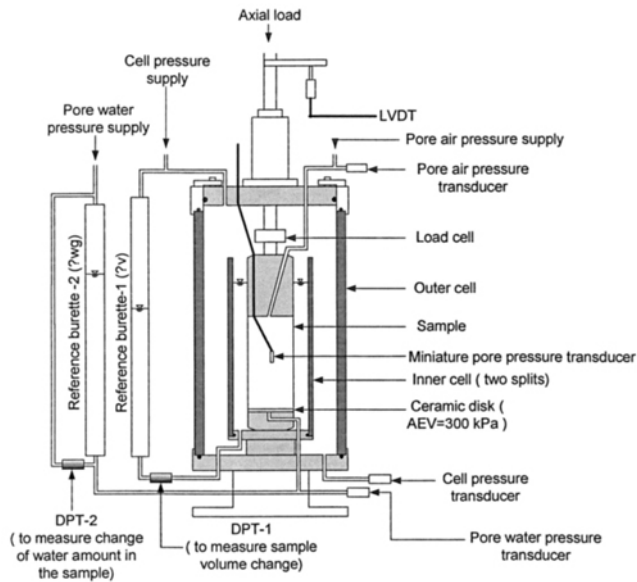
Fig.3. Modified triaxial apparatus for unsaturated soil testing

When the specimen reached zero matric suction (i.e. water pressure was equal to the air pressure), the assembly was disconnected from both pressure supplies and pressures were released simultaneously. The water content corresponding to zero suction on wetting curve was measured by oven-drying the soil specimen. This water content together with previous change in weight of the assembly was used to back-calculate the water contents corresponding to each suction value.

Triaxial Apparatus

A conventional triaxial apparatus, which was designed to test samples measuring 75 mm in diameter and 150 mm in height, was modified to test unsaturated soils. A simplified scheme of the modified apparatus and the associated system is drawn in Fig. 3.The suction is controlled by means of the axis translation technique (Hilf 1956). The pore air pressure is applied through the top cap. The pore water pressure is controlled at the sample bottom through the water drainage system, using a high air-entry value ceramic disk (AEV≈300 kPa) fixed to the pedestal. As shown in Fig. 3, the water drainage system consists of a burette and a differential pressure transducer (DPT-2) with the capacity of 6 kPa. The DPT-2 measures the pressure of the top and the bottom of the burette through which the pore water pressure is applied to the specimen. Then DPT-2 is then calibrated to measure change of weight of water in the reference burette-2 due to infiltration into the sample or to drain out from the sample.

   In addition to three pressure transducers, measuring the pore air pressure, the pore water pressure, and the cell pressure, the apparatus is equipped with a miniature pressure transducer to measure pore water pressure inside the sample. The miniature pressure transducer, which is going into the sample through the top cap, is modified with a small ceramic disk (AEV =100 kPa) in order to measure both positive and negative pore water pressures. This local measurement of pore water pressure is necessary to verify that the desired suction (by axis-translation) is achieved by following the wetting path or the drying path of SWCCs and to observe the equalization of the applied pore water pressure inside the sample.

   The axial displacement is measured externally by a LVDT. The overall volume change of the sample is measured by the double-cylinder technique. The double cylinder system in the triaxial apparatus consists of an inner cell (see Fig. 3) coaxial to the sample and filled with water. The variations in the level of water in the inner cell can be related to the volume change of the sample. The reference burette -1, filled with water and maintained at the same pressure as the cell, is used to fix a reference pressure. A very thin stratum of silicon oil on the water surface in both the inner cell and the burette reduces water evaporation (Tatsuoka 1988).The system can apply deviatoric stress in stress controlled condition and it is measured by the load cell with the capacity of 5 tons located above the top cap (see Fig. 3).

Testing procedure

All the tests were conducted on re-compacted specimens (75 mm diameter and 155 mm high)with the initial dry density of 1.5 g/cm^3(relative density of 1.31) and the initial molding gravimetric water content of 10%.

First, the ceramic disk attached to the pedestal and the associated system were fully saturated. After fixing the pedestal to the base plate of the triaxial cell, a 0.3 mm thick rubber membrane was fastened to the circumference of the pedestal. The membrane was then stretched with the help of the split mould and the specimen was directly prepared on the top of the saturated ceramic disk by the method of moist placement (wet tamping) in ten equal layers. The soil, mixed with 10 % of water, for each layer was poured into into the mould and compacted until the predetermined height was achieved. During the preparation, the pore water pressure in the sample was monitored at the bottom of the sample and the miniature pore pressure transducer, which was placed at two –third height (from the bottom) of the sample. After completing the setup shown in Fig. 3, predetermined net confining (σ_c-u_a) stress and the suction (u_a-u_w), by the axis-translation technique following either the wetting path or the drying path, were applied. It was allowed to equalize to the applied suction (pore water pressure) in the sample under an isotropic condition. The sample was then sheared under constant suction and net confining pressures (both the pore water and the pore air pressures were kept constant during shearing).

To achieve the desired suction by following the wetting process, negative pore water pressure in the sample was being observed (by pore water pressure transducer at the bottom and the miniature pore pressure transducer inside the sample) until it exceeded the negative pore water pressure corresponding to the desired suction. The axis-translation technique was then used to apply desired suction and the equalization of applied pore water pressure in the sample was ensured when the pore water pressure measurement of the miniature sensor was relatively equal to the applied pore water pressure or no water infiltration was observed. This equalization process required 7 ~ 10 days. Figure 4 depicts the pore water pressure (refer to next page)
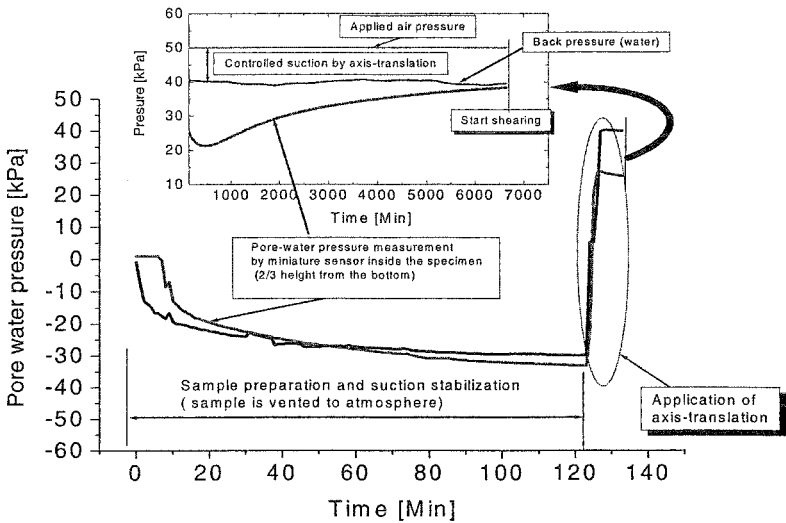
Figure 4. Sample preparation, axis-translation, and pore water pressure equalization at wetting

measurements during sample preparation and pore water pressure equalization after axis-translation application.

To achieve the desired suction by following the drying process, prepared sample with 10% initial water content was first saturated and air pressure (u_a) was then applied at the top of the sample and maintained at a higher value than the back pressure (u_w). The difference of applied air pressure and back pressure (u_a-u_w) was equal to the desired value. Water was driven out from the soil sample against the back water pressure, through the high air entry ceramic disk and into the back pressure controller, until equilibrium was established under the applied pressures. A total of 4 ~10 days was required to complete this consolidation and desaturation. Amount of water flow in and out from the sample and the pore water pressure measurement inside the sample were being recorded during the process of saturation and desaturation.

Results and discussions

Suction achieved by following the wetting process

A series of tests were conducted with constant suction, (u_a-u_w), which was achieved by following the wetting process explained under testing procedure, (i.e. u_a-u_w = 0 (saturated), 10, 20, 50 kPa). For each suction value, two or three tests were conducted varying net confining pressure, (σ_3-u_a), as 25, 50, 75 kPa. The peak deviator stress was considered as the failure of each specimen. Note that a new specimen was used for each u_a-u_w and σ_3-u_a values.

Figure 5 illustrates the deviator stress vs. axial strain curves obtained from tests under a constant suction (20 kPa). It can be observed that shear stress increases as net confining (σ_3-u_a) pressure increases. As shown in Fig. 6, contraction followed by dilation was observed during shearing and the amount of contraction was high at higher confining pressure. The similar behavior was observed from the results of tests under a constant suction of 0, 10, 50 kPa. The extended Mohr-Coulomb failure envelope at the matric suction of 20 kPa is presented in Fig. 7 (c) as a horizontal projection on the shear stress ($\tau = \dfrac{(\sigma_1 - \sigma_3)}{2}$) vs. net normal stress ($\sigma - u_a$) plane.

The failure envelope has an intercept (apparent cohesion) of 12 kPa and a slope angle (angle of internal friction angle) of 47.21^0. Figure 7 (a), (b) and (d) depict the extended mohr-Coulomb envelopes at the matric suction of 0, 10, and 50 kPa respectively.

Figure 8 (a) and (b) show the variation of the angle of internal friction (ϕ') and the apparent cohesion with the matric suction, respectively. The results suggest that the angle of internal friction of soil does not depend on low suction values. It implies that the unsaturated specimens have the value of ϕ' which is equal to that of saturated specimens. This finding led to the conclusion that the value of ϕ' for saturated CD tests can be used in the Equation (1) to predict the drained shear strength of the unsaturated soils (under low suction) as it is assumed when the equation (1) is proposed. As shown in Fig. 8 (b), the apparent cohesion vs. matric suction is not

linear as it is shown in the Equation (1). This finding is consistent with the results of other researchers such as (Fredlund et al 1986, Wheeler 1991, Ridley 1995, and Ridley et al 1995). However, the approximate linear relationship of the apparent cohesion vs. matric suction can be observed for the matric suction less than 20 kPa.
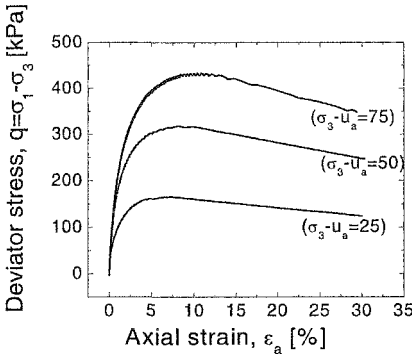
Figure 5. Deviator stress vs. axial strain curves from CD tests under constant matric suction of 20 kPa at wetting
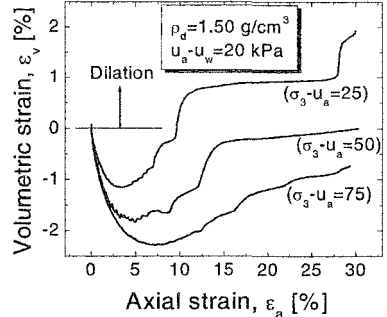
Figure 6. Volumetric strain vs. axial strain curves from CD tests under constant matric suction of 20 kPa at wetting
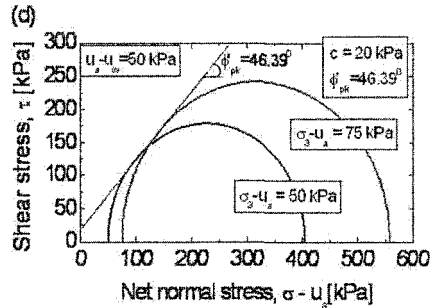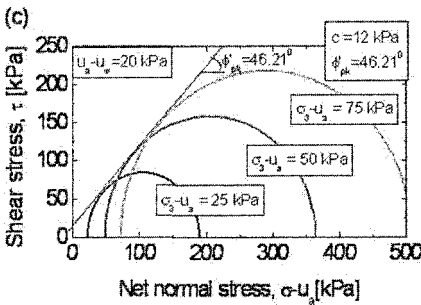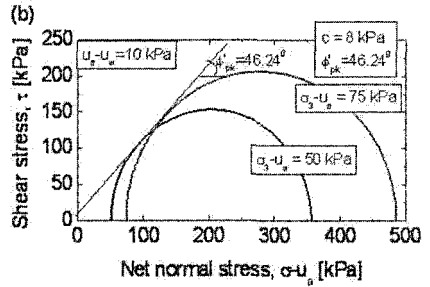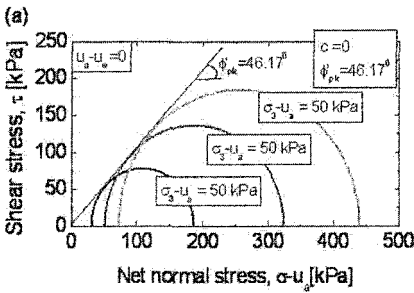
Figure 7. Mohr-Coulomb failure envelopes for CD tests under constant suction of (a) 0 kPa, (b) 10 kPa, (c) 20 kpa, and (d) 50 kPa at wetting.
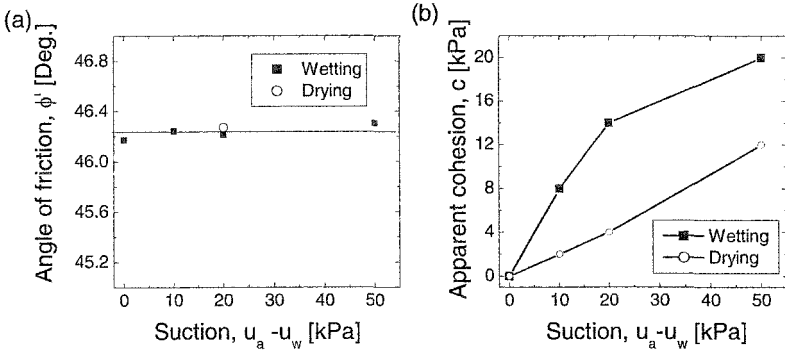
Figure 8. (a) Angle of internal friction vs. suction, (b) apparent cohesion vs. suction, at both wetting and drying
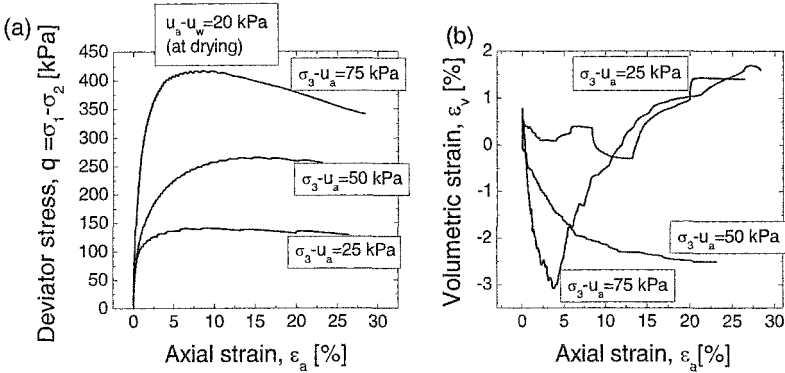
Figure 9. (a) Deviator stress vs. axial strain curves, (b) Volumetric strain vs. axial strain curves, from CD tests under constant matric suction of 20 kPa at drying

Suction achieved by following the drying process

A series of tests were conducted with constant suction, (u_a-u_w), (i.e. 10, 20, 50 kPa), which was achieved by following the drying process explained under the testing procedure, in order to investigate the effects of the hysteresis of SWCC on the unsaturated shear strength papameters.

First, three tests under a constant suction of 20 kPa were conducted varying net confining pressure, (σ_3-u_a), as 25, 50, 75 kPa. Figure 9(a) and (b) depict the deviator stress vs. axial strain curves and volumetric strain vs. axial strain curves respectively. As it was observed at wetting process, shear stress increases as net confining (σ_3-u_a) pressure increases and the overall volume of the specimen reduces during shearing

and the amount of contraction was high at higher confining pressure. Figure 10 shows the extended Mohr-Coulomb failure envelope at the matric suction of 20 kPa in drying process. The slope of the failure envelope is 46.27^0 and it is plotted in Fig. 9 (a). According to the results shown in Fig. 9(a), it can be concluded that the angle of internal friction (ϕ') of soil may not depend on the matric suction (or water content) and the hysteresis of SWCC. (For other tests, ϕ' is taken as 46.25^0).

In order to obtain the apparent cohesion (c)values for the suction of 10 and 50 kPa at the drying process, two tests were conducted under the matric suction of 10 and 50 kPa with the same net confining pressure (σ_3-u_a) of 50 kPa. Figure 12 shows the use of single Mohr circle with an assumed ϕ' of 46.25^0 to determine the apparent cohesion corresponding to each suction value (i.e : 10 and 50 kPa).

Figure 9 (b) summarizes the relationship of the apparent cohesion and the matric suction for both the wetting and the drying process. It can be seen that in the drying process, the soil possesses much lesser apparent cohesion values than that obtained at the wetting process under the same matric suction. In fact the single Mohr's circle approach in determination of the c in the drying process seems reasonable relative to other experiments; it is understandable more tests are needed in the drying to support the approach since the c values are quite small. Therefore, more experiments on the way in drying with the same dry density of 1.5 g/cm^3 and also another experimental program with the relative density of 1.20 g/cm^3.

As shown in Fig. 1, the air entry values for drying and wetting are 5 and 2 kPa, respectively. In fact some literature revealed that the relationship of the apparent cohesion and the matric suction is non linear when the matric suction is greater than air entry value of the soil. However this can not be concluded with the results shown in Fig. 8(b) since the tests were conducted under greater suction values than the air entry value of the soil. It seems that non-linearity when the suction is greater than 20 kPa in the wetting.
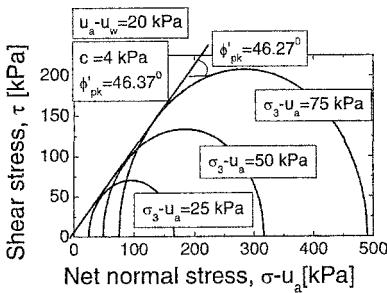
Figure10. Mohr-Coulomb failure envelope for CD tests under constant suction of 20 kPa at drying
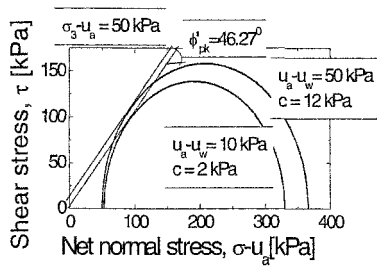
Figure 11. Mohr-Coulomb failure envelopes for CD tests under constant suction of 10 and 50 kPa at drying

Figure 12 (a) and (b) illustrate effects of the hyteresis of SWCC on the deviator stress vs. axial strain and volumetric strain vs. axial strain curves. It can be observed that the shear stress in the wetting process is higher than that in the drying process under the same matric suction and net confining pressure. This finding contradicts the results of (Han et al. 1995). The specimen at the wetting process exhibits more contractive behavior compared to the specimen at the drying process
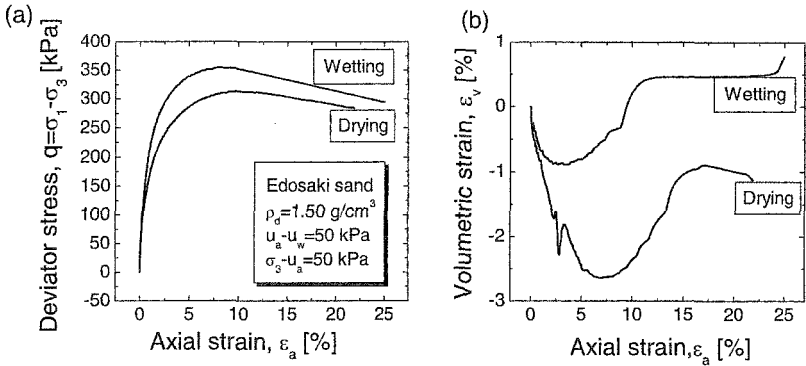
Fig.12. (a) Deviator stress vs. axial strain curves, (b) Volumetric strain vs. axial strain curves, from CD tests under constant matric suction of 50 kPa and constant net confining stress of 50 kPa under wetting and drying

Conclusions

The following conclusions can be drawn from the results of the experimental program:

(a) The shear strength and the volume change of unsaturated soil is affected by the change in net confining stress, shear strength increases and total volume decreases as the net confining stress increases.

(b) The effective friction angle of soil from the CD test seems to be independent on water content (or suction) and the hyteresis of SWCC. Thus, the ϕ' from saturated CD tests can be used to estimate the shear strength of unsaturated soils.

(c) The apparent cohesion (c) of unsaturated soils is affected by both the matric suction (water content) and the hysteresis of SWCC. The apparent cohesion increases with decreasing rate as the suction increases in the wetting process. However, it seems to be reasonable to assume a linear relationship between the c and the suction for the matric suction value less that 20 kPa.

(d) The apparent cohesion in the wetting process is higher than that in the drying process under the same suction value.

(e) It can be observed that the shear stress in the wetting process is higher than that of in the drying process under the same matric suction.

Acknowledgement

References

Blatz, J. A. Graham, J. & Chandler, N.A. (2002). "Influence of suction on the strength and stiffness of compacted sand-bentonite." Canadian Geotechnical Journal, 39, 1005-1015.
Brand, E.W., Premchitt, J. & Phillipson, H.B. (1984). "Relationship between rainfall and landslides in Hong Kong." Proc. 4th International Symposium on Landslides, Ontario, Canada, 377-384.
Escario, V. & Saez, J.(1986). "The shear strength of partly saturated soils." Geotechnique, 36(2), 453-456.
Fredlund, D.G., Morgenstern, N.R. & Widger (1978). "The shear strength of unsaturated soils." Canadian Geotechnical Journal, 15, 313-321.
Fredlund, D.G., Rahardjo, H. & Gan, J.K.M. (1987). "Non-linearity of strength envelope for unsaturated soils." Proc. 6th Int. Conf. Expansive soils, New delhi, pp 49-54, Rotterdam, Balkema.
Gan, J.K.M., Fredlund, D.G. & Rahardjo, H. (1988). "Determination of the shear strength parameters of an unsaturated soils using the direct shear test." Canadian Geotechnical Journal, 25(8), 500-510.
Gan, J.K.M. & Fredlund, D.G.(1996). "Shear strength characteristics two saprotic soils." Canadian Geotechnical Journal, 33, 595-609.
Han, K.K. & Rahardjo, H. (1995). "Effects of hysteresis on the shear strength of a residual soil." E.E. Alonso & P. Delage (Eds), Unsaturated soils, 2, 637-644, Rotterdam, Blackman.
Hilf, J.W. (1956). "An investigation of pore water pressure in compacted cohesive soils." U. S. Dept. Interior Bur. Reclamation tech. Memorandum 654.
Ho, D.Y.E. & Fredlund, D.G. (1982a). "A multistage triaxial test for unsaturated soils." ASTM, Geotechnical testing journal, 5(1), 18-25.
Ridley, A.M., Burland, J.B. & Monroe, A.S. (1995). "Unconfined compression tests with pore pressure measurements." Proc. 11th African regional conference. SMFE. Cario.
Ridley, A.M. (1995). "Strength-suction-moisture content relationships for Kaolin under normal atmospheric conditions." UNSAT 1995, 2, 645-651, Paris.
Tatsuoka, F.(1988). "Some recent development in triaxial testing system for cohesionless soils." ASTM STP 977, West Conshohoken, PA.
Wheeler, S.J.(1991). "An alternative framework for unsaturated soil behavior." Technical note Geotechnique. 41(2), 257-261.

Yielding of unsaturated compacted silty soil under anisotropic conditions

A. R. Estabragh[1] and A. A. Javadi[2]

[1]University of Tehran, Tehran, Iran, PH +98(21)44650896; FAX +44(1392)217965; email: aestabragh@yahoo.co.uk.
[2] Department of Engineering, School of Engineering and Computer science, University of Exeter, Exeter, EX4 4QF, UK, PH +44(1392)263640; FAX +44(1392)217965; email: a.a.javadi@ex.ac.uk

Abstract

Considerable attempts have been made in recent years to develop a better understanding of the mechanical behavior of unsaturated soils in terms of elasto-plastic critical state constitutive models. An important feature of the models is the suggestion of the existence of a yield surface in mean net stress: deviator stress: suction space. This paper presents the results of experimental tests for investigating the shape of yield surface for compacted silty soils. A comprehensive set of laboratory experiments has been undertaken in a double-walled triaxial cell. The method of axis translation was used to create the desired suction in the samples. The results show that constant suction cross sections of the yield surface were approximately elliptical in shape, and inclined to the axes; the size of the elliptical yield curves increased with increasing suction and the flow rule was non-associated.

Introduction

Yielding is an important feature of the stress-strain behavior of soils and can be defined as the limit of elastic deformations. It is expressed by a combination of stress states that cause yielding in the soil. The different combinations of effective stresses causing yielding in identical samples may be plotted in stress space as the yield envelope, which is a boundary separating the plastic and elastic regions, and is the theoretical limit of elasticity. In fact there is generally a gradual transition from elastic to plastic behavior. Yielding of soil has been studied by many investigators including Tavenas and Leroueil (1977), Tavenas et al. (1979), Graham et al. (1983) and Baracos et al. (1980). Most of these studies have concentrated on natural saturated soils.

In modeling terms, the flow rule describes the relationship between the volumetric and shear components of plastic strain during first time loading (Delage and Graham 1996). Many researchers such as Cui and Delage (1996), Zakaria et al. (1996) have investigated the flow rule for unsaturated soils. Alonso et al. (1990) suggested a non-associated flow rule, but Wheeler and Sivakumar (1995) adopted an associated flow rule in their elasto-plastic model of unsaturated soils. In what follows, the results of an experimental study on the shape of yield surface for an unsaturated compacted silty soil are presented.

Experimental study

Soil properties. The soil used in the testing program was a silty soil with medium plasticity. The soil comprised of 5% sand, 90% silt and 5% clay. A combination of sieve analysis and hydrometer test was used to determine the particle size distribution of the soil. The soil had a liquid limit of 29% and plasticity index of 19%. The optimum water content in the standard compaction test was 14.5% and the maximum dry density was 1.74 Mg/m^3.

Sample preparation. All the samples were prepared by static compaction at a water content of 10% (4.5% less than the optimum water content as determined by the standard compaction test). The samples were 38 mm in diameter and 76 mm high. In order to ensure adequately uniform samples and a repeatable test procedure, preliminary static compaction tests were carried out by preparing samples in one, three, six and nine layers in an Instron machine. Each layer was compacted by a static load at a fixed displacement rate of 1.5 mm/min to a maximum vertical total stress of 1600 kPa for each method of static compaction. The dry density was measured along the sample and the optimum number of layers for compaction of the samples was selected based on the variation of density (along the length of the sample) and uniformity of the sample. By considering the value of Standard Deviation (STD) of the values of dry densities along the sample and the presence of marked interfaces between the layers for different methods of sample preparation, it was concluded that the sample uniformity was greatly improved by compaction in nine layers. The samples prepared by this technique were very uniform and the interfaces between layers were minor and the repeatability of this method was found to be excellent.

Experimental apparatus. A Bishop and Wesley triaxial cell was modified to a double walled cell and used for measuring the volume change of the samples. The technique of axis translation proposed by Hilf (1956) was used for creating the desired suctions in the samples. Four GDS pressure controllers were connected to the apparatus and were controlled by a computer. The controllers were used to apply the pressure in the inner and outer cells, the pore water pressure and the axial stress. All the experimental data were recorded continuously by computer.

Experimental procedure

Equalization.   After setting up the apparatus, the first step of each test was equalization. The purpose of the equalization stage was to create a desired suction in the sample by allowing the pore air pressure and pore water pressure to equalize to the applied air pressure and back pressure respectively. During equalization, the suction in the sample changed from its initially unknown value after compaction to the required value.

Ramp consolidation and unloading. After the sample was equalized at a specified suction (100, 200 or 300 kPa) and a mean net stress, it was loaded isotropically (by a linear ramp procedure) under the constant suction to a pre-specified value of mean net stress (550 kPa). The process of ramped consolidation was used to limit the excess pore water pressure generated at the top face of the sample, and was followed by unloading to a pre-defined lower value of mean net stress.

Suction change.   The isotropic loading and unloading stages were performed at constant suction. At the end of the unloading stage, the suction in the sample was reduced continuously from its initial value to a pre-determined value while the mean net stress was kept constant. This was to study the effect of suction change on the yield point in the following isotropic reloading stage.

Isotropic reloading. This stage of the test program was carried out after the suction change stage. Three tests were conducted at different values of suction with an isotropic reloading stage ($\Delta q/\Delta p'=0$). The procedure for isotropic loading was similar to the ramp consolidation. The main objective of the isotropic reloading stage was to evaluate the yield point under isotropic stress at different values of suction.

Shearing (anisotropic reloading).   The final stage of the tests included drained shear at constant cell pressures. Five drained shear tests were conducted at cell pressures of 50, 100, 200, 300, and 400 kPa for each value of suction (100, 200 and 300 kPa). The purpose of conducting shear tests was to investigate yielding under anisotropic stress conditions ($\Delta q/\Delta p'=3$) and study the form of the flow rule after yielding.

Identification of yield points

The stresses at which yielding occurs can be estimated on the basis of empirical procedures. These should ideally be as general as possible and as free as possible from the influence of the observer (Graham et al. 1988). There is typically a region of transitional behavior between pre-yield and post-yield stressing. Consequently a degree of judgment must be exercised in selecting a yield stress. To assist in the identification of the yield point, the stress-strain (deviator stress q versus

axial strain ε_1, deviator stress q versus shear strain ε_s, and specific volume versus mean net stress p' (with p' on a logarithmic scale)) curves were used. Various other plots were also investigated, including p' versus energy per volume (as recommended by Graham et al. 1983). It was found, however, that yield was even more ambiguous in these additional plots than in the stress-strain and specific volume-mean net stress curves. The yield points were identified using the method of intersection of two linear segments of specific volume-mean net stress curves (see Fig. 1).
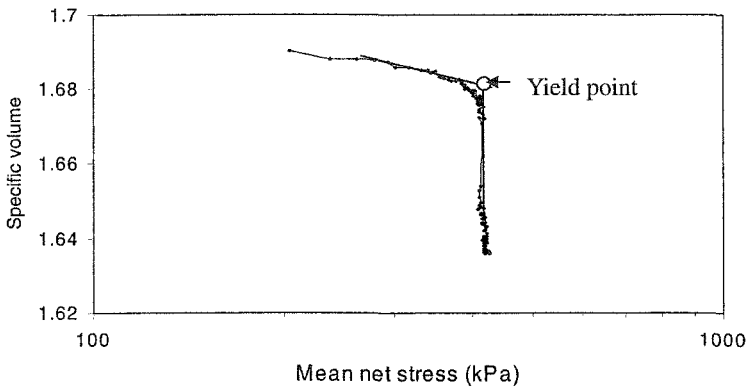
Figure 1. Determination of yield point from v:Lnp' plot.

Yield surface

The estimated values of yield stresses (q_y, p'_y), determined from the above procedure, were used to plot constant suction yield curves in the q: p' plane for suction values of 100, 200 and 300 kPa (see Fig. 2) including an isotropic yield point for each suction. Six to seven tests were conducted with different confining pressures at each value of suction.

Flow rule

The flow rule represents the relationship between the yield curve and the direction of the plastic strain increment vector. To obtain the direction of the plastic strain increment vector after yielding, plots of deviator stress q versus shear strain ε_s and mean net stress p' versus volumetric strain ε_v were used. The elastic and plastic shear strain increments ($\delta\varepsilon_s^e$ and $\delta\varepsilon_s^p$) were evaluated from $q : \varepsilon_s$ plots, whereas the elastic and plastic volumetric strain increments ($\delta\varepsilon_v^e$ and $\delta\varepsilon_v^p$) were determined from the $p' : \varepsilon_v$ plots. The plastic strain increment vectors were superimposed on the $q{:}p'$ plot by plotting the magnitudes of the plastic volumetric strain increment $\delta\varepsilon_v^p$ and plastic shear strain increment $\delta\varepsilon_s^p$ at the yield points with axes parallel to p' and q (see Figs. 3, 4 and 5).

Results and discussion

From Fig. 2 it can be seen that the yield curves for suctions 100, 200 and 300 kPa are ellipses inclined to the axes. This general shape of the yield curves is similar to that of natural soils. It can be concluded that the effect of the anisotropic stress history of the samples, produced by compaction, has not been erased during isotropic loading (consolidation). This does not agree with the models of Alonso et al. (1990) and Wheeler and Sivakumar (1995) which were based on elliptical yield curves at constant suction with the p' axis being the axis of symmetry for the ellipse. The effect of suction induces an expansion of the yield curve which exhibits a suction hardening effect as proposed by Alonso et al. (1990). The inclination of the yield curve indicates a clear anisotropic behavior of the compacted soil, which may be related to the stress state supported during compaction. This is similar to the effect of sedimentation in natural soft soils. Natural and compacted unsaturated soils are rarely isotropic and one can expect to see more anisotropic behaviors like those observed in saturated soil. Thus the relationship between isotropic and anisotropic unsaturated soils appears to be exactly analogous to that already established in saturated soils. Many researchers, such as Graham et al. (1983) have concluded that the inclination of the yield curve is an indication of fabric anisotropy arising from previous compaction. It can be concluded from Figs. 3 and 4 that the total plastic strain increment vectors $\delta\varepsilon^p$ at each yield point are not perpendicular to the yield curve, indicating that the flow rule is non-associated. This does not agree with the proposal of Wheeler and Sivakumar (1995) and Zakaria et al. (1996) who adopted an associated flow rule in their model. In contrast, Alonso et al. (1990) suggested a non-associated flow rule in their elasto-plastic model. It would be possible to derive an equation for inclined elliptic yield curve which can be incorporated in constitute modeling of unsaturated soils.
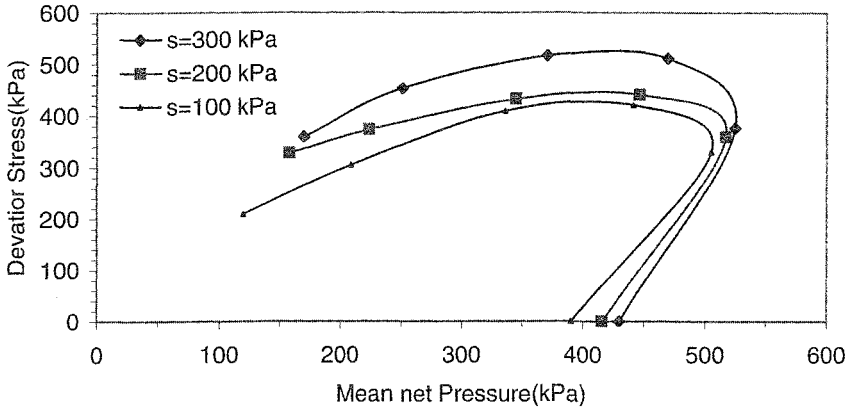
Figure 2. Yield curves for different suctions.

Conclusion

    The influence of anisotropy and suction on the yield surface and flow rule for a compacted unsaturated silty soil has been investigated through a number of triaxial (isotropic and anisotropic) loading tests. A comprehensive set of tests has been carried out and the results have been used to identify the yield points, the yield surface and the flow rule. The experimental results show that the anisotropic nature of the soil produced by the compaction process has not been eradicated by subsequent isotropic ramped consolidation and unloading. The results also indicate that the shape of the yield surface is an inclined ellipse in the $q : p'$ space and is a function of the stress history of the soil. This non-isotropic evolution of yield surface with increasing suction as a function of stress history also occurs for saturated soils. The total plastic strain increment vectors at the yield points are not perpendicular to the yield curve, indicating that the flow rule is non-associated. These findings support the results of Cui and Delage (1996) who suggested that the flow rule was non-associated for compacted Jossigny silt, because the direction of the plastic strain increment vectors showed large departures from being normal to the yield curves.
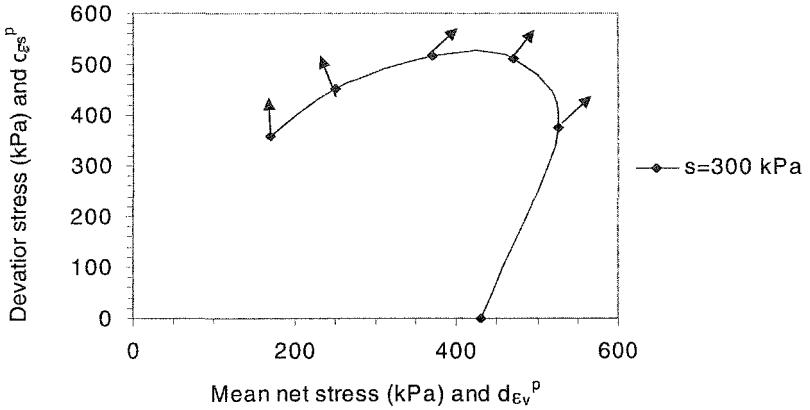
Figure 3. Yield curve at s **=300 kPa and plastic strain increment direction.**
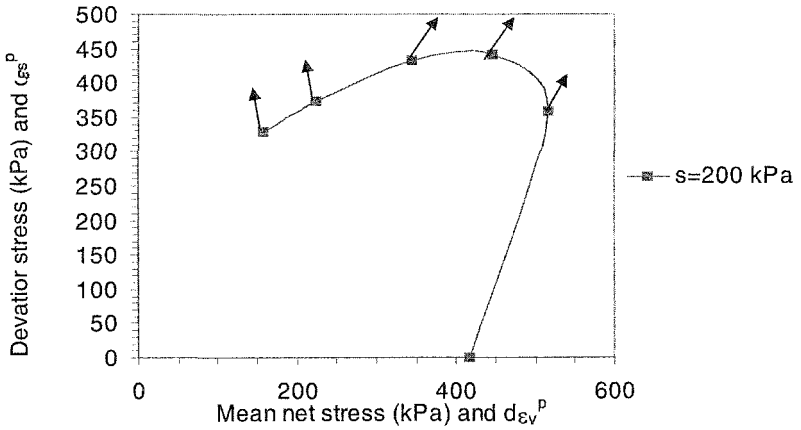
Figure 4. Yield curve at s **=200 kPa and plastic strain increment direction.**
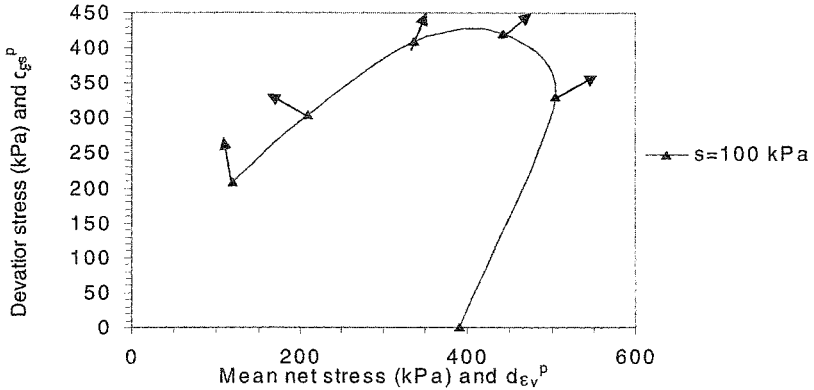
Figure 5. Yield curve at s =100 kPa and plastic strain increment direction.

References

Alonso, E. E., Gens, A., and Josa, A. (1990). "A constitutive model for partially saturated soils." *Geotechnique*, 40(3), 405-430.

Baracos, A., Graham., J. and Domaschuk, L. (1980). "Yielding and rupture in a Lacustrine clay." *Canadian Geotechnical Journal*, 17(4), 559-573.

Cui, Y. J. and Delage, P. (1996). "Yielding and plastic behaviour of an unsaturated compacted silt." *Geotechnique*, 46(2), 291-311.

Delage, P. and Graham, J. (1996). "Mechanical behavior of unsaturated soils: Understanding the behavior of unsaturated soils requires reliable conceptual models." *Proc. 1st Int. Conf. Unsaturated Soils*, Paris, 1223-1256.

Graham, J., Noonan, M.L., and Lew, K.V. (1983). "Yield states and stress strain relationship in a natural plastic clay." *Canadian Geotechnical Journal*, 20(3), 502-516.

Graham, J., Crooks, J. H. A., and Lau, S. L. K. (1988). "Yield envelopes: Identification and geometric properties." *Geotechnique*, 38 (1), 125-134.

Hilf, J. W. (1956). "An investigation of pore pressures in compacted cohesive soils." *Technical Memorandum No. 654*, Bureau of Reclamation, USDI, Denver, Colorado.

Tavenas, F. and Leroueil, S. (1977). "Effects of stresses and time on yielding of clay." *9th ICSMFE*, Tokyo, 1, 319-358.

Tavenas, F., Des Rossiers, J. P., Leroueil, S., LaRochelle, P. and Roy, M. (1979). "The use of strain energy as a yield and creep criterion for lightly overconsolidated clay." *Geotechnique*, 29(3), 285-303.

Wheeler, S. J., and Sivakumar, V. (1995). "An elasto-plastic critical state framework for unsaturated soil." *Geotechnique*, 45(1), 35-54.

Zakaria, I., Wheeler, S. J., and Anderson, W. F. (1996). "Yielding of unsaturated compacted kaolin." *Proc. 1st Int. Conf. Unsaturated Soils*, Paris, 1, 223-229.

Effects of matric suction on residual strength and deformation characteristics under low confining pressure

S. Kato[1], Y. Yoshimura[2] and T. Sakakibara[3]

[1] Department of Architecture and Civil Engineering, Kobe University, Rokkodai-cho 1-1, Nada-ku, Kobe, 857-8501, Japan; PH & FAX +81 78 803 6030; email: skato@kobe-u.ac.jp
[2] Department of Civil Engineering, Gifu National College of Technology, 2236-2 Kamimakuwa, Motosu, Gifu 501-0495, Japan; PH +81 58 320 1401; FAX PH +81 58 320 1409; email: yuji@gifu-nct.ac.jp
[3] CRC Solutions Corporation, 4-1-3 Kyutaro-cho, Tyuou-ku, Osaka, 541- 0056, Japan; PH +81 6 6241 4121; FAX +81 6 6241 4136; email: tatsuo@crc.co.jp

Abstract

Shear strength characteristics of unsaturated soils under low confining pressure are important in order to analyze the mechanism of slope failures induced by rainfall. In this paper, we studied the results of unconfined compression test and constant water content compression test on silt specimen under low confining pressure performed in the past and examined the residual strength and deformation characteristics. The residual stress states of specimens having different degrees of saturation and matric suctions at failure show a unique relationship for the confining pressure when the suction stress is considered. This means that "suction stress" affects the residual strength considerably. It is also found that when the specimens have nearly the same initial void ratio and expanded in shear process, critical state lines parallel to the original one is expected. From these results, it is inferred that in some cases, the extended Cam clay models proposed need to be modified when they are applied for low confining stress state.

Introduction

Usually, triaxial tests have been carried out under high confining pressures to study the strength characteristics of unsaturated soils, and little data exist for the condition under low confining pressure. In this study, we carried out unconfined compression test and unconsolidated and constant water compression test for

compacted specimen, and examined the residual strength and deformation characteristics under low confining pressures.

The following symbols and notations are used in this paper for stresses and strains; σ_1, σ_2, σ_3:total principal stress, σ_c: consolidation pressure under isotropic stress state, u_a, u_w: pore-air and pore-water pressure, $\sigma - u_a$: net normal stress, $s = u_a - u_w$: matric suction, $p = (\sigma_1 + \sigma_2 + \sigma_3)/3$:mean principal stress, $p' = p - u_w$, effective stress, $p_{net} = p - u_a$, mean net stress, $q = \sigma_1 - \sigma_3$:shear stress, ε_1, ε_2, ε_3 : principal strain, $\varepsilon_s = \varepsilon_1 - \varepsilon_3$:shear strain.

1.Effect of Matric Suction on Shear Strength of Unsaturated Soil. When matric suction is applied to the soil, water meniscus develops and it induces intergranular forces between soil particles. The intergranular forces increase shear resistance for slippages between the soil particles, and cause an increase of shear strength of unsaturated soil. Fredlund et al. (1978) proposed the shear strength equation for unsaturated soil as follows.

$$\tau_f = c_{sat} + (\sigma - u_a)\tan\phi_{net} + (u_a - u_w)\tan\phi^b \tag{1}$$

whereτ_f: shear stress on the failure plane,

  σ : total normal stress,

  ϕ_{net}: internal friction angle with respect to net normal stress,

  ϕ^b: parameter related to the increase of shear strength with matric suction increase.

The third term in left hand side of equation (1) represents the increase of shear strength related to matric suction. The value of ϕ^b is equal to the value of ϕ_{net} when matric suction is lower than the air entry value for soil, and is lower than that when matric suction becomes higher than the air entry value (Fredlund and Rahardjo, 1993).

Recent studies have reported that the increase of shear strength has a relation with the water characteristic curve, (Abe, 1994, Vanapalli et al., 1996). Karube et al.(1996) and Vanapalli et al., (1996) proposed the same equation for the relationship between the increase of shear strength, c* and the matric suction, s as follows.

$$c^* = \left(\frac{S_r - S_{r0}}{100 - S_{r0}} \cdot s\right)\tan\phi_{net}$$

where S_r, S_{r0} : degree of saturation and degree of saturation at residual state.

But these studies had only examined the peak strength of unsaturated soil. There are a few studies concerning the relationship between the residual strength and matric suction, and effects of matric suction on the residual strength are not known sufficiently.

To study the mechanism of the "rapid landslide" (Wang, F. et al., 2000) that can take place during earthquake, Kobari et al. (2005) carried out triaxial compression tests under constant volume state for unsaturated specimen. The samples were obtained from the places where slope failure or the "rapid landslide" occurred at earth quake. They showed that the degree of saturation has a relationship with the residual strength under constant volume state. Kawarada et al. (2005) carried out the ring shear test using unsaturated specimens, and studied the effects of initial degree of saturation on the residual strength. In these studies, matric suction was neither controlled nor measured.

2. Study for Critical State in Unsaturated Soil. In saturated clays under normally consolidated state, when shear process continues, the specimen reaches to the critical state (Scofield, A.W. and Wroth, C.P., 1968), in which shear strain develops in constant volume state without stress change. The relationship between void ratio and mean stress is represented as the critical state line on void ratio versus mean stress plane. The "Cam clay model" (Scofield, A.W. and Wroth, C.P., 1968) , which is based on the critical state concept, is an elasto-plastic model for saturated normally consolidated clay, and widely accepted for many researchers as simple and suitable one to predict behavior of normally consolidated clay.

For unsaturated soil, the extended Cam clay models, in which matric suction is treated as one of the stress parameter, have been presented (Alonso et al. 1990, Wheeler and Sivakumar, 1992 and Kohgo et al., 1993). In these models, the increase of stiffness of soil structure induced by matric suction is represented as expansion of yield surface in three dimensional stress space of p, q and s or in two dimensional stress plane of p' and q. And the contraction of yield surface induced by the decrease of matric suction represents deformation or collapse in wetting process. But relating to the critical state, which is fundamental base for the Cam clay model, only a few data is available (for example, Toll & Ong, 2003). The main reason is the difficulties in triaxial tests using unsaturated soils. For example, when compacted specimen is used, it is very difficult to keep the same initial state for each specimen. This difficulty affects the correctness of examination for the critical state line.

Soil Sample Used for the Tests and Test Procedures

A non-plastic silt with trace clay, having specific gravity (Gs) of 2.68, was used. The grain size distribution curve for sample is shown in Figure 1. After adding distilled water to the air-dried sample in order to adjust water content, it was stored for one day in a sealed container.

1.Preparation of Compacted Specimen. Dynamically compacted specimens were prepared in a mold of 10 cm diameter by using the rammer of 2.5 kg weight. Each sample was compacted in five layers and each layer was compacted with 25 times of tamping. Figure 2 shows the compaction curve for specimens prepared. The water contents in the unconfined compression tests were in the range of 11 to 23%. The

water contents in the unconfined compression tests were in the range of 11 to 23%. The optimum water content was about 20%. The compacted samples were kept in a closed container and trimmed before each test to a specimen size of 50 mm diameter and 100 mm height. These prepared specimens were used in the unconfined compression tests and the constant water content compression test.

2.Unconfined Compression Test and Constant Water Content Compression Test Measuring Matric Suction and Volume Change of Each Specimen. Figure 3 shows a sketch of the test cell used. After the specimen was set on the pedestal of the cell, the specimen was covered with a rubber membrane and a loading cap, and sealed with O-rings. The cell was filled with water before the test was carried out. During the test, the displacement of the cell water was measured with a weighing device that was connected to the inside of the cell. The volume change of the specimen was obtained by adjusting the recorded displacement of the cell water for the piston penetration into the cell. A ceramic disk, whose air entry value was 500 kPa, was sealed into the pedestal of the cell to measure the pore- water pressure in the specimen. In the loading cap, a porous metal plate was installed. An air line was connected to the loading cap and the pore-air pressure in the specimen was released
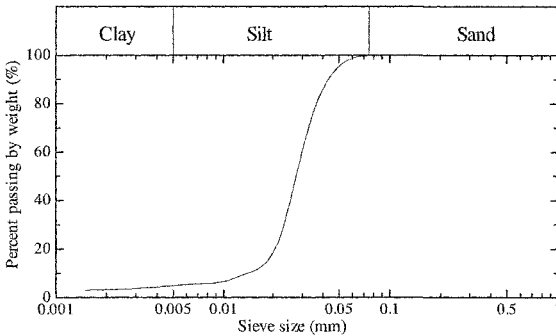
Figure 1. Grain size distribution curve sample used
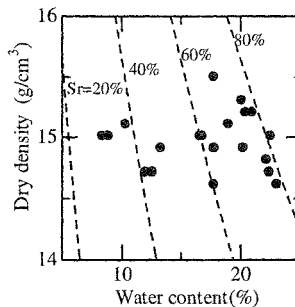
Figure 2. Compaction curve for specimen prepared
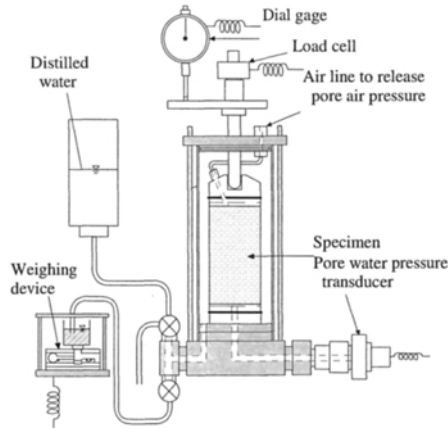
Figure 3. Sketch of test cell apparatus used

to atmosphere. The matric suction in the specimen was determined from the value of the measured pore-water pressure. The rate of axial strain was 0.1% per minute.

The unconfined compression test and the constant water content compression test under low confining pressure were carried out using the compacted specimen mentioned above. Both tests were carried out with almost the same procedure, but in the constant water content compression test, the confining pressures of 6, 10 and 50 kPa are applied before the shearing process. When these confining pressures were applied, both of the volume of the cell and the specimen will change. But in the calculation of volume of the specimen, these volume changes were ignored with the assumption that they were negligible. In the shearing process, the volume change of the specimen was measured with the displacement of the cell water. The shearing process in the constant water content compression test was carried out under undrained state which is the same condition as the unconfined compression test.

Stress-Strain Relation and Peak Strength Characteristics

All of the specimens expanded with the increase of axial strain in the shear process. The axial stresses showed peak values, and then reduced to the residual state as shown later in Figures 7 and 8. In the constant water content compression test, the specimen expanded more when the lower confining pressures were applied.

Figures 4 and 5 show the relationships between shear strain and matric suction for different test cases. Figure 4 shows results of the unconfined compression test for specimen compacted at different water contents. The legends of "Dry", "Opt" and "Wet" mean results of the specimen which compacted at the water contents of nearly 17%, 20% and 22%, respectively. From this figure, we can observe that matric

suction in the initial state becomes higher with the decrease in water content, and values of matric suction converge to almost the same value at residual state. Figure 5 shows the results for specimens compacted at the optimum water content under different confining pressures. The matric suction values in initial state are different with confining pressures, but the matric suction values in the residual state converge to the same value. These results show a tendency that the matric suction values converge to almost the same value in the residual state regardless of the initial states of specimen and the confining pressures.

Figure 6 shows relationship between the shear stress at failure and the stress parameter, p^* which is sum of p_{net} and the suction stress, p_s that is defined as follows (Karube et al. 1996).

$$p_s = \frac{S_r - S_{r0}}{100 - S_{r0}} \cdot s$$

where p_s : the suction stress.

From Figure 6, we can find that the stress states at failure state are arranged on a unique failure line. In this figure, the solid line shows the failure line for saturated specimen, which corresponds to 42 degrees of the internal friction angle. This result
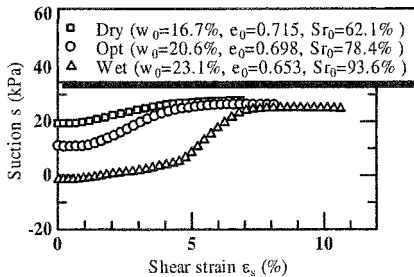
Figure 4. Relation between shear strain and matric suction for unconfined compression test
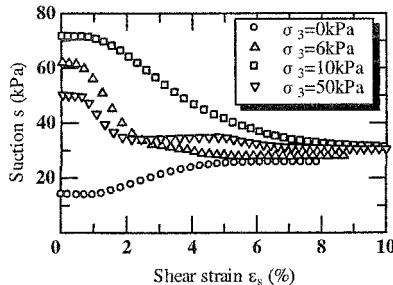
Figure 5. Relation between shear strain and matric suction for specimen compacted at optimum water content under different confining pressures
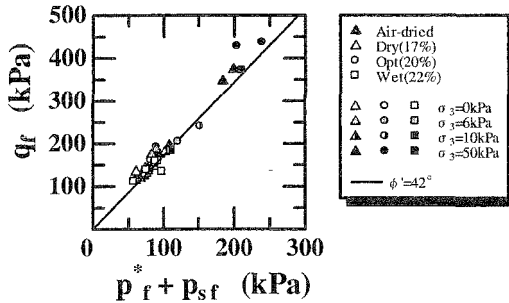
Figure 6. Relationship between shear stress at failure and p*

means that both the matric suction and the degree of saturation affect the peak strength of unsaturated soil (Kato et al. 2002).

Effects of Matric Suction on Residual Strength

Figure 7 and 8 show stress paths in q and ($p_{net} + p_s$) plane for the unconfined compression test and the constant water content compression test, respectively. In these figures, the solid lines show the failure line for saturated specimen, which corresponds to 42 degrees of the internal friction angle. From this figure, we find that the stress paths for all specimens show peak values of shear stress, q and then come around the failure line for saturated specimen. In Figure 8, the stress paths for the constant water content compression test show similar tendency under different applied confining pressures. These results show that the suction stress has influence on the stress states under residual state. This failure line was obtained by using the saturated compacted specimen that dilate during shear process, and was thought to correspond to the stress state for the peak shear strength. Therefore, the residual stress states for these test results reach to the failure line of peak stress state for saturated specimens. This phenomenon is different from the critical state for normally consolidated clay, because at the critical state, the stress state is on the failure line in which shear strain develops in constant volume state without stress change.

Karube et al. (1986) carried out triaxial compression tests on compacted kaolin specimen under constant matric suctions and mean net stress states in drained condition. From the test results, they pointed out effectiveness of the suction stress because the failure stress states obtained were arranged on a straight line on q vs. ($p_{net} + p_s$) plane. In their test results, the specimens contracted during the shear process. On the other hand, Kawai et al.(2002) carried out similar test for preconsolidated kaolin specimen. From the test results, they pointed out that the peak shear stresses for unsaturated specimen are higher than that for saturated specimen at the same value of ($p_{net} + p_s$). In their test results, the specimen first contracted, and then
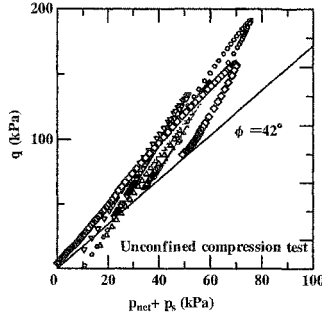
Figure 7. Stress paths with q and ($p_{net} + p_s$) in unconfined compression test
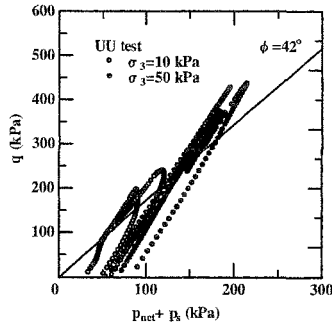
Figure 8. Stress paths with q and ($p_{net} + p_s$) in constant water content compression test

expanded during the shear process. Comparing these test results with those shown in Figures 7 and 8, we can understand the following behaviors; i) when an unsaturated specimen expands during shear process, it shows peak shear strength, and ii) the residual stress state reaches the failure line for saturated specimen, whether the peak value or the critical state is observed at the failure state.

Effects of Matric Suction on Change in Void ratio

Figure 9 shows relationship between void ratio and mean net stress. In this figure, the triangle plots show a compression curve obtained from slurry state specimen. From this figure, we can find that the specimens contracted firstly with the increase of mean net stress, but then expanded with decrease of mean net stress.

Figures 10 and 11 show relationships between void ratio and ($p_{net} + p_s$) in the unconfined compression test and constant water content compression test, respectively. Figure 10 shows that the decrease of void ratio is small in early stage of shear process, and that the specimen tends to expand when the stress state of ($p_{net} + p_s$) comes nearly to the maximum value and starts to decrease. And when the stress

state reaches to residual state, the plots come around the solid lines shown in each figures. We can understand that the slopes of the solid lines are bigger than the compression curve shown in the Figure 9. We can see that similar tendency is observed for the change in void ratio on the results shown in Figures 10 and 11. The solid line shown in Figure 11 has similar slope with that shown in Figure 10. The dotted lines shown in Figures 10 and 11 correspond to the residual state. When we compare Figure 11 with Figure 10, it is found that the doted line for the case $\sigma_3 = 50$ kPa shows different tendency from the other dotted lines.

Figures 12 and 13 show the similar relationships with Figures 10 and 11 for the cases when the void ratios "e_c" before shear process have nearly the same value in each case. In these figures, the triangle dots show compression curves shown in Figure 9 moving toward the vertical axis direction and parallel to the abscissa. From these figures, we can understand that when the void ratio before shear process has nearly the same value, the plots of residual states reach around the moved compression
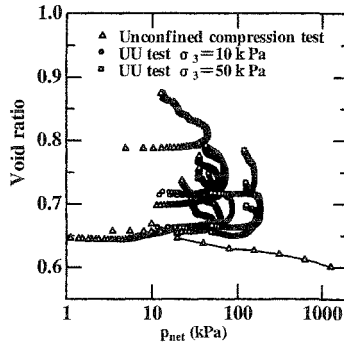
Figure 9. Relationship between void ratio and mean net stress
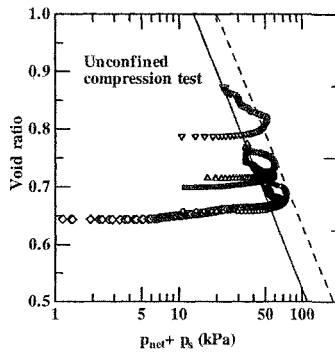
Figures 10. Relationship between void ratio and ($p_{net} + p_s$) in the unconfined compression test
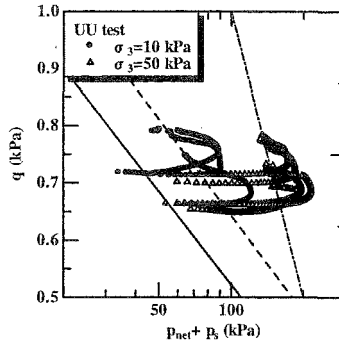
Figure 11. Relationship between void ratio and $(p_{net} + p_s)$ in constant water content compression test

curve even though the confining pressures are different. If we compare these results with the concept of critical state line for saturated soil, we can deduce that when the void ratio before shear process has different value, the critical state line moves parallel to the abscissa

The extended Cam clay models have been proposed and applied to the prediction of deformation for unsaturated soil. From the test results presented here, we find that the stress state in residual state corresponds to the peak stress state of saturated specimens, and also find a possibility that there exist parallel critical state lines for the specimens with different initial void ratio. These results mean that the proposed models for unsaturated soil need to be modified when they are applied for low confining stress state.

Conclusions

We studied the test data obtained in the past for silt specimen under low confining pressure (Kato et al., 2001 & 2002), and examined the residual strength and the deformation characteristics. From the examined results, it is found that the stress paths in q and $(p_{net} + p_s)$ plane for the unconfined compression test and the constant water content compression test reached the failure line for peak shear stress of saturated specimen. This result means that the suction stress, which is defined as a product of the matric suction and the relative degree of saturation, has an effect on the residual stress state.

When the void ratio before shear process has nearly the same value, the void ratios in residual states reach around the moved compression curve even though the confining pressures are different. It is also found that when the specimens have nearly the same initial void ratio and expanded in shear process, the parallel critical state lines could be recognized in the relations between the void ratio and the confining pressure that is taking account of the suction stress. This result is similar with that shown by Toll
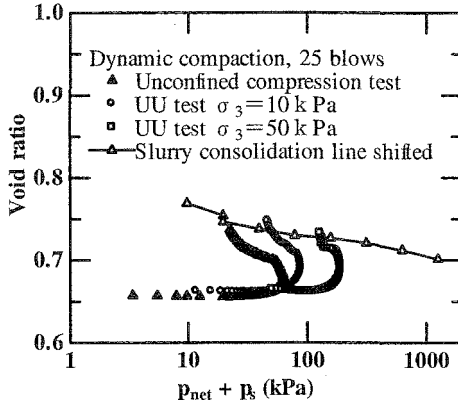
Figures 12. Relationship between void ratio and ($p_{net} + p_s$) for specimens with same initial void ratio (Case 1, $e_c = 0.65$)
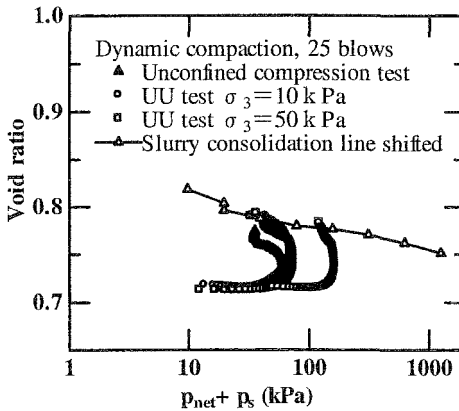
Figure 13. Relationship between void ratio and ($p_{net} + p_s$) for specimens with same initial void ratio (Case 2, $e_c = 0.70$)

& Ong (2003), and shows a possibility that the critical state exists under low confining pressure for unsaturated soil which expand in shear process. From these results, it is inferred that in some cases, the extended Cam clay models proposed need to be modified when they are applied for low confining stress state.

References

Abe, H.(1994). "Experimental study on the estimation of mechanical properties fro unsaturated soil." *Ph.D. thesis*, Tokyo University, Japan.

Alonso, E.E., Gens, A., and Josa, A.(1990)."A constitutive model for partially saturated soils." *Geotechnique*, 40(3), 405-430.

Karube, D., Kato, S., and Katsuyama, J. (1986). "Effective stress and soil constants of unsaturated kaolin." *J. Geotechnical Engineering*, JSCE, 370(III-5), 179-188.

Karube, D., Kato, S., Hamada, K., and Honda, M. (1996). "The relationship between shearing characteristics and the composition of pore-water in unsaturated soil." *J. Geotechnical Engineering*, JSCE, 575(III-40), 49-58.

Kato, S., Yoshimura, Y., Kawai, K., and Sunden W. (2001). "Effects of suction on strength characteristics of unconfined compression test for a compacted silty clay." *J. Geotechnical Engineering*, JSCE, 687(III-56), 213-218.

Kato, S., Yoshimura, Y., and Sunden W. (2002). "Effects of suction on unconfined compression strength and undrained shear strength of a compacted silty clay." *Proc. of the Third International Conference on Unsaturated Soils*, ISSMFE, Recife, 2, 513-519.

Kawaharada, T., Umezaki, T., and Kawamura, T. (2005). "Residual and peak strength of properties of unsaturated clay in ring shear test." *Proceedings of 40th annual conference of JGS,* JGS, 891-892.

Kawai, K., Karube, D., Kado, Y., and Kato, S. (2002). "The mechanical behavior of unsaturated soils and water retention characteristics on undrained triaxial compression test." *J. Geotechnical Engineering*, JSCE, 715(III-60), 287-296.

Kobari, Y., Nakamura, S., Nakamura, M., Ishihara, K., and Tsukamoto, Y. (2005). "Residual strength of partially saturated soils in triaxial compression tests with specimen's volume change control." *Proceedings of 40th   annual conference of JGS,* JGS, 889-890.

Kohgo, Y., Nakano, M., and Miyazaki, T. (1993). "Theoretical aspects of constitutive modeling for unsaturated soils." *Soils and Foundations*, 33(4), 49-63.

Fredlund, D.G., Morgenstern, N.R., and Widger, R.A. (1978). "The shear strength of unsaturated." *Canadian Geotechnical Journal*, 15, 313- 321.

Fredlund, D.G., and Rahardjo, H.(1993). *"Soil mechanics for unsaturated soils."* John Wiley & Sons, 220.

Scofield, A.W., and Wroth, C.P. (1968). "Critical state soil mechanics." London, McGraw-Hill.

Toll, D.G.., and Ong B.H. (2003). "Critical-state parameters for an unsaturated residual sandy clay." *Geotechnique*, 53(1), 93-103.

Vanapalli,S.K., Fredlund, D.G., Pufahl, M.D., and Clifton, A.W. (1996). "Model for prediction of shear strength with respect to soil suction." *Canadian Geotechnical. Journal*, 33(3), 379-392.

Wang, F., Sassa, K., and Fukuda, H. (2000), "Geotehcnical simulation test for the Nikawa landslide induced by January 17, 1955 Hyogoken-Nanbu earthquake." Soil and Foundations, 40(1), 35-46.

Wheeler, S.J., and Sivakumar, V. (1992), "Critical state concepts for unsaturated soil." *Proc. 7th Int. Conf. on Expansive Soils*, ISSMFE, 1, 167-172.

Residual strength of a low plasticity clay at high suctions

J. Vaunat[1], C. Amador[2], E. Romero[1]
and I. Djeran-Maigre[2]

[1]Technical University of Catalonia (UPC), c./ Jordi Girona, 1-3 Building D2, 08034, Barcelona, Spain; PH: (+34) 93.401.72.48; FAX: (+34) 93.401.72.51; email: *jean.vaunat@upc.edu*, *enrique.romero-morales@upc.edu*
[2]National Institute of Applied Sciences (INSA), Building J.C.A Coulomb, 34 avenue des Arts, 69621 Villeurbanne Cedex France
celine.amador@insa-lyon.fr, *irini.djeran-maigre@insa-lyon.fr*

Abstract: In this paper, tests conducted on a low plasticity clay in a Bromhead ring shear apparatus adapted to allow for suction control during the shearing phase are presented. Conclusions are drawn concerning the effect of suction on the residual strength of the material. Apparatus and test procedure are firstly detailed. Afterwards, a series of single and multi-stage shear tests performed on samples saturated, dried in one step, dried in several steps or wetted in several steps are described. It was concluded that suction does not introduce any cohesion-like component of strength but rather produces an increase in friction angle, possibly due to particle aggregation during drying.

Introduction

The residual strength is a parameter of significant importance in the design of structures founded on fissured and jointed clay materials because it gives the lower bound of the soil resistance mobilized along discontinuities. For example, Alonso (1998) cites the case of two earth dams, one founded on very soft clays and the second on claystones, with very similar cross sections and explains this similarity by the design constraints related to the low resistance mobilized in the claystones along horizontal continuous shearing bedding layers.

Since the early recognition of the importance of the residual strength by Skempton (1964), extensive investigations have been performed concerning the parameters that control its value. It is now of general acceptance that the residual strength is characterized by a null cohesion and a friction angle ϕ'_r that depends on stress level (Skempton, 1985; Stark & Eid, 1994), soil gradation (Skempton, 1964; Kenney, 1967; Lupini et al., 1981; Skempton, 1985), particle mineralogy (Mitchell, 1993),

rate of shearing (Tika et al., 1994) and pore water chemistry (Di Maio, 1996a, 1996b, Chighini et al., 2005). Lupini et al. (1981) proposed a framework to interpret the influence of soil grading on the basis of the type of shear mechanism (rolling, transitional or sliding) that develops during large displacements at the scale of soil particles. Mitchell (1993) pointed out that soil mineralogy should be added to this approach, in particular for the case of volcanic soils with large amounts of allophane that contains bulky-shaped particles rather than platy particles. The dependency of ϕ'_r on the salinity of pore water is another interesting phenomenon reported by Di Maio (1996a, 1996b) and Chighini et al. (2005) that highlights the importance of the microstructure and its changes on the residual strength.

In this paper, the influence of suction, another parameter likely to affect the residual strength through changes in soil microstructure, is analyzed. Residual strength is measured in a Bromhead ring shear apparatus adapted to allow for application of high suctions during shearing. Material tested is a low plasticity clay, a non-expansive material suitable for testing the apparatus developed in this work, before going through tests on more plastic clays. Equipment and procedures are described in a first part of the paper. In a second part, tests results are presented and discussed for the case of the material under study. The paper concludes with remarks concerning the influence of suction of the residual strength of the material.

Experimental device and procedure

Description of the apparatus: Tests have been conducted in a Bromhead (1979) ring shear apparatus adapted for allowing for suction control during the shearing phase. A picture of the general device is shown in Figure 1. A scheme describing the control of suction and the experimental set-up is depicted in Figure 2.
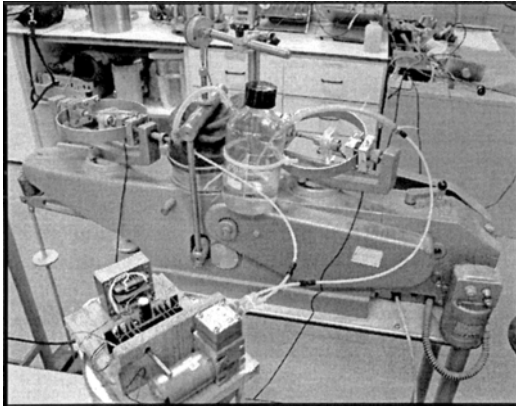
Figure 1. Picture of the apparatus.

The ring shear device is composed by two annular top and bottom plates. The bottom plate is connected to an electric motor and can rotate at a speed comprised between 0.025°/min and 60°/min. The top plate transmits the torque that is measured by two load cells and a torque arm. The shear resistance is then calculated as the force by unit area of soil sample that produces the same value of torque. The vertical load is applied through a frame and a lever mechanism. A micrometer is used to measure the vertical displacement of the top annular plate.

In order to apply suction to soil sample, the whole ring box is put inside a chamber isolated from the relative humidity of the room atmosphere by a vapour-tight rubber membrane. Two small tubes connect the chamber to the atmosphere prevailing above a saline solution in a closed recipient. A pump connected to one of the tube allows for establishing a forced convection of vapour in the circuit. A hygrometer equipped with an internal thermometer registers the values of relative humidity and temperature inside the chamber during the test.
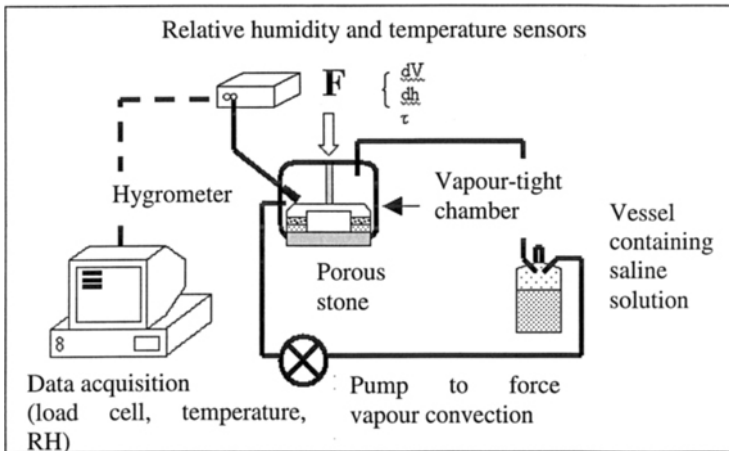
Figure 2. Scheme of the experimental set-up.

Tested material: Tested material is a low plasticity silty clay (Barcelona silty clay). Its liquid limit is equal to 30% and plasticity index to 14%. Particle density is equal to 2.71 Mg/m^3. Samples were prepared at a dry density equal to 1.9 Mg/m^3.

The retention curve of the material is depicted in Figure 3. Zone of interest for the present study is the zone where suction can affect the microstructure of the soil by changing content of microstructural water, bonded by absorption to soil particles. According to Romero (1999), this zone corresponds to a range of suction typically higher that 2 MPa. In that range, water content varies linearly with the logarithm of suction following two different slopes depending whether the soil is in the wetting or drying branch. The two lines intersect at a water content equal to 2.3% (see figure).

Below this water content value, water can be assumed to be strongly bonded to solid particles and very high suction changes are necessary to expel it.

Initial equilibrium: The soil is mechanically remolded close to its plastic limit and placed into the annular ring of inner radius 35 mm, outer radius 50 mm and height 5 mm. For the saturated tests, samples are then simultaneously loaded and flooded and the shearing stage started once consolidation displacement stabilized. For the unsaturated tests, the vertical load is first applied and vapour subsequently circulated in the circuit. In this case, shearing is launched once stabilized both the vertical displacement and the relative humidity measured inside the chamber by the hygrometer. The same procedure is repeated when load or saline solution are changed at intermediate times in multistage shear tests.

Three distinct saline solutions have been used: a saturated aqueous solution of NaCl to apply a relative humidity (RH) equal to 75%, a saturated solution of $Ca(NO_3)_2$ to apply RH = 51% and a saturated solution of LiCl for RH = 11%.
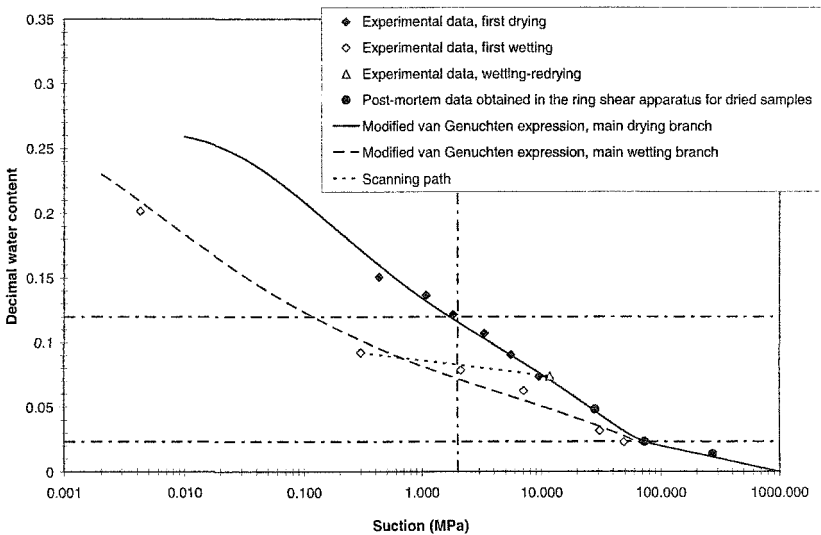
Figure 3. Retention curve of the material.

Time evolutions of vertical displacement and relative humidity inside the chamber during the equilibrium stage are depicted in Figure 4 for the case of an applied vertical stress equal to 300 kPa and a relative humidity controlled by LiCl solution. When loaded (t = 0), soil sample experiments an instantaneous displacement of 0.90 mm. Afterwards, consolidation starts accompanied with a differed increment of displacement equal to 0.21 mm at 1000 min. Between 0 and 1000 min, the chamber is connected to the vessel containing the saline solution, but the pump is not working. Change in relative humidity in the circuit is thus controlled only by the process of

vapour diffusion. As a consequence, RH increases inside the chamber, due to the fact that water evaporation from the sample is higher than vapour outflow. At time $t = 1000$ min, a forced convective flow of vapour is established in the circuit by turning on the pump. The relative humidity decreases then quickly in the chamber. At $t = 6500$ min, it reaches a stationary value equal to 14.5 %, slightly higher than the value imposed by the saline solution (11%). During all the drying process, the soil undergoes an increment of vertical displacement equal to 0.04 mm.

The same type of response is observed when other saline solutions are used. The final relative humidity attained in the chamber is equal to 79 % for NaCl solution and to 59 % for $Ca(NO3)_2$ solution. Approximate times to reach equilibrium are 3000 and 4000 min, respectively.
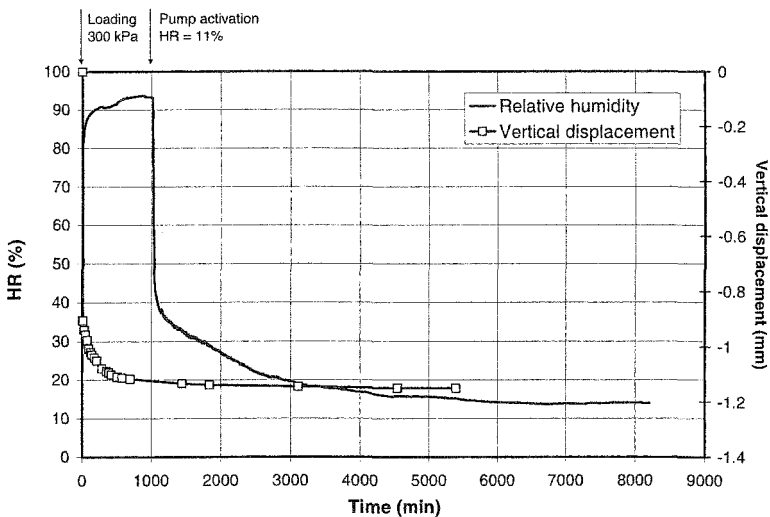
Figure 4. Time evolution of relative humidity and vertical displacement during the equilibrium stage of a sample submitted to a vertical stress equal to 300 kPa and a relative humidity controlled by LiCl aqueous solution.

Shearing stage: Once equilibrium is reached, shearing is carried out under the relative humidity applied by the saline solution and the applied vertical stress. To verify that shearing takes place under drained conditions, the effect of shear velocity has been studied. Two samples have been let to equilibrate under a relative humidity controlled by LiCl solution, which corresponds to the case of soil driest state and thus lowest unsaturated permeability. They have been then sheared at two rotational speeds: 0.024°/min and 0.12°/min. No differences have been detected in the value of shear strength. Consequently, all the tests have been performed at 0.12°/min.

Fluctuations of relative humidity and temperature inside the chamber have been registered during the shearing stage, which allows for a precise computation of the suction applied during the test. Figure 5 shows an example of the relative humidity and the temperature recorded during the shearing stage of a test performed under an atmosphere controlled by NaCl solution and a vertical stress equal to 300 kPa. In that particular case, relative humidity varies between 75.7 and 81.6 % and temperature between 23.8 and 26.6 °. From the psychrometric law, it comes then out that suction varies between 28.1 and 38.6 MPa. The range of suction variation is smaller for the other series of tests. Suction changes between 74.6 and 75.6 MPa when the relative humidity is controlled by $Ca(NO_3)_2$ solution and between 274 and 280 MPa when LiCl solution is employed.
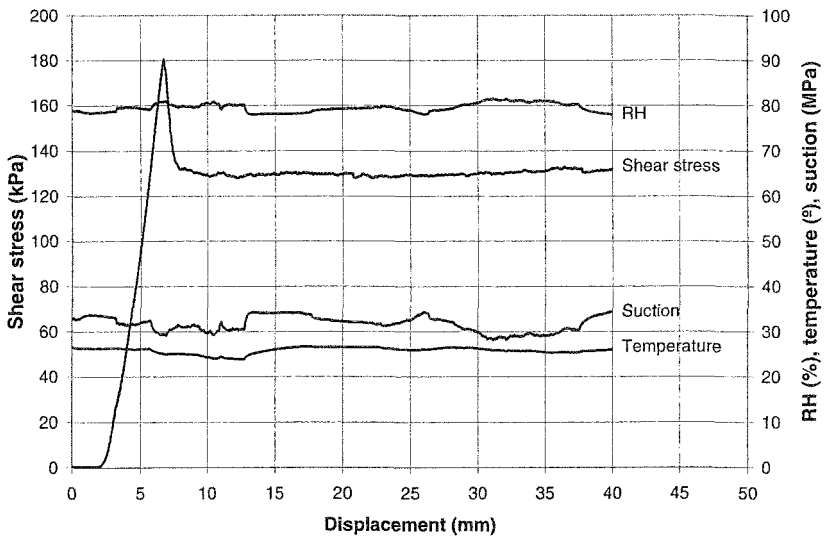
Figure 5. Data output during a shearing test performed under a relative humidity equal to 79% and a vertical stress equal to 300 kPa: evolution of relative humidity, temperature, suction and shear stress as a function of time.

Evolution of shear stress with displacement is also depicted in Figure 5 for the test described in the previous paragraph ($\sigma'_v = 300$ kPa, NaCl solution). After some delay due to gap closure in the system, the shear stress increases rapidly to a peak equal to 180 kPa for an increment of displacement of the order of 5 mm. Shear stress then decreases down to the residual value equal at 130 kPa at a displacement around 8 mm. Afterwards, shear stress varies between 127 and 135 kPa up to displacements of 40 mm, when test is stopped. The following remarks can be done: 1) the low value of displacement necessary to reach the residual state is consistent with the low plasticity of the clay; 2) suction fluctuations recorded during the tests affect only marginally the value of the residual strength that varies between ±2% of its average

value during the test. As a consequence and for the sake of simplicity, the series will be referred in the remaining text as being performed under suctions equal to 32, 75 and 277 MPa, respectively.

At the end of the test, sample is dismantled and water content measured. Points are reported on the retention curve shown in Figure 3 (black circles). They are in good agreement with the analytical expression used to fit experimental data obtained by psychrometer readings, which is an additional indication that shearing has been performed on soil samples in equilibrium with the above atmosphere.

Experimental results

Single-stage shear tests on dried samples: A series of four single-stage shear tests have been first carried out on samples dried from saturated conditions. Sample 1 has been sheared under saturated conditions, sample 2 at s = 32 MPa, sample 3 at s = 75 MPa and sample 4 at s = 277 MPa. The applied vertical stress is equal to 300 kPa. The displacement-shear stress curves obtained during the tests is represented in Figure 6.a. Sample sheared under saturated conditions exhibits a ductile response, characterized by a progressive increase of shear stress that reaches the residual strength without presenting any peak. Under unsaturated conditions, the response of the soil turns out to be more brittle. Strength passes through a peak before dropping towards the residual value. As the soil becomes drier, both values of peak and residual strength increase. Suction affects moreover the slope of the post-peak response of the material: at 32 MPa, a loss of strength equal to 50 kPa occurs for an increment of displacement of 0.66 mm. At higher suctions, the loss of strength takes place abruptly (vertical slope), suggesting a quasi-brittle type of response of the material. Evolution of vertical settlements is shown in Figure 6.b. It evidences that the ductile response in saturated conditions is associated with a compression of the sample whereas peak development in unsaturated conditions takes place at the moment of transition between sample contractancy and dilatancy, the latter increasing with suction. This would indicate that suction enhances the dilatancy of the material, a fact that has been already mentioned in triaxial tests by Barrera et al. (2002) and Cattoni et al. (2005) and in direct shear tests by Ng & Zhou (2005).

Multi-stage shear tests on dried and wetted samples: Multi-stage shearing tests have been performed in order to study the influence of suction and pre-shearing history on the value of residual strength. Two tests have been carried out: in the first test (labeled 5 in Fig. 7), a sample is sheared in saturated conditions and brought successively to suctions equal to 32, 75 and 277 MPa; in the second test (labeled 6), the sample is initially dried at a suction equal to 75 MPa, then wetted to a suction equal to 32 MPa and finally flooded. For each suction step, the soil is sheared three times under a vertical stress σ'_v equal respectively to 100, 200 and 300 kPa. The displacement - shear stress curves obtained at s = 0, 32 and 277 MPa and at a vertical stress equal to 300 kPa are compared in Figure 7 with the response registered at the same suctions and vertical stress during single-stage tests. Results indicate that: 1) the soil response is the same whether the sample has been submitted to a first-time

shear in saturated conditions (test 5) or sheared once flooded after six shearing stages at higher suctions (test 6); 2) the same response is also observed for the sample sheared at a suction of 32 MPa after having being sheared in saturated conditions (test 5) or at a suction equal to 75 MPa (test 6); 3) peak in strength at $s = 32$ and 277 MPa disappear for samples having known at least one pre-shearing stage; 4) residual strengths at any suction appear to be unchanged whatever are the number of pre-shearing stage and the history of suction.

Residual strengths are compiled in Figure 8 as a function of vertical stress and suction. They appear to depend linearly on the normal stress for the level of loads applied during the tests. Residual strength can be characterized by a null cohesion and a friction angle that increases from 19.6 to 24.5° when the soil passes from saturated to dry conditions.
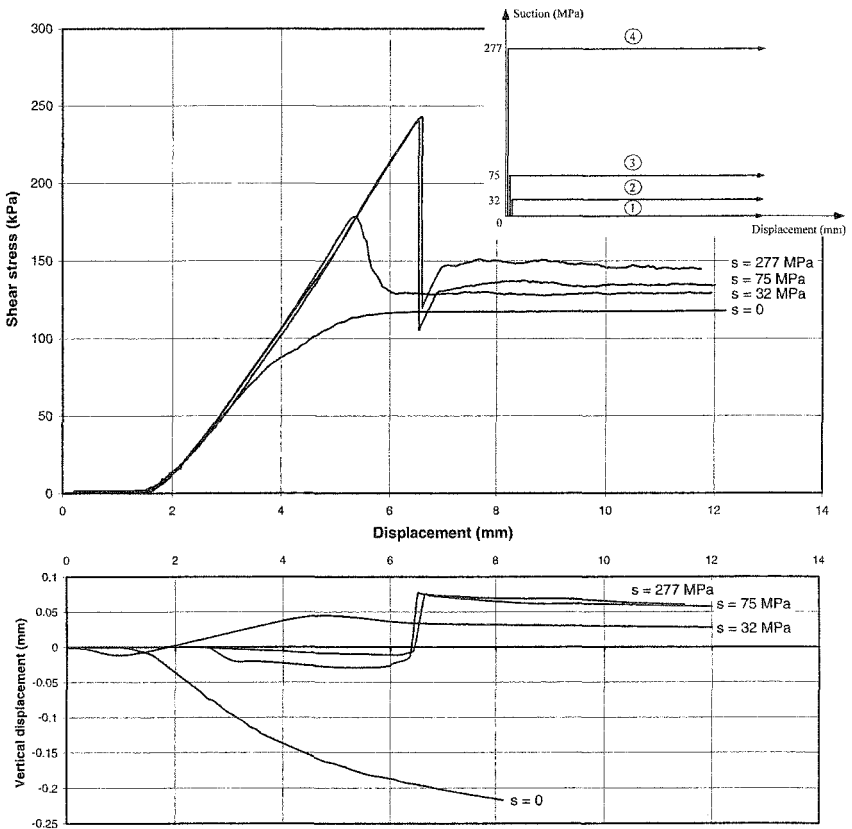
Figure 6. Experimental results obtained on samples dried to different suctions before shearing: a) displacement *vs* shear stress curves; b) displacement *vs* vertical settlement.
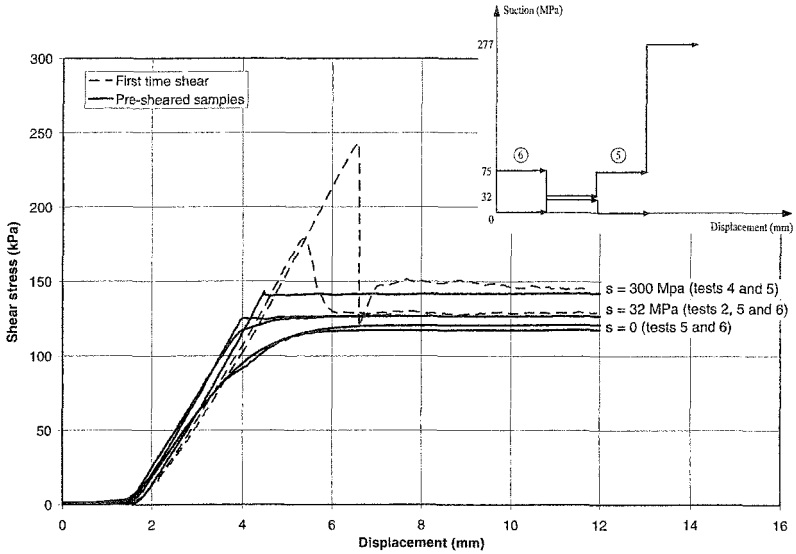
Figure 7. Comparison between displacement - shear stress curves obtained at different suctions during multi-stage (continuous line) and single-stage (dashed line) shear tests.
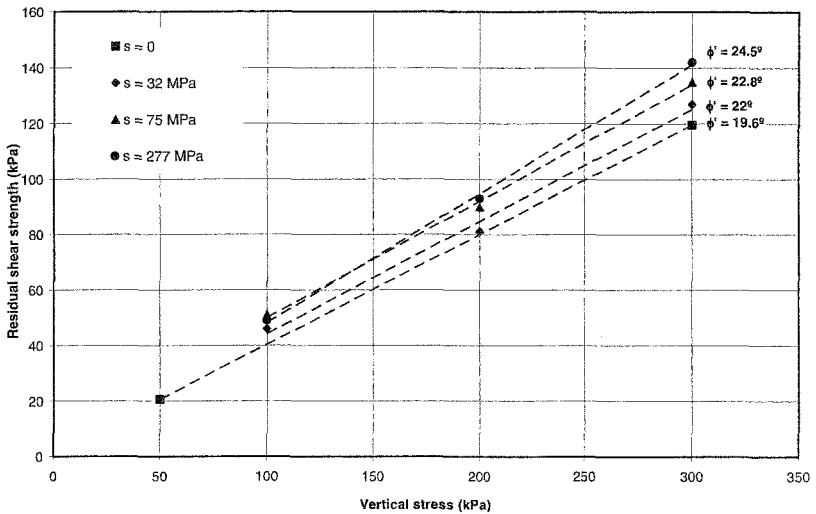
Figure 8. Residual shear strength envelopes.

Conclusions

A ring shear apparatus of Bromhead type has been adapted to apply suction during the shearing stages. Various controlled-suction tests have been performed on a low plasticity silty clay. Equipment and procedures insuring that sample is in equilibrium with the applied suction are described and results presented. They indicate thatsuction do not create a cohesive-like increase of residual strength but causes an increase of the friction angle. For the tested material, ϕ'_r passes from 19.6° in saturated conditions to 24.5° in the dry state. Measured residual strengths have been found to be independent of pre-shearing and suction history.

Tests provide moreover information about the volumetric response of the sample. When soil is dried in the shear box and a first-time shearing applied, soil presents a dilatant behaviour and its strength passes through a peak before reaching the residual value. This phenomenon can be seen as a genuine effect of suction, because, on the one hand, the same soil is contractant under saturated conditions and, on the other hand, there is no structure effect since the sample is placed remoulded in the apparatus. However, dilatancy disappears when the sample is pre-sheared before being dried.

These results tend to indicate that suction transforms the behaviour of the remoulded silt into that more characteristic of a granular material, possibly due to particle aggregation during drying, and that the aggregation process is different depending if the sample has been only remoulded or remoulded and pre-sheared in the ring apparatus. Tests on materials of increasing plasticity are now been performed to confirm this behaviour.

References

Alonso, E.E.. (1998). "General report. Cutting and natural slopes." *In Evangelista and Picarelli (eds), Proc. 2nd Int. Symp. The geotechnics of hard soils – soft rocks*, 1441-1481. Rotterdam : Balkema.

Barrera, M., Romero, E., Lloret, A. and Vaunat, J. (2002). "Hydro-mechanical behaviour of a clayey silt during controlled-suction shearing". *In Jucà et al. (eds), Proc. 3rd Int. Conf. on Unsaturated Soils*, 2, 485-490. Rotterdam : Balkema

Bromhead, E.N. (1979). "A simple ring shear apparatus". *Ground Eng.*, 12, 40-44.

Cattoni, E., Cecconi, M. & Jommi, C. (2005). "Soil dilatancy and suction: some remarks on their mutual effects on the shear strength of granular soils." *In Barla and Barla (eds), Proc. 11th Int. Conf. on Computer Methods an Advances in Geomechanics*, 2, 19-26. Bologna : Pàtron Editore.

Chighini , S. , Lancellotta, R., Musso, G. and Romero, E. (2005). "Mechanical behavior of Monastero Bormida clay: chemical and destructuration effects". *In Bilsel and Nalbantoğlu (eds), Proc. Int. Conf. on Problematic Soils*, Vol. 1, 381-388. Famagusta : Eastern Mediterranean University.

Di Maio, C. (1996a). "The influence of pore fluid composition on the residual shear strength of some natural clayey soils." *In K. Senneset (ed.), Proc. 7th Int. Conf. on Landslides*, 2, 1189-1194. Rotterdam : Balkema

Di Maio, C. (1996b). "Exposure of bentonite to salt solution: osmotic and mechanical effect." *Géotechnique*, 46(4), 695-707.

Kenney, T.C. (1967). "The influence of mineral composition on the residual strength of natural soils." *Proc. Geotech. Conf. on the Shear strength properties of natural soils and Rocks*, 1, 123-129.

Lupini, J.F., Skinner, A.E. and Vaughan, P.R. 1981. The drained residual strength of cohesive soils. *Géotechnique*, 31(2), 181-213.

Mitchell, J. K. (1993). *Fundamentals of soil behaviour. 2nd edition*, John Wiley & Sons, New York.

Ng, C.W.W. and Zhou, R.Z.B. (2005). "Effects of soil suction on dilatancy of an unsaturated soil." In *Proc. 16th Int. Conf. on Soil Mechanics and Geotechnical Engineering,* 2, 559-562. *Rotterdam : Millpress Science Publishers,*.

Romero, E. 1999. *Characterization and thermo-hydro-mechanical behaviour of unsaturated Boom clay: an experimental study.* Doctoral thesis, Universitat Politècnica de Catalunya, Barcelona.

Skempton, A.W (1964). "Fourth Rankine Lecture: long-term stability of clay slopes". *Géotechnique*, 14(1), 77-102.

Skempton, A.W. (1985). "Residual strength of clays in landslides, folded strata and the laboratory". *Géotechnique*, 35(1), 3-18.

Stark, T.D. and Eid, H.T. (1994). "Drained residual strength of cohesive soils". *J. of Geotech. Engng., ASCE*, 120(5), 856-871.

Tika, T. E., Vaughan, P. and Lemos, L. J. L. J. (1996). "Fast shearing of pre-existing shear zones in soil". *Géotechnique*, 46(2), 197-233.

Direct and Indirect Tensile Tests for Measuring the Equivalent Effective Stress in a Kaolinite Clay

L. F. Vesga, A.S.C.E. Member[1] and L. E. Vallejo, A.S.C.E. Member[2]

[1]Geomechanics, Inc. P.O. Box 386, Elizabeth, PA, 15037-0386; PH (724) 379-6300; FAX (724) 379-4242; email: vesgaluis@yahoo.com
[2]Department of Civil and Environmental Engineering, University of Pittsburgh, 3700 O'Hara St. Pittsburgh, PA, 15261; PH (412) 624-8188; FAX (412) 624-0135; email: vallejo@civ.pitt.edu

Abstract

Laboratory tests performed on unsaturated kaolinite clay show that the shear strength is function of the water content. Water contents used for the tests were obtained by drying the clay. Three different intervals of water contents in the clay were identified for which the shear strength varies in different way. When the clay has high water content, close to saturation, the shear strength increases as the water content is reduced. If the clay has a water content in an intermediate interval the shear strength is almost constant. For the interval of low water contents the clay presents lower shear strength as the water content is reduced, which is the opposite tendency for the interval of water contents that is close to saturation. In this article, the three water content intervals are related to three water distribution states of the water in the pores namely: the saturated-funicular state, the complete pendular state and the partial pendular state. On the other hand, the shear strength in the soil is represented as a function of the equivalent effective stress and the friction angle in the clay. The equivalent effective stress is determined through direct and indirect tensile tests. The friction angle that results from the above relationship is very similar to the friction angle of the clay when it is saturated.

Introduction

The evaluation of the tensile strength of unsaturated soils is an important area of research in geotechnical engineering because it permits to obtain the equivalent effective stress acting in the soil. In this study, Brazilian indirect tension tests (ASTM, D3967-95a) and direct tensile tests (Vesga, 2005) were performed on unsaturated

kaolinite clay samples to evaluate the equivalent effective stress, which was used to determine the shear strength of the unsaturated clay.

Air and Water Distribution in the Pores of the Clay

The air and water distribution in the pores of unsaturated clays can be used to explain the behavior of those clays when subjected to changes in stresses. German (1989) identified three forms of liquid distribution in the pores between packed particles: saturated, funicular and pendular states as shown in sections a-c of Figure 1, respectively. It can be seen that all the voids are filled with liquid in the saturated state (Figure 1a). Air bubbles are present in the voids in the funicular state, and the liquid phase is continuous (Figure 1b). There is no continuity in the water phase in the pendular state (Figure 1c). A ring of liquid (a capillary neck) exists at the contact points between neighboring particles, but the rings do not touch one another (German, 1989). Theoretical analyzes from Pierrat and Caram (1997) and Hotta et al (1974) show that the capillary force between two particles that are not in physical contact can drop to zero if the water volume in the capillary neck is reduced but the distance between particles is greater than zero. On the other hand, using the scanning force microscopy (SFM), He et al (2001) found that the capillary neck between particles in physical contact can disappear altogether when the relative humidity (*RH*) of the vapor phase around the capillary neck is lowered sufficiently below a critical value. As a result of these conditions under which capillary forces between particles can be lost, Vesga (2005) presented an additional stage added to Figure 1 in order to show a partial pendular state for which there are disconnected liquid contacts within the group of particles.
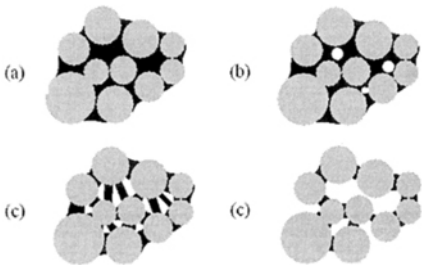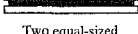
Figure 1. Stages of water distribution into a group of particles. a) Saturated state. b) Funicular state: air bubbles penetrate into the soil c) Complete Pendular state: all contacts with meniscus. d) Partial Pendular state: some liquid bridges break (Adapted from Vesga, 2005).

As is mentioned later, each the above states of water distribution inside the clay pores affects the overall strength of the clay. The clay behaves in different ways depending on the distribution of air and water. Vallejo (1989) showed that when using uniaxial compression tests on brittle kaolinite clay specimens prepared in the laboratory, a reduction in the strength occurred when the water content in the samples was reduced below $\omega=10\%$. Vallejo (1989) explained this behavior as a consequence of there have been more and more contacts between particles in the soil that lost their liquid contacts as the water content was reduced. His findings closely match the theoretical and experimental results mentioned below.

Inter-particle Attractive Forces and Equivalent Effective Stress

Saturated and Funicular States. In a saturated state (Figure 1a), the inter-particle attractive forces are due to the negative pore water pressure (u_w) in the pores, and the Terzaghi's effective stress principle applies (Terzaghi and Peck, 1948); correspondingly, the inter-particle attractive force increases as the negative pore water pressure increases. The effective stress (σ') is expressed as $\sigma'=\sigma - u_w$ (Eq. 1). If the level of matric suction ($s=u_a-u_w$) directly above the air entry value (AEV) is increased, air bubbles penetrate the soil (Fredlund and Rahardjo, 1993) and a funicular state (Figure 1b) is produced. In such cases, there is continuity in the water phase, and there remains an effective stress in the soil, caused by the combined effects of the total stress and the confinement of the matric suction; the equation for this relationship is given by $\sigma'=\sigma+s$ (Eq. 2). If the air pore pressure $u_a=0$ then Eq. 2 is equal to Eq. 1. When the soil is dried, the actual suction in the pores increases as a consequence of the water content having been reduced. In the saturated-funicular state, when the water content is reduced, both the effective stress increases and the shear strength increases.

CASE		AUTHORS
Two equal-sized spheres in contact	Two equal-sized parallel plates	Cho and Santamarina (2001)
Two equal-sized, separated spheres		Pierrat and Caram (1995)
Two different-sized spheres in contact		Mehrotra and Sastry (1979)
Two different-sized separated spheres	Sphere and a plate, separated	Hotta, Takeda and Iinoya (1974)
Sphere and a cone in contact	Sphere and a plate, separated	Ho et al (1974)
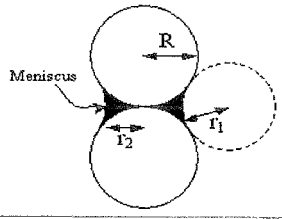
Figure 2. Theoretical cases for capillary contact force between two particles analyzed by several authors.

Figure 3. Pore water between two equal-sized spheres.

Complete Pendular State. In a complete pendular state (Figure 1c) the water phase in the soil is not continuous and the liquid bridges don't touch each other. As a result the effective stress cannot simply be attributed to the suction pressure in the meniscus. Several researches have analyzed theoretically the capillary force developed between two particles in the complete pendular state. Figure 2 offers an overview of studies of contact forces as they apply to spherical, planar, and conic-shaped particles. The various authors used different mathematical approaches to reach their respective solutions, but the shared of their analyses is that the capillary force between two

particles in a true-contact state tends to remain constant when the suction pressure in the meniscus is increased (identical results are obtained when the capillary neck volume is reduced and/or if the soil is dried). The simplest case of capillary force is the one between two equal-sized spheres in contact (Figure 3), in which the capillary force (F) -that the meniscus in a pendular state produces on the particles- results from two forces. One part of the attractive force is that produced by the unbalanced pressure (i.e., matric suction, $s=u_a-u_w$) acting on the cross sectional area of the meniscus. The second part is that produced by the liquid surface tension acting along the perimeter ($2\pi r_2$) of the capillary neck (Cho and Santamarina, 2001); F is given by

$$F=s(\pi r_2^2)+T_s(2\pi r_2) \qquad (3)$$

The combined effect of the matric suction s and the surface tension Ts of the water (0.0727 N/m at 20°C) is represented in Figure 4. The suction s and the surface tension Ts are related by the Laplace equation as

$$s = T_s\left(\frac{1}{r_1}+\frac{1}{r_2}\right) \qquad (4)$$

The Eq (3) shows a force F that remains constant as the actual suction pressure in the capillary neck is increased (as a result of the water content being reduced). If the contact forces inside the soil are constant when the actual suction pressure is changed, then the strength of the material should also be constant. As will be mentioned later, a constant uniaxial compression strength was observed in the kaolinite clay for an interval of water contents in the soil (different water contents in the soil correspond to different matric suctions). This expected behavior coincides with earlier theoretical analyses of the complete pendular state.
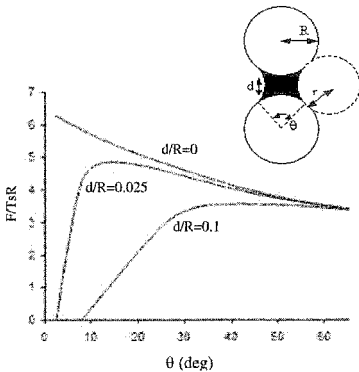
Figure 4. Effect of the separation d on the capillary force between two spheres (adapted from Pierrat and Caram, 1995).
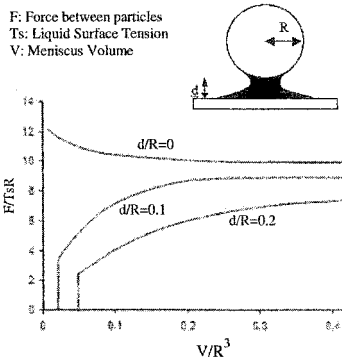
Figure 5. Effect of the separation d on the capillary force between sphere and a plate (adapted from Hotta et al, 1974).

Partial pendular state. Figure 4 shows two particles separated a distance d. Pierrat and Caram (1997) derived a mathematical expression to represent the capillary force for this case, which leads to the relationship shown in Figure 4. If the two particles are in contact, the distance d is zero and the force F reaches the maximum value possible. If, however, particles are not in contact then the contact force can be zero for low values of the contact angle θc (due to a low volume of the capillary liquid). As a result, the liquid bridge between particles can disappear and correspond to that partial pendular state. In addition, when capillary contact forces between particles are lost, the strength of the material of which the particles are part would diminish. Laboratory results shown below confirm that if the water content in the clay is reduced below a certain value, a resulting reduction in the overall strength can be expected. Another configuration that produces notable results is the one of a sphere and a plate (Figure 5), where once again, the capillary force can be deduced as a function of the suction pressure and the geometry of the liquid bridge. This would be the case of two plates having corner-to-face contact or edge-to-face contact. In cases like these, the capillary contact force can be zero even if the particles are separated from to each other. Contrary to the conclusion drawn from earlier research on this topic, it now appears that it is possible for the capillary neck between two particles in contact to disappear under two conditions: if there is a distance between the particles (as was explained above) or if the relative humidity (RH) in the vapor phase is low enough to produce this unexpected effect.

Figure 6, shows the relationship found by He et al (2001) of the pull-off force needed to separate two particles on the *RH* of the air surrounding the capillary neck; four zones can be identified from the relationship. In Zone 1, the force between particles increases as the relative humidity decreases. The force reaches a maximum and remains almost constant in Zone 2 and reduces progressively in the Zone 3 until the capillary neck disappears (in Zone 4). For the final residual condition, the inter-particle forces are dominated by the van der Waals interactions, and there is not capillary action after the capillary neck breaks.
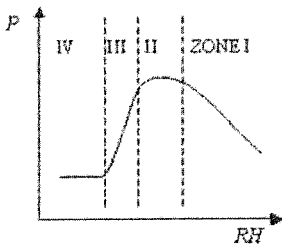
Figure 6. Relationship between the pull-off force (*P*) between two nanoparticles having a capillary neck, and the relative humidity of the vapor phase (*RH*) (Adapted from He et al, 2000).

The above conditions produce zero capillary force between particles, lead to a reduction in the equivalent effective stress in the surrounding soil that, in turn, translate to a reduction in the strength and an increase in the volume of the soil. As an illustration of the above, Vesga (2005) presented a simple test done using the triaxial chamber (see Figure 7). A drop of water was inserted into the tip of the loading piston, and a piece of foam was suspended and maintained in contact with the water;

then, the chamber was hermetically sealed, and a constant *RH* maintained (producing constant suction pressure in the foam). These conditions were maintained for 48 hr and then dry air was allowed to flow into the chamber to reduce the *RH*. As a result, the capillary contact force was reduced, and the foam fell, showing the reduction in the tensile strength of the contact.
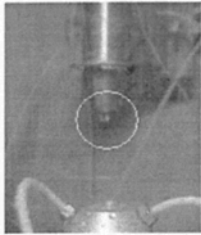
| (a) A drop of water in the piston tip that will provide the capillary forces. | (b) Foam suspended during 48 hr with suction pressure remaining constant in the triaxial chamber. | (c) The foam fell due to contact breakage after water evaporated (the suction was increased). |
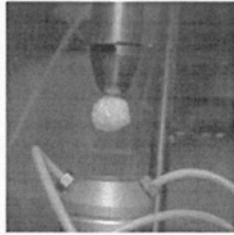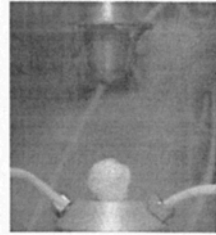
Figure 7. Simple test using a triaxial chamber to demonstrate that inter-particle capillary force lessens or disappears altogether when *RH* is reduced.

Plate stacks. Montmorillonite, kaolinite, and illite are clay minerals composed of plate-shaped particles (Lambe and Whitman, 1969). For parallel face-to-face plates, Cho and Santamarina (2001) developed a theoretical expression for the capillary force that depends on the actual matric suction pressure and the specific surface of the plates. According to Cho and Santamarina (2001), the capillary force increases progressively as the suction pressure increases. This would occur with a disperse structure in a clayey soil and could explain the high strength of high plasticity fine clays having low water content. However, clayey soils are composed of plates that can be arranged face to face and comprise/form stacks, as Figure 8 shows. The contact between two different plate stacks can be simulated by sphere-to-sphere or sphere-to-plate contacts, and lead to similar relationships, as Figures 4 and 5 show. This suggests that the capillary force between two stacks of plates would not be as strong as between two individual plates resting face-to-face; in addition, as explained above, the capillary force in clays can be very low or even zero if the amount of water in the capillary neck between stacks is reduced.
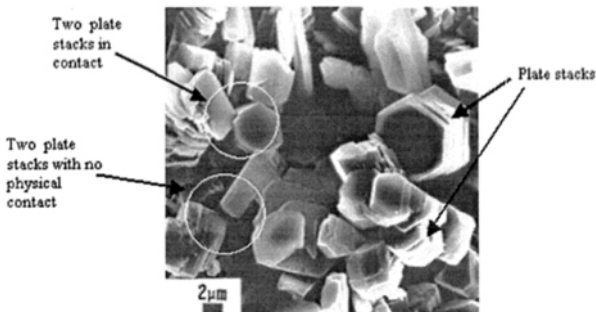
Figure 8. SEM picture of a kaolinite clay (adapted from Keller, 1985).

SEM photographs of the kaolinite clay used in the research. Scanning Electron Microscope (SEM) photographs were taken of samples of a number of kaolinite clay specimens used in this research. Figure 9 shows plate stacks of different sizes forming the clay. The differences in plate size, like the stack-to-stack contact mentioned earlier, could greatly influence the amount of capillary force between plates. This difference in plate size is illustrated in Figure 10, which shows large plates surrounding small plates. If, in fact, this apparent configuration is accurate, the distance between the large plates would be constant, and a pendular state could also exist simultaneously. In such a state, if the soil were dried, the resulting capillary neck could produce a capillary force of zero between large particles even though the large-plate-to-small-plate contact would still have a functioning capillary force. Breakage of capillarity necks in a soil leads to partial-pendular state (Vesga, 2005).

Equivalent Effective Stress and Shear Strength

The effective stress concept is useful for deriving the shear strength of saturated soils, but is not applicable when the soil is in pendular states. Rather, the equivalent effective stress is used instead to measure the effect of water distribution patterns in clay and, as such, relates to the effect of suction within the clay. For two particles with capillary force acting between them, the equivalent effective stress σ'_{eq} due to capillarity can be defined as the capillary force between the particles (F) divided by the effective afferent area that corresponds to that contact (A_{eff}) (Cho and Santamarina, 2001). The equivalent effective stress becomes

$$\sigma'_{eq} = \frac{F}{A_{eff}} \tag{5}$$

One of the problems associated with the Eq. 5 is that the force F depends not only on the surface water tension (Ts) but also on geometric conditions from each water bridge and from each particle in the soil; however, this information is not easy to obtain for a group of particles. Knowing the actual suction pressure in the meniscus is not enough to establish the shear strength of the entire group of particles; rather, the geometry of each meniscus in the soil, i.e., shape, arrangement, and distance of particles, is also needed. Instead of using the actual matric suction pressure acting on the meniscuses in a soil to study the behavior of unsaturated soil, Atkinson and Nocilla (2003) proposed the concept of equivalent suction pressure (s_{eq}) or equivalent pore pressure ($-u_{eq}$), which represents the mean stress caused by the capillary forces between individual particles. Indirect Brazilian tension tests (ASTM, D3967-95a) and direct tensile tests (Vesga, 2005) were used to measure the equivalent suction pressure in the clay, for this research. As there is no confinement in these tests, the total stress was zero and the equivalent suction pressure (s_{eq}) was equal to the equivalent effective stress in the soil σ'_{eq}. The equivalent effective stress in a cross section of a soil is defined as

$$\bar{\sigma}_{eq} = \frac{\sum F_c}{A} \tag{6}$$

where *Fc* is the component of a capillary inter-particle force that is parallel to the considered direction of σ'_{eq} and *A* is the total area of the section of the soil. This concept is very helpful in understanding the shear strength of soils subjected to suction. Using this concept, it is now possible to extend and apply the traditional effective stress concept for saturated soils proposed by Terzaghi (Terzaghi and Peck, 1948) more easily and to facilitate interpretations.

When the equivalent effective stress is known, the shear strength can also be obtained. The shear strength, in such a case would be the equivalent effective stress multiplied by the coefficient of friction between the particles plus the cohesion of the soil. As the equivalent effective stress σ'_{eq} depends on the attractive force between particles, the three states of water distribution in the pores would react as follows: a) for soil in the saturated-funicular state, the strength of a clay would increase as the water content is reduced, b) for soil in the complete pendular state, the strength of a clay would remain constant regardless of whether if the water content is changed or not, and c) for soil in the partial pendular state, the strength of a clay would diminish as the water content is reduced.
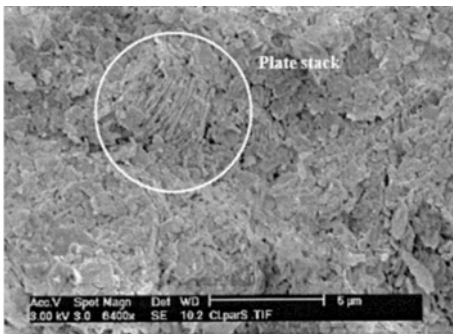
Figure 9. SEM pictures of the kaolinite used in the research. Plate-shaped particles of different sizes can be observed (Vesga, 2005).
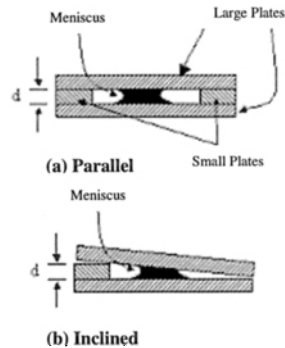
Figure 10. Meniscus formed between two large plates separated a distance *d* (Vesga, 2005).

Tensile Tests

Direct tensile tests. These tests were done on bowtie-shaped specimens as shown in Figure 11a. The specimen is subjected to a tensile force through two Plexiglass clamps that are pulled apart by a tensile force actuator Digital data regarding measurements of force and deformation were obtained using the data acquisition system DATAQ ID-194 and stored in a computer. The measurements of tensile strength (σ_t) from the direct tensile tests were based on the ratio between the force applied to produce the failure (F) of the specimen under tension and the cross-sectional area of the specimen neck $(\sigma_t = F/A)$.

Brazilian tension tests. The Brazilian test is an indirect type test that is used to determine the tensile strength of rocks (ASTM D3967-95a). This test uses a cylindrical sample of diameter D and length L that is diametrically compressed by two point loads (P) (see Figure 11b). The tensile strength σ_t of the cylindrical sample is obtained from $\sigma_t=2P/\pi LD$. A compression machine was used to apply the load.
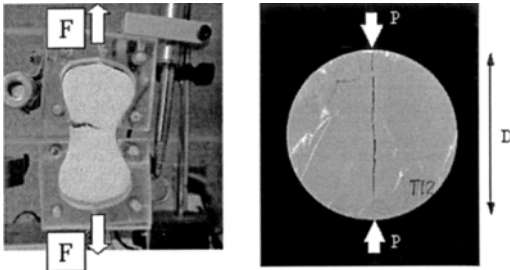
Figure 11. a) Result of a direct tensile test. b) Result of an indirect Brazilian tension test.

Specimens used in the tests. Cylindrical specimens were prepared for the Brazilian tests while bow-tie shaped specimens were prepared for the direct tensile tests. The liquid, plastic and shrinkage limits of the kaolinite are 44, 26 and 24 respectively and the specific gravity is 2.59. The specimens for the direct and indirect tensile tests had moisture contents between 3% and 32%, with intervals of around 3%. The sample preparation was done with the following process: a) Mixing the dry powdered kaolinite with distilled water to moisture content of 40% and until a smooth and uniform paste was obtained. b) Casting the paste into the molds (bow-tie shaped with 2.5 cm neck, 7 cm long and 2.2 cm thick and cylindrical 6.25 cm in diameter and 2 cm thick). c) Applying a vertical pressure of 30 kPa for consolidation during 24 hours in a closed environment with 75% of relative humidity (RH). d) Extracting the specimens and subjecting them to a drying process into an environment with a RH ~50%. e) After each specimen reached the desired moisture content (between 2% and 34%) it was stored into a plastic membrane during a 48 hour period in order to obtain a homogeneous moisture content through the samples.

Results. Figure 12 shows the results of the direct and indirect tensile tests, which measure the equivalent effective stress in clay having different water contents. In this figure, three clear zones can be identified. Zone I corresponds to the saturated-funicular state for moisture contents higher that 26%, Zone II corresponds to the complete pendular state for moisture contents between 12% and 26%, and the Zone III to the partial pendular state for moisture contents below 12%. The results show clearly that the equivalent effective stress concept adequately explains the strength of the clay. The tensile strength obtained with the Brazilian tests was found to be lower than that obtained with direct tensile tests. Compressed zones develop on the top and the bottom of the sample, close to the contact areas with the bearing plates. As a result, the diameter of the portion of the sample subjected to tension is reduced. Corrected values of the Brazilian tests using the actual diameter were determined.

Figure 12 compares the results and shows that direct tensile tests and the corrected Brazilian tests are close.

Shear strength

Traditional theories. The shear strength of unsaturated soils has traditionally been derived by one of two means. The first way is based on a relationship derived from the net pressure ($\sigma_f - u_a$) applied to the soil and on the actual matric suction pressure ($u_a - u_w$) to which the soil is subjected (Fredlund and Rahardjo, 1993); this equation is

$$\tau_f = c' + (\sigma_f - u_a)\tan\phi' + (u_a - u_w)\tan\phi^b \qquad (7)$$

where c': Cohesion intercept, σ_f: Normal stress at failure, u_a: Air pressure, u_w: Water pressure, ϕ', ϕ^b: Friction angles. Another commonly used equation to represent the shear strength of unsaturated soils is the following equation (Bishop and Blight, 1963):

$$\tau_f = c' + [(\sigma_f - u_a) + \chi(u_a - u_w)]\tan\phi' \qquad (8)$$

where χ is a parameter related to the degree of saturation of the soil. Although these means are commonly used, the shear strength of the unsaturated kaolinite clay used in this research could not be expressed using either Eq. 5 -or Eq. 6. This is because it was found that over a certain level of suction pressure ($u_a - u_w = 1 MPa$), the strength of the material was not affected by the degree of suction or the strength reduced as the suction was increased. This can be observed in Figures 13 and 14. The suction pressure increased remarkably but the increment is not reflected in the strength. As a result of these findings, the equivalent effective stress concept was used to explain the behavior of the unsaturated kaolinite clay as is presented below.
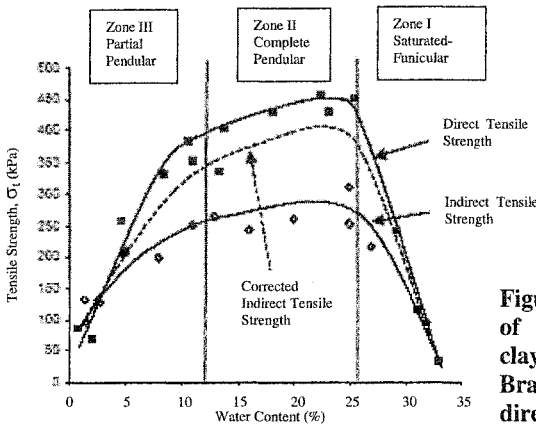
Figure 12. Tensile strength of unsaturated kaolinite clay from indirect Brazilian tension tests and direct tensile tests (Vesga,

Shear strength derived using the equivalent effective stress concept. As presented by Vesga and Vallejo (2005), the equivalent effective stress is the equivalent confinement applied to samples during the uniaxial compression tests and would be equal to the minor principal equivalent effective stress applied ($\sigma'_{3eq} = \sigma_t$). The values

of uniaxial strength presented in Figure 13, below, become the deviator stresses $(\sigma_u = \sigma'_{1eq} - \sigma'_{3eq})$, and the equivalent major principal stress can then be deduced as a function of the tensile strength $(\sigma'_{1eq} = \sigma_u + \sigma_t)$; this interpretation makes it possible to obtain the q-p plot at failure (Figure 15) by using the following equations

$$q = \frac{\sigma'_{1eq} - \sigma'_{3eq}}{2} = \frac{\sigma_u}{2} \quad \text{and} \quad p = \frac{\sigma'_{1eq} + \sigma'_{3eq}}{2} = \frac{\sigma_u + 2\sigma_t}{2} \quad \text{(9 and 10)}$$
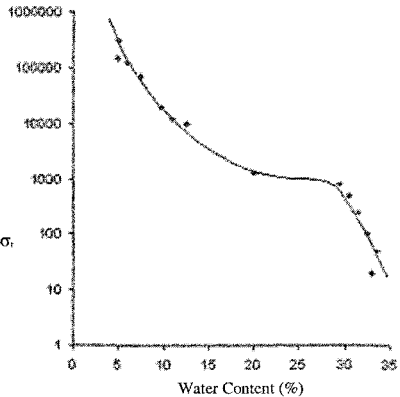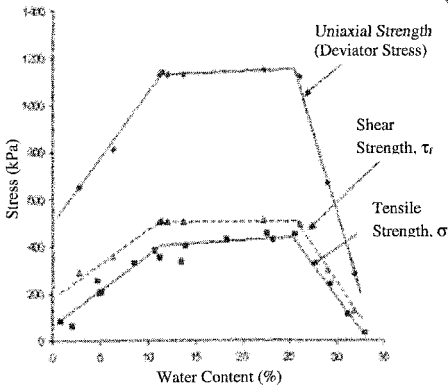
Figure 13. Uniaxial strength (σ_u), equivalent effective stress (tensile strength σ_t), and derived shear strength (τ_f) of kaolinite samples.

Figure 14. Water retention curve of the kaolinite clay for a drying path (the stress is the matric suction).

The data points shown in Figure 15 were derived from the values of the uniaxial compression strength (σ_u) and the correspondent tensile strength (σ_t) at the same water content obtained from Figure 12. The equivalent angle of internal friction (ϕ_{eq}) was established from the value of α using the relationship $tan(\alpha)=sin(\phi)$; $\phi_{eq} = 27°$. As Figure 15 indicates, this angle is very similar to the effective friction angle of the kaolinite clay used in the research $(\phi'=25°)$.
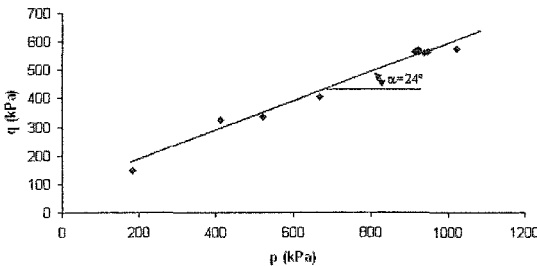
Figure 15. Diagram q-p derived from the uniaxial compression strength and the direct tensile strength (i.e., equivalent effective stress) of kaolinite clay samples.

Conclusions

Indirect Brazilian tension tests and direct tensile tests were performed on unsaturated kaolinite clay specimens prepared in the laboratory. Through the tensile strength of the clay the equivalent effective stress produced by the capillary forces between particles was obtained; this is a very important parameter that was used to derive the shear strength of the unsaturated clay using the concepts proposed by Terzaghi for saturated soils. Further research is necessary in order to apply these concepts to other soils.

References

ASTM (2001). "Standard Test Method for Splitting Tensile Strength of Intact Rock Core Specimens". Designation: D3967-95a (Reapproved 2001).

Atkinson, J and Nocilla, A. (2003). "Suction and strength in heavily compressed carbonate sand". *Geotechnique*, Vol. 53, No. 9, 831-832.

Bishop, A.W., and Blight, G.E. (1963). "Some aspects of effective stress in saturated and partially saturated soils". *Geotechnique*, Vol. 13, pp. 177-197.

Cho, G.C and Santamarina, J.C. (2001). "Unsaturated particulate materials - Particulate-level studies". *Journal of Geotechnical and Geoenvironmental Engineering. ASCE*. Vol. 127. No. 1. pp 84-96.

Fredlund, D.G., and Rahardjo, H. (1993). *Soil mechanics for unsaturated soils*. John Wiley and Sons. New York.

German, R. M. (1989). *Particle packing characteristics*. Metal Powder Industries Federation. Princeton, New Jersey.

He, M.; Szuchmacher, A.; Aston, D.E.; Buenviaje, C.; Overney, R.; Luginbuhl, R. (2001). "Critical phenomena of water bridges in nanoasperity contacts". *Journal of Chemical Physics*. Vol. 114. No. 3. pp 1355-1360.

Hotta, K; Takeda, K. and Iinoya, K. (1974). "The capillary binding force of a liquid bridge". *Powder Technology*. Elsevier Sequoia S.A., Vol. 10. 231-242.

Lambe, T.W and Whitman, R.V. (1969). *Soil Mechanics*. John Wiley & Sons, NY.

Mehrotra, V.P. and Sastry, K.V.S. (1980). "Pendular bond strength between unequal-sized spherical particles". *Powder Technology*. Elsevier Sequoia S.A., Vol. 25. 203-214.

Pierrat, P. and Caram, H.S. (1997). "Tensile Strength of wet granular materials". *Powder Technology*. Elsevier Science S.A., Vol. 91, 83-93.

Terzaghi, K., and Peck, R.B. (1948). *Soil mechanics in engineering practice*. John Wiley and Sons. New York.

Vesga, L.F. (2005). *Mechanics of crack propagation in clays under dynamic loading*. Unpublished PhD Dissertation. Department of Civil and Environmental Engineering. University of Pittsburgh.

Vesga, L.F. and Vallejo, L.E. (2005). "Strength of an Unsaturated Kaolinite Clay Under Suction Pressures". *16th International Conference on Soil Mechanics and Geotechnical Engineering*. ISSMGE. Osaka, Japan.

Vallejo, L.E. (1989). "Fissure parameters in stiff clays under compression". *Journal of Geotech. Eng., ASCE*, Vol. 115, No. 9, pp. 1303-1317.

This page intentionally left blank

Subject Index

Page number refers to first page of paper

This page intentionally left blank

Author Index

Page number refers to first page of paper